NASA TM X-3334

COLLECTED WORKS OF ROBERT T. JONES

CASE

National Aeronautics and
Space Administration

Ames Research Center
Moffett Field, California 94035

1. Report No.	2. Government Accession No.	3. Recipient's Catalog No.
TM X-3334		

4. Title and Subtitle	5. Report Date
Collected Works of Robert T. Jones	February 1976
	6. Performing Organization Code
7. Author(s)	8. Performing Organization Report No.
Ames Research Center, Moffett Field, Calif. 95035	A-6140
	10. Work Unit No.
9. Performing Organization Name and Address	
Ames Research Center Moffett Field, Calif. 95035	11. Contract or Grant No.
	13. Type of Report and Period Covered
12. Sponsoring Agency Name and Address	Technical Memorandum
National Aeronautics and Space Administration Washington, D.C. 20546	14. Sponsoring Agency Code

15. Supplementary Notes

16. Abstract

This collection includes papers on a variety of topics, especially aeronautics. Early work of the National Advisory Committee for Aeronautics on aircraft stability and control appears in the first section and is followed by original contributions in airfoil theory, including theories of sweptback and slender airfoils. Several papers are devoted to the theory of minimum drag and to the theory of the oblique wing.

Papers on geometrical optics appear next. Perhaps the most significant of these is the design of a fast (F/.66) monochromatic lens based on an inversion of the Schmidt arrangement.

Several papers based on work at Avco-Everett Research Laboratory on cardiac assist devices are included and show elementary applications of fluid dynamics to the design of blood pumps and in particular the intra-aortic balloon pump.

The last section presents some simple heuristic techniques in relativistic kinematics — based on conformal coordinates in two dimensions. Here the application to space-like motions provides an interesting duality with Einsteinian kinematics.

17. Key Words (Suggested by Author(s))		18. Distribution Statement
Aeronautics	Geometric optics	Unlimited
Aircraft stability	Blood pumps	
Wing theory	Relativistic kinematics	STAR Cat 02
Minimum drag		

19. Security Classif. (of this report)	20. Security Classif. (of this page)	21. No. of Pages	22. Price*
Unclassifie d	Unclassified	1,041	$15.25

For sale by the National Technical Information Service, Springfield, Virginia 22161

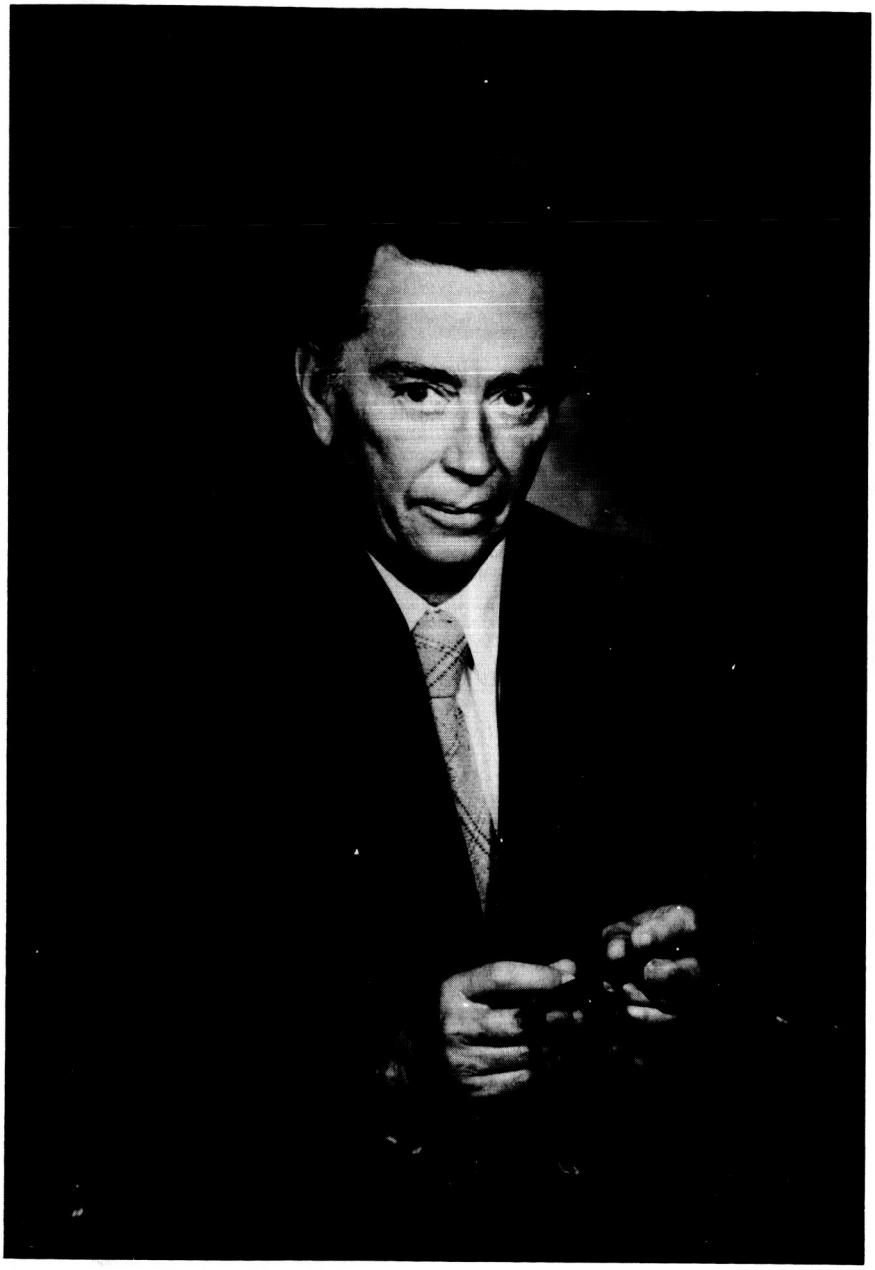

Robert T. Jones

FOREWORD

This volume is a tribute to a very remarkable man. It has been my great pleasure to have been associated with him for the past six years and, since I came late to the business of aeronautics, I had never had the pleasure of meeting Dr. Robert T. Jones before. During the period that I have had the opportunity to work with him I have developed an enormous respect for his technical abilities and also for his character as a man. His grasp of the physical sciences is as broad as that of anyone I know. It ranges from practical aeronautical engineering to the most advanced and abstruse statistical mechanics. What is more remarkable is that R. T.'s understanding is not superficial. In an amazingly short time R. T. can master a field to the point where he can make original contributions. R. T. is also an excellent teacher. He has a profound influence on those around him. In addition, his critical faculties are also exceedingly sharp. The Ames Research Center is indeed fortunate to count R. T. as one of us. He is unique and his work has added greatly to the Center's scientific and technical reputation. It is a genuine pleasure as well as an honor to have him here.

Hans Mark
Director

Ames Research Center

INTRODUCTION

The publication of this remarkable collection commemorates the 65th birthday of a very remarkable man, Dr. Robert Thomas Jones, Aeronautical Engineer, who first went to work for NACA 41 years ago. During this long Civil Service career, he has become one of the world's leading aerodynamicists, made discoveries that have changed the history of aeronautics, and received important honors. What sort of man is this, whose career has been so long and whose contributions have been so many and so important?

This question is, of course, a loaded one - as many will realize who know him - for nothing about Bob Jones is commonplace!

First, consider how he got into aeronautics. A fascination with aviation in the 1920's was, to be sure, commonplace among us who were schoolboys then. In Macon, Missouri, where he lived, young Bob read *Aero Digest*, treasured its cover pictures of the airplanes of the day, and pored over its technical articles on performance estimation, stability and control, and stress analysis. Assembling these and NACA Reports, he began the design and construction of a small, motorcycle-engined airplane, upstairs in his house. An unusual high-school mathematics teacher, Iva Z. Butler, helped him to understand stress and strain, but high-school graduation intervened, the airplane remained unfinished, and Bob went off to the University of Missouri in 1927.

But the aviation bug had bitten him badly. He discovered Walter Diehl's famous *Engineering Aerodynamics* and found it more exciting than the required courses of his freshman year. He left the university after that first year and entered the aviation industry - by working for Charles Fower's flying circus, which flew Standard J-1 biplanes; Bob carried gasoline cans, patched wing tips, and was paid in flying lessons!

In about 1929, there was considerable activity in aviation in the United States, including the Middle West. There were names like Alexander-Eaglerock, Beech, Cessna, Travel-Air, and Waco - some still around in 1975 and others nearly forgotten. A great demand for a "family flivver of the air" was expected. In Marshall, Missouri, the Nicholas-Beazley Company began manufacture of the Barling NB 3, a sporty, three-place, low-wing, cantilever monoplane. Bob, with his highly practical (if brief) background in the flying circus and a good recommendation from Charles Fower, landed a job there. It was not, at first, an engineering job, but young Jones made it clear that the engineering office was where he wanted to be - and when a vacancy suddenly occurred, there he was! Together with the company's chief engineer, Thomas Kirkup, Bob applied Diehl's aerodynamics, carried out stress analyses, and performed (late into the night) static tests to failure. But Nicholas-Beazley, with many others, was wiped out in 1930 by the business collapse.

The aviation industry recovered later in the '30's, and surely Bob's first jobs had prepared him admirably - even typically - to become an aircraft manufacturer or chief engineer - another Glenn Martin, Donald Douglas, or John K. Northrop. But whatever fates control the destinies of aeronautical engineers, with or without college degrees, had other plans for Robert Jones.

When Nicholas-Beazley folded, he returned home to study Glauert's *Aerofoil and Airscrew Theory* and Munk's *Fundamentals of Fluid Dynamics for Aircraft Designers*. His father was chairman of the local Democratic committee, and this helped young Bob get a job running an elevator in the House Office Building in Washington, D.C. Surely the above-mentioned fates had a hand in this, for the building was across the street from the Library of Congress. Bob paid visits to Dr. Albert F. Zahm, the Library's Director and once a member of the NACA. They must have talked about mathematics, for Bob decided to study that field. He began with Hamilton's quaternions! And when a Congressman, Honorable David J. Lewis, went to Dr. Zahm to request instruction in mathematics and physics - the Congressman was 65 and had finished with law and government - Dr. Zahm sent him to the bright elevator boy across the street. Bob taught the Congressman algebra and calculus.

At about this time, Bob made another friend whose influence on his career was tremendous: Dr. Max M. Munk, who had left the NACA, set up an office in Washington as consultant and patent attorney, and was giving evening courses at Catholic University. (He had also studied law, passed the bar exams, and learned Russian.) When he discovered that the elevator boy had studied his book, he suggested that he take his evening course - a graduate course. When Bob said that he might not be prepared for it (a suggestion that was certainly not characteristic of young Bob!), Dr. Munk gave him a little oral exam and enrolled him. Bob took Munk's evening courses for about three years - vector analysis, airfoil theory, and relativity theory - and drew upon this sound early teaching throughout his career. Thus Bob is truly one of the "Prandtl grandchildren" and an heir to that great tradition, with its deep, intuitive appreciation of the power of applied mathematics, without attraction to mathematics or mathematical elegance for its own sake.

The election of Franklin D. Roosevelt (1932) brought the Public Works Administration, and PWA opened up emergency jobs at Langley Memorial Aeronautical Laboratory. Dr. Zahm and Congressman Lewis saw Dr. George W. Lewis, NACA Head, and recommended Robert Jones for one of these jobs; Bob went to Langley, reporting to Carl J. Wenzinger, Charles Zimmerman, and Fred Weick, on a nine-month assignment as Scientific Aid. The fates had their way: It required a sequence of unlikely events and remarkable people, but Robert T. Jones was embarked on a career in research in the NACA and under the supervision of some unusually capable bosses.

Not surprisingly, ordinary linear differential equations was a subject missing from Bob's informal educational background - although he did know the quaternions and had read Grassmann's *Ausdehnungslehre* and similar classics in the original - so with Weick's and Zimmerman's guidance, he "learned by doing" differential equations. He published some of the earliest results of step-by-step solutions of the equations of airplane motion (obtained on desk calculating machines), such as the transient motions following abrupt, unit-step control deflections and gusts. He recalls that he became a sort of local authority on linearity after once calculating the transient motion following a two-unit step input, and comparing the results with unit-step results! He was also one of the first to apply Heaviside's operators to problems of airplane dynamics.

But the nine-month temporary appointment was about to expire. Bob's bosses, Fred Weick, and Henry Reid, Director of the Langley Laboratory, tried to arrange for him to take a Civil Service exam so they could hire him permanently, but the Civil Service rules specified a Bachelor's degree. Weick and Reid then thought to issue a special Civil Service exam that would require everything that Bob knew. In due course a special Civil Service examination was issued with questions on Hamilton's quaternions, operational calculus, aircraft stability and control, wing theory, and a few other subjects. To the surprise of those at Langley, a fellow showed up who offered this exotic combination and a Bachelor's degree as well. Weick assigned him to Bob Jones, who put him to work. Bob finally got a permanent appointment on a subprofessional grade. Some years later, when he approached the first professional grade P-1, he again encountered the requirement for the Bachelor's degree. This time the NACA was more ingenious - the stated requirements for grade P-2 did not mention any degree, so NACA promoted him directly to that grade!

By the time World War II began, Bob had published important papers, including a most ingenious way to find the transient lift on finite-span wings (page 193). He had become deservedly well-known in aeronautical circles, expecially as an expert in stability and control. At Northrop Aircraft we were struggling with the problems of the all-wing airplanes - XB 35, YB 49, etc. - and every trip to Langley Field, for wind-tunnel tests or other business, included a visit to Bob to discuss stability and control, and especially the properties of sweptback wings. When the first guided missiles were developed, Bob worked closely with the Army Special Weapons unit. In those days the missiles were actually pilotless airplanes, and one of them was a Northrop all-wing design with turbojet power (a rebuilt turbo-supercharger). The autopilot was made by the Hammond Organ Company. Mr. Laurens Hammond startled us by proposing one black box in the right wing with a pitch gyro, and another in the left wing with a tilted gyro for lateral control. Each of these controlled only its own "elevon" (combined elevator and aileron); there was no connection between the two autopilots and no connection between the two elevons. Even Bob Jones was horrified by the idea, but the little aircraft flew with faultless stability and control; there was, after all, aerodynamic coupling between its left and right sides, although the dynamics of the system could certainly not be divided into lateral and longitudinal motions. Bob was impressed with the unimportance of bilateral symmetry!

He first worked out his famous theory of low-aspect-ratio wings in 1944 (page 369). He was embarrassed when it was referred to under his name, because he thought it was an obvious extension of Dr. Munk's classical and well-known work. The rest of us have never found that the extension, involving as it does the recognition and treatment of the trailing vortices that lie behind all trailing edges, is at all "obvious". Bob did not even publish it at first, but later realized that it applied to high-speed flow, including supersonic, as well as to low-speed, because the flow near the axis of the Mach cone is similar to incompressible flow.

At about the same time, he remembered from an old NACA Technical Note of Munk's - T.N. 177 (1924) - that you can calculate the effects of sweepback and dihedral angle in a wing by an "independence principle": The two-dimensional flow around the wing due to the stream component perpendicular to the wing

axis is independent of the flow due to the stream component along this axis. Bob realized that this independence principle did not depend upon incompressibility, and thus he discovered the "theory of simple sweepback" (page 377), which is certainly one of the most important discoveries in the history of aerodynamics. At first he made the mistake of putting the low-aspect-ratio and the sweep theories in the same paper, but the NACA editorial committee, which had to approve the paper, believed the former and not the latter. As Bob says, "It has to be remembered that at that time there was thought to be a very great difference between subsonic and supersonic flow," so that it seemed, to some skeptics, impossible to render a supersonic flow essentially subsonic by such a simple device as sweepback.

While the argument with the editorial committee was still in progress, Bob's colleague, Robert Hess, read Adolph Busemann's 1935 paper concerning supersonic flow, and they realized that Busemann's argument would lead to the same result as Jones's, if the wing was swept behind the Mach cone. But Busemann had not discussed this case in his paper, so the editorial committee remained unconvinced. Bob divided the troublesome paper in two parts, and the low-aspect-ratio part was published. NACA began experiments in an effort to confirm the startling conclusions of the simple-sweep theory. Before the experiments were completed, V. E. Day occurred, Allied engineers went into Germany, and the news came back that the Germans knew about the effect of sweep and were using it on all of their new designs.

For his discovery of the sweep effect and other contributions, Bob was given the Sylvanus Albert Reed Award by the Institute of the Aeronautical Sciences in 1946. It was also in 1946 that he left the Langley Laboratory and moved to Ames.

About the time he moved to the West Coast, Bob acquired a new interest: telescopes. In characteristic fashion, this led him to a deep study of geometrical optics. He learned the art of grinding spherical mirrors and set up an impressive optical shop in the garage of his Palo Alto home. Also typically, he made inventions and original discoveries (which he calls "minor") in this field. The lens described starting on page 917 had a speed of f/0.66 and was "a sort of conjugate of the Schmidt telescope."

When the Space Age began in 1957, Bob and his wife expected telescopes to be much in demand. They formed the Vega Instrument Company, and went into production on a six-inch telescope of the type described starting on page 895, selling for about $800. They sold about ten of these and went on to a more elegant instrument: a six-inch Newtonian-Maksutov, selling for $1700. The idea was to make fewer telescopes and more money. Bob's son, Edward, worked for the Vega Instrument Company, as did a machinist and an optician. Although thirty of the Maksutovs were made, the company's profits hovered near zero.

Of course, Bob's interest and knowledge in astronomy was very timely: NACA became NASA, the "space agency," and Bob was one of the few aeronautical engineers who knew his way around the sky. He served for several years on the Astronomy Subcommittee. He had been fascinated by relativity theory since taking Munk's night courses in Washington. Now that space travel at great

speeds was a real possibility, he followed up a number of original ideas in this field (pages 927-956).

But he also continued to make profound discoveries in aerodynamics. One was the "supersonic area rule" which correctly carries into the supersonic regime the concept of equivalent body of revolution, which had been found so useful in the transonic regime (page 609). He thought about the effects of sweepback on boundary-layer behavior (page 473) and discovered an "independence principle" here, as well. (Professor Prandtl, V. V. Struminskii, and the present writer all came independently to this result at the same time! Dr. Munk was somewhat skeptical but told me, "Bob Jones says the same thing, so it must be right.") Another discovery was the existence of a new kind of leading-edge singularity in thin-wing theory (page 533). All of these papers are typical examples of Bob's insight and his direct, intuitive style of writing. Lesser aerodynamicists often find his arguments too concise, and the literature of the field includes papers in which authors re-do Bob's work, providing longer proofs, and discover again Bob's results.

In 1956 Bob and Doris Cohen were asked to write an important section of the Princeton Series, *High Speed Aerodynamics and Jet Propulsion*. This collaboration produced the section entitled "Aerodynamics of Wings at High Speeds." One of the features of this section is the analysis of the drag of elliptical wings, including those that fly at an angle of yaw. Thus Bob returned to the consideration of sweepback effects and asymmetrical configurations.

The analysis showed Bob that elliptic wings are ideal and that, at high speeds, they should be yawed. He remembered the unimportance of bilateral symmetry. In a series of papers (pages 657-883), he has pointed out the attractive properties - both aerodynamical and structural - of yawed (oblique) wings for supersonic aircraft. The spars of such wings carry the bending moment right across; it is not put into the variable-sweep mechanism. Bob and his NASA colleagues are pursuing this idea vigorously. The aeronautical world still seems hesitant to accept configurations without symmetry. Nevertheless, I, for one, fully expect to see future transport airplanes with "Jones oblique wings."

Here again are examples of Bob's insight into engineering problems: The aeroelastic properties of the oblique wing have frightened a number of engineers, for the upstream panel surely wants to deflect aeroelastically upward and the downstream panel downward. To Bob it seems obvious that these effects simply do not occur in flight. A study of the equilibrium of rolling moments will confirm that he is right. The details are left to the reader; it must be said that the conclusion is not quite "obvious," even to most aeronautical engineers!

Pages 957-1017 represent still another facet of R. T. Jones's career: studies of the bio-mechanics of blood flow. These were investigations carried out at the Avco Everett Research Laboratories.

But there is still another, most important side of Bob Jones, and one that this all-too-brief biographical sketch has ignored to this point. He is the father of six children (two adopted), of whom the eldest, Eddy, is now a

man of 41 years. Bob's relationship to them has been exceptionally warm and rewarding. A typical example comes to mind: Daughter Patty is a violinist, and by about 1956 had progressed so well that she needed a good violin. Her remarkable father agreed, and decided that he would study the acoustics of good violins and make one for Patty! Here, in his own words, is the story:

> "Milton Van Dyke gave me some reprints of scientific articles on the violin by his old physics professor, W. A. Saunders of Harvard. Saunders had made electronic-acoustic tests of many violins, including some valuable old Italian ones, and had elicited the help of Jascha Heifetz. By following Saunders' frequency-response curves, I should be able to make Patty a super-violin! So I set up the electronic testing, bought the wood, and after some months of spare-time work turned out a very good-looking violin. Unfortunately its tone seems to have deteriorated with time, or perhaps it wasn't as good as we thought at the time, and so I had to make her a second one (see page 1019). The second one seems to be really good, and Patty plays it at recitals and in the LaJolla Civic Symphony. I am now (1975) finishing number 6, but No. 2 has been the best until now. Am experimenting with 1500-Hz vibration dampers (this is the "nasal" range) and have made an electronic violin which my friend Irwin Hahn of the Berkeley Physics Department, and a violinist, thinks is very good."

In 1971, Bob was awarded the degree of Doctor of Science, *honoris causa*, by the University of Colorado, "in acknowledgement of his scientific eminence and his service to society." In 1973 he was elected to the National Academy of Engineering.

Aeronautical engineer, applied mathematician, astronomer, designer of telescopes, bio-mechanicist, maker of violins, inventor, author, discoverer of profound principles, civil servant, devoted father - our friend Bob is all of these. He is also a man of exemplary character and a most delightful companion on any occasion, whose intelligence and intellectual honesty shine brightly from those clear, big, blue eyes. No one really believes he has reached 65 years, for he is obviously ageless! He has no intention of retiring for some time. We can be certain that airplanes, fluid flow, violins, the stars, and perhaps many other things will continue to fascinate him and lead him to new truths in the future!

William R. Sears
University of Arizona

TABLE OF CONTENTS

	Page
FOREWORD	v
INTRODUCTION	vii
WING ANALYSIS: POBJOY RACEPLANE	1
CALCULATION OF THE MOTION OF AN AIRPLANE UNDER THE INFLUENCE OF IRREGULAR DISTURBANCES	21
A SIMPLIFIED APPLICATION OF THE METHOD OF OPERATORS TO THE CALCULATION OF DISTURBED MOTIONS OF AN AIRPLANE	31
THE EFFECT OF LATERAL CONTROLS IN PRODUCING MOTION OF AN AIRPLANE AS COMPUTED FROM WIND-TUNNEL DATA	45
A STUDY OF THE TWO-CONTROL OPERATION OF AN AIRPLANE	73
THE REDUCTION OF AILERON OPERATING FORCE BY DIFFERENTIAL LINKAGE	91
RÉSUMÉ AND ANALYSIS OF N.A.C.A. LATERAL CONTROL RESEARCH	117
THEORETICAL STABILITY AND CONTROL CHARACTERISTICS OF WINGS WITH VARIOUS AMOUNTS OF TAPER AND TWIST	147
THE INFLUENCE OF LATERAL STABILITY ON DISTURBED MOTIONS OF AN AIRPLANE WITH SPECIAL REFERENCE TO THE MOTIONS PRODUCED BY GUSTS	167
OPERATIONAL TREATMENT OF THE NONUNIFORM-LIFT THEORY IN AIRPLANE DYNAMICS	179
THE UNSTEADY LIFT OF A WING OF FINITE ASPECT RATIO	193
TRANSIENT EFFECTS OF THE WING WAKE ON THE HORIZONTAL TAIL	203
AN ANALYSIS OF THE STABILITY OF AN AIRPLANE WITH FREE CONTROLS	221
A GRAPHICAL METHOD OF DETERMINING PRESSURE DISTRIBUTION IN TWO-DIMENSIONAL FLOW	235
THEORETICAL CORRECTION FOR THE LIFT OF ELLIPTIC WINGS	245
NOTES ON THE STABILITY AND CONTROL OF TAILLESS AIRPLANES	251

WIND-TUNNEL INVESTIGATION OF CONTROL-SURFACE CHARACTERISTICS V - THE USE OF A BEVELED TRAILING EDGE TO REDUCE THE HINGE MOMENT OF A CONTROL SURFACE 281

DETERMINATION OF OPTIMUM PLAN FORMS FOR CONTROL SURFACES 307

EMERGENCY MEASURES FOR INCREASING THE RANGE OF FIGHTER AIRPLANES 315

EFFECT OF HINGE-MOMENT PARAMETERS ON ELEVATOR STICK FORCES IN RAPID MANEUVERS 335

WIND-TUNNEL INVESTIGATION OF A BEVELED AILERON SHAPE DESIGNED TO INCREASE THE USEFUL DEFLECTION RANGE 345

A METHOD FOR STUDYING THE HUNTING OSCILLATIONS OF AN AIRPLANE WITH A SIMPLE TYPE OF AUTOMATIC CONTROL 363

PROPERTIES OF LOW-ASPECT-RATIO POINTED WINGS AT SPEEDS BELOW AND ABOVE THE SPEED OF SOUND 369

WING PLAN FORMS FOR HIGH-SPEED FLIGHT 377

FLOW OVER A SLENDER BODY OF REVOLUTION AT SUPERSONIC VELOCITIES 385

THIN OBLIQUE AIRFOILS AT SUPERSONIC SPEED 403

SUBSONIC FLOW OVER THIN OBLIQUE AIRFOILS AT ZERO LIFT 415

ESTIMATED LIFT-DRAG RATIOS AT SUPERSONIC SPEED 425

EFFECTS OF SWEEPBACK ON BOUNDARY LAYER AND SEPARATION 473

THE USE OF CONICAL AND CYLINDRICAL FIELDS IN SUPERSONIC WING THEORY. . . 483

ECONOMY OF FLIGHT AT SUPERSONIC SPEEDS 499

A METHOD FOR PREDICTING THE STABILITY IN ROLL OF AUTOMATICALLY CONTROLLED AIRCRAFT BASED ON THE EXPERIMENTAL DETERMINATION OF THE CHARACTERISTICS OF AN AUTOMATIC PILOT 515

LEADING-EDGE SINGULARITIES IN THIN-AIRFOIL THEORY 533

THE SPANWISE DISTRIBUTION OF LIFT FOR MINIMUM INDUCED DRAG OF WINGS HAVING A GIVEN LIFT AND A GIVEN BENDING MOMENT 539

THE MINIMUM DRAG OF THIN WINGS IN FRICTIONLESS FLOW 557

THEORETICAL DETERMINATION OF THE MINIMUM DRAG OF AIRFOILS AT SUPERSONIC SPEEDS 567

POSSIBILITIES OF EFFICIENT HIGH-SPEED TRANSPORT AIRPLANES 579

MINIMUM WAVE DRAG FOR ARBITRARY ARRANGEMENTS OF WINGS AND BODIES 593

SOME RECENT DEVELOPMENTS IN THE AERODYNAMICS OF WINGS FOR HIGH SPEEDS 601

THEORY OF WING-BODY DRAG AT SUPERSONIC SPEEDS 609

THE COMPRESSIBILITY RULE FOR DRAG OF AIRFOIL NOSES 619

AERODYNAMIC DESIGN FOR SUPERSONIC SPEEDS 625

THREE-DIMENSIONAL WINGS OF MINIMUM PRESSURE DRAG 645

REDUCTION OF WAVE DRAG BY ANTISYMMETRIC ARRANGEMENT OF WINGS AND BODIES 657

NEW DESIGN GOALS AND A NEW SHAPE FOR THE SST 665

AN EXPERIMENTAL INVESTIGATION OF THREE OBLIQUE-WING AND BODY COMBINATIONS AT MACH NUMBERS BETWEEN 0.60 AND 1.40 673

TRANSONIC TRANSPORT WINGS - OBLIQUE OR SWEPT? 849

AIRCRAFT DESIGN FOR FLIGHT BELOW THE SONIC BOOM SPEED LIMIT 859

AEROELASTIC CHARACTERISTICS OF AN OBLIQUE WING 867

COMA OF MODIFIED GREGORIAN AND CASSEGRAINIAN MIRROR SYSTEMS 885

A PORTABLE 12-INCH 891

A WIDE-FIELD TELESCOPE WITH SPHERICAL OPTICS 895

SPACE SCIENCE - SOME SELECTED PROBLEMS AND ACCOMPLISHMENTS 903

WIDE ANGLE LENSES WITH ASPHERIC CORRECTING SURFACES 917

TIMES FOR INTERPLANETARY TRIPS 923

EXTENDING THE LORENTZ TRANSFORMATION BY CHARACTERISTIC COORDINATES 927

ANALYSIS OF ACCELERATED MOTION IN THE THEORY OF RELATIVITY 933

CONFORMAL COORDINATES ASSOCIATED WITH UNIFORMLY ACCELERATED MOTION . . 939

CONFORMAL COORDINATES ASSOCIATED WITH SPACE-LIKE MOTIONS 943

MOTIONS OF A LIQUID IN A PULSATING BULB WITH APPLICATION TO PROBLEMS OF BLOOD FLOW 957

ELEMENTARY THEORY OF SYNCHRONOUS ARTERIO-ARTERIAL BLOOD PUMPS 967

BLOOD FLOW 975

FLUID DYNAMICS OF HEART ASSIST DEVICES 999

A SIMPLE VIOLIN OSCILLATOR 1019

WING ANALYSIS: POBJOY RACEPLANE

Robert T. Jones

January 1930

WING ANALYSIS: POBJOY RACEPLANE*

R. T. Jones

The Pobjoy Raceplane is a light, low winged monoplane designed for high speed, maneuverability, and general high performance. The estimated characteristics are:

Gross Weight,	576#
Net Weight,	511#
Wing Span,	21.75'
Wing Area,	60'

The wing designed for this plane is of a new type being patented by Mr. H. G. Landis, and possesses many novel and unconventional features. The general arrangement of the structure will be seen in figures (1) and (2). Since it is of the multispar type and not subject to a rigorous analysis resort was made to an approximate calculation supplemented by a static test on a section of the wing (see "TEST ON A METAL WING").

The approximate method was completely verified and sufficient data obtained to design a wing for the racer. Several minor changes were made as follows: The shear bracing was changed from a Pratt trussing with tension strips to Warren truss of channel members, the truss members were centered on the outside of the beam flanges instead of on its neutral axis as before, the gauge of the material was increased and the size of the members decreased. These changes were thought desirable from the results of the test and serve to strengthen the structure by reducing the possibility of local failure and increasing the allowable stress in the material.

---

*Engineering Report: Nicholas-Beasley Airplane Co., Marshall, Mo., Dec. 1929-Jan. 1930.

The wing is constructed of aluminum alloy (25 ST) having the following properties: Yield Point, 30,000#/"; Tensile Strength, 55,000#/". The gauge used is .040".

Since the method of analysis used does not take into account the travel of the center of pressure, only the high angle of attack condition will be investigated. The validity of this assumption was also demonstrated by the test. The ultimate load sustained by the structure is not appreciably affected by twisting since the moments of inertia of the spars decrease progressively from the centroid as shown in Fig. (2). In the analysis the moments carried by the individual spars are proportional to their moments of inertia. All of the spars being of the same cross section, the end load carried by each can be determined in terms of the total moment across the section of wing. (See Fig. 1.)

$$M_o = \frac{M_t}{I_t} \cdot I_o \quad ; \quad P_o = \frac{M_o}{Y_o}$$

$$I_t = \sum_{8}^{1} ay^2 = (ay_1^2 + ay_2^2 + ay_3^2 + \ldots ay_8^2)$$

$$a = c \qquad \therefore \quad I_t = a \sum_{8}^{1} y^2$$

and

$$M_o = \frac{M_t a y_o^2}{a \sum_{8}^{1} y^2} \quad , \quad = \frac{M_t y_o^2}{\sum_{8}^{1} y^2} \quad ; \quad P_o = \frac{y_o}{\sum_{8}^{1} y^2} \cdot M_t$$

$y_1^2 = 1.05^2$	1.103	$P_1 = .0465\ M_t$	$M_1 = .0487\ M_t$
$y_2^2 = 1.75^2$	3.06	$P_2 = .0775\ M_t$	$M_2 = .135\ M_t$
$y_3^2 = 1.95^2$	3.80	$P_3 = .0860\ M_t$	$M_3 = .168\ M_t$
$y_4^2 = 1.80^2$	3.24	$P_4 = .0795\ M_t$	$M_4 = .143\ M_t$
$y_5^2 = 2.00^2$	4.00	$P_5 = .0884\ M_t$	$M_5 = .177\ M_t$
$y_6^2 = 1.75^2$	3.06	$P_6 = .0775\ M_t$	$M_6 = .135\ M_t$
$y_7^2 = 1.50^2$	2.25	$P_7 = .0663\ M_t$	$M_7 = .0995\ M_t$
$y_8^2 = 1.45^2$	2.10	$P_8 = .0640\ M_t$	$M_8 = .0930\ M_t$

$$\sum_{8}^{1} y^2 = 22.6$$

Knowing the proportional moment carried by each spar it is only necessary to determine the total moment at the section and, in the bay, the end load produced by the pull of the lift wires. The two stresses are then added and the margin of safety of the critical spar determined.

An elliptical lift distribution is assumed for the tip, which is elliptical in plan view. (See Fig. 2.)

LOADING PER INCH SPAN

tip length: 45" elliptical tip load: $\frac{X^2}{45^2} + \frac{W^2}{W_1^2} = 1$

uniform load in bay length of bay = 76.5"

gross weight = 576# net weight = 511#

$$\frac{45\pi W_1}{4} + 76.5\ W_1 = 255.5\#$$

$$W_1 = \frac{255.5}{\frac{45\pi}{4} + 76.5} = 2.275\#/" \text{ span}$$

Load Factor = 10 $\therefore$ $W_1 = 22.75\#/"$ span

MOMENT AT BRACE WIRES (M_b)

$\bar{X}$ (centroid of tip load) = 19.3", load on tip = $\frac{45\pi W_1}{4}$ = 803#

$$M_b = 803\# \times 19.3'' = 15500''\#$$

In determining the end loads in the spars and brace wires the shears at the fuselage and wire fittings will first be found by taking the moments of the elliptical tip load and the rectangular load in the bay separately and equating to equilibrium at the two points. The truss will then be solved by resolutions and checked graphically.

The bracing wires attach to the landing gear and make an angle of approximately 19 degrees with the wing spars. (See Figs. 2 and 3.)

e-b (end load in spars) = $R_1 \cot 19° = 1885\# \times 2.9042 = 5450\#$

e-a (end load in wires) = $R_1 \csc 19° = 1885\# \times \frac{1}{.32557} = 5750\#$

which agrees within the error of the graphical construction.

The bending moments in the bay produced by the combined side and end load will next be found. The wing is continued through the fuselage, making it necessary to first determine the fixing moment at that point. The Berry equations will be used together with a graphical solution.

FIXING MOMENT (M_a) (See Fig. 3.)

Berry Equation:

$$M_b L_1 f(\alpha_1) + M_a L_2 f(\alpha_2) + 2M_a [L_1 \phi(\alpha_1)] + L_2 \phi(\alpha_2) = \frac{W_1 L_1^3}{4} \psi(\alpha_1)$$

Solve for M_a:

$$M_a = \frac{\frac{1}{4} W_1 L_1^3 \psi(\alpha_1) - M_b L_1 f(\alpha_1)}{L_2 f(\alpha_2) + 2L_1 \phi(\alpha_1) + 2L_2 \phi(\alpha_2)}$$

M_b = 15500"#

W_1 = 22.75#/" span

$L_1 = 76.5''$

$L_2 = 18''$

E (duralumin) = 10,000,000

$$I = a \sum_{8}^{1} y^2 = 1.571'' \times .040'' \times 22.6''^2 = 1.4''^4$$

P = e-b = 5450#

$$\alpha = \sqrt{\frac{P}{EI}} \cdot \frac{L}{2}, \quad \alpha_1 = \sqrt{\frac{5450}{14,000,000}} \times 38.25'', \quad \alpha_2 = \sqrt{\quad} \times 9''$$

$$\alpha_1 = \sqrt{.00039} \times 38.25 = .0197 \times 38.25 = .755 = 43°$$

$$\alpha_2 = .0197 \times 9'', \quad = .1775 = 10°$$

$$f(\alpha_1) = \frac{6(2\alpha_1 \csc 2\alpha_1 - 1)}{(2\alpha_1)^2} = 1.344$$

$$\phi(\alpha_1) = \frac{3(1 - 2\alpha_1 \cot 2\alpha_1)}{(2\alpha_1)^2} = 1.1918$$

$$\psi(\alpha_1) = \frac{3(\tan \alpha_1 - \alpha_1)}{\alpha_1^3} = 1.2918$$

$f(\alpha_2) = 1.0144$

$\phi(\alpha_2) = 1.0082$

$\psi(\alpha_2) = 1.0123$

$$M_a = \frac{.25 \times 22.75 \times 76.5^3 \times 1.2918 - 15500 \times 76.5 \times 1.344}{18 \times 1.0144 + 2 \times 76.5 \times 1.1918 + 2 \times 18 \times 1.0082}$$

log .25	=	9.39790 - 10
log 22.75	=	1.35698
3·log 76.5	=	5.65098
log 1.2918	=	0.11126
antilog		(16.51712 - 10) = 3289000

$$\log 15500 = 4.19033$$
$$\log \quad 76.5 = 1.88366$$
$$\log \quad 1.344 = \underline{0.12840}$$
$$\text{antilog} \qquad 6.20239 = 1593500$$
$$3289000 - 1593500 = 1695500$$

$$18 \times 1.0144 = 18.28$$
$$2 \times 76.5 \times 1.1918 = 182$$
$$2 \times 18 \times 1.0082 = 36.30$$
$$18.28 + 182 + 36.30 = 236.58$$

$$M_a = \frac{1695500}{236.58} = 7170.0''\#$$

The restraining moments Ma and Mb, and the loading, Wl determine the bending moments in the bay. These will be found by a simple graphical method. This method has not yet been published and was discovered in England. The present use is due to Mr. T. A. Kirkup, who is chief engineer for the Nicholas-Beasley Airplane Company. As shown in Fig. 4 this method consists in laying off a segment, 2α, of a circle of radius $\frac{W_1}{P/EI}$, measuring toward the center a distance Ma on one side and Mb on the other. A circle passing through the origin (center), Ma, and Mb is then drawn. The distances between the arc 2α and the circle defined by the three points, along normals in the arc, determine the moment curve for the beam.

The bending of the tip beyond the brace wire attachment is neglected inasmuch as the gauge material and size of spars is continued the whole length and the bending moments necessarily decrease faster than the strength of the spars.

These reactions neglect the effect of the fixing moment, Ma, at the fuselage. This fixing moment produces an additional shear at the wire fittings tending to reduce R1.

Total shear at a-b- R1 - Sf

Sf shear due to fixing

The Ma determined from the uncorrected R1 is 7170#/" and is applied at a distance of 76.5" from the point a-b. Its effect is to reduce R1 by approximately 94#. In reducing R1, the end load, P, and the fixing moment itself are also reduced. The effect, however, is obviously small and is not considered in the calculation.

From Fig. 4 the bending moment in the bay is approximately 6000"#, Ma is 7170"#, and Mb 15500"#. Immediately to the left of the wire attachment the end load is being added to the end load produced by Mb. This will then be the portion of the wing receiving the greatest stress. For this reason a reinforcement will be added to the spars at this point extending in the bay to where the moment becomes of the order of Ma, approximately 10 inches. This reinforcement also serves to strengthen the wire attachment which is a tubular beam extending through the webs of the spars. (See Fig. 5.)

The margins of safety of the critical spars will be determined at four points: to the right and left of the wire attachment, at the maximum in the bay, and at the fuselage attachment. The pull of the wires is assumed to be equally distributed among the spars, the tubular wire attachment being sufficiently rigid to distribute the load.

From Fig. 1 it will be seen that spar No. 5 is critical for the restraining moments while spar No. 4 is so for the maximum in the bay.

At Ma

Spar No. 5

$$P_5 = .0884\ M_t = .0884 \times 7170 = 633\#$$

$$P_{t5} = 633\# + \frac{5450\#}{8} = 633\# + 681\# = 1314\#$$

$$f_b + f_c = \frac{1314\#}{.0628''^2} = 21000\#/''^2$$

$$M.S. = \frac{30000}{21000} - 1 = .43$$

At M_{max}

Spar No. 4

$$P_u = .0795\ M_t = .0795 \times 6000 = 475\#$$

$$P_{tu} = 475\# + 681 = 1156\#$$

$$f_b + f_c = \frac{1156\#}{.0628''^2} = 18400\ \#/''^2$$

$$M.S. = \frac{30000}{18400} - 1 = .63$$

To left of Mb

Spar No. 5

$$P_5 = .0884\ M_t = .0884 \times 15500''\# = 1370\#$$

$$P_{t5} = 1370\# + 681\# = 2051\#$$

$$f_b + f_c = \frac{2051}{.1256} = 1600\#/''^2 \text{ (.0628 sq. in. reinforcement)}$$

$$M.S. = \frac{30000}{16000} - 1 = .875$$

To right of Mb

Spar No. 5

$$P_5 = .0884\ M_t = 1370\# \text{ (end load not added)}$$

$$f_b = \frac{1370}{.0845} = 16000\#/''^2 \text{ (.0217 sq. in. reinforcement)}$$

$$M.S. = \frac{30000}{16000} - 1 = .875$$

The margins of safety of the spar flanges may seem unnecessarily high. Since little time was available for experimentation and the requirements of the particular case necessitated the utmost caution as regards strength of structure, it was not thought desirable to go below these figures.

The shearing forces in the wing will be considered next. A plan view of the shear webs together with a diagram showing the location of the struts with respect to the vertical shear load is given in Fig. 5. In finding the loads in these struts the shear across a section is divided among the webs of the spars in proportion to the bending moment carried by the spars. A maximum load will occur in one particular strut, located at the section of maximum shear and in the web of the deepest spar. This web connects spars No. 4 and 5 and makes an angle of approximately 25 with the chord line. This angle, together with the angle (45) in the plane of the web, serves to determine the inclination of the strut with respect to the vertical shear load as shown in Fig. 5. The maximum shear 1 load occurs at the wire attachment and is 1885# (see Fig. 3).

TEST OF SHEAR BRACING

The purpose of this test was to determine the margin of safety of the shear trusses in the multispar wing designed for the Pobjoy Raceplane. This wing (see Wing Analysis) consists of arc flanges or spars connected by inclined Warren trusses of channel section members, the whole being blanked and formed from a single sheet of aluminum alloy. In forming the channel members it was necessary to leave a considerable area of unstiffened material at the panel points. These members are centered on the outside of the flange in order to prevent local failure of the free edges by relieving the stress in them. Because of this intentional eccentricity and the fixity of the strut ends it was thought advisable to determine the strength of the channels by actual test.

The test was carried out in the following manner: A sample frame of the shear bracing was made up, using the same material (.040-25 ST) and dies used for the actual wing. This frame was bolted to a steel angle at two points and the load applied at the apex of the frame as shown in Fig. 6. This application of the load simulates the conditions existing in the wing, corresponding to the transmission of end load into the flanges and producing the same effects at the joints. The P/A stress in the struts is relatively small (see Wing Analysis) and little doubt was felt as to the ability of the channel to take the load, the main purpose of the test being to determine the effects of the secondary stress.

The load consisted of iron weights and was suspended from the frame by means of two steel straps pinned through with a 3/16 bolt. The location of the bolt and the application of the load are shown in Fig. 6. Using all the weights available, a load of 320# was applied to the structure and produced no visible deformation. Since this was in excess of the requirements of the wing and it was not thought desirable to reduce the size of the members for structural reasons, the test was not carried further. The load carried by each strut was approximately 227# and the P/A stress developed, 9080#/".

The material was the Aluminum Company of America's 25 ST alloy and has the following properties: Min. Yield Point, 30,000#/", Min. Tensile Strength, 55,000#/". Due to lack of data on open dural sections it is difficult to obtain a comparison but it is believed that with the slenderness ratio used the results are satisfactory.

A RACING PLANE THAT WEIGHS 355 POUNDS.

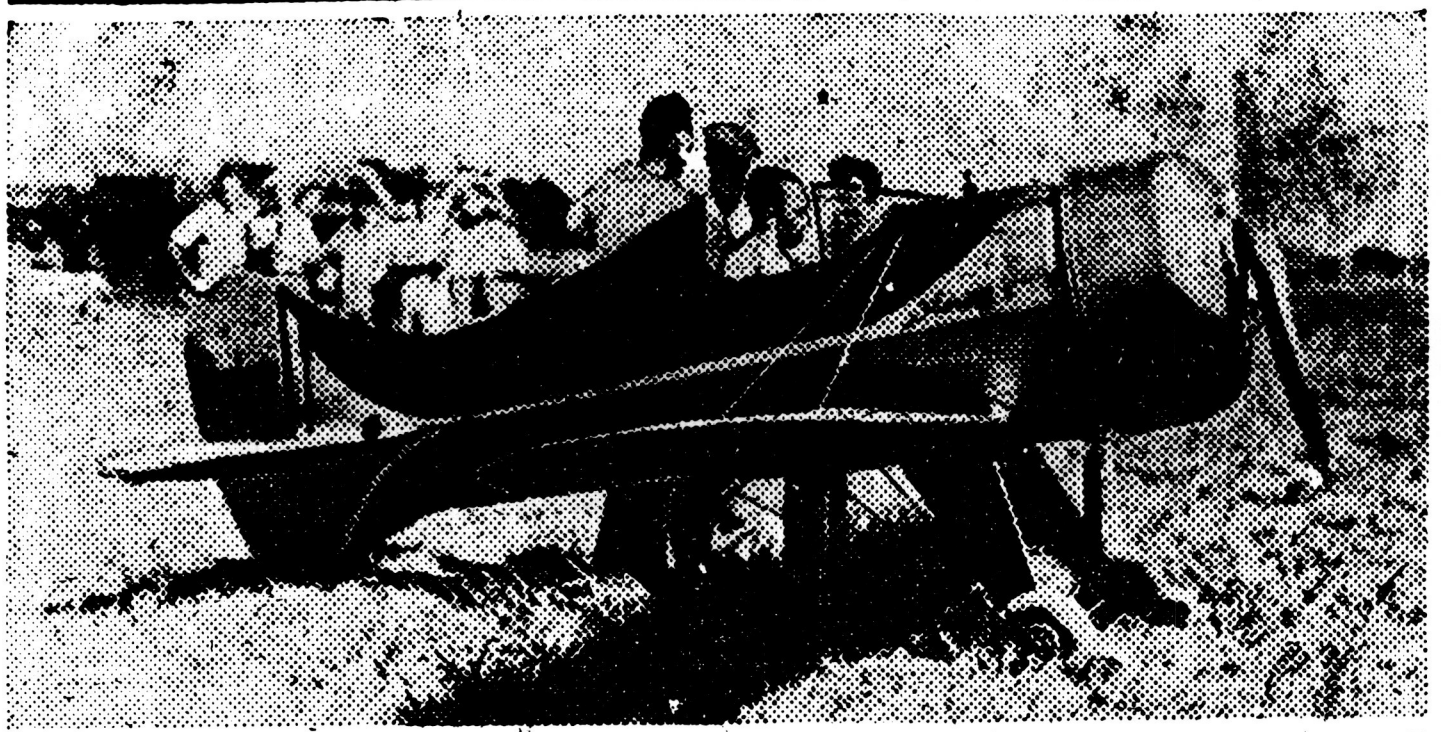

The "Phantom I," miniature racing plane built by the Marshall, Mo., Aircraft Laboratories, has been entered in the national air races in Chicago August 23 to September 1 The craft, which is capable of making more than 200 miles an hour, will be flown by D A. Fowlie of Morris, Ill.

Of low wing, all metal construction, the Phantom I is powered with a Popjoy motor which develops 72 horsepower and weighs 115 pounds. The total weight of the monoplane is 355 pounds. It has a patented wing of unusual construction with a spread of 21 feet and 9 inches and its fuselage is 12 feet and 9 inches in length.

It has been given an "R" license by the federal government.

m_n = moment exerted by single spar (flange)
p_n = load " " " " " "
For bending only: (subscript "t" indicates total)
$m_n = (m_t/Y_t) \times Y_n$; $p_n = m_n/y_n$
$Y_t = \sum$ area $\times y^2$, but area = a constant; $Y_t = a \sum y^2$
and $m_n = m_t y_n^2 / \sum y^2$, and $p_n = m_t y_n / \sum y^2$

$y_1^2 = 1.95^{in} = 1.10$	$p_1 = .0445^{p} \; m_t$	
$y_2^2 = 1.75^{in} = 3.06$	$p_2 = .0775^{p} \; m_t$	
$y_3^2 = 1.95^{in} = 3.80$	$p_3 = .0860^{p} \; m_t$	
$y_4^2 = 1.80^{in} = 3.24$	$p_4 = .0795^{p} \; m_t$	
$y_5^2 = 2.00^{in} = 4.00$	$p_5 = .0885^{p} \; m_t$	
$y_6^2 = 1.75^{in} = 3.06$	$p_6 = .0775^{p} \; m_t$	
$y_7^2 = 1.50^{in} = 2.25$	$p_7 = .0665^{p} \; m_t$	
$y_8^2 = 1.45^{in} = 2.10$	$p_8 = .0690^{p} \; m_t$	
$\sum y^2 =$	22.6^{in}	

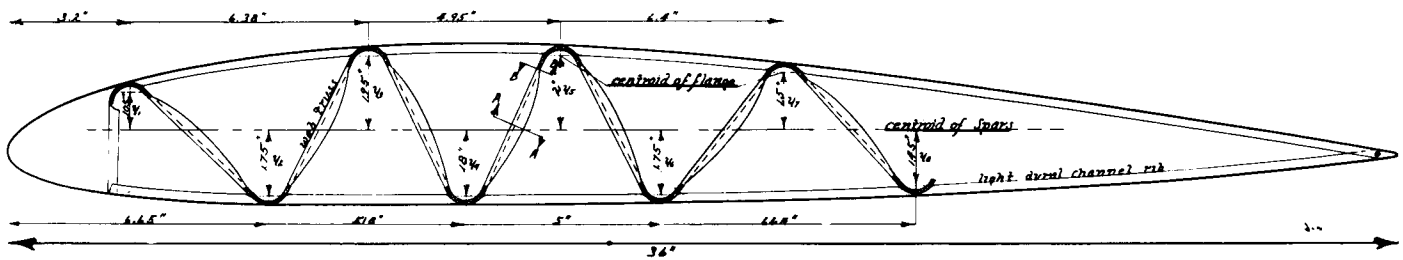

Fig. 1.– SECTION of WING
Showing Approximate Method of Analysis
1/4 Scale: Material 25ST (Dural)

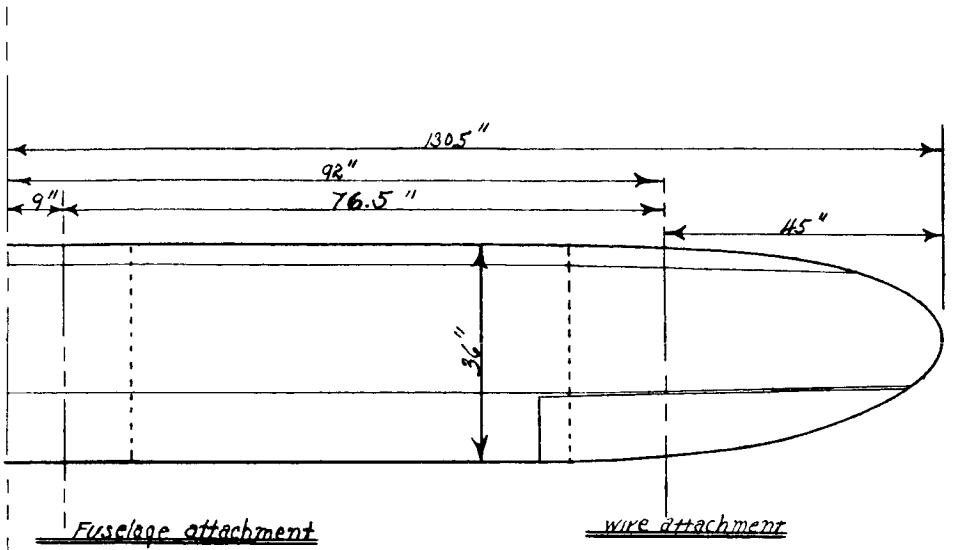

PLAN

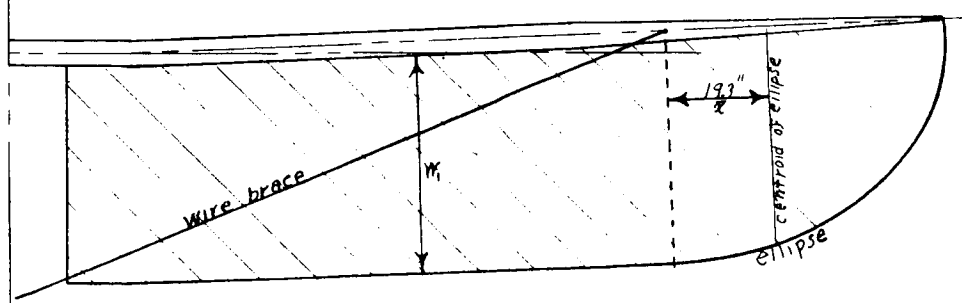

LOADING CURVE

FIG. 2

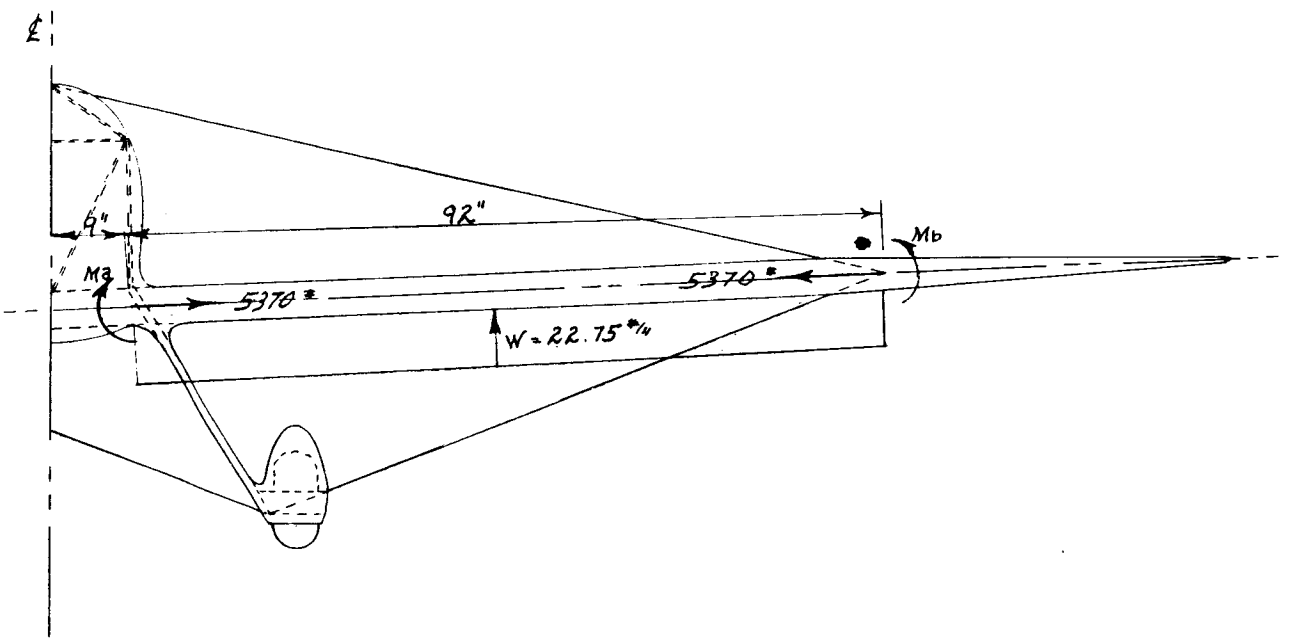

Fig. 3

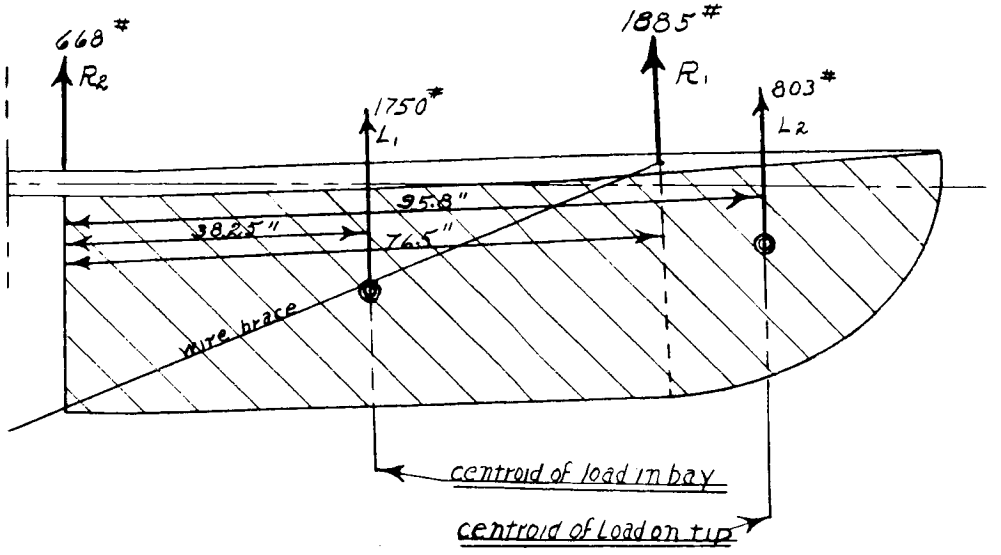

— Reactions at Supports —

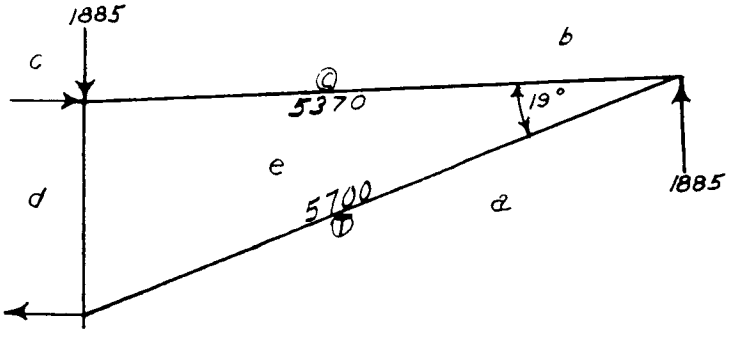

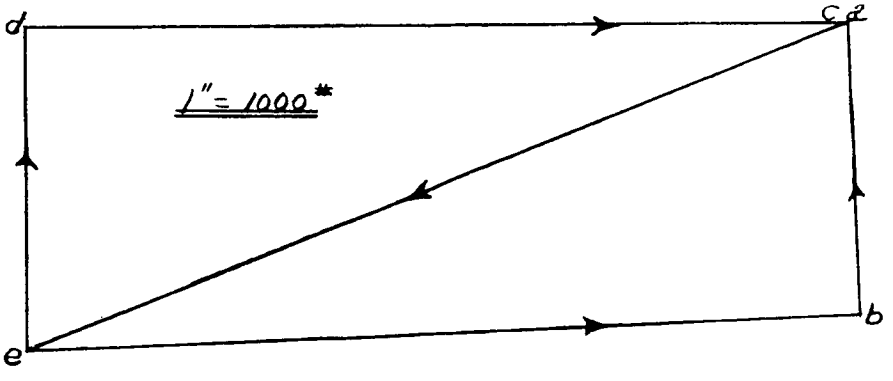

— End loads in Spars & wires —

Fig. (3) – Concluded.

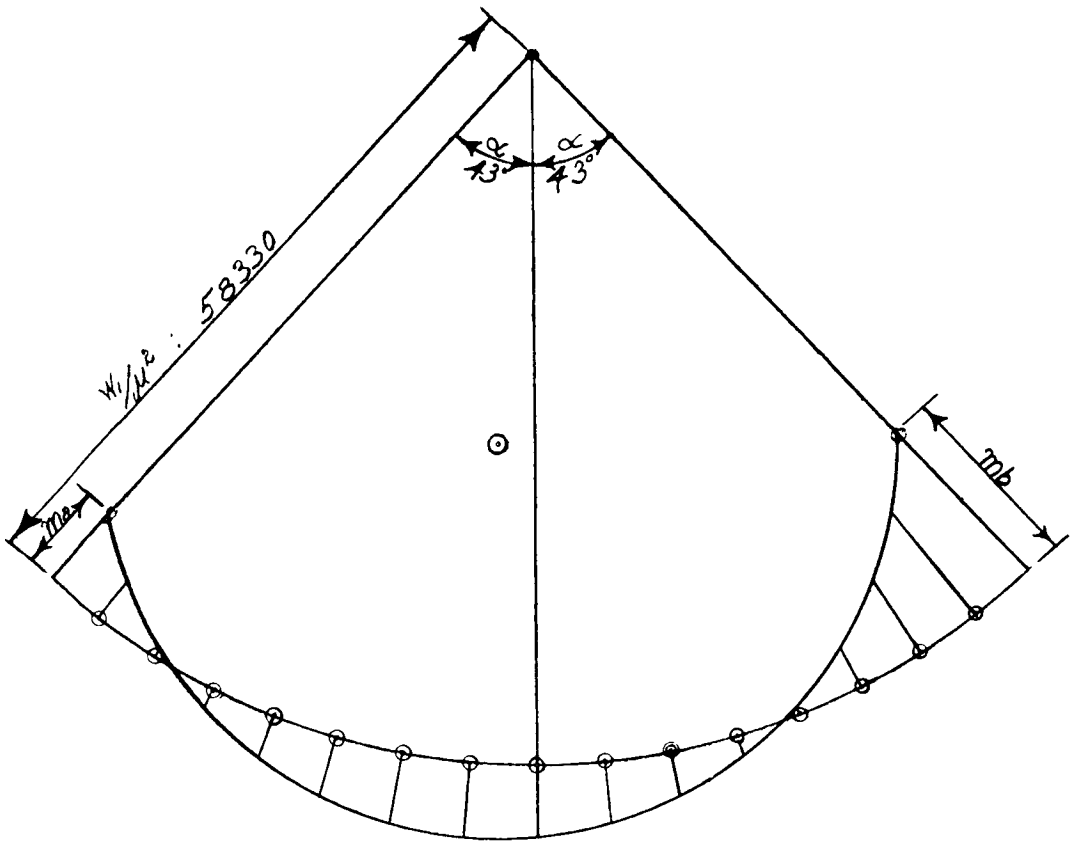

GRAPHICAL SOLUTION OF BERRY EQUATION

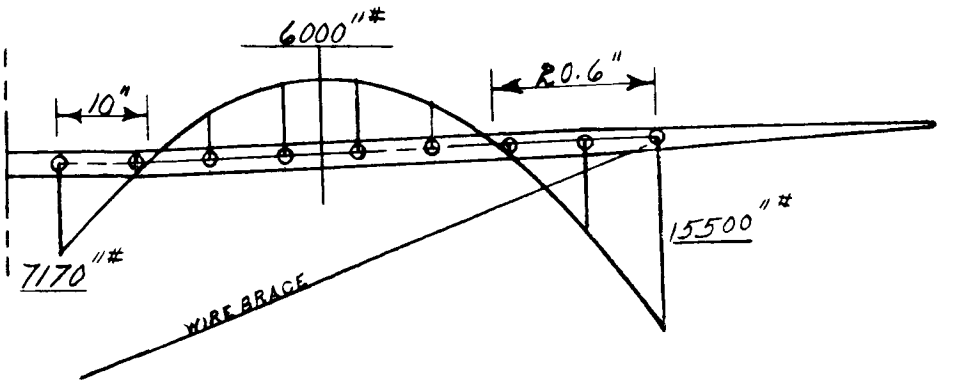

BENDING MOMENTS IN BAY

1 CM = 5000"#

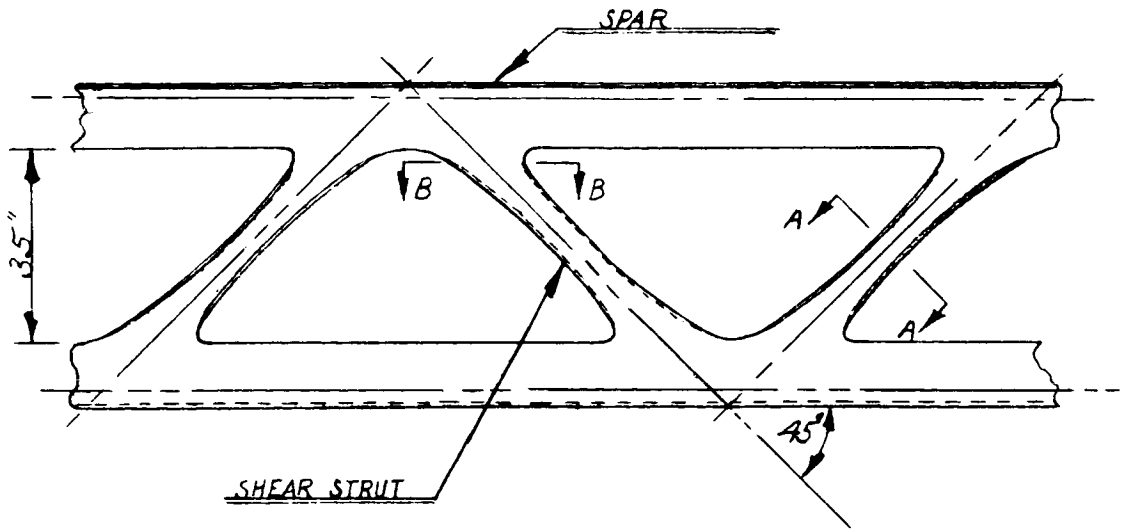

PLAN OF WEB TRUSS

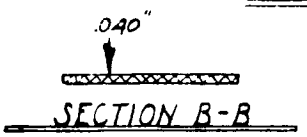

SECTION B-B

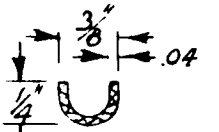

SECTION A-A

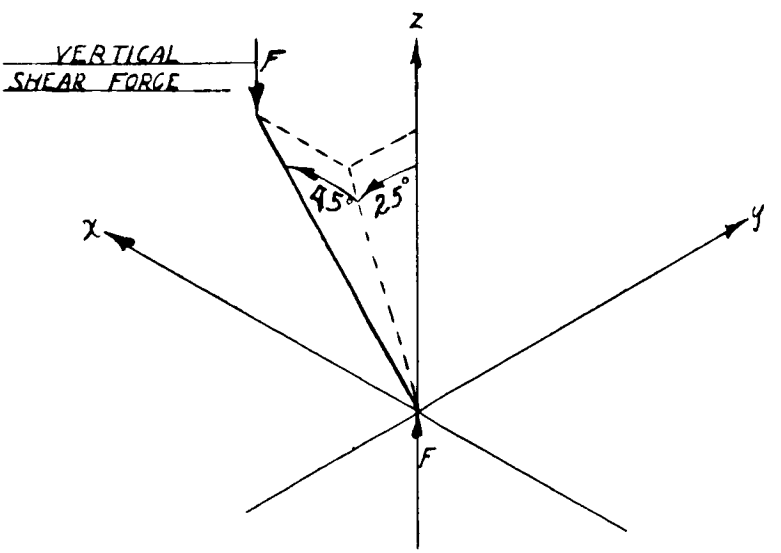

INCLINATION OF STRUT

(Fig. 5)

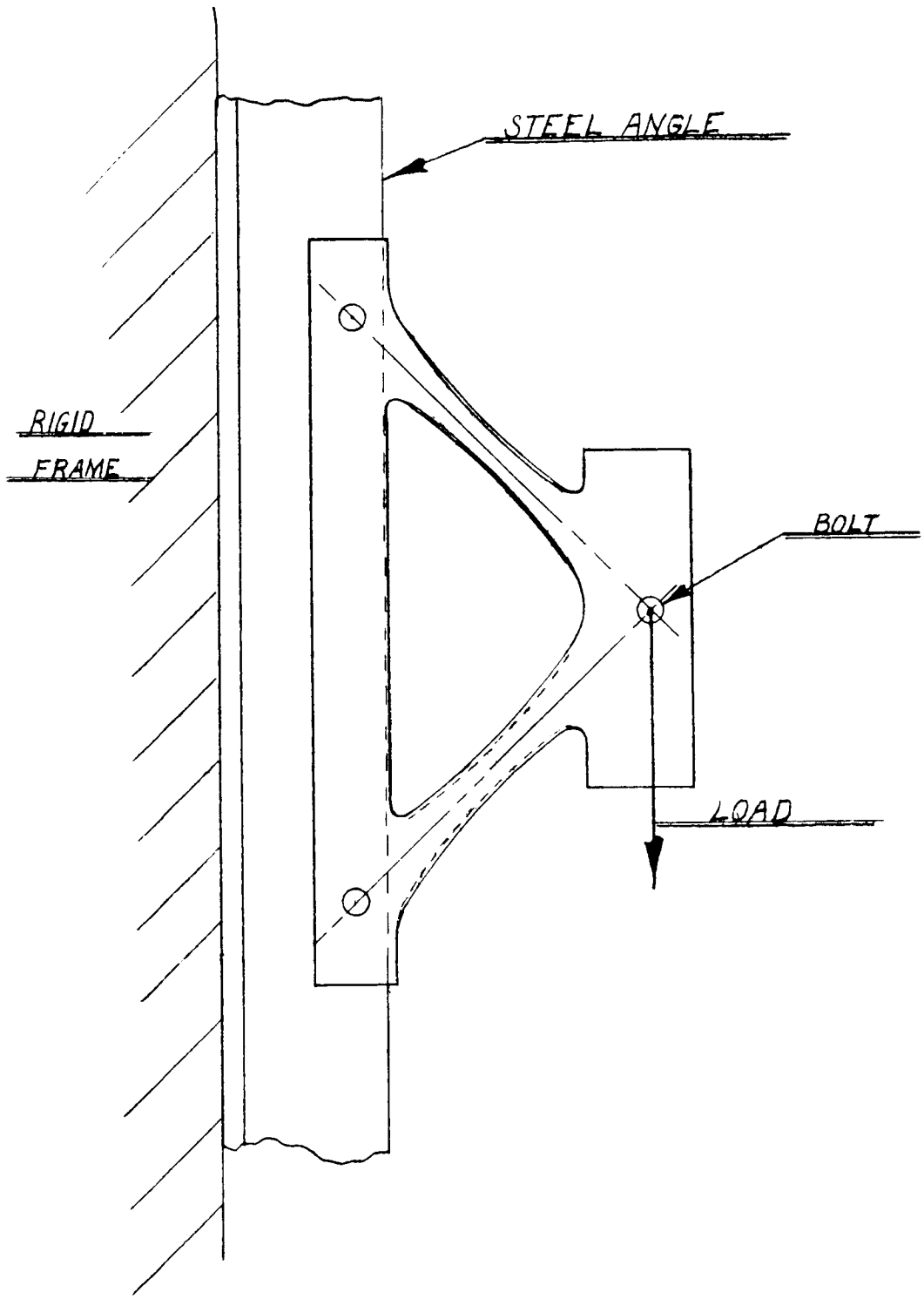

STATIC TEST OF SHEAR STRUTS

Fig. 6

CALCULATION OF THE MOTION OF AN AIRPLANE UNDER THE INFLUENCE OF IRREGULAR DISTURBANCES

Robert T. Jones

Langley Field, Virginia

October 1936

JOURNAL OF THE
AERONAUTICAL SCIENCES

Volume 3 OCTOBER, 1936 Number 12

Calculation of the Motion of an Airplane Under the Influence of Irregular Disturbances

ROBERT T. JONES, *Langley Field, Virginia*

(Received August 17, 1936)

SUMMARY

THE paper illustrates the application of mathematical advances made in electricity and other branches to problems of airplane dynamics. The Heaviside-Bromwich methods of solution of linear differential equations are described and it is shown how these methods avoid the consideration of boundary conditions and of particular or complementary integrals. It is pointed out that if the solution of the differential equation is obtained for the case of a unit disturbance, the effect of varying disturbances may be found therefrom by Carson's Theorem. A graphical solution of Carson's Integral for irregular disturbances is given.

The procedure of obtaining unit solutions of the equations is then taken up and the analogy between Heaviside's symbolic series solution and a physical procedure of approximation is shown. It is suggested that a fictitious impulsive disturbance be used in the treatment of initial motions. Bromwich's interpretation of the operational method is briefly described and the expression of the irregular disturbance functions by definite integrals is shown.

DEFINITIONS

U_0—Equilibrium flight velocity.

w—Linear velocity in plane of symmetry of airplane and normal to U_0.

p—Rolling angular velocity of airplane. (About U_0 as axis).

q—Pitching angular velocity of airplane. (About axis normal to U_0 and to the plane of symmetry).

L—Rolling moment per unit moment of inertia of airplane.

Z—Force per unit mass of airplane. (Along w).

L_p, Z_w, . . . etc., $= \frac{dL}{dp}, \frac{dZ}{dw}$, etc.

The use of some mathematical discipline in the study of disturbed motions of airplanes seems essential if a consistent advance in the improvement of airplane flying and handling qualities is to be made. The study of stability alone has thus far not been of very great usefulness in this respect partly because it has been difficult to establish the interpretation of the mathematical definition of stability in terms of control and flying qualities.

A study of the specific effects of disturbances and control manipulations is in many respects more instructive than the study of stability alone. A calculation of the motion of the airplane gives a comprehensible result; in terms of velocities, accelerations, etc., while the stability calculation must be considered incomplete as it yields only an indication of the character of the free motion. Thus it appears that the study of airplane dynamics may be more profitable if the question of stability is subordinated to specific questions involving the effects of gusts and control manipulations.

It has been considered that the representation of the motions of an airplane under the influence of irregular disturbances would require a prohibitive labor of cal-

culation. Such differential equations as occur in airplane dynamics are, however, of the same form as those used in certain problems of electricity and in other branches and many of the advances made there can be adapted to aeronautical problems. It will be seen that these advances result in very practical simplifications of the mathematical procedure.

The question of the solution of differential equations arises in the study of airplane dynamics because it is easier to write expressions for the detailed component accelerations of an airplane in motion than it is to write expressions giving the movements directly. The analysis of the problem, the expression of equations for the component accelerations, consists simply in attributing a component of reaction in each degree of freedom of the airplane to each component of motion or displacement. The analysis need not be restricted to the airplane as a rigid body, for component deformations of the machine may often be treated as additional degrees of freedom.

According to Bryan's theory of airplane stability the component reactions are considered to be directly proportional to the displacements or motions. Originally this assumption was used in application to vanishingly small motions since the consideration of such motions was sufficient to etablish the stability of steady flight. The latter advance of aerodynamics has shown that the simple linear laws of variation of aerodynamic reactions with the motions should give good approximation for movements of the airplane such as are encountered in ordinary maneuvering. Hence the theory was extended to the caluculation of unsteady motions of aircraft in general.

The assumption of linear laws of aerodynamic reaction (together with other commonly used simplifying assumptions) leads to the representation of the accelerations of a disturbed airplane by linear differential equations. It is usually necessary to consider several component motions simultaneously, since a movement of the airplane in one degree of freedom generally reacts on and modifies the movements in other degrees. Thus one is led to a set of simultaneous equations. The parameters of these equations, expressing the proportions between motions and air forces or moments, are termed "stability derivatives."

The set of equations containing only the reactions that the airplane naturally receives when displaced from equilibrium flight are the so-called "complementary equations" and are those used in the study of stability. This set of equations has a whole family of possible solutions. The possible solutions of a set of complementary equations do have one unique characteristic however, and that is the indication as to whether or not the natural free oscillations of the airplane tend to diminish with time.

If it is desired to calculate the motion of an airplane due to some disturbing influence, such as a gust or a

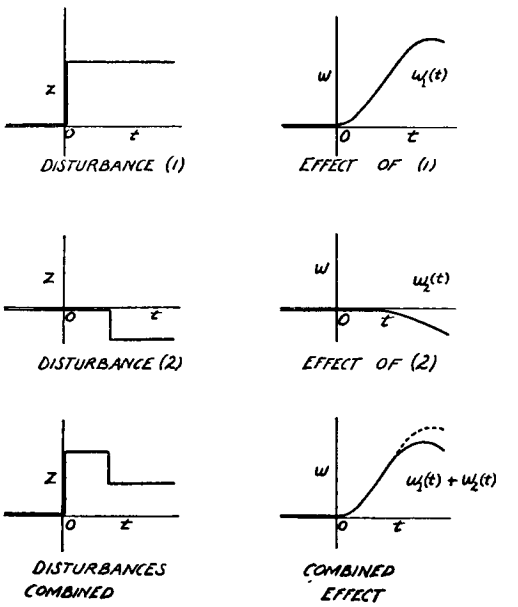

FIG. 1. The superposition of disturbed motions.

manipulation of the control, it is necessary to include terms in the equations that express the component accelerations attributed to the disturbance. Thus in the case of a deflected control the known moment exerted (per unit moment of inertia of the airplane) is added to the other terms in the appropriate equation. Such disturbing reactions must be given in terms of the time before the equations can be solved. The equation expressing the acceleration in free pitching motion is:

$$\frac{dq}{dt} - wM_w - qM_q = 0$$

If, however, a disturbing pitching moment due to the elevator, say, is acting, the equation is written:

$$\frac{dq}{dt} - wM_w - qM_q = M(t)$$

and it is implied that the right hand side is a function of t.

Although the component motions of the airplane mutually interfere and must be calculated simultaneously (that is, by simultaneous differential equations), the effects of component disturbances may be calculated separately and later added in any desired proportion. Thus if a given impressed rolling moment, acting alone, causes a 20° bank of the airplane in one second and a given yawing moment, also acting alone, produces 5° of bank in the same time the combined effect of both acting simultaneously will be a 25° bank.

A somewhat similar statement may be made with regard to the effects of disturbances that are not applied simultaneously, viz.; that if a given disturbance which arises at the time $t = 0$ is later augmented in some amount the effect of the increment of disturbance will

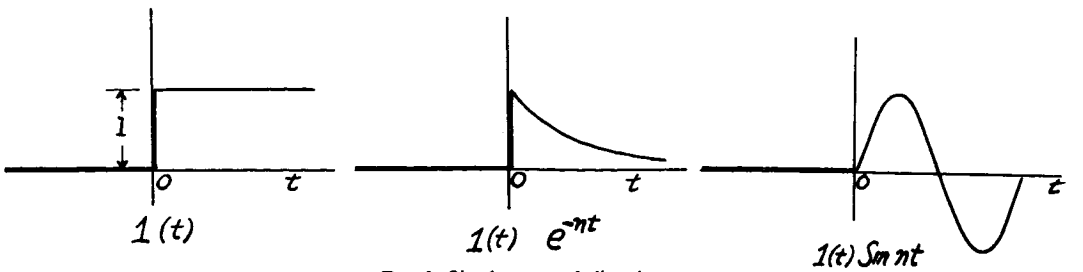

FIG. 2. Simple types of disturbances.

run its course independently of the effect of the original disturbance. Thus in a problem involving the correction of a gust disturbance by a manipulation of the control a history of the motion due to the uncorrected gust may be calculated and an entirely independent motion, due to the assumed corrective control manipulation, added later at any desired point. Fig. 1 illustrates this principle.

These important characteristics of the dynamical system regarding the superposition of effects of disturbances lead to the consideration of the effect of a simple "unit disturbance." The concept of a disturbing acceleration of unit magnitude applied instantly at the time $t = 0$ to a dynamical system otherwise at rest is attributed to Heaviside, who employed it in the development of his Operational Calculus. Carson[1] utilized this concept to calculate the effect of a varying disturbance of arbitrary form.

The unit disturbance, otherwise known as the "unit function," is defined by:

$$\begin{aligned} \mathbf{1}(t) &= 0 \text{ when } t < 0 \\ \mathbf{1}(t) &= 1 \text{ when } t > 0 \end{aligned} \qquad (1)$$

(see Fig. 2).

In Electricity this symbol is used to denote a unit e.m.f. instantly applied at $t = 0$. The corresponding use in Aeronautics would be to denote a unit impulsive linear or angular acceleration.

As an example of the application of this concept suppose that it is required to find the combined pitching motion (q) and the vertical translation (w) of an airplane due to the sharp edged vertical gust of (constant) velocity w_0. The simultaneous equations for these motions are:

$$\begin{aligned} \frac{dw}{dt} - wZ_w - q(Z_q + U_0) &= w_0 Z_w = Z_0 \\ \frac{dq}{dt} - wM_w - qM_q &= w_0 M_w = M_0 \end{aligned} \qquad (2)$$

The procedure is to perform the calculation with a unit disturbance substituted into the first equation, thus

$$\begin{aligned} \frac{dw}{dt} - wZ_w - q(Z_q + U_0) &= \mathbf{1}(t) \\ \frac{dq}{dt} - wM_w - qM_q &= 0 \end{aligned} \qquad (3)$$

[1] J. R. Carson, *Electric Circuit Theory and Operational Calculus*, McGraw-Hill Book Company, 1926.

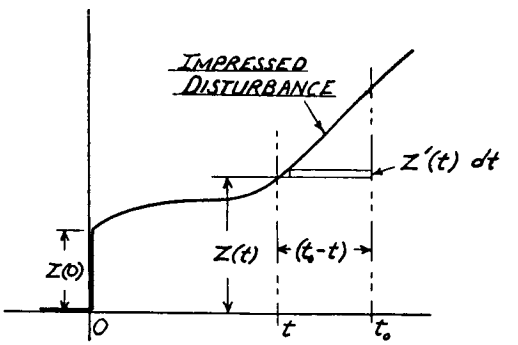

FIG. 3. Carson's integral.

If the motions thus calculated are

$$w_{1Z}(t) \text{ and } q_{1Z}(t)$$

and the motions calculated for a unit disturbance substituted into the second equation are

$$w_{1M}(t) \text{ and } q_{1M}(t),$$

then the motions due to the gust w_0 may be found from:

$$\begin{aligned} w(t) &= Z_0 w_{1Z}(t) + M_0 w_{1M}(t) \\ q(t) &= Z_0 q_{1Z}(t) + M_0 q_{1M}(t) \end{aligned} \qquad (4)$$

Carson's Theorem[1], which enables the calculation of motion due to any irregular variation of disturbance, is simply a statement of the generalized superposition theorem in terms of a definite integral. Let $w_1(t)$ be the motion calculated for a unit disturbance $\mathbf{1}(t)$, and suppose that it is desired to find the motion $w(t)$ due to some varying disturbance, say $Z(t)$. According to Carson's Theorem

$$w(t_0) = w_1(t_0)\, Z(0) + \int_0^{t_0} w_1(t_0 - t)\, Z'(t)\, dt, \qquad (5)$$

where $w_1(t_0 - t)$ is the motion at the time $(t_0 - t)$ after the impression of the unit disturbance. (See Fig. 3.)

In the most general case the impressed disturbance will be given as a function of the time simply by a curve, as in Fig. 4 (curve B). If the "indicial motion," or motion of the system due to a unit disturbance, is also given by a curve (curve A) the two may be combined by a simple artifice and the general solution obtained by a graphical integration.[2] For this purpose

[2] This novel graphical construction is due to the author's associate, Mr. A. I. Nerken.

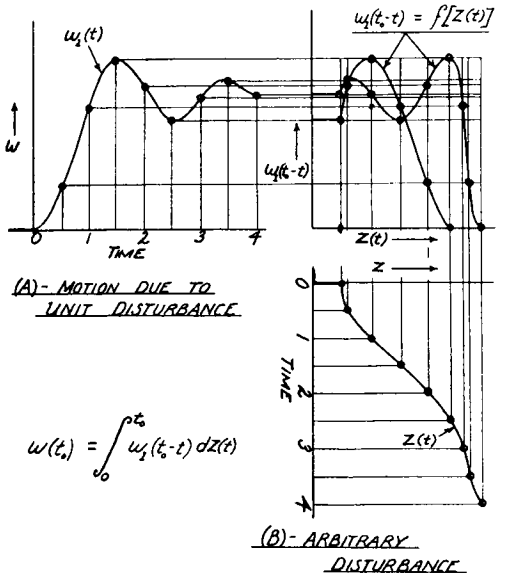

FIG. 4. Diagram illustrating calculation of motion by Carson's theorem.

the integral of Eq. (5) is expressed in the alternative form;

$$w(t_0) = \int_0^{Z(t_0)} w\,(t_0 - t)\, dZ(t) \tag{6}$$

The procedure of finding the motion at several instants consists in plotting curves of

$$w_1(t_0 - t) = f[Z(t)] \tag{7}$$

for various values of the parameter t_0. The area under any one of these curves is obviously $w(t_0)$. (See Fig. 4.)

Points of the curves of Eq. (7) may be readily located if the two diagrams $w_1(t)$ and $Z(t)$ have equal time scales and are placed with these scales at 90°, as in Fig. 4. Lines from the ordinates of the $Z(t)$ curve corresponding to various values of t are projected upward from this diagram and similar lines corresponding to equal time intervals on the $w_1(t)$ curve are projected across, intersecting the former lines at right angles. Lines of both sets are identified by the time instants to which they correspond. A series of intersections such that the time instants sum to t_0 can then be located and they define the curve $w_1(t_0 - t)$ *vs.* $Z(t)$. Fig. 4 shows such curves for $t_0 = 2\frac{1}{2}$ and 4.

It is evident from the foregoing considerations that solutions of the differential equations of airplane motion need be obtained only for the case of a unit disturbance. The motion caused by any arbitrary or irregular disturbance then follows by simple principles.

For an illustration of this solution of the equations let us take the simple case of an airplane free to move only in rolling. The rolling motion p following the application of a unit disturbance must satisfy the following differential equation:

$$\frac{dp}{dt} - pL_p = \mathbf{1}\,(t) \tag{8}$$

where L_p is the damping derivative in rolling. Obviously the motion will start with the angular acceleration 1 and, as a definite rate of rolling is acquired, will be decelerated in an amount proportional to the rate at each instant. The solution of this equation may be demonstrated by a process of successive approximations. Suppose that for the first approximation we calculate the rolling by neglecting the damping factor entirely; the value thus found will be

$$p = \int_0^t \mathbf{1}\,(t)\, dt \tag{9}$$

or, simply, $p = t$. As a second approximation we use the value of p thus found to calculate a damping deceleration, viz: pL_p. The integral of this deceleration gives a decrement of p which may then be applied to the first approximation. The new approximation again requires correction because the value of p assumed in calculating the damping was too high. The successive steps may be represented by the following series:

$$p = \int_0^t \mathbf{1}\,(t)\, dt + \int_0^t L_p \int_0^t \mathbf{1}\,(t)\, dt^2 + \int_0^t L_p \int_0^t L_p \int_0^t \mathbf{1}\,(t)\, dt^3 \tag{10}$$

The result of the integrations is obvious since L_p is a constant.

$$p = t + \frac{L_p t^2}{2!} + \frac{L_p^2 t^3}{3!} + \ldots\ldots +, \text{ etc.} \tag{11}$$

The similarity between this series and the series for $e^{L_p t}$ is recognized. A factor L_p is needed and a term 1, hence

$$p = \frac{e^{L_p t} - 1}{l_p} \tag{12}$$

Heaviside's power series soultion may be considered as a shorthand method of arriving at the foregoing result. In order to apply this method to more complex equations it is found convenient to introduce an abbreviated notation for differentiation and integration with respect to time, viz:

$$\begin{gathered} \frac{d}{dt} = D, \frac{d^2}{dt^2} = D^2; \text{ etc.} \\ \int \ldots\ldots dt = D^{-1}, \int\int \ldots\ldots dt^2 = D^{-2}; \text{ etc.} \end{gathered} \tag{13}$$

It is to be noted that the operation indicated by this symbol obeys the formal laws of algebra so long as the derivative of a square or product is not required. The latter possibility is avoided in our equations since they are *linear*.

With this preparation Eq. (8) may be written as

$$Dp - L_p p = \mathbf{1}(t) \tag{14}$$

or

$$p = \frac{\mathbf{1}(t)}{D - L_p}$$

The fraction $(D-L_p)^{-1}$ is then expanded by the binomial theorem:

$$(D - L_p)^{-1} = D^{-1} + L_p D^{-2} + L_p^2 D^{-3} +, \text{ etc.} \quad (15)$$

This result is obviously the same series of operations that were led to in obtaining successive approximations to the solution (Eq. (10)). Either result may be summarized by the formula

$$(D - L_p)^{-1} \mathbf{1}(t) = \mathbf{1}(t) \frac{e^{L_p t} - 1}{L_p}. \quad (16)$$

A number of other symbolic formulas, each of which bears a relation to the solution of some linear differential equation, may be devised by similar algebraic procedure.

The recovery of an airplane from a given initial motion or displacement may be treated very simply by the consideration of another special type of disturbance. Consider the fictitious disturbance that would result in the airplane suddenly acquiring a unit velocity or displacement at the time $t = 0$:

$$\begin{aligned} D\,\mathbf{1}(t) &= 0 \text{ when } t < 0 \\ D\,\mathbf{1}(t) &= \infty \text{ when } t = 0 \\ D\,\mathbf{1}(t) &= 0 \text{ when } t > 0 \end{aligned} \quad (17)$$

This function may be termed the "unit impulse" and may be used to represent a quantity of very large magnitude but of such short duration that its time integral is finite. Obviously the time integral of the unit impulse is the unit function $\mathbf{1}(t)$.

The solution of Eq. (8) for the condition of a unit initial angular velocity in rolling may be obtained by a method analogous to that previously given. Here one can write

$$\begin{aligned} Dp - L_p p &= D\mathbf{1}(t) \\ p &= \frac{D}{D-L_p}\mathbf{1}(t) \end{aligned} \quad (18)$$

Algebraic expansion of the right hand side gives simply:

$$p = \mathbf{1}(t)\, e^{L_p t} \quad (19)$$

The solution of complex systems of equations such as are frequently met in airplane dynamics is based on an extension of the algebraic manipulation of the "operator" D .. For simplicity the solution of Eqs. (3) can be illustrated: the extension of the procedure to equations of greater complexity will be obvious.

Rewriting the equations in the new terminology,

$$\begin{aligned} (D - Z_w)\, w - (Z_q + U_0)q &= \mathbf{1}(t) \\ -M_w w + (D - M_q)q &= 0 \end{aligned} \quad (20)$$

The algebraic resolution of the equations for w is:

$$w = \frac{D - M_q}{D^2 - (Z_w + M_q)D + Z_w M_q - M_w (Z_q + U_0)} \times \mathbf{1}(t) \quad (21)$$

which is of the form

$$w = \frac{f(D)}{F(D)}\mathbf{1}(t) \quad (22)$$

The fraction $\frac{(fD)}{F(D)}$ may be expanded algebraically into a series of simpler operations just as the fraction $\frac{1}{D-L_p}$ was. A simple procedure is to resolve it into partial fractions. According to the partial fractions theorem (a theorem of algebra):

$$\frac{f(x)}{F(x)} = \sum_{\lambda} \frac{f(\lambda)}{F'(\lambda)\,(x-\lambda)} \quad (23)$$

where the λ's are the roots of the polynomial equation $F(x) = 0$. The restrictions on this theorem are (1) that the roots λ be distinct and (2) that the polynomial $F(x)$ be of higher degree in x than $f(x)$. Applying this theorem to our fraction $\frac{f(D)}{F(D)}$, we obtain:

$$\frac{f(D)}{F(D)}\mathbf{1}(t) = \sum_{\lambda} \frac{f(\lambda)}{F'(\lambda)} \frac{\mathbf{1}(t)}{D-\lambda} \quad (24)$$

The part $\mathbf{1}(t) / (D-\lambda)$ has already been evaluated by the binomial expansion, Eq. (16), and the substitution of that result gives

$$\frac{f(D)}{F(D)}\mathbf{1}(t) = \mathbf{1}(t)\left[\sum_{\lambda} \frac{f(\lambda)}{\lambda F'(\lambda)} e^{\lambda t} - \sum_{\lambda} \frac{f(\lambda)}{\lambda F'(\lambda)}\right] \quad (25)$$

It is only necessary to note that the second term on the right is

$$\sum_{\lambda} \frac{f(\lambda)}{F'(\lambda)\,(0-\lambda)} = \frac{f(0)}{F(0)} \quad \text{(See Eq. (23))}$$

Then

$$w = \frac{f(D)}{F(D)}\mathbf{1}(t) = \mathbf{1}(t)\left[\frac{f(0)}{F(0)} + \sum_{\lambda} \frac{f(\lambda)}{\lambda F'(\lambda)} e^{\lambda t}\right] \quad (26)$$

This general formula is known as the "Heaviside Expansion Theorem" and is subject to the same restrictions that apply to the algebraic theorem for expansion into partial fractions.

The methods of solution thus demonstrated avoid the complication of adjustment to boundary conditions as well as the consideration of particular and complementary integrals. They depend on the consideration of discontinuous or irregular functions of the time. That these methods have a counterpart expressible in conventional mathematical language was shown by Bromwich[3], who gave a rigorous form for the older Operational Calculus of Heaviside. The principle of Bromwich's method is the expression of the solution of the linear differential equation as a definite integral in which the independent variable (t) appears under the integral sign as a parameter.

For an elementary illustration of this method suppose that it is desired to find a solution $w(t)$ of Eqs. (2) with an impressed vertical acceleration $Z(t)$. The equations are written

$$\begin{aligned} Dw - Z_w w - (Z_q + U_0)q &= Z(t) \\ Dq - M_w w - M_q q &= 0 \end{aligned} \quad (27)$$

[3] T. A. I'J. Bromwich, *Normal Coordinates in Dynamical Systems*, Proc. Lond. Math. Soc. (2) 15, 401–408, 1916.

Solving the second equation for w and substituting in the first equation results in:

$$D^2w - (Z_w + M_q)Dw - [M_wZ_q - M_qZ_w + M_w U_0]\, w = DZ(t) - M_qZ(t) \quad (28)$$

or:

$$D^2w + aDw + bw = \phi(t) \quad (29)$$

It happens to be fairly easy to devise an expression for w that will satisfy this equation if the definite integral of an auxiliary variable, $\lambda = x + iy$, is introduced. Such an integral, viz:

$$w = \int_{(closed\ contour)} \frac{f(\lambda)}{F(\lambda)} e^{\lambda t}\, d\lambda \quad (30)$$

is seen to be a particular solution if

$$F(\lambda) = \lambda^2 + a\lambda + b \text{ (See Eq. (29))} \quad (31)$$

and if

$$\int_{(closed\ contour)} f(\lambda)\, e^{\lambda t}\, d\lambda = \phi(t) \quad (32)$$

for the successive differentiations (see Eq. (29)) of Eq. (30) reproduce $F(\lambda)$ in the numerator.

The essential step of the method is then the expression of the irregular disturbance function $\phi(t) = \mathbf{1}(t)$ in the form of such a definite integral. The required integral may be shown to be

$$\frac{1}{2\pi i}\int_{-\infty i}^{+\infty i} \frac{e^{\lambda t}}{\lambda}\, d\lambda = \mathbf{1}(t) \quad , \quad (33)$$

giving the value zero for negative t and the value 1 for positive t. Here the limit, or path, of integration extends along the imaginary axis and to the right of the singular point at the origin. With the limit of the integral thus specified it is permissible to integrate in addition along any other path provided it is shown that the additional path does not change the value of the integral as defined. Then it is easy to prove that a closure of the path along a semicircle to the left of the imaginary axis does not contribute to the integral if t is positive. The path then encloses one singular point, 0, and the value of the integral is, by the residue theorem[4]

$$\frac{1}{2\pi i}\int_{(closed\ contour)} \frac{e^{\lambda t}}{(\lambda - 0)}\, d\lambda = e^{0t} = 1 \quad (34)$$

For t negative, however, the closure of the path to the left avoids the definition; but it is seen that the path can then be closed to the right of the imaginary axis without altering the value of the integral as defined. (See Fig. 5.) This contour now encloses no singular point, and, the integrand being analytic, the integral is zero.

The integrand of the expression for $\mathbf{1}(t)$ thus has a singular point at $\lambda = 0$. By modifying the integrand so that the singularity occurs at another point, say n, the expression for another irregular disturbance is obtained, namely:

$$\frac{1}{2\pi i}\int_{-\infty i}^{+\infty i} \frac{e^{\lambda t}}{\lambda - n}\, d\lambda = \mathbf{1}(t)\, e^{nt} \quad (35)$$

[4] E. R. Hedrick and Otto Dunkel, *Goursat's Mathematical Analysis*, Vol. II, Part I, Ginn & Co., 1916.

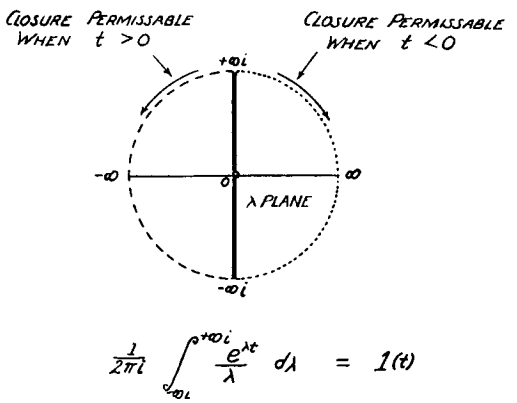

FIG. 5. Evaluation of definite integral giving the unit function.

The result is multiplied by $1(t)$ to indicate that it is zero when t is negative. Writing (in) for n gives a disturbance of the form

$$\mathbf{1}(t)\, (\cos nt + i \sin nt)$$

The real part of a solution is then the solution for $\mathbf{1}(t) \cos nt$, and the coefficient of the imaginary is the solution for $\mathbf{1}(t) \sin nt$, (see Fig. 2).

It has been pointed out in previous paragraphs that the solution of the equations of motion need only be obtained for the elementary unit disturbance. The effect of any other disturbance, whether given by a mathematical expression or not, may then be obtained by Carson's Theorem. The procedure of finding the "unit solution" by Bromwich's method may now be made more definite. Suppose $Z(t)$ is replaced by $\mathbf{1}(t)$ in Eq. (28). The right hand side of this equation becomes $(D - M_q)\ (\mathbf{1}t)$ whence (see Eq. (32)),

$$\int_{(closed\ contour)} f(\lambda)\, e^{\lambda t}\, d\lambda = \frac{1}{2\pi i}\int_{-\infty i}^{+\infty i} \frac{\lambda - M_q}{\lambda} e^{\lambda t} d\lambda = (D - M_q)\ \mathbf{1}(t) \quad (36)$$

The solution for w is simply

$$w_1(t) = \int_{-\infty i}^{+\infty i} \frac{\lambda - M_q}{F(\lambda)} \frac{e^{\lambda t}}{\lambda}\, d\lambda \quad (37)$$

where

$$F(\lambda) = \lambda^2 - (Z_w + M_q)\,\lambda - (M_wZ_q - M_qZ_w + M_wU_0) \quad (38)$$

as before.

For the evaluation of the integral of Eq. (37) by the residue theorem the singular points of the integrand are needed. These points are values of λ that make the denominator equal to zero. The denominator is usually termed the "stability polynomial", hence these points are simply the roots of the stability equation (in addition to the point $\lambda = 0$). Rewriting the polynomial in terms of these roots λ_1, λ_2, one obtains

$$w_1(t) = \frac{1}{2\pi i}\int_{-\infty i}^{+\infty i} \frac{(\lambda - M_q)}{(\lambda - \lambda_1)(\lambda - \lambda_2)(\lambda - 0)} e^{\lambda t} d\lambda \quad (39)$$

The value of the integral is the sum of the residues:

$$w_1(t) = \frac{\lambda_1 - M_q}{(\lambda_1 - \lambda_2)\lambda_1} e^{\lambda_1 t} + \frac{\lambda_2 - M_q}{(\lambda_2 - \lambda_1)\lambda_2} e^{\lambda_2 t} + \frac{0 - M_q}{(0 - \lambda_1)(0 - \lambda_2)} e^{0t} \quad (40)$$

Since $(\lambda_1 - \lambda_2) = F'(\lambda_1)$, and $(\lambda_2 - \lambda_1) = F'(\lambda_2)$ etc., this result may be expressed somewhat differently, viz;

$$w_1(t) = \sum_{\lambda n} \frac{f(\lambda)}{\lambda F'(\lambda)} e^{\lambda t} + \frac{f(0)}{F(0)} \quad , \quad (41)$$

which is the Heaviside Expansion theorem. The residue theorem is not subject to the restrictions that apply to the partial fractions theorem, however, and the residues corresponding to multiple roots may be readily found. Thus motions due to periodic disturbances that are synchronous with the natural oscillations of the airplane may be calculated.

REPORT NO. 560

A SIMPLIFIED APPLICATION OF THE METHOD OF OPERATORS TO THE CALCULATION OF DISTURBED MOTIONS OF AN AIRPLANE

Robert T. Jones

Langley Memorial Aeronautical Laboratory

1936

E R R A T A

NATIONAL ADVISORY COMMITTEE FOR AERONAUTICS

TECHNICAL REPORT NO. 560

A SIMPLIFIED APPLICATION OF THE

METHOD OF OPERATORS TO THE CALCULATION OF

DISTURBED MOTIONS OF AN AIRPLANE

Page 5, column 1, equation (15):

For	Read
$= \frac{R_2}{R_1 R_3} e^{\lambda 1 t} + i(\theta_2 - \theta_1 - \theta_3)$	$= \frac{R_2}{R_1 R_3} e^{\lambda_1 t + i(\theta_2 - \theta_1 - \theta_3)}$
$= R_o e^{\lambda 1 t} + i\theta_o$	$= R_o e^{\lambda 1 t + i\theta_o}$

Page 6, legend of figure 3:

For	Read
$\frac{f(\lambda)}{F'(\lambda)}$	$\frac{f(\lambda)}{\lambda F'(\lambda)}$

Page 8, column 2, second line of equation (32):

For	Read
$(D - L_o)p$	$(D - L_p)p$

REPORT No. 560

A SIMPLIFIED APPLICATION OF THE METHOD OF OPERATORS TO THE CALCULATION OF DISTURBED MOTIONS OF AN AIRPLANE

By Robert T. Jones

SUMMARY

A simplified treatment of the application of Heaviside's operational methods to problems of airplane dynamics is given. Certain graphical methods and logarithmic formulas that lessen the amount of computation involved are explained.

The problem of representing a gust disturbance or control manipulation is taken up and it is pointed out that in certain cases arbitrary control manipulations may be dealt with as though they imposed specific constraints on the airplane, thus avoiding the necessity of any integration whatever.

The application of the calculations described in the text is illustrated by several examples chosen to show the use of the methods and the practicability of the graphical and logarithmic computations described.

INTRODUCTION

The theory of airplane dynamics in its present form is due mainly to the original researches of Lanchester and Bryan on the stability of airplanes. Later investigators, notably Bairstow and Wilson (reference 1), applied and extended the original conceptions of the theory. Bryant and Williams (reference 2) have recently shown how the operational mathematics of Heaviside may be used in applying the theory to problems of the disturbed motions of airplanes.

Although the calculation of disturbed motions of aircraft is important in problems of flight safety, little experience has been gained in the practical application of the theory owing to its mathematical complexity. The present paper gives the results of researches in the mathematical application of the theory. It has been found, as suggested by Bryant and Williams, that the Heaviside method affords the simplest and most direct solution of these problems. In order to bring out the advantages of this method, a treatment of its application is given and certain formulas and graphical constructions are explained that make the calculations easier.

In their usual form, problems of airplane dynamics depend for solution on the integration of simultaneous linear differential equations. Methods for the integration of such equations are given by Wilson and Routh (references 1 and 3) and in mathematical textbooks. The problems met in airplane dynamics are often more complex than the examples treated in textbooks and, when an attempt is made to apply the given methods to their solution, difficulties of computation arise.

In view of the importance of investigating these problems and since their solutions involve lengthy calculations, it is desirable that as many mathematical simplifications as possible be employed. Heaviside's method gives such a simplification, the solution of the differential equations being accomplished symbolically by a single "expansion theorem."

THE DIFFERENTIAL EQUATIONS FOR THE DISTURBED MOTIONS

An airplane in uniform flight may be thought of as a free rigid body in equilibrium. Deviations of the airplane from this equilibrium condition may be caused by reactions due to control movement, gustiness in the air, or by some influence such as the stopping of an engine. The motions of the airplane following such a disturbance may be calculated if the momentary accelerations or forces are known. It is obvious that this computation may be performed by taking small intervals of the time and caculating the velocities and displacements generated by the known accelerations step by step, assuming the accelerations momentarily constant.

The component linear and angular motions of the airplane in its deviations from equilibrium are given exact definition by constructing a set of axes rigidly fixed in the machine and considering its motions as being those of the axes themselves. The motions spoken of are then velocities and displacements of the airplane axes relative to the earth or the air. When the airplane is in steady flight, it maintains a certain equilibrium attitude with respect to the air and to the earth. Thus for climbing flight at a given engine speed a definite angle of attack and a definite angle of pitch must be preserved. Deviations from equilibrium in either sense will introduce reactions; hence motions of the airplane axes relative to both air and earth must be considered.

The aerodynamic reactions to the motions arise from changed relative air velocities over the different parts of the airplane. The calculation or measurement of these component aerodynamic reactions leads to quantities known as "resistance derivatives" or "stability derivatives," which are taken as constant factors of proportionality between the reactions and the velocities or displacements of the motions. For a more detailed exposition of the concept of stability derivatives, the reader is referred to standard textbooks on aeronautics.

On account of the bilateral symmetry of the airplane it is customary to divide the motions into two independent groups, the lateral and the longitudinal, each consisting of three degrees of freedom:

(A) Lateral motions: Rolling. Yawing. Sideslipping.

(B) Longitudinal motions: Pitching. Vertical translation. Forward translation.

Presumably the reactions to small increments of longitudinal speed or displacement do not sensibly influence the lateral motions and the two groups may be independently treated. In order to illustrate the calculation of the history of a motion due to a given disturbance, examples of lateral motions are chosen although the methods used are equally applicable to any set of degrees of freedom of the airplane. The quantities that arise in the consideration of the lateral motions are defined in the following table:

Velocities and displacements of airplane axes:

U_0, equilibrium flight velocity along X axis.

v, component of flight velocity along Y axis (sideslipping).

p, component of angular velocity about X axis (rolling).

r, component of angular velocity about Z axis (yawing).

φ, angle of bank (relative to gravity).

Forces and moments resolved along airplane axes:

Y, component of force along Y axis.

L, component of moment about X axis (rolling moment).

N, component of moment about Z axis (yawing moment).

Accelerations of airplane:

$Y_0=Y/m$ (force per unit mass).

$L_0=L/mk_X^2$ (moment per unit moment of inertia).

$N_0=N/mk_Z^2$ (moment per unit moment of inertia).

Gust velocities resolved along airplane axes:

v_0, component of gust velocity directed along Y axis.

r_0, component of angular velocity of gust about Z axis.

p_0, component of angular velocity of gust about X axis.

NOTE.—The signs of the gust velocities are so chosen that a positive gust produces the same aerodynamic reaction on the airplane as a positive velocity of the airplane in still air. The resolution of gust velocities along the moving axes is exact only to the first order of the small quantities involved.

Airplane characteristics used as parameters:

Y_v, Y_r, L_p, L_v, L_r, N_v, N_p, N_r: Stability derivatives in terms of accelerations of airplane, thus:

$$Y_v=\frac{\partial Y}{\partial v}\Big/m$$

$$L_r=\frac{\partial L}{\partial r}\Big/mk_X^2$$

$$N_p=\frac{\partial N}{\partial p}\Big/mk_Z^2$$

With the definition of the component motions that are to be considered, the stability derivatives will be of the form:

$$\frac{\partial L}{\partial p}, \frac{\partial N}{\partial v}, \frac{\partial Y}{\partial r}, \text{etc.}$$

where L, N, Y, respectively, are the rolling moment, the yawing moment, and the sidewise force, as they are customarily defined.

It has been found convenient to transform all stability derivatives and disturbing effects into terms of accelerations of the airplane rather than retaining them as moments and forces. This transformation is accomplished by dividing out the appropriate moments of inertia and the mass of the machine. For example, $\frac{\partial L}{\partial p}\Big/mk_X^2$ may be written simply as L_p; similarly $\frac{\partial N}{\partial v}\Big/mk_Z^2=N_v$ and $\frac{\partial Y}{\partial r}\Big/m=Y_r$.

If the flight path is assumed to be horizontal (or nearly so) and the main forward velocity U_0 to be substantially constant, the equations of motion in a lateral disturbance may be written:

$$\left.\begin{aligned}&\text{(In sideslipping)}\quad \frac{dv}{dt}=g\varphi-rU_0+vY_v+rY_r+Y_0\\&\text{(In rolling)}\quad \frac{dp}{dt}=vL_v+pL_p+rL_r+L_0\\&\text{(In yawing)}\quad \frac{dr}{dt}=vN_v+pN_p+rN_r+N_0\end{aligned}\right\}\qquad (1)$$

In these equations the terms Y_0, L_0, and N_0 represent known disturbing or controlling accelerations, assumed to be given as functions of the time t. In the first equation the terms $g\varphi$ and $-rU_0$ are, respectively, the accelerations due to gravity and to the rotation of the moving axes. Since the axes chosen will ordinarily lie

near the axes of the principal moments of inertia of the airplane, terms involving the products of inertia have been neglected.

INTEGRATION OF EQUATIONS FOR VELOCITIES AND DISPLACEMENTS

As previously mentioned, equations (1) may be integrated by taking small intervals of the time and calculating the velocities, and finally the displacements, by assuming the accelerations $\frac{dv}{dt}$, etc., to be momentarily constant. Although this method is sometimes useful, it naturally leads to extensive numerical work. The operational mathematics of Heaviside appear to offer the most promising means of performing these integrations.

The first step in integrating the equations of motion by the operational method is to replace the symbol $\frac{d}{dt}$ by the so-called "differential operator" D, which is to be treated as though it were an ordinary algebraic quantity; the equations are then rearranged with the known disturbance effects on the right-hand side:

$$\begin{aligned}(D-Y_v)v-g\varphi+(U_0-Y_r)r&=Y_0\\ -L_v v+(D-L_p)p-L_r r&=L_0\\ -N_v v-N_p p+(D-N_r)r&=N_0\end{aligned}\tag{2}$$

Since $D\varphi=p$, the first equation may be operated on throughout by D, reducing all to the same variables (v, p, r):

$$\begin{aligned}D(D-Y_v)v-gp+D(U_0-Y_r)r&=DY_0\\ -L_v v+(D-L_p)p-L_r r&=L_0\\ -N_v v-N_p p+(D-N_r)r&=N_0\end{aligned}\tag{2a}$$

With the equations in this form, they may be solved for v, p, or r by ordinary algebraic means; thus,

$$v=\frac{\begin{vmatrix} DY_0 & -g & D(U_0-Y_r)\\ L_0 & (D-L_p) & -L_r\\ N_0 & -N_p & (D-N_r)\end{vmatrix}}{\begin{vmatrix} D(D-Y_v) & -g & D(U_0-Y_r)\\ -L_v & (D-L_p) & -L_r\\ -N_v & -N_p & (D-N_r)\end{vmatrix}}\tag{3}$$

The expansion of the determinant of the numerator in terms of minors results in:

$$\begin{vmatrix}(D-L_p) & -L_r\\ -N_p & (D-N_r)\end{vmatrix}DY_0+\begin{vmatrix}D(U_0-Y_r) & -g\\ (D-N_r) & -N_p\end{vmatrix}L_0+\begin{vmatrix}-g & D(U_0-Y_r)\\ (D-L_p) & -L_r\end{vmatrix}N_0\tag{4}$$

In the calculation of any of the velocity components the same denominator appears; if this determinant is denoted by $F(D)$, the forms of these components are:

$$\begin{aligned}v&=\frac{f_{11}(D)}{F(D)}Y_0+\frac{f_{12}(D)}{F(D)}L_0+\frac{f_{13}(D)}{F(D)}N_0\\ p&=\frac{f_{21}(D)}{F(D)}Y_0+\frac{f_{22}(D)}{F(D)}L_0+\frac{f_{23}(D)}{F(D)}N_0\end{aligned}\tag{5}$$

etc.

Thus far the solution of the equations of motion has progressed simply on algebraic grounds, the required quantities (v, p, etc.) having been found explicitly in terms of the symbol D. The symbol D was defined as the operation of derivation with respect to the time t, expressed by writing

$$D=\frac{d}{dt}$$

The terms of the solution $f(D)/F(D)$ indicate that the formal operations are to be performed on whatever functions follow them as factors. Since they contain the symbol D in their denominators, it becomes necessary to define the operation indicated by $1/D$ *or* D^{-1}. As D is an operation and not a number, its reciprocal is defined as the inverse of the operation of differentiation, rather than as the derivative itself divided into 1. The inverse of differentiation is integration: thus,

$$D^{-1}=\int \ldots dt$$

The operations indicated by the ratios of polynomials in D that occur in the terms of our solution then consist of a succession of differentiations, $[f(D)]$, and a succession of integrations, $[F(D)]^{-1}$. It is clear that the nature of the problems at hand requires that the resultant of these operations be an integration, which is shown by the fact that the polynomial $F(D)$ is invariably of higher degree in D than any of the polynomials $f(D)$.

THE EXPANSION EQUATION

By treating the disturbances (such as Y_0, N_0, L_0) as discontinuous functions of the time, Heaviside obtained solutions of equations similar to the foregoing by a simple theorem. The substitution of Y_0 into Heaviside's theorem results in

$$\frac{f(D)}{F(D)}Y_0=Y_0\left[\frac{f(0)}{F(0)}+\sum_{\lambda}\frac{f(\lambda)}{\lambda F'(\lambda)}e^{\lambda t}\right]\tag{6}$$

where the λ's are the roots of the polynomial equation $F(D)=0$. This polynomial, $F(D)=0$, is used in the study of the stability of motion, being called the "stability equation." Its roots, $\lambda_1\ \lambda_2\ \ldots\ \lambda_n$, give an

indication of the natural tendencies of an airplane's motion and are used in the definition of stability.

In order to apply the foregoing theorem to the integration of equations of airplane motion it is necessary to assume that the disturbance terms (Y_0, N_0, etc.) due to the control or gust in question are instantly applied at the assumed origin of the time scale ($t=0$) and remain constant thereafter. In the general case the disturbance terms in the equations of motion cannot be thus represented as remaining constant although in practical problems they may almost invariably be represented by means of functions of the form $Y_0 e^{nt}$. The interpretation of Heaviside's theorem equation (6) when this form of function is used is (see reference 2):

$$\frac{f(D)}{F(D)}Y_0e^{nt}=Y_0\left[\frac{f(n)}{F(n)}e^{nt}+\sum_{\lambda}\frac{f(\lambda)}{(\lambda-n)F'(\lambda)}e^{\lambda t}\right] \quad (7)$$

When dealing with variable disturbance terms, it is important to note that a discontinuity of the function representing the disturbance at $t=0$ is implied as in equation (6).

By the substitution of (in) for n in equation (7), expressions that can be used when the disturbances

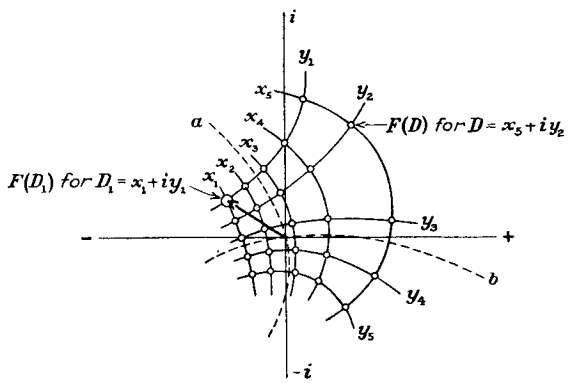

FIGURE 1.—Map of polynomial. $F(D)=D^4+aD^3+bD^2+cD+d$ near zero. $F(D)\rightarrow F(\lambda)=0$ when $D\rightarrow a\pm ib$.

are represented by forms involving sin nt or cos nt are obtained

$$\frac{f(D)}{F(D)}Y_0e^{int}$$
$$=Y_0\left[\frac{f(in)}{F(in)}(\cos nt+i\sin nt)+\sum_{\lambda}\left(\frac{\lambda+in}{\lambda^2+n^2}\right)\frac{f(\lambda)}{F'(\lambda)}e^{\lambda t}\right] \quad (7a)$$

If $\frac{f(in)}{F(in)}=A+iB$, then the expressions for the sine and cosine forms separately become

$$\frac{(fD)}{F(D)}Y_0\sin nt$$
$$=Y_0\left[A\sin nt+B\cos nt+\sum_{\lambda}\left(\frac{n}{\lambda^2+n^2}\right)\frac{f(\lambda)}{F'(\lambda)}e^{\lambda t}\right] \quad (8)$$

$$\frac{f(D)}{F(D)}Y_0\cos nt$$
$$=Y_0\left[A\cos nt-B\sin nt+\sum_{\lambda}\left(\frac{\lambda}{\lambda^2+n^2}\right)\frac{f(\lambda)}{F'(\lambda)}e^{\lambda t}\right] \quad (9)$$

These latter forms are particularly useful because almost any arbitrary variation of gust or control may by expressed as a sum of sine or cosine terms. Thus if

$$Y_0=K_1\sin n_1t+K_2\sin n_2t+\ \ldots\ +\text{etc.}$$
$$\frac{f(D)}{F(D)}Y_0=\frac{f(D)}{F(D)}K_1\sin n_1t+\frac{f(D)}{F(D)}K_2\sin n_2t+\ \ldots\ +\text{etc.} \quad (10)$$

Each of these terms may be evaluated by equation (8).

SOLUTION OF OPERATIONAL EQUATIONS

FINDING THE ROOTS OF THE EQUATION $F(D)=0$

The expansion equations given for the forms $f(D)/F(D)$ require the roots of the complementary equations $F(D)=0$ for their solution. In cases of airplane motions this equation is normally of the fourth degree in D; hence it is not practicable to find the roots directly. Although a number of methods for approximating the roots of such equations have been devised, the most direct way is to draw a curve of the function $F(D)$ against D, locating the real roots as the points crossing the D axis. Usually in equations of this type near roots may be isolated by separating the equation into two parts. Thus, if

$$F(D)=D^4+aD^3+bD^2+cD+d=0 \quad (11)$$

there will usually be a large real root near $D^4=-aD^3$, or $D=-a$, and a small one near $D=-\frac{d}{c}$. This division follows from the consideration that large roots are more dependent on the coefficients of the higher powers of D and small roots, on the lower powers.

If the natural motion of the airplane contains oscillatory components, as it usually does, there will be pairs of conjugate complex roots of the polynomial $F(D)=0$ in addition to the real roots. The determination of these roots is naturally more difficult, although if real roots have been previously found they may be used to reduce the degree of the equation by synthetic division and the determination of further roots will become progressively easier. Complex roots of such an equation may be directly found by plotting a map of the polynomial $F(D)$ for various values of D using the coordinates $D=x+iy$ and finding the zero point, or root, by interpolation, as is shown in figure 1. If a very accurate value of the root is required it may be convenient to plot the region of $F(D)$ near the origin to a magnified scale. Since the polynomial is what is known as an "analytic function" (reference 4),

$$\frac{\partial F(D)}{\partial x}=-i\frac{\partial F(D)}{\partial y} \quad (12)$$

and the map in its smallest parts will consist of squares. In this way a more accurate interpolation may be made or a process analogous to Newton's method may be applied.

It will be found most convenient to calculate the various values of $F(D)$ by means of a vector diagram

as shown in figure 2. If trial values of D are expressed in the form R (cos $\theta+i$ sin θ) or $Re^{i\theta}$, vectors representing each of the terms of the polynomial may be simply calculated. The problem is to make all terms of the polynomial balance each other and it is readily seen how this may be accomplished by varying θ to change the relative inclinations of the vectors and by varying R to change their relative lengths. The advantage of this method is that it enables a close approximation of the value of a root with a minimum number of trials, the diagram making apparent how nearly all the vectors cancel each other.

SOLUTION OF EXPANSION EQUATIONS

The numerical operations indicated in the expansion equations (6) to (9) call for calculations with complex numbers (i. e., roots of $F(D)=0$). A great deal of the labor involved in these computations may be saved by the use of graphical and logarithmic methods.

Thus, if it is desired to calculate values of the complex terms occurring in equation (6), the logarithmic formula

$$\log\frac{f(\lambda_1)}{\lambda_1 F'(\lambda_1)}e^{\lambda_1 t}=\lambda_1 t+\log f(\lambda_1)-\log\lambda_1-\log F'(\lambda_1) \quad (13)$$

is used. For the purpose of calculating these logarithms, it is convenient to express the complex numbers (λ_1, $f(\lambda_1)$, etc.) as vectors of radius R and angle θ, writing, for example,

$$\lambda_1=a+ib=R_1(\cos\theta_1+i\sin\theta_1)=R_1e^{i\theta_1} \quad (14)$$

by De Moivre's formula.

A complex term of equation (6) may then be written,

$$\frac{f(\lambda_1)}{\lambda_1 F'(\lambda_1)}e^{\lambda_1 t}=\frac{R_2e^{i\theta_2}}{R_1e^{i\theta_1}R_3e^{i\theta_3}}e^{\lambda_1 t}$$

$$=\frac{R_2}{R_1R_3}e^{\lambda_1 t+i(\theta_2-\theta_1-\theta_3)} \quad (15)$$

$$=R_0e^{\lambda_1 t+i\theta_0}$$

Then

$$\log\frac{f(\lambda_1)}{\lambda_1 F'(\lambda_1)}e^{\lambda_1 t}=\lambda_1 t+\log R_0+i\theta_0 \quad (16)$$

and the resultant logarithm may be plotted as a straight line $\lambda_1 t+$constant, which is then divided or extended to represent any division or extension of the time t over which the calculation is made. (See fig. 3.) The final vectors will represent the complex values of

$$\frac{f(\lambda_1)}{\lambda_1 F'(\lambda_1)}e^{\lambda_1 t}$$

and it is seen that the ordinates of the points of the line $\lambda_1 t+$constant are the angles of these final vectors while the abscissas are the logarithms of their radii.

By a separation of the two components of the imaginary root $\lambda=a+ib$, the logarithmic formula may be reduced to

$$\log\frac{f(a+ib)}{(a+ib)F'(a+ib)}e^{(a+ib)t}=(a+ib)t+\log R_0+i\theta_0$$

$$=(\log R_0+at)+i(\theta_0+bt) \quad (17)$$

The final formula, where $\lambda_1=a+ib$, then becomes

$$\frac{f(\lambda_1)}{\lambda_1 F'(\lambda_1)}e^{\lambda_1 t}=R_0e^{at}e^{i(bt+\theta_0)} \quad (18)$$

or, by De Moivre's theorem,

$$\frac{f(\lambda)}{\lambda F'(\lambda)}e^{\lambda t}=R_0e^{at}[\cos(bt+\theta_0)+i\sin(bt+\theta_0)] \quad (19)$$

The points thus plotted will lie on a logarithmic spiral (fig. 3); the deviation of this spiral from a circle

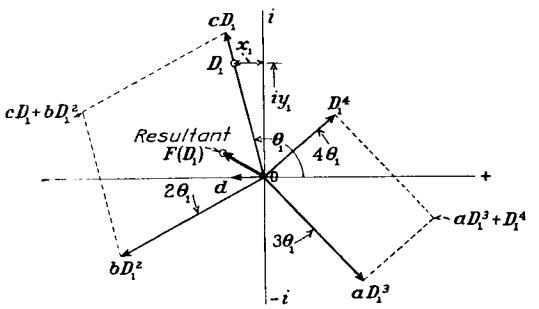

FIGURE 2.—Graphical method of locating values of $F(D)$ near zero, where $F(D)=D^4+aD^3+bD^2+cD+d$. $D_1=x_1+iy_1=R_1e^{i\theta_1}=R_1(\cos\theta_1+i\sin\theta_1)$

shows the influence of damping on the natural motion of the airplane.

The summation indicated in equation (6) calls for the plotting of such a logarithmic spiral for each of the complex roots. Since these roots always occur in conjugate pairs, the calculation may be carried out for one of such a pair and a spiral calculated for the second would be exactly conjugate to the first. Thus, it is only necessary to perform the foregoing calculations for one root of each pair, the summations indicated in the equations being carried out in effect by merely doubling the abscissas of the points of one of the conjugate spirals. If $\lambda_1=a+ib$ and $\lambda_2=a-ib$, this summation may be written:

$$\sum_{\lambda_1}^{\lambda_2}\frac{f(\lambda)}{\lambda F'(\lambda)}e^{\lambda t}=2R_0e^{at}\cos(bt+\theta_0) \quad (20)$$

The formulas for the integration of terms containing sin nt and cos nt may be put into a more convenient form for the graphical or logarithmic calculations, i. e.,

$$\frac{f(D)}{F(D)}Y_0\sin nt=Y_0\left[\text{imaginary coordinate of }\frac{f(in)}{F(in)}e^{int}+\sum_{\lambda}\frac{n}{\lambda^2+n^2}\frac{f(\lambda)}{F'(\lambda)}e^{\lambda t}\right] \quad (21)$$

$$\frac{f(D)}{F(D)}Y_0\cos nt=Y_0\left[\text{real coordinate of }\frac{f(in)}{F(in)}e^{int}+\sum_{\lambda}\frac{\lambda}{\lambda^2+n^2}\frac{f(\lambda)}{F'(\lambda)}e^{\lambda t}\right] \quad (22)$$

In these forms the graphical construction of the terms $\frac{f(in)}{F(in)}e^{int}$ proceeds along the same lines as that of the terms involving complex roots λ. Here the resulting diagrams will be circles, divided into equal angles as nt may be divided. In case λ is complex the plot of an $e^{\lambda t}$ term will be a logarithmic spiral as before and it is important to remember that the summation

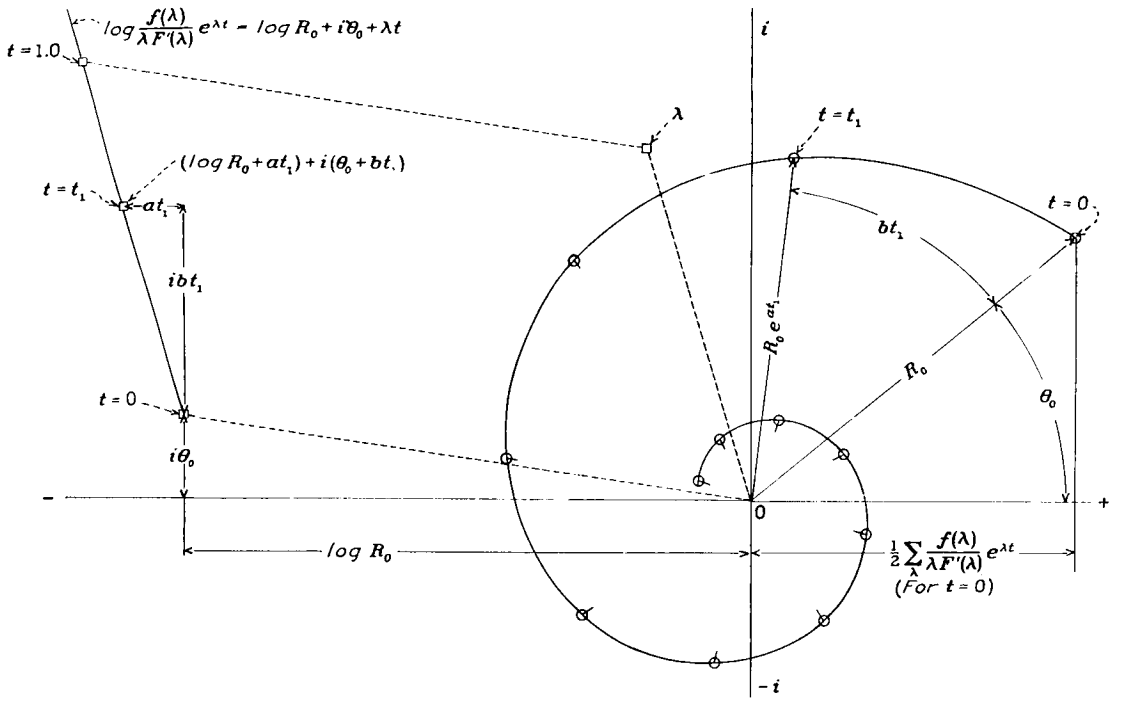

FIGURE 3.—Graphical construction of $\sum_{\lambda}\frac{f(\lambda)}{\lambda F'(\lambda)}e^{\lambda t}$ where $\lambda = a \pm ib$. Log $f(\lambda)$ − log λ − log $F'(\lambda)$ = log $R_0 + i\theta_0$

over each of a pair of conjugate roots is accomplished by doubling the abscissas of the spiral obtained for one.

WAYS OF REPRESENTING GUSTS AND CONTROL MANIPULATIONS

GUST DISTURBANCES

If the disturbances to be considered are due to gusts, the terms Y_0, L_0, etc. of equations (1) will be of the form

$$\begin{aligned} Y_0 &= v_0 Y_v + r_0 Y_r \\ N_0 &= v_0 N_v + p_0 N_p + r_0 N_r \end{aligned} \tag{23}$$

where r_0, p_0, and r_0 are the component velocities of the gust, which may vary with the time. As given, the reference system for specifying these gusts has been chosen so that a positive gust velocity may be considered as producing the same aerodynamic reaction on the airplane as a positive airplane velocity in still air. All such gusts must be assumed to be moderate so that second-order effects may be neglected. (See reference 1.)

For the velocities of an assumed gust, forms involving e^{nt} are useful. Thus, if the gust is considered a "transient" one, disappearing rapidly from an arbitrary initial value, the form (A) (fig. 4)

$$v_0 = v_1 e^{-nt} \tag{24}$$

may be used. Here v_1 is the initial value and $-n$ is chosen to make the gust diminish in any required way.

If the gust is to be made to start from an initial value of zero and to persist with the time, the form (B)

$$v_0 = v_1(1 - e^{-nt}) \tag{25}$$

may be used. (See reference 1.)

For the purpose of representing gusts that arise with any degree of sharpness from zero velocity to a given peak value and then diminish, the form (C) may be used:

$$v_0 = Ke^{-nt}(1 - e^{-mt}) \tag{26}$$

The sharpness of the rise of this gust is governed by $-m$ and the decrease by $-n$, since its curve approaches that of $(1-e^{-mt})$ near the origin and finally becomes asymptotic to e^{-nt}.

In the case of a rotating gust it is probably more logical to use the transient forms that represent the gust as disappearing in time instead of being persistent.

CONTROLLED MOTIONS

When considering controlled motions, it is often just as reasonable to assume that the airplane is under a

kinematic constraint, or prescribed acceleration, imposed by the control as to assume that the pilot uses the control in an arbitrary way. This assumption leads to the inversion of the integration problems heretofore considered, because the motion of the airplane is itself predetermined and the forces and moments (or, more properly, accelerations) required to be supplied by the controls are calculated by differentiation. The ability of various control devices to produce a given maneuver of the airplane may thus be compared and the degree of coordination required of the other controls may be studied.

The foregoing procedure is a particularly useful way of studying the lateral-control effectiveness in turns. Turn maneuvers, which usually begin and end in level

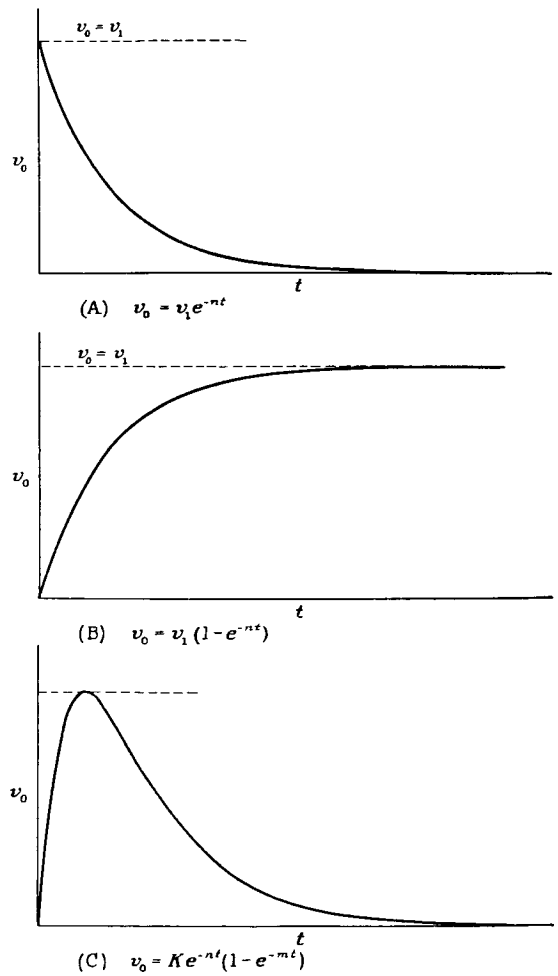

FIGURE 4.—Curves of different formulas for representing gusts.

flight, may be described by means of a few sine or cosine terms. For example, the angle of bank φ may be given by

$$\varphi = \text{constant} + A_1 \cos nt + A_2 \cos 2nt + \text{etc.} \quad (27)$$

(See fig. 5.) The rate of rolling at every instant naturally follows by differentiating this equation. If the turn is to be "perfect," that is, with no sideslipping, the rate of yawing throughout must bear a definite relation to the angle of bank, namely,

$$r = \frac{g}{U_0} \sin \varphi \quad (28)$$

or, simply,

$$r = \frac{g}{U_0}\varphi \text{ if } \varphi \text{ is under } 30°$$

Differentiating the expressions for p and r gives the accelerations in rolling and yawing and hence the

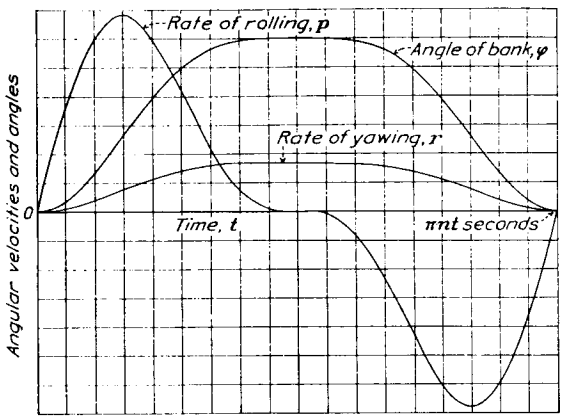

FIGURE 5.—Specifications for a turn maneuver in which the constraints are given by $\varphi = 1\frac{1}{4}A_1 + A_1 \cos nt + \frac{1}{4}A_1 \cos 2nt$; $p = \frac{d\varphi}{dt}$; $r = \frac{g}{U_0}\varphi$.

moments, which will arise from two sources: the reactions due to natural stability and the reactions produced by the displaced controls. The reactions arising from the motions are found by combining the known stability derivatives with the angular velocities p and r, obtained from the specification equations (27) and (28). The parts of the moments necessarily supplied by the controls are then obtained by deducting these from the total moments. In the case of the aileron control, secondary moments in yaw result from the application of rolling moment, which modify the amount of rudder control displacement necessary.

CONTROL AGAINST GUSTS OR ENGINE FAILURE

In order to deal with attempted control of a given disturbance it is important to consider that there is invariably a lag in the pilot's reaction in countering the motion. In these cases it is possible to assume that the disturbance arises instantly, or nearly so (whether persistent or not), and that the pilot's displacement of the corrective control takes place according to the law

$$\delta = \delta_0(1 - e^{-nt}) \quad (29)$$

(see fig. 4(B)) where δ_0 is the assumed maximum control deflection, which occurs more or less quickly as $-n$ is made large or small.

63689—38——2

EXAMPLES SHOWING APPLICATION OF OPERATIONAL METHODS TO PROBLEMS OF AIRPLANE MOTION

The following examples illustrate the application of the various methods to specific problems of airplane motion. The airplane assumed in these calculations is a typical 2-passenger machine having the following characteristics:

CHARACTERISTICS OF TYPICAL AIRPLANE

Type: Monoplane; aspect ratio 6; rectangular, rounded tip, Clark Y wing; dihedral angle, 1°.

Dimensions:

Gross weight	1,600 lb.
Wing span	32 ft.
Wing area	171 sq. ft.
mk_x^2	1,216 slug-ft.^{2}
mk_z^2	1,700 slug-ft.^{2}

Stability derivatives:

U_0 (ft./sec.)	C_L	L_v	L_r	U_0L_v	N_p	N_r	U_0N_v
150	0.35	−5.44	1.11	−2.16	−0.207	−0.913	5.52
88.5	1.0	−3.23	1.88	−1.11	−.301	−.663	2.04
66	[b]1.8	−2.46	2.51	−1.66	−.310	−.977	1.46

[b] Flaps down.

The calculated principal lateral-stability derivatives of this machine given with the other characteristics refer to motions of a set of axes fixed in the airplane but so inclined that the X axis points in the direction of the relative wind in straight flight at the lift coefficient specified. The axes, nevertheless, move with the machine during the small oscillations considered and hence depart slightly from instantaneous reference axes fixed in the wind direction.

ILLUSTRATION OF SOLUTION WITH CONSTANT DISTURBANCE TERM

Example I, Rolling motion produced by deflecting ailerons at low speed:

(a) Assume the machine to be in level steady flight at a speed of 88.5 feet per second ($C_L=1.0$) and that a rolling moment corresponding to $C_l=0.04$, with an adverse yawing moment $C_n=-0.01$, is applied suddenly at the time $t=0$. This condition corresponds approximately to a full deflection of ordinary ailerons at this speed.

(b) The equations of the motion in the three degrees of lateral freedom may be set up without including the expressions for the lateral air force, since this force is small and may be neglected in this case. The equations are:

$$\left.\begin{aligned}\frac{dv}{dt}&=g\varphi-rU_0\\ \frac{dp}{dt}&=vL_v+pL_p+rL_r+L_0\\ \frac{dr}{dt}&=vN_v+pN_p+rN_r+N_0\end{aligned}\right\}\qquad(30)$$

The terms L_0 and N_0 represent the accelerations due to the constant control moments suddenly applied at $t=0$. They are

$$\left.\begin{aligned}L_0&=\frac{C_lqSb}{mk_x^2}\\ N_0&=\frac{C_nqSb}{mk_z^2}\end{aligned}\right\}\qquad(31)$$

The substitution of D for d/dt, and the rearrangement of the equations result in

$$\left.\begin{aligned}&D^2v-gp+DU_0r=0\\ &-L_vv+(D-L_p)p-L_rr=L_0\\ &-N_vv-N_pp+(D-N_r)r=N_0\end{aligned}\right\}\qquad(32)$$

Since the rolling motion is desired, the equations will be solved for p. The algebraic solution is:

$$p=\frac{\begin{vmatrix}D^2 & 0 & DU_0\\ -L_v & L_0 & -L_r\\ -N_v & N_0 & (D-N_r)\end{vmatrix}}{\begin{vmatrix}D^2 & -g & DU_0\\ -L_v & (D-L_p) & -L_r\\ -N_v & -N_p & (D-N_r)\end{vmatrix}}\qquad(33)$$

which is then reduced to the form required for expansion in equation (6),

$$p=\frac{f_1(D)}{F(D)}L_0+\frac{f_2(D)}{F(D)}N_0\qquad(34)$$

The calculation of the various polynomials in D results in:

$$\left.\begin{aligned}f_1(D)&=D^3-N_rD^2+U_0N_vD\\ f_2(D)&=L_rD^2-U_0L_vD\\ F(D)&=D^4-(L_p+N_r)D^3+(L_pN_r-L_rN_p+U_0N_v)D^2\\ &+U_0\left(L_vN_p-L_pN_v-\frac{g}{U_0}L_v\right)D+g(L_vN_r-L_rN_v)\end{aligned}\right\}\qquad(35)$$

At the assumed speed of 88.5 feet per second ($C_L=1.0$), the constant rolling and yawing accelerations are

$$\left.\begin{aligned}L_0&=\ \ 1.68\\ N_0&=-0.301\end{aligned}\right\}\qquad(36)$$

Using these numerical values, combined with those given for the stability derivatives, the polynomials in D become

$$\left.\begin{aligned}f_1(D)&=D^3+0.663D^2+2.04D\\ f_2(D)&=1.88D^2+1.11D\\ F(D)&=D^4+3.89D^3+4.75D^2+10.33D-1.13\end{aligned}\right\}\qquad(35a)$$

In order to perform the expansion of $\frac{f(D)}{F(D)}$ by Heaviside's theorem it is necessary to determine the roots of the complementary equation $F(D)=0$. When the

polynomial $F(D)$ is plotted as a function of a real variable (D), two real roots of this equation are found:

$$\left.\begin{aligned}\lambda_1&=-3.41\\ \lambda_2&=\ \ 0.104\end{aligned}\right\} \tag{37}$$

By the use of vector diagrams (see fig. 2) and the plotting of a map of the polynomial considered as a function of a complex variable ($D=x+iy$), the following root was found by interpolation:

$$\lambda_3=1.78\ (\cos 1.73+i\sin 1.73) \tag{38}$$

An additional complex root that is the conjugate of λ_3 is known to exist and completes the four roots of the fourth-degree equation,

$$\lambda_4=1.78\ (\cos 1.73-i\sin 1.73) \tag{39}$$

The next step is to set up the integration equation and perform the indicated operations. Since the applied control moments L_0 and N_0 are constants, form (6) will be used

$$p=\frac{f_1(D)}{F(D)}L_0+\frac{f_2(D)}{F(D)}N_0=L_0\left[\frac{f_1(0)}{F(0)}+\sum_{\lambda}\frac{f_1(\lambda)}{\lambda F'(\lambda)}e^{\lambda t}\right]+N_0\left[\frac{f_2(0)}{F(0)}+\sum_{\lambda}\frac{f_2(\lambda)}{\lambda F'(\lambda)}e^{\lambda t}\right] \tag{40}$$

The various terms to be substituted in this formula are found to be:

$$\left.\begin{aligned}&\frac{f_1(0)}{F(0)}L_0+\frac{f_2(0)}{F(0)}N_0=0\\ &f_1(\lambda)L_0+f_2(\lambda)N_0=1.68\lambda^3+0.54\lambda^2+3.09\lambda\\ &\lambda F'(\lambda)=4\lambda^4+11.67\lambda^3+9.49\lambda^2+10.33\lambda\end{aligned}\right\} \tag{41}$$

These terms are to be calculated for the four (real and complex) values of the roots. In the case of the real roots the calculation is made without resorting to graphical methods. For $\lambda_1=-3.41$, the value

$$\frac{f_1(\lambda_1)L_0+f_2(\lambda_1)N_0}{\lambda_1F'(\lambda_1)}=-0.484 \text{ results,} \tag{42}$$

and for $\lambda_2=0.104$

$$\frac{f_1(\lambda_2)L_0+f_2(\lambda_2)N_0}{\lambda_2F'(\lambda_2)}=0.277 \tag{43}$$

It will be convenient to perform graphical calculations to determine the other parts of the solution, corresponding to the complex terms. This result is accomplished by calculating the square, cube, and fourth power of the absolute length of λ_3 and by multiplying each of these values by the proper coefficients in the polynomials $f(D)$ and $F(D)$. By vector addition the value of the first polynomial was determined as

$$f_1(\lambda_3)L_0+f_2(\lambda_3)N_0=3.99\ (\cos 5.23+i\sin 5.23) \tag{44}$$

and the second

$$\lambda_3F'(\lambda_3)=40.6\ (\cos 5.60+i\sin 5.60). \tag{45}$$

Since the quotient of these values is to be multiplied into $e^{\lambda_3 t}$ for a series of values of t it will be convenient to use the logarithm of this quotient, simply adding to it the various values of $\lambda_3 t$ for which the calculation is to be made. This logarithm is

$$\log\frac{f_1(\lambda_3)L_0+f_2(\lambda_3)N_0}{\lambda_3F'(\lambda_3)}=(\log 3.99-\log 40.6)+i(5.23-5.60)=-2.32-0.38\,i \tag{46}$$

The logarithm of the result naturally occurs in the form $x+iy$. Plotting this point on the paper and constructing from it a line parallel to λ_3, we obtain the locus of

$$\log\frac{f_1(\lambda_3)L_0+f_2(\lambda_3)N_0}{\lambda_3F'(\lambda_3)}e^{\lambda_3 t}$$

for various values of t (see fig. 3). The angles of the final points are given by the ordinates of these logarithms and the absolute lengths by the antilogarithms of the abscissas. The final points are found to lie on a logarithmic spiral whose radius decreases with the time (time measured as angle) showing the damping of this component of the motion. The summation over the two conjugate roots λ_3 and λ_4 is accomplished without any further calculation by merely doubling the abscissas of the points plotted above, as has been pointed out. The values thus obtained are listed in the following table:

Table of values obtained from graphical construction

t (Seconds)	$\sum_{\lambda}\frac{f_1(\lambda)L_0+f_2(\lambda)N_0}{\lambda F'(\lambda)}e^{\lambda t}$
	(For λ_3 and λ_4)
0	0.184
.2	.186
.4	.166
.6	.130
.8	.082
1.0	−.030
1.5	−.080
2.0	−.110

At the time $t=0$, $e^{\lambda t}$ will be unity so that the initial condition of zero rate of rolling should be given by the sum of its coefficients. The summation

$$-0.484+0.277+0.184=-0.023$$

shows how nearly this condition is attained. Figure 6 shows the resultant rate of rolling and the components of the solution corresponding to each of the four roots, λ_n. In addition to the rolling curve obtained by the foregoing methods, other curves obtained by step-by-step integrations of the same equations of motion are given. In the calculation of these curves, steps of one-tenth and one-twentieth second were taken, which resulted in the differences shown.

ILLUSTRATION OF SOLUTION WITH VARIABLE DISTURBANCE TERMS

Example II, Sideslipping during 2-control turn maneuver:

(a) Assume the airplane to perform a specified banking maneuver by application of a variable rolling moment. If no yawing moments (from either rudder or

ailerons) are applied, the natural stability of the airplane will cause it to turn in a direction appropriate to the direction banked. Such a turn is called a "2-control turn," inasmuch as only two (ailerons and elevator) of the three available controls are used. Since there will not be a very perfect coordination between the banking and yawing, some sideslip will result. It is of interest to know the approximate amount of this

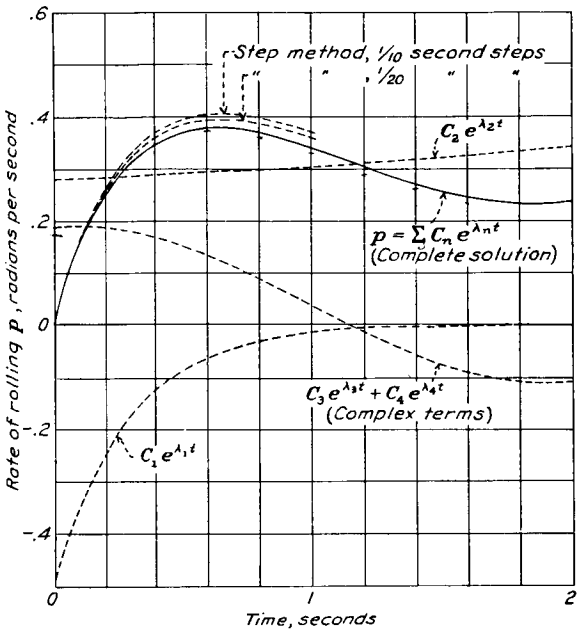

FIGURE 6.—Result of sample computation compared with step-by-step integrations; example I. Rolling motion following sudden deflection of ailerons. Typical 1,600-pound airplane. $C_L=1.0$; $C_l=0.04$; $C_n=-0.01$.

sideslip during such a turn in studying the practicability of 2-control operation.

(b) The first step in this problem is the determination of a suitable expression for the banking part of the maneuver. It was considered that the pilot would naturally conform his use of the control to the desired motion of the airplane rather than move the control in a predetermined way and accept whatever motion of the machine followed. Hence it seems more logical to specify the banking motion itself rather than to try to predetermine a law of application of rolling moment.

The airplane is thus assumed to be constrained in banking by the aileron control so as to follow a well-executed bank maneuver and recovery. The usual procedure in making a turn is to bank the machine up to a definite angle, holding this angle steadily for a short time while in the steady part of the turn, and then to recover to level flight on the completion of the desired angle of turn. A curve representing such a relation of bank angle against time may be represented by a series of only two cosine terms with a constant defining the initial and terminal conditions of level flight, or zero bank angle. (See fig. 7.) For a fairly sharp turn with this small airplane the time required will be about 6 seconds if the maximum angle of bank is 30°. The specification decided on is:

$$\text{Bank angle, } \varphi=0.327-0.262\ [\cos t+\tfrac{1}{4}\cos 2t] \qquad (47)$$

which reaches a steady value of 30°, and gives level flight at $t=0$ and $t=2\pi$ seconds. The rate of rolling is the rate of change of this angle of bank; or

$$p=\frac{d\varphi}{dt}=0.262\sin t+0.131\sin 2t \qquad (48)$$

A constraint of the machine in one of its degrees of freedom having thus been specified, it is only necessary to consider the equations for free motion in the remaining two degrees. As before, the lateral motion will be assumed to be independent of the longitudinal. There remain only the sideslipping and yawing motions to be considered. Their equations are:

$$\left.\begin{aligned}\frac{dv}{dt}&=g\varphi-rU_0\\ \frac{dr}{dt}&=vN_v+pN_p+rN_r\end{aligned}\right\} \qquad (49)$$

Although the equations contain the rate of rolling and the angle of bank, these are to be considered as known

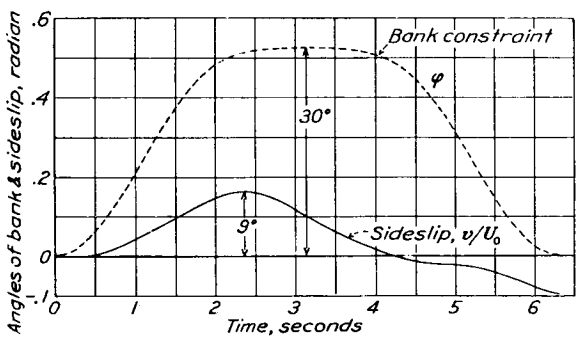

FIGURE 7.—Result of computation; example II. Sideslip during a 2-control turn maneuver.

from equations (29) and (30) and are, in fact, to be used as the disturbance terms. Calling

$$\left.\begin{aligned}Y_0&=\frac{g}{U_0}\varphi\\ N_0&=pN_p\end{aligned}\right\} \qquad (50)$$

and rearranging the equations as in the other problems:

$$\left.\begin{aligned}D\frac{v}{U_0}+r&=Y_0\\ -U_0N_v\frac{v}{U_0}+(D-N_r)\,r&=N_0\end{aligned}\right\} \qquad (51)$$

Solving algebraically for v/U_0:

$$\frac{v}{U_0}=\frac{\begin{vmatrix} Y_0 & 1 \\ N_0 & (D-N_r) \end{vmatrix}}{\begin{vmatrix} D & 1 \\ -U_0N_v & (D-N_r) \end{vmatrix}} \tag{52}$$

or

$$\frac{v}{U_0}=\frac{f_1(D)}{F(D)}Y_0+\frac{f_2(D)}{F(D)}N_0 \tag{52a}$$

where

$$\left.\begin{aligned} f_1(D)&=D-N_r \\ f_2(D)&=-1 \\ F(D)&=D^2-N_rD+U_0N_v \end{aligned}\right\} \tag{53}$$

If the airplane is to maintain its altitude while turning, the speed must be adjusted to give a higher lift than that at an equal lift coefficient in level flight. At an assumed lift coefficient of 1 the speed necessary to maintain altitude while turning at 30° bank is found to be 95 feet per second. Actually, if this speed is held throughout the specified maneuver, the longitudinal path will be accelerated somewhat; this condition will be neglected in the present problem. The necessary stability derivatives calculated for the new condition are:

$$\left.\begin{aligned} N_r&=-0.712 \\ U_0N_v&=2.40 \\ N_p&=-0.323 \end{aligned}\right\} \tag{54}$$

The "disturbance effects" Y_0 and N_0 are (see equations (46), (47), and (49))

$$\left.\begin{aligned} Y_0&=0.111-0.0888\cos t-0.0222\cos 2t \\ N_0&=-0.0846\sin t-0.0423\sin 2t \end{aligned}\right\} \tag{55}$$

and, finally,

$$\begin{aligned} \frac{v}{U_0}=&0.111\frac{f_1(D)}{F(D)}-0.0888\frac{f_1(D)}{F(D)}\cos t \\ &-0.0222\frac{f_1(D)}{F(D)}\cos 2t-0.0846\frac{f_2(D)}{F(D)}\sin t \\ &-0.0423\frac{f_2(D)}{F(D)}\sin 2t \end{aligned} \tag{56}$$

For the expansion of these terms in the integration equations (6), (8), and (9), it is necessary to know the roots of $F(D)=0$. These are

$$\left.\begin{aligned} \lambda&=\frac{N_r\pm\sqrt{N_r^2-4U_0N_v}}{2} \\ \lambda&=-0.356\pm 1.51i \end{aligned}\right\} \tag{57}$$

Since both these roots are complex, the operations indicated in the integration equations were performed graphically in the manner previously shown.

The results of these calculations are shown in figure 7. The fact that the error in meeting the zero sideslip condition at the start of the maneuver was very small (even though the graphical construction of several terms was required) gives an indication of the accuracy of the calculation.

LANGLEY MEMORIAL AERONAUTICAL LABORATORY,
NATIONAL ADVISORY COMMITTEE FOR AERONAUTICS,
LANGLEY FIELD, VA., *February 19, 1936.*

APPENDIX

EVALUATION OF ELEMENTARY OPERATORS

A simple differential equation may be used to illustrate briefly Heaviside's method of evaluating more elementary operational forms. Consider the case of an airplane executing pure rolling motion under the influence of a suddenly applied rolling moment of magnitude $mk_X^2L_0$, which produces the impulsive acceleration L_0 in roll. The equation of motion may be written:

$$\frac{dp}{dt}=pL_p+L_0 \tag{58}$$

in which both p and L_0 are supposed to have the value zero at the time $t=0$.

The solution of this equation as ordinarily found will consist of two parts, one of which is a solution of

$$\frac{dp}{dt}-pL_p=0 \tag{59}$$

the "complementary equation." In effect, Heaviside wrote both equations, (58) and (59), as one by introducing a discontinuous function of t into (58). Thus, (substituting the usual D)

$$Dp-L_pp=1(t)L_0 \tag{60}$$

where the symbol $1(t)$ is termed the "unit function," and is supposed to have the value zero until the time $t=0$ and to take the value 1 thereafter. The algebraic solution of (60) is then written

$$p=\frac{1}{D-L_p}1(t)L_0 \tag{60a}$$

and it is required to evaluate the form

$$\frac{1}{D-L_p}1(t)$$

The procedure is to expand the fraction by the binomial theorem in ascending powers of L_p, thus,

$$(D-L_p)^{-1}=D^{-1}+D^{-2}L_p+D^{-3}Lp^2+\ldots+\text{etc.} \tag{61}$$

Since

$$\begin{aligned}D^{-1}1(t)&=\int 1(t)dt=1(t)t\\ D^{-2}1(t)&=\int\int 1(t)dtdt=1(t)\frac{t^2}{2!};\ \text{etc.},\end{aligned} \tag{62}$$

performing the indicated integrations results in

$$(D-L_p)^{-1}1(t)=1(t)\left(t+\frac{L_pt^2}{2!}+\frac{L_p^2t^3}{3!}+\ldots+\text{etc.}\right) \tag{63}$$

If this series is multiplied throughout by L_p it becomes identically the series for e^{L_pt} except for the term 1, that is

$$[L_p(D-L_p)^{-1}+1]1(t)=1(t)e^{L_pt} \tag{64}$$

or

$$(D-L_p)^{-1}1(t)=\frac{1(t)}{L_p}(e^{L_pt}-1) \tag{65}$$

The final solution of the original equation (1) follows as

$$p=1(t)\frac{L_0}{L_p}(e^{L_pt}-1) \tag{66}$$

Such forms as the left side of equation (60), involving the symbol D, are termed "operators." Equations (6) to (9) of the text are to be considered as evaluations of the more complex operators $f(D)/F(D)$ along the above-indicated lines. The evaluation of a number of such forms is given in reference 5.

Equation (6) of the text is a shorthand method of arriving at the foregoing solution. For the present problem this formula is:

$$p=\frac{f(D)}{F(D)}1(t)L_0=1(t)\left[\frac{f(0)}{F(0)}L_0+\sum_{\lambda}\frac{f(\lambda)L_0}{\lambda F'(\lambda)}e^{\lambda t}\right] \tag{67}$$

and the various terms are:

$$\left.\begin{aligned}f(D)&=1\\ F(D)&=D-L_p\\ f(0)&=1\\ F(0)&=-L_p\\ \lambda&=L_p\\ f(\lambda)&=1\\ F'(\lambda)&=1\end{aligned}\right\} \tag{68}$$

The substitution of these terms in (67) results in

$$p=1(t)\frac{L_0}{L_p}(e^{L_pt}-1) \tag{69}$$

as before.

REFERENCES

1. Wilson, Edwin Bidwell: Theory of an Aeroplane Encountering Gusts. T. R. No. 1, Part 2, 1915; II, T. R. No. 21, 1917; and III, T. R. No. 27, N. A. C. A., 1918.
2. Bryant, L. W., and Williams, D. H.: The Application of the Method of Operators to the Calculation of the Disturbed Motion of an Aeroplane. R. & M. No. 1346, British A. R. C., 1931.
3. Routh, E. J.: Advanced Rigid Dynamics, vol. II. The MacMillan Company, 1905.
4. Goursat, Edouard: Functions of a Complex Variable. Translated by E. R. Hedrick and Otto Dunkel, Ginn & Co., 1916.
5. Bush, V.: Operational Circuit Analysis. John Wiley and Sons, Inc., 1929.

REPORT NO. 570

THE EFFECT OF LATERAL CONTROLS IN PRODUCING MOTION OF AN AIRPLANE AS COMPUTED FROM WIND-TUNNEL DATA

Fred E. Weick and Robert T. Jones

Langley Memorial Aeronautical Laboratory

1936

REPORT No. 570

THE EFFECT OF LATERAL CONTROLS IN PRODUCING MOTION OF AN AIRPLANE AS COMPUTED FROM WIND-TUNNEL DATA

By Fred E. Weick and Robert T. Jones

SUMMARY

An analytical study of the lateral controllability of an airplane has been made in which both the static rolling and yawing moments supplied by the controls and the reactions due to the inherent stability of the airplane have been taken into account. The investigation was undertaken partly for the purpose of coordinating the results of a long series of wind-tunnel investigations with phenomena observed in flight tests; for this reason a hypothetical average airplane, embodying the essential characteristics of both the wind-tunnel models and the full-size test airplanes, was assumed for the study.

Stability derivatives for the average airplane and for several of the actual flight-test airplanes were computed, and computations were made in an attempt to reproduce by the theory the conditions of several actual flight tests. Computations made of forced rolling and yawing motions of an F–22 airplane caused by a sudden deflection of the ailerons were found to agree well with actual measurements of these motions.

The conditions following instantaneous full deflections of the lateral control have been studied, and some attention has been devoted to the controlling of complete turn maneuvers. A portion of the work was devoted to a study of controllability at stalling angles, and the results of this application of theory were found to agree qualitatively with flight-testing experience.

The angle of bank produced in 1 second, φ_1, by a deflection of the rolling control may be taken as a relative measure of the control effectiveness. In the analysis of controllability below the stall, it was found that a simple measure of the rolling effectiveness of a control is given by the sum of a constant times the rolling moment and a constant times the yawing moment. Thus a relative weight or importance is given to the secondary yawing moment produced by the rolling control. It was concluded that the importance of such secondary moments can be minimized by alteration of the moments of inertia of the airplane. Increasing the yawing moment of inertia reduces the effectiveness of a given yawing control in producing either yawing or rolling motion. Changes of rolling moment of inertia have little direct effect on either the rolling or yawing motion produced by a given rolling control moment.

The study of conditions above the stall indicated that satisfactory control could not be expected without some provision to maintain the damping in rolling and that a dangerous type of instability would arise if the damping were insufficient. The quantity $L_p N_r - L_r N_p < 0$ was found to give a good measure of this type of instability.

INTRODUCTION

For some time the N. A. C. A. has been conducting a program of research on lateral control for the specific purpose of obtaining information that would lead to improvement of control at the low speeds and high angles of attack above the stall, a region in which present conventional ailerons are known to be unsatisfactory. Several series of wind-tunnel investigations have been completed and an attempt has been made to compare a number of widely different lateral-control devices on the basis of what has been considered their primary function—the provision of rolling moment. Some of the secondary characteristics, such as the yawing moments given by the controls and their effect on the damping in rolling, were considered but only by comparing the various values separately. Flight

tests were then made with the devices that seemed to promise the best lateral control at the stall. Some of them did not perform as had been expected from the wind-tunnel tests (see reference 1), indicating that the first approximation, based largely on the rolling moments given by the devices, was an insufficient basis for comparison and that the complete interaction of the secondary factors must very likely be considered.

References 2 to 5 describe important work that has been done on the lateral control of airplanes in both normal and stalled flight. Reference 2 gives a general account of the problem of control of the stalled airplane; references 3 and 4 describe investigations of the lateral control and stability of different biplane types.

The present report contains the results of a study of control effectiveness made by means of computations that take into account the secondary factors including the yawing moments given by the controls, their effect on the damping in rolling, the other lateral-stability derivatives, and the moments of inertia of the airplane.

Two methods of computation are used. In the first, the rolling and yawing motions are computed step by step for the conditions following a sudden deflection of the lateral control; in the second method a complete turn is arbitrarily specified and the control moments and deflections necessary to perform the maneuver are found. The first method is used to compare the effectiveness below the stall of various lateral-control devices and to investigate primarily the effects of changed stability characteristics above the stall.

The results of calculations made for normal unstalled conditions are compared with measurements made in flight using different types of lateral-control devices. The effects of certain changes in the lateral-stability characteristics below the stall are also studied. The method used in the study of complete turn maneuvers has proved to be a very practical way of dealing with specific control problems. Here all the stability characteristics of the airplane are taken into account but the lengthy and tedious integration of the equations of motion is avoided by predetermining the actual movements of the airplane in the form of some desired maneuver and then finding the manipulation of the controls that would be necessary to execute the specified maneuver. The coordination of the rudder with different types of ailerons has been studied in this way.

MOTION FOLLOWING SUDDEN CONTROL APPLICATION

The method used for calculating the motion following a sudden application of the controls consists of a step-by-step integration. In most cases the control moments were assumed to be applied constantly throughout the motion.

Assumptions and symbols.—The assumptions usually made in the study of airplane stability were used here, including:

1. That the air forces and moments arising from displacements of the airplane, relative to its steady condition of flight, are proportional to the displacements or to their rates.

2. That the components of moment due to the different components of motion are additive (i. e., the rolling moment due to the combined rolling and sideslipping may be computed as though the rolling and sideslipping had occurred separately).

The axes used in specifying the moments, angular velocities, etc., are fixed in the airplane and therefore move relatively to the air and to the earth. The X axis passes through the center of gravity of the airplane in the plane of symmetry and is chosen to point directly into the line of the relative wind when the airplane is flying steadily. In other respects the axes form a conventional trihedral system, intersecting at the center of gravity of the airplane, the Z axis pointing downward in the plane of symmetry and the Y axis pointing along the direction of the right wing. The motions discussed are those of the moving axes relative to the undisturbed air with the exception of the angle of bank, which is measured relative to the horizontal.

The symbols used in the various formulas are defined as follows:

U_0, velocity along X axis in steady flight.
v, velocity of sideslip.
p, angular velocity in rolling.
r, angular velocity in yawing.
φ, angle of bank.

$\beta=\frac{v}{U_0}$, angle of sideslip.

δ, angle of control setting.
Y, component of force along Y axis.
L, rolling moment (about X axis).
N, yawing moment (about Z axis).

$L_p=\frac{\frac{\partial L}{\partial p}}{mk_x^2}$, rolling acceleration due to rolling.

$N_p=\frac{\frac{\partial N}{\partial p}}{mk_z^2}$, yawing acceleration due to rolling.

etc.

$\delta L_\delta=\frac{C_l qSb}{mk_x^2}$, where C_l is the control rolling-moment coefficient.

$\delta N_\delta=\frac{C_n qSb}{mk_z^2}$, where C_n is the control yawing-moment coefficient.

b, wing span.
c, wing chord.
S, wing area.
l, tail length (distance from c. g. to tail post).
mk_X^2, moment of inertia of airplane about X axis.
mk_Z^2, moment of inertia of airplane about Z axis.
Γ, dihedral angle.
Λ, sweepback angle.

Equations of motion.—The moments acting on the airplane during its maneuvers are considered to be divided into two main groups: (1) Those due to the deflected controls, and (2) those arising from the motions of the airplane. The motions are usually supposed to be started by the action of the controls alone but, at each succeeding instant, to be conditioned by factors that vary directly in magnitude with the motions or displacements relative to the air. The effects of the motions are described by quantities known as "resistance," or "stability," derivatives. The part of a rolling moment due to rolling motion is calculated by the expression $p\frac{\partial L}{\partial p}$; the partial rolling moment due to combined yawing and rolling is given by:

$$p\frac{\partial L}{\partial p}+r\frac{\partial L}{\partial r}$$

It will be found convenient to replace the actual moments by their corresponding angular accelerations, which are proportional to them. Since

$$\frac{\frac{\partial L}{\partial p}}{mk_X^2}=L_p$$

the component of rolling acceleration due to rolling motion is simply

$$pL_p$$

If the airplane is moving in all its degrees of lateral freedom with deflected controls, the total acceleration in rolling is expressed by

$$\frac{dp}{dt}=\delta L_\delta+pL_p+rL_r+\beta L_\beta \qquad (1)$$

where δL_δ is the part of the acceleration due to the control. Likewise the sum of the components of yawing acceleration is

$$\frac{dr}{dt}=\delta N_\delta+pN_p+rN_r+\beta N_\beta \qquad (2)$$

The equation for the angle of sideslip contains both the centrifugal effect due to turning and the effect of gravity,

$$\frac{d\beta}{dt}=\frac{g}{U_0}\sin\varphi-rU_0 \qquad (3)$$

It is to be noted that, when the angle of sideslip β was computed, the component accelerations due to the sidewise air forces (i. e., terms containing Y) were neglected. The most important term here is Y_β; a rough estimate shows that its greatest probable effect would be negligible for the type of maneuver investigated.

Since the axes changes their orientation in the airplane with different lift coefficients, they will not be directly in line with the axes of the principal moments of inertia. The corrections are small, however, and have been neglected.

Integration of equations.—The equations show that in order to calculate the acceleration of the motion at any time, the velocities p, r, and the angle of sideslip β must be known. This knowledge is, of course, available only when all accelerations before the time in question are known; an integration is therefore necessary. This integration may be conveniently performed by dividing the time during which the motion occurs into very small steps and by assuming that the velocities remain constant over these small intervals. If a particular instant is denoted by the subscript n, the accelerations at this instant may be calculated by the formulas

$$\left.\begin{aligned}\left(\frac{dp}{dt}\right)_n&=(\delta L_\delta)_n+p_nL_p+r_nL_r+\beta_nL_\beta\\ \left(\frac{dr}{dt}\right)_n&=(\delta N_\delta)_n+p_nN_p+r_nN_r+\beta_nN_\beta\end{aligned}\right\} \qquad (4)$$

If the preceding time instant is denoted by n–1, the accelerations at each succeeding instant may be calculated step by step, using the velocities computed from the previous instant. Thus:

$$\left.\begin{aligned}p_n&=\left(\frac{dp}{dt}\right)_{n-1}\times\Delta t+p_{n-1}\\ \varphi_n&=p_{n-1}\times\Delta t+\varphi_{n-1}\\ r_n&=\left(\frac{dr}{dt}\right)_{n-1}\times\Delta t+r_{n-1}\\ \beta_n&=\left(\frac{d\beta}{dt}\right)_{n-1}\times\Delta t+\beta_{n-1}\end{aligned}\right\} \qquad (5)$$

The right-hand sides of these equations contain only quantities known from the preceding instant. At the start, $n=0$, all the velocities and angles are taken as zero, and the accelerations are caused by the control moments alone,

$$\left.\begin{aligned}\left(\frac{dp}{dt}\right)_0&=\delta L_\delta=\frac{C_lqSb}{mk_X^2}\\ \left(\frac{dr}{dt}\right)_0&=\delta N_\delta=\frac{C_nqSb}{mk_Z^2}\\ \left(\frac{d\beta}{dt}\right)_0&=0\end{aligned}\right\} \qquad (6)$$

A typical example illustrating the step-by-step computation is given in table I.

Comparison of computed and measured motions.—The results of a number of flight tests of the F–22 airplane equipped with several widely different lateral-

control devices have been used as checks of the computations. These tests were conducted by gliding the airplane at various steady speeds and suddenly deflecting the aileron control to its full extent. Instrument records of the resulting rolling and yawing angular

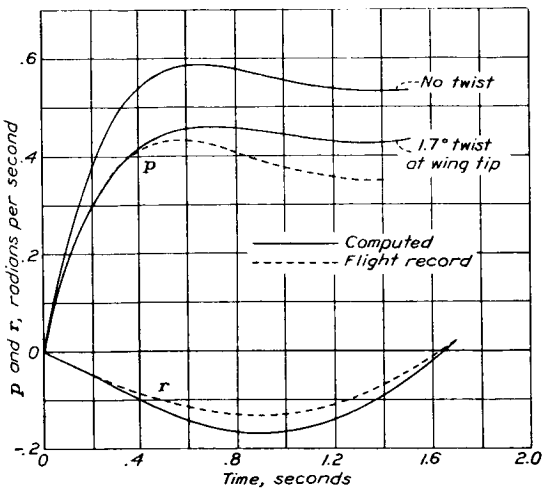

FIGURE 1.—Rolling and yawing motion of F–22 airplane with long narrow ailerons. Flaps up; C_L=1.0.

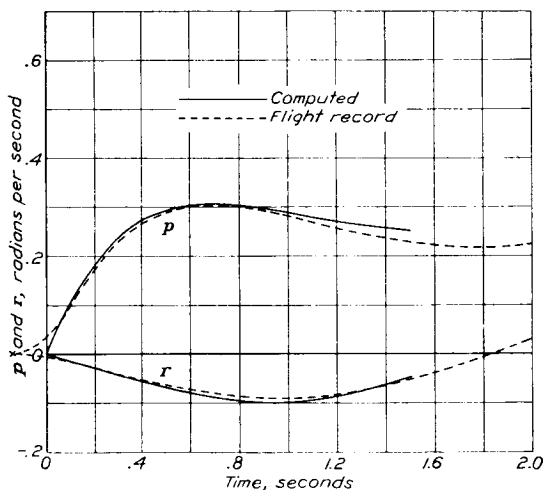

FIGURE 2.—Rolling and yawing motion of F–22 airplane with long narrow ailerons. Flaps down; C_L=1.75.

velocities were made as a measure of the effectiveness of the various controls. (See references 1 and 6.)

The procedure in these experiments simulated very closely the conditions assumed in the computations, although the flight records showed that about 0.15 second was actually required to accomplish the full deflection of the control, which was assumed to be instantaneous in the computations. In the comparisons included, this discrepancy was eliminated by appropriate shifts of the time scales.

The flight tests were intended to supplement a program of tests made in the 7- by 10-foot wind tunnel of a series of lateral-control devices (reference 7). The wind-tunnel program included experiments to determine several important lateral-stability characteristics as well as the static rolling and yawing moments produced by the control devices; the results of these

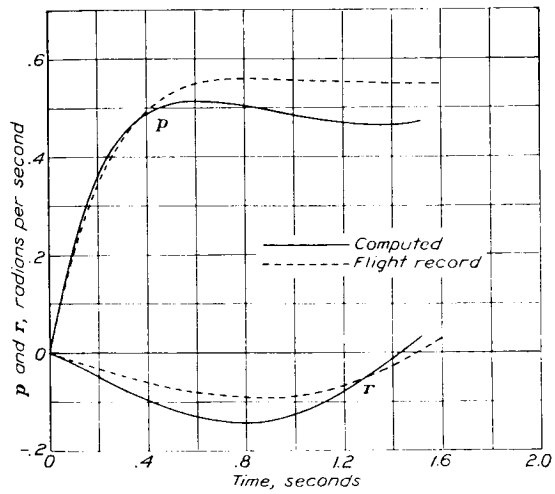

FIGURE 3.—Rolling and yawing motion of F–22 airplane with balanced short wide ailerons. Flaps up; C_L=1.10.

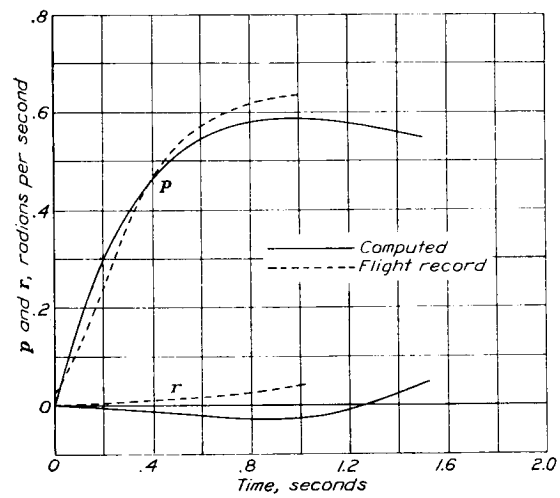

FIGURE 4.—Rolling and yawing motion of F–22 airplane with retractable ailerons. Flaps up; C_L=1.0.

experiments furnished the necessary basis for reproducing the conditions of the flights in the computations. The quantities needed in the computations, including the resistance derivatives, were determined from the known dimensions of the F–22 airplane by the methods given in appendix I.

When computed motions and flight records were first compared, it was found that in many cases the initial accelerations in roll predicted from the rolling moments obtained in the wind tunnel were larger than those shown by the motions recorded in flight. Thus, the full value of the rolling moment measured on the

models was apparently not realized in flight. Examination showed this lack of agreement to be especially apparent in the cases of devices that would be expected to exert the greatest twisting effect on the wings and, since appreciable twisting of the actual wings had been observed in full-scale wind-tunnel experiments, the discrepancy was attributed to this effect. Calculation showed that in the most extreme case (that of ordinary narrow-chord ailerons) a linearly distributed angle of twist reaching 1.7° at the wing tip would account for the observed difference and that the rolling-moment coefficient would be reduced from 0.056 to 0.043. In this case the flight test was made at a dynamic pressure of 9 pounds per square foot. With this first correction as a basis, a general correction formula was used in which the reduction in rolling moment was given as a proportion of the dynamic pressure and the change in section pitching-moment coefficient produced by deflecting the controls.

Figures 1 and 2 show the rolling and yawing motions of the F–22 equipped with long, narrow ailerons. This particular airplane was also equipped with flaps that retracted into the wing ahead of the ailerons. (See reference 6.) Figure 1 illustrates the effect attributed to twisting of the wings. The higher curve was obtained when a value of the rolling-moment coefficient based on a wind-tunnel test of a solid wooden model was used. The yawing angular velocity curves showed remarkably good agreement in these two cases, especially as regards the period of the oscillation of this motion.

The comparison of the yawing curves in figures 3 and 4 is not so favorable as in the former cases. In figure 3 it appears that the yawing-moment coefficient as computed from the wind-tunnel data was slightly greater than that recorded. In this case the control moment coefficients used in the computations were obtained from full-scale wind-tunnel tests of the actual airplane; hence no correction for wing twist was applied. The curves of figure 4 apply to a modified F–22 airplane equipped with retractable ailerons. It is possible that this control device, which is similar to a spoiler, has some effect on the yawing moment due to rolling. The disagreement in the yawing curves would seem to indicate that too large a negative value was assumed in the computations.

The curves of computed rolling motion show no consistent disagreements with the curves plotted from the flight measurements, the differences being of opposite sign in several cases. It seems probable that these comparisons represent the general accuracy obtainable either in the experiments or in the calculations.

COMPUTATIONS FOR AVERAGE AIRPLANE IN UNSTALLED FLIGHT

The results of the flight experiments with the F–22 airplane were not suitable for direct comparisons of the effectiveness of the various controls used because the airplane was modified considerably during the progress of the experiments (see references 1 and 6) so that different sets of stability derivatives and moments of inertia had to be used in the computations to represent the different individual tests. In order to secure data of more general significance and to make a more systematic investigation of control effectiveness than was possible in the flight experiments, it was thought desirable to make a series of computations based on a standard set of airplane characteristics, including standard resistance derivatives and moments of inertia. At the same time it was desired to retain the basic dimensions of the F–22 machine so that there would be at least a partial check with the flight-test work at all times.

Specifications of average airplane.—With these considerations in mind the specifications of an arbitrary standard airplane were devised. The weight and the wing area and span of the F–22 airplane were retained but, since other dimensions were obtained from statistical averages, the machine was called an "average airplane." These statistical averages were obtained by studying the specifications of a number of conventional airplanes of different sizes, weights, and types. Data from 20 to 40 airplanes were used for the determination of average values of the following characteristics:

1. The ratio of the total fin and rudder area to the wing area.
2. The ratio of the tail length (i. e., distance from *c. g.* of airplane to the tail post) to the wing span.
3. The ratios of the radii of gyration in rolling and yawing to the wing span.

The moments of inertia were obtained from data listed in reference 8. That the characteristics thus obtained did not differ appreciably from those of the F–22 is shown by the following table:

	Range of characteristics of F–22 airplane used in flight tests	Characteristics of average airplane
Weight.....pounds..	1,500–1,650	1,600
Wing span.....feet..	30– 32.8	32
Wing area.....square feet..	161– 172	171
Area of fin and rudder.....do....	10.1	10.8
Tail length.....feet..	14.5	14.6
mk_x^2.....	696–1,554	1,216
mk_z^2.....	1,520–2,118	1,700

Computations based on a purely dimensionless average airplane were considered, but it was thought that the results would have a more concrete meaning if they were presented in terms of an airplane of particular size, especially since they could then be directly compared with the flight results.

Unstalled-flight computations.—Most of the lateral-control devices tested in the wind tunnel did not cause any change in the stability derivatives of the wings (spoiler devices are a notable exception). In such cases the sole effect of the control in producing motions can

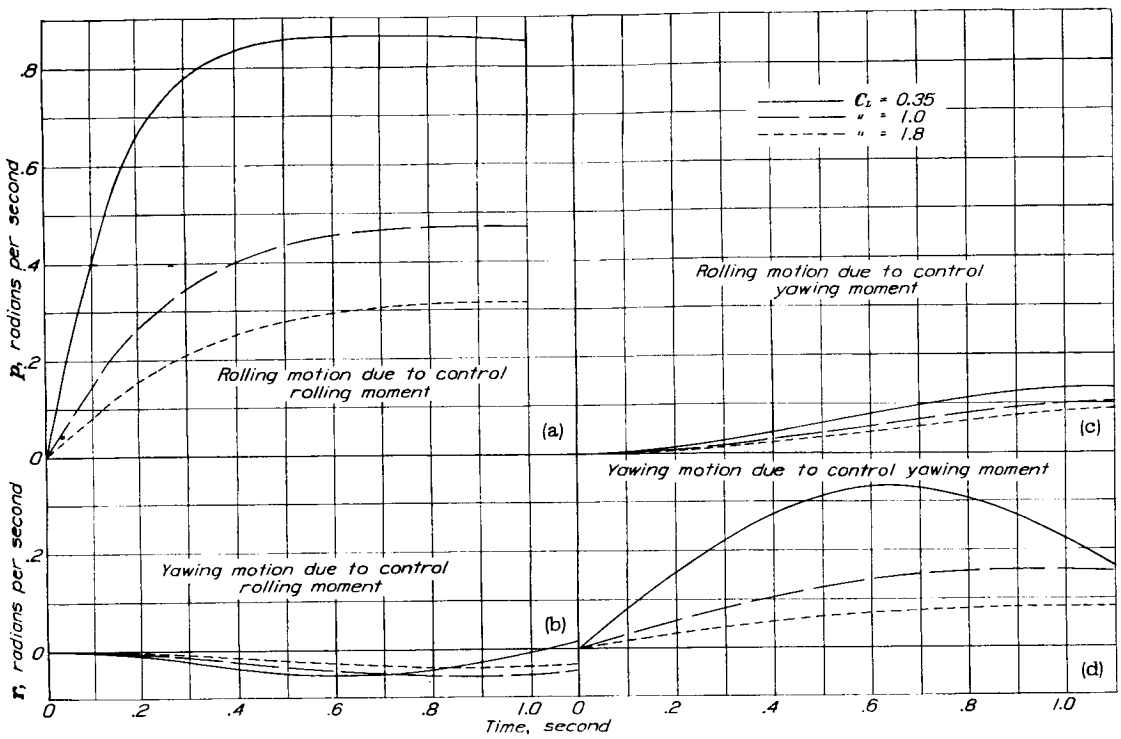

(a) (b) C_l=0.04 C_n=0 (c) (d) C_l=0 C_n=0.01

FIGURE 5 (a, b, c, d).—Computed rolling and yawing motions of average airplane.

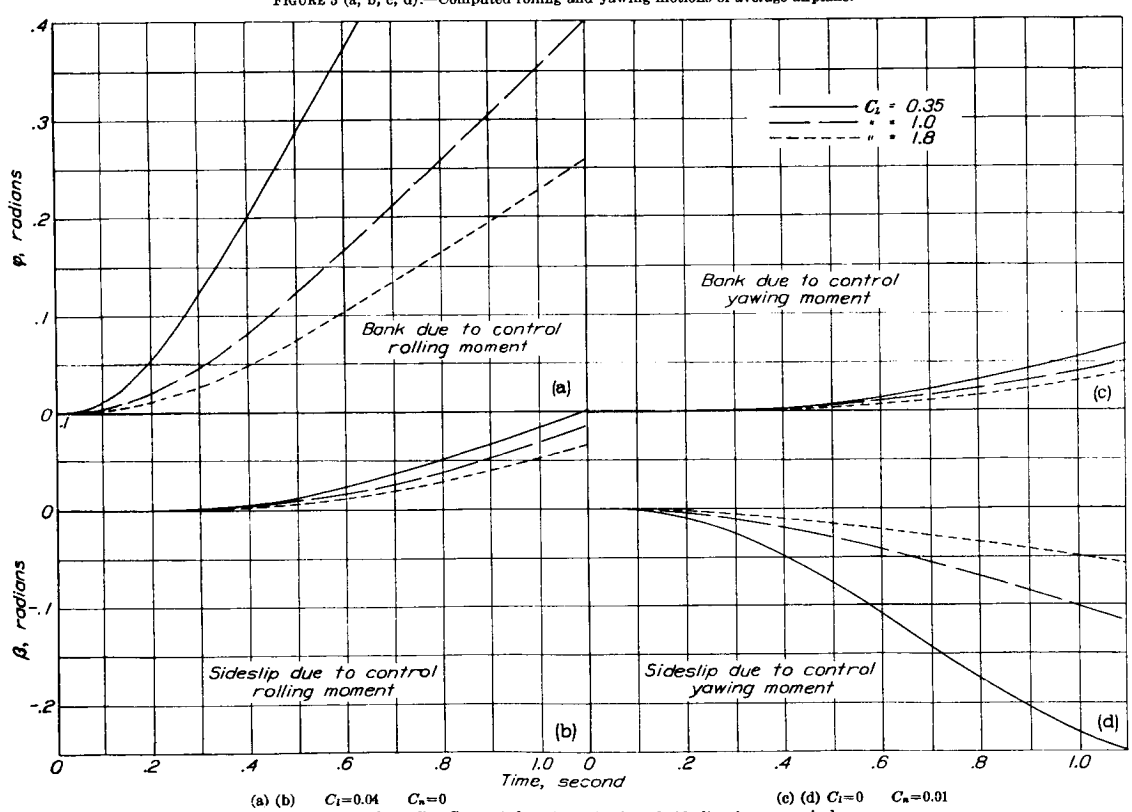

(a) (b) C_l=0.04 C_n=0 (c) (d) C_l=0 C_n=0.01

FIGURE 6 (a, b, c, d).—Computed angles of bank and sideslip of average airplane.

be attributed to the static rolling and yawing moments produced; consequently, a large class of devices could be investigated, in effect, by extending computations over a suitable range of combinations of static rolling and yawing moments.

On account of the linearity of the equations of motion it was possible to calculate the effects of yawing moments and rolling moments separately and later to add them in any desired proportion. Thus, at each of the three lift coefficients two computations were made, one to determine the motion due to a yawing moment and the other to determine the motion due to a rolling moment. The following table lists the values of the coefficients that were used:

C_L : 0.35; 1.0; and 1.8 (20 percent c split flaps, full span).

C_n : 0.01 and 0.

C_l : 0 and 0.04.

In these cases the dihedral angle assumed for the average airplane was 1°. Several additional computations were made to investigate the effect of variation of this factor, assuming angles of 5° and 9°.

Stability derivatives of average airplane.—The stability derivatives used in these computations were obtained by methods described in appendix I and are given in the following table; in the calculation the average airplane was assumed to have rounded-tip wings with 1° dihedral.

	L_p	L_r	L_β	N_p	N_r	N_β
$C_L=0.35$ Cruising speed $U_0=150$ feet per second	−5.44	1.11	−2.16	−0.207	−0.913	5.52
$C_L=1.0$ Gliding speed $U_0=88.5$ feet per second	−3.23	1.88	−1.11	−.301	−.663	2.04
$C_L=1.8$ Low speed (flaps) $U_0=66$ feet per second	−2.46	2.51	−1.66	−.310	−.977	1.46

Results of below-stall computations.—The results of the series of computations for the condition below the stall are shown in figures 5 to 9. Calculated examples of the complete motion are given in figures 5 and 6, which show the rates of rolling and yawing and the angles of bank and sideslip plotted against time for the different flight speeds.

It was thought that the amount of motion produced in 1 second would be a reasonable measure of the control effectiveness. As previously mentioned, the motion produced by a given yawing moment can be added to that produced by a given rolling moment to get the simultaneous effect of both. Thus the formulas for the motion produced in 1 second by any combination of rolling and yawing moments are

$$\left.\begin{aligned} p_1&=C_l\frac{\partial p_1}{\partial C_l}+C_n\frac{\partial p_1}{\partial C_n}\\ \varphi_1&=C_l\frac{\partial \varphi_1}{\partial C_l}+C_n\frac{\partial \varphi_1}{\partial C_n}\\ r_1&=C_l\frac{\partial r_1}{\partial C_l}+C_n\frac{\partial r_1}{\partial C_n}\\ \beta_1&=C_l\frac{\partial \beta_1}{\partial C_l}+C_n\frac{\partial \beta_1}{\partial C_n}\end{aligned}\right\} \quad (7)$$

where $\frac{\partial p_1}{\partial C_n}$, $\frac{\partial \varphi_1}{\partial C_l}$, etc., are parameters that depend on the speed of flight and the stability characteristics of the airplane. These parameters are shown plotted against lift coefficient (as a measure of the flight speed) in figures 7 and 8 and represent the principal results of the series of computations for unstalled flight.

Discussion of below-stall computations.—The factors shown in figures 7 and 8 may be used to compare the effectiveness of various lateral-control devices on the basis of the motions and displacements they would produce on a 1,600-pound airplane of average stability characteristics. By showing the effect of secondary control moments in producing motion of the airplane, they give a measure of the relative weight to be assigned such secondary moments in comparing different devices. These factors will, of course, be somewhat different for airplanes of different stability characteristics and the relative effects of secondary control moments will be expected to be somewhat different also. The average airplane is simply a convenient yardstick in this respect.

If the factors given in figures 7 and 8 are used as absolute measures of the amount of motion produced in 1 second (aside from their use simply in comparing various control devices), a greater error will be committed in applying them to airplanes of different size than in applying them to airplanes of somewhat different stability characteristics. Reference 9 gives the necessary rules for correctly applying the present data to airplanes of any size or weight in which certain definite aspects of similarity are preserved. The theory requires that the airplanes be geometrically similar although they may have different densities. Practically, this requirement necessitates that the outward forms of the airplanes be similar and that the ratios of the radii of gyration about each axis to the wing span be the same. The motions of the different sized airplanes are compared at equal values of the lift coefficient. With equal values of the wing loading the angular velocities are inversely proportional to the spans: Thus,

76746—37——2

and

$$\left.\begin{aligned}\frac{p'_1 b'}{2U_0}&=\frac{p_1 b}{2U_0}\\ \frac{\varphi'_1 b'}{2U_0}&=\frac{\varphi_1 b}{2U_0}\end{aligned}\right\} \tag{8}$$

With similar airplanes of different wing loadings the state of motion existing at a given time for one will generally pertain to a different instant for another, which is also true of an airplane of the same size and loading but flying in air of different density. Given the motion of the average airplane at 1 second, the instant to which this state of motion (as indicated by

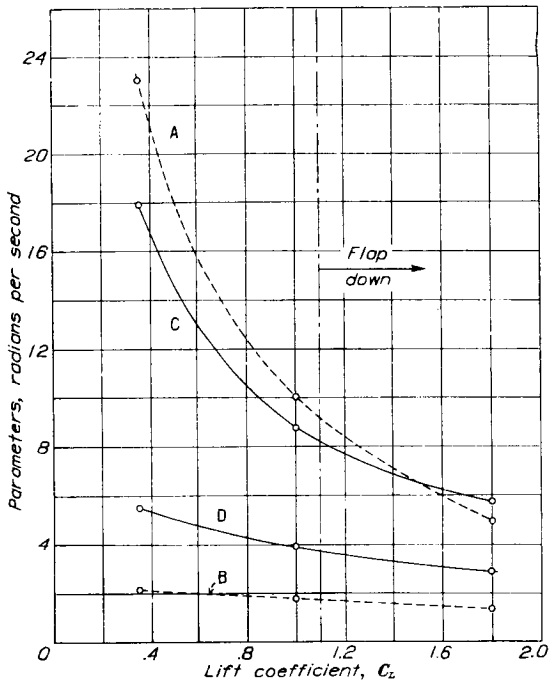

$-\frac{\partial \beta_1}{\partial C_n}$ curve A, $\frac{\partial \beta_1}{\partial C_l}$ curve B, $\frac{\partial \varphi_1}{\partial C_l}$ curve C, $\frac{\partial \varphi_1}{\partial C_n}$ curve D

$\varphi_1 = C_l\frac{\partial \varphi_1}{\partial C_l} + C_n\frac{\partial \varphi_1}{\partial C_n}$, $\beta_1 = C_l\frac{\partial \beta_1}{\partial C_l} + C_n\frac{\partial \beta_1}{\partial C_n}$

FIGURE 7.—Parameters for computing displacement of average airplane at end of 1 second with various combinations of rolling and yawing moments.

the value of $pb/2U_0$) pertains on a similar airplane may be found from:

$$t' = 1 \times \frac{S\frac{\rho}{2}\frac{U_0}{m}}{S'\frac{\rho'}{2}\frac{U_0'}{m'}} \tag{9}$$

Plots representing the motion of an airplane in non-dimensional terms have as abscissa

$$\frac{S\frac{\rho}{2}U_0}{m} \times t$$

and as ordinate

$$\frac{pb}{2U_0}$$

or

$$\frac{S\frac{\rho}{2}b}{\varphi\frac{}{2m}}$$

etc.

In the case of the average airplane the influence of moderate dihedral on the lateral controllability below

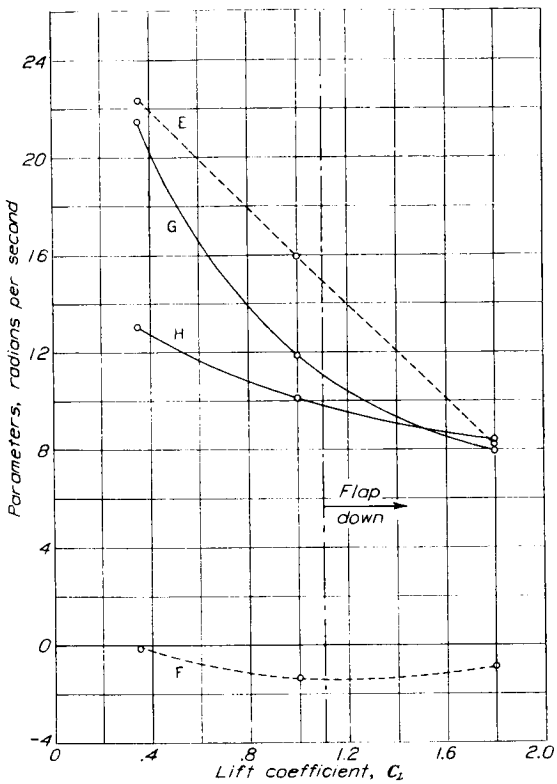

$\frac{\partial r_1}{\partial C_n}$ curve E, $\frac{\partial r_1}{\partial C_l}$ curve F, $\frac{\partial p_1}{\partial C_l}$ curve G, $\frac{\partial p_1}{\partial C_n}$ curve H

$p_1 = C_l\frac{\partial p_1}{\partial C_l} + C_n\frac{\partial p_1}{\partial C_n}$, $r_1 = C_l\frac{\partial r_1}{\partial C_l} + C_n\frac{\partial r_1}{\partial C_n}$

FIGURE 8.—Parameters for computing motion of average airplane at end of 1 second with various combinations of rolling and yawing moments.

the stall was small, as is shown in figure 9. If, however, a large dihedral effect is combined with considerable adverse yawing tendency from the ailerons, the lateral control may become ineffective. This condition is most likely to occur at low speeds with flaps deflected because under these conditions the wings show their greatest tendency to roll when yawed (dihedral effect) and because the aileron yawing moment is usually greatest at high lift coefficient. Figure 9 shows that with a dihedral angle of 9° and an adverse yawing moment of one-fourth of the rolling moment, the aver-

age airplane actually reversed its normal roll, rolling against the ailerons less than 2 seconds after they were applied. The magnitude of the tendency for a given adverse yawing moment to render the lateral control ineffective depends to some extent on all the stability characteristics of the airplane, but principally on the ratio of rolling to yawing moments in sideslip, i. e., on $\frac{dC_l/d\beta}{dC_n/d\beta}$. For the various cases depicted in figure 9 these ratios were:

Dihedral angle, degrees	$\frac{dC_l/d\beta}{dC_n/d\beta}$
1	0.8
5	1.2
9	2.4

Large values of this ratio decrease the aileron control effectiveness if the secondary yawing moments are adverse but will tend to increase it if they are favorable. The curves of rolling motion given in figures 1 to 5 show that the rate of rolling rises quickly at the start on account of the relatively great rolling moment but soon becomes almost steady. This steady rate is attained in about 0.3 second at high speed and occurs when the air damping of the rolling motion is large enough to overcome the control moment. Obviously the lateral moment of inertia (mk_X^2) cannot have much influence on this portion of the curve since the airplane is not accelerating appreciably, and its effect will be shown mainly on the starting slope of the curve. (See fig. 10.) It may be seen that the area under the curve at, say, 1 second would not be appreciably affected by changes in this slope; hence the angle of bank reached in 1 second would not be much affected by the moment of inertia in rolling. This fact has been borne out by flight experiments made by the N. A. C. A. in which the test pilots were unable to detect with certainty the effects of changes in rolling moment of inertia of as high as 50 percent. (See also reference 10.)

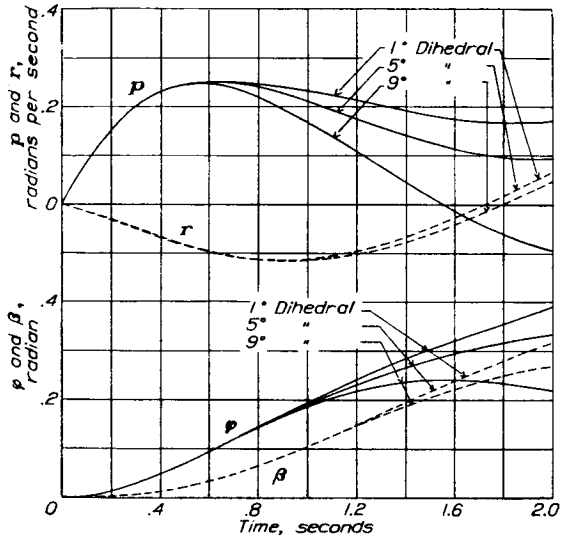

FIGURE 9.—Effect of dihedral combined with adverse yawing moment on rolling control. Flaps down; C_L=1.8; C_l=0.04 ; C_n=−0.01.

The yawing-motion curves indicate a different phenomenon. Here the damping is relatively small and the effects of moment of inertia in yaw are fairly large. Thus it appears that the magnitude of the rudder moments should be accommodated to the airplane moment of inertia, while the principal consideration determining the rolling-control moments should be the air-damping factor.

Since the amount of yawing motion produced by a given yawing moment is primarily governed by the moment of inertia in this motion, it appears that the unfavorable influence of secondary aileron yawing moments could be effectively reduced by increasing this moment of inertia. Furthermore, since the direct effect of roll moment of inertia on the rolling motion is apparently slight, it is possible that increasing mk_Z^2 by distributing weight along the wing span would actually increase the aileron effectiveness if considerable adverse yawing moment were present.

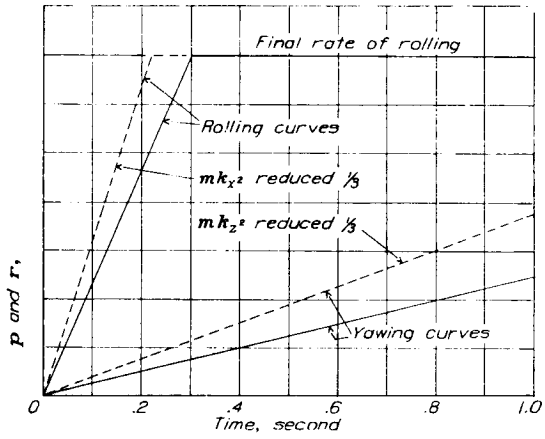

FIGURE 10.—Diagram illustrating effect of change of moments of inertia on rolling and yawing control.

COMPUTATIONS FOR STALLED FLIGHT

Experiments with lateral control at angles of attack above the stall having been made both in the flight and the wind-tunnel research projects, it was desired to extend the present investigation to cover this condition also. Accordingly, a study of the results of both series of tests was made with the object of determining whether the conditions encountered in practice could be reproduced in theory.

Unfortunately, the wind-tunnel experiments showed that no certain determination of the factors (resistance derivatives) involved in the motion of a stalled airplane was possible. On the other hand, the flight experiments indicated that these factors apparently had no definite values (according to their usual definition), inasmuch

as the action of the airplane could not be foretold from one experiment to the next. For example, the outcome of a simple aileron movement might in one instance be a roll in the direction urged by the control; whereas at another time, under practically the same conditions, the roll would be the reverse of that intended.

Stability derivatives above stalling angles.—The reasons for the apparently contradictory results of the flight tests may be found in the wind-tunnel measure-

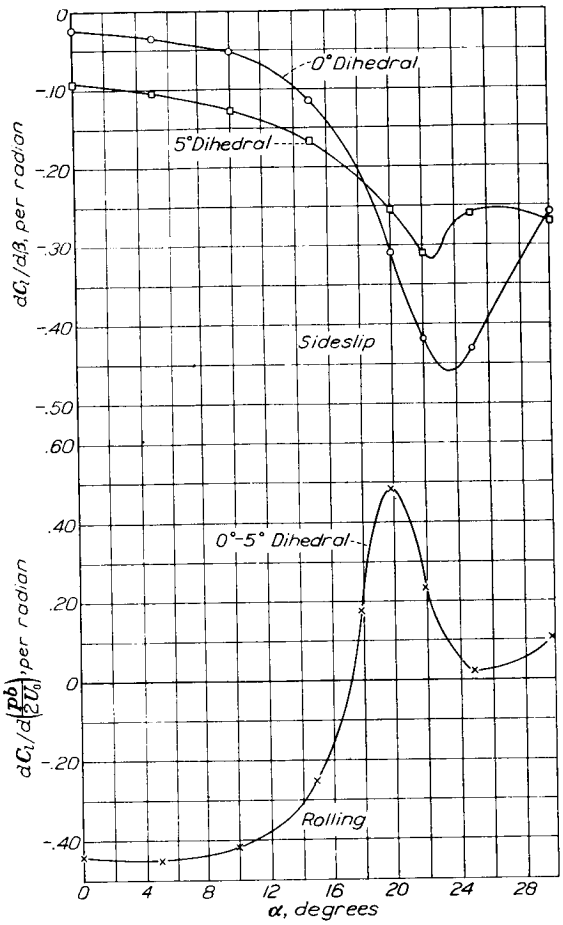

FIGURE 11.—Coefficients of rolling moment due to rolling and sideslip at various angles of attack. Rectangular Clark Y monoplane; data from tests in the 7- by 10-foot wind tunnel.

ments of the stability characteristics made at these high angles; these measurements show that motions of the wings may develop unstable moments, which could quickly overpower static rolling or yawing moments given by the controls. Figure 11 shows typical measurements of coefficients by which these quantities are determined. These curves show that the rolling moment due to sideslip of a straight wing increases enormously as the stall is approached, reaching values 7 or 8 times as great as those at medium angles below stalling. Under the same conditions the damping moment in rolling changes sign and becomes an "aiding" (autorotational) moment.

Obviously many of the assumptions of the method as used in investigating unstalled-flight phenomena are not true in the case of stalled flight. In particular, the assumed independence of small longitudinal and lateral motions, which is supported by both experience and reason for the ordinary-flight range, cannot be said to hold under these new conditions because the values of the derivatives change very rapidly with small changes of longitudinal attitude (angle of attack). The assumption that the components of a moment arising from different sources may be added together as though their causes occurred separately is apparently borne out only in the abstract sense of representing the average condition.

In spite of these limitations of the method, it was considered feasible to extend the computations to the condition of stalled flight in the study of the general conditions encountered in controlling such flight, although the results of the computations made for these conditions do not have the same significance as those made for conditions below the stall. The former results gave quantitative estimates of the amount of motion produced by given control moments; the extension of the computations to stalled flight will only illustrate the various phenomena that may result from the conditions predicted by the wind-tunnel experiments.

Experience in attempting controlled flight above the stall has shown that the possibility of controlling such flight depends as much on the natural stability characteristics of the airplane as on the possibility of securing adequate controlling moments. Because of this fact the present computations were made primarily to investigate the effects of changed stability characteristics (derivatives). Another important reason for choosing various combinations of stability derivatives is the fact that no very definite values can be assigned to them for a particular lift coefficient, as was possible in the unstalled-flight range.

For these reasons the investigation of controllability above the stall is necessarily presented in a manner different from that used in the cases of ordinary flight. The wind-tunnel measurements were studied to find the approximate variation of the resistance derivatives over a range of angles of attack definitely above the stall, chosen to include the region of most violent instability. The particular lift coefficient assumed was necessarily somewhat loosely defined (C_L=1.2); it was so taken to represent extreme stalling as well as intermediate conditions. The calculation of the stability derivatives at these angles is given in appendix I.

In the variation of the stability characteristics to take account of the range of possible conditions, the effects of the parts of the airplane other than the wings were not considered. The wing characteristics which

show the greatest variation in this region and which apparently have the greatest effect on the stability are:

1. The damping in rolling, L_p.
2. The rolling reaction due to sideslip, L_β.
3. The yawing reaction due to rolling, N_p.

Accordingly, three values for each of these were chosen, covering the range shown by the wind-tunnel data and representing two extremes and one mean condition. These values were designated a, b, and c and are listed in table II.

TABLE II.—VALUES OF STABILITY DERIVATIVES USED ABOVE STALL

Designation	L_p	L_β	N_p
a	−1.75	−7.4	−0.20
b	0	−11.4	.53
c	3.50	−14.4	1.06

In each case it will be noted that letter c denotes the most extreme condition likely to be encountered. Condition a may be fairly assumed to apply only to cases where some provision is made to prevent the wing tips from stalling, which may be accomplished by washout or twist or by means of some such device as tip slots. (See appendix I for determination of these derivatives.)

The computations were made to cover more than a dozen different combinations of these values of the derivatives in conjunction with a given fixed pair of control rolling and yawing moments. These arbitrary controlling moments were chosen to represent rolling- and yawing-moment coefficients somewhat greater than those obtained with ordinary ailerons but which might be attained in practice with rather large ailerons, especially those of the short, wide type described in reference 7, I. As in the previous computations (below stall), the sign of the standard yawing-moment coefficient was alternated, giving the effect of favorable and adverse, as well as zero, secondary yawing moment.

Range of investigation of stalled flight.—Since in these computations the plan was to study the *possibility of control* rather than to obtain any numerical measure of control effectiveness, the procedure of the computations was sometimes varied in such a way as to represent attempts of the control to check motions of the airplane as well as to start them. In some cases the motion was assumed to be due to some external cause and to exist at the start of the computations, while in other cases the initial setting of the control was reversed after a short interval in an attempt to check the motion it had already produced. The effects of both favorable and adverse yaw were tried in these cases.

Results of computations.—Figure 12 shows rolling motions resulting from suddenly applied and continuously maintained aileron deflections giving a rolling-moment coefficient of 0.04 and an adverse yawing-moment coefficient of −0.02. The different angular-velocity curves are the results of assuming different combinations of the stability derivatives listed in table II. In accordance with the plan of table II, the first letter in each symbol designation attached to the curves indicates the value of the damping factor L_p used; the second, the value of L_β; and the last, N_p.

These curves appear to represent the same erratic phenomena as were observed in the flight experiments. It will be noted that in some instances the direction of motion of the airplane after a short interval was the reverse of that urged by the rolling control, while in other instances it rolled with increasing acceleration in the direction urged. Either of these phenomena

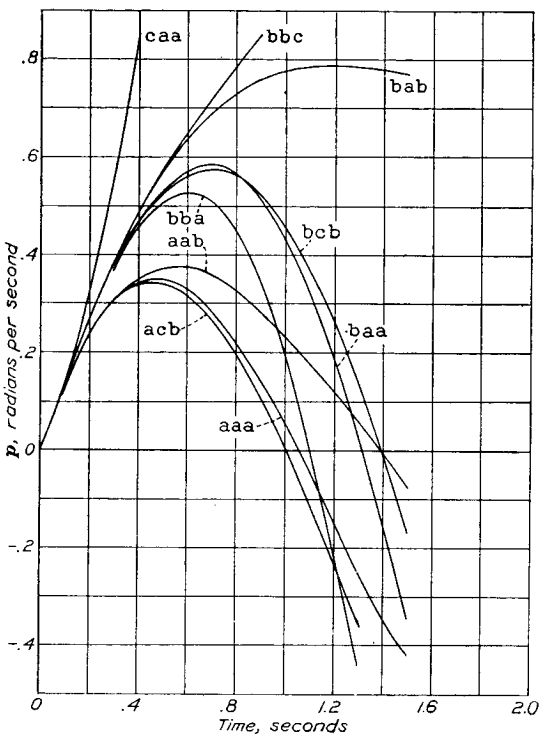

FIGURE 12.—Rolling motions resulting from application of adverse-yaw aileron control in stalled flight with different combinations of stability derivatives; $C_l=0.04$; $C_n=-0.02$.

occurred within the predictable range of the stability derivatives.

The effects of smaller control rolling and yawing moments may be visualized simply by reducing the scales of the motions. Thus in figure 12 the motions calculated for $C_l=0.02$ and $C_n=-0.01$ would be just half those plotted.

Figure 13 shows the results of attempts to check an initial disturbance in rolling with both favorable- and adverse-yaw ailerons. The failure of the adverse-yaw ailerons is due mainly to the yawed attitude they produce, although the actual yawing motion accounts for an appreciable effect. Figure 14 differs from figure 13 in that it includes also conditions in which the initial

motion countered by the ailerons was assumed to be due to the action of the control rather than to an external disturbance in rolling. Here the ailerons were called upon to check whatever yawing motion they had previously produced. In this case it will be noted that the favorable-yaw ailerons encountered difficulty because it was hard to recover from the initial motion they had produced.

Figure 15 shows the effect of a delay in attempting to recover from rolling and yawing motion. Because of the instability of the airplane, the motion could not be checked even though the yawing moment of the ailerons was favorable. Thus, for the particular case illustrated, a delay of 0.1 second in reversing the control changed the action from one in which the airplane followed the

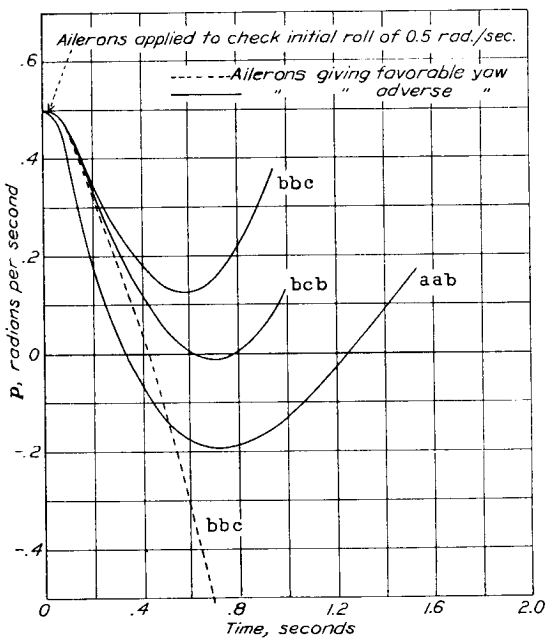

FIGURE 13.—Rate-of-rolling curves illustrating attempts to control initial motion in pure rolling. Stalled flight; $C_l=-0.04$; $C_n=\pm 0.02$.

control to one in which it continued to roll against it.

Discussion in terms of stability derivatives.—The motion of the average airplane in stalled flight is apparently governed more by its natural tendencies than by the applied control moments, a condition illustrated by the curves previously described which showed that the airplane developed tendencies that were uncontrollable in some instances. When using the step-by-step method, it was found convenient to tabulate each separate component of the rolling and yawing accelerations due to the stability factors as well as the components of motion. (See table I.) In this way a complete history of the contribution of each factor was obtained, thus enabling a study of the controllability in terms of the stability derivatives.

Undoubtedly the most important single factor contributing to the uncontrollable instability above the stall is the loss of the damping in rolling. Below the stall this damping is the most powerful constraint of the airplane, and the effects produced by its sudden drop to zero or to a negative value exert a great influence on the behavior of the machine. Apparently no airplane can be considered safely controllable above the stall if the autorotational tendencies observed in wind-tunnel tests of plain wings are retained.

During a roll maneuver in stalled flight there may be, in addition to the control moment, certain other factors that tend to accelerate the rolling. These factors arise because the rolling motion by itself usually tends to

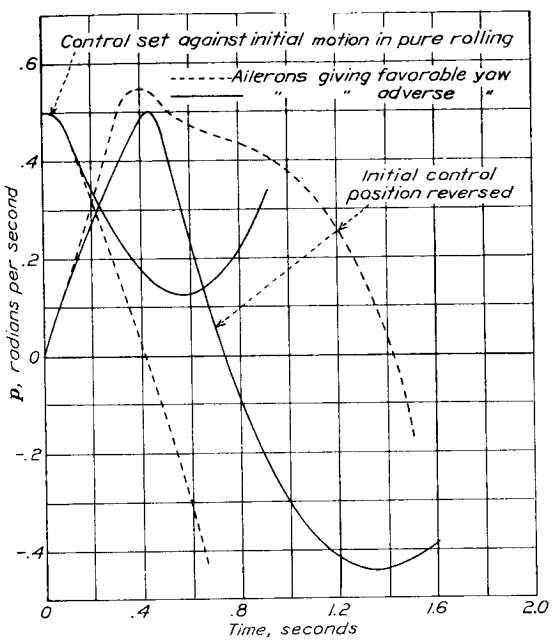

FIGURE 14.—Rate-of-rolling curves showing effect of favorable and adverse aileron yawing moments in attempting to control initial motion in pure rolling and in reversing initial control position. Case bbc; $C_l=0.04$; $C_n=\pm 0.02$.

induce a favorable yawing action above the stall. Thus when the right wing is dropping, its added drag causes a yaw to the right, retarding the wing tip and causing a loss of lift due to decreased speed and tending to aggravate the dropping of the wing. The factors that directly oppose these rolling and yawing motions by damping tend to check this sequence if they are present. The first two effects, which aid the angular motion indirectly, relate to L_r and N_p, proportional, respectively, to the rolling moment due to yawing and the yawing moment due to rolling. Evidently if these moments overcome the direct damping tendencies, the angular motion will tend to accelerate of its own accord or will diverge. Suppose for the moment that these opposing tendencies just balance each other, that is,

$$\left.\begin{aligned} pL_p+rL_r=0 \\ pN_p+rN_r=0 \end{aligned}\right\} \qquad (10)$$

Inasmuch as p and r are simultaneous, there will exist a relation between the derivatives that is independent of p and r; i. e.,

$$L_pN_r - L_rN_p = 0 \tag{11}$$

If this sum is zero, L_r and N_p are sufficiently large to equilibrate the stabilizing damping terms; and, if it is negative, any combined rolling and yawing motion will tend to diverge with increasing acceleration even though the direct dampings are present. The relation between this criterion and the behavior of the airplane in lateral motions above the stall is shown in table III, which gives values for the cases shown in figures 12 to 16.

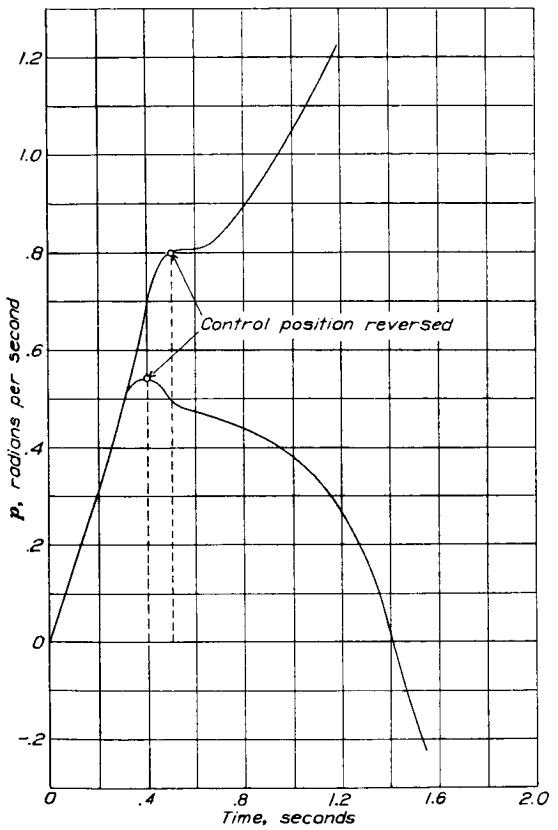

FIGURE 15.—Effect of delay in attempting to recover from motion started by ailerons with favorable yaw. Stalled flight. Case bbc; C_l=0.04; C_n=0.02.

It will be noted that the curves of figure 12 which indicate the greatest tendency toward continued rolling in the direction started correspond to the greatest negative values of $L_pN_r - L_rN_p$. In the curves shown, the rolling control was assumed to give an adverse yawing moment that served to oppose the tendency toward divergence indicated by negative values of this criterion. If a rolling moment with no secondary yawing moment had been assumed in these cases, each curve would have shown an increasing acceleration in rolling greater than that given by the control and according to the magnitude of the tendency exhibited by the value of the criterion, as shown in figure 16. After a definite interval this tendency would have exceeded the power of the controls, and recovery would have been impossible.

Below the stall this criterion appears to be in every case positive, indicating stability. Relatively large positive values indicate relatively great damping of combined rolling and yawing motion.

The foregoing considerations do not take account of any sideslipping effects. These considerations, when combined with the factors determining the sideslipping tendency, give a more complete idea of the controllability characteristics of the airplane at high angles of attack and in stalled flight.

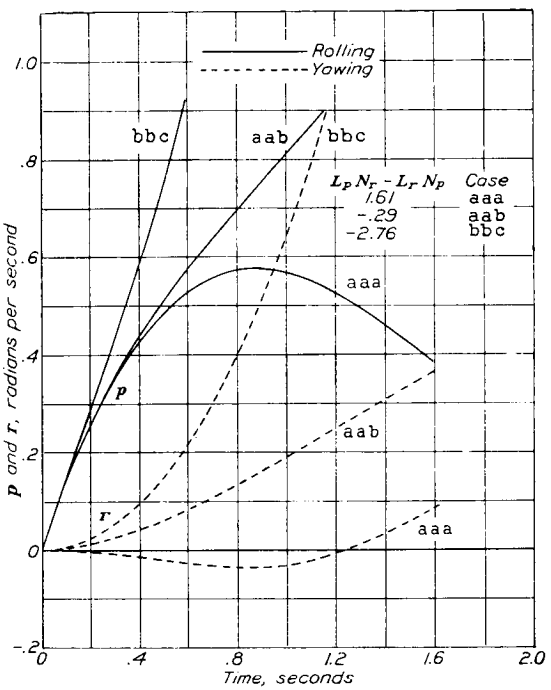

FIGURE 16.—Rolling and yawing motions resulting from application of rolling moment without secondary yawing moment showing effect of different degrees of damping; $L_pN_r - L_rN_p$; C_l=0.04, C_n=0.

It may be shown that the question of whether the airplane tends to sideslip inward or outward at the beginning of a rolling motion depends on the magnitude of N_p compared with g/U_0. As rolling commences from level flight the yawing tendency due to the rolling (which is usually positive above the stall) causes the downgoing wing to be dragged back, creating an outward sideslipping tendency. This tendency is opposed by the action of gravity when the plane is banked, tending to produce inward sideslip. The condition that the outward and inward accelerations cancel is that

$$rU_0 = g\varphi \tag{12}$$

assuming sin φ equal to φ. The angular acceleration in yawing requisite to this condition is

$$\frac{dr}{dt}=\frac{g}{U_0}p \tag{13}$$

In a rolling disturbance the yawing angular acceleration will be due only to N_p, or:

$$\frac{dr}{dt}=pN_p \tag{14}$$

Hence the condition that a rolling disturbance from level flight result in neither outward nor inward sideslipping is that

$$N_p=\frac{g}{U_0} \tag{15}$$

and the relative magnitudes of these quantities may be taken as an indication of the resultant tendency.

The airplane may diverge in the combined rolling and yawing motion previously discussed without sideslipping although such will not generally be the case. Near stalling angles the magnitude of the dihedral effect of the wings increases enormously (especially if the actual dihedral angle is small) and, if the tendency of the airplane is to sideslip outward while rolling and turning, any divergence in the rolling and yawing motion (indicated by negative $L_pN_r-L_rN_p$) will be greatly aggravated. The question of whether the dihedral effect will increase the instability is determined by the sign of the quantity (N_p-g/U_0). The magnitude of the effect of the sideslipping tendency thus determined obviously depends on the stability derivatives in sideslip L_β and N_β or, more conveniently, on L_β/N_β. The values of N_p computed for the stalled-flight conditions b and c were considerably larger than g/U_0, indicating that the natural tendency would be toward outward sideslip during a lateral maneuver. In such cases N_β would exert a stabilizing influence, tending to straighten out the skid. The values of these sideslipping criterions for the cases shown in figures 12 to 16 are given in table III.

TABLE III.—CONTROLLABILITY CRITERIONS FOR CASES SHOWN IN FIGURES 12 TO 16

Designation (see fig. 12)	Damping of rolling L_p	Combined damping $L_pN_r-L_rN_p$	Sideslip indication N_p-g/U_0	Sideslip stability factor $-\frac{L_\beta}{N_\beta}$
	(1)	(2)	(3)	
aaa	−1.75	1.61	−0.60	2.73
aab	−1.75	−.29	.13	2.73
acb	−1.75	−.29	.13	3.76
baa	0	.52	−.60	2.73
bab	0	−1.38	.13	2.73
bba	0	.52	−.60	3.40
bcb	0	−1.38	.13	3.76
caa	3.50	−1.65	.60	2.73
bbc	0	−2.76	.66	3.40

[1] Positive values indicate instability.
[2] Negative values indicate instability.
[3] Positive values indicate outward sideslipping tendency.

Possible modifications of characteristics to improve stability above the stall.—Of the factors influencing the lateral controllability, the stability characteristics that depend on the moments developed by the wings appear to be most important, since it is to be expected that they will be changed most by stalling. In addition to the damping in rolling, the wing moment characteristics that show marked change at the stalling point and contribute to the instability are L_r, L_β, and N_p. The factor L_r, proportional to the rolling moment due to yawing, depends on the lift coefficient and on the spanwise distribution of lift. Obviously, the greater the lever arm of the supporting lift, the greater L_r will be and, since it is desired to make L_r smaller, tapering the wings or shortening their span should help. The factor L_β at normal angles of attack depends also on this spanwise lever arm of the lift and on the dihedral angle. At stalling angles different tip shapes have considerable effect and the relation between the dihedral angle and the rolling moment reverses, the greatest moment being shown by the straight wing with square or upturned tips. (See fig. 11.) Here also, shortening the span and tapering the wing should improve conditions. The use of a moderate dihedral angle appears desirable in the stalled condition. The other wing characteristic, N_p, would be favorably affected by shortening the span of the wings. Here its magnitude depends mainly on the rate of increase of the profile drag of the wings and on the effective arm of the increase. If no damping in rolling (L_p) is present, there will be no induced N_p but in this case the slope of the wing profile-drag curve is almost certain to be very great, more than accounting for the induced effect. (See appendix I.) Taper or washout of the wings should help this situation. The provision of damping in rolling calls for keeping the wing tips from stalling; this requirement is compatible with all the others mentioned except that for small L_r. The desirability of maintaining the damping, however, far outweighs this consideration.

In the consideration of modifications of wing design to improve the controllability at high angles, it is important to take account of the premature tip-stalling phenomena exhibited by tapered wings. As was pointed out in the previous discussion, reducing the lift and the slope of the drag curve near the tips would lead to improved conditions. If this improvement is effected simply by tapering the wings, however, the net result may be detrimental to controllability on account of the premature loss of roll damping due to the stalling of the tips. In the case of any wing with an extreme reduction of chord, the downwash distributes itself in such a manner as to tend to maintain a more uniform distribution of the actual lift, so that the lift coefficient, and hence the effective angle of attack, of the reduced-chord sections is greater than at other sections. Pressure-distribution tests show that the tip portions of a 5:1 tapered wing reach their maximum lift coefficients at angles as much as 5° below the stalling angle of the center portions of the wing. Thus,

tapering the wings cannot be expected to improve the controllability at low speeds unless the taper is accompanied by some washout, or unless other provision is made to prevent the tips from stalling.

It may be inferred from the foregoing discussions that the effects of high aspect ratio will be detrimental to controllability and stability above the stall. It is easily seen how the unstable tendencies of the wings would be more unfavorable to controllability if the wings were of large span. If the span is large in proportion to the lever arm of the rudder control, the wings may easily develop yawing tendencies that will completely overpower the rudder moments. Furthermore, since rapid yawing motion induces a rolling moment through L_r, it is important to provide a large damping in yawing as an indirect check on the rolling as well as on the yawing motions. Thus it appears that considerable tail length and fin area are desirable to increase both N_r and N_β. Inasmuch as there ordinarily exists a great disproportion between the dampings in rolling and yawing below the stall, it is probable that fairly large increases in N_r would be permissible without causing undesirable stiffness of the rudder control at high speeds. Increasing N_β by using larger vertical tail surfaces is especially desirable because in that way the available rudder control is increased. Data on conventional airplanes show that the rudders used produce the weakest of the three controlling moments; their maximum moment is often smaller than the secondary yawing moment of the ailerons, yet the rudder deals with the largest moment of inertia of the airplane and should be the most effective control in checking the unstable yawing tendencies of the wings (as, for instance, in spinning). It appears that considerable improvement in these characteristics could be effected by enlarging the fin surface of conventional machines. If the increased rudder control is found to be undesirable at high speed because of too great sensitiveness, a corresponding increase in N_r, the damping in yawing, should remedy this trouble and still further improve the controllability at high angles. Thus if the tail is made longer as the vertical surface is increased, the control characteristics at high speed should not be unfavorably affected. It appears unlikely, however, that such improvements could result in the retention of satisfactory control above the stall if the autorotational tendencies shown by ordinary wings in wind-tunnel experiments are developed.

TURN MANEUVERS

The foregoing computations were designed to represent the procedure employed in a particular type of flight test to compare the efficiency of various control devices purely on the basis of their independent action in producing roll. Another type of flight test, qualitative in nature, consisted of performing normal turn maneuvers with the airplane, using the device in conjunction with the other controls and observing the amount of coordination that was required.

The first type of computation together with the flight tests showed that the roll-producing effectiveness of some devices would be influenced by the occurrence of considerable incidental sideslipping, much of the apparent improvement due to favorable secondary yaw being obtained by the production of outward sideslipping.

Since it was not known in any quantitative way how the presence of this sideslipping tendency due to the secondary aileron moments would affect the controllability in making actual turn maneuvers, it was decided to make an analysis of these conditions, representing analytically as nearly as possible the second stage of the flight tests.

EXPLANATION OF METHOD OF COMPUTATIONS

In certain instances in the former computations a simple sort of controlled maneuver was used in which an initial deflection of the ailerons was reversed, representing an attempt to check a motion previously produced by them. (See fig. 13.) It was realized that an extension of this procedure could be applied to the present problem by means of step-by-step integrations of the motion due to any arbitrarily specified way of applying the controls. This adaptation of the former method would have required a knowledge of the control manipulations necessary to perform a normal turn, as well as lengthy step-by-step calculations. For these reasons it was considered more feasible to predetermine the actual motion of the airplane than to fix on an arbitrary way of applying the controls. Furthermore it seemed reasonable to presume that the pilot of an airplane would conform his use of the controls to suit a desired maneuver, rather than to prescribe beforehand his use of the control and accept whatever motion of the airplane followed. He would then judge the effectiveness of the control by the way it had to be used to obtain a desired result.

As the outcome of these considerations, the problem of investigating turn maneuvers presented itself in a way inverse to the previous problems. Here the motion of the airplane was given and the requisite use of the controls was sought. Previously the airplane motions had been determined from the controlling accelerations by integration, whereas here the accelerations incident to a given motion were to be determined; thus the process would simply be a differentiation.

Periodic or trigonometric functions of the time naturally suggested themselves for the representation of the angular velocities and displacements during a turn maneuver. By the use of trigonometric functions of the time, any conceivable maneuver of the airplane that begins and ends in level flight may be specified; that is, any given manner of varying the attitude or

angular velocity of the airplane during a given interval may be described by a formula such as

$$p, \text{ or } \varphi, \text{ or } \ldots \text{ etc.}$$
$$=A_1 \sin nt+A_2 \sin 2nt+A_3 \sin 3nt+\text{etc.} \quad (16)$$

By a suitable choice of n the maneuver may be made to extend over as long or as short a time as desired.

In the present case it was intended that the airplane roll up to a moderate angle of bank, starting with the wings level, and check its rate of rolling so as to maintain this bank angle steadily, then roll back to the level condition after a definite time interval. Throughout this interval the airplane was to be yawing appropriately while banking and in the correct amount to prevent sideslipping during every part of the maneuver. Thus the turn was to be "perfect" in that no sideslip was permitted and the coordination of the lateral controls (ailerons and rudder) necessary to accomplish such a maneuver was to be studied.

A few trials in plotting cosine curves against time showed that the expression

$$\varphi=-A_1 \cos nt-\tfrac{1}{4} A_1 \cos 2nt+\text{constant} \quad (17)$$

would represent a bank that assumed a steady angle at the midpoint of the maneuver, starting with zero at the time $t=0$ and becoming zero again at $t=\pi/n$. Arranging for the bank to become steady at the midpoint of the maneuver and choosing nt so as not to coincide with the natural period of the free motions of the airplane obviated the possibility of any reinforced oscillation phenomena during the maneuver. The form of the curve of bank angle against time plotted to this formula is shown in figure 17.

In order to attain the specified bank at every instant, a definite rate of rolling is required at all times, which is obviously found by differentiating the bank equation; thus

$$p=\frac{d\varphi}{dt}=nA_1 \sin nt+\frac{2n}{4}A_1 \sin 2nt \quad (18)$$

In order for the airplane to turn without sideslipping, there must be a coordination between the banking and yawing at all times. The outward and inward accelerations must cancel, that is:

$$rU_0=g \sin \varphi \quad (19)$$

(See equation (12).)

This equation enables the calculation of r from φ, assuming the condition that

$$r=\frac{g}{U_0} \sin \varphi \quad (20)$$

is satisfied. The curve of yawing angular velocity plotted against time is thus very similar in shape to the bank-angle curve, reaching a steady value at its midpoint.

The specification of the angular velocities and angles of the airplane in the foregoing manner is analogous to the specification of constraints of the motion. The total accelerations necessary to constrain the airplane to the specified motions are calculated by differentiating the expressions for the angular velocities, p and r. (See equations (17) and (18).)

$$\frac{dp}{dt}=\frac{d^2\varphi}{dt^2}=n^2A_1 \cos nt+\frac{4n^2}{4}A_1 \cos 2nt \quad (21)$$

and

$$\frac{dr}{dt}=\frac{g}{U_0}p \cos \varphi \quad (22)$$

These accelerations are not furnished altogether by the controls but have components due to the air reactions on the moving airplane. The air reactions are calculated from the resistance derivatives and, when deducted from the total accelerations, give the components necessarily supplied by the deflected controls. Thus the acceleration supplied by the rolling control will be

$$\delta L_\delta=\frac{dp}{dt}-pL_p-rL_r \quad (23)$$

If the application of rolling control is accompanied by a secondary (adverse or favorable) yawing moment, the rudder control will have to accommodate this moment as well as the residual acceleration of the yawing motion. This secondary yawing moment may be considered to be a function of the rolling moment and its acceleration written as $f(\delta L_\delta)$; then

$$\delta N_\delta=\frac{dr}{dt}-pN_p-rN_r-f(\delta L_\delta) \quad (24)$$

Equation (24) gives the amount of rudder coordination necessary with a given aileron-control device. The rolling- and yawing-moment coefficients corresponding to these accelerations may be calculated by known means from the speed of flight and the airplane dimensions.

In the derivation of the equations for the turn maneuvers no account was taken of the pitching motion involved. Obviously if a banked airplane is turning without loss of altitude there will be a component of pitching involved in the motion. As was explained in the description of the step-by-step method of computation the pitching motion may be considered separately and independently of the lateral motions since the airplane is symmetrical about the plane in which pitching occurs. Presumably, the only ways in which pitching motions can influence the lateral motions are by a change of speed or attitude introducing changes in the lateral-stability derivatives or by gyroscopic couples. In the case of a prescribed turn maneuver the maximum gyroscopic couple may be estimated in advance and the relative importance of its effect may be foreseen. The other secondary influence may be partly accounted for

by assuming a certain increased speed throughout the turn. Either the air speed or the attitude will, in general, vary continuously throughout the turn if no altitude is lost or gained. For turns up to 30° angle of bank the change in stability derivatives thus produced will be slight and may be satisfactorily compensated by assuming an average value of the speed U somewhat greater than that for level flight. This speed may be calculated from the relation:

$$q = \frac{q_0}{\cos \varphi} \tag{25}$$

where q_0 is the dynamic pressure at steady-flight speed and φ is the angle of bank at which the airplane is assumed to lose or gain no altitude.

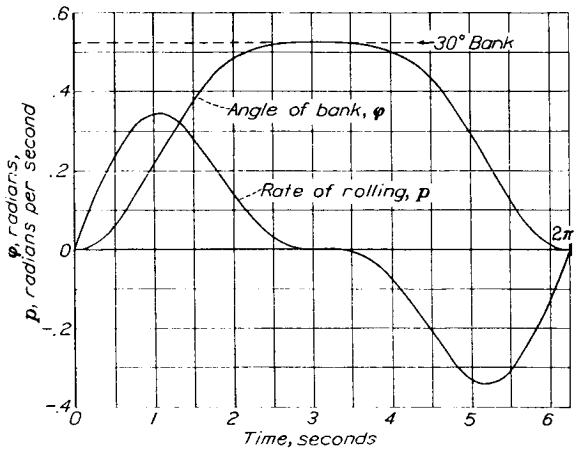

FIGURE 17.—Angle of bank and rate of rolling during specified turn maneuver. $\varphi = -0.262[\cos t + \frac{1}{4} \cos 2t] + 0.327$; $p = d\varphi/dt$.

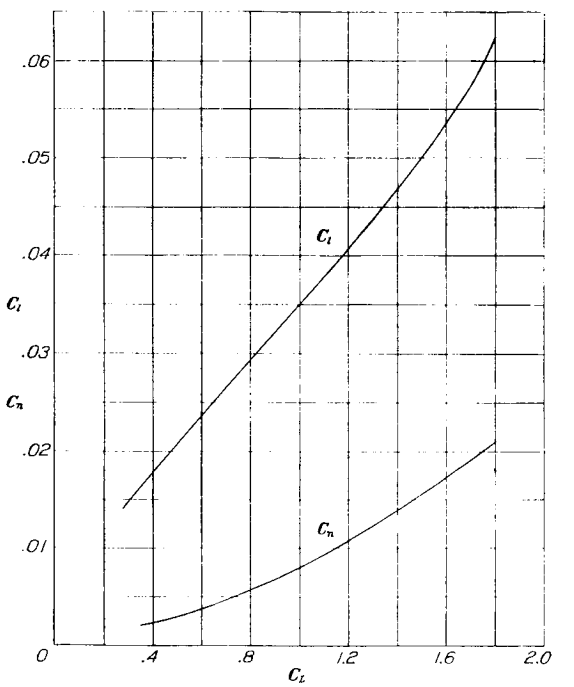

FIGURE 19.—Maximum control-moment coefficients required in performing a turn maneuver at various lift coefficients; average airplane (for 30° bank turn completed in 6.28 seconds).

RESULTS AND DISCUSSION

The foregoing procedure was applied to the case of the average airplane performing 30° banked turns at various speeds. The time taken to complete the specified maneuver was chosen as approximately 6.28 (2π) seconds, since at the lowest speeds under consideration comparatively large rolling and yawing moments were required to execute the maneuver with this rapidity. Inasmuch as the angle-of-bank relation was held the same for all speeds, the rate of yawing was necessarily different and hence the actual angle of turn, or the changed heading of the airplane, was different for the different speeds. As in the previous computations, lift coefficients of 0.35, 1.0, and 1.8 were assumed, although the corresponding speeds were increased somewhat over those in the previous computations to account for the additional lift while turning, as previously explained. With the assumption of no loss of altitude at 30° bank, the speeds were increased by the factor

$$\sqrt{\frac{1}{0.866}} = 1.074$$

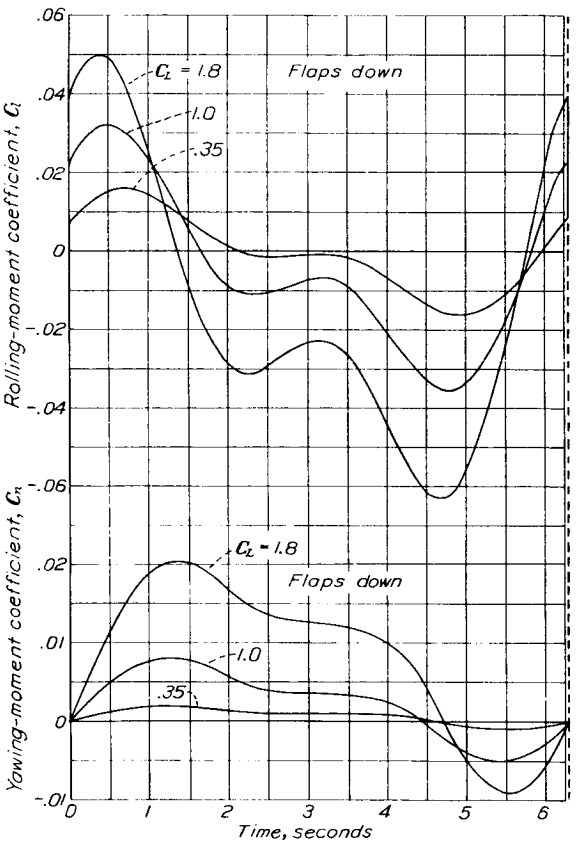

FIGURE 18.—Control rolling- and yawing-moment coefficients necessary to perform 30° bank turn without sideslipping at various lift coefficients.

The values of L_p, L_r, N_p, N_r, corresponding to the given lift coefficients, were also multiplied by this factor. (See appendix I.)

The curves of rolling motion and angle of bank calculated for these maneuvers are those shown in figure 17. The formula for the bank angle was

$$\varphi = -0.262\ (\cos t + 1/4\ \cos 2t) + 0.327 \qquad (26)$$

reaching a maximum of 30° at π seconds. This formula determined the angular velocities and accelerations by the principles already demonstrated. Inasmuch as the turn reaches a steady rate at its midpoint, the whole

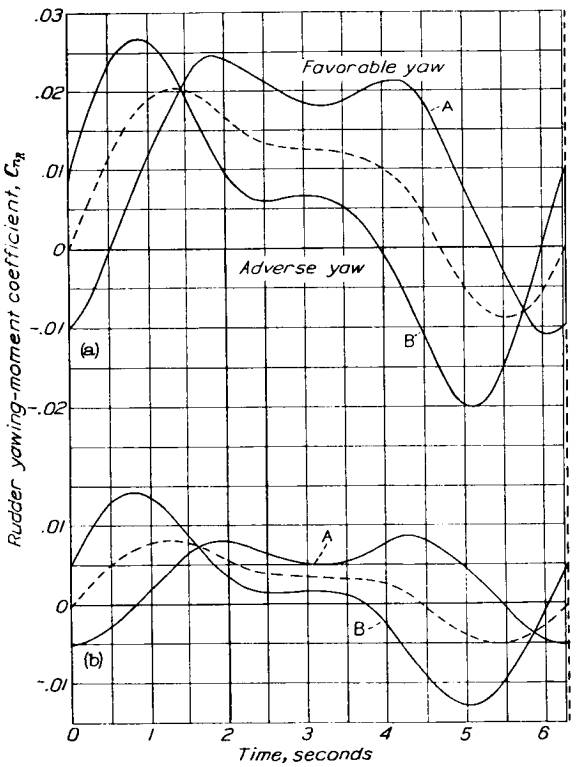

(a) Low speed, flaps down, $C_L = 1.8$.
(b) Gliding speed, $C_L = 1.0$.

FIGURE 20. Rudder control-moment coefficients during 30° bank turn, showing effect of secondary aileron yawing moments on rudder control necessary to perform a turn maneuver without sideslipping. Assumed aileron yawing moment, $\pm 1/4$ aileron yawing moment. C_{n_A} is secondary aileron yawing-moment coefficient.
$C_{n_A} = 1/4 C_{l_A}$ curve A $\qquad C_{n_A} = -1/4 C_{l_A}$ curve B

maneuver may be presumed to be of any time extent by assuming a continuation of this steady point, which occurs at π seconds.

The results of a series of these computations showed principally the effect of flight speed on the degree of control deflection necessary to perform a given maneuver and the effect of favorable-yaw and of adverse-yaw ailerons on the amount of rudder control required. Figure 18 shows the rolling- and yawing-moment coefficients necessary to accomplish the maneuver at speeds corresponding to the three different lift coefficients. For the average airplane these were:

C_L	U
0.35	161 feet per second.
1.0	95 feet per second
1.8	71 feet per second (flaps deflected).

In this case no secondary aileron yawing moments were included and such moment coefficients would have to be added to or deducted from the yawing-moment curves. These computations showed that the maximum yawing moment necessary at the lowest speed was 10 times as great as that at high speed, while the maximum rolling-moment coefficient increased only 4 times under the same circumstances. Figure 19 illustrates this increase of coefficient necessary to perform the specified maneuver in the same time at the lower speeds.

Figure 20 shows the effects of favorable and adverse secondary aileron yawing moments on the rudder control necessary throughout the turn. Positive yawing moments indicate a setting of the rudder in a direction to aid the turning. It will be noted that the existence of any secondary aileron moment calls for a counteracting movement of the rudder applied simultaneously with the ailerons at the beginning of the turn. With no secondary aileron moments the curves show that the simultaneous initial deflection of both ailerons and rudder is not required, the turn being initiated by the ailerons alone with the rudder being applied after the start. In the case of favorable secondary yawing moments an initial setting of the rudder opposite to the direction of the turn is required, while on beginning the recovery the rudder has to be moved slightly in a direction that would normally tend to continue the turning. It appears that ailerons giving no secondary yawing moments of either sign would require the least rudder coordination in making turns without sideslipping.

CONCLUSIONS

1. The agreement of the computations with the results of flight tests verifies the usefulness of the method utilizing stability derivatives for the study of controllability both above and below the stall.

2. The angle of bank produced in 1 second, φ_1, by a full deflection of the lateral control may be taken as a relative measure of the control effectiveness. In the case of a conventional airplane this measure is given by a simple formula involving the static rolling and yawing moments produced by the control, namely:

$$\varphi_1 = \text{constant} \times C_l + \text{constant} \times C_n$$

3. The effect of secondary adverse yawing moments on the aileron control may be moderated by increasing the moment of inertia about the yaw axis, although it is to be expected that the power of the rudder will be correspondingly reduced. Increasing the moment of inertia about the roll axis should have little direct

influence on the lateral-control effectiveness with a given rolling-control moment.

4. The tendency for a given adverse yawing moment to render the lateral control ineffective becomes greater with increasing dihedral. In no case should the ratio of the control adverse yawing moment to the rolling moment be allowed to exceed (in absolute magnitude) either:

(a) The ratio of yawing to rolling moment acting on the airplane in sideslip; or

(b) The ratio of yawing to rolling moment acting on the airplane in yawing.

5. It appears that ailerons giving nearly zero yawing moment would require the least coordination of the rudder control in executing turn maneuvers without sideslip.

6. The study of conditions above the stall indicates that satisfactory control cannot be expected unless some provision is made to maintain the damping in rolling at these angles.

7. For control at high angles of attack it is important that the damping in both rolling and yawing be maintained above a definite minimum to avoid an uncontrollable form of instability arising from the interaction of these motions. The minimum damping is given by the condition that

$$L_p N_r > L_r N_p$$

This condition appears to be next in importance to direct damping in rolling.

LANGLEY MEMORIAL AERONAUTICAL LABORATORY,
NATIONAL ADVISORY COMMITTEE FOR AERONAUTICS,
LANGLEY FIELD, VA., *April 20, 1936.*

TABLE I.—STEP-BY-STEP COMPUTATION OF MOTION OF AVERAGE AIRPLANE

[C_L=1.0; C_l=0.04; C_n=0]

Time	$\left(\frac{dp}{dt}\right)_n$ $\delta L_\delta + \Sigma L_i$ (δL_δ=1.68)	p_n $\left(\frac{dp}{dt}\right)_{n-1} \times \Delta t + p_{n-1}$	φ_n $p_{n-1} \times \Delta t + \varphi_{n-1}$	$\left(\frac{v'}{U_0}\right)_n$ $\frac{32.2}{88.5} \times \Delta t \times \sin \varphi_{n-1} + \left(\frac{v'}{U_0}\right)_{n-1}$	$\left(\frac{dr}{dt}\right)_n$ $\delta_{n-1} + \Sigma N_i$ $\delta N_\delta = 0$	r_n $\left(\frac{dr}{dt}\right)_{n-1} \times \Delta t + r_{n-1}$	β_n' $-r_{n-1} \times \Delta t + \beta_{n-1}$	β_n $\beta_n' + \left(\frac{v'}{U_0}\right)_n$	ΣL_i $p_n L_p + r_n L_r + \beta_n L_\beta$			ΣN_i $p_n N_p + r_n N_r + \beta_n N_\beta$		
									$p_n \times -3.23$	$r_n \times 1.88$	$\beta_n \times -1.11$	$p_n \times -0.301$	$r_n \times -0.663$	$\beta_n \times 2.04$
sec.														
0	1.680	0	0	0	0	0	0	0	0	0	0	0	0	0
.05	1.409	.084	0	0	−.025	0	0	0	−.271	0	0	−.025	0	0
.10	1.181	.154	.004	0	−.045	−.001	0	0	−.497	−.002	0	−.046	.001	0
.20	−.790	.272	.019	0	−.078	−.006	0	0	−.879	−.011	0	−.082	.004	0
.30	.518	.351	.046	.001	−.093	−.014	.001	.002	−1.134	−.026	−.002	−.106	.009	.004
.40	.329	.403	.081	.003	−.096	−.023	.002	.005	−1.302	−.043	−.006	−.121	.015	.010
.50	.199	.436	.121	.006	−.089	−.033	.004	.010	−1.408	−.062	−.011	−.131	.022	.020
.60	.109	.456	.165	.010	−.074	−.042	.007	.017	−1.473	−.079	−.019	−.137	.028	.035
.70	.050	.467	.211	.016	−.054	−.049	.011	.027	−1.508	−.092	−.030	−.141	.032	.055
.80	.009	.472	.257	.024	−.024	−.054	.016	.040	−1.525	−.102	−.044	−.142	.036	.082
.90	−.013	.473	.304	.033	.005	−.056	.021	.054	−1.528	−.105	−.060	−.142	.037	.110
1.00	−.027	.472	.351	.044	.039	−.055	.027	.071	−1.525	−.103	−.079	−.142	.036	.145

APPENDIX I

CALCULATION OF STABILITY DERIVATIVES [1]

In the report all moments and angular velocities are measured from axes fixed in the airplane along the directions perpendicular and parallel to the relative wind in the steady flight just previous to the maneuver computed.

In the computations of the stability derivatives as well as in the consideration of their modification by alteration of the design of an airplane, it is convenient to separate those governed by the wing characteristics from those depending mainly on the body and the tail.

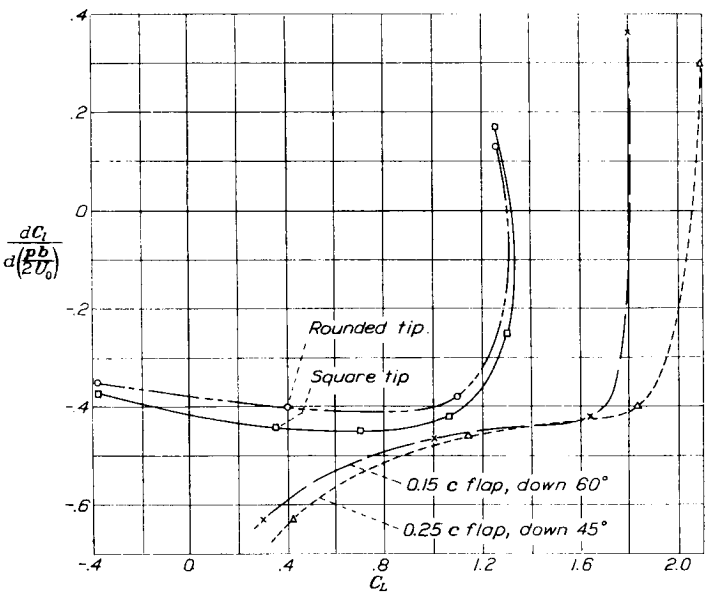

FIGURE 21.—Damping in rolling of rectangular wing. Aspect ratio, 6; 7- by 10-foot wind-tunnel measurements.

In the case of conventional airplanes, the derivatives that depend almost wholly on the wings are

$$L_p,\ L_r,\ L_\beta, \text{ and } N_p$$

The other two factors considered in the report, N_r and N_β, depend primarily on the disposition and area of the vertical tail and on the fuselage.

ROLLING ACCELERATION DUE TO ROLLING, L_p

The factor L_p may be determined from the results of tests of the damping in rolling of wings, such as the tests that have been made in the 7- by 10-foot wind tunnel. The test results are given in the form of the coefficient $\frac{dC_l}{d\left(\frac{pb}{2U_0}\right)}$ and are summarized in figure 21, which shows values of the coefficient measured on rectangular Clark Y wings of aspect ratio 6. The effects of deflected split flaps and tip rounding are also shown. Correction factors to convert these values to those for tapered wings and wings of different aspect ratio are given in figure 22. These correction factors are based on theoretical calculations of the load distribution on wings having a uniform twist which, in effect, reproduced the conditions encountered by a rolling wing as far as the rolling moment is concerned. The data for these corrections were deduced from calculations given in reference 11.

The actual damping moment of a full-size wing calculated from the coefficient is

$$L=p\times\frac{dC_l}{d\left(\frac{pb}{2U_0}\right)}S\frac{\rho}{2}U_0\frac{b^2}{2} \qquad (27)$$

The derivative, as used in the report, is obtained by dividing the coefficient of p by the moment of inertia of the airplane in rolling: i. e.,

$$L_p=\frac{dC_l}{d\left(\frac{pb}{2U_0}\right)}S\frac{\rho}{2}U_0\frac{b^2}{2mk_X^2} \qquad (28)$$

It will be readily appreciated that parts of the airplane other than the wings contribute only a negligible amount of this damping; for example, if the tail plane has an area 15 percent of that of the wing and a span of 25 percent b, its contribution will be less than

$$0.15\times(0.25)^2=0.019, \text{ or 2 percent}$$

of that due to the wing.

The rolling moment due to rolling of a biplane may be estimated by using its equivalent monoplane aspect ratio in figure 22.

For the damping of rolling above stalling angles, wind-tunnel tests show that there is no consistent linear relation between the damping moment and the rate of rolling even at very slow rates; hence there actually exists no definite L_p in the sense previously defined. Arbitrary values may be assumed to repre-

[1] The authors desire to acknowledge valuable aid received from Mr. C. H. Zimmerman of the laboratory staff in the preparation of this section.

sent roughly certain conditions, as was done in the described stalled-flight computations. In the case of wings with devices to prevent stalling at the tips, recourse must be had to wind-tunnel tests.

ROLLING ACCELERATION DUE TO YAWING, L_r

The rolling moment developed by a wing in circling flight may be easily calculated from the consideration that this motion brings about a difference in velocity along the span. If the yawing velocity is r and the spanwise distance from the reference origin (center of gravity) is y, this additional velocity will be ry. The lift on an element of the wing is proportional to the square of the whole velocity, or:

$$(U_0 \pm ry)^2 = U_0^2 \pm 2ryU_0 + (ry)^2 \tag{29}$$

The rolling moment produced by the change in lift on either side of the wing is directly proportional to r. A

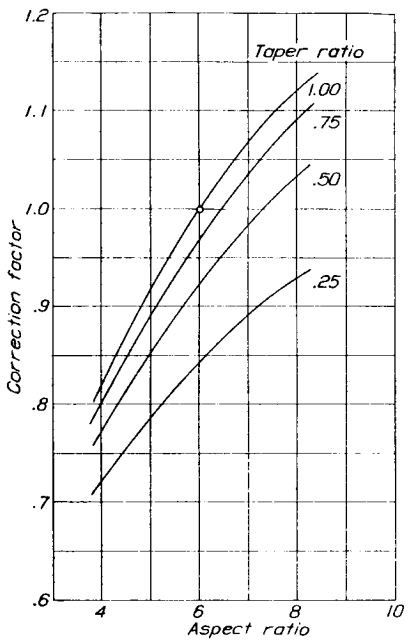

FIGURE 22.—Factors for correcting wind-tunnel values of $dC_l/d\left(\frac{pb}{2U_0}\right)$ for aspect ratio and taper.

simple integration shows the moment for a straight wing to be:

$$L = r\frac{b^2}{6}S\frac{\rho}{2}U_0C_L \tag{30}$$

if the lift is distributed uniformly along the span. Such a distribution is approximated in the case of a rectangular wing at stalling angles, hence the foregoing formula was used in the stalled-flight computations. Below the stall the actual distribution of lift on the wings in circling flight should be taken into account. This distribution is modified somewhat by the fact that the induction of the circular trail of vortices differs from the induction in straight flight. These phenomena have been treated by Glauert and Wieselsberger for the cases of rectangular and elliptical wings in circling flight and curves derived from their calculations are shown in figure 23. (See reference 12.) The derivative L_r is obtained from the coefficient by the formula

$$L_r = F_1C_LS\frac{\rho}{2}U_0\frac{b^2}{2mk_x^2} \tag{31}$$

It appears that the value of $\frac{1}{2}F_1$ previously calculated from simple integration as one-sixth should be more nearly one-eighth for aspect ratio 6, as indicated by the chart. Although no calculations have been made for tapered wings, it may be presumed that the interpolated curves given in figure 23 will apply with good approximation. The part of L_r due to the body and tail will be treated in a later paragraph.

ROLLING ACCELERATION DUE TO SIDESLIP, L_β

Measurements of the rolling moment due to sideslip have been made on a large number of wing models in the 7- by 10-foot wind tunnel. The results of these

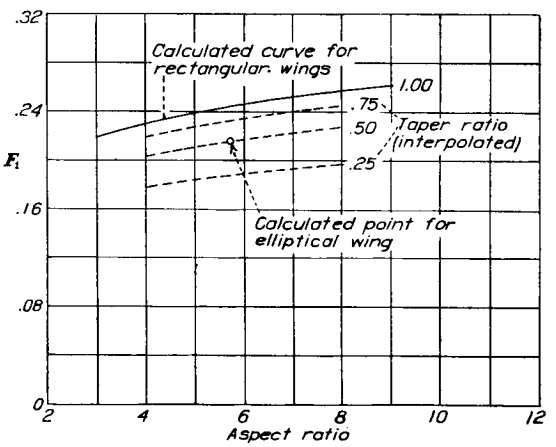

FIGURE 23.—Factors for calculating rolling moment in circling flight.

$$dC_l/d\left(\frac{rb}{2U_0}\right) = F_1C_L$$

tests are summarized in figure 24, which shows the influence of tip rounding and deflected split flaps on the dihedral effect of Clark Y wings without actual dihedral angle. Further tests made on wings with varying degrees of dihedral showed that the additional effect due to this angle was the same regardless of the tip shape or the lift coefficient of the wing (below the stall). Sweepback of the wings is known to have an effect similar to dihedral, although comparatively few tests have been made. Unlike the rolling moment due to dihedral angle, however, the rolling effect of sweepback appears to be approximately proportional to the lift coefficient, disappearing at zero lift as would be expected. Presumably, its effect may be added to the others as in the case of the dihedral. These considerations result in the following formula for the total rolling moment in sideslip

$$\frac{dC_l}{d\beta}=\left(\frac{dC_l}{d\beta}\right)_{\Gamma,\Lambda=0}+\Gamma\frac{\partial}{\partial\Gamma}\left(\frac{dC_l}{d\beta}\right)+\Lambda\frac{\partial}{\partial\Lambda}\left(\frac{dC_l}{d\beta}\right) \quad (32)$$

where Γ is dihedral angle and Λ is angle of sweepback.

An analysis of the available data indicates the following values for the parameters:

$$\left.\begin{aligned}\frac{\partial\left(\frac{dC_l}{d\beta}\right)}{\partial\Gamma}&=-0.012\\ \text{(see reference 13), and}\\ \frac{\partial\left(\frac{dC_l}{d\beta}\right)}{\partial\Lambda}&=-0.0045C_L\end{aligned}\right\} \quad (33)$$

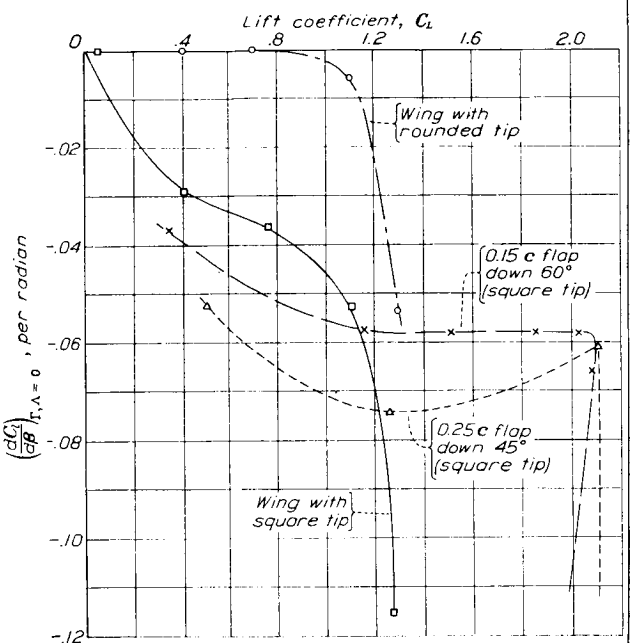

FIGURE 24.—Rolling moment due to sideslip. Untapered wings without dihedral; aspect ratio, 6; 7- by 10-foot wind-tunnel measurements.

where $dC_l/d\beta$ is in terms of radians and Γ and Λ are measured in degrees. The derivative L_β follows from the formula:

$$L_\beta=\frac{dC_l}{d\beta}Sq\frac{b}{mk_x^2} \quad (34)$$

Inasmuch as the wind-tunnel tests were of rectangular wings of aspect ratio 6, the formula (33) applies directly to them. Correction factors for calculating the rolling moment due to the dihedral of yawed wings of different aspect ratios and taper ratios are given in figure 25. These corrections were deduced from theoretical calculations made at the Laboratory (reference 11) on the span load distribution of wings having their right and left semispan portions set at different angles of attack and are somewhat different from those deduced previously for the damping in rolling.

Above stalling angles none of the given formulas or correction factors apply. In this region a straight wing shows a far greater rolling tendency when yawed than wings with either sweepback or dihedral. Adding either sweepback or dihedral tends to reduce this tendency and may on this account be desirable to a certain degree. Tests of wings with very large sweepback, such as are used on tailless airplanes, have been made in which the rolling moment due to yaw actually reversed its sign when the stall was reached.

YAWING ACCELERATION DUE TO ROLLING, N_p

It is assumed that the effect of a rolling motion of the wing can be replaced by a relative rolling motion

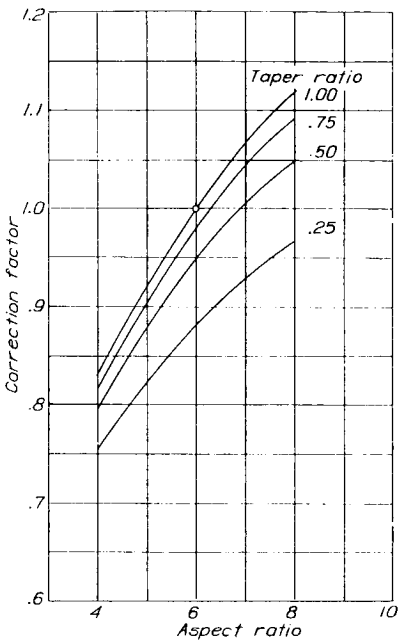

FIGURE 25.—Factors for correcting wind-tunnel value of $\partial\left(\frac{dC_l}{d\beta}\right)/\partial\Gamma$ for aspect ratio and taper.

of the air about the X axis of the airplane. Thus in positive rolling the relative air stream is rising toward the right wing tip and descending on the left. The lift vectors, being perpendicular to the relative wind at each point of the span, are inclined forward with respect to the Z axis on the right and backward on the left, resulting in a negative yawing moment for positive rolling of the wing. (This varying resolution of the lift vectors along the span is unimportant in computing the rolling moment due to rolling since the angle $pb/2U_0$ is small.)

In addition to the changed resolution of the lift vectors along the span, there is an increased drag on the downgoing wing that tends to reduce the negative yawing tendency. It should be noted that an asymmetrical change in the lift distribution, such as that caused by rolling, results in greater changes in the induced drag at various sections of the wing than would be produced by symmetrical lift changes. (See

reference 14.) Hence the uncorrected results of measurements made on the wing in direct lifting cannot be used in computing the rolling or yawing moments of a rolling wing.

Figure 26 shows the resolution of the lift at a point of the span y on the downgoing side of the wing. The air stream initially rising toward the section at the inclination py/U_0 is deflected somewhat by the resulting increased lift at that point so that the air meets the wing at the additional effective angle of attack, $\Delta\alpha_0=\frac{py}{U_0}-\Delta\frac{w}{U_0}$. This additional angle of attack may be found at each point of the span if the corresponding lift increment is known, since

$$\Delta\alpha_0=\frac{\Delta C_L}{\left(\frac{dC_L}{d\alpha}\right)_0} \tag{35}$$

where $\left(\frac{dC_L}{d\alpha}\right)_0$ is the slope of the lift curve for infinite aspect ratio. The lift vector on the wing in straight flight C_L is increased by the amount ΔC_L and inclined forward through the angle $\Delta\alpha_0$. If the usual assumptions regarding small angles are made, the total effect may be integrated along the span as

$$N=-2\frac{\rho}{2}U_0^2\int_0^{b/2}C_L\times\Delta\alpha_0\times c\times y\times dy \tag{36}$$

It will be noted that it is unnecessary to consider the resolution of the lift increments ΔC_L by the angles $\Delta\alpha_0$ since they are sensibly equal and opposite on either side of the wing and their yawing effects cancel, resulting simply in a bending moment about the midpoint. Replacing $\Delta\alpha_0$ by $\frac{\Delta C_L}{\left(\frac{dC_L}{d\alpha}\right)_0}$ and calculating the coefficient

$$C_n=-\frac{2}{Sb\left(\frac{dC_L}{d\alpha}\right)_0}\int_0^{b/2}C_L\times\Delta C_L\times c\times y\times dy \tag{37}$$

Since $\frac{2}{Sb}\times\Delta C_L\times c\times y\times dy=dC_l$, an approximate expression of this formula is

whence
$$\left.\begin{aligned}C_n&=\frac{C_L}{\left(\frac{dC_L}{d\alpha}\right)_0}C_l\\ \frac{dC_n}{d\left(\frac{pb}{2U_0}\right)}&=\frac{C_L}{\left(\frac{dC_L}{d\alpha}\right)_0}\frac{dC_l}{d\left(\frac{pb}{2U_0}\right)}\end{aligned}\right\} \tag{38}$$

This approximation is based on the assumption of constant lift coefficient across the span and hence corresponds to an elliptical wing. The resolution of this yawing moment along the general wind direction results in:

$$\frac{dC_n}{d\left(\frac{pb}{2U_0}\right)}=\frac{dC_l}{d\left(\frac{pb}{2U_0}\right)}\left[\frac{C_L}{\left(\frac{dC_L}{d\alpha}\right)_0}-\frac{C_L}{\pi R}\right] \tag{39}$$

Reference 11 gives the lift and lift-increment distributions for both rectangular and tapered wings and these may be used in conjunction with the foregoing formulas if a more accurate theoretical value of N_p is desired.

A component of N_p due to the profile-drag effect may be estimated by a simple integration, assuming the slope of profile-drag coefficient with effective angle of attack to be constant across the span. Thus, if $\left(\frac{dC_D}{d\alpha}\right)_0$ is the slope of the drag curve for infinite aspect ratio at the lift coefficient in question

$$\Delta N=2\frac{\rho}{2}U_0^2\int_0^{b/2}\Delta\alpha_0\left(\frac{dC_D}{d\alpha}\right)_0 cydy \tag{40}$$

or, making the same substitutions as before, the coefficient giving the effect of profile drag is

$$\frac{dC_n}{d\left(\frac{pb}{2U_0}\right)}=-\frac{dC_{D_0}}{dC_L}\frac{dC_l}{d\left(\frac{pb}{2U_0}\right)} \tag{41}$$

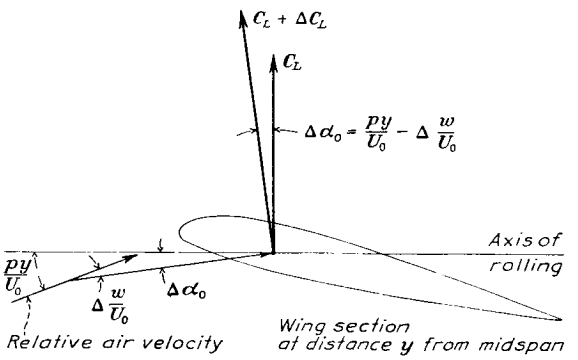

FIGURE 26.—Resolution of air velocity and lift at section of rolling wing

where C_{D_0} is the profile-drag coefficient of the airfoil section. The final formula for N_p is

$$N_p=\frac{dC_n}{d\left(\frac{pb}{2U_0}\right)}S\frac{\rho}{2}U_0\frac{b^2}{2mk_Z^2} \tag{42}$$

where $\frac{dC_n}{d\left(\frac{pb}{2U_0}\right)}$ is the sum of the portions given by equations (39) and (41).

Above stalling angles the slope of the profile-drag coefficient with angle of attack reaches large values, and it is to be expected that N_p will change its sign. The foregoing theoretical formulas cannot be used at these angles, because the lift is no longer proportional to the angle of attack. A tentative formula for $\frac{dC_n}{d\left(\frac{pb}{2U_0}\right)}$ in the stalled condition is

$$\frac{dC_n}{d\left(\frac{pb}{2U_0}\right)}=\left[\left(\frac{dC_D}{d\alpha}\right)_0-C_L\right]\frac{4}{Sb^2}\int_0^{b/2}cy^2dy \tag{43}$$

or simply

$$\frac{dC_n}{d\left(\frac{pb}{2U_0}\right)}=\frac{1}{6}\left[\left(\frac{dC_D}{d\alpha}\right)_0-C_L\right] \tag{44}$$

for rectangular wings.

In the case of an airplane with a long fuselage, a certain increment of N_p at high angles of attack due to the effect of the body and fin must be considered, as will be explained later.

YAWING ACCELERATION DUE TO YAWING, N_r

Unlike the damping in rolling, the damping in yawing N_r, cannot be attributed to any single predominant factor. It is convenient, however, to consider it as primarily effected by the disposition and area of the vertical tail surface. Since only a few isolated experiments have been made for the determination of this derivative and since it is not known

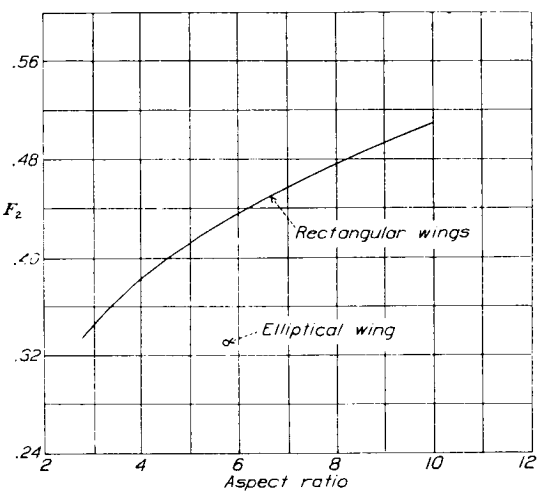

FIGURE 27.—Factors for calculating the yawing moment due to the induced-drag distribution in circling flight.

$$dC_{n_i}/d\left(\frac{rb}{2U_0}\right)=-F_2C_{D_i}$$

to what extent certain incalculable factors influence it, only a rough estimate of its value in any given case is possible.

The part of the damping of yawing due to the wings may be calculated from considerations similar to those employed in the determination of L_r. Here the changed drag distribution along the span in circling flight is to be considered and the resulting yawing moment found. The theoretical calculations of Glauert and Wieselsberger that were employed in the determination of L_r may be applied in this case as well. Here, however, it will be necessary to include the effect of profile drag of the wings and their attachments, since it is the actual magnitude of the drag that counts in determining N_r and not its rate of increase with angle of attack. On the assumption that the profile-drag coefficient is normally the same at all sections of the span, a simple integration (see L_r) gives the formula

$$\frac{dC_{n_0}}{d\left(\frac{rb}{2U_0}\right)}=-\frac{1}{3}C_{D_0} \tag{45}$$

for the part due to the profile drag of a rectangular wing. Figure 27 shows the results of the previously mentioned calculations, which were extended to the determination of the distribution of induced drag while circling. With the factor shown in the figure included, the formula for the total wing effect becomes

$$\frac{dC_n}{d\left(\frac{rb}{2U_0}\right)_w}=-F_2C_{D_i}-\frac{1}{3}C_{D_0} \tag{46}$$

where C_{D_i} is the induced-drag coefficient, i. e.,

$$C_{D_i}=\frac{C_L^2}{\pi R} \tag{47}$$

The part of N_r due to the vertical tail surfaces may be very simply calculated. The yawing angular velocity r about an axis through the center of gravity produces an effective sidewise velocity of the vertical tail equal to rl. Its change in angle of attack relative to the air stream is then rl/U_0. The yawing moment due to this effect is

$$N=\frac{rl}{U_0}\left(\frac{dC_y}{d\beta}\right)_f\frac{S_f}{S}S\frac{\rho}{2}U_0^2l \tag{48}$$

where $(dC_y/d\beta)_f$ is the slope of the normal-force coefficient of the fin against the sidewise angle of attack β and S_f is the area of the fin. An average value for $dC_y/d\beta$ is -2.2. Combining these factors and writing the expression in a form involving the span as the fundamental length results in

$$\frac{dC_n}{d\left(\frac{rb}{2U_0}\right)_f}=\frac{dC_y}{d\beta}\left(\frac{l}{b}\right)^2\frac{S_f}{S}\times 2 \tag{49}$$

Expressing the various factors thus calculated in the form of a single dimensionless coefficient, the formula for the total damping derivative in yawing becomes

$$N_r=\frac{dC_n}{d\left(\frac{rb}{2U_0}\right)}S\frac{\rho}{2}U_0\frac{b^2}{2mk_z^2} \tag{50}$$

in which $\dfrac{dC_n}{d\left(\frac{rb}{2U_0}\right)}$ may be determined from an aerodynamic test of a complete model or may be estimated from the sum of several contributing factors.

It is not known how the body of the airplane influences its damping in yawing, although it is unlikely that its effect is as powerful as that of the vertical fin. In the case of the average airplane treated in this

report, an allowance equal to 60 percent of the fin effect was made for the fuselage and parts of the airplane other than the wings.

YAWING ACCELERATION DUE TO SIDESLIP, N_β

Measurements of the yawing moments in sideslip have been made on a large number of complete models in the course of routine wind-tunnel testing of military airplanes. A study of the results of these tests indicated that at low angles of attack the yawing moment may be estimated from the area and disposition of the vertical fin with a suitable allowance for the fuselage effect. Although airplane bodies when tested alone almost invariably show an unstable yawing tendency about the center of gravity, when tests of a complete model are made the results may show an additional stabilizing influence of the fuselage, possibly due to interference effects. At high lift coefficients the wings may exert considerable influence. The effect of the fuselage depends, of course, on its disposition with respect to the center of gravity and also on the nose shape. Models, especially those with uncowled radial engines, often show only 40 or 50 percent of the righting moment calculated for the fin and rudder alone.

The part of the yawing moment in yaw due to the vertical fin surface may be estimated by means of the data previously used for the calculation of N_r,

$$N_{\beta_f} = -\left(\frac{dC_y}{d\beta}\right)_f \frac{l}{b}\frac{S_f}{S} Sq \frac{b}{mk_z^2} \tag{51}$$

In cases of airplanes having wings set at a dihedral angle some provision must be made for an additional yawing moment in yaw that arises as a consequence of the setting of the wings. In straight flight, lift vectors drawn on each wing half, being inclined inward by the angle of dihedral, would intersect on the Z axis vertically above the center of gravity. These lift vectors remaining at the same time perpendicular to the leading-edge lines and to the relative wind direction do not intersect when the wing is yawed, giving rise to a couple. A simple approximation results in

$$C_n = -\frac{1}{5}\Gamma\beta C_L \tag{52}$$

Since this component of yawing moment is attributed to dihedral setting, it may be represented by

$$\frac{\partial}{\partial\Gamma}\frac{dC_n}{d\beta} = -\frac{1}{5}C_L \tag{53}$$

for calculation.

In addition to the simple dihedral effect, an induced yawing moment on the yawed wing must be considered as a secondary effect of the rolling moment. An approximate formula for this yawing moment derived from data given in reference 13 is

$$\left.\begin{aligned} C_n &= -\frac{1}{4}C_L C_l \\ \text{or} \qquad \frac{dC_n/d\beta}{dC_l/d\beta} &= -\frac{1}{4}C_L \end{aligned}\right\} \tag{54}$$

These formulas agree with the results of tests made in the 7- by 10-foot wind tunnel except near the region of zero lift. A formula for the total yawing-moment coefficient of the wings is

$$\left(\frac{dC_n}{d\beta}\right)_w = -C_L\left(0.0035\Gamma + \frac{1}{4}\frac{dC_l}{d\beta}\right) \tag{55}$$

where Γ is given in degrees.

CERTAIN CORRECTING TERMS AT HIGH ANGLES OF ATTACK

At high angles of attack the body of the airplane will be inclined appreciably to the reference axis about which the rolling moments are measured. The formulas given for the effects of the fin (and body) on the damping in yawing and yawing moment in yaw should for exactness have included the factor cos α, since the lever arm of the moment-producing effects will actually be shortened somewhat by the inclination. This correction is of no importance, however, and need not be considered. The same is true of the logical correction that should be applied to the wind-tunnel measurements of rolling moment in yaw, which were actually made about an axis pointing directly upstream and hence not quite in line with the axes considered in the report. The only correcting terms that are of sufficient magnitude to be considered here are those affecting L_r, L_β, and N_p and arising from the fact that the fin and body surfaces are disposed below the rolling axes. These terms are

$$\left.\begin{aligned} \Delta L_r &= N_r \sin\alpha \times \frac{k_z^2}{k_x^2} \\ \Delta L_\beta &= N_\beta \sin\alpha \times \frac{k_z^2}{k_x^2} \\ \Delta N_p &= N_r \sin\alpha \end{aligned}\right\} \tag{56}$$

Only the components of N_r and N_β attributed to the fuselage and vertical fin of the airplane should be used here.

REFERENCES

1. Weick, Fred E., Soulé, Hartley A., and Gough, Melvin N.: A Flight Investigation of the Lateral Control Characteristics of Short Wide Ailerons and Various Spoilers with Different Amounts of Wing Dihedral. T. R. No. 494, N. A. C. A., 1934.
2. Jones, B. Melvill: Research on the Control of Airplanes. T. M. No. 485, N. A. C. A., 1928.
3. Halliday, A. S., and Burge, C. H.: Lateral Stability Calculations for the Bristol Fighter Aeroplane. R. & M. No. 1306, British A. R. C., 1930.
4. Jones, B. Melvill, and Trevelyan, A.: Step-by-Step Calculations upon the Asymmetric Movements of Stalled Aeroplanes. R. & M. No. 999, British A. R. C., 1925.
5. Stability and Control Panel: The Lateral Control of Stalled Aeroplanes. R. & M. No. 1000, British A. R. C., 1926.
6. Soulé, H. A., and McAvoy, W. H.: Flight Investigation of Lateral Control Devices for Use with Full-Span Flaps. T. R. No. 517, N. A. C. A., 1935.
7. Wind-Tunnel Research Comparing Lateral Control Devices, Particularly at High Angles of Attack.
   I. Ordinary Ailerons on Rectangular Wings, by Fred E. Weick and Carl J. Wenzinger. T. R. No. 419, N. A. C. A., 1932.

II. Slotted Ailerons and Frise Ailerons, by Fred E. Weick and Richard W. Noyes. T. R. No. 422, N. A. C. A., 1932.

III. Ordinary Ailerons Rigged up 10° When Neutral, by Fred E. Weick and Carl J. Wenzinger. T. R. No. 423, N. A. C. A., 1932.

IV. Floating Tip Ailerons on Rectangular Wings, by Fred E. Weick and Thomas A. Harris. T. R. No. 424, N. A. C. A., 1932.

V. Spoilers and Ailerons on Rectangular Wings, by Fred E. Weick and Joseph A. Shortal. T. R. No. 439, N. A. C. A., 1932.

VI. Skewed Ailerons on Rectangular Wings, by Fred E. Weick and Thomas A. Harris, T. R. No. 444, N. A. C. A., 1932.

VII. Handley Page Tip and Full-Span Slots with Ailerons and Spoilers, by Fred E. Weick and Carl J. Wenzinger. T. N. No. 443, N. A. C. A., 1933.

VIII. Straight and Skewed Ailerons on Wings with Rounded Tips, by Fred E. Weick and Joseph A. Shortal. T. N. No. 445, N. A. C. A., 1933.

IX. Tapered Wings with Ordinary Ailerons, by Fred E. Weick and Carl J. Wenzinger. T. N. No. 449, N. A. C. A., 1933.

X. Various Control Devices on a Wing with a Fixed Auxiliary Airfoil, by Fred E. Weick and Richard W. Noyes. T. N. No. 451, N. A. C. A., 1933.

XI. Various Floating Tip Ailerons on Both Rectangular and Tapered Wings, by Fred E. Weick and Thomas A. Harris. T. N. No. 458, N. A. C. A., 1933.

XII. Upper-Surface Ailerons on Wings with Split Flaps, by Fred E. Weick and Carl J. Wenzinger. T. R. No. 499, N. A. C. A., 1934.

XIII. Auxiliary Airfoils Used as External Ailerons, by Fred E. Weick and Richard W. Noyes. T. R. No. 510, N. A. C. A., 1935.

8. Miller, Marvel P., and Soulé, Hartley A.: Moments of Inertia of Several Airplanes. T. N. No. 375, N. A. C. A., 1931.

9. Glauert, H.: A Non-Dimensional Form of the Stability Equations of an Aeroplane. R. & M. No. 1093, British A. R. C., 1927.

10. Aerodynamics Staff of the R. A. E.: The Effect upon the Control of an Aeroplane of Carrying Load Distributed along the Planes. R. & M. No. 849, British A. R. C., 1922.

11. Pearson, H. A.: Theoretical Span Loading and Moments of Tapered Wings Produced by Aileron Deflection. T. N. No. 589, N. A. C. A., 1937.

12. Glauert, H.: Calculation of the Rotary Derivatives Due to Yawing for a Monoplane Wing. R. & M. No. 866, British A. R. C., 1923.

13. Shortal, Joseph A.: Effect of Tip Shape and Dihedral on Lateral-Stability Characteristics. T. R. No. 548, N. A. C. A., 1935.

14. Munk, Max M.: A New Relation between the Induced Yawing Moment and the Rolling Moment of an Airfoil in Straight Motion. T. R. No. 197, N. A. C. A., 1924.

REPORT NO. 579

A STUDY OF THE TWO-CONTROL OPERATION OF AN AIRPLANE

Robert T. Jones

Langley Memorial Aeronautical Laboratory

1936

REPORT No. 579

A STUDY OF THE TWO-CONTROL OPERATION OF AN AIRPLANE

By Robert T. Jones

SUMMARY

The two-control operation of a conventional airplane is treated by means of the theory of disturbed motions. The consequences of this method of control are studied with regard to the stability of the airplane in its unconstrained components of motion and the movements set up during turn maneuvers.

It is found that the motion of a conventional airplane is more stable when an arbitrary kinematic constraint is imposed in banking than when such constraint is imposed in yawing. Several hypothetical assumptions of piloting procedure, each of which is considered to represent a component of the actual procedure, are studied. Different means of two-control operation are also discussed and it is concluded that a reliable rolling-moment control that does not give the usual adverse secondary yawing moment should be most satisfactory. Several special modifications intended to make the airplane more suitable for two-control operation are also discussed, and it is found that relatively great weathercock stability (N_v) would be desirable.

INTRODUCTION

A number of flights have been made with airplanes utilizing both the aileron-elevator and the elevator-rudder combinations for two-control operation. Some question exists as to which of these modes of operation is likely to prove the better and also whether either of them is capable of affording the controllability requisite to safety in flight. Such questions must, of course, be eventually decided by experience, no mathematical analysis being sufficiently broad to deal with all aspects of the problem. It is believed, nevertheless, that certain conceptions gained from an analysis of the problem may be useful in furthering development along these lines.

One of the purposes of the present work was to ascertain on theoretical grounds which of the two possible modes of operation was more likely to prove satisfactory. It was also desired to find what changes might be effected in a conventional airplane to make it more suitable for two-control operation.

The analysis of the various dynamical problems that arise makes use of many concepts that are discussed at length in reference 1. The treatment of airplane motion as a problem of dynamics is based primarily on the assumptions of the theory of airplane stability as developed by Bryan and others; for the elucidation of this theory the reader is referred to text books on aeronautics.

MATHEMATICAL TREATMENT OF CONTROLLED MOTION

The motion of an airplane with adequate control about its three axes may, in one sense, be regarded as a purely constrained motion. From this point of view, the act of piloting the airplane must be considered to be the use of the available control means for overcoming the inherent aerodynamic and inertial reactions of the airplane, causing it to follow a more or less definitely constrained motion induced by the controls. The natural oscillation and damping of the free motion of the airplane do not appear, then, in the controlled motion because the pilot has accommodated his use of the available control to the governing of these inherent tendencies. Accordingly the stability or instability of the airplane will be apparent only in the requisite use of the controls to perform a given maneuver.

It has been found by experience that the lateral-stability characteristics of an ordinary airplane are such that it is feasible to abandon one of the direct constraints of the lateral motion in ordinary flight maneuvers. All lateral maneuvers that are to be performed with a minimum of sideslipping or sidewise acceleration require a definite coordination between the banking and yawing motions; it appears that a conventional airplane will naturally tend to fulfill this requisite relation in greater or less degree, on account of the inherent stability, even when one of the lateral controls is abandoned.

Under the conditions of two-control operation the motion of the airplane cannot be considered as an entirely constrained motion. The pilot of such a machine can exercise direct constraint in only one of the three components of lateral movement and must depend on the natural tendencies of the airplane for the requisite coordination of the other motions. In order to show this coordination the airplane need not be entirely stable with all controls released, but it is imperative that there be satisfactory stability in those components in which the machine is unconstrained. Thus, if an

airplane is to be controlled by the ailerons and elevator alone, it must be satisfactorily stable in combined yawing and sideslipping, in which it is free; if control is by rudder and elevator, corresponding stability in combined banking and sideslipping is necessary.

If the controls are considered to impress constraints in those components of motion in which they operate directly, the movements of a two-control airplane may be studied by the method of forced oscillations. Thus, if the airplane controlled by ailerons is caused to follow a definite course in banking, in which it is considered to be constrained, this motion will impress disturbing forces and couples leading indirectly to yawing and sideslipping motions. The yawing and sideslipping motions must, however, be considered to be unconstrained and to be conditioned by the natural stability of the machine as well as by the impressed disturbances.

The disturbing forces or couples impressed in those components in which the airplane is unconstrained are caused by the constrained movements and are considered proportional to them. The factors of proportionality are simply the appropriate stability derivatives of the airplane. Thus, if the machine is constrained to follow a definite sequence of rolling motions by the application of a suitable control moment, a disturbing acceleration in yawing that is proportional to the given rate of rolling at each instant will be impressed, namely:

$$\text{impressed } \frac{dr}{dt}=p\times N_p$$

In order to express the foregoing ideas definitely it will be necessary to resort to mathematical treatment of the motions. It is convenient for this purpose to choose a set of axes rigidly fixed in the airplane at its center of gravity and inclined at the angle of attack α, so that the X axis points into the direction of the relative wind in steady flight at the specified lift coefficient. The following notation and diagram define the quantities used in the subsequent equations.

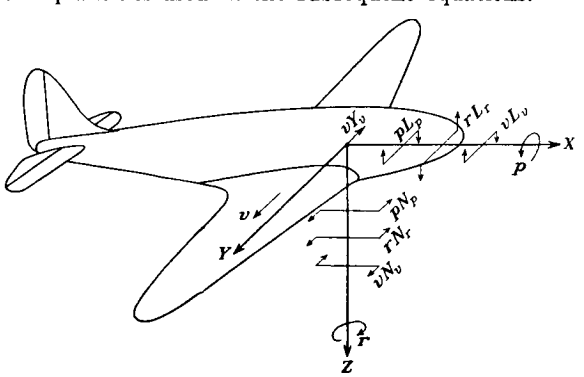

U_0, forward (X-wise) velocity in steady flight.

p, rolling component of angular velocity.

r, yawing component of angular velocity.

v, component of flight velocity along Y axis (sideslip).

φ, angle of bank (relative to gravity).

β, angle of sideslip v/U_0, approximately.

δ, angle of rudder or aileron deflection.

Y, force component along the direction of the Y axis.

L, rolling-moment component.

N, yawing-moment component.

$\delta L_\delta=L/mk_X^2$, $\delta N_\delta=N/mk_Z^2$, Control moments per unit moment of inertia of airplane.

Y_v, L_p, L_r, L_v, N_p, N_r, N_v Stability derivatives in terms of unit mass or moment of inertia of airplane, thus:

$$Y_v=\frac{\partial Y}{\partial v}/m$$

$$L_r=\frac{\partial L}{\partial r}/mk_X^2, \text{ etc.}$$

A number of secondary considerations will be neglected in the mathematical analysis of the problems to make the mathematical expressions as simple as possible and because it is not considered important to secure exact numerical results for studying the general problem. For these approximate calculations the lateral and longitudinal motions of the airplane will be considered separable during turning flight. A check of the maximum gyroscopic couples encountered shows that they are negligible for the present study, although it is probable that the longitudinal and lateral oscillations in turning flight can be separated for only a relatively short time after the passing of a disturbance. Another assumption made is that the effect of a component torque applied to the airplane is an angular acceleration about the axis of the torque. In general, the angular acceleration does not have the same axis as the applied torque but in the present case the reference axes chosen lie near the assumed principal axes of inertia, and the difference of moments of inertia taken about various axes is not great. In addition, the flight of the airplane is assumed to be horizontal and the speed not to vary appreciably from the average (U_0) in a given case.

According to the previously outlined treatment, the movement of the airplane in at least one of the lateral coordinates will be modified by a constraint. The complete set of three degrees of freedom is not in this case expressed in the usual three simultaneous equations of motion, for this procedure would imply that each component of the motion was affected by the other two, whereas the present problem calls for an independent expression of one of them. Thus, it is assumed that the available control is sufficiently powerful to force any desired motion in the controlled component. When setting up the equations, this

motion will be considered to be given as a function of the time.

It is important to emphasize in the interpretation of the mathematical analysis the practical significance of the assumptions used. The solution of the equations requires that the complete history of the variation of one of the components of the motion (or the control setting) be known beforehand. This variation is not subsequently altered to accommodate the variation of the other motions as would be the case if an intelligent pilot were at the controls. It may be imagined that the pilot has only one degree of attention. Having fixed on a procedure of rolling the airplane, he concentrates on the execution of this alone, paying no attention to the consequences in yawing or sideslipping. It would be feasible to assume that the pilot concentrated his attention on carrying out a predetermined manipulation of the controls, without regard to any of the motions set up. This assumption is, however, considered to be too far removed from actuality to be of much use in analyzing the problem. It would be of more practical interest to assume that the pilot had sufficient skill to enforce a desired motion in every respect, taking no account of the control manipulations. The control manipulations required could then be calculated and an idea of the degree of skill necessary to attain a perfect result could be derived therefrom.

With two-control operation a perfect coordination of the motions is, of course, not possible. If the pilot enforces complete control over one component of the airplane's motion, he must do so at the expense of control in some other component. The residual component is then considered to be free. In practice the pilot can exercise an indirect influence on all lateral motions with only a single lateral control. Hence, it is possible to assume that a skilled pilot could enforce complete control over the yawing motion even though his available control exerted only rolling moments directly. Then the rolling motion must be considered free and not subject to the pilot's attention although his available control operates directly on this motion. Such an assumption obviously cannot give an accurate description of anything occurring in practice. The same is true in some degree of any other assumed procedure that can be mathematically treated. The actual procedure of a pilot is undoubtedly an indeterminate and variable synthesis of such elementary procedures. The study of a single assumption of this nature is therefore incomplete, constituting simply a part in the analysis of the problem.

In order to illustrate the variety of assumptions that may be treated, four equations, containing movements both of the airplane and of the control surface, will be set down:

$$\left.\begin{aligned} &\frac{dv}{dt}-g\varphi+rU_0-vY_v &&=0\\ &\frac{dp}{dt}-pL_p-rL_r-vL_v-\delta L_\delta &&=0\\ &\frac{dr}{dt}-pN_p-rN_r-vN_v-\delta N_\delta &&=0\\ &\frac{d\varphi}{dt}-p &&=0 \end{aligned}\right\}(1)$$

These equations are to be satisfied simultaneously and, since there are more variables than equations, one of the variables must be given in terms of the time to effect a solution. Any assumption of the kind considered may be applied by setting one of the variables equal to a function of t. Thus the equations of motion with an arbitrarily prescribed course in rolling are:

$$\left.\begin{aligned} &\frac{dv}{dt}+rU_0-vY_v &&=g\varphi(t)\\ &-rL_r-vL_v-\delta L_\delta &&=L_p p(t)-\frac{d}{dt}p(t)\\ &\frac{dr}{dt}-rN_r-vN_v-\delta N_\delta &&=N_p p(t) \end{aligned}\right\}(2)$$

Similarly, if the pilot uses the control to enforce some given motion in yawing, the equations are:

$$\left.\begin{aligned} &\frac{dv}{dt}-g\varphi-vY_v &&=-U_0 r(t)\\ &\frac{dp}{dt}-pL_p-vL_v-\delta L_\delta &&=L_r r(t)\\ &-pN_p-vN_v-\delta N_\delta &&=N_r r(t)-\frac{d}{dt}r(t)\\ &\frac{d\varphi}{dt}-p &&=0 \end{aligned}\right\}(3)$$

Solutions of the foregoing differential equations have the general form

$$v, p, \delta, \text{ or } r=(C_1e^{\lambda_1 t}+C_2e^{\lambda_2 t}+\ \ldots\ C_ne^{\lambda_n t})+\zeta(t) \quad (4)$$

This type of solution has two significant components; the part enclosed by parentheses represents the occurrence of the natural oscillations and damping in the resultant motion. If the natural modes of motion are stable, this component will disappear with time and the solution will be represented by $\zeta(t)$. If the impressed disturbance is periodic, the motion will at first be conditioned by the natural period but, if this is damped, will later follow the impressed period in accordance with Herschel's theorem. In these cases the term $\zeta(t)$ may be called the "steady-state solution."

Under the assumed conditions of two-control operation the pilot enforces one component of the motion and relies on the reaction of this motion on the uncontrolled component to induce an appropriate

motion there. As seen in equation (4), this accompanying motion is at first conditioned by the natural oscillations. Obviously for satisfactory two-control operation it is desirable that the natural oscillations in the uncontrolled components quickly die away. It also appears that if any reasonable coordination of the motions is to be obtained the period of the free oscillation must be short compared with the duration of the maneuver.

STABILITY OF A CONVENTIONAL AIRPLANE OPERATED WITH TWO CONTROLS

From the foregoing considerations it is apparent that the airplane must have certain degrees of stability for satisfactory two-control operation. Operation with constraint in yawing calls for stability in combined rolling and sideslipping, whereas operation with rolling constraint requires stability in combined yawing and sideslipping, as indicated by equations (2) and (3). In order to illustrate the degree of stability of a conventional airplane in these motions, data from an assumed average airplane (described in reference 2) have been used and several calculations made for the two cases. The principal characteristics of the assumed airplane are given in the table I.

TABLE I

CHARACTERISTICS OF ASSUMED AVERAGE AIRPLANE

Type	Monoplane, 2-passenger.
Gross weight	1,600 lb.
Wing area	171 sq. ft.
Wing span	32 ft.
mk_X^2	1,216 slug-ft.^{2}
mk_Z^2	1,700 slug-ft.^{2}

Stability derivatives at various lift coefficients:

C_L	L_v	L_r	$^a L_v$	N_v	N_r	N_v	Y_v
0.35	−5.44	1.11	−0.0544	−0.207	−0.913	0.0368	−0.172
1.0	−3.23	1.88	−.0415	−.301	−.663	.0231	−.145
^{b} 1.8	−2.46	2.51	−.0461	−.310	−.977	.0221	−.224

^{a} 5° dihedral.
^{b} Flaps down.

STABILITY WHEN CONSTRAINED IN ROLLING

The stability of the motion of the airplane (or of the movement of the control, δ) when the rolling component is arbitrarily constrained may be calculated from the complementary equations of (2):

$$\left.\begin{aligned} \frac{dv}{dt}+rU_0-vY_v &=0 \\ -rL_r-vL_v-\delta L_\delta &=0 \\ \frac{dr}{dt}-rN_r-vN_v-\delta N_\delta &=0 \end{aligned}\right\} \tag{5}$$

The complementary equations express only a part of the complete motion. They show the influence of stability on the manipulations of the control required to enforce the desired constraint in bank as well as the stability of the free yawing and sideslipping oscillations. Whatever rolling motion is assumed, a solution of the complementary equations will appear as a component of the final solution.

The third equation of (5) may be solved for v and the resulting expression substituted into the first equation, etc. The same procedure may be carried out for r or δ; in either case the so-called "auxiliary" equation is:

$$\begin{aligned} &L_\delta[\lambda^2-(N_r+Y_v)\lambda+N_rY_v+U_0N_v] \\ &+N_\delta[L_r\lambda-L_rY_v-U_0L_v]=0 \end{aligned} \tag{6}$$

The equation is conveniently divided into two parts to show the effects of control rolling and yawing moments. If the rolling motion is constrained by a direct rolling-moment control, the second part of the equation (containing N_δ) is eliminated. Since the first polynomial is a quadratic, its roots are:

$$\lambda=\frac{(N_r+Y_v)\pm\sqrt{(N_r+Y_v)^2-4(N_rY_v+N_vU_0)}}{2} \tag{7}$$

If the airplane shows an average degree of weathercock stability ($N_v>0$), the roots will be conjugate complex numbers and the terms

$$C_1e^{\lambda_1 t}+C_2e^{\lambda_2 t}$$

of equation (4) will represent a damped oscillation. If $\lambda_1=a+ib$ and $\lambda_2=a-ib$, the period of this oscillation is

$$T_1=\frac{2\pi}{b} \tag{8}$$

and the time to damp to one-half amplitude:

$$T_2=-\frac{\log 0.5}{a}=\frac{0.7}{a} \tag{9}$$

provided that a is negative.

Neglecting the first part of equation (6) (containing L_δ) amounts to the assumption that the banking motion is constrained by the application of a rudder control. The solution of this part of the equation alone is:

$$\lambda=Y_v+\frac{U_0L_v}{L_r} \tag{10}$$

The auxiliary equation thus has only one real root and it is negative, indicating stability. The assumption is that a sidewise disturbance (v) causes the pilot to give the airplane a rate of yawing such that

$$rL_r=-vL_v \tag{11}$$

As L_r is positive, this yawing reduces the sideslip and must then itself be reduced in proportion to prevent rolling, thus resulting in a convergence. This control procedure, although stable and nonoscillatory, represents a more artificial assumption than the control of

the rolling motion by direct rolling moments, for here the pilot in order to check a sudden disturbance must move the airplane as a whole with equal suddenness while with direct control he is only called upon to deflect the control surface suddenly.

Although the motion that occurs when the rolling is controlled—either directly by a variable rolling moment alone or indirectly by a yawing moment—is stable, a control device that gives both rolling and yawing moments in combination may cause instability. Inasmuch as conventional ailerons do give secondary yawing moments, this case is of considerable interest. Denoting the ratio:

$$\frac{N_\delta}{L_\delta}=\kappa$$

where each δ denotes aileron deflection, the following resolution of equation (6) is obtained

$$\lambda^2-[(N_r-\kappa L_r)+Y_v]\lambda+(N_r-\kappa L_r)Y_v +U_0(N_v-\kappa L_v)=0 \tag{12}$$

The solution of this equation differs from that of the first component of equation (6) in that the quantities N_v and N_r are replaced by $(N_v-\kappa L_v)$ and $(N_r-\kappa L_r)$, respectively. Thus it is concluded that an effect of a secondary *adverse* yawing moment in an attempted rolling maneuver will be an apparent reduction of both the *weathercock stability* (N_v) and the damping in yawing (N_r).

Calculation shows that the motion becomes unstable when

$$\kappa>\frac{N_r+Y_v}{L_r} \tag{13}$$

or when

$$\kappa>\frac{Y_vN_r+U_0N_v}{Y_vL_r+U_0L_v} \tag{14}$$

in negative magnitude. Such instability would indicate that an arbitrary constraint in rolling (such as attempted level flight) could not be maintained by the ailerons alone.

Conventional ailerons give rise to adverse yawing moments in an amount approximately independent of the speed of flight while the rolling moments and stabilizing factors are much reduced at the lower speeds. The result is that the ratio κ approaches the foregoing undesirable magnitude at the highest lift coefficients. It is therefore considered that ordinary ailerons working on a part of the wing surface that sustains a high lift would not be desirable for two-control operation.

Table II lists the results of calculations of the stability indexes of the average airplane in free yawing and sideslipping motions at several lift coefficients. Since these calculations were to be used later in investigating the motions set up during turning maneuvers, a certain increase in the steady-flight speed at a given lift coefficient was assumed. The increase amounted to 7½ percent and the stability derivatives at each lift coefficient were multiplied by this factor.

TABLE II

INDEXES OF STABILITY OF MOTION WITH CONSTRAINT IN ROLLING

	C_L	Roots of stability equation	Period of oscillation	Time to damp ½
			Seconds	*Seconds*
$\kappa=0$	0.35	$-0.383\pm2.50i$	2.51	1.18
	1.0	$-.435\pm1.51i$	4.16	1.60
	1.8	$-.645\pm1.23i$	5.10	1.08
Adverse yaw $\kappa=-0.15$	1.0	$-.283\pm1.31i$	4.80	2.5
Favorable yaw $\kappa=0.15$	1.0	$-.585\pm1.67i$	3.76	1.2

The combined yawing and sideslipping motion under consideration is, in general, very stable. Further calculations have shown that the stability of the motion when free only in yawing and sideslipping is much greater than the stability of the completely free motion, the oscillations having a shorter period and greater damping.

STABILITY WHEN CONSTRAINED IN YAWING

Calculation of the stability of the rolling and sideslipping motions when the airplane is constrained in yawing is similar to that given for constraint in banking. Here the complementary equations of (3) are used. The corresponding auxiliary equation is

$$N_\delta[\lambda^3-(L_p+Y_v)\lambda^2+L_pY_v\lambda-gL_v] +L_\delta[-N_p\lambda^2+N_pY_v\lambda-gN_v]=0 \tag{15}$$

The complementary part of the general solution (4) will be of the form

$$p,\ v,\ \text{or}\ \delta=C_1e^{\lambda_1 t}+C_2e^{\lambda_2 t}+C_3e^{\lambda_3 t} \tag{16}$$

since there are now three roots. In case the yawing motion is constrained directly by the application of control yawing moments, only the first part of the equation will be in force. Calculation shows that two of the roots will then be of the conjugate complex type previously discussed and that the third root will be very nearly equal to L_p. Table III gives these roots as calculated for the average airplane under conditions similar to those assumed in table II.

TABLE III

STABILITY OF MOTION OF AVERAGE AIRPLANE WITH CONSTRAINT IN YAWING

C_L	Real root	Complex roots	Period of oscillation	Time to damp ½ (complex roots)
			Seconds	*Seconds*
0.35	−5.90	$-0.064\pm0.562i$	11.2	10.8
1.0	−3.59	$-.019\pm.636i$	9.9	36.6
1.8	−2.67	$-.015\pm.716i$	8.8	46.3

The fact that the auxiliary equation for the case of free rolling and sideslipping motion with yawing control has roots of such widely different magnitude is an indication that the motion may be separated into distinct modes. The large real root (nearly equal to L_p) indicates the sharp damping of an initial rolling motion and is of such magnitude that the wings may be considered to be in a measure constrained against rolling relatively to the air. A possible rolling motion, however, that will not be appreciably damped consists in rolling about an instantaneous center some distance above the center of gravity of the airplane. For rotation of the airplane as a rigid body about this point the rolling moment due to sideslip will balance the damping of the rolling.[1] The height, $\bar{z}_L$, of the instantaneous center above the center of gravity is found from:

$$vL_v=-pL_p$$

where

$$v=-pz$$

whence

$$\bar{z}_L=\frac{L_p}{L_v} \tag{17}$$

The mode of motion represented by the small complex roots (table III) thus consists in a swinging oscillation of the airplane about the metacenter $\bar{z}$ as a pendulum suspended from that point. The characteristic roots for the pendulum motion would be

$$\pm\sqrt{-\frac{g}{z}}=\pm i\sqrt{\frac{qL_v}{L_p}} \tag{18}$$

which are seen to be approximate roots of equation (15) ($L_\delta=0$).

From these considerations it appears that the two-control airplane constrained in yawing with the rudder would be subject to swinging oscillations of long period and slight damping. If the airplane is given an initial angle of sideslip, it will be restrained against banking directly by the relatively great damping in rolling L_p and the banking that occurs will conform nearly to a rotation of the airplane about the metacenter $\bar{z}_L$. It will be of interest to calculate this height, using the stability derivatives given in table I:

C_L	$z_L=\frac{L_p}{L_v}$
	Feet
0.35	100
1.0	92.5
1.8	53

Physical considerations indicate that the damping of this mode of motion is almost entirely dependent on Y_v; hence, for two-control operation with the rudder, it should be desirable to have a large value of this derivative.

It is possible for the pilot to apply a yawing moment either through the secondary influence of an aileron control or indirectly by rolling the airplane as a whole. If the latter effect were used to constrain the yawing, the resulting motion would be excessively unstable. Thus, in order to prevent a sidewise disturbance from yawing the airplane ($r=0$), the pilot must execute a roll such that the forward wing is depressed ($pN_p=-vN_v$). This roll provides the occasion for an increase of sideslip due to the bank and requires, in turn, more rapid rolling so that the motion diverges quickly. Secondary aileron yawing moments of either sign moderate this instability and the motion may become stable if the yawing moment is favorable.

These considerations indicate that the pilot could not maintain an exact yawing constraint by the use of ailerons alone. On the other hand, this inability is probably not of great importance since the assumption of piloting procedure is obviously artificial and since the former calculations (stability with constraint in rolling) indicated that, if the ailerons were used to hold the wings level, the free yawing oscillations would be short and quickly damped. (See table II.) Thus it appears that, in order to prevent any yawing whatever during a disturbance, the pilot would have to execute a divergent bank whereas if he merely held the wings level the yawing motion might be unnoticeable. The divergent bank consists in a rotation of the airplane about the metacenter

$$\bar{z}_N=\frac{N_p}{N_v} \tag{19}$$

which is now situated below the airplane. The motion is like that of a pendulum placed at this height above its point of support.

TWO-CONTROL OPERATION IN STEADY TURNS

The two-control average airplane, showing stability both in combined yawing and sideslipping (rolling control) and in combined rolling and sideslipping (yawing control), should reach a definite condition of equilibrium with some fixed setting of the lateral control. In general, the equilibrium condition corresponding to a definite rudder or aileron setting will be a steady turn at a definite angle of bank. If the components of rolling and yawing angular acceleration produced by the deflected controls are δL_δ and δN_δ, as before, the equations of lateral equilibrium at a fixed angle of bank may be written:

$$\left.\begin{aligned} g\varphi-rU_0+vY_v &=0\\ rL_r+vL_v+\delta L_\delta &=0\\ rN_r+vN_v+\delta N_\delta &=0 \end{aligned}\right\} \tag{20}$$

In case control is by ailerons giving secondary (adverse or favorable) yawing moments, the term N_δ is replaced by κL_δ; and, in case control is by rudder alone, L_δ is dropped from the equations. In any case it has

[1] This mode of oscillation has been discussed by Lanchester.

to be assumed that the longitudinal control is properly manipulated for maintaining altitude and speed while turning.

Two special conditions of equilibrium are of interest. Solving the equations for the angle of bank

$$\varphi=\frac{(Y_v L_r+L_v U_0)\delta N_\delta-(Y_v N_r+N_v U_0)\delta L_\delta}{g(L_r N_v-L_v N_r)} \quad (21)$$

The necessary condition for the bank angle to be zero with deflected controls is:

$$\frac{1}{\kappa}=\frac{L_\delta}{N_\delta}=\left(\frac{Y_v L_r+L_v U_0}{Y_v N_r+N_v U_0}\right) \quad (22)$$

(See equation (14).)

In case the applied control rolling and yawing moments are in this ratio, the steady state of motion of the airplane will be a flat turn without bank. This limiting ratio may be compared with the ratio of the secondary aileron yawing moments to the rolling moments. If the secondary moment is adverse and exceeds a certain proportion of the rolling moment, an equilibrium condition in which the ailerons do not produce a bank of the airplane becomes possible. In this condition a gradual deflection of the ailerons would merely cause the airplane to assume a yawed attitude, turning slowly under the influence of the side pressure vY_v. Such a condition should be especially avoided in a two-control airplane utilizing aileron operation.

Another simpler condition of equilibrium that is also of interest is the condition for zero rate of yawing with deflected controls. The resolution of the equations in this case is:

$$r=\left(\frac{L_v N_\delta-N_v L_\delta}{L_r N_v-L_v N_r}\right)=0 \quad (23)$$

This is the condition for an ordinary sideslip and the ratio of yawing to rolling moment requisite to this condition is simply

$$\frac{1}{\kappa}=\frac{L_\delta}{N_\delta}=\frac{L_v}{N_v} \quad (24)$$

Obviously it should be considered undesirable to allow the secondary adverse yawing moment of the ailerons to approach this proportion of the rolling moment.

By a similar resolution of the equations another condition, namely,

$$\frac{1}{\kappa}=\frac{L_\delta}{N_\delta}=\frac{L_r}{N_r} \quad (25)$$

is obtained for the case of steady turning without sideslipping. This equilibrium is possible with aileron control alone in the case of secondary adverse yawing moments and furnishes another criterion for the magnitude of these secondary moments. In this case it would be expected that a gradual application of the rolling control would lead to turning at a progressively greater rate with the angle of bank opposite in sense to the applied rolling moment.

The main point of interest in the condition of steady turning with two-control operation is the angle of sideslip incident to the turn at various angles of bank. The resolution of the equations for v results in:

$$v=g\varphi\frac{N_r-\kappa L_r}{\kappa(Y_v L_r+U_0 L_v)-(Y_v N_r+U_0 N_v)} \quad (26)$$

In the case of rudder control, where $L_\delta=0$ the expression for v reduces to:

$$v=\frac{-g\varphi}{\left(Y_v+U_0\frac{L_v}{L_r}\right)} \quad (27)$$

while in the case of pure rolling-moment control (ailerons giving no secondary yawing moments)

$$v=\frac{-g\varphi}{\left(Y_v+U_0\frac{N_v}{N_r}\right)} \quad (28)$$

Thus the sideslip incident to turning with only rudder control is mainly dependent on the ratio of L_v/L_r while with rolling-moment control the important factor is

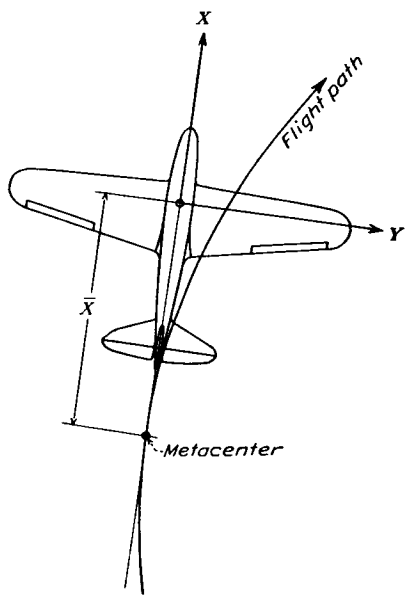

FIGURE 1.—Diagram illustrating combined yawing and sideslipping motion during a steady two-control turn. Metacenter for yawing moment $\bar{x}_N=\frac{N_r}{N_v}$; metacenter for rolling moment $\bar{x}_L=\frac{L_r}{L_v}$.

N_v/N_r. In both cases the sideslip will ordinarily be positive (toward the center of the turn) although the airplane does not necessarily lose altitude on this account.

Figure 1 illustrates the combined sideslipping and yawing of a two-control airplane during a steady turn.

102277—37——2

In the case of rudder control the inward sideslip must be such that $vL_v = -rL_r$ to prevent rolling. This combined sideslipping and yawing motion may be ascribed to a rotation of the airplane about some point aft of the center of gravity. If the distance of this point behind the center of gravity is denoted by $\bar{x}_L$

$$r\bar{x}_L L_v = -rL_r$$

or

$$\bar{x}_L = -\frac{L_r}{L_v} \tag{29}$$

for the case of rudder-controlled turns. For rotation of the airplane about this point the rolling moment vanishes, hence the point is a metacenter for the rolling moment. The X axis will be tangent to the flight path at this point in rounding a turn, as shown in figure 1.

Similar considerations apply in the case of operation with a rolling-moment control with fixed rudder. Here the metacenter is for a vanishing yawing moment, the amount of sideslip being that necessary for $vN_v = -rN_r$. The distance of the metacenter aft of the center of gravity is found from

$$r\bar{x}_N N_v = -rN_r$$

or

$$\bar{x}_N = -\frac{N_r}{N_v} \tag{30}$$

An interesting point arises in connection with the relation of the two metacenters ($\bar{x}_L$ and $\bar{x}_N$). For positive rotation of the airplane about a point nearer the center of gravity than $\bar{x}_N$ the residual yawing moment will be negative; hence if the metacenter $\bar{x}_L$ is nearer the center of gravity than $\bar{x}_N$, steady turning with rudder operation will require a positive setting of the rudder, i. e., in a direction to aid the turn. Conversely, if control is by rolling moments, the steady motion will be a rotation about $\bar{x}_N$ and, if the residual rolling moment for rotation about this point is negative ($\bar{x}_L < \bar{x}_N$), the rolling control setting will be positive, also in a sense aiding the turn. Obviously, the condition $\bar{x}_N < \bar{x}_L$ corresponds to *instability* since in this case with either mode of two-control operation the control setting during a steady turn would be one appropriate to recovery from the turn. This condition is analogous to the spiral instability discussed by Lanchester. The following table gives the metacenters $\bar{x}_L$ and $\bar{x}_N$ for the average airplane at various lift coefficients:

C_L	$\bar{x}_L$	$\bar{x}_N$
	Feet	*Feet*
0.35	20	25
1.0	45	29
1.8	55	44

At the lowest speeds ($C_L = 1.0$ and 1.8) $\bar{x}_N$ is less than $\bar{x}_L$, indicating that negative rudder and aileron settings will be required during steady positive turns. Figure 2 shows results of calculations of the control-moment coefficients for equilibrium in turning at various angles of bank that give an indication of the fixed control settings.

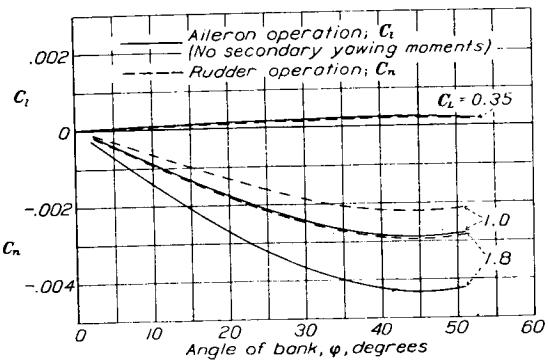

FIGURE 2.—Moment coefficients indicating control settings during steady turns at various angles of bank.

Equilibrium angles of sideslip in steady turning with both modes of two-control operation are shown in figure 3. It is to be noted that the angle of sideslip is not greatly different in steady turning with either type of control and in every case is positive.

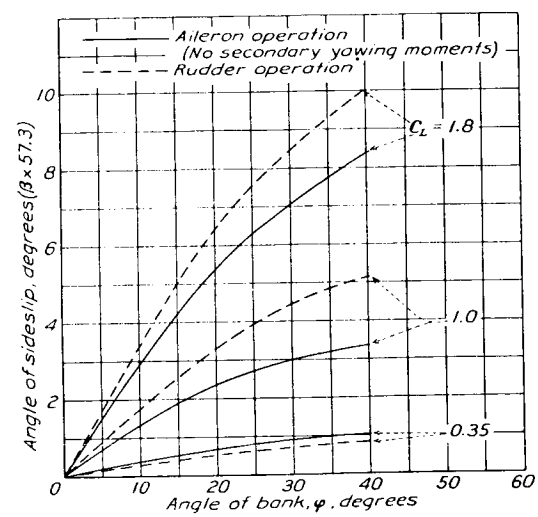

FIGURE 3.—Angles of sideslip during steady turns at various angles of bank with different modes of two-control operation.

The only possibility of outward or negative sideslip during the steady turn occurs when rolling and yawing moments are applied in combination. Such an occurrence is illustrated in figure 4, which shows the effect of secondary aileron yawing moments on the equilibrium during 30° bank turns. At $C_L = 1.0$ the sideslip becomes

negative, or outward, when the ratio N_δ/L_δ exceeds negatively N_r/L_r, i. e.:

$$\kappa=\frac{C_n}{C_l}\frac{I_X}{I_Z}=\frac{N_\delta}{L_\delta}>\frac{N_r}{L_r} \tag{31}$$

(See equation (25).)

Whether or not a given secondary aileron yawing moment will reduce or increase the equilibrium sideslip angle during a steady turn depends on the spiral stability of the airplane, for this characteristic determines the sign of the equilibrium control setting.

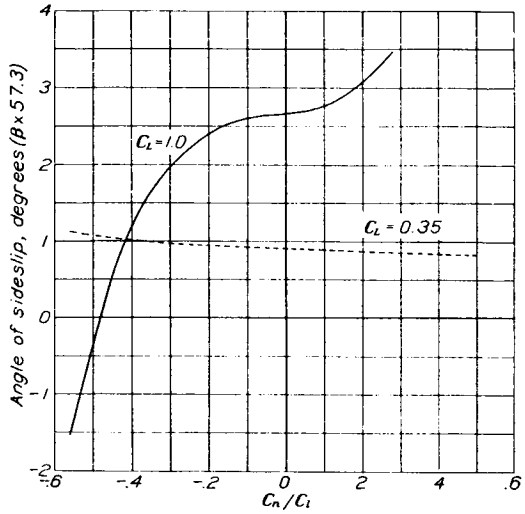

FIGURE 4.—The effect of secondary yawing moments on sideslip during a 30° bank steady turn; two-control operation with ailerons.

Thus, in the case of a spirally unstable machine the aileron setting will be appropriate to recovery from the bank and an adverse yawing moment will act in a positive direction, aiding the turn. In any event, spiral stability, if present, must be considered as a small effect (with conventional airplanes); and the control setting during steady turns is, if positive, almost certain to be small so that secondary moments will have little effect. (See fig. 4, C_L=0.35.)

TWO-CONTROL OPERATION IN UNSTEADY TURNS

The consideration of the equilibrium state is sufficient for the study of conditions during slowly executed maneuvers of sufficient duration for the natural free oscillations of the airplane to die out. In the case of rapid maneuvers performed by more or less quick movements of the control the equilibrium conditions are of secondary importance and the primary consideration is the oscillation and damping of the free motion.

According to the previously outlined treatment, the motions of the two-control airplane set up during unsteady turns will be studied by considering a constraint impressed on the motion in the particular coordinate in which the available control operates. Thus in one case of rudder control a definite sequence of yawing motions appropriate to the turn maneuver under consideration will be assumed. The free rolling motion that the airplane takes up during the maneuver will then be studied and compared with the rolling motion that would be considered appropriate for the execution of the maneuver.

The investigation of unsteady conditions during various maneuvers required that the equations of motion (equations (1) to (3)) be solved for different types and variations of the impressed disturbances. The first step in the procedure consisted in obtaining solutions of the equations for "unit disturbances" substituted into each coordinate of freedom.

The unit disturbance is defined by

$$\left.\begin{aligned} 1(t)&=0 \text{ when } t<0\\ 1(t)&=1 \text{ when } t>0\end{aligned}\right\} \tag{32}$$

(see reference 3) and is taken to represent a disturbing acceleration of unit magnitude applied instantly at $t=0$.

The solutions of the equations of motion for this type of disturbance were found by methods described in reference 4. The result thus obtained is analogous

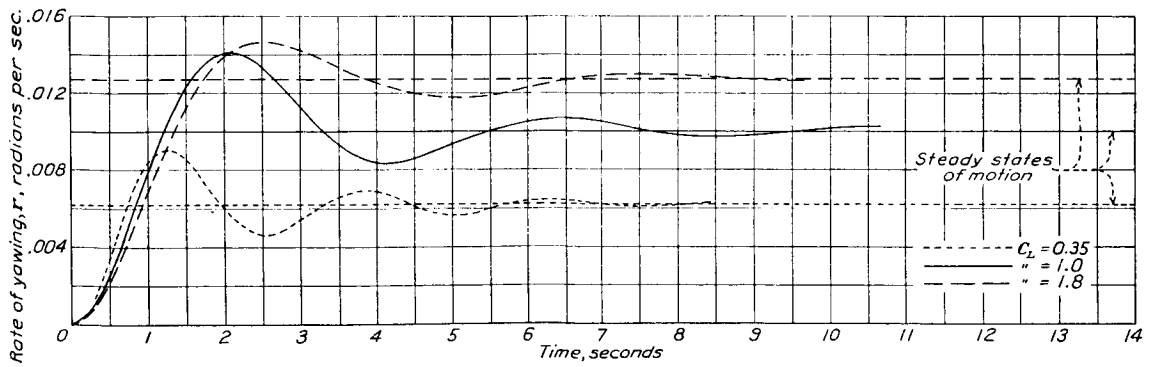

FIGURE 5.—Yawing motion due to unit *side* disturbance; two-control airplane constrained in rolling (aileron operation; κ=0).

to the so-called "indicial admittance" of the electric-circuit theory and was combined with Carson's generalized expansion theorem (see reference 5) to obtain the motion due to the varying forms of disturbance. If $v_1(t)$ is the motion calculated for a unit disturbance $1(t)$, and $v(t)$ is the motion due to a varying disturbance, say $\varphi(t)$ (see equation (2)), then Carson's theorem may be written

$$v(t_n)=v_1(t_n)\varphi(0)+\int_0^{t_n} v_1(t_n-t)\frac{d\varphi}{dt}\,dt \qquad (33)$$

It was found convenient to evaluate this integral graphically.

Figures 5 and 6 show the motions of the two-control airplane constrained in rolling (aileron operation) due to unit disturbances acting in each of the two remaining degrees of freedom. Figure 5 shows the yawing motions resulting from a suddenly impressed sidewise acceleration of 1 foot per second per second. The conditions here may be assumed to represent the effect of an initial and constantly maintained angle of bank of approximately

$$\varphi=\frac{1}{g} \qquad (34)$$

In order to maintain this bank angle without sideslipping, the airplane should immediately acquire a uniform rate of yawing of approximately

$$r=\frac{1}{U_0} \qquad (35)$$

As the curves show, the actual yawing is delayed for an instant but in each case oscillates about the mean value given by (35). The most favorable condition is that at high speed ($C_L=0.35$) since the appropriate yawing motion occurs with the least delay and the oscillations are most quickly damped.

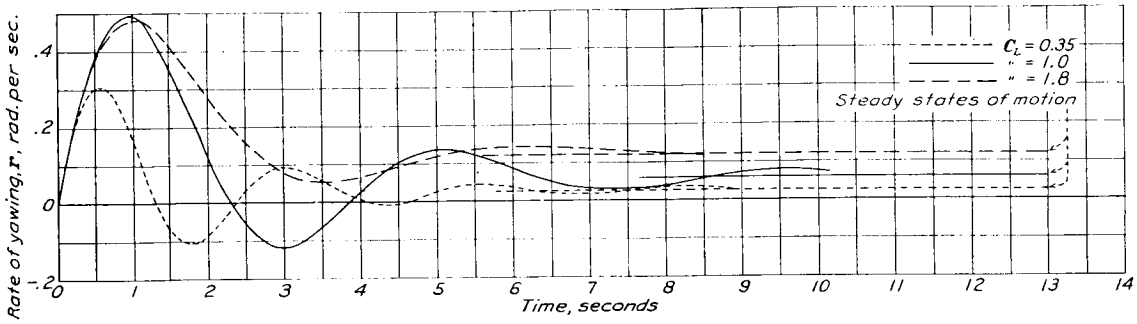

FIGURE 6.—Yawing motion due to unit *yawing* disturbance; two-control airplane constrained in rolling (aileron operation; $\kappa=0$).

As stated previously, the unit motions, or motions due to unit disturbances, were utilized in calculating the effects of varying disturbances assumed during turn maneuvers. Thus the curves given in figure 5 were used to find the motions due to a varying angle of bank by means of Carson's integral (33). Actually, in constraining the airplane to a definite bank angle as was assumed, a varying aileron rolling moment has to be applied and, if this moment is accompanied by a secondary yawing moment, additional disturbances in yawing will be introduced. The rolling motion will also introduce a secondary disturbance in yawing equal to $N_p\times p(t)$. Figure 6 shows the yawing motion produced by a unit disturbance in yawing that was used in calculating the effects of such impressed yawing disturbances. This curve may be considered to represent the yawing motion following the sudden application of a control yawing moment. The final effect of this disturbance is to cause the machine to assume a yawed attitude, turning slowly under the influence of the side force vY_v.

Figures 7 and 8 show the corresponding solutions of the equations of motion (3) for the case of the airplane constrained in yawing by a rudder control. Figure 7

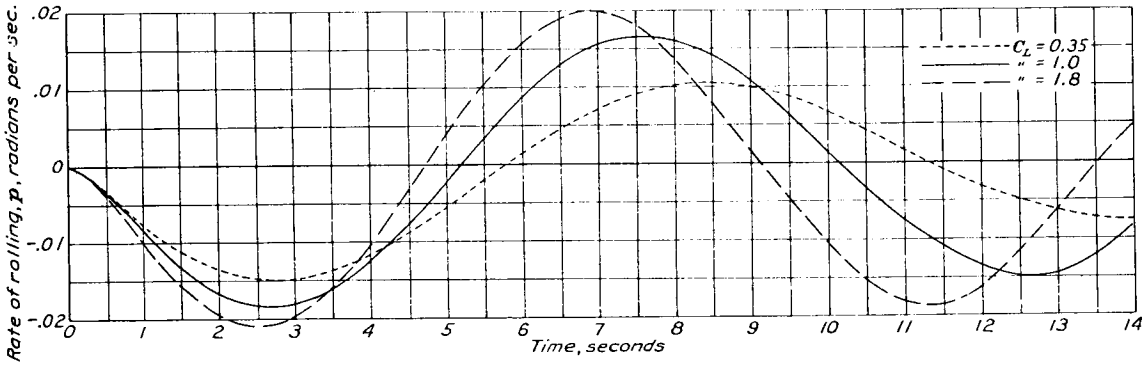

FIGURE 7.—Rolling motion due to unit *side* disturbance; two-control airplane constrained in yawing (rudder operation).

may be taken to represent the rolling motion following an initial bank angle. Presumably the ideal condition would be a rapid diminishing of this bank angle to zero. The integrated areas under the curves shown would then approach a definite value after a few oscillations, which area should be equal to the initial bank angle, namely approximately

$$\varphi=\frac{1}{g} \tag{36}$$

Instead, the airplane continues to roll one way and then the other, executing the pendulum-like oscillations described in the discussion of the stability of this motion. The damping of these oscillations is slight and is most apparent at the lowest lift coefficient, $C_L=0.35$.

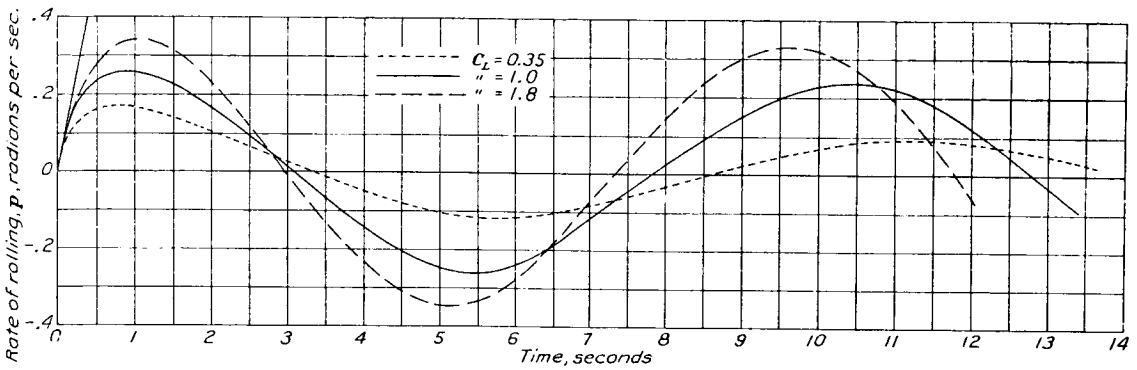

FIGURE 8.—Rolling motion due to unit *rolling* disturbance; two-control airplane constrained in yawing (rudder operation).

Figure 8 is similar to figure 7 except that here the rolling motion is due to a suddenly impressed angular acceleration in rolling. These curves were used in calculating the effect of varying rolling moments impressed indirectly by yawing motion $L_r \times r(t)$. (See equation (3).) Figure 8 is of interest in illustrating the two more or less distinct modes of motion in free rolling and sideslipping. It will be noted that the rolling starts very rapidly (with an initial angular acceleration of one radian per second per second) but soon takes up the slow swinging oscillation. As in the previous case of rolling motion, the steady state finally approached is a definite angle of bank.

The foregoing calculations are of interest in indicating how the different types of two-control airplanes may be expected to respond to attempted maneuvers. The first step in the calculation of an actual complete maneuver is to arrive at a specification for that part of the motion which is assumed to be constrained. It will be of interest to compare the motions executed by the two-control airplane with the most perfect possible coordination of the motions that might be obtained with three-control operation. Obviously, it will be necessary to specify a maneuver that is within the power of the control to produce and it will be desirable to conform the specification to a type of turn likely to be followed in practice. In other respects, it was thought that any smooth curve representing the banking or yawing of the machine up to a definite angle or rate maintained steadily for a short time and followed by a smooth recovery to straight flight would serve the purpose. Figure 9 shows the time history of the ideal three-control turn that was assumed in the subsequent investigation. In most cases the manuever was assumed to be completed in 6.28 seconds and this time is taken to represent about the maximum rapidity with which the maneuver could be performed at the lowest speed using conventional-type controls. Figure 10 shows the control-moment coefficients necessary to constrain the rolling and yawing motions to the specified maneuver with perfect three-control operation. Under the conditions of two-control operation the turns will not be perfect owing to the sideslipping and it is to be expected that this sideslipping will in some degree modify the control settings.

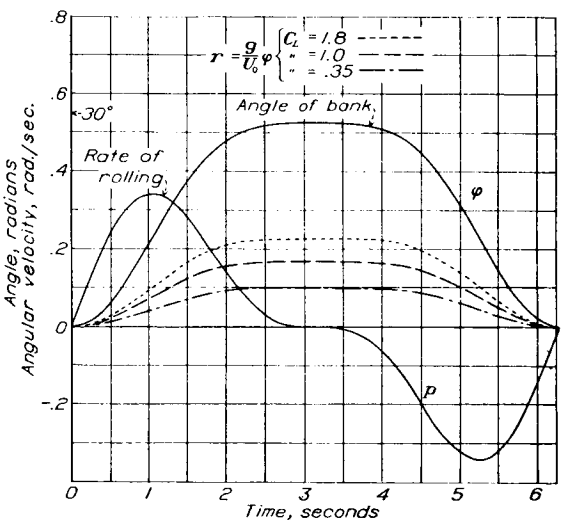

FIGURE 9.—Angle of bank and rates of rolling and yawing specified for 30° bank two-control turn maneuvers.

In the calculations illustrated in figure 11 the banking motion was assumed to be forced to follow the ideal bank by means of a rolling control and the resultant free yawing motions were computed. The reaction of the machine was evidently favorable in this case. This result could have been anticipated from the calcu-

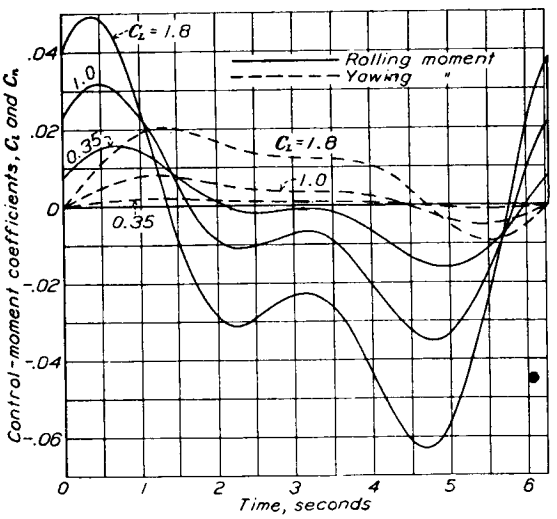

FIGURE 10.—Control-moment coefficients necessary to produce specified manuever with zero sideslip.

lations of stability, which showed that the free yawing motion was of short period and strongly damped.

The curves of figure 11, although indicating the advantage of rolling-moment control, also bring out an imperfection in the coord nation of the yawing motion. The rolling motion itself tends to induce an unfavorable

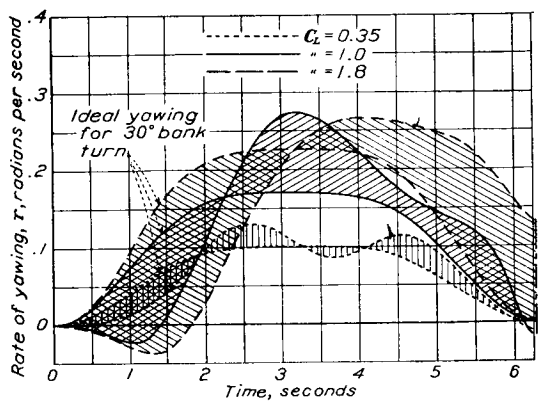

FIGURE 11.—Free yawing motion during 30° bank maneuvers performed with rolling control.

yawing motion at the start of the maneuver due to the adverse sign of N_p. This effect becomes more pronounced at the higher lift coefficients and, in the worst case (C_L=1.8), produces an adverse change in the heading of the machine of 2.0°. The total change in heading produced by the maneuver at this speed is approximately 50°.

From the foregoing considerations, it appeared that a certain amount of favorable secondary aileron yawing moment might be desirable to overcome the adverse yaw caused by the rolling motion at the start of the

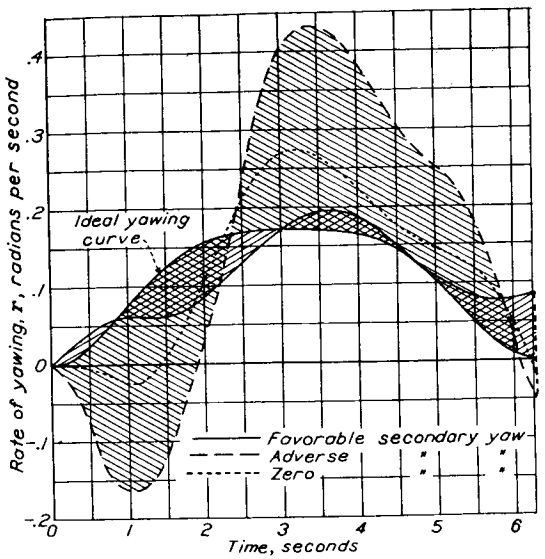

FIGURE 12.—The effect of secondary yawing moments on yawing motions during 30° bank maneuver performed with rolling control; C_L=1.0. C_n=± 0.21C_l, (κ=± 0.15).

turn. The effects of secondary yawing moments of both favorable and adverse sign applied in proportion to the control rolling moment are illustrated in figures 12, 13, and 14.

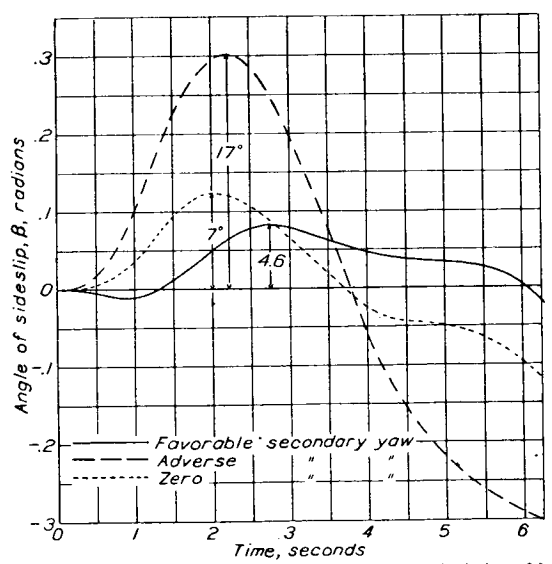

FIGURE 13.—The effect of secondary yawing moments on sideslip during 30° bank maneuver performed with rolling control; C_L=1.0. C_n=±0.21C_l (κ=±0.15).

The curves shown were calculated by equation (2) and take account of the increments of control displacement necessary to accommodate the rolling moments introduced by the yawing and sideslipping oscillations.

The effect of these increments of control displacement is to modify the stability of the yawing and sideslipping motions, an adverse yawing moment reducing the damping and lengthening the period. The results indicate especially the disadvantage of adverse yaw and show that some improvement may be had from a favorable yawing moment.

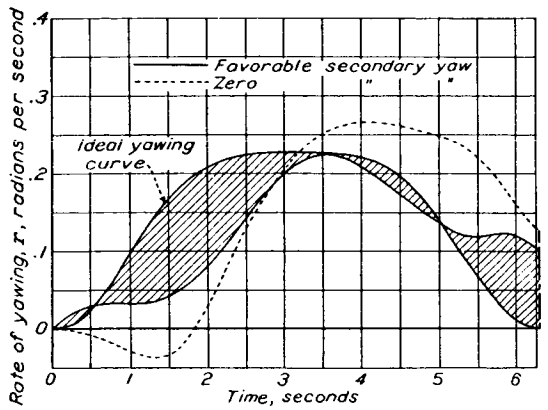

FIGURE 14.—The effect of favorable secondary yawing moment on yawing motion during 30° bank maneuver performed with rolling control; $C_L=1.8$. $C_n=0.21C_l$ ($\kappa=0.15$).

In order to study more closely the possible beneficial effects of a favorable aileron yawing moment, it is of some interest to analyze further the control application into several components. The component that results in modification of the stability through the action of the secondary yawing moment may be considered to be directly favorable to improved coordination of the

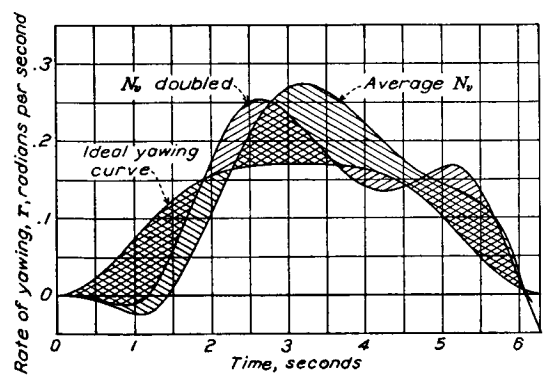

FIGURE 15.—The effect of increased N_v on yawing motion during 30° bank maneuver; aileron operation (no secondary yawing moment); $C_L=1.0$.

yawing motion because it shortens the natural oscillation period and increases the damping. With a given proportion of favorable yawing moment, increasing the dihedral angle should result in further improvement in this respect since the apparent weathercock stability ($N_v-\kappa L_v$) is increased in that way. Another component of the applied rolling control is directed to overcoming the damping of the rolling incident to the maneuver. The secondary yawing disturbance thus introduced is of the same form as pN_p and may be calculated as

$$N_p'=(N_p-\kappa L_p) \tag{37}$$

The condition for perfect coordination of banking and yawing motion during the turn requires that the acceleration in yawing be very nearly proportional to the rate of rolling; namely,

$$\frac{dr}{dt}=\frac{g}{U_0}\times p \tag{38}$$

The component of rolling control directed toward opposing the damping in rolling is applied in this way

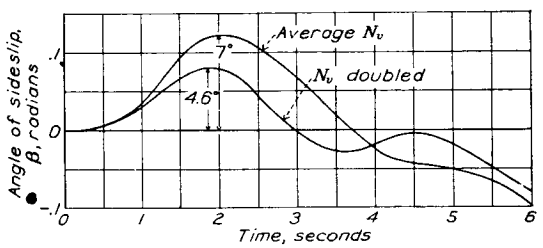

FIGURE 16.—The effect of increased N_v on sideslip during two-control 30° bank maneuver; aileron operation (no secondary yawing moment); $C_L=1.0$.

and it is seen that this component of the secondary favorable yawing moment is properly directed toward improved coordination of the yawing motion. The component of control application necessary to accelerate the rolling motion does not, however, lead to a desirable secondary yawing acceleration since this acceleration is not proportioned to the rolling velocity.

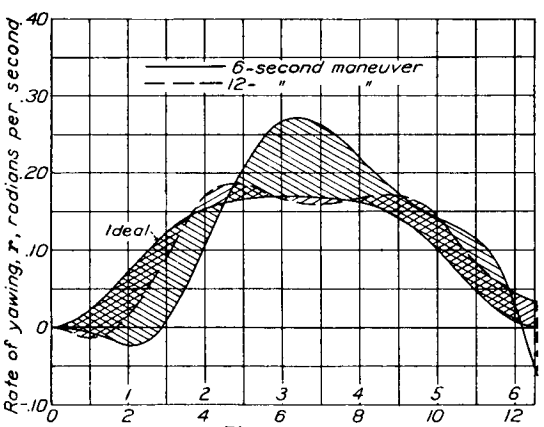

FIGURE 17.—Comparison of yawing motions during maneuvers of different time extents; aileron operation (no secondary yawing moment); $C_L=1.0$.

This component results in the primary disadvantage associated with favorable-yaw ailerons. Quick or irregular movements of the control may lead to pronounced yawing oscillations if the secondary moment is very great.

It appears that a decisive method of improving the aileron-operated two-control airplane would be to

increase the weathercock-stability factor N_v. This method would serve directly to reduce the sideslipping to a minimum both in steady turning and in rapidly executed turn maneuvers. Figure 15 shows the effect of doubling N_v on the yawing motion during the maneuver performed at $C_L=1.0$. This modification of the airplane shortened the natural period of the oscillation and resulted in the yawing action taking place more quickly. The effect on sideslip is shown in figure 16. Although the maneuver ends with about 5° of outward sideslip, this value will be quickly reduced to zero on account of the natural stability of the motion. With different timing of the maneuver it may, of course, be brought to an end with no residual sideslip. The following table shows the effect of arbitrarily increasing N_v on the natural period of the yawing oscillations:

Ratio of N_v to that of average airplane	Period
	Seconds
1	4.16
2	2.92
4	2.05

It is to be noted that an increase in vertical-fin area will increase the derivative N_r as well as N_v and will thus result in greater damping of the motion.

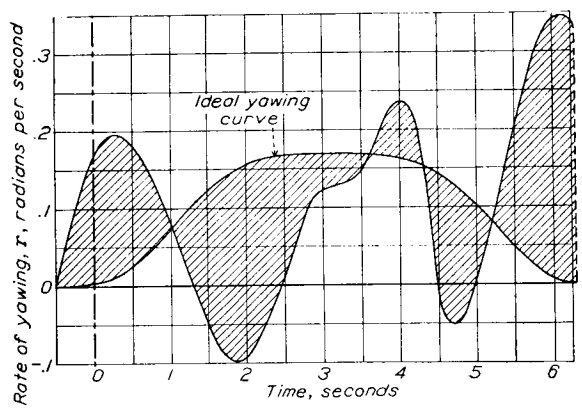

FIGURE 18.—Yawing motion necessary to enforce assumed 30° bank maneuver with rudder operation; $C_L=1.0$.

A certain disadvantage associated with increased N_v is the relatively greater tendency for spiral instability and the consequent necessity for holding the control against the steady turn. It may be expected, however, that this undesirable tendency could be overcome by properly proportioning the dihedral of the wings. The greatest possible effect of increase of vertical-fin area would be to cause the metacenter for yawing moments $\bar{x}_N$ (see discussion of stability) to approach coincidence with the fin; it would then appear necessary to arrange the metacenter for rolling moments ahead of this point in order to accommodate any desired increase of vertical-fin area and secure spiral stability.

Further improvement in the operation of the aileron-controlled machine could be had by decreasing the yawing derivative in rolling N_p. Alteration of this derivative apparently would require fundamental changes in wing design, improvement being in the direction of lower aspect ratio, which might, of course, conflict with other requirements.

As pointed out, the maneuvers assumed in these calculations are considered to be more rapid than usual in

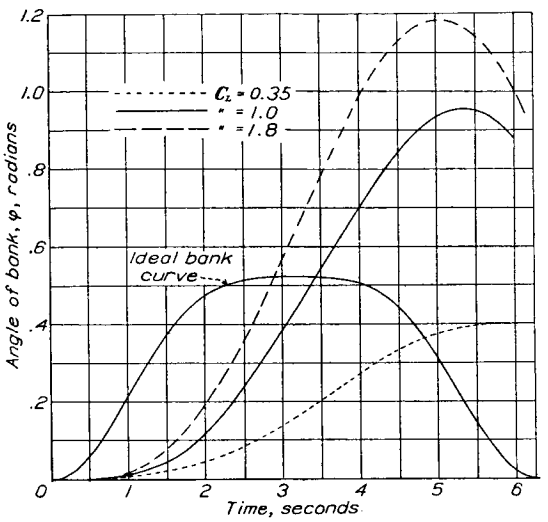

FIGURE 19.—Free angles of bank during turn maneuvers performed with rudder compared with ideal bank curve; yawing constraints for 30° bank maneuver.

normal flight, since they represent the use of a large proportion of the control power ordinarily available at the lower speeds. With slower maneuvers the coordination of the motions of the two-control airplane would be expected to be much better, especially when the duration of the maneuver becomes large relative to the natural period of oscillation of the airplane. Figure 17 shows the result of a calculation in which the duration of the 6.28-second maneuver was doubled.

It is worth noting that the actual deflection of the flight path of an airplane relative to the earth is accomplished much more directly by banking than by steering. Regardless of the sideslipping and coordination of angular motions, any decided acceleration of the path must be brought about by inclination of the lift and is not directly affected to any great extent by rotating the airplane in yaw. Such deflection of the path would be the principal objective in turning to avoid an obstacle. Thus the airplane with rolling-moment control should be capable of avoiding obstacles equally as quickly as a conventional three-control airplane. As is the case with three-control operation, the tendency of a two-control airplane to accelerate downward when banked must be counteracted by a movement of the elevator.

If the airplane is assumed to execute a sharp turn to avoid an obstacle, the primary consideration will thus be the ability to produce a specified bank. Under such

conditions the pilot of the rudder-operated airplane would be expected to make an effort at indirect control of the bank without regard to the coordination of the yawing motion. The question then arises as to what yawing motion would have to be prescribed in the case of the rudder-controlled machine to enforce the desired motion in banking.

Figure 18 shows the yawing motion that results in a bank curve similar to that given in figure 9. It appears that, in order to attain the bank angle as shown, a relatively powerful rudder control would have to be applied about one-half second in advance of the usual start of the turn. Further calculations showed that the prescribed yawing motion could be attained throughout if a rather large amount of rudder control were available. That such an attempt to follow a definite course in banking would require a vigorous use of the rudder is evident from the oscillation of the yawing curve.

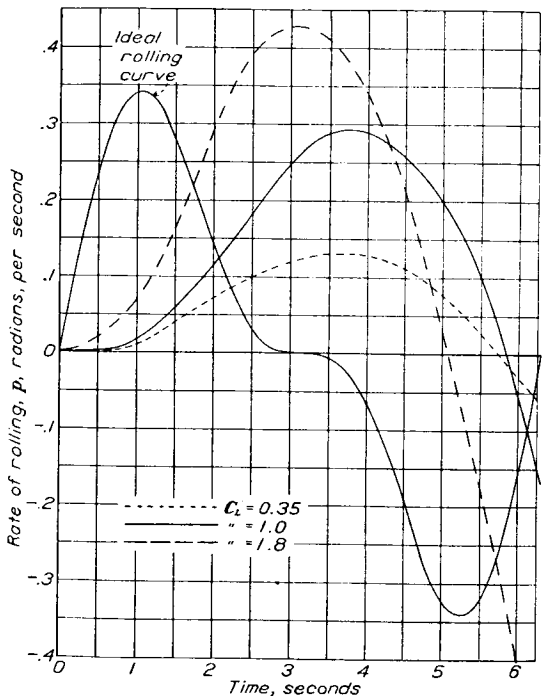

FIGURE 20.—Free rolling motion during turn maneuvers performed with rudder; yawing constraints for 30° bank maneuver.

In the case of two-control operation with a constraint in yawing by means of the rudder, the yawing motions shown in figure 9 were assumed and the resulting free rolling motions were calculated. Figures 19 and 20 show the results of such calculations made at different lift coefficients. The angles of bank and rates of rolling attained are compared with those that would be appropriate to the constrained yawing motion. It is apparent from these and the preceding figures that the two-control airplane operated with the rudder cannot be expected to perform rapid maneuvers of the type considered. The natural reaction of the rolling motion is too slow and the damping is too slight to enable even an approximate coordination of the motions within the short time of duration of the maneuver.

Figure 21 shows the angles of sideslip attained with the various modes of operation considered, summarizing the results of the calculations.

The reasons for the inability of the rudder-controlled airplane to execute rapid turns are: First, that the secondary rolling reaction due to yawing motion is insufficient to overcome the relatively great damping of direct rolling motion; second, that for a rapid turn the rate of rolling required on entry and recovery greatly exceeds the maximum rate of yawing; and third, that the free rolling and sideslipping oscillations set up are not very well damped. The greatest possibility for improvement would appear to be in increasing the derivatives L_v and Y_v. The first (L_v) would call for increased dihedral angle and would serve to shorten the natural period of the rolling and sideslipping motion, while the second (Y_v) would call for increased area of the side projection of the airplane and should improve the damping of the oscillations. The following table shows the effects of changing these derivatives on the natural period and damping of the oscillations at C_L=1.0.

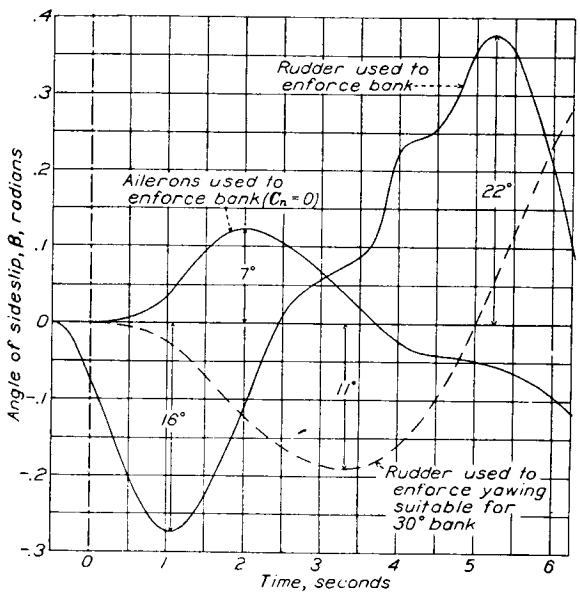

FIGURE 21.—Angles of sideslip during two-control turn maneuvers with different modes of operation; 30° bank turn maneuver.

	Ratio of derivative to that of average airplane				
	L_v			Y_v	
	½	1	2	1	2
Time to damp ½, seconds	12.4	36.6	∞	36.6	6.25
Period, seconds	15.3	9.9	7.65	9.9	10.9

CONCLUSION

The lateral motion of a conventional airplane is more stable when constrained in rolling than when constrained in yawing. The stability of the free yawing and sideslipping motion is greater than that of the entirely free motion; the stability of the free rolling and sideslipping is less than that of the entirely free motion.

If a rolling-moment control is used to enforce an arbitrary constraint in banking, the free yawing that results will be approximately coordinated to the bank if the airplane has the average degree of weathercock stability (N_v). The yawing in this case is also approximately adjusted to the speed of flight so that with a given bank maneuver a more rapid rate of yawing is attained at low speed than at high speed, as is desirable. The deviation of the yawing from the ideal is greater, however, at lower speeds and is also greater in quick turns than in more slowly executed ones. If the rolling control were designed to give a moderate favorable yawing moment, the coordination of the motions would be improved. Improvement may also be effected by increasing the weathercock stability. If, however, the aileron control gives the usual proportion of secondary adverse yawing moment, the coordination of the yawing with the banking will be relatively very poor. The motions may then become unstable and uncontrollable in an extreme case at high lift coefficient. These latter statements are particularly applicable to conventional-type ailerons which are considered as undesirable on this account for use at low flight speed unless compensated by the rudder.

A rudder control may be used to enforce a constraint either directly on the yawing motion or indirectly on the rolling motion provided that the maneuver specified is not too rapid nor the disturbances encountered too severe. In the former case the free banking motion occurs as a series of long oscillations that do not begin to approximate the desired bank until some time after the start of a maneuver or after the passing of a disturbance. During a rapid yawing maneuver the bank that occurs is greater at low flight speed than at high, indicating that the coordination of the centrifugal and the gravitational accelerations is not adapted to the desired variation with flight speed.

Although the coordination of the motions with aileron control grows worse as the flight speed is reduced, the coordination with rudder control improves somewhat at the lower speeds. This effect would be especially apparent if the rudder were applied in such a way as to enforce indirectly a desired banking motion. Such indirect control requires, however, that the rudder be deflected in advance of the desired effect. The yawing that arises when the bank is indirectly controlled with the rudder is a very poor approximation to the ideal yawing and calls for large and irregular control movements.

The amount of sideslipping during *steady* turns is not greatly different with either mode of operation. In either case it appears desirable that the free motion of the airplane show spiral stability so that control settings opposing the turn will not be required.

In general, it is concluded that a reliable rolling-moment control that does not give a secondary adverse yawing moment would afford the most satisfactory means for two-control operation. It appears that a moderate amount of favorable secondary yaw would be desirable although certain disadvantages appear if the proportion is too great.

The disadvantage in two-control operation lies not so much in the imperfection of control of the flight path of the airplane relative to the earth as in the sideslipping and sidewise accelerations that arise through the imperfect coordination of the yawing and banking motions. It appears possible that this tendency may be so reduced by the use of suitable control organs and properly modified stability characteristics as to be unobjectionable.

LANGLEY MEMORIAL AERONAUTICAL LABORATORY,
NATIONAL ADVISORY COMMITTEE FOR AERONAUTICS,
LANGLEY FIELD, VA., *August 12, 1936.*

REFERENCES

1. Routh, E. J.: Advanced Rigid Dynamics, vol. II. The Macmillan Co.,1905.
2. Weick, Fred E., and Jones, Robert T.: The Effect of Lateral Controls in Producing Motion of an Airplane as Computed from Wind-Tunnel Data. T. R. No. 570, N. A. C. A., 1936.
3. Bush, V.: Operational Circuit Analysis. John Wiley and Sons, Inc., 1929, p. 41.
4. Jones, Robert T.: A Simplified Application of the Method of Operators to the Calculation of Disturbed Motions of an Airplane. T. R. No. 560, N. A. C. A., 1936.
5. Carson, J. R.: Electric Circuit Theory and Operational Calculus. McGraw-Hill Book Co., Inc., 1926.

TECHNICAL NOTE 586

THE REDUCTION OF AILERON OPERATING FORCE BY DIFFERENTIAL LINKAGE

Robert T. Jones and Albert I. Nerken

Langley Memorial Aeronautical Laboratory

December 1936

NATIONAL ADVISORY COMMITTEE FOR AERONAUTICS

TECHNICAL NOTE NO. 586

THE REDUCTION OF AILERON OPERATING FORCE BY DIFFERENTIAL LINKAGE

By Robert T. Jones and Albert I. Nerken

SUMMARY

It is shown that the control force of ordinary ailerons may be reduced to zero over a range of deflections and at a given flight condition by the use of an appropriate differential movement. Approximations to the ideal motion obtainable with a simple linkage are discussed and a chart that enables the selection of an appropriate crank arrangement is presented. Various aspects of the practical application of the system are discussed and it is concluded that a small fixed tab, deflected to trim both ailerons upward, would be advantageous.

INTRODUCTION

One of the most exacting requirements of a lateral-control system is the provision of an adequate degree of control with a small expenditure of operating effort. It appears that a differential linkage can, when properly designed, be a very effective means of reducing the operating force of ordinary ailerons. Several other advantages accrue to the differential and such systems are widely used. The possible reduction of control force appears to be of primary importance, however, and it is therefore of interest to discuss some rules for the design of a linkage that will afford the greatest advantage in this respect.

The reduction of operating force with a differential linkage is accomplished by taking advantage of the up-floating tendency of the ailerons. This floating tendency is apparent in measurements of aileron hinge moments, which generally show an offset moment (C_{h_o}) at the neutral setting. (See fig. 1.) This moment varies with angle of attack and with airfoil profile.

With a differential linkage the ailerons on opposite tips of the wing begin to move at different rates immediately after they are deflected from neutral, the downgoing aileron moving more slowly than the upgoing one. Thus with the ailerons deflected the upward pressure on the upgoing aileron, which tends to increase the deflection, has a greater mechanical advantage at the control stick than does the upward pressure of the downgoing aileron. The combination of a reduced upward pressure and an increased mechanical advantage of the upgoing aileron tends to nullify the effect of the increased upward pressure and reduced mechanical advantage of the downgoing aileron to the extent that within certain limits the operating force may be reduced or even reversed.

If the ailerons are connected to the control stick with nondifferential gearing, the effect of the initial hinge moment at the neutral setting is not felt in the stick force required to deflect them. In this case the mechanical advantage of one aileron with respect to the other remains the same, so that the initial offset moment (C_{h_o}) on one aileron is exactly balanced by that on the other. The only force experienced at the stick is that due to the difference of the aerodynamic hinge moments of the two ailerons brought about by their deflection.

DEFINITIONS OF SYMBOLS

c_w, chord of wing.

c_a, chord of aileron.

c_t, chord of tab.

C_h, aileron hinge-moment coefficient.

C_{h_o}, aileron hinge-moment coefficient at zero deflection (normally negative).

C_{h_s}, resultant hinge-moment coefficient acting at control stick (negative when moment opposes deflection).

C_ℓ, rolling-moment coefficient.

C_n, yawing-moment coefficient.

C_L, lift coefficient.

ϕ_1, angle of bank 1 second after deflection of aileron control.

δ_N, angular setting of aileron crank when neutral.

θ_N, angular setting of control-stick crank when neutral.

$\Delta\theta$, angular movement of control-stick crank.

δ_u, upward deflection of aileron

δ_d, downward deflection of aileron

δ_{uf}, upfloating angle of aileron

δ_{td}, downward deflection of tab

} Taken as positive numbers.

CALCULATION OF CONTROL FORCE AND WORK OF DEFLECTION

A calculation of the effective moment coefficient acting at the control stick will show how the characteristics of the differential linkage affect the operating force. The hinge-moment coefficient of an ordinary aileron may be calculated with sufficient accuracy by the formula (neglecting weight of aileron),

$$C_h = C_{h_o} + \delta \frac{dC_h}{d\delta} \tag{1}$$

This formula applies to a single aileron. The effective moment coefficient acting at the control stick or wheel due to the up aileron is

$$C_{h_s} = \left(\delta_u \frac{dC_h}{d\delta} - C_{h_o}\right) \frac{d\delta_u}{d\theta} \tag{2}$$

and that due to the down aileron

$$C_{h_s} = \left(\delta_d \frac{dC_h}{d\delta} + C_{h_o}\right) \frac{d\delta_d}{d\theta} \tag{3}$$

The rates of change of the up and the down aileron angles throughout the range of the stick deflection are determined by the characteristics of the particular differential linkage used.

The various terms of equations (2) and (3) may be so collected as to represent two components of the total moment, one tending to return the control to neutral and the other tending to displace the control away from neutral. Thus,

$$C_{h_s} = - C_{h_o} \left[\frac{d\delta_u}{d\theta} - \frac{d\delta_d}{d\theta}\right] + \frac{dC_h}{d\delta} \left[\delta_u \frac{d\delta_u}{d\theta} + \delta_d \frac{d\delta_d}{d\theta}\right] \qquad (4)$$

The term containing C_{h_o} represents the reduction of C_{h_s} due to the difference of mechanical advantages.

With regard to the reduction of operating force, it is seen that the problem is to secure the proper relationship between the two components of equation (4). A large upfloating angle (indicated by large C_{h_o}) and a rapidly increasing difference between the mechanical advantages of the two ailerons make for the displacing tendency, whereas a large slope of the hinge-moment curve and a large average mechanical advantage of both ailerons (large $d\delta/d\theta$) make for a large restoring force. If the control stick is to tend to return to neutral when displaced, C_{h_s} must be at least slightly negative.

An examination of the hinge-moment curve (fig. 1) will show that the balancing effect of the differential can be simply described in terms of the work of deflecting the ailerons. Work is gained by allowing the aileron to rise. The resultant work is found by deducting that exerted on the down side from that gained on the up side. The two components are represented by the areas under the hinge-moment curve on either side of neutral. The formula for the resultant work is

$$C_{h_o}\ \delta_d + \frac{dC_h}{d\delta} \frac{\delta d^2}{2} - C_{h_o}\ \delta_u + \frac{dC_h}{d\delta} \frac{\delta u^2}{2} \qquad (5)$$

If the work of deflection is made zero at every point, the stick force (which may be calculated as the slope of the curve of work against deflection) will also be zero at every point. Hence an idealized differential motion of the ailerons that gives complete balance may be calculated by means of this expression for the work of deflection. By equating the work to zero and rearranging

$$\delta_d = \frac{-C_{h_o} \pm \sqrt{{C_{h_o}}^2 - \frac{dC_h}{d\delta}\left[\frac{dC_h}{d\delta}\ \delta u^2 - 2C_{h_o}\ \delta_u\right]}}{\frac{dC_h}{d\delta}} \qquad (6)$$

If C_{h_o} and $dC_h/d\delta$ are known, this formula may be used to calculate the simultaneous upward and downward positions of the ailerons for which the work of deflection is zero. A differential linkage arranged to give these simultaneous positions of the ailerons would thus require no operating effort.

A decidedly simpler formula than (6) results if the aileron characteristics C_{h_o} and $dC_h/d\delta$ are expressed in terms of the upfloating angle

$$C_{h_o} \frac{d\delta}{dC_h} = \delta_{uf} \tag{7}$$

(See fig. 1.) The resultant formula is

$$\delta_d = \sqrt{(\delta_{uf} + \delta_u)^2 - 2\delta_u{}^2} - \delta_{uf} \tag{8}$$

The ratio of the rates of travel of the two ailerons is simply

$$\frac{d\delta_d}{d\delta_u} = \frac{(\delta_{uf} - \delta_u)}{(\delta_{uf} + \delta_d)} \tag{9}$$

(Note that δ_{uf}, δ_u, and δ_d are taken as positive numbers.) Curves of such idealized differential motions for ailerons having different floating angles are shown in figure 2. It is probable that a number of more or less complicated mechanical linkages that would give the ailerons motions approximating these curves could be devised. The ordinary simple linkage consisting of two properly set cranks connected by a rod is of most interest, however, and the following discussion is devoted chiefly to the problem of approximating the limiting degree of balance with such a simple arrangement.

METHOD OF APPROXIMATING LIMITING DEGREE OF BALANCE

The preceding discussion led to the determination of curves of aileron deflection giving zero stick force derived without reference to the limitations of mechanical linkages. Although the discussion was confined to ailerons showing a straight-line hinge-moment variation, the procedure of deriving a curve similar to those of figure 2

for the case of a more irregular hinge-moment variation will be obvious. Once the limiting curve showing the deflections that result in zero operating force is determined, it becomes necessary to devise a geometrical arrangement of levers that will approximate this motion.

Although it is not thought desirable completely to eliminate the control force at any flight condition, it is useful to consider this condition as a limiting adjustment of the differential. In a given case the stick force can be balanced out at only one angle of attack and, since the floating angle becomes smaller, the effectiveness of the balancing diminishes as the angle of attack is reduced. Hence if the stick force is made to become zero at an angle of attack higher than normally encountered in flight, overbalance of the control in normal flight will be guarded against and, at the same time, the greatest permissible reduction of control force will be approached.

The ideal curves given in figure 2 cannot, of course, be exactly reproduced by a simple mechanical linkage. Figure 3 illustrates the simplest type of linkage used in practice. Movement of the control causes the stick cranks to move oppositely through equal angles $\Delta\theta$ from their neutral positions. The diagram shows the downgoing crank in the dead-center position. Figure 4 illustrates the computation of the mechanical characteristics of such a simple linkage. Here it is assumed that the lengths of the various levers are known. The formula then gives δ in terms of θ.

Such linkages can be adjusted to give aileron movements similar to those shown in figure 2 and can, in fact, be made to satisfy as many as four conditions in approaching such a curve, since four independent adjustments of the linkage may be made. The reduction of the stick force to zero at four points would, however, eliminate all possible linkages but one and would require a definite spacing of the crank centers and definite radii of the cranks, as well as specific neutral settings.

When trying to approximate the ideal differential motion by means of a simple mechanical linkage, it is not feasible to satisfy all the possible conditions. If only two minimizing conditions are imposed on the stick-force curve, it may be ascertained that the differential chosen is reasonably near the limiting one and, at the same time, an arbitrary choice of two of the geometric parameters of

the linkage may be made. The spacing of the crank centers and the relative radii of the two cranks may therefore be left to be dictated by other considerations.

Figure 5 shows a type of stick-force curve that satisfies two very simple criterions. First, the slope of the curve is zero at the beginning of the deflection; and, second, the force is zero at a deflection of the up aileron equal to the floating angle. The last criterion is satisfied by arranging for the downgoing aileron to reach dead center at this point or, algebraically expressed,

$$(\delta_u)_{\delta_d=\delta_{d_{max}}} = \delta_{uf} \tag{10}$$

In order to show how the first of the two criterions may be satisfied, it will be necessary to calculate the slope of the stick-force coefficient curve at zero deflection ($\theta = \theta_N$). If there is an infinitesimal displacement of the control from neutral, the difference of the mechanical advantages of the two ailerons will be

$$2d\ \theta\ \frac{d^2\delta}{d\theta^2} \tag{11}$$

This difference multiplied by the initial or offset hinge moment (C_{h_o}) will give the infinitesimal displacing moment at the start of the deflection. The changes of aerodynamic hinge moment, $d\delta_u \frac{dC_h}{d\delta}$ and $d\delta_d \frac{dC_h}{d\delta}$, do not contribute to this quantity. The restoring or stabilizing tendency for infinitesimal deflection is simply

$$2d\ \theta\ \frac{d\delta}{d\theta}\ \frac{dC_h}{d\delta}\ \frac{d\delta}{d\theta} \tag{12}$$

Here the infinitesimal changes of mechanical advantages play no part. The starting slope of the curve is then

$$\left(\frac{dC_{h_s}}{d\theta}\right)_{\theta=\theta_N} = 2\left[\frac{dC_h}{d\delta}\left(\frac{d\delta}{d\theta}\right)^2 - C_{h_o}\frac{d^2\delta}{d\theta^2}\right] \tag{13}$$

Since $C_{h_o} = \delta_{uf}\frac{dC_h}{d\delta}$ this result may be expressed

$$\left(\frac{dC_{h_s}}{d\theta}\right)_{\theta=\theta_N} = 2\frac{dC_h}{d\delta}\left[\left(\frac{d\delta}{d\theta}\right)^2 - \delta_{uf}\frac{d^2\delta}{d\theta^2}\right]_{\theta=\theta_N} \tag{14}$$

The condition for zero initial slope is then simply

$$\left(\frac{d\delta}{d\theta}\right)^2_{\theta=\theta_N} = \delta_{uf}\left(\frac{d^2\delta}{d\theta^2}\right)_{\theta=\theta_N}$$

(Note that δ_{uf} must now be expressed in radian measure.)

CHARTS FOR SELECTION OF LIMITING DIFFERENTIAL

It will be noted that the only characteristic of the ailerons appearing in either of the two criterions is the floating angle δ_{uf} (neglecting the implied assumption of a straight-line hinge-moment variation). It thus appears that the choice of differential as defined by these two criterions depends only on the floating angle. With the essential aileron characteristics thus limited, it was found feasible to make a series of calculations that would show the adjustment of a differential necessary to satisfy both criterions for a minimum stick force.

Figure 6 shows the results of such a series of calculations. This chart shows directly the angular settings of stick and aileron cranks to be used for a given up-floating angle at several spacings of the crank centers. It was assumed that the cranks were of equal radius. The maximum down-aileron deflection is shown in each case and it is to be noted that, if the maximum deflection of the upgoing aileron exceeds the floating angle, the down aileron will pass beyond dead center and return toward neutral. Since a differential selected by means of these charts will give what amounts to complete balance at the flight condition corresponding to the assumed floating angle, it is essential that this angle be at least as large as the maximum encountered in flight, which, as might be expected, usually occurs at or beyond maximum lift.

IMPROVEMENT OF BALANCE AT LOW ANGLES OF ATTACK BY MEANS OF A FIXED TAB

It is evident that the same degree of balance cannot be attained at all flight speeds with any type of differential, inasmuch as the floating angle varies. At higher speeds the degree of balance becomes less and the control

force correspondingly greater. Calculations have shown, however, that a considerable advantage usually accures to the differential system even at the highest flight speeds.

Although the possibility of securing complete balance at any one flight condition does not depend to a great extent on the characteristics of the aileron, modification of these characteristics can be very effective in improving the balance over a range of flight conditions. Thus, an aileron that shows only a small variation of floating angle over the flight range will be nearly ideally balanced under all conditions.

Wing-section theory indicates that the floating tendency of a flap may be characterized by two effects, namely:

1. A constant floating tendency due to camber of the airfoil and influenced mainly by the degree of camber near the flap trailing edge. This effect varies with the flap chord and is measured by the floating angle at zero lift of the airfoil.

2. A floating tendency varying with angle of attack of the wing section. This effect is the same for all airfoil shapes but varies with flap chord.

It is the latter tendency that is significant in causing the undesirable increase in stick force as the angle of attack is reduced. In general, the variation of floating angle with angle of attack can be reduced by reducing the chord of the aileron. This procedure, however, reduces the maximum floating angle in proportion so that the change in percentage with angle of attack remains about the same. Wind-tunnel tests show that a large constant floating effect can be produced by a relatively small camber of the trailing edge of the aileron (e.g., by a tab). The most nearly ideal arrangement for balance would thus incorporate a bent trailing-edge tab with an aileron of small chord.

Figure 7 shows the variation of floating angle with flap chord and angle of attack. The angles shown were computed by finding the moments of the pressure acting on rear portions of Clark Y and N.A.C.A. 23012 wing sections (reference 1 and unpublished data). This procedure gave the hinge moments at zero deflection and the floating angles were computed therefrom by using an empirical value of the slope of the hinge-moment curve $\left(\frac{dC_h}{d\delta} = -0.0085\right)$.

Figure 8 shows results of experiments (reported in reference 2) with a 2.5-percent c_w tab on a 25-percent-c_w aileron. Deflecting the tab 10° had the effect of nearly doubling the maximum floating angle. The undesirable variation of floating angle with angle of attack, expressed in terms of percentage of the maximum, decreased accordingly. Figure 9 summarizes the results of some experiments made with tabs in the N.A.C.A. 7- by 10-foot wind tunnel.

CALCULATED EXAMPLE

Some calculations have been made to illustrate the application of the principles discussed. The results are summarized in figure 10, which shows the reduction of operating force that can be attained with a suitable differential both with and without a fixed tab. The chart has as ordinate the resultant moment coefficient acting at the control-stick crank divided by the lift coefficient $-\Sigma C_h/C_L$. This quantity is taken as a measure of the operating force. Division by the lift coefficient is made to take account of the increase in dynamic pressure corresponding to a reduction in angle of attack of steady flight. The abscissa represents a measure of the deflection of the control and is the computed angle of bank that a small average airplane (1,600 pounds) would attain in 1 second after the instantaneous partial deflections of the ailerons thus indicated. Such a conversion was necessary in order to compare equal up-and-down deflections with various degrees of differential movement of the ailerons on an impartial basis. Such deflections are thus measured by the banking effect they produce. The computation of banking effect is given in reference 3 by a simple formula,

$$\phi_1 = \left(\frac{\partial \phi_1}{\partial C_l}\right) C_l + \left(\frac{\partial \phi_1}{\partial C_n}\right) C_n \qquad (16)$$

where $\left(\frac{\partial \phi_1}{\partial C_l}\right)$, etc., are constants for a given airplane at a given flight speed. The curves of aileron hinge moment given in figure 8 were used and data on the rolling- and yawing-moment coefficients were taken from reference 4. As no limit was set on the maximum deflection of the control and no gearing ratio of the control stick to the stick crank of the differential was assumed, the values given are only comparative. The maximum degree of control

usually shown by airplanes of this size corresponds to $\phi_1 = 20°$ or $25°$ at a lift coefficient of 1.0.

The top pair of curves of figure 10 was computed for equal up-and-down ailerons without balance of any kind. The middle pair of curves shows the degree of balance that can be attained by a differential linkage without modification of the aileron floating characteristics. The differential linkage was selected with the aid of the chart (fig. 6). A crank spacing of four times the crank radius (R = 1/4) was assumed. The floating angles of the aileron without the tab are indicated in figure 8. Since the maximum floating angle in this condition was only 12°, the downward deflection of the ailerons was limited to slightly under 5°. (See fig. 6.) Thus a reversal of the motion of the down aileron occurred at this angle. Further deflection of the system then gave reduced control effectiveness and resulted in the sharp upward sloping of the stick-force curve ($C_L = 1.0$) that is apparent near $\phi_1 = 22°$. It appears that, in general, the best results will be obtained when the maximum deflection permitted does not greatly exceed this reversal point.

The bottom pair of curves of figure 10 gives an indication of the remarkable effect of a small fixed tab. The tab and deflection assumed (2.5 percent wing chord, down 10°) would give the trailing edge of a 5-foot-chord wing a downward displacement of only 1/4 inch. This modification served to increase the maximum floating angle of the ailerons from 12° to 20°, thereby permitting the use of a differential with a greater maximum downward deflection. It will be noted, in addition, that the stick force required for control at high speed ($C_L = 0.35$) is much less, and is also more nearly coincident with the force required at low speed ($C_L = 1.0$), than was the case with the unmodified ailerons. The beneficial effect of a fixed tab would be expected to be even more apparent in the case of narrow-chord ailerons.

Inasmuch as the floating angles corresponding to 15° angle of attack (fig. 8) were used in the selection of the differentials, the control will begin to show overbalance at this angle of attack. The form of the curves of stick force against deflection will be similar to those given but the curve will lie more nearly along the axis.

One difficulty that might arise in practice was brought out in the sample computation given. Here, in the

case of the aileron without the tab, the maximum upfloating angle was less than the maximum angle of deflection that might be required for control. The down aileron will, in this case, reverse its motion before the maximum deflection of the control stick is reached. It was observed in the computation that the stick-force curve rose sharply after this deflection was reached, showing that further deflection of the system was inefficient. The differential selected on the basis of the given assumptions was such as to impose a minimizing condition at this deflection. It is evident that a slightly different linkage might give better results at higher deflections; hence it might have been better to have chosen a different criterion. In such a case it would be advisable to make several trial computations, assuming fictitious floating angles higher than the actual angle. The desirability of keeping the maximum deflection of the stick cranks low should be especially emphasized. Since the maximum angular travel of the control stick or wheel is naturally limited, a large deflection of the stick crank of the differential means that the pilot will have to operate the system at a large mechanical disadvantage. When a deflection such that the down aileron reverses its motion is reached, further deflection does not cause the control rolling moment to increase very rapidly; hence a relatively larger maximum deflection will be needed for the requisite amount of control than would be the case if the reversal did not occur.

Wind-tunnel experiments show that the floating angles of ailerons are considerably influenced by insignificant details of construction. It is difficult, for instance, to establish any definite relation between the floating angle and the chord of a flap from small-scale wind-tunnel observations. The presence of a gap between the aileron and wing affects the floating angle and is also known to be decidedly detrimental to control. Furthermore, motions of the airplane such as rolling or sideslipping affect the pressure on the ailerons and thereby change the action of the differential to some extent. In view of these considerations, it would seem advisable to incorporate in differential ailerons either an adjustable tab or a deformable trailing edge so that unpredictable defects of the system may be remedied during trial.

Langley Memorial Aeronautical Laboratory,
National Advisory Committee for Aeronautics,
Langley Field, Va., November 13, 1936.

REFERENCES

1. Wenzinger, Carl J.: Pressure Distribution over an Airfoil Section with a Flap and a Tab. T.R. No. 574, N.A.C.A., 1936.

2. Harris, Thomas A.: Reduction of Hinge Moments of Airplane Control Surfaces by Tabs. T.R. No. 528, N.A.C.A., 1935.

3. Weick, Fred E., and Jones, Robert T.: The Effect of Lateral Controls in Producing Motion of an Airplane as Computed from Wind-Tunnel Data. T.R. No. 570, N.A.C.A., 1936.

4. Weick, Fred E., and Wenzinger, Carl J.: Wind-Tunnel Research Comparing Lateral Control Devices, Particularly at High Angles of Attack. I - Ordinary Ailerons on Rectangular Wings. T.R. No. 419, N.A.C.A., 1932.

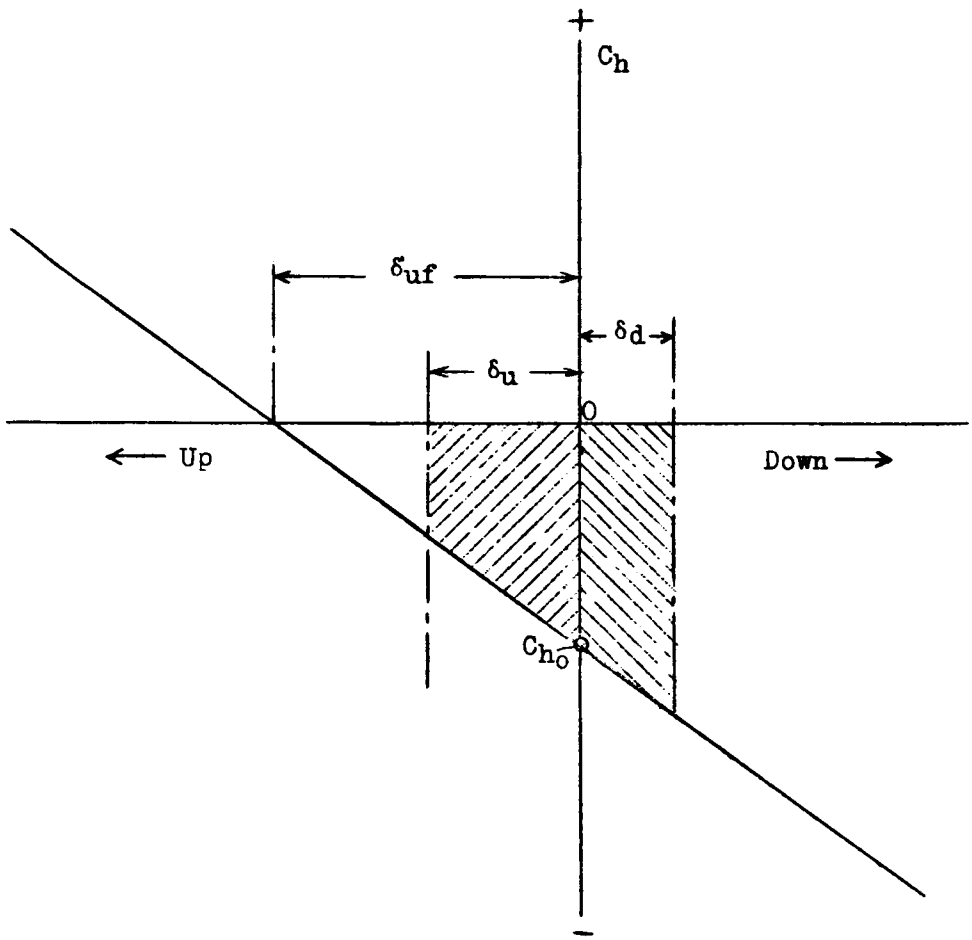

Figure 1.- Plot of aileron hinge-moment coefficient showing work of deflection.

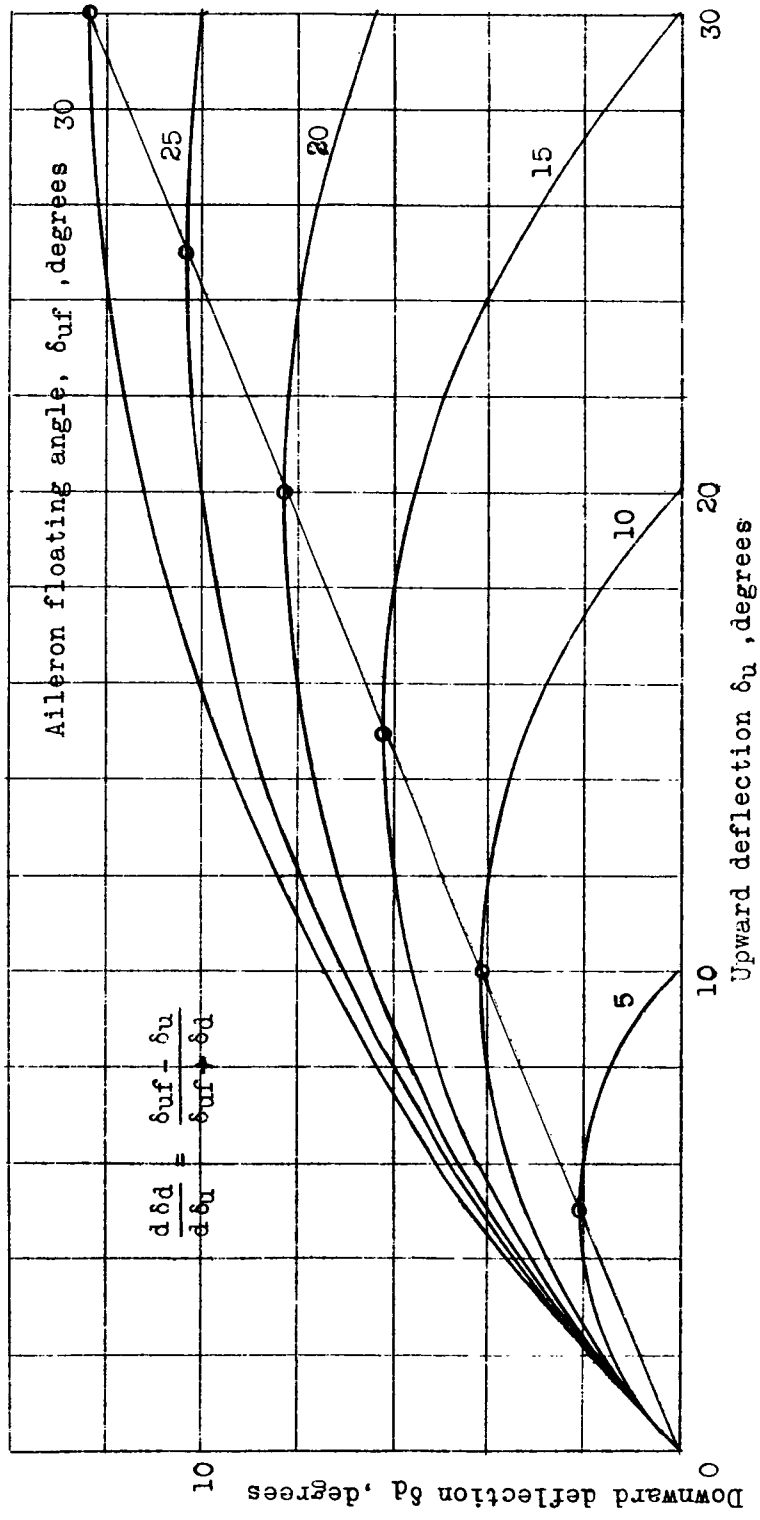

Figure 2.- Simultaneous positions of ailerons for which the work of deflection is zero.

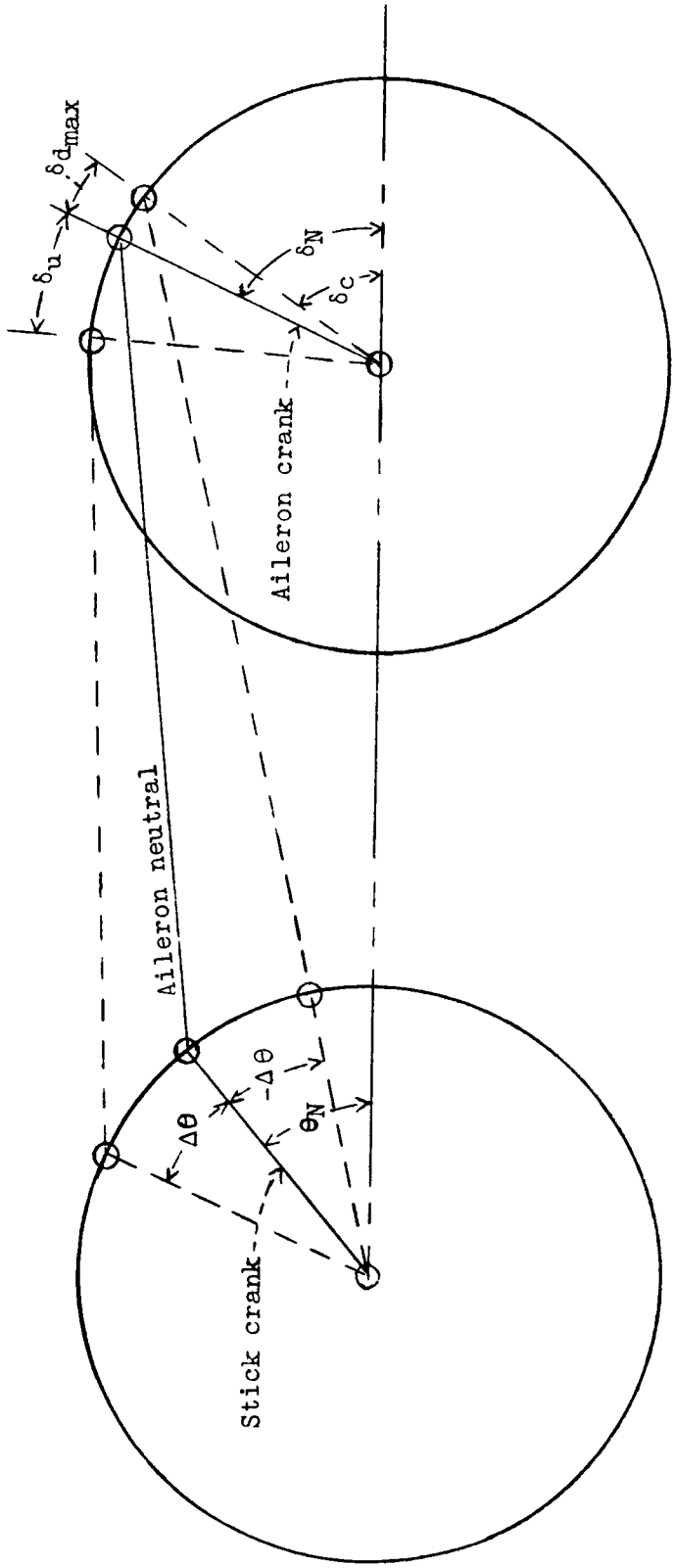

Figure 3.- Diagram representing simple differential linkage.

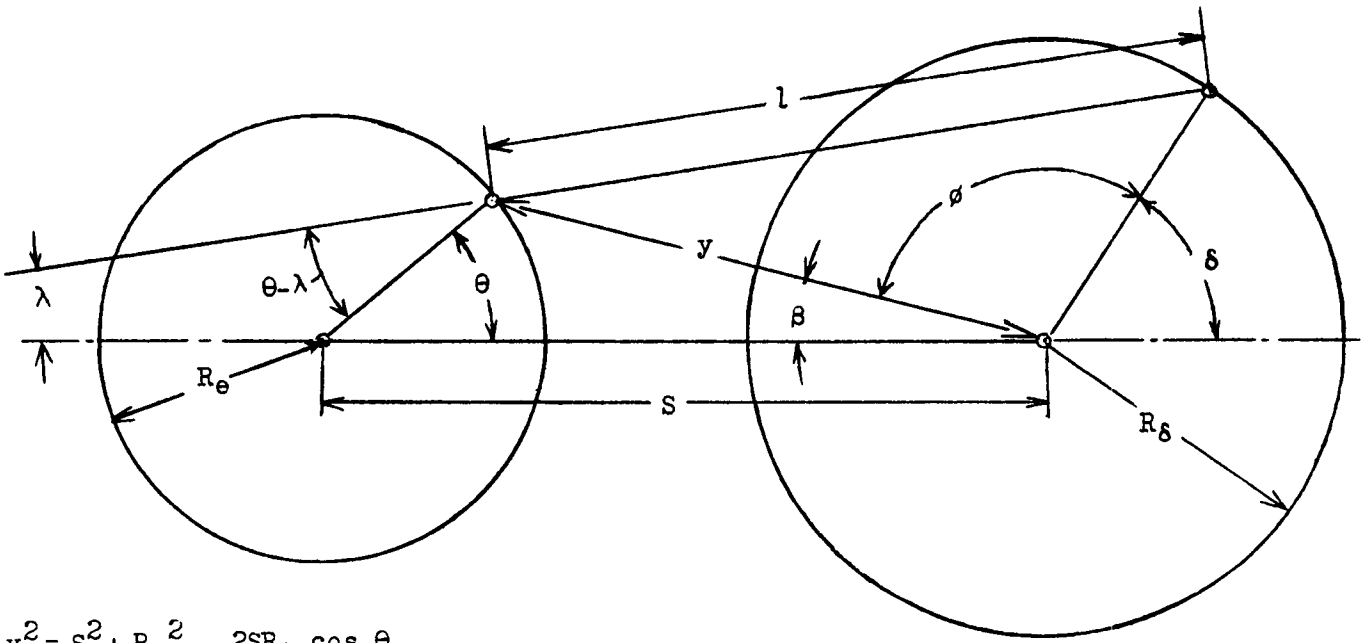

$$y^2 = S^2 + R_e^2 - 2SR_e \cos\theta$$

$$\sin\beta = R_e \sin\theta / y$$

$$\cos\phi = (y^2 + R_\delta^2 - l^2) / 2yR_\delta$$

$$\delta = 180^\circ - (\beta + \phi)$$

$$\sin\lambda = (R_\delta \sin\delta - R_e \sin\theta) / l$$

$$\frac{d\delta}{d\theta} = \frac{R_e}{R_\delta} \frac{\sin(\theta-\lambda)}{\sin(\delta-\lambda)}$$

Note: S , l , R_e , R_δ are assumed to be known: θ is then varied as desired and the corresponding values of δ are found.

Figure 4.- Diagram and formulas for calculating the characteristics of a differential linkage.

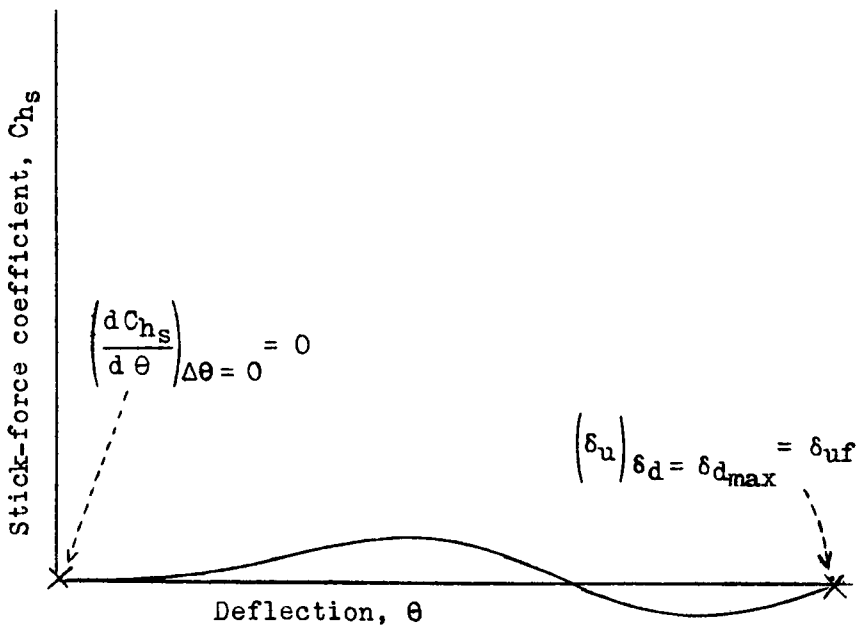

Figure 5.- Type of curve that satisfies simple criterions for minimum stick force.

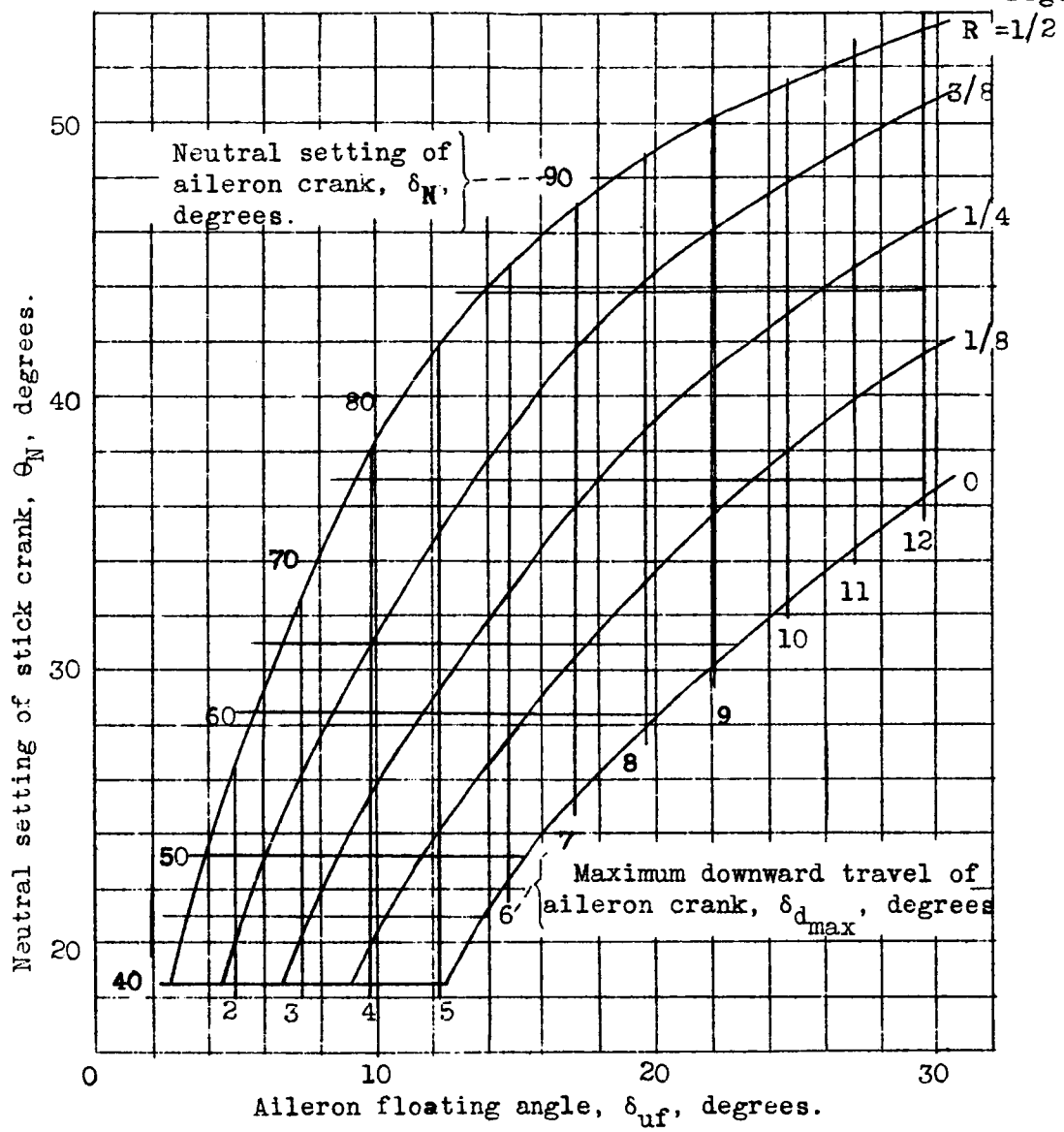

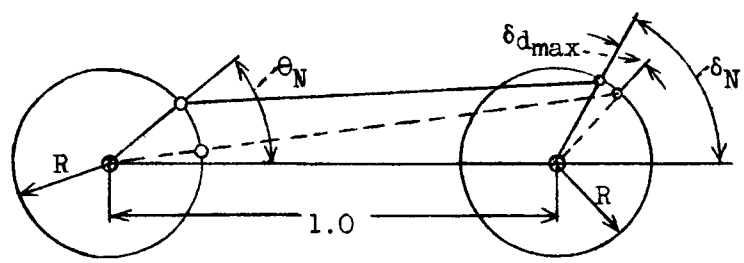

Figure 6.- Specifications of differentials that satisfy criterions for minimum stick force: $(dC_{h_s}/d\theta)_{\theta=\theta_N} = 0$; $(\delta_u)_{\delta_d=\delta_{d_{max}}} = \delta_{uf}$.

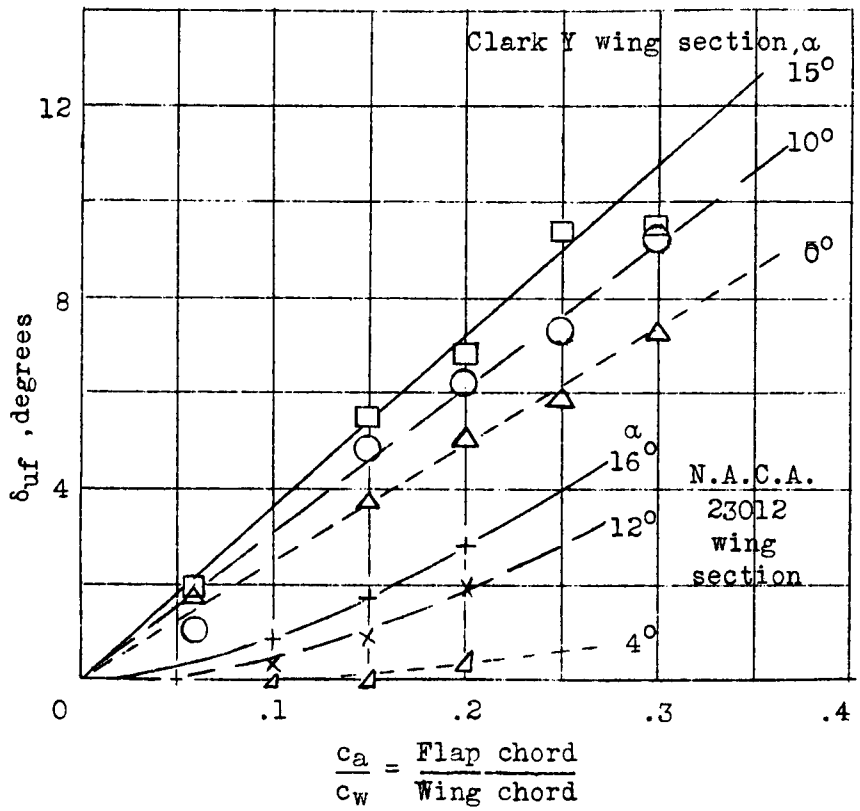

Figure 7.- Floating angles of flaps of different chords computed from pressure-distribution measurements.

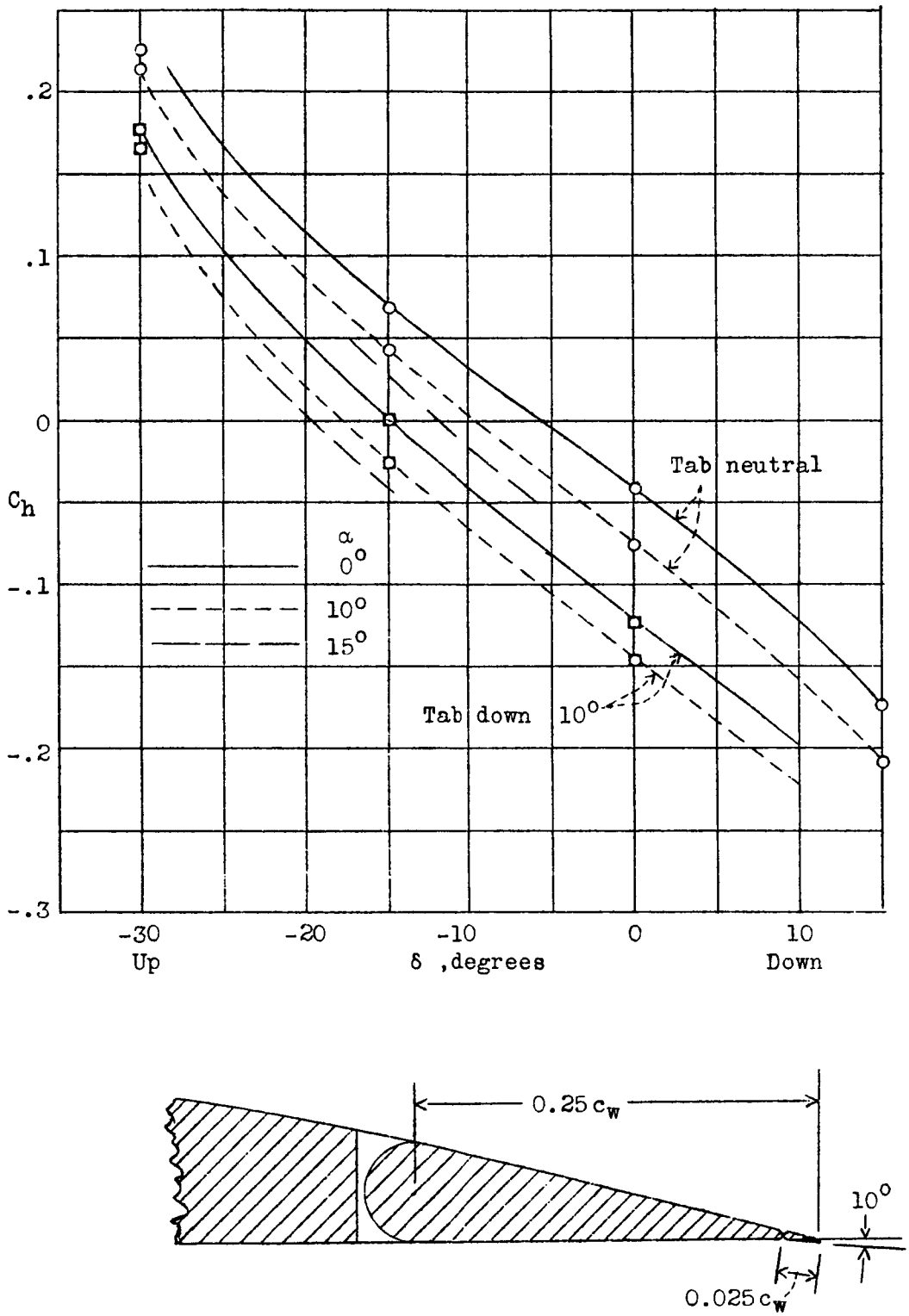

Figure 8.- Hinge-moment coefficients of aileron with tab. (reference 2).

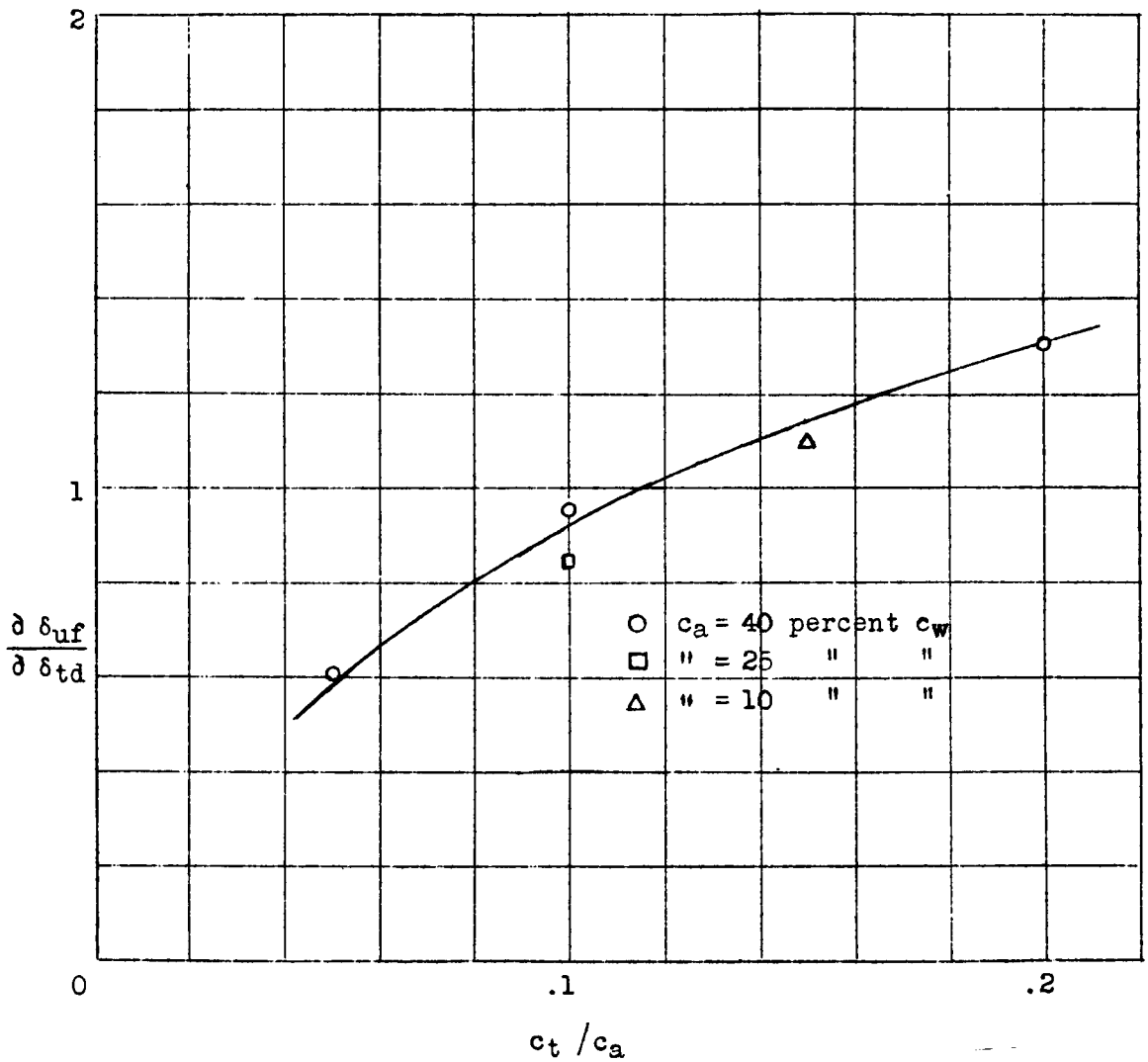

Figure 9.- Effect of tabs on aileron floating angles at small deflections ($\delta_t < 15^o$); 7 by 10 foot wind tunnel experiments.

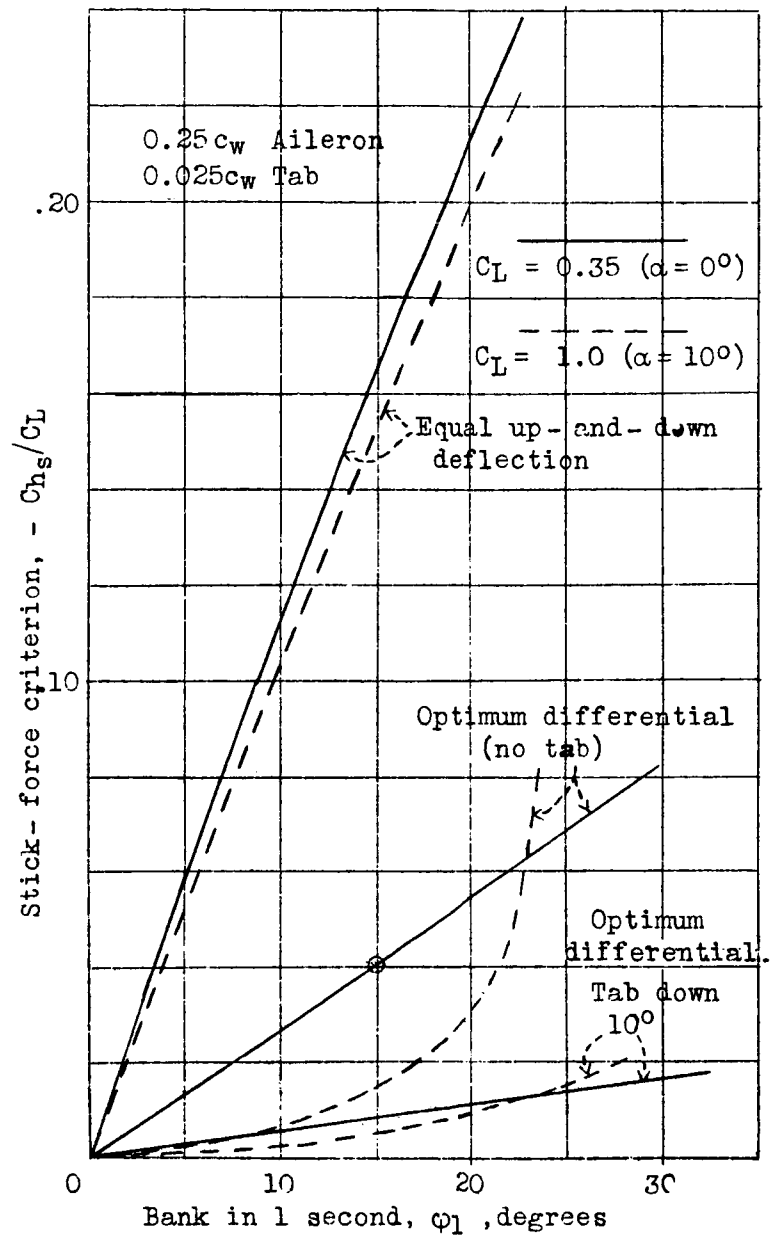

Figure 10.- Example showing reduction of stick force accomplished by suitable differential. The effect of a tab deflected downward to increase the floating angle is also shown.

REPORT NO. 605

RÉSUMÉ AND ANALYSIS OF N.A.C.A. LATERAL CONTROL RESEARCH

Fred E. Weick and Robert T. Jones

Langley Memorial Aeronautical Laboratory

1937

REPORT No. 605

RÉSUMÉ AND ANALYSIS OF N. A. C. A. LATERAL CONTROL RESEARCH

By Fred E. Weick and Robert T. Jones

SUMMARY

An analysis of the principal results of recent N. A. C. A. lateral control research is made by utilizing the experience and progress gained during the course of the investigation. Two things are considered of primary importance in judging the effectiveness of different control devices: The (calculated) banking and yawing motion of a typical small airplane caused by a deflection of the control, and the stick force required to produce this deflection. The report includes a table in which a number of different lateral control devices are compared on these bases.

Experience gained while testing various devices in flight with a Fairchild 22 airplane indicated that, following a sudden deflection of the control at low speed, an angle of bank of 15° in 1 second represented a satisfactory minimum degree of effectiveness for this size of airplane. Some devices capable of giving this degree of control were, however, considered to be not entirely satisfactory on account of sluggishness in starting the motion. Devices located near the trailing edge of the wings had no detectable sluggishness. Lateral control forces considered desirable by the test pilots varied from 2 to 8 pounds; 15 pounds was considered excessive.

Test flights demonstrated that satisfactory lateral control at high angles of attack depends as much on the retention of stability as on aileron effectiveness.

The aerodynamic characteristics of plain sealed ailerons could be accurately predicted by a modification of the aerodynamic theory utilizing the results of experiments with sealed flaps. Straight narrow-chord sealed ailerons covering 60 to 80 percent of the semispan represented about the most efficient arrangement of plain unbalanced ailerons from considerations of operating force. The stick force of plain ailerons can be effectively reduced by the use of a differential linkage in conjunction with a small fixed tab arranged to press the ailerons upward.

INTRODUCTION

In 1931 the Committee started a systematic wind-tunnel investigation of lateral control with special reference to the improvement of control at low air speeds and at high angles of attack. Many different ailerons and other lateral control devices have been subjected to the same systematic investigation in the 7- by 10-foot wind tunnel. (See reference 1.) The devices that seemed most promising were tested in flight (references 2 and 3). In many cases, however, devices that produced what seemed to be satisfactory rolling moments and favorable yawing moments did not give satisfactory control.

An analytical study of control effectiveness was therefore made (reference 4) taking into account a number of secondary factors, including the yawing moments produced by the controls, the effect of the controls on the damping in rolling, the lateral-stability derivatives of the airplane, the moments of inertia, and the time required for the control moments to become established after the deflection of the surfaces. The computations consisted of step-by-step solutions of the equations of rolling and yawing motion for the conditions following a deflection of the controls. The results of these computations based on aerodynamic data obtained from wind-tunnel tests of wings incorporating various devices agreed satisfactorily with the results measured in flight for widely different forms of control, such as ailerons and spoilers.

The study of conditions above the stall indicated that satisfactory control could not be expected without some provision to maintain the damping in rolling and that a dangerous type of instability would arise if the damping were insufficient. Since damping in rolling depends on an increase in the lift of the airfoil with increasing angle of attack, it follows that, in order to obtain satisfactory lateral control, the outer or tip portions of the wing, which govern the rolling moments, must remain unstalled. If damping in rolling is retained, it is practically insured that control moments will be retained as well.

The progress of the investigation has thus led to a more accurate interpretation of the results of the wind-tunnel tests. In the present paper the experience gained during the course of the investigation is made the basis of a revised method of comparison of lateral control devices. Wind-tunnel measurements of control and stability factors (reference 1) are utilized in computations to show the banking and yawing motions that would be produced by the controls acting on a small typical airplane. These computations follow the method of analysis given in reference 4. In section I of the report the new basis of comparison is explained and

a number of the devices that were tested in reference 1 are analyzed and compared. The principal items of comparison are collected into a table. Section II presents an analysis of the rolling, yawing, and hinge moments of plain flap-type ailerons and deals with the application of these data in the design of control systems.

I. COMPARISON OF LATERAL CONTROL DEVICES

REVISED BASIS OF COMPARISON

AIRPLANE USED IN COMPARISON

The procedure adopted in the lateral control investigation has comprised a wind-tunnel test program followed by flight tests of the different devices on the Fairchild 22 airplane. Not all of the devices tested in reference 1 have been tried in flight, however, and the present report may be considered an analytical extension of the flight-test procedure that was applied to some of the devices. The procedure employed to test lateral controls in flight is simulated by means of computation. Thus, the comparative criterions used herein are based on application of the devices to a hypothetical Fairchild 22 type of airplane, which is the type used in the flight tests.

The Fairchild 22 airplane was necessarily somewhat modified for each different flight test and wings of different moment of inertia, plan form, and section were used in some cases. The wing of the hypothetical airplane assumed in the computations represents an average of the tested wings. Furthermore, since the characteristic ratios of dimensions (tail length, tail area, radii of gyration about various axes, etc.) used agree very closely with statistical averages of these quantities, the assumed airplane may be considered to embody average stability characteristics. The principal characteristics of the assumed airplane are as follows:

Weight, W	1,600 lb.
Wing span, b	32 ft.
Wing area, S	171 sq. ft.
Wing loading, W/S	9.4 lb. per sq. ft.
Area of fin and rudder	10.8 sq. ft.
Tail length	14.6 ft.
I_X	1,216 slug-ft.^{2}
I_Z	1,700 slug-ft.^{2}

ROLLING ACTION

It is recognized that different types of airplanes require different amounts of control. At the start of the wind-tunnel investigation of lateral control devices (reference 1) a rolling criterion ($RC=C_l/C_L$) representing a conservative lower limit of rolling control for all types was assumed. The assumed satisfactory value of the rolling criterion was 0.075, which corresponds to a lateral movement of the center of pressure of 7.5 percent of the wing span. Recent experience indicates that this value is likely to be ample for any condition of flight that might be encountered and is therefore a desirable value to attain. Where a compromise must be made between the rolling moment and some other characteristic of the control system, particularly the control force, a decidedly lower value of the rolling criterion may be used. It appears that a value possibly as low as half the original one may be found reasonably satisfactory for practically all conditions of flight with nonacrobatic airplanes.

The criterion of rolling control used in the present analysis is the angle of bank attained in 1 second following a sudden deflection of the control. This criterion shows the actual amount of motion produced and depends on both the acceleration at the start and the final rate of roll. It includes the effect of yawing moment given by the control as well as the stability characteristics and moments of inertia of the airplane. The values of the criterion are found by computation and as such are applicable only to the particular type of airplane (F–22) that has been assumed.

Experience gained in flight tests of the Fairchild 22 airplane with various lateral control devices indicated a minimum satisfactory amount of rolling control corresponding to about 15° of bank in 1 second. (See fig. 1.) Ailerons capable of giving this amount of bank

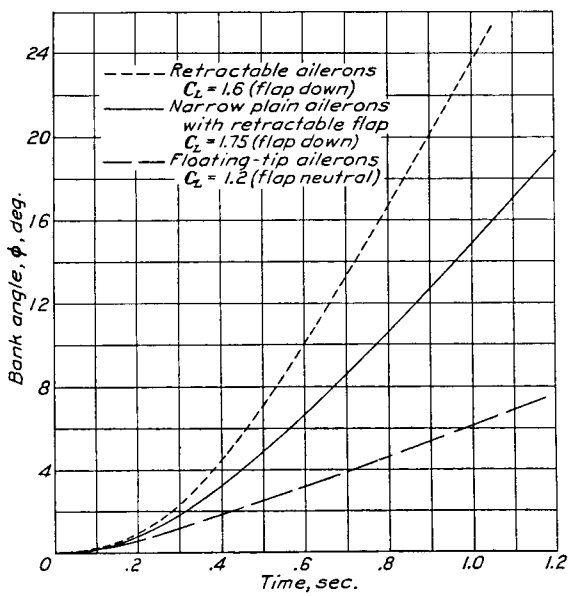

FIGURE 1.—Banking of Fairchild 22 airplane after sudden deflection of lateral control devices at low speed. (The narrow plain ailerons and the retractable ailerons were considered to give a satisfactory amount of control; the floating-tip ailerons were reported as weak.)

at low speed have been found reasonably satisfactory in practice with this type of airplane. Owing to the present general use of high-lift flaps on airplane wings, the size and deflection of ailerons are usually determined by the low-speed condition of flight with the flaps deflected. For comparative computations, in the present report, a lift coefficient of $C_L=1.8$ is assumed as representative of the low-speed condition of flight with

flaps. The sizes or deflections of the lateral controls are selected in each case to give an angle of bank of 15° in 1 second at C_L=1.8.

In addition to providing a sufficient amount of banking motion, two further desirable characteristics of the rolling action are: (1) The response of the airplane in roll to any movement of the lateral control surface should be immediate, any noticeable delay or hesitation in the action being objectionable; and (2) the action should be so graduated that the acceleration and maximum rate of roll increase smoothly and regularly as the stick deflection is increased. Conventional ailerons or similar lateral control devices located near the trailing edge of the wing easily meet these requirements and show, in analyses of motions recorded in flight, practically instantaneous response of rolling acceleration to control-surface movement. From 0.1 to 0.2 second is ordinarily required to deflect the surfaces and, during this interval, the rolling acceleration apparently keeps pace, although only a slight amount of rolling motion is accumulated by the time of full deflection. Comparison shows that good synchronization of the calculated motion with the flight records was obtained when the assumed full deflection was taken at the instant the actual deflection reached half its ultimate value. This assumption was used in the computations for plain ailerons and other devices that gave no indication of sluggish response characteristics.

CONTROL FORCE

During the course of the lateral control investigation it became apparent that the force required to move the controls is of extreme importance in obtaining satisfactory lateral control. As shown by the flight tests of references 2 and 3, an airplane that requires a light control force is likely to seem more controllable to a pilot than one that requires a heavy control force, even though with full deflection the heavier control may be considerably more powerful than the lighter one. It seems desirable to have the control force as light as possible and yet to maintain the feeling of a definite neutral position. This characteristic is especially important in the aileron control since the effort expended in moving the stick sidewise is relatively greater than for other control movements. (See reference 5.) Correlation of test-flight reports and control-force records indicates that the forces required to operate the ailerons should not exceed about 8 pounds in order to be considered desirable. A lower limit of stick force of about 2 pounds at full deflection is apparently considered essential so that there may be a noticeably regulated increase of force with deflection. Friction of the control mechanism plays an increasingly important part as the operating force is reduced and should in no case be great enough to mask the "feel" of the control. It is probable that with sufficiently little friction a force not greatly in excess of 2 pounds would be considered most desirable. A force of 15 pounds is to be considered excessive.

As previously stated, the size or maximum deflection of the control devices compared in this paper have been selected to give an angle of bank of 15° in 1 second following full deflection and, considering the average airplane fitted with a high-lift flap and flying at a lift coefficient of 1.8, the ailerons are compared (see table I) on the basis of the stick force required to attain this angle of bank of 15° in 1 second at lift coefficients of 0.35, 1.0, and 1.8, which compose the usual flight range. The lift coefficient of 0.35 represents the conditions of high-speed and cruising flight. The lift coefficient of 1.0 is considered to represent two conditions, the first being that of low-speed flight without a flap, such as is used in an approach to a landing with an unflapped airplane, and the second being one with a flap fully deflected, which represents as high a speed as is usually attained in that condition. The value C_L=1.8 can be obtained only with the flap deflected and represents the low-speed flight condition with the high-lift device in use. When representative values of this nature are used, it is necessary to examine the complete original data to show that the critical values are representative of conditions throughout the flight range. Such an examination has been made for the comparisons of the present report.

The stick force for a 15° bank in 1 second is used as the basis of comparison at all flight speeds and lift coefficients even though the conventional ailerons will produce a decidedly greater bank in 1 second at higher speeds. The 15° value is taken throughout because it is considered to represent the maximum control likely to be used in ordinary flight at any speed and is therefore of greater interest as a basis for stick forces required than the maximum possible deflection, as long as the force at maximum deflection does not approach the strength of the pilot.

The data for some of the ailerons were obtained with plain unflapped wings with which a lift coefficient of 1.8 could not be attained and, in order to have all the lateral control devices on a comparable basis whether mounted on flapped or unflapped wings, their sizes and maximum deflections were selected to give essentially the same rolling effect as the others at a lift coefficient of 1.0. The analysis showed that conventional ailerons which give an angle of bank of 15° in 1 second on a flapped wing at a lift coefficient of 1.8 could, when fully deflected, give an angle of bank of 22.5° with the flap retracted at a lift coefficient of 1.0. The ailerons on the unflapped wings were therefore selected to be capable of giving 22.5° bank in 1 second at a lift coefficient of 1.0, but the values of the stick forces required were computed for partial deflections giving a 15° bank in 1 second at lift coefficients of both 1.0 and 0.35. The first aileron of table I is of the conventional unbalanced flap type on a rectangular wing of aspect ratio 6. It has a chord 0.25 c_w and a span 0.40 $b/2$ and has equal

up-and-down linkage. It will be noted that, for an airplane equipped with these ailerons, the stick force computed for a 15° bank in 1 second at the cruising-flight condition is 4.7 pounds with aileron deflections of only ±3.4°. At a lift coefficient of 1.0, representing the low-speed flight condition for the unflapped wing, the same amount of control was obtained with a stick force of 3.6 pounds and aileron deflections of ±7.4°. All the stick forces are given for an assumed aileron linkage such that at the maximum deflection the control stick, which has a length of 20 inches on the Fairchild 22 airplane and is so assumed for the average airplane, is deflected 25° from neutral. The maximum aileron deflection is 11.2° and is the deflection required to produce a bank of 22.5° in 1 second at $C_L=1.0$. Here the ailerons are not being taxed to their fullest extent.

The maximum amount of control specified in a design has a predominating effect on the operating force. Figure 2 shows a calculated example of the variation of

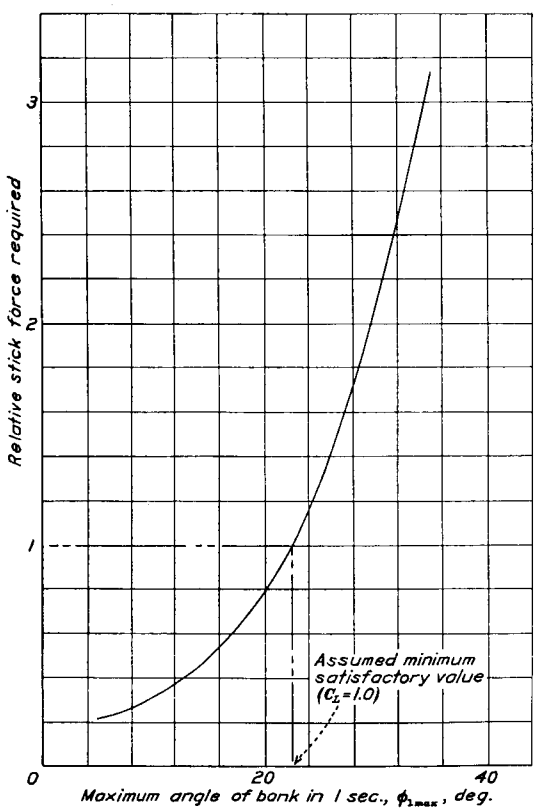

FIGURE 2.—Relation between stick force and maximum amount of control obtained. Fairchild 22 type airplane; 0.80 $\frac{b}{2}$ sealed ailerons deflected ±20°; aileron chord varied.

operating force with specified control in which it was assumed that ailerons with equal up-and-down motion and the most efficient length and deflection (±20°) were used in each case. The rate of increase of operating force with amount of control depends on the manner in which the increase of control is obtained, as will be more fully developed in a later section.

YAWING MOTION AND SIDESLIP

The effect of the yawing moment produced by the ailerons is considered in two ways. First, the secondary effect of yaw on the rolling motions is inherently included in the computed banking effectiveness. Thus, the bank in 1 second is that produced by the ailerons without aid from the rudder. If it is assumed that a sufficiently powerful rudder were used in such a way as to prevent sideslip, a given aileron device would, in general, produce a somewhat greater banking effect. This assumption is not used here, however, and the deflections of the control surfaces given in table I are those required to produce the specified angle of bank in 1 second with the particular combination of rolling and yawing moments produced by the aileron in question.

The second effect considered is the sideslip produced by the sudden use of the aileron control for banking. In flight the rudder is used to avoid sideslipping and the amount of rudder action necessary for this purpose is in direct proportion to the sideslip incurred by the ailerons alone.

The angle of sideslip accompanying a 15° bank in 1 second following the sudden displacement of the lateral controls is also given in table I. The first aileron listed, it will be noted, produces a sideslip of 7° at $C_L=1.0$ and of 3° at $C_L=0.35$ when the rudder is not used to correct for this condition.

LATERAL STABILITY

In the ordinary unstalled-flight range the effects of the lateral-stability factors on the lateral control obtained are included in the computations of the angle of bank reached in unit time. The angle of bank ϕ_1 is the angle that would be produced by the control operating on the average airplane. The effect of a given control on an airplane of greatly different lateral-stability characteristics might, of course, be considerably different than indicated in this case.

One of the most important factors in the interaction of lateral stability and control below the stall is the effect of the secondary yawing moment induced by the control and an allowance for this effect should be made in the proportioning of the airplane for lateral stability. Modifications that tend to increase spiral stability in free flight (namely, reduced vertical-fin area and increased dihedral) tend to render the airplane uncontrollable under the action of ailerons giving adverse yawing moment. The degree of "weathercock" stability should be sufficient to restore the airplane from a yawed attitude when the wings are held level by use of the ailerons. For safety in this respect the ratio of adverse yawing to rolling moment given by the ailerons should not be allowed to approach the ratio of yawing to rolling moments that naturally act on the airplane either

in pure sideslipping or pure yawing motion. (See reference 6.)

One of the lateral-stability factors, the damping in rolling, has been shown by the analysis in reference 4 to have a critical effect on the controllability obtained, satisfactory lateral control requiring that positive damping exist. Since the damping in rolling depends on a positive slope of the left curve, the damping exists only at angles of attack of the outer portions of the wing that are below the maximum lift coefficient. While some semblance to control may be obtained at angles of attack above the stall if controls giving favorable yawing moments as well as sufficiently powerful rolling moments are used, the instability associated with uneven stalling and autorotation is so violent that it is necessary for the pilot to use the controls continually to keep the airplane near the desired attitude. If sufficiently rapid rolling is once started, either by the controls themselves or as the result of gusty air, it cannot be stopped. The angle of attack at which the damping in rolling becomes zero and above which autorotation takes place ($\alpha_{L_p=0}$) is used herein as an indication of the limit of the flight attitude above which satisfactory lateral control cannot be obtained. This value was given in the reports of reference 1 for both the angle of attack at which autorotation was selfstarting and the angle of attack at which the damping became zero when the wing was rotating at the rate $pb/2V=0.05$, a value representative of the rolling likely to be caused by gusty air. The latter value of α has ordinarily been found to be about 1° lower than the former value and, being therefore more decisive, is used in the present report. The difference between the angle of attack for zero damping and the angle of attack for the maximum lift coefficient of the entire wing $(\alpha_{L_p=0}-\alpha_{C_{L_{max}}})$ has been tabulated under Lateral Stability to show whether the maximum lift coefficient can be expected to be reached in flight before satisfactory lateral control is lost. It will be noted that for ailerons 3 and 4 the wing loses its damping in roll at an angle of attack 1° higher than that at which the maximum lift coefficient is reached. Thus, as far as the stability is concerned, lateral control should be possible throughout the entire unstalled-flight range, including the angle of attack for maximum lift coefficient.

WING PERFORMANCE CHARACTERISTICS

The same criterions used throughout the reports of reference 1 to show the relative performance characteristics of the wings are used in the present report and are tabulated in the last three columns of table I. The maximum lift coefficient $C_{L_{max}}$ is given as an indication of the wing area required for a desired minimum speed. The ratio $C_{L_{max}}/C_{D_{min}}$ is an indication of the speed range and, for a given minimum speed, shows the relative effects of the wings on the maximum speed attainable. The ratio L/D taken at a value of the lift coefficient $C_L=0.70$ is an indication of relative merit in climbing flight. In a series of performance computations made for airplanes of different wing loadings and power loadings and with both plain and slotted wings, this criterion was found to be satisfactory throughout the entire range. It should be noted that the comparative values used in the present report are based on tests made in the 7- by 10-foot atmospheric wind tunnel and hence do not coincide in absolute value with results of tests made at different Reynolds Numbers.

APPLICATION TO AIRPLANES OF DIFFERENT SIZES AND LOADINGS

Because the flight experience that led to the specification of a satisfactory degree of control was restricted to the Fairchild 22 type of airplane, there is some doubt about the application of this experience to other types and especially to large or very small airplanes. The Fairchild 22 type of airplane, of course, serves as well as any other when different aileron devices are simply compared among themselves. The principles governing the extension of the computations of motion to geometrically similar airplanes of different sizes and loadings are well known and can be applied here, but this extension of the computations does not definitely answer the question as to what constitutes a satisfactory degree of control for large (or very small) airplanes.

According to the principles of dynamical similarity, large or small similar airplanes of the same wing loading would show the same linear rise and fall of the wing tips $\left(\frac{\phi_1 b}{2}\right)$ during a 1-second banking motion. Large and small airplanes do actually show a tendency toward similarity in important dimensions and size of control surfaces, and it seems logical to assume that a given value of the vertical distance described by the wing tips within 1 second following a sudden control deflection that represents a satisfactory amount of control for the Fairchild 22 airplane should be satisfactory for any size of airplane.

For similar airplanes the linear distance described by the wing tips in banking $\left(\frac{\phi_1 b}{2}\right)$ is independent of the size. Figure 3 shows this distance plotted against wing loading and gives the separate effects of rolling and yawing moments of coefficient 0.01 at different lift coefficients. The banking effect of any combination of rolling and yawing moment may be found by superposition, i. e.,

$$\frac{\phi_1 b}{2}=\frac{C_l}{0.01}\left(\frac{\phi_1 b}{2}\right)_{C_l=0.01}+\frac{C_n}{0.01}\left(\frac{\phi_1 b}{2}\right)_{C_n=0.01} \qquad (1)$$

The ordinates of the figure give directly the circumferential displacement of the wing tip in feet for a unit of 0.01 rolling- or yawing-moment coefficient. It is important to note that the banking effects of rolling and yawing moments can be separately considered and later added in any desired proportion to obtain the total combined effect.

The computations show that, in general, smaller values of the control-moment coefficients are required to produce a given wing-tip displacement in a unit of time for the more heavily loaded airplanes. Another point of interest in connection with the secondary adverse yawing moments produced by conventional-type controls is that these moments are more effective in hindering the control with lightly loaded airplanes than with heavily loaded ones. Note that in the usual case the banking effect of the yawing moment is to be deducted in equation (1) since this moment is usually adverse and therefore negative.

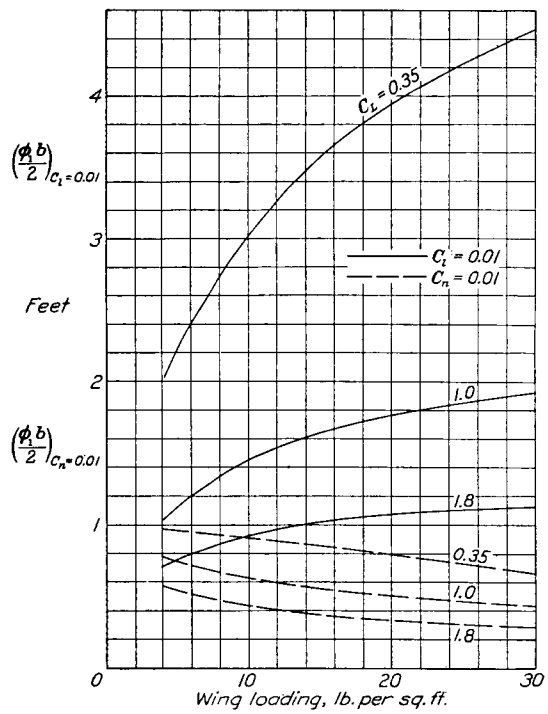

FIGURE 3.—Wing-tip displacement produced in 1 second by suddenly applied rolling and yawing moments for different wing loadings and flight speeds.

$$\frac{\phi_1 b}{2} = \frac{C_l}{0.01}\left(\frac{\phi_1 b}{2}\right)_{C_l=0.01} + \frac{C_n}{0.01}\left(\frac{\phi_1 b}{2}\right)_{C_n=0.01}$$

The variation of control force with size and loading of the airplane may be determined from general rules as in the case of the variation of the amount of rolling motion. As shown by figure 3, heavily loaded airplanes require smaller control-moment coefficients for a comparable amount of control than do lightly loaded airplanes. In general, a heavily loaded airplane that is otherwise similar to a lightly loaded one will have smaller control surfaces. On the other hand, the heavily loaded airplane will fly at a higher speed so that the dynamic pressure will be greater. Figure 4 shows a calculated example of the variation of stick force with wing loading at a given lift coefficient and for a given maximum amount of control. Here, as in figure 2, the most efficient combination of size and deflection is assumed for each point. Figure 4 shows that the stick force required to obtain a given angle of bank in 1 second is practically the same for all wing loadings up to 10 pounds per square foot but that it increases somewhat as the wing loading increases further.

With moderately large airplanes, somewhat higher stick forces are apparently tolerated by pilots without serious objection. With extremely large airplanes, however, the operating force becomes too great to be satisfactorily overcome by the pilot and either servo controls or auxiliary power is required. With auxiliary power, the pilot might presumably operate a valve or easily deflected controller governing a special power source that deflected the control surfaces. Under such conditions the magnitude and variation of the hinge moments would be relatively less important and the maximum deflection of the control surfaces would very likely be determined by the maximum rolling and yawing moments they could produce rather than by the hinge moments and the resultant deflecting force required. Although some indication of the relative performance of the various lateral control devices compared in this report can be obtained from the data as given, it would be desirable to reanalyze the original data given in references 1, 7, 8, 9, and 10 if a comparison on the basis of ailerons operated by auxiliary power were desired.

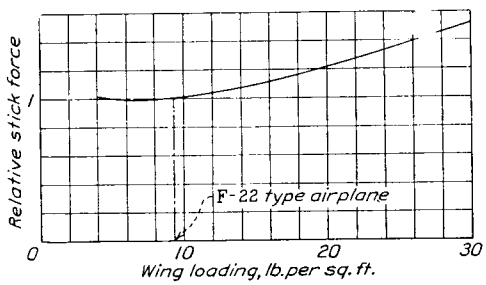

FIGURE 4.—Relation between the wing loading and the stick force required for a given amount of control ($\phi_{1_{max}}=22.5°$; $C_L=1.0$).

COMPARISONS OF VARIOUS DEVICES

PLAIN AILERONS

Effect of aileron and wing plan form.—The tests of reference 1, part I, were made with rectangular wings having ailerons of three different proportions: 0.25 c_w by 0.40 $b/2$ (which were taken as the standard for comparison throughout the series), 0.15 c_w by 0.60 $b/2$, and 0.40 c_w by 0.30 $b/2$. These sizes were selected to give approximately equal rolling moments with the same angular deflection. These ailerons are numbered 2, 3, and 4, respectively, in table I. With equal up-and-down deflection, the stick force is much larger for the short, wide ailerons than for the long, narrow ones and is, in each case, slightly less for the low-speed condition than for high speed. If a suitable differential linkage is employed, the stick forces at the low-speed

condition, where the wide ailerons have the advantage of a large floating angle, are quite low for all three sizes of aileron. At the high-speed condition, however, the 0.40 c_w by 0.30 $b/2$ aileron requires a rather high stick force, even with the best differential.

The sideslip incurred by an angle of bank of 15° in 1 second is not greatly different for the different aileron plan forms either with or without differential linkages. The values are slightly lower at C_L=1.0 with the differential linkages than with the equal up-and-down, and with the 0.25 c_w by 0.40 $b/2$ plan form than with either of the others.

It is possible by methods to be described in section II to compute an optimum size of the aileron, i. e., the size giving the desired amount of control with the least stick force. The effect of varying the aileron span and chord is shown in figure 5, the chord for each span value being

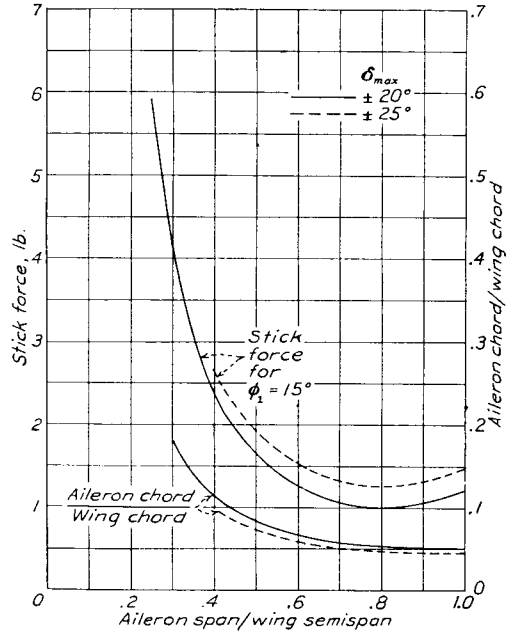

FIGURE 5.—Variation of stick force with aileron span. Aileron chord proportioned to give $\phi_{1_{max}}$=22.5° with maximum deflection of ±25° and ±20°; rectangular wing; average airplane; C_L=1.0; sealed ailerons.

the smallest that will give an angle of bank of 15° in 1 second with the assumed average airplane. From this figure it is apparent that with equal up-and-down deflection an aileron span of 80 percent of the wing semispan will give the lowest stick force, but the variation is small for ailerons between 60 percent and 100 percent of the wing semispan. Other computations not shown lead to the same conclusion for ailerons having differential linkages.

The relations of aileron chord and span, considering especially that the hinge moment increases with the square of the chord while the rolling moment increases only as the square root of the chord, are such that lower stick forces are obtained with narrower chords. The narrower ailerons require greater deflections and the reduction in chord size is limited by the fact that deflections greater than about ±20° are inefficient. Marked separation of the air flow takes place at about this angle of deflection on all the conventional flap-type ailerons tested and, as shown by the typical curves of figure 6, the rolling-moment coefficients increase at a lower rate beyond 20° deflection. If it is attempted to

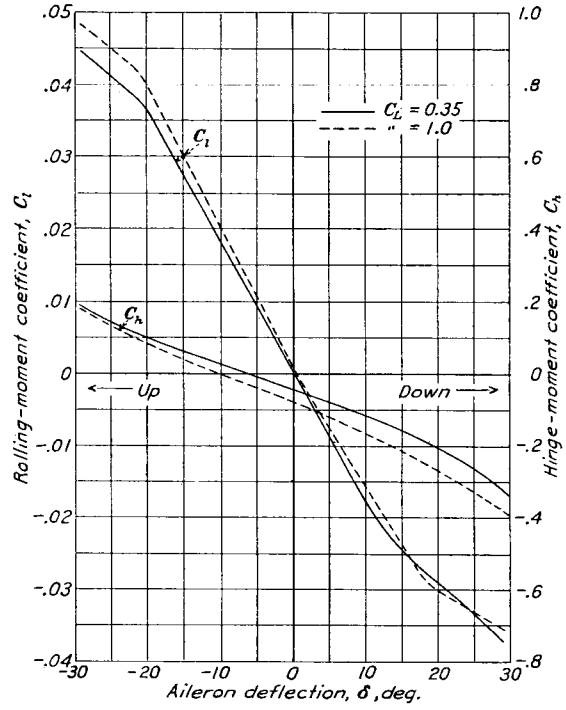

FIGURE 6.—Typical rolling- and hinge-moment coefficient curves for plain ailerons.

reduce further the chord of the aileron by extending the deflection beyond this break, the stick force will be higher because of the loss in mechanical advantage. Figure 5 illustrates this point, for when an aileron deflection of ±25° is assumed, narrower ailerons are required but the stick force is larger for all aileron spans than with a deflection of ±20°.

Aileron 5 (table I) represents the narrowest sealed aileron covering 80 percent of the wing semispan that gives the required control with a deflection of ±20°. The aileron chord in this case is only 5.3 percent of the wing chord, and the stick forces are lower than for any of the previous ailerons. If a differential motion is used, a somewhat wider aileron is required. With narrow ailerons the floating angle is very small, and a tab is required to make the ailerons float at a sufficiently high angle that the differential linkage will be effective in reducing the stick force. (See reference 11.) Aileron 6 of table I is the smallest one covering 80 percent of the semispan that will give the required

amount of control with a differential motion and with suitable aileron tabs. The assumed tab covers the entire trailing edge of the ailerons, has a chord 1.5 percent of the wing chord, and is permanently bent downward 14°. For this case the entire aileron chord including the tab is 7.8 percent of the wing chord and the stick force is only 0.5 pound for the high-speed condition and 0.1 for low speed.

These values of stick force are lower than are considered desirable for the Fairchild 22 airplane but are interesting in showing the possibility of obtaining a satisfactorily low stick force in larger and heavier airplanes. For small airplanes, one satisfactory method of increasing the stick force to the value desired would be to use greater up travel than 20° with differential ailerons, thus getting into the range of inefficient stick force although obtaining the advantage of slightly smaller adverse yawing moments.

In many practical cases the chord of the aileron varies along the span. Inasmuch as the hinge moment varies as the square of the chord and the control effectiveness only about as the square root of the chord of an aileron element, the stick force required to give a certain amount of control is inherently greater if the chord of the aileron varies appreciably along the span. This relation is true in spite of the fact that the portion of the aileron nearer the tip of the wing has a greater lever arm, which suggests that it might be advantageous to increase the chord of the aileron as the wing tip is approached. Thus, it is possible to state as a general rule that to obtain the lowest stick force, ailerons should have an essentially constant chord over their entire span.[1]

On wings having rounded tips it is sometimes the practice to use ailerons having skewed hinge axes like aileron 7 in table I. This aileron corresponds in span, area, and gap to the 0.25 c_w by 0.40 $b/2$ aileron 2, but the stick force is decidedly higher for the skewed ailerons on account of the variation of the aileron chord along the span.

Ailerons 8 and 9 of table I are of tapered plan form and are mounted on tapered wings. In the computations of the rolling effect with the tapered wings the reduction in the moments of inertia due to the taper are taken into account. For example, for the wing with 5:1 taper, the value of I_X was changed from 1,216 slug-feet^2 for the original average airplane to 860, and the value of I_Z from 1,700 to 1,400 slug-feet^2. The lateral-stability derivatives were also changed to take account of the taper. (See reference 4.)

A comparison of ailerons 8 and 9 with aileron 1, which has the same relative chord size but is attached to a rectangular wing, shows that the stick force becomes lower as the taper of the wing is increased. The sideslip or adverse yawing effect is also smaller with the tapered wings than with the rectangular. The lateral-stability factor, damping in roll, is reduced to zero at an angle of attack 3° below the stall with the 5:1 tapered wing, indicating that the airplane could not be safely maintained at the maximum lift condition in flight.

The ailerons on tapered wings dealt with up to this point have had chords that were the same percentage of the wing chord at each position along the span, the ailerons tapering with the wings. It has been stated that the lowest stick force would be obtained with constant-chord ailerons. Computations have been made comparing the straight or constant-chord ailerons on a tapered wing with the ailerons that taper with the wing, and the results are shown in figure 7. The straight

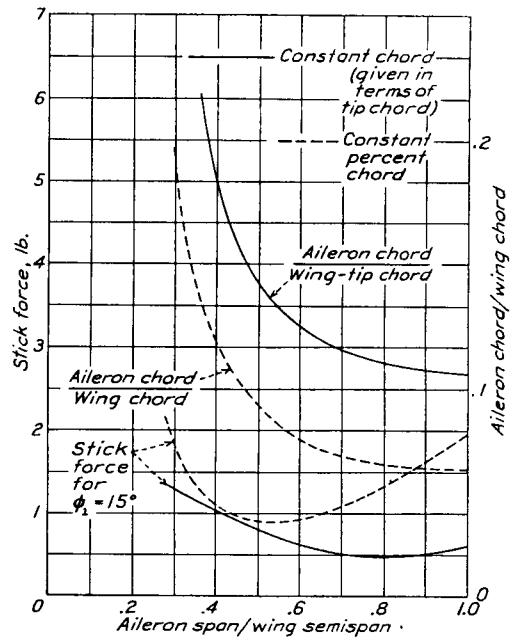

FIGURE 7.—Variation of stick force with aileron span and chord for straight and tapered ailerons on 5:1 tapered wing. Aileron chord proportioned to give $\phi_{1_{max}}$ = 22.5° with maximum deflections of ±20°; C_L=1.0; sealed ailerons.

or constant-chord ailerons require lower stick forces for any given aileron span. It is interesting to note that with tapered ailerons the aileron span giving the lowest stick force is about half the wing semispan; whereas with constant-chord ailerons the best aileron span is 80 percent of the wing semispan, as it is in the case of rectangular wings. Ailerons 10 and 11 are the optimum sizes for the tapered and straight ailerons, respectively, on a 5:1 tapered wing. With equal up-and-down deflections, the stick forces for the straight ailerons are about half those for the tapered. In either case the stick forces could be nearly counterbalanced by means of a suitable differential linkage and tab, as will be developed more fully in section II.

Effect of hinge gap.—Wind-tunnel tests have shown that even a slight gap between ordinary unbalanced ailerons and the wing upon which they are mounted

[1] The greatest taper mathematically compatible with a minimum stick force is less than about 3 percent of the aileron chord.

causes a relatively large loss in rolling moment. This loss for unbalanced flaps having a gap of one thirty-second inch on a wing of 10-inch chord was found to be approximately 30 percent. The hinge moment is also reduced by the gap but to a much lesser extent and the resultant stick force for a given amount of lateral control is greater because a larger aileron deflection is required, which necessitates a linkage having a poorer mechanical advantage. The effect on the stick force is shown in table I by a comparison of the values for aileron 2, which has a gap, with those for aileron 1, which is sealed.

BALANCED AILERONS

Balanced ailerons of the Frise and Handley Page types are widely used at the present time, the particular forms of aerodynamic balance incorporated in these ailerons giving improved yawing moments as well as reduced hinge moments. Good results are obtained with proper designs but the exact shape of these ailerons has a critical effect on the rolling and hinge moments, and each different installation is likely to require considerable individual development. Figure 8 shows typical curves of rolling and hinge-moment coefficients for Frise type ailerons. The rolling-moment coefficient for the example shown increases less rapidly with deflection after an upward angle of 7° to 10° has been reached, which is considerably lower than the 20° critical deflection for plain unbalanced ailerons (fig. 6). Thus, it is uneconomical with respect to stick force to use large up deflections and, owing to the smaller maximum deflections, larger ailerons are required for efficiency than when ailerons of the plain unbalanced sealed type are used. The break in the curve of rolling-moment coefficient against deflection is associated in the case of the Frise and Handley Page types of aileron with the downward projection of the nose of the aileron and the resultant breaking away of the flow from the under side of the aileron. This effect can be reduced or possibly eliminated by using a raised-nose portion.

The Frise and Handley Page types of aileron have gaps between the aileron and the wing, and the effectiveness of the ailerons cannot be assumed equal to that of smoothly sealed flaps.

The hinge-moment curves as shown in figure 8 have very low and even negative slopes at places, and extreme differential linkage cannot be used because overbalance would occur with medium or small deflections of the up aileron. Because the hinge-moment curves are far from straight, it is more difficult to select suitable differential linkages for ailerons of this type than for plain unbalanced ailerons. Satisfactory linkages have often been obtained in practice, however, and there are many excellent examples in which a nice balance of conditions has been obtained with satisfactory control and light stick forces.

Ailerons 12 and 13 are examples of the Frise type. A comparison of aileron 12 with the same size of plain unbalanced but sealed ailerons shows that the stick forces at the low-speed condition are about the same for both types of aileron, both with equal up-and-down and with differential motion. At the high-speed condition the Frise ailerons have somewhat lower stick forces than they have for the same control at low speed. It is worthy of note that, although the deflections are small in both cases, the Frise ailerons are apparently not greatly oversized for, in their case, substantially greater deflections would be inefficient. The plain ailerons, on the other hand, have maximum deflections well under the limiting 20° value and are decidedly oversized, considering the amount of control specified.

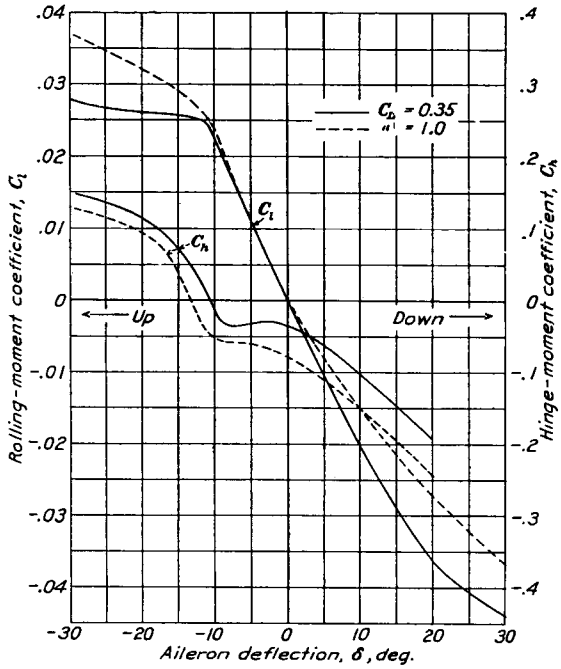

FIGURE 8.—Typical rolling- and hinge-moment coefficient curves for Frise ailerons.

If a fixed tab is used to trim the ailerons upward, lower values of stick force can be obtained with the plain unbalanced ailerons (reference 11). The tab will not give the same improvement with the Frise ailerons because of the varying slopes of the hinge-moment curves.

The 0.40 c_w by 0.30 $b/2$ Frise aileron 13 has a different sectional form than aileron 12 in that the nose portion is raised, and this aileron gives smoother curves of rolling and hinge-moment coefficients. The Frise aileron with the raised nose shows no improvement in yawing effect over the plain unbalanced ailerons of the same size, but the 0.25 c_w by 0.40 $b/2$ Frise aileron, which has the more typical Frise sharp nose, gives a slight improvement in this respect.

The drag of all commonly used forms of Frise and Handley Page ailerons is sufficiently great to be considered a serious disadvantage in connection with

modern high-performance airplanes. For this reason, the development of a type of aerodynamic balance that does not add to the drag is desirable.

FLOATING-TIP AILERONS

Conventional ailerons operating on a lifting portion of the wing suffer several fundamental disadvantages. First, the production of rolling moment by a lifting wing gives rise to the adverse yawing moment; and, second, the loss of lift at the stall is accompanied by a loss of effectiveness of the ailerons. It has become apparent during the investigation, however, that the stall of the wing or, at any rate, of the outer portions of the wing, is accompanied by such a loss of stability that it is hardly an advantage to retain aileron rolling moments in this condition.

In the case of floating-tip ailerons, control is secured by surfaces that contribute no lift. This arrangement avoids both the adverse yawing moment of ordinary ailerons and the loss of rolling moment associated with stalling of the main wing; but it increases the drag of the airplane and adds to the over-all dimensions. If the airplane is designed to fulfill certain performance specifications, such as landing speed, climb, ceiling, etc., the floating-tip ailerons cannot be considered an integral part of the main wing as they do not contribute effectively to the area or span so far as induced drag and lift are concerned.

A number of floating-tip aileron devices were tested in the course of the investigation of reference 1. Apparently the most usable of these are the tip ailerons on the 5:1 tapered wing. Two methods of comparison have been followed. In one case (aileron 14) the ailerons were included within the over-all dimensions of the 5:1 tapered-wing average airplane. The values given in the table for this case (short wing) were based directly on the results of tests made in the 7- by 10-foot wind tunnel (reference 1, part XI). The criterions show the effect of reduced area and span of the lifting portion of the wing as a reduction of the climb and maximum lift.

In order to take account of the effect of simply adding a tip aileron to a normal-size wing, further calculations were made. In this case (aileron 15) it was assumed that the over-all span of the average airplane was increased by the additional span of the tip ailerons; hence, the aspect ratio of the lifting portion of the wing remained the same. The added span of the wing, although it contributed practically no lift and hardly modified other stability characteristics of the airplane, considerably increased the damping in rolling. This fact was accounted for in the computations, data on damping of the tested 5:1 tapered wing with floating-tip ailerons included in the original plan form being extrapolated for this purpose. It would be natural to assume that the floating-tip ailerons would be just as effective as the main portion of the wing in contributing damping. The tests showed, however, that the damping of the 5:1 tapered wing with floating tips was only 85 percent of that with the tips rigid.

The rolling moments produced by floating-tip ailerons can be predicted with good accuracy by the conventional aileron theory. The induced yawing moments correspond to those given by plain ailerons with an extreme uprigging or negative droop corresponding to the neutral floating positions of the tip ailerons. Ordinarily, the tip ailerons, on account of the local upwash at the end of the rigid wing, float at a negative angle of attack relative to the mean direction of flight and hence give slight favorable induced yawing moments with respect to the wind axes. The yawing and hinge moments used in table I for the long-wing airplane (aileron 15) were predicted from the results of the wind-tunnel tests on the short 5:1 tapered wing.

The tabulated results of the computations show that the stick forces required for satisfactory control are reasonably low in the case of the short 5:1 tapered wing. It will be noted that only relatively small deflections of these ailerons are required for control, a fact that can be attributed partly to the reduced damping in rolling shown by this wing. On the other hand with the long wing, when the tip ailerons were added to the regular wing span, the damping in rolling and moment of inertia were increased and, hence, larger stick forces were required to produce the given bank. The same hinge-axis location, and hence the same degree of balance of the ailerons, were assumed in both cases. It will be noted that about the same force was required to produce 15° bank at high and low lift coefficients.

Although the floating-tip ailerons give small favorable yawing moments, it will be noted that their use results in some inward sideslip during the 15° bank. The rolling motion of the wing induces a small adverse yawing effect as is indicated by the adverse sign of the yawing moment due to rolling. This cause combined with the inward acceleration due to gravity is sufficient to bring about the inward sideslip in spite of the favorable yawing moment of the floating ailerons.

It has often been suggested that tip ailerons be trimmed by tabs so as to float downward and give some lift. Such an arrangement should improve the performance characteristics but would void the advantage of these ailerons in giving favorable yawing moments. If the tip ailerons were trimmed so as to produce as much lift as the adjacent rigid portion of the wing, it is to be expected that they would show the same proportion of adverse yawing moment to rolling moment as do conventional ailerons.

At stalling angles of attack for the main wing the floating tips remain unstalled. Hence, they should be expected to aid in preventing the loss of damping in rolling at or near the stall. The only floating aileron device that effectively prevented the loss of damping in rolling in the wind-tunnel experiments was the long nar-

row aileron attached to a rectangular wing. (See reference 1, part XI.) In this particular case the performance characteristics were so poor that the device as tested could not be considered practical for application.

As noted in table I, the lateral-stability characteristics of the 5:1 tapered wing with the floating-tip ailerons are almost as bad as those on the conventional rigid 5:1 wing and are somewhat worse than those of the rigid rectangular wing. Inasmuch as the damping in rolling is lost at an angle of attack 2° below the angle for maximum lift, the airplane could not be safely maintained in flight above this angle even though the ailerons continue to give undiminished rolling moments. Flight tests of floating-tip ailerons on a tapered wing fitted to a Fairchild 22 airplane support this conclusion.

Wind-tunnel results with floating-tip ailerons showed a smaller adverse effect on the performance characteristics of the 5:1 tapered wing than on any of those tested. The effect of reducing the span and area of the rigid portion of a given wing is shown by the comparison of the performance criterions of the short 5:1 tapered wing, having an over-all aspect ratio of 6, with those tabulated for the conventional rigid 5:1 tapered wing, having the same over-all span and area. Here the maximum speed of the airplane will be hardly affected while the climb and maximum lift will be reduced, as indicated. Simply adding the tip portions to the normal-size wing will increase the parasite drag at high speed but, as shown by the tabulated criterions for this case, will probably slightly improve the climb.

SPOILERS

Spoilers in the form of small flaps or projections raised from the upper surface of the wing have presented attractive possibilities as lateral control devices because they give positive or favorable yawing moments and large rolling moments at the high angles of attack through the stall. (See fig. 9.) As spoilers giving apparently satisfactory rolling and yawing moments had been developed in the 7- by 10-foot wind-tunnel investigation (reference 1, part V), they were tested in flight on a Fairchild 22 airplane (reference 2). When the spoilers were first tried in flight, the pilots noticed that the airplane apparently did not react until the control stick had been given a medium amount of deflection, after which the rolling velocity suddenly built up to a much higher value than had been experienced with any previously tested control system. This characteristic made it impossible to perform smooth maneuvers requiring the coordination of the spoilers with the elevator or rudder and led to overcontrolling when an attempt was made to keep the wings level in gusty air. Closer inspection of the spoiler action, however, disclosed that for any spoiler movement there was actually an appreciable delay between the movement of the spoiler itself and the start of the desired rotation in roll of the airplane. In order to substantiate the pilot's findings, records were made of the rotation of the airplane in roll immediately following a movement of the stick and a specimen

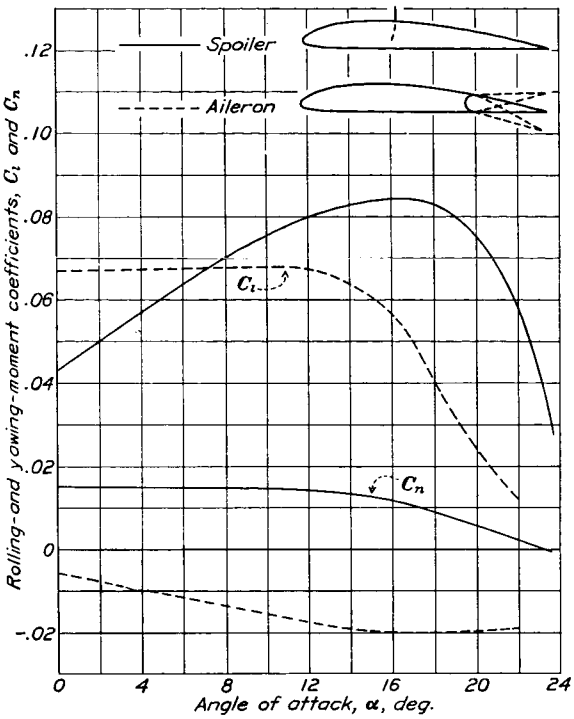

FIGURE 9.—Comparison of rolling- and yawing-moment coefficients obtained with ailerons and spoilers.

time history of the motion is shown in figure 10, together with similar information for other lateral con-

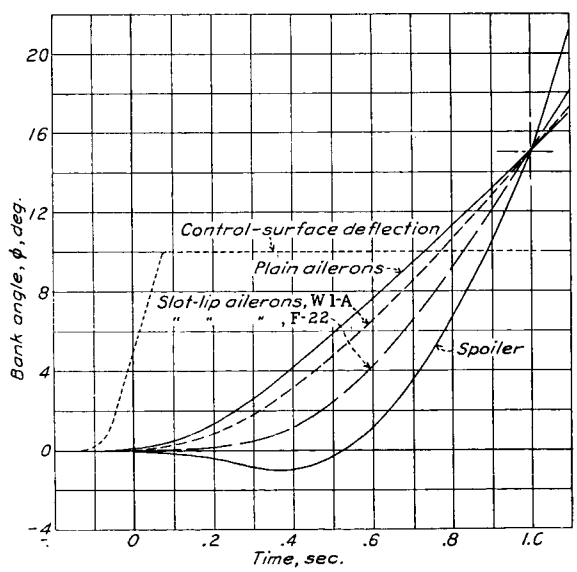

FIGURE 10.—Bank curves derived from flight records illustrating response characteristics of various lateral control devices.

trol devices including conventional ailerons. The records showed that the delay before rotation started

in the desired direction was of the order of half a second. This lag seems surprisingly short to have much effect on the control obtained with spoilers, but apparently it is sufficient to prohibit the use of the spoilers close to the ground because of the danger of overcontrolling.

The lag of spoilers was then studied by means of a special hinged wing model of 4-foot chord mounted in the 7- by 10-foot wind tunnel (reference 12). This installation reproduced the conditions encountered in the flight tests. The tests with spoilers located in different positions along the chord of the wing showed that the lag was relatively large with the spoilers near the leading edge and became less after the spoiler was moved to the rear until it was zero for normal trailing-edge flap-type ailerons.

The spoiler located near the rear of the wing was found to act with a negligible amount of lag (less than one-tenth second could not be detected by the pilots) and seemed to give some promise of making a satisfactory lateral control device. Flight tests were therefore made of a retractable spoiler located 83 percent of the wing chord back of the leading edge which, because of its rearward position, was referred to as a "retractable" aileron. The aileron was made in the form of a plate curved in a circular arc to form a segment of a cylinder and was moved in and out through a slit in the upper surface of the wing and about an axis at the center of the cylinder. This arrangement produced no aerodynamic hinge moment and was found to operate satisfactorily in flight on a Fairchild 22 airplane (reference 3). The retractable aileron mounted on the assumed average airplane is number 16 in table I. The stick-force characteristic (zero force) is not the most desirable but could be brought up to a desired value either by the addition of a spring in the aileron linkage or by an off-center location of the hinge axis of the aileron. A large amount of control is available from ailerons of this type and the yawing characteristics are more satisfactory than those of conventional ailerons.

Combinations of conventional ailerons with spoilers located ahead of them and deflected simultaneously showed some promise in the wind-tunnel investigation (reference 1, part V) and were found to give satisfactory control free from lag when tested in flight on the Fairchild 22 airplane (reference 2). With the spoiler deflected in front of the aileron, the floating angle of the aileron is raised and, if properly developed, certain combinations seem very promising in regard to both yawing effect and stick force. Estimated characteristics of one such combination are given in table I, aileron 17.

Another possible combination that has been tested and may deserve further development is one in which two spoilers are located in tandem and deflected simultaneously. The tests with this arrangement (reference 12) showed that the lag of the combination was no greater than that for the rear spoiler alone, whereas the final rolling moment was the same as for the front one when used without a flap. Later tests indicate that spoilers located on the forward portion of the wing may be rendered ineffective by the action of a split flap. One other point has not yet been completely determined, namely, whether the rolling motion would get under way with sufficient acceleration immediately after the start. This point will be dealt with further in the next section on slot-lip ailerons.

SLOT-LIP AILERONS

Means for the elimination of the lag of spoilers were investigated in the 7- by 10-foot tunnel and it was found that the lag could be eliminated by providing a slot or passage through the wing back of the spoiler. This investigation has resulted in the development of what have been termed the "slot-lip" ailerons (references 8 and 12). The slot-lip aileron is a combination of a spoiler-type flap located on the upper surface of the wing and a continuously opened slot, the flap forming the upper portion or lip of the slot. The computed control performances for two arrangements of slot-lip ailerons in different positions along the chord of the wing are listed 18 and 19 in table I.

The slot-lip ailerons satisfactorily eliminate or reduce to a negligible value the actual lag intervening before the wing starts moving in the desired direction, and they give a very high maximum rate of rolling; but the rolling nevertheless increased less rapidly immediately after the start of the motion than with conventional trailing-edge flap-type ailerons. This condition is illustrated in figure 10, which includes curves from flight records of slot-lip ailerons on the Fairchild 22 airplane and slot-lip ailerons on the W1–A airplane. It will be noticed that with the W1–A the rate of roll increases nearly as rapidly as with conventional ailerons but with the Fairchild 22 the action was considerably more sluggish. The differences in the behavior of these two airplanes have been studied (reference 8) and it has been concluded that the superior response characteristics shown by the W1–A are due in large measure to the relatively great dihedral (5°) and to the smaller moments of inertia of this airplane. The secondary yawing action of the slot-lip ailerons is favorable, hence the dihedral effect increases the rolling action. Other differences favorable to improved response of the W1–A are: (1) The more rearward location of the aileron (0.30 c_w compared with 0.20 c_w tested on the Fairchild 22) and (2) the slightly greater size of the slot.

The lateral control with the slot-lip ailerons on the W1–A seemed satisfactory to the pilots, but on the Fairchild 22 it was found to be too sluggish and to give somewhat the same feeling as a slight amount of lag. This comparison, aided by several others of a pertinent nature, indicates that an additional point must be

covered in a specification for a completely satisfactory lateral control dealing with the acceleration or rate at which the rolling increases during the first half second or so following the actual start. It may be stated in simple quantitative terms, applying to the conditions for the assumed average airplane, that the angle of bank one-half second after a sudden deflection of the controls should be at least one-third the angle of bank reached at 1 second. Thus, if a bank of 15° is reached in 1 second, at least 5° of this should be attained in the first half second.[2]

The sluggishness of the slot-lip ailerons is a great handicap in the method of comparison of control effectiveness used in the present report, in which a certain angle of bank must be obtained in a time of 1 second. Even though these ailerons give a high final rate of roll, excessively great deflections are required to attain an angle of bank of 15° in 1 second at a lift coefficient of 1.8, and the stick forces are excessively high. This particular disadvantage might be overcome by the use of a suitable aerodynamic balance but, even so, the sluggishness of the slot-lip ailerons might prevent them from being considered satisfactory if it were of the magnitude found on the Fairchild 22 instead of that found on the W1–A.

The sideslip accompanying a 15° bank in 1 second is negligible with the 0.55 c_w slot-lip ailerons in the usual flight range with unflapped wings. With more forward locations the yawing moment becomes decidedly positive, resulting in outward sideslip. Because of the action of the slots at high angles of attack, the damping in rolling is retained to an angle of attack beyond that for maximum lift coefficient and, for this reason, it should not be difficult to design an airplane incorporating these ailerons in such a manner that lateral control and stability would be reasonably satisfactory at all angles of attack that could be maintained in flight. The continuously open slot, however, results in a high drag, which reduces the high-speed and climbing performance to a noticeable extent. The drag is less for the rear positions of the slot-lip ailerons and a special investigation has been made in the 7- by 10-foot tunnel to develop slots with reduced drags. Some success has been attained but, considering the best results to date, these ailerons do not seem suitable for modern high-performance airplanes.

LATERAL CONTROL WITH HIGH-LIFT FLAPS

Since the inception of the research program of reference 1, wing flaps have come into very general use and have further complicated the problem of lateral control. In steady flight ordinary ailerons give rolling moments that vary almost inversely with the lift coefficient; hence, wings equipped with high-lift devices require relatively large control surfaces. The installation of an effective flap then becomes more difficult.

Another problem introduced by the use of high-lift devices concerns the adverse yawing moment of the ailerons. The ratio of induced yawing to rolling moment increases (adversely) in direct proportion to the lift coefficient. Furthermore, the effect of a given yawing moment on the rolling control is usually greater with flaps in use on account of the increased dihedral effect due to the flap. Thus it appears almost necessary to use some device that causes large changes of profile drag resulting in a favorable component of yawing moment or to use wings with washout at the tip portions (partial-span flaps) so that the induced yawing moment is reduced. Many of the devices developed in reference 1 for use with full-span flaps show satisfactory yawing moments on account of the profile-drag increments caused. Comparisons of a number of the most promising devices have been made and are listed in section B of table I.

Plain ailerons on wings with partial-span flaps.—On account of the general use of partial-span split flaps with ordinary ailerons, some tests of this arrangement were made in the 7- by 10-foot wind tunnel (reference 7). The tests were made with tapered wings because they represent the most efficient application of the arrangement and are most used in practice. The most interesting result of these tests was the small loss of maximum lift coefficient entailed by the substitution of ailerons for the tip portions of the flap, particularly in the case of ailerons 21 and 23 as listed in table I, where only 30 percent of the semispan was used for the aileron portion. The indicated reduction amounted to less than 10 percent of the maximum lift shown by the same tapered wings with full-span split flaps. The reduction was about the same for the two taper ratios tried. It will be noted that the 5:1 tapered wing gave more efficient control as regards stick forces under all conditions. In each case the stick force is slightly less for the longer ailerons, although of course the wings with shorter ailerons showed better performance characteristics. Both sizes of ailerons on the 5:1 tapered wings showed a marked diminution of effectiveness above about 10° angle of attack, presumably due to flow separation at the tip portions.

The deflection of the partial-span flap introduces a large relative washout of the aileron portions so that at a given over-all lift coefficient the ratio of yawing to rolling moments is less with flap down than with flap neutral. It will be noted that the tabulated values of sideslip remain about the same at $C_L=1.8$ as at $C_L=1.0$. The sideslip at $C_L=1.0$ would have been appreciably less than indicated if a flap-down condition had been assumed here.

Although the lateral-stability characteristics of the highly tapered wing are unfavorable, there are indica-

[2] As mentioned previously, in order to simplify the computations and to make possible a comparison with flight records, the starting time has been arbitrarily taken as the instant at which the control surfaces reached half their final deflection.

tions that the use of a partial-span flap may not aggravate the instability in every case. The results of the aileron tests, as well as visual observations of the flow by means of tufts, show that the effect of the upwash at the tips introduced by lowering the flap may be compensated by a strong spanwise flow, which inhibits the stalling of these portions. The indications are that the angle of attack for autorotational instability would be about the same with the flaps as without for the wings tested, although rolling experiments were not tried.

Plain ailerons with retractable flap.—A plain aileron with a split flap retracting ahead of it was developed as a means of control with a full-span flap. This device has been tested in flight with a modified Fairchild 22 airplane and is one of the few lateral control systems incorporating full-span flaps that has proved entirely satisfactory in flight (reference 3). This device is so designed that the retracted flap does not interfere with the ailerons in any way and hence the control characteristics with flap neutral are those of plain ailerons. With the flap deflected, however, the characteristics are similar to those of the upper-surface ailerons tested in the 7- by 10-foot wind tunnel (reference 1, part XII).

Although the deflected flap is in such a position as to shield the under surface of the ailerons entirely, it was observed in the tests that the ailerons in this condition were nearly as effective as conventional ailerons with unsealed gaps. The effectiveness of downward deflection, however, falls off rapidly at an angle of about 8°.

The rolling-moment characteristics of the plain ailerons with retractable flaps are such as to favor a differential motion, since the upgoing aileron is more effective than the downgoing one at high lift coefficients. The hinge-moment characteristics are, however, distinctly unfavorable for this mode of operation inasmuch as the ailerons show a downward floating tendency with the flap down. Relatively large deflections of the ailerons are required to meet the control requirements at low speed on account of the shielding effect of the flap, and consequently a relatively high gearing ratio of ailerons to control stick is needed. The result is that the stick forces required for the specified banking control are somewhat higher than those for conventional ailerons throughout the flight range. These forces (see aileron 24, table I) are well within the desirable range for the Fairchild 22 airplane, although they indicate undesirably high values for larger airplanes.

The yawing action of these ailerons is about the same as that of the conventional ailerons with partial-span flaps. Although the induced yawing moment of the ailerons with the full-span flap is greater than that with the partial-span flap, the ailerons cause larger compensating changes of profile drag.

Several possible means of improving the control-force characteristics of these devices suggested themselves. The device listed next in table I (aileron 25) shows the calculated effects of such improvements. First, the span of the aileron was increased to what has previously been found the most efficient value and the chord of the aileron was reduced as much as seemed practical. Second, it was assumed that a trailing-edge tab (0.02 c_w bent down 15°) was attached to the aileron so as to avoid the downward-floating tendency. It was assumed that lowering the flap caused the same change in floating angle with the tab as without. Since the deflection of the flap caused a large change in the floating position of the aileron, it was desirable to change the balancing characteristics of the differential with flap deflection. Consequently, it was assumed that the differential cranks were rotated into new positions as the flap was deflected. The resulting stick forces tabulated give an indication of the improvement that might be effected by such development of the device.

Retractable ailerons (spoilers).—Tests of spoilers (reference 12) showed that for locations behind about 80 percent of the wing chord the lag in rolling action would probably be negligible. Flight tests were subsequently made of a Fairchild 22 airplane equipped with a curved-plate spoiler that moved edgewise into and out of the wing through a narrow slit in the upper surface at 83 percent of the airfoil chord. This plate was arranged to rotate about a hinge at the center of curvature, so that the air pressure (being normal to the plate) caused no resultant hinge moment. The test airplane incorporated a full-span split flap and, inasmuch as the downward motion of the spoiler took place entirely within the wing, the flap and spoiler did not interfere.

The flight tests showed very promising results, although the feature of zero hinge moment was not found especially desirable. Angular-velocity and control-position records taken simultaneously in flight showed no definite lag or sluggishness in the response to control movements. (See reference 3.) The devices as tested (0.15 c_w by 0.50 $b/2$) were somewhat larger than necessary to give the assumed satisfactory degree of control. As is indicated in the table, a maximum deflection causing a 7.4 percent c_w projection of the spoiler should be sufficient for control in the flap-down condition.

An important advantage of the retractable ailerons (aside from their advantage in permitting the use of a full-span flap) is that they give small favorable yawing moments throughout the greater portion of the flight range. At high lift coefficients with the flap in use, however, small adverse yawing moments result. (See reference 13.)

Although the deflected spoiler causes quite an increase of profile drag, it is not expected that the incidental deflections required for control in normal flight would appreciably affect the performance. The performance criterions listed are, of course, for undeflected controls.

External-airfoil flap-type ailerons.—The external-airfoil (Junkers or Wragg) type flap has been studied as a possible means for improving the take-off and

ceiling characteristics of airplanes in addition to providing the high-lift features of ordinary and split flaps. As this device showed promise of improved performance, several methods of securing lateral control with such a flap have been studied.

A simple method of providing lateral control with full-span external-airfoil flaps is to move the flaps themselves independently as ailerons. (See reference 10.) Thus the ailerons are used simultaneously as a high-lift device and to provide rolling moments without sacrificing a special part of the wing span. In order to employ these flaps to their best advantage, it is necessary to deflect them downward over the entire wing span, thereby avoiding excessive induced drag. The action of the flaps deflected downward as ailerons is similar to the action of ordinary ailerons with droop. The external-airfoil flaps show a superiority over ordinary flaps for this purpose, however, in that they retain their lift-changing effectiveness at greater downward deflections (in excess of 20°).

Aileron 27 in the table is an arrangement of these flaps whereby the entire span is deflected downward 20° and the semispan portions are moved differentially from this downward position to provide rolling control.

This arrangement was tested in flight with the Fairchild 22 airplane and was found to give unsatisfactory yawing characteristics, although the rolling moments seemed to be ample. The computations made for the average airplane indicated an adverse sideslip of 10° accompanying a 15° bank at low speed with the flaps down.

A possible way of improving the adverse-yaw characteristics of these devices is to make use of the effect of washout. This method was used in the case of aileron 28, where the flap was considered to extend unbroken over the middle portion of the wing with the parts of the flap used as ailerons covering the outer 50 percent of the semispan portions. Wind-tunnel tests (reference 10) showed that, with the inner portion down 30° and the outer, or aileron, portions down only 10°, the performance criterions were about the same as with the whole flap down 20°. This change reduced the yawing effect considerably, as shown by the table, although the sideslip is still somewhat worse than is the case with most of the other devices.

When the stick forces and deflections for these two arrangements are compared, it will be noted that the deflection required with the full semispan aileron is almost as great as that required when only half the flap is used for control. This fact is partly accounted for by the difference in yawing effects.

In the low-speed conditions (C_L=1.8) the ailerons are lowered 20° in one case and 10° in the other and the effective floating angles are thereby increased by these amounts. This fact introduces a difficulty into the design of a suitable differential linkage. A linkage designed to accommodate the floating tendency with flaps neutral will overbalance when the flaps are deflected. In the computations it was assumed that the additional floating tendency was neutralized by a long spring that came into action as the flaps were lowered.

The external-airfoil flaps permit high lift coefficients to be attained without excessive profile drag. The advantage over a split flap begins to be apparent at lift coefficients in excess of 0.7, aiding the take-off and the low-speed climb but hardly affecting the maximum rate of climb. Hence, in this particular case, the performance criterions listed in table I do not fully indicate the differences to be expected with these devices.

Ailerons with external-airfoil flaps.—A logical extension of the development of the slot-lip aileron has led to a device in which the aileron forms the lip of the slot between an ordinary external-airfoil-type flap and the main wing. (See aileron 29, table I.) This arrangement avoids the excessive drag entailed by other forms of slot and, on account of the rearward position of the aileron, should give good response characteristics (except, possibly, under certain conditions noted later).

The device as tested (see reference 9) comprised an aileron 0.12 c_w wide and $b/2$ long. The tests showed that, in general, the effectiveness of the aileron was reduced by the presence of the flap, in accordance with the theoretical consideration that any change in slope of the wing section ahead of the trailing edge is less effective than a corresponding change at the trailing edge itself. When the flap is lowered, however, an upward deflection of the aileron apparently causes separation of flow over the flap, thus greatly reducing the lift and developing a large rolling moment. With the flap down 30° this change occurs at the beginning of the aileron deflection, while at intermediate flap deflections the change occurs at greater up aileron angles. This more or less sudden change of conditions, in addition to giving a large increase of rolling moment, also caused a reduction or a reversal of hinge moment; hence, the device may be impracticable for use at intermediate flap settings. (See reference 9.)

In the device as shown in table I the downward deflection of the aileron is limited by the presence of the flap nose to a maximum of about 7°, and it is consequently necessary to use a differential movement. Change of setting of the flap has a pronounced effect on the floating angle of the aileron. With the flap set at 30° a differential giving no more than 7° downward deflection of the aileron will be overbalanced by this floating tendency. In the computation it was assumed that a spring tending to turn each aileron downward (with a torque of 8.7 foot-pounds acting at the aileron hinge) was brought into action by lowering the flap. With the flap neutral the floating angle of the aileron is too small for satisfactory balance, although wind-tunnel tests showed that it could be effectively increased by a tab. Consequently, the device was assumed to incor-

porate such a tab (0.018 c_w, down 5°) and the spring tension was adjusted to accommodate the effect of the tab with flap down.

The resulting stick forces, together with the deflections required for control, appear in the table. It will be noted that the greatest deflection required is that at $C_L=1.0$. In this condition the aileron does not produce the previously discussed change in flow over the flap. At $C_L=1.8$ the deflection required is small because a small upward movement of the aileron in the flap-down condition produces a large rolling moment. The yawing effect is adverse but is not excessive.

The performance characteristics of this wing (with the N. A. C. A. 23012 airfoil flap) are somewhat better than those of the two wings previously considered, which had flaps of Clark Y section.

II. ANALYSIS OF CONVENTIONAL FLAP-TYPE AILERONS

The practical advantages of plain ailerons are well known, and, since they are universally used in more or less modified form, the following section is devoted to an analysis of factors involved in their design.

One of the conclusions of the lateral control investigation has been that no decisive benefit was to be gained from a device that continued to give rolling moments when the major outer portions of the wings were stalled. If stalling of the aileron portions of the wing is prohibited, plain ailerons or other devices located near the trailing edge of the wing will retain their effectiveness.

If the loss of rolling effect on a stalled wing is discounted, it appears that the primary disadvantage to be associated with plain ailerons is their adverse yawing effect. For this reason the yawing action of plain ailerons will be rather fully analyzed.

ROLLING MOMENT

For the purpose of calculating the coefficients of rolling and yawing moment, the effect of a deflected aileron may be ascribed to a change of angle of attack of the wing sections comprising the aileron portions. Thus, the localized effect of the deflected aileron is measured by the change in the angle of zero lift. This change is proportional to the angle of deflection of the aileron for deflections below about ±20° and the factor of proportionality (denoted by $\Delta\alpha/\Delta\delta$) depends on the chord of the aileron. Thus, the plain flap-type aileron is considered merely as a device for changing the angle of attack. The section lift increment is not used to characterize the effect of the flap because this increment cannot, in general, be specified, being dependent on the plan form of the wing. The effective change in angle of attack per unit change of flap deflection is, however, theoretically independent of the aspect ratio and the plan form.

Figure 11 summarizes the results of a number of wind-tunnel experiments with plain flaps (references 14, 15, and 16) and shows the measure of flap effectiveness ($\Delta\alpha/\Delta\delta$) as a function of the relative flap chord. A curve predicted by wing-section theory (reference 17) is also shown for comparison. The surprisingly powerful effect of a narrow flap should be noted. Thus, deflecting a 0.20 c_w flap is about half as effective as deflecting the entire wing section.

Since the effective angle of attack of a wing section is a linear function of the camber (reference 17), the curve of figure 11 may be used to predict the effect of a multiply hinged flap, such as an aileron equipped with a balancing tab. The combined effect of a succession of bends along the wing section may be found by calculating the separate effects of each bend and adding them. Thus the effect of a 0.20 c_w aileron equipped with a 0.05 c_w tab is (using values from fig. 11)

$$\Delta\alpha=0.51\delta_a+0.21\delta_t \qquad (2)$$

where δ_a is the deflection of the aileron with respect to the wing and δ_t is the deflection of the tab with respect to the aileron. This simple relation should not be expected to apply beyond ±20° deflection and, in the case of very narrow tabs, beyond about ±15°

Deflected ailerons thus cause, in effect, a discontinuous change of angle of attack across the wing span. The lift change caused by the ailerons cannot be discontinuous, however, because of the natural equalization of pressure along the span. Ailerons covering only a portion of the span influence the lift at every spanwise point and this effect appears to be satisfactorily predicted by the airfoil theory. Calculations of the effects of ailerons based on this theory have been made, the most extensive series being reported in reference 18. Figure 12 shows the rolling-moment coefficient C_l caused by a 1° difference in angle of attack of various right and left portions of a rectangular wing of aspect ratio 6. The abscissa of this diagram represents a semispan of the wing with the midspan point at the origin and the tip at the point 1.0. The ordinate gives directly the rolling- (or yawing-) moment coefficient due to a unit change of angle of attack extending from the point indicated on the abscissa out to the tip. The rolling effect of two ailerons is twice as great as that of a single one and hence the difference of the increments of equivalent angle of attack, as indicated, should be used. The rolling moment is not appreciably changed by differential deflection.

The curves give the values predicted by the theory and the points indicate values obtained in various experiments as noted on the figure. The wing-section characteristic $\Delta\alpha/\Delta\delta$ of the devices tested was determined from figure 11.

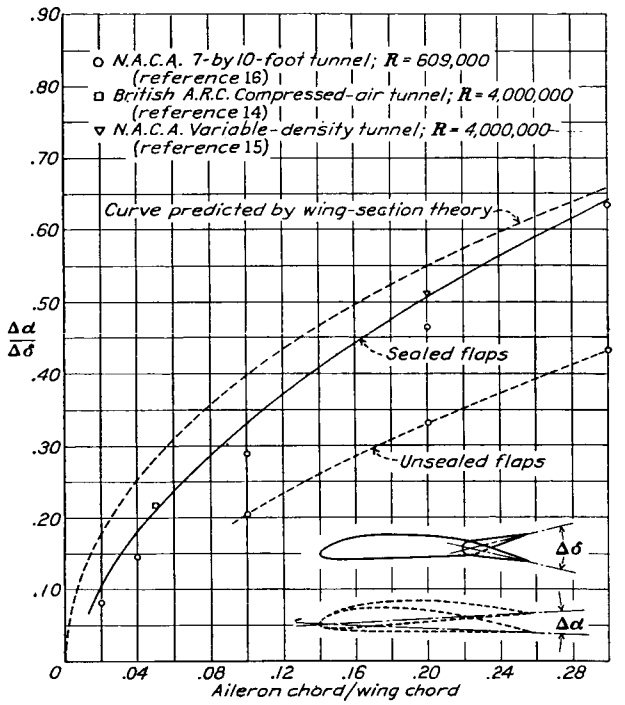

FIGURE 11.—Change of effective angle of attack of a wing section per unit change of flap angle. Plain flaps of various chords at small deflections; $\delta < \pm 20°$.

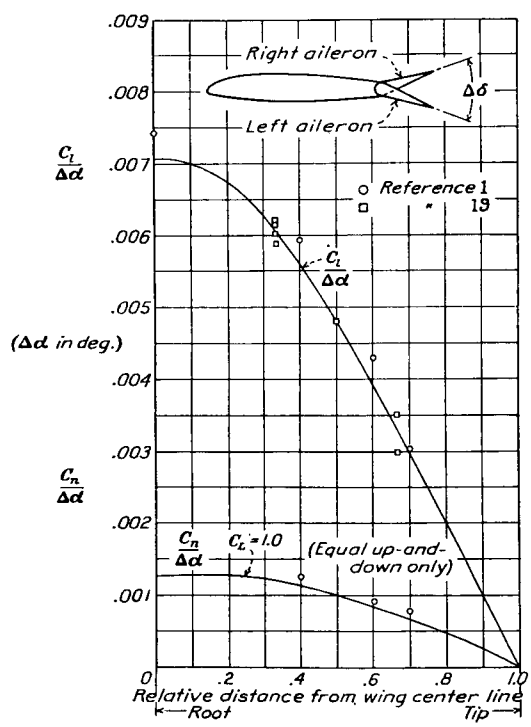

FIGURE 12.—Variation of rolling- and yawing-moment coefficients with aileron span and a comparison of theoretical and experimental values. Rectangular wings; $b^2/S = 6$; $\Delta\delta < \pm 20°$.

The rolling-moment characteristics of the plain 0.25 c_w by 0.40 $b/2$ sealed ailerons (aileron 1 of table I) were calculated with the aid of figures 11 and 12. Reference to figure 11 shows that the equivalent change in angle of attack produced by a 0.25 c_w sealed flap is 57.5 percent of the angle of deflection of the flap. Thus, a deflection of $\pm 7.4°$ (see table I) is equivalent to a change in angle of attack of

$$0.575 \times 7.4° = 4.26° \qquad (3)$$

or a difference of angle of the right and left aileron portions of 8.52°. According to figure 12 the rolling-moment coefficient per degree of this difference for a 0.40 $b/2$ aileron portion extending to the wing tip is 0.0039; hence, the coefficient predicted is

$$C_l = 8.52 \times 0.0039 = 0.0332 \qquad (4)$$

Working charts for predicting the rolling moment of plain ailerons of any size on monoplane wings of various aspect ratios and different degrees of taper are given in figure 13. In order to use these charts it is necessary to ascertain from figure 11 the section characteristic $\Delta\alpha/\Delta\delta$, which is a function of the relative chord of the aileron. The charts may be used for differential ailerons merely by taking the difference of angle of attack of the right and left aileron portions. The theoretical rolling moment is independent of any initial washout of the wing sections along the span; hence, the rolling-moment curves are applicable to wings with partial-span flaps. The charts cannot be used with devices that change the slope of the lift curve nor for excessive deflections that introduce disturbed air flow. In this connection it appears that a deflection of plain ailerons involving disruption of the air flow is inefficient from considerations of stick force.

It will be noted that two sets of curves are given for tapered wings. The solid lines apply to ailerons that are not tapered with the wing, i. e., ailerons of constant actual chord. For this type the change of equivalent angle of attack should be calculated on the basis of the wing-tip chord (whether or not the aileron extends to the wing tip). The long-dash curves are for the particular case in which the aileron chord is a constant proportion of the wing chord along the span, in which case the change of equivalent angle of attack does not vary along the aileron portion. The additive effect of an element of aileron covering any spanwise portion of the wing may be determined from the increment of the $C_l/\Delta\alpha$ curve over that portion. Although the curves of figure 13 show increasing rolling-moment coefficients with increased aspect ratios of the wings, the control requirement (rolling-moment coefficient for a given banking effect) also increases with aspect ratio and, on account of the damping, in nearly the same way as does the coefficient. (See reference 4.) In general, it may be said that the relative proportions of the ailerons

should not be reduced on account of increased aspect ratio.

YAWING MOMENT

Yawing moment with equal up-and-down deflection.—The results of experiments indicate that the primary source of adverse yawing moment given by plain ailerons at small deflections is the theoretical, or induced, yawing moment. The production of rolling moment results in an induced twisting flow analogous to the downwash in direct lift. The yawing moment arises from the resultant inclination of the supporting lift vectors along the span. If the wing is supporting no lift, the production of rolling moment by equal and opposite lift increments on the two wing halves will not result in a yawing moment because the lift increment vectors are all inclined backward by the induction, resulting in a drag. Hence, only the interaction of an initial lift and a rolling moment give rise to an induced yawing moment.

A more specific treatment of this theory is given in reference 18. The formula for yawing moment that results for equal up-and-down deflections is

$$C_n = KC_L \times C_l \tag{5}$$

where K is a factor dependent on the aspect ratio and the plan form of the wing, and to some extent, on the spanwise position of the aileron. It is interesting to note that with a given equal up-and-down aileron deflection the induced yawing *moment* is the same throughout the speed range, while the rolling moments and the stabilizing factors are greatly reduced at the lower speeds.

Figure 12 gives a comparison of theoretical and experimental values of $\frac{C_n/\Delta\alpha}{C_L}$ for a rectangular wing of

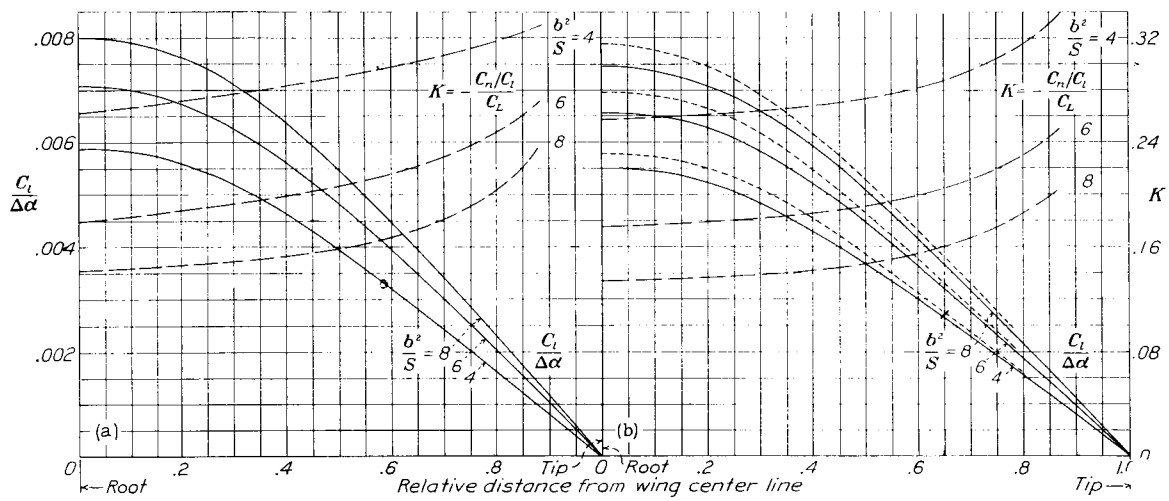

(a) Rectangular. (b) 4:3 taper.

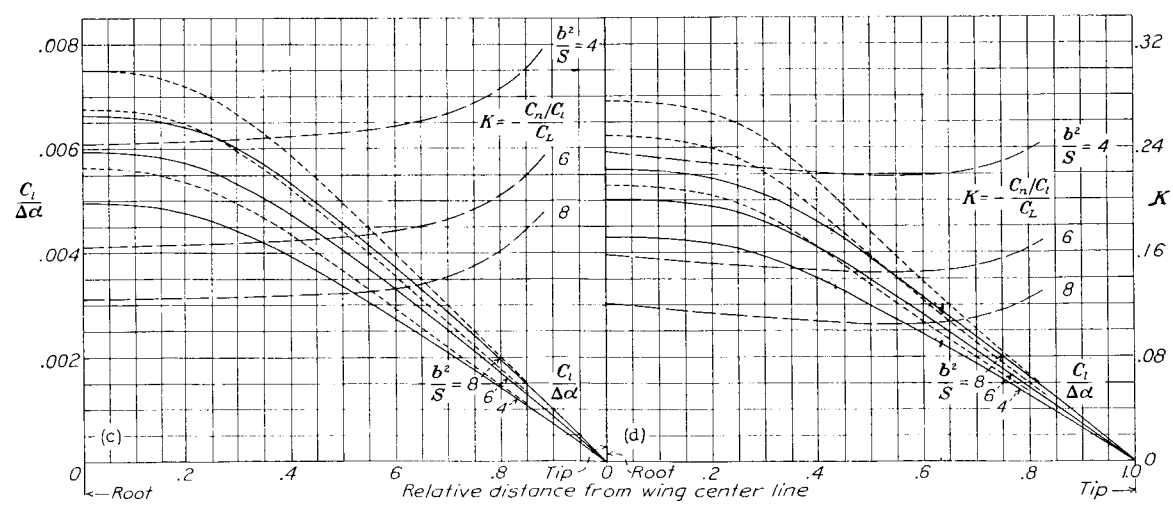

(c) 2:1 taper. (d) 4:1 taper.

FIGURE 13.—Charts for calculation of rolling and yawing moments of plain ailerons, showing the effects of span and spanwise location of ailerons with straight and tapered wings.

aspect ratio 6. Deviation from the theory is to be expected at excessive deflections of ordinary ailerons and with special types of devices, since important changes of profile drag may be introduced. If complete wing section data are available, however, the profile-drag part of the yawing moment may be readily estimated.

As in the case of rolling moment, the yawing moment of an aileron at any spanwise position may be calculated by taking the difference of ordinates at abscissas corresponding to the ends of the aileron. Unlike the rolling moment, however, the yawing moment of differential ailerons is not the same as that of ailerons with equal deflections. In the general charts given in figure 13 the ratio of yawing to rolling moments at $C_L = 1.0$ is given rather than $C_n/\Delta\alpha$. In this case the differences between two points cannot be used directly to give the yawing moment of an aileron extending between these two points. The yawing moment caused by an aileron ending inboard of the tip may be found, however, by taking the difference of the yawing moments given by two ailerons, one extending from the inboard end of the actual aileron to the wing tip and the other extending from the outboard end to the tip. The straight and tapered ailerons should give yawing moments in practically the same ratio to the rolling moment; hence, only a single set of values of $K = -\frac{C_n/C_l}{C_L}$ is given.

Referring again to the 0.25 c_w by 0.40 $b/2$ plain aileron (aileron 1) of table I, it is found that the ratio of yawing- to rolling-moment coefficients for this case is

$$\frac{C_n}{C_l} = -0.216 \tag{6}$$

at $C_L = 1.0$. (See fig. 13.) At the deflection given the rolling-moment coefficient previously found is

$$C_l = 0.0332 \tag{7}$$

Hence, the yawing-moment coefficient at $C_L = 1.0$ is

$$C_n = -0.216 \times 0.0332 = -0.0072 \tag{8}$$

The values of both yawing- and rolling-moment coefficients for these ailerons having been obtained, it is now possible to calculate their rolling effectiveness by means of figure 3. The wing loading of the average airplane assumed in table I is 9.4 pounds per square foot; hence, at $C_L = 1.0$ the banking effect of a rolling moment of coefficient 0.01 acting for 1 second is

$$\left(\frac{\phi_1 b}{2}\right)_{C_l = 0.01} = 1.42 \text{ feet} \tag{9}$$

and for a rolling-moment coefficient of 0.0332

$$\frac{\phi_1 b}{2} = 1.42 \times 3.32 = 4.7 \text{ feet} \tag{10}$$

The effect of the yawing moment of coefficient -0.0072 is calculated in the same way, i. e.,

$$\frac{\phi_1 b}{2} = -0.72 \times 0.65 = -0.47 \text{ foot} \tag{11}$$

The effect of these rolling and yawing moments applied simultaneously is

$$\frac{\phi_1 b}{2} = 4.7 - 0.47 = 4.23 \text{ feet} \tag{12}$$

Thus, deflecting the ailerons suddenly to $\pm 7.4°$ causes a 4.23-foot displacement of the wing tips in 1 second. The angle of bank for the average airplane ($b/2 = 16$ feet) is

$$\phi_1 = \frac{\frac{\phi_1 b}{2}}{\frac{b}{2}} \times 57.3 = 15° \tag{13}$$

as appears in the table.

Yawing moment with differential deflection or droop.—The effect of an unequal movement of the ailerons may be taken into account by considering an equivalent equal up-and-down deflection from a mean upward position of the ailerons. Thus, deflections of 15° up and 5° down may be considered as equivalent to 10° equal up-and-down from a mean position 5° up. Inasmuch as a differential deflection of the ailerons changes the mean lift of the wing, figure 13 cannot be used without correction to calculate the yawing moment due to unequal deflection. As was brought out in the preceding discussion, the yawing moment is caused by the interaction of the wing lift and the induced flow caused by the rolling moment. Hence, the yawing moment incident to a given rolling moment depends on the distribution of the basic or symmetrical part of the lift. The basic lift distribution upon which the yawing moment depends is, then, the distribution for a wing with both ailerons raised. The adverse yawing moment will, in this case, be reduced because of the lessened lift over the tip portions. For the conditions following sudden aileron deflections the average upward movement of both ailerons will entail an actual reduction for a short time of the lift of the wing without correspondingly increasing either the flight speed or the angle of attack. The conditions will, of course, be different for steady flight with ailerons held over. For practical purposes it is sufficient to calculate an increment of C_n/C_l due to the increment of lift produced by the symmetrical droop or uprigging of both ailerons. This increment would be the yawing moment incident to a unit rolling moment when the entire lift of the airfoil was due to the droop of the ailerons. The ratio of yawing to rolling moment thus found will be a constant additive contribution to equation (5) at all lift coefficients.

Figure 14 shows the reduction of the ratio of adverse yawing to rolling moment in terms of the reduction of

over-all lift coefficient for a rectangular wing of aspect ratio 6. The experimental points indicated were derived by taking the differences of yawing moment measured with equal up-and-down deflections and up-only deflections and dividing these differences by the measured reduction in total lift coefficient caused by the up-only deflection.

If C_L is the lift of the wing with ailerons undeflected and $\Delta\alpha_m$ is the equivalent angle of washout of the

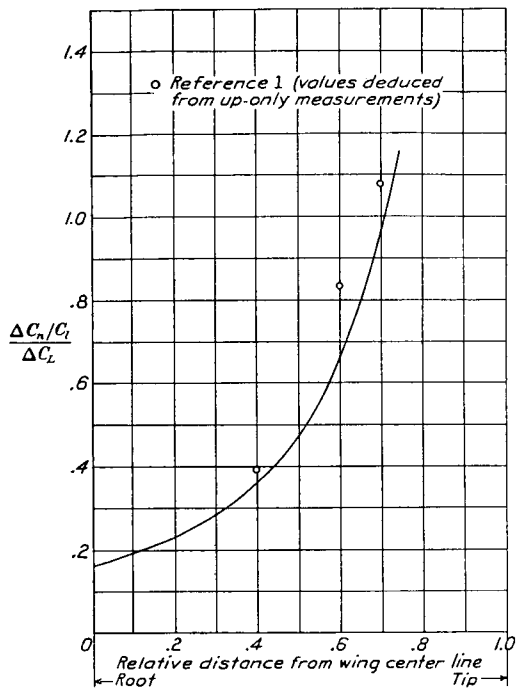

FIGURE 14.—Increment of induced yawing moment due to differential deflection of ailerons; ΔC_L is the reduction of lift coefficient due to differential deflection. Rectangular wing; $b^2/S=6$.

aileron portions introduced by the unequal aileron deflections, then

$$\Delta\frac{C_n}{C_l}=\kappa\Delta\alpha_m \tag{14}$$

since the reduction of lift is proportional to $\Delta\alpha_m$. The factor κ, like the factor K, depends on the wing plan form and the relative length of the aileron portion.

Figure 15 shows theoretical values of κ for wings of aspect ratio 6 and various plan forms. It should be remembered that C_L as used in equation (14) is the lift coefficient with ailerons undeflected. Correction of the values given in figure 15 for wings of different aspect ratio may be made by considering that κ is very nearly inversely proportional to the aspect ratio.

It is evident that the foregoing remarks apply equally as well to wings having washout at the tips or to wings with partial-span flaps. For wings with partial-span flaps $\Delta\alpha_m$ is simply the reduction of the effective angle of attack at the tips due to removal of the tip portions of the flap. It should be remembered that droop of the outer portions (negative $\Delta\alpha_m$) increases the adverse (negative) yawing moment while washout (positive $\Delta\alpha_m$) decreases it.

The increment of yawing moment due to the sum of two distributions of droop or washout is equal to the sum of the increments associated with each separate distribution. This property may be used to compute quite accurately, though not exactly, the yawing

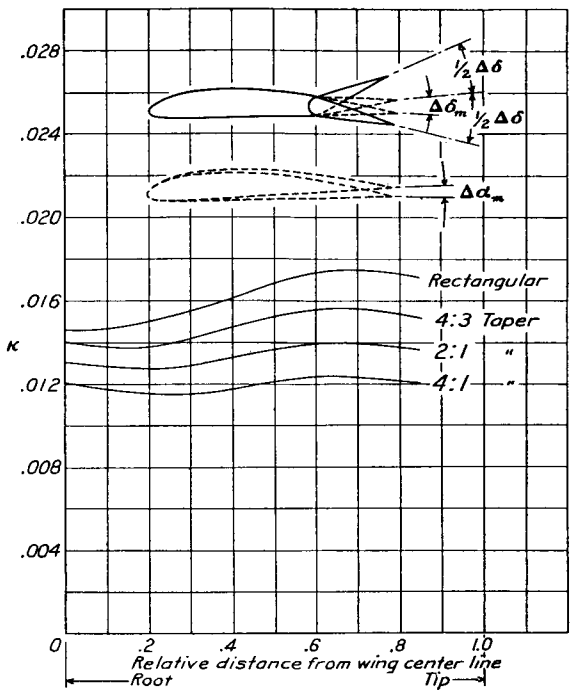

FIGURE 15.—Ratios for calculating additional induced yawing moments of differential ailerons or ailerons on wings with washout; $b^2/S=6$; $\Delta\alpha_m$ is in degrees.

$$(1+\Delta)\frac{C_n}{C_l}=-KC_L+\kappa\Delta\alpha_m$$

moment of differential ailerons that end inboard of the wing tip.

CONTROL FORCES

Hinge moment.—The available experimental data indicate that the hinge-moment coefficient C_h of an ordinary aileron can be treated with sufficient accuracy as a characteristic of the wing section, that is, as a characteristic independent of the plan form of the aileron or the wing. An average experimental value for the slope of the hinge-moment curve against deflection is

$$\frac{dC_h}{d\delta}=-0.0085 \text{ per degree} \tag{15}$$

for sealed ailerons of chord c_a and span b_a, where

$$C_h=\frac{\text{hinge moment of aileron element}}{qc_a^2b_a}$$

Thus, the actual hinge moment at a given deflection varies as the aileron span and as the square of the aileron chord.

Strictly speaking, the hinge moment of a deflected flap should be calculated in two parts. The primary part arises from that component of the distributed pressure change which does not contribute to the lift of the airfoil section. Since no lift is involved, this component is independent of the aspect ratio. The second component of the hinge moment, proportional to the lift change, is subject to the ordinary aspect-ratio correction. The correction is, however, small except for wide flaps.

Some additional considerations arise in the application of aileron hinge moments to the calculation of control force. The angular travel and the length of the control stick (or radius of the control wheel) are limited in practice. Thus, ailerons requiring large deflections must be geared to the control stick or wheel in a high ratio. In the case of the average airplane the total circumferential movement of the end of the control stick was assumed to be 0.73 foot in the case of each of the control devices. This value corresponds to a $\pm 25°$ deflection of a 20-inch stick corresponding to that available in the Fairchild 22 airplane.

If reference is made to the tabulated results for aileron 1, it is seen that the total deflection necessary to insure the assumed satisfactory degree of control ($\phi_1 = 22.5°$ at $C_L = 1.0$, in this case) is $\pm 11.2°$. The work of deflecting ailerons of chord c_a and span b_a is

$$\frac{dC_h}{d\delta}\,\delta\,\frac{\delta}{57.3}\,qc_a^2 b_a = -0.0085 \times \frac{11.2 \times 11.2}{57.3} \times 9.4 \times (0.25 \times 5.3)^2 \times 0.4 \times 16 = 1.97 \text{ foot-pounds} \qquad (16)$$

The control force is equal to twice the total work divided by the linear travel of the end of the stick, or

$$\text{Stick force} = \frac{3.94}{0.73} = 5.4 \text{ pounds} \qquad (17)$$

The stick force at the partial deflection required for $\phi_1 = 15°$ is

$$2.31 \times \frac{\delta 15°}{\delta 22.5°} = 2.31 \times \frac{7.4°}{11.2°} = 3.6 \text{ pounds} \qquad (18)$$

These simple relations apply, of course, only to linear variation of the hinge moment and to nondifferential gearing.

Differential linkages.—It appears that a differential linkage can, when properly designed, be a very effective means of reducing the operating force of flap-type ailerons (reference 11). The reduction of operating force is accomplished by taking advantage of the upfloating tendency of the ailerons. With differential linkage the ailerons on opposite tips of the wing begin to move at different rates immediately after they are deflected from neutral, the downgoing aileron moving more slowly than the upgoing one. The upgoing aileron thus has the greater mechanical advantage at the control-stick connection. It is evident that the reduced upward pressure of the upgoing aileron is partly compensated by its increased mechanical advantage and that the increased upward pressure on the downgoing aileron is also partly compensated by its reduced mechanical advantage. At a certain deflection the downgoing aileron reaches dead center and, regardless of its aerodynamic pressure, cannot contribute to the stick force; if the upgoing aileron is then at the floating angle (i. e., angle of zero hinge moment), the stick force will be zero.

Ordinary ailerons show nearly straight-line hinge-moment curves $\left(\frac{dC_h}{d\delta} = -0.0085\right)$ and in this case the balancing effect of a given differential linkage depends only on the upfloating angle. A formula for a differential motion that gives zero operating force over a range of deflections may be obtained by writing the expression for the work of deflection of the ailerons and equating it to zero at every point.

$$\delta_d = \sqrt{(\delta_{uf} + \delta_u)^2 - 2\delta_u^2} - \delta_{uf} \qquad (19)$$

where δ_u and δ_d are the upward and downward deflections of the ailerons and δ_{uf} is the floating angle measured upward from the neutral position. A practical limitation of this formula is reached when $d\delta_d/d\delta_u$ approaches -1, for then both ailerons begin to move in the same direction and at the same rate.

It should be appreciated that a differential designed in accordance with equation (19) will give complete balance at the specified floating angle. It is, however, considered desirable not to eliminate completely the control force at any flight condition, as the pilots' feel of the control would be taken away. This condition can be avoided by designing the linkage for a fictitious floating angle somewhat higher than the maximum actually reached in flight. If $\Delta\delta_{uf}$ is the difference between the floating angle at which the differential gives complete balance and the actual floating angle of the aileron in the given flight condition, the resultant stick coefficient C_{h_s} will be

$$\frac{\text{Stick moment}}{qc_a^2 b_a} = C_{h_s} = \Delta\delta_{uf}\,\frac{dC_h}{d\delta}\left(\frac{d\delta_u}{d\theta} + \frac{d\delta_d}{d\theta}\right) \qquad (20)$$

where θ is the angular deflection of the control stick.

In any given case the stick force can be balanced out at only one angle of attack and, in general, the balancing effect diminishes as the angle of attack is reduced. Hence, if the stick force is made to become zero at an angle of attack above maximum lift, overbalance of the control in normal flight will be avoided.

A more or less complicated mechanical linkage that would give aileron movements approximating equation (19) could be devised. The ordinary simple linkage consisting of two properly set cranks connected by a rod can, however, be arranged to give the desired motion with close approximation, and such an arrangement will be given primary consideration.

Such a simple linkage can be made to satisfy two conditions for a minimum stick force. Figure 16 shows a type of stick-force curve that satisfies two very simple criterions. First, the slope of the curve is zero at the beginning of the deflection and, second, the resultant stick force is zero at a stick deflection corresponding to the floating angle of the up aileron. As was stated earlier, the latter condition is satisfied by arranging for the downgoing aileron to reach dead center when the upgoing aileron reaches the floating angle. Figure 17 shows geometrical arrangements of linkages that satisfy these two criterions for a minimum stick force. If the spacing of the crank centers is known in terms of the crank radius, the figure gives directly the neutral settings of the two cranks. The differential thus chosen will give what amounts to complete balance at the specified floating angle. The maximum downward

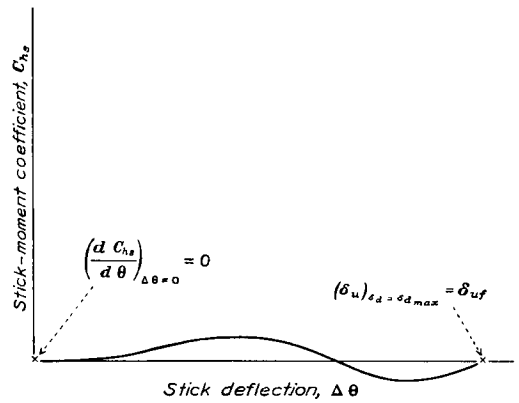

FIGURE 16.—Type of curve that satisfies simple criterions for minimum stick force.

travel of the aileron is shown in each case and it is to be noted that, if the maximum deflection of the upgoing aileron exceeds the assumed floating angle, the downgoing aileron will pass dead center and return toward neutral.

Since the floating tendency of a given aileron has a primary influence on the design of the differential linkage, it will be necessary to devote some study to this aileron characteristic. It appears that the floating angle of a plain flap-type aileron can be attributed to two effects: (1) a hinge moment proportional to the angle of attack of the wing, this moment being greater for large flap chords but independent of the shape of the wing section; and (2) a hinge moment attributed to the camber of the wing section, which remains constant as the angle of attack is changed. This second moment is primarily influenced by the camber of the aileron portion itself and is greatly affected by small changes at the extreme trailing edge. Thus, a small fixed tab can be used to introduce a large constant floating moment.

Figure 18 shows the variation of floating angle with flap chord and lift coefficient for the Clark Y wing section. The floating angles shown were indirectly computed from floating moments that were found by integration of pressure-distribution diagrams for a smooth wing (reference 20) and hence correspond to smoothly sealed flaps.

For the comparisons given in table I, infinite linkages ($R=0$ in fig. 17) were assumed to simplify the computations of control force. In most cases of differential ailerons listed, several trial computations of stick force were made to ascertain the optimum differential arrangement. These trial computations included the

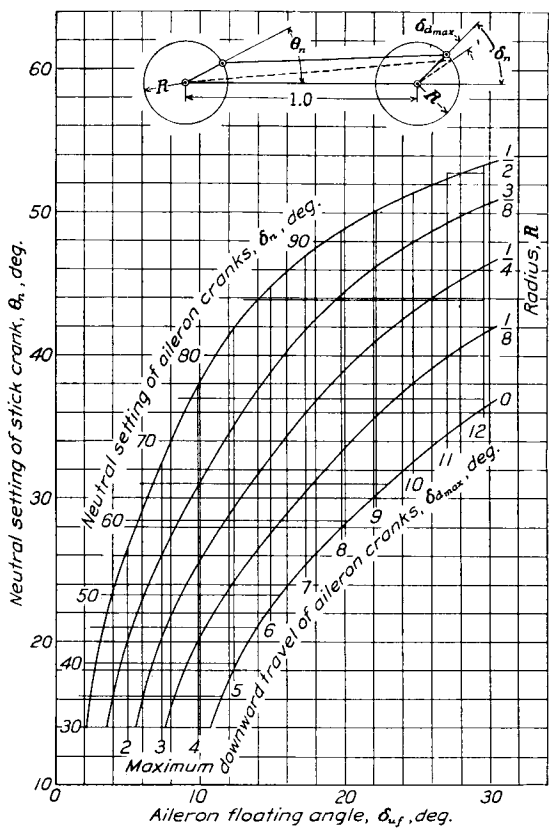

FIGURE 17.—Specifications of simple differential linkages that satisfy criterions for minimum stick force.

$\left(\frac{dC_{h_e}}{d\theta}\right)_{\theta=\theta_n}=0;\ (\delta_u)_{\delta_d=\delta_{d_{max}}}=\delta_{uf}$

determination of the curve of stick force against deflection to insure that no reversals of slope of the stick-force curve occurred at any point.

Aileron 1 may be used to illustrate the use of figure 17 in the selection of a differential. Assuming that the greatest possible reduction in stick force is desired, a floating angle only slightly higher than the maximum shown by figure 18 will be assumed. On the assumption that it is permissible to allow the control force to become zero at $C_L=1.25$ ($\delta_{uf}=11°$), the differential chosen by means of the chart will have neutral settings of $\theta_n=15°$ and $\delta_n=30°$, approximately. As indicated by figure 17, the maximum downward deflection obtain-

able with this arrangement will be about 4½° and this angle will be reached when the upgoing aileron reaches 11° deflection. For greater deflections the downgoing aileron will return, reaching neutral when the up aileron is at 22°.

Effect of a fixed tab used in conjunction with a differential linkage.—Figure 18 shows that the floating angles of plain ailerons are reduced as the lift coefficient is reduced. It is on this account that the balancing effect of the differential diminishes. The stick forces tabulated for the differentially linked aileron 1 show this effect as an increase of stick force at high speed. It is possible to introduce a large constant floating moment by means of a properly formed fixed tab. The effect of such a tab is to increase the floating angle at all flight speeds by a constant amount so that the per-

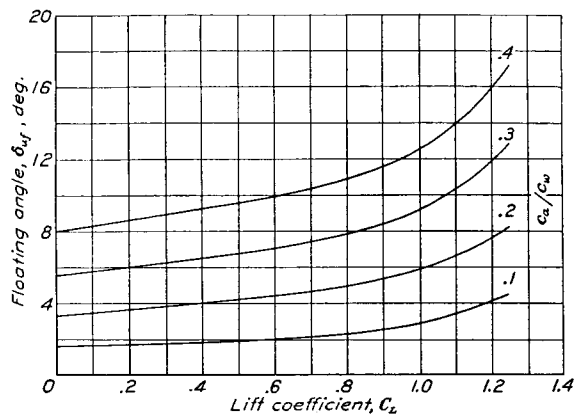

FIGURE 18.—Floating angles of sealed flaps of various chords on a Clark Y wing as computed from pressure-distribution data (reference 20).

centage variation with flight speed is reduced. This effect is especially pronounced in the case of very narrow ailerons, which do not show a very great variation of floating angle with angle of attack.

Furthermore, the maximum floating angle shown by very narrow ailerons is not great enough to permit the use of a differential to the best advantage. Thus, if the floating angle is considerably smaller than the maximum upward deflection required to produce sufficient control, the stick force may rise considerably after this point is reached on account of the return of the downgoing aileron and the consequent extra deflection required of the upgoing aileron. Advantageous use of a differential in such cases can be accomplished by incorporating a fixed tab (or a small amount of camber) arranged to trim both ailerons upward. In order to secure satisfactory results with a tab, a reasonably smooth inset type with a sealed juncture should be used. Attached tabs or tabs set at large angles ($\delta_t > \pm 15°$) have been found to cause an adverse increase in the slope of the hinge-moment curve.

Figure 19 shows the summarized results of experiments with tabs made in the 7- by 10-foot wind tunnel. As was stated before, the tab produces an essentially constant change in floating angle. The variation of floating angle with angle of attack can be found from figure 18. Figure 19 gives the change of aileron floating angle with tab deflection. (See references 9 and 21.) The experiments indicated that this ratio depended primarily on the ratio of tab chord to aileron chord independently of the chord of the aileron, although this relation can not be expected to apply as the aileron chord is indefinitely increased. At the Reynolds Number of the tests the tabs began to lose effectiveness when

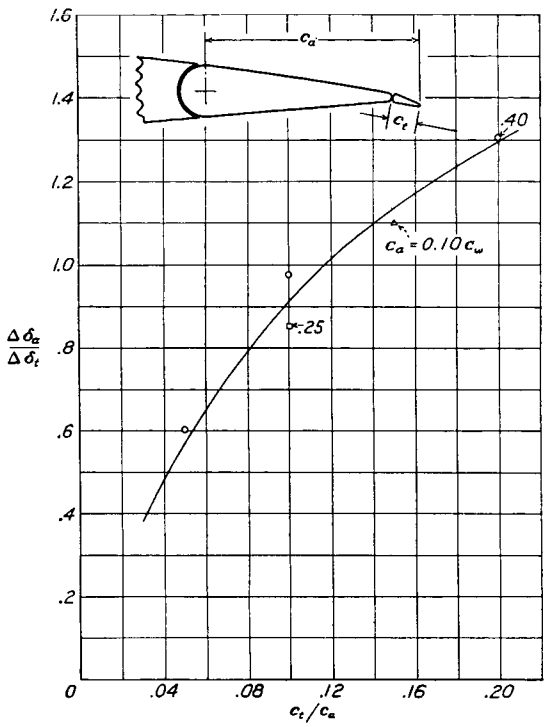

FIGURE 19.—Effect of inset tabs on aileron floating angles (references 9 and 21); $\delta_t < \pm 15°$.

deflected past 15°; hence, the ratios given should be considered applicable to tab deflections not exceeding this angle. Figure 19 may also be used to estimate the balancing effect of a movable tab.

It appears from figure 19 that a very large floating angle can be obtained by the use of a relatively small inset tab and deflection. Thus, the floating angle can very easily be altered to suit a given set of conditions. It has been pointed out that it is desirable to have the floating angle at least as large as the maximum upward deflection required for control so that the stick-force curve will lie reasonably near the minimum throughout the range. The smaller the percentage variation of floating angle with angle of attack, the smaller will be the variation of the actual stick force with flight speed. It would therefore appear desirable to trim the ailerons up as far as possible by means of a tab. On the other

hand, inasmuch as the deflected tab is made an inherent part of the airfoil camber, the size and deflection of the tab cannot be indefinitely increased without adversely affecting the pitching-moment and drag characteristics of the airfoil.

Reference to figure 19 shows that a 0.10 c_a (2½ percent c_w) tab deflected downward 10° will change the floating angles of aileron 1 by approximately 9°, raising the maximum floating angle to about 20°. This tab on the average airplane would be only 1.6 inches wide and the deflection of 10° would displace the trailing edge of the wing section by only one-third inch and would consequently not be expected to make a noticeable change in the drag or the pitching moment of the wing as a whole. The differential linkage giving complete balance at $\alpha=15°$ with this floating angle can be found from figure 17. The neutral settings of the cranks are

$$\theta_n=28°,\ \delta_n=59° \tag{21}$$

The maximum downward deflection found on the chart is about 8°, but in this case the aileron is not required to reach this deflection (20° up and 8° down) to produce a sufficient bank. Reference to figure 18 shows that the reduction in floating angle between $C_L=1.25$ (maximum) and $C_L=1.0$ is 2.5° so that, with the tab assumed, the floating angle at $\alpha=10°$ ($C_L=1.0$) will be

$$20°-2.5°=17.5° \tag{22}$$

Similarly, the new floating angle at $\alpha=0°$ ($C_L=0.35$) will be

$$20°-4.8°=15.2° \tag{23}$$

These values indicate that the balancing effect of the differential will not be greatly reduced at the higher speeds. Table I gives the actual stick forces as computed at these lift coefficients and indicates the reduction possible with a tab. An even better degree and range of balance could be attained with narrower ailerons on account of the smaller variation of floating angle with angle of attack.

CONCLUDING REMARKS

The provision of control rolling moments at high angles of attack or beyond the stall is not sufficient to secure control in flight at these angles unless the damping in rolling is retained. This requirement necessitates that at least the tip portions of the wing remain unstalled; hence, it cannot be considered a decided advantage to retain control rolling moments far above the stall with conventional wings.

The flight-testing experience gained throughout the course of the lateral control investigation has led to more or less definitely quantitative ideas regarding the desired effectiveness of the lateral control and the desirable variation of the control forces in normal flight.

From considerations of operating force required for a given amount of control, plain narrow sealed ailerons with deflections limited to 20° seem about the most efficient. Very great taper, or change of aileron chord along the span, leads to inefficiency whether used with a straight or a tapered wing. A differential linkage can be so designed as to reduce considerably the operating force of ordinary unbalanced ailerons, especially if a small fixed tab is used to increase the floating angle.

Several devices, notably the plain ailerons with flap retracting ahead, and the retractable aileron or spoiler located at 0.80 c_w have been developed and proved in flight to be suitable for use with full-span flaps. It was found, however, that the maximum lift of a tapered wing with split flaps was reduced less than 10 percent by the removal of the outer 0.30 $b/2$ portions of the flap, so that a conventional aileron could be used over that portion of the wing without great loss.

Aerodynamic theory can be successfully applied to the calculation of rolling and yawing moments of plain ailerons provided that experimental section characteristics are used in the computation of the local changes in angle of attack along the wing span caused by the ailerons. Further calculations involving the airplane stability characteristics can be applied to the prediction of the actual resultant motions caused by a given deflection of the control, thus giving a measure of effectiveness in controlling the movements of the airplane.

LANGLEY MEMORIAL AERONAUTICAL LABORATORY,
NATIONAL ADVISORY COMMITTEE FOR AERONAUTICS,
LANGLEY FIELD, VA., *April, 20, 1937.*

REFERENCES

1. Wind-Tunnel Research Comparing Lateral Control Devices, Particularly at High Angles of Attack.
   I. Ordinary Ailerons on Rectangular Wings, by Fred E. Weick and Carl J. Wenzinger. T. R. No. 419, N. A. C. A., 1932.
   II. Slotted Ailerons and Frise Ailerons, by Fred E. Weick and Richard W. Noyes. T. R. No. 422, N. A. C. A., 1932.
   III. Ordinary Ailerons Rigged up 10° When Neutral, by Fred E. Weick and Carl J. Wenzinger. T. R. No. 423, N. A. C. A., 1932.
   IV. Floating Tip Ailerons on Rectangular Wings, by Fred E. Weick and Thomas A. Harris. T. R. No. 424, N. A. C. A., 1932.
   V. Spoilers and Ailerons on Rectangular Wings, by Fred E. Weick and Joseph A. Shortal. T. R. No. 439, N. A. C. A., 1932.
   VI. Skewed Ailerons on Rectangular Wings, by Fred E. Weick and Thomas A. Harris. T. R. No. 444, N. A. C. A., 1932.
   VII. Handley Page Tip and Full-Span Slots with Ailerons and Spoilers, by Fred E. Weick and Carl J. Wenzinger. T. N. No. 443, N. A. C. A., 1933.

VIII. Straight and Skewed Ailerons on Wings with Rounded Tips, by Fred E. Weick and Joseph A. Shortal. T. N. No. 445, N. A. C. A., 1933.

IX. Tapered Wings with Ordinary Ailerons, by Fred E. Weick and Carl J. Wenzinger. T. N. No. 449, N. A. C. A., 1933.

X. Various Control Devices on a Wing with a Fixed Auxiliary Airfoil, by Fred E. Weick and Richard W. Noyes. T. N. No. 451, N. A. C. A., 1933.

XI. Various Floating Tip Ailerons on Both Rectangular and Tapered Wings, by Fred E. Weick and Thomas A. Harris. T. N. No. 458, N. A. C. A., 1933.

XII. Upper-Surface Ailerons on Wings with Split Flaps, by Fred E. Weick and Carl J. Wenzinger. T. R. No. 499, N. A. C. A., 1934.

XIII. Auxiliary Airfoils Used as External Ailerons, by Fred E. Weick and Richard W. Noyes. T. R. No. 510, N. A. C. A., 1935.

2. Weick, Fred E., Soulé, Hartley A., and Gough, Melvin N.: A Flight Investigation of the Lateral Control Characteristics of Short Wide Ailerons and Various Spoilers with Different Amounts of Wing Dihedral. T. R. No. 494, N. A. C. A., 1934.
3. Soulé, H. A., and McAvoy, W. H.: Flight Investigation of Lateral Control Devices for Use with Full-Span Flaps. T. R. No. 517, N. A. C. A., 1935.
4. Weick, Fred E., and Jones, Robert T.: The Effect of Lateral Controls in Producing Motion of an Airplane, as Computed from Wind-Tunnel Data. T. R. No. 570, N. A. C. A., 1936.
5. Gough, M. N., and Beard, A. P.: Limitations of the Pilot in Applying Forces to Airplane Controls. T. N. No. 550, N. A. C. A., 1936.
6. Jones, Robert T.: A Study of the Two-Control Operation of an Airplane. T. R. No. 579, N. A. C. A., 1936.
7. Wenzinger, Carl J.: Wind-Tunnel Investigation of Tapered Wings with Ordinary Ailerons and Partial-Span Split Flaps. T. R. No. 611, N. A. C. A., 1937.
8. Shortal, J. A.: Wind-Tunnel and Flight Investigation of Slot-Lip Ailerons. T. R. No. 602, N. A. C. A., 1937.
9. Platt, Robert C., and Shortal, J. A.: Wind-Tunnel Investigation of Wings with Ordinary Ailerons and Full-Span External-Airfoil Flaps. T. R. No. 603, N. A. C. A., 1937.
10. Platt, Robert C.: Aerodynamic Characteristics of Wings with Cambered External-Airfoil Flaps, Including Lateral Control with a Full-Span Flap. T. R. No. 541, N. A. C. A., 1935.
11. Jones, Robert T.; and Nerken, Albert I.: The Reduction of Aileron Operating Forces by Differential Linkage. T. N. No. 586, N. A. C. A., 1936.
12. Weick, Fred E., and Shortal, Joseph A.: Development of the N. A. C. A., Slot-Lip Aileron. T. N. No. 547, N. A. C. A., 1935.
13. Shortal, J. A.: Effect of Retractable-Spoiler Location on Rolling- and Yawing-Moment Coefficients. T. N. No. 499, N. A. C. A., 1934.
14. Williams, D. H., and Brown, A. F.: Experiments on a Small-Chord Flap on a Clark YH Aerofoil in the Compressed Air Tunnel. R. & M. No. 1681, British A. R. C., 1936.
15. Higgins, George J., and Jacobs, Eastman N.: The Effect of a Flap and Ailerons on the N. A. C. A.—M6 Airfoil Section. T. R. No. 260, N. A. C. A., 1927.
16. Wenzinger, Carl J.: Wind-Tunnel Investigation of Ordinary and Split Flaps on Airfoils of Different Profile. T. R. No. 554, N. A. C. A., 1936.
17. Munk, Max M.: Elements of the Wing Section Theory and of the Wing Theory. T. R. No. 191, N. A. C. A., 1924.
18. Pearson, H. A.: Theoretical Span Loading and Moments of Tapered Wings Produced by Aileron Deflection. T. N. No. 589, N. A. C. A., 1937.
19. Heald, R. H., and Strother, D. H.: Effect of Variation of Chord and Span of Ailerons on Rolling and Yawing Moments in Level Flight. T. R. No. 298, N. A. C. A., 1928.
20. Wenzinger, Carl J., and Harris, Thomas A.: Pressure Distribution over a Rectangular Airfoil with a Partial-Span Split Flap. T. R. No. 571, N. A. C. A., 1936.
21. Harris, Thomas A.: Reduction of Hinge Moments of Airplane Control Surfaces by Tabs. T. R. No 528, N. A. C. A., 1935.

TABLE I (A).—COMPARISON OF VARIOUS LATERAL CONTROL DEVICES

Device / Criterion		Linkage	Control forces and aileron deflections to produce specified bank in 1 second				Maximum deflection (degrees) $\phi_1=22.5°$ $C_L=1.0$	Sideslip with 15° bank in 1 second (degrees)		Lateral stability $\alpha_{L_p=0}$ minus $\alpha_{C_{L_{max}}}$ (degrees)	Performance		
			$\phi_1=15°$										
			$C_L=0.35$		$C_L=1.0$			$C_L=0.35$	$C_L=1.0$		Maximum lift $C_{L_{max}}$	Speed range $\frac{C_{L_{max}}}{C_{D_{min}}}$	Climb $\frac{L}{D}$ at $C_L=0.7$
			Stick force (lb.)	Aileron angles (degrees)	Stick force (lb.)	Aileron angles (degrees)							
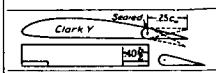	1. Plain ailerons sealed [a] $0.25c_w \times 0.40\frac{b}{2}$.	Equal	4.7	±3.4	3.6	±7.4	±11.2	3	7				
		Diff	2.1	3.9×2.7	1.1	11.0×4.1	20.0×2.0	3	7				
		Diff. with tab.	.9	3.7×3.0	.3	9.0×6.0	14.0×7.7	3	7				
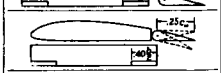	2. Plain ailerons $0.25c_w \times 0.40\frac{b}{2}$.	Equal	6.4	±3.8	5.6	±9.4	±14.5	3	8	0	1.27	91	18.7
		Diff	2.6	4.5×3.0	1.6	11.0×4.8	18.0×5.0	3	7	0	1.27	91	18.7
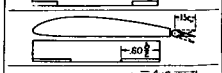	3. Plain ailerons $0.15c_w \times 0.60\frac{b}{2}$.	Equal	3.2	±3.8	2.6	±7.9	±13.0	4	8	1	1.22	85	18.5
		Diff	2.5	4.5×3.0	1.2	11.0×4.8	23.0×4.0	4	8	1	1.22	85	18.5
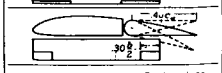	4. Plain ailerons $0.40c_w \times 0.30\frac{b}{2}$.	Equal	14.0	±4.2	11.0	±9.0	±14.0	4	9	1	1.25	87	18.2
		Diff	7.0	4.8×3.5	2.0	12.0×7.0	18.0×8.0	4	8	1	1.25	87	18.2
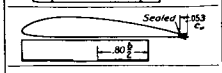	5. Optimum plain sealed ailerons [a] $0.053c_w \times 0.80\frac{b}{2}$.	Equal	1.4	±6.1	1.0	±13.0	±20.0	3	7				
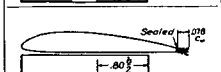	6. Optimum differential sealed ailerons [a] $0.078c_w \times 080.\frac{b}{2}$; $0.015c_w$ fixed tab, down 14°.	Diff	0.5	4.5×3.6	0.1	12.0×7.4	20.0×8.6	3	7				
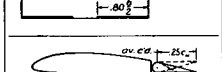	7. Skewed ailerons. Rounded tip wing [b] $0.25c_w \times 0.40\frac{b}{2}$; 20° skew.	Equal	10.0	±4.8	9.2	±12.0	±18.0	5	8	2	1.26	87	18.5
		Diff	5.2	6.1×3.8	4.7	16.0×5.0	27.0×3.2	4	7	2	1.26	87	18.5
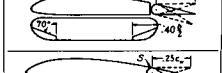	8. Tapered ailerons 5:3 tapered wing $0.25c_w \times 0.41\frac{b}{2}$.	Equal	4.0	±3.0	3.7	±7.5	±11.6	3	7		1.88	125	19.5
		Diff	2.4	3.4×2.6	1.5	8.4×4.8	15.0×5.6	3	7		1.88	125	19.5
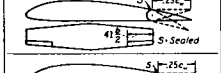	9. Tapered ailerons 5:1 tapered wing $0.25c_w \times 0.50\frac{b}{2}$.	Equal	2.4	±2.8	2.2	±7.4	±11.7	3	6	−3	1.81	129	18.2
		Diff	1.4	3.1×2.5	1.2	8.2×6.0	13.0×7.8	3	6	−3	1.81	129	18.2
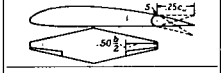	10. Optimum tapered sealed ailerons 5:1 tapered wing [a] $0.086c_w \times 0.53\frac{b}{2}$.	Equal	1.4	±7.3	0.9	±14.5	±20.0	3	6				
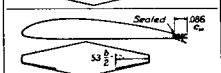	11. Optimum straight sealed ailerons 5:1 tapered wing [a] $0.112c_w$ (at tip)$\times 0.80\frac{b}{2}$.	Equal	0.8	±6.8	0.5	±13.5	±20.0	3	6				
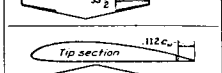	12. Frise ailerons $0.25c_w \times 0.40\frac{b}{2}$.	Equal	3.2	±2.6	3.8	±7.5	±14.5	3	7	0	1.28	85.0	18.5
		Diff	1.8	2.6×2.5	1.1	8.0×7.0	18.0×12.0	3	6	0	1.28	85.0	18.5
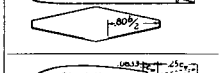	13. Frise ailerons (modified) $0.40c_w \times 0.30\frac{b}{2}$.	Equal	5.1	±4.2	8.1	±10.0	±14.3	5	9				
		Diff	1.7	4.3×4.0	2.3	11.0×8.5	16.0×11.0	5	8				
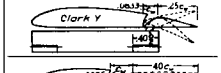	14. Floating-tip ailerons 5:1 tapered wing $1.06c_w \times 0.28\frac{b}{2}$.	Equal	2.5	4.8	2.2	8.6	13.0	2	2	−2	1.18	91.0	12.6
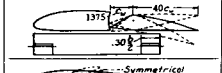	15. Floating-tip ailerons 5:1 tapered special wing [a] $1.00c_w \times 0.20\frac{b}{2}$.	Equal	4.8	7.4	4.9	15.8	25.0	1	2		1.27	84.0	19.5
	16. Retractable ailerons $0.15c_w \times 0.50\frac{b}{2}$.	Up only	0	$0.025c_w$ [f]	0	$0.062c_w$ [f]	$0.074c_w$ [f]	1	4		1.27	91.0	18.1
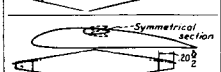	17. Ailerons and spoiler: [a,d] Ailerons $0.25c_w \times 0.40\frac{b}{2}$. Spoiler $0.07c_w \times 0.40\frac{b}{2}$.	Equal	2.3	±2.0	1.2	±4.4	±6.5	3	4	0	1.27	91.4	18.7
		Diff	1.4	2.4×2.2	.2	6.0×4.4	9.6×5.6	3	4	0	1.27	91.4	18.7
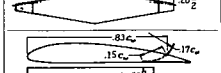	18. Slot-lip ailerons [d] $0.30c_w$ location $0.10c_w \times 0.50\frac{b}{2}$.	Unbalanced	32.0	23.0×14.0	18.0	55.0×0	55.0×0	−5	−2	4	1.22	75.0	15.0
		Balanced	20.0	23.0×14.0	16.0	55.0×0	55.0×0	−5	−2	4	1.22	75.0	15.0
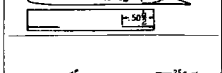	19. Slot-lip ailerons [d] $0.55c_w$ location $0.10c_w \times 0.50\frac{b}{2}$.	Unbalanced	12.0	19.0×12.0	9.3	43.0×3.0	47.0×0	−1	2	4	1.23	83.0	16.0
		Balanced	8.5	19.0×12.0	8.5	43.0×3.0	47.0×0	−1	2	4	1.23	83.0	16.0

[a] Computed or estimated results.
[b] Hinge moments computed or estimated.
[d] Device may not give satisfactory response characteristics.
[f] Deflection given in percentage of wing chord.

TABLE I (B).—COMPARISON OF VARIOUS LATERAL CONTROL DEVICES

Device / Criterion		Linkage	Control force and aileron deflection to produce specified bank in 1 second, $\phi_1=15°$						Sideslip with 15° bank in 1 second (degrees)			Performance		
			$C_L=0.35$		$C_L=1.0$		$C_L=1.8$							
			Stick force (lb.)	Aileron angles (degrees)	Stick force (lb.)	Aileron angles (degrees)	Stick force (lb.)	Aileron angles (degrees)	$C_L=0.35$	$C_L=1.0$	$C_L=1.8$	Maximum lift $C_{L_{max}}$	Speed range $\frac{C_{L_{max}}}{C_{D_{min}}}$	Climb $\frac{L}{D}$ at $C_L=0.7$
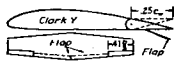	20. Tapered ailerons, sealed. 5:3 tapered wing. Partial-span split flap: Ailerons $0.25c_w \times 0.41\frac{b}{2}$. Flap $0.15c_w \times 0.59\frac{b}{2}$.	Equal Diff.	4.0 2.4	±3.0 3.4×2.6	3.7 1.5	±7.5 8.4×4.8	3.5 .8	±12.0 15.0×5.6	3 3	7 7	8 7	1.88 1.88	125 125	19.5 19.5
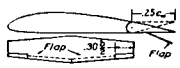	21. Tapered ailerons, sealed. 5:3 tapered wing. Partial-span split flap: Ailerons $0.25c_w \times 0.30\frac{b}{2}$. Flap $0.15c_w \times 0.70\frac{b}{2}$.	Equal Diff.	4.0 2.1	±4.3 5.0×3.6	3.6 1.1	±9.6 13.0×5.1	4.5 1.3	±16.0 25.0×1.5	3 3	7 6	8 6	1.97 1.97	130 130	19.5 19.5
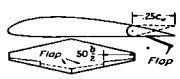	22. Tapered ailerons, sealed. 5:1 tapered wing. Partial-span split flap: [e] Ailerons $0.25c_w \times 0.50\frac{b}{2}$. Flap $0.15c_w \times 0.50\frac{b}{2}$.	Equal Diff.	2.4 1.4	±2.8 3.1×2.5	2.2 1.2	±7.4 8.2×6.0	1.9 .1	±11.7 13.0×7.8	3 3	6 6	6 6	1.81 1.81	129 129	18.2 18.2
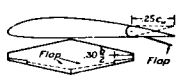	23. Tapered ailerons, sealed. 5:1 tapered wing. Partial-span split flap: Ailerons $0.25c_w \times 0.30\frac{b}{2}$. Flap $0.15c_w \times 0.70\frac{b}{2}$.	Equal Diff.	2.4 1.5	±4.2 4.5×3.6	2.5 1.4	±12.0 14.0×18.0	2.8 1.5	±20.0 26.0×10.0	2 2	6 5	6 5	1.97 1.97	141 141	18.2 18.2
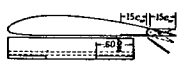	24. Plain ailerons. Retractable flap: Ailerons $0.15c_w \times 0.60\frac{b}{2}$. Flap $0.15c_w \times 1.00\frac{b}{2}$.	Equal Diff.	6.2 5.7	±3.8 4.0×3.5	4.7 3.7	±7.8 8.7×7.1	6.7 5.4	±25.0 28.0×11.0	4 4	8 8	8 7	2.05 2.05	143 143	18.5 18.5
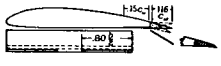	25. Plain sealed ailerons. Retractable flap: [a] Ailerons $0.116c_w \times 0.80\frac{b}{2}$. Flap $0.15c_w \times 1.00\frac{b}{2}$.	Diff. with tab.	1.4	3.4×4.2	0.9	8.4×6.6	2.7	35.0×0.6	3	8	6	2.05	143	18.5
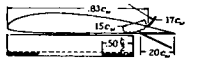	26. Retractable ailerons. Split flap: Ailerons $0.15c_w \times 0.50\frac{b}{2}$. Flap $0.20c_w \times 1.00\frac{b}{2}$.	Up only.	0	$0.025c_w$[f]	0	$0.062c_w$[f]	0	$0.074c_w$[f]	1	4	6	2.19	149	18.1
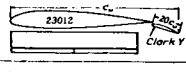	27. External-airfoil flaps [c] $0.20c_w \times 1.00\frac{b}{2}$.	Diff.	5.5	3.2×3.0	3.1	6.0×5.5	0.2	13.0×11.0	3	7	10	1.83	172	18.7
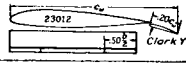	28. External-airfoil flap ailerons [c] $0.20c_w \times 0.50\frac{b}{2}$.	Diff.	0.9	3.7×3.7	0.8	7.6×7.3	0.3	16.0×9.2	3	7	8	1.80	172	18.7
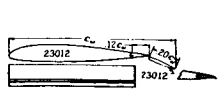	29. Slot-lip ailerons. External-airfoil flap: [e, d] Ailerons $0.12c_w \times 1.00\frac{b}{2}$. Flap $0.20c_w \times 1.00\frac{b}{2}$.	Diff. with tab.	2.4	10.0×6.0	2.3	25.0×6.5	1.4	14.0×6.8	3	6	7	1.92	202	19.0

[a] Computed or estimated results.
[e] C_L slightly below 1.8.
[d] Device may not give satisfactory response characteristics.
[c] Spring mechanism assumed to avoid overbalance with flap down.
[f] Deflection given in percentage of wing chord.

REPORT NO. 635

THEORETICAL STABILITY AND CONTROL CHARACTERISTICS OF WINGS WITH VARIOUS AMOUNTS OF TAPER AND TWIST

Henry A. Pearson and Robert T. Jones

Langley Memorial Aeronautical Laboratory

1938

REPORT No. 635

THEORETICAL STABILITY AND CONTROL CHARACTERISTICS OF WINGS WITH VARIOUS AMOUNTS OF TAPER AND TWIST

By HENRY A. PEARSON and ROBERT T. JONES

SUMMARY

Stability derivatives have been computed for twisted wings of different plan forms that include variations in both the wing taper and the aspect ratio. Taper ratios of 1.0, 0.50, and 0.25 are considered for each of three aspect ratios: 6, 10, and 16. The specific derivatives for which results are given are the rolling-moment and the yawing-moment derivatives with respect to (a) rolling velocity, (b) yawing velocity, and (c) angle of sideslip. These results are given in such a form that the effect of any initial symmetrical wing twist (such as may be produced by flaps) on the derivatives may easily be taken into account.

In addition to the stability derivatives, results are included for determining the theoretical rolling moment due to aileron deflection and a series of influence lines is given by which the loading across the span may be determined for any angle-of-attack distribution that may occur on the wing plan forms considered. The report also includes incidental references to the application of the results.

INTRODUCTION

Although a formal theory for the dynamics of airplane motions has been available for many years, airplane designers have not been in a position to utilize this theory to its fullest advantage on account of lack of knowledge of the basic physical quantities involved. It is true that the physical quantities, or stability derivatives, have been determined by test or calculation in a number of instances, but there exists no systematic series or correlation of tests sufficient to guide the designer in the prediction of these factors.

As is well known, the calculations involved in aerodynamic wing theory have been developed and refined to such an extent that it is possible to predict quite accurately the air moments and forces on the isolated wing at a fixed speed and incidence. Since several of the airplane lateral-stability derivatives depend almost entirely on the aerodynamic characteristics of the wing and since it would be desirable in any case to know the separate effects of variation of wing form on stability, it was thought worth while to extend the calculations to the determination of the moments developed by the wings when the airplane is disturbed from steady flight. This report gives theoretical stability derivatives for a variety of wing shapes including nine different plan forms and covering, in most cases, an arbitrary distribution of twist.

Past work on the stability characteristics of wings has, except in isolated cases, been confined to analysis by the "strip method," wherein the effects of aerodynamic induction were neglected. The main effects of the induction are included in the present computations, although the secondary influence of distortion or curvature of the wake is neglected.

DEFINITIONS

The axes used in specifying moments, angular velocities, etc., are fixed in the wing and therefore move relatively to the air and to the earth. The X axis passes through the wing aerodynamic center in the plane of symmetry and is so chosen as to point directly into the line of the relative wind when the wing is moving steadily. Otherwise the axes form an orthogonal system as shown in the back cover of the report.

The derivatives that may be obtained enable an estimate to be made of the variation of both rolling moment and yawing moment with (1) rolling velocity, (2) yawing velocity, and (3) sideslip angle. These factors, designated by C_{l_p}, C_{n_r}, etc., are to be used in the following general formulas to determine the wing rolling and yawing moment in combined rolling, yawing, and sideslipping motion:

$$\frac{L}{qSb}=C_{l_p}\left(\frac{pb}{2V}\right)+C_{l_r}\left(\frac{rb}{2V}\right)+C_{l_\beta}\beta \qquad (1)$$

$$\frac{N}{qSb}=C_{n_p}\left(\frac{pb}{2V}\right)+C_{n_r}\left(\frac{rb}{2V}\right)+C_{n_\beta}\beta \qquad (2)$$

Subscripts p and r are used to designate the partial derivatives of the well-known wing rolling-moment and yawing-moment coefficients, C_l and C_n, with respect to instantaneous rolling and yawing angular velocities (expressed as helix angles) and β is used to designate the partial derivatives of these coefficients with respect to instantaneous sideslip angles. In this manner the notation is considerably shortened from the usual more cumbersome expressions $\partial C_l/\partial\left(\frac{pb}{2V}\right)$, $\partial C_n/\partial\left(\frac{rb}{2V}\right)$, etc. Expressing the rolling and yawing moments as the sums

of partial linear factors is considered valid for motions that are slow relative to the flight speed V and for small displacements, such as occur in ordinary unstalled maneuvers and such as are considered in the study of stability.

α, angle between the zero-lift direction of the wing section and the air velocity at infinity, radians.

θ, parameter defining spanwise position, $y=-\frac{b}{2}\cos\theta$ $\left(\text{when } \theta=0,\ y=-\frac{b}{2};\ \theta=\pi,\ y=\frac{b}{2}\right)$.

C_0, C_2, C_4, coefficients of cosine series expressing wing plan form.

C_l, rolling-moment coefficient.

C_n, yawing-moment coefficient.

p, angular velocity in roll, radians per sec.

r, angular velocity in yaw, radians per sec.

V, flight velocity of wing along X, f. p. s.

β, angle of sideslip, radians.

δ, aileron deflection, radians.

C_{l_p}, rate of change of rolling-moment coefficient C_l with the helix angle $pb/2V$.

C_{n_p}, rate of change of yawing-moment coefficient C_n with the helix angle $pb/2V$.

C_{l_r}, rate of change of rolling-moment coefficient C_l with the helix angle $rb/2V$.

C_{n_r}, rate of change of yawing-moment coefficient C_n with the helix angle $rb/2V$.

C_{l_β}, rate of change of rolling-moment coefficient C_l with sideslip angle β.

C_{n_β}, rate of change of yawing-moment coefficient C_n with sideslip angle β.

C_{l_δ}, rate of change of rolling-moment coefficient C_l with aileron angle δ.

C_{n_δ}, rate of change of yawing-moment coefficient C_n with aileron angle δ.

L, total wing rolling moment, ft.-lb.

N, total wing yawing moment, ft.-lb.

q, dynamic pressure, lb. per sq. ft.

S, wing area, sq. ft.

c, chord length at any section, ft.

c_t, chord length at plane of symmetry, ft.

m_0, section slope of the lift curve, per radian.

b, wing span, ft.

A, wing aspect ratio, b^2/S.

A_n, B_n, C_{2n}, coefficients of Fourier series. (See reference 2.)

c_i, section lift coefficient, section lift/$qcdy$.

C_L, wing lift coefficient, wing lift/qS.

c_{d_0}, section profile-drag coefficient.

c_{d_i}, section induced-drag coefficient.

C_{D_0}, wing profile-drag coefficient.

λ, taper ratio: i. e., ratio of the fictitious tip chord, obtained by extending the wing leading and trailing edges to the tip, to the root chord.

Γ, dihedral angle, radians.

CONDITIONS RELATING TO THE COMPUTATIONS

PLAN FORMS

The particular chord distributions for which the computations were made are illustrated in figure 1. Table I gives the coefficients of the cosine series used to express these chord distributions in terms of θ. Although the quarter-chord line is shown to be straight, it is permissible to apply the results to wings with similar chord distributions but with the different plan forms that

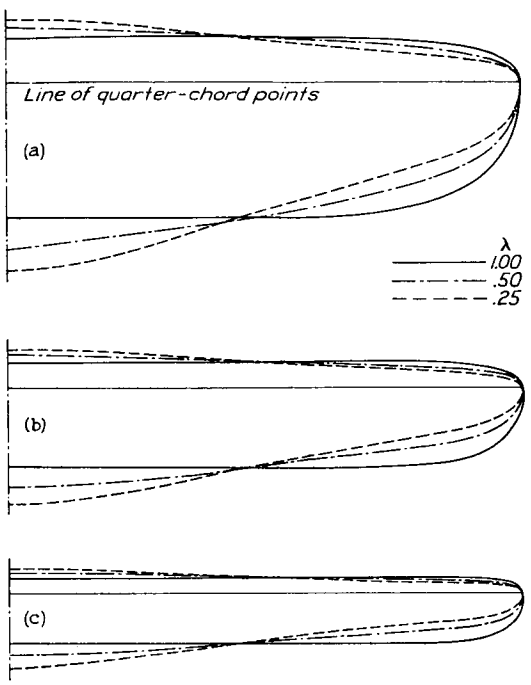

(a) $A=6$.
(b) $A=10$.
(c) $A=16$.

FIGURE 1.—Wing plan forms considered.

may be obtained by small alterations of the shape of the quarter-chord line. The computations were made for three aspect ratios, 6, 10, and 16, and for three taper ratios, 1.00, 0.50, and 0.25. The wing plan forms used only approximate those of linearly tapered wings with rounded tips.

LIFT DISTRIBUTIONS

Rolling, yawing, and sideslipping motions introduce varying resolutions of the relative-wind velocity over the wing. It is evident that these variations can, to a certain extent, be replaced by a fictitious warp or twist of the wing in straight flight. The procedure followed here is to calculate the spanwise lift and drag distributions for the fictitious twist (i. e., that replacing the effect of motion) in the ordinary way, but to incline the

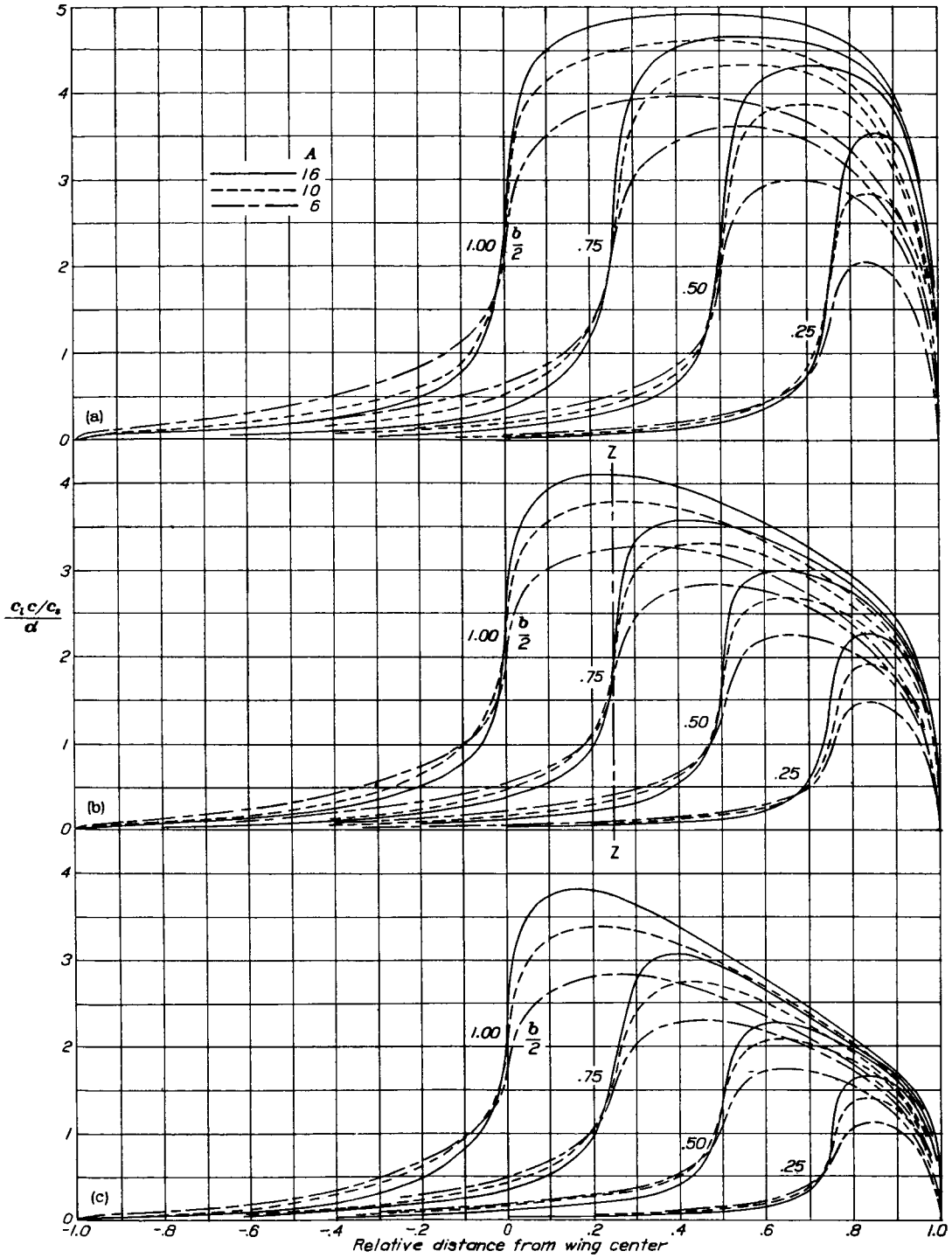

(a) λ=1.00. (b) λ=0.50. (c) λ=0.25.

FIGURE 2.—Load distribution due to unit angles of attack extending inward from the tip.

lift and drag components so as to maintain them along the perpendicular and the parallel to the actual local relative-wind velocity. A further refinement of the theory would involve the influence of the curvature of the wing wake. Since the helix angles involved in the motions are small ($pb/2V<0.1$ and $rb/2V<0.1$) and since that region of the wake nearest the wing is of predominant influence, this correction may be neglected.

Inasmuch as the various stability derivatives thus depend upon a summation of appropriate components of the lift and the drag loading along the span, it was necessary to determine these distributions for each of the wings with several different angle-of-attack distributions. For this purpose the Lotz method of calculation (references 1 and 2) was used. In order to keep the computations from becoming too lengthy, the chord-distribution function that occurs in this method was expressed by, at most, three terms of a cosine series (as in table I). Although this expression caused the chord distributions of the actual wings (fig. 1) to differ slightly from those for linearly tapered wings with rounded tips, such a procedure was justified because these slight departures in plan form had only a small effect on the characteristics but permitted a large saving in the computations required. Thus only the terms near the diagonal running through equations (19) of reference 2 entered into the computations. As the various derivatives for the elliptical wing could be obtained relatively easily, they were sometimes computed in order to determine the shape of the various derivative curves; it was therefore possible to use fewer points in fairing similar curves for the tapered wings.

The wing theory was applied in a special way so as to obtain results applicable to any arbitrary twist of the wings. The theoretical span loading being a linear function of the angle-of-attack distribution, the loading due to arbitrary twist can be built up, as will be indicated later, from certain elementary loadings by superposition. The elementary loadings considered were those caused by simple unit jumps of angle of attack occurring at different points of the span.

For each of the nine tapered wings, the first 20 Fourier coefficients determining the load distributions were computed (10 odd and 10 even) for the cases of unit angles of attack extending inward from the wing tip and covering various amounts of the semispan. The rest of the wing was in each case assumed to be at zero angle of attack. The portions thus covered were 0.25, 0.50, 0.75, and 1.00 of the semispan.

In spite of the great number of harmonic terms retained, the conditions near the points of discontinuity in the angle of attack required special treatment. The problem of these end conditions has been solved by Betz and Petersohn (reference 3) and their results were utilized in fairing the load curves through this region. Figure 2 shows the elementary loadings that were calculated, including the modified fairing. The results pertain specifically to the chord distributions illustrated in figure 1 but interpolation might be made for intermediate plan forms.

It is evident that any angle-of-attack distribution, symmetrical or unsymmetrical, may be built up of elemental steps of the type used in deriving figure 2. Figure 3 illustrates the procedure of finding the resultant load distribution. Thus, the loading contributed by element 10 of figure 3 (a) is obtained by deducting the load curve due to an increment of angle of attack extending between B and C from that due to an increment extending between A and C. Although this process could be continued until the load distribution was completely determined, the same results can be more easily obtained from influence lines, which give the load at a particular spanwise station due to the effect of unit angle-of-attack changes extending inward various

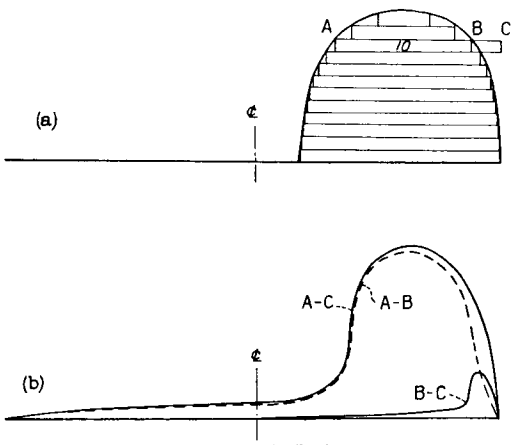

(a) Angle-of-attack distribution.
(b) Load distribution for element (10).
FIGURE 3.—Load components for an element.

amounts from the right wing tip. Such influence lines are given in figures 4, 5, and 6 for eight evenly spaced points across the wing semispan. Each line was obtained by cross-plotting the values of $\frac{c_l c/c_a}{\alpha}$ at the intersections of the loading curves of figure 2 with vertical lines drawn at the particular stations. (For example, the points of intersection of line Z—Z, fig. 2 (b), with the various curves represent the load induced at the 0.25-semispan point by uniform angle-of-attack increments that extend in varying amounts from the wing tip. These intersections identify the corresponding curves of figs. 4 to 6.)

In order to illustrate the use of the influence lines in determining the lift distribution as well as to show the degree of accuracy with which they may be used, the influence lines will be applied to predict the loading for a tapered wing ($\lambda=0.25$, $A=6$) corresponding to the angle-of-attack distribution shown in figure 7 (a). The particular angle-of-attack distribution used is defined by the equation

$$\alpha=\left(\frac{c_s}{c}+\frac{3c_s m_0}{4b\sin\theta}\right)\sin 3\theta \qquad (3)$$

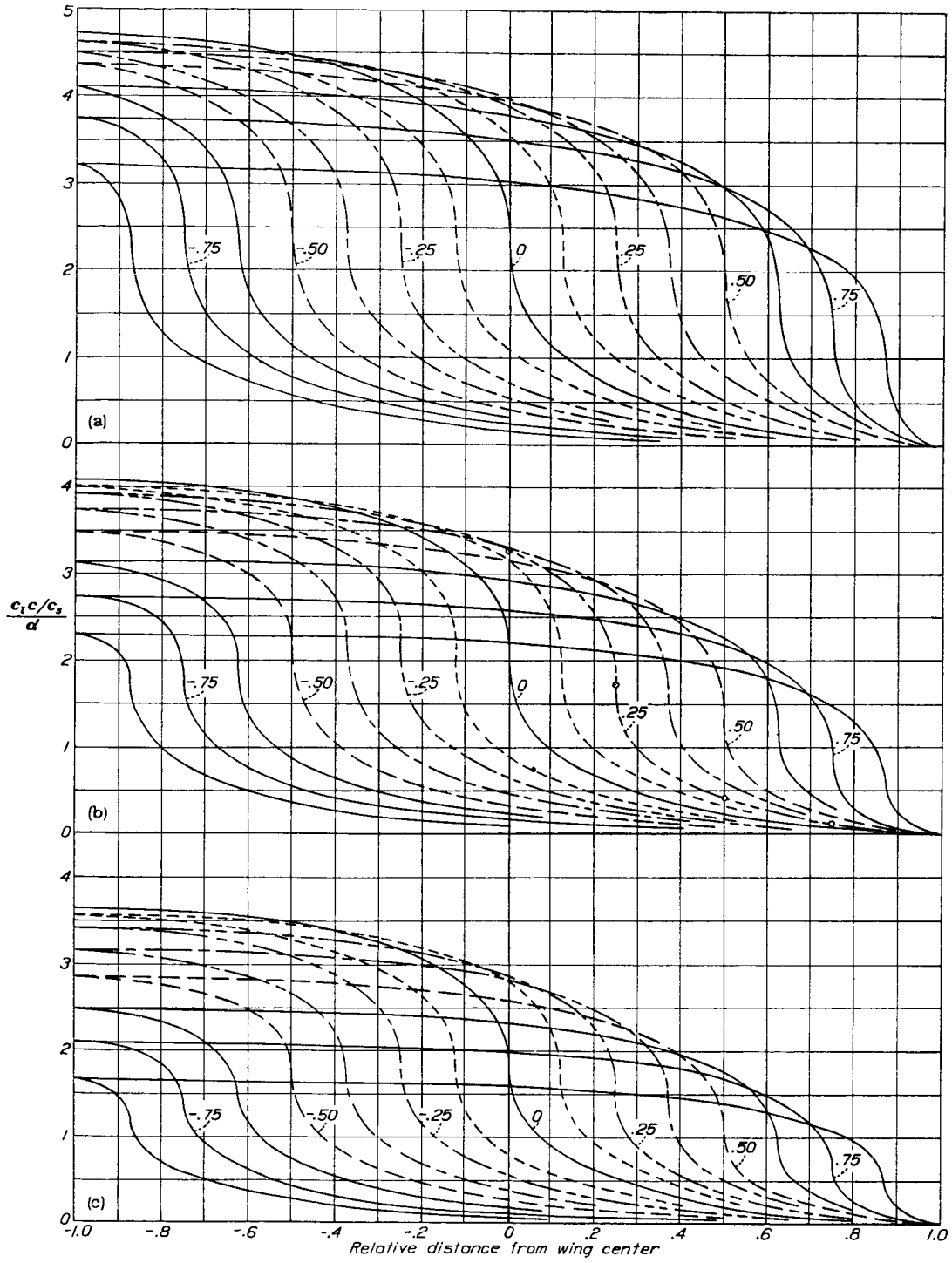

(a) λ=1.00. (b) λ=0.50. (c) λ=0.25.

FIGURE 4.—Influence lines for determining the load distribution. $A=6$. The number identifying a given line refers to the particular spanwise station at which the load is to be computed.

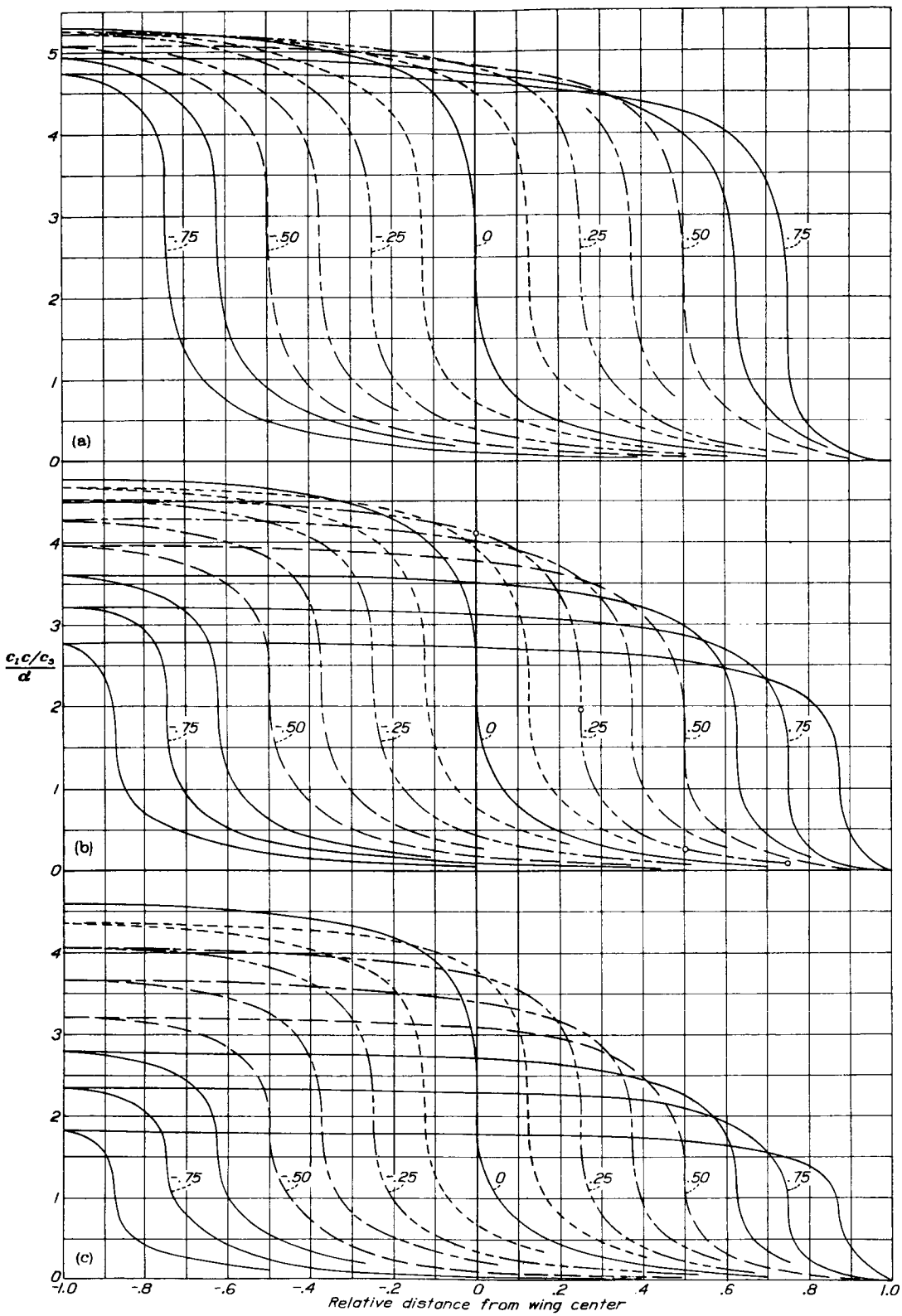

(a) $\lambda = 1.00$ (b) $\lambda = 0.50$. (c) $\lambda = 0.25$.

FIGURE 5.—Influence lines for determining the load distribution. $A = 16$. The number identifying a given line refers to the particular spanwise station at which the load is to be computed.

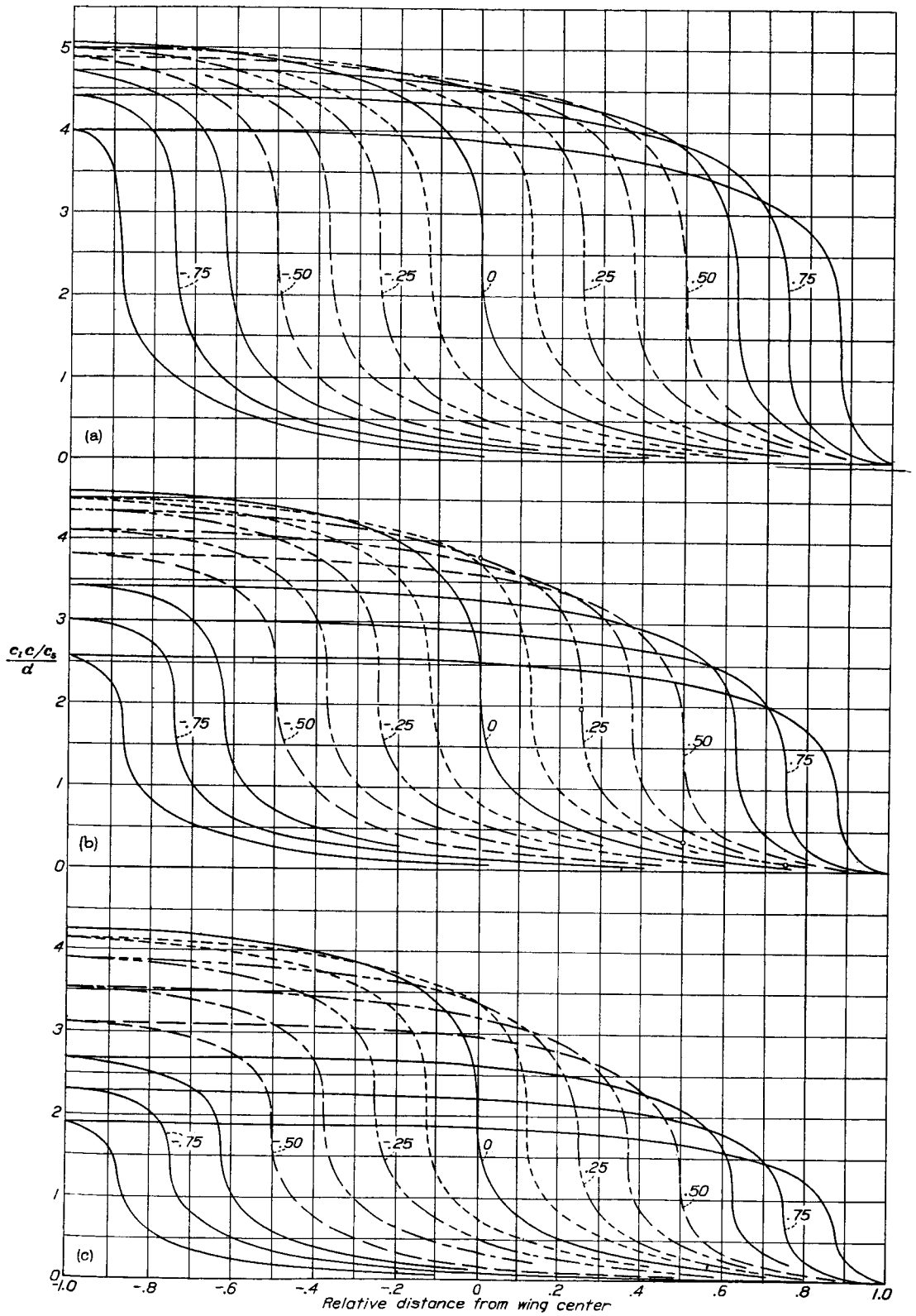

(a) λ=1.00. (b) λ=0.50. (c) λ=0.25.

FIGURE 6.—Influence lines for determining the load distribution. $A=16$. The number identifying a given line refers to the particular spanwise station at which the load is to be computed.

This particular distribution is employed because it is possible thereby to compute exactly the corresponding theoretical distribution as a check, without the usual approximations of a Fourier series. The following procedure illustrates the use of the influence lines to determine the lift at the 0.75-semispan point due to this distribution of twist: (1) The influence curve labeled 0.75 in figure 4 (c) is reproduced beneath the angle distribution to the same spanwise scale; (2) a base line with a range from α_{max-} to α_{max+} is laid out as in figure 7 (c) with the origin of the ordinates at α equal to zero; (3) the effect of any length of elemental angle-of-attack change, $d\alpha$, in figure 7 (a) is found by projecting the length of the element onto figure 7 (b) and plotting the increments (Δ_1) and ($\Delta_2+\Delta_2'$) at the angles of attack for which these elements are drawn, as in figure 7 (c). Because a negative angle would induce a negative load at the point in question, Δ_1 is plotted as a negative value. This process is continued from α_{max-} to α_{max+} and the resulting curve (fig. 7 (c)) is integrated to obtain the total effect at 0.75, which is then plotted in figure 7 (d). The load distribution over the entire span is obtained by repeating the same procedure for a number of points along the span.

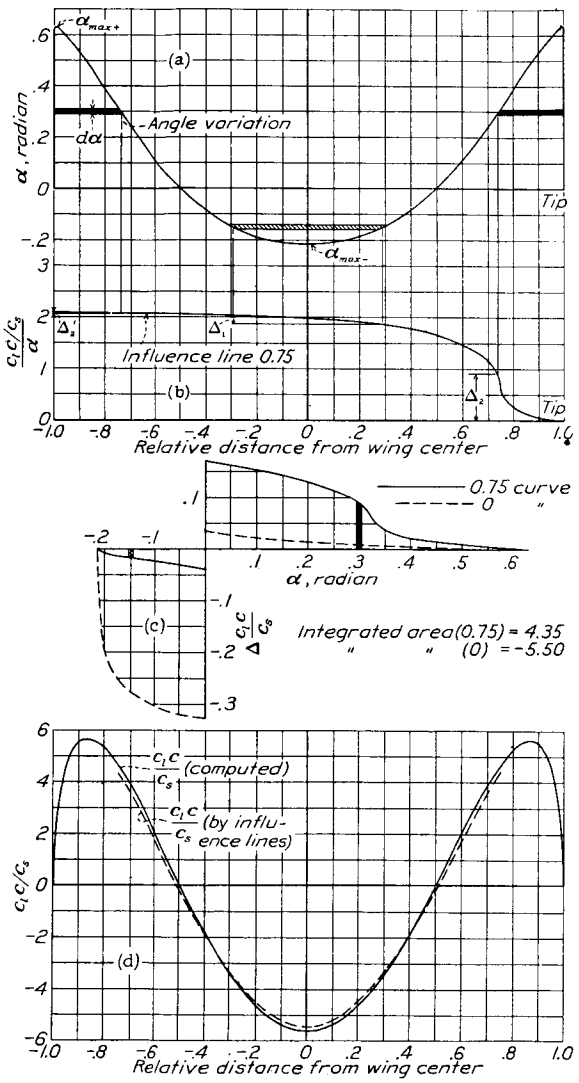

FIGURE 7.—Determination of lift distribution.

With the lift loading thus determined, the induced-drag distribution may be found by a simple operation, namely

$$c_{d_i}=c_l\left(\alpha-\frac{c_l}{m_0}\right) \tag{4}$$

Figure 7 (d) gives the comparison of the load-distribution curve obtained from the influence lines with that computed directly by the wing theory using equation (3). Although the agreement is not precise, it must be remembered that the solid curve represents a case where no series approximation was necessary; hence it may be concluded that the influence-line method of determining the lift distribution is as accurate as any other for practical purposes.

Aside from other possible applications, the load distribution may be used to determine the stability derivatives for certain cases not specifically covered by the calculations. In the subsequent charts, it is sometimes necessary to stipulate either that the initial angle-of-attack distribution be symmetrical about the wing center line or that the dihedral angle be constant along the span. With a knowledge of the complete load distribution, however, values of the derivatives or their respective moments might be found for particular cases where the charts do not apply.

STABILITY DERIVATIVES

Although it is possible, in the general case, to obtain the stability derivatives from the lift distribution, such a procedure will not usually be necessary because the charts to be presented cover all cases likely to be of interest. The results are presented in such a form that the effect of flaps on the derivatives may easily be determined.

ROLLING MOMENT DUE TO ROLLING

The first derivative considered is the rolling moment due to rolling. In unstalled flight, when the wing rolls about the longitudinal wind axis, a damping or restoring moment is set up. This moment $L_{rolling}$ varies directly with the angular velocity p and is defined by the equation

$$L_{rolling}=C_{l_p}\frac{pb}{2V}qSb \tag{5}$$

where the product $C_{l_p}\frac{pb}{2V}$ is simply a rolling-moment coefficient that varies linearly with the angular velocity.

The computed variation of the derivative C_{l_p} with aspect ratio and taper is given in figure 8. In the usual lift range below the stall, this derivative may be considered to be independent of either initial wing twist or angle of attack and of the wing dihedral. In conventional cases, practically the entire damping moment for the airplane may be attributed to the wings. It can be seen that the moment contributed by a tail surface, geometrically similar to the wing but with only one-

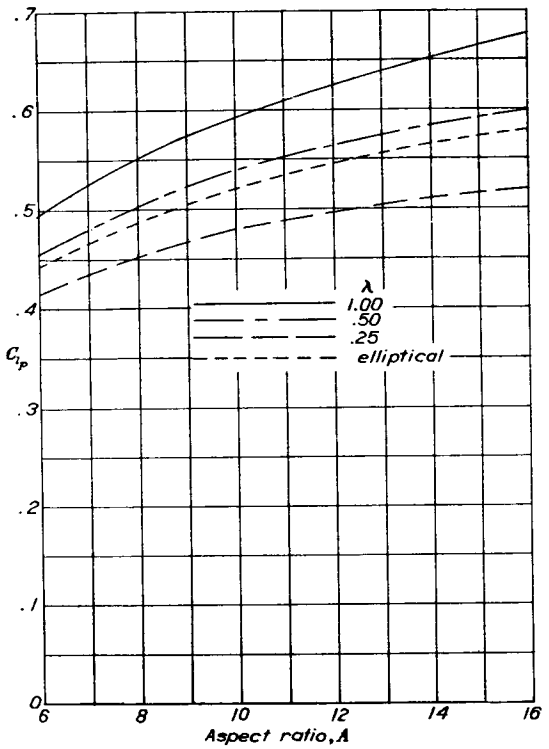

FIGURE 8.—Rolling derivative due to rolling. $L_{rolling}=C_{l_p}\frac{pb}{2V}qSb$

fourth the span, would be $\frac{1}{256}$ of that contributed by the wing, inasmuch as $L_{rolling}$ for a given angular velocity varies as the fourth power of a linear dimension.

Reducing the aspect ratio or increasing the taper tends to reduce the derivative C_{l_p}, as may be seen from the curves given in figure 8. Comparison of the present values of C_{l_p} with similarly derived values given in reference 4 indicates that the effect of rounding the wing tips is to reduce the theoretical restoring moment by about 6 percent for wings of aspect ratio 6.

YAWING MOMENT DUE TO ROLLING

During a rolling motion, the wing experiences a linear antisymmetrical change in angle of attack along the span and, as a result, antisymmetrical loadings are added to those that originally were on the wing. The resulting yawing moment is due to components of the lift as well as to the drag along the span, the lift components being the more important. With the specified system of axes, positive rolling produces a negative yawing moment or, for any case, with positive lift coefficients the falling wing tends to advance owing to the predominating influence of the lift vectors.

The yawing moment due to rolling, unlike the rolling moment due to rolling, depends upon both the initial wing twist and the angle of attack. For untwisted wings, however, the yawing moment is zero at zero lift and increases linearly with the wing lift coefficient. For a twisted wing, the yawing moment due to rolling, although varying linearly with the over-all lift coefficient, is not necessarily zero when C_L is zero but may have either a small positive or a small negative value depending upon the initial angle-of-attack distribution. Owing to this circumstance, it is most convenient to express the derivative C_{n_p} as a ratio in terms of unit partial-span angle-of-attack changes.

Figure 9 shows the computed variation of the ratio C_{n_p}/α for unit symmetrical angle-of-attack changes that extend out from the wing center so as to cover various amounts of the wing span. Thus, if it is desired to determine C_{n_p} for an untwisted rectangular wing of aspect ratio 6 at an angle of attack of 0.1 radian, the value 0.195 (for an angle of attack of 1 radian), read from the solid line of figure 9 (a) at the relative distance of 1.0, is multiplied by 0.1 to give a value of C_{n_p} equal to 0.0195. If, now, a half-span flap of constant chord ratio were displaced an amount sufficient to cause an additional change in angle equal to 0.1 radian over the portion with flaps, the new value of C_{n_p} would be

$$(0.1\times 0.195)+(0.1\times 0.134)=0.0329$$

This value of C_{n_p} is then inserted into the equation

$$N_{rolling}=C_{n_p}\frac{pb}{2V}qSb \qquad (6)$$

to determine the yawing moment due to a rolling angular velocity.

Although the curves given in figure 9 can be directly used to determine the effect on C_{n_p} of deflecting partial-span flaps of constant flap-chord ratio, they are also readily adapted to the determination of C_{n_p} for a wing with any initial twist provided that the twist distribution is symmetrical about the wing center line. The process is illustrated in the following example where it is desired to find the value of C_{n_p} for a rounded-tip rectangular wing of aspect ratio 6 with the symmetrical angle-of-attack distribution shown in figure 10 (a). The contribution of the element of angle of attack $d\alpha$, shown at the point $\alpha=0.15$ radian, to the total value of the wing C_{n_p} is equivalent to that caused by a full-span elemental flap minus the contribution of the cross-hatched portions. The contribution of this element $d\alpha$ is denoted by $\left(\frac{C_{n_p}}{\alpha}\right)d\alpha$ and may be obtained

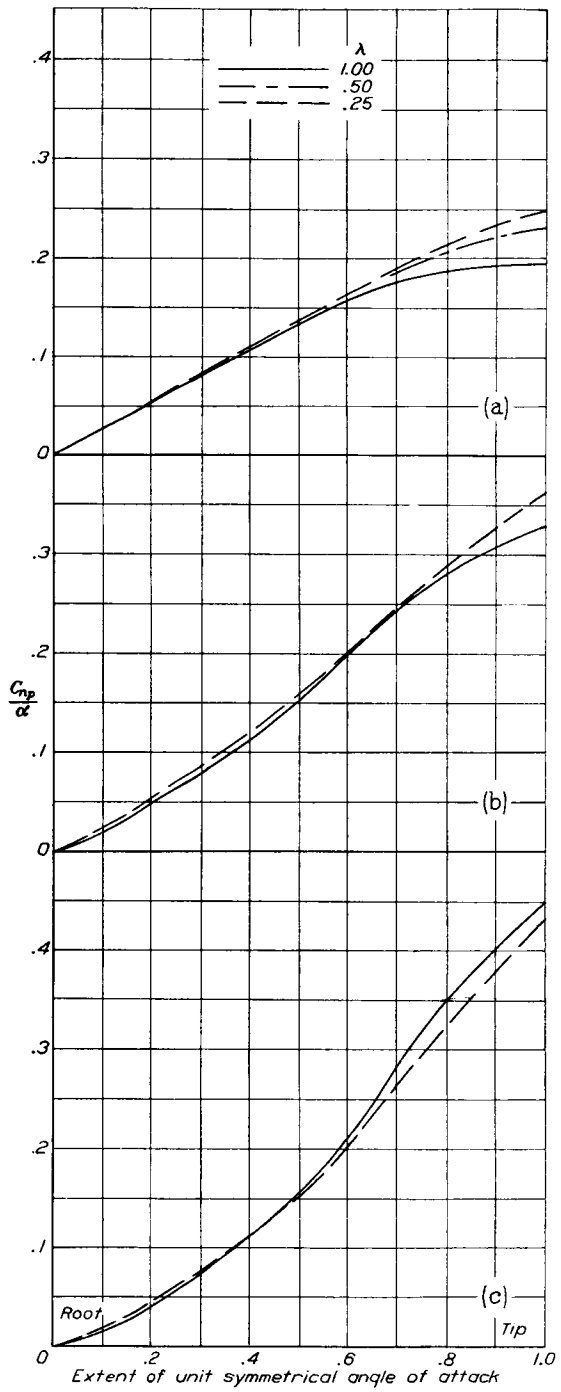

(a) $A=6$.
(b) $A=10$.
(c) $A=16$.

FIGURE 9.—Yawing derivative due to rolling. $N_{rolling}=C_{n_p}\frac{pb}{2V}qSb$

by projecting the various small flap portions onto the appropriate C_{n_p}/α curve (taken from fig. 9) as in figure 10 (b), and adding the increments Δ_1 and Δ_2. The sum of these increments is then plotted in figure 10 (c) at the value of α for which the element is drawn. The value of C_{n_p} for the complete wing is obtained by performing the integration

$$C_{n_p}=\int_0^{\alpha_{max+}}\left(\frac{C_{n_p}}{\alpha}\right)d\alpha \qquad (7)$$

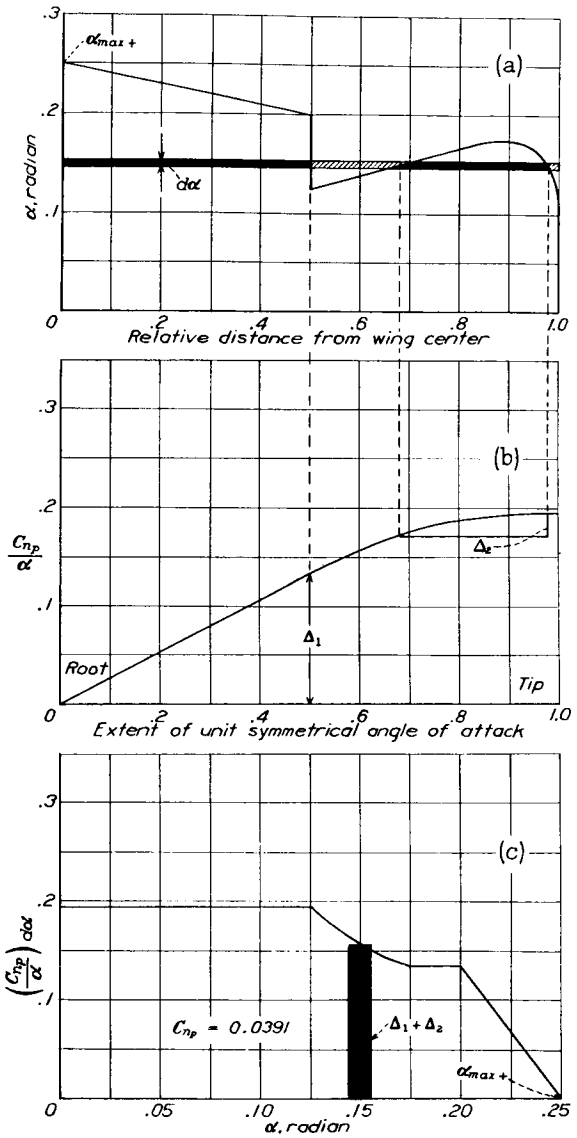

FIGURE 10.—Application of C_{n_p} curves to an example.

These curves apply to wings with symmetrical twist and it is necessary to consider only half the wing, the factor 2 being included in the curves. The evaluation in the case of figure 10 (c) yields 0.0391.

The curves of figure 9 indicate that, for a given angle-of-attack distribution, there is relatively little change in the value of C_{n_p} with the taper ratios investigated. Changes in taper ratio did, however, have an appreciable effect on the value of C_{l_p} (fig. 8) with the result that the ratio of the yawing to the rolling moment in roll will, in general, increase with increase in taper.

Inasmuch as the inclination of the lift vectors at the outer portions of the span has such a predominating effect on the yawing moment, the most effective means of reducing C_{n_p} for a given wing lift coefficient is to give the wings washout toward the tips.

The yawing moment due to rolling is, in conventional designs, largely due to the wings. The tail surfaces contribute very little to this moment both because of their short span and because of the small angles of attack relative to the wing.

ROLLING MOMENT DUE TO YAWING

During a yawing motion, increments of velocity are added along the forward-moving half of the wing and similar increments are deducted along the rearward-moving half. The difference in velocity of the two halves causes a rolling moment which, for an untwisted wing, varies directly with the initial angle of attack as well as with the angular velocity. The velocity increments vary linearly with the distance from the wing center line and are small relative to the flight speed; it is therefore permissible to make certain mathematical approximations in deriving the necessary equations for the determination of the yawing derivatives. When these approximations are used and the velocity along the span is expressed as a variable, the new downwash equation becomes

$$w=\frac{V}{4\pi b}\int_0^{\pi}\frac{\left[\frac{d(c_l\alpha)}{d\theta}\left(1+\frac{rb}{2V}\cos\theta\right)-(c_l\alpha)\frac{rb}{2V}\sin\theta\right]}{\cos\theta-\cos\theta_0}d\theta \quad (8)$$

The system of simultaneous equations derived for the approximate solution of this integral equation is

$$\Sigma C_{2n}\cos 2n\theta\,\Sigma A_n\sin n\theta+\frac{c_s m_0}{4b}\Sigma nA_n\sin n\theta$$

$$+\frac{c_s m_0}{4b}\frac{rb}{4V}\Sigma(A_{n-1}-A_{n+1})\sin n\theta=\Sigma B_n\sin n\theta=\alpha\sin\theta \quad (9)$$

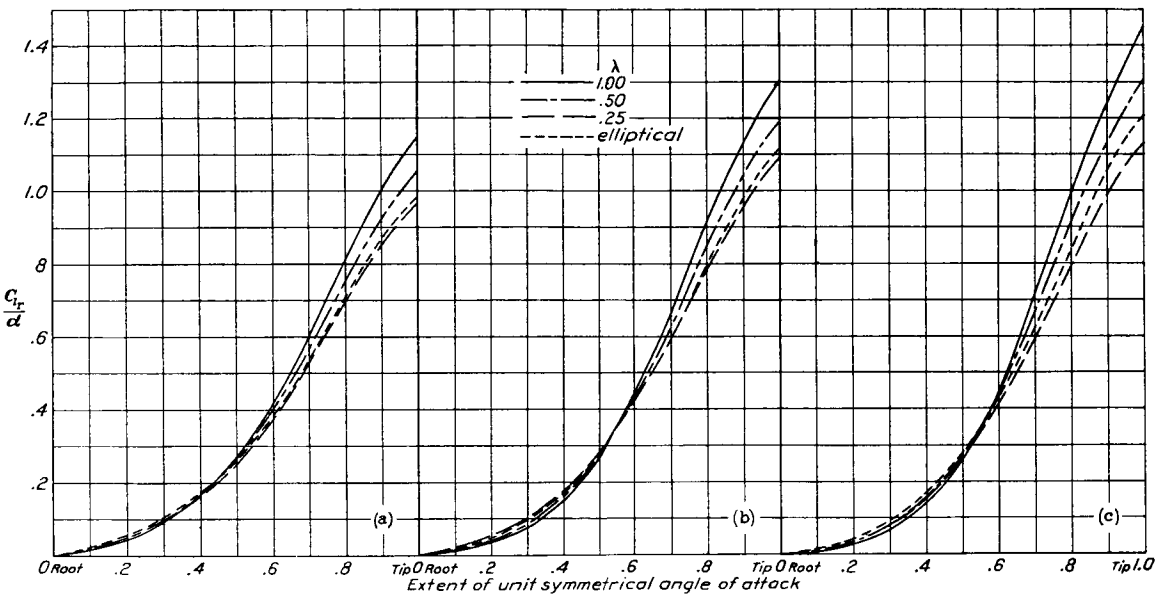

(a) $A=6$.
(b) $A=10$.
(c) $A=16$.

FIGURE 11.—Rolling derivative due to yawing. $L_{yawing}=C_{l_r}\frac{rb}{2V}qSb$

By means of equation (9), Fourier coefficients were computed for the nine tapered wings with two different initial angle-of-attack distributions: (1) a distribution due to a unit angle of attack extending over the whole span, and (2) a unit angle of attack at the wing center covering half the span. In order to obtain the correct fairing of the final curves of figure 11, similar results were computed for elliptical wings with six angle-of-attack distributions covering 0, ¼, ½, ¾, ⅞, and all of the wing span.

As was the case with the derivative C_{n_p}, it is most convenient to give the derivative of rolling moment

due to yawing C_{l_r} as a ratio in terms of a partial-span unit angle of attack. The values of C_{l_r} may be obtained from figure 11 and are to be inserted into the equation

$$L_{yawing}=C_{l_r}\frac{rb}{2V}qSb \tag{10}$$

By the process described in the previous section, values of C_{l_r} may be obtained for wings with any initial twist distribution that is symmetrical about the center line.

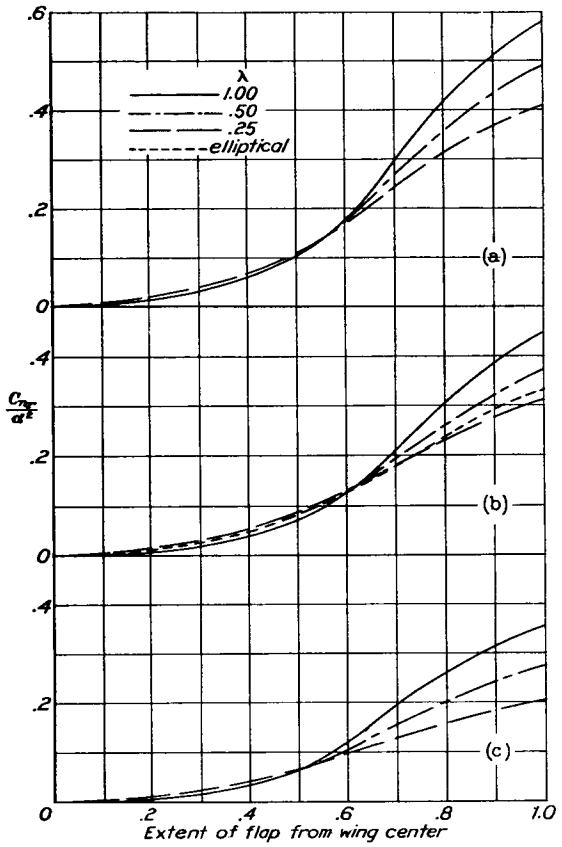

(a) $A=6$.
(b) $A=10$.
(c) $A=16$.

FIGURE 12.—Yawing derivative due to yawing for partial-span flap.

$N_{yawing}=C_{n_r}\frac{rb}{2V}qSb$

The curves of figure 11 fall in the order that would be expected for the various taper ratios, i. e., the moment for an untwisted tapered wing would be expected to be less than that for a rectangular wing of the same span and area because the tapered wings have a smaller proportion of the wing area at the tip. On account of the induced velocities along the span, the reduction, for the tapered wings, is not so great as would be obtained by an application of the ordinary strip theory.

The direction of the moment is such that, with the system of axes used, a positive rolling moment generally results from a positive yawing velocity when the wing is giving positive lift. By the use of considerable washout, such as is obtained with partial-span flaps, it is possible not only to reduce the value of this moment but also to make it slightly negative for low wing lift coefficients.

As was the case with C_{l_p} and C_{n_p}, the value of C_{l_r} for the entire airplane is due almost wholly to the wings because the side area of the airplane contributes relatively little moment as compared with the wings in curvilinear flight.

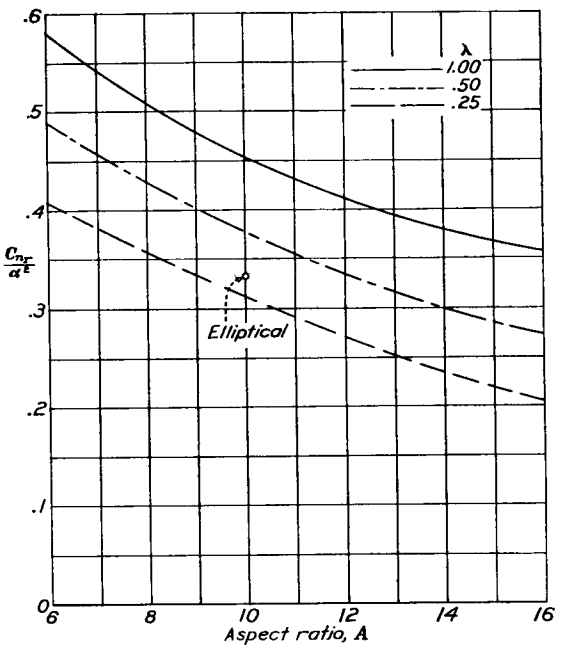

FIGURE 13.—Yawing derivative due to yawing for untwisted wing.

$N_{yawing}=C_{n_r}\frac{rb}{2V}qSb$

YAWING MOMENT DUE TO YAWING

A part of the wing yawing moment due to yawing results from the change in the induced-drag distribution that accompanies the change in the lift distribution across the span of a yawing wing. The rest of the yawing moment is due to the difference in the distribution of profile drag resulting from the variation in velocity along the span. Both parts, however, produce damping moments in the unstalled-flight range.

The part of the wing yawing moment due to the induced drag is defined by the equation

$$N_{yawing}=C_{n_r}\frac{rb}{2V}qSb \tag{11}$$

where the derivative C_{n_r} may be obtained from figure 12 for certain types of angle-of-attack distribution. The special distributions for which the derivatives of figure 12 apply are both uniform and symmetrical about the

wing center line. Such distributions occur only when partial-span flaps of constant-chord ratio are deflected, the rest of the span being at zero angle of attack. This limitation in the applicability of these curves as compared with the previous ones is due to the fact that the principle of superposition does not apply in cases where the variation is not linear with α. The computed results may, however, be used to determine the variation of C_{n_r} for the most useful case, namely, that of a wing without twist. For this purpose, the proper values of C_{n_r}/α^2 obtained from figure 13, which is a cross plot of the end points of figure 12, are multiplied by the square of the actual angle of attack.

The part of the yawing moment due to the profile drag can be determined from the easily derived equation

$$\Delta N_{yawing}=q\int_{-\frac{b}{2}}^{\frac{b}{2}} c_{d_0}c\left(1+\frac{2ry}{V}\right)y\,dy \qquad (12)$$

where c_{d_0} and c are functions of the distance y along the span. It is possible, by assuming c_{d_0} constant and by neglecting terms of the second order, to obtain a coefficient ΔC_{n_r} that may be used with the equation

$$\Delta N_{yawing}=\Delta C_{n_r}\frac{rb}{2V}qSb \qquad (13)$$

to compute the part of the yawing moment due to the profile drag. The values of the profile yawing moment, as given by equation (13), are sufficiently accurate for most wings since c_{d_0} generally varies only slightly across the span. The variation of the coefficient $\Delta C_{n_r}/C_{D_0}$ with taper ratio is given in figure 14.

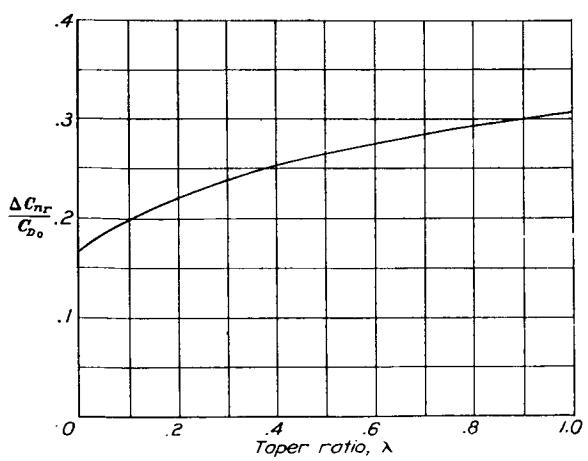

FIGURE 14.—Profile-drag yawing derivative. $\Delta N_{yawing}=\Delta C_{n_r}\frac{rb}{2V}qSb$

The total wing yawing moment due to yawing is the sum of the moments given by equations (11) and (13). At low lift coefficients, the profile drag contributes the greater portion of the wing damping moment in yawing. At moderate or high lift coefficients, however, the part due to the induced drag exceeds that due to the profile drag. If it is assumed that $\alpha=0.3$ and $C_{D_0}=0.01$, then the respective values of C_{n_r} and ΔC_{n_r} would be 0.0522 and 0.0031 for a rectangular wing of aspect ratio 6.

The damping moment contributed by the wings in yawing motion is, in most cases, secondary but is not

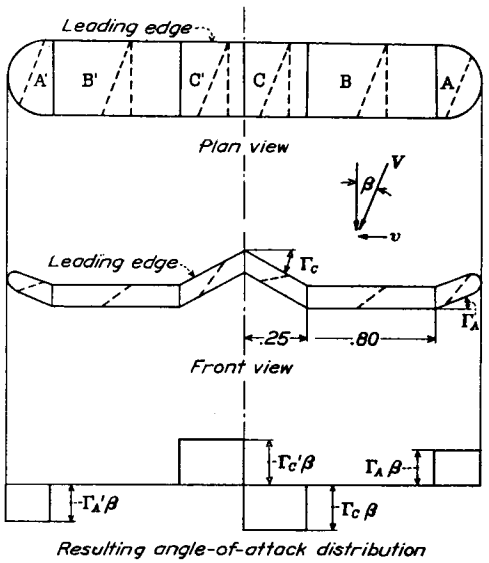

FIGURE 15.—Effect of irregular dihedral on sideslip.

negligible with respect to the damping moment contributed by the fuselage and the vertical tail surfaces. The damping in yawing due to the wings depends upon the angle of attack as well as upon the plan form; therefore the relative amounts contributed by the wings and tail surfaces may vary considerably.

Although it was not possible to give a general chart for determining the damping in yawing for symmetrically twisted wings as was done with the previous derivatives, it can nevertheless be said that the addition of load toward the tips, whether by washing or by an increase in taper ratio, would increase the wing damping moment due to a yawing angular velocity.

ROLLING MOMENT DUE TO SIDESLIP

The manner in which the changes in angle of attack that cause a rolling moment are brought about during a sideslipping motion is shown in figure 15 by a sketch of a wing having positive, negative, and zero dihedral over various portions of the span. For simplicity, the wing is assumed to have no initial twist and the dihedral angles are assumed constant over each of the portions A, B, and C. For small angles of sideslip β, the increase in angle at tip A is, to a first approximation, equal to $\Gamma_A\beta$; whereas, at the opposite tip A', there is an equal decrease of the angle of attack. The portions B—B', having no dihedral, contribute no change in angle of attack when the wing is sideslipping. At the center,

however, owing to the negative angle of dihedral Γ_C, there is an effective decrease in angle of attack over part C equal to $\Gamma_C\beta$ and on C′ there is a similar increase in angle. Figure 15 shows the resulting effective angle-of-attack distribution for the particular shape of dihedral assumed.

The effect of this distribution is similar to that caused by two pairs of ailerons equally and oppositely deflected with the inner pair opposing the rolling action of those at the tip. Positive areas of dihedral on the advancing wing tend to add load onto that wing. For the system of axes chosen, all areas with positive dihedral produce a negative rolling moment with a positive angle of sideslip. This moment, like the rolling moment due to roll, is independent of the initial wing twist as long as no portion of the wing becomes stalled.

The rolling-moment derivative due to sideslip C_{l_β} may be determined from figure 16, which gives the variation of C_{l_β}/Γ for various unit antisymmetrical angle-of-attack distributions (i. e., symmetrical portions with constant dihedral) that extend out from the wing center and cover various relative amounts of the wing semispan. In the usual case, where the dihedral angle Γ is constant along each semispan, the value of the rolling moment due to a sideslip angle β can be obtained from the equation

$$L_{sideslip}=C_{l_\beta}\beta qSb \qquad (14)$$

where the appropriate values of C_{l_β}/Γ, obtained from figure 16 at the relative distance equal to 1.0, are multiplied by the dihedral angle in radians. In more unusual cases as, for example, where only the tips are turned up or where the wing is given a gull shape for any reason, it is still possible to determine a coefficient of rolling moment due to sideslip simply by adding the effects of the various parts in the way previously described. Thus, for the wing shown in figure 15, let $A=6$, $\lambda=1.0$, Γ_A and $\Gamma_C=0.1$ radian and assume that it is desired to find the proper value of C_{l_β} to use in equation (14). The part due to the tip portions A—A′ is Δ_1 (from fig. 16 (a)) $\times$ $\Gamma_A=0.195\times 0.1=0.0195$. The part due to the center portions C—C′ is $\Delta_2\times\Gamma_C=0.065\times 0.1=0.0065$. The resulting value of C_{l_β} to be used in equation (14) is thus 0.0130. The extension of this method to a curvilinear variation of Γ along the span may be easily made by plotting the values of Γ at each point of the span and using the method given in a previous section for integrating for the total effect.

The results of figure 16 indicate that equivalent angle-of-attack changes caused by unit lengths of dihedral portion near six-tenths of the relative distance from the center are, in general, slightly more effective in producing rolling moment than unit lengths of dihedral at the tips. Such a result is due partly to the fact that the load curves near the tips are rounded and partly to the fact that, for the tapered wings, the larger areas affected by lengths of dihedral near the 0.6 point tend to compensate for the shorter moment arms through which the change in loading acts.

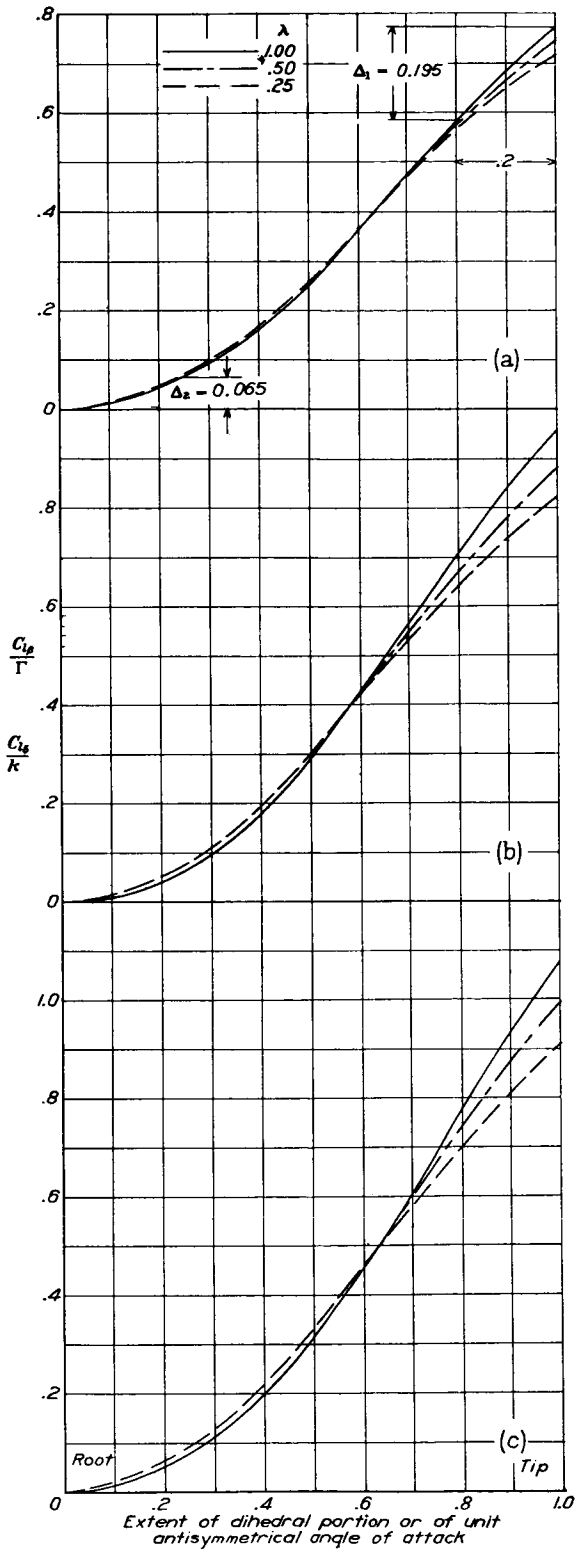

(a) $A=6$. (b) $A=10$. (c) $A=16$.

FIGURE 16.—Rolling derivative due to sideslip with dihedral. $L_{sideslip}=C_{l_\beta}\beta qSb$

Although, during a sideslipping motion, positive dihedral produces a righting moment, a similar though generally smaller effect may also be produced by the addition of vertical area above the longitudinal wind axis. Also, on account of interference effects, the proportion of the airplane rolling moment contributed by the wings may vary considerably with the external appearance of the airplane.

It is usually considered, in practice, that a straight wing will have some dihedral effect, but tests of wings with well-rounded tips (reference 5) do not support this view. In cases of wings with blunt tips or in cases where chords of the sections near the tip do not lie in one plane, some dihedral action is shown.

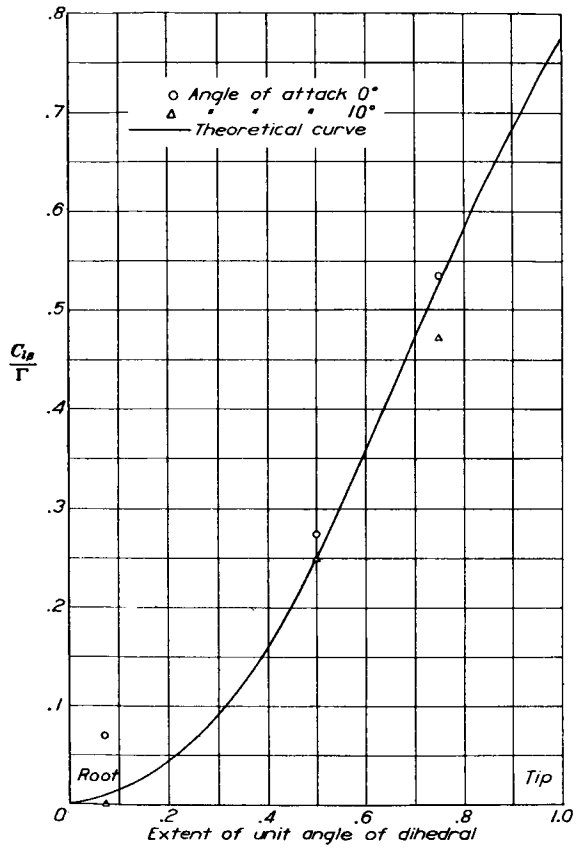

FIGURE 17.—Comparison between experimental and computed values of C_{l_β}/Γ (experimental data from reference 5).

Figure 17 shows a comparison of experimental and computed values of C_{l_β}/Γ. The experimental values have been obtained from figure 23 of reference 5 and the coefficients given therein have been converted to the form used in this report. In the tests reported in reference 5, a rounded-tip rectangular wing of aspect ratio 6 was given various lengths of dihedral by turning up the outer portions of the wing. Each wing was then tested throughout the angle-of-attack range for various sideslip and dihedral angles.

It will have been apparent from the preceding discussion that the results of figure 16 may also be applied to predict the rolling moment caused by an aileron deflection in unyawed flight since ailerons, equally and oppositely deflected, cause changes in the angle-of-attack distribution that are similar to the changes caused by dihedral. Strictly speaking, however, the change in angle of attack due to dihedral cannot have quite the same effect as a similar change produced by ailerons because the ordinary lifting-line theory, when applied to yawed or sweptback wings, omits the effect of the stagger of the trailing vortices and the inclination of the bound vortex. Although the present theory has not been modified to take this effect into account, there

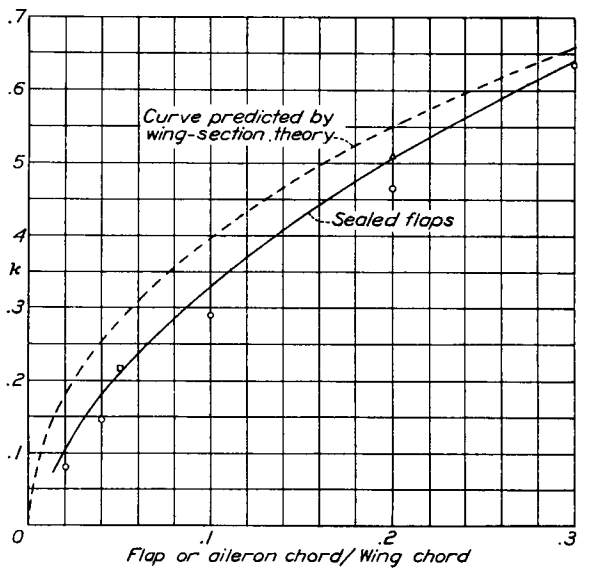

FIGURE 18.— Variation of k with ratio of flap or aileron chord to wing chord.

is ample justification for omitting it in the computations as experiments indicate only second-order differences (see reference 5) for the usual angles of yaw and sweepback.

For the computation of the rolling moment due to an aileron deflection δ, the appropriate value of C_{l_δ} to be inserted in the equation

$$L_{ailerons} = C_{l_\delta} \delta q S b \qquad (15)$$

may also be found from figure 16. The derivative C_{l_δ} is given as a ratio in terms of k, the theoretical change of α with aileron deflection. Although the value of k has been theoretically determined for thin wings, it is better to use values of k determined from an analysis of experimental data. For this purpose, figure 18 is included, which shows the variation of k for values of the ratio of aileron or flap chord to wing chord up to 0.3. This variation of k has previously been given in figure 11 of reference 6 and holds for sealed flaps deflected up to approximately 20°.

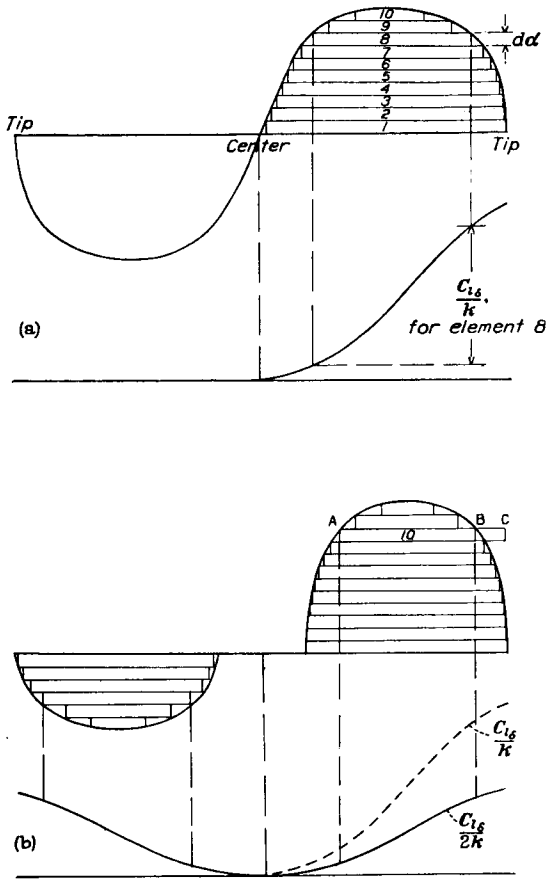

(a) Ailerons deflected equally.
(b) Ailerons deflected differentially.

FIGURE 19.—Addition of effect of aileron elements.

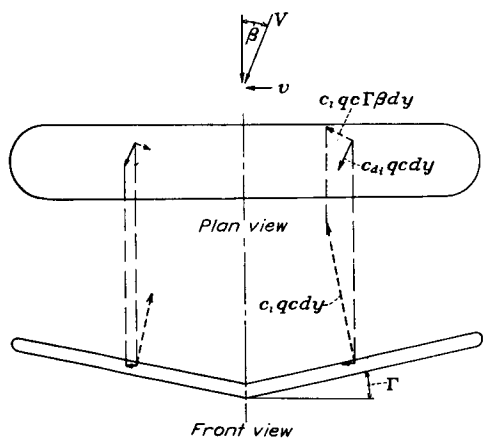

FIGURE 20.—Action of dihedral in producing yawing moment in sideslip.

If the angle-of-attack change caused by deflecting the ailerons is antisymmetrical about the wing center line, the proper value of C_{l_δ} to be used with equation (15) (for the rolling moment only) can be found by an integration or summation of the effects of elemental ailerons of various lengths and positions along the span as indicated in figure 19 (a). The values of C_{l_δ}/k are obtained from figure 16 for the wing plan form used. If the ailerons are differentially operated, then it may be better to divide the ordinates of figure 16 by 2 and to determine the value of the moment given by each aileron as indicated in figure 19 (b).

YAWING MOMENT DUE TO SIDESLIP

The yawing moment of a wing with dihedral in sideslipping motion may be conveniently divided into two parts, the first part being due to the unsymmetrical

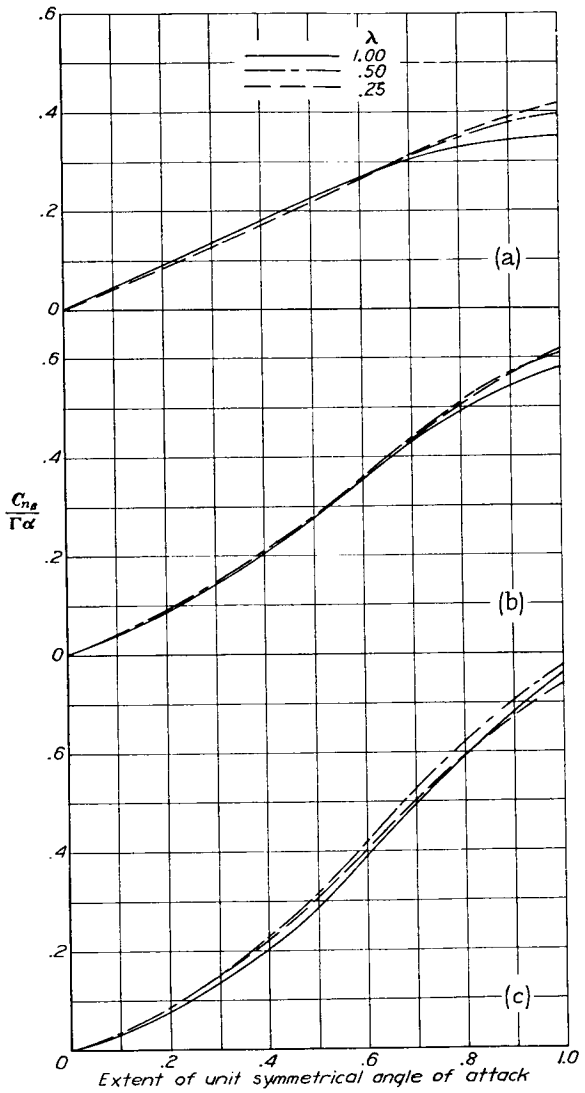

(a) $A=6$.
(b) $A=10$.
(c) $A=16$.

FIGURE 21.—Yawing derivative due to sideslip (dihedral constant).
$N_{\text{sideslip}}=C_{n_\beta} qSb$

induced-drag distribution over the span and the second part due to a shift of the lift vectors acting so as to produce a moment about the vertical axis. Figure 20 illustrates the components of the section lift and drag vectors that produce yawing moments. The advanced wing having the larger lift will also have a larger induced drag and hence a component moment is set up that tends to turn the wing so as to reduce the sideslip; at the same time, however, the contrary moment due to the components of the lift acts to advance the forward half of the wing still more. As was the case with the yawing derivative due to rolling, the moments caused by the lift components predominate and, as a result, the net theoretical moment is an unstable one; or, in other words, with the system of axes chosen, a negative yawing moment results when the dihedral and sideslip angles are positive.

The explanations advanced in some textbooks neglect the inward slope of the lift vectors and lead to an incorrect sign of the yawing moment.

The yawing moment in sideslip is given by the equation

$$N_{sideslip}=C_{n_\beta}\beta qSb \tag{16}$$

The derivative C_{n_β} is given in figure 21 as a ratio in terms of $\Gamma\alpha$ because its value depends linearly upon the magnitude of the product of these variables. The values of $C_{n_\beta}/\Gamma\alpha$ have been computed for unit symmetrical angle-of-attack distributions that extend out on either side of the center line and cover 0.25, 0.50, 0.75, and all of the wing span. These curves may be used to determine values of C_{n_β} for any initial angle-of-attack distribution symmetrical about the wing center line, provided also that the angle of dihedral is constant across the wing span. Although the rolling derivative due to sideslip can be obtained (from fig. 16) for a curvilinear variation of dihedral along the span, it is necessary to stipulate that either α or Γ remain constant if the principle of superposition is to be applied in the determination of C_{n_β}. The combination of variable symmetrical twist and uniform dihedral being more common than the converse, the computations were shortened by including curves for only the case of uniform dihedral.

The resultant value of C_{n_β} (to be used in equation (16)) is found by either an integration or a summation of the effects of elements of angle of attack extending along the span. The process to be followed where graphical evaluation is necessary has been illustrated in figure 10, with the ordinates of figure 10 (a) changed to $\Gamma\alpha$. The ordinates and abscissas of the remaining parts are to be changed as required. For untwisted wings with uniform dihedral, the value of $C_{n_\beta}/\Gamma\alpha$ is obtained by multiplying the value read at a relative distance of 1.0 by the wing angle of attack and, in turn, by the dihedral angle.

The curves of figure 21 being generally steeper beyond the 0.5 point, the deduction of increments of angle of attack at the tip, i. e., giving the wing washout, would be the simplest means of decreasing the unstable yawing moment caused by the wings in a sideslipping motion.

Although the predicted variation of the yawing moment with dihedral is confirmed, experiments show a residual stable yawing moment at zero dihedral that is not predicted by the ordinary theory. This residual moment is greater for wings with blunt tips and is greater at zero or negative lifts. It will be noted that the theoretical yawing moment is itself the small resultant of two large contrary effects and is thus of the same order as a number of possible secondary influences.

LANGLEY MEMORIAL AERONAUTICAL LABORATORY,
NATIONAL ADVISORY COMMITTEE FOR AERONAUTICS,
LANGLEY FIELD, VA., *April 19, 1938.*

REFERENCES

1. Lotz, Irmgard: Berechnung der Auftriebsverteilung beliebig geformter Flügel. Z. F. M., 22.Jahrg., 7.Heft, 14.April 1931, S. 189–195.
2. Pearson, H. A.: Span Load Distribution for Tapered Wings with Partial-Span Flaps. T. R. No. 585, N. A. C. A., 1937.
3. Betz, A., and Petersohn E.: Contribution to the Aileron Theory. T. M. No. 542, N. A. C. A., 1929.
4. Pearson, H. A.: Theoretical Span Loading and Moments of Tapered Wings Produced by Aileron Deflection. T. N. No. 589, N. A. C. A., 1937.
5. Shortal, Joseph A.: Effect of Tip Shape and Dihedral on Lateral-Stability Characteristics. T. R. No. 548, N. A. C. A., 1935.
6. Weick, Fred E., and Jones, Robert T.: Résumé and Analysis of N. A. C. A. Lateral Control Research. T. R. No. 605, N. A. C. A., 1937.

TABLE I.—VALUES OF COEFFICIENTS DEFINING WING CHORD DISTRIBUTION

$$\frac{c_s}{c}\sin\theta=\Sigma\, C_n\cos n\,\theta$$

C_0

A \ λ	1.00	0.50	0.25	Elliptical
6	0.730	1.000	1.300	1.000
10	.700	.956	1.270	1.000
16	.677	.952	1.240	1.000

C_2

A \ λ	1.00	0.50	0.25	Elliptical
6	−0.260	−0.149	----------	----------
10	−.320	−.218	----------	----------
16	−.368	−.259	−0.121	----------

C_4

A \ λ	1.00	0.50	0.25	Elliptical
6	----------	−0.074	−0.207	----------
10	----------	−.140	−.220	----------
16	−0.040	−.154	−.323	----------

REPORT NO. 638

THE INFLUENCE OF LATERAL STABILITY ON DISTURBED MOTIONS OF AN AIRPLANE WITH SPECIAL REFERENCE TO THE MOTIONS PRODUCED BY GUSTS

Robert T. Jones

Langley Memorial Aeronautical Laboratory

1938

REPORT No. 638

THE INFLUENCE OF LATERAL STABILITY ON DISTURBED MOTIONS OF AN AIRPLANE WITH SPECIAL REFERENCE TO THE MOTIONS PRODUCED BY GUSTS

By Robert T. Jones

SUMMARY

Disturbed lateral motions have been calculated for a hypothetical small airplane with various modifications of fin area and dihedral setting. Special combinations of disturbing factors to simulate gusts are considered and the influence of lateral stability on the motions is discussed.

The modifications of the airplane include changes of dihedral from 0° to 10° and changes of the weathercock stability from zero to $C_{n_\beta}=0.137$ (the equivalent of a fin as large as 10 percent of the wing area). The positions of the modified airplanes on the lateral-stability charts are shown.

Fin area and wing dihedral were found to be of primary importance in side gusts. It was found that the rolling action of the wing with as much as 5° dihedral was distinctly unfavorable, especially when the weathercock stability was small. It is pointed out that the greatest susceptibility to lateral disturbances lies in the inherent damping and coupling moments developed by the wing.

INTRODUCTION

Inherent stability, as defined in mathematical treatment, must be considered only one of several essential flying qualities of an airplane. Other important qualities belonging in this category are steadiness in rough air and responsiveness to control. Although the different flying qualities depend largely on the same governing factors, they may not call for similar proportionings of the factors. It is known, for instance, that the requirements for stability and control may conflict.

What is ultimately desired, or course, is a definite understanding of the individual requirements for stability, control, and steadiness in rough air. Most of the earlier work has been devoted primarily to the study of stability alone. A noteworthy early work on the effects of gusts is that of Wilson (reference 1). More recently the results of an investigation dealing with the effects of different degrees of stability on the motions following assumed initial conditions have been published (reference 2). The purpose of the present work is to study the amplitudes of the motions set up by gusts or other disturbances, particularly insofar as these motions are affected by the lateral-stability characteristics. It is hoped that the study will be useful in indicating combinations of stability characteristics that result in good riding qualities.

The mathematical treatment employed is, in principle, an extension of that used by Wilson and other early writers. The methods of calculation are, however, more concise and the development is not restricted to special types of gust. The operational method of resolving the effects of disturbances was used. (See reference 3.)

According to the theory, the motion caused by any random variation or sequence of the disturbing factors may be built up by superposing the effects of abrupt unit increases of the disturbance, which corresponds, in the case of gusts, to the effects of elementary sharp-edge cross-currents. Thus the effects of random gusts can be largely visualized in the effect of a unit sharp-edge gust.

STABILITY FACTORS ASSUMED

The chief differences of lateral stability considered were assumed to be brought about by changing the fin area and dihedral of a hypothetical small monoplane. Differences in other proportions of most airplanes of conventional form have only secondary effects (in unstalled flight) and, furthermore, are not usually dictated by considerations of stability. The exact arrangement of the hypothetical airplane, such as the vertical disposition of the wing with respect to the fuselage, may be taken as indefinite. Differences of arrangement can, of course, have large secondary influences on the action of the fin or dihedral, which are usually attributed to aerodynamic interference. It is reasonable to assume that the effects of such interference will be similar to the effects of actual changes in the size of the fin or the amount of dihedral.

The airplane assumed in the calculations is a small 1,600-pound monoplane having rectangular wings with rounded tips. The other proportions, including the radii of gyration about various axes, the tail length, etc., are based on average values of these quantities for a number of conventional machines. The stability derivatives and other characteristics of the airplane are essentially the same as those used in reference 4, except for the differences of fin area and dihedral, and apply to power-off flight. The axes and symbols employed throughout are given in detail in reference 4. Additional symbols that occur in this report are given in the following list:

X, Y, and Z, axes fixed in the airplane so that X points into the relative wind in steady flight. (See report cover.)

U_0, steady-flight velocity.

$\beta=\tan^{-1} v/U_0$.

Derivatives (see report cover for formulation of coefficients):

$C_{Y_\beta}=\frac{\partial C_Y}{\partial \beta}$, side force due to sideslip.

$C_{l_\beta}=\frac{\partial C_l}{\partial \beta}$, rolling moment due to sideslip.

$C_{n_\beta}=\frac{\partial C_n}{\partial \beta}$, yawing moment due to sideslip.

$C_{l_p}=\frac{\partial C_l}{\partial \frac{pb}{2U_0}}$, rolling moment due to rolling.

$C_{n_p}=\frac{\partial C_n}{\partial \frac{pb}{2U_0}}$, yawing moment due to rolling.

$C_{l_r}=\frac{\partial C_l}{\partial \frac{rb}{2U_0}}$, rolling moment due to yawing.

$C_{n_r}=\frac{\partial C_n}{\partial \frac{rb}{2U_0}}$, yawing moment due to yawing.

$L_v=\frac{1}{mk_X^2}\frac{\partial L}{\partial v}$.

$N_v=\frac{1}{mk_Z^2}\frac{\partial N}{\partial v}$.

It was found convenient to designate the five cases of modification by symbols representing the different front views of the airplane. Table I gives the stability coefficients assumed in each case for flight at three different lift coefficients.

TABLE I.—ASSUMED STABILITY COEFFICIENTS

(b, 32 ft.; m, 49 slugs; S, 171 sq. ft.; k_X, 0.150b; k_Z, 0.183b)

Case	Ratio of vertical fin area to wing area	Dihedral angle (deg.)	C_L	U_0 (f. p. s.)	$C_{l_p}=\frac{\partial C_l}{\partial \frac{pb}{2U_0}}$	$C_{l_r}=\frac{\partial C_l}{\partial \frac{rb}{2U_0}}$	$C_{l_\beta}=\frac{\partial C_l}{\partial \beta}$	$C_{n_p}=\frac{\partial C_n}{\partial \frac{pb}{2U_0}}$	$C_{n_r}=\frac{\partial C_n}{\partial \frac{rb}{2U_0}}$	$C_{n_\beta}=\frac{\partial C_n}{\partial \beta}$	$C_{Y_\beta}=\frac{\partial C_Y}{\partial \beta}$
	0.04	5.0	0.35	150.0	−0.425	0.086	−0.067	−0.022	−0.076	0	−0.226
			1.00	88.5	−.420	.250	−.088	−.055	−.091	0	−.356
			1.80	66.0	−.442	.442	−.130	−.074	−.196	0	−.772
	.06	5.0	.35	150.0	−.425	.086	−.067	−.022	−.097	.064	−.274
			1.00	88.5	−.420	.250	−.088	−.055	−.109	.067	−.410
			1.80	66.0	−.442	.442	−.130	−.074	−.220	.086	−.808
	.10	5.0	.35	150.0	−.425	.086	−.067	−.022	−.130	.102	−.378
			1.00	88.5	−.420	.250	−.088	−.055	−.146	.108	−.464
			1.80	66.0	−.442	.442	−.130	−.074	−.246	.137	−.920
	.06	0	.35	150.0	−.425	.086	0	−.022	−.097	.064	−.274
			1.00	88.5	−.420	.250	0	−.055	−.109	.067	−.410
			1.80	66.0	−.442	.442	0	−.074	−.220	.086	−.808
	.06	10.0	.35	150.0	−.425	.086	−.137	−.022	−.097	.064	−.274
			1.00	88.5	−.420	.250	−.177	−.055	−.109	.067	−.410
			1.80	66.0	−.442	.442	−.259	−.074	−.220	.086	−.808

These coefficients were estimated from the outward characteristics of the airplane by methods described in reference 41. The derivatives C_{n_β}, C_{n_r}, and C_{Y_β} (corresponding to the yawing moments in sideslip and in yawing and to the side force in sideslip) were assumed to be affected by the changes of fin area. Only the derivative C_{l_β} (corresponding to the rolling moment in sideslip) was assumed to be affected by changes of dihedral. The effect of dihedral on the lateral force in sideslip was neglected inasmuch as it was found that a compensating error was introduced by the absence of the side force due to rolling in the equations of motion. Another omission is the small adverse effect of dihedral angle on the weathercock-stability factor C_{n_β}. This effect is small, particularly in view of the wide variation of C_{n_β} assumed. At a lift coefficient of 1.8, representing low-speed flight, a full-span flap was assumed. Tests show that the effect of such a flap is to increase the weathercock-stability factor somewhat for the wing alone. In practice, the flap might interfere with the air flow over the fin so that the increase of C_{n_β} assumed in this condition would not be realized.

Figure 1 shows the positions of the modified airplanes on the lateral-stability diagrams. These diagrams are essentially similar to those given in reference 5 except that a simultaneous increase of C_{n_r} with C_{n_β} was assumed to show directly the effect of increasing the fin area.

The value recommended by Diehl (reference 6) for C_{n_β} works out to about 0.03 for the wing loading assumed here. Limits mentioned by Millikan (reference 7) correspond to $0.08>C_{n_\beta}>0.05$. Nearly all designers are familiar with the limits of L_v/N_v for satisfactory lateral stability given by Korvin-Kroukovsky (reference 8). Figure 1 (a) shows these limits in terms of C_{l_β} and C_{n_β}. It should be mentioned that Korvin-Kroukovsky's formulas are more suited to the empirical-statistical analysis in which they were employed than to the determination of absolute values of C_{n_β}/C_{l_β} for this stability chart. In most cases, wind-tunnel tests show values of C_{n_β} smaller than those predicted so that

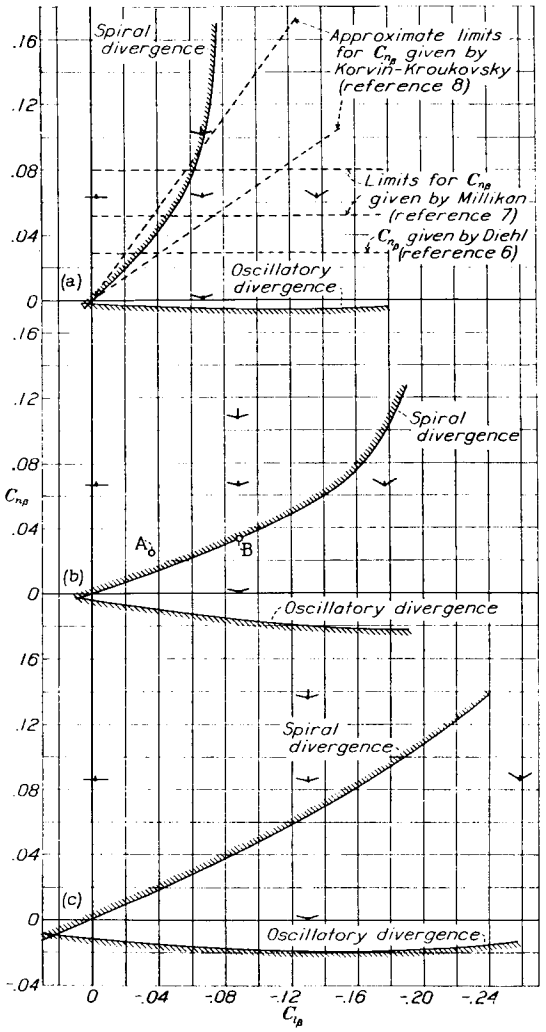

(a) C_L=0.35; U_0=150 f. p. s.
(b) C_L=1.0; U_0=88.5 f. p. s
(c) C_L=1.8; U_0=66 f. p. s.

FIGURE 1.—Stability chart showing positions of the assumed airplanes.

the specified range, if given in wind-tunnel values, would probably fall somewhat lower than indicated in figure 1.

The value $C_{n_\beta}=0$ does not, of course, correspond to an airplane with no vertical tail surface. Experience has shown that the unstable yawing moment of a large well-streamlined fuselage may entirely offset the stabilizing action of a fair-size fin. This occurrence is naturally more probable if the fin area is originally small; hence the smallest area likely to be used in a modern design (4 percent of the wing area) was chosen to represent the condition.

It is, in general, difficult to predict the values of either C_{n_β} or C_{l_β} for a given design. It will be realized that the corresponding values of fin area and dihedral, as referred to in this report, apply only under certain idealized conditions and are employed primarily as a matter of convenience in fixing ideas on the problem Reference 9 gives a summary of test values of C_{n_β}, including a discussion of pertinent factors and drawings of the models tested. The data included in that paper should aid the designer in judging the weathercock stability.

INFLUENCE OF LATERAL STABILITY ON MOTIONS DUE TO ARBITRARY DISTURBANCES

GENERAL DESCRIPTION OF LATERAL MOTIONS

The equations of lateral stability generally show two real roots together with one conjugate complex pair, indicating three "modes" of motion. Different disturbances will result in motions compounded of these three modes in different proportions.

Table II lists the roots, or stability indices, for the various cases considered. The first mode (corresponding to the root λ_1), represents primarily the heavy damping of any movement involving rolling of the wings relative to the air. At normal flight speeds, this damping is such that the wings are in a large measure constrained against such relative movement normal to their chords.

TABLE II.—STABILITY INDICES, RATES OF DAMPING, AND PERIODS

[$\lambda_2=a+bi$]

Case	C_L	λ_1	$\frac{-0.69}{\lambda_1}$ (a)	λ_2	$\frac{(0.095 \text{ or } -0.105)}{\lambda_2}$ (b)	a	$\frac{-0.69}{a}$	b	$\frac{\pi}{2b}$ (c)
	0.35	−5.477	0.126	−0.4190	[d] 1.645	−0.1720	4.01	0.708	2.22
	1.0	−3.255	.212	−.2974	[d] 2.32	−.1386	4.98	.8241	1.907
	1.8	−2.533	.273	−.6080	[d] 1.13	−.1794	3.85	.8568	1.83
	.35	−5.472	.126	−.0070	15.0	−.495	1.39	2.45	.641
	1.0	−3.280	.210	.0615	1.55	−.3637	1.90	1.676	.937
	1.8	−2.633	.262	.0624	1.53	−.5247	1.315	1.546	1.02
	.35	−5.466	.126	0	∞	−.680	1.01	3.03	.518
	1.0	−3.294	.209	.0838	1.133	−.4797	1.44	2.013	.780
	1.8	−2.670	.258	.1347	.706	−.6075	1.14	1.829	.858
	.35	−5.369	.129	.0420	2.27	−.571	1.21	2.35	.668
	1.0	−3.070	.225	.1770	.537	−.529	1.30	1.519	1.034
	1.8	−2.320	.297	.2900	.328	−.795	.868	1.415	1.110
	.35	−5.573	.124	−.0504	2.08	−.423	1.63	2.55	.616
	1.0	−3.460	.199	−.0184	5.71	−.235	2.94	1.826	.860
	1.8	−2.872	.240	−.1045	1.005	−.3219	2.14	1.697	.925

[a] The value $-0.69/\lambda$ represents time to diminish by ½.
[b] Use $-0.105/\lambda_2$ for time to diminish by 1/10 when λ_2 is negative; use $0.095/\lambda_2$ for time to increase by 1/10 when λ_2 is positive.
[c] Quarter period.
[d] For this case, $-0.69/\lambda_2$ has been used.

The second mode distinguishable in the lateral motions (corresponding to λ_2) is a practically continuous turning motion, which may either converge or diverge. Normal stability of this mode represents the slow natural recovery from a banked turn. The rate of increase or decrease of the turning motion is slow, primarily on account of the insensitiveness of the airplane to displacement in bank and the strong resistance to rolling motion. The slow spiral always occurs with inward sideslip.

The third mode (λ_3) is the familiar oscillation, consisting usually of a yawing and sideslipping motion. Such rolling as occurs in the oscillation is determined by the tendency of the wings to follow a path outlined by the dihedral in front view. The wing, when sideslipping, tends strongly to roll in a way involving the least angle-of-attack change along the span. Thus the oscillations involve a "weathercock" motion combined with a rolling nearly in phase with the sideslip.

With fairly large fin area, the oscillations are rapid and are quickly damped. Under most conditions the amplitude is small. As the fin area is reduced, however, the period becomes slower and, with normal dihedral, the oscillation takes on the character of a swinging in bank and sideslip under the action of gravity. The point of instability is reached when the oscillation degenerates to an almost pure rolling and sideslipping motion, so that the damping derivative in yawing, C_{n_r}, has little effect on the occurrence of undamped oscillations. As has been shown (reference 4), unstable oscillations can readily occur if the airplane is constrained in yawing.

Although both the oscillation and the slow mode of convergence are largely governed by the fin area and the dihedral, the rapid convergence λ_1 is practically independent of either of these factors. The damping comes, of course, from the wings and is an inherent characteristic of conventional airplanes. This damping is excessive and is undesirable, since it indicates great sensitiveness to rolling gusts or to vertical gusts with a gradient along the wing span. The damping of rolling can be reduced by increasing the lateral moment of inertia, but the possible improvement appears to be small.

CALCULATED MOTIONS

The equations of motion of the airplane form a linear system so that the effects of disturbances can be compounded by addition. Thus, if any sequence of application of forces or couples to the airplane is given, it is possible to compute the resultant theoretical motion at any instant by addition, or integration, of separate effects. The impressed forces or couples may be due to control manipulation or to gusts, alone or in combination.

The foregoing statement refers to a resolution of the impressed disturbances along the axes fixed in the airplane. The disturbances are assumed to take on preassigned values independent of the movements of the airplane. With conventional control devices, the disturbances do remain practically independent of the motions. The orientation of the gusts is not dependent on the motion of the airplane, and deviations caused by such outside disturbances will introduce changes in the magnitudes of the disturbing factors themselves. For small displacements, these changes are of second order and are negligible. For large displacements in gusts it may, however, be necessary to carry out the calculation in several steps, altering the magnitude of the disturbance as the orientation of the relative wind changes.

The data needed for the computation of motion under any given set of conditions are the histories of motions following sudden unit disturbances. Computations of such unit motions were made during the course of the investigation reported herein and the results were used as the basis for the more complete calculations given later.

Specifically, the unit disturbance referred to is a force (Y) or a couple (L or N) having the value zero up to the time $t=0$ and maintaining a constant value thereafter. The magnitude is such as to cause a unit linear or angular acceleration of the airplane. According to well-known mathematical rules, the motions under such conditions are given by equations of the form

$$p_Y(t) = p_{Y0} + p_{Y1}e^{\lambda_1 t} + p_{Y2}e^{\lambda_2 t} + p_{Y3}e^{at}\cos b(t + t_{pY}) \quad (1)$$

where p_{Y0}, p_{Y1}, and t_{pY} are constants, calculated values of which are given in table III, and λ_1, λ_2, $a+ib$, and $a-ib$ are the roots, or stability indices. (See table II.) Three components of motion for each of three component disturbances are given. Thus, $p_Y(t)$ denotes the rolling velocity due to a unit side disturbance and $r_L(t)$ denotes the yawing velocity due to a unit rolling disturbance.

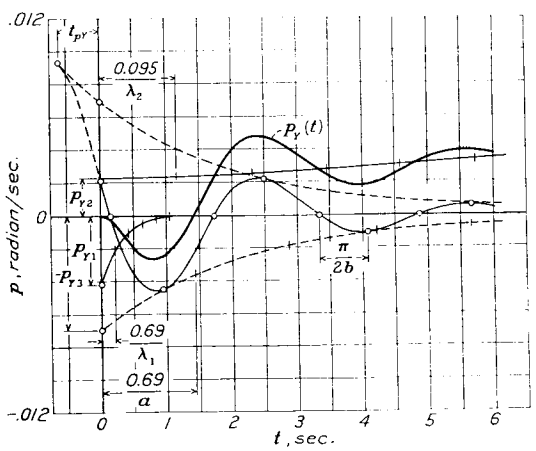

FIGURE 2.—Example showing use of data given in table III for plotting motions.

$p_1(t) = p_{Y1}e^{\lambda_1 t} + p_{Y2}e^{\lambda_2 t} + p_{Y3}e^{at}\cos b(t+t_{pY})$

Plots of these equations were made with scarcely any additional computation. The procedure is illustrated by figure 2. First the coefficients, as given in

TABLE III.—EQUATIONS OF MOTION FOR UNIT DISTURBANCES

$[v_L(t) = v_{L0} + v_{L1}e^{\lambda_1 t} + v_{L2}e^{\lambda_2 t} + v_{L3}e^{at}\cos b(t + t_{vL})$; etc.]

Case	C_L	Sideslip					Rolling					Yawing				
		a—Due to side disturbance														
		v_{Y0}	v_{Y1}	v_{Y2}	v_{Y3}	t_{vY}	p_{Y0}	p_{Y1}	p_{Y2}	p_{Y3}	t_{pY}	r_{Y0}	r_{Y1}	r_{Y2}	r_{Y3}	t_{rY}
	0.35	0.	−0.0041	0.5685	−1.6820	1.735	0	−0.00178	−0.00533	0.01683	1.600	0	−0.00007	0.00380	−0.00380	0.284
	1.0	0	−.0237	.5558	−1.3410	1.413	0	−.00374	−.00408	.01683	1.320	0	−.00041	.00605	−.00565	−.080
	1.8	0	−.067	.627	−1.416	1.360	0	−.00658	−.00497	.02360	1.235	0	−.00113	.00777	−.00668	.138
	.35	0	−.0033	.1390	−.3980	.500	0	−.00171	−.00021	.00393	.433	0	−.00005	.00581	−.00589	−.088
	1.0	0	−.021	.274	−.532	.652	0	−.00414	.00159	.00804	.743	0	−.00030	.00878	−.00888	−.175
	1.8	0	−.053	.446	−.565	.618	0	−.00734	.001502	.0121	.690	0	−.00060	.00975	−.0102	−.297
	.35	.1271	−.0027	0	−.3310	.391	−.00015	−.00169	0	.00322	.318	.00625	−.00040	0	−.00638	−.076
	1.0	0	−.0199	.2350	−.4570	.537	0	−.00433	.00224	.00698	.629	0	−.00022	.00908	−.00930	−.155
	1.8	0	−.048	.342	−.459	.479	0	−.00770	.00323	.0110	.629	0	−.00037	.00970	−.0103	−.238
	.35	0	−.0005	.1687	−.4200	.493	0	−.00026	.00128	−.00134	−.302	0	−.00001	.00635	−.00656	−.110
	1.0	0	−.0087	.3510	−.5940	.630	0	−.00153	.00480	−.00581	−.641	0	−.00010	.00854	−.00939	−.301
	1.8	0	−.044	.489	−.529	.402	0	−.00485	.00660	−.0105	−.993	0	−.00035	.00738	−.00928	−.502
	.35	0	−.0056	.1293	−.3830	.487	0	−.00305	−.00142	.00746	.403	0	−.00010	.00607	−.00600	−.069
	1.0	0	−.0278	.2080	−.5060	.660	0	−.00601	−.00044	.01236	.557	0	−.00041	.00846	−.00824	−.115
	1.8	0	−.057	.329	−.537	.612	0	−.00909	−.00226	.01755	.511	0	−.00075	.00996	−.00952	−.149
		b—Due to rolling disturbance														
	C_L	v_{L0}	v_{L1}	v_{L2}	v_{L3}	t_{vL}	p_{L0}	p_{L1}	p_{L2}	p_{L3}	t_{pL}	r_{L0}	r_{L1}	r_{L2}	r_{L3}	t_{rL}
	0.35	18.490	−0.401	2.985	−22.035	−0.419	0	−0.17602	−0.02753	0.22000	−0.552	0	−0.0074	0.01959	−0.04996	−1.870
	1.0	23.809	−1.7368	2.2288	−26.332	−.480	0	−.2787	−.0163	.3338	−.591	0	−.03029	.02409	−.11120	−1.832
	1.8	21.688	−3.452	5.385	−26.215	−.523	0	−.3341	−.0431	.4385	−.625	0	−.0576	.0672	−.1257	−1.744
	.35	114.003	−.338	−112.570	−1.698	−.355	0	−.1769	.1659	.0195	−.397	4.682	−.0050	−4.6992	.02997	.301
	1.0	−32.398	−1.4005	37.3	−5.98	−.563	0	−.2761	.2186	.0843	−.490	−1.244	−.019	1.198	.093	.476
	1.8	−66.222	−2.236	70.067	−7.340	−.874	0	−.3067	.2338	.1577	−.705	−1.6167	−.0248	1.5269	.1317	.333
	.35	.943	−.314	.732t	−1.138	−.326	.1732	−.1782	0	.0106	−.356	−.01256	−.00398	.0360t	.00226	.247
	1.0	−21.747	−1.2602	24.768	−3.9301	−.550	0	−.2736	.2368	.0605	−.455	−1.0078	−.0142	.9500	.0860	.289
	1.8	−24.096	−1.873	26.642	−4.953	−.784	0	−.2979	.2514	.1184	−.638	−.8434	−.0142	.7554	.1107	.215
	.35	−22.128	−.3679	23.738	−1.999	−.383	0	−.18612	.17915	.00700	.074	−.9088	−.00530	.8934	.0310	.357
	1.0	−13.715	−1.8440	18.444	−7.4601	−.773	0	−.3250	.2521	.0729	.023	−.5266	−.0223	.4493	.1177	.370
	1.8	−16.375	−3.485	18.276	8.721	.981	0	−.3911	.2473	.1726	−.414	−.4000	−.0287	.2751	.1545	.078
	.35	15.508	−.313	−14.033	−1.637	−3.066	0	−.16874	.15318	.03290	−.422	.6369	−.0048	−.6469	.0254	.372
	1.0	89.459	−1.1249	−85.096	−4.700	−.410	0	−.2433	.1819	.1142	−.549	3.435	−.016	−3.464	.076	.500
	1.8	32.402	−1.613	−27.849	−5.801	−.612	0	−.2571	.1904	.1905	−.715	.7916	−.0211	−.8409	.1032	.485
		c—Due to yawing disturbance														
	C_L	v_{N0}	v_{N1}	v_{N2}	v_{N3}	t_{vN}	p_{N0}	p_{N1}	p_{N2}	p_{N3}	t_{pN}	r_{N0}	r_{N1}	r_{N2}	r_{N3}	t_{rN}
	0.35	29.084	−0.035	−292.010	284.729	0.556	0	−0.0154	2.7364	−2.8476	0.423	1.429	−0.001	−1.948	0.644	−0.894
	1.0	90.505	.434	−222.037	142.701	.493	0	.0719	1.6312	−1.8012	.402	1.999	.007	−2.415	.600	−.997
	1.8	68.0192	2.398	−144.835	109.323	.959	0	.2299	1.149	−1.8340	.840	1.250	.040	−1.795	.519	−.269
	.35	139.162	−.026	−163.417	24.673	.073	0	−.0135	.2433	−.2420	−.130	6.836	0	−6.834	−.372	.640
	1.0	−102.736	.307	70.750	32.050	−.090	0	.0590	.4128	−.4752	.067	−2.270	.004	2.268	−.515	.934
	1.8	−184.052	1.202	151.993	31.509	−.132	0	.1631	.5074	−.6713	−.029	−3.382	.014	3.316	.557	−.955
	.35	−15.600	−.019	.672t	15.980	−.068	.1583	−.0191	0	−.1541	−.146	.0129	−.0001	.0330t	−.3160	.505
	1.0	−51.788	.251	29.799	22.169	−.098	0	.0549	.2846	−.3395	−.004	−1.144	.003	1.152	−.452	.768
	1.8	−60.316	.890	38.791	21.305	−.137	0	.1414	.3660	−.5075	−.012	−1.108	.007	1.099	.491	−.857
	.35	−27.012	.073	.961	26.769	−.104	0	.0370	.00732	−.0860	.438	0	.0010	.0362	−.4202	.631
	1.0	−43.492	1.104	5.154	39.990	−.246	0	.1949	.0683	−.3948	.553	0	.0133	.1214	−.6383	.894
	1.8	−45.455	4.110	11.236	36.908	−.436	0	.4632	.1533	−.7250	.392	0	.033	.168	−.645	.885
	.35	18.930	.107	−41.150	22.326	−.054	0	−.0579	.4548	−.4372	−.170	1.894	−.002	−1.904	.353	−.603
	1.0	283.675	−.112	−310.046	26.484	−.001	0	−.0242	.6604	−.6476	−.103	12.538	−.002	−12.598	.430	−.781
	1.8	90.055	.135	−114.774	24.680	.052	0	.0215	.7855	−.8099	−.050	3.309	.002	−3.466	.437	−.711

table III, were marked off on the ordinate scale. The time intervals within which the various modes diminish or increase by one-half, or by one-tenth in the case of λ_2 (see table II), were then spaced off on the abscissa and points on the curves were found by diminishing or increasing the ordinates successively as indicated by the sign of the root. The oscillatory mode was obtained by drawing in the envelope (given by $\pm p_{V3}$, say) and spacing off the quarter periods, beginning at the point indicated by the phase angle of this mode. The cosine curve was then simply sketched in as shown. The final curves were found to give remarkably good checks when applied in the original differential equations of motion. Such a check shows the correctness of both the method of plotting and the analytical solutions (equation (1) and table III).

If the impressed disturbance is given as a function of t by a curve, it will usually be sufficient to approximate this curve by the addition of a number of successive positive and negative steps. The combination of steps necessary to reproduce the disturbance leads directly to the addition of the elementary motions for the resultant motion. Otherwise, for example, if the variation of disturbance is given by $L(t)$, then the resultant motion $p(t)$ at any time t due to $L(t)$ beginning at $t=0$ may be found by Duhamel's theorem, thus

$$p(t)_{\text{due to variable rolling moment}} = p_L(t)\ L(0) + \int_0^t p_L(t-t_1)\ L'(t_1)\ dt_1 \qquad (2)$$

where $p_L(t)$ and $p_L(t-t_1)$ are obtained from table III. An explanation and a graphical method for evaluation of such integrals are given in reference 3.

MOTIONS IN SIDE GUSTS

The motion caused by a unit increment of gust velocity is found by compounding elementary disturbances in such a way as to simulate the disturbing action of the gust. Thus, in a side gust of velocity v_0, the disturbing acceleration along Y will be $v_0 Y_v$ and angular disturbances will be $v_0 L_v$, $v_0 N_v$.

As explained before, the effects of any usual variation of gustiness can be largely foretold from the effect of a unit sharp-edge gust. The variable gust can be built up from small increment jumps of gust velocity corresponding to sharp-edge cross-currents and the final motion will approach that obtained by superposing the motions due to the individual elements.

The effect of a sharp gust from the side is similar to, although not exactly the same as, the effect of an initial angle of sideslip. For the side gust, it is necessary to take account of the period of penetration of the airplane into the current. The first effect will be to push the nose of the airplane downwind whereas an instant later the current will strike the fin, turning the machine into the gust. The action of dihedral in causing the machine to roll away from the gust will also occur before the fin is affected. These effects are, however, of short duration and do not alter the motion to any great extent after the first fraction of a second, except in cases of small weathercock stability where the fuselage contributes a large unstable yawing moment.

The computations that follow are based on the assumption that the rolling action of the gust begins at $t=0$ and that the yawing action begins when the airplane has traveled far enough to carry the fin into the current. The case of $C_{n_\beta}=0$ was treated by assuming a yawing couple equal and opposite to that of the 4-percent fin applied when $t=0$, this couple being neutralized at the instant the fin entered the gust.

A possible further refinement of the calculations would involve the delay in building up the full lift forces on the various surfaces. Mathematical methods for dealing with various lags or rates of growth of the aerodynamic reactions have been developed, but their description is beyond the intended scope of the present report. It may be said, however, that, for motions as slow as the natural oscillations of a rigid airplane, this effect (judging by the theoretical predictions) is quite negligible.

Figure 3 illustrates the results of the calculations based on a 10-foot-per-second sharp-edge side gust. The curves shown are for flight at $C_L=1.0$ but the same general trends appeared in the calculations made for other lift coefficients.

The most noteworthy difference shown is the effect of deficiency of fin area on the banking motion (figs. 3 (a) and 3 (b)). The airplane with 10° dihedral and average fin was not displaced so much in bank by the side gust as was the airplane with 5° dihedral and a small fin. The initial rate of rolling, however, was greater with the greater dihedral.

With a given dihedral an increase of fin area cuts down the banking motion although, after a certain size is reached, the gain becomes slight, as is illustrated by figure 3 (a). With neutral weathercock stability (fig. 3 (c)) the change of heading on entering the gust is at first small and, although the motion is stable, the oscillation in azimuth seems to be reinforced for a time by the rolling. This action is to be attributed to the phase lag between the rolling and the yawing effects upon penetrating the sharp-edge current. It seems probable that an appearance of inherent instability may be reached at a point considerably above the mathematical limit for undamped oscillations. (See fig. 1.) It is known, for instance, that unstable oscillations may result from an attempt to hold the wings level with ordinary ailerons unless C_{n_β} has a definite positive value.

The side gust is equivalent to a sudden shift in the wind direction, corresponding to a change in azimuth ψ_0 as indicated in figure 3 (c). The normal airplane swings about and tends to approach this heading. It will be noted that the airplane with the large fin turns fairly sharply into the wind and, since the banking

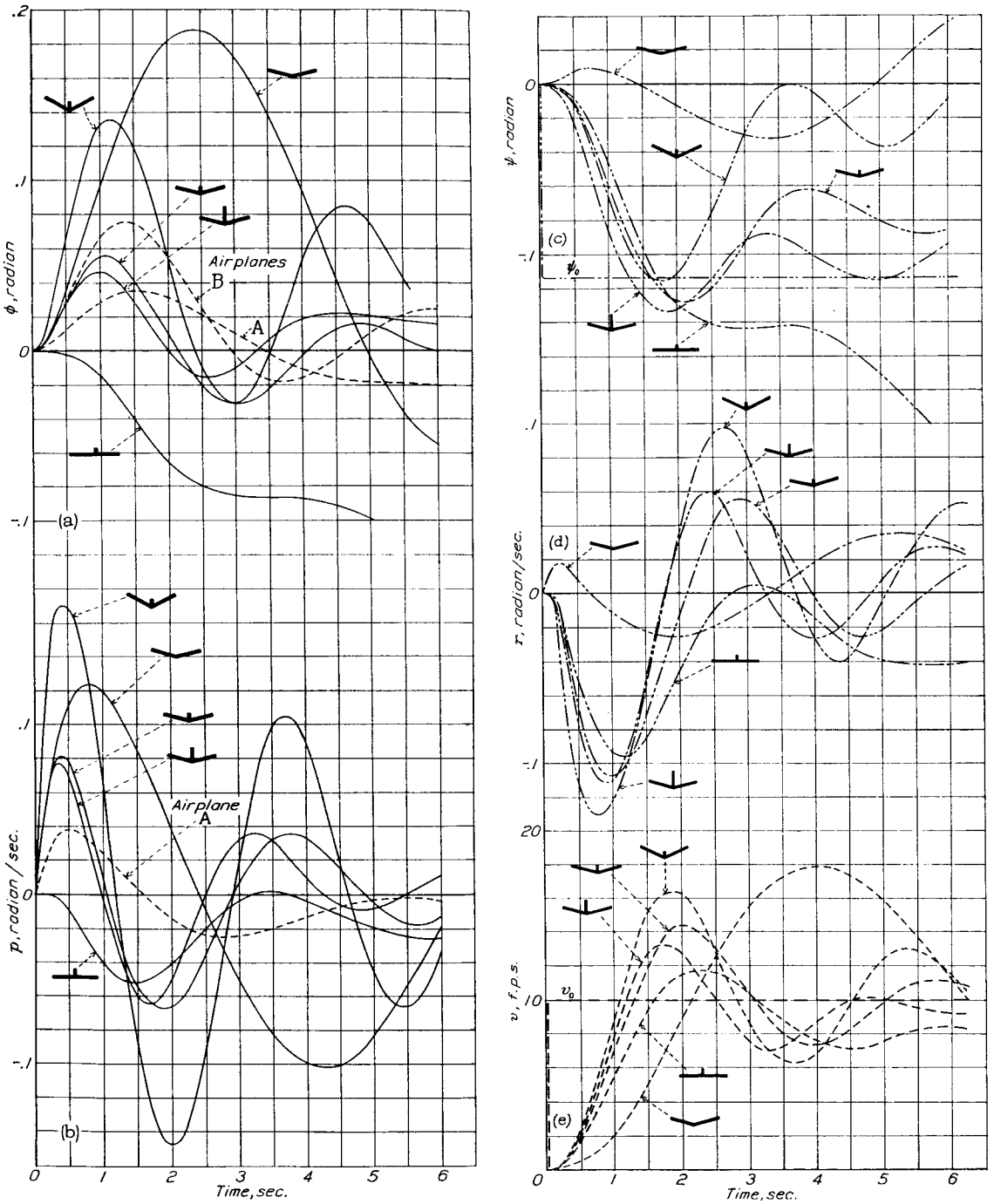

(a) Banking.
(b) Rolling motion.
(c) Azimuth.
(d) Yawing motion.
(e) Sideslip velocity.

FIGURE 3.—Motions caused by a sharp-edge side gust.
$C_L = 1.0$; $\rho_0 = 10$ f. p. s.; $U_0 = 88.5$ f. p. s.

motion is small, tends to keep the same flight path relative to the earth for a short time. After about 6 seconds, however, the spiral divergence begins to be apparent and the motion finally results in turning downwind.

An example of extreme spiral divergence is illustrated by the airplane with no dihedral. In this case, however, the airplane banks and turns directly upwind. The airplane with large dihedral illustrates the opposite condition and shows the predominance of oscillations that generally characterizes the effect of dihedral. Here the airplane tends back toward its original azimuth heading, drifting sidewise with the gust.

The airplane with 5° dihedral banked rather sharply away from the gust, whereas the airplane with zero dihedral showed an undesirable tendency to bank and slide into the gust. It was therefore a matter of interest to try some modifications lying in between these two conditions. It was realized that the rolling could not be entirely suppressed by such modifications on account of the phase relationships involved in the motions.

It appeared that 1° or 2° of effective dihedral would give about the least banking motion in the side gust and hence this condition was investigated. Inasmuch as the airplane might have shown a noticeable spiral divergence at low speeds with the normal fin area, this area was arbitrarily reduced, bringing the weathercock-stability factor C_{n_β} down in about the same proportion as the dihedral factor C_{l_β}. The values selected were $C_{n_\beta}=0.025$ and $C_{l_\beta}=-0.035$, which corresponds to 2° effective dihedral. The position of this airplane on the lateral-stability chart is denoted by the point A in figure 1 (b).

The results for airplane A are compared with the others in figures 3 (a) and 3 (b). It will be noted that the bank is somewhat smaller than in the case with 5° dihedral and a large fin but that the bank persists for a longer time. The difference made by the change from 5° dihedral to 2° seems surprisingly small. A somewhat greater difference would be expected if the fin had not been reduced. It should be borne in mind that the yawing disturbance is reduced by cutting down the fin.

The curve for airplane B (fig. 3 (a)) shows the result of attempting to secure spiral stability (at $C_L=1.0$) by cutting down the fin of the airplane with 5° dihedral. (Note that airplane A is slightly unstable.) The value of C_{n_β} in this case is about half that assumed for the mean condition. (See fig. 1 (b).) The banking displacement seems undesirably large (comparatively) in this case.

OTHER TYPES OF GUST

The flight velocity of the airplane being normally large with respect to gust velocities, it is permissible to consider the gusts as being stationary in time with respect to the flight path. Thus the gusts are considered to exist as a fixed pattern in the air ahead of the airplane and not to vary in time within the short space required for the machine to travel its own length.

As mentioned before, when the airplane enters a cross-current in level flight, a gradient of sidewise velocity along the length of the fuselage will exist. The effect of this gradient is similar to the effect of a relative yawing motion superposed on the side velocity. For a uniform gradient the additional yawing moment would be $(-dv_0/dx)\times N_r$. The calculations involved this factor by virtue of the time lag assumed in application of the yawing moment due to the fin, and upon this basis they should be applicable to any reasonable variation or gradient of sidewise velocity.

A somewhat different situation arises when the airplane is climbing or descending through a cross wind that varies with height, as, for instance, when descending through the earth boundary layer for a cross-wind landing, for then no perceptible gradient of sidewise velocity along the length of the airplane will exist. The motions that arise in these cases can be compounded by integration from the motion following an initial angle of sideslip. This motion is not greatly different from that caused by entering a sharp cross-current and the same general conclusions will apply.

It appears that a true yawing gust, consisting of pure angular relative motion of the air, could act only momentarily on the airplane. The sidewise velocity would predominate after the first two- or three-tenths of a second with the airplane flying at normal speed. Gradients of velocity along the wing span, however, might persist for longer periods.

Away from the ground influence, gradients of forward velocity and of vertical velocity along the wing span must be considered as being about equally probable. At normal flight speeds, the vertical gradients produce by far the greater effects. As was mentioned before, the damping of relative rolling motion is such that the airplane very quickly takes on the angular velocity of the gust gradient.

Figure 4 shows the rolling motion calculated for the medium airplane (5° dihedral and 6 percent fin) in a momentary rolling gust $p_0b/2U_0=0.05$. It will be noted that the airplane takes on approximately half the rolling velocity of the gust within one-fifth second.

As might be expected, observations have shown that vertical currents tend to diminish near flat ground. Thus side gusts and yawing gradients are more likely to affect the airplane while it is landing and taking off. At very low speeds with flaps down, the rolling derivative due to yawing becomes as great as that due to rolling (see table I) so that in this condition the airplane is affected as much by spanwise gradients of longitudinal velocity as it would be by the rolling gradients. (Note also that the effect of the rolling gradients is less at low speed.)

Figure 5 shows the banking reactions of the various airplanes in a sudden, persistent yawing-gradient gust.

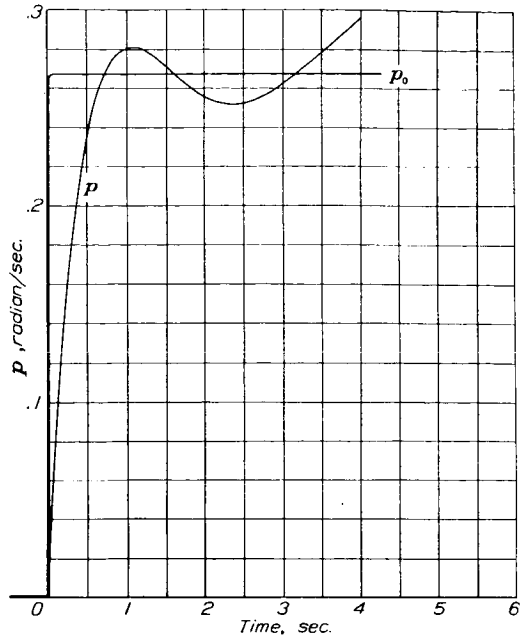

FIGURE 4.—Typical rolling motion caused by a sudden rolling gradient.

$\frac{p_0 b}{2U_0}=0.05(t>0)$; $U_0=88.5$ f. p. s.

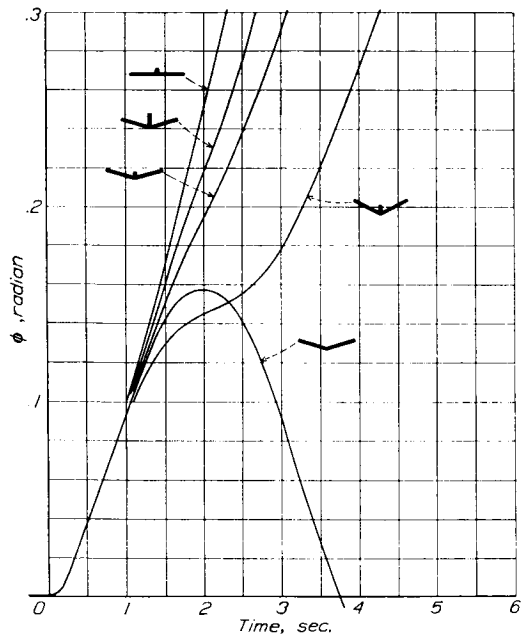

FIGURE 5.—Bank caused by a yawing gradient along the wing span.

$\frac{r_0 b}{2U_0}=0.05(t>0)$; $U_0=88.5$ f. p. s.

The gust assumed corresponded to a difference of longitudinal velocity between the two wing tips of about 9 feet per second ($r_0 b/2U_0=0.05$). All the examples show roughly the same banking tendency within the first second, since the disturbing factors (rolling moments due to yawing velocity) are the same in all cases. The subsequent motions show the influence of different degrees of spiral stability and instability.

The primary disturbing factor in the yawing-gradient gust being proportional to the derivative L_r (rolling moment due to yawing), the greatest room for improvement would be to reduce this derivative. Taper and washout (such as are attained with a partial-span flap) are beneficial in this respect. It is estimated that L_r might have been reduced by one-third of the given value (see table I) at $C_L=1.8$ if a 50-percent-span flap had been assumed. The effect of plan form is not so pronounced, leading to a reduction of one-sixth for a 4:1 taper.

In general, a reduction of the rolling moment due to yawing seems desirable from considerations of lateral stability. The magnitude of this derivative with controls fixed is, like that due to rolling, primarily a consequence of the general lay-out of the airplane and is not dictated by considerations of stability. It appears, however, that the magnitude of L_r with controls free (or loosely held) could be reduced or reversed by making use of an appropriate combination of ailerons with increased upward pressure (attained by cambering the ailerons) and a differential linkage, as described in reference 10. An appropriate linkage would eliminate the necessity of applying contrary aileron pressure during steady turns and would also eliminate the spiral instability with controls free.

CONCLUDING REMARKS

A study of the effects of gusts gives different indications depending on the interval of time considered. During the first stages, the upsetting movements of the stable airplane may be more severe than those of a slightly unstable one. If the airplane is under control and if the gusts are of noticeable magnitude, then the motion during the first 2 or 3 seconds is of primary concern. For uncontrolled flight or for flight in relatively calm air where disturbances could become apparent only through introducing a divergence, the later stages of the motion are of interest.

In a consideration of the early stages of the motion, it is evident that the requirements of fin area and dihedral for spiral stability at low speed conflict somewhat with the requirements for steadiness in side gusts. If spiral instability is present, the rates of divergence introduced by various disturbances appear to be small as long as there is a moderate dihedral action present. The condition of zero (effective) dihedral leads, however, to definitely undesirable rates of divergence.

If average weathercock stability ($C_{n_\beta}=0.05$ to 0.07) is assumed, the optimum magnitude of the rolling derivative due to sideslip for steadiness in side gusts appears to be about $C_{l_\beta}=-0.01$ to -0.04, corresponding to an effective dihedral of 1° or 2°. Spiral stability

throughout the flight range could be secured with this dihedral by cutting down the fin effect. The latter change would lead to somewhat greater banking displacements in the gusts and would also be detrimental to aileron control, unless such control were obtained without adverse yawing moments.

The damping of rolling is such that the airplane very quickly takes on any rolling component of gust velocity. The usual modifications of the lateral-stability factors have but little influence on the immediate effects of the rolling gust. An automatic device, acting so as to cut down the damping of rolling (relative to the air), should be advantageous from considerations of riding comfort.

The effects of longitudinal gradients of gust velocity become fairly large at low flight speeds. Noticeable improvement can be obtained by the use of partial-span flaps or by otherwise concentrating the lift toward the center of the wing, but this conclusion applies, of course, only as long as no portion of the wing is brought near the stalling point.

LANGLEY MEMORIAL AERONAUTICAL LABORATORY,
NATIONAL ADVISORY COMMITTEE FOR AERONAUTICS,
LANGLEY FIELD, VA., *June 8, 1938.*

REFERENCES

1. Wilson, Edwin Bidwell: Theory of an Aeroplane Encountering Gusts.
   I. T. R. No. 1—Part 2, N. A. C. A. First Annual Report, 1915, pp. 52–75.
   II. T. R. No. 21, N. A. C. A. Third Annual Report, 1917, pp. 405–431.
   III. T. R. No. 27, N. A. C. A. Fourth Annual Report, 1918, pp. 83–89.
2. Haus, Fr.: Theoretical Study of Various Airplane Motions after Initial Disturbance. T. M. No. 867, N. A. C. A., 1938.
3. Jones, Robert T.: Calculation of the Motion of an Airplane under the Influence of Irregular Disturbances. Jour. Aero. Sci., vol. 3, no. 12, Oct. 1936, pp. 419–425.
4. Jones, Robert T.: A Study of the Two-Control Operation of an Airplane. T. R. No. 579, N. A. C. A., 1936.
5. Zimmerman, Charles H.: An Analysis of Lateral Stability in Power-Off Flight with Charts for Use in Design. T. R. No. 589, N. A. C. A., 1937.
6. Diehl, Walter Stuart: Engineering Aerodynamics. The Ronald Press Co., 1936, p. 206.
7. Millikan, Clark B.: On the Results of Aerodynamic Research and Their Application to Aircraft Construction. Jour. Aero. Sci., vol. 4, no. 2, Dec. 1936, pp. 43–53.
8. Korvin-Kroukovsky, B. V.: Proportioning the Plane for Lateral Stability. Aero. Eng. Supplement to Aviation, vol. 26, Jan. 1929, pp. VIII–XII.
9. Imlay, Frederick H.: The Estimation of the Rate of Change of Yawing Moment with Sideslip. T. N. No. 636, N. A. C. A., 1938.
10. Jones, Robert T., and Nerken, Albert I.: The Reduction of Aileron Operating Force by Differential Linkage. T. N. No. 586, N. A. C. A., 1936.

TECHNICAL NOTE 667

OPERATIONAL TREATMENT OF THE NONUNIFORM-LIFT THEORY IN AIRPLANE DYNAMICS

Robert T. Jones

Langley Memorial Aeronautical Laboratory

October 1938

NATIONAL ADVISORY COMMITTEE FOR AERONAUTICS

TECHNICAL NOTE NO. 667

OPERATIONAL TREATMENT OF THE NONUNIFORM-LIFT THEORY IN AIRPLANE DYNAMICS

By Robert T. Jones

SUMMARY

The method of operators is used in the application of nonuniform-lift theory to problems of airplane dynamics. The method is adapted to the determination of the lift under prescribed conditions of motion or to the determination of the motions with prescribed disturbing forces.

INTRODUCTION

Problems in airplane dynamics are usually treated on the assumption that the air forces are instantly adjusted to each motion of the airplane. Since the development of recent theories for the nonuniform motion of airfoils, it has become possible to consider more exact laws for the adjustment of the lift.

The nonuniform-lift theory has already been applied to certain dynamical problems, notably to the problem of flutter. These applications have, however, been confined either to approximate solutions or to cases in which the type of motion is prescribed beforehand. The more usual problem, in which the resulting motion is unknown, requires the solution of integral equations. The present paper shows how solutions of these equations may be obtained fairly simply by operational methods.

SUPERPOSITION OF LIFTS

In nearly every aerodynamic problem, the approximations that must be made to effect solutions are such as to lead to linear relations. Thus, in the case of the unsteady lift of a wing, Laplace's equation combined with the assumption of

an undistorted wake leads to a linear relation between the lift and the angle of attack. Such a relation means that the lift due to the sum of two variable motions is equal to the sum of the lifts for the two motions taken independently.

In particular, if the lift following a sudden unit jump of angle of attack is known (see reference 1), then the lift for any variable motion is easily obtained by breaking the given motion down into a succession of small jumps or steps and adding the lifts incident to each one. The case treated by Wagner thus becomes the key to the calculation of lift for any variable motion.

Wagner's function (reference 1) giving the lift after a sudden unit jump of angle of attack (two-dimensional case) may be denoted by $c_{l_1}(s)$. The superposition of lifts for any variable motion $\alpha(s)$, as previously explained, is accomplished by the integration of Duhamel's integral

$$\int_0^s c_{l_1}(s - s_0)\, \alpha'(s_0)\, ds_0 \qquad (1)$$

(See reference 2.)

OPERATIONAL SOLUTION OF INTEGRAL EQUATIONS

It is evident that, in order to take account of unsteady air-flow phenomena in the theory of airplane dynamics (including stability and related problems) the customary instantaneous equations of motion must be replaced by equations involving the integral (1). The equations of motion then become linear integral equations. Solutions of these equations may be conveniently obtained by operational methods.

Let D represent the operator d/ds and let $1 = 1(s)$ represent the unit jump function, that is, a function of s having the value 1 at $s > 0$ and having the value 0 at $s < 0$. Then a function of s may be represented by a combination of operations on the unit jump function

$$\phi(s) = \overline{\phi}(D)1 \qquad (2)$$

The combination of operations $\overline{\phi}(D)$ on 1 necessary to reproduce the function $\phi(s)$ is called the "operational equivalent" of the function $\phi(s)$. The operational equivalent $\overline{\phi}$ of a given function ϕ may be found by the infinite-integral theorem (reference 2)

$$\overline{\phi}(a) = a \int_0^\infty \phi(x)\, e^{-ax}\, dx \tag{3}$$

A general operational equivalent is

$$s^n = \Gamma\,(1 + n)\, D^{-n}\, 1(s) \tag{4}$$

(See Peirce's table, p. 63, no. 493.)

The operational treatment of integral equations is based on the proposition that an integral of the form

$$\phi(s) = Z(s)\, X(0) + \int_0^s Z(s - s_o)\, X'(s_o)\, ds_o \tag{5}$$

may be regarded as the solution of a linear differential equation. As such, its operational equivalent is

$$\phi(s) = \overline{Z}(D)\, X(s) = \overline{Z}(D)\, \overline{X}(D)\, 1(s) \tag{6}$$

where $\overline{Z}$ and $\overline{X}$ are the operational equivalents of the functions Z and X.

In order to illustrate the operational solution, let it be required to find the function $X(s)$ from

$$\int_0^s \frac{X'(s_o)}{\sqrt{s - s_o}}\, ds_o - 2X(s) = \frac{4}{3}s^{3/2} - s^2 \tag{7}$$

assuming that $X(0) = 0$. Here the function corresponding to $Z(s)$ in equation (5) is $1/\sqrt{s}$. With the aid of equation (4), the various components are written in operational form

$$Z(s) = \Gamma(1/2)\ \sqrt{D}\ 1(s) \tag{8}$$

$$-4/3s^{3/2} + s^2 = -\left(\frac{\Gamma(1/2)}{D\sqrt{D}} - \frac{2}{D^2}\right) 1(s) \tag{9}$$

Equation (6) becomes

$$\Gamma(1/2)\ \sqrt{D}\ X(s) - 2X(s) = \left(\frac{\Gamma(1/2)}{D\sqrt{D}} - \frac{2}{D^2}\right) 1(s)$$

or

$$X(s) = \frac{\dfrac{\Gamma(1/2)}{D\sqrt{D}} - \dfrac{2}{D^2}}{\Gamma(1/2)\ \sqrt{D} - 2}\ 1(s)$$

Simplifying:

$$X(s) = \frac{1}{D^2}\,\frac{\Gamma(1/2) - \dfrac{2}{\sqrt{D}}}{\Gamma(1/2) - \dfrac{2}{\sqrt{D}}}\ 1 = \frac{1}{D^2}\ 1 = \frac{1}{2}\ s^2 \tag{10}$$

It will be helpful to review certain aspects of the theory of unsteady lift before proceeding to the application of this theory in airplane dynamics. It is found convenient to think of the lift on the airfoil as composed of three parts: (1) A part due to instantaneous acceleration of the noncirculatory potential flow. This lift is equal to the virtual additional mass of the wing ($\pi \frac{c^2}{4} \rho$ per unit span, for infinite aspect ratio) times the rate of increase of the relative wind velocity normal to the chord. (2) A part due to the circulatory flow and dependent on the angle-of-attack variation, i.e., the lift given by $c_{l_1}(s)$. (3) A part due to the circulatory

flow and ascribed to a relative curvature or camber of the airfoil in pitching motion. The third component will be automatically included with the second if the angle of attack is obtained by resolving velocities at the 75-per-cent-chord point.

With these provisions, the instantaneous lift of an airfoil in combined pitching and vertical motion may be written (see fig. 1)

$$c_l(s) = \mu[\alpha'(s) + l_{50}\,\theta''(s)]$$

$$+ [\alpha(0) + l_{75}\theta'(0)]c_{l_1}(s) + \int_0^s c_{l_1}(s - s_o)[\alpha'(s_o) + l_{75}\theta''(s_o)]ds_o \tag{11}$$

where μ is a coefficient for the virtual additional mass of the wing ($\mu = \pi$ for infinite aspect ratio). Now let $\overline{c}_{l_1}$ be the operational equivalent of Wagner's function c_{l_1}:

$$c_l(s) = \mu[D\alpha + l_{50}D^2\theta] + \overline{c}_{l_1}(D)[\alpha + l_{75}D\theta] \tag{12}$$

No concise formula for $c_{l_1}(s)$ is known although it is found that Wagner's curve is[1] reproduced almost exactly by the equation

$$c_{l_1}(s) = C_o + C_1e^{\lambda_1 s} + C_2e^{\lambda_2 s} \tag{13}$$

where

$$C_o = 2\pi$$

$$C_1 = -0.330\,\pi$$

$$C_2 = -0.670\,\pi$$

$$\lambda_1 = -0.0455$$

$$\lambda_2 = -0.300$$

and where s refers to the half-chord as unit, that is

$$s = \frac{Vt}{c/2}$$

In this form, the operational equivalent is readily found from the relation

$$e^{\lambda s} = \frac{D}{D - \lambda} 1(s) \qquad \text{(See reference 2)} \qquad (14)$$

whence

$$\overline{c}_{l_1}(D) = C_o + C_1 \frac{D}{D - \lambda_1} + C_2 \frac{D}{D - \lambda_2} \qquad (15)$$

The calculation of lift under a prescribed variation of angle of attack can be illustrated by assuming that the airfoil is given a sinusoidal motion

$$\alpha(s) \text{ (or } \theta(s)) = \text{R.P. or I.P. of } e^{ins} \qquad (16)$$

This variation is reduced to operational form (see equation (14)):

$$\overline{\alpha}(D) = \frac{D}{D - in} \qquad (17)$$

$$c_{l_n}(s) = \mu D \frac{D}{D - in} 1 + \left(C_o + C_1 \frac{D}{D-\lambda_1} + C_2 \frac{D}{D-\lambda_2}\right) \frac{D}{D-in} 1 \qquad (18)$$

(See equations (12) and (15).)

The resulting operator may be evaluated by the Heaviside expansion theorem:

$$\frac{f(D)}{F(D)} 1 = \frac{f(0)}{F(0)} + \sum_{\lambda} \frac{f(\lambda)}{\lambda F'(\lambda)} e^{\lambda s} \qquad (19)$$

where the λ's are the roots of $F(D) = 0$.

$$c\zeta_n(s) = \mu\, ine^{ins} + \left[C_o + C_1 \frac{in}{in - \lambda_1} + C_2 \frac{in}{in - \lambda_2}\right] e^{ins}$$

$$+ C_1 \frac{\lambda_1}{\lambda_1 - in} e^{\lambda_1 s} + C_2 \frac{\lambda_2}{\lambda_2 - in} e^{\lambda_2 s} \quad (20)$$

The terms involving $e^{\lambda s}$ disappear in time and hence may be disregarded in a continuous oscillation. The terms

$$\left[C_o + \frac{in}{in - \lambda_1} C_1 + \frac{in}{in - \lambda_2} C_2\right] e^{ins} = 2\pi[F + iG]\, e^{ins} \quad (21)$$

yield approximate expressions of the lift functions for the oscillating airfoil introduced by Theodorsen (reference 3):

$$2\pi F(n) = C_o + C_1 \frac{n^2}{\lambda_1^2 + n^2} + C_2 \frac{n^2}{\lambda_2^2 + n^2}$$

$$2\pi G(n) = - C_1 \frac{\lambda_1 n}{\lambda_1^2 + n^2} - C_2 \frac{\lambda_2 n}{\lambda_2^2 + n^2} \quad (22)$$

As pointed out by Garrick (reference 4), Theodorsen's function for sinusoidal motion

$$C(in) = F(n) + iG(n) \qquad \text{(equation (21))}$$

may be regarded as the operational equivalent of Wagner's curve, i.e.,

$$2\pi C(D)1 = \overline{c}_\zeta(D)\ 1 = c\zeta_1(s) \quad (23)$$

This fact may be verified by referring to equation (15). This relation is especially interesting because it shows a connection between the Fourier and the operational analyses.

Thus, if the response of a linear system to a continuous sinusoidal excitation is known,

$$R_n(s) = f(in)\, e^{ins} \tag{24}$$

Then the function f furnishes immediately the operational equivalent of the unit response so that for any variable excitation $Z(s)$,

$$R(s) = f(D)\, Z(s) = f(D)\, \overline{Z}(D)\, 1 \tag{25}$$

In general, the motion of the airfoil or airplane will not be prescribed beforehand but must be determined from dynamical equations. This type of problem can be illustrated simply by considering the disturbed vertical motion of the airplane without pitching. The dynamical equation in this case is

$$m \frac{dw}{dt} - \text{resisting force} = \text{impressed force, } Z \tag{26}$$

where w is the vertical velocity of the airplane and m is the mass including the virtual additional mass of the wing. Since

$$\frac{dw}{dt} = \frac{V^2}{c/2} \frac{d\alpha}{ds} \tag{27}$$

$$m \frac{dw}{dt} = \frac{2m}{S\ \rho/2\ c} \times S\ \rho/2\ c/2 \times \frac{V^2}{c/2} \frac{d\alpha}{ds} \tag{28}$$

Making the substitution

$$\frac{2m}{S\ \rho/2\ c} = \sigma \tag{29}$$

and writing the equation in coefficient form,

$$\sigma D\alpha + \overline{c}_{l_1}(D)\, \alpha = c_{l_o}(s) \tag{30}$$

where c_{l_o} is the lift coefficient of the given disturbing force. The operational solution is

$$\alpha(s) = \frac{1}{\sigma D + \overline{c}_{l_1}(D)} c_{l_o}(s) \tag{31}$$

Again, as in the case of the lift, the solution for the elementary jump is the key to solutions for variable conditions.

$$\alpha_1(s) = \frac{1}{\sigma D + \overline{c}_{l_1}(D)} 1 \tag{32}$$

Replacing $\overline{c}_{l_1}(D)$ by (15) and simplifying:

$$\alpha_1(s) = \frac{(D - \lambda_1)(D - \lambda_2)}{aD^3 + bD^2 + cD + d} 1 = \frac{f(D)}{F(D)} 1 \tag{33}$$

which is in standard form for evaluation by the expansion theorem (19). Finally,

$$\alpha(s) = c_{l_o}(o)\, \alpha_1(s) + \int_o^s \alpha_1(s - s_o)\, c_{l_o}'(s_o)\, ds_o \tag{34}$$

The extension of this treatment to problems involving the number of degrees of freedom will be evident.

Langley Memorial Aeronautical Laboratory,
National Advisory Committee for Aeronautics,
Langley Field, Va., September 12, 1938.

REFERENCES

1. Wagner, Herbert: Über die Entstehung des dynamischen Auftriebes von Tragflügeln. Z.f.a.M.M., Bd. 5, Heft 1, Feb. 1925, S. 17-35.

2. Carson, J. R.: Electric Circuit Theory and Operational Calculus. McGraw-Hill Book Co., Inc., 1926.

3. Theodorsen, Theodore: General Theory of Aerodynamic Instability and the Mechanism of Flutter. T.R. No. 496, N.A.C.A., 1934.

4. Garrick, I. E.: On Some Reciprocal Relations in the Theory of Nonstationary Flows. T.R. No. 629, N.A.C.A., 1938.

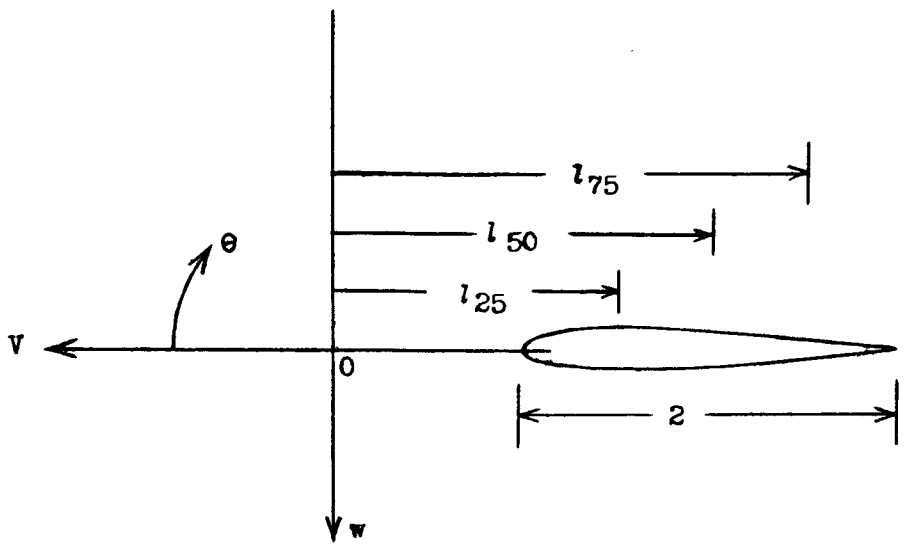

Figure 1.- Moving axes. $\alpha = w/V$; $s = Vt/c/2$.

REPORT NO. 681

THE UNSTEADY LIFT OF A WING OF FINITE ASPECT RATIO

Robert T. Jones

Langley Memorial Aeronautical Laboratory

1940

E R R A T A

NATIONAL ADVISORY COMMITTEE FOR AERONAUTICS

TECHNICAL REPORT NO. 681

THE UNSTEADY LIFT OF A WING OF FINITE ASPECT RATIO

By Robert T. Jones

Page 3, equation (10):
Last term should read: $-\frac{1}{x}$

Page 4, equation (13):
Second integral sign should read: $\int_0^{\pi/2}$

$\left(k\ \frac{1}{k}\right)$ should read: $\left(k - \frac{1}{k}\right)$

Page 4, equation (14):
Second line should read: $+\frac{1}{k}E(k) - 1\Big]\Big\}$

Page 8, equation (49) should read:

$$\mu D\alpha + \overline{C}_{L_\alpha}(D)\alpha = \overline{C}_{L_g}(D)\alpha g$$

REPORT No. 681

THE UNSTEADY LIFT OF A WING OF FINITE ASPECT RATIO

By Robert T. Jones

SUMMARY

Unsteady-lift functions for wings of finite aspect ratio have been calculated by correcting the aerodynamic inertia and the angle of attack of the infinite wing. The calculations are based on the operational method.

The starting lift of the finite wing is found to be only slightly less than that of the infinite wing; whereas the final lift may be considerably less. The theory indicates that the initial distribution of lift is similar to the final distribution.

Curves showing the variation of lift after a sudden unit change in angle of attack, during penetration of a sharp-edge gust, and during a continuous oscillation are given. Operational equivalents of these functions have been devised to facilitate the calculation of lift under various conditions of motion. As an application of these formulas, the vertical acceleration of a loaded wing caused by penetrating a gust has been calculated.

INTRODUCTION

The two-dimensional potential theory of airfoils in nonuniform motion was given by Wagner (reference 1) and has been extended to problems involving the motion of hinged or flexible airfoils by Theodorsen (reference 2) and Küssner (reference 3).

In the case of steady motion, a correction is known to be necessary before the results of the two-dimensional theory can be applied to wings of finite aspect ratio. A theory for the unsteady lift of finite wings was developed in reference 4. This theory has since been somewhat improved mathematically by making use of operational methods in the solution of the integral equations. (See reference 5.) The present report combines this previous work and extends the theory to show the effects of gusts.

THE INDICIAL LIFT

INFLUENCE OF THE WAKE

Owing to the presence of circulation, the lifting wing leaves in its path a surface of discontinuity, the local vortex strength of which is determined by the rate of change of circulation taken both across the span and along the flight path. (See fig. 1.) The distribution of vorticity in the wake is determined by the assumption that the flow field at each instant conforms to the Kutta condition. An essential feature of the problem is the determination of the influence of this wake on the flow at the wing.

It is important to note that the wake is supposed to remain plane and undistorted. As a consequence of this assumption, the effects of different wakes are additive, permitting the various flows to be built up by superposition. Thus, if the solution for the growth of the increment of lift following a sudden change of normal velocity—or, what amounts to the same thing under the assumptions involved, a sudden change in the angle of attack—is known, this solution may be used as the element in an integral that gives the lift in any variable motion. With this point in mind, attention will at first be directed to the special case in which the wing starts suddenly from rest at $t=0$ with the

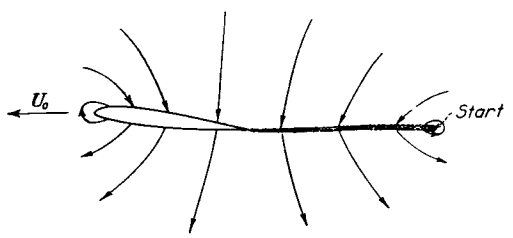

FIGURE 1.—Flow caused by wing starting from rest.

normal velocity w and the flight velocity U_0, the velocities remaining constant thereafter.

LIFT NEAR THE START

The starting lift of any wing may be expressed by a simple theorem based directly on the Kutta condition. As a consequence of this condition, the portion of the wake adjacent to the trailing edge must move as an impermeable extension of the wing surface. Thus, the first element of wake formed must move with the same normal velocity as the wing. The flow produced at the first instant is what might be caused by the wing in process of growing wider at the rate U_0 while moving downward with the velocity w. The starting lift may then be thought of as the reaction to uniform motion of the wing as a body with increasing mass:

$$L=w\frac{dm'}{dt} \tag{1}$$

where m' is the mass representing the aerodynamic inertia of the wing in normal motion.

In order to apply equation (1) to the finite wing, the inertia factor for such a wing must be known as a function of the width. Solutions for elliptic plates are given by the classical hydrodynamic theory, and these solutions can be used to represent approximately the initial rates of increase of inertia of wings of oval or elliptic plan form.

The distribution of potential over each chordwise section of an elliptic plate in normal motion has the same form as the corresponding two-dimensional potential. Thus

$$\phi=\frac{w}{E}\sqrt{1-x^2} \tag{2}$$

where E is the elliptic integral giving the ratio of the semiperimeter to the span. At the normal velocity $w=E$, the potential distribution over any chord is represented by a circle having the chord as diameter. (See fig. 2.) If the edge of the plate distorts into a slightly wider ellipse, the change in potential arising at any point will be measured by the difference between the original and the slightly expanded circles. (The change in the factor E during widening may be neglected for ordinary aspect ratios.) The pressure difference across the plate with changing potential is given by the formula

$$p=-2\rho\left(U_0\frac{\partial\phi}{\partial x}+\frac{\partial\phi}{\partial t}\right) \tag{3}$$

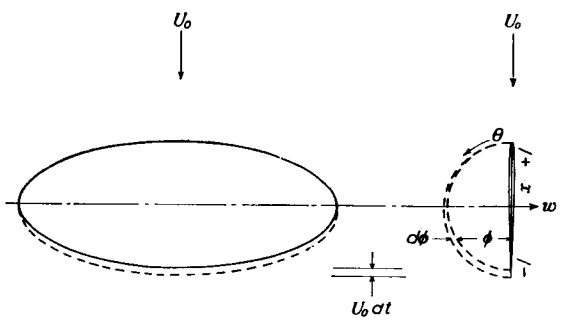

FIGURE 2.—The wake and the distribution of potential over the chord shortly after the start.

For $w=E$

$$\phi=\sqrt{1-x^2}=\sin\theta \tag{4}$$
$$\frac{\partial\phi}{\partial x}=\frac{-x}{\sqrt{1-x^2}}=-\cot\theta$$

and, from the geometry of the circle,

$$\left.\frac{\partial\phi}{\partial t}\right|_{t=0}=\frac{\partial\phi}{\partial\Delta c}\left.\frac{d\Delta c}{dt}\right|_{t=0}=U_0\left.\frac{\partial\phi}{\partial\Delta c}\right|_{\Delta c=0}=U_0\frac{1}{2}\cot\frac{\theta}{2} \tag{5}$$

The pressure across the plate with the normal velocity $w=E$ and the flight velocity U_0 is, therefore,

$$p_{t=0}=\rho U_0\left(2\cot\theta-\cot\frac{\theta}{2}\right) \tag{6}$$

Integration of this pressure over any section gives the lift coefficient for angle of attack α of the plate,

$$C_{L_{t=0}}=\frac{\pi}{E}\frac{w}{U_0}=\frac{\pi}{E}\alpha \tag{7}$$

with each local center of pressure at the quarter-chord point.

The start of the plane elliptic wing being equivalent to a uniform lengthening of each chord, the true elliptic outline is not preserved. Such a change, however, may be shown to conform very nearly to a change into another, slightly larger, ellipse at all points except those very near the tips. Furthermore, if the wing is assumed to distort in any of a number of ways into a slightly different elliptical plan form, the change of aerodynamic inertia will be found to be but little affected by the change in shape and to depend primarily on the over-all change in size. Each such distortion can be thought of as representing a certain distribution of the starting velocity U around the edge of the wing. Equation (5) is exact for all distortions of this class. Inasmuch as they may be made to fall on either side of the distortion represented by U=constant (representing the start of the rigid wing), the equation is also considered applicable to this case.

THE DOWNWASH CORRECTION

A reasonably accurate curve of the growth of lift might now be drawn by connecting the starting value

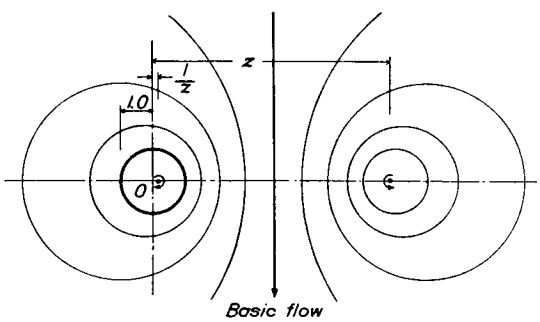

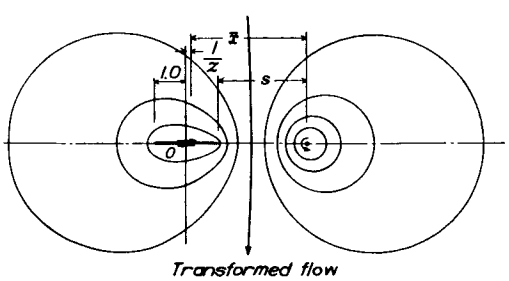

FIGURE 3.—Element of circulatory flow.

(equation (7)) asymptotically to the known steady value given by the Prandtl theory. Calculations have

shown, however, that, after the wing has progressed a distance of the order of one semispan, the effect of finite width of the wake can be treated simply as a modification of the angle of attack of the entire wing, as in the steady-lift theory. A closer approach to the true form of the curve may be obtained by proceeding on this basis.

Before the three-dimensional problem is considered, it will be helpful to review certain aspects of the two-dimensional theory (reference 1). In order to make the analysis nondimensional, all velocities are expressed in terms of the flight velocity U_0 and all lengths, in terms of the half chord.

Figure 3 shows the elementary two-dimensional flow used as a starting point by Wagner (reference 1). This flow is caused by two vortices, representing, respectively, an element of circulation around the wing and the vortex left in the wake when this circulation originated. The streamlines of this flow are eccentric circles. One such circle (of unit radius) is chosen to represent the wing section and the axes are so placed that this circle has its center at the origin. The geometry of the resulting pattern is such that, when the wake vortex is at z, the wing vortex will be at $1/z$. This spacing preserves the unit circle as a streamline of the flow.

Transformation of the pattern by the formula

$$2\zeta = z + \frac{1}{z} \tag{8}$$

flattens the unit circle into a thin-line wing section and distorts the originally circular streamlines into oval Joukowski figures. The transformed pattern thus represents the circulatory flow around a flat wing section with an associated countervortex in the wake. In the transformation, the centroid of wing vorticity remains at the position of the original bound vortex while the wake vortex is shifted forward somewhat as shown (fig. 3).

Each elementary flow of the type shown contributes a certain velocity around the trailing edge of the airfoil. The flow due to an instantaneous change of angle of attack of the airfoil may be superposed on these flows and will contribute a trailing-edge velocity of opposite sense. On this basis, the problem of circulation with varying angle of attack may be solved by an inverse procedure. Assume some convenient distribution of wake vorticity and calculate (by integration) the trailing-edge velocity at each point along the flight path corresponding to the prescribed wake. The particular variation of angle of attack necessary to cancel this trailing-edge flow at each instant (Kutta condition) can then be determined. If a number of such curves are found, they may be added in various ratios so as to approximate some prescribed variation of angle of attack; the corresponding circulation curves are added in like ratios.

In essentially the manner described, Wagner (reference 1) calculated the two-dimensional flow around a wing section following a sudden unit change in angle of attack. The integrated pressures over the airfoil give a lift coefficient that asymptotically approaches the known steady value 2π; whereas the starting lift coefficient is found to be exactly one-half this value. The center of pressure remains at the quarter-chord point throughout the motion.

In the case of the finite wing, an element of the wake will be as depicted in figure 3 but will, in addition, contain vortices completing each circuit to the wing through the tips. The length of the tip vortices may be approximated by assuming that they extend to the chordwise centroid of the wing circulation. After some

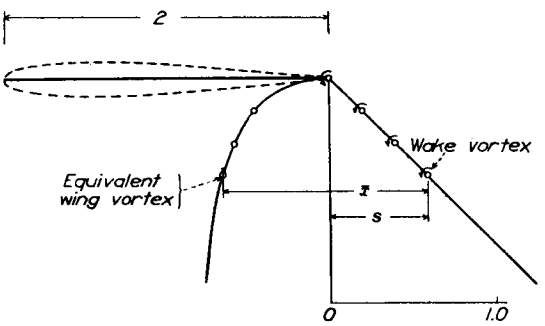

FIGURE 4.—Position of the centroid of discontinuity in the wing for different positions of the wake vortex.

calculation, the equivalent length $\bar{x}$ of the tip vortices in terms of the distance traveled s reduces to

$$\bar{x} = \sqrt{s(s+2)} \tag{9}$$

Figure 4 illustrates the rapid travel of the centroid of discontinuity within the wing subsequent to its initial position at the trailing edge.[1] It is seen that, after a travel of several chord lengths, the centroid may be taken at the middle of the wing section. This assumption will later be used.

Figure 5 shows how an elementary loop vortex in the wake of a finite wing can be formed by cancelation from an element of the wake of an infinite wing. The downwash induced by segments CD and FH accounts for the aspect-ratio effect. Since a uniform distribution of the downwash flow is assumed, the calculations will be restricted to the center of the wing. By the application of Biot-Savart's rule, the downwash velocity due to elements CD and FH is found to be

$$\frac{1}{2\pi}\left[\left(\frac{x}{y}+\frac{y}{x}\right)\frac{1}{\sqrt{x^2+y^2}}-\frac{1}{x}\right] \tag{10}$$

This expression for downwash may be integrated in

[1] At $s=0$, the tip vortices are lengthening at an infinite rate and, although the vortex strength is zero at the beginning of the motion, the limiting calculation shows that the induced downwash flow has a certain rate of acceleration at this instant. As a result, the starting lift of the finite wing is diminished, in accordance with the result of the previous calculation.

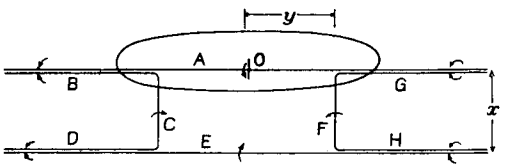

FIGURE 5.—Superposition of vortices to obtain finite loop.

the case of elliptic spanwise loading. Let γ represent the circulation around any chordwise section; then

$$\gamma=\Gamma \sin\theta \tag{11}$$

where $y=\frac{b}{2}\cos\theta$, and Γ is the value of γ at the center section.

$$y^2+x^2=\left(\frac{b}{2}\right)^2\left[1+\left(\frac{x}{b/2}\right)^2\right](1-k^2\sin^2\theta) \tag{12}$$

where $k^2=\dfrac{1}{1+\left(\dfrac{x}{b/2}\right)^2}$

Then the induced velocity due to a series of finite loops of the form CEF (fig. 5) is given by

$$\frac{\Gamma}{\pi b}\int_0^{\pi/2}\left(\frac{x}{\frac{b}{2}\sqrt{1+\left(\frac{x}{b/2}\right)^2}}+\frac{b/2\cos^2\theta}{x\sqrt{1+\left(\frac{x}{b/2}\right)^2}}\right)\frac{d\theta}{\sqrt{1-k^2\sin^2\theta}}$$

$$=\frac{\Gamma}{\pi b}\frac{1}{\sqrt{1+\left(\frac{x}{b/2}\right)^2}}\int_0^{\pi/2}\left(\frac{x}{b/2}+\frac{b/2}{x}\cos^2\theta\right)\frac{d\theta}{\sqrt{1-k^2\sin^2\theta}}$$

$$=\frac{\Gamma}{\pi b}\left\{\frac{x}{b/2}kK(k)+\frac{b/2}{x}\left[K(k)\left(k\frac{1}{k}\right)+\frac{E(k)}{k}\right]\right\} \tag{13}$$

where $K(k)$ and $E(k)$ are the complete elliptic integrals. (See Peirce's table.)

Subtracting the two-dimensional vortex E gives the effect of a series of segments of the form of DC and FH, distributed along the span according to the elliptic loading.

$$\frac{dw}{d\Gamma}=w_\Gamma=\frac{1}{\pi b}\left\{\frac{x}{b/2}kK(k)+\frac{b/2}{x}\left[\left(k+\frac{1}{k}\right)K(k)+\frac{1}{k}E(k)=1\right]\right\} \tag{14}$$

Figure 6 shows the variation of downwash velocity with increasing length of the wake as determined by this formula. Some additional rough calculations have shown that the downwash becomes practically uniform over the entire wing before the wake has attained a length of one semispan.

Figure 7 shows downwash curves derived from equation (14) for elliptic wings of aspect ratios A of 3 and 6. In this derivation, the unit of length was taken as half the central chord of the wing. Thus, the wings have the same chords ($c_{max}=2$) but are of different spans. In order to define the later portions of the curve, the wake was assumed to start with length equal to the mean chord b/A in each case. This assumption, though somewhat arbitrary, makes allowance for the curvature of the trailing edges of the wings.

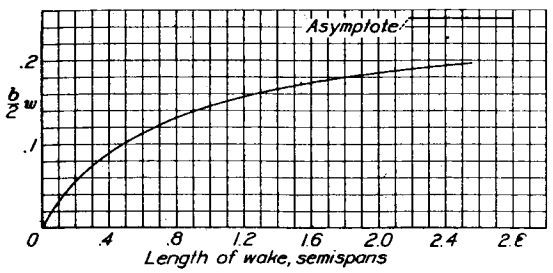

FIGURE 6.—Growth of downwash with increasing length of the wake. $\Gamma_0=1.0$; elliptical span load.

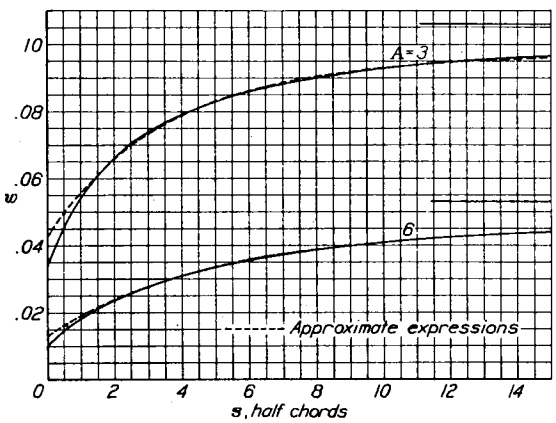

FIGURE 7.—Downwash functions, $w_\Gamma(s)$.

The induced downwash w_i with any variation of circulation $\Gamma(s)$ along the flight path may be determined from the curves given in figure 7 by superposition; thus

$$w_{iw}(s)=w_\Gamma(s)\Gamma_w(0)+\int_0^s w_\Gamma(s-s_0)\Gamma_w'(s_0)ds_0 \tag{15}$$

The growth of circulation following a sudden start of the motion will be determined from the two-dimensional theory by using the effective normal velocity

$$w_e=w-w_i=1-w_i \tag{16}$$

Let Γ_{0w} be the rise of circulation following a sudden start with unit normal velocity as given by the two-dimensional theory. Then, for the finite wing,

$$\Gamma_w(s)=\Gamma_{0w}(s)-\Gamma_{0w}(s)w_i(0)-\int_0^s\Gamma_{0w}(s-s_0)w_i'(s_0)ds_0 \tag{17}$$

The determination of the effective normal velocity and the circulation for the finite wing thus depends on the simultaneous solution of integral equations (15) and (17). This solution may be conveniently obtained by operational methods.

OPERATIONAL SOLUTION OF INTEGRAL EQUATIONS

Let D represent the operator d/ds and let $1=1(s)$ represent the unit jump function, that is, a function of s having the value zero at $s<0$ and having the value 1 at $s>0$. A function of s may be represented by a combination of operations on the unit jump function

$$\Phi(s)=\bar{\Phi}(D)1 \tag{18}$$

The combination of operations $\bar{\Phi}(D)$ necessary to reproduce the function $\Phi(s)$ is called the operational equivalent of the function $\Phi(s)$.

Rules for finding such equivalents are discussed in reference 6. The most general rule for proceeding either from $\bar{\Phi}$ to Φ, or vice versa, is:

$$\bar{\Phi}(a)=a\int_0^\infty \Phi(z)e^{-az}dz$$

$$\Phi(a)=\frac{1}{2\pi i}\int_{-\infty i}^{\infty i}\frac{\bar{\Phi}(z)}{z}e^{az}dz$$

The rule needed in the following development is the Heaviside expansion theorem:

$$\Phi(s)=\bar{\Phi}(D)1=\frac{f(D)}{F(D)}1=\frac{f(0)}{F(0)}+\sum_{\lambda}\frac{f(\lambda)}{\lambda F'(\lambda)}e^{\lambda s} \tag{19}$$

where f and F are algebraic polynomials and the λ's are the roots of $F(\lambda)=0$.

The operational treatment of integral equations is based on the proposition that an integral of the form of (15) may be regarded as the linear superposition of the effects of a succession of small jump functions. The operational form of (15) is

$$\bar{w}_{tw}(D)=\bar{w}_\Gamma(D)\bar{\Gamma}_w(D) \tag{20}$$

and that of (17)

$$\bar{\Gamma}_w(D)=\bar{\Gamma}_{0w}(D)[1-\bar{w}_{tw}(D)] \tag{21}$$

Solving algebraically for $\bar{w}_{tw}(D)$:

$$\bar{w}_{tw}(D)=\frac{\bar{w}_\Gamma(D)\bar{\Gamma}_{0w}(D)}{1+\bar{w}_\Gamma(D)\bar{\Gamma}_{0w}(D)} \tag{22}$$

The induced velocity $w_{tw}(s)$ gives the variation of the effective angle of attack of the finite wing when the geometric angle of attack is held constant. The lift at later stages of the motion is then found by combining the effective angle-of-attack variation

$$w_{ew}(s)=1-w_{tw}(s) \tag{23}$$

with the two-dimensional indicial-lift function given by Wagner. Let $C_{L_{0w}}(s)=C_{L_{0\alpha}}(s)$ be the lift in two-dimensional flow following a sudden unit jump of angle (the curve given by Wagner is for $\alpha=1/2\pi$); then, for the finite wing:

$$C_{L_\alpha}(s)=C_{L_{0\alpha}}(s)-C_{L_{0\alpha}}(s)w_{tw}(0)-\int_0^s C_{L_{0\alpha}}(s-s_0)w_{tw}'(s_0)ds_0 \tag{24}$$

or, in operational form:

$$\bar{C}_{L_\alpha}(D)=\bar{C}_{L_{0\alpha}}(D)-\bar{C}_{L_{0\alpha}}(D)\bar{w}_{tw}(D) \tag{25}$$

Substitution of the expression for $\bar{w}_{tw}(D)$ from equation (22) gives the operational form of the lift function for the finite wing in terms of the known functions

$$w_1(s),\ \Gamma_{0w}(s),\text{ and } C_{L_{0\alpha}}(s)$$

Because no concise expressions of the required functions are known, approximate formulas must be devised. The function $e^{\lambda s}$ has a simple operational equivalent, namely,

$$e^{\lambda s}=\frac{D}{D-\lambda}1 \tag{26}$$

and, since the curves to be fitted are asymptotic in character, series of such functions were chosen as follows:

$$\left.\begin{aligned}\Gamma_{0w}(s)&=5.75-3.75e^{-0.239s}-1.50e^{-1.970s}\\ C_{L_{0\alpha}}(s)&=2\pi-0.330\pi e^{-0.045s}-0.670\pi e^{-0.300s}\\ w_\Gamma(s)_{A=3}&=0.096-0.053e^{-0.281s}\\ w_\Gamma(s)_{A=6}&=0.045-0.032e^{-0.203s}\end{aligned}\right\} \tag{27}$$

Figures 7 and 8 show the degree of exactness attained with these expressions. It was considered not important to fit the curves accurately near the origin.

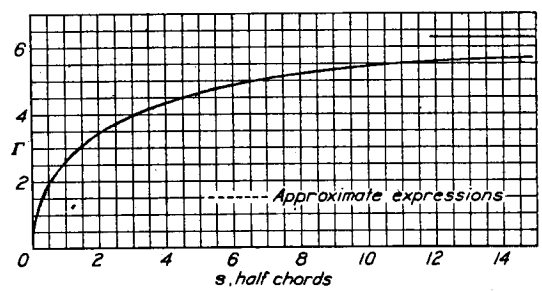

FIGURE 8.—Growth of circulation in two-dimensional flow, $\Gamma_{0w}(s)$.

The operational equivalents $\bar{\Gamma}_{0w}(D)$, $\bar{w}_{tw}(D)$, etc., are easily written down from (26). The substitution of these equivalents into equations (22) and (25) and the evaluation of the resulting operators by the Heaviside expansion theorem are quite lengthy and will not be reproduced. The resulting expressions for $C_{L_\alpha}(s)$ were found to be

$$\left.\begin{aligned}C_{L_{\alpha_{A=3}}}&=\pi[1.288-0.190e^{-0.045s}+0.055e^{-0.300s}\\ &\quad+0.043e^{-2.071s}+0.915e^{-0.293s}\cos 0.095(s-19.135)]\\ C_{L_{\alpha_{A=6}}}&=\pi[1.589-0.242e^{-0.045s}-0.403e^{-0.300s}\\ &\quad+0.008e^{-1.998s}+0.872e^{-0.234s}\cos 0.0724(s-21.117)]\end{aligned}\right\} \tag{28}$$

Because the curves given by these formulas are considered invalid near the start of the motion, new curves having the correct starting values given by equation (7) were drawn in as shown (fig. 9). These final curves have the useful approximate expressions:

$$\left.\begin{aligned}C_{L_{\alpha_{A=3}}}(s)&=1.200\pi(1.000-0.283e^{-0.540s})\\ C_{L_{\alpha_{A=6}}}(s)&=1.48\pi(1.000-0.361e^{-0.381s})\end{aligned}\right\} \tag{29}$$

An analogous expression for infinite aspect ratio is

$$C_{L_{0\alpha}}(s)=2\pi(1.000-0.165e^{-0.045s}-0.335e^{-0.300s}) \quad (30)$$

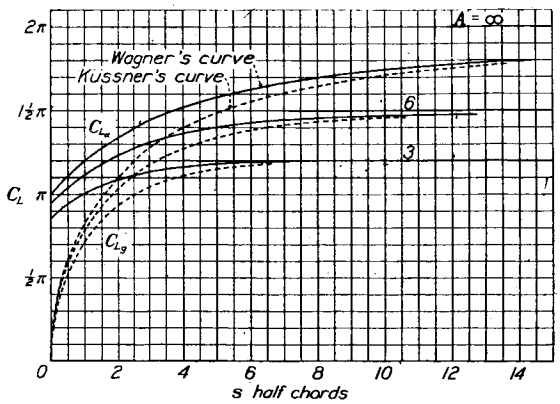

FIGURE 9.—Indicial lift functions, $C_{L_\alpha}(s)$ and $C_{L_\theta}(s)$.

LIFT IN VARIABLE MOTION

In addition to the lift given by the lift function $C_{L_\alpha}(s)$, the airfoil experiences a reaction equal to the instantaneous rate of change of the normal-velocity component times the virtual additional mass of the wing in normal motion. In coefficient form:

$$\Delta C_{L_{inertia}}=\frac{\pi}{E}\frac{d\alpha}{ds} \quad (31)$$

Furthermore, if the wing is rotating in pitch, the effect of an additional relative camber is introduced. A simple integration, making use of well-known results of thin-airfoil theory, shows

$$\Delta\alpha_{pitching}=l\frac{d\theta}{ds} \quad (32)$$

where the factor l is ½ for a straight rectangular wing. For the elliptic wing, $\frac{1}{2}>l>\frac{\pi}{8}$, approximately, being somewhat smaller than ½ because the rotation introduces a smaller relative camber at the narrower sections toward the tip.

The effects of combined vertical motion $\left(\alpha=\frac{w}{U_0}\right)$ and rotation ($\alpha=\theta$) may be conveniently treated by the use of moving axes as shown in figure 10. With these points in mind, the following operational formula for the total lift may be derived:

$$C_L(s)=\frac{\pi}{E}D\alpha(s)+\overline{C}_{L_\alpha}(D)[\alpha(s)+lD\theta(s)] \quad (33)$$

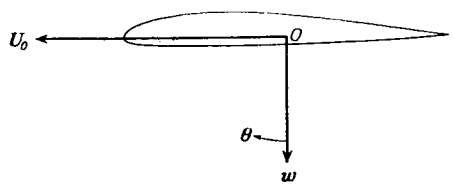

FIGURE 10.—Moving axes, $\alpha=w/U_0$.

LIFT FUNCTIONS FOR AN OSCILLATING AIRFOIL

The lift in sinusoidal motion where

$$\alpha=e^{ins} \text{ and } \theta=0 \quad (34)$$

is given by

$$C_{L_n}(s)=\frac{\pi}{E}ine^{ins}+\overline{C}_{L_\alpha}(D)e^{ins} \quad (35)$$

Since

$$e^{ins}=\frac{D}{D-in}1$$

$$\overline{C}_{L_\alpha}(D)e^{ins}=\overline{C}_{L_\alpha}(D)\frac{D}{D-in}1 \quad (36)$$

Expansion of this operator gives, with the exception of transient terms,

$$C_{L_n}(s)=\overline{C}_{L_\alpha}(in)e^{ins} \quad (37)$$

The function $\overline{C}_{L_\alpha}(in)$ corresponds to the lift function $C(n)$ introduced by Theodorsen (reference 2) for the oscillating two-dimensional airfoil, that is, in Theodorsen's terminology

$$\overline{C}_{L_\alpha}(in)=2\pi C(n)=2\pi[F(n)+iG(n)] \quad (38)$$

The expressions for $F+iG$ found from the operational equivalents of (29) are:

$$\left.\begin{aligned}(F+iG)_{A=3}&=0.600-0.170\frac{in}{in+0.540}\\(F+iG)_{A=6}&=0.740-0.267\frac{in}{in+0.381}\end{aligned}\right\} \quad (39)$$

Figure 11 shows these functions plotted against the wave length $2\pi/n$ of the oscillation.

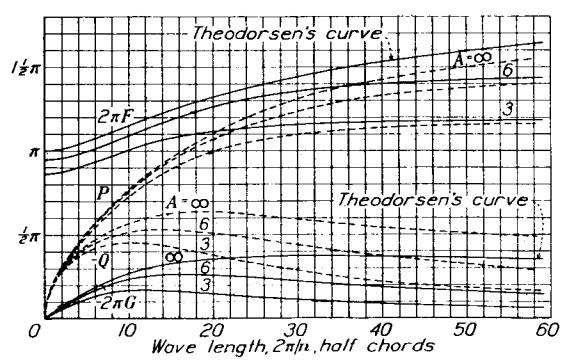

FIGURE 11.—Oscillating-lift functions, $\overline{C}_{L_\alpha}(in)=2\pi(F+iG)$ and $\overline{C}_{L_\theta}(in)=P+iQ$.

Relation (37) is especially interesting (see reference 7) because it shows a connection between the Fourier and the operational analyses. Thus, if the response of a linear system to a continuous sinusoidal excitation is known,

$$R_n(s)=f(in)e^{ins} \quad (40)$$

then, the function f immediately furnishes the opera-

tional equivalent of the unit response so that, for any variable excitation $z(s)$,

$$R(s)=f(D)z(s)=f(D)\bar{z}(D)\,1 \tag{41}$$

LIFT IN GUSTS

The foregoing calculations provide the basis for the determination of lift under any prescribed conditions of motion of the wing. These results may also be used in conjunction with the equations given by Theodorsen (reference 2) to predict the air forces on wings with hinged flaps.

In all cases treated, the airfoil has been considered as moving in air that would otherwise be at rest. Another problem of considerable interest is the prediction of lift during passage of the airfoil through gusts. The two-dimensional theory for this case was developed by Küssner (reference 3) and has since been corrected in certain details by von Kármán and Sears (reference 8).

The basic solution required in the gust problem is the solution for a unit sharp-edge gust of uniform upward velocity. In order to obtain this solution, it is useful to substitute for the change in direction of the relative air velocity an equivalent fictitious bending of the airfoil in still air such that it has at every point an angle of attack equal to the angle that would otherwise be produced by the gust.

The effect of a bend progressing along the chord of the airfoil may be calculated by thin-airfoil theory (reference 9, chs. III and IV). A part of the effect appears as a change in angle of attack of the airfoil as a whole, namely:

$$\Delta\alpha_g=1-\frac{\cos^{-1}(s-1)+\sqrt{s(2-s)}}{\pi} \tag{42}$$

The corresponding part of the lift is obtained from the indicial-lift function $C_{L_\alpha}(s)$ by superposition. In addition, a reaction caused by acceleration of the noncirculatory potential flow exists during the time the airfoil is partly immersed in the gust. In two-dimensional flow, the additional reaction is

$$\Delta C_{L_g}=2\sqrt{s(2-s)} \tag{43}$$

No corresponding expression for the finite wing is known, but it may be reasoned that the maximum correction will be no greater than that indicated by the inertia factor of the rigid elliptic disk, $1/E$. Hence, the formula

$$\Delta C_{L_g}=\frac{2}{E}\sqrt{s(2-s)} \tag{44}$$

was used for the finite wings as an approximation.

The consideration of wings with curvature or sweepback introduces another difficulty into the analysis, since the sections of such wings will not strike the edge of the gust simultaneously. It is obviously impractical to attempt to include in the analysis the effects of the many possible variations of plan form, and the calculations were therefore made on the assumption that all sections entered the gust simultaneously. Such an analysis may be considered sufficiently exact for the usual variations of plan form but is, of course, not applicable to wings with considerable sweep.

Figure 9 shows the functions, designated $C_{L_g}(s)$, thus calculated. These curves have the useful approximate expressions:

$$\left.\begin{aligned}
C_{L_g}(s)_{A=3}&=1.200\pi(1.000-0.679e^{-0.558s}-0.227e^{-3.20s})\\
C_{L_g}(s)_{A=6}&=1.500\pi(1.000-0.448e^{-0.290s}\\
&\qquad -0.272e^{-0.725s}-0.193e^{-3.00s})\\
C_{L_g}(s)_{A=\infty}&=2.000\pi(1.000-0.236e^{-0.058s}\\
&\qquad -0.513e^{-0.364s}-0.171e^{-2.42s})
\end{aligned}\right\} \tag{45}$$

As in the case of the functions $C_{L_\alpha}(s)$, the exponential forms were used to give simple operational equivalents. The operational equivalents of the indicial-gust functions, $\bar{C}_{L_g}$, give directly functions determining the alternating lift of a stationary wing in an oscillating air stream. Thus

$$C_L(s)=\bar{C}_{L_g}(in)e^{ins}=[P(n)+iQ(n)]e^{ins} \tag{46}$$

Figure 11 shows these functions in comparison with the corresponding functions for the oscillating airfoil.

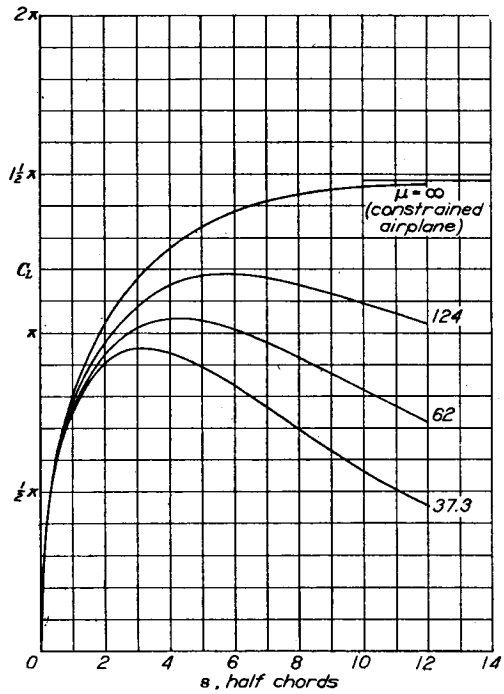

FIGURE 12.—Variation of the lift during passage through unit sharp-edge gust. $A=6$.

MOTION OF AIRPLANE IN GUST

In most problems that arise in practice, the motion of the airfoil, or airplane, will not be prescribed beforehand but must be determined from dynamical equations. The rising motion of an airplane (or, as it shall

be considered here, a loaded wing) while entering a sharp-edge gust presents such a problem and will be used to illustrate the application of the operational formulas.

The dynamical equation for this case (neglecting pitching motion) is:

$$m\frac{dw}{dt}+\text{resisting force}=\text{impressed force} \tag{47}$$

where the impressed force is that part of the lift caused by the gust. Since

$$\frac{dw}{dt}=\frac{U_0^2}{c/2}\frac{d\alpha}{ds}$$

$$m\frac{dw}{dt}=\frac{2m}{S\frac{\rho}{2}c}s\frac{\rho}{2}\frac{c}{2}\frac{U_0^2}{c/2}\frac{d\alpha}{ds}=\mu s\frac{\rho}{2}U_0^2\frac{d\alpha}{ds} \tag{48}$$

where $\mu=\frac{2m}{S\frac{\rho}{2}c}$. In coefficient form,

$$\mu D\alpha-\overline{C}_{L_\alpha}(D)\alpha=\overline{C}_{L_g}(D)\alpha_g \tag{49}$$

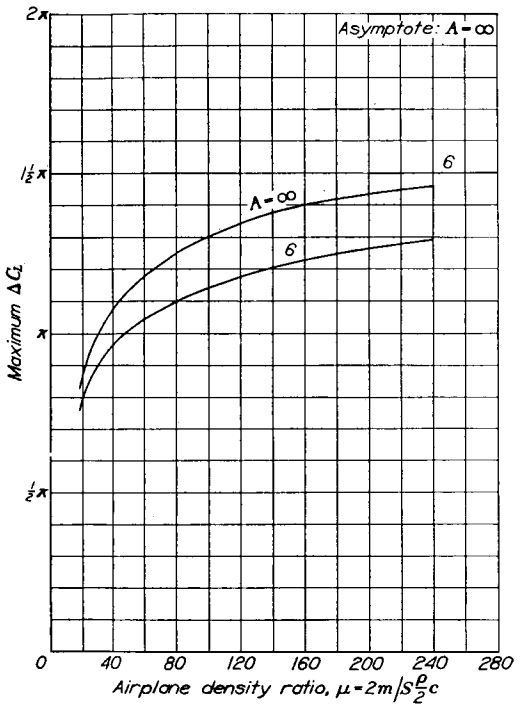

FIGURE 13.—Maximum-lift increments developed in flying through a unit sharp-edge gust.

where α_g is the change in angle of attack represented by the gust.

For a unit sharp-edge gust, $\alpha_g=1$; then (solving for α),

$$\alpha(s)=\frac{\overline{C}_{L_g}(D)}{\mu D+\overline{C}_{L_\alpha}(D)}1 \tag{50}$$

By the use of the approximate expressions given for C_{L_α} and C_{L_g} (equations (29) and (45)), this operator may be reduced to the form (19).

Figure 12 shows the lift coefficient $C_L(s)=\mu D\alpha(s)$ computed from equation (50) for several values of the density ratio μ and for $A=6$. Figure 13, derived from similar calculations, gives maximum lift loads attained in the sharp-edge gust as functions of the relative density.

LANGLEY MEMORIAL AERONAUTICAL LABORATORY,
NATIONAL ADVISORY COMMITTEE FOR AERONAUTICS,
LANGLEY FIELD, VA., *June 15, 1939.*

REFERENCES

1. Wagner, Herbert: Über die Entstehung des dynamischen Auftriebes von Tragflügeln. Z. f. a. M. M., Bd. 5, Heft 1, Feb. 1925, S. 17–35.
2. Theodorsen, Theodore: General Theory of Aerodynamic Instability and the Mechanism of Flutter. T. R. No. 496, N. A. C. A., 1935.
3. Küssner, H. G.: Zusammenfassender Bericht über den instationären Auftrieb von Flügeln. Luftfahrtforschung, Bd. 13, Nr. 12, 20. Dec. 1936, S. 410–424.
4. Jones, Robert T.: The Unsteady Lift of a Finite Wing. T. N. No. 682, N. A. C. A., 1939.
5. Jones, Robert T.: Operational Treatment of the Nonuniform-Lift Theory in Airplane Dynamics. T. N. No. 667, N. A. C. A., 1938.
6. Jeffreys, Harold: Operational Methods in Mathematical Physics. Cambridge Tracts in Math. and Phys. No. 23, Cambridge Univ. Press, 1927.
7. Garrick, I. E.: On Some Reciprocal Relations in the Theory of Nonstationary Flows. T. R. No. 629, N. A. C. A., 1938.
8. von Kármán, Th., and Sears, W. R.: Airfoil Theory for Non-Uniform Motion. Jour. Aero. Sci., vol. 5, no. 10, Aug. 1938, pp. 379–390.
9. Munk, Max M.: Fundamentals of Fluid Dynamics for Aircraft Designers. The Ronald Press Co., 1929.

TECHNICAL NOTE 771

TRANSIENT EFFECTS OF THE WING WAKE ON THE HORIZONTAL TAIL

Robert T. Jones and Leo F. Fehlner

Langley Memorial Aeronautical Laboratory

August 1940

NATIONAL ADVISORY COMMITTEE FOR AERONAUTICS

TECHNICAL NOTE NO. 771

TRANSIENT EFFECTS OF THE WING WAKE ON THE HORIZONTAL TAIL

By Robert T. Jones and Leo F. Fehlner

SUMMARY

An investigation was made of the effect of the wing wake on the lift of the horizontal tail surfaces. In the development of expressions for this effect, the growth of wing circulation and wing wake, the time interval represented by the tail length, and the development of lift by the tail were considered. The theory has been applied to a specific case to show the magnitude of the effect to be expected.

It is shown that, for motions below a certain frequency, the development of lift by the tail may be represented by a simple lag function. The lag is, however, somewhat greater than that indicated by the tail length.

INTRODUCTION

During unsteady motions of the airplane, the wing leaves in its wake a sheet of vortices of varying strength. The velocity induced by these vortices may have a pronounced effect on the direction of the air flow near the tail, particularly during motions involving rapid changes of lift such as oscillations of short period or passage through gusts.

An approximation to the effect of the wing wake has been used by Cowley and Glauert (reference 1). They assumed that the downwash associated with a change in lift is equal to the corresponding steady value but that the effect at the tail is delayed by the time required for the airplane to travel a distance equal to the tail length. It is known, however, that during increases of circulation the wing develops counterrotating vortices which must, for a time, at least, induce a strong upwash, increasing the

lift of the tail. In addition to the time lag considered by Cowley and Glauert, both the variation of vertical velocity and the delay in the development of lift by the tail are considered in the present paper.

The flow around the wing, hence the wake produced by the wing, is assumed to be uninfluenced by the presence of the tail surface. The interference is thus confined to the effect of the wing on the tail and, since the wake formed by an isolated wing is known, the interference can be directly calculated for any relative position of the two surfaces.

Although the theory is thus applicable to a variety of arrangements, computations to cover all conditions were not considered to be worth while. In particular, the exact vertical location of the tail surface (within the usual range) was not expected to be critical. The tail surface was therefore considered to be located directly in the wake where the effect is a maximum. The effect of tail length was investigated and it was found that the results obtained from computations covering a typical case could be extrapolated to take account of this factor in a satisfactory manner.

LIFT FUNCTIONS

As in other problems involving unsteady flow, it is convenient to assume at first a sudden unit jump in the angle of attack of the wing and to develop more general solutions by operational methods (reference 2). The lift of the tail surface under these conditions is due solely to interference from the wing and is to be added to the lift independently developed.

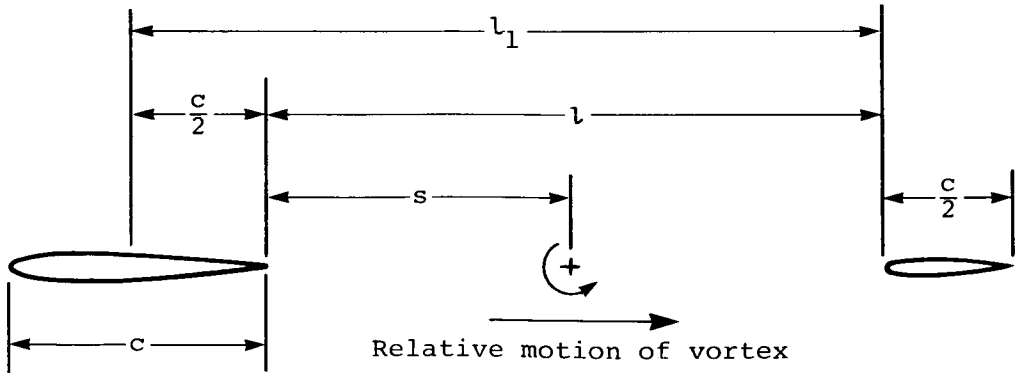

Figure 1.

Figure 1 shows the notation used in the development. Variable quantities are expressed in terms of the distance along the flight path, $s = \frac{U_o t}{c/2}$, where t represents time. The analysis is kept nondimensional by expressing all velocities in terms of the flight velocity, U_o, and all lengths in terms of the half chord, $c/2$.

The rate of development of vorticity by the wing following a sudden unit increase in angle of attack α ($\alpha = 1(s)$) is given in reference 3 and shows directly the distribution of vortices in the wake. The total circulation at any instant after such a change is denoted by $\Gamma_\alpha(s)$. The vertical velocity of air in the vicinity of the tail induced by a unit wake vortex, $w_\Gamma(s)$, (fig. 2) may be calculated from the Biot-Savart rule. The resultant variation of vertical velocity following a unit change of angle of attack of the wing follows from the combination of these two functions, i.e.,

$$w_w(s) = w_\Gamma(s)\ \Gamma_\alpha(0) + \int_o^s w_\Gamma(s - s_o)\ \Gamma_\alpha'(s_o)\ ds_o \qquad (1)$$

The effect of the vertical velocity, w_w, on the tail surface may be treated as the effect of a varying gust. The lift on an airfoil penetrating this gust is given by

$$C_{L_{t_w}}(s) = C_{L_g}(s)\ w_w(0) + \int_o^s C_{L_g}(s-s_o)\ w_w'(s_o)\ ds_o \qquad (2)$$

where $C_{L_g}(s)$ is the gust lift function for the tail surface (reference 3).

The integrations (1) and (2) may be carried out in a single step by using the operational equivalents of the functions involved. Thus

$$C_{L_{t_w}}(s) = \overline{C}_{L_{t_w}}(D)\ 1(s) = \overline{C}_{L_g}(D)\ \overline{\Gamma}_\alpha(D)\ \overline{w}_\Gamma(D)\ 1(s) \qquad (3)$$

The function $C_{L_{t_w}}(s)$ is the lift on the tail surface due solely to a unit change in the angle of attack of the wing and is to be added to the lift developed independently by the tail surface.

The function $\Gamma(s)$ denotes the circulation around the wing (or the equal and opposite circulation measured around the wake) in the plane of symmetry. The spanwise distribution of vorticity is assumed to remain elliptical. A unit increment of $\Gamma(s)$ thus involves a single wing and wake vortex of unit strength at the center, the strength falling off toward the tips in accordance with the elliptic loading. The two vortices are connected by a sheet containing only the spanwise component of discontinuity. This arrangement can be derived by the superposition of vortices of the type shown in figure 3.

The centroid of wing circulation is assumed to remain stationary at the center of the wing chord. Although the wing circulation originates at the trailing edge, little error is incurred through this assumption because the travel of the centroid to the center of the chord is very rapid (reference 3). If the wing circulation is replaced by a single vortex A (fig. 3), the vertical velocity at the tail due to vortices A and B is given by

$$w_{\Gamma_{AB}}(s) = \frac{1}{2\pi}\left(\frac{1}{l - s} - \frac{1}{l_1}\right) \tag{4}$$

The operational equivalent of this function is

$$\overline{w}_{\Gamma_{AB}}(D) = \frac{1}{2\pi}\left[D\, e^{-lD}\, Ei(lD) - \frac{1}{l_1}\right] \tag{5}$$

where the symbol Ei represents the exponential integral function, i.e.,

$$Ei(x) = \int_{\infty}^{-x} \frac{e^{-u}}{u}\, du$$

The downwash due to the spanwise component of discontinuity (vortices C and D, fig. 3) may be determined from figure 6 of reference 3, which shows the downwash at the edge of a sheet of discontinuity of varying length. The downwash in the region of the tail corresponding to any position or extent of the wake may be obtained by adding the effects of two sheets of different lengths, as indicated in figure 4.

APPLICATION OF THEORY

In order to illustrate the application of the theory and to show the order of magnitude of the results to be expected, the lift functions are determined for a specific example. The proportions considered are as follows. (See fig. 1.)

Aspect ratio of wing - - - - - - 6

Aspect ratio of tail surface - - 3

l - - - - - - - - - - - - - - - - 5.54

l_1 - - - - - - - - - - - - - - - - 6.54

Chord of tail surface - - - - - 1.0

The effect of the noncirculatory component of the flow about the wing is neglected, its influence at the tail being small and constant in value.

The approximate expressions used for the functions $\overline{C}_{L_g}(D)$ and $\overline{\Gamma}_\alpha(D)$ are:

$$\overline{C}_{L_g}(D) \cong 3.77 - \frac{2.56\ D}{D + 1.116} - \frac{1.044\ D}{D + 6.40} \tag{6}$$

$$\overline{\Gamma}_\alpha(D) \cong 4.71 - \frac{2.11\ D}{D + 0.290} - \frac{1.25\ D}{D + 0.690} - \frac{0.800\ D}{D + 0.276} \tag{7}$$

It should be noted that the function C_{L_g} is in terms of the half-wing chord which, in the example chosen, is twice the corresponding dimension of the tail surface itself. There is a slight change in the expression as given in reference 3 to make it more closely approximate the starting value.

If the proper values are substituted in equations (4) and (5), the function $w_{\Gamma_{AB}}$ becomes

$$w_{\Gamma_{AB}}(s) = \frac{1}{2\pi}\left(\frac{1}{5.54 - s} - \frac{1}{6.54}\right) \tag{8}$$

and

$$w_{\Gamma_{AB}}(D) = \frac{1}{2\pi}\left[D\, e^{-5.54D}\, Ei(5.54D) - \frac{1}{6.54}\right] \tag{9}$$

No concise expression for the spanwise component of the downwash, $w_{\Gamma_{CD}}$, can be given. The curve can be approximated, however, by a series of exponential terms of the form $Ae^{\lambda s}$. For the proportions considered

$$w_{\Gamma_{CD}}(s) \cong -0.083 + 0.047e^{-0.067S} + 0.145e^{-0.354S} - 0.156e^{-0.742S} + 0.047e^{-1.45S} \tag{10}$$

$$\overline{w}_{\Gamma_{CD}}(D) \cong -0.083 + \frac{0.047\ D}{D + 0.067} + \ldots \tag{11}$$

These expressions are to be added to equations (8) and (9), respectively, to give the function $\overline{w}_{\Gamma}(D)$ required in the evaluation of equation (3).

The calculation of $C_{L_{t_w}}$ according to equation (3) results in the lift of the tail surface, as a function of the distance traveled following a sudden unit jump in the angle of attack of the wing, i.e., the "indicial lift"; it is shown in figure 5.

For a unit change in angle of attack of the airplane as a whole, the lift developed independently by the tail must be added. This lift increment is given by equation (29) of reference 3 for an airfoil of aspect ratio 3 but it must be expressed in terms of the wing cord. The function $C_{L_{t_\alpha}}(s)$ (fig. 6) shows the lift resulting from the unit change of angle of attack of the entire airplane.

Although the indicial lift curves (figs. 5 and 6) show infinite values, it is to be noted that the integration of the expressions by superposition for any probable disturbance results in finite lift at all points. Furthermore, when the effects of moderate rates of change in the angle of attack are integrated, the exact form of the indicial response curve is not critical.

This point is best illustrated by integrating the response to a continuous oscillatory variation of angle of attack. If $\alpha = e^{ins}$,

$$C_{L_{(\alpha=e^{ins})}}(s) = \overline{C}_L(D)\ e^{ins} = \overline{C}_L(in)\ e^{ins} = [A(n)+iB(n)]\ e^{ins}$$

The real part, A, is the component of the response in phase with the disturbance, and the imaginary part, B, is the component 90° out of phase with the disturbance.

The evaluation of the exponential integral with an imaginary argument is given in reference 4, page 80.

$$Ei(in) = Ci(n) + i\left[Si(n) + \frac{\pi}{2}\right]$$

where Ci and Si are, respectively, the cosine-integral and the sine-integral functions.

Figure 7 shows the A and the B components of the oscillatory lift function, $C_{L_{t_w}}(in)$, the lift on the tail surface induced by a continuous sinusoidal oscillation of the wing. For a continuous vertical oscillation of the airplane as a whole (changes of angle of attack without rotation), the function $C_{L_{t_\alpha}}(in)$ (fig. 8) shows the resulting lift.

If the oscillatory lift functions are approximated by a Fourier series, this series will be found to correspond to an approximation of the indicial lift function in the form of steps. Thus the function $C_{L_{t_w}}(in)$ is closely approximated, as shown by broken lines in figure 7, by the expression

$$C_{L_{t_w}}(in) \cong 0.30 - 2.20\ e^{-7.14in} \qquad (12)$$

for values of n less than 0.35. If the argument (in) is replaced by the operator D, the resulting function is the operational equivalent of a simple step function, which is an approximation of the corresponding indicial lift function. Thus

$$C_{L_{t_w}}(s) \cong \left[0.30 - 2.20\ e^{-7.14D}\right] 1(s) \cong$$
$$0.30 - 2.20\ [1(s - 7.14)] \qquad (13)$$

This approximation is shown by the broken line in figure 5.

Similarly, the approximation shown by the broken line in figure 8 is

$$C_{L_{t_\alpha}}(in) \cong 3.85 - 1.98\, e^{-7.48in} \tag{14}$$

and

$$C_{L_{t_\alpha}}(s) \cong \left[3.85 - 1.98\, e^{-7.48D}\right] 1(s) \cong 3.85 - 1.98\, [1(s - 7.48)] \tag{15}$$

and is shown by the broken line in figure 6.

In the case of an airplane executing pitching motions during which the angle of attack of the wing does not change, the component of response out of phase with the disturbance is insignificant. The response may therefore be considered instantaneous. Although the general case involves motions that combine changes of angle of attack, α, and of angular displacement, θ, the lift increments resulting from each motion have been separately treated. In this form, the results are directly applicable to the differential equations of motion of the airplane.

CONCLUDING REMARKS

Although the indicial lift of the tail surface actually shows a pronounced variation, it is permissible to consider the effect of a simple lag if only moderate rates of motion are involved. The lag functions shown in figures 5 and 6 give the lift quite accurately during any motion that can be compounded of frequencies lower than one cycle in 18 half chords ($n < 0.35$).

It will be noted that these expressions differ from those assumed by Cowley and Glauert in two ways. First, the value of the function from 0 to l is not zero but is a positive value, which accounts for the upwash that the tail initially encounters. Second, the distance after which the value of the function becomes negative is not equal to the tail length, l, but occurs at a distance somewhat greater than the tail length. This distance accounts for the lag in the growth of downwash and the lag in the development of lift by the tail and may be called the effective tail length.

Although the results thus far have been obtained for one specific wing and tail arrangement, the effective tail length and the magnitude of the effect to be expected may be determined for other cases.

According to the theory, the pattern of the wake formed by the wing remains unchanged as it passes downstream. In addition, the rapid changes of induced velocity at the tail occupy a fairly short distance immediately ahead of and back of the edge of the wake. For any usual tail length, therefore, the time history of the lift on the tail is not substantially altered in relation to the instant at which the wake strikes the tail. This point is illustrated by figure 9, where the induced vertical velocity, w_Γ, following a unit change in wing circulation ($\Gamma = 1(s)$) is shown for different positions of the wing ahead of the tail surface. The principal effect of a change in tail length is to shift the origin along the relatively flat portion of the indicial lift curves shown in figures 5 and 6. This change in tail length then corresponds to an equal change in effective tail length. The effective tail length for any case is thus determined.

If the wing wake passes either above or below the tail surface, the lift functions will not show infinite values as they do in the case considered. The peak value of the lift function is lowest when the wake passes below the tail surface. The final value of the lift is but little affected by the vertical displacement as long as this displacement is small relative to the span.

The theory may be extended to show the effects of vertical gusts. The lift of the tail surface due to interference from the wing during penetration of the gust may be calculated with the aid of the curves of figure 5, provided that the variation of the angle of attack of the wing is known. A close approximation to this variation of angle of attack during penetration of a varying gust is obtained by measuring the angle of attack with respect to the relative wind direction at a point one-fourth of the chord ahead of the trailing edge of the wing. This approximation is based on a well-known result of the thin-airfoil theory and is valid as long as the rate of change of gust velocity along the flight path is less than that represented by an oscillation of one cycle in 18 chord lengths. The lift independently developed by the action of the gust on the tail surface may be determined from reference 3. This lift is directly added to that developed by interference from the wing.

As noted earlier, only in cases of extremely rapid changes in wing lift ($n > 0.35$) is the exact form of the indicial lift curve important. Such changes may occur, however, in sharp gusts and it is believed that the extension of the present investigation to cover the effect of vertical position of the tail surface in these cases would be worth while.

Langley Memorial Aeronautical Laboratory,
National Advisory Committee for Aeronautics,
Langley Field, Va., July 23, 1940.

REFERENCES

1. Cowley, W. L., and Glauert, H.: The Effect of the Lag of the Downwash on the Longitudinal Stability of an Aeroplane and on the Rotary Derivative M_q, R. & M. No. 718, British A.R.C., 1921.

2. Jones, Robert T.: Operational Treatment of the Nonuniform-Lift Theory in Airplane Dynamics. T.N. No. 667, NACA, 1938.

3. Jones, Robert T.: The Unsteady Lift of a Wing of Finite Aspect Ratio. T.R. No. 681, NACA 1940.

4. Jahnke, Eugen, and Emde, Fritz: Tables of Functions. 2d ed., B. G. Teubner (Leipzig and Berlin), 1933.

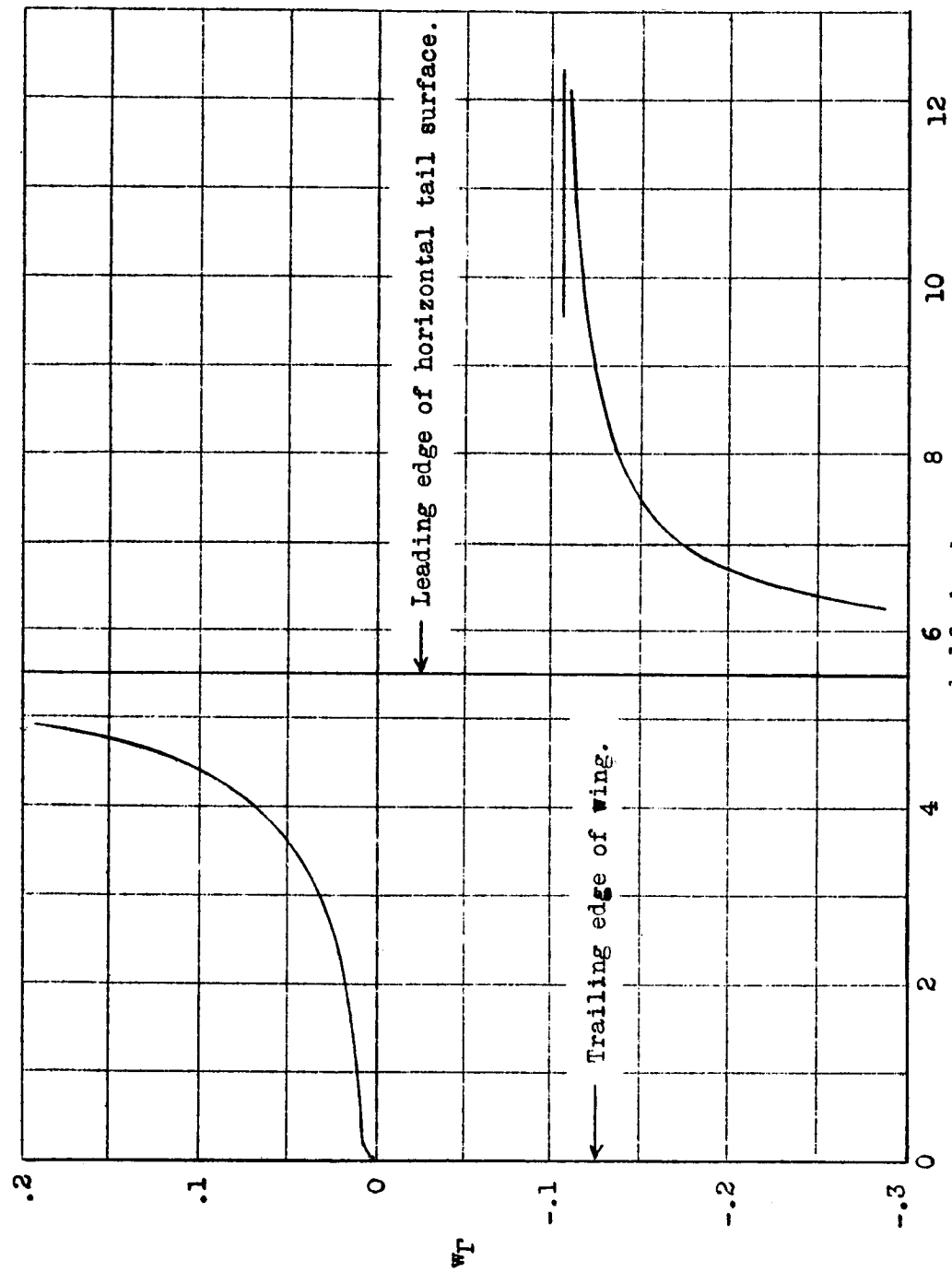

Figure 2.- Variation of vertical velocity at the horizontal tail following a unit increase in wing circulation, $w_T(s)$.

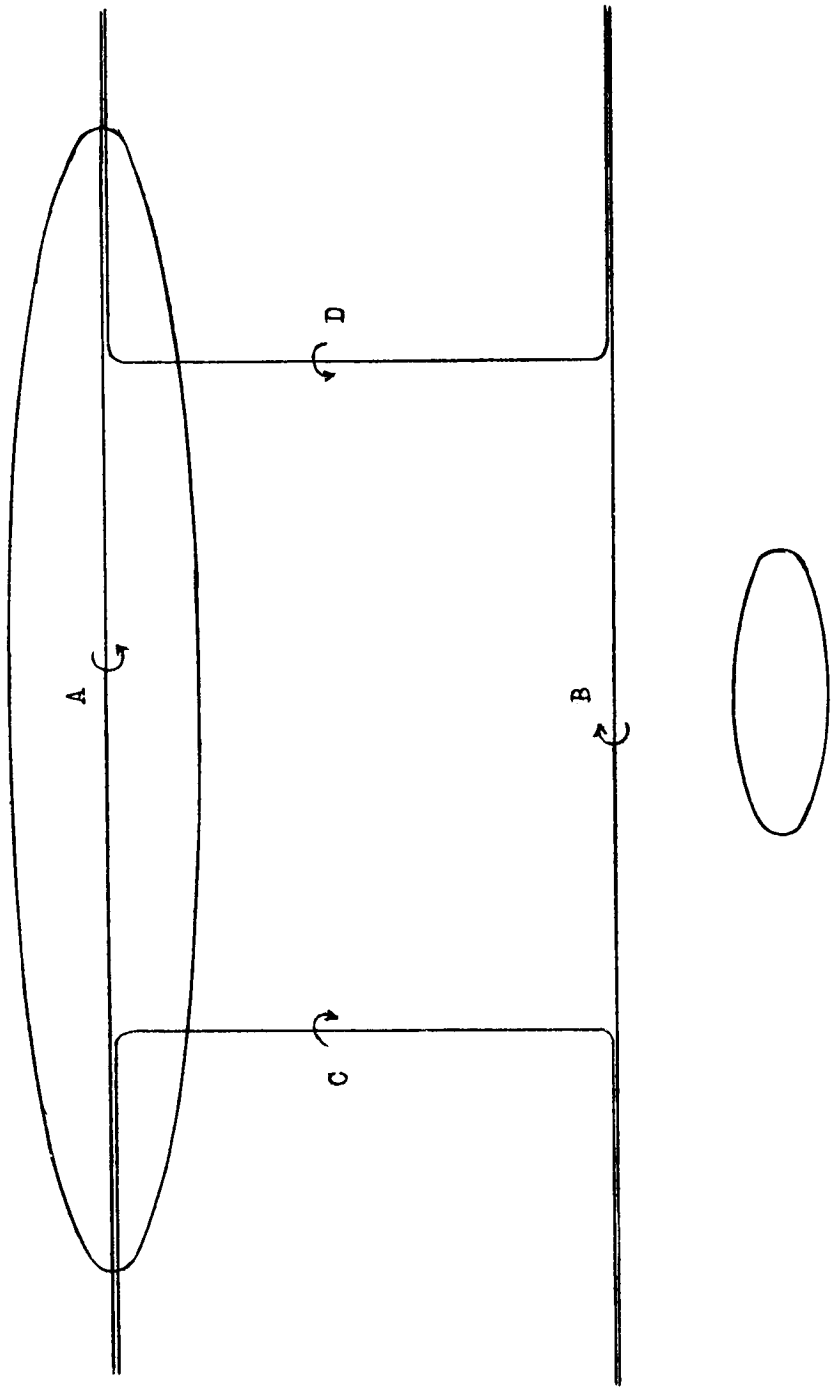

Figure 3.- Superposition of vortices to obtain finite loop.

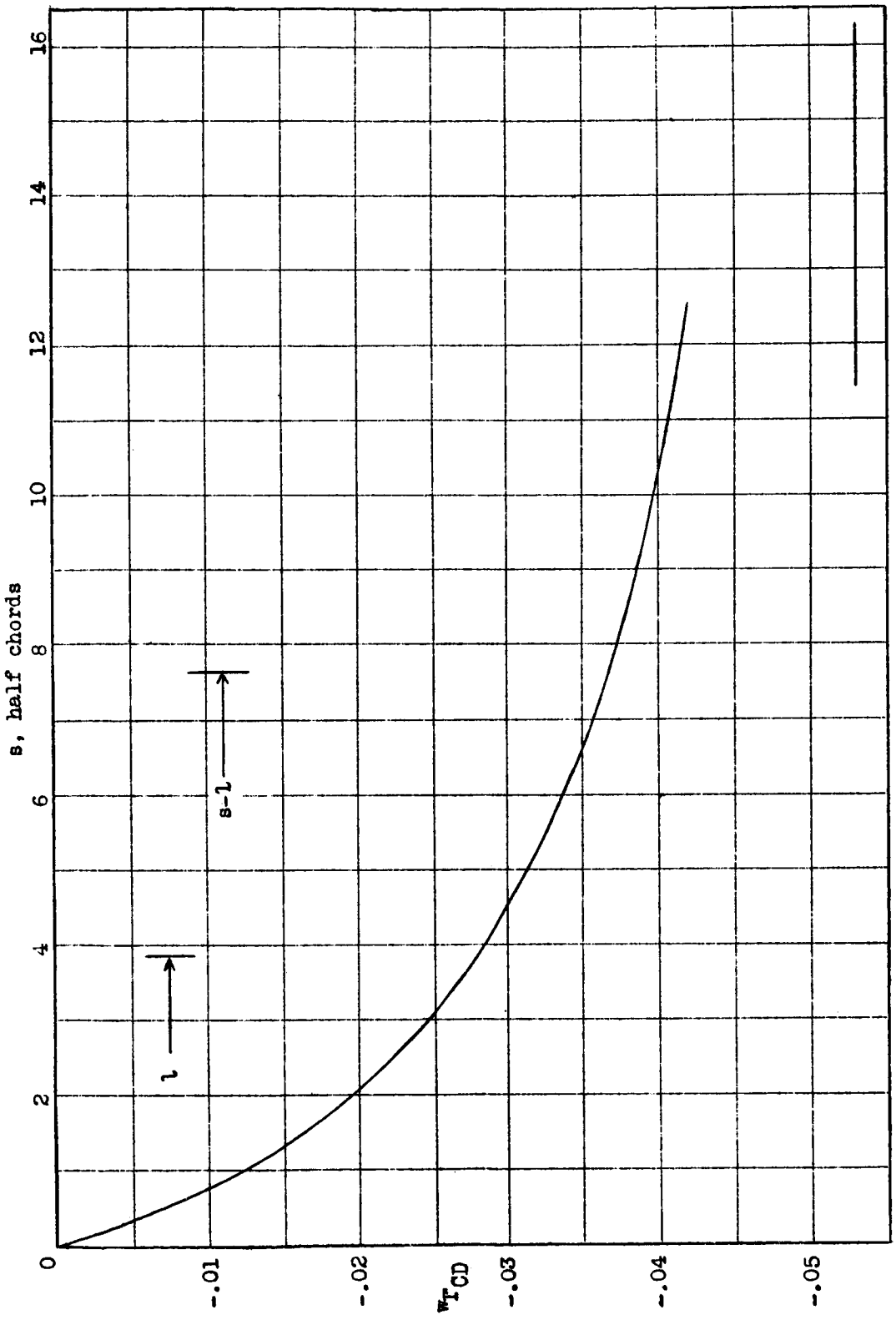

Figure 4.- Variation of downwash in the plane of symmetry with increasing length of the wake. Spanwise component of discontinuity. $w_{T_{CD}}(s) = w_{T_{CD}}(1) + w_{T_{CD}}(s-1)$

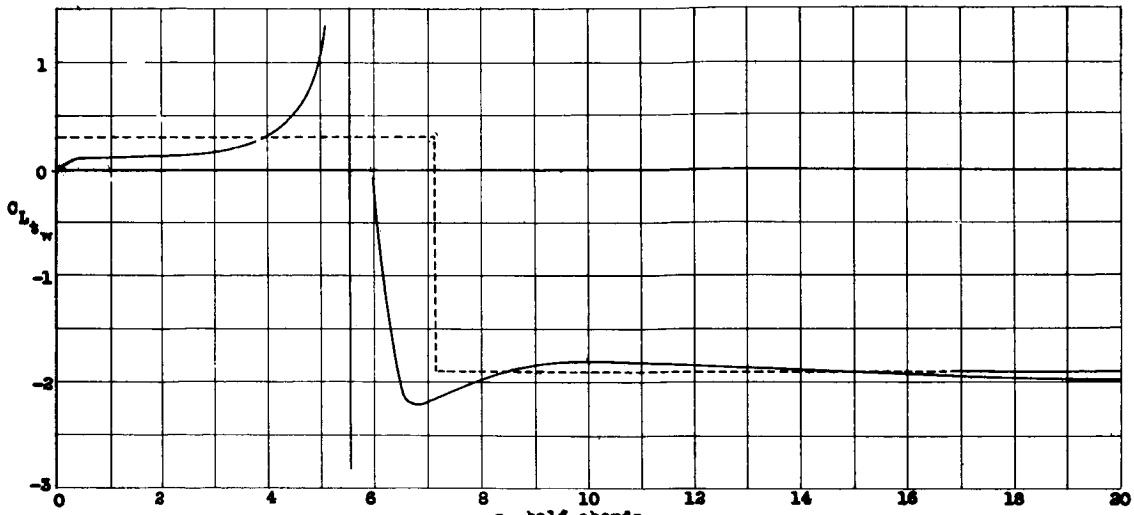

Figure 5.- Variation of lift on horizontal tail following an instantaneous unit change of angle of attack of the wing.

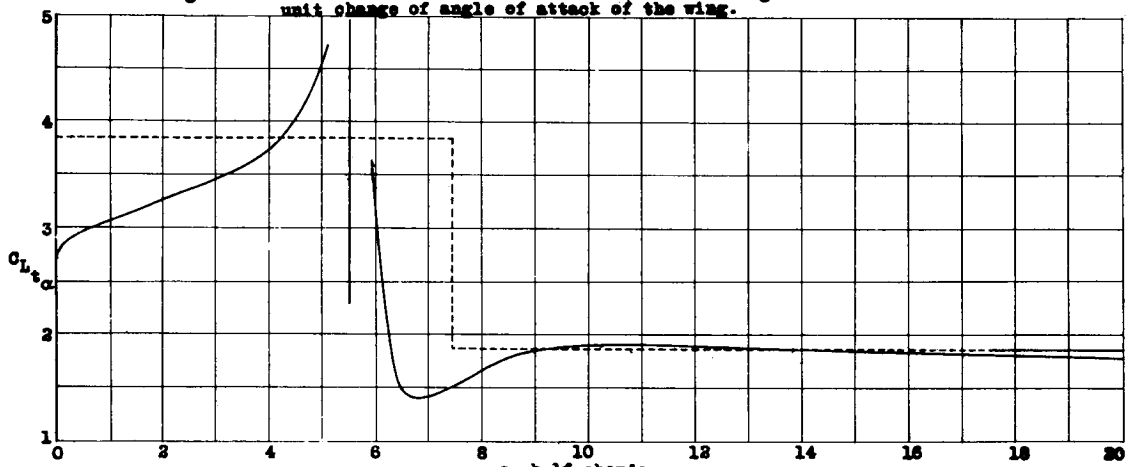

Figure 6.- Variation of lift on horizontal tail following an instantaneous unit change of angle of attack of the airplane.

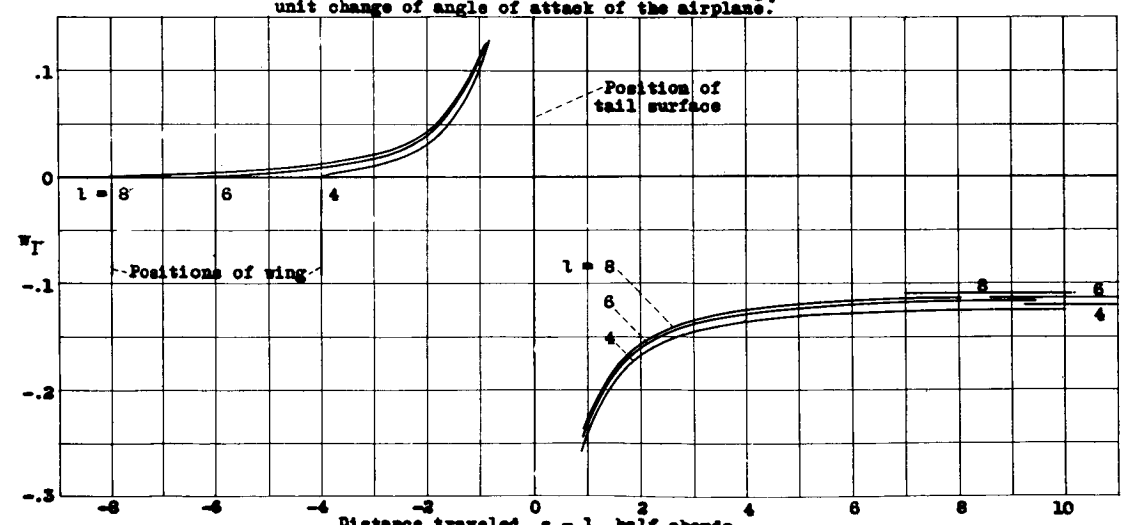

Figure 9.- Effect of tail length on the vertical velocity at the horizontal tail following a unit increase in wing circulation, $w_T(s)$.

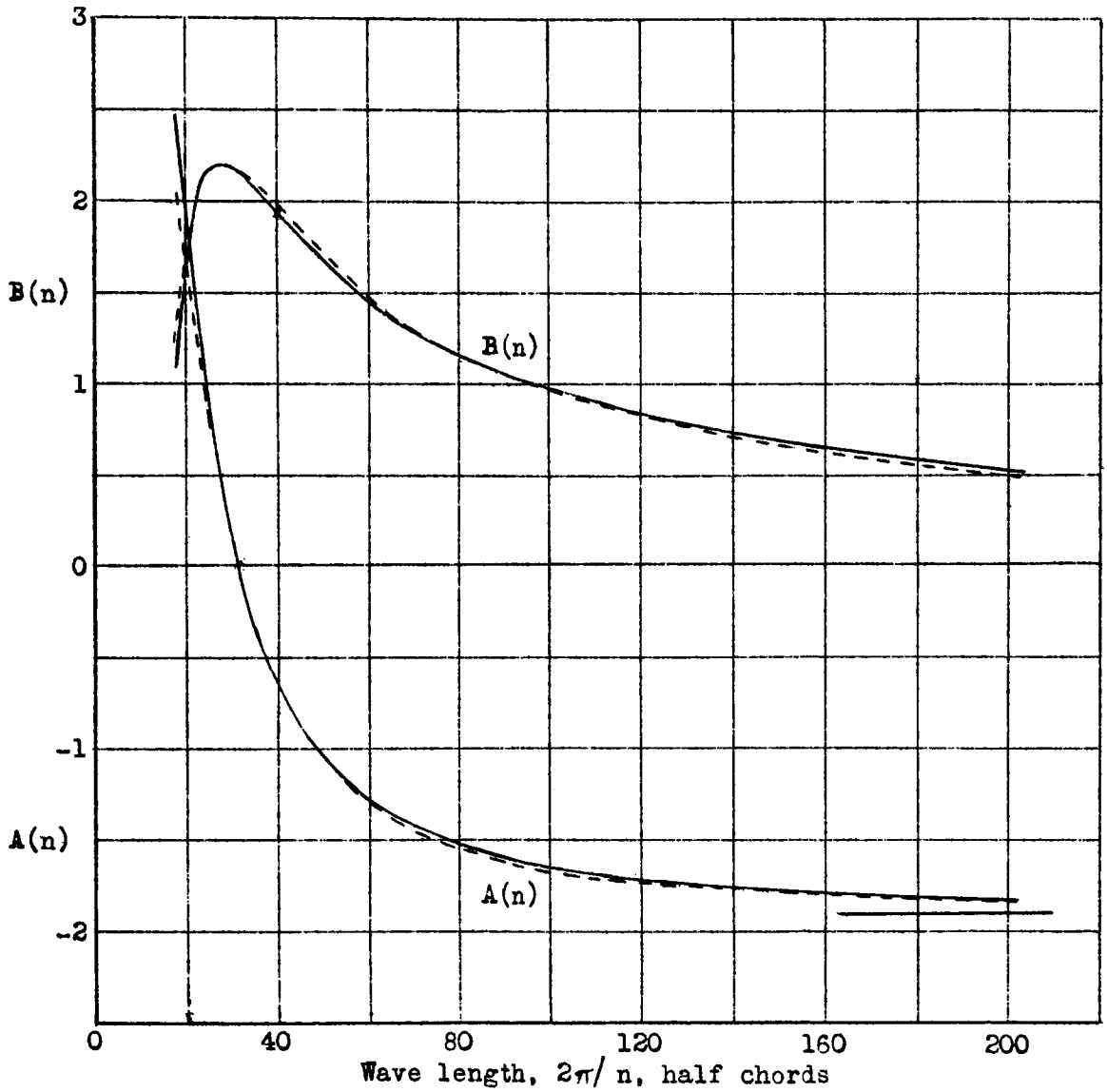

Figure 7.- Influence of wing oscillation on the lift of the horizontal tail. $C_{L_{t_w}}(in) = A(n) + iB(n)$

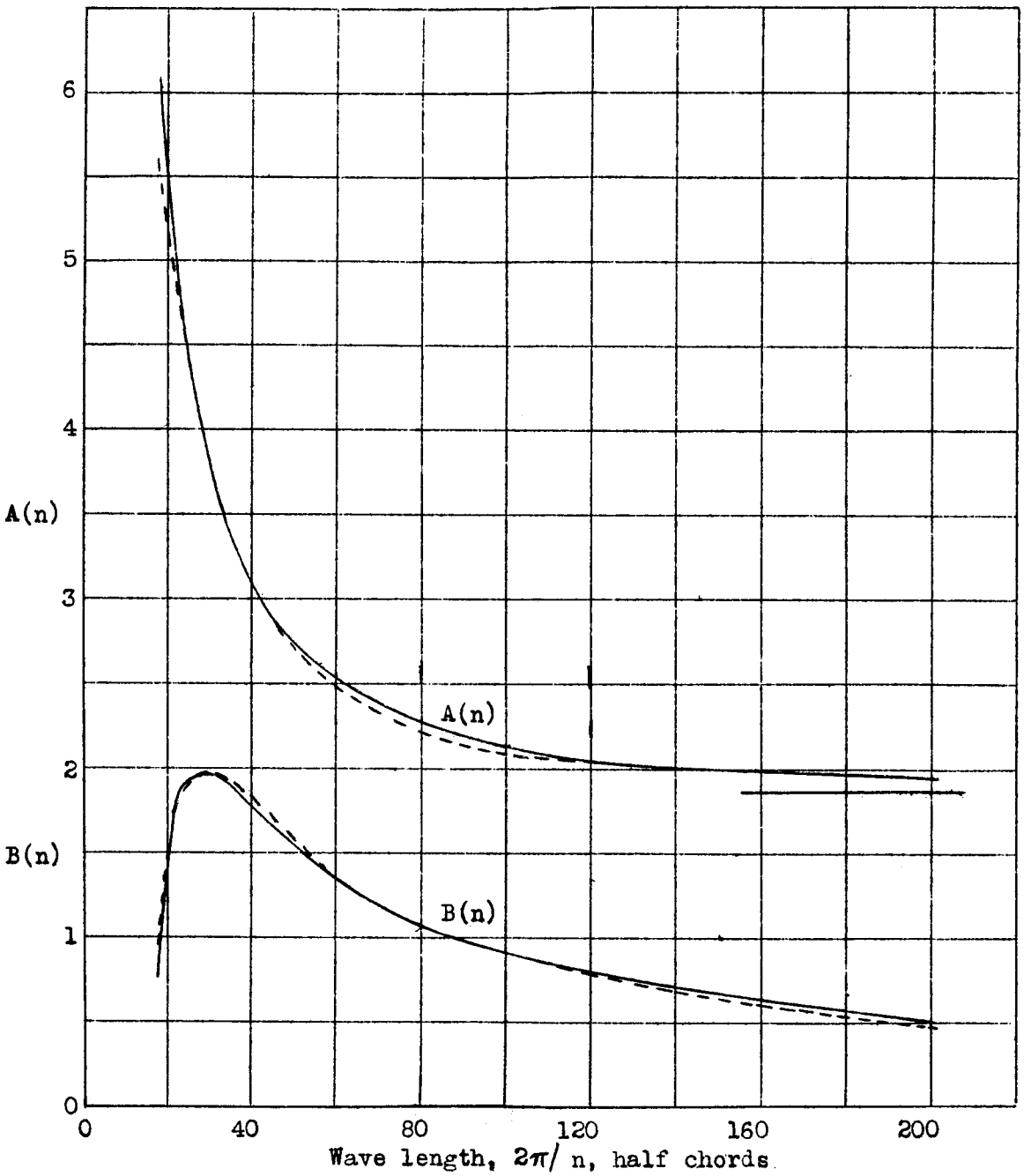

Figure 8.- Lift functions for horizontal tail of airplane in vertical oscillation without pitching. $C_{L_{t_\alpha}}(in) = A(n) + iB(n)$

REPORT NO. 709

AN ANALYSIS OF THE STABILITY OF AN AIRPLANE WITH FREE CONTROLS

Robert T. Jones and Doris Cohen

Langley Memorial Aeronautical Laboratory

1941

E R R A T A

NACA REPORT NO. 709

AN ANALYSIS OF THE STABILITY OF AN AIRPLANE WITH FREE CONTROLS
By Robert T. Jones & Doris Cohen

Page 7, Figures 10 to 13: All values of C_{n_β} given in figures 10 through 13 should be reduced by dividing by 6; that is, the values on the curves should read C_{n_β} = .102, .064, and .026 instead of .612, .384, and .156.

Page 8: In the second equation of the two bracketed as (12), the sign of the third term should be changed from minus to plus; thus the equation should read:

$$m_a k_a^2 \frac{d^2\delta}{dt^2} - p\frac{\partial H}{\partial p} + \frac{dp}{dt}(m_a\overline{yx} + \ldots .$$

Pages 8 and 9: Figure 14, containing the aileron-free stability boundaries, has been found to be incorrect and should not be used. The paragraph referring to this figure, beginning at the bottom of page 8 and continuing through equation (15) on page 9, is therefore also in error. The correct boundaries for oscillatory stability with ailerons free are given in the enclosed new figure 14. The boundary for divergence is that given by equation (16). Statement 3 under "Concluding Remarks," page 9, no longer applies to ailerons.

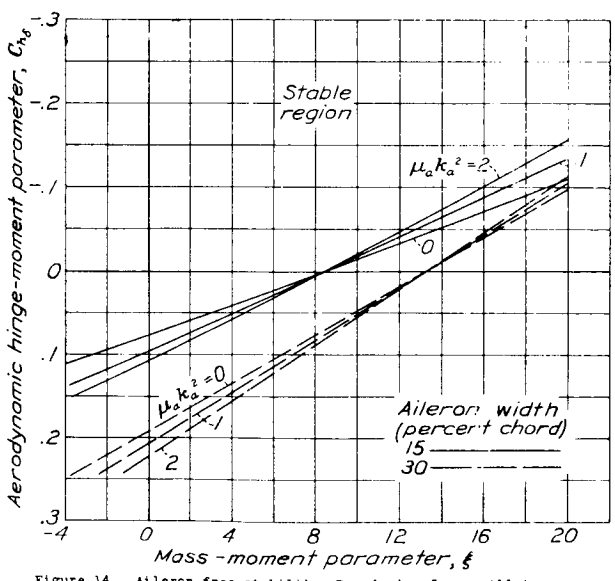

Figure 14.- Aileron-free stability. Boundaries for oscillatory stability. μ, 45; k_x, 1.80.

REPORT No. 709

AN ANALYSIS OF THE STABILITY OF AN AIRPLANE WITH FREE CONTROLS

By Robert T. Jones and Doris Cohen

SUMMARY

An investigation is made of the conditions essential to the stability of an airplane with free control surfaces. Calculations are based on typical airplane characteristics with certain factors varied to cover a range of current designs. Stability charts are included to show the limiting values of the aerodynamic hinge moments and the weight hinge moments of the control surfaces for various positions of the center of gravity of the airplane and for control systems with various moments of inertia. The effects of reducing the chord and of eliminating the floating tendency of the surface, of changing the wing loading, and of decreasing the radius of gyration of the airplane are also indicated. An investigation has also been made of the nature of the motion of the airplane with controls free and of the modes of instability that may occur.

Stability with the controls free generally depends more critically on the design of the control system than on the stability characteristics of the airplane. In particular, too great a weight moment, combined with a high degree of aerodynamic balance, may cause undamped oscillations. Regardless of the weight moment, it appears difficult to secure stability when the aerodynamic balance exceeds 75 percent of the hinge moment.

INTRODUCTION

During recent investigations by the NACA of the flying qualities of several airplanes of different types, a tendency toward longitudinal instability was noted that involved pitching of the airplane reinforced by movements of the elevator. In other flight tests, lateral instability accompanied by oscillations of the rudder or of the ailerons has been noticed. The oscillations observed were rapid enough to be influenced by the inertia of the control surfaces but were not believed to be sufficiently rapid to involve the elasticity of the structure. The problem is thus concerned with motions intermediate between flutter and movements of the airplane as a rigid body.

It was thought that a theoretical analysis of the stability of an airplane with the controls free might shed some light on the cause of these undesirable motions and might indicate how they could be avoided in design. Of the previous publications on the subject, the most detailed is that of E. Bartsch on lateral motions of an airplane with free rudder and ailerons (reference 1). In order to make specific recommendations applicable to modern design, a study of stability more complete and detailed than any available was undertaken. Calculations were made covering both longitudinal and lateral motions and the elevator-free, the rudder-free, and the aileron-free conditions. The computations were based on a set of typical airplane characteristics, except for parameters introduced to cover such variations in control-surface design as seem most likely to affect stability. The results that might be expected under corresponding conditions in airplanes with different over-all mass characteristics have also been indicated.

SYMBOLS AND COEFFICIENTS

The following symbols are used in addition to those defined in the report covers. (See figs. 1 and 2.)

The subscript c refers to a control-surface characteristic and is replaced in the various sections of the report by e for elevator, r for rudder, and a for ailerons; the subscript s refers to the control stick or wheel mechanism.

A length equal to one-half the mean wing chord is used as the fundamental unit of length in order to obtain the results in a form applicable to geometrically similar airplanes of any size or loading. Conversion to this system is made by dividing all lengths measured in ordinary units by the length of the half-wing chord. Quantities entering into nondimensional expressions do not, of course, require such conversion.

U_0 steady-flight speed

β angle of sideslip

k_c radius of gyration of control mechanism about control-surface hinge axis

$\bar{x}_c$ moment arm of center of gravity of control system about hinge axis, positive when center of gravity is behind hinge

$\bar{y}$ distance from center of gravity of aileron to plane of symmetry

A aspect ratio

l tail length of airplane

$x_{a.c.}$ projection on X axis of distance between center of gravity of airplane and its aerodynamic center (with controls fixed)

$\mu = \frac{m}{S\frac{\rho}{2}c}$ airplane density ratio

$\mu_c = \frac{m_c}{S_c\frac{\rho}{2}c_c}$ control-surface density ratio

ξ aileron weight-moment parameter. (See equation (14).)

H control-surface hinge moment

η control gearing ratio

$C_h = \frac{H}{S_c\frac{\rho}{2}U_0^2 c_c}$

$s = U_0 t$ distance along flight path

$\dot{w}$, $\dot{\delta}$, etc. $= \frac{dw}{dt}, \frac{d\delta}{dt}$, etc.

$\ddot{\theta}$, $\ddot{\delta}$, etc. $= \frac{d\theta}{dt}, \frac{d^2\delta}{dt^2}$, etc.

$D = \frac{d}{ds}$ differential operator

$C_{L_\alpha} = \frac{\partial C_L}{\partial \alpha}$; $C_{n_\beta} = \frac{\partial C_n}{\partial \beta}$; $C_{n_{D\delta}} = \frac{\partial C_n}{\partial D\delta}$; etc.

STABILITY WITH ELEVATOR FREE

Pitching motions sufficiently rapid to be affected by the inertia of the elevator control probably will not involve sensible changes in the forward speed of the airplane. Accelerations of the airplane along the flight path will therefore be neglected. The rapidity of the oscillations makes it advisable, on the other hand, to include certain aerodynamic effects not retained in the equations of motion in their usual form. In addition to the moments developed in response to the displacements of the tail surfaces, moments due to angular velocities of these surfaces are also considered. Thus, the pitching moment due to angular velocity of the elevator about its hinge $\partial M/\partial\dot{\delta}$, the pitching moment due to the aerodynamic inertia of the surfaces $\partial M/\partial\dot{w}$, and the aerodynamic damping of the elevator $\partial H/\partial\dot{\delta}$ will be included in the present analysis. Secondary factors entering into the equations, such as the vertical acceleration at the center of gravity due to the lift of the horizontal tail, are neglected. The equations of motion take the following form:

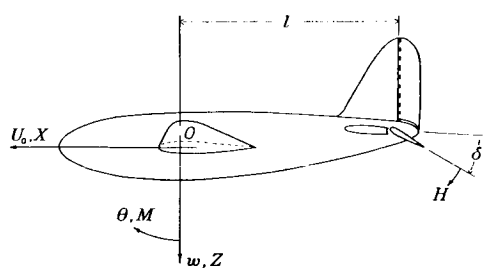

FIGURE 1.—Notation for longitudinal motions.

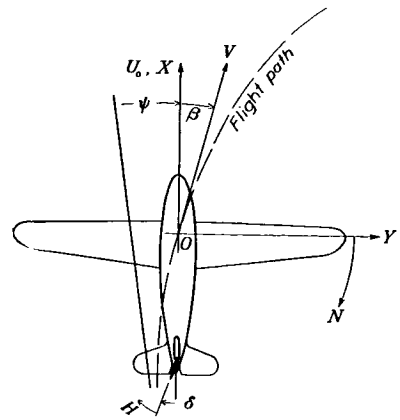

FIGURE 2.—Notation for lateral motions.

$$\left.\begin{aligned}
&m(\dot{w} - U_0\dot{\theta}) - w\frac{\partial Z}{\partial w} && = 0\\
&mk_Y^2\ddot{\theta} - \dot{\theta}\frac{\partial M}{\partial \dot{\theta}} - w\frac{\partial M}{\partial w} - \dot{w}\frac{\partial M}{\partial \dot{w}} - \delta\frac{\partial M}{\partial \delta} - \dot{\delta}\frac{\partial M}{\partial \dot{\delta}} && = 0\\
&m_e k_e^2(\ddot{\delta} + \ddot{\theta}) + m_e\bar{x}_e(l\ddot{\theta} + \dot{w} - U_0\dot{\theta}) - w\frac{\partial H}{\partial w} - \dot{\theta}\frac{\partial H}{\partial \theta}\\
&\qquad - \delta\frac{\partial H}{\partial \delta} - \dot{\delta}\frac{\partial H}{\partial \dot{\delta}} && = 0
\end{aligned}\right\} \quad (1)$$

If the following substitutions are made

$$\mu = \frac{m}{S\frac{\rho}{2}c}$$

$$\mu_e = \frac{m_e}{S_e\frac{\rho}{2}c_e}$$

$$t = \frac{s}{U_0}$$

$$D = \frac{d}{ds} = \frac{1}{U_0}\frac{d}{dt}$$

$$w = \alpha U_0$$

$$\frac{c}{2} = 1$$

and the stability derivatives are replaced by the equivalent coefficients, equations (1) are reduced to the following nondimensional form:

$$\left.\begin{aligned}
&\left(\mu D+\frac{C_{L_\alpha}}{2}\right)\alpha-\mu D\theta &&=0\\
&-(C_{m_{D\alpha}}D+C_{m_\alpha})\alpha+(\mu k_Y{}^2D-C_{m_{D\theta}})D\theta\\
&\qquad-(C_{m_{D\delta}}D+C_{m_\delta})\delta &&=0\\
&(\mu_c\bar{x}_eD-C_{h_\alpha})\alpha+[\mu_e(\bar{x}_el+k_e{}^2)D-\mu_e\bar{x}_e-C_{h_{D\theta}}]D\theta\\
&\qquad+(\mu_ek_e{}^2D^2-C_{h_{D\delta}}D-C_{h_\delta})\delta &&=0
\end{aligned}\right\} \quad (2)$$

It is to be noted that, with the exception of the independent variable s, equations (2) involve no quantities dependent on the steady-flight speed. Motions plotted against the distance s are therefore applicable to any initial flight condition within the unstalled range.

The equations of motion are based on the assumption of a constant forward velocity and therefore do not show the possibility of a phugoid oscillation of increasing amplitude or the possibility of a certain type of slow divergence from the steady-flight attitude. Experience has shown that the unstable phugoid motion is not likely to cause trouble under ordinary operating conditions because its period is of the order of 2500 chord lengths; the oscillations of interest in control-free stability have periods of the order of 50 chord lengths. The slow divergence corresponds simply to a loss of static stability when the control is free. Static stability with the elevator free is assured if the following condition is fulfilled:

$$C_{h_\delta}C_{m_\alpha}>C_{m_\delta}C_{h_\alpha} \quad (3)$$

In this paper the divergence treated is of a more rapid type.

Because the pitching that enters into the equations of motion was expected to be quite rapid, it was thought that the lag in the effect of the wing wake at the tail would be an important factor. Under steady conditions, the wing wake diminishes the relative angle of attack at the tail to about one-half. After a sudden change of angle, however, the tail will at first receive a strong upwash due to vortices shed by the wing in consequence of its additional circulation. The result is a rather complex transient variation of the vertical velocity. This variation affects both the lift of the horizontal tail and the floating moment of the elevator.

The possible effect of the transient-flow phenomenon at the tail was estimated by making several calculations in which a simple fixed lag in the action of the downwash was assumed, expressed by setting [1]

$$C_{m_\alpha}=C_{m_{\alpha_{wing}}}+C_{m_{\alpha_{tail}}}(1-\epsilon_\alpha e^{-lD}) \quad (4)$$

$$C_{h_\alpha}=C_{h_{\alpha_{tail}}}(1-\epsilon_\alpha e^{-lD}) \quad (5)$$

A comparison of the resulting motions with corresponding results obtained when the lag function was entirely omitted showed that the lag, although having a noticeable effect on certain stable modes of oscillation, caused only a small change in the slower type of oscillation in which instability occurs first. Revision of the computations to include a more accurate representation of the lag was therefore considered not worth while and all calculations were allowed to stand with $\epsilon_\alpha e^{-lD}$ as the lag operator. In order to combine this operator with other terms of the equations, the expression was expanded into a power series in D.

The stability of the motions is indicated by the nature of the roots of the characteristic equation, which is obtained from equations (2) by setting the determinant formed from the coefficients equal to zero. If $D\theta$, rather than θ, is considered one of the variables, this equation is

$$\begin{vmatrix}
\mu D+\frac{1}{2}C_{L_\alpha} & -\mu & 0\\
-C_{m_{D\alpha}}D-C_{m_\alpha}(D) & \mu k_Y{}^2D-C_{m_{D\theta}} & -C_{m_{D\delta}}D-C_{m_\delta}\\
\mu_c\bar{x}_eD-C_{h_\alpha}(D) & \mu_e(\bar{x}_el+k_e{}^2)D & \mu_ek_e{}^2D^2\\
 & -\mu_e\bar{x}_e-C_{h_{D\theta}} & -C_{h_{D\delta}}D-C_{h_\delta}
\end{vmatrix}=0 \quad (6)$$

The equation is thus a quartic, and terms introduced by the expansion of $C_{m_\alpha}(D)$ and $C_{h_\alpha}(D)$ that would increase its degree were discarded because the roots are always small and higher powers are negligible in value.

The roots of the stability equation were found for several typical cases. Apparently, in the usual case the motion is oscillatory and of two fairly distinct modes. One of the modes of oscillation, although more rapid than the modes encountered with the controls fixed, is nevertheless slow enough (with a period of the order of 60 chord lengths) to involve coupling and reinforcing movements of the airplane. The damping is consequently light, and instability will occur first in this slower mode. It is undoubtedly this mode that has been observed in flight in the cases mentioned in the introduction. The second mode is much more rapid but heavily damped. The short period (about 15 chord lengths) suggests that the motion is essentially limited to a flapping of the elevator and may become unstable only as flutter involving elastic deformations of the structure.

It was expected that variations in the aerodynamic hinge-moment slope C_{h_δ}, the mass-moment coefficient $\mu_e\bar{x}_e$, the moment-of-inertia coefficient $\mu_ek_e{}^2$, and the static stability coefficient C_{m_α} would be most important from the designer's point of view. These quantities were therefore retained in the equations as parameters, and numerical values were substituted for the remaining quantities. Limiting conditions for stability are then in the form of relations connecting the four variables.

Of the conditions for stability, only two were found to be effective within the practical range of the parameters. A boundary beyond which straight divergence

[1] For the use of the operator e^{-lD} to show the effect of lag, see reference 2, page 26. Subsequent investigation (reference 3) has shown the complex transient effect to be more nearly approximated by the operator $\epsilon_\alpha e^{-(l+\Delta)D}$.

occurs is obtained by setting the constant term of the stability equation

$$\mu(C_{h_\delta}C_{m_\alpha}-C_{m_\delta}C_{h_\alpha})+\frac{C_{L_\alpha}}{2}[C_{h_\delta}C_{m_{D\theta}}-C_{m_\delta}(C_{h_{D\theta}}+\mu_c\bar{x}_e)] \quad (7)$$

equal to zero. This expression is independent of the elevator moment of inertia. The second boundary is the limit for oscillatory stability and is obtained by applying Routh's discriminant to the stability quartic. This boundary was found to shift only a negligible amount with a large change in the static-stability coefficient C_{m_α} and was therefore considered to be independent of C_{m_α}. Partial elimination of the parameters in this way made possible the presentation of the results in a simplified form.

The computations of figure 3 were based on the characteristics of generally used types of balance and on a set

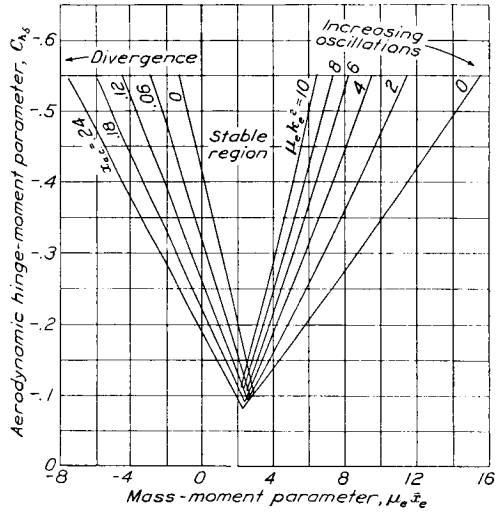

FIGURE 3.—Elevator-free stability regions. 50-percent-chord elevator; μ, 45; k_Y, 1.79.

of typical airplane characteristics. (See table I of the appendix.) The effect of variation of the moment of inertia was subsequently investigated. Figure 4 covers the case of an airplane with the radius of gyration reduced to make the moment of inertia half the average assumed for figure 3. An investigation was also made of the stability of a more heavily loaded airplane by doubling the density factor μ and comparing (fig. 5) a representative stability boundary (in terms of $\mu_c k_c^2$ and $\mu_c\bar{x}_c$) with the corresponding curve for the conditions of figure 3. The particular variations chosen were considered representative of the trends in modern airplane design.

Of the over-all characteristics of an airplane, the radius of gyration seems most likely to affect its stability. The results show that an airplane with a small radius of gyration will not permit so wide a range of the elevator design parameters as will the assumed average airplane. Its greater responsiveness to elevator deflection will cause it to reinforce more readily the movements of the elevator leading to oscillatory instability. The boundary for divergence (equation (7)) is independent of variations in the radius of gyration.

As shown in figure 5, the relative density or loading

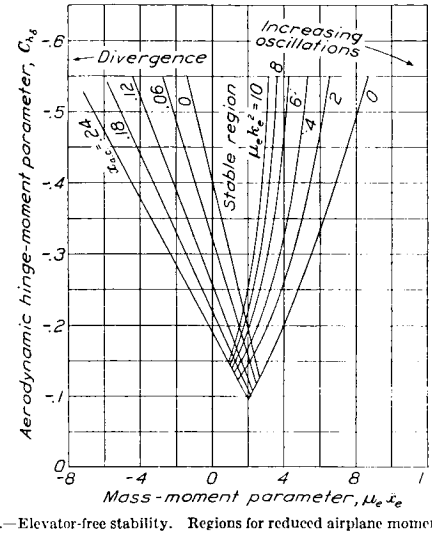

FIGURE 4.—Elevator-free stability. Regions for reduced airplane moment of inertia. 50-percent-chord elevator; μ, 45; k_Y, 1.27.

of the airplane is not a critical factor, which may be attributed to the fact that the normal relation between the lift-curve slope and the loading is such that the airplane is effectively constrained against relative motions normal to the wing surface. Differences in the

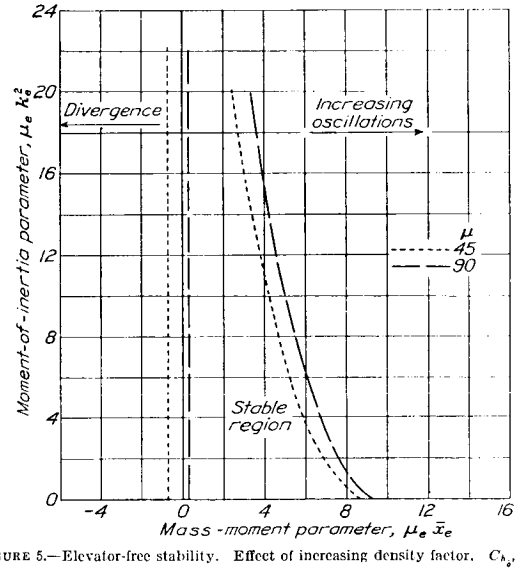

FIGURE 5.—Elevator-free stability. Effect of increasing density factor. C_{h_δ}, −0.3; $x_{a.c.}$, 0.12; k_Y, 1.79.

degree of this constraint, as caused by ordinary variations in either C_{L_α} or μ, are unimportant.

In general, it may be concluded that the design of the elevator itself is of critical importance in obtaining control-free stability. A large mass moment or moment of inertia of the control surface is seen to be unfavorable

to stability. Of primary concern, however, is the adverse effect of aerodynamic balance, especially because it is found necessary to resort to a high degree of balance with many modern airplanes.

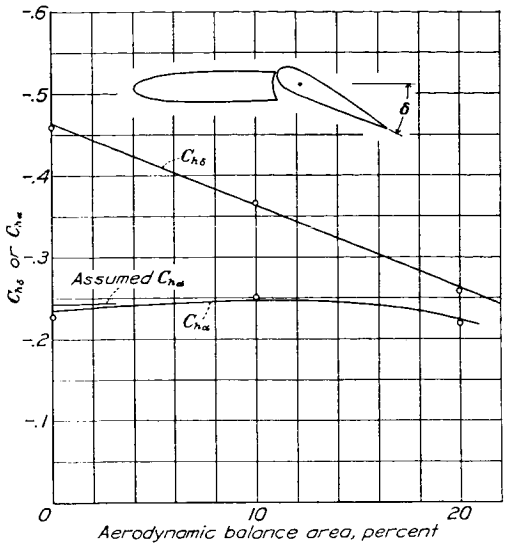

FIGURE 6.—Typical variation of C_{h_δ} and C_{h_α} with aerodynamic balance area for small deflections (from reference 4).

Figure 6 (taken from data of reference 4) shows typical hinge-moment-coefficient curves for a control flap having the inset-hinge type of balance used in most modern control systems. In these experiments, the hinge moment due to a unit change in the angle of attack

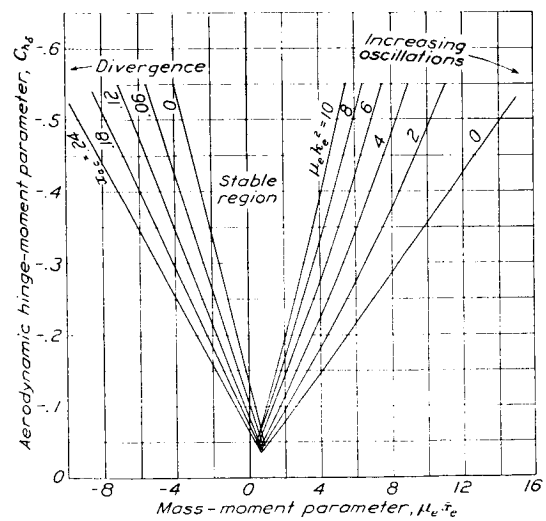

FIGURE 7.—Elevator-free stability. Regions for nonfloating elevator. 50-percent-chord elevator; μ, 45; k_Y, 1.79.

remained practically constant as the balance area was increased. This form of balance thus would not provide compensation for the floating moment C_{h_α} in the same proportion as for the restoring moment C_{h_δ} and, as the degree of balance was increased, the equilibrium floating angles would become increasingly large, so that there would be greater danger of static instability with controls free, as shown in equation (3). The same considerations apply to the balancing tab.

On the other hand, it should be possible to compensate for the floating pressure in the same or, perhaps, in a greater proportion than the proportion of reduction of the restoring moment. Thus, with a horn type of balance, for example, the equilibrium floating angles may be held constant or may even be reduced, which results in greater static stability.[2] A comparison of figure 3 ($C_{h_{\alpha_{tail}}} = -0.24$) with figure 7 ($C_{h_{\alpha_{tail}}} = 0$) shows that decreasing the floating moment also decreases the likelihood of rapid divergence. The boundary for oscillatory stability is hardly influenced by this factor.

The computations for either type of balance apply to an elevator operated by a servo tab, provided that

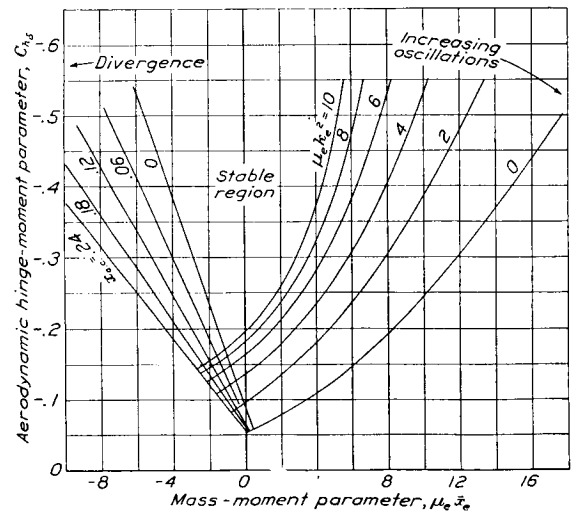

FIGURE 8.—Elevator-free stability. Regions for reduced elevator chord. 25-percent-chord elevator; μ, 45; k_Y, 1.79.

the tab remains fixed relative to the elevator during the oscillations. Thus, as far as stability is concerned, servo operation with controls fixed corresponds to the ordinary control-free condition. The stability with both elevator and servo tab free is not covered in the present study.

Future designs will probably show a trend toward narrower control surfaces, whether balanced or not, because the basic hinge moments can be markedly reduced with a small loss of effectiveness. If the chord of the elevator is reduced from 50 percent to 25 percent of that of the horizontal tail surface, its effectiveness is reduced by only 30 percent; whereas, the basic hinge moment is divided by 4.

Figure 8 shows the regions of stability with a reduced

[2] Another advantage of the horn type of balance is that the hinge gap may be sealed. The subject of horn balances is discussed further by Hemphill in reference 5.

elevator chord. The differences between these regions and those of figure 3 are principally due to changes in the coefficients $\partial C_h/\partial\alpha$, $\partial C_h/\partial D\delta$, and $\partial C_m/\partial D\delta$. As previously noted, the control moment (proportional to $\partial C_m/\partial\delta$) is reduced by only 30 percent. In the interpretation of this figure, it should be borne in mind that the ratios $\bar{x}_e$ and k_e would naturally be smaller for the narrower elevator. If account were taken of this scale factor, the region of stability would appear much wider than the region for the 50-percent elevator.

An effective method of obtaining greater stability in the control-surface motions is the introduction of additional damping into the system. If the responsiveness of the control surface is reduced, a considerably larger degree of aerodynamic balance may be used (fig. 9). The permissible mass unbalance is also increased, although to a lesser extent. The results

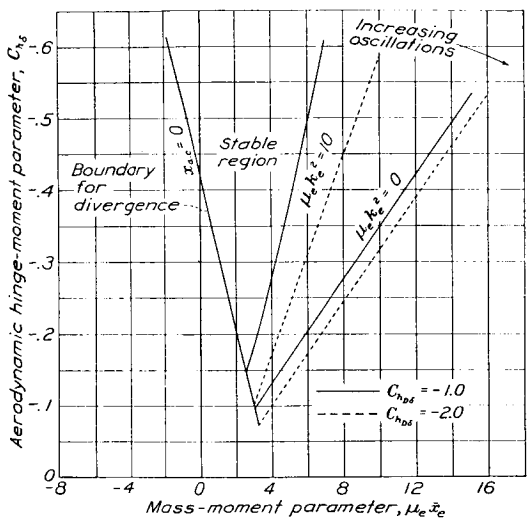

FIGURE 9.—Elevator-free stability regions. Effect of additional damping in the control system. 50-percent-chord elevator; μ, 45; k_Y, 1.79.

shown are for a comparatively small amount of damping ($\Delta C_{h_{D\delta}} = -1.0$), which corresponds, for a rate of deflection of 20° per second, to the force required of the pilot to maintain 1° of elevator deflection.

STABILITY WITH RUDDER FREE

Because the lateral motions involve two controls and five degrees of freedom, the analysis is more complex than for the longitudinal motion, which has one control and three degrees of freedom. Fortunately, the rudder and the ailerons exert their principal influences on different modes and only a slight loss in accuracy is incurred if each mode is treated separately.

Oscillation of the rudder control will be primarily influenced by coupling with the yawing oscillations of the airplane. The small rolling oscillations simultaneously induced will generate neither very strong yawing moments nor very strong rudder hinge moments; hence, the rolling degree of freedom will be neglected in the examination of rudder-free stability. This assumption, which has been checked quantitatively by Bartsch (reference 1), reduces the simultaneous equations of motion to the following form:

$$\left.\begin{aligned} &mU_0(\dot{\psi}+\dot{\beta})-\beta\frac{\partial Y}{\partial\beta} &&=0\\ &mk_z^2\ddot{\psi}-\dot{\psi}\frac{\partial N}{\partial\dot{\psi}}-\beta\frac{\partial N}{\partial\beta}-\delta\frac{\partial N}{\partial\delta}-\dot{\delta}\frac{\partial N}{\partial\dot{\delta}} &&=0\\ &m_r k_r^2(\ddot{\psi}+\ddot{\delta})-m_r\bar{x}_r U_0(\dot{\psi}+\dot{\beta})+lm_r\bar{x}_r\ddot{\psi}-\beta\frac{\partial H}{\partial\beta}-\delta\frac{\partial H}{\partial\delta}\\ &\qquad -\dot{\delta}\frac{\partial H}{\partial\dot{\delta}}-\dot{\psi}\frac{\partial H}{\partial\dot{\psi}} &&=0 \end{aligned}\right\} \quad (8)$$

If substitutions corresponding to those introduced in the elevator calculations are made, the equations are reduced to the following nondimensional form:

$$\left.\begin{aligned} &\left(\mu D-\frac{C_{Y_\beta}}{2}\right)\beta+\mu D\psi &&=0\\ &-C_{n_\beta}\beta+\left(\frac{\mu k_Z^2 D}{A}-C_{n_{D\psi}}\right)D\psi-(C_{n_{D\delta}}D+C_{n_\delta})\delta &&=0\\ &-(\mu_r\bar{x}_r D+C_{h_\beta})\beta+[\mu_r(k_r^2+\bar{x}_r l)D-(C_{h_{D\psi}}+\mu_r\bar{x}_r)]D\psi\\ &\qquad +(\mu_r k_r^2 D^2-C_{h_{D\delta}}D-C_{h_\delta})\delta &&=0 \end{aligned}\right\} \quad (9)$$

The stability equation is

$$\begin{vmatrix} -\mu D+\frac{C_{Y_\beta}}{2} & \mu & 0\\ C_{n_\beta} & \frac{\mu k_Z^2 D}{A}-C_{n_{D\psi}} & -(C_{n_{D\delta}}D+C_{n_\delta})\\ \mu_r\bar{x}_r D+C_{h_\beta} & \mu_r(k_r^2+\bar{x}_r l)D-(C_{h_{D\psi}}+\mu_r\bar{x}_r) & \mu_r k_r^2 D^2-C_{h_{D\delta}}D-C_{h_\delta} \end{vmatrix}=0 \quad (10)$$

This equation is closely analogous to equation (6) for longitudinal motion. The corresponding coefficients have similar values with the exception of C_{Y_β}, which is much smaller than the corresponding term C_{L_α} because the normal force that is developed by the wing in pitching is absent in the lateral motions.

The roots of the stability equation again indicate two modes of motion. Thus, in a typical case, the roots are $-0.008\pm0.035i$ and $-0.25\pm0.28i$. In this instance, the modes are both oscillatory. The first pair of roots indicates a lightly damped oscillation of such a frequency (period≅90 chord lengths) as to involve sensible coupling between the yawing of the airplane and the swinging of the rudder. The second mode is of much higher frequency and undoubtedly represents the natural oscillation of the rudder with the airplane acting as a practically rigid support. When the restoring moment C_{h_δ} is reduced, the second mode becomes aperiodic and eventually divergent as the motion becomes less rapid. Oscillatory instability appears first in the slower mode, as in the case of the elevator.

The calculations of the stability boundaries covered changes in rudder chord, changes in the airplane moment of inertia mk_Z^2, and changes in the weathercock stability factor C_{n_β}. Additional calculations were made to show the action of a nonfloating type of rudder.

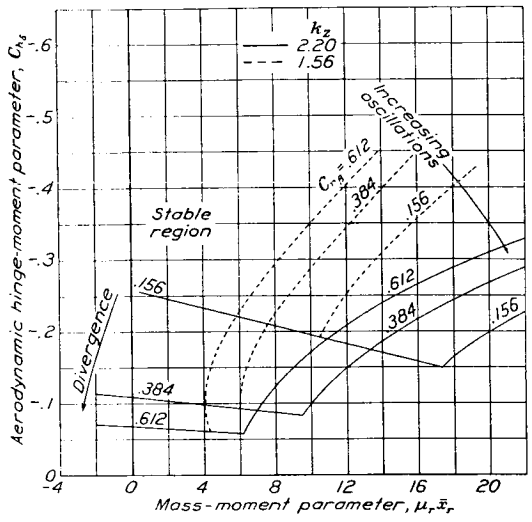

FIGURE 10.—Rudder-free stability. Minimum regions ($0<\mu_r k_r^2<8$). 50-percent-chord rudder; μ, 45.

Variations in the density factor μ were considered insignificant, this quantity entering the equations independently only in conjunction with the small side-force derivative C_{Y_β}.

A simplification corresponding to the elimination of

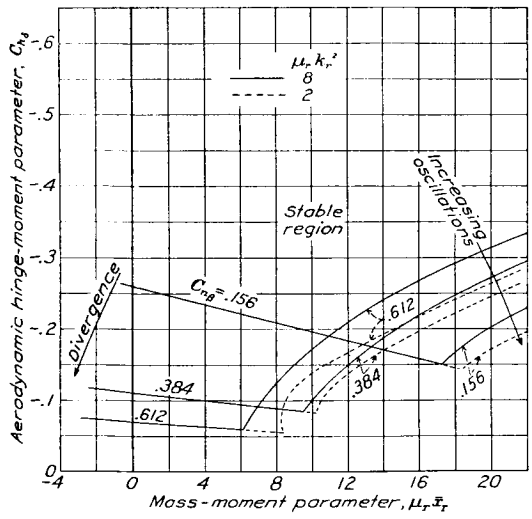

FIGURE 11.—Rudder-free stability. Variation of boundaries with moment of inertia of rudder. 50-percent-chord rudder; μ, 45; k_Z, 2.20.

C_{m_α} as a parameter of the oscillatory stability boundary was not found possible in these equations. Plots of Routh's discriminant for rudder-free motion show it to be noticeably dependent on all four parameters, the least effective being the moment of inertia of the rudder system. Since the permissible mass moment is smaller for larger values of $\mu_r k_r^2$, an upper practical limit ($\mu_r k_r^2<8$) was assumed for this parameter and the resulting family of curves was plotted to give the minimum regions for stability in terms of C_{h_δ}, $\mu_r\bar{x}_r$,

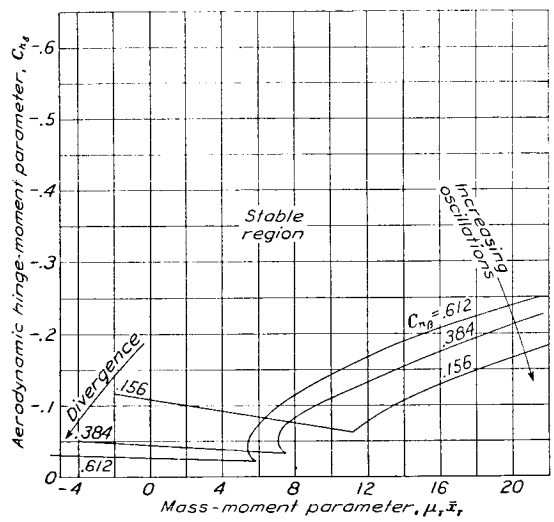

FIGURE 12.—Rudder-free stability. Minimum regions for reduced rudder chord ($0<\mu_r k_r^2<8$). 25-percent-chord rudder; μ, 45; k_Z, 2.20.

and C_{n_β} (figs. 10, 12, and 13). The margin beyond these minimum regions, for values of $\mu_r k_r^2$ less than 8, is indicated by figure 11, in which the corresponding curves for $\mu_r k_r^2=8$ and $\mu_r k_r^2=2$ are plotted.

The charts show the weathercock stability of the air-

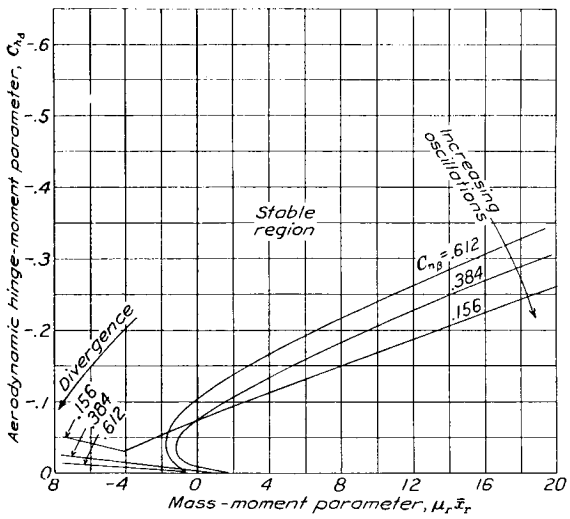

FIGURE 13.—Rudder-free stability. Minimum regions for nonfloating rudder. ($0<\mu_r k_r^2<8$). 50-percent-chord rudder; μ, 45; k_Z, 2.20.

plane to be of greater importance in the case of lateral motion than in the case of longitudinal motion. The effect of the moment of inertia of the control surface, which determined the degree of oscillatory stability in longitudinal motion, is small relative to the effect of

C_{n_β}. The greater the value of C_{n_β}, the less is the allowable mass moment with any given amount of aerodynamic balance. On the other hand, if the mass moment is small enough to insure damping of the oscillations, a larger value of C_{n_β} will increase the aerodynamic balance that may be introduced without causing divergence. The radius of gyration of the airplane is of considerable importance, shifting the boundary for oscillatory stability so as very nearly to double the stable region when the moment of inertia is doubled. (See fig. 10.)

Instability with the rudder free is likely to occur in the form of a divergence. The criterion is practically the same as the condition for weathercock stability with the control free, which is

$$C_{h_\delta}C_{n_\beta}-C_{h_\beta}C_{n_\delta}\geqq 0 \tag{11}$$

This criterion is independent of the moments of inertia of the airplane and of the control surface. The greatest

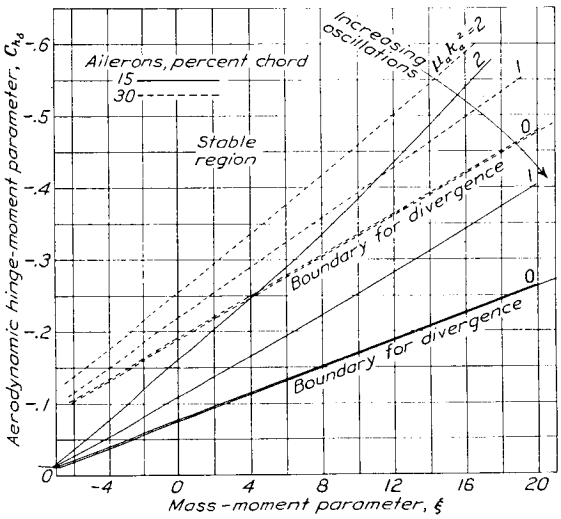

FIGURE 14.—Aileron-free stability boundaries. μ, 45; k_X, 1.80.

gain in this margin of stability is obtained by increasing C_{n_β} and reducing the floating tendency C_{h_β} of the rudder. Reducing the chord of the rudder decreases both C_{h_β} and C_{n_δ} and hence considerably widens the margin of stability. (See fig. 12.) Complete elimination of C_{h_β} by the use of a nonfloating type of balance eliminates the likelihood of divergence within the normal range of weight distribution (fig. 13). Such a gain, however, would be achieved only by sacrificing some margin of oscillatory stability.

The lateral oscillations of an airplane with controls fixed are known to be influenced by coupling between the rolling and the yawing motions. These oscillations tend to become undamped when the weathercock stability C_{n_β} approaches zero. Freeing the rudder control diminishes C_{n_β} and may thus lead to this type of oscillatory instability. The condition for zero weathercock stability is approximately that for straight divergence in the control-free condition (equation (11)) and the boundaries for divergence (figs. 10 to 13) can therefore be interpreted also as boundaries for stability of the slow lateral oscillation, when the airplane is free to roll. The absence in the criterion of terms involving the mass of the rudder may be explained by the fact that, as the limit of stability is approached, the oscillation becomes very slow and the yawing component tends to disappear.

STABILITY WITH AILERONS FREE

The stability of an airplane with the ailerons free is examined by including in the equations the interaction between rolling motions of the airplane and movements of the ailerons. Small simultaneous yawing and sideslipping motions will also occur but, because their reactions on the rolling and the hinge moments are small, they may be neglected. The resulting equations are:

$$\left.\begin{aligned} mk_X^2\frac{dp}{dt}-p\frac{\partial L}{\partial p}-\delta\frac{\partial L}{\partial \delta}-\dot{\delta}\frac{\partial L}{\partial \dot{\delta}} &=0\\ m_ak_a^2\frac{d^2\delta}{dt^2}-p\frac{\partial H}{\partial p}-\frac{dp}{dt}(m_a\overline{yx}+\eta m_sk_s^2)-\delta\frac{\partial H}{\partial \delta}-\dot{\delta}\frac{\partial H}{\partial \dot{\delta}} &=0\end{aligned}\right\} \tag{12}$$

or, in nondimensional form,

$$\left.\begin{aligned} \left(\frac{\mu k_X^2}{A}D-C_{l_{D\phi}}\right)D\phi-(C_{l_{D\delta}}D+C_{l_\delta})\delta &=0\\ (\xi D-C_{h_{D\phi}})D\phi+(\mu_ak_a^2D^2-C_{h_{D\delta}}D-C_{h_\delta})\delta &=0\end{aligned}\right\} \tag{13}$$

In the aileron control, a part of the mechanism normally rotates about an axis at right angles to the aileron hinge axis. As a result, a part of the aileron torque produced by angular acceleration of the airplane is proportional to the product of inertia of the aileron itself and another part is proportional to the moment of inertia of the control stick or wheel. Both quantities are included in the parameter ξ. Thus:

$$\xi=\frac{m_a\overline{yx}+\eta m_sk_s^2}{S_a\frac{\rho}{2}c_a} \tag{14}$$

where the subscript s refers to the control stick and η is a constant inserted to take account of any difference of gearing between the control and the aileron.

The calculations, based on values of the derivatives given in the appendix, cover two aileron widths: 15 percent and 30 percent of the wing chord. In both cases, the ailerons were assumed to cover 50 percent of the wing semispan.

Variations in the floating tendency of the aileron were also considered but were found to have little effect on the stability. The results given may therefore be applied to any of the existing types of balance that give smooth hinge-moment curves.[3]

The boundaries for stability in the two possible modes are presented in figure 14. Instability appears

[3] Certain ailerons of the Frise type that show a reversal of the hinge-moment slope may develop uncontrollable oscillations of fixed amplitude. This condition is discussed in reference 6.

in the form of increasing oscillations and is most likely to occur when the ailerons have a high degree of aerodynamic balance and too great a mass moment or moment of inertia. As the moment of inertia decreases, the boundary for undamped oscillations approaches that for straight divergence (which is itself independent of the moment of inertia), and it becomes possible for both types of instability to exist simultaneously. The condition to prevent straight divergence,

$$C_{l_\delta}\xi - C_{h_{D_\phi}}C_{l_{D\delta}} - C_{l_{D\phi}}C_{h_{D\delta}} - \frac{1}{A}C_{h_\delta}\mu k_X^2 > 0 \qquad (15)$$

is, however, always satisfied when there is damping of the oscillations.

Straight divergence, as encountered in the elevator-free and the rudder-free conditions, is indicated when the constant term of the stability equation is negative, that is, when

$$C_{l_{D\phi}}C_{h_\delta} \gtrless C_{h_{D\phi}}C_{l_\delta} \qquad (16)$$

This condition is not likely to occur unless the aerodynamic balance is nearly complete.

CONCLUDING REMARKS

Experience has shown that, before the actual limit of stability is reached, the airplane undergoes oscillations which, although damped, are still persistent enough to be undesirable. The boundaries given in the stability charts are therefore of value chiefly as indications of the effect of certain design factors; they are useful quantitatively only as outside limits, not to be approached too closely. Further experiments will be necessary to determine the margin of stability required for smooth operation in gusty air.

On the other hand, the charts are to a certain extent conservative because they do not take into account the possibility of friction of the control system, a factor that would widen the margin of stability.

The indications of the present study may be summarized as follows:

1. There is a limit to the effectiveness of the aerodynamic balance that may be safely employed with any conventional control system. In most cases, it appears difficult to secure stability with the hinge moment reduced to less than 25 percent of its value for the unbalanced surface.

2. Reduction of the floating moment C_{h_α}, if it can be brought about independently of a reduction of the aerodynamic balance, causes a shift of the boundary for divergence. (Cf. figs. 3 and 7 and figs. 12 and 13.) The effect is particularly noticeable in the case of the rudder, where the likelihood of this form of instability is materially decreased.

3. Within the usual range of characteristics, the elevator and the aileron controls are more susceptible to oscillatory instability than to the rapid form of divergent instability. The stability with either of these controls free may be improved by (*a*) using a less effective aerodynamic balance, (*b*) decreasing the mass moment and the moment of inertia of the control, or (*c*) using a control surface of narrow chord.

4. Divergence is a more likely form of instability for the rudder control (figs. 10 and 11) and may be avoided by reducing the effectiveness of the aerodynamic balance or, as has been suggested, by using a balance that reduces the floating tendency of the rudder, although a highly effective balance of a type that reduces the floating tendency may result in oscillatory instability.

5. The oscillatory stability of the elevator-free system is but little affected by the restoring moment of the airplane in pitch (C_{m_α}). In the case of the yawing motions, however, the existence of a strong restoring moment (C_{n_β}) increases the likelihood of oscillatory instability. (See, for example, fig. 10.)

6. In all cases, an increase in the relative radius of gyration of the airplane results in an increased range of stability (cf. figs. 3 and 4; see also fig. 10), but changes in weight without corresponding changes in the rotary inertia have little effect. (See fig. 5.)

7. The use of a narrow control surface is recommended as a means of increasing the control-free stability as well as from other considerations. The marked effect of reducing the chord is shown by a comparison of figure 8 with figure 3 and of figure 12 with figure 10.

LANGLEY MEMORIAL AERONAUTICAL LABORATORY,
NATIONAL ADVISORY COMMITTEE FOR AERONAUTICS,
LANGLEY FIELD, VA., *August 15, 1940.*

APPENDIX

STABILITY DERIVATIVES

The geometric and the aerodynamic characteristics used in the stability calculations are given in tables I to IV.

TABLE I.—GENERAL AIRPLANE CHARACTERISTICS

$\frac{\text{Tail length}}{\text{Wing chord}}$	2.75
$\frac{\text{Horizontal-tail area}}{\text{Wing area}}$	.153
$\frac{\text{Vertical-tail area}}{\text{Wing area}}$	.06
$\frac{\text{Horizontal-tail chord}}{\text{Wing chord}}$	.50
$\frac{\text{Vertical-tail chord}}{\text{Wing chord}}$	.333
$\frac{\text{Aileron chord}}{\text{Wing chord}}$	.15
$\frac{\text{Aileron span}}{\text{Wing semispan}}$	.50
Wing aspect ratio	6
Horizontal-tail aspect ratio	3.75
Vertical-tail aspect ratio	3.00

TABLE II.—ELEVATOR-FREE STABILITY COEFFICIENTS

	50-percent-chord elevator	25-percent-chord elevator
C_{L_α}	4.3	4.3
$C_{m_{D\theta}}$	−9.26	−9.26
$C_{m_{\alpha_{wing}}}$	4.3(0.135−$x_{a.c.}$)	4.3(0.135−$x_{a.c.}$)
$C_{m_{\alpha_{tail}}}$	−1.121	−1.121
$C_{m_{D\alpha}}$	−1.450	−1.450
C_{m_δ}	−.960	−.672
$C_{m_{D\delta}}$	−.57	−.23
$C_{h_{D\delta}}$	−1.00	−.50
$C_{h_{D\theta}}$	−1.33	−.406
$C_{h_{\alpha_{tail}}}$	−0.24 and 0	−.075

TABLE III.—RUDDER-FREE STABILITY COEFFICIENTS

	50-percent-chord rudder	25-percent-chord rudder
C_{Y_β}	−0.274	−0.274
$C_{n_{D\psi}}$	−.582	−.582
C_{n_δ}	−.0567	−.0397
$C_{n_{D\delta}}$	−.0460	−.0175
$C_{h_{D\psi}}$	−.883	−.276
C_{h_β}	.123	.075
$C_{h_{D\delta}}$	−1.00	−.50

TABLE IV.—AILERON-FREE STABILITY COEFFICIENTS

	15-percent-chord aileron	30-percent-chord aileron
$C_{l_{D\phi}}$	−2.94	−2.94
C_{l_δ}	−.229	−.352
$C_{l_{D\delta}}$	−.110	−.295
$C_{h_{D\phi}}$	−.184	−.322
$C_{h_{D\delta}}$	−.650	−1.587

The aerodynamic coefficients are, in most cases, based on experimental results; theoretical values are used only where such results were not established. Discussions of the more commonly used derivatives will be found in references 7, 8, and 9. Several of the unfamiliar coefficients are developed in the following paragraphs.

Damping in pitching $C_{m_{D\theta}}$.—The principal component of damping in pitching, furnished by the horizontal tail, is

$$-\frac{l\dot{\theta}}{U_0}\frac{S_t l}{Sc}C_{L_{\alpha_t}}$$

In addition, the pitching motion introduces a relative camber of the wing section, giving rise to a moment coefficient

$$-\frac{\pi}{4}\frac{\dot{\theta}c}{2U_0}$$

Thus

$$C_m=-\frac{l\dot{\theta}}{U_0}\left(\frac{S_t l}{Sc}C_{L_{\alpha_t}}+\frac{\pi}{4}\frac{c}{2l}\right)$$

Then, since

$$\frac{l\dot{\theta}}{U_0}=\frac{2l}{c}D\theta$$

$$C_{m_{D\theta}}=-\left[2\frac{S_t}{S}\left(\frac{l}{c}\right)^2 C_{L_{\alpha_t}}+\frac{\pi}{4}\right]$$

Pitching-moment slope C_{m_α}.—The pitching-moment slope is given by

$$C_{m_\alpha}=-C_{L_\alpha}\frac{x_{a.c.}}{2}+C_L\frac{z_{a.c.}}{2}$$

where $x_{a.c.}$ and $z_{a.c.}$ are the distances of the aerodynamic center of the complete airplane behind and below the center of gravity. The location of the aerodynamic center for the airplane as a whole is estimated by taking the centroid of the aerodynamic centers of the various components. Thus, if terms in $z_{a.c.}$ (which is usually small) are neglected,

$$x_{a.c.}=x_{a.c._{wing}}+\frac{\alpha_t}{\alpha}\frac{C_{L_{\alpha_t}}}{C_{L_\alpha}}\frac{S_t}{S}\quad x_{a.c._{tail}}$$

Pitching-moment coefficient due to vertical acceleration $C_{m_{D\alpha}}$.—The pitching-moment coefficient due to vertical acceleration arises from the aerodynamic inertia of the wing and the horizontal tail surfaces in motion normal to their chords. The force on each surface is equal to the reaction of a body of air described by rotating the surface about its midchord line. Thus, the pitching moment

$$M=\left[\pi\rho\left(\frac{c}{2}\right)^2 bx_{50}+\pi\rho\left(\frac{c_t}{2}\right)^2 b_t x_{50_t}\right]\frac{dw}{dt}$$

and

$$C_m=\left[\frac{x_{50}}{c}+\frac{x_{50_t}}{c}\left(\frac{b_t c_t}{bc}\right)^2\right]\pi D\alpha$$

where x_{50} is the distance from the 50-percent-chord point of the wing to the center of gravity of the airplane and x_{50_t} is the same distance measured from the corresponding point of the horizontal tail.

Pitching moment due to elevator deflection C_{m_δ}.—The pitching moment due to elevator deflection is given by the formula

$$C_{m_\delta}=\frac{\partial C_m}{\partial\delta}=\frac{\partial\alpha_e}{\partial\delta}C_{L_{\alpha_t}}\frac{-S_t}{S}\frac{l}{c}$$

where α_e is the angle of zero lift of the elevator.

Theoretical and experimental values for $\partial\alpha_e/\partial\delta$, for flaps with sealed hinges, are given in figure 15. The coefficients used in these calculations (C_{n_δ} and C_{l_δ} as well as C_{m_δ}) were, however, based on the experimentally determined changes of lift produced by a flap with open gaps at the hinges. The effect of a small gap is to reduce the effectiveness of the flap by about 30 percent. At a large deflection, the flap with inset-hinge balance shows a still greater loss because of the protruding balance portion.

Pitching-moment coefficient due to angular velocity of the elevator $C_{m_{D\delta}}$.—The pitching-moment coefficient due to angular velocity of the elevator is

$$C_{m_{D\delta}}=\frac{dC_{L_t}}{dD\delta}\frac{S_t}{S}\frac{l}{c}$$

where

$$\frac{dC_{L_t}}{dD\delta}=\frac{\partial C_{L_t}}{\partial D\delta}+\frac{\partial\alpha_e}{\partial D\delta}\frac{dC_{L_t}}{d\alpha_t}$$

The parameters $\partial C_{L_t}/\partial D\delta$ and $\partial\alpha_e/\partial D\delta$ may be found as functions of the chordwise position of the hinge from figure 15. The figure is based on the theoretical treatment of Theodorsen (reference 7), with the assumption of long oscillations (greater than 20 chord lengths). It must be remembered that $D\delta$ involves the distance traveled by the airplane measured in terms of its half-wing chord, and the quantities given must be multiplied by the ratio c_t/c_w to convert them to half-wing chord lengths.

Damping moment of elevator $C_{h_{D\delta}}$.—The hinge moment due to angular velocity is treated theoretically by Theodorsen in reference 7. Figure 16, derived from the theory, gives the component parameters of the damping moment as functions of the chordwise position of the hinge. The same considerations are effective here as in the application of figure 15.

Hinge moment due to pitching $C_{h_{D\theta}}$.—Positive pitching motion causes an increase in the angle of attack of the tail surface equal to $l\dot{\theta}/U_0$. The resulting hinge-moment coefficient is

$$\frac{l\dot{\theta}}{U_0}C_{h_{\alpha_{tail}}}$$

and, since

$$\frac{l\dot{\theta}}{U_0}=\frac{2l}{c}D\theta$$

$$C_{h_{D\theta}}=\frac{2l}{c}C_{h_{\alpha_{tail}}}$$

Inasmuch as rotation of the airplane about its center of gravity does not appreciably change the lift of the wing, the downwash correction may be neglected.

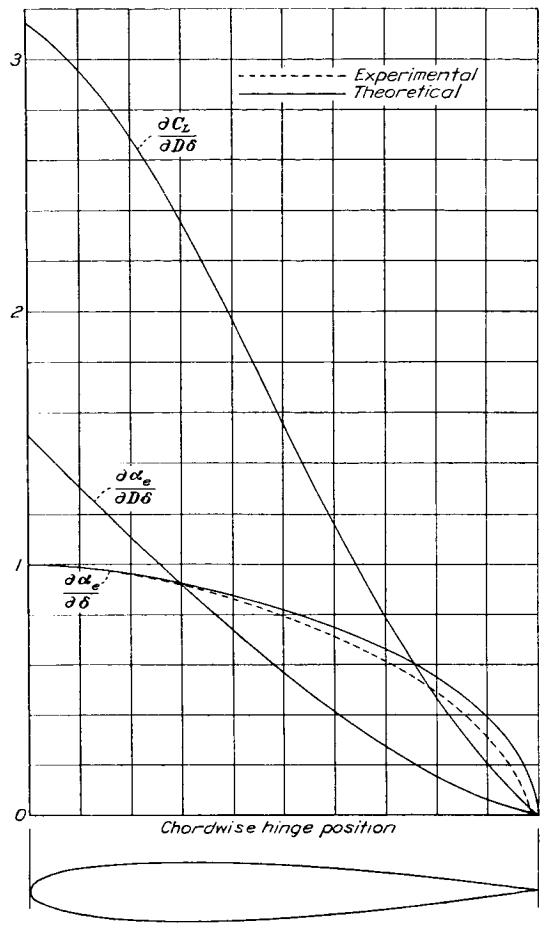

FIGURE 15.—Parameters for determining the effects of angular velocity and deflection of flaps on the lift.

$$C_L=D\delta\frac{\partial C_L}{\partial D\delta}+D\delta\frac{\partial C_L}{\partial\alpha}\frac{\partial\alpha_e}{\partial D\delta}+\delta\frac{\partial C_L}{\partial\alpha}\frac{\partial\alpha_e}{\partial\delta}$$

Hinge moment due to change in angle of attack C_{h_α}.—In accordance with the indications of tests by Goett and Reeder (reference 4), the aerodynamic floating moment $C_{h_{\alpha_{tail}}}$ was assumed independent of the degree of aerodynamic balance of the control surface

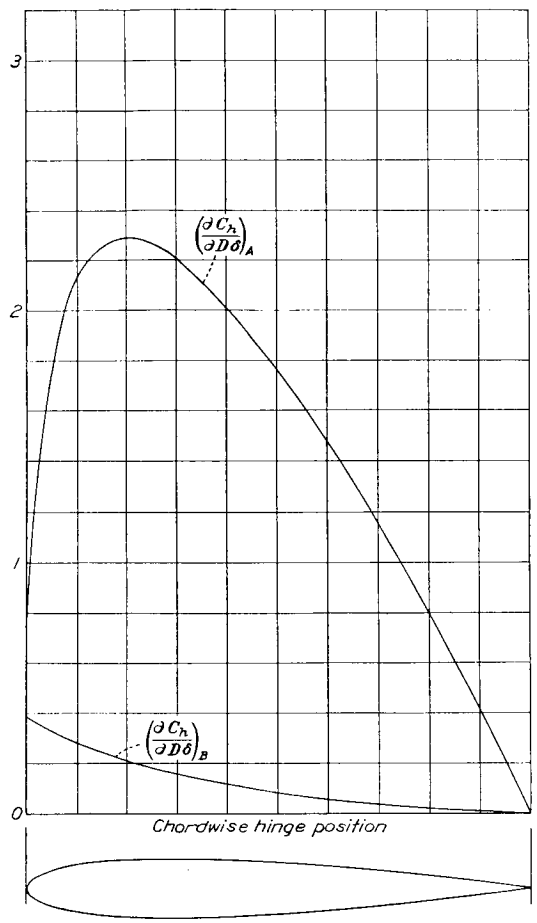

FIGURE 16.—Parameters for determining the damping moments of flaps.

$$C_{h_D} = \left(\frac{\partial C_h}{\partial D\delta}\right)_A + \frac{dC_L}{d\alpha}\left(\frac{\partial C_h}{\partial D\delta}\right)_B$$

(fig. 6). The assumption is valid for the inset-hinge type of balanced flap shown in this figure. The floating moment will vary with the type of balance, however, as discussed in the text, and additional computations were therefore made in which $C_{h_{\alpha_{tail}}}$ was assumed equal to zero.

The lateral-stability derivatives C_{Y_β}, C_{n_β}, $C_{n_{D\psi}} = \frac{\partial C_n}{\partial \frac{rc}{2U_0}}$, and $C_{l_{D\phi}} = \frac{\partial C_l}{\partial \frac{pc}{2U_0}}$ are discussed in references 8 and 9. The other coefficients for the lateral motions are derived in a manner closely analogous to the derivation of the corresponding longitudinal coefficients.

The values of the mass moment and the moment-of-inertia coefficients of several representative elevator-control systems were determined experimentally in order to find the magnitude and the range to be expected in practice. The experiments were made by attaching a spring of known stiffness to the control column, oscillating the system, and recording the frequency and the damping. The mass moment was measured directly with a spring scale. The interpreted results are given in the following table:

Airplane	$\mu_e \overline{x}$	$\mu_e k_e^2$
North American BT-9	2.70	1.35
Curtiss P-36	0	.90
Lockheed 12	9.5	4.5
Fairchild 22	3.0	1.1

REFERENCES

1. Bartsch, Edmund: Wende- und Rollschwingungen eines Flugzeugs. Jahrb. 1938 der deutschen Versuchsanstalt für Luftfahrt, E. V., Berlin-Adlershof, pp. 179–194.
2. Jeffreys, Harold: Operational Methods in Mathematical Physics. Cambridge Tracts in Mathematics and Mathematical Physics, No. 23, 2d ed., Cambridge Univ. Press, 1931.
3. Jones, Robert T., and Fehlner, Leo F.: Transient Effects of the Wing Wake on the Horizontal Tail. T. N. No. 771, NACA, 1940.
4. Goett, Harry J., and Reeder, J. P.: Effects of Elevator Nose Shape, Gap, Balance, and Tabs on the Aerodynamic Characteristics of a Horizontal Tail Surface. Rep. No. 675, NACA, 1939.
5. Hemphill, T. M.: Control Surface Hinge Moments and Their Relation to Stability. Paper presented before Inst. Aero. Sci., New York, Jan. 26, 1940.
6. Pugsley, A. G.: Aileron Stability, with Special Reference to Rolling-Aileron Motion and the Influence of Frise Type Hinge Moment Curves. R. & M. No. 1595, British A. R. C., 1934.
7. Theodorsen, Theodore: General Theory of Aerodynamic Instability and the Mechanism of Flutter. Rep. No. 496, NACA, 1935.
8. Zimmerman, Charles H.: An Analysis of Lateral Stability in Power-Off Flight with Charts for Use in Design. Rep. No. 589, NACA, 1937.
9. Weick, Fred E., and Jones, Robert T.: The Effect of Lateral Controls in Producing Motion of an Airplane as Computed from Wind-Tunnel Data. Rep. No. 570, NACA, 1936.

REPORT NO. 722

A GRAPHICAL METHOD OF DETERMINING PRESSURE DISTRIBUTION IN TWO-DIMENSIONAL FLOW

Robert T. Jones and Doris Cohen

Langley Memorial Aeronautical Laboratory

1941

REPORT No. 722

A GRAPHICAL METHOD OF DETERMINING PRESSURE DISTRIBUTION IN TWO-DIMENSIONAL FLOW

By Robert T. Jones and Doris Cohen

SUMMARY

By a generalization of the Joukowski method, a procedure is developed for effecting localized modifications of airfoil shapes and for determining graphically the resultant changes in the pressure distribution. The application of the procedure to the determination of the pressure distribution over airfoils of original design is demonstrated. Formulas for the lift, the moment, and the aerodynamic center are also given.

INTRODUCTION

It is possible, by a simple geometric construction, to modify any given streamline shape in such a way that the effect of the modification on the pressure distribution, the lift, and the moment can be readily determined. The construction is essentially that used in deriving the familiar Joukowski airfoils from a circle (reference 1) although it may be applied to an airfoil shape to introduce modifications of the outline. The method is based on the concept of complex numbers but its application requires no familiarity with them.

By two or more successive applications of the construction to a circle, it is possible to derive shapes of such diversity as to permit the approximation of nearly any airfoil of current design. For the airfoil derived in this way the pressure distribution can be determined exactly, so that the only error likely to occur is in the reproduction of the exact airfoil shape. Any inaccuracy in this approximation is immediately apparent and can be made as small as is considered desirable.

MODIFICATION OF AN AIRFOIL

The method consists entirely in applications of a single construction; desired effects are obtained by the proper choice of a parameter k and of the location of the axes with respect to the figure to be transformed. This basic construction applied to an airfoil surface is demonstrated in figure 1. In order to find the point z_a on the modified airfoil to correspond to a point z on the original airfoil, the vector Oz is drawn from the origin and the vector $O\frac{k^2}{z}$ is added to it. The vector $O\frac{k^2}{z}$, which will be termed the "reciprocal" vector, is constructed with its length equal to k^2 times the reciprocal of the length of Oz and at an angle $-\phi$ with the x-axis, where ϕ is the angle made with this axis by Oz. A point of the modified airfoil, then, is located by the resultant of the vector Oz and its reciprocal vector.

The construction by which a figure is modified applies equally well to all its streamlines, altering them to conform to the distortion. The change in spacing of the streamlines near the boundary of the figure will show directly the effect of the transformation on the velocity in that region because the velocity varies inversely with the spacing. The factor by which the elements of length near a point z are changed may be shown to be the ratio of the length of the diagonal from

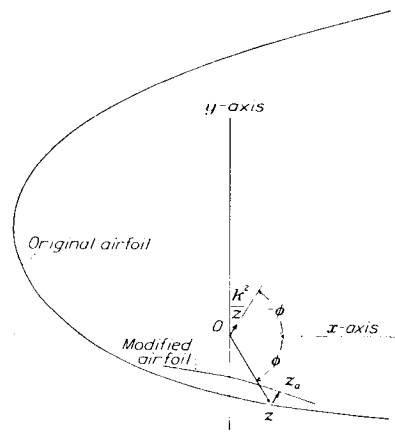

FIGURE 1.—Construction to determine a point on the modified airfoil.

k^2/z to z (the vector $z-k^2/z$) to the vector Oz. Then the ratio of the velocity at a point $z+k^2/z$ to the velocity at the corresponding point z of the original figure is the inverse of this factor.

The problem of determining the pressure distribution is reduced by Bernoulli's relation $P=P_0-\rho V^2/2$ to that of finding the distribution of the velocity. If the velocity distribution over the original figure is known, the velocity distribution over the modified figure may then be found by applying the ratio $\frac{|z|}{\left|z-\frac{k^2}{z}\right|}$ at each point used in the construction. The vectors z and $z-k^2/z$ have already been used in transforming these points and are therefore directly measurable.

Strictly speaking, the method as outlined is applicable only to potential flows. It is reasonable to suppose, however, that the actual velocity distribution over the modified airfoil may be obtained with good accuracy

from a distribution experimentally determined for the original airfoil, provided that: (1) the experimental and the theoretical distributions do not differ too greatly and (2) the modification itself does not introduce too great a change in the distribution.

The requirements of each problem will suggest the proper choice of the axes and of k. A few general observations may be helpful in this connection. It is evident that the origin must be in the neighborhood of

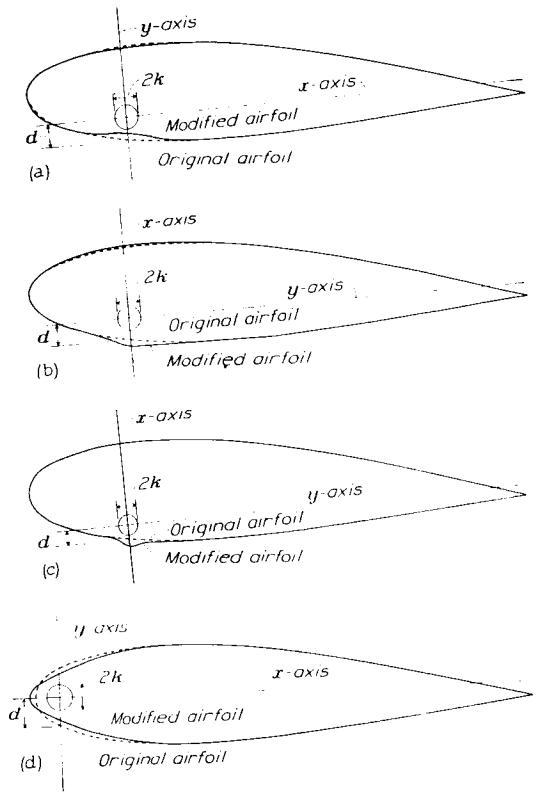

FIGURE 2.—The effect of varying the parameters of the construction.

the section to be modified since the point nearest the origin is shifted the greatest distance. The direction in which a point is shifted depends on the inclination of its vector to the axes, and the shift may have a relatively small component normal to the airfoil boundary. If one axis is roughly parallel to the section of the surface to be modified, the point of greatest deviation will usually be very near the intersection of the surface with the other axis. It will therefore be useful to note that the displacement of a point on either axis is k^2/d, where d is the distance of the origin from the point. Points on or near the x-axis are shifted outward from the origin; points near the y-axis are moved inward. The transformations of figure 2 show the nature of the modifications to be obtained by various choices of the axes and of k. Sharp modifications occur when the airfoil intersects either axis at a distance from the origin only slightly greater than k.

It is expected that the method as outlined will be useful in ascertaining the effect on the velocity distribution of a localized modification of an airfoil. It is possible, however, to approximate a more extensive modification to any desired degree of accuracy by successive applications of the same transformation, the velocity being calculated at each stage by the rule already given.

APPROXIMATION OF A GIVEN AIRFOIL

The foregoing discussion is concerned with the problem of effecting small modifications of existent airfoils for which the velocity distribution is known. It is sometimes required to predict the theoretical characteristics of an airfoil not derived in this way. In such a case, it is customary to use the known flow around a circle as a starting point. If the transformation discussed here is applied to a circle, the result is an oval shape with circular-arc camber, as demonstrated by Joukowski. (See reference 1.) It should be possible to proceed to modify this figure (or its special form, a Joukowski airfoil) as was done in the preceding section to an experimentally known airfoil. In general, however, it would require many steps to reproduce an arbitrary airfoil in this way because modifications of the shape already approaching an airfoil would, of necessity, be small and localized. On the other hand, if the procedure were reversed, it would be found that any airfoil may be derived by a single step from a figure closely approximating a circle, a figure which will hereinafter be called the "distorted circle" of the airfoil. The distorted circle may then be considered the result of modifying a circle, a result obtained in the same way as were the slightly modified airfoils of the preceding section.

For the first step in this process, the determination of the distorted circle corresponding to the desired airfoil, reference could be made to Theodorsen and Garrick (reference 2) or von Kármán and Burgers (reference 3), who give exact formulas for the distorted circle in terms of the airfoil coordinates. A graphical method based on the simpler transformation that is being used in this paper makes it possible, however, to obtain the distorted circle merely by trial.

The entire procedure is illustrated step by step in figure 3. In order to achieve a considerable simplification of the construction, the airfoil is considered in this figure and in the following discussion to have been drawn through the midpoints rather than through the terminals of the vectors $z+k^2/z$, so that they appear here as if to half scale.

The axes and the parameter k for the first step are found from the airfoil dimensions according to the relations given in figure 3(a). The x-axis is made to pass through the leading and the trailing edges to reduce to a minimum the distortion that will later have to be reproduced.

The axes and k having been chosen, the intersections of the distorted circle with the axes, X_N, X_T, Y_U, and

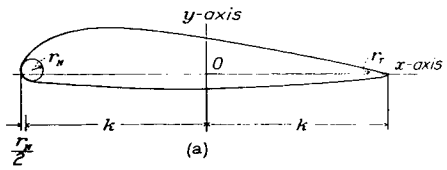

(a) Location of the axes and determination of the parameter k from the airfoil.

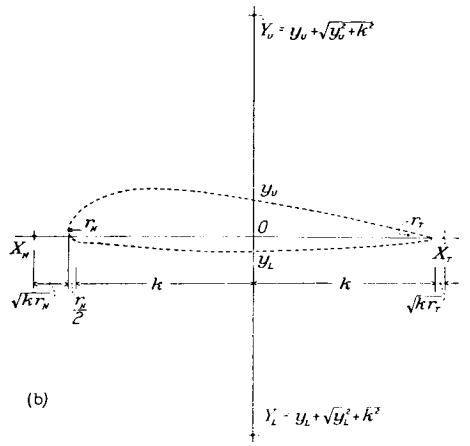

(b) Location of the intersections of the distorted circle with the axes.

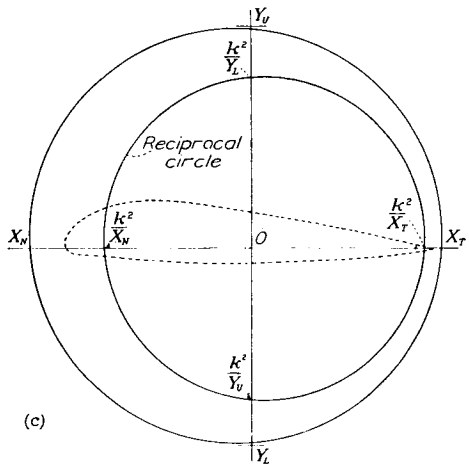

(c) Construction of the circle to serve as a first approximation of the distorted circle; the reciprocal circle.

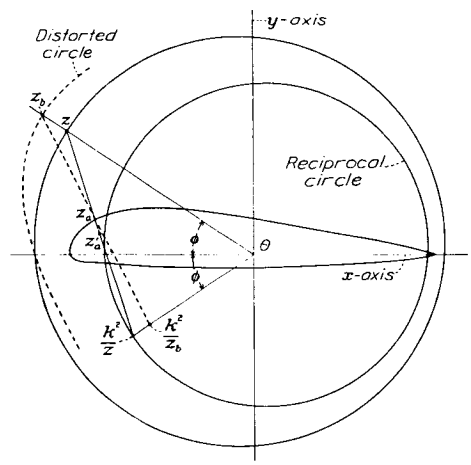

(d) Construction of the distorted circle of the airfoil.

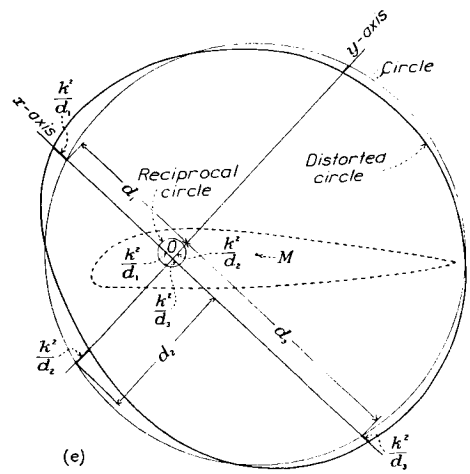

(e) Approximation of the distorted circle by a small modification of a circle.

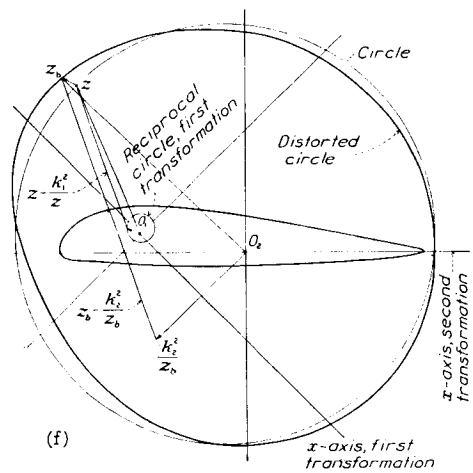

(f) Reconstruction of the airfoil from the circle, showing the lines needed in computing the velocity distribution.

FIGURE 3.—Steps in the approximation of a given airfoil by the transformation of a circle.

V_L, are easily calculated (fig. 3(b)). The construction then proceeds as follows:

In order to serve as a first approximation of the distorted circle, a circle is drawn to fit the four intersections with the axes as closely as possible. It should be remembered that, because this step is a first approximation, great accuracy is not a consideration. When the vectors z follow this circle, the vectors k^2/z, constructed as previously described, are found to terminate in a smaller circle, which is termed for convenience the "reciprocal" circle. This reciprocal circle may be easily located from its intersections with the axes (fig. 3 (c)). Vectors Oz and $O\frac{k^2}{z}$ are then drawn from the origin to the circle and to the reciprocal circle at equal angles below and above the x-axis (fig. 3(d)). The midpoint z_a' of the diagonal $z-k^2/z$ connecting the ends of these vectors will not, in general, fall exactly on the airfoil. A point of the distorted circle z_b is located by adjusting with dividers the length of Oz_b along Oz so that the diagonal to its reciprocal is bisected by the airfoil. The point of the airfoil z_a at which this bisection occurs will actually be indistinguishable from the intersection of the first diagonal with the airfoil: this fact is useful in making the correction. Because the corrections to the vectors Oz and $O\frac{k^2}{z}$ are in approximately the same ratio as the vectors, the decrease in k^2/z that corresponds to an increase in the length of Oz may be estimated and the reciprocal relation be maintained by eye. Any desired degree of accuracy may be obtained by checking numerically the lengths of the vectors.

The distorted circle obtained in this way must now be approximated by applying a transformation of the form $z+k^2/z$ to the circle most nearly approximating it. For this purpose the circle already drawn for the preceding step will usually be satisfactory, although it may have to be shifted slightly to obtain a more convenient distribution of the distortion. Depressions should occur as nearly as possible on opposite sides of the circle, with distended portions between them. (See fig. 3(e).) The x-axis should then be passed through the distended portions and the y-axis, through the depressions. Some adjustment will be needed to satisfy the condition that the segments of the axes cut off by the circle and the corresponding distortions be approximately in inverse proportion, that is, that their product at each intersection be constant. The parameter k for the transformation is then the square root of this product.

Carrying out the transformation of the circle at this point serves at once to check the estimated parameters or to suggest an adjustment and to provide the construction lines that will be needed to determine the velocity distribution. Similarly, the distorted circle thus obtained from the circle should be reduced to the desired airfoil.

In figure 3(f) the complete double transformation and the lines necessary for the computation of the velocity distribution are shown applied to a point of the circle of figure 3(e).

Occasionally an airfoil will give rise to a distorted circle that cannot be obtained by a single modification of a circle. In such a case an additional transformation may be applied either to achieve the desired distortion of the circle or to modify locally an airfoil that can be derived by two transformations.

VELOCITY DISTRIBUTION OVER AN AIRFOIL DERIVED FROM A CIRCLE

It is apparent that a large variety of useful airfoil shapes can be obtained by two or more successive applications to a circle of the transformation $z+k^2/z$. (Two typical examples are shown in fig. 4.) The first transformation primarily determines the general outline of the airfoil. The second transformation reduces the figure to the dimensions of an airfoil and determines the nose radius, the thickness, and the camber. It may be of interest to note that in the first transformation k is small relative to the radius of the circle; in the second transformation the ratio of k to the radius of the circle is only slightly less than 1.

The method of finding the velocity at a point on an airfoil derived in this manner is deduced from the following considerations:

The velocity at a point z on the circle is given by the formula

$$V_z=2V_0 \sin \theta+\frac{\Gamma}{2\pi r}$$

where r is the radius of the circle, V_0 is the wind velocity, and θ is the angle that the radius to the point z makes with the direction of the air stream. The circulation Γ is determined by the Kutta condition. Then

$$V_z=2V_0(\sin \theta-\sin \theta_0)$$

where θ_0 equals the angle between the air stream and the radius to $z_{T.E.}$, the point of the circle that transforms to the trailing edge of the airfoil. This expression for V_z lends itself readily to graphical evaluation as a part of the construction; the velocity factor $(\sin \theta-\sin \theta_0)$ is proportional to the ordinate of the circle measured from a line drawn through $z_{T.E.}$ and parallel to the wind velocity V_0.

The velocity at the corresponding point of the transformed figure has been shown in a preceding section to be $\left|\frac{z}{z-\frac{k^2}{z}}\right| V_z$. The "stretching factor" $\left|\frac{z}{z-\frac{k^2}{z}}\right|$ will have to be applied again to the velocities over the distorted circle to transform the flow to that over the airfoil. A simple procedure is to plot the stretching factor alone for the first transformation, as a function of the angular position of the transformed point, with the lengths $|z|$ and $\left|z-\frac{k^2}{z}\right|$ measured from the construction. The stretching factor for the second transformation could then be applied at convenient points to values of the

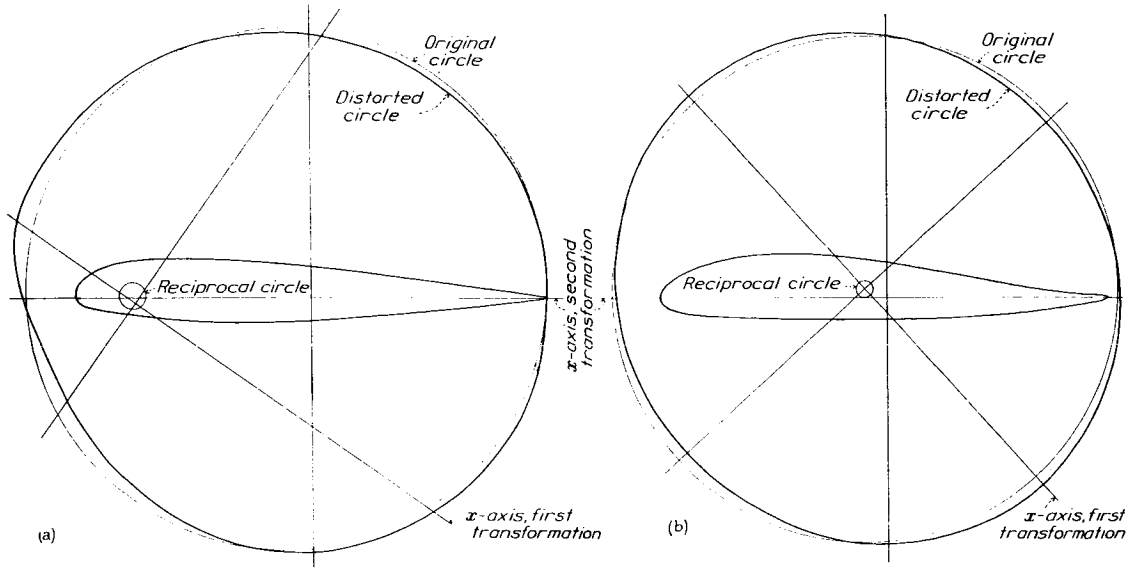

FIGURE 4.—Airfoils derived by two applications of transformation to circle. Airfoils are shown half scale with respect to circles.

stretching factor for the first transformation read from the plot. The resultant stretching factor obtained in this way can be directly applied to the velocity at points of the circle to give the velocity distribution over the airfoil at any angle of attack.

Figure 5 shows a sample pressure distribution over an airfoil (the NACA 4412 airfoil) approximated by two transformations of a circle. Comparison is made with the distribution derived by the theory of reference 2 and with experimental results taken from reference 4. The theoretical distributions were computed at an angle of attack of 6.4°, which corresponds to a geometric angle of attack of 8.5° for the finite-span airfoil of reference 4.

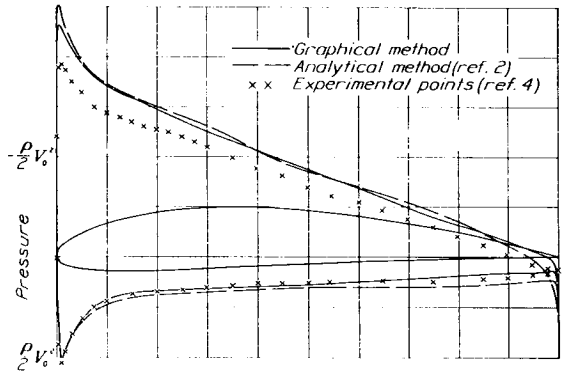

FIGURE 5.—Theoretical and experimental pressure distributions over NACA 4412 airfoil. $\alpha_a = 6.4°$.

CONCLUSION

The method of this paper has been found useful in determining the effect of small modifications of airfoil shapes on the pressure distribution. It is apparent that a family of related shapes can be derived in this way with greater simplicity than by standard methods because the effect of the modification alone can be calculated for each shape. It is also possible to foresee the manner in which a shape must be modified to produce a desired change in the pressure distribution. The method is, in fact, reversible and by it an airfoil may be designed to have a predetermined pressure distribution, provided that a somewhat similar airfoil is already known. The modified pressure distributions obtained in this way have closely checked with experiment.

LANGLEY MEMORIAL AERONAUTICAL LABORATORY,
NATIONAL ADVISORY COMMITTEE FOR AERONAUTICS,
LANGLEY FIELD, VA., *November 12, 1940.*

APPENDIX

FORMULAS FOR LIFT AND MOMENT

In the case of an airfoil derived from a circle, the method of derivation, interpreted in terms of complex numbers, makes it possible to give concise formulas for the lift and the moment in terms of the parameters used in the construction and to locate by simple geometric methods the theoretical aerodynamic center. The general theory for a transformation of the form

$$z_a=z+\frac{a_1}{z}+\frac{a_2}{z^2}+\cdot\ \cdot\ \cdot \tag{1}$$

has been developed by von Mises (reference 5, ch. VII). In order to apply the formulas of von Mises, it is necessary to express the resultant of two successive transformations in a series of the foregoing form.

Let $z_b=z+k_1^2/z$ express the first transformation, z being a point on the circle or one of its streamlines and z_b, the corresponding point associated with the distorted circle. The axes for the second transformation are described by the complex parameter z_1, which locates the origin, and β, the angle between the two sets of axes.

Then, if primes denote the vectors drawn to the new origin,

$$z_b'=(z_b-z_1)e^{-i\beta} \tag{2}$$

Substitute

$$z_b=z+\frac{k_1^2}{z}$$

Then

$$z_b'=\left(z+\frac{k_1^2}{z}-z_1\right)e^{-i\beta} \tag{3}$$

which is the point on the distorted circle located with respect to the axes for the second transformation. Apply the second transformation to z_b'; then

$$z_a'=z_b'+\frac{k_2^2}{z_b'} \tag{4}$$

gives the corresponding point associated with the airfoil. Substitute for z_b' from equation (3). Equation (4) then becomes

$$z_a'=\left(z+\frac{k_1^2}{z}-z_1\right)e^{-i\beta}+\frac{k_2^2e^{i\beta}z}{z^2-z_1z+k_1^2} \tag{5}$$

In order to restore the wind velocity V_0 to its original magnitude and direction, it is necessary to return to the original axes.

$$z_a'=(z_a-z_1)e^{-i\beta} \tag{6}$$

and the inverse transformation is

$$z_a=z_a'e^{i\beta}+z_1 \tag{7}$$

Then

$$z_a=z+\frac{k_1^2}{z}+\frac{k_2^2e^{2i\beta}z}{z^2-z_1z+k_1^2} \tag{8}$$

This expression for the complete transformation can be expanded, by carrying out the division of the last term, into the series

$$z_a=z+\frac{k_1^2+k_2^2e^{2i\beta}}{z}+\frac{k_2^2e^{2i\beta}z_1}{z^2}+\ \cdot\ \cdot\ \cdot \tag{9}$$

which is in the form of equation (1), where

$$\left.\begin{aligned}a_1&=k_1^2+k_2^2e^{2i\beta}\\ a_2&=k_2^2e^{2i\beta}z_1\end{aligned}\right\} \tag{10}$$

The formulas for the lift and the moment as given by Glauert (reference 5, pp. 84 and 85) may now be applied. The circulation, and consequently the lift, is unchanged by the transformation. Thus the lift depends only on the radius of the original circle.

$$L=\rho V_0\Gamma=8\pi r\frac{\rho}{2}V_0^2\sin\theta_0 \tag{11}$$

or $4\pi r\frac{\rho}{2}V_0^2\sin\theta_0$ for the half-scale airfoil. The value of M_0, the moment about O (fig. 6), is given by the imaginary part of the expression (reference 5, p. 84)

$$\pi\rho\left[2a_1V_0^2e^{2i\alpha}-2r^2V_0^2-\frac{mV_0\Gamma}{\pi}ie^{i(\alpha-\delta)}-\frac{\Gamma^2}{4\pi^2}\right] \tag{12}$$

where the quantities not already defined are as defined by the figure. Substitution for a_1 from equation (10) gives

$$\pi\rho\left[2(k_1^2+k_2^2e^{2i\beta})e^{2i\alpha}-\frac{mV_0\Gamma}{\pi}ie^{i(\alpha-\delta)}\right] \tag{13}$$

for expression (12), or

$$M_0=2\pi\rho V_0^2[k_1^2\sin 2\alpha+k_2^2\sin 2(\alpha+\beta)] -m\rho V_0\Gamma\cos(\alpha-\delta) \tag{14}$$

Since

$$\Gamma=4\pi rV_0\sin(\alpha-\alpha_0) \tag{15}$$

$$M_0=2\pi\rho V_0^2[k_1^2\sin 2\alpha+k_2^2\sin 2(\alpha+\beta) -2rm\cos(\alpha-\delta)\sin(\alpha-\alpha_0)] \tag{16}$$

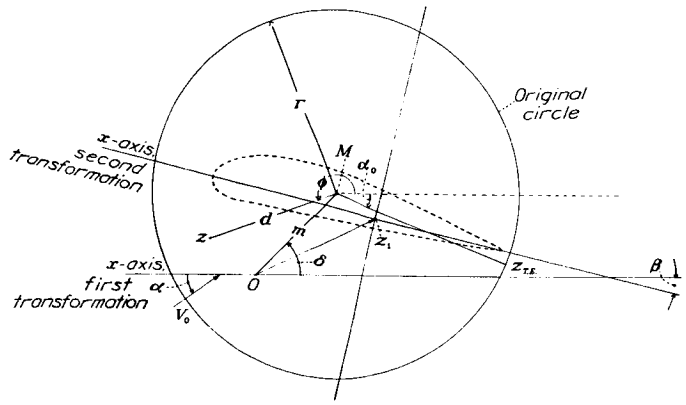

FIGURE 6.—Symbols used in development of lift and moment formulas.

In general, the moment about any point z (see fig. 6) is given by

$$M_z=2\pi\rho V_0^2[k_1^2 \sin 2\alpha+k_2^2 \sin 2(\alpha+\beta) +2rd \cos(\alpha-\phi) \sin(\alpha-\alpha_0)] \quad (17)$$

or

$$\frac{M_z}{2\pi\rho V_0^2}=[k_1^2+k_2^2 \cos 2\beta+rd \cos(\phi+\alpha_0)] \sin 2\alpha +[k_2^2 \sin 2\beta-rd \sin(\phi+\alpha_0)] \cos 2\alpha +rd \sin(\phi-\alpha_0) \quad (18)$$

The location of the aerodynamic center (or focus) is determined by the condition that the moment about that point be independent of the angle of attack. In order to satisfy this condition, the coefficients of $\cos 2\alpha$ and of $\sin 2\alpha$ in equation (18) must vanish simultaneously.

Thus

$$\frac{1}{r}(k_1^2+k_2^2 \cos 2\beta)=-d \cos(\phi+\alpha_0) \quad (19)$$

$$\frac{1}{r}k_2^2 \sin 2\beta=d \sin(\phi+\alpha_0) \quad (20)$$

and

$$\left.\begin{aligned}(\phi+a_0)&=\tan^{-1}\frac{-k_2^2 \sin 2\beta}{k_1^2+k_2^2 \cos 2\beta}\\ d^2&=\frac{1}{r^2}(k_1^4+2k_1^2k_2^2 \cos 2\beta+k_2^4)\end{aligned}\right\} \quad (21)$$

Equations (21) are found to have a simple geometric representation. If k_1^2/r and k_2^2/r are two sides of a triangle and $(180°-2\beta)$ is the angle between them, then d is the length of the third side and $(\phi+\alpha_0)$ is the supplement of the angle opposite k_1^2/r. This triangle may be used to locate the aerodynamic center directly on the construction, as shown in figure 7. As in the preceding illustrations, this airfoil has been drawn to half scale with respect to the circle and the distance d has therefore been bisected. The moment about the aerodynamic center

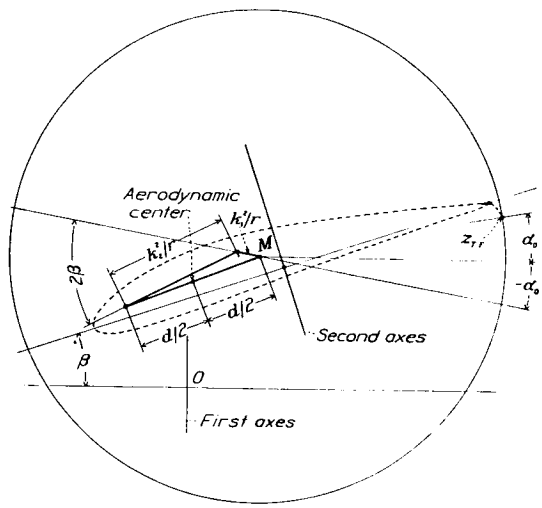

FIGURE 7.—Construction to find the aerodynamic center.

$$M_0=2\pi\rho V_0^2rd \sin(\phi-\alpha_0) \quad (22)$$

is obtained directly from equation (18). The moment for the half-scale airfoil is one-quarter of this value.

REFERENCES

1. Trefftz, E.: Graphic Construction of Joukowski Wings. Pt. II of T. M. No. 336, NACA, 1925.
2. Theodorsen, Theodore, and Garrick, I. E.: General Potential Theory of Arbitrary Wing Sections. Rep. No. 452, NACA, 1933.
3. von Kármán, Th., and Burgers, J. M.: Application of the Theory of Conformal Transformation to the Investigation of the Flow around Airfoil Profiles. Vol. II, div. E, ch. II, pt. B of Aerodynamic Theory, W. F. Durand, ed., Julius Springer (Berlin), 1935, pp. 58–83.
4. Pinkerton, Robert M.: Calculated and Measured Pressure Distributions over the Midspan Section of the N. A. C. A. 4412 Airfoil. Rep. No. 563, NACA, 1936.
5. Glauert, H.: The Elements of Aerofoil and Airscrew Theory. The Univ. Press (Cambridge), 1926.

THEORETICAL CORRECTION FOR THE LIFT OF ELLIPTIC WINGS

Robert T. Jones

National Advisory Committee for Aeronautics

November 1941

Theoretical Correction for the Lift of Elliptic Wings

ROBERT T. JONES†

National Advisory Committee for Aeronautics

IN THE WING section theory the magnitude of the circulation, and hence of the lift, is determined by the velocity that would be induced near the trailing edge of the section in a non-lifting potential flow. In three-dimensional flow the problem is complicated by the presence of the wake and no simple basic solution has been found. Treatment of the problem of a wing of finite span has therefore been on the basis of the two-dimensional theory, corrected for the effect of the wake.*

The correction commonly applied is that introduced by Prandtl and known as the lifting-line theory. The downflow induced by the wake is considered, in this theory, to reduce the relative normal velocity and hence the edge velocity of the wing. It is assumed, however, that once the true angle of attack is determined for any section of the wing its effect in producing circulation and lift is the same as in two-dimensional flow. This assumption is expressed by the equation

$$C_L = 2\pi(\alpha - \alpha_i) \tag{1}$$

where 2π is the slope of the lift curve for the thin wing of infinite aspect ratio, α is the angle of attack of the section, and α_i is the induced angle of downflow.

Eq. (1) takes into account the effect of the wake in diminishing the relative normal velocity of the wing. A further correction is indicated by the fact, established in hydrodynamic theory, that the surface velocities induced by a given relative motion of a body in three-dimensional flow are generally smaller than those in two. For example, the maximum, or "edge" velocity around an infinite cylinder is 1, while that around a sphere of the same cross-section is $1/2$. Similarly, if the velocity around the edge of an endless thin plate is taken as unity, the corresponding velocity around the edge of a circular disc is found to be $2/\pi$, or 0.637.

In the case of an elliptic disc the velocity at every point is reduced by the factor $1/E$, where E is the ratio of the semiperimeter of the ellipse to the span. (See appendix.) Further investigation shows that the chordwise cross-sections of the non-lifting potential flow are similar all along the span of the elliptic plate and are the same as those obtained from the wing-section theory except for this constant reduction factor.

Received July 31, 1941.

† Assistant Aeronautical Engineer.

* More recently the problem has been treated on the basis of the acceleration potential, which vanishes in the wake.[1] The method is still one of considerable difficulty, however.

If the velocity distributions of the circulatory flow are also assumed to be similar to those given by the wing-section theory, the circulation required to satisfy the Kutta condition at each section should be reduced by the same factor. The corrected formula for the lift is then

$$C_L = (2\pi/E)(\alpha - \alpha_i) \tag{2}$$

This correction may be given a physical interpretation by considering that a finite wing offers a longer edge around which the air may escape (see Fig. 1),

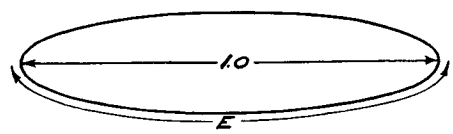

FIG. 1. Correction factor E for the effect of the perimeter ratio on the lift: $C_L = (2\pi/E)(\alpha - \alpha_i)$.

and that the air velocities are therefore less in the proportion that the length of the edge is greater. The rule is not exact for plan forms other than the elliptical.

Since the velocity of the non-lifting potential flow is constant all around the edge of the elliptic plate, the circulation required will be proportional to the chord at each section. The circulation is thus elliptically distributed spanwise. Such a distribution, with the chordwise distribution assumed earlier, leads, as in the lifting-line theory, to the relation

$$\alpha_i = C_L/\pi A \tag{3}$$

where A is the aspect ratio.

Substitution of this value into Eq. (2) gives

$$C_L = 2\pi\alpha A/(EA + 2) \tag{4}$$

Since the chordwise distribution of the circulation in three-dimensional flow is assumed similar to that in two, and since the similarity is only proved for the non-circulatory flow, Eq. (4) must be considered a correction of the wing-section theory rather than a solution of the three-dimensional problem. The assumption of similarity, although its validity is subject to somewhat the same limitations in general, appears to be a more justifiable one than the assumption of equality made in the lifting-line theory.

The problem of *three-dimensional* flow around a lifting elliptical plate has been treated by Krienes[2] using

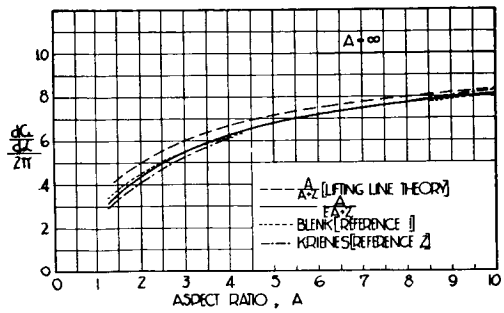

FIG. 2. Theoretical variations of lift-curve slope with aspect ratio.

Prandtl's concept of the acceleration potential. The calculations involve the superposition of a series of solutions of $\Delta^2\phi = 0$ in ellipsoidal coordinates (Lamé functions), the coefficients of the series being obtained from simultaneous equations. Although the overall lift depends on only one coefficient, calculations of the span loading and the drag would require all the terms of the infinite series and was therefore not considered practicable.

The lift coefficients obtained by Krienes' method are shown in Fig. 2. Results obtained by correcting the wing-section theory in accordance with Eq. (4) are compared with Krienes', and the agreement is seen to be good for ordinary aspect ratios.

A curve derived from Blenk's calculation of the vortex distribution in a rectangular plate[3] also agrees closely with Eq. (4).

It is found that the additional correction to the wing-section theory accounts for an appreciable fraction of the loss in lift that is usually attributed to viscosity. It has been difficult to reconcile the magnitude of the inefficiency with the observed dimensions of the wake, which in the case of smooth wings, is extremely narrow at the trailing edge. The foregoing correction accounts for as much as half of this discrepancy in cases of wings with sharp trailing edges. (See Fig. 3.)

According to Munk's theorem, the induced drag is not affected by a displacement of the lifting elements in the direction of the chord; hence the relation between the lift and the induced drag may be derived on the basis of the lifting-line theory. Also, since the pitching moment of the elliptic wing involves the same correction as the lift, no change of aerodynamic center location with aspect ratio is indicated.

The three-dimensional potential flow around the elliptic disc may be used also as the basis for calculating the lift of an elliptic wing with varying angle of attack. On account of the linearity of the equations, the general problem may be reduced to a determination of the growth of lift following a sudden start of the motion with the flight velocity V and the normal velocity $w = V\alpha$.*

* The infinite force implied by the sudden start leads, in practice, to a finite value during the continuous motions to which the formulas are applied.

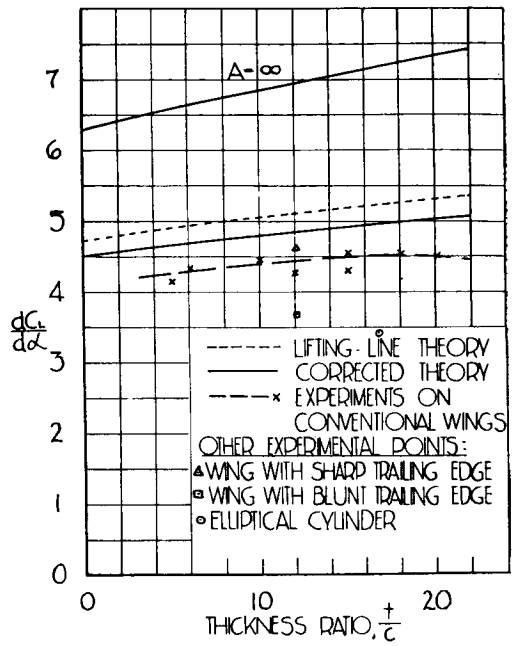

FIG. 3. Experimental and theoretical lift-curve slopes. Aspect ratio, 6.

Since the steady or asymptotic value of the lift is already known, the most important point is the determination of the lift near the start of the motion.

As a consequence of the Kutta condition, the layer of air leaving the wing at the trailing edge must satisfy the same boundary condition as the adjacent wing surface for a short distance downstream. Thus the layer of air in contact with the wing retains the motion imparted by the wing and for a short distance after the start this layer (the vortex wake) behaves as an impermeable extension of the wing surface.[4] The flow at the first instant after the start is thus what might be caused by the wing in process of growing wider at the rate V while moving with the normal velocity w. The starting lift $L_{t=0}$ may then be thought of as the reaction to uniform motion of the wing acting as a body with increasing mass:

$$L_{t=0} = w\,(dm'/dt) = w\,(dm'/dc)\,V \qquad (5)$$

where m' is the mass representing the aerodynamic inertia of the flow and c is the apparent length of the chord. In two-dimensional flow

$$m' = \pi\,(c^2/4)\rho \qquad (6)$$

so that

$$C_{L_{t=0}} = \pi\alpha \qquad (7)$$

In the case of the elliptic wing the starting process is pictured as a change into a similar but slightly wider ellipse. For normal aspect ratios this change fulfills the required conditions everywhere except near the extreme tips. The aerodynamic inertia of the elliptic

wing is the same as if the sections were in two-dimensional flow except for the factor E. Hence:

$$C_{L_{l=0}} = \pi\alpha/E$$

According to some approximate calculations (based on the lifting-line theory) made by the author,[4] the lift of the elliptic wing approaches its final value more rapidly than would be suggested by the two-dimensional theory.

In the case of $A = 3$, or in the equivalent case of $A = 6$ with the wing vibrating symmetrically in torsion, the development of lift appears to be nearly instantaneous.

Appendix

The problem of the fluid motion produced by translation of a solid ellipsoid was first solved by Green in an investigation of the vibration of pendulums. Formulas given for this problem in textbooks on hydrodynamics become indeterminate when applied to the case of an elliptic disc. The following short discussion is therefore presented to show the application to the present problem.

As explained in ref. 5, the surface potential of an ellipsoid can be given by a very simple formula. For motion along a principal axis, the potential at any point on the surface is proportional to the coordinate of the point in the direction of motion. Thus, if the ellipsoid with semiaxes $a > b > c$ along x, y, and z, respectively, is moving with unit velocity in the direction of z, the surface potential is simply

$$\phi = Cz \tag{3}$$

The equipotential lines are the similar ellipses formed by the intersection of the ellipsoidal surface with a series of equidistant parallel planes perpendicular to z. The constant C depends on the axis ratio and its evaluation involves a special class of transcendental function known as "Green's Integrals." The solution for the surface potential appears in the form:

$$\phi = [\gamma_0/(2 - \gamma_0)]\, z \tag{4}$$

where

$$\gamma_0 = abc \int_0^\infty \frac{d\lambda}{(c^2 + \lambda)\sqrt{(a^2 + \lambda)(b^2 + \lambda)(c^2 + \lambda)}}$$

is Green's integral.

The reduction of these integrals to the standard elliptic functions is given in ref. 5. Following equation (6.1) of ref. 5 and substituting $\lambda = 0$, in order to restrict the solution to the surface of the ellipsoid, will give

$$\gamma_0 = \frac{2abc}{\sqrt{(a^2 - c^2)^3}} \frac{a^2 - c^2}{b^2 - c^2}\left[\frac{b}{ac}\sqrt{a^2 - c^2} - E\right]$$

where E is the complete elliptic integral with the modulus $k = \sqrt{(a^2 - b^2)/a^2}$. The integral E is equal to the perimeter of a quadrant of the ellipse ab divided by the semiaxis a.[6]

$$\gamma_0 \longrightarrow 2\,[1 - (c/b)E]$$

As $c \longrightarrow 0$

Since Eq. (4) becomes indeterminate ($z \longrightarrow 0$ and $\gamma_0 \longrightarrow 2$), it is necessary to express the solution in terms of x and y, which are related to z through the equation of the ellipsoidal surface:

$$\frac{x^2}{a^2} + \frac{y^2}{b^2} + \frac{z^2}{c^2} = 1 \tag{5}$$

or

$$z = c\sqrt{1 - \frac{x^2}{a^2} - \frac{y^2}{b^2}} \tag{6}$$

Substitution for γ_0 and z in Eq. (4) gives

$$\phi = \frac{b}{E}\sqrt{1 - \frac{x^2}{a^2} - \frac{y^2}{b^2}} \tag{7}$$

or

$$(x^2/a^2) + (y^2/b^2) + [\phi^2/(b/E)^2] = 1 \tag{8}$$

Hence the distribution of the surface potential over the disc may be represented by the ordinates of a circumscribed ellipsoid having the vertical axis $2b/E$. For infinite axis ratio, $E = 1$ and the chordwise cross-sections of the potential distribution are circles of radius b.

In order to illustrate the analogy to two-dimensional flow, it is convenient to introduce the angle θ defined, at a particular value of x, by

$$\cos\theta = y/y_e \tag{9}$$

where $y_e = b\sqrt{1 - (x^2/a^2)}$ is the ordinate of the edge of the disc. Then, from Eq. (8),

$$\phi = (y_e/E)\sin\theta \tag{10}$$

which is the potential function of the two-dimensional case except for the factor $1/E$. It follows then that the edge velocity is also reduced from that in two-dimensional flow by the factor $1/E$.

References

[1] Prandtl, L., *Recent Work on Airfoil Theory*, N.A.C.A. Technical Memorandum No. 962, 1940.

[2] Krienes, Klaus, *The Elliptic Wing Based on the Potential Theory*, N.A.C.A. Technical Memorandum No. 971, 1941.

[3] von Kármán, Th., and Burgers, J. M., Vol. II, *division E of Aerodynamic Theory*, W. F. Durand, ed., Julius Springer (Berlin), 1935.

[4] Jones, Robert T., *The Unsteady Lift of a Wing of Finite Aspect Ratio*, N.A.C.A. Technical Report No. 681, 1939.

[5] Munk, Max M., *Fluid Mechanics*, Part II, Vol. I, Div. C of Aerodynamic Theory, W. F. Durand, ed., Julius Springer (Berlin), 1935, pages 293–304.

[6] Wilson, Edwin Bidwell, *Advanced Calculus*, Ginn and Co., page 514. 1912.

TECHNICAL NOTE 837

NOTES ON THE STABILITY AND CONTROL OF TAILLESS AIRPLANES

Robert T. Jones

Langley Memorial Aeronautical Laboratory

December 1941

NATIONAL ADVISORY COMMITTEE FOR AERONAUTICS

TECHNICAL NOTE NO. 837

NOTES ON THE STABILITY AND CONTROL OF TAILLESS AIRPLANES

By Robert T. Jones

SUMMARY

Problems involved in the stability and control of tailless airplanes are discussed. Such factors as the location of the aerodynamic center and its effect on the longitudinal stability, longitudinal trim with high-lift devices, the effects of various changes in the shape of the wing on lateral stability, and the effects of nacelles are covered.

It appears that sufficient stability and controllability can be secured without sweepback. With sweepback, a flap over the center section of the wing may be used to serve the dual purpose of elevator control and high-lift device. Sweepback introduces undesirable stalling characteristics, however, and may require auxiliary devices to prevent stalling of the tips.

INTRODUCTION

The advantage in arrangement and performance that the tailless airplane has over the conventional type has already been the subject of considerable discussion. The present paper is chiefly concerned with aerodynamic factors as they affect the stability and control of tailless airplanes.

With the aerodynamic information available at present, the designer should be able to predict with confidence the behavior of an airplane that resembles in design a reasonably conventional wing. There is still, however, a lack of information on the loading of wings with large angles of sweepback and on the loading of wings of very low aspect ratio.

SYMBOLS

A	aspect ratio
α	angle of attack
b	wing span
β	angle of sideslip
c	wing chord
$C_L = \frac{\text{Lift}}{S_w \frac{\rho}{2} U_o^2}$	lift coefficient
$C_l = \frac{L}{S_w \frac{\rho}{2} U_o^2 b}$	rolling-moment coefficient
$C_m = \frac{M}{S_w \frac{\rho}{2} U_o^2 c}$	pitching-moment coefficient
$C_n = \frac{N}{S_w \frac{\rho}{2} U_o^2 b}$	yawing-moment coefficient
$C_Y = \frac{Y}{S_w \frac{\rho}{2} U_o^2}$	side-force coefficient

$$C_{L_\alpha} = \frac{\partial C_L}{\partial \alpha}, \quad C_{m_{D\theta}} = \frac{\partial C_m}{\partial D\theta} = \frac{\partial C_m}{\partial \frac{qc}{U_o}}, \text{ etc.}$$

$$C_{n_r} = \frac{\partial C_n}{\partial \frac{rb}{U_o}}, \quad C_{l_p} = \frac{\partial C_l}{\partial \frac{pb}{U_o}}, \quad C_{l_\beta} = \frac{\partial C_l}{\partial \beta}, \text{ etc.}$$

$D = \frac{d}{ds}$ derivative with respect to distance along flight path

δ	elevator or rudder deflection
k_X, k_Y, k_Z	radii of gyration about axis indicated by subscript
l	length of fuselage
m	mass of airplane
p	angular velocity in rolling
q	angular velocity in pitching
r	angular velocity in yawing
$s = \frac{U_o t}{c}$	distance along flight path
X, Y, Z	airplane axes

LONGITUDINAL STABILITY AND CONTROL

An ordinary wing with a slight reflex camber and dihedral has all the aerodynamic characteristics necessary for both lateral and longitudinal stability. As in the conventional airplane, longitudinal stability in gliding flight is practically assured if the center of gravity is located slightly ahead of the aerodynamic center of the wing (fig. 1). For wings of normal aspect ratio and dimensions the aerodynamic center is located at about 24 percent of the mean chord. At very low aspect ratios the aerodynamic center moves ahead and upward, and the attainment of stability and balance becomes more difficult. The location is also appreciably changed by the addition of a streamline nacelle or by sweepback. Changes in wing section generally have only a slight effect. An extreme reduction in thickness toward the trailing edge may cause a backward displacement of 2 or 3 percent. Conversely, it is possible to produce a forward shift of the same amount by abnormal thickening of the rear portion.

The addition of a streamline fuselage or nacelle causes a forward shift of the aerodynamic center, thus necessitating a more forward location of the center of grav-

ity. Figure 2 (plotted from data given in reference 1) shows the movement of the aerodynamic center actually caused by a relatively large fuselage in combination with the wing. It will be noted that, when the wing intersection was near the nose of the fuselage, the interference was sufficient to nullify the unstable moment; that is, the aerodynamic center was not shifted. A comprehensive analysis of the effects of the fuselage and nacelles on both the longitudinal and the lateral stability parameters will be found in a recent article by Multhopp (reference 2).

The stability characteristics of a tailless airplane differ from those of a conventional airplane chiefly in the reduced kinematic damping of the pitching motion. Figure 3 shows the estimated damping coefficients

$$C_{m_{D\theta}} = \frac{\partial C_m}{\partial D\theta} = \frac{\partial C_m}{\partial \frac{qc}{U_o}} \tag{3}$$

for several airfoil arrangements. It is to be noted that the addition of the tail surface increases the kinematic damping nearly 10 times. Both theory and experiment indicate that the effect of the fuselage on the damping is not important. (The value of $\Delta C_{m_{D\theta}}$ is of the order of -0.2 for a fuselage of the proportions illustrated in fig. 2).

If the tailless airplane is statically stable (that is, has its center of gravity ahead of the aerodynamic center), the free rotations in pitch will be coupled with motions normal to the chord and the damping of these motions will be effective in reducing the pitching.

Figure 4 shows the calculated periods and rates of damping of the short-period longitudinal oscillations, for varying degrees of static stability. In addition to the reduced damping coefficient $\left(C_{m_{D\theta}} = -\frac{1}{2}\right)$, the all-wing airplane was assumed to have a reduced moment of inertia in pitch $\left(k_Y = \frac{1}{2}\,c\right)$. The curves shown apply to a wing chord of 10 feet at a loading of 20 pounds per square foot and are typical of the results of an extensive series of calculations. The dotted lines indicate locations of the center of gravity for aperiodic motion in this mode.

It is remarkable that, although the rotary damping coefficient $C_{m_{D\theta}}$ of the tailless airplane is only one-tenth that of the conventional airplane, the resultant damping of oscillations in flight is nearly as great. The additional damping is obtained through coupling with the vertical motion. The lack of direct damping appears to alter the sequence of the motions in such a way as to make this coupling more effective in the case of the tailless airplane.

In slow longitudinal motions involving changes of flight speed, the stability of the conventional airplane is usually impaired by the action of the slipstream on the tail surface. In the usual arrangement, the lift of the wings acts behind the center of gravity and a downward trimming load is carried by the tail surface, which is in the slipstream. Since the velocity in the slipstream tends to remain more nearly constant than the flight velocity, the forces on the wing and on the tail surfaces will not vary with flight speed in the same proportion. Thus if the airplane noses up and loses flying speed, the wings, having most of their area outside the slipstream, will lose lift at a rate greater than the rate of reduction of the downward trimming load and the airplane may continue to nose up in an unstable manner. The tailless arrangement affords a definite advantage in that such adverse effects can be easily eliminated.

In the gliding condition, the damping of the phugoid motion of a tailless airplane is less than that of a conventional airplane and there is, in general, somewhat greater likelihood of phugoid instability with the tailless airplane. (See fig. 5.) With power on, the conventional airplane is more unstable because of the destabilizing influence of the slipstream. Inasmuch as the period of this oscillation is very long and the damping slight in any case, the differences shown are considered unimportant.

A decided change in the character of the longitudinal motion will occur if the center of gravity is allowed to shift to a position behind the aerodynamic center. In this condition the rate of divergence of the tailless airplane is much more rapid than that of the conventional type and may become uncontrollable at relatively small negative values of $\bar{x}$. Figure 6 shows typical variations of the damping factors at small values of $\bar{x}$. As the condition of neutral static stability ($\bar{x} = 0$) is approached,

the complex roots are replaced by real roots, one of which becomes positive at $\bar{x} = 0$, indicating a rapid divergence of the tailless airplane in the region of static instability.

It should be possible to secure satisfactory longitudinal control with a straight wing simply by utilizing the pitching action of narrow flaps. Because trim at higher angles of attack would be attained by raising the flap and thus reducing the camber, the arrangement would entail some reduction in maximum lift, the amount depending on the degree of static stability. Figure 7 shows the elevator angles and corresponding reductions in $C_{L_{max}}$ for several flaps with a straight wing. The curves were based on the reductions in C_L (below $C_{L_{max}}$) and the pitching moments obtained in experiments with flaps. It is to be noted that the narrower flap is the more efficient (though less powerful) elevator. The computations were made for a rectangular wing of aspect ratio 6. Very high lift coefficients could be attained only with the aid of some device that did not displace the center of pressure.

Figure 8 shows elevator deflections necessary to produce a specified curvature of the flight path and illustrates the increased maneuverability of the tailless airplane. The elevators are designed to give equal pitching moments in order that both the conventional and the tailless airplanes would require the same elevator deflections to produce equal changes in trim. The increased path curvature or normal acceleration possible with the tailless airplane is a consequence of the smaller damping in pitching.

If sufficient sweepback is employed, it becomes possible to use cambered sections or sections with flaps designed to increase the lift over the center sections of the wing. In such an arrangement the lift developed by the flap or by the camber is placed sufficiently far ahead to offset the pitching moment. Furthermore, if the flapped portion of the wing is placed somewhat farther ahead, so as to bring the centroid of its load forward of the center of gravity, the flap may be used directly as an elevator. (See fig. 9.) Downward deflection of the flap will then increase the lift and the angle of attack simultaneously, as illustrated in figure 10.

If the angle of sweepback is small, it may be assumed

that the spanwise loading is not altered but is merely rotated backward through the angle of sweep. The pitching moment due to a small amount of sweep thus depends on the spanwise location of the load centroid of the straight wing. Figure 11 shows the calculated locations of this centroid corresponding to flaps of various lengths extending from the middle of the wing. The centroid for a flap of 100-percent span is the same as that for a change in angle of attack of the wing as a whole and thus locates the spanwise position of the aerodynamic center. It is preferable to assume that the lift loads act along the quarter-chord line and to take account of the backward displacement of the flap lift load by calculating the integrated pitching moment of the flapped sections, because this moment is more independent of aspect-ratio effects than is the lift. For rough estimates, the lift added by the flap may be assumed to act at about 45 percent of the chord of those sections inboard of the flap tip and along the quarter-chord line outboard of the flap tip.

A small damping coefficient $C_{m_{D\theta}}$ is a definite advantage in that the pitching disturbances produced by gusts are smaller. According to calculations made by Küssner (reference 3), a straight wing moving into an increasing gust will experience no pitching moment whatever about the quarter-chord line. Although it might be expected that the nose of the wing, being in a region of greater velocity than the rest of the wing, would be deflected upward, there will be at the same time an acceleration of the average normal velocity over the entire chord, which will lead to an aerodynamic inertia force acting at the 50-percent-chord point and which, calculations show, is just sufficient to balance the moments about the aerodynamic center. The argument may be extended to include any arbitrary variation of vertical velocity along the path of the airplane.

Because the wing will actually have its center of gravity ahead of the aerodynamic center for stability, it follows that the action of a rising gust will be to reduce the angle of attack and thus automatically to diminish the force of the gust. In figure 12 are plotted some curves, calculated by the method of reference 4, to show the effect of a gust on tailless and conventional airplanes. The gust was assumed to have uniformly increasing velocity. In the case of the conventional airplane, the initial pitching motion is in a direction that increases the angle

of attack because of the difference in the gust velocities at the wing and at the tail.

LATERAL STABILITY AND CONTROL

With careful design, the tailless airplane should be able to approach the conventional airplane in its lateral stability and control characteristics. The main difficulty is undoubtedly in the provision of sufficient weathercock stability and damping in yawing. The required degree of such stability is essentially the same as that for a conventional airplane and in either case is greatly reduced if the adverse yaw of the ailerons is eliminated. For this reason it seems desirable to use a lateral control having a zero or a slightly favorable yawing action. Favorable action is probably best achieved by a linkage between the aileron and the rudder controls or by a linkage between the ailerons and a servo tab on the rudder. With the aileron yaw compensated, the fin area required will be about in proportion to the size of the nacelles because the wing alone has marginal weathercock stability and damping. The unstable moment of the nacelles may be estimated by Munk's formulas (reference 5).

Different static yawing-moment characteristics may be obtained by altering the plan and elevation shapes of the wing. Changes of plan form alone do not, however, have a pronounced effect on the lateral-stability characteristics except insofar as they modify the stalling behavior of the wing. Weathercock stability may be secured by the use of sweepback combined with negative dihedral or with end plates at the tips. The negative-dihedral arrangement results in a favorable combination of rolling and yawing moments if the control is made to act on the turned-down tips. The yawing moment due to the rolling motion produced is adverse, however, and of such magnitude as to counteract the favorable effect, unless extreme negative dihedral is employed. If extreme negative dihedral is used, the controllers on the tips act primarily as rudders and separate ailerons must be provided on the main wing surface. The tips then correspond to end plates on the under side of the wing.

End plates on the under side of the wing will experience an outward force as a continuation of the lift of the wing. It might be thought that the outward lift of

such end plates would be unfavorable to weathercock stability, because a sideslip would increase the lift, and hence the drag, on the down-wind plate. In the true resolution of forces, however, it is found that the resultant tends to turn, maintaining a direction nearly enough at right angles to the wind to outweigh the drag increase. There is, therefore, actually a favorable weathercock action, as shown in figure 13. Similar considerations apply in determining the yawing moment of a wing with dihedral. In this case the customary setting, which inclines the lift inward, results in adverse weathercock action. For a more complete analysis of the lateral-stability characteristics of wings, the reader is referred to reference 6.

The requirement of dihedral for stability is essentially the same for a tailless airplane as for a conventional airplane. If spiral stability is not considered essential at all speeds (as is usually the case), it seems advisable to limit the dihedral to 1° or 2° in order to reduce lateral oscillations in rough air.

As in the case of pitching motion, elimination of the tail greatly reduces the rotational damping. Figure 14 shows the estimated damping coefficients of yawing motion $C_{n_r} = \frac{\partial C_n}{\partial \frac{rb}{U_o}}$ for some typical arrangements. The damping of a well-streamlined fuselage of round or oval cross section will be very small. One set of oscillation experiments gave a value equivalent to $C_{n_r} = -0.005$ for a fuselage having a length equal to two-thirds the wing span. In this case, however, the fuselage terminated in a vertical wedge, a feature which may well have accounted for the greater part of its damping. The damping of the wing is due to the distribution of drag along the span and becomes greater at higher lift coefficients. Within the usual limits of dihedral and weathercock effects, the damping of the free lateral oscillations is invariably greater than is indicated by the damping of pure yawing motion alone C_{n_r}. The additional damping is provided by C_{Y_β} and C_{l_p} and is introduced through the coupling of these motions (sideslipping and rolling) with the yawing motion. Because both C_{Y_β} and C_{n_r} as well as the coupling between yawing and rolling motions tend to diminish at lower angles of attack, the lateral oscillation is more likely to be troublesome at high speed. Figure 15 shows calculated

rates of damping of the free lateral oscillations for typical values of the stability derivatives. The value of C_{l_β} used corresponds to a dihedral angle of approximately 2°. An indication of the variation of lateral stability with C_{n_β} and C_{l_β} at low values of C_{n_r} may be obtained from the charts given in reference 7.

If sweepback is employed, the fact should be borne in mind that a pronounced rolling or pitching instability may develop at high angles of attack because of premature tip stalling associated with a lateral flow of the boundary layer. The effect of sweep is to introduce a component of the relatively great chordwise pressure gradient into a direction at right angles to the main stream velocity over the wing. The viscous drag of the stream then cannot act to prevent flow of the boundary layer laterally into regions of lower pressure over the forward portions of adjacent wing sections. The result is that the boundary layer flows toward the tips of a swept-back wing and premature separation occurs. Figure 16, plotted from data given in reference 8, shows this effect on sections near the tips of two rectangular wings with sweep. The existence of this effect may also be inferred from the tests of reference 9, in which the swept-back wings tended to nose up when stalled. (See fig. 17.) With 30° sweepback this tendency persisted even when the wing was given 8.5° washout. Little is know about the variation with angle of sweep, although the tests of reference 9 showed an appreciable effect at an angle of 15°. From these indications, it would seem advisable to incorporate some auxiliary boundary-layer control device, such as leading-edge slots, in the design of a tailless airplane having considerable sweepback.

CONCLUSIONS

1. With careful design it should be possible to secure satisfactory stability and control in a tailless airplane. The small rotational damping hardly affects the short-period longitudinal oscillations, although the damping of the stable lateral oscillation is likely to be reduced somewhat, particularly at high speeds.

2. Although the damping in pitching has a small effect on the stability with normal center-of-gravity locations, the tailless airplane is in greater danger of in-

stability due to an abnormal backward shift of the center of gravity because this instability becomes more serious as the damping is reduced.

3. As the weathercock stability or the damping in yawing is reduced by elimination of the tail surfaces, it becomes more important to overcome the aileron yaw and the yaw due to rolling.

4. A considerable reduction of the disturbances produced by vertical gusts is possible in the case of a tailless airplane without sweepback. This effect, which is due to a favorable pitching motion, depends on the static stability and the moment of inertia of the airplane.

5. The use of sweepback makes it possible to employ a partial-span flap as a high-lift device. It also simplifies the problem of securing weathercock stability and damping in yawing. Wind-tunnel tests of wings with sweepback show, however, that it is necessary to guard against a pronounced rolling and pitching instability near the stall.

Langley Memorial Aeronautical Laboratory,
National Advisory Committee for Aeronautics,
Langley Field, VA., October 2, 1941.

REFERENCES

1. Jacobs, Eastman N., and Ward, Kenneth E.: Interference of Wing and Fuselage from Tests of 209 Combinations in the N.A.C.A. Variable-Density Tunnel. Rep. No. 540, NACA, 1935.

2. Multhopp, H.: Zur Aerodynamik des Flugzeugrumpfes. Luftfahrtforschung, Bd. 18, Lfg. 2/3, 29 March, 1941, pp. 52-56.

3. Küssner, H. G.: Zusammenfassender Bericht über den instationären Auftrieb von Flügeln. Luftfahrtforschung, Bd. 13, Nr. 12, 20 Dec., 1936, pp. 410-424.

4. Jones, Robert T.: The Unsteady Lift of a Wing of Finite Aspect Ratio. Rep. No. 681, NACA, 1940.

5. Munk, Max M.: Fundamentals of Fluid Dynamics for Aircraft Designers. The Ronald Press Co., 1929, pp. 27-41.

6. Pearson, Henry A., and Jones, Robert T.: Theoretical Stability and Control Characteristics of Wings with Various Amounts of Taper and Twist. Rep. No. 635, NACA, 1938.

7. Zimmerman, Charles H.: An Analysis of Lateral Stability in Power-Off Flight with Charts for Use in Design. Rep. No. 589, NACA, 1937.

8. Knight, Montgomery, and Noyes, Richard W.: Span Load Distribution as a Factor in Stability in Roll. Rep. No. 393, NACA, 1931.

9. Anderson, Raymond F.: Determination of the Characteristics of Tapered Wings. Rep. No. 572, NACA, 1936.

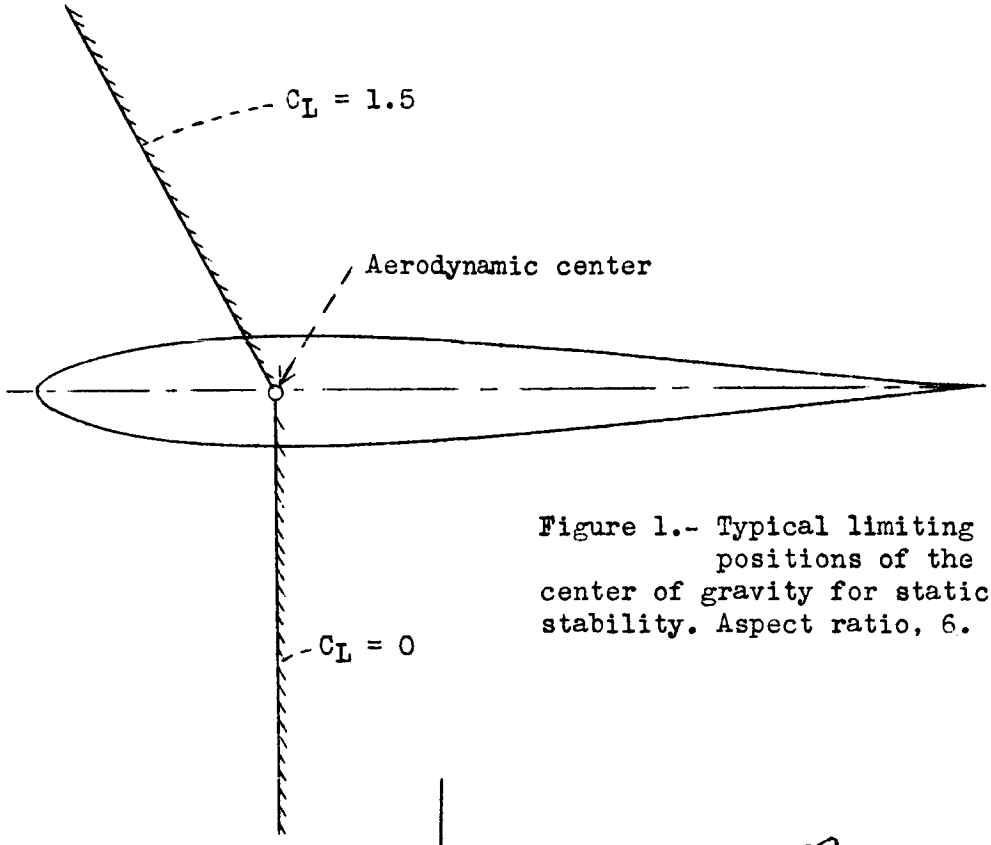

Figure 1.- Typical limiting positions of the center of gravity for static stability. Aspect ratio, 6.

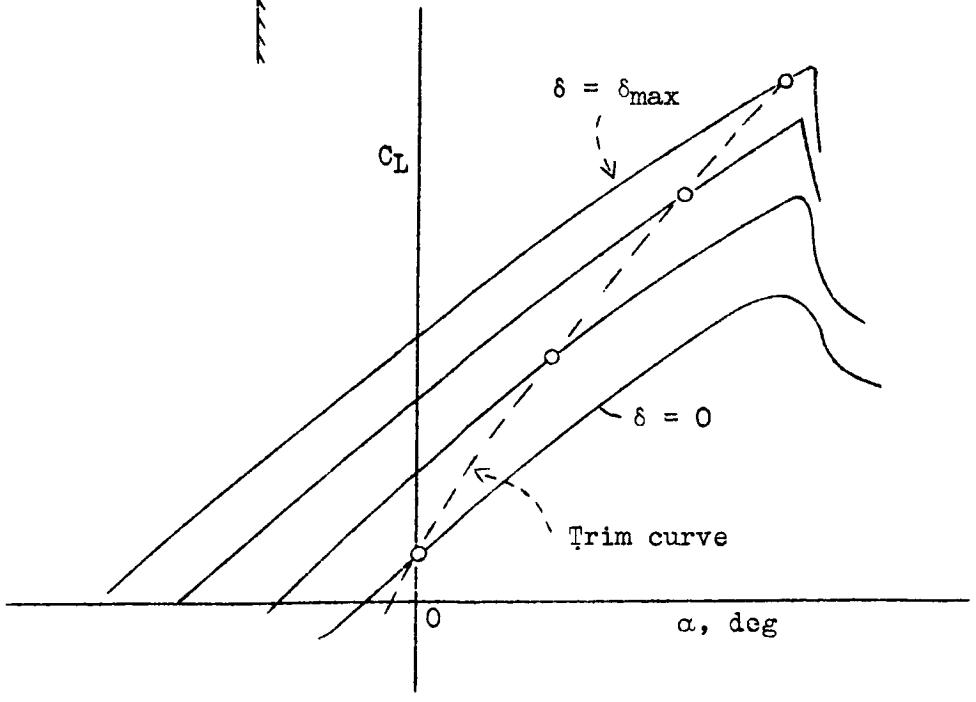

Figure 10.- Simultaneous change in lift and angle of attack produced by a flap on a wing with sweepback.

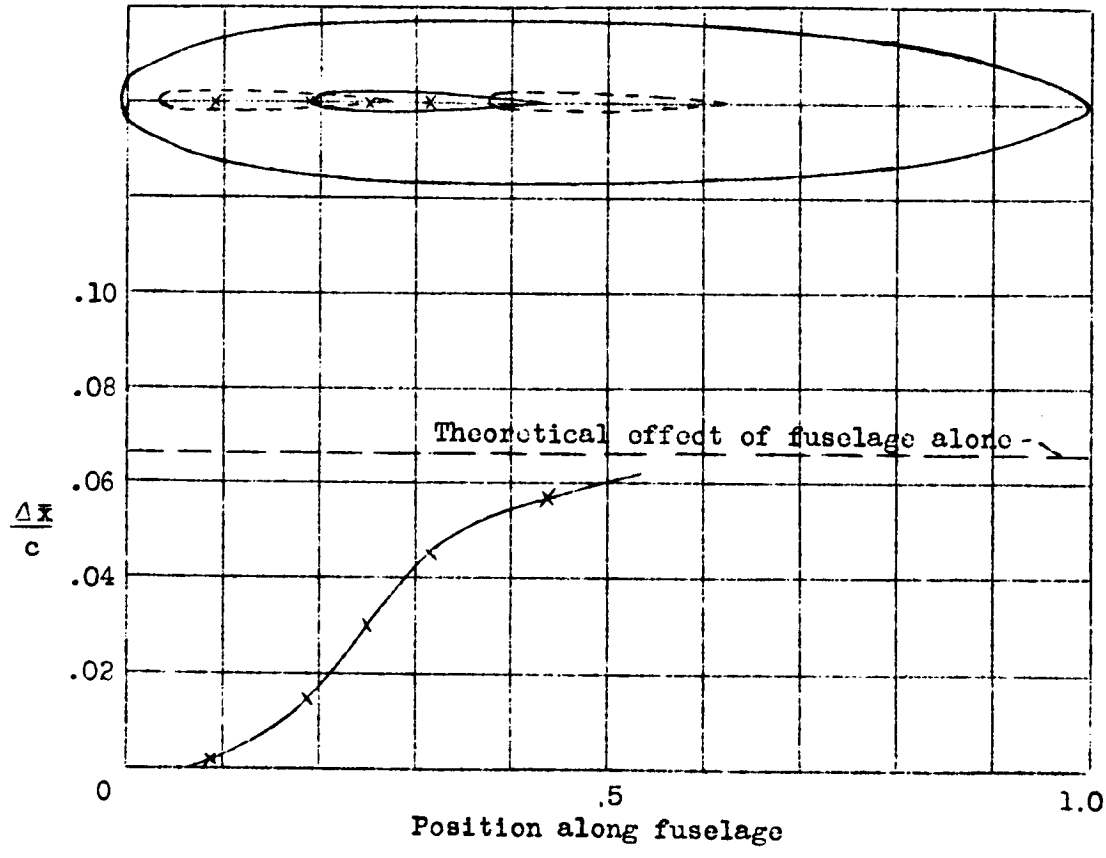

Figure 2.- Forward displacement of the aerodynamic center caused by the fuselage in combination with the wing. Wing span, 1.5. Data from reference 1.

$C_{m_{D\theta}} = -0.5$

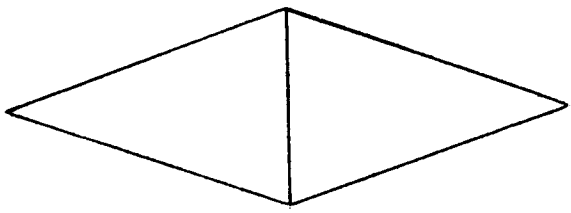

$C_{m_{D\theta}} = -0.6$

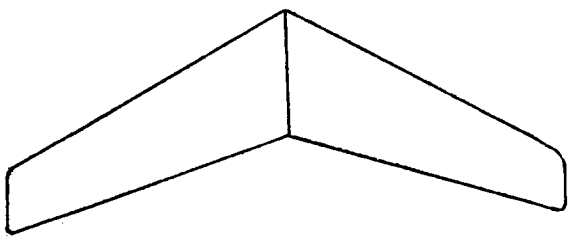

$C_{m_{D\theta}} = -1.2$

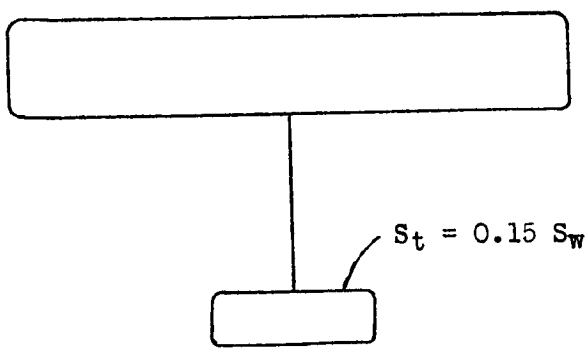

$C_{m_{D\theta}} = -4.6$

Figure 3.- Representative damping coefficients. $C_{m_{D\theta}} = \frac{\partial C_m}{\partial \frac{qc}{U_o}}$

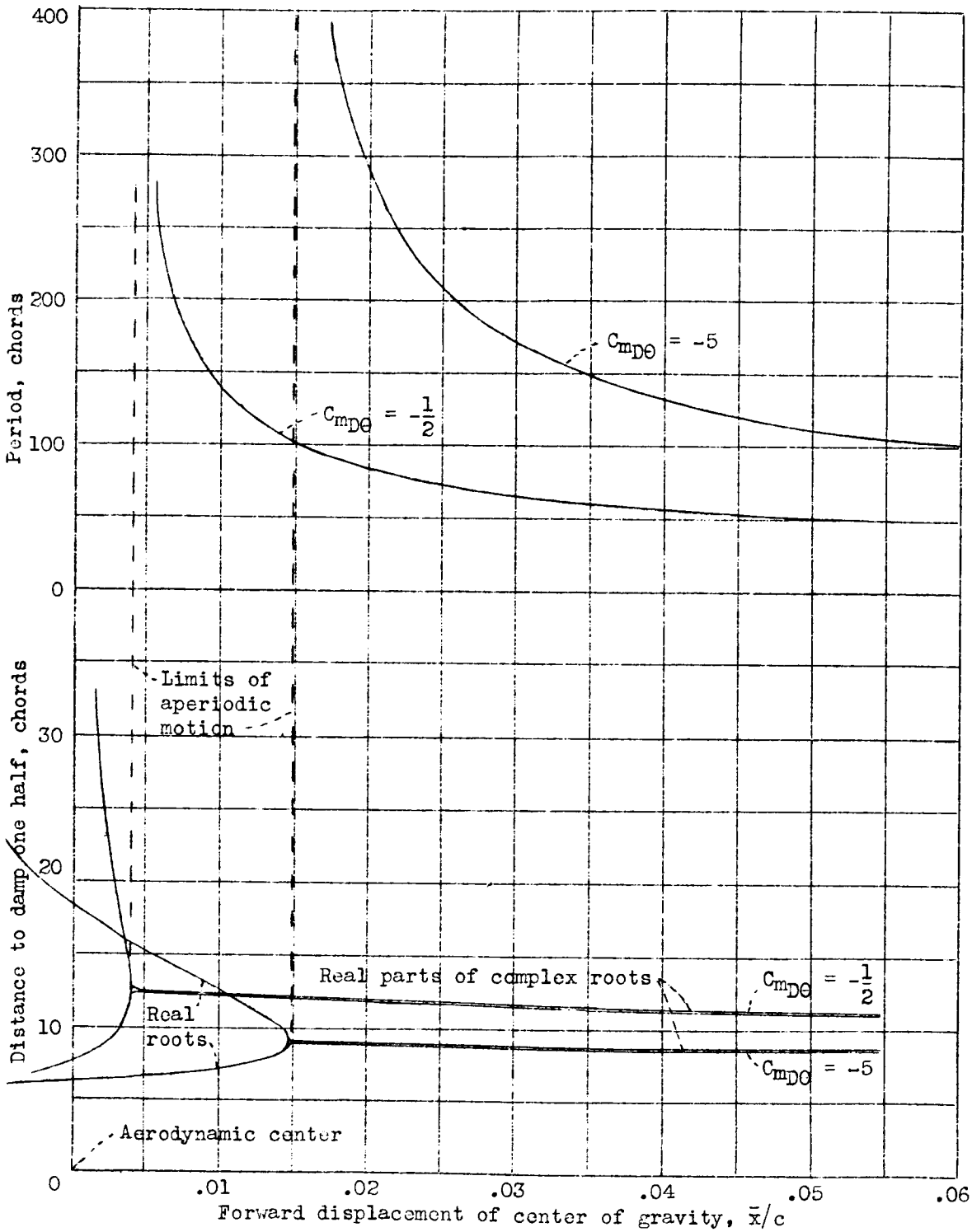

Figure 4.- Characteristics of the short-period longitudinal oscillation.

$$\frac{m}{S\frac{\rho}{2}c} = 50$$

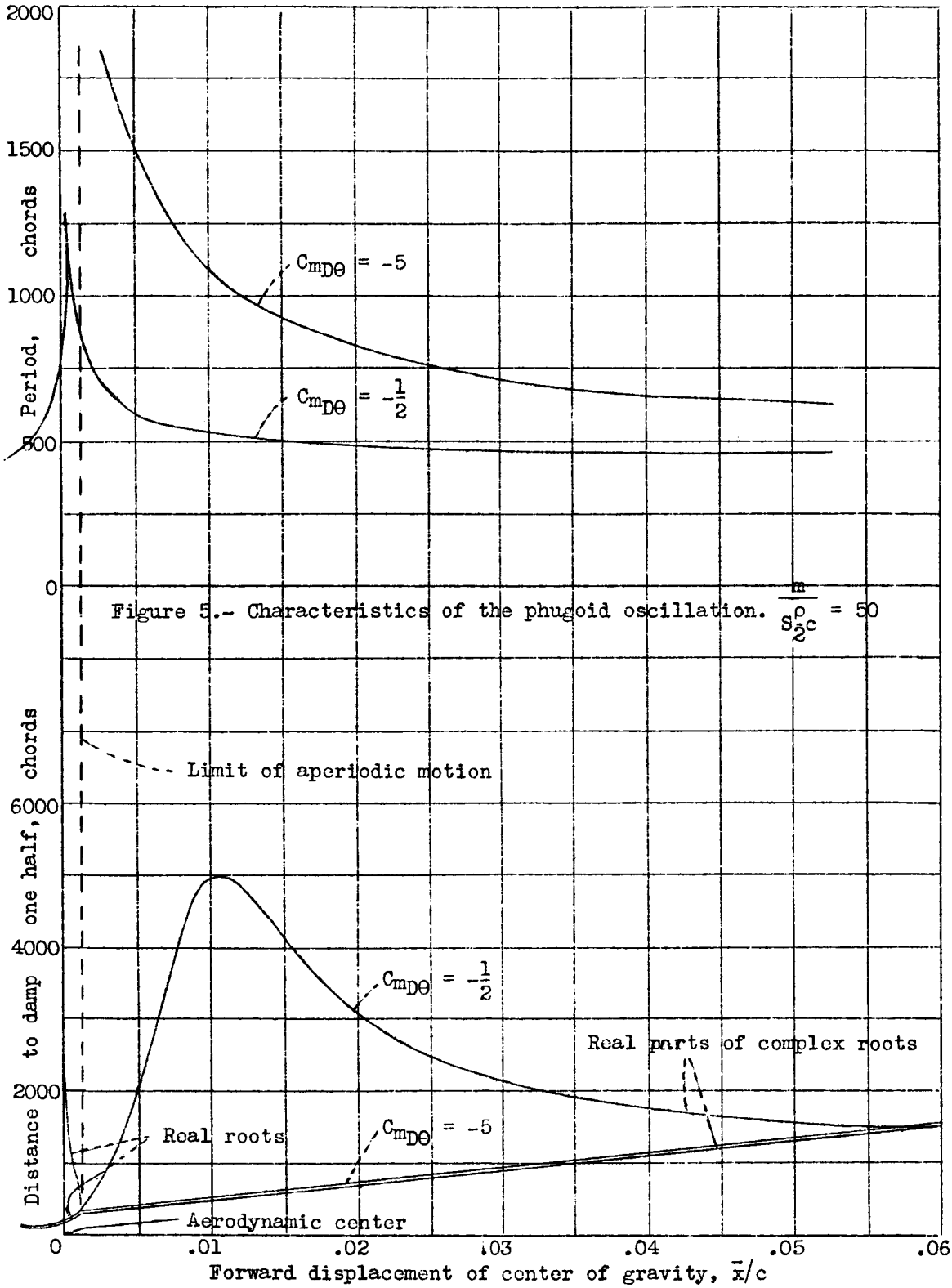

Figure 5.- Characteristics of the phugoid oscillation. $\frac{m}{S\frac{\rho}{2}\bar{c}} = 50$

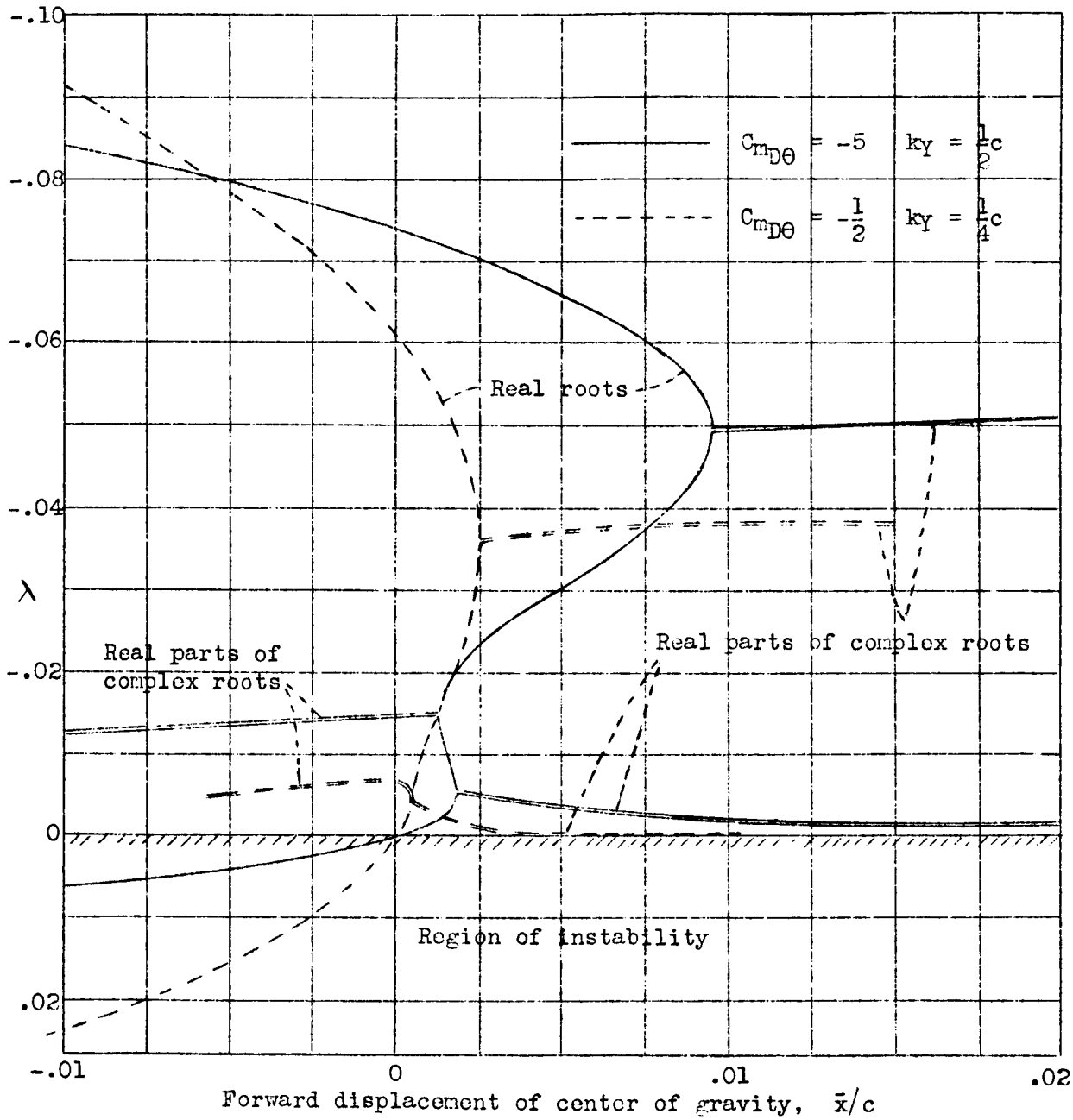

Figure 6.- Variations of stability with small displacements of the center of gravity from the aerodynamic center. Root of stability equation, λ; $\frac{m}{S\frac{\rho}{2}c} = 150$; $C_L = 2.0$.

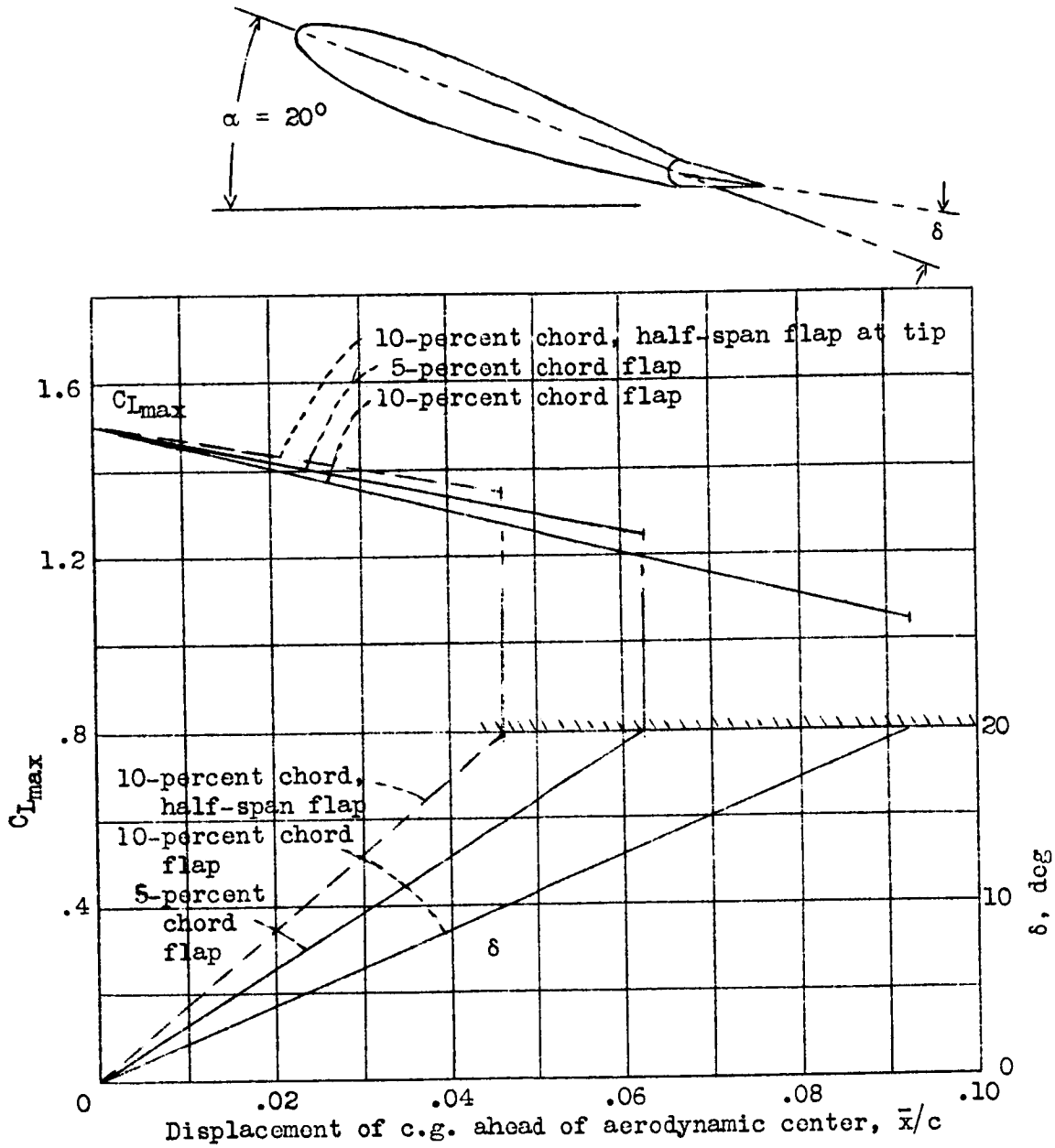

Figure 7.- Elevator deflections and corresponding reductions in $C_{L_{max}}$ for trim at $\alpha = 20^{\circ}$. Rectangular wing, aspect ratio, 6.

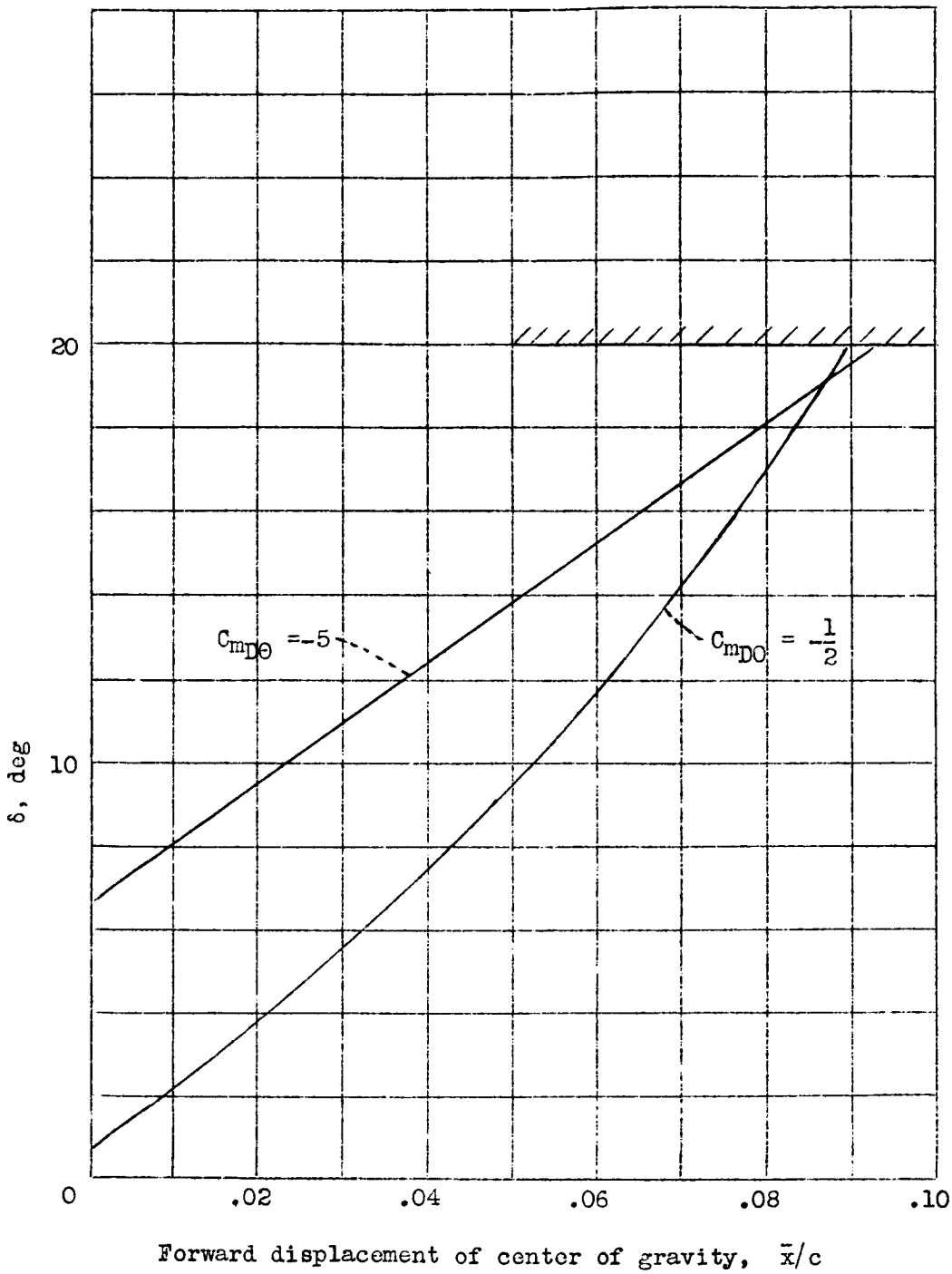

Figure 8.- Typical elevator deflections required to produce specified acceleration in pull-up. (Elevators designed to give equal pitching moments.)

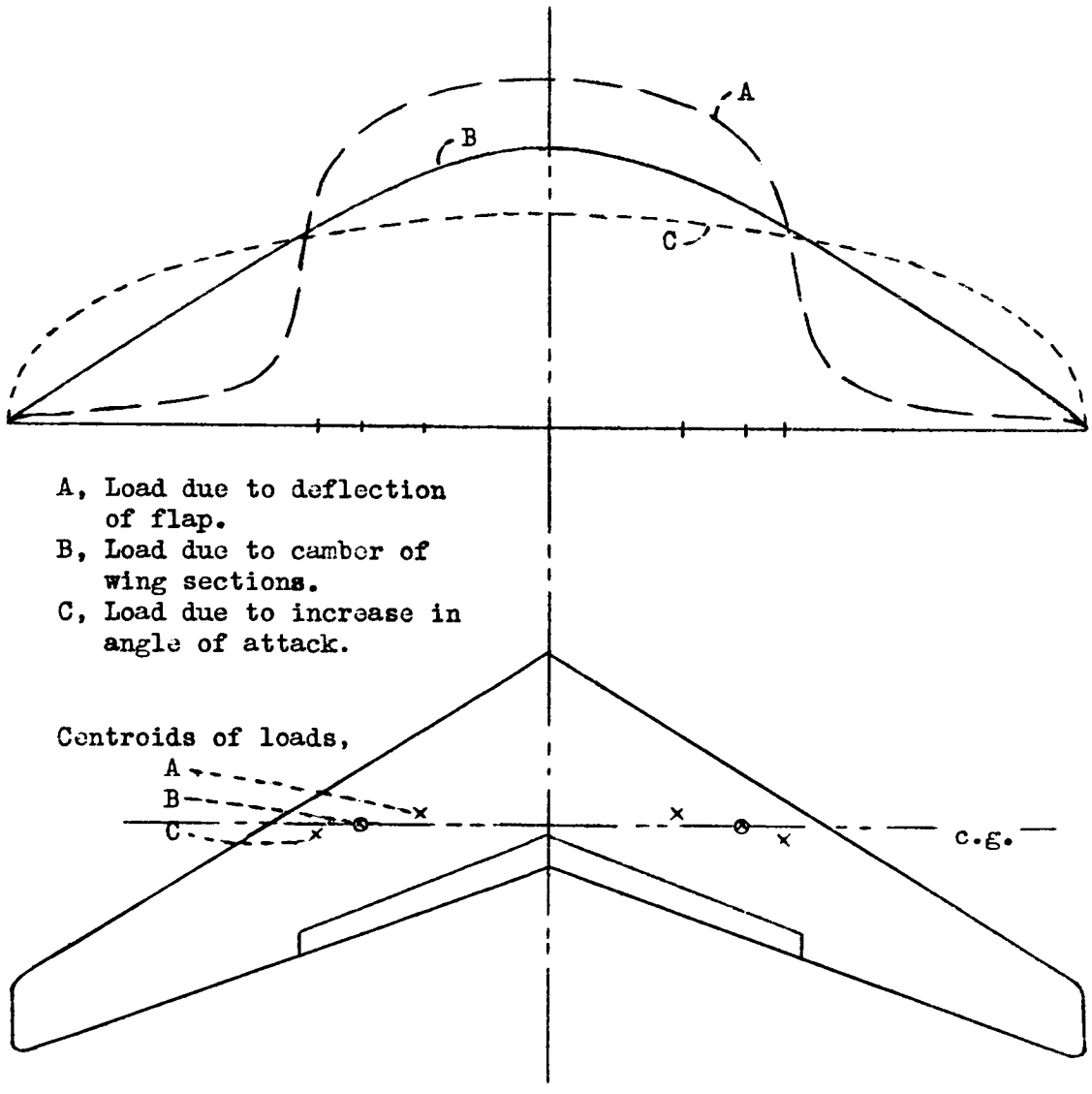

Figure 9.- Diagram illustrating the use of sweepback to secure trim with a partial-span flap.

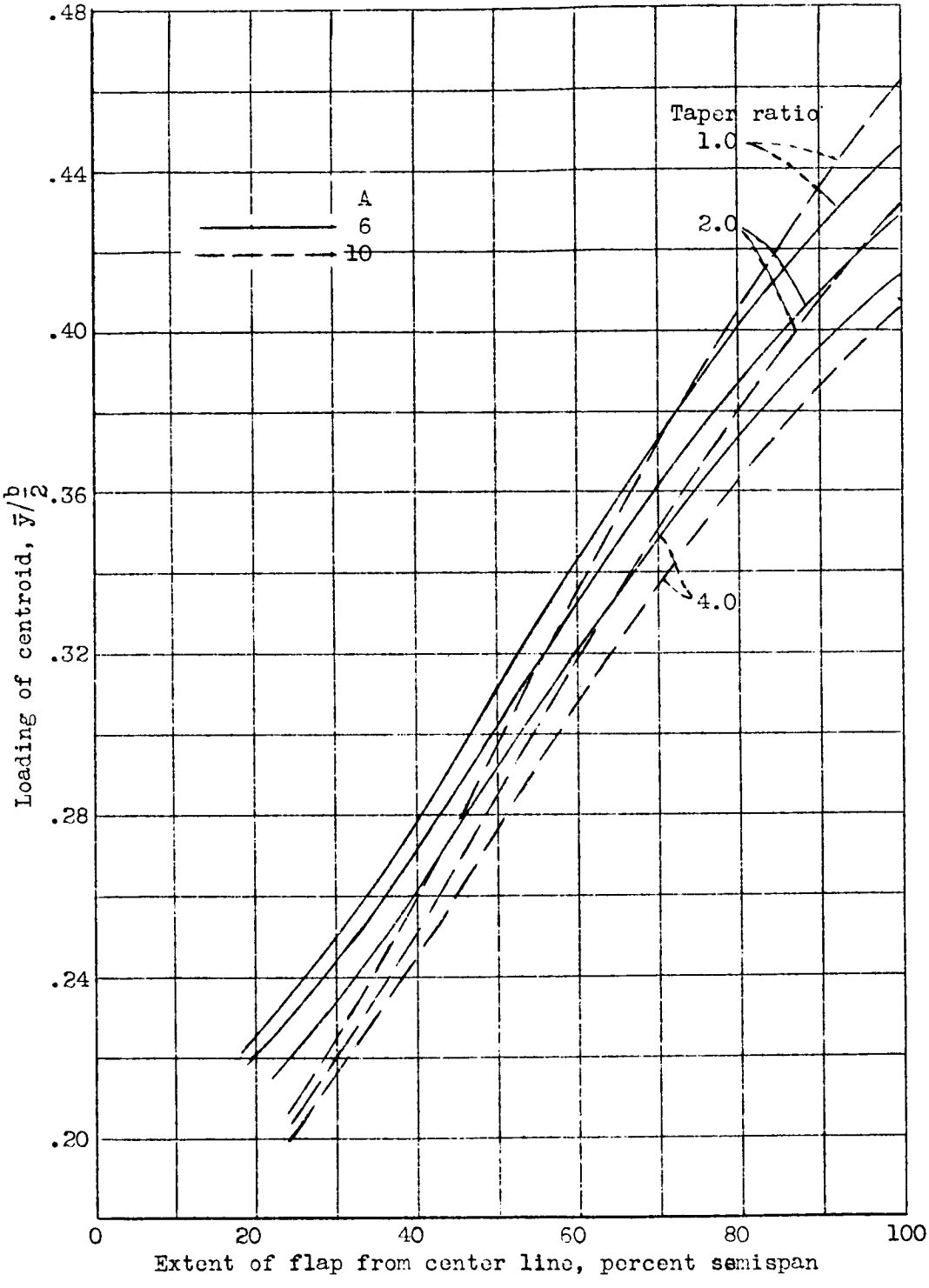

Figure 11.- Spanwise location of the centroid of the loading due to deflection of partial-span flaps. (Loading A, figure 9.)

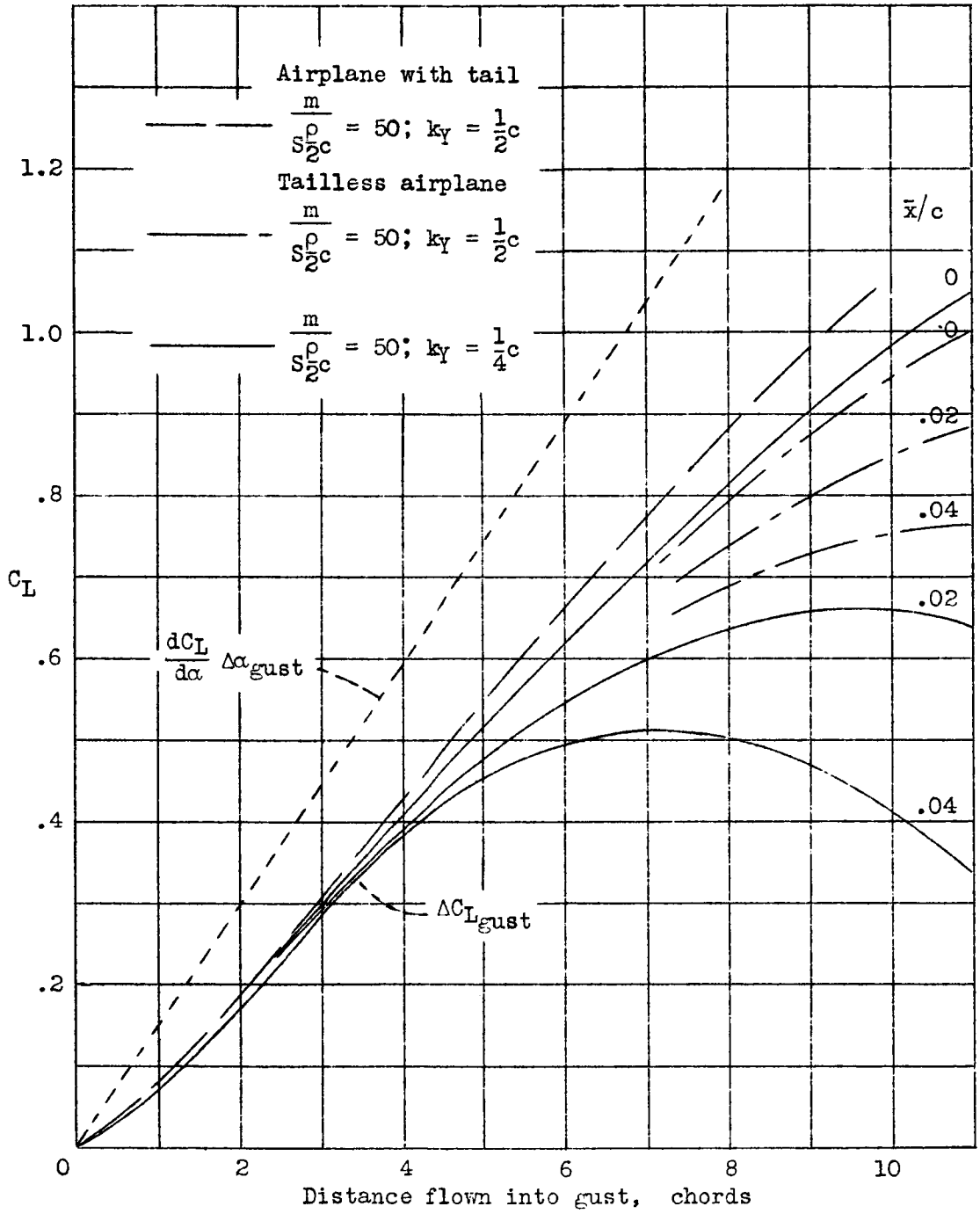

Figure 12.- Gust-alleviating action due to pitching motion and to lag in the development of lift.

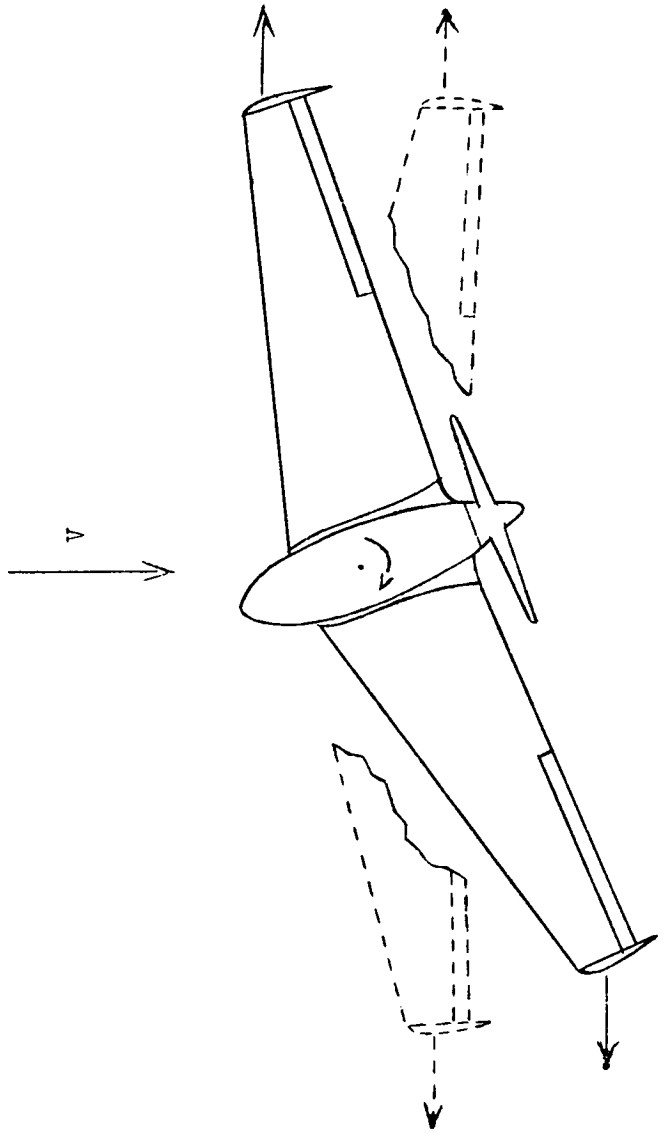

Figure 13.- Weathercock action of end plates set to give outward lift.

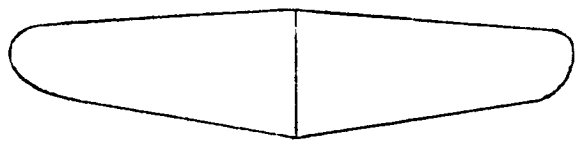

$C_{n_r} = -.003$

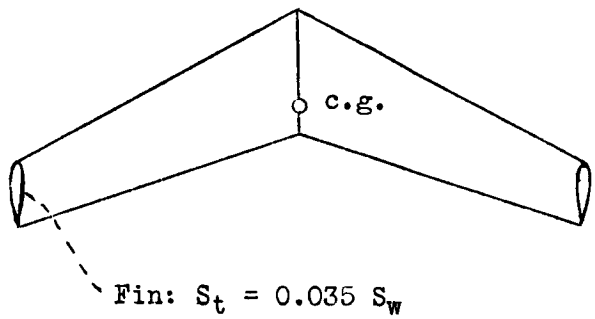

$C_{n_r} = -.005$

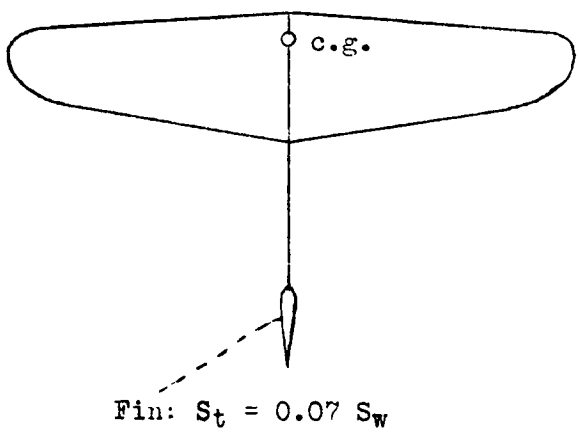

$C_{n_r} = -.050$

Figure 14.- Representative damping coefficients. $C_{n_r} = \frac{\partial C_n}{\partial \frac{rb}{U_o}}$

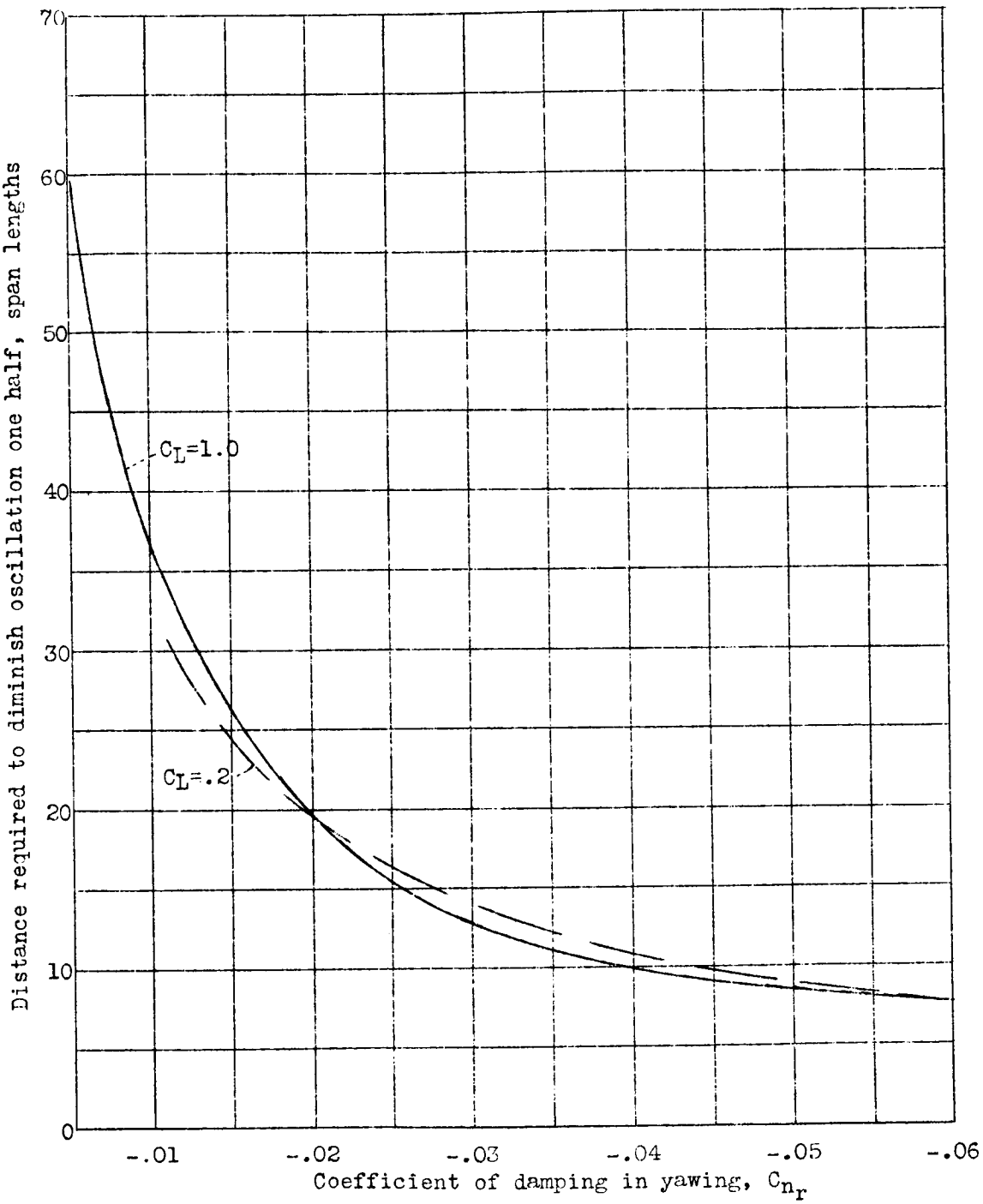

Figure 15.- Variation of damping of lateral oscillations with C_{n_r}.

$\frac{m}{S\frac{\rho}{2}b} = 8\frac{1}{3}$; $\frac{k_X}{b} = \frac{1}{8}$; $\frac{k_Z}{b} = \frac{1}{7}$; $C_{l_\beta} = -0.026$; $C_{n_\beta} = 0.020$.

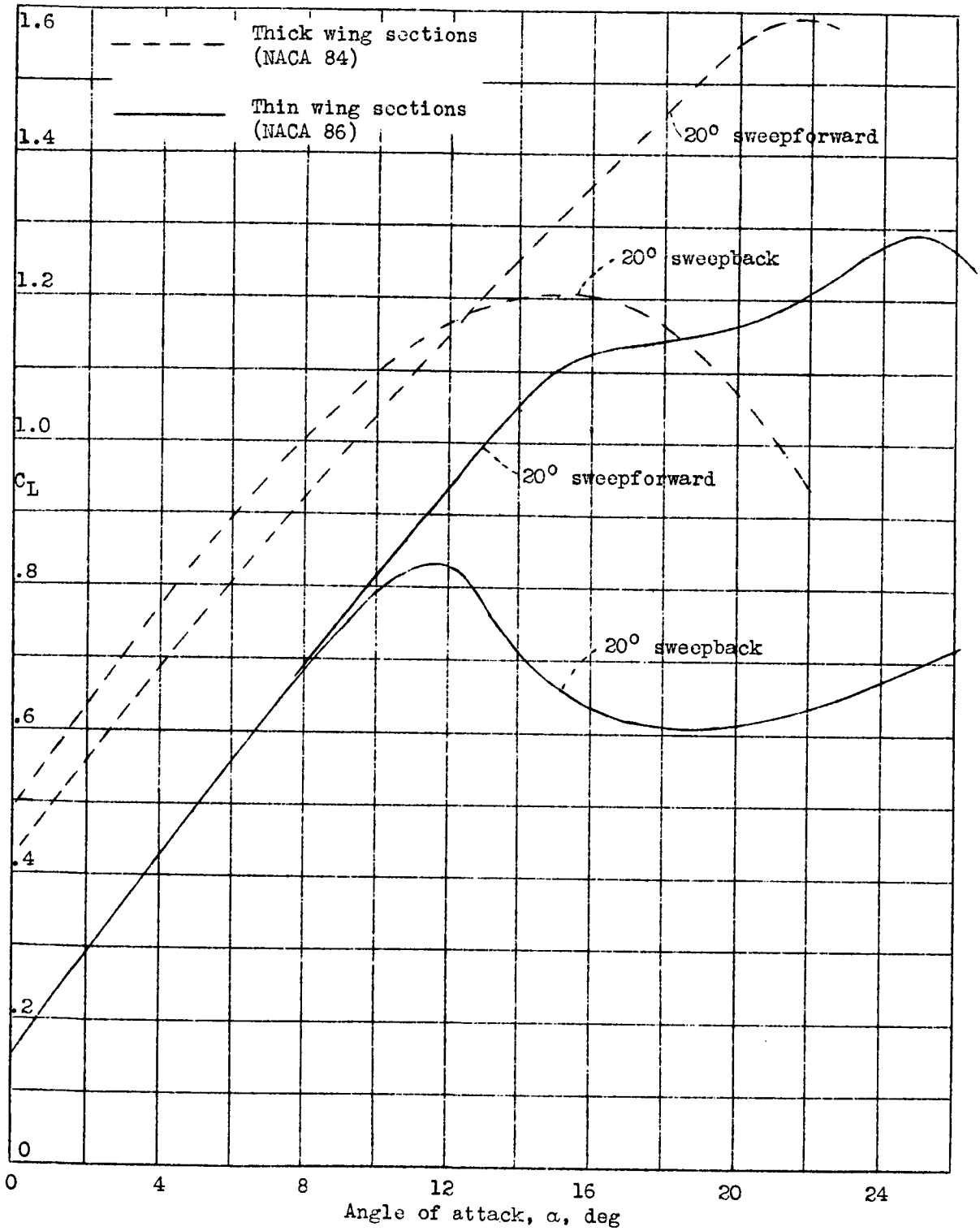

Figure 16.- Effect of sweep on the lift of a wing section near the tip (80 percent semispan stations). Data from reference 8.

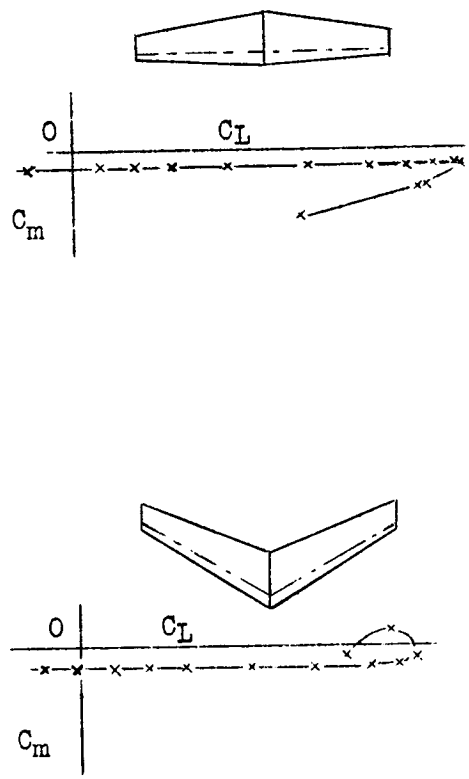

Figure 17.- Test results showing pitching instability of swept-back wing at $C_{L_{max}}$. Data from reference 9.

WARTIME REPORT L-464

WIND-TUNNEL INVESTIGATION OF CONTROL-SURFACE CHARACTERISTICS V—THE USE OF A BEVELED TRAILING EDGE TO REDUCE THE HINGE MOMENT OF A CONTROL SURFACE

Robert T. Jones and Milton B. Ames, Jr.

Langley Memorial Aeronautical Laboratory

March 1942

WIND-TUNNEL INVESTIGATION OF CONTROL-SURFACE CHARACTERISTICS

V - THE USE OF A BEVELED TRAILING EDGE TO REDUCE THE HINGE MOMENT OF A CONTROL SURFACE

By Robert T. Jones and Milton B. Ames, Jr.

SUMMARY

Wind-tunnel tests have been made to investigate the possibility of reducing the hinge moments of a control surface by beveling the trailing edge. The tests were made with a 9-percent-thick airfoil having a 30-percent-chord plain flap. A faired beveled shape, 5 percent of the airfoil chord in width and having a thickness of 2½ percent of the airfoil chord, was found to give approximately 50-percent reduction in the hinge moment caused by a given deflection of the flap and 80-percent reduction in the hinge moment due to the angle of attack of this airfoil for a wide range of angles. A blunter beveled portion of the same thickness gave overbalance and reversal of the floating tendency over a small angular range. Elliptical trailing-edge shapes were also tried but were found to be somewhat less effective than the shapes ending in an acute angle. A semicircular trailing edge produced only a slight change in the hinge moments but caused a drag increment much greater than that of an efficient beveled shape.

INTRODUCTION

The hinge moments obtained in tests of airfoils with plain flaps have often been observed to fall considerably below the values predicted by the potential-flow theory. It has also been noted that the hinge moments obtained in different tests show wider discrepancies than do other airfoil characteristics.

Several years ago the NACA had occasion to test a flap with a particularly thin, sharp trailing edge. In this case the hinge moments were higher than usual and agreed better with the theory. Thus, it appeared that the discrepancies in the hinge moments obtained in the usual tests might have been due to minor differences in the shapes of the trailing

edge. This phenomenon led to speculation concerning the nature of the flow near the trailing edge and the effect of small departures from the Kutta condition.

In the ideal flow, the Kutta condition requires that the air leaving the trailing edge maintain the direction of the mean camber for a short distance downstream. The velocities on the upper and lower surfaces approach the same value with the result that the pressure difference or lift vanishes at the trailing edge. The curve marked "a" in figure 1 shows the lift distribution over an airfoil section with the flow conforming perfectly to this condition. The guiding action of a slightly blunt or beveled trailing edge will not be perfect, however, and in such a case a relatively great negative lift will be developed across the edge, as shown by curve "b" in figure 1. A deliberate thickening of the airfoil, designed to permit further deviation from the Kutta condition, might therefore lead to the type of pressure distribution represented by curve "b" in figure 1. It was thought that the effect might be used to provide aerodynamic balance for a control surface and in order to test this theory a series of wind-tunnel experiments was planned. These tests have recently been made and form the subject of the present paper.

TESTS

Apparatus and Models

In figure 2 are shown the shapes tested. These shapes are of two types - beveled and elliptical. In the case of the beveled flap, the point at which the beveling of the flap began was faired into an arc in order to allow smooth flow. The portion of the flap extending from the center of this arc to the trailing edge will be referred to hereinafter as the "bevel." Because the action of the blunt trailing edge is in some ways similar to that of an automatic balancing tab (see fig. 3), the beveled shapes were designed to approximate the outline of such tabs in the balancing position. The 20-percent bevel corresponds to a 20-percent c_f tab deflected 10°. The elliptical shapes are of somewhat similar proportions. A flap having a bulged portion near the hinge was also tried. With the exception of the bulged flap, all shapes tested were obtained by interchanging trailing-edge blocks having these shapes on a standard 2-foot-chord by 4-foot-span model of laminated mahogany.

Table I gives the ordinates of the standard section (derived from the NACA 0009 airfoil by drawing straight lines from the 55-percent station back to the removable tail block). The dimensions of the removable tail portions are shown in figure 2 and the ordinates of the bulged flap are given in table II. As shown in figure 2, the flap was of the plain unbalanced type, 30 percent of the airfoil chord in width. The tests were made with the gap both sealed and open.

The procedure of the tests was similar to that followed in reference 1. They were made in the NACA 4-foot by 6-foot vertical tunnel, modified as described in reference 2. The lift, the drag, and the pitching moments were measured on a three-component balance. The hinge moments were measured electrically with a calibrated torque rod built into the model. The model extended completely across the closed test section of the tunnel, so that the flow was very nearly two-dimensional. The tests were made at a dynamic pressure of 15 pounds per square foot, corresponding to a velocity of about 76 miles per hour and a test Reynolds number of 1,430,000. The flap deflection was varied in 5° increments from 0° to 30°. In some cases check points at ±2° from neutral were obtained. Lift, drag, airfoil pitching moment, and flap hinge moments were measured throughout the angle-of-attack range, from positive to negative stall of the airfoil, at 2° intervals of angle of attack.

Precision

The maximum error in the angle of attack or in flap setting appears to be about ±0.2°. An experimentally determined correction has been applied to the lift but not to the hinge moments. The hinge moments are probably slightly higher than would be obtained in free air. It should be noted that the drag of the basic 0009 airfoil is somewhat higher than is obtained in other tests at the same Reynolds number.

RESULTS AND DISCUSSION

Symbols

c_l airfoil section lift coefficient (l/qc)

c_{d_o} airfoil section profile-drag coefficient (d_o/qc)

c_m airfoil section pitching-moment coefficient (m/qc^2)

c_h flap section hinge-moment coefficient (h/qc_f^2)

α_o angle of attack of infinite aspect ratio

α_e equivalent angle of attack

δ_f flap angle with respect to airfoil

l airfoil section lift

d_o airfoil section profile drag

m airfoil section pitching moment about quarter-chord point of airfoil

h flap section hinge moment

c chord of airfoil with flaps neutral

c_f flap chord

c_b chord of beveled portion of flap

Section data are plotted in figure 4. Figures 5 and 6, cross-plotted from the section data, show typical variations of lift and hinge moment and illustrate the magnitude of the effect obtainable with a moderate and with an extremely blunt bevel. It will be noted that the reduction in hinge moment outweighs the loss in lift and also that the reduction in $\partial c_h/\partial \alpha_o$ is greater than the reduction in $\partial c_h/\partial \delta_f$. The lift of the airfoil with the control free is therefore actually greater for the blunt trailing edge than for the plain flap. The results for the plain flap are taken from reference 1, part I.

The results given for the flap with beveled trailing edge are for the gap-sealed condition. The tests with the gap open showed no noteworthy results beyond the loss in efficiency usually associated with this condition.

Table III summarizes several important characteristics of the shapes tested. The values given in the table apply to a fairly wide angular range. An idea of the deviations from linearity may be obtained by inspection of figure 4.

The results show an interesting difference in the behavior of the elliptical and the beveled trailing edges. The bluntest elliptical shape, which was simply a circular

rounding, increased the floating tendency and the drag but had no appreciable effect on $\partial c_h/\partial \delta_f$ or $\partial c_l/\partial \alpha_o$. In this case the curvature of the surface is so great that the flow apparently leaves the airfoil as if the end had been cut off square. The increment of drag coefficient in this case is approximately 0.0028. The moderately beveled or tapered shapes, the 0.20 c_f and 0.15 c_f bevels, on the other hand, showed less than 0.0004 increase in drag coefficient, indicating fairly complete closure of the flow behind the airfoil. This small drag increase, together with the regularity of the hinge-moment variation, indicates that the balancing action of the moderate shapes does not depend on a pronounced separation of flow but on more or less progressive changes in the boundary-layer thickness on the two sides of the bevel. As the angle of the bevel becomes steeper, the closure of the flow becomes less complete and the balancing action becomes more pronounced though somewhat irregular and may involve complete separation on one side or the other. The critical angle in the present tests was that of the 0.13 c_f bevel.

As will be noted in table III, the airfoil pitching moments follow the variation that might be expected from the hinge moments. In the most extreme case (0.10 c_f bevel), the aerodynamic center was shifted 0.051c ahead of the quarter-chord point.

From a practical standpoint the most interesting results are those obtained with the moderately beveled and elliptical shapes (0.15 c_f to 0.20 c_f bevels). Thus the 0.20 c_f bevel shows nearly 50-percent reduction in $\partial c_h/\partial \delta_f$ and more than 50-percent reduction in $\partial c_h/\partial \alpha_o$, as compared with the plain flap. The drag increments are not so great as those obtained in comparable tests (reference 1) of the conventional inset-hinge balance with the medium or tapered nose but are greater than those obtained with the blunt nose balance. Inasmuch as the beveled trailing edge is effective in reducing the floating moment, the lift of the airfoil is greater with the control free than with the plain or the inset-hinge flap.

It is frequently found that full balance cannot be obtained in a satisfactory manner by the use of a single device; for example, a large degree of balance with the inset-hinge type of control surface requires such a long overhang that the permissible deflection of the flap is limited. The use of a large horn balance introduces structural difficulties. It is helpful, therefore, to

have available several independent means of reducing hinge moments. The beveled trailing edge should be especially useful in combination with other types of balance, because it involves no additional linkages. Also, it is occasionally found desirable to increase the hinge moments slightly as a final adjustment during flight tests. Such an adjustment might be provided by the addition of a thin, sharp edge.

The present tests are too limited to furnish more than very general information on the effects of trailing-edge shape. Thus, the variations with flap chord, Reynolds number, or airfoil section have not been explored. In any event, it is to be expected that the effect of trailing-edge shape will be greatly magnified as the chord of the flap is reduced - a fact that makes it necessary to employ a certain amount of care in the construction of the trailing edge.

CONCLUSIONS

The beveled trailing edge provides a convenient means of reducing the hinge moments of control surfaces. In the present tests, a moderate bevel on a 30-percent-chord flap produced a 50-percent reduction in the hinge moment cause by a given deflection of the flap. This balancing effect extended over a wide angular range and showed a smooth variation with angle of attack and with flap deflection. The profile-drag coefficient showed an increase of 0.0004.

Overbalance and reversal of the floating tendency over a small angular range were obtained when rather blunt bevels were tested. The effect of trailing-edge shape is expected to be even more pronounced as the chord of the flap is reduced, indicating the necessity for careful construction of narrow flaps.

National Advisory Committee for Aeronautics,
Langley Memorial Aeronautical Laboratory
Langley Field, Va.

REFERENCES

1. Sears, Richard I.: Wind-Tunnel Investigation of Control-Surface Characteristics. I. Effect of Gap on the Aerodynamic Characteristics of an NACA 0009 Airfoil with a 30-Percent-Chord Plain Flap. NACA A.R.R., June 1941.

   Sears, Richard I. and Hoggard, H. Page, Jr.: Wind-Tunnel Investigation of Control-Surface Characteristics. II. A Large Aerodynamic Balance of Various Nose Shapes with a 30-Percent-Chord Flap on an NACA 0009 Airfoil. NACA A.R.R., Aug. 1941.

   Ames, Milton B., Jr.: Wind-Tunnel Investigation of Control-Surface Characteristics. III. A Small Aerodynamic Balance of Various Nose Shapes with a 30-Percent-Chord Flap on an NACA 0009 Airfoil. NACA A.R.R., Aug. 1941.

   Ames, Milton B., Jr. and Eastman, Donald R. Jr.: Wind-Tunnel Investigation of Control-Surface Characteristics. IV. A Medium Aerodynamic Balance of Various Nose Shapes Used with a 30-Percent-Chord Flap on an NACA 0009 Airfoil. NACA A.R.R., Sept. 1941.

2. Ames, Milton B. Jr. and Sears, Richard I.: Pressure-Distribution Investigation of an N.A.C.A. 0009 Airfoil with a 30-Percent-Chord Plain Flap and Three Tabs. T. N. No. 759, NACA, 1940.

3. Sears, Richard I.: Wind-Tunnel Data on the Aerodynamic Characteristics of Airplane Control Surfaces. NACA ACR No. 3L08, 1943.

TABLE I

ORDINATES OF MODIFIED NACA 0009 AIRFOIL

[Stations and ordinates in percent airfoil chord]

	Stations	Ordinates
NACA 0009 airfoil section	0	0
	1.25	±1.42
	2.5	±1.96
	5.0	±2.67
	7.5	±3.15
	10	±3.51
	15	±4.01
	20	±4.30
	25	±4.46
	30	±4.50
	40	±4.35
	50	±3.97
Straight portion	60	±3.42
	70	±2.83
	80	±2.25
	90	±1.67
	100	±1.08

L. E. radius: 0.89

TABLE II

ORDINATES OF BULGED FLAP

[Stations and ordinates in percent airfoil chord]

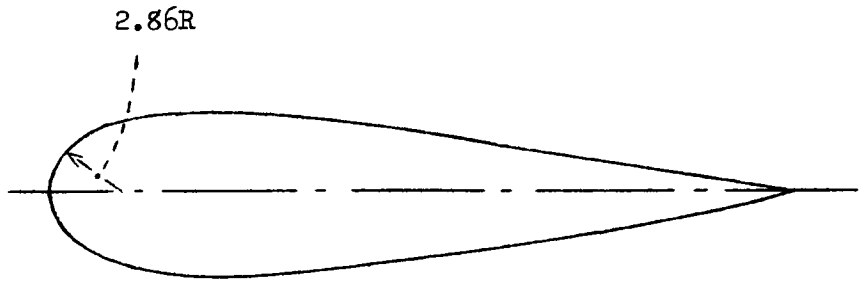

Stations (from hinge axis)	Ordinates
0	±2.96
1.94	±3.38
4.82	±3.62
7.85	±3.43
10.80	±3.03
15.25	±2.37
19.70	±1.69
25.15	±1.02
30.00	±0.10

TABLE III.- SUMMARY OF CHARACTERISTICS OF TRAILING-EDGE SHAPES TESTED

Modifications	$\left(\frac{\partial c_h}{\partial \delta_f}\right)$	$\left(\frac{\partial c_h}{\partial \alpha_o}\right)_{\delta_f}$	$\left(\frac{\partial c_l}{\partial \alpha_o}\right)_{\delta_f}$ (Control fixed)	$\left(\frac{\partial c_l}{\partial \alpha_o}\right)_{c_h=0}$ (Control free)	$\left(\frac{\partial \alpha_o}{\partial \delta_f}\right)_{c_l}$	$\left(\frac{\partial c_m}{\partial \delta_l}\right)_{\delta_f}$	$\left(\frac{\partial c_m}{\partial \delta_f}\right)_{c_l}$	$c_{d_{o_{min}}}$ (Uncorrected)
Plain	-0.012	-0.006	0.098	0.066	0.57	0.001	-0.010	0.0096
$0.20c_f$ bevel	-.007	-.003	.092	.070	.56	.033	-.009	.0100
$0.15c_f$ bevel	-.005	-.001	.091	.080	.56	.038	-.008	.0100
$0.13c_f$ bevel	-.003	.001	.090	.106	.54	.048	-.008	.0105
$0.10c_f$ bevel	.000	.002	.088	Unstable	.50	.051	-.007	.0110
$0.20c_f$ elliptical	-.006	-.003	.091	.068	.50	.036	-.008	.0105
$0.10c_f$ elliptical	-.011	-.008	.099	.060	.54	.011	-.008	.0118
Semicircular	-.012	-.009	.101	.059	.56	.002	-.010	.0124
Bulged	-.010	-.005	.095	.071	.50	.016	-.010	.0102

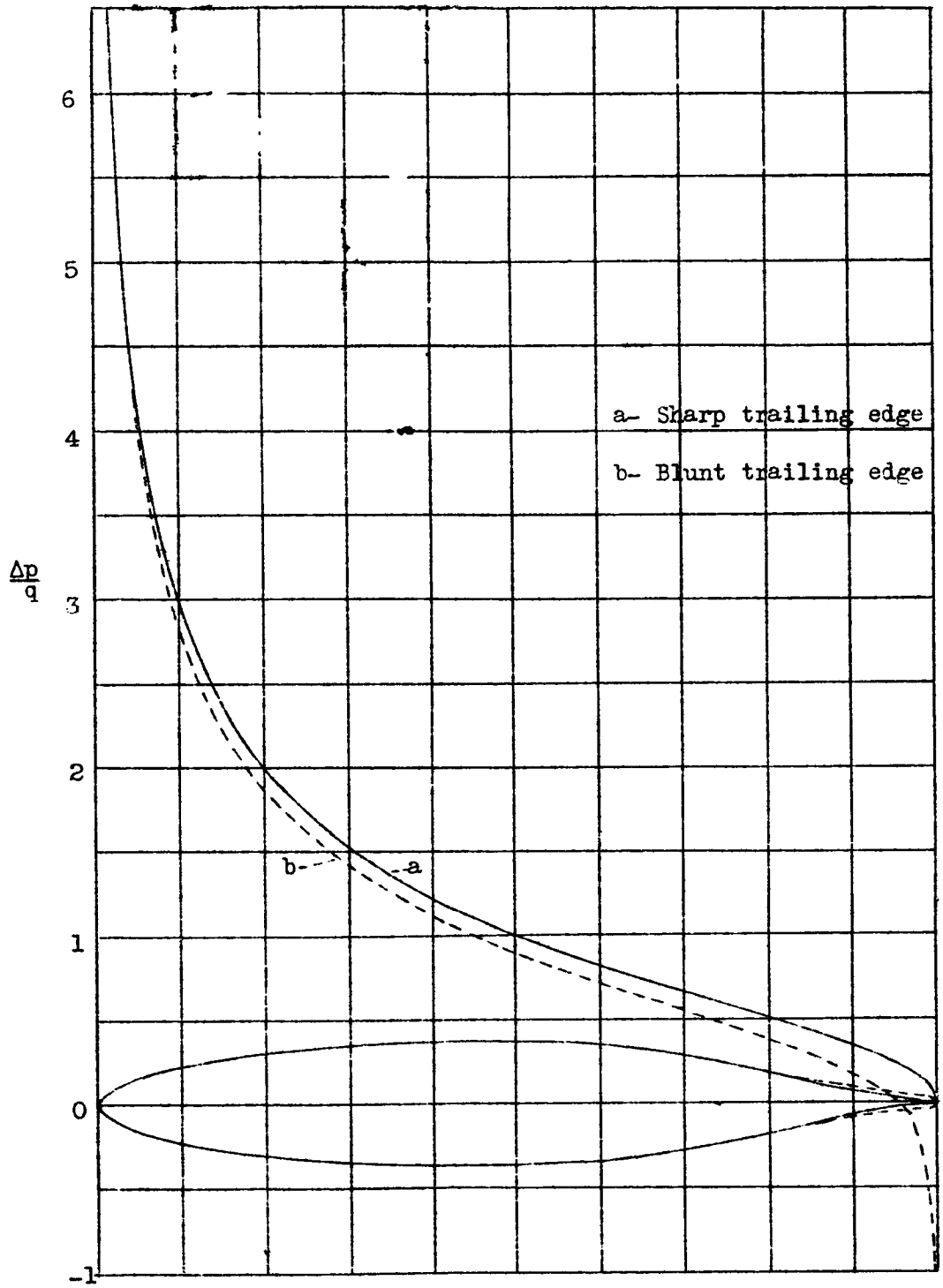

Figure 1.- The effect of flow around the trailing edge on the lift distribution.

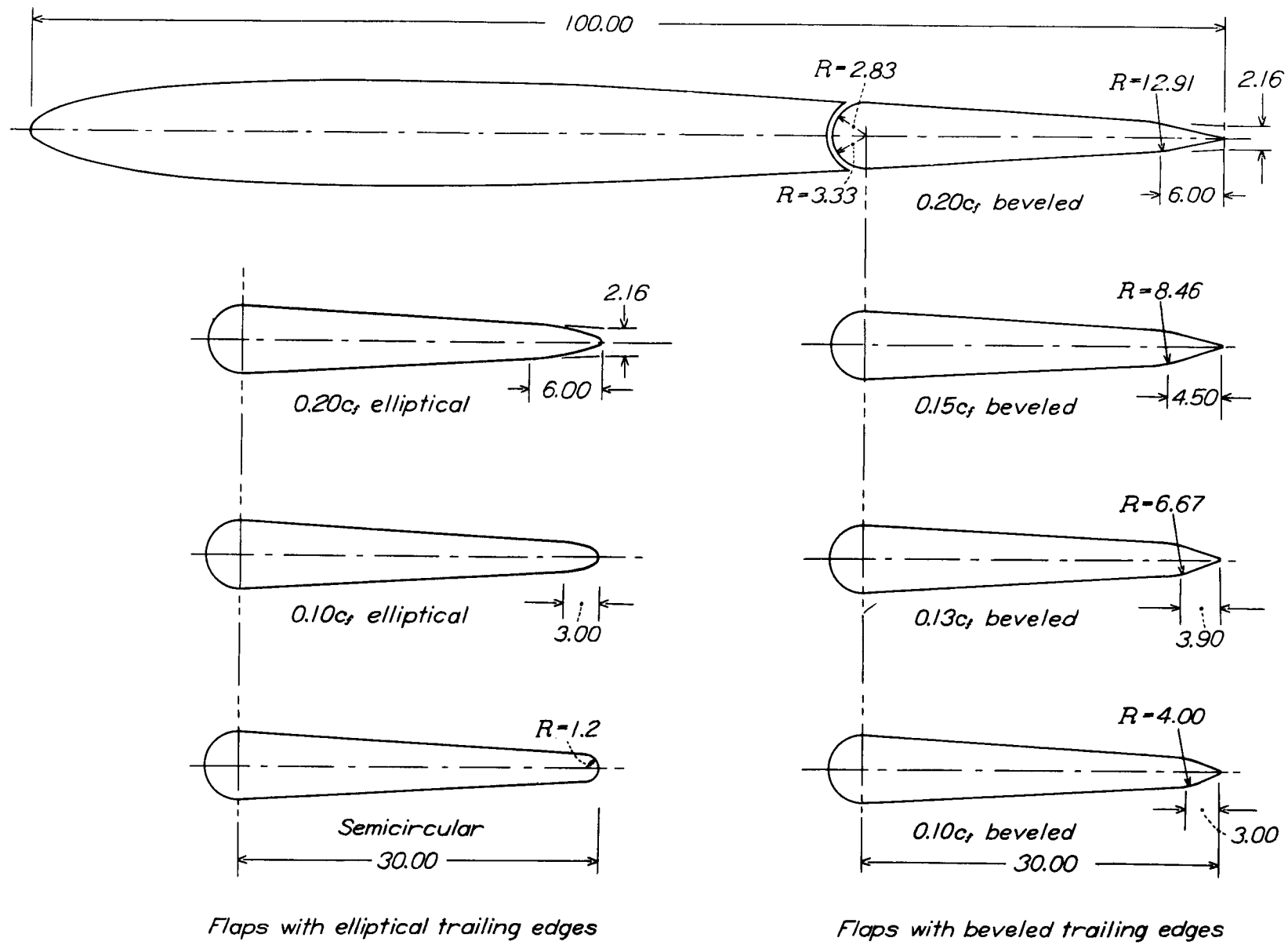

Figure 2.- Trailing-edge modifications. Dimensions are in percent of airfoil chord.

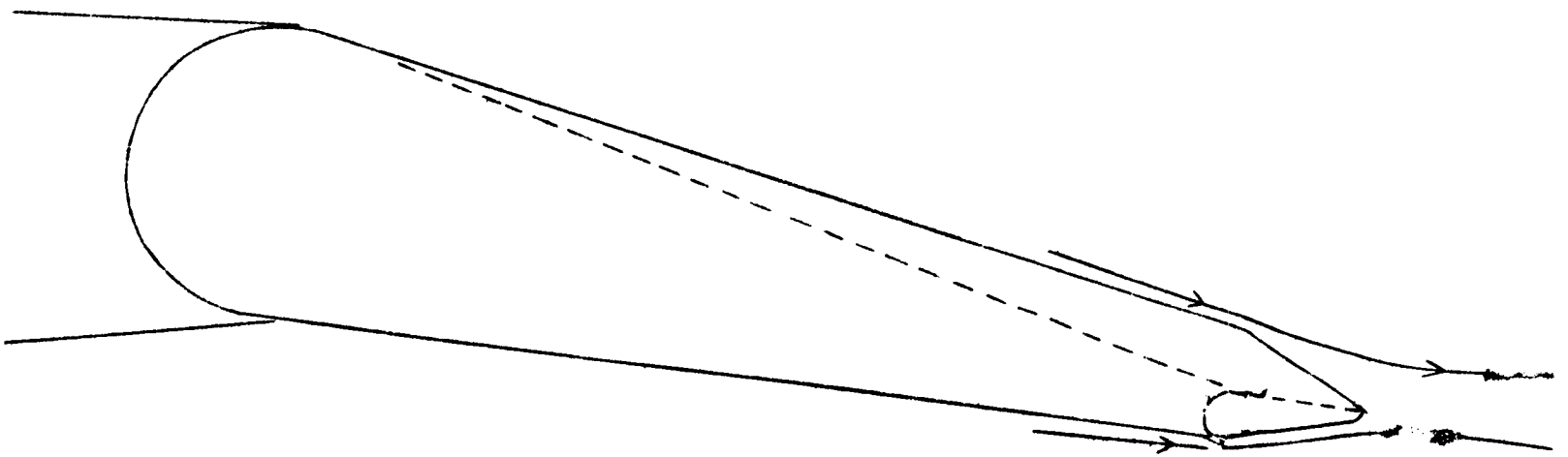

Figure 3.- Flow around beveled trailing edge showing similarity to the effect of a balancing tab.

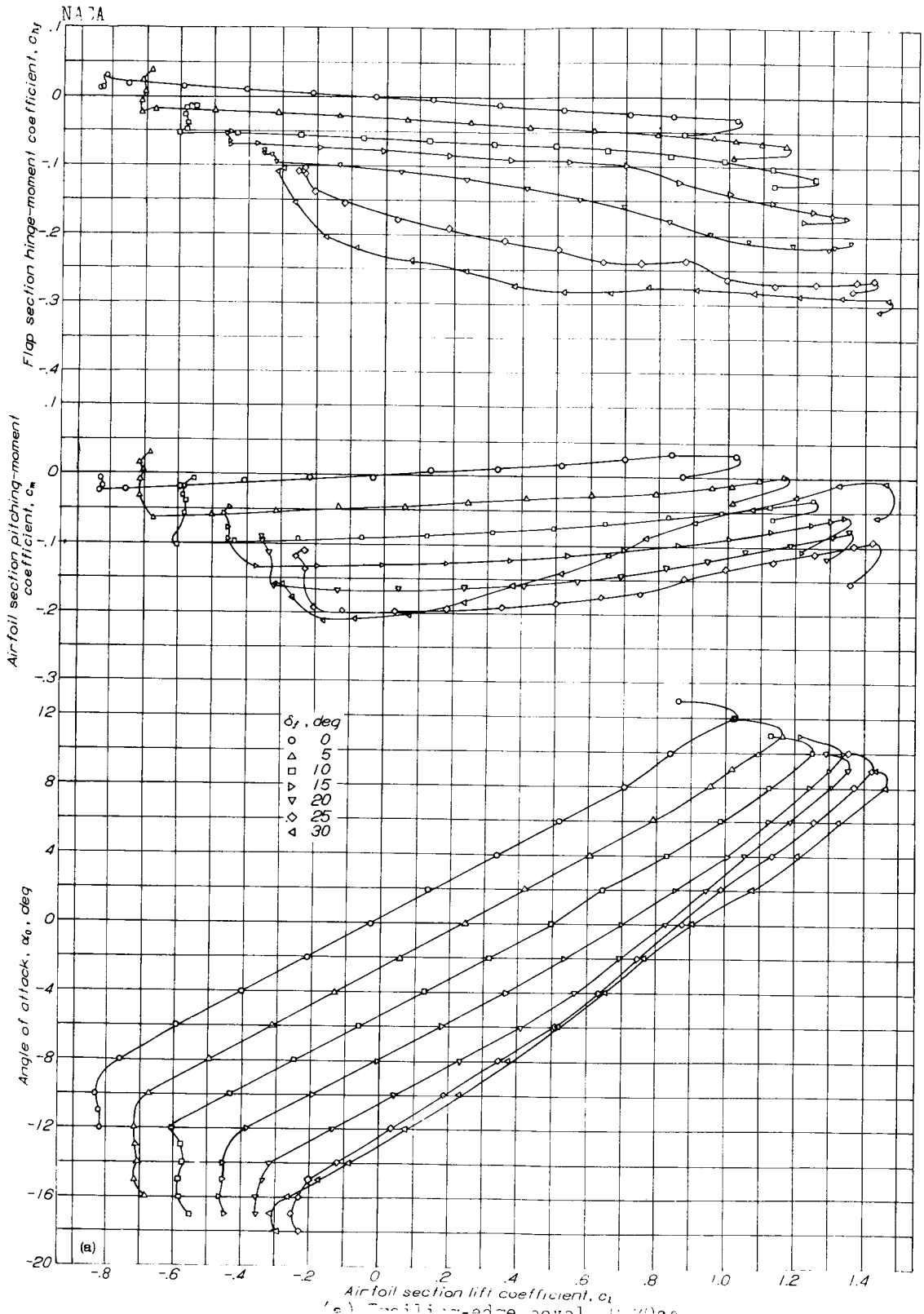

(a) Trailing-edge bevel, 0.20c_f.

Figure 4(a to h).- Aerodynamic [illegible] characteristics of airfoil and 0.[illegible]c flap.

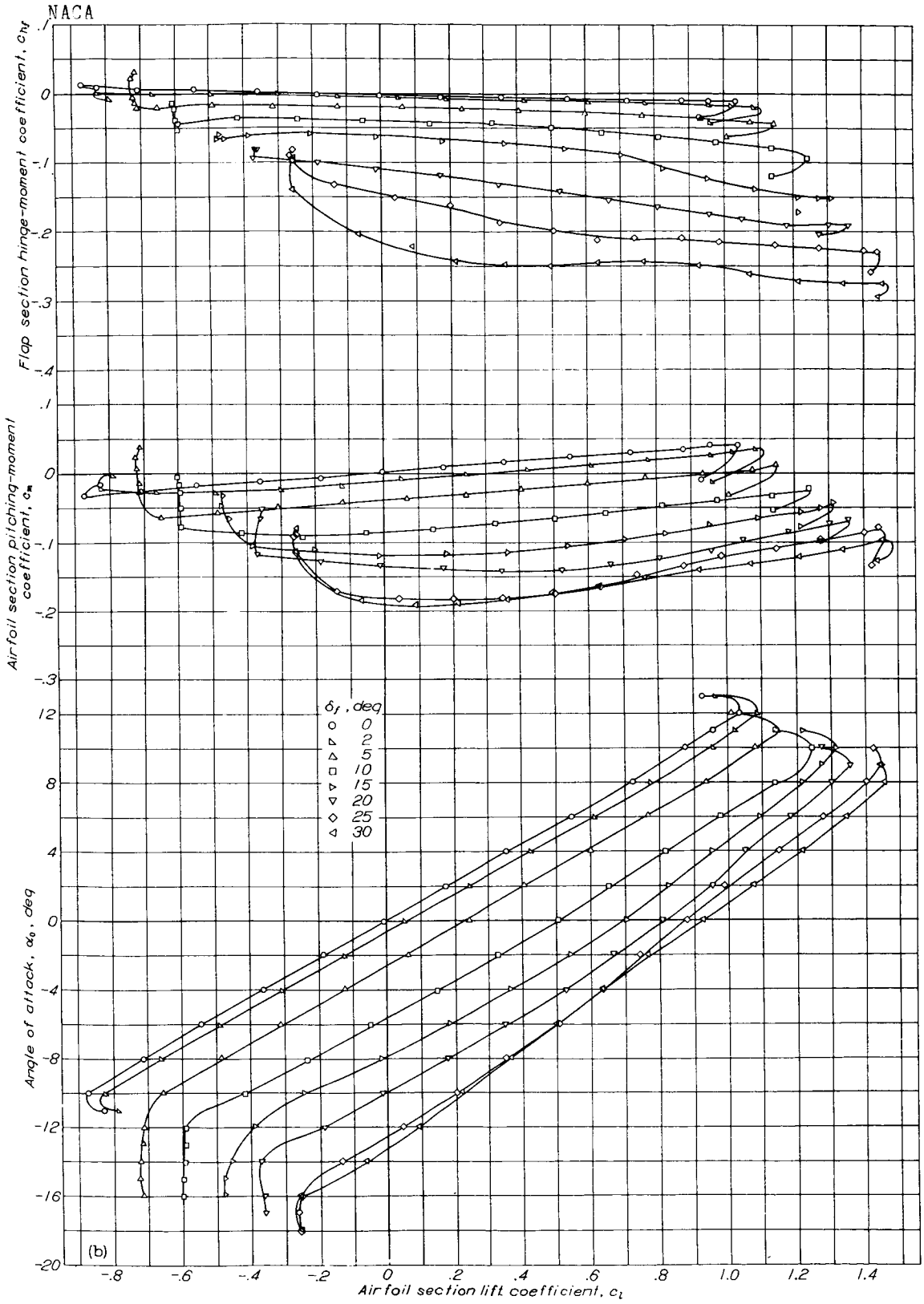

Figure 4b.- Trailing-edge bevel, 0.15c_f.

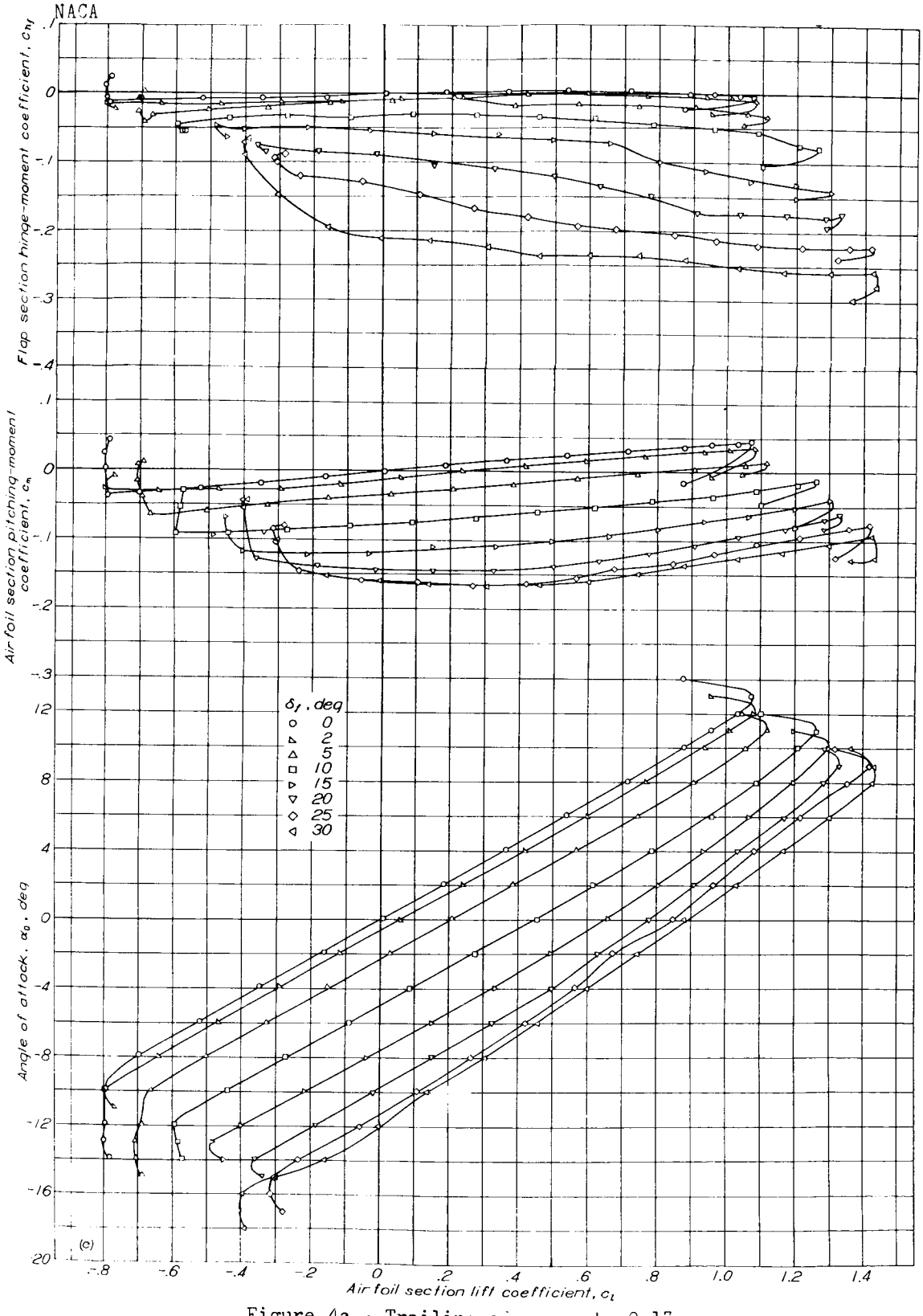

Figure 4c.- Trailing-edge bevel, 0.13c_f.

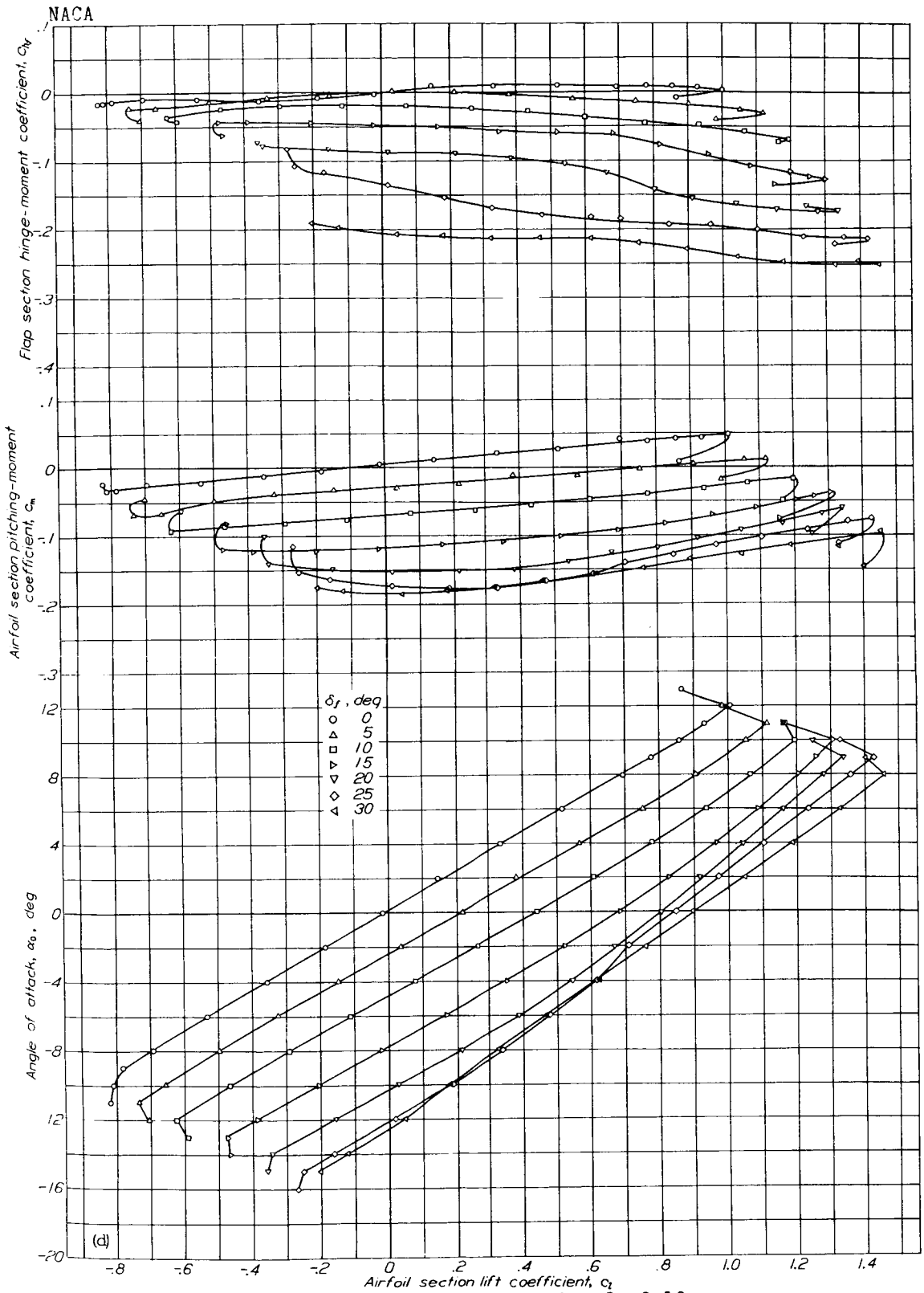

Figure 4d.- Trailing-edge bevel. $0.10c_f$.

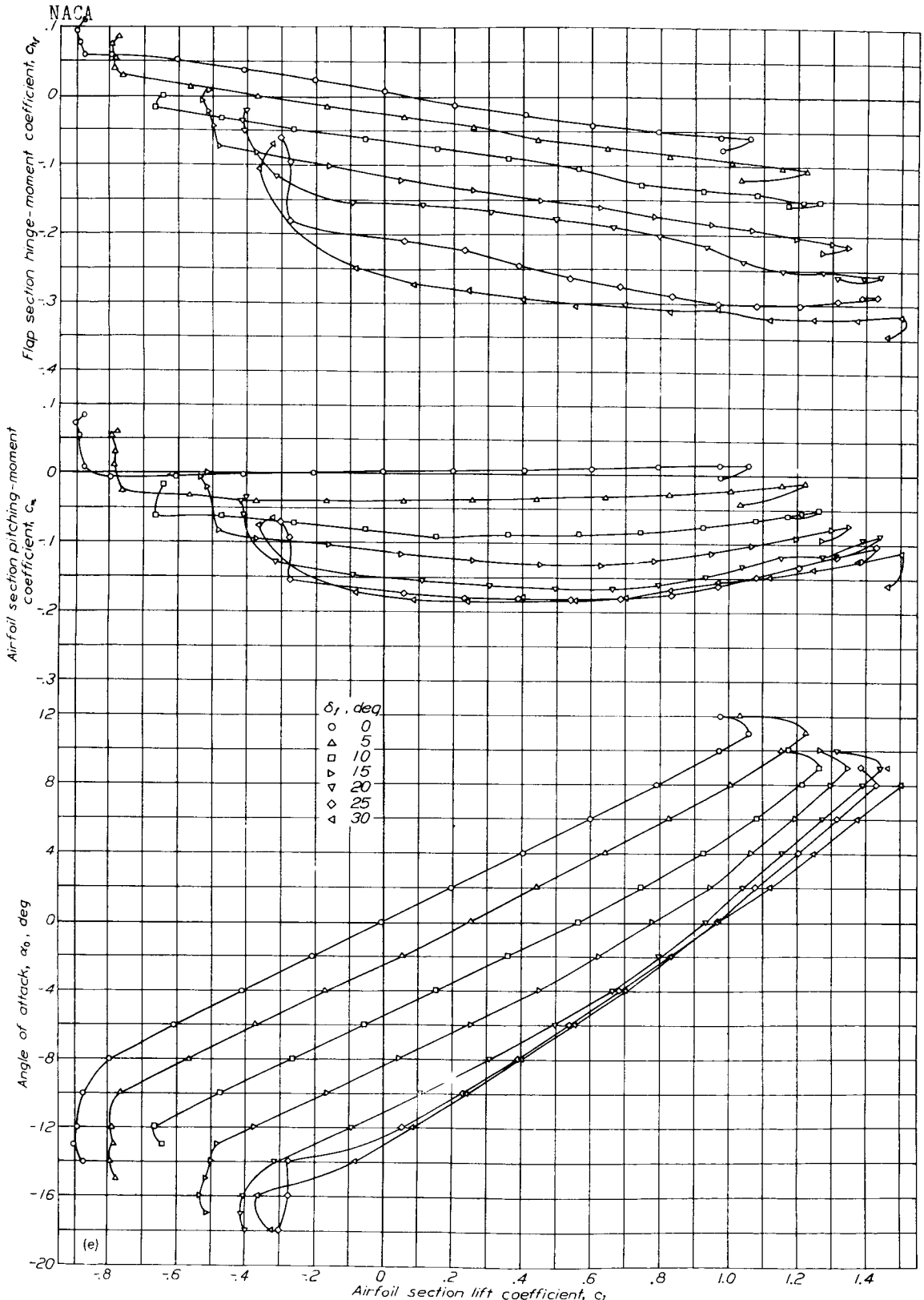

Figure 4e.- Elliptical trailing edge, 0.10c_f.

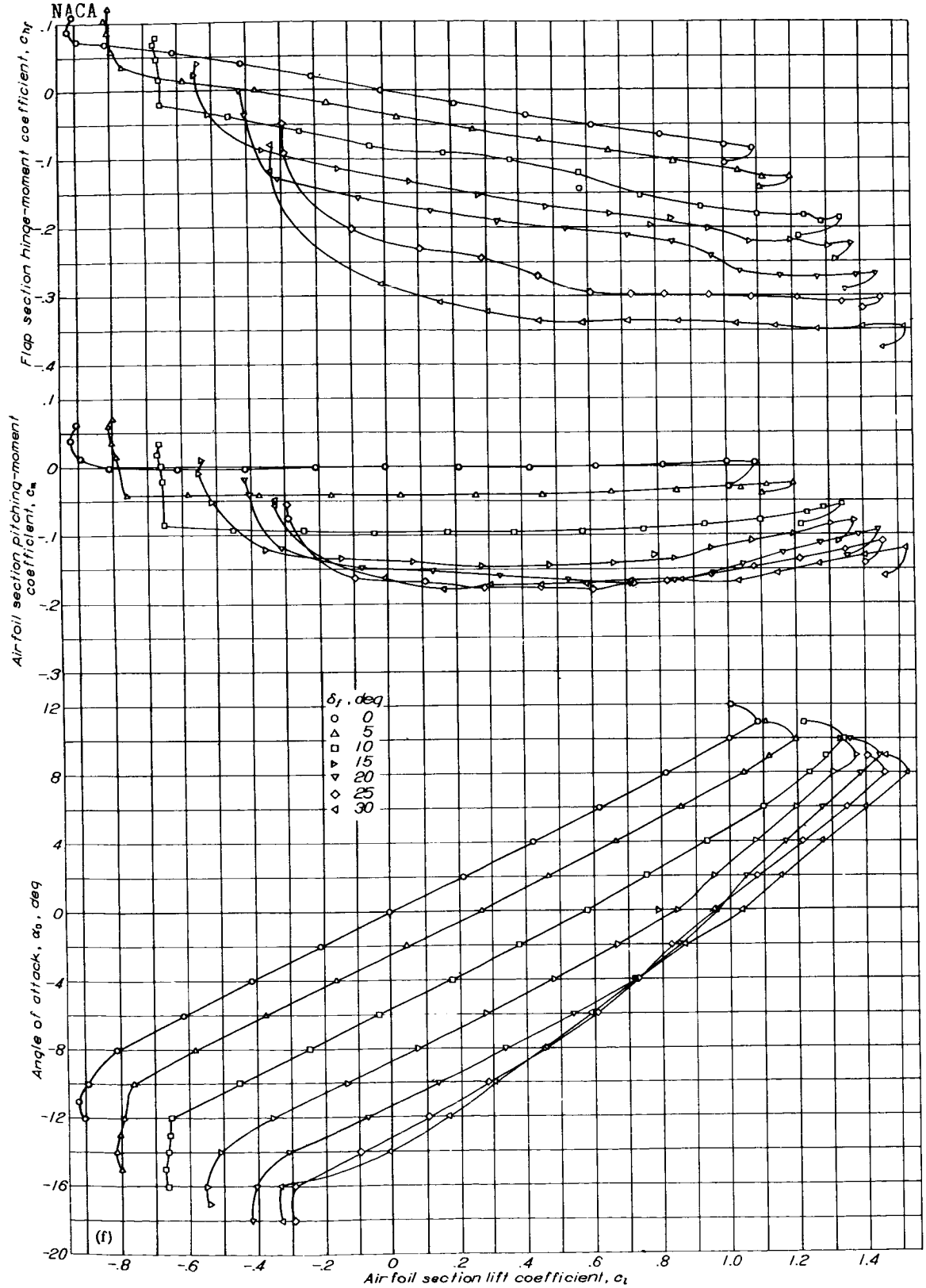

Figure 4f.- Semicircular trailing edge; radius, 0.036c.

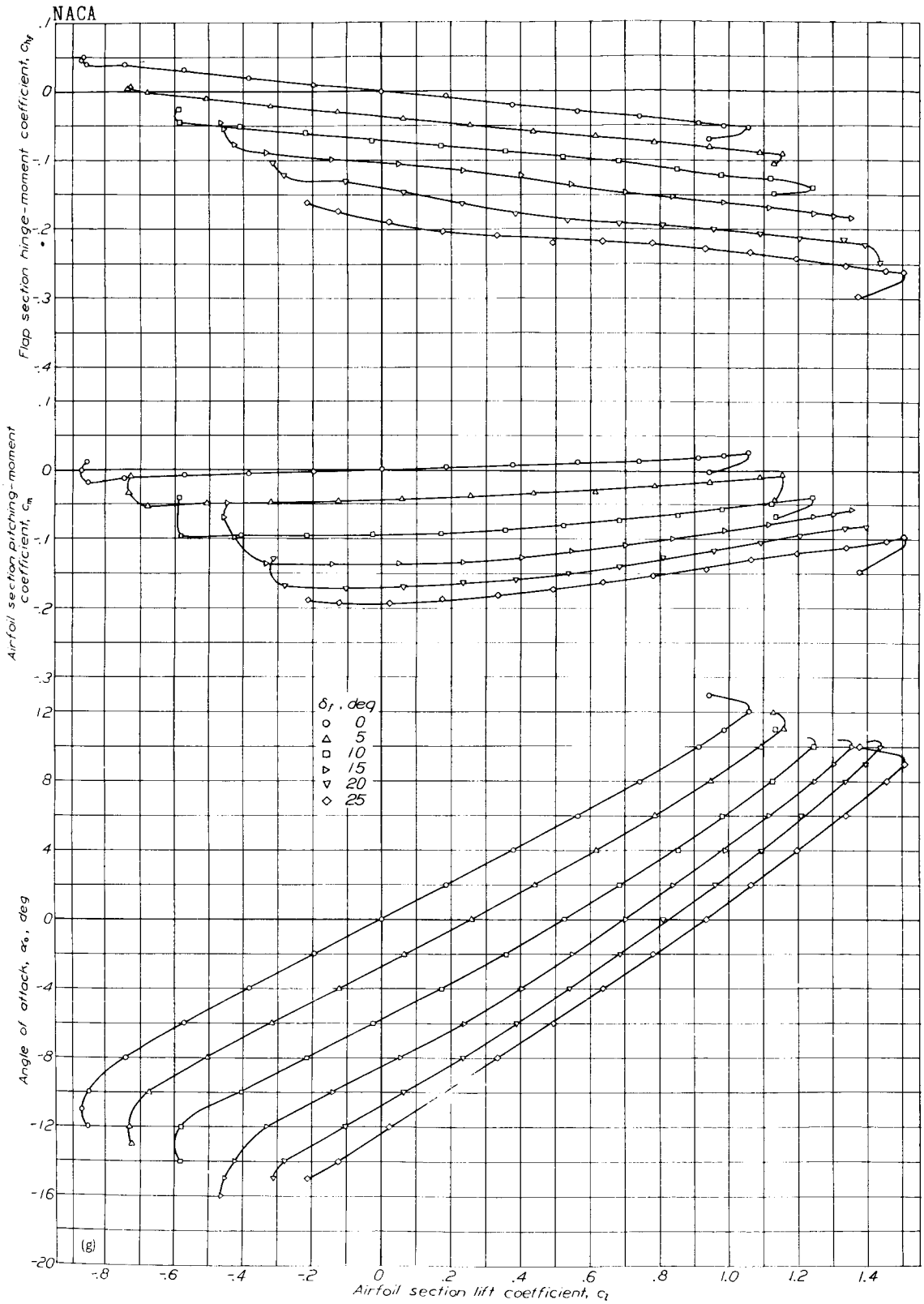

Figure 4g.- Bulged flap.

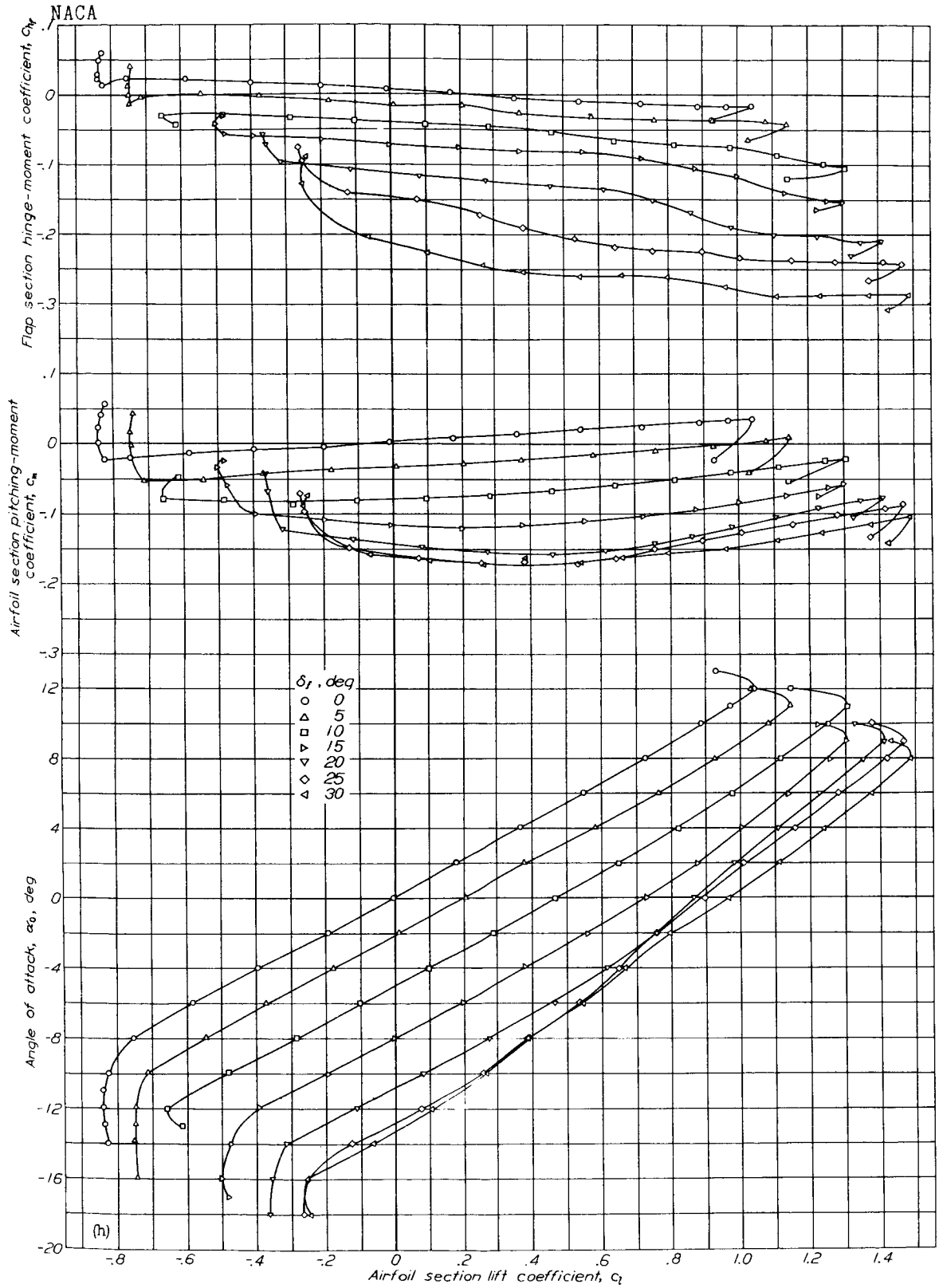

Figure 4h.-Elliptical trailing edge, 0.20c_f.

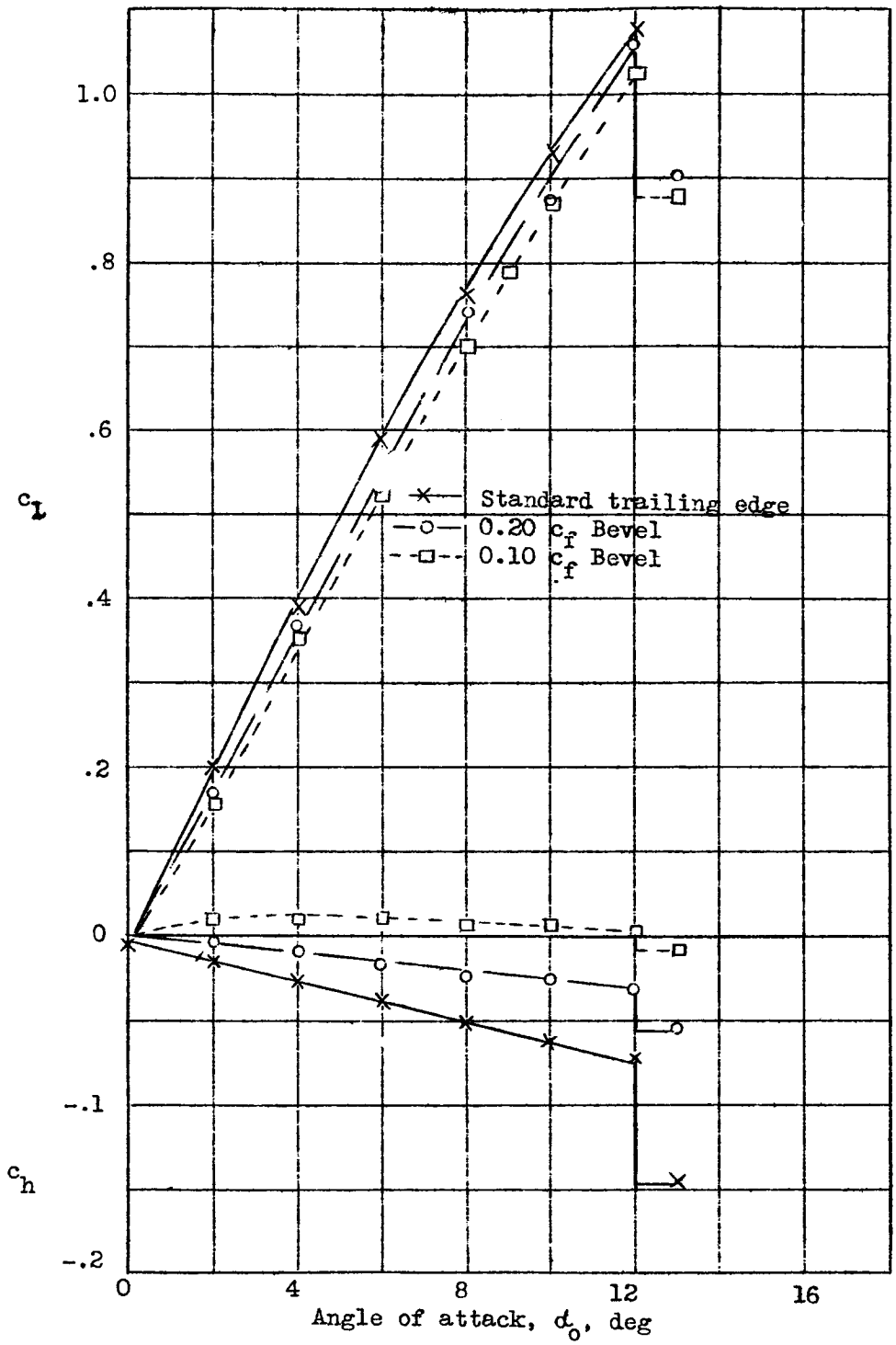

Figure 5.- Typical variations of lift and hinge moment with angle of attack. $\delta_f=0^o$.

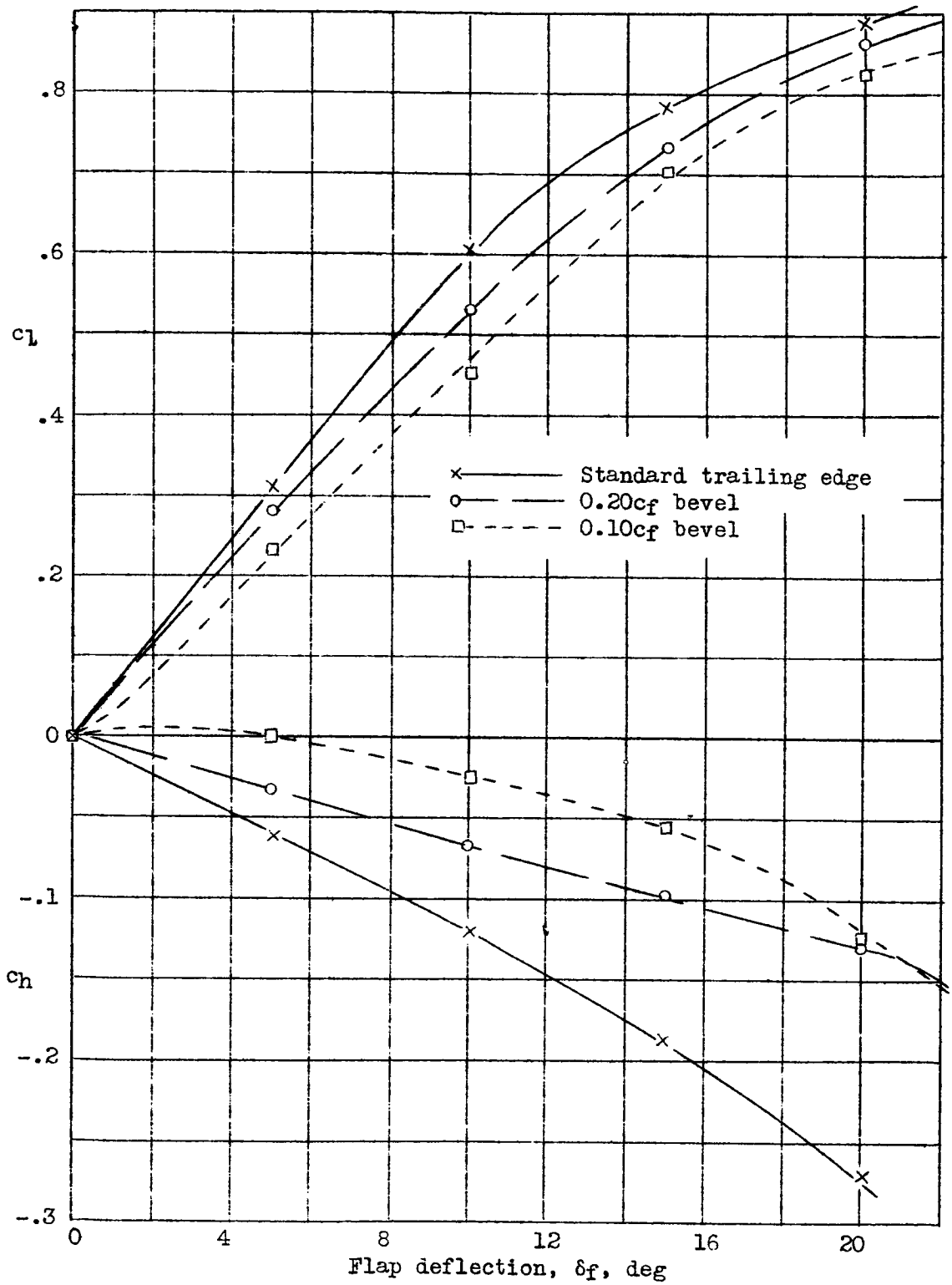

Figure 6.- Typical variations of lift and hinge moment with flap deflection. $\alpha = 0^\circ$.

REPORT NO. 731

DETERMINATION OF OPTIMUM PLAN FORMS FOR CONTROL SURFACES

Robert T. Jones and Doris Cohen

Langley Memorial Aeronautical Laboratory

1942

REPORT No. 731

DETERMINATION OF OPTIMUM PLAN FORMS FOR CONTROL SURFACES

By Robert T. Jones and Doris Cohen

SUMMARY

A theoretical analysis is made to determine the optimum chord distribution, location, and extent of control surfaces, with the ratio of hinge moment to effectiveness as the criterion. Expressions for the effectiveness — for ailerons, the rolling moment, and for tail surfaces, the change of lift on the tail due to deflection of the surface—were derived from lifting-line theory.

Solutions found for a range of airfoil plan forms indicate that, regardless of the characteristics of the tail surface, the chord of the rudder or of the elevator should be very nearly constant over its span. The optimum ailerons are also of a characteristic shape, varying little with the plan form of the wing.

INTRODUCTION

One of the primary difficulties in airplane design has been to keep the stick forces required to deflect the control surfaces at reasonably low values. This problem has inevitably increased in seriousness with the size and the speed of modern airplanes. There is as yet, however, no basic principle of control-surface design that engineers will agree minimizes the ratio of stick force to effectiveness. Examination of typical designs indicates that hinge-moment reductions as great as 40 percent may be achieved in some cases without lowering the effectiveness of the flap; that is, the efficiency may be increased by two-thirds.

The present study, which neglects structural and similar considerations, is a mathematical analysis leading to the plan forms for rudder, elevator, and ailerons that will be most effective in producing a given amount of control with the least operating force. The solutions are applicable to any airfoil of conventional plan form to the same extent as are the usual assumptions of the aerodynamic theory of airfoils, on which the analysis is based. Further discussion covers the extent, the location, and the shape of partial-span control surfaces to give the greatest efficiency.

THEORETICAL ANALYSIS

It is required to find the plan forms for rudder, elevator, and ailerons that will require the least stick force to produce a fixed amount of control per unit deflection of the surface. This is a problem in the calculus of variations, in which the expression for the effectiveness is the integral to be kept constant; the expression for the hinge moment is the integral to be minimized; and the hinge line, defined by a relation between the spanwise station and the ratio of flap chord to airfoil chord, may be considered the path of integration to be determined so as to satisfy the foregoing conditions. In the case of a rudder or an elevator, the effectiveness is measured by the change of lift on the tail surface produced by deflection of the flap; in the case of ailerons, it is measured by the rolling moment produced.

It will be seen in the course of the discussion that all constant factors may be combined in the final result into a single factor of proportionality. All the functions and relations discussed hereinafter will therefore be treated without regard to such factors.

The following symbols will be used in the development:

b	span of airfoil
$\frac{y}{b/2}$	spanwise station measured from plane of symmetry
$\theta=\cos^{-1}\frac{y}{b/2}$	parameter indicating spanwise station
Δl_1	lift per unit span at any section due to unit flap deflection
$\Delta\alpha_1$	change in effective angle of attack at any section due to unit flap deflection
c_l	section lift coefficient
c	chord of airfoil
c_f	chord of flap
r	ratio of flap chord to airfoil chord (c_f/c)
c_s	chord of airfoil at plane of symmetry
δ_f	angle of flap deflection
a_0	section lift-curve slope
$\mu=c_s a_0/4b$	aspect-ratio parameter
H	hinge moment
A_i,B_j,C_k	Fourier series coefficients
A_1	Fourier series coefficient proportional to lift
A_2	Fourier series coefficient proportional to moment
K_n	constants determined by C's and μ
λ	arbitrary proportionality factor

The expression for effectiveness is obtained with the aid of the Lotz method, an outline of which is found in reference 1. Results obtained by this method check reasonably well with experiment except for aspect ratios less than 2.

If the lift distribution over the airfoil is given by the Fourier series

$$\Delta l_1 \propto \sum_{i=1}^{\infty} A_i \sin i\theta \tag{1}$$

the angle-of-attack distribution, by the series

$$\Delta\alpha_1 \sin\theta \propto \sum_{j=1}^{\infty} B_j \sin j\theta \tag{2}$$

and the chord distribution of the airfoil, by

$$\frac{\sin\theta}{c} = C_0 + \sum_{k=1}^{\infty} C_{2k} \cos 2k\theta \tag{3}$$

then the coefficients of the series are connected by the relation

$$\sum_k C_{2k} \cos 2k\theta \sum_i A_i \sin i\theta + \mu \sum_i i A_i \sin i\theta \equiv \sum_j B_j \sin j\theta \tag{4}$$

or

$$\sum_k \sum_i A_i C_{2k} [\sin (i+2k)\theta + \sin (i-2k)\theta] + 2\mu \sum_i i A_i \sin i\theta \equiv 2 \sum_j B_j \sin j\theta \tag{5}$$

This identity is equivalent to the set of simultaneous equations obtained by equating coefficients of terms in the same multiple of θ; thus, for each value of j,

$$(-1)^{(i+2k)} \sum_{k=0}^{\infty} \sum_{i=1}^{\infty} A_i C_{2k} + (C_0 + 2j\mu) A_j = 2B_j \tag{6}$$

where i and k are limited to values such that $i \pm 2k = \pm j$.

The plan form of the airfoil under consideration will determine the values for C_{2k} and will probably be approximated closely enough with a series of two or three terms. (It should be noted that the values of C_{2k} depend only on the distribution of the chord length rather than on the actual plan form.) The B's can be expressed as functions of the ratio r of flap chord to airfoil chord. This ratio will be considered the dependent variable, to be found as a function of the spanwise station $\frac{y}{b/2}$, or of θ. The set of simultaneous equations may now be solved for A_1, which is proportional to the total change in lift due to deflection of the flap, and for A_2, which is proportional to the rolling moment.

It should be possible to limit the number of equations to six or eight without introducing any noticeable inaccuracies. Only odd values of j, moreover, are involved in the solution for A_1 and only even values are involved in the solution for A_2. The value of A_1 will be found to be proportional to an expression of the form

$$K_1 B_1 + K_3 B_3 + \ldots + K_{2n-1} B_{2n-1} \ldots \tag{7}$$

and A_2 will be proportional to $\sum K_{2n} B_{2n}$, where K_n is a constant determined by the C's and μ. From equation (2)

$$B_n \propto \int_0^{\pi} \Delta\alpha_1(r) \sin\theta \sin n\theta \, d\theta \tag{8}$$

Substitute in expression (7); then

$$A_1 \propto \int_0^{\pi} \Delta\alpha_1(r) \sin\theta \, F_1(\theta) \, d\theta \tag{9}$$

where

$$F_1(\theta) = \sum_n K_{2n-1} \sin (2n-1)\theta \tag{10}$$

Similarly,

$$A_2 \propto \int_0^{\pi} \Delta\alpha_1(r) \sin\theta \, F_2(\theta) \, d\theta \tag{11}$$

where

$$F_2(\theta) = \sum_n K_{2n} \sin 2n\theta \tag{12}$$

A curve for $\Delta\alpha_1$ as a function of r, representing a summary of available experimental data on sealed-hinge flaps, is given in figure 1. (A theoretical curve

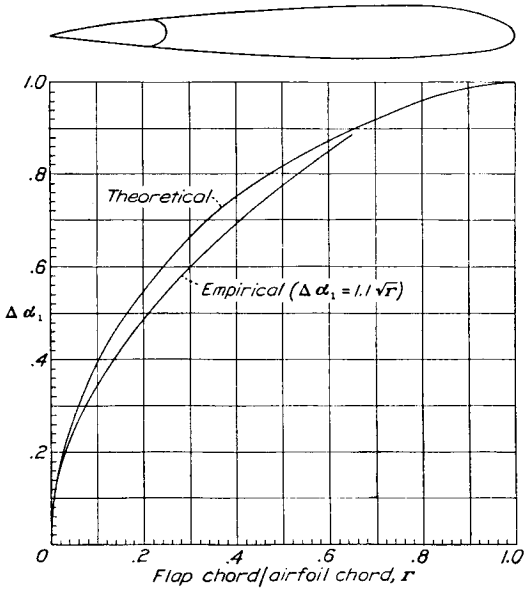

FIGURE 1.—Flap-effect curves for flaps with sealed hinges. (Theoretical curve from reference 2.) $\delta_f < \pm 20°$.

taken from reference 2 has been included in fig. 1 for comparison.) This empirical curve is closely approximated, for flaps up to 70-percent chord, by the equation

$$\Delta\alpha_1 = 1.1\sqrt{r} \tag{13}$$

Then

$$A_1 \propto \int_0^{\pi} \sqrt{r} \sin\theta \, F_1(\theta) \, d\theta \tag{14}$$

and

$$A_2 \propto \int_0^{\pi} \sqrt{r} \sin\theta \, F_2(\theta) \, d\theta \tag{15}$$

The expressions for the lift and the rolling moment obtained by this method take into account the important effect of the aerodynamic induction associated with airfoils of finite span. In the expression for the hinge moment, this factor will be neglected; that is, the end loss in aerodynamic loading and a variation,

caused by the floating tendency of the flap, in the hinge moment developed by the induced downwash will be omitted. Both of these effects are small for narrow-chord flaps. Without these effects the hinge moment is simply proportional to the square of the flap chord at each section. Thus,

$$H \propto \int_0^{\pi} c^2 r^2 \sin\theta \, d\theta \tag{16}$$

This assumption checks reasonably well with experiments.

The problem may now be restated in more specific terms: to find r as a function of θ so that H is a minimum for a fixed value of A_1 (or A_2). Clearly, an equivalent condition would be that $H+\lambda A$ be rendered a minimum, where λ is a parameter associated with the value of A required. This condition is satisfied only if the variation of the integrand of the sum with the dependent variable is equal to zero.

Thus,

$$\frac{\partial}{\partial r}[r^2c^2 \sin\theta + \lambda\sqrt{r} \sin\theta \; F(\theta)=0] \tag{17}$$

Then

$$2rc^2 \sin\theta + \frac{\lambda}{2\sqrt{r}} \sin\theta \; F(\theta)=0 \tag{18}$$

or

$$r \propto c^{-\frac{4}{3}}[F(\theta)]^{\frac{2}{3}} \tag{19}$$

and

$$c_f \propto \sqrt[3]{\frac{[F(\theta)]^2}{c}} \tag{20}$$

which is the most general form of the desired solution. In particular, if airfoils defined by two coefficients C_0 and C_2 are considered,

$$c=\frac{\sin\theta}{C_0+C_2\cos 2\theta} \tag{21}$$

$$F_1=\left[(C_0+7\mu)(C_0+5\mu)(C_0+3\mu)-\frac{C_2^2}{2}(C_0+5\mu)\right]\sin\theta$$
$$-\frac{C_2}{2}\left[(C_0+7\mu)(C_0+5\mu)-\left(\frac{C_2}{2}\right)^2\right]\sin 3\theta$$
$$+\left(\frac{C_2}{2}\right)^2(C_0+7\mu)\sin 5\theta-\left(\frac{C_2}{2}\right)^3\sin 7\theta \tag{22}$$

and

$$F_2=\left[(C_0+8\mu)(C_0+6\mu)(C_0+4\mu)-\frac{C_2^2}{2}(C_0+6\mu)\right]\sin 2\theta$$
$$-\frac{C_2}{2}\left[(C_0+8\mu)(C_0+6\mu)-\left(\frac{C_2}{2}\right)^2\right]\sin 4\theta$$
$$+\left(\frac{C_2}{2}\right)^2(C_0+8\mu)\sin 6\theta-\left(\frac{C_2}{2}\right)^3\sin 8\theta \tag{23}$$

RESULTS AND DISCUSSION

The method just developed has been applied to airfoils with the following chord distributions:

$$\frac{\sin\theta}{c}=2.071-0.6904\cos 2\theta \qquad \text{(blunt)}$$

$$\frac{\sin\theta}{c}=2.356 \qquad \text{(elliptical)}$$

$$\frac{\sin\theta}{c}=2.926+0.9755\cos 2\theta \qquad \text{(tapered)}$$

The elliptical distribution and the degrees of taper represented by the relations $C_2/C_0=\pm 1/3$ were chosen to give an inclusive indication of the range and the manner of variation of the solutions. Particular values of C_0 were determined by the condition that the airfoils

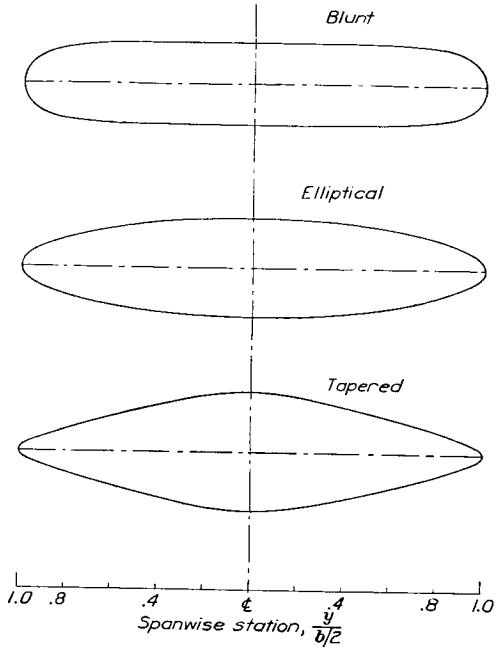

FIGURE 2.—Airfoil plan forms defined by the two-term series: $\frac{\sin\theta}{c}=C_0+C_2\cos 2\theta$. Aspect ratio, 6.

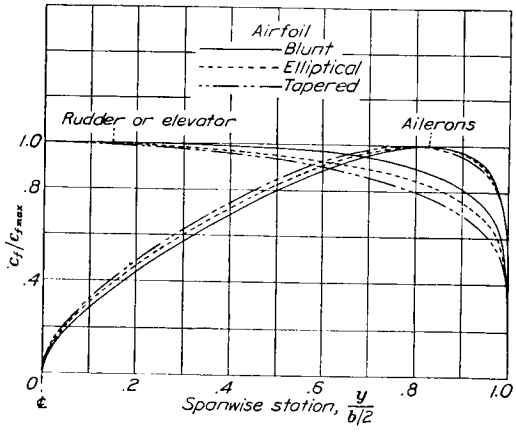

FIGURE 3.—Optimum chord distribution for control surfaces.

be of unit semispan and aspect ratio 6. The resulting chord distributions, plotted about a straight 50-percent chord line, are shown in figure 2.

The solutions were found to be strikingly independent of the form of the airfoil. In figure 3, the shapes for the movable surfaces are shown for the three airfoils just described. The optimum ailerons are seen to vary hardly at all from airfoil to airfoil. The outlines for maximum lift efficiency, although differing slightly,

nevertheless suggest the general conclusion that the most desirable control surfaces in this respect are of nearly constant chord.

From this result it follows that the most efficient airfoil plan form for longitudinal control is also one of nearly constant chord, because such a combination of airfoil and flap will have a nearly uniform distribution

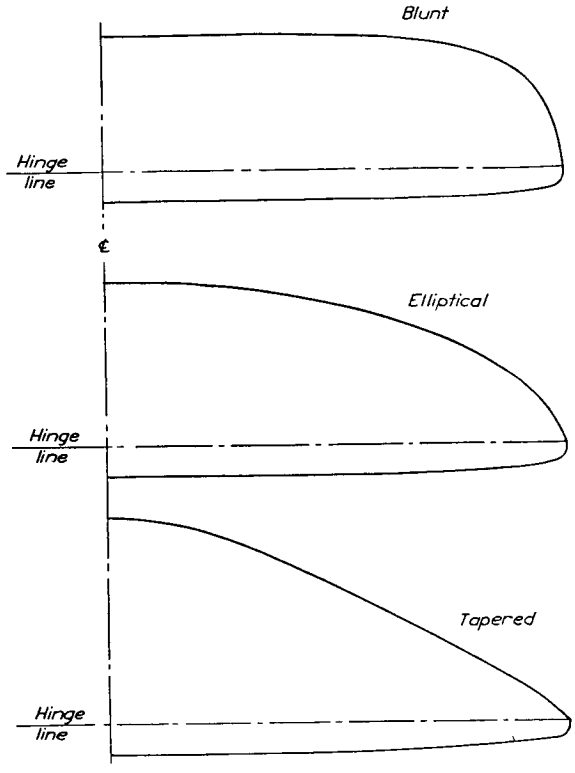

FIGURE 4.—Airfoils of figure 3 with flaps of optimum plan form for lift. Average chord ratio, 20 percent.

of effective angle of attack. Calculations also show that, if each of the airfoils given by the foregoing distributions were provided with a flap of optimum shape, a somewhat smaller movable surface, and hence a smaller hinge moment, would be required to increase the lift on the blunt wing a given amount per unit deflection than on either of the other two. On the other hand, since aileron effectiveness depends on the ratio of rolling moment to damping moment, a tapered wing is seen to be most efficient for lateral control.

In figure 4 the flaps are plotted in relation to the airfoils. The flaps as drawn are 20 percent of the mean chord of the airfoil. It will be noted that, for the tapered airfoil, this is the maximum width at which the shape of the flap can be maintained. Ordinarily as high a taper as shown would not be used and a 20-percent or wider flap would be possible. It is not important, in any case, to hold rigidly to the optimum shape at the extreme tip if such a design introduces a cusp in the fixed portion of the surface.

The corresponding presentation of the solution for the ailerons is given in figure 5. The ailerons shown are approximately 15 percent of the mean chord of the airfoil. Seen in this aspect ratio, the ailerons appear not to vary greatly in width over their span. As is to be expected, however, they do taper off somewhat toward the center where the small moment arm would obviously make a larger area inefficient.

The choice of a straight hinge line has led to the introduction of sweepback in these plan forms. It should be remembered, however, that the solutions as expressed by figure 3 are mathematically very general ones and cover, within the limits of accuracy of the lifting-line theory, any width of flap, any shape of hinge line or quarter-chord line, and any normal aspect ratio. The

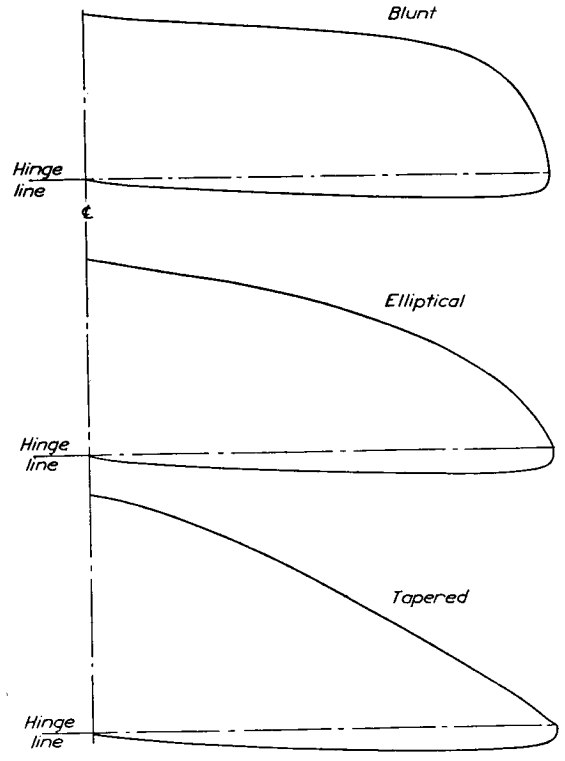

FIGURE 5.—Airfoils of figure 3 with ailerons of optimum plan form. Average chord ratio, 15 percent.

aspect ratio, in μ, affects the expressions for $F(\theta)$ in equations (22) and (23), but calculations made for an aspect ratio of 2 resulted in outlines that could not be differentiated in plotting from those given in figure 3. Thus, the aspect ratio enters the solutions only in so far as it limits the applicability of the lifting-line theory. The solutions are also expected to apply in a general way to

unsealed flaps which, although less effective than sealed flaps, may be supposed to show similar variations of effectiveness with chord.

A separate investigation was made to determine on which of the airfoils considered the derived control surfaces would produce the most lift for a given hinge moment, with a view to estimating the loss resulting from the use of a tapered stabilizer. The calculated difference of 8 percent between the tapered and the blunt airfoils was not so great as might have been expected. It is supplemented, however, by other aerodynamic effects such as fuselage interference, which may make the use of area near the fuselage inefficient.

Ailerons on a blunt wing would similarly give more rolling moment for a certain hinge moment than on a more tapered wing. Since the tapered wing requires less powerful ailerons because of the small damping moment, the actual rate of rolling would be definitely greater for a given hinge moment; thus in the last analysis, the tapered wing must be considered the most efficient from considerations of aileron control.

PARTIAL-SPAN FLAPS

At this point a question arises as to the design of partial-span flaps, their shape, optimum length, and location. The most efficient shape for such flaps can be deduced from a review of the preceding development. If a portion of the airfoil span has no movable area, the value of $\Delta\alpha_l$ will be zero over that region and the expressions for A_1 and A_2 given in equations (14) and (15) will reduce to integrals covering only flapped portions of the span. The limits for H given in equation (16) may be similarly changed. Then the reasoning remains the same; only the limits of integration are changed to agree with the extent of the flap and, these limits being identical for the functions involved, the relations between the integrands may be expressed as before and the same solutions will be obtained. It follows that flaps extending over a part of the span of an airfoil should have the same shape as the portion of a flap of optimum shape covering that same part of the span.

Another interesting characteristic of these shapes, one from which further deductions concerning partial-span flaps may be made, appears when the solution given in equation (19) is substituted in expressions (14), (15), and (16) for the effectiveness and the hinge moment. It is seen that the integrands of these expressions are identical except for the discarded factors of proportionality. This fact may be interpreted as meaning that the surfaces found have, for any particular solution, a constant ratio of effectiveness to hinge moment all along the span, or that any portion of a given flap of optimum shape is as efficient as any other portion.

This characteristic leads again to the conclusion that partial-span flaps should be segments of the optimum full-span shapes. The extent and the location of the flaps for greatest efficiency are also indicated by these considerations. If the ratio for a given shape is everywhere the same, the greatest lift or rolling moment must be contributed by the element of the flap that has the maximum chord (and therefore the maximum hinge moment). If any other element of equal span is to be used to develop the same lift, that element must either be deflected through a greater angle or increased in width. It is assumed that the maximum degree of control possible within the efficient range of flap deflection, which is about $\pm 20°$, is desired, and the control should therefore not be increased at the expense of

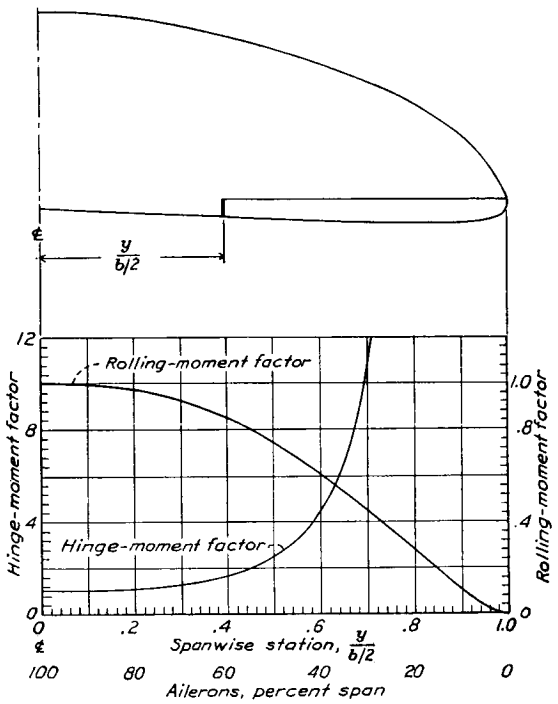

FIGURE 6.—Rolling-moment and hinge-moment curves for partial-span ailerons. Elliptical wing; aspect ratio, 6.

flap deflection. If the chord is increased, it will be with the square of the lift (equation (13)) and the hinge moment will then be increased with the square of the chord (equation (16)) or the fourth power of the lift. The conclusion is obvious: The most efficient flap of a given span will cover the portion over which the ordinates of figure 3 are the greatest. This result is of particular significance as applied to ailerons, which should therefore extend inward from the tips.

It also follows that the greatest efficiency is obtained by using the longest possible control surfaces. Shorter flaps must of necessity be wider to produce the same effect, and the increase in chord causes a sharp drop in efficiency. This consideration should influence not only the design of the flaps but also the design of the tail surfaces themselves.

Figures 6 and 7 are a quantitative representation of

the situation. In these figures, the "hinge-moment factor" is the number by which the hinge moment of the partial-span control surfaces would be multiplied if their effectiveness were increased (by increasing the chord) to equal that of the full-span surfaces. The "rolling-moment factor" is the rolling moment developed by partial-span ailerons (to the tip) of optimum shape, expressed as a fraction of the moment developed by the full-span ailerons of which they are a part.

In the case of ailerons, the loss of efficiency is not very great if the extreme inboard portion is dispensed with, but the rate at which the efficiency drops increases rapidly as the span of the ailerons is lessened. For example, if on a particular wing only the outer 60 percent of the optimum ailerons of a certain percentage chord were used, approximately 16 percent of the rolling moment would be sacrificed. If it were desired, however, to retain the full power of the control, a 60-percent increase in hinge moment would be incurred; or, from another point of view, a 60-percent aileron will always require an operating force 60 percent greater than is entirely necessary for the same effectiveness. If only 40 percent of the span is used for control, the hinge moment required will be almost three times as great as for equally effective 60-percent-span ailerons and 4.4 times as great as for full-span ailerons.

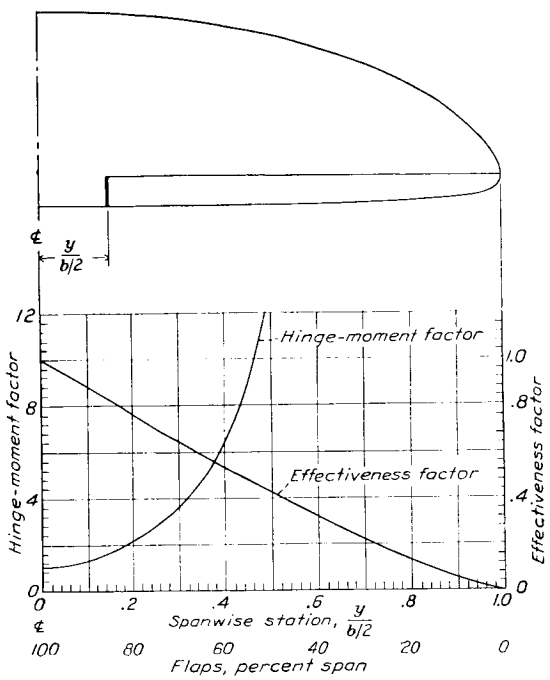

FIGURE 7.—Hinge-moment and effectiveness curves for partial-span flaps. Elliptical tail surface; aspect ratio, 6.

The corresponding curves for the elevator (fig. 7) show a much sharper decline in efficiency as the flaps are shortened along the span. Because the fixed surface between flaps (or the cut-out) is seldom more than 15 percent, however, the resultant increase of control force is not so great as for partial-span ailerons.

Application of the principles outlined has been made to a modern airplane, with ailerons as shown in figure 8. Calculations indicate a 30-percent reduction in hinge moment (with no loss of rolling moment) due to improvement of the plan form of the ailerons alone. If an additional 10 percent of the semispan were allotted to each aileron, the required operating force would be reduced to 45 percent of that for the original ailerons, and the efficiency would be more than doubled.

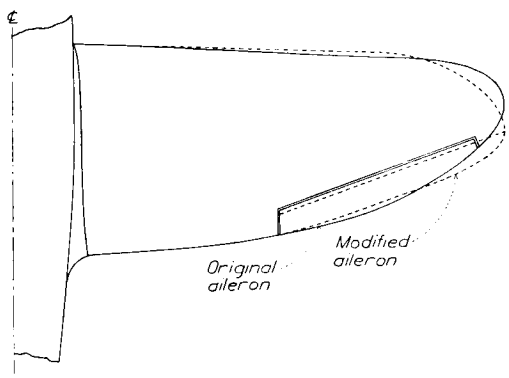

FIGURE 8.—Modification of a typical aileron to reduce the hinge moment.

CONCLUSIONS

Control surfaces of maximum efficiency (requiring a minimum operating force to achieve a given amount of control) may be designed almost without regard to the characteristics of the wings or tail surfaces to which they are to be attached. Except, perhaps, on very low-aspect-ratio tail surfaces (aspect ratio less than 2), flaps should be of almost constant chord over the span. The optimum shape for ailerons is of maximum width near the tip of the wing and has a slightly convex curvature as it tapers toward the center. Partial-span control surfaces should be sections of these optimum shapes and should include the regions of maximum chord. For maximum efficiency, however, because the hinge moment increases as the fourth power of the lift when the gain in lift must be achieved by increasing the chord, flaps and ailerons should be as long and narrow as is compatible with structural and other design considerations.

LANGLEY MEMORIAL AERONAUTICAL LABORATORY,
NATIONAL ADVISORY COMMITTEE FOR AERONAUTICS,
LANGLEY FIELD, VA., *January 30, 1941.*

REFERENCES

1. Pearson, H. A.: Span Load Distribution for Tapered Wings with Partial-Span Flaps. Rep. No. 585, NACA, 1937.
2. Munk, Max M.: Fundamentals of Fluid Dynamics for Aircraft Designers. The Ronald Press Co., 1929, p. 75.

WARTIME REPORT L-223

EMERGENCY MEASURES FOR INCREASING THE RANGE OF FIGHTER AIRPLANES

Robert T. Jones and Joseph W. Wetmore

Langley Memorial Aeronautical Laboratory

May 1943

NATIONAL ADVISORY COMMITTEE FOR AERONAUTICS

EMERGENCY MEASURES FOR INCREASING THE RANGE OF FIGHTER AIRPLANES

By Robert T. Jones and Joseph W. Wetmore

SUMMARY

An analysis was made to show the relative effectiveness of streamline external fuel tanks, a fuel tank in the form of a wing mounted in a biplane position, and auxiliary wing panels attached at the wing tips to increase the span as temporary means for increasing the range of a fighter-type airplane. The airplane considered is representative of either an Army or Navy single-engine heavy fighter. Figures and charts for the various devices considered show the results of calculations of range, duration of flight, and take-off distance for both land-base and carrier operation.

The results indicated that the wing-tip extensions were the most promising of the devices considered. It was estimated that 10-foot tip extensions - that is, an increase in span of 20 feet - used in conjunction with a streamline external fuel tank would increase the range of the airplane 125 to 130 percent without any increase in the distance required to take off from either a land base or a carrier. With 5-foot tip extensions, the range would be increased 65 to 70 percent, under the same limitations. The tank wing was found to cause some reduction in the efficiency of the airplane in terms of miles per gallon. The added area would permit a greater fuel load to be carried, however, for a given take-off distance and the range would thereby be increased. For a given take-off distance from a land base, the calculated increase in range due to the tank wing was about 45 percent. The increase for a given carrier take-off would be about 20 percent. Increasing the range 50 percent by carrying extra fuel in a streamline external tank without any other modifications to the airplane would require an

increase of 20 percent in take-off distance from a land base and 32 percent from a carrier.

INTRODUCTION

The range of fighter-type airplanes is ordinarily relatively short because of high span loading and limitations on the space available for fuel. Permanent modifications in the design of the airplane to achieve longer ranges would not be acceptable because of the consequent impairment of other characteristics that are ordinarily of greater importance. Under certain circumstances, however - for example, for ferrying purposes - it would be of great value to increase the range of fighter airplanes by temporary devices, despite sacrifices in other performance characteristics.

Considerable increases in range may be obtained by carrying streamline external fuel tanks but only at the cost of a possibly prohibitive increase in take-off distance. Several methods, designed to increase the range without increasing the take-off distance, have been suggested. One of these methods consists essentially in making the external tank in the shape of an airfoil to increase the total wing area. Another method consists in adding area at the wing tips, which has the advantage of increasing not only the wing area for take-off but also the span and, thereby, the efficiency in terms of miles per gallon of fuel. Such area might be added in the form of temporary extensions attached in place of the removable fairings on the original wings.

Determination of the most expedient method will depend on a number of factors outside the field of the present investigation, such as pilot endurance, area available for take-off, and structural considerations. The following analysis is intended to provide a comparison of the suggested methods on the basis of maximum attainable range, flying time required, and take-off distances from either a land base or a carrier. The calculations were made for an airplane the characteristics of which may be considered representative of either an Army or Navy single-engine heavy fighter.

ANALYSIS

Airplane.- The characteristics of the airplane considered in the analysis are:

Wing area, square feet	310
Wing span, feet	41
Wing incidence angle, degrees	2
Ground angle (longitudinal axis), degrees	12
Empty weight (design gross weight less normal fuel load), pounds	11,000
Engine displacement, cubic inches	2800
Supercharger	two-stage, gear-driven
Propeller	three-blade, constant-speed
Propeller gear ratio	2:1
Maximum speed at sea level, miles per hour	317
Capacity of internal fuel tank, gallons	300

A sketch of the airplane with a tank wing of 300-gallon capacity (4-ft chord by 20-ft span) is shown in figure 1. In figure 2 the airplane is shown with 10-foot wing-tip extensions (area increase, approx. 80 sq ft) and a 300-gallon streamline external tank.

Calculation of range.- The range was calculated by the Breguet formula, which takes account of the continuous reduction in power required to operate at constant lift-drag ratio. The equation is

$$R = 375 \frac{\eta}{C} \frac{L}{D} \log_e \frac{W_t}{W_e}$$

where

R range, miles

η average propulsive efficiency during flight

C average specific fuel consumption during flight, pounds per horsepower-hour

L/D lift-drag ratio of airplane

W_t weight of airplane at take-off

W_e weight of airplane with tanks empty

Calculation of aerodynamic efficiency L/D.- The values of aerodynamic efficiency L/D for use in the range equation were computed from the relation

$$\frac{L}{D} = \frac{1}{\frac{1.075f}{W/\rho V^2} + \frac{W/\rho V^2}{1.075\ \pi b_e^2}}$$

where

f parasite area of airplane

W weight of airplane

ρ mass density of air

V true airspeed, miles per hour

b_e effective span

For the original airplane, the value of f was calculated from consideration of the maximum speed and corresponding power output of the engine. Increments in parasite area due to the external tanks, the tank wing, and the wing-tip extensions were estimated by determining the wetted areas of these additions and multiplying by a skin-friction coefficient of 0.005, representative of a turbulent boundary layer. For the streamline external tanks, the wetted area was assumed to be that of an ellipsoid of revolution having a fineness ratio of 5 and providing the desired volume. The

drag of a faired tank has been found to be slightly less than that obtained by this method.

For the normal airplane and the airplane with wing-tip extensions, the effective span b_e was assumed to be 90 percent of the actual span. For the tank wing, the effective span was taken as the effective span of the original airplane multiplied by Munk's span factor; the value of the factor for the configuration assumed (fig. 1) was taken from reference 1; and the assumption that the lift would be distributed between the two wings in proportion to their respective areas was used.

The curves of L/D against $\frac{V}{\sqrt{W/W_e}}$, where W is the airplane weight with any fuel load and V is the true airspeed at an altitude of 10,000 feet, are plotted in figure 3(a) for the various modifications of the airplane. The curve for a given airplane configuration is independent of loading when plotted in this manner.

Calculation of engine-propeller efficiency η/C.- Values of propulsive efficiency η were computed from full-scale test data on a suitable propeller-nacelle combination. Specific fuel consumption C was determined from manufacturer's performance charts for the engine considered. It was assumed that the engine was operating in low blower and subject to the limitations on engine speed and manifold pressure specified for the cruising power condition. The values of C were increased 5 percent to take account of oil consumption. The maximum value of the ratio η/C was determined for several values of brake horsepower at each of a number of airspeeds; an altitude of 10,000 feet was assumed. It was found that the maximum value of η/C at a given airspeed is practically unaffected by considerable variations in power, with the result that a single curve of η/C against true airspeed, given in figure 3(b), could be used for all the airplane modifications considered.

Determination of loading.- The weight of fuel carried was estimated on the basis of 6 pounds per gallon. This value was increased 5 percent to allow for oil consumption. The weight of the streamline external fuel tanks and the weight of the tank wing were assumed to be 15/85 of the weight of the fuel the tanks are capable of carrying. The weight of the wing-tip extensions was taken as 3 pounds per square foot of area added. The loadings used for the several modifications of the airplane that were considered in

the calculations are given in the following table:

Condition	Total fuel capacity (gal)	Empty weight (lb)	Take-off weight (lb)	W_t/W_e
Normal airplane	300	11,000	12,890	1.172
300-gallon external tank added	600	11,319	15,092	1.333
5-foot wing tips added	300	11,155	13,043	1.168
5-foot wing tips and 300-gallon external tank added	600	11,474	15,247	1.328
10-foot wing tips added	300	11,300	13,188	1.166
10-foot wing tips and 300-gallon external tank added	600	11,619	15,392	1.324

Calculation of take-off distance.- Take-off distances from both a land base and a carrier were computed for the various airplane conditions. For the land-base take-offs, the distance required to clear a 50-foot obstacle was included. It was assumed that flaps would not be used and that there was no wind. The ground-run distances were computed by the method of reference 2. The take-off speed was taken as 5 percent in excess of the power-off stalling speed and the rolling-friction coefficient, as 0.05. Air-run distances were estimated from the results of step-by-step integrations of the air-run flight path, based on the assumption that the lift coefficient at which the airplane takes off would be maintained up to the 50-foot height. For the carrier take-offs, only the distance required to attain take-off speed was calculated. Estimation of take-off speed was based on the assumption that the tail wheel would be in contact with the deck at take-off. The airplane was assumed to be equipped with partial-span slotted flaps that would be deflected 30° for carrier take-offs. The deck-wind velocity was taken as 25 knots and the rolling-friction coefficient, as 0.02. The method of refer-

ence 2 was used for the calculation of the take-off distances.

For both land-base and carrier take-offs, account was taken, as well as possible, of the effects of slipstream and proximity of the ground. Lift increments due to the slipstream were estimated from the semiempirical formulas given in reference 3. The parasite drag of parts of the airplane in the slipstream was assumed to be increased in proportion to the increase in dynamic pressure in the slipstream. It was assumed that the induced drag associated with the lift increment due to the slipstream would be the same as though this lift increment were obtained with a flap having a span equal to the slipstream diameter. The effects of ground interference on the lift-curve slope and induced drag were estimated on the basis of Wieselsberger's adaptation of biplane theory (reference 4).

RESULTS AND DISCUSSION

Chart for range and take-off distance.- A chart, from which the range, mean speed or duration of flight, and take-off distances from a land base or a carrier may be estimated for any of the cases considered, has been constructed from the results of the calculations of range and take-off distance and is given in figure 4. Values of the range efficiency factor $\frac{\eta}{C}\frac{L}{D}$ are plotted in the upper left-hand section of the chart against a variable speed scale just below. This plot shows lines of constant mean speed sloping to the left with increasing values of the ratio of take-off weight to empty weight, given on the diagonal scale to the right, and thereby takes account of the fact that the speed corresponding to a given point on the $\frac{\eta}{C}\frac{L}{D}$ curve for a given condition increases with increasing weight. Inasmuch as the value of η/C (fig. 3) for a given speed is found to be practically independent of loading for the engine-operating conditions assumed, the value corresponding to a given value of L/D will vary somewhat with loading. The variation, however, is small and values of η/C for the airspeed corresponding to the average of the full and empty loading for each airplane condition were therefore used in determining the $\frac{\eta}{C}\frac{L}{D}$ curves.

In the upper right-hand section of the chart, curves defining the relation between $\frac{\eta}{C}\frac{L}{D}$ and W_t/W_e for constant values of range are plotted. The lower part of the chart shows the variation with W_t/W_e of take-off distance from a land base or a carrier for the various airplane configurations.

The method of using the chart is indicated in figure 4 by the dashed lines drawn between the small circles on the curves and scales. The case illustrated is that of estimating the maximum range and duration of flight of the normal airplane for which the take-off distance from a land base is limited to 2500 feet. A line is drawn vertically from the 2500-foot point on the land-base take-off curve for the normal airplane through the W_t/W_e scale and up to the range section. Another line is drawn horizontally from the peak of the proper $\frac{\eta}{C}\frac{L}{D}$ curve to intersect the vertical line. (It will be noted that the value of $\frac{\eta}{C}\frac{L}{D}$ is between the peaks of the no-external-tank and the 300-gallon-external-tank curves to take account of the fact that an intermediate external-tank size is required for the case assumed in the example.) The intersection of the horizontal and vertical lines gives the value of maximum range - about 2050 miles for the example. In order to estimate the mean velocity, a vertical line is drawn down from the point corresponding to the value of $\frac{\eta}{C}\frac{L}{D}$ used in determining the range. The point of intersection of this line with a horizontal line drawn from the previously established point on the W_t/W_e scale gives the mean speed of the flight - about 206 miles per hour for the example. The duration of the flight is given by dividing the range by the mean speed and is found to be about 9.95 hours. The same procedure would be followed for the case of take-off from a carrier, using the carrier take-off curves instead of the land-base curves.

Figures 5 and 6 have been prepared from the chart in figure 4 to provide a more direct comparison of the various means for increasing the range. Figure 5 shows the minimum take-off distances and the corresponding duration of flight plotted against range. Figure 6 gives the variation of take-off distances with range when the duration of flight for a given range is the same for all cases as that for the original airplane operating at maximum efficiency.

Streamline external tank.- In figure 5 it is shown that, by increasing the fuel capacity of the airplane from 300 to 600 gallons through the use of a streamline external tank, the maximum range would be increased from about 1450 to 2600 miles or about 80 percent. The take-off distance from a land base would be increased from 2160 feet to 2960 feet or about 35 percent. From a carrier, the take-off distance would be increased from 308 to 500 feet or about 62 percent. The extent to which an increase in take-off distance from a land base would be acceptable depends, of course, on the size of airfield available. For carrier operation, however, any material increase in take-off distance would probably be a serious disadvantage.

Tank wing.- The tank wing is essentially a temporary means of providing added wing area in order that the airplane may take off with a greater fuel load for certain long-range missions and, at the same time, provides tank space for this extra fuel. This auxiliary wing would probably be mounted as the upper wing of a biplane as shown in figure 1. With such an arrangement, it would be theoretically possible to increase the effective span of the airplane to some extent but the high aspect ratio that would be required for the auxiliary wing would probably unduly complicate the structural problems. For the purposes of this analysis, it was assumed that a tank wing of aspect ratio 5 with an area of 80 square feet and a fuel capacity of 300 gallons would represent a reasonably practicable case. This arrangement entails a reduction in the effective span of the combination of about 2 percent in comparison with the original airplane. The wetted area and hence the parasite-drag increase due to the tank wing, furthermore, is about twice that of a body of revolution of equal volume. As a result, the airplane with the tank wing is somewhat less efficient than the airplane with a streamline external tank. (See figs. 3 and 4.)

The effect of this reduced efficiency shows in figure 5 as a reduction in range from 2600 to 2440 miles with a 600-gallon fuel load. The tank wing does, however, give an increase in range for a given take-off distance, because of the greater fuel load that can be carried. For land-base operation, the tank wing increases the range from 1440 to 2100 miles or about 45 percent for the same take-off distance as for the original airplane with the normal full fuel load of 300 gallons. For carrier operation, the range would be increased to 1750 miles or about 20 percent. The effectiveness of the tank wing for carrier operation in comparison

with that for land-base operation is reduced because the flap on the original wing is used for the carrier take-offs and the added wing area due to the tank wing does not, in this case, proportionately increase the take-off lift.

Wing-tip extensions.- Increasing the span of an airplane, other things remaining equal, will proportionately increase the maximum range attainable with a given fuel load. This fact suggests the use of auxiliary panels, attached to the wing tips in place of the removable tip fairings (see fig. 2), as a promising means for increasing the range.

Inasmuch as the greatest range is attained at moderate speeds, it is possible that these temporary tip extensions could be constructed of fairly light wood or plastic. Furthermore, because the wing of a fighter airplane is designed for loadings much greater than those encountered in level flight, major changes in the main wing structure might not be necessary. It is suggested that, by using a greater taper in the tip extensions as shown in figure 2 and at the same time suitably increasing the camber of the airfoil sections, the gust loads imposed on the main wing structure by the tip extensions can be considerably reduced without materially affecting the range or the take-off distance.

The tip extensions would considerably reduce the lateral maneuverability of the airplane. For the airplane considered, it is estimated that tip extensions of 10-foot span (over-all span increased from 41 to 61 ft) would decrease the maximum value of the tip helix angle $pb/2V$ attainable with the ailerons about 30 percent. It is believed that this loss in control effectiveness would not be too serious for the maneuvers which might be required in a long-range flight. Flight tests have shown that the moment of inertia of an airplane about its longitudinal axis can be at least doubled without materially affecting lateral maneuverability; accordingly, the added moment of inertia due to the tip extensions should have no noticeable effect on the response to aileron control.

The relatively low stability that is normally characteristic of fighter-type airplanes would tend to increase pilot fatigue on a long-range flight. The temporary devices used for increasing the range should therefore be designed, insofar as possible, to improve the stability. Increased longitudinal stability could be obtained by providing sweep-

back in the wing-tip extensions or by properly disposing the fuel load carried in external tanks. Wing-tip extensions might be designed with sufficient dihedral angle to improve spiral stability, if necessary, in order that the pilot could fly with rudder alone in smooth air.

The use of wing-tip extensions, either alone or in conjunction with streamline external fuel tanks, appears to be the most effective of the means considered for increasing the range attainable with fighter airplanes. Not only is the efficiency of the airplane increased, as shown in figures 3 and 4, with the result that the range with a given fuel load is greater, but also the added wing area will give a substantial improvement in take-off distance. In figure 5, the maximum range of the airplane with 600 gallons of fuel is shown to be increased from 2600 to 3030 miles with 5-foot tip extensions and to 3450 miles with 10-foot tip extensions. It is also shown that, without exceeding take-off distance of the original airplane from either a land base or a carrier, the range is increased from 1440 to about 2400 miles or almost 70 percent with 5-foot tip extensions and to about 3300 miles or between 125 and 130 percent with 10-foot tip extensions. The wing-tip extensions, in contrast with the tank wing, appear equally effective in increasing the range for a given take-off distance from either a land base or a carrier because the increased lift-curve slope with the wing-tip extensions gives a relatively higher take-off lift for the fixed angle of attack of the carrier take-offs than is obtained with the tank wing.

Inasmuch as an increase in span reduces the airspeed at which maximum efficiency is attained, the time of flight over a given distance will be greater with the wing-tip extensions than with the original airplane or with the tank wing, if the primary consideration is the attainment of a given range with the least possible fuel load or take-off distance. This case is represented in figure 5. When the distance to be flown is so great as to tax the pilot's endurance, it may be desirable to fly at speeds higher than those at which maximum efficiency occurs, even though a greater fuel load and take-off distance will be required. Comparison of figures 5 and 6 shows that the flying speed for the airplane equipped with wing-tip extensions could be increased to the extent that the duration of flight for a given range is the same as for the original airplane without seriously increasing the take-off distances for a given range or, conversely, without greatly reducing the range attainable for a given take-off distance.

CONCLUDING REMARKS

Of the methods considered for temporarily increasing the range of fighter-type airplanes, the use of auxiliary wing-tip extensions appears the most promising. For the airplane considered, it was estimated that 10-foot extensions - that is, an increase in span of 20 feet - used in conjunction with an external fuel tank would increase the range of the airplane 125 to 130 percent without any increase in the distances required to take off from either a land base or a carrier. With 5-foot tip extensions, the range would be increased 65 to 70 percent, under the same limitations.

An auxiliary wing of 4-foot chord and 20-foot span mounted above the main wing and providing tank capacity for 300 gallons of extra fuel, was shown to give somewhat lower efficiency in terms of miles per gallon than the original airplane with the extra fuel carried in a streamline external tank. The tank wing would permit a greater fuel load to be carried for a given take-off distance because of the added wing area, and the range would thereby be increased. For a given take-off distance from a land base, the increase in range was estimated to be about 45 percent. The increase for a given carrier take-off would be about 20 percent.

Increasing the range 50 percent by carrying extra fuel in streamline external tanks without any other modifications to the airplane would entail an increase of 20 percent in take-off distance from a land base and 32 percent from a carrier.

Selection of the most suitable method for a particular application will of course depend on other factors besides the attainable range and take-off performance, such as structural problems, pilot endurance, and area available for take-off. For example, if in a given case the duration of flight with external tanks alone is equal to the endurance of the pilot and if the area and the span available for take-off are adequate, there will be little advantage in the use of more efficient methods.

Langley Memorial Aeronautical Laboratory,
National Advisory Committee for Aeronautics,
Langley Field, Va.

REFERENCES

1. Diehl, Walter S.: Engineering Aerodynamics. The Ronald Press Co., 1928, pp. 36-40.

2. Hartman, Edwin P.: Considerations of the Take-Off Problem. T.N. No. 557, NACA, 1936.

3. Smelt, R., and Davies, H.: Estimation of Increase in Lift due to Slipstream. R. & M. No. 1788, British A.R.C., 1937.

4. Wieselsberger, C.: Wing Resistance near the Ground. T.M. No. 77, NACA, 1922.

Figure 1.- Fighter airplane with 300-gallon tank wing.

Figure 2.-
Fighter airplane with 10-foot wing-tip extensions and 300-gallon external fuel tank.

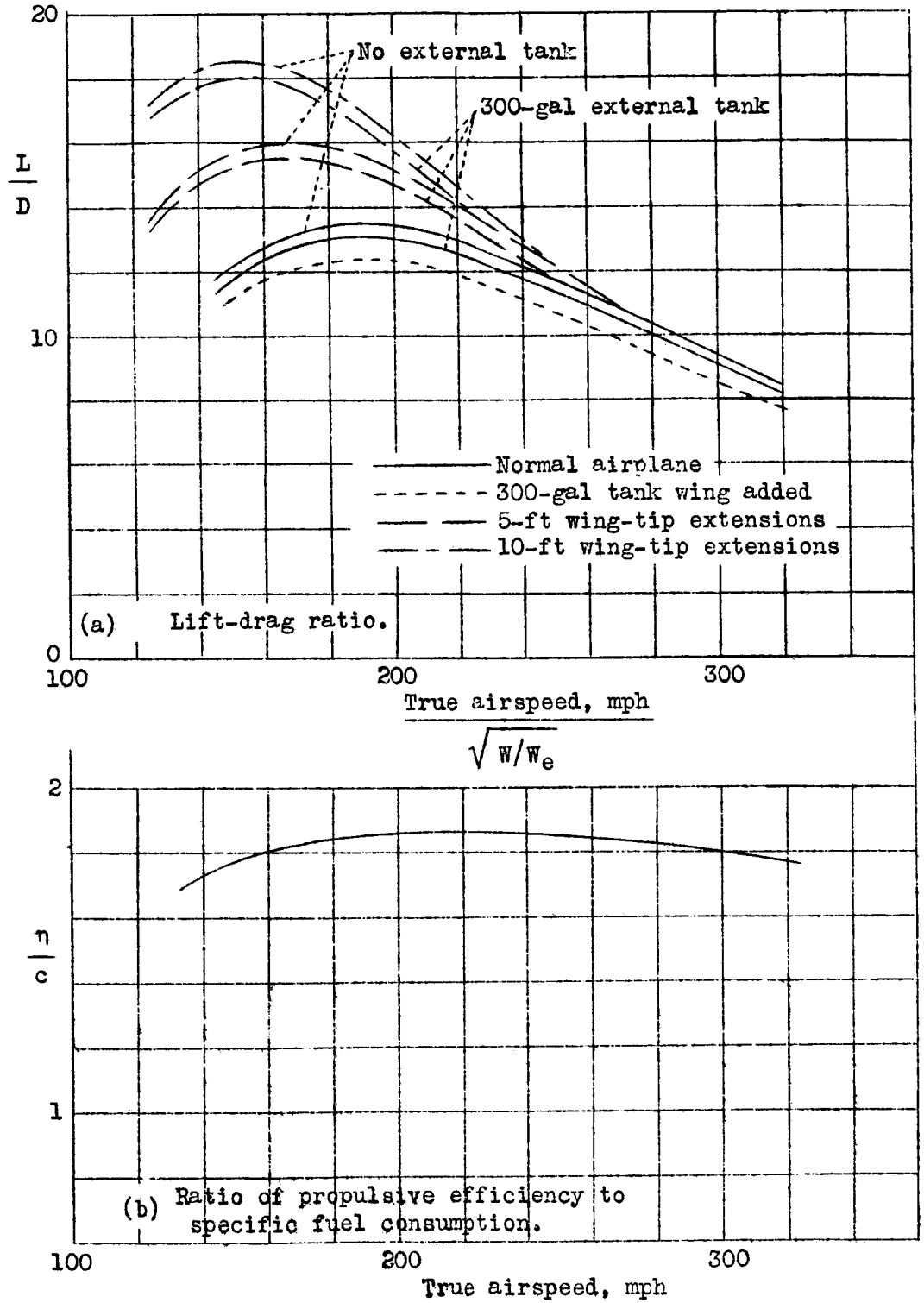

Figure 3.- Variation with true airspeed of lift-drag ratio and ratio of propulsive efficiency to specific fuel consumption for various modifications of fighter airplane. Altitude = 10,000 feet.

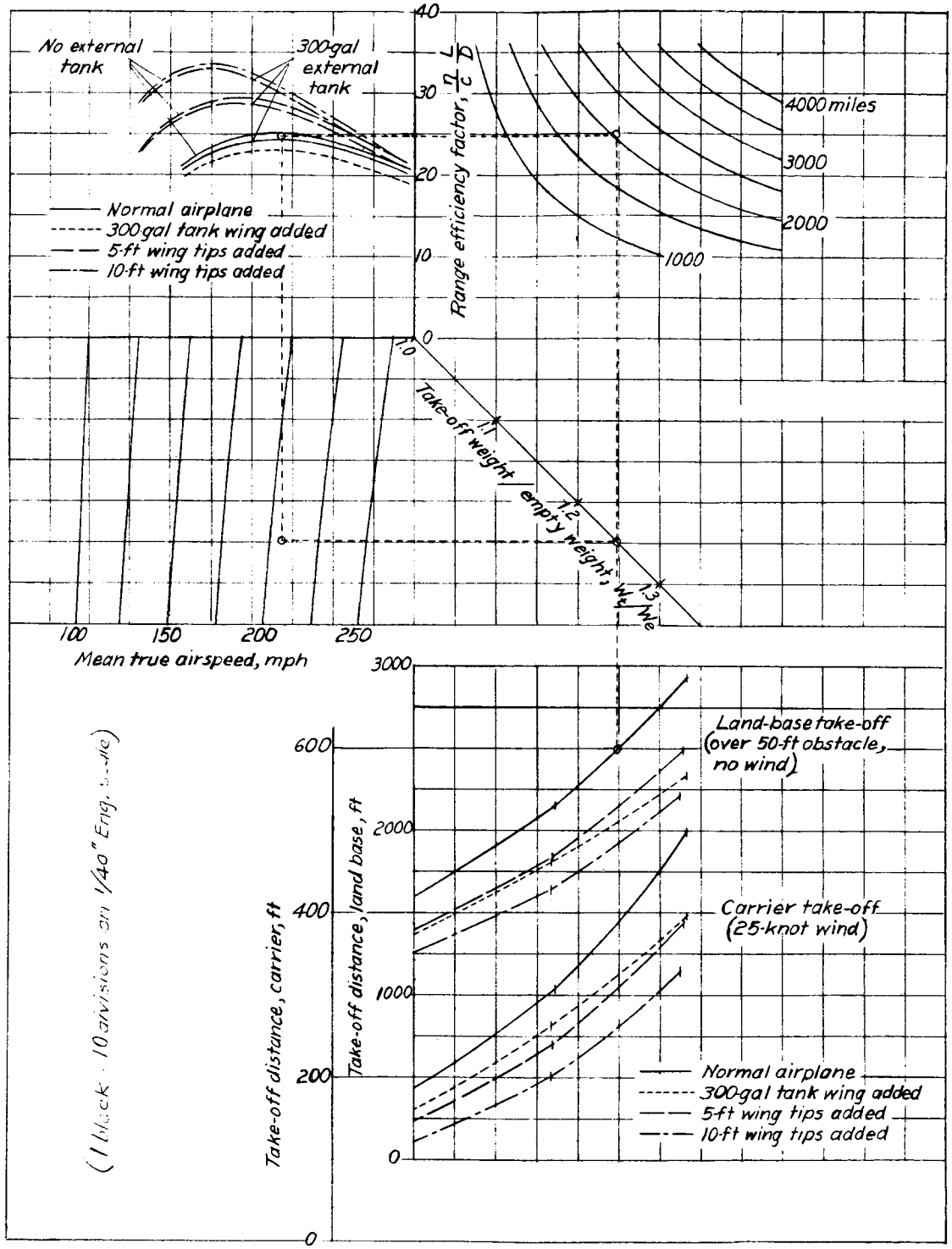

Figure 4.- Chart for estimating range, duration of flight and take-off distance for various modifications of fighter airplane. Altitude = 10,000 feet. Vertical marks on take-off curves denote 300- and 600-gallon fuel loads.

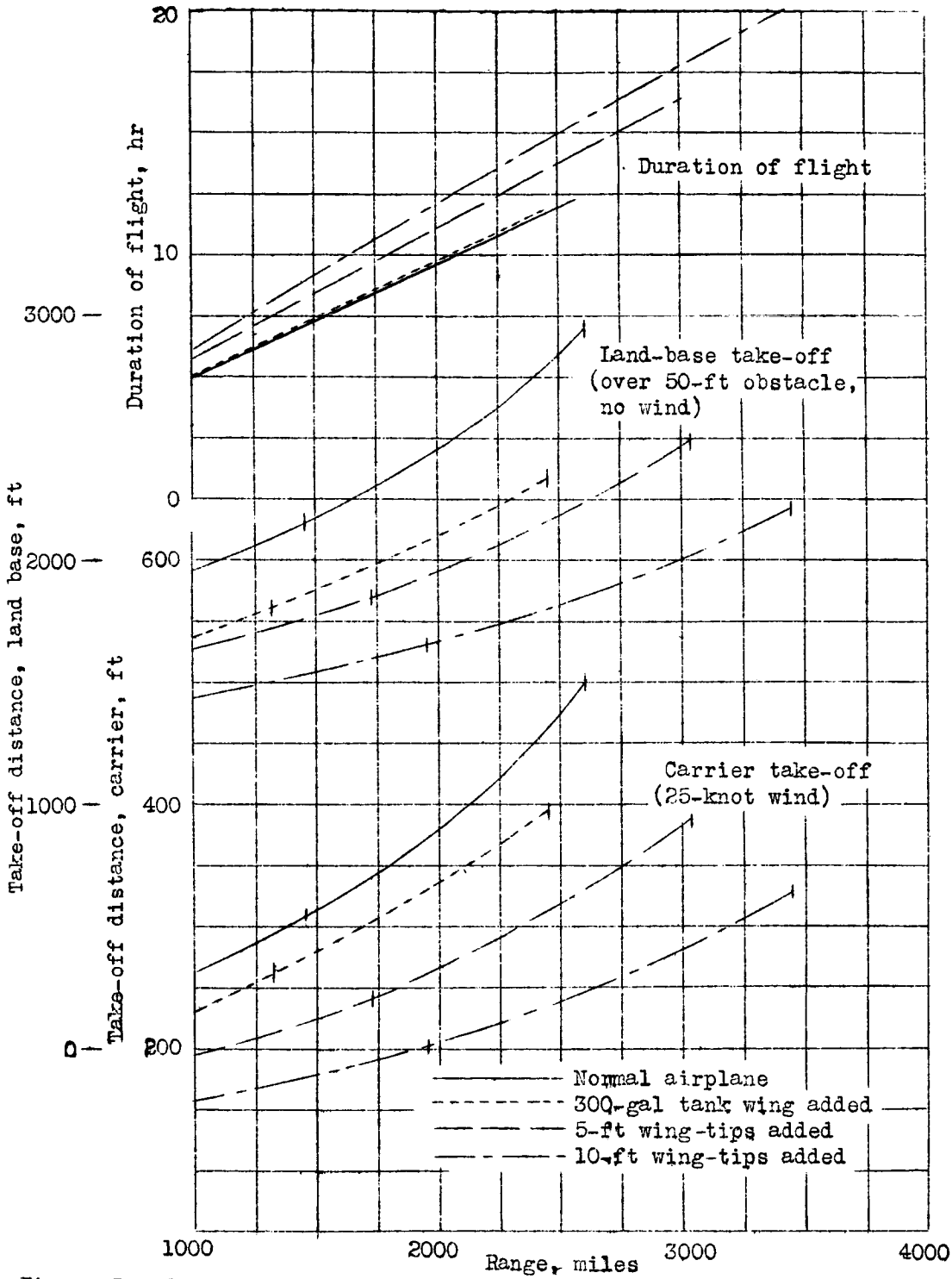

Figure 5.- Variation with range of take-off distances from a land base and a carrier and duration of flight for various modifications of fighter airplane. Flight at 10,000 feet at speed of maximum η/C L/D for each condition. Vertical marks on curves of take-off distance against range denote take-off distance and range with 300- and 600-gallon fuel loads.

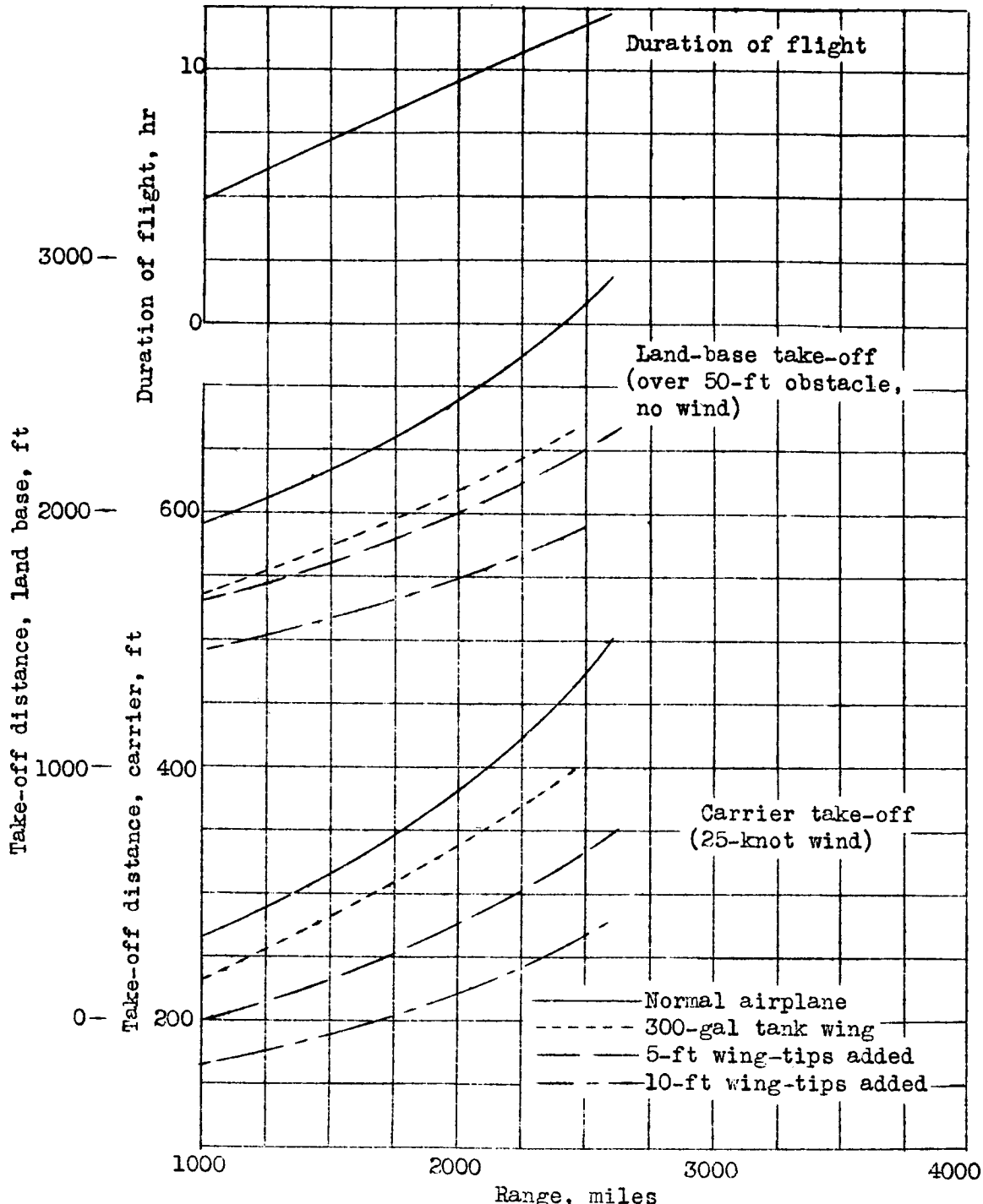

Figure 6.- Variation with range of take-off distances from a land base and a carrier and duration of flight for various modifications of fighter airplane. Flight at 10,000 feet at speed of maximum $\eta/C \quad L/D$ of normal airplane for all conditions.

REPORT NO. 798

EFFECT OF HINGE-MOMENT PARAMETERS ON ELEVATOR STICK FORCES IN RAPID MANEUVERS

Robert T. Jones and Harry Greenberg

Langley Memorial Aeronautical Laboratory

1944

REPORT No. 798

EFFECT OF HINGE-MOMENT PARAMETERS ON ELEVATOR STICK FORCES IN RAPID MANEUVERS

By Robert T. Jones and Harry Greenberg

SUMMARY

The importance of the stick force per unit normal acceleration as a criterion of longitudinal stability and the critical dependence of this gradient on elevator hinge-moment parameters have been shown in previous reports. The present report continues the investigation with special reference to transient effects for maneuvers of short duration.

The analysis made showed that different combinations of elevator parameters which give the same stick force per unit acceleration in turns give widely different force variations during the entries into and recoveries from steady turns and during maneuvers of short duration such as abrupt pull-ups. A combination of relatively large negative values of the restoring tendency C_{h_δ} and the floating tendency $C_{h_{\alpha_t}}$, approaching those of an unbalanced elevator, results in a stick force that is high during the initial stage of a pull-up and then decreases, and may even reverse, as the acceleration is reduced at the end of the maneuver. The stick force per unit acceleration is greater for abrupt than for gradual control movements.

If the negative value of C_{h_δ} is reduced so that the corresponding value of $C_{h_{\alpha_t}}$ becomes slightly positive, the reversal of force may be eliminated and the force may be brought nearly in phase with the acceleration. There is a limit to the permissible reduction of the value of C_{h_δ}, however, because as C_{h_δ} approaches zero the stick force per unit acceleration may become lower for abrupt than for gradual maneuvers and may thus lead to undesirably low stick forces at the beginning of the maneuver.

INTRODUCTION

The stick force per unit normal acceleration as measured in steady turns or pull-outs, which was proposed as a criterion of longitudinal handling in reference 1, is now generally accepted as a basic measure of longitudinal stability. The critical dependence of this stick-force gradient on elevator hinge-moment parameters and on mass unbalance of the control system was shown in reference 2. It was found that a given stick-force gradient can be obtained by any of a series of combinations of these parameters satisfying certain prescribed relations.

Further consideration of the problem and some recent flight experience, however, have shown the need for investigating the transient effects that occur during the change from steady unaccelerated flight to steady accelerated flight. These transient effects cause a difference between the stick-force gradients in a steady turn and in a maneuver of short duration such as a pull-up.

The purpose of the present report is to investigate the variation of elevator stick force and normal acceleration during the transition interval preceding the steady turn and also during turns or pull-ups of short duration. The effect of combinations of hinge-moment parameters is considered; each combination is chosen to give the same stick-force gradient in a steady maneuver. Time histories of the stick force and normal acceleration are found for predetermined variations of elevator deflection. An attempt is made to explain and to suggest a remedy for the large variations of stick force with time observed during pull-ups of short duration on different airplanes in flight. A previous analysis, somewhat similar to the present one, was made in England (reference 3) but included a smaller range of hinge-moment parameters.

SYMBOLS

A	aspect ratio of wing
b	wing span
C_h	elevator hinge-moment coefficient $\left(\frac{H}{qS_e\bar{c}_e}\right)$
C_L	airplane lift coefficient $\left(\frac{\text{Lift}}{qS}\right)$
C_m	pitching-moment coefficient about airplane center of gravity $\left(\frac{\text{Pitching moment}}{qS\bar{c}}\right)$
c	wing chord
c_e	elevator chord
D	differential operator (d/ds)
F_s	stick force, pounds
$F_1, \ldots F_5$	cases representing particular combinations of hinge-moment parameters
F_n	stick-force gradient in maneuvers $\left(\frac{dF_s}{dn}\right)$
g	acceleration of gravity
H	hinge moment; positive when tends to lower elevator
H_0	mass moment of elevator control system about elevator hinge; positive when tends to lower elevator
$h=\frac{4H_0}{\rho S_e c_e c}$	
k_Y	radius of gyration of airplane about Y-axis
l_h	tail length, half-chords
m	mass of airplane
n	normal acceleration per g of airplane due to curvature of flight path; accelerometer reading minus component of gravity force
q	dynamic pressure
S	wing area

746006—47

S_e	elevator area
s	distance traveled, half-chords ($2Vt/c$)
T	period of elevator motion
t	time
u	independent variable used in Duhamel's integral
V	velocity
$x_{a.c.}$	distance between center of gravity and aerodynamic center; positive when stable
$d\delta/dx$	deflection of elevator per unit movement of stick, radians per foot
α	angle of attack, radians
α_t	angle of attack at tail, radians
δ	deflection of elevator; positive downward
θ	angle of pitch of airplane
λ	root of stability equation
μ	airplane-density parameter ($m/\rho Sb$)
ρ	mass density of air

Subscript:

max	maximum

Subscripts α, $D\alpha$, $D^2\alpha$, α_t, $D\theta$, δ, and $D\delta$ indicate derivatives; for example, $C_{m_{D\theta}}=\frac{\partial C_m}{\partial D\theta}$. A dot over a symbol indicates differentiation with respect to time.

METHOD OF ANALYSIS

The following assumptions are made in the present analysis:

(1) Variation in forward speed is negligible

(2) Stability derivatives are constant; that is, any possible nonlinearity of coefficients is negligible

(3) Effects of power are negligible

(4) Effects of control-system moment of inertia are negligible

(5) Control-system mass unbalance is all located at airplane center of gravity

The equations of motion of an airplane subjected to a prescribed elevator motion can be obtained from reference 2. If forward speed is assumed constant, there are three equations of motion. The first two equations determine the motion of the airplane if the control motion is specified. The third equation determines the hinge-moment coefficient, which depends on the motion of the control surface and the airplane. These equations are

$$\left(\frac{C_{L_\alpha}}{2}+2A\mu D\right)\alpha-2A\mu D\theta=0 \tag{1}$$

$$(C_{m_\alpha}+C_{m_{D_\alpha}}D+C_{m_{D^2_\alpha}}D^2)\alpha+(C_{m_{D\theta}}-2A\mu k_Y{}^2D)D\theta=-C_{m_\delta}\delta \tag{2}$$

$$[C_{h_\alpha}+(C_{h_{D_\alpha}}D-h)D+C_{hD^2_\alpha}D^2]\alpha+(C_{h_{D\theta}}+h)D\theta+(C_{h_\delta}+C_{h_{D\delta}}D)\delta=C_h \tag{3}$$

Equations (1) and (2) are used to solve for α in terms of δ. The solution can be expressed in determinant form as

$$\frac{\alpha}{\delta}=\frac{-2A\mu C_{m_\delta}}{\begin{vmatrix}\frac{C_{L_\alpha}}{2}+2A\mu D & -2A\mu\\ C_{m_\alpha}+C_{m_{D_\alpha}}D+C_{m_{D^2_\alpha}}D^2 & C_{m_{D\theta}}-2A\mu k_Y{}^2D\end{vmatrix}} \tag{4}$$

If δ is given as a function of time, the solution for α is found by the method of operational calculus as follows: First α is found for a unit change in δ. This solution is obtained from

$$\alpha=\frac{-2A\mu C_{m_\delta}}{F(D)}=-2A\mu C_{m_\delta}\left[\sum\frac{e^{\lambda s}}{\lambda F'(\lambda)}+\frac{1}{F(0)}\right] \tag{5}$$

where $F(D)$ is the determinant given in equation (4) and λ represents the roots of $F(D)=0$. The solution for α (equation (5)) may be denoted by $\bar{\alpha}(s)$. The value of α for a given variation of δ is then given by Duhamel's integral, which is

$$\alpha=\bar{\alpha}(s)\delta(0)+\int_0^s\bar{\alpha}(s-u)\delta'(u)\,du$$

By a similar procedure $D\theta$ can be found for a prescribed variation of δ. The angle of attack at the tail can then be found from

$$\alpha_t=\frac{\partial\alpha_t}{\partial\alpha}\alpha+l_hD\theta$$

The normal acceleration, which is considered positive upward, is proportional to the change in angle of attack α and is given by

$$n=\frac{V^2}{cg}\frac{C_{L_\alpha}}{2A\mu}\alpha$$

The value of the stick force can be obtained by substituting the derived values of α and $D\theta$ and the given value of δ in the hinge-moment equation (equation (3)). The relation between the stick force and C_h is simply

$$F_s=\frac{1}{2}\rho V^2S_ec_eC_h\frac{d\delta}{dx}$$

The assumed variation of elevator deflection with time is illustrated in figure 1 and can be represented analytically by

$$\delta=\delta_{max}\left(\frac{1}{2}-\frac{1}{2}\cos\frac{2\pi}{T}t\right)$$

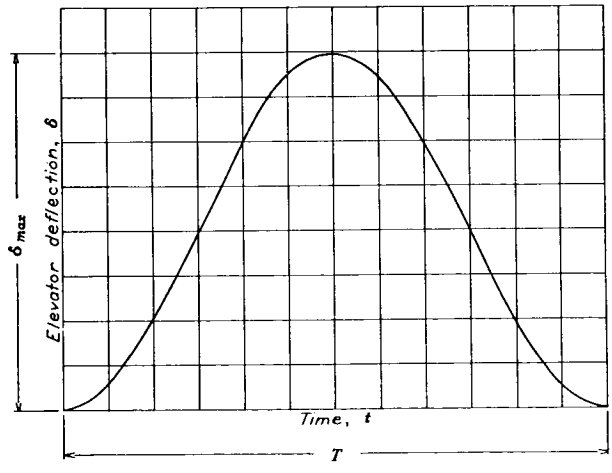

FIGURE 1.—Shape of curve of elevator deflection against time assumed in the analysis.

The calculations were made for a pursuit airplane for five different combinations of the hinge-moment parameters $C_{h_{\alpha_t}}$, C_{h_δ}, and h; for three different durations of the maneuver T; and for three different center-of-gravity locations. These five different combinations of the hinge-moment parameters were selected to give, for one center-of-gravity location, the same stick-force gradient in a steady turn, as determined by the formula for stick-force gradient in a gradual pull-up or steady turn given in reference 2, which is

$$F_s=\frac{\rho S_e c_e c g}{4}\frac{d\delta}{dx}\left(\frac{4A\mu C_{h_\alpha}}{C_{L_\alpha}}+C_{h_{D\theta}}-\frac{4A\mu C_{h_\delta}C_{m_\alpha}}{C_{L_\alpha}C_{m_\delta}}-\frac{C_{h_\delta}C_{m_{D\theta}}}{C_{m_\delta}}+h\right)$$

The locus of points in the $C_{h_{\alpha_t}}C_{h_\delta}$ plane corresponding to a value of the stick-force gradient of 5 pounds per g and a center-of-gravity location 7½ percent chord ahead of the aerodynamic center is shown in figure 2 for a mass-balanced and also for a mass-unbalanced elevator. The amount of unbalance corresponding to the line marked $h=5$ would require a pull of 15 pounds on the control stick for balance. The five points marked F_1, . . . F_5 represent the combinations of the hinge-moment parameters used in the calculations.

NUMERICAL VALUES USED IN ANALYSIS

The following parameters were used in the analysis:

C_{L_α}	4.3
μ	12.5
A	6
C_{m_α}	−0.348, −0.195, or −0.0464
$x_{a.c.}$	0.075c, 0.042c, or 0.01c
$C_{m_{D\alpha}}$	−8.9
$C_{m_{D^2\alpha}}$	23.2
$C_{m_{D\theta}}$	−15.3
k_Y, half-chords	1.5
C_{m_δ}	−1.54
l_h, half-chords	6.6
$d\delta/dx$, radian of elevator motion per foot of stick travel	0.5
C_{h_α}	$0.514C_{h_{\alpha_t}}$
$C_{h_{D\alpha}}$	$3.22C_{h_{\alpha_t}}$
$C_{h_{D^2\alpha}}$	$-10.55C_{h_{\alpha_t}}$
$C_{h_{D\delta}}$	−1

The following dimensions and density were assumed:

c, feet	7
c_e, feet	2
S_e, square feet	30
ρ, slug/cu ft; at altitude of 10,000 feet	0.00176

The foregoing airplane derivatives are for an airplane having a wing loading of 30 pounds per square foot. Five combinations of hinge-moment parameters selected to give a stick-force gradient of 5 pounds per g in a steady pull-up when the center-of-gravity location is 7½ percent chord ahead of the aerodynamic center (see fig. 2) are as follows:

Case	$C_{h_{\alpha_t}}$	C_{h_δ}	h
F_1	−0.1	−0.230	0
F_2	0	−.065	0
F_3	.039	0	0
F_4	−.1	−.035	5
F_5	0	0	1.65

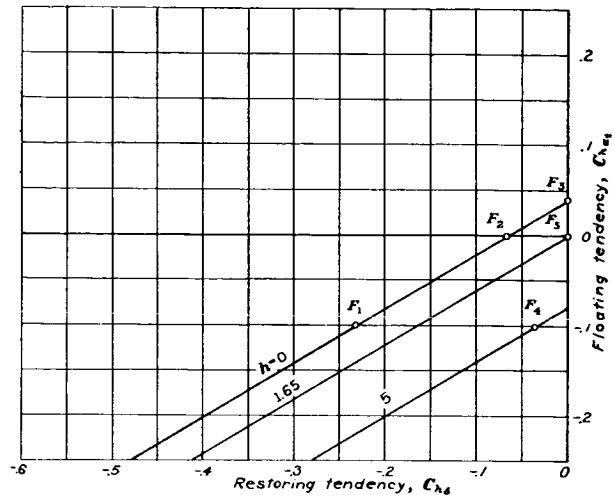

FIGURE 2.—Lines of constant stick-force gradient showing combinations of hinge-moment parameters used. F_s=5 pounds per g; $x_{a.c.}$=0.075c.

All these values were used in calculating the variation in stick force during a maneuver for $x_{a.c.}=0.075c$. For qualitative comparison, case F_1 may be taken to represent a normal elevator with a fairly high trailing tendency and a moderate amount of blunt-nose inset-hinge balance. The characteristics of F_2 or F_3 could be achieved by the use of a sharp-nose inset-hinge balance, a horn balance, or a beveled trailing edge; F_4 combines a large amount of inset-hinge balance with a bobweight at the control stick; F_5 is the case in which the stick force is due entirely to the bobweight. Two more-rearward center-of-gravity locations ($x_{a.c.}=0.042c$ and $0.01c$) were also assumed, and the stick force in maneuvers was worked out for cases F_1, F_2, and F_5.

RESULTS

Curves of stick force and normal acceleration for a varying elevator deflection are shown in figures 3, 4, and 5 for T=4, 2, and 1 seconds, respectively, for V=400 miles per hour, and for $x_{a.c.}=0.075c$. In these curves, the stick force for F_1 reaches a maximum value before the peak acceleration and reverses direction in the latter part of the cycle. This effect becomes more pronounced as the duration of the maneuver becomes shorter. The curves for F_2, F_3, F_4, and F_5 show a progressively smaller phase difference between the stick force and the acceleration. The stick-force curve for F_4 is most nearly in phase with the acceleration curve.

The effect of center-of-gravity location on the stick-force gradient in steady turns or pull-ups can be shown in diagrams of the type of figure 2. Figure 6, for example, shows that the "maneuver point" (*e.g.* location for zero stick force per g) for case F_1 is 4.2 percent chord ahead of the aerodynamic center (point where $C_{m_\alpha}=0$). For center-of-gravity locations behind the maneuver point, the stick-force gradient for case F_1 is negative. The stick forces for F_3 and F_5, however, are unaffected by center-of-gravity location.

The time histories of the stick forces in a 2-second maneuver for the cases shown in figure 6 for $x_{a.c.}=0.042c$ and $0.01c$

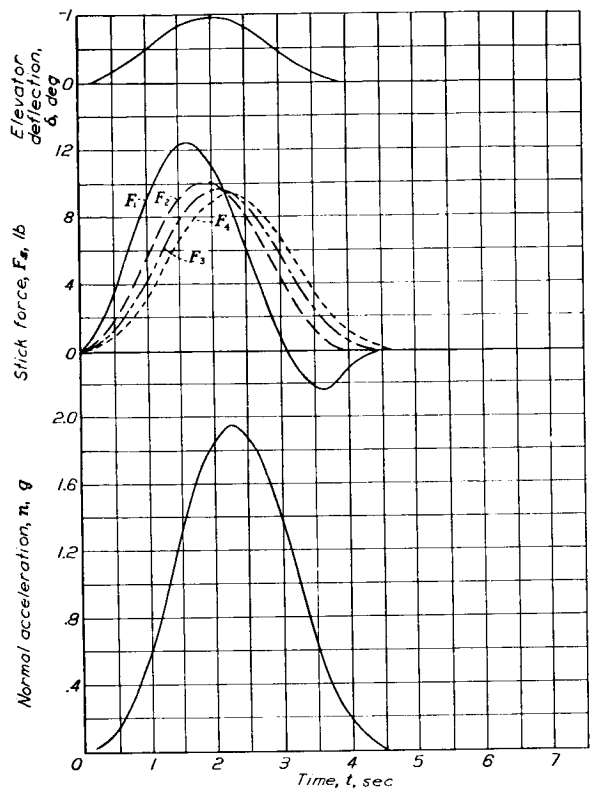

FIGURE 3.—Stick force and normal acceleration due to rapid elevator motion. T=4 seconds V=400 miles per hour; $r_{a.c.}$=0.075c.

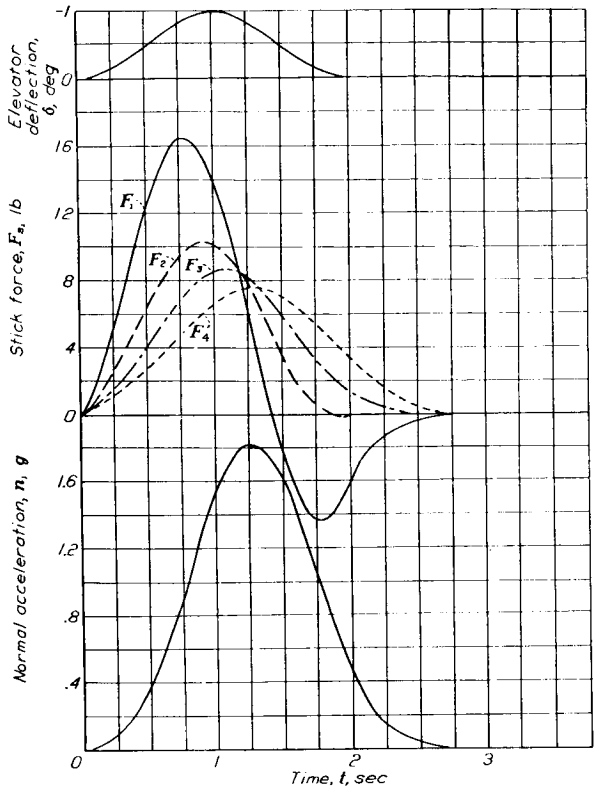

FIGURE 4.—Stick force and normal acceleration due to rapid elevator motion. T=2 seconds; V=400 miles per hour; $r_{a.c.}$=0.075c.

are plotted in figures 7 and 8. In figure 7, the stick force corresponding to F_1 (*c.g.* at maneuver point) is positive at first and then reverses and becomes negative. The maximum values of the positive and negative forces are approximately equal. As the center of gravity is moved behind the maneuver point for F_1 (fig. 8), the negative maximum force is greater than the positive; this increase would be expected since a negative force is required to hold the airplane in a steady turn. The stick forces for F_3 and F_5 remain positive. The elevator deflection required to produce a given acceleration, however, decreases as the center of gravity moves rearward.

Airplane speed has no effect on the shape of the stick-force and acceleration curves, if compressibility effects are neglected and if the product of speed and duration of maneuver is held constant; for example, the shape of the curves of figures 3 to 5 is unchanged if the speed is halved and the duration is doubled. The effect of increasing speed therefore is the same as the effect of increasing duration in the same ratio.

DISCUSSION

Before the various elevator cases and degrees of stability for which the computations were made are discussed, it appears desirable to explain the effects of the separate parameters that combine to give the resultant elevator forces in pull-ups. These effects, as already stated, are the variation of hinge-moment coefficient with elevator deflection, as indicated by C_{h_δ}; the variation of hinge-moment coefficient with angle of attack at the tail, as indicated by $C_{h_{\alpha_t}}$; the variation of hinge moment with angular velocity of the elevator about its hinge; the mass unbalance (bobweight effect); and the effective moment of inertia of the elevator system.

Because preliminary computations indicated that the inertia of the elevator system had a negligible effect on the stick force for the shortest maneuver assumed, it was neglected in the analysis. For airplanes larger than the one considered in this report and for other special cases, inertia of the elevator system may be an important factor.

The influence of the important parameters is shown in figure 9, which gives a breakdown of the factors contributing to the stick-force curve for case F_4 in figure 5. Case F_4 was chosen because it was the only condition in which all the parameters were combined.

Figure 9 shows that the effect of C_{h_δ} is to produce a component of stick force in phase with elevator deflection. The magnitude of this component of the stick force depends solely on the elevator deflection at a given speed and is independent of the duration of the maneuver.

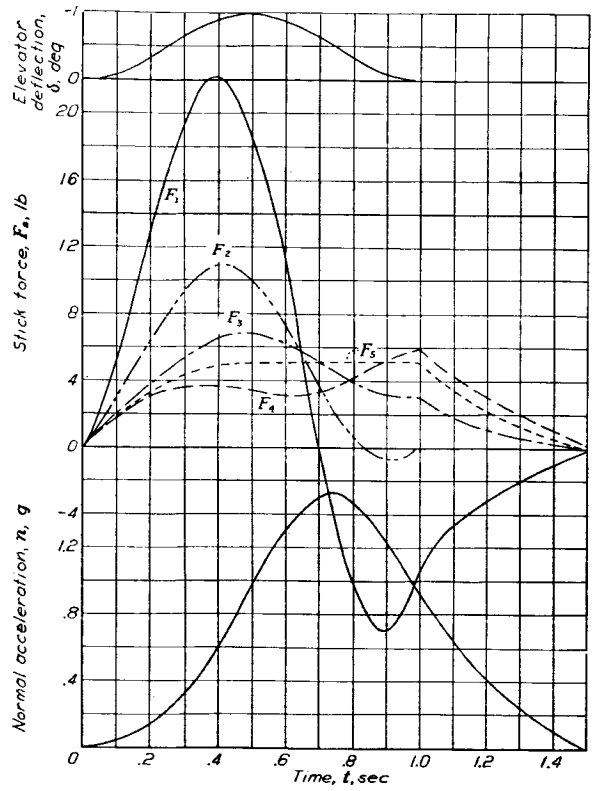

FIGURE 5.—Stick force and normal acceleration due to rapid elevator motion. T=1 second; V=400 miles per hour; $x_{a.c.}$=0.075c.

The normal acceleration produced by the elevator decreases as the duration of the maneuver is made shorter. The stick force per unit acceleration due to the C_{h_δ} term therefore increases as the maneuver becomes more rapid.

The effect of the mass unbalance of a bobweight is to contribute a component of force that is in phase with and solely dependent on the normal acceleration of the airplane. The stick-force gradient due to the bobweight is therefore independent of duration of maneuver. Although figure 9 deals with a mass unbalance that tends to depress the trailing edge of the elevator, in the general case the unbalance may be of the opposite sign so that push instead of pull forces result.

The effect of $C_{h_{\alpha_t}}$ is similar to that of the bobweight since the component of force caused by $C_{h_{\alpha_t}}$ is nearly in phase with the acceleration. The slight difference in phase between the values of α_t and n is the effect of the rate of change of airplane angle of attack. For maneuvers of short duration, this slight phase shift causes a noticeable difference between the action of $C_{h_{\alpha_t}}$ and of a bobweight.

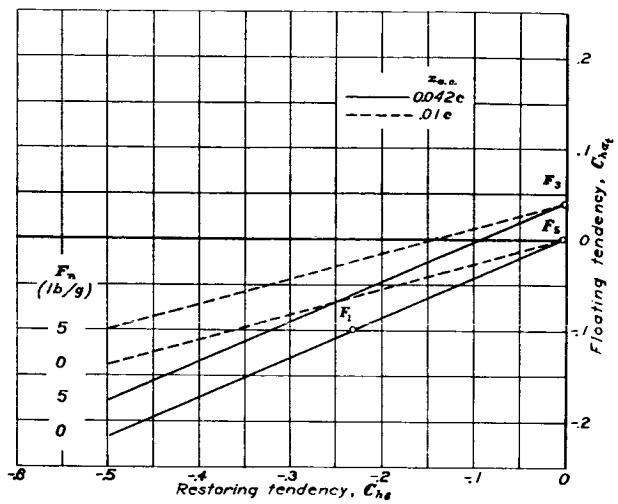

FIGURE 6.—Lines of constant stick-force gradient. F_s=0 and 5 pounds per g.

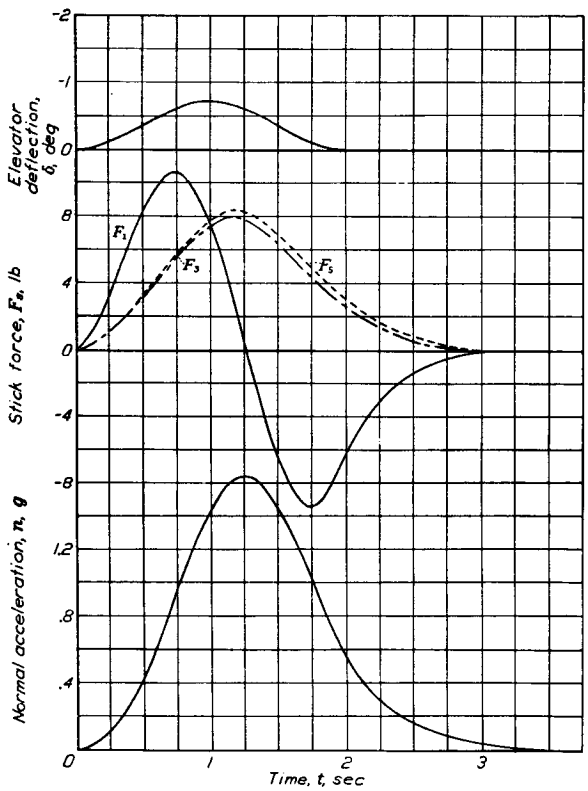

FIGURE 7.—Stick force and normal acceleration due to rapid elevator motion. T=2 seconds; V=400 miles per hour; $x_{a.c.}$=0.042c.

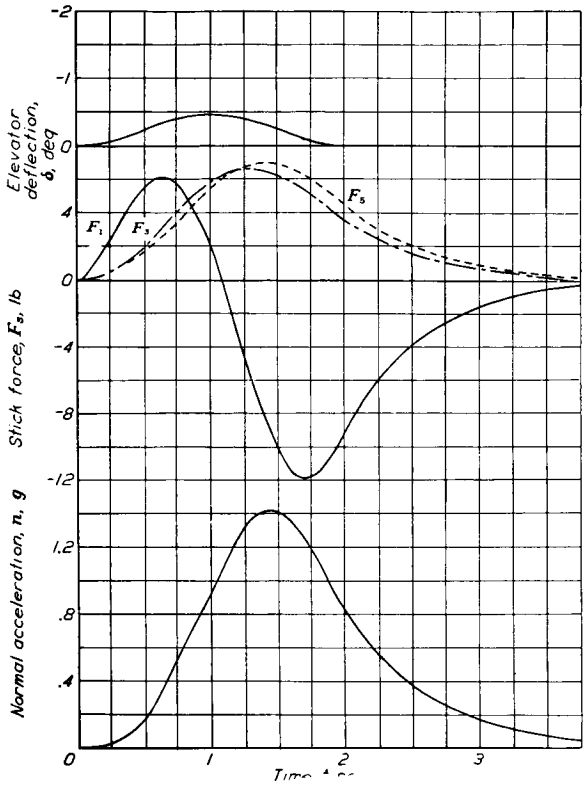

FIGURE 8.—Stick force and normal acceleration due to rapid elevator motion. $T=2$ seconds; $V=400$ miles per hour; $x_{a.c.}=0.01c$.

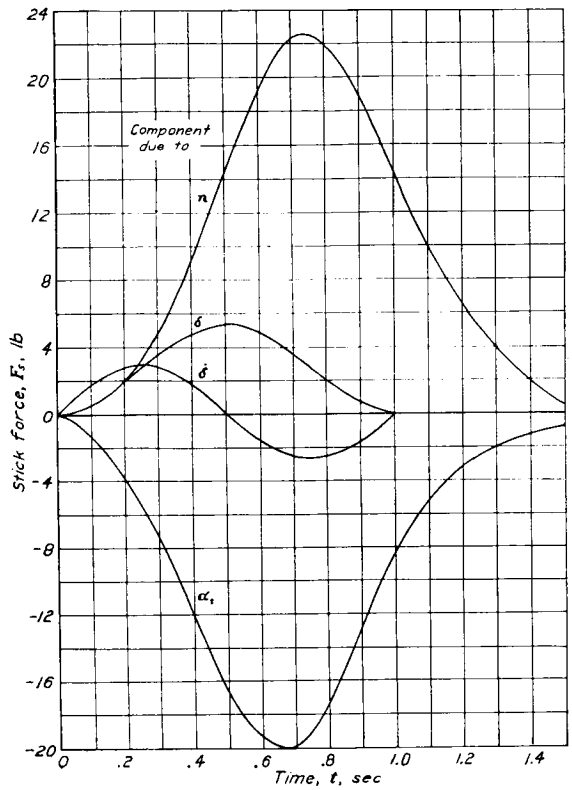

FIGURE 9.—Components of stick force for case F_1 in figure 5.

The component of force due to the angular velocity of the elevator may be very important for maneuvers of short duration. It has the effect of reducing the stick-force gradients in cases in which the maximum force occurs after the elevator has reached maximum deflection.

The cases for which the results are presented in figures 3 to 5 were chosen to show the effects of different combinations of the hinge-moment parameters subject to the designer's control. The parameter $C_{h_{D\delta}}$ is the same for all cases. In case F_1, the desired stick force for a steady turn is achieved by a balance of relatively large negative values of C_{h_δ} and $C_{h_{\alpha_t}}$. The stick forces due to these two parameters are in opposite directions so that the net value in a steady turn is due to the difference in their effects. In a maneuver of the type shown in figure 1, the elevator-deflection curve leads the normal-acceleration curve; hence C_{h_δ} has the predominating effect in the initial stages of the maneuver and the negative $C_{h_{\alpha_t}}$ in the later stages. This fact accounts for the high stick forces in the first half of the maneuver and the reversal of force in the second half for case F_1. The difference is more noticeable in the shorter maneuvers. As the duration of the maneuver decreases, the lag between airplane motion and elevator deflection becomes greater and the maximum value of the acceleration for the given elevator deflection becomes smaller. Both of these factors tend to reduce the importance of the $C_{h_{\alpha_t}}$ component in the early part of the maneuver and to increase the maximum force required for a given maximum acceleration. This variation of maximum force per unit maximum acceleration shown in figure 10 is quite large.

For case F_2, the desired stick force for steady turns is achieved through the action of C_{h_δ} alone. All curves for F_2 would have the same magnitude for any duration of maneuver and would be in phase with the elevator-deflection curve but for the contribution of $C_{h_{D\delta}}$. The effect of $C_{h_{D\delta}}$ increases with the rapidity of the elevator movement and causes a phase shift in the force curve relative to the elevator deflection, which results in a slight increase in the maximum value for the shortest maneuver. A slight push force near the end of the maneuver is produced by $C_{h_{D\delta}}$. Figure 10 shows that in case F_2 the maximum force per unit maximum acceleration increases as the maneuver is shortened although not so much as in case F_1.

The balance is achieved in case F_3 through action of

$C_{h_{\alpha_t}}$ alone. In this case, the maximum stick force attributed to $C_{h_{\alpha_t}}$ is nearly in phase with the acceleration and, consequently, the maximum value occurs after maximum elevator deflection when the elevator is being moved back to its original position. The forces at the beginning of the maneuver are consequently smaller than in cases F_1 and F_2 and may be too small for satisfactory handling qualities. The effect of $C_{h_{D\delta}}$ is to decrease the maximum force by an increasing amount as the maneuver becomes shorter. The discontinuity in the F_3 curve (and also in the F_4 and F_5 curves) for the 1-second maneuver results from the disappearance of the $C_{h_{D\delta}}$ component at the completion of the elevator motion. Figure 10 shows that the maximum force per unit maximum acceleration for case F_3 decreases as the maneuver is shortened; this effect is primarily a result of the action of $C_{h_{D\delta}}$.

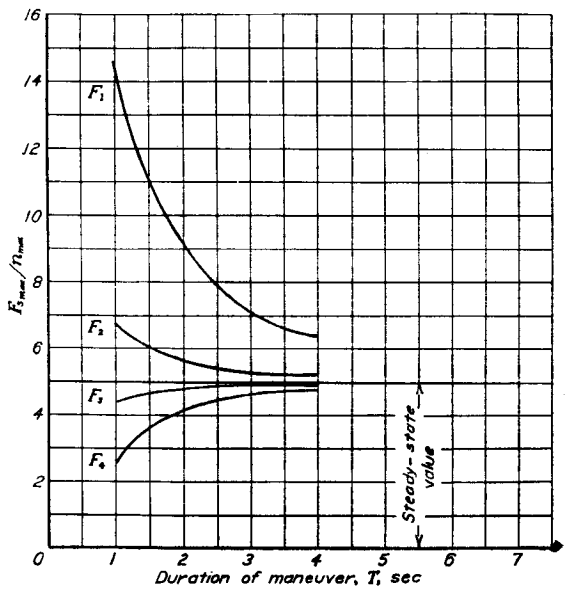

FIGURE 10.—Maximum stick force per unit maximum acceleration against duration of maneuver. $x_{a.c.}=0.075c$.

For case F_4, the stick force for steady turns is achieved mainly by a balance of negative $C_{h_{\alpha_t}}$ and bobweight effects. As a result of the large mass unbalance required, the maximum force in the 1-second maneuver occurs at the end of the elevator motion.

The stick force is achieved solely through the action of mass unbalance, or a bobweight, in case F_5. Computations have been made for only the 1-second maneuver. The action of the bobweight, as previously mentioned, is similar to that of $C_{h_{\alpha_t}}$ but for a slight phase shift. The phase shift for a maneuver of short duration is sufficient to reduce the adverse influence of $C_{h_{D\delta}}$. This case would show a slightly greater decrease of maximum force per unit maximum acceleration than case F_3 with decreased duration of the maneuver.

The change of stick force with center-of-gravity location for case F_1, shown in figures 7 and 8, is caused by the greater angular response of the airplane to a given elevator deflection that occurs with reduced stability. The greater response changes the balance between the $C_{h_{\alpha_t}}$ and C_{h_δ} components. If the stick force is independent of C_{h_δ}, as in case F_3 and F_5, the form of the stick-force curves is unchanged by variation of the center-of-gravity location. Figure 11 shows that the variation of maximum force per unit maximum acceleration in a rapid maneuver with center-of-gravity location becomes less as the value of C_{h_δ} is reduced.

The adjustment of the elevator parameters so that the stick forces for steady turns are directly proportional to the normal acceleration produced and independent of center-of-gravity location is generally conceded to be desirable. It appears possible from the analysis to accomplish these conditions by making the stick forces depend primarily on $C_{h_{\alpha_t}}$ or on a bobweight, provided the entrance and recovery are made slowly. It is not definitely known whether this condition of strict proportionality is desired in maneuvers of short duration. In these cases, however, when the entry

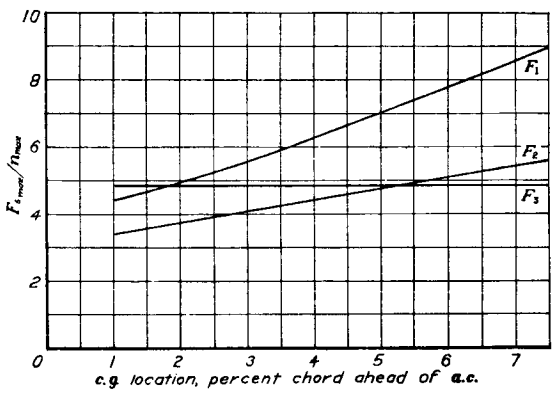

FIGURE 11.—Variation of maximum stick force per unit maximum acceleration with center-of-gravity location. $T=2$ seconds; $V=400$ miles per hour.

and recovery are of necessity rapid, strict proportionality between stick force and acceleration appears impossible because of the action of $C_{h_{D\delta}}$. According to figure 10, a stick-force gradient that is independent of duration of maneuver but varies somewhat with center-of-gravity location can be obtained for a case intermediate between F_2 and F_3. This case would correspond to a certain amount of negative C_{h_δ} and positive $C_{h_{\alpha_t}}$ and would also result in higher stick forces at the start of the maneuver. A bobweight that increases the stick forces can be substituted for the positive $C_{h_{\alpha_t}}$.

CONCLUDING REMARKS

A small stick-force gradient in steady turns can be obtained with fairly large negative values of the restoring tendency C_{h_δ} and the floating tendency $C_{h_{\alpha_t}}$, approaching those of an unbalanced elevator. Although suitable for slow maneuvers, this combination of parameters leads to a high initial value followed by a reversal of the stick force in abrupt maneuvers. This difficulty can be avoided and the stick force can be made

to follow closely in phase with the airplane normal acceleration during both abrupt and slow maneuvers by decreasing the value of C_{h_δ} and by making $C_{h_{\alpha_t}}$ slightly positive.

If C_{h_δ} is made zero, the stick-force gradient depends entirely on a positive value of $C_{h_{\alpha_t}}$ and is unaffected by the location of the airplane center of gravity. In this condition, however, the stick force required to initiate a maneuver may be undesirably light. In order to prevent undesirably light stick forces at the beginning of a maneuver, a small negative C_{h_δ} must be retained.

The use of a bobweight in the elevator control system has an effect similar to that of increasing $C_{h_{\alpha_t}}$ although, in rapid maneuvers, there are slight phase differences in the stick-force variations.

LANGLEY MEMORIAL AERONAUTICAL LABORATORY,
NATIONAL ADVISORY COMMITTEE FOR AERONAUTICS,
LANGLEY FIELD, VA., *October 12, 1944.*

REFERENCES

1. Gilruth, R. R.: Requirements for Satisfactory Flying Qualities of Airplanes. NACA Rep. No. 755, 1941.
2. Greenberg, Harry, and Sternfield, Leonard: A Theoretical Investigation of Longitudinal Stability of Airplanes with Free Controls Including Effect of Friction in Control System. NACA Rep. No. 791, 1944.
3. Tye, W.: Control Forces during Recovery from Dive. J. A. C. Paper No. 69, British R. A. E., April 1941.

WARTIME REPORT L-651

WIND-TUNNEL INVESTIGATION OF A BEVELED AILERON SHAPE DESIGNED TO INCREASE THE USEFUL DEFLECTION RANGE

Robert T. Jones and W. J. Underwood

April 1944

NATIONAL ADVISORY COMMITTEE FOR AERONAUTICS

MEMORANDUM REPORT

for the

Army Air Forces, Materiel Command

WIND-TUNNEL INVESTIGATION OF A BEVELED AILERON SHAPE DESIGNED TO INCREASE THE USEFUL DEFLECTION RANGE

By R. T. Jones and W. J. Underwood

INTRODUCTION

The useful range of deflection of a control surface is ordinarily limited by the occurrence of flow separation on the convex side of the surface behind the hinge. After this separation occurs the hinge moment increases rapidly, making it extremely difficult to deflect the aileron beyond this point at high speed. An aileron following the shape of the original airfoil forms an outside corner on one side of the flap hinge when it is deflected through a small angle. The increased local velocity around this corner, which is followed by an adverse pressure gradient, is responsible for the flow separation.

When beveled ailerons were constructed for the XP-51 airplane, the bevel was built up by spreading the upper and lower surfaces apart behind the hinge (see fig. 1, configuration B, and fig. 2 of reference 1), making a slight inside corner on each surface. During the flight tests, it was noted that these ailerons showed a somewhat greater useful range of deflections and gave slightly better control at low speed than did the original ailerons.

In an attempt to further increase the useful range of angular deflections, the aileron shown in figure 1, configuration C, was designed. The more pronounced inside corner at the aileron hinge point causes an initial positive pressure peak, so that a certain amount of deflection is possible before the pressure curve becomes flat. The purpose of the present investigation made in the Langley Memorial Aeronautical Laboratory two-dimensional low-turbulence tunnel was to determine the general

aerodynamic characteristics of this aileron and, in particular, to determine its useful angular range.

APPARATUS AND METHODS

A scale model having a 36-inch wing chord and 35.75-inch span was made to correspond to the measured ordinates of an intermediate section of the aileron portion of the wing (16 inches outboard from the inboard end of the right aileron) of the XP-51 airplane. The wing section was modified aft of the 70-percent chord point in order to fair in the 0.150-chord aileron. (See fig. 1, configuration C.) The ordinates of the modified wing section forward of the aileron hinge line and the original measured ordinates of the plain wing are given in table I.

The aileron shapes tested are shown in figure 2. The three ailerons were hinged at the 85-percent chord point. Therefore, with the 0.145-chord aileron the wing chord was reduced approximately 0.2 inch. In the sealed condition, the aileron nose gap was sealed with thin rubber dam.

For the low-drag condition, the model was finished with number 400 waterpaper to produce aerodynamically smooth surfaces. For the high-drag condition, the model surfaces were the same as in the low-drag condition; but roughness strips, made of carborundum grains embedded in glue on a 1-inch strip of Scotch tape, were placed on the upper and lower surfaces near the leading edge of the model.

Lift and drag measurements of the model were made by the methods described in reference 2. The profile-drag and lift coefficients were based on a nominal wing chord of 36 inches. The aileron hinge moments were measured by means of a calibrated torque rod and the coefficient is based on the actual chord and span of the aileron.

All tests were made at a dynamic pressure of 59.7 pounds per square foot, which corresponds to a velocity of about 150 miles per hour and a test Reynolds number of approximately 4,000,000. The test program is given in the following table.

Aileron deflection, ±30°, for all runs

Run no.	Aileron	α_o (deg)	Gap condition	Surface condition
1	1	0	Seal	Smooth
2	1	0	No seal	Smooth
3	1	0	Seal	Roughness strips
4	2	0	Seal	Smooth
5	2	0	Seal	Roughness strips
6	3	0	Seal	Smooth
7	3	0	Seal	Roughness strips
8	3	0, ±4.1 8.3	Seal	Roughness strips

RESULTS AND DISCUSSION

Effect of hinge-gap seal.- The effects of sealing the hinge gap on the aileron characteristics can be seen from the results presented in figure 3. With the gap open there is a tendency for aileron 1 to overbalance for small deflections. A similar tendency has been found in other tests on beveled-trailing-edge ailerons. As shown in figure 3, this tendency to overbalance was eliminated by sealing the gap to stop the flow of air. Apparently the pressure difference resulting from a small deflection of the aileron is sufficient to cause a large portion of the boundary layer to flow from one side of the airfoil to the other through the hinge gap, accentuating the effect of the bevel. In addition to eliminating the overbalance, sealing the gap also reduced the increment in lift for the larger aileron deflections. This is not in agreement with the usually favorable effect of sealing the gap of contour ailerons or less severely shaped ailerons. In a practical installation the effect of the hinge gap may, of course, be influenced by the internal pressure in the wing.

Effect of surface condition and Reynolds number.- Because the balancing action of the bevel depends on the boundary-layer thickness and profile, it is to be expected that the amount of balance obtained may vary considerably with surface roughness and Reynolds number. Because the boundary-layer thickness near the trailing edge of the airfoil is intimately related to the drag coefficient and because the form of the boundary-layer profile near the trailing edge varies little for thin airfoils at small angles of attack, it is to be expected that the balancing action of the bevel can be related to the drag coefficient of the section. The effects of Reynolds number, position of transition, and surface condition on aileron characteristics may therefore be correlated with their known effects on profile drag.

The effect of changes in profile drag on the aileron characteristics is indicated by the results presented in figure 4. The presence of the roughness strips approximately doubles the drag of the airfoil section in each case. A comparison between the high- and low-drag conditions for the three configurations shows that the slope of the hinge-moment curve is reduced for small deflections and the increment of lift is reduced for almost all aileron deflections by the addition of the roughness strips near the leading edge of the model.

For a conservative design, the control surface should be proportioned so as to avoid overbalance with the highest profile-drag coefficient the wing would be expected to have in service.

Although these results (fig. 4) may be taken as an indication of the effect of drag on a moderately thin airfoil, it is not thought that the results can be safely applied to airfoils of greater thickness. On thicker airfoils the boundary layer at the trailing edge is often considerably nearer the separation point, and the behavior of the aileron under these circumstances may be quite different.

Effect of aileron profile.- The effects of aileron profile on the aileron characteristics are presented in figures 4 and 5.

In figure 4(a) the hinge moment and lift characteristics are given for aileron 1, which had a trailing-edge bevel angle of 27°. In the smooth condition, the

results show that for this moderate bevel angle the hinge-moment and lift characteristics are approximately linear until a down deflection of 25° is reached. For upward deflections near -10°, an abrupt change occurs in the slope of the hinge-moment curve. Although aileron 1 would give the required lateral control at low speeds, the large negative value (-0.0053) of $(\partial c_h/\partial \delta_a)_\alpha$ combined with the characteristic positive value of $(\partial c_h/\partial \alpha)_{\delta_a}$ for beveled-trailing-edge ailerons would result in too large stick forces at high speeds to suit present-day control requirements. The results in figure 4(b), wing smooth, show that aileron 2 with a bevel angle of 30°, an increase of 3° in the bevel angle of aileron 1, would also fail to give the required lateral control at high speed because of the too large negative value (-0.0044) of $(\partial c_h/\partial \delta_a)_\alpha$. The results in figure 4(c), wing smooth, show that aileron 3 with a bevel angle of 33°, an increase of 3° in the bevel angle of aileron 2, combined with a reduction in aileron chord of 0.005c had a value of -0.0020 for $(\partial c_h/\partial \delta_a)_\alpha$ which should be low enough to give the required lateral control at high speeds on a pursuit plane of conventional size.

A comparison of figures 4(a), 4(b), and 4(c) shows that by increasing the bevel angle from 27° to 33° the slope of the hinge-moment curve is progressively reduced at small deflections, resulting in considerable curvature of the hinge-moment curve, while the lift-characteristic curves remain about the same for the three ailerons.

No contour aileron was tested for comparison with the modified aileron; hence, it is not possible to state definitely that the results of these tests show an increase in the range of useful deflection over the usual contour aileron, although low values of the hinge moment appear to be extended to greater deflections than is ordinarily found for conventional shapes.

Figure 5 gives a comparison of drag polars for the modified aileron section and the plain wing section with and without a 0.187c contour aileron. This comparison shows that in the range of test Reynolds number an increase in minimum profile drag $c_{d_{o_{min}}}$ of about

0.0002 resulted from deforming the plain section with a contour aileron to form the modified section and aileron.

Because the results given in figure 6, wing leading edge rough, showed that a 33° bevel angle would just balance out the aileron hinge moments with the model at 0° angle of attack, tests were made to determine the characteristics of aileron 3 with the model, leading edge rough, at other angles of attack. These results (fig. 6) show that, as the angle of attack was increased from 0° to 4.1° and to 8.3°, aileron 3 showed positive hinge-moment slopes in the negative deflection range. It will be noted, however, that the combination of right and left ailerons is not overbalanced.

Langley Memorial Aeronautical Laboratory,
National Advisory Committee for Aeronautics,
Langley Field, Va., April 8, 1944.

REFERENCES

1. White, M. D., and Hoover, Herbert H.: Flight Tests of Modifications to Improve the Aileron Control Characteristics of a North American XP-51 Airplane (A. C. No. 41-38). NACA MR, June 20, 1942.

2. Abbott, Ira H., von Doenhoff, Albert E., and Stivers, Louis S., Jr.: Summary of Airfoil Data. NACA ACR No. L5C05, 1945.

3. Abbott, Frank T., Jr., and Underwood, William J.: Wind-Tunnel Investigation of Profile Drag and Lift of an Intermediate Wing Section of the XP-51 Airplane with Beveled Trailing-Edge and Contour Ailerons. NACA MR, Jan. 27, 1943.

TABLE I

AIRFOIL ORDINATES OF INTERMEDIATE WING SECTION OF XP-51 AIRPLANE

Plain wing section			Modified wing section		
x/c	y_U/c	y_L/c	x/c	y_U/c	y_L/c
0	0	0	0	0	0
.0125	.0184	-.0134	.0125	.0184	-.0134
.025	.0267	-.0181	.025	.0267	-.0181
.05	.0368	-.0249	.05	.0368	-.0249
.075	.0438	-.0304	.075	.0438	-.0304
.10	.0500	-.0349	.10	.0500	-.0349
.15	.0598	-.0412	.15	.0598	-.0412
.20	.0664	-.0464	.20	.0664	-.0464
.25	.0717	-.0506	.25	.0717	-.0506
.30	.0763	-.0546	.30	.0763	-.0546
.35	.0787	-.0550	.35	.0787	-.0550
.40	.0793	-.0552	.40	.0793	-.0552
.45	.0790	-.0545	.45	.0790	-.0545
.50	.0769	-.0530	.50	.0769	-.0530
.60	.0675	-.0447	.60	.0675	-.0447
.70	.0520	-.0319	.70	.0520	-.0319
.80	.0338	-.0168	.80	.0328	-.0173
.805	.0326	-.0163	.85	.0220	-.0080
.8125		-.0156			
.815		-.0154			
.8175		-.0151			
.82		-.0143			
.85	.0228	-.0113			
.90	.0133	-.0066			
.95	.0056	-.0024			
.998	.0011	-.0011			
1.000	0	0			

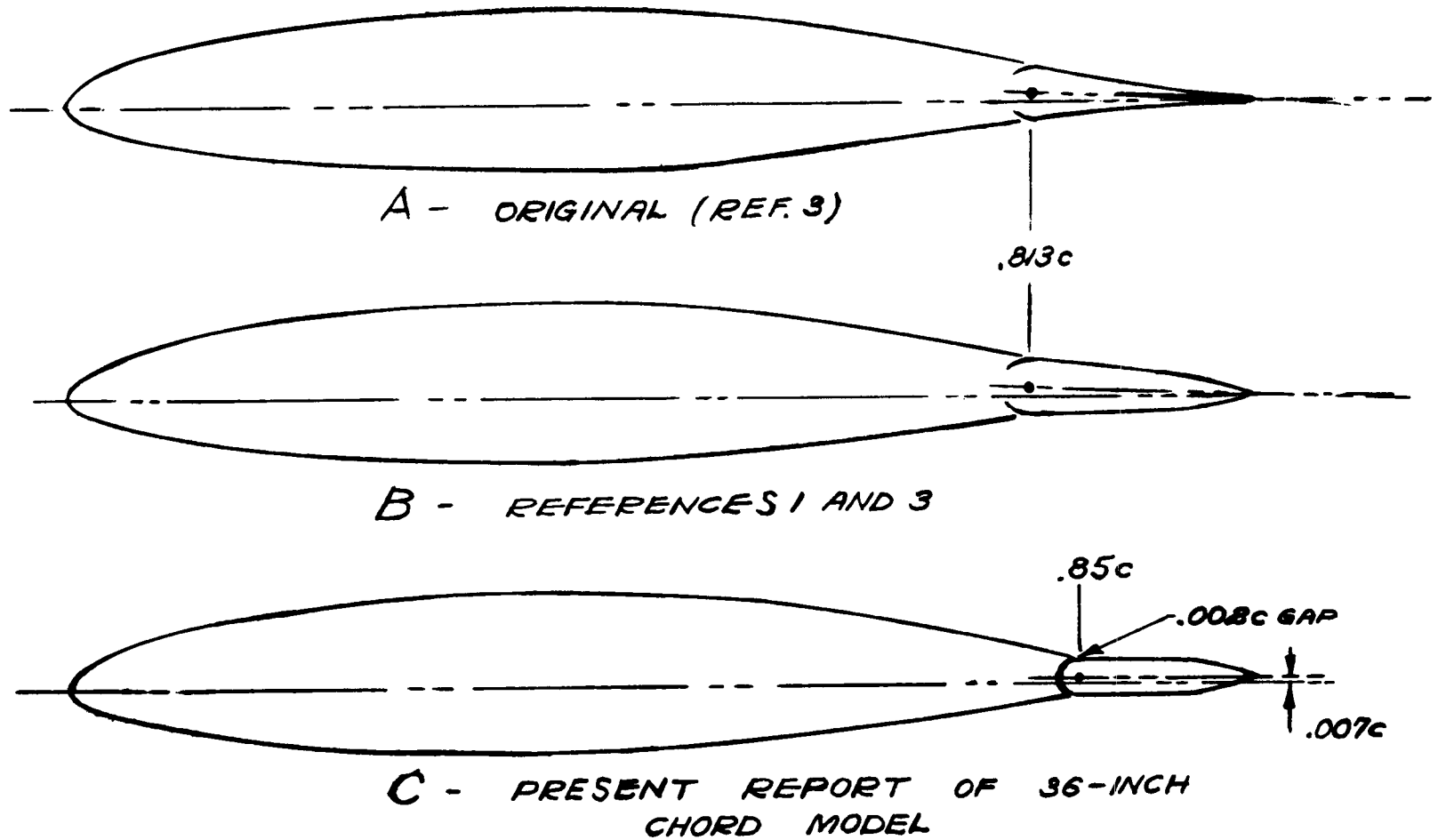

Figure 1.- Comparison of aileron shapes tested for XP-51 airplane. Configuration C is model configuration reported herein.

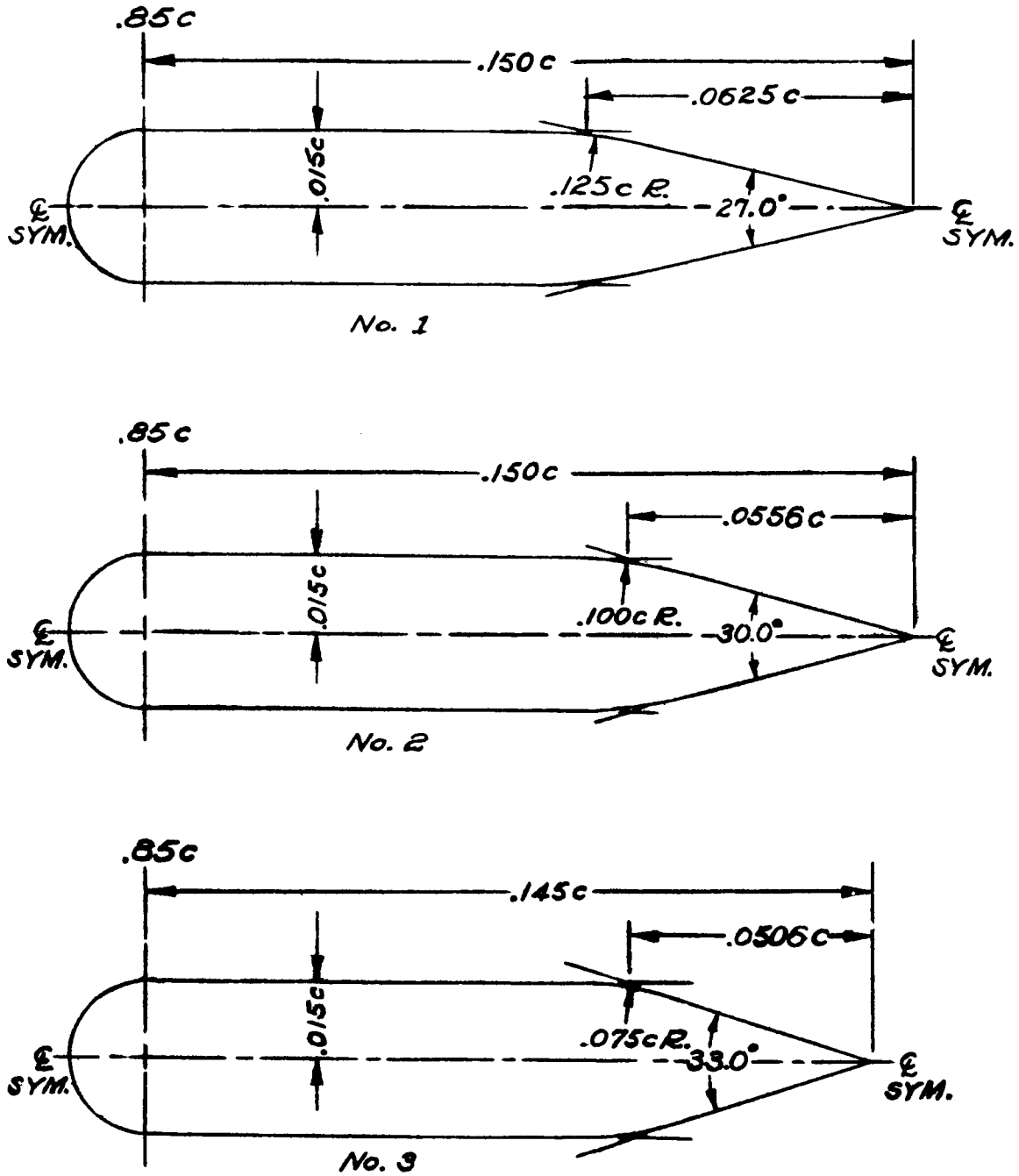

Figure 2.— Aileron shapes tested on 36-inch chord model of XP-51 wing section.

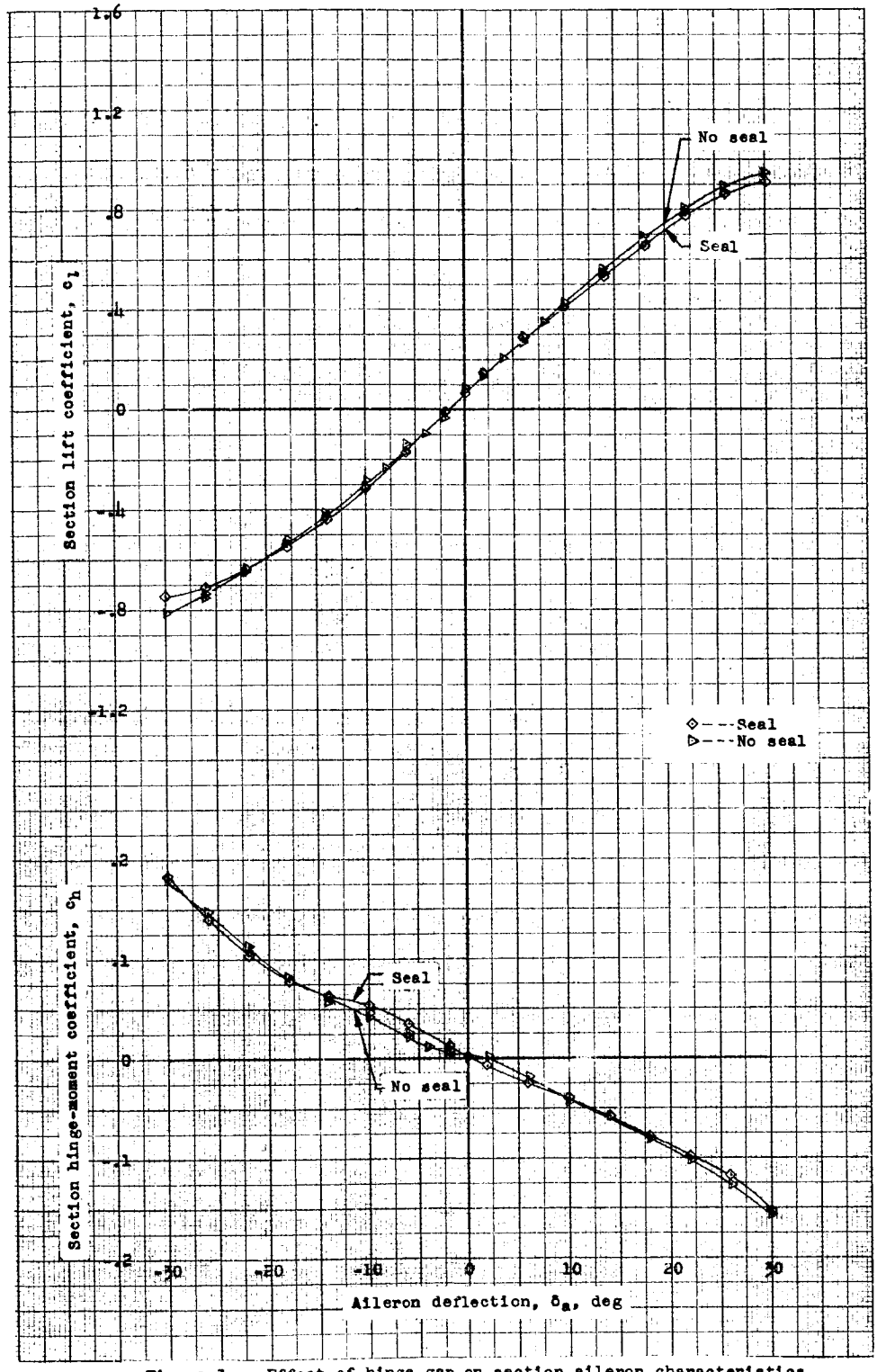

Figure 3.- Effect of hinge gap on section aileron characteristics of aileron 1 on a scale model of the intermediate wing section of the XP-51 airplane. α_o,0°; wing smooth ($c_{d_o} \cong .0045$); R, 4 × 10^6.

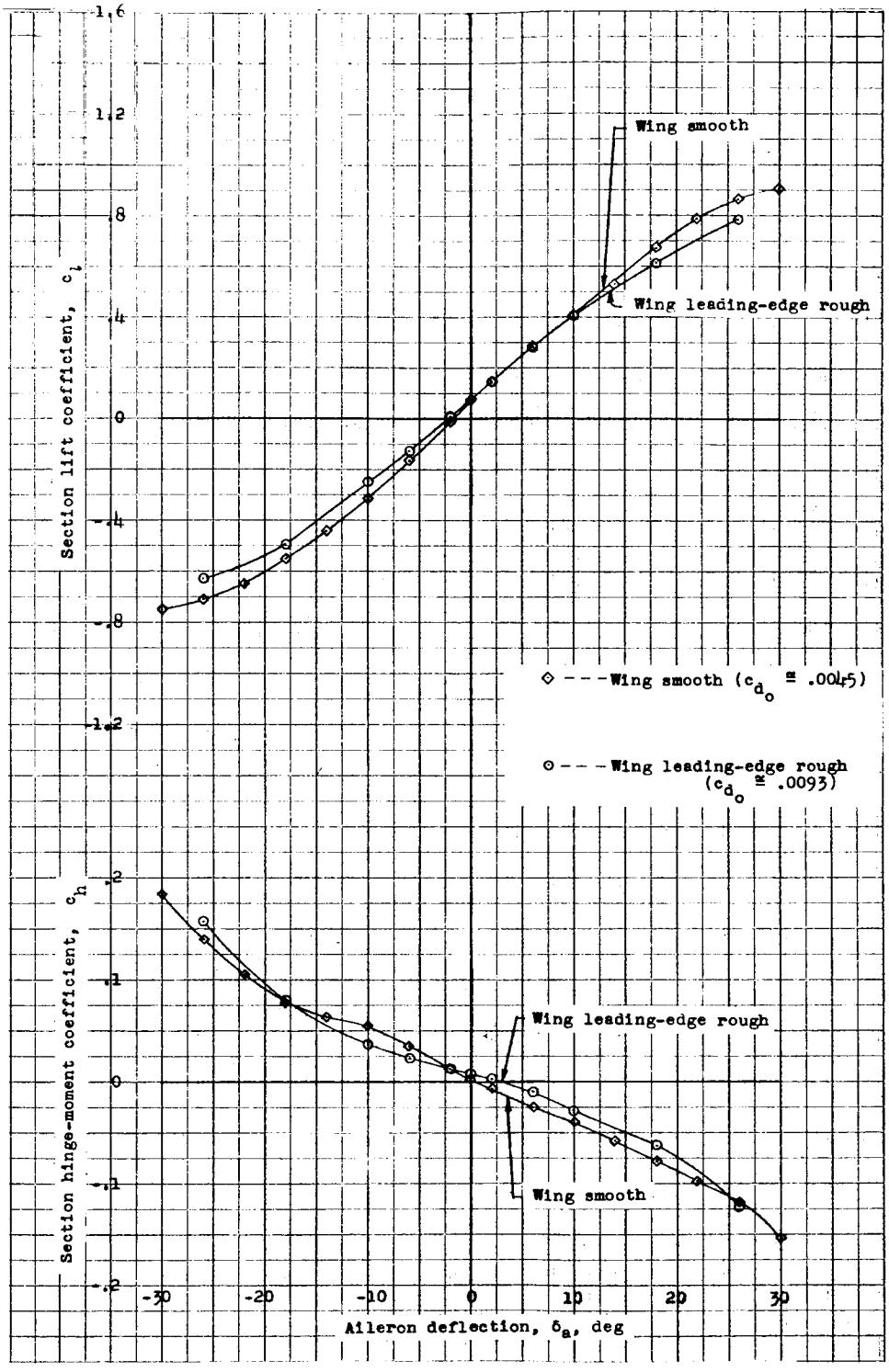

(a) (Aileron 1.

Figure 4.- Effect of wing leading-edge roughness on section aileron characteristics of a modified aileron on a scale model of the intermediate wing section of the XP-51 airplane. α_o, 0°; sealed; R, 4 × 10^6.

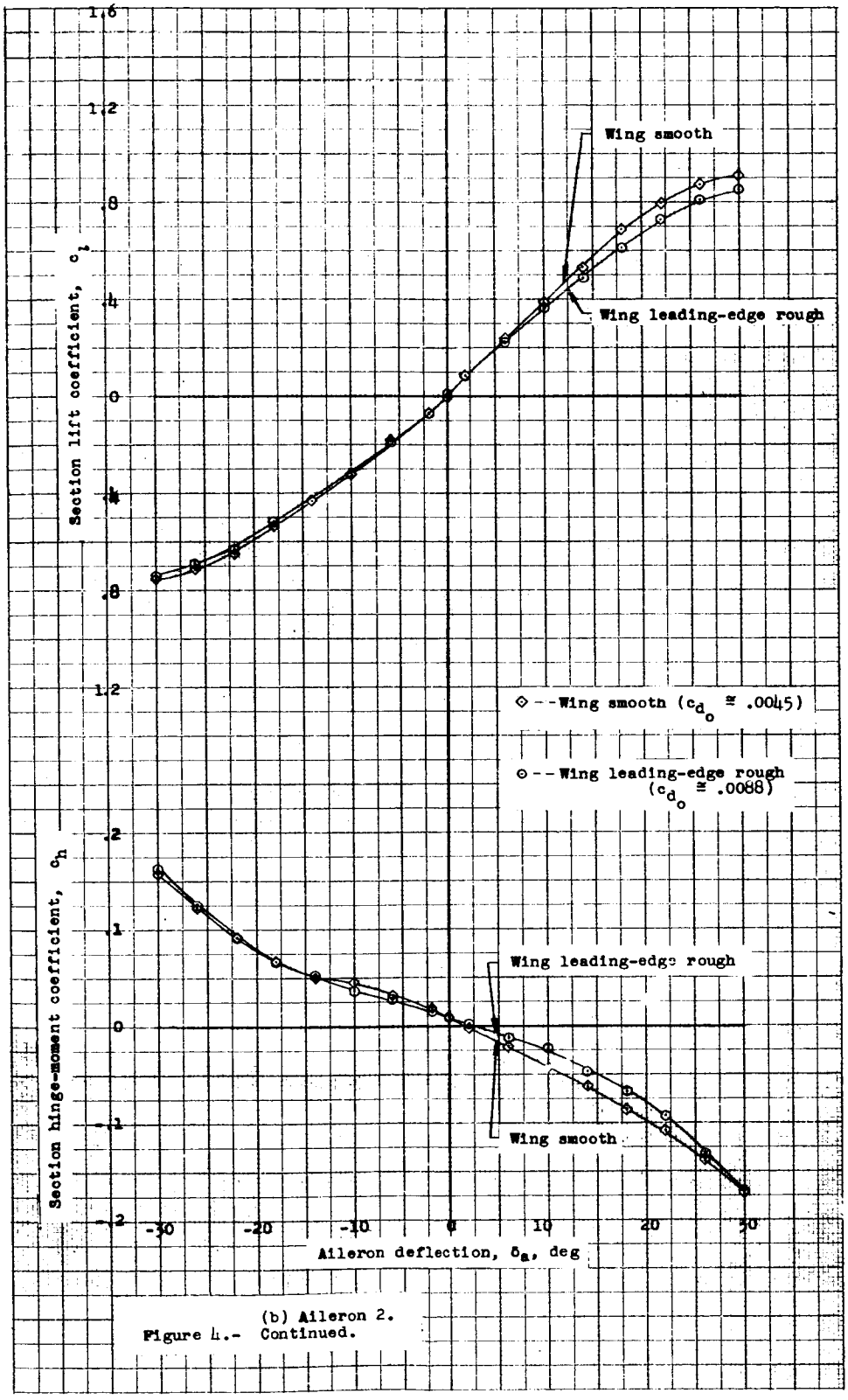

(b) Aileron 2.

Figure 4.- Continued.

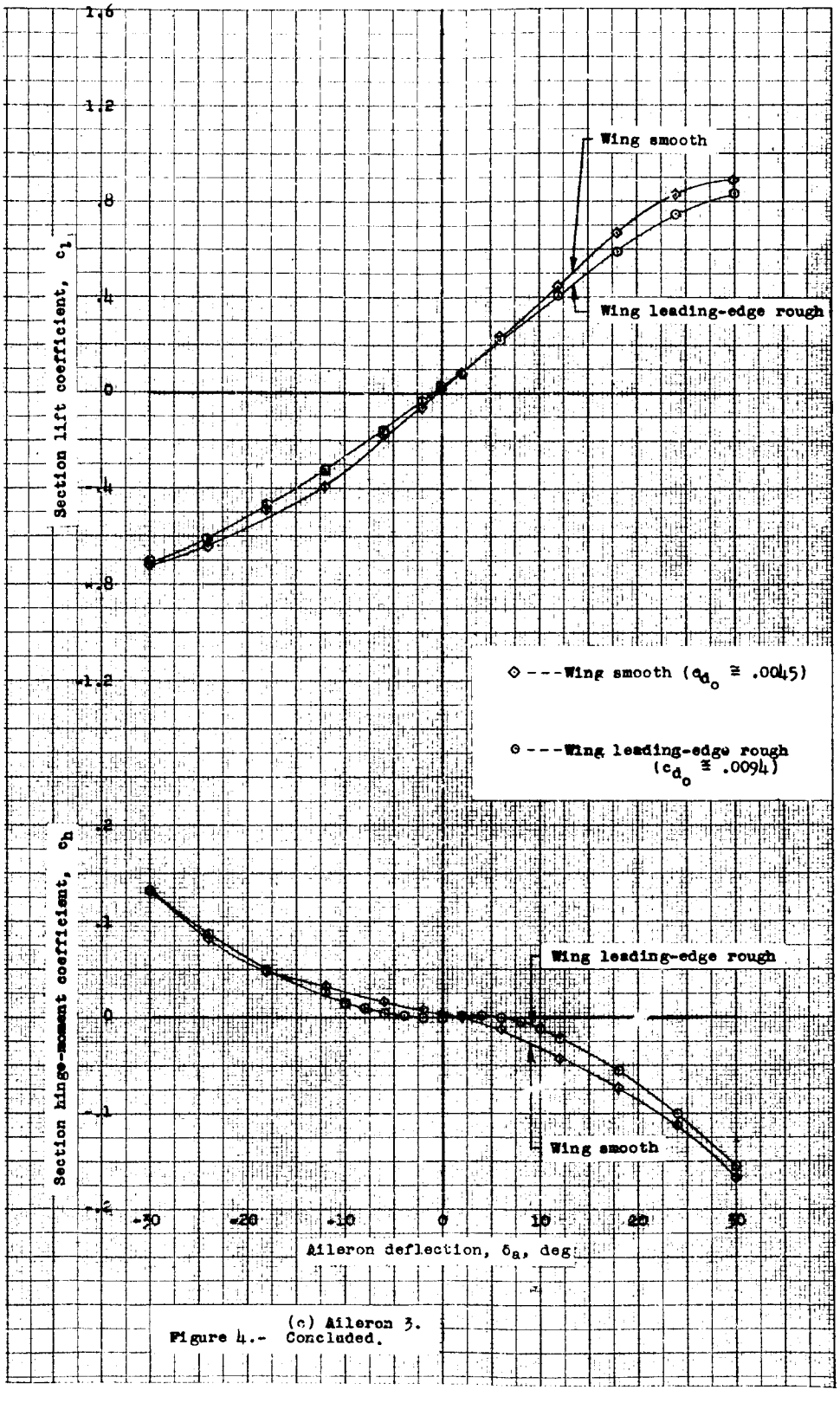

(c) Aileron 3.

Figure 4.- Concluded.

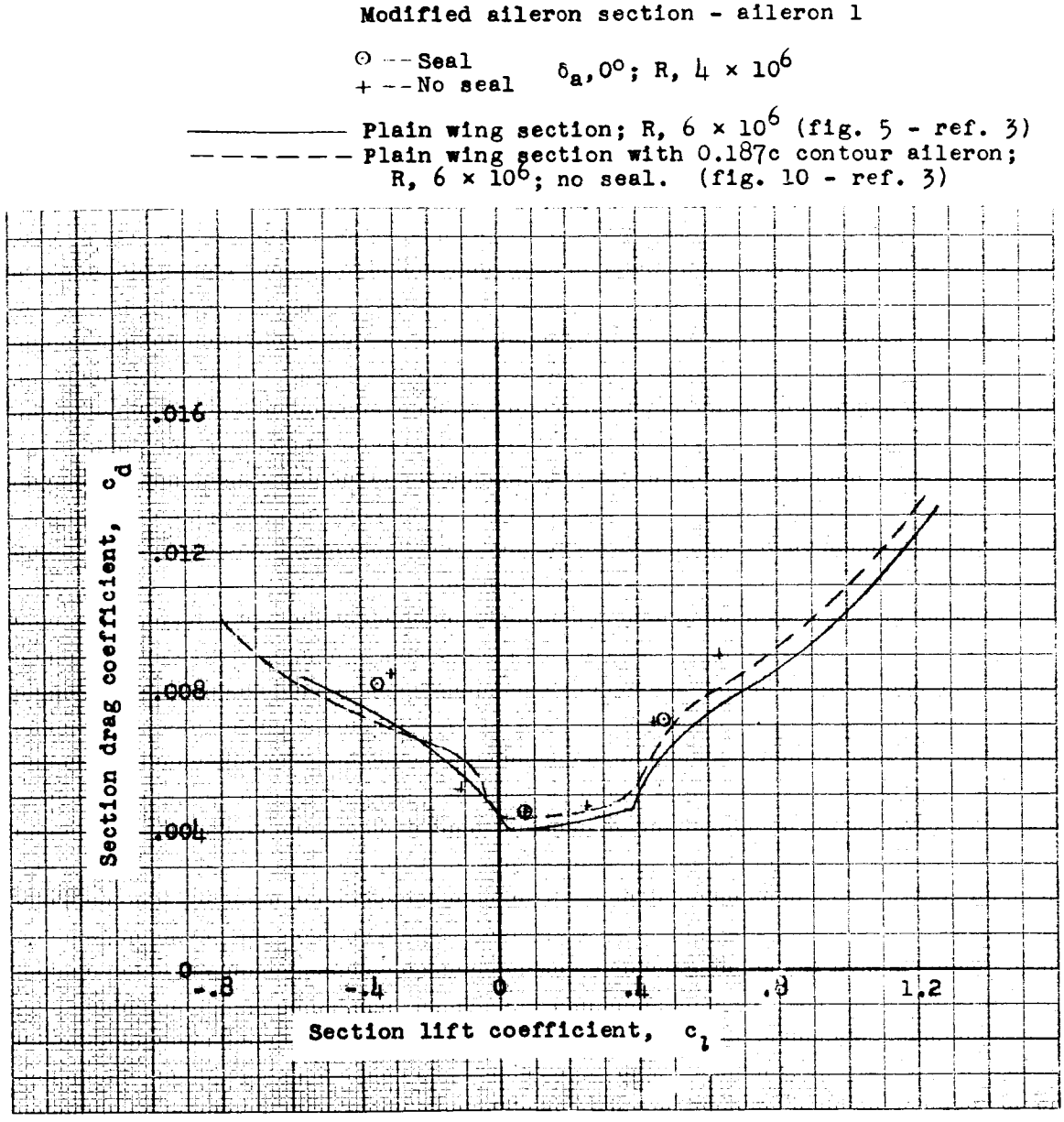

Figure 5.- Comparison of the drag polars of the modified wing section with aileron 1 and the plain wing with and without a contour aileron.

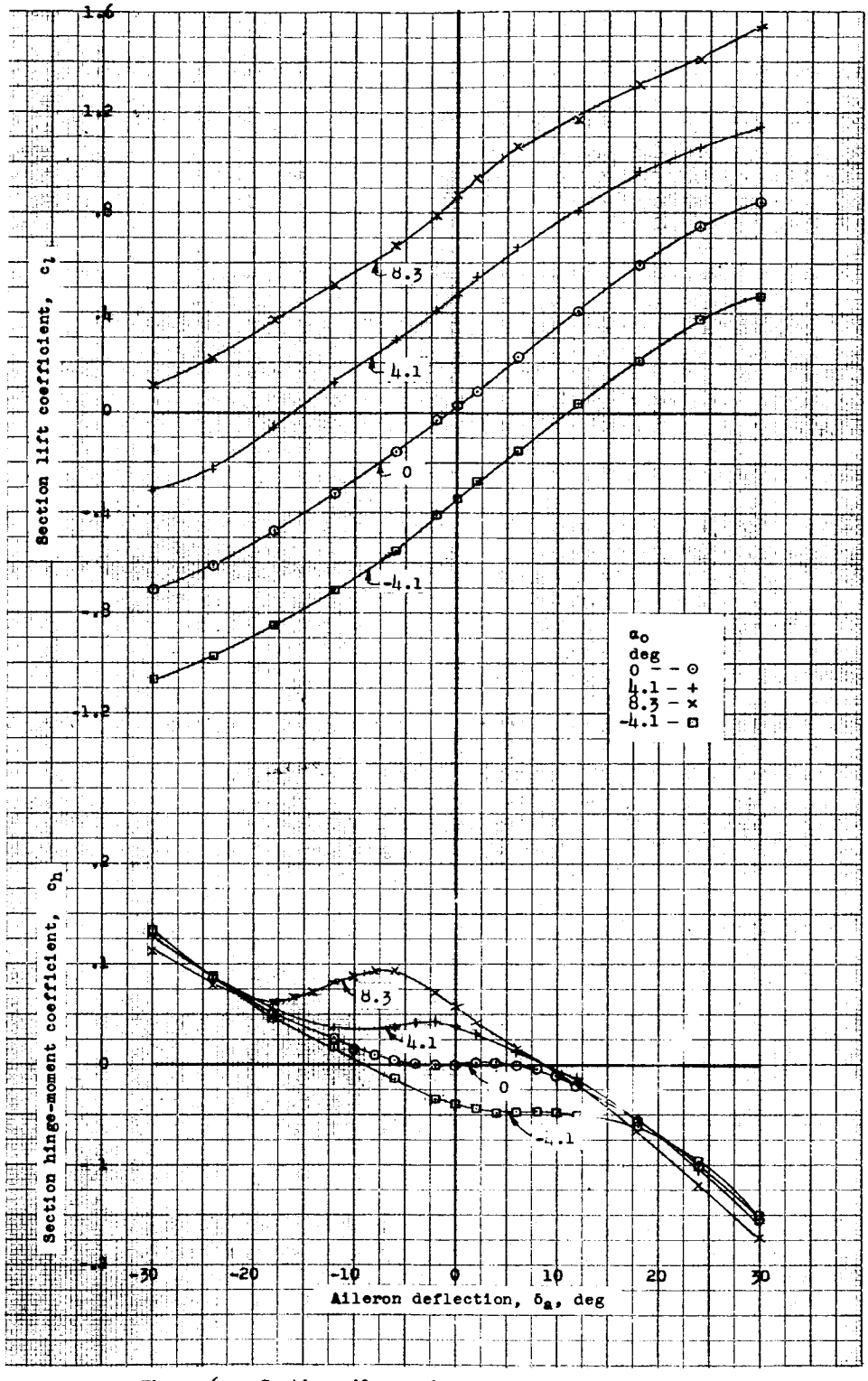

Figure 6.- Section aileron characteristics of aileron 3 on a scale model of the intermediate wing section of the XP-51 airplane. Wing leading-edge rough, sealed; R, 4×10^6.

REPORT NO. 801

A METHOD FOR STUDYING THE HUNTING OSCILLATIONS OF AN AIRPLANE WITH A SIMPLE TYPE OF AUTOMATIC CONTROL

Robert T. Jones

Langley Memorial Aeronautical Laboratory

1944

REPORT No. 801

A METHOD FOR STUDYING THE HUNTING OSCILLATIONS OF AN AIRPLANE WITH A SIMPLE TYPE OF AUTOMATIC CONTROL

By Robert T. Jones

SUMMARY

A method is presented for predicting the amplitude and frequency, under certain simplifying conditions, of the hunting oscillations of an automatically controlled aircraft with lag in the control system or in the response of the aircraft to the controls. If the steering device is actuated by a simple right-left type of signal, the series of alternating fixed-amplitude signals occurring during the hunting may ordinarily be represented by a "square wave." Formulas are given expressing the response to such a variation of signal in terms of the response to a unit signal. A more complex type of hunting, which may involve cyclic repetition of signals of varying duration, has not been treated and requires further analysis. Several examples of application of the method are included and the results discussed.

INTRODUCTION

When an airplane or other aircraft is directed by a simple right-left signal from an automatic steering device, the result is usually a maintained hunting oscillation about the desired path. The amplitude of this oscillation is influenced by the amount of backlash or "dead spot" in the control system and by the damping of the motion of the airplane. In the following analysis the amplitude and frequency of these oscillations is investigated in terms of the response characteristics of the airplane.

ANALYSIS

The analysis is based on consideration of the response of the airplane (in terms of angle of yaw or pitch) to a continued (unit) signal (fig. 1). This response may be calculated by the ordinary theory of dynamical stability and is conveniently represented in operational form (references 1 and 2) as follows:

$$R_1(t)=\overline{R}_1(D)1(t) \tag{1}$$

The unit response ordinarily occurs in the form

$$\overline{R}_1(D)=\frac{f(D)}{F(D)}$$

from which is obtained

$$R_1(t)=C(t)+(C_1e^{\lambda_1 t}+C_2e^{\lambda_2 t}+\ \ldots) \tag{2}$$

where $C(t)$ is the steady-state motion, C_1 and C_2 are the constant coefficients of the Heaviside expansion, and λ_1, λ_2, and so forth, are the nonzero roots of the characteristic equation defining the natural periods of oscillation and the damping of the aircraft without signal. The function $f(D)$ and the particular solution $C(t)$ depend on the time variation of control displacement produced by a signal and on the stability characteristics of the airplane in the degrees of freedom in which the control operates. (See reference 3.) In the case of a continued signal, the usual form of the function $C(t)$ is

$$C(t)=C_{-1}+C_0t$$

where C_0 is the steady rate of turn called for by the signal and C_{-1} is a constant. (See fig. 1.)

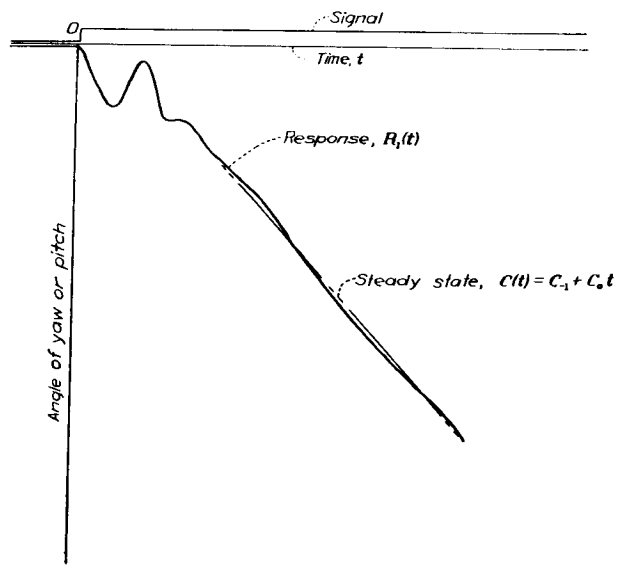

FIGURE 1.—Typical response to continued signal.

During a hunting oscillation, the automatic steering device reverses the signal periodically as the airplane swings through the desired heading. A typical hunting oscillation is shown in figure 2. Here it is assumed that the reversal of signal is delayed either because of a "dead spot" in the steering device or because of backlash in the control mechanism or a combination of the two. As indicated, the oscillation will have a fundamental period $2\pi/\omega$ (where ω is the angular frequency of the hunting oscillation) but may also involve

components of higher frequency, depending on the natural modes of oscillation of the airplane. Ordinarily, the shorter-period components do not have sufficient amplitude to cause a reversal of the signal during a half cycle. In these cases the variation of signal with time will be represented by a simple "square wave," which may be expressed as a function of time by

$$\frac{4}{\pi}\sum_n \frac{1}{n}\sin n\omega t \qquad (n=1, 3, 5, \ldots) \quad (3)$$

or, more conveniently, by the imaginary part of the corresponding exponential series; that is,

$$I.\ P.\ \frac{4}{\pi}\sum_n \frac{1}{n} e^{in\omega t} \quad (4)$$

where $t=0$ is taken to represent a time at which the signal becomes positive.

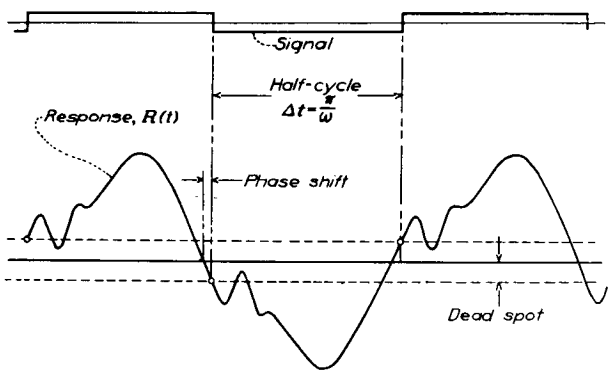

FIGURE 2.—Hunting oscillation with "square" signal.

The response to the alternating signal is obtained by substituting expression (4) for the unit function $1(t)$ in equation (1). Thus,

$$R(t)=I.\ P.\ \overline{R}_1(D)\frac{4}{\pi}\sum_n \frac{1}{n} e^{in\omega} \quad (5)$$

If the airplane is inherently stable, so that transient effects following the start of an oscillation disappear with time, the remaining steady oscillation will be represented by

$$R(t)=I.\ P.\ \frac{4}{\pi}\sum_n \frac{1}{n}\overline{R}_1(in\omega)e^{in\omega t} \quad (6)$$

Equation (6) gives the forced oscillation of the airplane in response to an alternating signal in the form of a square wave of any frequency ω.

By investigating the form of these forced oscillations at various frequencies it will be possible to ascertain whether such oscillations, under the conditions of automatic control, will give rise to the assumed alternating signals of equal duration, and thus to establish certain ranges of ω over which hunting of this type can occur. It will also be possible to establish, in these ranges, a correspondence between the frequency of the hunting oscillation and the magnitude of the dead spot. With the frequency determined, it is possible also to find the amplitude of the oscillation and the maximum deviation of the airplane from its path.

In the simplest cases the required information may be obtained directly from equation (6). In the case of more complex motions, further analysis will be required as follows:

As a first step, separate $\overline{R}_1(in\omega)$ into its real and imaginary parts

$$\overline{R}_1(in\omega)=A(n\omega)+iB(n\omega)$$

The functions A and B may be plotted against $n\omega$ as in figure 3. These functions will show peaks near values of $n\omega$

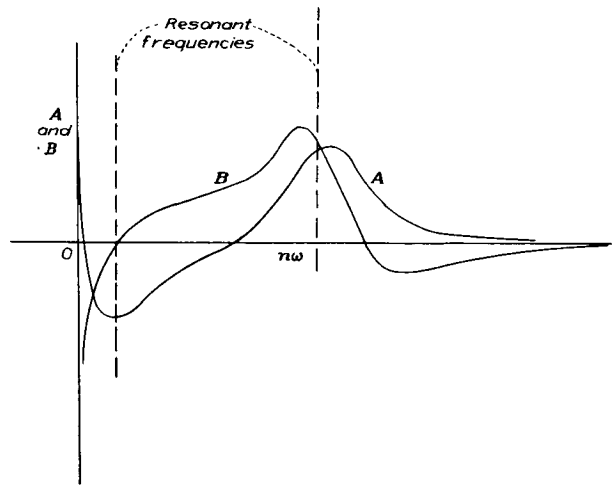

FIGURE 3.—Curves showing in-phase and out-of-phase components of response to periodic signal.

corresponding to the resonant frequencies of the airplane. Then, for any particular hunting frequency ω,

$$R(t)=\frac{4}{\pi}\sum_n \frac{1}{n}[A(n\omega)\sin n\omega t+B(n\omega)\cos n\omega t] \quad (7)$$

At the time of reversal of the signal $\sin n\omega t=0$ and $\cos n\omega t=\pm 1$, the sign depending on whether the signal is becoming positive or negative. The amplitude of the response at this instant is therefore

$$\pm\frac{4}{\pi}\left[B(\omega)+\frac{1}{3}B(3\omega)+\frac{1}{5}B(5\omega)+\ldots\right]$$

This amplitude will also be the amplitude of the dead spot. (See fig. 2.) A plot of

$$R_b(\omega)=\frac{4}{\pi}\sum_n \frac{1}{n}B(n\omega) \qquad (n=1, 3, 5, \ldots)$$

can readily be obtained from the curve of B in figure 3 and will show the periods of the hunting oscillation corresponding to various widths of dead spot.

The slope of the response curve at this same instant is

$$R'_B=\left(\frac{dR}{dt}\right)_B=\frac{4\omega}{\pi}[A(\omega)+A(3\omega)+A(5\omega)+\ldots]$$

If the response to a positive signal is negative (as in fig. 1), in order that the motion represent a possible hunting oscillation (that is, be consistent with the assumed variation of signal), it is necessary that

(I) $$R_B \geqq 0$$

for a positive dead spot, and that

(II) $$R'_B > 0$$

indicating that the airplane crosses the dead spot in the proper direction. A further condition is that no more than one complete crossing of the dead spot occurs within one-half cycle; that is,

(III) $$R(t) > -R_B$$

(See fig. 2.) The value of $R(t)$ in the middle of a half cycle is relatively simple to obtain

$$R_A = \frac{4}{\pi}\left[A(\omega) - \frac{1}{3}A(3\omega) + \frac{1}{5}A(5\omega) - \ldots\right]$$

and may be used as a criterion, though R_A is not necessarily the maximum or minimum value of $R(t)$ (see fig. 4) and condition III may not be satisfied even though $R_A > -R_B$.

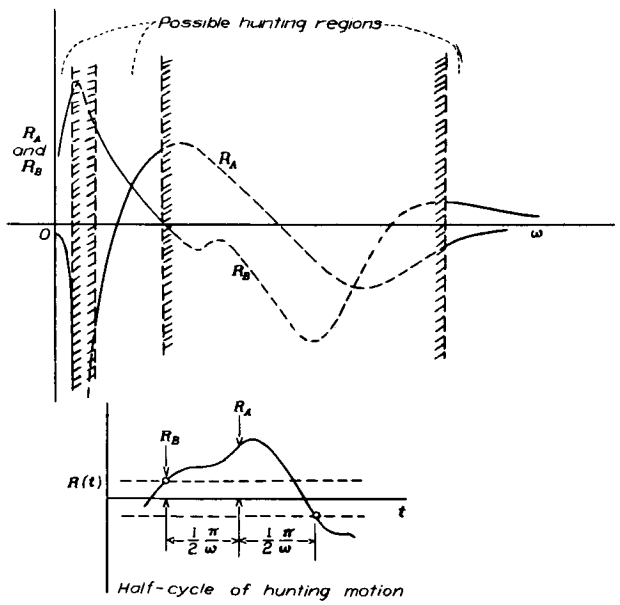

FIGURE 4.—Plot of R_A and R_B against frequency, showing approximate regions in which hunting oscillations are possible and width of dead spot in those regions.

It should be noted that, in the regions excluded by the foregoing conditions, a more complex type of hunting oscillation involving a sequence of signals of different durations may occur. In these regions, the curves of R_A and R_B derived for the square-wave signal no longer apply to the condition of automatic control. These oscillations require analysis beyond that presented in this report.

EXAMPLES

In order to demonstrate and check the procedure described, assume a simple response characteristic in which the airplane immediately starts turning at a constant rate, as directed by the signal. With this response

$$\bar{R}_1(D) = -\frac{C_0}{D}$$

$$\bar{R}_1(n\omega i) = \frac{C_0}{n\omega}\, i$$

and, from equation (7),

$$R(t) = \frac{4}{\pi}\sum_n \frac{C_0}{n^2\omega}\cos n\omega t$$

which is the Fourier series for a "saw-tooth" wave 90° out of phase with the signal. (See fig. 5.) In this case the response occurs without lag and the amplitude of the hunting is exactly equal to the dead spot. The frequency ω is $\pi C_0/2$ divided by the width of the dead spot.

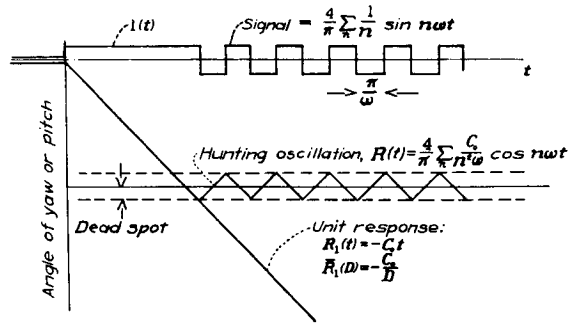

FIGURE 5.—Example in which response is instantaneous.

A simple example nearer the practical case is one in which the signal causes a force F to act on a mass m. In this case the response to a unit signal is

$$\bar{R}_1(D) = -\frac{F}{m}\frac{1}{D^2}$$

and the hunting oscillation is seen to be

$$R(t) = \frac{4}{\pi}\frac{F}{m}\sum_n \frac{1}{n^3\omega^2}\sin n\omega t$$

The expression is recognized as the Fourier series for a succession of parabolic segments (fig. 6). It should be noted that there is no component out of phase with the signal, with the result that R_B is zero for all values of ω. Hence the calculation shows no possibility of hunting with a finite dead spot. In fact, it can be seen from energy considerations that if a dead spot existed the oscillation would be divergent.

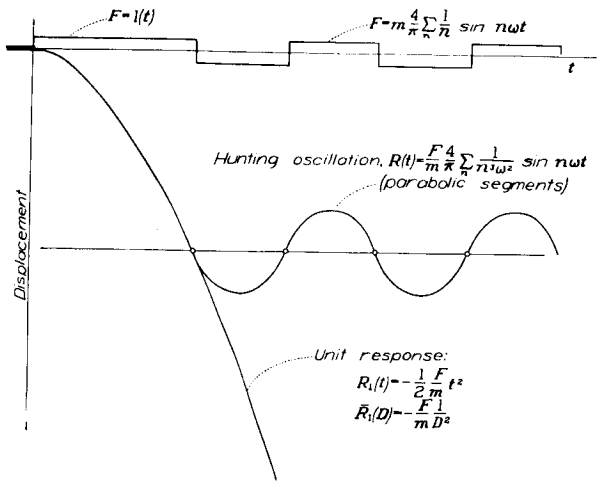

FIGURE 6.—Hunting oscillation of mass acted on by force.

Interesting applications of the method are furnished by cases in which the response to a signal shows a lag, possibly due to backlash in the control mechanism, in addition to a dead spot. A simple example of this kind is illustrated in figure 7. Here the response is similar to that in the first example (fig. 5) except for the time lag τ. Use is made of the well-known lag operator $e^{-\tau D}$. Thus,

$$e^{-\tau D} f(t) = f(t-\tau)$$

Applying this operator to the response in figure 5 gives

$$\bar{F}_1(D) = -e^{-\tau D} \frac{C_0}{D}$$

$$\bar{R}_1(in\omega) = \frac{C_0}{n\omega} (\sin n\omega\tau + i \cos n\omega\tau) = A + iB$$

and, finally (equation (7)),

$$R(t) = \frac{4}{\pi} \sum_n \frac{C_0}{n^2\omega} (\sin n\omega\tau \sin n\omega t + \cos n\omega\tau \cos n\omega t)$$

$$= \frac{4}{\pi} \sum_n \frac{C_0}{n^2\omega} \cos n\omega(t-\tau)$$

With the lagging response, the hunting oscillation is not confined to the amplitude of the dead spot and, in fact, hunting will occur with no dead spot. It is easily seen by

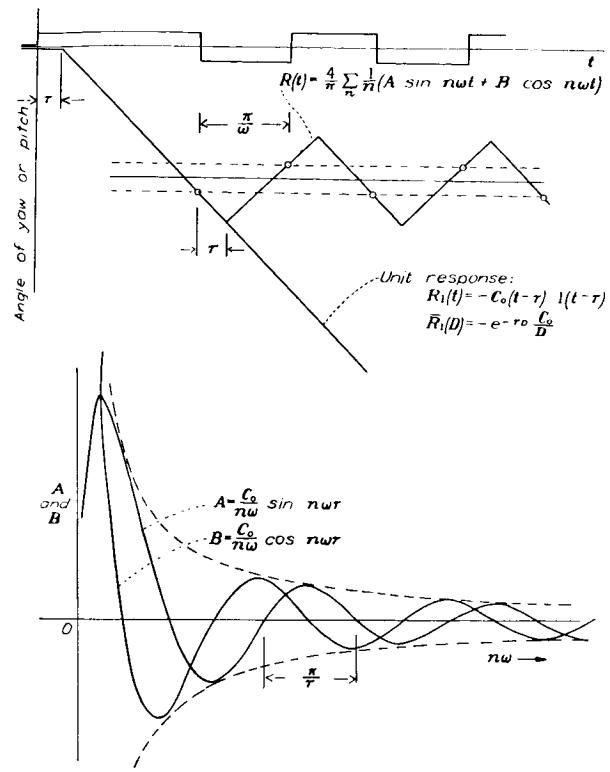

FIGURE 7.—Example in which response shows lag

reference to figure 7 that the half period of the oscillation in this case (no dead spot) is

$$\frac{\pi}{\omega} = 2\tau$$

LANGLEY MEMORIAL AERONAUTICAL LABORATORY,
NATIONAL ADVISORY COMMITTEE FOR AERONAUTICS,
LANGLEY FIELD, VA., *May 5, 1944.*

REFERENCES

1. Jeffreys, Harold: Operational Methods in Mathematical Physics. Cambridge Tracts in Mathematics and Mathematical Physics, No. 23. Second ed., Cambridge Univ. Press, 1931.
2. Jones, Robert T.: A Simplified Application of the Method of Operators to the Calculation of Disturbed Motions of an Airplane. NACA Rep. No. 560, 1936.
3. Jones, Robert T.: Calculation of the Motion of an Airplane under the Influence of Irregular Disturbances. Jour. Aero. Sci., vol. 3, no. 12, Oct. 1936, pp. 419–425.

REPORT NO. 835

PROPERTIES OF LOW-ASPECT-RATIO POINTED WINGS AT SPEEDS BELOW AND ABOVE THE SPEED OF SOUND

Robert T. Jones

Langley Memorial Aeronautical Laboratory

1946

REPORT No. 835

PROPERTIES OF LOW-ASPECT-RATIO POINTED WINGS AT SPEEDS BELOW AND ABOVE THE SPEED OF SOUND

By Robert T. Jones

SUMMARY

Low-aspect-ratio wings having pointed plan forms are treated on the assumption that the flow potentials in planes at right angles to the long axis of the airfoils are similar to the corresponding two-dimensional potentials. For the limiting case of small angles of attack and low aspect ratios the theory brings out the following significant properties:

(1) The lift of a slender pointed airfoil moving in the direction of its long axis depends on the increase in width of the sections in a downstream direction. Sections behind the section of maximum width develop no lift.

(2) The spanwise loading of such an airfoil is independent of the plan form and approaches the distribution giving a minimum induced drag.

(3) The lift distribution of a pointed airfoil traveling pointforemost is relatively unaffected by the compressibility of the air below or above the speed of sound.

A test of a triangular airfoil at a Mach number of 1.75 verified the theoretical values of lift and center of pressure.

INTRODUCTION

The assumption of small disturbances in a two-dimensional potential flow leads to the well-known thin-airfoil theory of Munk (reference 1) and the Prandtl-Glauert rule (references 2 and 3) at speeds less than sonic. At speeds above the speed of sound, application of the same assumptions leads to the Ackeret theory (reference 4) according to which the wing sections generate plane sound waves of small amplitude. As is well known, the Ackeret theory predicts a radical change in the properties of such wings on transition to supersonic velocities and these changes have been verified by experiments in supersonic wind tunnels (reference 5).

Both the Ackeret theory and the Munk theory apply to the case of a wing having a large span and a small chord. The present discussion is based on assumptions similar to those used by Ackeret and Munk but covers the opposite extreme, namely, the wing of small span and large chord. In the latter case the flow is expected to be two dimensional when viewed in planes perpendicular to the direction of motion.

A theory for the rectangular wing of small aspect ratio has been given by Bollay (reference 6). Bollay assumes a separated, or discontinuous, potential flow similar to the well-known Kirchoff flow and shows that under these circumstances the lift is proportional to the square of the angle of attack. Bollay does not consider the effect of compressibility. The present treatment covers other plan forms and, although based on different assumptions, is not inconsistent with Bollay's theory in the limiting case of small angles of attack.

By limiting the plan forms to small vertex angles, the properties of the wings in compressible flow at high subsonic and at supersonic speeds are also covered. Tsien (reference 7) has pointed out that Munk's airship theory (reference 8) applies to a slender body of revolution at speeds greater than sonic. The lift and moment of such a body are not expected to change appreciably with Mach number. The present paper gives an analysis of the low-aspect-ratio airfoil based on similar assumptions and shows that little change of the lift distribution of an airfoil of pointed plan form lying near the center of the Mach cone is to be expected.

SYMBOLS

V	flight velocity
α	angle of attack
S	wing area
A	aspect ratio $\left(\frac{b_{max}^2}{S}\right)$
x	distance along axis of symmetry of pointed airfoil, measured downstream from nose
y	spanwise distance, measured from axis of symmetry
z	vertical distance from plane of wing
t	time
m'	additional apparent mass (spanwise section)
b	local span
c	chord
ρ	density of air
q	dynamic pressure $\left(\frac{1}{2}\rho V^2\right)$
l	local lift force (per length dx)
c_l	local lift coefficient $\left(\frac{l}{qb\,dx}\right)$
D_i	induced drag
C_{D_i}	induced-drag coefficient $\left(\frac{D_i}{qS}\right)$
L	total lift
C_L	lift coefficient $\left(\frac{L}{qS}\right)$
ϕ	surface potential
θ	spanwise-location parameter $\left(\cos^{-1}\frac{y}{b/2}\right)$
Δp	local pressure difference
M	Mach number, ratio of flight velocity to speed of sound
$x_{c.p.}$	distance of center of pressure from nose of airfoil
C_m	pitching-moment coefficient $\left(\frac{\text{Pitching moment}}{qSc_{max}}\right)$
L_M	lift at Mach number M
L_0	lift at zero Mach number
max	maximum (used as subscript)

788875—49

THEORY FOR WINGS OF LOW ASPECT RATIO

The flow about an airfoil of very low aspect ratio may be considered two dimensional when viewed in cross sections perpendicular to the longitudinal axis. With this idealization, the treatment of the low-aspect-ratio airfoil becomes exceedingly simple; formulas are obtained that are similar in some respects to those derived by Munk (reference 8) and Tsien (reference 7) for an elongated body of revolution.

Perhaps the simplest case from the analytical point of view is that of the long, flat, triangular airfoil traveling point-foremost at a small angle of attack. Viewed from a reference system at rest in the undisturbed fluid, the flow pattern in a plane cutting the airfoil at a distance x from the nose is the familiar two-dimensional flow caused by a flat plate having the normal velocity $V\alpha$. (See fig. 1.) Observed in this plane, the width of the plate and hence the scale of the flow pattern continually increase as the airfoil progresses through the plane. This increase in the scale of the flow pattern requires a local lift force l equal to the downward velocity $V\alpha$ times the local rate of increase of the additional apparent mass m', or

$$l=V\alpha\frac{dm'}{dt}$$

$$=V^2\alpha\frac{dm'}{dx}$$

since

$$V=\frac{dx}{dt}$$

By a well-known formula from two-dimensional-flow theory,

$$m'=\pi\frac{b^2}{4}\rho\,dx$$

where b is the local width of the plate. Hence

$$\frac{dm'}{dx}=\pi\frac{b}{2}\rho\,dx\frac{db}{dx}$$

and the lift l per length dx will be given by the expression

$$l=\pi\alpha\frac{\rho}{2}V^2b\frac{db}{dx}dx$$

Dividing by $\frac{\rho}{2}V^2$ and by the area $b\,dx$ gives the local lift coefficient

$$c_l=\pi\alpha\frac{db}{dx} \tag{1}$$

When this flow is considered in more detail, it is found from the two-dimensional theory that the surface potential ϕ is distributed spanwise according to the ordinates of an ellipse, that is,

$$\phi=\pm V\alpha\sqrt{\left(\frac{b}{2}\right)^2-y^2}$$

$$=\pm V\alpha\frac{b}{2}\sin\theta \tag{2}$$

where $\cos\theta=\frac{y}{b/2}$ and the sign changes in going from the upper to the lower surface of the airfoil. (See fig. 2.) An instant later, in the same plane, the ordinates are those of a slightly larger ellipse, corresponding to an increase of ϕ. The local pressure difference is given by the local rate of increase of ϕ, that is,

$$\Delta p=2\rho\frac{\partial\phi}{\partial t}$$

$$=2\rho V\frac{\partial\phi}{\partial x}$$

$$=2\rho V\frac{\partial\phi}{\partial b}\frac{db}{dx} \tag{3}$$

where $\partial\phi/\partial b$ is a function of y. Differentiation of ϕ yields the equation

$$\Delta p=2\rho V^2\frac{b}{\sqrt{\left(\frac{b}{2}\right)^2-y^2}}\frac{db}{dx}\frac{\alpha}{4}$$

or

$$\frac{\Delta p}{q}=\frac{2\alpha}{\sin\theta}\frac{db}{dx} \tag{4}$$

The pressure distribution thus shows an infinite peak along the sloping sides of the airfoil similar to the pressure peak at the leading edge of a conventional airfoil. The distribution along radial lines passing through the vertex of the triangle $\left(\text{lines of constant }\frac{y}{b/2}\right)$ is uniform (fig. 3), however, and the center of pressure coincides with the center of area.

Equations (1) and (4) show that the development of lift by the long slender airfoil depends on an expansion of the sections in a downstream direction; hence a part of the surface having parallel sides would develop no lift. Furthermore, a decreasing width would, according to equation (4), require negative lift with infinite negative pressure peaks along the edges of the narrower sections. In the actual flow, however, the edge behind the maximum cross section will lie in the viscous or turbulent wake formed over the surface ahead; and for this reason it will be assumed that the infinite pressure difference indicated by equation (3) cannot be developed across these edges. It is this assumption, corresponding to the Kutta condition, which gives the plate the properties of an airfoil as distinct from another type of body, such as a body of revolution.

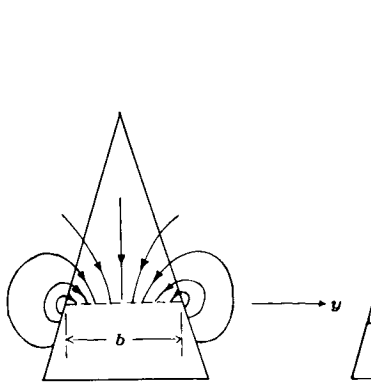

FIGURE 1.—Flow pattern.

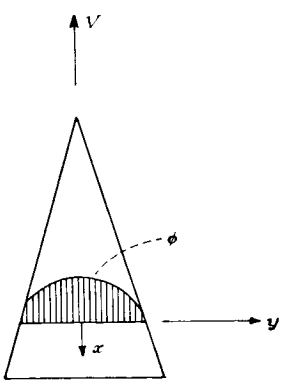

FIGURE 2.—Potential.

With the aid of the Kutta condition, it may easily be shown that sections of the airfoil behind the section of greatest width develop no lift. A potential flow satisfying both the boundary condition and the Kutta condition may be obtained by the introduction of a free surface of discontinuity behind the widest section. This surface of discontinuity (fig. 4) would be composed of parallel vortices extending downstream from the widest section of the airfoil as prolongations of the vortices representing the discontinuity of potential over the forward part of the airfoil. This sheet, although possibly wider than the downstream sections of the airfoil, still satisfies their boundary condition, since the lateral arrangement of the vortices is such as to give uniform downward velocity equal to $V\alpha$ over the entire width of the sheet including the rearward portion of the airfoil. Since the pressure difference across the airfoil is proportional to $\partial\phi/\partial x$ and since this gradient disappears as soon as the vortices become parallel to the stream, no lift is developed on the rearward sections.

Integration of the pressures in a chordwise direction from the leading edge downstream to the widest section will give the span load distribution and the induced drag. The span load distribution is

$$\frac{\partial L}{\partial y}=\int \Delta p\, dx$$

or, from equation (3),

$$\frac{\partial L}{\partial y}=2\rho V\phi$$

From equation (2),

$$\phi=V\alpha\frac{b_{max}}{2}\sin\theta$$

Hence $\partial L/\partial y$ is elliptical and independent of the plan form. With the elliptical span load the induced drag is a minimum and is equal to

$$D_i=\frac{L^2}{\pi q b_{max}^2} \tag{5}$$

A second integration of $\frac{\partial L}{\partial y}dy$ across the widest section gives the total lift, which is

$$L=\frac{\pi}{4}\rho V^2\alpha b_{max}^2 \tag{6}$$

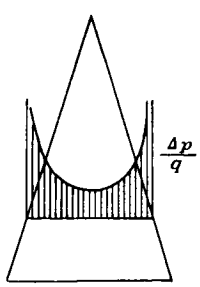

FIGURE 3.—Pressure distribution.

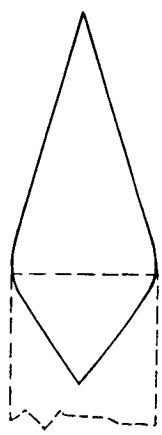

FIGURE 4.—Wake.

The lift of the slender airfoil therefore depends only on the width and not on the area. If the lift is divided by $\frac{1}{2}\rho V^2 S$ and if the aspect ratio A is considered to be $\frac{b_{max}^2}{S}$, then

$$C_L=\frac{\pi}{2}A\alpha \tag{7}$$

and the induced-drag coefficient is

$$C_{D_i}=\frac{C_L^2}{\pi A}$$

$$=C_{L_2}^{\alpha} \tag{8}$$

From equation (8) it appears that the resultant force lies halfway between the normal to the surface and the normal to the air stream.

It is seen that in the case of a rectangular plan form the simplified formula (equation (4)) gives an infinite concentration of lift at the leading edge and no lift elsewhere, whereas a more accurate theory would show some distribution of the lift rearward. If the rate of increase of the width becomes too great, the flow cannot be expected to remain two dimensional. It can be shown by examination of the known three-dimensional (nonlifting) potential flow around an elliptic disk (reference 9), however, that the two-dimensional theory gives a good approximation in the case of an elliptical leading edge, which indicates that the theory

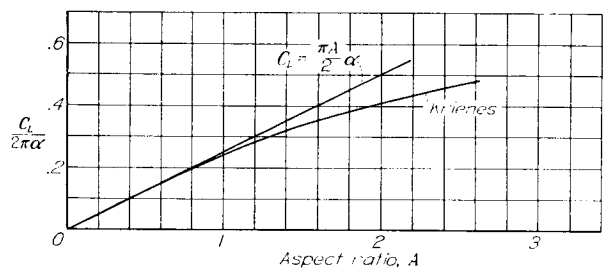

FIGURE 5.—Comparison of lift calculated by present theory for elliptical wings of low aspect ratio with results of Krienes (reference 10).

is applicable over a large range of nose shapes. In figure 5 is shown a comparison of the lift calculated by the present theory for elliptical wings of low aspect ratio with the results of the more accurate three-dimensional potential-flow calculations of Krienes (reference 10). The results are in good agreement up to aspect ratios approaching 1. Application of equation (4) gives a center of pressure on the elliptical plan form at one-sixth of the chord. Figure 6 also shows this value compared with values given by Krienes' theory. In this respect it appears that the agreement is not so good as for the lift.

EFFECT OF COMPRESSIBILITY

In order to show the effect of compressibility, use will be made of the theory of potential flow with small disturbances. Glauert (reference 2) and Prandtl (reference 3) have demonstrated that, at subsonic speeds, a distribution of potential satisfying Laplace's equation will satisfy the linearized compressible-flow equation if the distribution $\phi(x, y, z)$ is

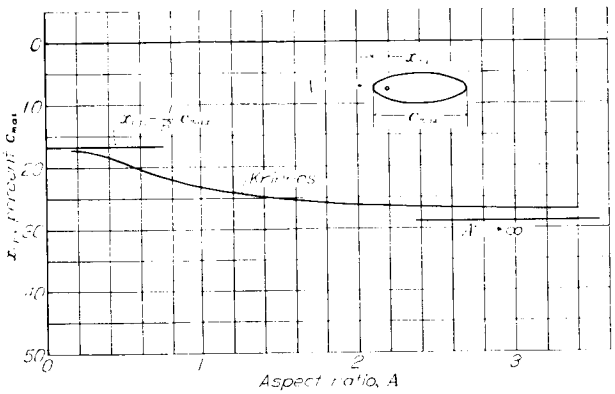

FIGURE 6.—Comparison of center of pressure calculated by present theory for elliptical wings of low aspect ratio with results of Krienes (reference 10).

foreshortened along the direction of motion by the transformation

$$x'=\frac{x}{\sqrt{1-M^2}} \qquad y'=y \qquad z'=z$$

This fact may be applied in a calculation procedure by starting with a fictitious airfoil longer in the x-direction than the true one and calculating the potential distribution for this airfoil by methods of incompressible flow. The correct dimensions and correct distribution of ϕ are then obtained when the transformation is applied.

For the long slender airfoil, the potential distribution at each section is similar to that for an infinitely long body; therefore $\partial\phi/\partial x$ and hence the local pressures vary in inverse proportion to the length. The foregoing calculation procedure gives a null result in this case, since the pressures calculated for the fictitious airfoil at $M=0$ will be reduced in the same ratio that the length is increased and the Lorentz transformation to restore the correct length will also restore the same pressures as those obtained at $M=0$. Since $\partial\phi/\partial z$ is unchanged by the transformation, the normal velocity component and hence the angle of attack are unchanged also. These results can be obtained by referring directly to the linearized equation for the potential

$$(1-M^2)\frac{\partial^2\phi}{\partial x^2}+\frac{\partial^2\phi}{\partial y^2}+\frac{\partial^2\phi}{\partial z^2}=0 \qquad (9)$$

(See reference 3.) If the airfoil is sufficiently slender, $\partial^2\phi/\partial x^2$ can be neglected in comparison with $\partial\phi/\partial x$ except near the edge. Since the lift is proportional to $\partial\phi/\partial x$, the increase of the lift with Mach number can therefore be neglected in comparison with the lift.

It is important to note that the theory of small disturbances is not limited to subsonic velocities and that, so long as the term $(1-M^2)\frac{\partial^2\phi}{\partial x^2}$ in equation (9) remains small, the solution in the region of the wing will continue to be given by the potential (equation (2)). Evidently the Mach number cannot be increased indefinitely, for then the coefficient of $\partial^2\phi/\partial x^2$ will become so large that the first term will no longer be negligible. The required condition will be satisfied, however, by adopting a pointed plan form with the vertex angle so small that the entire surface lies near the center of the Mach cone (fig. 7). The condition of a small vertex angle is also necessary in order that the potential distribution of equation (2) may apply. In the case of a wing with a blunt-leading-edge plan form, abrupt changes in the flow arise on transition to supersonic velocities, and potential flow of the subsonic type no longer exists.

The lift and lift distribution for rectangular surfaces at supersonic speeds have been calculated by Schlichting (reference 11). Figure 7 shows the variation of lift-curve slope with Mach number as obtained from Schlichting's results for rectangular wings of two different aspect ratios and for the range of speeds in which the two Mach cones from the tips do not reach the center of the wing. In the subsonic range, values given by the Prandtl-Glauert rule are shown. These curves are compared with the values indicated by the present theory for a triangular wing lying near the center of the Mach cone. Figure 8 shows the travel of the center of pressure for these plan forms. It is to be noted that, with the blunt-leading-edge plan forms, the center of pressure travels from a point near the quarter chord to a point near the mid-chord when the velocity is increased above the speed of sound.

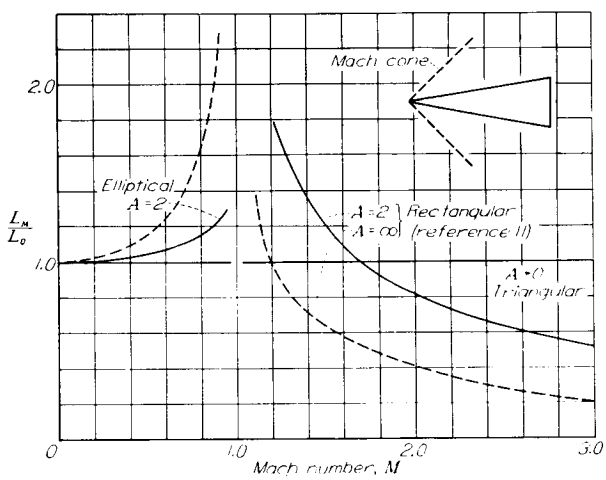

FIGURE 7.—Variation of lift with Mach number for different plan forms.

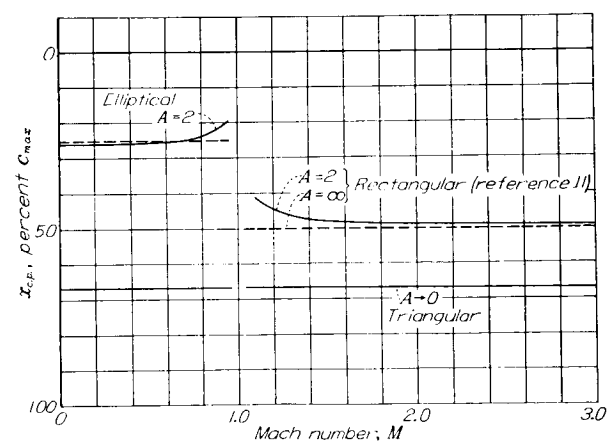

FIGURE 8.—Travel of center of pressure with Mach number for different plan forms.

TESTS OF A TRIANGULAR AIRFOIL AT SUPERSONIC SPEED

As a test of the foregoing analysis, a small triangular airfoil in the form of a steel plate with rounded leading edges was constructed and tested in the Langley model supersonic tunnel. The tests were made at a Mach number of 1.75. Figure 9 shows the details of the model and figure 10 summarizes the results of the test. At zero angle of attack a small lift and a small pitching moment occur, which are presumably the result of the camber given the airfoil by rounding off the leading edges in the manner shown by section A–A in figure 9. In general, the results are in good agreement with the theory if an allowance is made for this camber, as shown in figure 10.

CONCLUSIONS

1. The lift of a slender, pointed airfoil moving in the direction of its long axis depends on the increase in width of the sections in a downstream direction. Sections behind the section of maximum width develop no lift.

2. The spanwise loading of such an airfoil is independent of the plan form and approaches the distribution giving a minimum induced drag.

3. The lift distribution of a pointed airfoil traveling pointforemost is relatively unaffected by the compressibility of the air below or above the speed of sound.

LANGLEY MEMORIAL AERONAUTICAL LABORATORY,
NATIONAL ADVISORY COMMITTEE FOR AERONAUTICS,
LANGLEY FIELD, VA., *May 11, 1945.*

REFERENCES

1. Munk, Max M.: Elements of the Wing Section Theory and of the Wing Theory. NACA Rep. No. 191, 1924.
2. Glauert, H.: The Effect of Compressibility on the Lift of an Aerofoil. R. & M. No. 1135, British A. R. C., 1927.
3. Prandtl, L.: General Considerations on the Flow of Compressible Fluids. NACA TM No. 805, 1936.
4. Ackeret, J.: Air Forces on Airfoils Moving Faster Than Sound. NACA TM No. 317, 1925.
5. Taylor, G. I.: Applications to Aeronautics of Ackeret's Theory of Aerofoils Moving at Speeds Greater Than That of Sound. R. & M. No. 1467, British A. R. C., 1932.
6. Bollay, William: A Theory for Rectangular Wings of Small Aspect Ratio. Jour. Aero. Sci., vol. 4, no. 7, May 1937, pp. 294–296.
7. Tsien, Hsue-Shen: Supersonic Flow over an Inclined Body of Revolution. Jour. Aero. Sci., vol. 5, no. 12, Oct. 1938, pp. 480–483.
8. Munk, Max M.: The Aerodynamic Forces on Airship Hulls. NACA Rep. No. 184, 1924.
9. Lamb, Horace: Hydrodynamics. Sixth ed., Cambridge Univ. Press, 1932, pp. 146–153.
10. Krienes, Klaus: The Elliptic Wing Based on the Potential Theory. NACA TM No. 971, 1941.
11. Schlichting, H.: Airfoil Theory at Supersonic Speed. NACA TM No. 897, 1939.

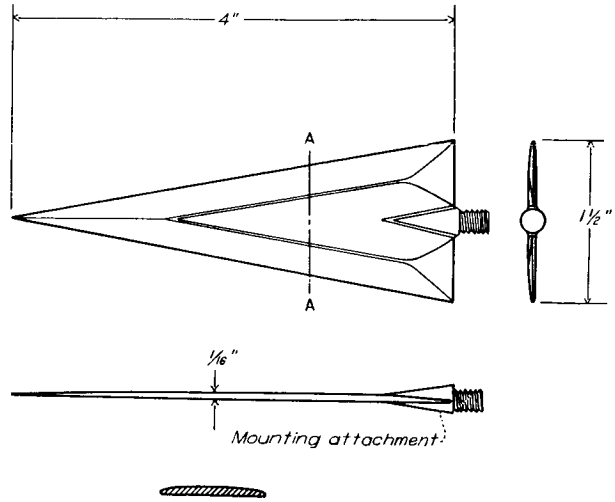

FIGURE 9.—Airfoil tested in Langley model supersonic tunnel.

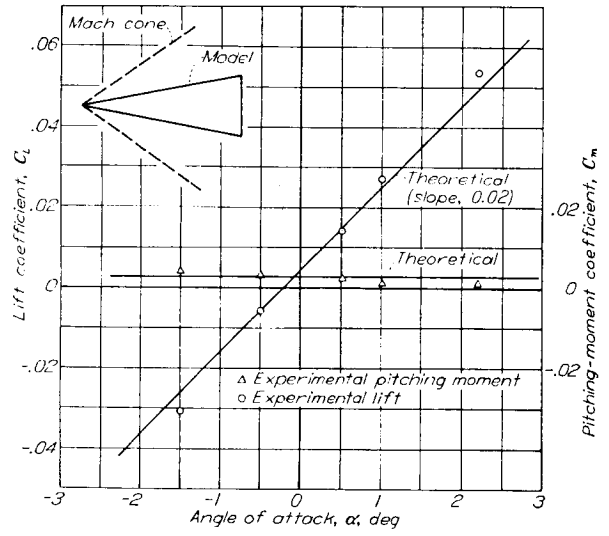

FIGURE 10.—Test of triangular airfoil in Langley model supersonic tunnel. Mach number, 1.75; Reynolds number, 1,600,000.

REPORT NO. 863

WING PLAN FORMS FOR HIGH-SPEED FLIGHT

Robert T. Jones

Langley Memorial Aeronautical Laboratory

1947

REPORT No. 863

WING PLAN FORMS FOR HIGH-SPEED FLIGHT

By Robert T. Jones

SUMMARY

It is pointed out that, in the case of an airfoil of infinite aspect ratio moving at an angle of sideslip, the pressure distribution is determined solely by that component of the motion in a direction normal to the leading edge. It follows that the attachment of plane waves to the airfoil at near-sonic or supersonic speeds (Ackeret theory) may be avoided and the pressure drag may be reduced by the use of plan forms in which the angle of sweepback is greater than the Mach angle.

The analysis indicates that for aerodynamic efficiency, wings designed for flight at supersonic speeds should be swept back at an angle greater than the Mach angle and the angle of sweepback should be such that the component of velocity normal to the leading edge is less than the critical speed of the airfoil sections. This principle may also be applied to wings designed for subsonic speeds near the speed of sound, for which the induced velocities resulting from the thickness might otherwise be sufficiently great to cause shock waves.

INTRODUCTION

The theory of potential flows with small disturbances is particularly suited for application to aeronautical problems because the assumptions of small disturbances and isentropic flows on which this theory is based agree with the requirements for efficient flight. Theories of large disturbances, which deal with the formation of shock waves, are of lesser practical interest since such theories describe the losses of energy and the large drags associated with unsuitable forms.

At subsonic speeds the assumption of small disturbances leads to the well-known thin-airfoil theory and the Prandtl-Glauert rule (references 1 and 2); whereas at supersonic velocities this assumption leads to the Ackeret theory (reference 3), according to which the wing sections generate plane sound waves of small amplitude. The assumption of small disturbances, although mathematically valid in the limiting case, does not, of course, insure that such a condition will exist with an actual body of finite thickness. Fortunately, experiments have been made that show in a general way the limits of applicability of this assumption. Of particular interest are the experiments of Ferri (reference 4) and Stanton (reference 5).

At present both the experiments and the theory have been restricted primarily to the two-dimensional flow caused by motion of the wing at right angles to its long axis. For this case the theory shows a radical change in the properties of the wing on transition from subsonic to supersonic speeds. At subsonic speeds the air flows smoothly over the wing section and no pressure drag arises. At angles of attack a suction force is developed on the nose of the airfoil of sufficient magnitude to bring the resultant air force forward relative to the chord axis to a position nearly at right angles to the relative wind. As soon as the speed of sound is exceeded, however, the nature of the flow changes and these favorable characteristics disappear. Instead there arise a pressure drag proportional to the square of the thickness and an additional drag equal to the lift times the angle of attack. These adverse effects are associated with the formation of plane sound waves by the airfoil. Predictions of the theory are borne out by experiments in supersonic wind tunnels.

The purpose of the present report is to show how the adverse effects of high speed may be minimized by the use of a relatively large angle of sweepback, so that the type of flow described in the Ackeret theory no longer occurs. Certain effects of sweepback have, of course, been known for some time (references 6 to 9). Küssner (reference 8) mentions compressibility effects of sweepback at subsonic speeds. Busemann (reference 9) considers the effect of sweepback at supersonic speeds and points out that the drag associated with flows of the Ackeret type may be reduced by the use of sweepback. Busemann does not, however, consider angles of sweepback greater than the Mach angle, which result in a different type of flow.

SYMBOLS

α	angle of attack
β	angle of sideslip or sweepback
u, v, w	velocity components along x, y, z
x, y, z	coordinates
y'	transformed coordinate
b	wing span
c	wing chord; velocity of sound
t	thickness
V	velocity of flight
ϕ	disturbance-velocity potential
L	lift
D	drag
C_L	lift coefficient
C_D	drag coefficient
M	Mach number
Δp	local pressure difference
q	dynamic pressure
θ	spanwise-location parameter $\left(\cos^{-1}\frac{y}{b/2}\right)$

816587—49

THEORY OF WING AT AN ANGLE OF SIDESLIP

The primary effects of sweepback may be illustrated by considering the problem of a long and approximately cylindrical airfoil at an angle of sideslip. Two such airfoils may then be combined (with due allowance for their interference) to give a sweptback plan form.

First consider the airfoil with its long axis parallel to the x-axis and with the relative wind at an angle β to the coordinate system as in figure 1. By following equation (9a) of reference 2 the differential equation of the flow may be written

$$\left(1-\frac{u^2}{c^2}\right)\frac{\partial u}{\partial x}+\left(1-\frac{v^2}{c^2}\right)\frac{\partial v}{\partial y}+\left(1-\frac{w^2}{c^2}\right)\frac{\partial w}{\partial z}-2\frac{uv}{c^2}\frac{\partial v}{\partial x}-2\frac{vw}{c^2}\frac{\partial v}{\partial z}-2\frac{uw}{c^2}\frac{\partial w}{\partial x}=0 \tag{1}$$

The Prandtl-Glauert rule follows from the assumption that only the velocity component u is comparable to the velocity of sound. In the present example both u and v, since they contain components of the flight velocity, are of the order of magnitude of the sound velocity c. On the other hand, if the flow patterns in planes perpendicular to the long axis of the wing are similar (two-dimensional flow), the terms $\partial u/\partial x$ and $\partial v/\partial x$ vanish.

If small velocity disturbances are assumed, the term w/c may be neglected and the term $1-\frac{v^2}{c^2}$ may be replaced by $1-\left(\frac{V\cos\beta}{c}\right)^2$ where $V\cos\beta$ is the component of the flight velocity in the direction normal to the long axis of the wing. By using this relation and introducing the disturbance potential ϕ, there is obtained

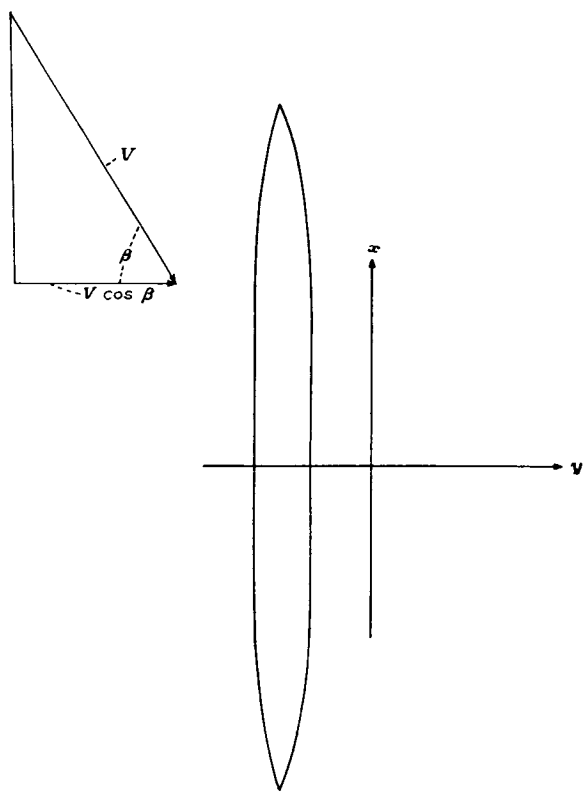

FIGURE 1.—Plan view of airfoil showing axes used in equation (1).

$$\left[1-\left(\frac{V\cos\beta}{c}\right)^2\right]\frac{\partial^2\phi}{\partial y^2}+\frac{\partial^2\phi}{\partial z^2}=0 \tag{2}$$

It is important to note that the derivation of this equation involves no restriction on the flight velocity V, which may be subsonic or supersonic. The restriction is that the disturbance velocities $\partial\phi/\partial y$ and $\partial\phi/\partial z$ be small relative to c.

If $V\cos\beta$ is less than the sound velocity c, the substitution

$$y'=\frac{y}{\sqrt{1-\left(\frac{V\cos\beta}{c}\right)^2}} \tag{3}$$

yields Laplace's equation

$$\frac{\partial^2\phi}{\partial y'^2}+\frac{\partial^2\phi}{\partial z^2}=0 \tag{4}$$

and it follows that the flow patterns are similar to those occurring in an incompressible fluid except for an increase of the pressures in the ratio

$$\frac{1}{\sqrt{1-\left(\frac{V\cos\beta}{c}\right)^2}}$$

If $V\cos\beta$ is greater than c, the substitution

$$y'=\frac{y}{\sqrt{\left(\frac{V\cos\beta}{c}\right)^2-1}} \tag{5}$$

results in the hyperbolic equation

$$\frac{\partial^2\phi}{\partial z^2}-\frac{\partial^2\phi}{\partial y'^2}=0 \tag{6}$$

which is the basis of the Ackeret theory.

The derivation of equations (4) and (6) is actually a special case of a more general statement, namely, that the component of translation of a cylindrical body in the direction of its long axis has no effect on the motion of a frictionless fluid. In the case of a wing of constant section moving through still fluid, the flow is determined by the normal components of velocity of its solid boundaries and these components in turn are completely specified by the component of motion in planes perpendicular to the axis $V\cos\beta$. When the normal component of velocity $V\cos\beta$ is less than sonic, then the wing-section flows are determined by solutions of Laplace's equation. As is well known, these flows show no pressure drag due to thickness of the airfoil. On the other hand, if the normal component exceeds the velocity of sound, the flow patterns are of a different type and are characterized by plane sound waves. In this case a pressure drag arises and the suction for ϕ at the leading edge disappears (fig. 2 (a)).

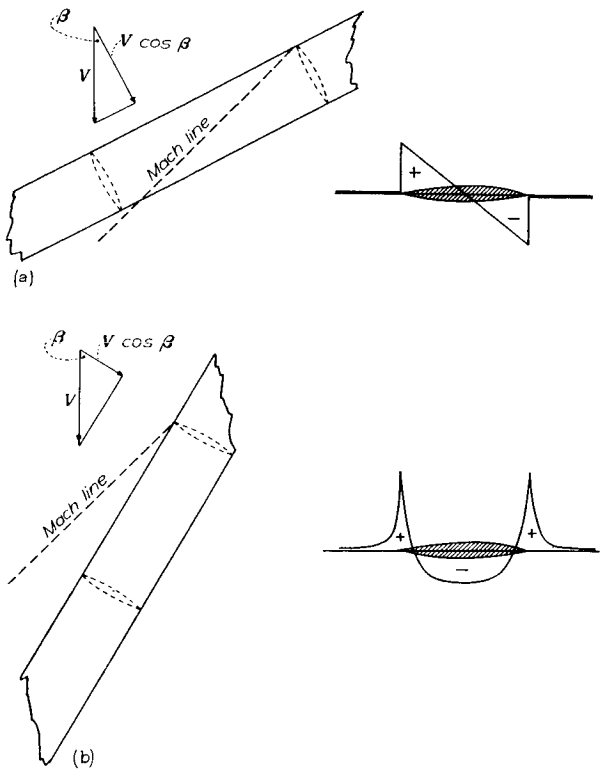

(a) $V \cos \beta > c$.
(b) $V \cos \beta < c$.

FIGURE 2.—Effect of leading-edge angle on pressure distribution.

A physical explanation of the occurrence of smooth flow patterns and pressure distributions at supersonic velocities is as follows: If V is greater than c but $V \cos \beta$ is less, then the angle of sideslip or sweepback is greater than the Mach angle (see fig. 2 (b)) and the airfoil will lie behind the characteristic lines along which pressure influences are transmitted (Mach lines). Thus, although the fluid directly upstream from a given section can receive no pressure signal from this section, the flow behaves as though it did receive such signals because of the successive influence of similar sections farther upstream along the airfoil. The streamlines will thus be caused to curve and follow paths appropriate to a subsonic flow, although the speed is everywhere supersonic.

Figure 3 illustrates the effect of sweepback on the change in cross section of a stream tube passing near the upper surface of a cambered airfoil. As is well known, the equations of fluid motion show a reduction in the area of a stream tube in the region of increased velocity above the airfoil when the velocity of flight is subsonic but show an increase in the cross section when the velocity of flight is supersonic. In figure 3 the component normal to the leading edge $V \cos \beta$ is subsonic; and hence in section view the streamlines, following the pattern for subsonic velocities, appear to contract as they flow over the upper surface. In plan view, however, the resolution of velocities shows that the flow lines bend as

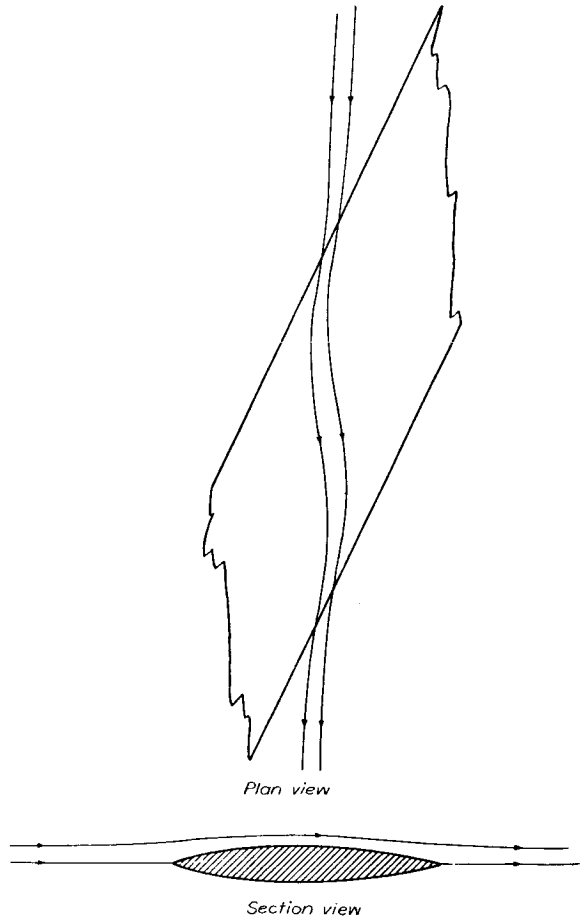

FIGURE 3.—Change in area of stream tube over upper surface of sweptback wing.

they pass over the wing in such a way as to increase the stream-tube area. In case the velocity of flight is supersonic, the latter effect must predominate, as is required by the equations of motion.

The order of magnitude of the pressure-drag coefficient and its variation with angle of sweepback are indicated by figure 4. The calculations were made by applying the Ackeret theory and formulas (4) and (5) to a wing of infinite aspect ratio. A simple biconvex wing section was assumed and the angle of attack was varied so as to maintain a constant lift coefficient of 0.5. The calculations were made for a Mach number of 1.4, with the result that at 45° the angle of sweepback becomes equal to the Mach angle and the factor

$$\frac{1}{\sqrt{\left(\frac{V \cos \beta}{c}\right)^2 - 1}}$$

becomes infinite. At this point the pressure drag due to thickness becomes infinite and the drag due to angle of attack (shown by the curve marked $\frac{t}{c}=0$) vanishes.

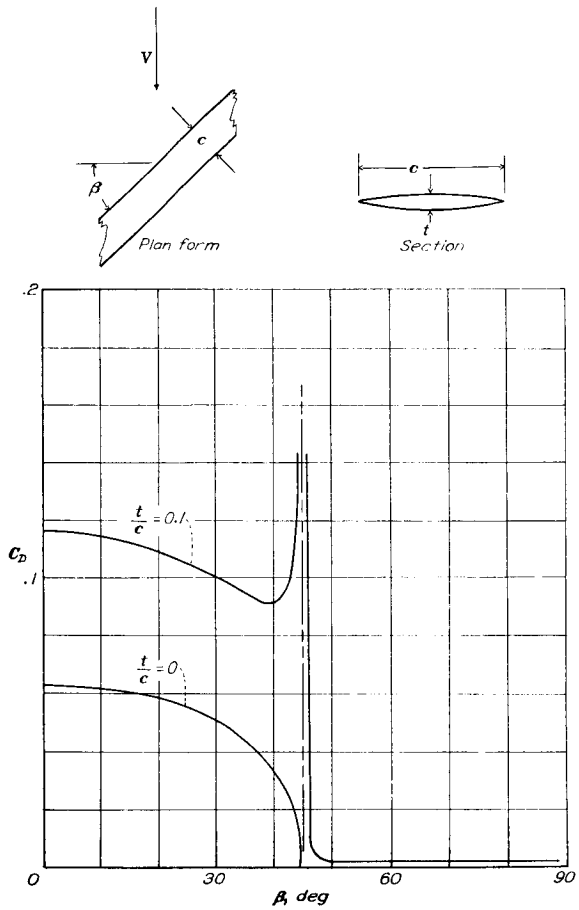

FIGURE 4.—Variation of pressure drag with angle of sweepback for infinite aspect ratio. $M=1.4$; $C_L=0.5$.

In the case of a wing of finite aspect ratio, it seems probable that in the regions of the center section and the tips pressure drags of the same order as those indicated for these sections by the Ackeret theory will appear. If the wing is of sufficiently high aspect ratio, however, the fraction of the wing area affected will be negligible and the pressure drag will be nearly that given in figure 4. The other drags involved are: (1) skin-friction drag, which may be of the order of 0.01, and (2) induced drag, which for an aspect ratio of 8 is also about 0.01.

WINGS OF FINITE SPAN AND THICKNESS

Schlichting (reference 10) proposes a trapezoidal plan form with tips cut away at the Mach angle as the ideal supersonic wing, since in this case the wake has no influence on the lifting surface and the drag is no greater than that of a wing of infinite span. In the plan forms proposed by Schlichting, however, the resultant force remains at right angles to the chord; hence the pressure drag is equal to the lift times the angle of attack. With this type of flow there is no favorable effect of aspect ratio.

It is interesting to note that a favorable interference may be obtained by separating the wing into lifting elements and staggering the elements in a rearward direction behind the Mach lines as in figure 5. In the staggered arrangement the upflow outside the vortices trailing from element A will be effective at the position of B and, although the lift of each element is at right angles to its chord, the upflow permits the angle of atatck of element B to be reduced for the same lift and hence the lift-drag ratio will be improved.

According to Munk's stagger theorem (reference 11) the over-all drag of a lifting system in an incompressible flow would not be altered by changing the relative positions of the lifting elements along the direction of flight. In the type of flow considered by Munk, therefore, a reduction in the drag

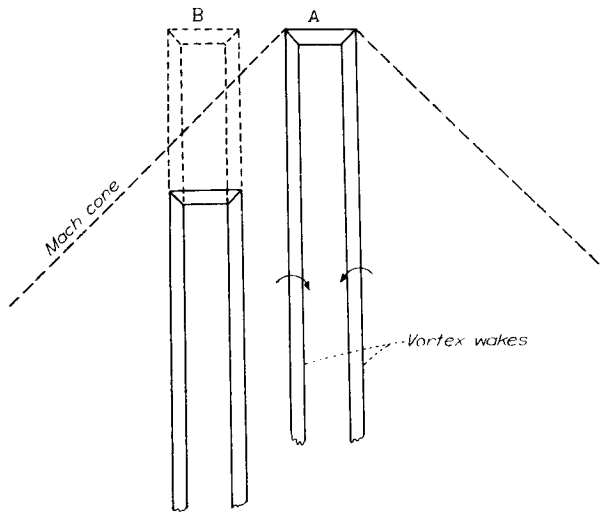

FIGURE 5.—Staggered lifting elements in supersonic flow.

of element B, caused by moving it into a position of greater upwash (that is, moving it backward relative to A), would be compensated by an equal increase in the drag of element A, resulting from the loss of upwash at A. (See fig. 5.) In supersonic flow, however, this reciprocal relation does not exist since a lifting element can produce no upwash ahead of its Mach cone. Lifting elements spaced at right angles to the direction of flight therefore have no favorable interference, and it is evident that the lift-drag ratio cannot be improved merely by increasing the aspect ratio of the lifting system. Favorable interference can be obtained only by arranging the lifting elements behind the Mach lines, as shown in figure 5.

Further analysis is needed to determine the flow near the center section of the sweptback wing because in this region the flow will not remain two-dimensional, as has been assumed. Departures from cylindrical flow caused by the tips will be small since their influence cannot extend forward of the Mach lines drawn from the points at which these departures originate in the plan form. As pointed out by Busemann and Schlichting (references 9 and 10), cylindrical flow may be preserved right up to the tips by cutting them off along the Mach lines. (See fig. 6.)

At large angles of sweepback the flow near the vertex is expected to be similar to that over the low-aspect-ratio triangular airfoil discussed in reference 12. Figure 7 shows the lift distribution obtained in reference 12 and shows qualitatively the type of approximation involved.

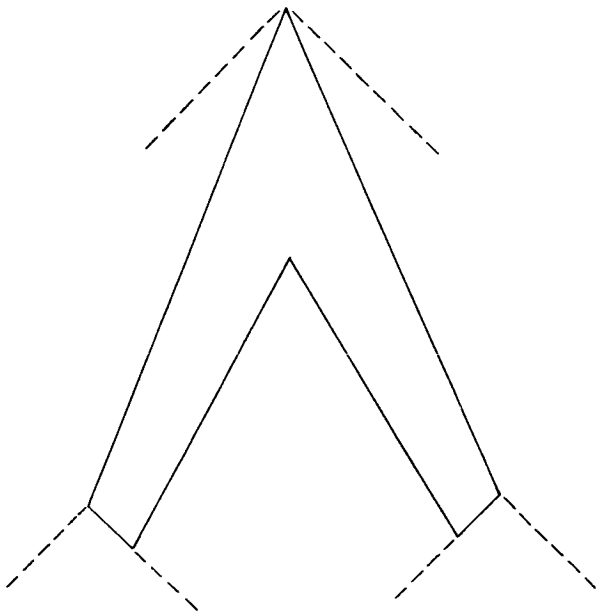

FIGURE 6.—Wing with tips cut away along the Mach lines.

Finite thickness is expected to result in a pressure drag on those sections near the center of the wing and further study is also required to establish the flow due to thickness in this region. Some insight into the problem of flow near the center section may be furnished by the known solutions for supersonic flow in three dimensions (reference 13). Finite thickness may also cause pressure drag in regions where the flow is two-dimensional if the induced velocities are great enough to cause shock waves. This effect may be avoided by increasing the angle of sweepback so that the normal component of velocity not only is subsonic but is less than the critical speed of the airfoil sections. This principle may also be applied to wings designed for subsonic speeds near the speed of sound.

LANGLEY MEMORIAL AERONAUTICAL LABORATORY,
NATIONAL ADVISORY COMMITTEE FOR AERONAUTICS,
LANGLEY FIELD, VA., *June 23, 1945.*

REFERENCES

1. Glauert, H.: The Effect of Compressibility on the Lift of an Aerofoil. R. & M. No. 1135, British A. R. C., 1927.
2. Prandtl, L.: General Considerations on the Flow of Compressible Fluids. NACA TM No. 805, 1936.
3. Ackeret, J.: Air Forces on Airfoils Moving Faster Than Sound. NACA TM No. 317, 1925.
4. Ferri, Antonio: Experimental Results with Airfoils Tested in the High-Speed Tunnel at Guidonia. NACA TM No. 946, 1940.
5. Taylor, G. I.: Applications to Aeronautics of Ackeret's Theory of Aerofoils Moving at Speeds Greater Than That of Sound. R. & M. No. 1467, British A. R. C., 1932.
6. Munk, Max M.: Note on the Relative Effect of the Dihedral and the Sweep Back of Airplane Wings. NACA TN No. 177, 1924.
7. Betz, A.: Applied Airfoil Theory. Unsymmetrical and Non-Steady Types of Motion. Vol. IV of Aerodynamic Theory, div. J, ch. IV, sec. 2, W. F. Durand, ed., Julius Springer (Berlin), 1935, pp. 97–99.
8. Küssner, H. G.: General Airfoil Theory. NACA TM No. 979, 1941.
9. Busemann, A.: Aerodynamischer Auftrieb bei Überschallgeschwindigkeit. Luftfahrtforschung, Bd. 12, Nr. 6, Oct. 3, 1935, pp. 210–220.
10. Schlichting, H.: Airfoil Theory at Supersonic Speed. NACA TM No. 897, 1939.
11. Munk, Max M.: The Minimum Induced Drag of Aerofoils. NACA Rep. No. 121, 1921.
12. Jones, Robert T.: Properties of Low-Aspect-Ratio Pointed Wings at Speeds below and above the Speed of Sound. NACA Rep. No. 835, 1946.
13. Von Kármán, Th.: The Problem of Resistance in Compressible Fluids. GALCIT Pub. No. 75, 1936. (From R. Accad. d'Italia, cl. sci. fis., mat. e nat., vol. XIV, 1936.)

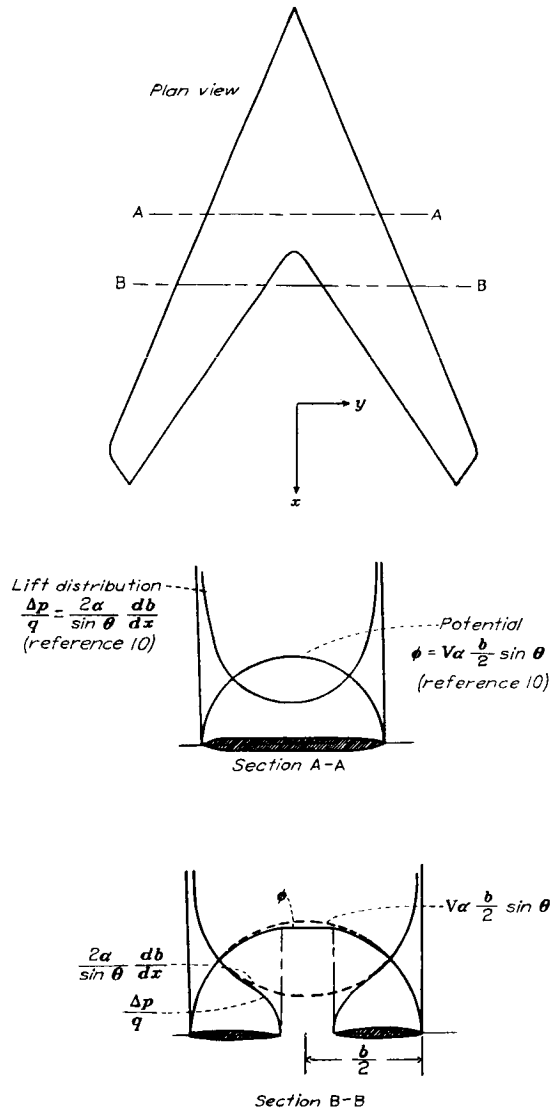

FIGURE 7.—Approximate distribution of lift near vertex of wing with large angle of sweepback.

TECHNICAL NOTE 1081

FLOW OVER A SLENDER BODY OF REVOLUTION AT SUPERSONIC VELOCITIES

Robert T. Jones and Kenneth Margolis

Langley Memorial Aeronautical Laboratory

August 1946

NATIONAL ADVISORY COMMITTEE FOR AERONAUTICS

TECHNICAL NOTE No. 1081

FLOW OVER A SLENDER BODY OF REVOLUTION AT SUPERSONIC VELOCITIES

By Robert T. Jones and Kenneth Margolis

SUMMARY

The theory of small disturbances is applied to the calculation of the pressure distribution and drag of a closed body of revolution traveling at supersonic speeds. It is shown that toward the rear of the body the shape of the pressure distribution is similar to that for subsonic flow. For fineness ratios between 10 and 15 the theoretical wave drag is of the same order as probable values of the frictional drag.

INTRODUCTION

Methods for calculation of the flow over a body of revolution traveling at supersonic velocities have been known for some time. (See references 1 and 2.) Investigations along these lines have, however, been confined chiefly to bodies having the form of artillery projectiles. Such bodies, because of their blunt forms, show relatively high drags and are thus not suited for use on high-speed aircraft. The drag of slender bodies and the effects of fairing the rear of these bodies are therefore of considerable interest in connection with the problem of flight at speeds above the speed of sound.

In view of the interest in possible aeronautical applications it was thought worth while to apply the known methods to a particular case of a closed body having both a tapered nose and a tapered tail. Slender shapes described by the rotation of parabolic arcs were chosen and the resulting pressure distributions calculated. The results are compared with those obtained for similar shapes in an incompressible fluid and also in one case with a two-dimensional body having a similar cross section.

SYMBOLS

x, y, z	Cartesian coordinates
V	undisturbed fluid velocity
a	speed of sound in fluid
M	Mach number (V/a)
$B = \sqrt{M^2 - 1}$	
$r = \sqrt{y^2 + z^2}$	
ρ	density of fluid
q	dynamic pressure $\left(\frac{1}{2}\rho V^2\right)$
Δp	pressure increment
ϕ_o	velocity potential of single source
ϕ	velocity potential of continuous distribution of sources along x-axis
ζ	abscissa of individual sources
R	radius of body
d	maximum diameter of body
L	length of body
S_{max}	maximum cross-sectional area
D	drag
C_{D_a}	drag coefficient based on maximum cross-sectional area (D/qS_{max})
$C_{D_{vol}}$	drag coefficient based on 2/3 power of volume $\left(\frac{D}{q(\text{Volume})^{2/3}}\right)$
c, C	constants

METHODS OF CALCULATION

The method used herein follows closely that of reference 1. Figure 1 shows the shape of the body and the orientation of the axes. The disturbance produced by the body is assumed to be small and the flow isentropic so that the linearized equation for the potential of the disturbance velocities ϕ will apply. This equation is (see reference 2)

$$\left(1 - M^2\right)\phi_{xx} + \phi_{yy} + \phi_{zz} = 0 \tag{1}$$

As in the case of an incompressible fluid the flow over the body can be obtained by the addition of flows due to an infinite number of sources distributed along the axis. The potential of a single source in a supersonic stream is

$$\phi_o = \frac{CV}{\sqrt{x^2 - B^2(y^2 + z^2)}}$$

$$= \frac{CV}{\sqrt{x^2 - B^2 r^2}} \tag{2}$$

where

$$B = \sqrt{M^2 - 1}$$

and

$$r = \sqrt{y^2 + z^2}$$

Figure 2 shows the equipotential lines for the supersonic source compared with those for a source in an incompressible flow. In the case of a source in an incompressible flow the equipotential surfaces are spheres, given by the expression

$$\phi_o = \frac{CV}{\sqrt{x^2 + y^2 + z^2}} \tag{3}$$

In the supersonic case the equipotential surfaces are hyperboloids of two sheets contained within the Mach cones. Although the mathematical expression has values in two cones, one ahead of and one behind the source, only the values behind have physical significance.

It will be noted that the distribution of velocities along the x-axis is the same for the supersonic source (equation (2)) as for the subsonic or incompressible source (equation (3)). Since the forward cone is to be disregarded in the supersonic case, however, it is found that the coefficient C in equation (2) must be doubled in order to produce the same flux, or intensity, as equation (3). The result is that the velocities along the axis behind a supersonic source are exactly twice those of a subsonic source having the same intensity.

The sources and sinks are assumed to be continuously distributed with intensity $2\pi Vf(\xi)$ per unit length along the x-axis from -1 to 1. The abscissas of the individual sources are denoted by ξ. Positive values of $f(\xi)$ denote sources and negative values denote sinks. By adding the potentials due to the single elementary sources $f(\xi)d\xi$ the resulant flow

$$\phi = V\int_{-1}^{x-Br} \frac{f(\xi)d\xi}{\sqrt{(x-\xi)^2 - B^2r^2}} \tag{4}$$

is obtained.

The problem is to determine a source distribution in such a way that

$$\frac{1}{V}\left(\frac{\partial\phi}{\partial r}\right)_{r=R} = \frac{dR}{dx} \tag{5}$$

where dR/dx gives the shape of the meridian curve of the body of revolution. It is shown in reference 1 that to a first approximation for a slender body the source strength is proportional to the rate of change of the cross section of the body, that is

$$f(x) = R\frac{dR}{dx} \tag{6}$$

a similar approximation can be applied to obtain the source distribution for a body in subsonic flow. The distributions are, in fact, the same in the two cases with the exception that in the supersonic flow the value of $f(x)$ must be doubled to account for the elimination of the flux through the forward cones.

By choosing $f(x) = c(x^3 - x)$ and solving equation (6), the following expression for R was obtained:

$$R = \frac{c}{2}(1 - x^2) \tag{7}$$

This expression may be recognized as the equation of a surface obtained by revolving a parabolic arc about its chord. The fineness ratio of the body is determined by the value assigned the factor c.

On substituting $c(\xi^3 - \xi)$ for $f(\xi)$ in equation (4), the velocity increment $\partial\phi/\partial x$ at point (x,r) is found to be (see equation (9.5), p.39, reference 1)

$$\frac{\partial\phi}{\partial x} = V\int_{-1}^{x-Br} \frac{f'(\xi)\,d\xi}{\sqrt{(x-\xi)^2 - B^2r^2}}$$

$$= cV\int_{-1}^{x-Br} \frac{(3\xi^2 - 1)}{\sqrt{(x-\xi)^2 - B^2r^2}}\,d\xi$$

$$= cV\left[\frac{(3 - 9x)}{2}\sqrt{(x+1)^2 - B^2r^2} + \left(3x^2 - 1 + \frac{3}{2}B^2r^2\right)\cosh^{-1}\left(\frac{x+1}{Br}\right)\right] \tag{8}$$

over the body.

Along the axis behind the body the integration gives

$$cV\left[(3x^2 - 1)\log\frac{x+1}{x-1} - 6x\right] \tag{9}$$

The pressure coefficients were calculated by the formula

$$\frac{\Delta p}{q} = \frac{2}{V}\frac{d\phi}{dx} \tag{10}$$

RESULTS

Calculations have been made for a Mach number of 1.4 and for three thickness ratios d/L of 0.0667, 0.10, and 0.15 corresponding to fineness ratios L/d of 15, 10, and 6.67, respectively. The results for the three bodies are shown in figures 3, 4, and 5, respectively, and are compared with the theoretical pressure distributions over these bodies in an incompressible fluid. A discussion of the errors involved in the linear theory and the variation of the pressures with Mach number will be found in reference 3.

Comparison of the distributions in a compressible fluid and in an incompressible fluid shows a certain similarity, especially toward the rear of the body. The effect of supersonic speed appears to be similar to the effect of a lag inasmuch as the negative pressure peak and the region of pressure recovery are displaced rearward. The pressures along the axis behind the body are just twice those produced by an incompressible fluid, as may be seen by referring to the velocity field of a single source.

The results obtained herein for the three-dimensional body are in marked contrast to the results obtained for two-dimensional bodies, or wing sections, having similar cross sections. As is well known, in the two-dimensional case no pressure recovery takes place at supersonic speeds, the pressure at a point being determined solely by the inclination of the surface at that point so that positive pressures occur wherever the cross section is expanding and negative pressures occur wherever the cross section is diminishing. Figure 6 shows the comparison of the two-dimensional and three-dimensional bodies for the 0.10 thickness ratio.

The essential difference between the two- and three-dimensional flows corresponds to the difference noted by Lamb (reference 4) between the characteristics of a plane sound wave and an axially symmetrical wave diverging from a center. As noted by Lamb, the plane wave, which corresponds in the present case to the flow produced by the two-dimensional wing section, is propagated indefinitely without change of form; whereas the axially symmetrical wave, which approximates that produced by an element of the slender body of revolution, does not follow the form of the disturbing motion but leaves a "tail" of diminishing intensity and indefinite extent. Thus the wing section leaves no pressure disturbance in its wake, whereas the axially symmetrical body is followed by an indefinite region of positive pressure. Integration of the axial components of the pressures

acting on the body, however, shows that the positive pressure at the rear of the three-dimensional body is sufficient to cancel only a small fraction of the total pressure or wave drag.

The wave-drag coefficients based on the maximum frontal area were found to be 0.049, 0.11, and 0.24 for the bodies with thickness ratios of 0.0667, 0.10, and 0.15, respectively. Figure 7 shows a comparison of these values with the wave drags of corresponding two-dimensional wing sections. It will be noted that the wave drag of the fuselage form is approximately proportional to the square of the thickness ratio.

An approximate estimate of the total drag of a body may be obtained by adding values of the frictional drag to the wave drag. A rather complete treatment of the frictional drag of bodies of revolution at subsonic speeds is available from reference 5. By use of values from reference 5 corresponding to a fully turbulent boundary layer and a Reynolds number of 10^8, the following estimates of the total drags of the bodies were obtained:

Thickness ratio	C_{D_a}	$C_{D_{vol}}$
0.0667	0.14	0.032
.10	.17	.051
.15	.29	.11

where C_{D_a} is the drag coefficient based on the frontal area and $C_{D_{vol}}$ is the drag coefficient based on the volume of the body to the 2/3 power.

The drag of a given volume is an important criterion in the case of an airplane fuselage and it will be of interest to compare these values with a typical value attainable at subsonic speeds. For a Reynolds number of 10^8 and a turbulent boundary layer, the best value given by Young (reference 5) corresponds to a thickness ratio of 0.2 and is approximately

$$C_{D_{vol}} = 0.016$$

CONCLUDING REMARKS

The theoretical pressure distribution over a closed body of revolution traveling at supersonic velocities shows a pressure recovery at the rear of the body similar to that occurring at

subsonic speeds. The extent of the region of positive pressure is, however, not sufficient to have a pronounced effect on the wave drag. It appears to be necessary to use extremely slender shapes to obtain total drag values comparable to those of a conventional airplane fuselage at subsonic speeds. For fineness ratios between 10 and 15 the theoretical wave drag is of the same order as probable values of the frictional drag.

Langley Memorial Aeronautical Laboratory
National Advisory Committee for Aeronautics
Langley Field, Va., July 8, 1946

REFERENCES

1. von Kármán, Th.: The Problem of Resistance in Compressible Fluids. GALCIT Pub. No. 75, 1936. (From R. Accad. d'Italia, cl. sci. fis., mat. e nat., vol. XIV, 1936.)

2. Prandtl, L.: General Considerations on the Flow of Compressible Fluids. NACA TM No. 805, 1936.

3. Taylor, G. I., and Maccoll, J. W.: The Air Pressure on a Cone Moving at High Speeds. Proc. Roy. Soc. (London), ser. A, vol. 139, no. 838, Feb. 1, 1933, pp. 278-311.

4. Lamb, Horace: Hydrodynamics. Sixth ed., Cambridge Univ. Press, 1932, pp. 298-301 and 524-527.

5. Young, A. D.: The Calculation of the Total and Skin Friction Drags of Bodies of Revolution at Zero Incidence. R. & M. No. 1874, British A.R.C., 1939.

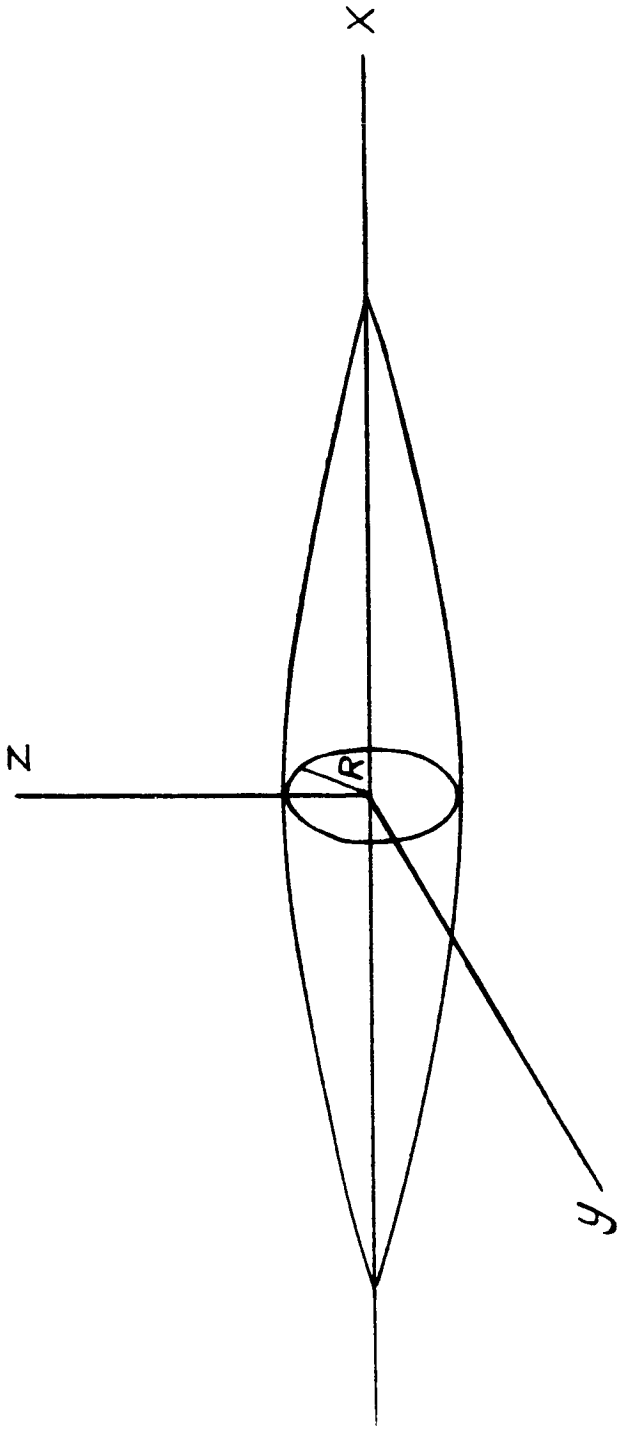

Figure 1.- Orientation of axes and shape of body.

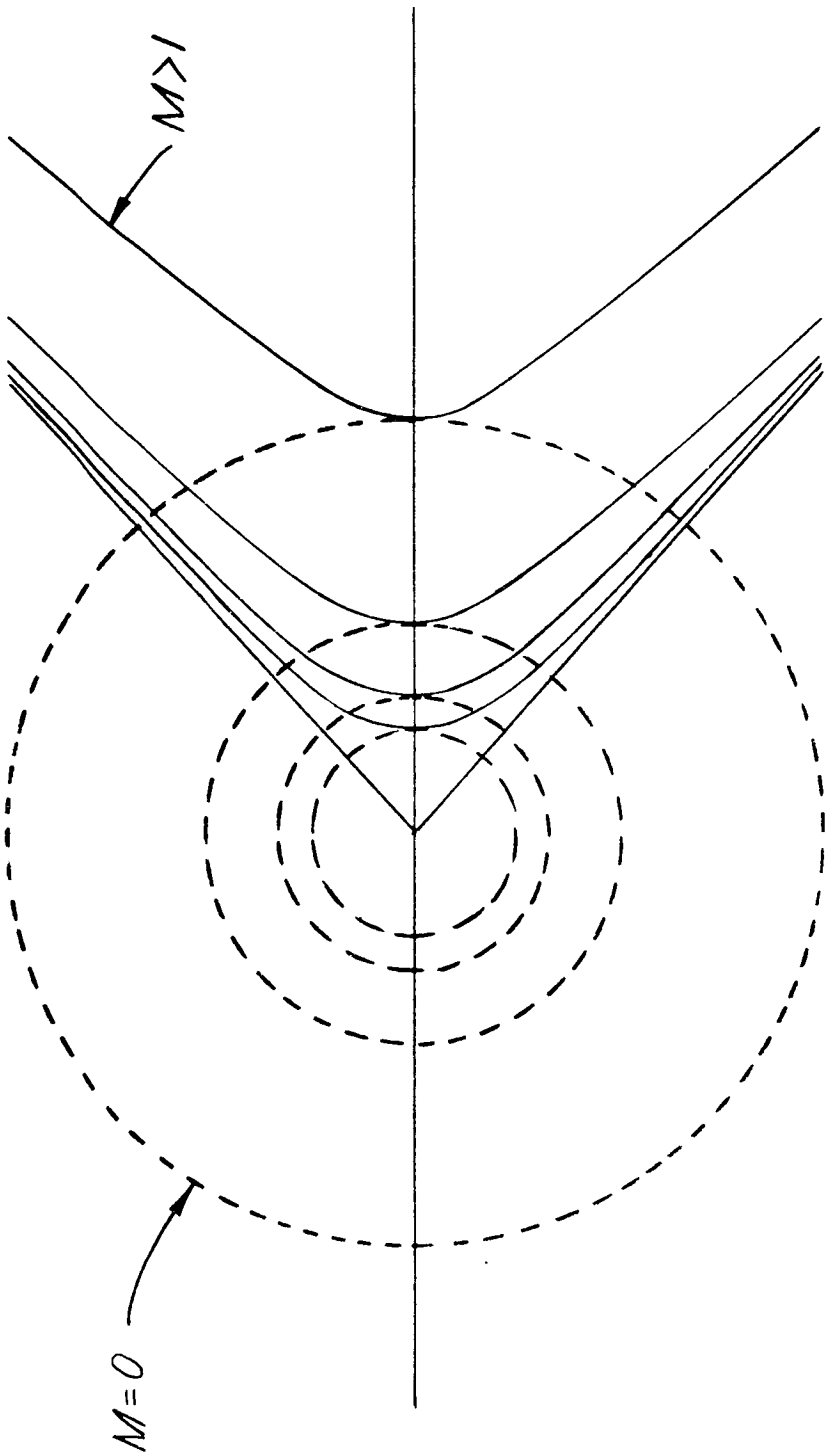

Figure 2.- Equipotential lines for a supersonic source compared with those for a source in an incompressible flow.

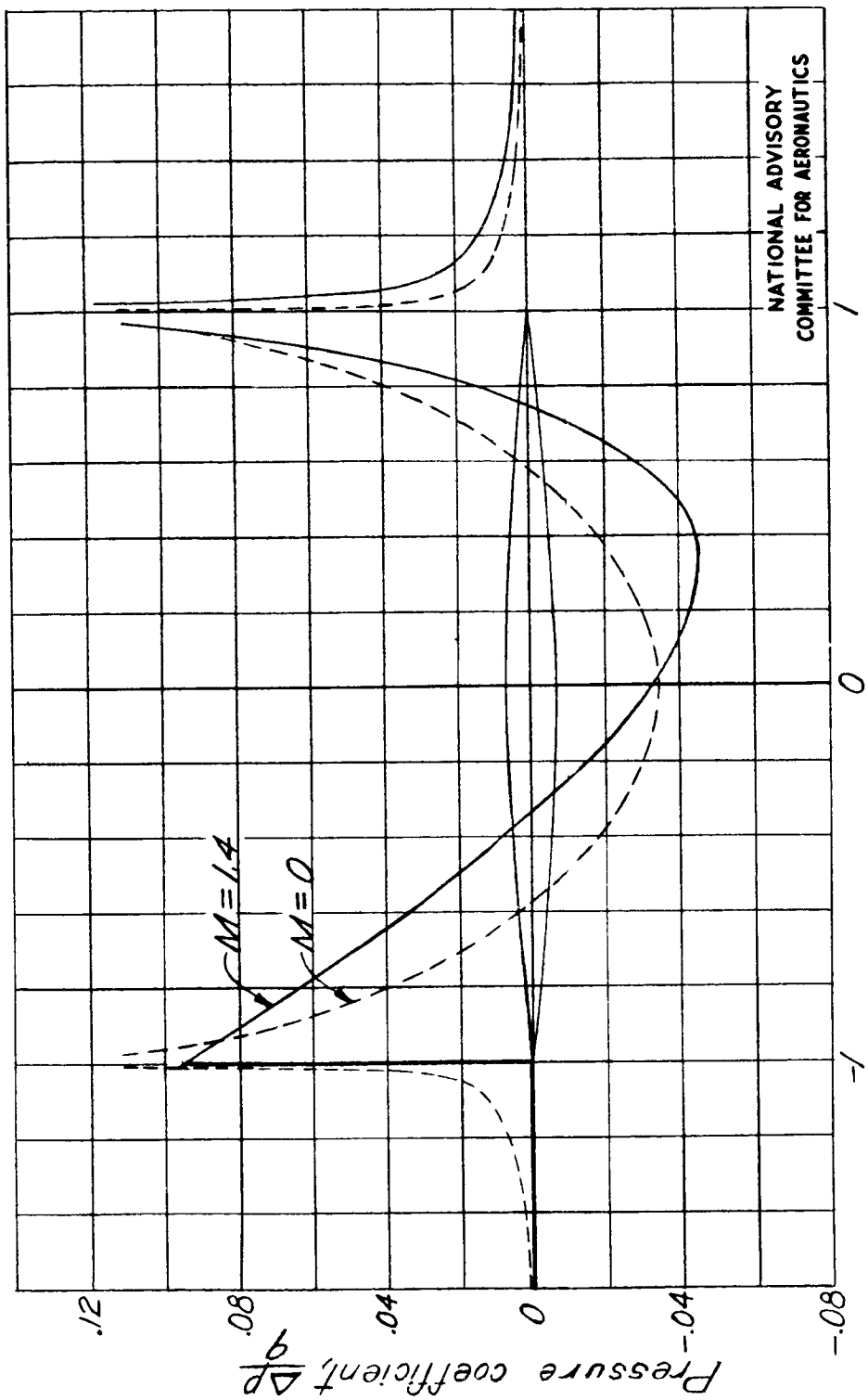

Figure 3.- Calculated pressure distributions for a thickness ratio of 0.0667.

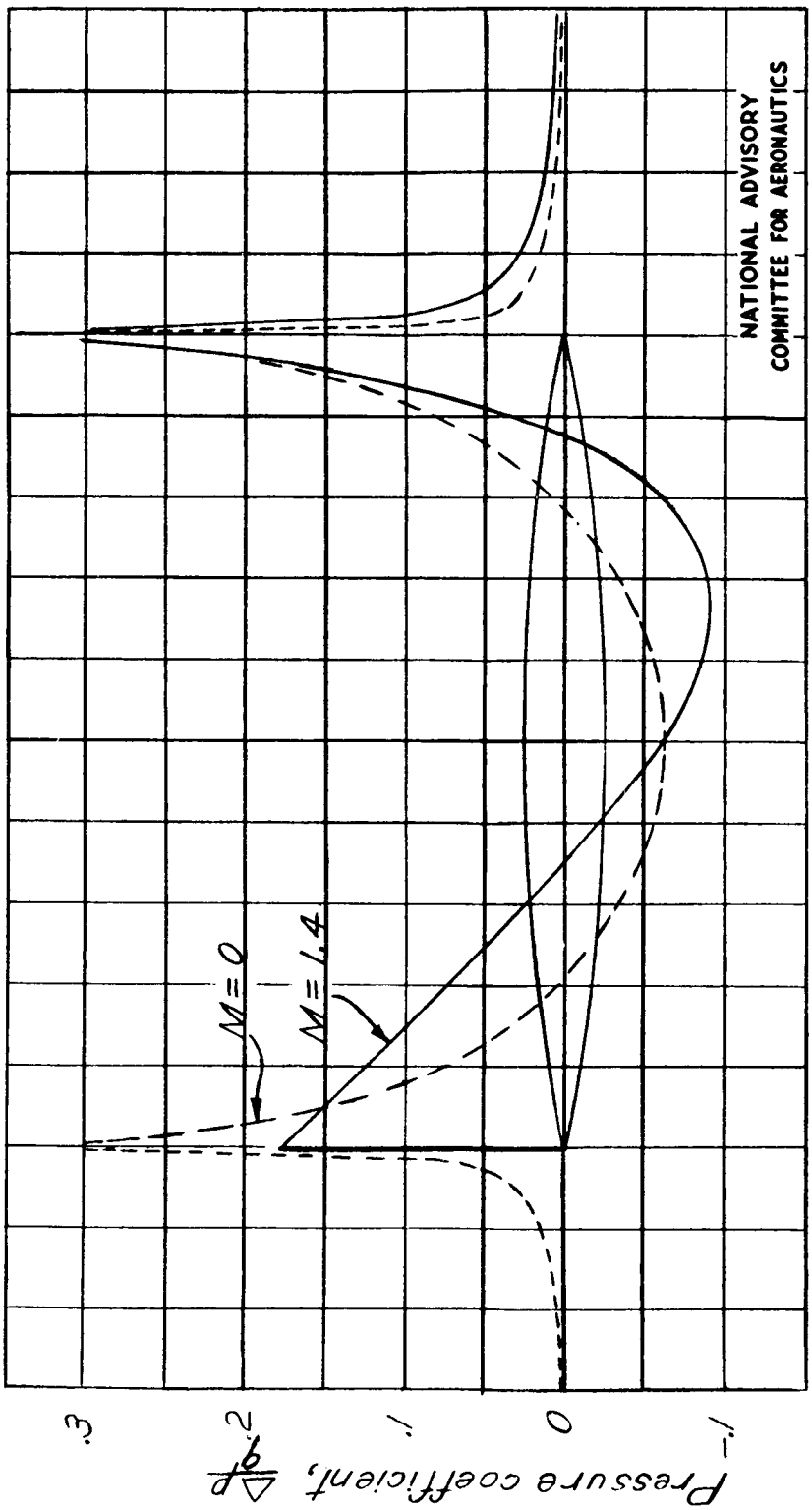

Figure 4.- Calculated pressure distributions for a thickness ratio of 0.10.

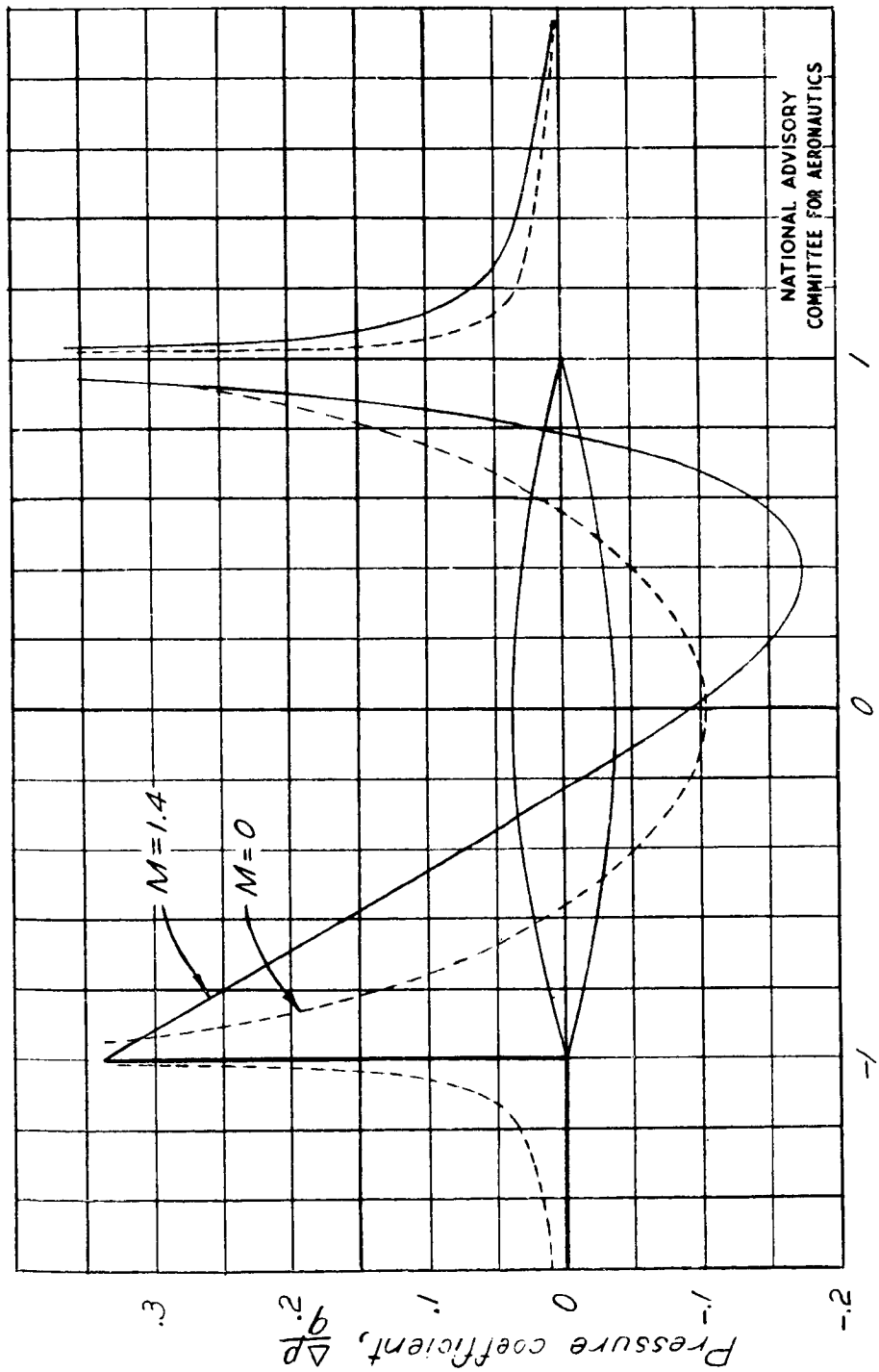

Figure 5.- Calculated pressure distributions for a thickness ratio of 0.15.

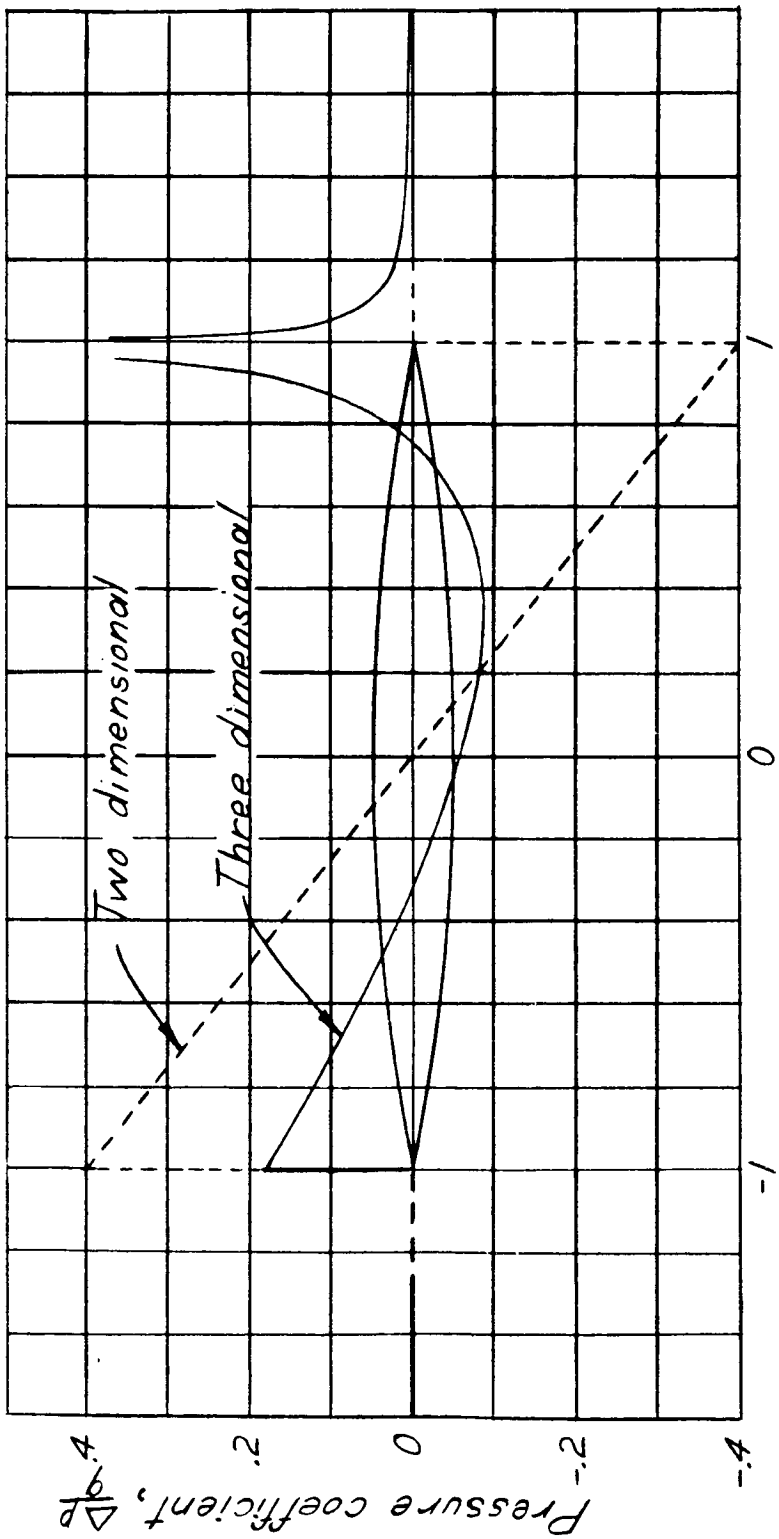

Figure 6.- Comparison of pressures for two- and three-dimensional bodies at a Mach number of 1.4 for a thickness ratio of 0.10.

NATIONAL ADVISORY COMMITTEE FOR AERONAUTICS

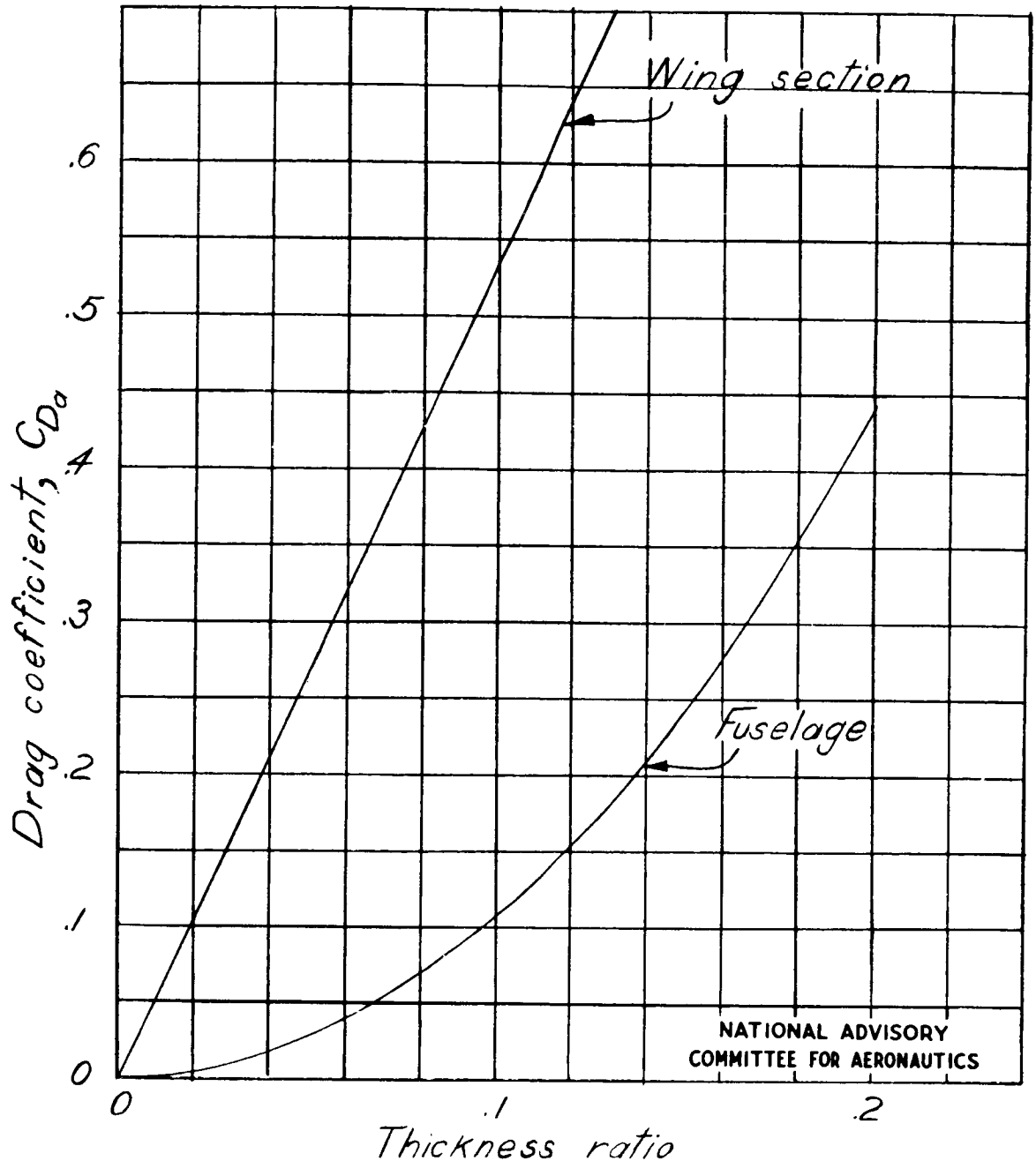

Figure 7.- Comparison of wave drags of two- and three-dimensional bodies for a Mach number of 1.4.

REPORT NO. 851

THIN OBLIQUE AIRFOILS AT SUPERSONIC SPEED

Robert T. Jones

Langley Memorial Aeronautical Laboratory

1946

REPORT No. 851

THIN OBLIQUE AIRFOILS AT SUPERSONIC SPEED

By ROBERT T. JONES

SUMMARY

The well-known methods of thin-airfoil theory have been extended to oblique or sweptback airfoils of finite aspect ratio moving at supersonic speeds. The cases considered thus far are symmetrical airfoils at zero lift having plan forms bounded by straight lines. Because of the conical form of the elementary flow fields, the results are comparable in simplicity to the results of the two-dimensional thin-airfoil theory for subsonic speeds.

In the case of untapered airfoils swept back behind the Mach cone the pressure distribution at the center section is similar to that given by the Ackeret theory for a straight airfoil. With increasing distance from the center section the distribution approaches the form given by the subsonic-flow theory. The pressure drag is concentrated chiefly at the center section and or long wings a slight negative drag may appear on outboard sections.

INTRODUCTION

In reference 1 it was pointed out that the wave drag of an infinite cylindrical airfoil disappears when the airfoil is yawed to an angle greater than the Mach angle. This observation led to the conclusion that the drag of a finite airfoil could be greatly reduced by the use of sufficient sweepback. With such a sweptback wing the wave drag would be associated with departures from the ideal two-dimensional flow at the root or tip sections and would thus be a function of the aspect ratio. The present report extends the theory of reference 1 to take account of these effects.

The treatment is based on the theory of small disturbances in a frictionless compressible fluid. The idealized fluid and its equations of motion are identical with those employed in acoustics in the theory of sound waves of small amplitude. The application of the theory is thus limited to bodies having thin cross sections so that the velocity of motion imparted to the fluid is small relative to the velocity of sound and so that the pressure disturbances produced are small relative to the ambient pressure.

The adaptation of the sound-wave theory to the aerodynamics of moving bodies was suggested many years ago by Prandtl. The theory was applied by Ackeret (reference 2) to thin airfoils moving at supersonic speed. Ackeret's treatment is limited, however, to infinitely long cylindrical airfoils moving transversely. The present theory may be considered an extension of Ackeret's theory to take into account wings of finite span and wings having tapered or sweptback plan forms. In the case of sweptback plan forms the results are markedly different from those obtained by the Ackeret theory and approach the values indicated in references 1 and 3.

In reference 4 Busemann describes a method for calculating the supersonic flow over bodies which produce a conical pressure field. Busemann shows that the flow around cones of circular cross sections as well as the flow around the tip of a rectangular lifting surface satisfies this condition. The fact that a great variety of three-dimensional flows can be constructed by the superposition of conical and cylindrical flow fields leads to an essential simplification of the airfoil theory at supersonic speeds.

The present treatment differs from Busemann's in that it is further limited to flat bodies, that is, bodies which are thin in both longitudinal and transverse sections. This additional restriction leads to a much simpler mathematical treatment and one which is applicable to a wide variety of airfoil shapes. Symmetrical nonlifting bodies are also treated in reference 5 where use is made of integral expressions corresponding to the velocity potential of plane-source distribution.

SYMBOLS

V	flight velocity
M	Mach number
x, y, z	coordinates
ξ	point on X-axis
x_1	limit of integration
ϕ	disturbance-velocity potential
u, v, w	disturbance-velocity components
u_1	value of u at x_1
$\bar{u}$	value of u for conjugate arrangement
p	local pressure
q	dynamic pressure $\left(\frac{1}{2}\rho V^2\right)$
ρ	density of air
P_n, Q_n	Legendre functions
I	source-strength factor
D	differential operator
C_D	drag coefficient
t	thickness of wing
m	slope of line source (absolute value)
c	chord of wing

795249—49

THE OBLIQUE LINE SOURCE

The assumptions of small disturbances and a constant velocity of sound throughout the fluid lead to the well-known linearized equation for the velocity potential ϕ (see reference 6)

$$(1-M^2)\phi_{xx}+\phi_{yy}+\phi_{zz}=0 \tag{1}$$

The analysis is simplified by introducing the coordinates

$$\left.\begin{aligned} x_1&=x \\ y_1&=\sqrt{M^2-1}\,y \\ z_1&=\sqrt{M^2-1}\,z \end{aligned}\right\} \tag{2}$$

Dropping the subscripts from the transformed coordinates gives

$$\phi_{xx}-\phi_{yy}-\phi_{zz}=0 \tag{3}$$

According to the thin-airfoil theory the pressures on the transformed airfoil are given by

$$\frac{\Delta p}{q}=2\frac{u}{V}$$

$$=\frac{2}{V}\frac{\partial\phi}{\partial x} \qquad (z\to 0) \tag{4}$$

and the slope of the airfoil surface $\frac{dz}{dx}$ is equal to the slope of the streamlines near the chord plane; that is,

$$\frac{dz}{dx}=\frac{w}{V}$$

$$=\frac{1}{V}\frac{\partial\phi}{\partial z} \qquad (z\to 0) \tag{5}$$

The use of the coordinate transformation, equation (2), will be understood in the following development. The results are therefore applicable directly to a Mach number of $\sqrt{2}$. For an equivalent airfoil at another Mach number the y- and z- coordinates of the surface will be multiplied by $\sqrt{M^2-1}$ while the pressure coefficients at corresponding points will be divided by the quantity M^2-1.

The elementary solution of equation (3) for a point source is

$$\phi_0=\frac{1}{\sqrt{x^2-y^2-z^2}}$$

This solution is directly related to the subsonic potential

$$\phi_0=\frac{1}{\sqrt{x^2+y^2+z^2}}$$

In the subsonic case the equipotential surfaces are, however, ellipsoids, whereas in the supersonic case the equipotential surfaces are hyperboloids limited by the Mach cone. (See reference 6 for the derivation of these elementary solutions.)

Because of the linearity of equation (1) a solution may be used to denote one of the velocity components rather than the velocity potential. The specification of one component in this manner actually describes the whole flow field since the other components may be obtained by integrating the given component to obtain the velocity potential and then differentiating the results along the desired directions to obtain the desired components. This procedure is especially useful in the thin-airfoil theory, where the complete velocity field may not be required.

Adopting the foregoing procedure, one may write

$$u_0=\frac{1}{\sqrt{x^2-y^2-z^2}}$$

Since u is proportional to the pressure, such a solution corresponds to a point source in the pressure field. The solution for an oblique line source may be obtained by integrating for the effect of a row of point sources along the line $y=mx$. It will be shown that such a line source satisfies the boundary condition for a thin wedge-shape body. This solution, as well as other expressions relating to oblique airfoils, can be most conveniently expressed by referring to the oblique coordinates

$$x'=x-my$$

$$y'=y-mx$$

$$z'=\sqrt{1-m^2}\,z$$

(See fig. 1.) It may be shown that if any function $f(x, y, z)$ is a solution of

$$f_{xx}-f_{yy}-f_{zz}=0$$

then $f(x', y', z')$ is also a solution. In particular, the point-source solution becomes

$$\frac{1}{\sqrt{x'^2-y'^2-z'^2}}=\frac{1}{\sqrt{1-m^2}}\frac{1}{\sqrt{x^2-y^2-z^2}}$$

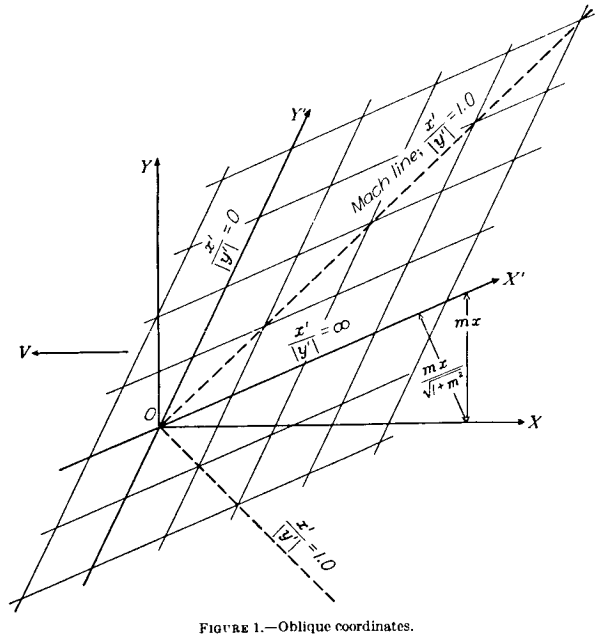

FIGURE 1.—Oblique coordinates.
$x'=x-my$
$y'=y-mx$
$z'=\sqrt{1-m^2}\,z$

Hence the integration for the effect of an inclined line of sources may be performed directly along the oblique x'-axis; thus, for $m<1.0$

$$u=I\int_0^{\xi'_1}\frac{d\xi'}{\sqrt{(x'-\xi')^2-y'^2-z'^2}}$$

$$=I\cosh^{-1}\frac{x'}{\sqrt{y'^2+z'^2}} \tag{6}$$

where ξ'_1 is the position of the last source whose Mach cone includes the point (x', y', z') and is given by

$$\xi'_1=x'-\sqrt{y'^2+z'^2}$$

When m approaches 1.0 the source line approaches coincidence with the Mach cone, corresponding to a transverse velocity component equal to the velocity of sound.

For values of m greater than 1.0 the integration yields

$$u=-Ii\cos^{-1}\frac{x'}{\sqrt{y'^2+z'^2}} \tag{7}$$

It will be seen that in this case I is imaginary.

The vertical velocity near $z=0$, which determines the shape of the boundary, may be determined by integrating u with respect to x and then differentiating the resulting velocity potential with respect to z; thus (see appendix),

$$w=\frac{\partial\phi}{\partial z}$$

$$=\frac{\partial}{\partial z}\int u\,dx$$

$$=\pm\pi\frac{I}{m}\sqrt{1-m^2} \tag{8}$$

if $z\to 0$ and $y'<0$. If $y'>0$, $w=0$. There is thus a discontinuity in the vertical velocity of the streamlines when they cross the line source at $y'=0$. For small values of I/m this discontinuity in vertical velocity agrees with the boundary condition for a simple wedge shape having a small wedge angle. (See fig. 2.)

If the source strength I is held constant and m is allowed to approach zero, the wedge angle ultimately becomes large. At $m=0$ the line source actually satisfies the boundary condition for the circular cone (reference 7), but it is found that the slope of the conical boundary does not agree with the slope of the streamlines near $z=0$ and hence the theory no longer holds. The condition $\frac{m}{I}\to 0$ thus represents the transition from an oblique airfoil to a body of revolution and will be avoided in the present analysis by restricting the formulas to flat bodies, that is, airfoils that are thin in both longitudinal and transverse section.

AIRFOIL OF WEDGE SECTION

Over the wedge section near the plane $z=0$, the formula (6) becomes simply

$$u=I\cosh^{-1}\frac{x'}{|y'|} \tag{9}$$

795249—49——2

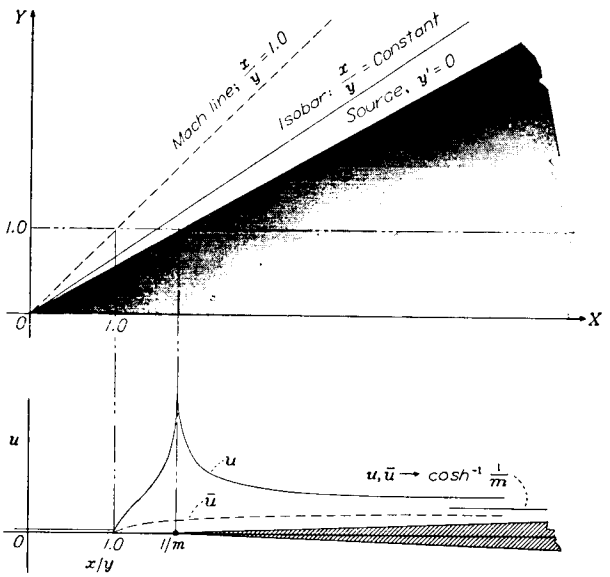

FIGURE 2.—Pressure field for oblique wedge where $m<1.0$. $\frac{\Delta p}{q}=\frac{2u}{V}$.

$$u=\cosh^{-1}\frac{x-my}{|y-mx|}$$

$$\bar{u}=\cosh^{-1}\frac{x+my}{|y+mx|}$$

where $|y'|$ denotes the absolute magnitude of $y'=y-mx$. The pressure is thus constant along the radial lines

$$\frac{x'}{y'}=\text{Constant} \tag{10}$$

and is conveniently represented by the variation along a line parallel to the X-axis. Figure 2 shows the oblique wedge-shape figure corresponding to a line source with $m<1.0$. In this case the pressure field is confined to the interior of the Mach cone $x^2-y^2-z^2=x'^2-y'^2-z'^2=0$ and the theory, unlike the Ackeret theory, indicates a stagnation point along the leading edge. (Actually, of course, the thin-airfoil theory shows an infinite velocity at such points, but this is to be interpreted as a velocity of the order of magnitude of the flight velocity V. The pressure to be expected along the leading edge is the stagnation pressure corresponding to the transverse velocity component.)

Given $\frac{dz}{dx}=\frac{w}{V}$, the wedge angle measured in downstream sections, the source strength must vary with m according to

$$I=\frac{V}{\pi}\frac{m}{\sqrt{1-m^2}}\frac{dz}{dx} \tag{11}$$

(from equation (7)). Then

$$\frac{\Delta p}{q}=\frac{2}{\pi}\frac{dz}{dx}\frac{m}{\sqrt{1-m^2}}\cosh^{-1}\frac{x'}{|y'|} \tag{12}$$

If m exceeds 1.0, the leading edge of the airfoil will lie outside the Mach cone. In this case

$$\frac{\Delta p}{q}=\frac{2}{\pi}\frac{dz}{dx}\frac{m}{\sqrt{m^2-1}}\cos^{-1}\frac{x'}{\sqrt{y'^2+z'^2}} \tag{13}$$

In the region between the leading edge and the Mach cone $\cos^{-1}\frac{x'}{|y'|}$ is constant and equal to π; hence the pressure in this region is constant, that is,

$$\frac{\Delta p}{q}=2\frac{dz}{dx}\frac{m}{\sqrt{m^2-1}} \tag{14}$$

Figure 3 illustrates this result.

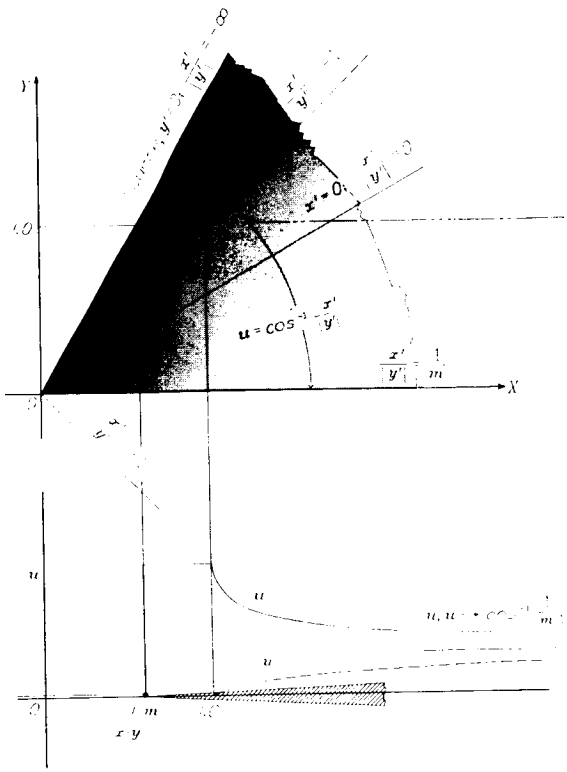

FIGURE 3.—Pressure field for oblique wedge where $m>1.0$. $\frac{\Delta p}{q}=\frac{2u}{V}$.

If $m\to\infty$ a semi-infinite airfoil with its leading edge at right angles to the direction of flight is obtained; here

$$\frac{x-my}{\sqrt{(y-mx)^2+(1-m^2)z^2}}=\frac{-y}{\sqrt{x^2-z^2}} \tag{15}$$

and $\frac{\Delta p}{q}=2\frac{dz}{dx}$ wherever $y>\sqrt{x^2-z^2}$. This value agrees with the Ackeret theory.

AIRFOILS BOUNDED BY PLANE SURFACES

The distribution of pressure over symmetrical airfoils bounded by plane surfaces can be obtained by superimposing the pressure fields for several line sources and sinks. This superposition is greatly simplified by the conical form of the pressure field for each single line source. Because of this form, the whole distribution in the plane $z=0$ is, in effect, represented by a single curve. If the velocity field for a line source beginning at the origin (equation (6)) is denoted by u and that beginning at $x=-1$ is denoted by u_{-1}, and so forth, the sum

$$u_{-1}-u_{+1}$$

represents the velocity over a plate of uniform thickness having a beveled leading edge of constant width. (See fig. 4.) Similarly

$$u_{-1}-2u+u_{+1}$$

represents the pressure field for an airfoil having diamond-shape cross sections.

The superposition required for several sources or sinks can be accomplished by manipulation of a single curve if it is remembered that u is a function of the ratio x/y. Figure 4 illustrates this process for a source and a sink. In terms of the ratio x/y the separation of source and sink and hence the scale of the chord length continually diminishes with increasing distance from the root section.

At large distances from the vertex ($x'\to\infty$) the expression (for $m<1.0$)

$$u_{-1}-u_{+1}\propto \cosh^{-1}\frac{x'+1}{|y'-m|}-\cosh^{-1}\frac{x'-1}{|y'+m|} \tag{16}$$

is found to approach the value

$$\log\frac{y'+m}{y'-m}=2Q_0\left(\frac{y'}{m}\right) \tag{17}$$

where Q_0 is the Legendre function. (See reference 7.)

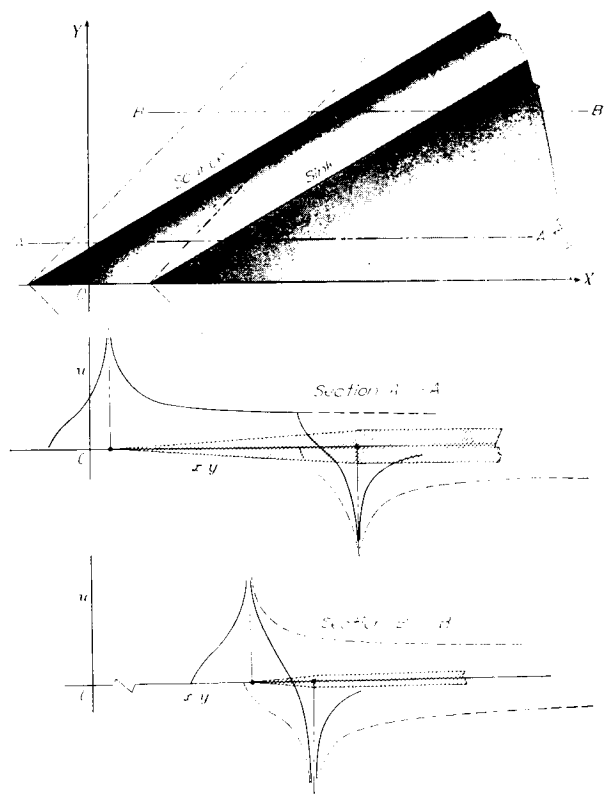

FIGURE 4. Superposition of source and sink to obtain plate with beveled edge.

In the thin-airfoil theory for subsonic speeds it can be shown that if

$$w \propto P_n(x)$$

$$\propto V\frac{dz}{dx} \tag{18}$$

then

$$u \propto Q_n(x) \tag{19}$$

since Neumann's formula (reference 8, p. 116)

$$Q_n = \frac{1}{2}\int_{-1}^{+1} \frac{P_n(\xi)}{(x-\xi)}\, d\xi \tag{20}$$

may be interpreted as the integration for the velocity distribution due to an array of sources of strength

$$w\, d\xi = P_n(\xi)\, d\xi$$

along the chord of the airfoil. The expression $Q_0 \frac{y'}{m}$ of equation (17) thus represents the subsonic pressure distribution over the beveled edge.[1]

At the root section ($y=0$) only the forward source need be considered since the airfoil surface is ahead of the Mach cone originating at the rear source. Here

$$u_{-1} - u_{+1} \propto \cosh^{-1}\frac{x+1-my}{|y-m(x+1)|}$$

$$\propto \cosh^{-1}\frac{1}{m} \tag{21}$$

and the pressure over the root section is thus constant, as given by the Ackeret theory, but is altered in magnitude by the obliquity.

The oblique wing lying behind the Mach lines thus shows the Ackeret type of pressure distribution over the foremost section and a progressive change along the span from this distribution to the subsonic type of distribution. Since the subsonic type of distribution shows no pressure drag, there is a continuous falling off of the pressure drag with increasing distance from the root section. The pressure drag of the oblique wing thus arises chiefly on the foremost section, and it follows that the drag coefficient of the wing as a whole diminishes with increasing aspect ratio. It will be shown subsequently that the effect of cutting the wing off along a line y=Constant to produce a downstream tip causes a reduction of the pressure drag on the adjacent sections; and if the aspect ratio is sufficiently high, the pressure drag in the region of the downstream tip may actually be negative.

If the wing lies ahead of the Mach lines ($m>1.0$) the Ackeret type of pressure distribution occurs and a pressure drag arises over the whole length. In this case both u and w are constant over the beveled part at a distance from the origin.

[1] Similarly if $P_n(\xi)\, d\xi$ is taken as the chordwise distribution of vorticity.

$$u \propto P_n(x)$$

$$w \propto Q_n(x)$$

$$\propto \frac{dz}{dx}$$

The first of this series of airfoils is the camber shape curved to support a uniform load.

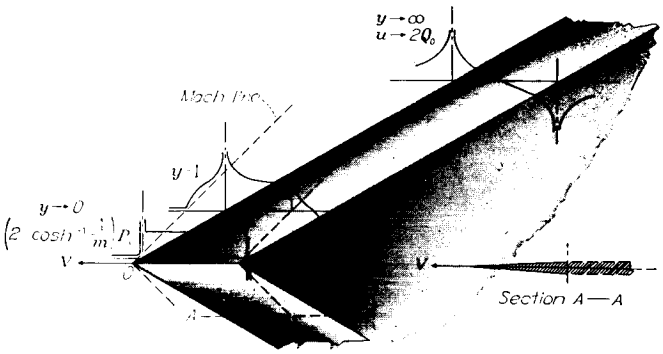

FIGURE 5.—Variation of pressure distribution along span of sweptback wing. m=tan 30.°

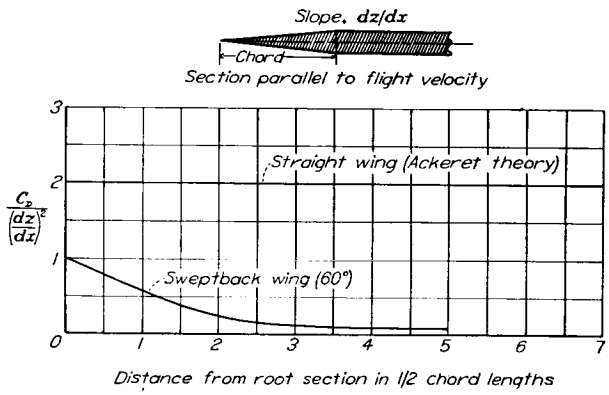

FIGURE 6.—Variation of drag coefficient with distance from root section for sweptback wing. Wedge section; M=1.4.

The treatment thus far applies to semi-infinite cylindrical wings having root sections near the origin. A complete sweptback wing may be obtained by the addition of a symmetrical or conjugate arrangement of source lines below the X-axis. Values of u for this conjugate arrangement may be denoted by $\overline{u}$. Figures 2 and 3 show $\overline{u}$ for a single inclined source and figure 5 shows calculated pressure distributions at several sections along the span for a complete sweptback airfoil having beveled sections. The addition of the conjugate source lines doubles the pressure at the root section, but this interference effect falls off rapidly along the span. It is noted that, as in figure 4, the most significant change in pressure distribution occurs along the expansion wave originating at the trailing edge of the root section. Figure 6 shows the variation in pressure drag along the span for this airfoil obtained by integrating the chordwise components of pressure at the different sections.

The addition of a reversed source-sink distribution having its origin displaced to a point 0_2 (see fig. 7) will show the effect of cutting the wing off in a direction parallel to the direction of flight. It will be evident that the effect of such a tip is characterized by the subtraction of the curves $\overline{u}$ and is limited to the area lying within the Mach cone which originates at the tip. It is interesting to note that pressure distributions of the Ackeret type, except reversed in sign, are added near the tip; hence, cutting the tip off in this manner reduces the drag of adjacent sections.

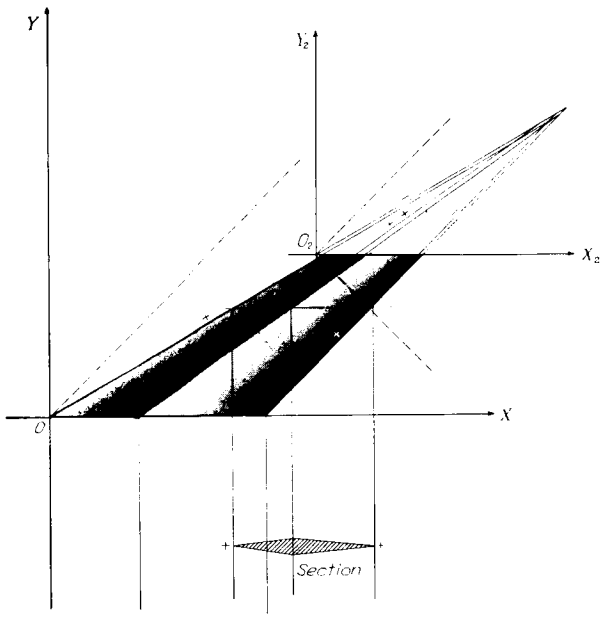

FIGURE 7.—Addition of reversed source-sink distribution to produce tip.

Figure 8 shows the pressure distributions over a rectangular airfoil having a leading edge at right angles to the flow. In the triangular area ahead of the Mach cones originating at the tips the pressure is constant, as given by the Ackeret theory, whereas behind these Mach cones the pressure drops sharply.

AIRFOIL OF BICONVEX SECTIONS

Curved surfaces require a continuous distribution of sources and sinks alined with the generators of the surface. Each elementary source line causes an infinitesimal change in direction of the surface and hence the slope at any point may be obtained by adding up the effects of all sources ahead of that point. Thus

$$\frac{dz}{dx}=\frac{\pi}{V}\int_{x_0}^{x}\frac{\sqrt{1-m^2}}{m}\frac{dI}{d\xi}\,d\xi \tag{22}$$

or

$$\frac{d^2z}{dx^2}=\frac{\pi}{V}\frac{\sqrt{1-m^2}}{m}\frac{dI}{dx}$$

For airfoils of constant chord, m will be a constant and the integrations can be performed without difficulty. The simplest case is that of constant curvature, which leads to profiles formed from circular arcs.

In order to obtain a biconvex profile, it is necessary to introduce finite sources of strength sufficient to form the desired angle of intersection of the arcs at the leading and trailing edges, together with a uniform distribution of sinks along the chord line between the two sources. These profiles thus require a uniform distribution of sources or sinks, which may be obtained by integrating the elementary solution for the line source (equation (6)). The resulting solution may be denoted by $\frac{1}{D}u$ and is, for $m<1$,

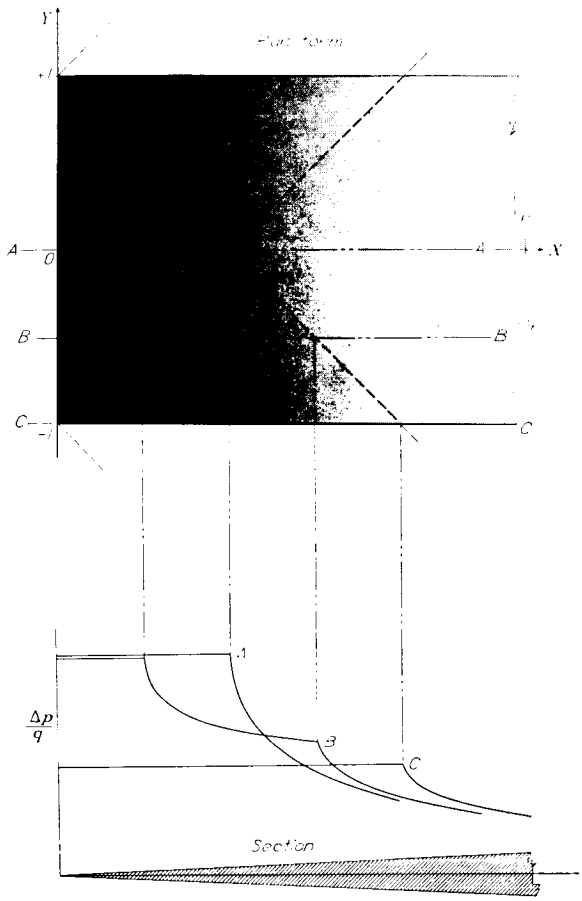

FIGURE 8.—Pressure distribution over airfoil of rectangular plan form.
$\frac{\Delta p}{q}=\sin^{-1}\frac{1-y}{x}+\sin^{-1}\frac{1+y}{x}$.

$$\frac{1}{D}u=I\int_{|y|}^{x}\cosh^{-1}\frac{\xi-my}{|y-m\xi|}\,d\xi$$
$$=I\left(\frac{\sqrt{1-m^2}}{m}\,y\cosh^{-1}\frac{x}{|y|}-\frac{1}{m}\,y'\cosh^{-1}\frac{x'}{|y'|}\right) \tag{23}$$

Inasmuch as the elementary solution u is of the form $f\left(\frac{x}{y}\right)$, the integrated solution appears in the form

$$\frac{1}{D}u=yg\left(\frac{x}{y}\right)$$

and will be conveniently represented by a curve typical of all spanwise stations, namely,

$$\frac{1}{yD}u=g\left(\frac{x}{y}\right)$$

For a closed profile intersecting the X-axis at the points ± 1 there is obtained

$$\Sigma u=u_{-1}+u_{+1}-y\left(\frac{1}{yD}u_{-1}-\frac{1}{yD}u_{+1}\right) \tag{24}$$

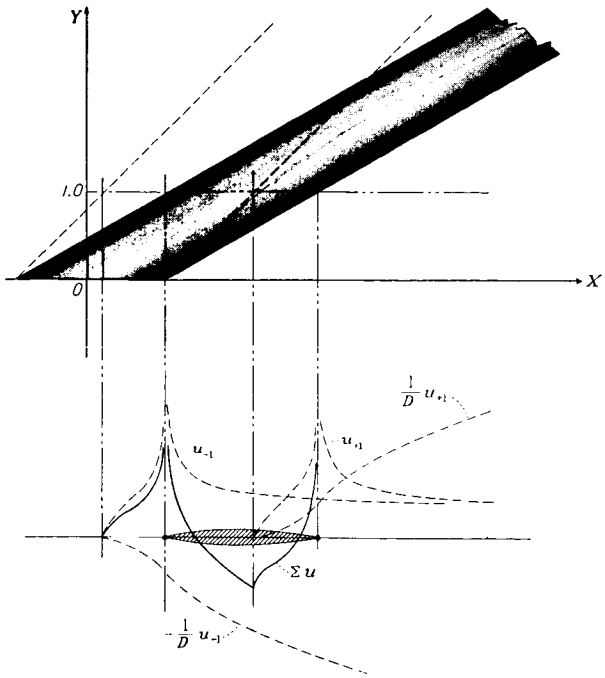

FIGURE 9.—Pressure distribution over wing of biconvex section. $\frac{\Delta p}{q}=\frac{2\Sigma u}{V}$.

This superposition may be accomplished conveniently by transposing and adding the typical curves u and $\frac{1}{yD}u$. (See fig. 9.)

It will be found that if m is less than 1.0 the velocity distribution approaches, with increasing distance from the root section, the form given by the subsonic-flow theory for an airfoil of biconvex section, that is,

$$\left.\begin{aligned} w &\propto P_1\left(\frac{y'}{m}\right) \\ u &\propto Q_1\left(\frac{y'}{m}\right) \end{aligned}\right\} \tag{25}$$

At the root section, however, the form is simply that given by the Ackeret theory for a straight airfoil although the values are reduced in magnitude by the factor $\frac{m}{\sqrt{1-m^2}}\cosh^{-1}\frac{1}{m}$.

The pressure distribution and the variation of drag along the span for the bilaterally symmetrical wing are shown in figures 10 and 11.

CONICAL SURFACES

For tapered airfoils both m and I will be functions of ξ. It is easily seen that closed surfaces can be obtained only if the relation between m and ξ is such that the line sources have a common point of intersection, as in figure 7. If this point is denoted by x_0, y_0

$$m=\frac{y_0}{x_0-\xi}$$

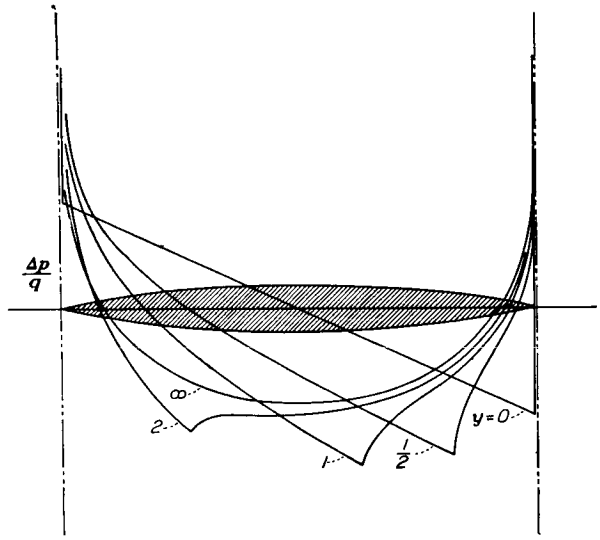

FIGURE 10.—Pressure distribution at different points along span. Biconvex wing.

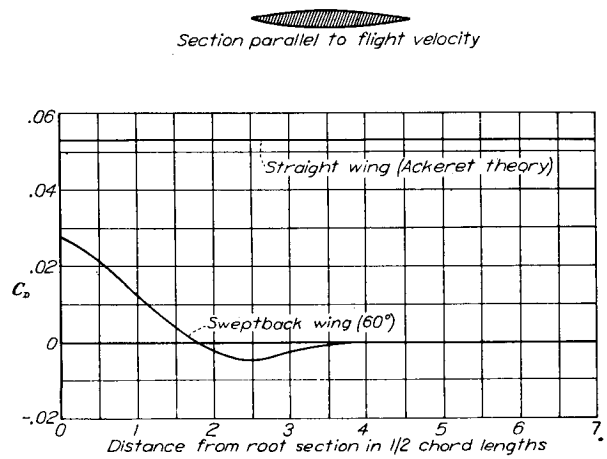

FIGURE 11.—Variation of drag coefficient with distance from root section for wings of biconvex section. $M=1.4$; $\frac{t}{c}=10$ percent.

The surface obtained is one generated by a line passing through the fixed point x_0, y_0 and hence is a conical surface.

The pressure over the tapered airfoil requires the integration of

$$u=\int_{\xi_1}^{x-y}\left[\cosh^{-1}\frac{x-\xi-my}{|y-m(x-\xi)|}\right]\frac{dI}{d\xi}\,d\xi$$
$$=\int_{\xi_1}^{x-y}u_\xi\frac{dI}{d\xi}d\xi$$

where ξ_1 is the location of the vertex of the airfoil and

$$\frac{dI}{d\xi}=\frac{V}{\pi}\frac{m}{\sqrt{1-m^2}}\frac{d^2z}{d\xi^2}$$

In conclusion it should be noted that the pressures have been derived for an airfoil transformed according to equations (2). The pressures at corresponding points of the original airfoil are to be obtained by dividing by M^2-1.

LANGLEY MEMORIAL AERONAUTICAL LABORATORY,
NATIONAL ADVISORY COMMITTEE FOR AERONAUTICS,
LANGLEY FIELD, VA., *May 23, 1946.*

APPENDIX

EVALUATION OF INTEGRAL OF EQUATION (8)

For $m<1.0$ the disturbance is zero outside the Mach cone and the range of integration should be extended only from $x_i=\sqrt{y^2+z^2}$ to x, that is,

$$\int_{-\infty}^{x} u\,dx=\int_{\sqrt{y^2+z^2}}^{x}\cosh^{-1}\frac{x'}{\sqrt{y'^2+z'^2}}\,dx \tag{A1}$$

(for unit source strength). Furthermore,

$$\frac{\partial}{\partial z}\int_{\sqrt{y^2+z^2}}^{x} u\,dx=\int_{\sqrt{y^2+z^2}}^{x}\frac{\partial u}{\partial z}\,dx \tag{A2}$$

since the integrand is zero at the lower limit. Now

$$\frac{\partial}{\partial z}\cosh^{-1}\frac{x'}{\sqrt{y'^2+z'^2}}=\frac{-x'z'\sqrt{1-m^2}}{(y'^2+z'^2)\sqrt{x'^2-y'^2-z'^2}} \tag{A3}$$

and hence the integral

$$w=\int_{\sqrt{y^2+z^2}}^{x}\frac{-x'z'\sqrt{1-m^2}}{(y'^2+z'^2)\sqrt{x'^2-y'^2-z'^2}}\,dx \tag{A4}$$

must be evaluated.

First it is noted that the integral vanishes with z except in the neighborhood of the Mach cone ($\sqrt{x'^2-y'^2-z'^2}=0$) and in the neighborhood of the line source ($y'=0$). Near the Mach cone $y'^2+z'^2\to x'^2$, so that

$$\int\frac{-x'z'dx}{(y'^2+z'^2)\sqrt{x'^2-y'^2-z'^2}}\to\int\frac{-z\,dx}{x'\sqrt{x^2-y^2-z^2}} \tag{A5}$$

Since the latter integral approaches zero with z, there is no contribution to equation (A4) in the region of the Mach cone. On the other hand, near the line source $y'\to 0$ and $\sqrt{x'^2-y'^2-z'^2}\to x'$; hence, as $z'\to 0$,

$$\int\frac{-x'z'dx}{(y'^2+z'^2)\sqrt{x'^2-y'^2-z'^2}}\to\int\frac{-z'}{y'^2+z'^2}\,dx=$$

$$\frac{1}{m}\tan^{-1}\frac{y'}{z'}+\text{Constant} \tag{A6}$$

The value of the integral changes from 0 to π in crossing over the line source at $y'=0$ and is positive or negative depending on whether z' approaches zero from the positive or negative side of the xy-plane. Hence

$$w=\pm\frac{\pi}{m}\sqrt{1-m^2}$$

If m is greater than 1.0,

$$u=\cos^{-1}\frac{x'}{\sqrt{y'^2+z'^2}} \tag{A7}$$

and the flow disturbance extends outside the Mach cone to a region bounded by plane waves extending from the line source and tangent to the Mach cone. (See fig. 12.) The equation of these planes can be easily shown to be $y'^2+z'^2=0$; hence for $m>1.0$ the lower limit of integration is given by

$$y'^2+z'^2=0$$

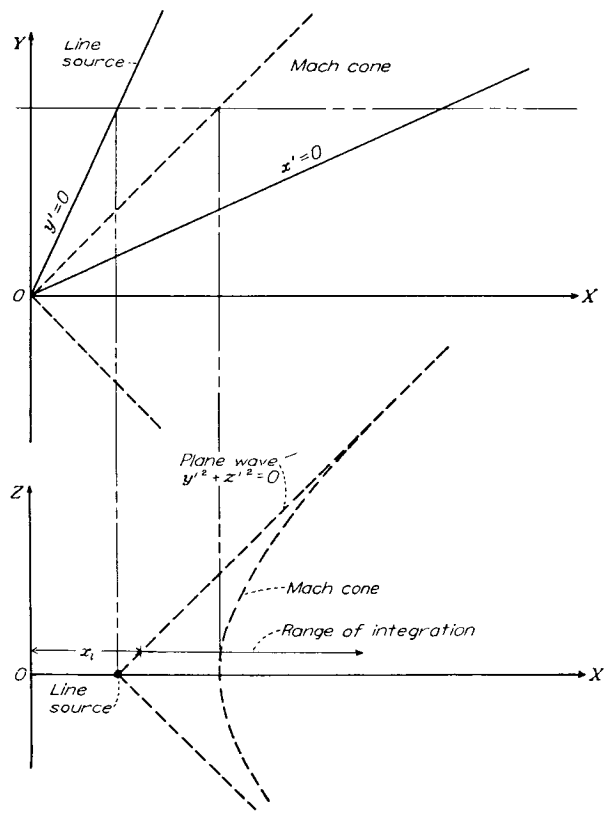

FIGURE 12.—Information pertinent to evaluation of equation (8) for $m>1.0$. (See appendix.)

or

$$x_1=\frac{y-\sqrt{m^2-1}z}{m} \tag{A8}$$

Then

$$\frac{\partial}{\partial z}\int_{x_1}^{x} u\,dx=\frac{\partial}{\partial z}\int_{x_1}^{x}\cos^{-1}\frac{x'}{\sqrt{y'^2+z'^2}}\,dx \tag{A9}$$

In this case u does not go to zero at the lower limit but is equal to π. In all other regions, however, the integral approaches zero uniformly with z as in the preceding case; hence

$$\begin{aligned} w&=\frac{\partial}{\partial z}\int_{x_1}^{x} u\,dx \\ &=u_1\frac{\partial x_1}{\partial z} \\ &=\pm\frac{\pi}{m}\sqrt{m^2-1} \end{aligned} \tag{A10}$$

as before.

REFERENCES

1. Jones, Robert T.: Wing Plan Forms for High-Speed Flight. NACA TN No. 1033, 1946.
2. Ackeret, J.: Air Forces on Airfoils Moving Faster Than Sound. NACA TM No. 317, 1925.
3. Jones, Robert T.: Properties of Low-Aspect-Ratio Pointed Wings at Speeds below and above the Speed of Sound. NACA Rep. No. 835, 1946.
4. Busemann, Adolf: Infinitesimale kegelige Überschallströmung. Sonderdruck aus dem Jahrb. 1942/43 der Deutschen Akademie der Luftfahrtforschung. (Available as NACA TM No. 1100, 1947.)
5. Puckett, Allen E.: Supersonic Wave Drag of Thin Airfoils. Jour. Aero. Sci., vol. 13, no. 9, Sept. 1946, pp. 475–484.
6. Prandtl, L.: General Considerations on the Flow of Compressible Fluids. NACA TM No. 805, 1936.
7. Von Kármán, Theodor, and Moore, Norton B.: Resistance of Slender Bodies Moving with Supersonic Velocities, with Special Reference to Projectiles. Trans. A. S. M. E., vol. 54, no. 23, Dec. 15, 1932, pp. 303–310.
8. Jahnke, Eugene, and Emde, Fritz: Tables of Functions with Formulae and Curves. Rev. ed., Dover Publications (New York), 1943, pp. 107–117.

REPORT NO. 902

SUBSONIC FLOW OVER THIN OBLIQUE AIRFOILS AT ZERO LIFT

Robert T. Jones

Ames Aeronautical Laboratory

1948

REPORT No. 902

SUBSONIC FLOW OVER THIN OBLIQUE AIRFOILS AT ZERO LIFT

By Robert T. Jones

SUMMARY

A previous report gave calculations for the pressure distribution over thin oblique airfoils at supersonic speed. The present report extends the calculations to subsonic speeds.

It is found that the flows again can be obtained by the superposition of elementary conical flow fields. In the case of the swept-back wing the pressure distributions remain qualitatively similar at subsonic and supersonic speeds. Thus a distribution similar to the Ackeret type of distribution appears on the root sections of the swept-back wing at $M=0$. The resulting positive pressure drag on the root section is balanced by negative drags on outboard sections.

INTRODUCTION

So far as is known, attempts to extend airfoil pressure-distribution calculations to three-dimensional flow have been confined to cases of thin lifting surfaces. It has generally been assumed that the component of the pressure distribution arising from the thickness of the airfoil will be but little affected by the finite span, or aspect ratio, of the wing. This supposition is borne out by the known incompressible-flow solutions for flat ellipsoids. These solutions show that the usual variations of aspect ratio produce small effects.

Compressible-flow theory shows, however, that the effects of plan form become more pronounced at higher speeds. The theory indicates a progressive reduction of the equivalent aspect ratio as the Mach number approaches 1.0. Hence at these speeds the three-dimensional character of the flow can no longer be neglected. Of particular interest are the deviations from two-dimensional flow near the root sections of a swept-back wing, since the adverse effects of compressibility may arise first in this region.

In the present report three-dimensional flows are obtained from a distribution of "pressure sources" in the chord plane of the airfoil. The shapes thus obtained are symmetrical airfoils at zero lift. The calculations are simplified by considering airfoils composed of conical or cylindrical surfaces. In these cases the sources can be arranged into lines of uniform strength following the generators of the surface. The relation between the strengths of the line sources and the shape of the airfoil is the same as in reference 1; that is, each line source produces a deflection of the streamlines crossing over the source. The pressure field of the line source again can be represented by systems of straight rays of equal pressure (isobars) radiating from the ends of the line source.

843314—49

In general, the present development follows closely that of reference 1 and the reader should consult that report for additional details of the method. The solutions are given explicitly for $M=0$ but are extended to other Mach numbers by the well-known Prandtl transformation.

THE OBLIQUE LINE SOURCE

It is well known that an individual velocity component of a potential flow will satisfy the same differential equation as the potential. In the approximation of the thin-airfoil theory the pressure depends only on the individual component u, that is,

$$\frac{\Delta p}{q}=\frac{2u}{V} \tag{1}$$

while the slope of the surface depends only on the individual component w, that is

$$\frac{dz}{dx}=\frac{w}{V} \tag{2}$$

(See appendix for symbols.) Hence in the thin-airfoil theory it is often more convenient to deal directly with the velocities u and w as solutions of Laplace's equation than to derive these components from a velocity potential φ.

Since u is proportional to the pressure, a solution of Laplace's equation can represent directly the pressure distribution, hence the term "pressure potential." In this terminology, the fundamental solution

$$u=\frac{1}{r}=\frac{1}{\sqrt{x^2+y^2+z^2}} \tag{3}$$

represents a point source of pressure rather than a point source of fluid.

To get the effect of a row of sources, or a line source, along the x axis between the points a and b, it is necessary to integrate equation (3):

$$u=\int_a^b \frac{d\xi}{\sqrt{(x-\xi)^2+y^2+z^2}}$$

$$=\sinh^{-1}\frac{x-b}{\sqrt{y^2+z^2}}-\sinh^{-1}\frac{x-a}{\sqrt{y^2+z^2}} \tag{4}$$

The pressure field of the finite line source thus consists of the sum of two conical pressure fields radiating from the ends of the line source. (See fig. 1.) In the supersonic case (reference 1), the radial isobars forming the conical field were

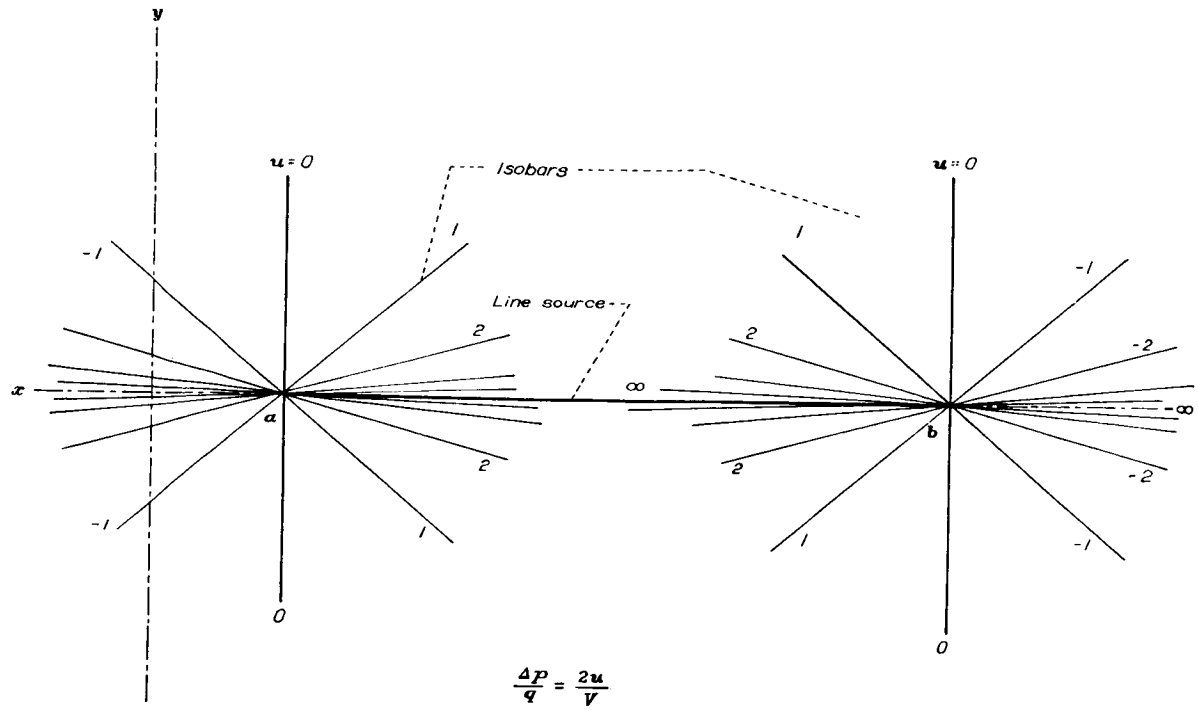

FIGURE 1.—Pressure field for line source of length $(b-a)$.

confined to the downstream Mach cone. Here, however, the isobars extend over the whole space.[1]

If the direction of flight is along the axis of the source (x axis), the flow will satisfy the boundary condition for a body of revolution. However, if the line source is turned out to a position oblique to the stream, the boundary shape will be distorted and, if the angle of obliquity is large enough to place the line source well outside the diameter of the original body, the figure formed will be an oblique wedge. The nose angle of the wedge is formed where the streamlines of the main flow cross the line source.

At supersonic speeds the expression for the oblique line source was obtained by applying an equivalent of the Lorentz transformation, for which the wave equation is invariant. The equivalent transformation for Laplace's equation is a rotation of the axes, given by

$$x' = x + my$$
$$y' = y - mx$$
$$z' = z\sqrt{1+m^2}$$

where m is the slope of the new axes relative to the old. (Note that a change of scale is admitted for convenience.) The geometry of the pressure field relative to the line source is not altered in any way by this rotation and the isobars behave as though they were rigidly attached to the ends of the source. For a line source with one end at the origin, we have

$$u = \sinh^{-1}\frac{x'}{\sqrt{(y')^2+(z')^2}} \tag{5}$$

This field is illustrated in figure 2 for the plane $z=0$. As $m\to\infty$ the x and y axes interchange and there is obtained

$$u = \sinh^{-1}\frac{y}{\sqrt{x^2+z^2}} \tag{6}$$

for a line source along y.

The vertical velocity w near $z=0$, which determines the shape of the boundary, may be found by integrating u with respect to x and then differentiating the resulting velocity potential with respect to z.

$$w = \frac{\partial\phi}{\partial z} = \frac{\partial}{\partial z}\int_{-\infty}^{x} u\,dx \tag{7}$$

Evaluation of this integral for the overlapping fields from two ends of a line source gives

$$w = \pm 2\pi\frac{\sqrt{1+m^2}}{m} \tag{8}$$

over the area of the xy plane behind the line source.

[1] The conical pressure field for either the subsonic or the supersonic line source may be obtained directly from the general solutions of Laplace's equations of zero degree in x, y, z given by W. F. Donkin. (See reference 2, page 357.) The general solution is

$$u = f\left(\frac{y \pm iz}{x+\sqrt{x^2+y^2+z^2}}\right)$$

The solution corresponding to the subsonic line source is

$$u = -R.P.\log\frac{y+iz}{x+\sqrt{x^2+y^2+z^2}} = \sinh^{-1}\frac{x}{\sqrt{y^2+z^2}}$$

while the field for the supersonic source is given by

$$u = -R.P.\log\frac{y+iz}{x+\sqrt{x^2-y^2-z^2}} = \cosh^{-1}\frac{x}{\sqrt{y^2+z^2}}$$

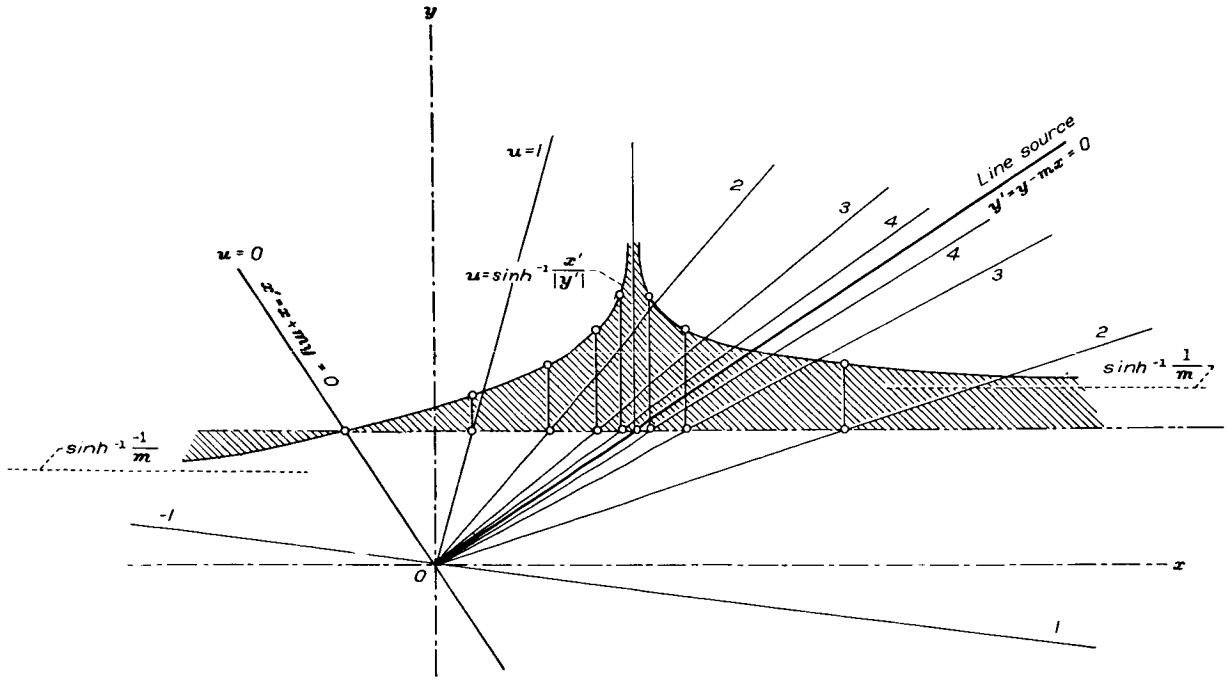

FIGURE 2.—Pressure field due to one end of oblique line source.

The figure formed by the streamlines crossing a line source is thus a wedge-shaped body having an oblique leading edge and extending indefinitely downstream. It is evident from equation (3) that the infinitely wide wedge cannot be treated in subsonic flow, since it creates an infinite pressure disturbance at all points.

The slope of the wedge surface away from the chord plane is given by

$$\frac{dz}{dx}=\frac{w}{V} \tag{9}$$

With this relation and equation (8) the pressure coefficient near the plane $z=0$ may be expressed in terms of the slope

$$\frac{\Delta p}{q}=\frac{1}{\pi}\frac{m}{\sqrt{1+m^2}}\frac{dz}{dx}\left(\sinh^{-1}\frac{x'-b'}{|y'|}-\sinh^{-1}\frac{x'-a'}{|y'|}\right) \tag{10}$$

where $|y'|$ indicates the absolute magnitude of y'. Following the thin-airfoil theory, the pressure over the chord plane ($z\to 0$) is taken as the pressure over the actual airfoil surface.

AIRFOILS BOUNDED BY PLANE SURFACES

It was seen that the effect of a line source in the pressure field is to cause a deflection of the streamlines crossing the source. The deflection thus produced is equal and opposite at points above and below the chord plane, so that the source spreads the streamlines apart. If the source is followed by a sink of equal strength, an equal opposite deflection of the streamlines will occur as they cross over the sink. The figure formed by the streamlines near the plane $z=0$ will thus be a plate of uniform thickness with a beveled leading edge.[2] (See fig. 3.)

[2] According to the thin-airfoil theory the thickness of the figure ends abruptly at the ends of the source lines. A more exact consideration would be expected to show some rounding at the tips of the wedge as indicated in figure 3.

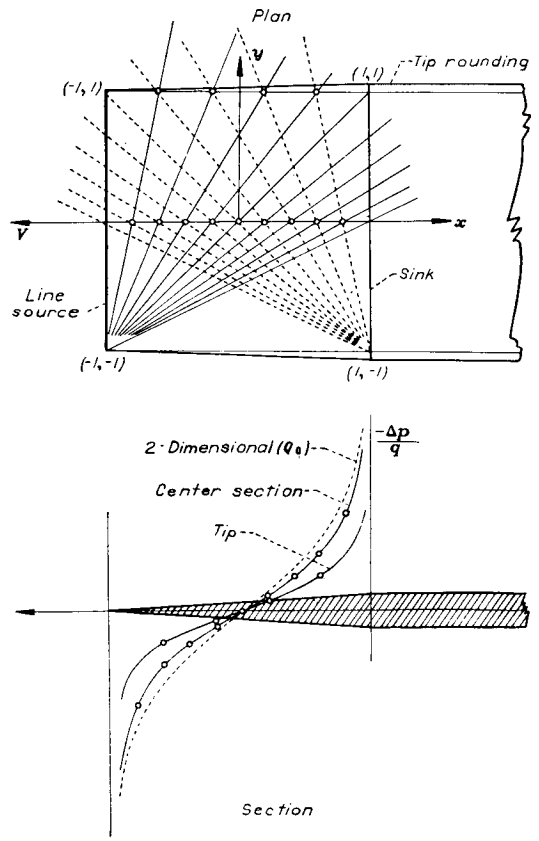

FIGURE 3.—Construction of the pressure distribution over a beveled leading edge.

The pressure distribution over such a beveled edge may be obtained very simply by superimposing the pressures laid off on radial isobars originating from the four corners of the bevel. Figure 3 illustrates this process for a bevel having a square plan form. Only isobars from one tip are shown because of the symmetry of the figure.

In figure 3, the line source and the line sink are parallel to the y axis, hence

$$u=\sinh^{-1}\frac{y+1}{|x+1|}-\sinh^{-1}\frac{y-1}{|x+1|}-\sinh^{-1}\frac{y+1}{|x-1|}+\sinh^{-1}\frac{y-1}{|x-1|} \tag{11}$$

It can be seen that if the aspect ratio of the figure is increased to a large value the ends of the line sources will be separated by a great distance and the isobars in intermediate regions will approach parallel straight lines, hence the flow field approaches a cylindrical or two-dimensional form. At the same time the arguments $y\pm1/|x\pm1|$ in equation (11) become $y\pm\eta/x\pm1$ and η takes on very large values so that

$$\sinh^{-1}\frac{y\pm\eta}{|x\pm1|}\rightarrow\pm\log 2\frac{y\pm\eta}{|x\pm1|}$$

and equation (11) is found to approach the Legendre function Q_0, that is

$$u=2\log\frac{|x-1|}{|x+1|}=-4\,Q_0(x) \tag{12}$$

(See reference 3, p. 110.)

This expression when combined with equation (8) agrees with the two-dimensional potential function for the wedge, that is,

$$-(u-iw)=4\,Q_0(x)\pm2\pi i\,P_0(x) \tag{13}$$

(See fig. 4.)

The isobars at right angles to the axis of the line source are lines of zero pressure, hence the rays originating at the tip of a rectangular wing contribute nothing to the pressure distribution at this tip. The whole pressure distribution at one tip is thus obtained by considering only those isobars radiating from the opposite tip. It is evident that in the case of a long narrow rectangular wing the pressures at either tip will be approximately one-half the pressures over the middle portion of the wing.

In case the wing is oblique the tip sections will no longer be at right angles to the axes of the source lines and the rays originating from the adjacent ends of the source lines *will* contribute to the pressure over the tip. It can be shown that this component of the tip pressure distribution is similar in form to the Ackeret type of distribution, that is, the pressure at any point of the surface is proportional to the slope of the surface at that point.

Consider first the sloping surface formed by a pair of oblique source-sink lines. The tip section lies along the lines of constant pressure of magnitude proportional to $\sinh^{-1}1/m$. Between the source and sink the pressures are additive, so that

$$\frac{\Delta p}{q}=\frac{2}{\pi}\frac{m}{\sqrt{1+m^2}}\frac{dz}{dx}\sinh^{-1}\frac{1}{m} \tag{14}$$

Ahead of or behind this section the pressures cancel.

In case of a curved airfoil surface the chord can be divided into elements composed of source-sink pairs, the strengths of which are proportional to the slope of the surface at the point in question. Each pair then contributes a pressure proportional to the local slope and contributes no pressure at other points. Hence, equation (14) applies when dz/dx is variable along the chord.

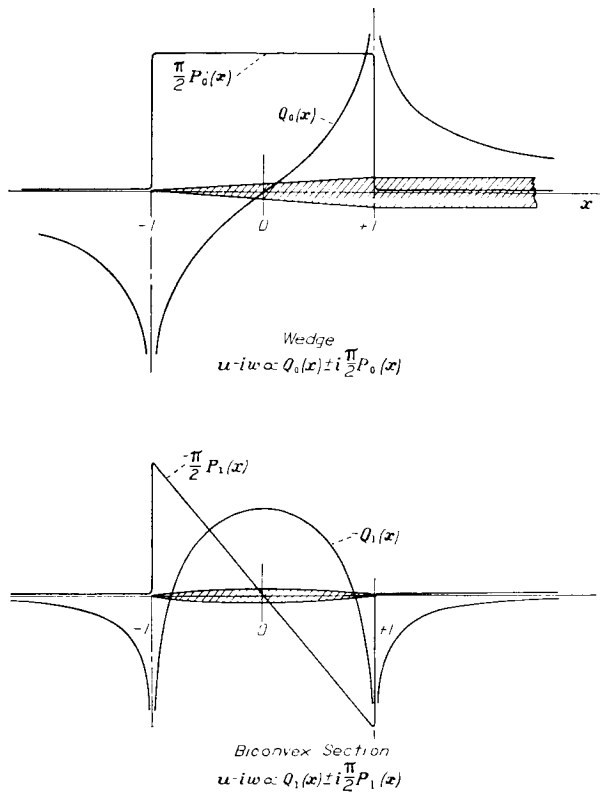

FIGURE 4.—Two-dimensional velocity functions for wedge and biconvex sections.

The foregoing arguments of course apply only at the tip section of the oblique wing. At some distance from the tip section the overlapping isobars radiating from the tip again produce a quasi-cylindrical pressure field as in the case of the rectangular wing. Thus the resultant pressure distribution at either tip of a long oblique wing consists of two components, one given by equation (14) and of the Ackeret type while the other component is equal to one-half the normal two-dimensional pressure distribution associated with the airfoil section.

Figure 5 shows the pressures over a beveled-edge profile having 45° sweepback. The pressure distribution over the root section is given by

$$\frac{\Delta p}{q}=-\frac{4}{\pi}\frac{m}{\sqrt{1+m^2}}\frac{dz}{dx}\left[Q_0(x)-\sinh^{-1}\frac{1}{m}P_0(x)\right] \tag{15}$$

at a great distance from either root or tip by

$$\frac{\Delta p}{q}=\frac{-4}{\pi}\frac{m}{\sqrt{1+m^2}}\frac{dz}{dx}Q_0(x) \tag{16}$$

and at the tip by

$$\frac{\Delta p}{q}=\frac{-2}{\pi}\frac{m}{\sqrt{1+m^2}}\frac{dz}{dx}\left[Q_0(x)+\sinh^{-1}\frac{1}{m}P_0(x)\right] \tag{17}$$

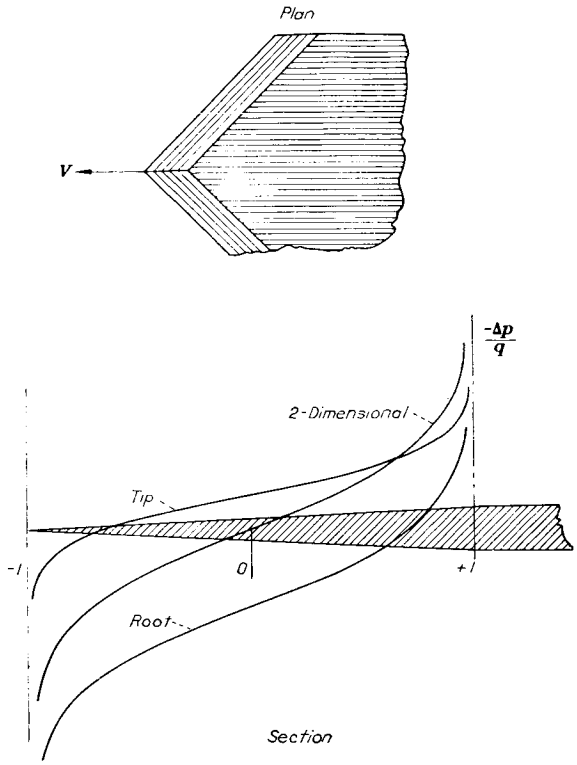

FIGURE 5.—Pressure distribution over beveled edge with 45° sweepback.

To take account of the effect of compressibility we make use of the Prandtl transformation, increasing both the x dimensions and the pressure coefficients by the factor $\frac{1}{\sqrt{1-M^2}}$. Replacing m by $\sqrt{1-M^2}\cot\Lambda$, where Λ is the angle of sweepback, equation (16) reduces to

$$\frac{\Delta p}{\rho/2(V\cos\Lambda)^2}=\frac{-4}{\pi}\frac{1}{\sqrt{1-(M\cos\Lambda)^2}}\frac{dz}{d(x\cos\Lambda)}Q_0(x) \tag{18}$$

Thus, at a great distance from either root or tip, the pressures follow a variation indicated by the normal component of velocity $V\cos\Lambda$.

At the root section, a component representing the Ackeret type of pressure distribution is added to equation (18). This component is

$$\frac{4}{\pi}\frac{1}{\sqrt{1-(M\cos\Lambda)^2}}\frac{dz}{d(x\cos\Lambda)}\sinh^{-1}\left(\frac{1}{\sqrt{1-M^2}\cot\Lambda}\right)P_0(x) \tag{19}$$

The factor $\sinh^{-1}\frac{1}{\sqrt{1-M^2}\cot\Lambda}$ shows a logarithmic infinity at $M=1.0$. Hence the pressure on the root section increases more rapidly with Mach number than do the pressures at other sections of the swept-back wing. Furthermore, the shape of the pressure distribution over the root section approaches the Ackeret shape more closely as the Mach number approaches 1.0. As shown in reference 1, the pressure distribution on the root section is exactly this shape at supersonic speeds, that is,

$$\frac{\Delta p}{q\cos^2\Lambda}=\frac{4}{\pi}\frac{1}{\sqrt{1-(M\cos\Lambda)^2}}\frac{dz}{d(x\cos\Lambda)}\cosh^{-1}\left(\frac{1}{\sqrt{M^2-1}\cot\Lambda}\right)P_0(x) \tag{20}$$

Since $\sinh^{-1}\to\cosh^{-1}$ for large values of the argument, the swept-back airfoil shows no discontinuity in the type of pressure distribution on passing through the speed of sound. It will be evident that similar reasoning can be applied to the tip sections.

AIRFOIL OF BICONVEX SECTION

The use of a finite number of sources and sinks results in airfoil sections composed of straight segments. Such sections are undesirable, since they show infinite pressure peaks at the bends in the surface. Surfaces having continuous curvature require continuous distribution of sources and sinks alined with the generators of the surface. The simplest of these is the biconvex profile in which the upper and lower surfaces are parabolic arcs and have constant curvature. Such a profile requires line sources of finite strength to form the desired angles of intersection of the arcs at the leading and trailing edges together with a uniform distribution of sinks along the chord plane between the two sources.

The pressure field for a uniform sheet of line sources is obtained by integrating the field of a single line source in the x direction. This integral is

$$\frac{1}{D}u=\int\sinh^{-1}\frac{x'}{|y'|}dx=\frac{\sqrt{1+m^2}}{m}y\sinh^{-1}\frac{x}{|y|}-\frac{1}{m}y'\sinh^{-1}\frac{x'}{|y'|} \tag{21}$$

The integration for a source sheet is actually somewhat simpler if the interference of a bilaterally symmetrical arrangement of sources is considered simultaneously. The influence of the symmetrical, or conjugate, arrangement is obtained by substituting $-m$ for m in equation (21). Denoting $x-my$ by $\bar{x}'$ and $y+mx$ by $\bar{y}'$ we have

$$\frac{1}{D}(u+\bar{u})=\int\left(\sinh^{-1}\frac{x'}{|y'|}+\sinh^{-1}\frac{\bar{x}'}{|\bar{y}'|}\right)dx=\frac{1}{m}\left(\bar{y}'\sinh^{-1}\frac{\bar{x}'}{|\bar{y}'|}-y'\sinh^{-1}\frac{x'}{|y'|}\right) \tag{22}$$

To obtain a complete swept-back wing it is necessary to add a number of component pressure fields as explained in

reference 1. For an infinite swept-back wing with leading and trailing edges at $y'=+m$ and $-m$, respectively, on one side, and at $\overline{y}'=+m$ and $-m$, respectively, on the other side, there is obtained

$$\frac{\Delta p}{q}=\frac{2}{\pi}\frac{m}{\sqrt{1+m^2}}\left(\frac{t}{c}\right)_{max}\left[\frac{y'}{m}\left(\sinh^{-1}\frac{x'+1}{|y'-m|}-\sinh^{-1}\frac{x'-1}{|y'+m|}\right)+\frac{\overline{y}'}{m}\left(\sinh^{-1}\frac{\overline{x}'-1}{|\overline{y}'-m|}-\sinh^{-1}\frac{\overline{x}'+1}{|\overline{y}'+m|}\right)+2Q_1\left(\frac{y'}{m}\right)+2Q_1\left(\frac{\overline{y}'}{m}\right)\right] \quad (23)$$

where $\left(\frac{t}{c}\right)_{max}$ is the thickness-chord ratio of the biconvex profile. The terms $Q_1\left(\frac{y'}{m}\right)$ represent the pressure distribution on the biconvex airfoil in two-dimensional flow. The appearance of these terms is the result of the assumption that the tips are removed to a great distance.

At the root section ($y=0$) equation (23) reduces to

$$\frac{\Delta p}{q}=\frac{2}{\pi}\frac{m}{\sqrt{1+m^2}}\left(\frac{t}{c}\right)_{max}\left[4Q_1(x)-4\sinh^{-1}\frac{1}{m}P_1(x)\right] \quad (24)$$

Figure 6 shows pressure distributions at various stations along the span for a biconvex wing with 60° sweepback. The curves assume the two-dimensional form at a relatively short distance ($y\geqq\frac{1}{2}c$) from the root section, and similar behavior is to be expected near the tips. Hence the assumption of infinite aspect ratio should apply very nearly at any section situated more than one-half chord length from either root or tip.

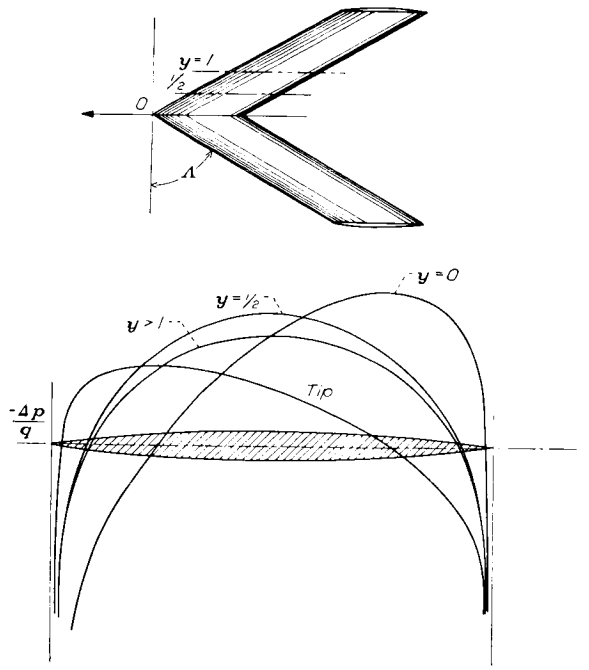

FIGURE 6.—Pressure distribution at various spanwise stations on swept-back wing, $\Lambda=60°$, $M=0$.

Figure 7 shows the effect of Mach number on the pressures over the root section and illustrates the progressive change to the supersonic type as the Mach number approaches 1.0. It can be seen that an increase in Mach number will not only increase the distortion of the pressure distribution but will increase the extent of the distortion along the span.

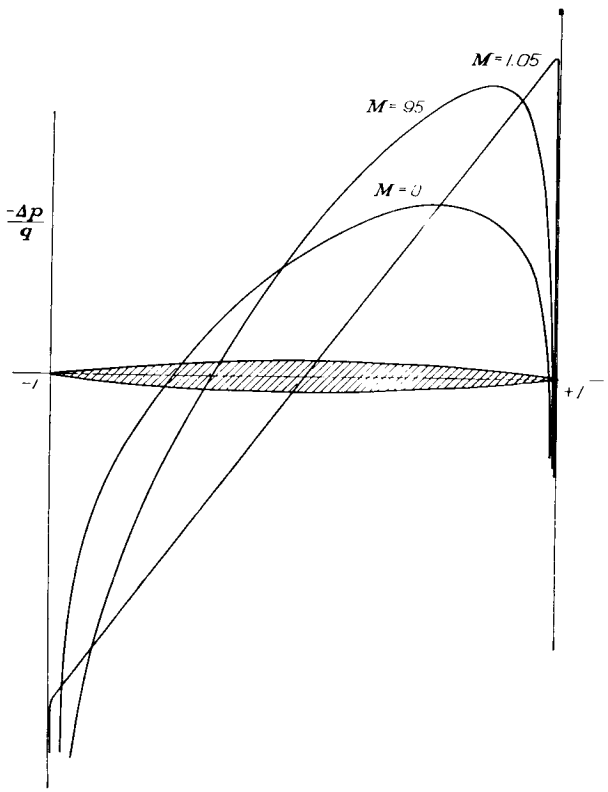

FIGURE 7.—Effect of Mach number on pressure distribution over root section of swept-back wing, $\Lambda=60°$, biconvex section.

An interesting point to be noted is that not all sections of the swept-back wing have zero pressure drag. A positive drag appears on the root sections and a negative drag on the tip sections. Hence the spanwise drag distribution is qualitatively similar to that at supersonic speeds though, of course, the net subsonic pressure drag is zero.

AMES AERONAUTICAL LABORATORY,
NATIONAL ADVISORY COMMITTEE FOR AERONAUTICS,
MOFFETT FIELD, CALIF., *May 1947*.

APPENDIX

SYMBOLS

V	flight velocity
M	Mach number
x, y, z	coordinates
ξ	point on x axis
η	point on y axis
ϕ	disturbance-velocity potential
u, v, w	disturbance-velocity components
p	local pressure
q	dynamic pressure $\left(\frac{1}{2}\rho V^2\right)$
ρ	air density
P_n, Q_n	Legendre functions
D	differential operator (d/dx)
t	thickness of wing
c	chord of wing (measured along x)
m	slope of line source (absolute value)
x'	$x+my$
y'	$y-mx$
$\bar{x}'$	$x-my$
$\bar{y}'$	$y+mx$
$R.\ P.$	Real part

REFERENCES

1. Jones, Robert T.: Thin Oblique Airfoils at Supersonic Speed. NACA Rep. No. 851, 1946.
2. Bateman, H.: Partial Differential Equations of Mathematical Physics. Dover Pub., 1944, p. 357.
3. Jahnke, Eugene, and Emde, Fritz: Tables of Functions with Formulas and Curves. Rev. Ed., Dover Pub., New York, 1943, pp. 107–117.

TECHNICAL NOTE 1350

ESTIMATED LIFT-DRAG RATIOS AT SUPERSONIC SPEED

Robert T. Jones

Ames Aeronautical Laboratory

July 1947

NATIONAL ADVISORY COMMITTEE FOR AERONAUTICS

TECHNICAL NOTE NO. 1350

ESTIMATED LIFT-DRAG RATIOS AT SUPERSONIC SPEED

By Robert T. Jones

SUMMARY

Recent developments in supersonic flow theory are applied to obtain estimates of the lift-drag ratios that may be achieved by aircraft employing swept-back wings. Lift-drag ratios greater than 10 to 1 can be maintained up to a Mach number of 1.4 by the use of large angles of sweep and high aspect ratios. As the speed increases in the supersonic range the attainable lift-drag ratios decrease and the gain due to sweepback also appears to diminish. An efficient configuration for $M = 1.4$ would require about 60° sweepback, an aspect ratio of 4 and a wing loading of one-third the atmospheric pressure. For a wing loading of 50 pounds per square foot the cruising altitude would be 60,000 feet and the indicated airspeed 290 miles per hour.

INTRODUCTION

The work required to propel an airplane a given distance in steady flight is equal to its weight times the distance travelled divided by the lift-drag ratio of the airplane. Hence the fuel expenditure per mile of flight need not increase with speed so long as the lift-drag ratio of the airplane can be maintained. However, with present shapes a prohibitive loss of lift-drag ratio occurs on passing beyond the speed of sound and it is evident that a radical change in configuration will be necessary for efficient flight at higher speeds.

The problem of an efficient configuration for flight at supersonic speeds was investigated by Busemann in 1935 (reference 1). Busemann concluded that an improvement in the lift-drag ratio at supersonic speeds could be obtained by sweeping the wing back at an angle just ahead of the Mach cone. Relatively much greater

efficiencies are obtainable when the wing is swept back behind the Mach cone. The change in the type of flow when the wing lies inside the Mach cone, and the resulting increase in efficiency have been brought out in reference 2. However, both reference 1 and reference 2 are restricted to considerations of two-dimensional flow and hence aspect-ratio effects could not be determined. Recent developments in aerodynamic theory have overcome this difficulty, making it possible to estimate the lift-drag ratio obtainable with practical configurations.

The present report applies these new theoretical results to obtain estimates of the lift-drag ratios that may be achieved with an efficient aircraft at supersonic speeds. The estimates are all based on the theory of small disturbances, first because this is the only adequate theory available, and second because it is reasoned that an aircraft producing a large disturbance in the external flow would be inherently inefficient.

At very high Mach numbers even thin bodies and small angles of attack cause relatively large pressure disturbances and consequent heating of the fluid. Here the heating effect of friction becomes no longer negligible. (Such conditions are likely to be encountered by rockets; however, in these cases the efficiency of steady flight may not be of primary concern.) The present analysis is therefore limited to more moderate speeds where the efficiency in steady flight is of primary importance and where it is evident that such efficiency can be achieved by known means.

FUNDAMENTAL RELATIONS FOR WING LOADING, ALTITUDE AND MAXIMUM LIFT-DRAG RATIO

The lift-drag ratio of a conventional airplane depends primarily on its external configuration and on the angle of attack and does not vary greatly with speed provided the correct relation between wing loading and altitude is maintained. For maximum efficiency the airplane should be flown at that lift coefficient $C_{L_{opt}}$ for which lift-drag ratio is a maximum. An increase in speed, then, necessitates an increase in altitude, since with fixed lift coefficient

(For a complete list of symbols see appendix.)

$$\frac{V}{V_o} = \sqrt{\frac{\rho_o}{\rho}} \tag{1}$$

where the subscript o refers to conditions at sea level.

With lift-drag ratio fixed, higher speed does not involve any increase in the thrust required for level flight; this thrust is simply

$$T = \frac{W}{(L/D)_{max}} \tag{2}$$

If the propulsive efficiency of the engine does not drop off with altitude, the increase in speed will thus be accomplished without any increase in the fuel consumption per mile of flight. Furthermore, the increase in speed is not accompanied by any significant change in the air loads or pressures on the airplane and hence no increase in structural stiffness is required. An obvious advantage of this method of increasing the cruising speed is that it does not interfere with the ability of the airplane to slow down at lower altitudes and land on short runways. A more complete discussion of these factors will be found in reference 3.

The altitude and speed of the airplane, of course, cannot be increased indefinitely at constant thrust, since eventually a critical Mach number will be exceeded and the lift-drag ratio of the airplane will begin to decrease. The limiting speed and the corresponding altitude may be determined from the relations

$$V = M_1 a \tag{3}$$

and

$$\frac{W/S}{\frac{\rho}{2}V^2} = C_{L_{opt}} \tag{4}$$

where M_1 is the Mach number at which, for $C_L = C_{L_{opt}}$, the drag begins to rise abruptly, a is the velocity of sound and W/S is the wing loading.

Equations (3) and (4) may be combined in the form

$$\frac{W/S}{p} \quad \frac{\gamma}{2} C_{L_{opt}} M_1^2 \tag{5}$$

where

p atmospheric pressure at altitude

γ ratio of specific heats for air (1.4).

Equation (5) gives the relation between wing loading and atmospheric pressure for maximum speed without loss of aerodynamic efficiency. This condition can hardly be attained at low altitudes since with an atmospheric pressure of 2000 pounds per square foot, for $M_1 = 0.75$ and the usual values of $C_{L_{opt}}$, the wing loading required would be of the order of 400 pounds per square foot. At 60,000 feet, however, the required wing loading works out to be the more practical value of 30 pounds per square foot.

Later calculations will show that similar considerations apply to supersonic aircraft; that is, the best lift-drag ratios are obtained when the wing loading is an appreciable fraction of the atmospheric pressure.

At subsonic speeds it is customary to divide the drag into two parts, one the result of friction (including the friction drag of the fuselage) and the other - the induced drag - the result of the lift. The friction drag is considered nearly independent of the angle of attack. Thus

$$C_D = C_{D_o} + C_{D_i} \tag{6}$$

where C_{D_o} is the drag at zero lift, and for subsonic flow equals C_{D_f}, the friction drag. If the velocity and pressure disturbances produced by the airplane are small, the drag arising from the lift will be satisfactorily represented by the well-known formula

$$C_{D_i} = \frac{C_L^2}{\pi A} \tag{7}$$

or

$$\frac{C_{D_i}}{C_L^2} = \frac{1}{\pi A} \tag{8}$$

and the friction drag will be nearly independent of the angle of attack. The lift-drag ratio at any angle is then

$$\frac{L}{D} = \frac{C_L}{C_{D_o}+C_{D_i}} \tag{9}$$

Solving for the lift coefficient at maximum lift-drag ratio results in

$$C_{L_{opt}} \quad \sqrt{\frac{C_{D_o}}{C_{D_i}/C_L^2}} \tag{10}$$

and therefore

$$\left(\frac{L}{D}\right)_{max} = \frac{1}{2}\sqrt{\frac{1}{C_{D_o}\ (C_{D_i}/C_L^2)}} \tag{11}$$

In calculating lift-drag ratio for supersonic speed the drag may again be divided into two components, one independent of the lift and one proportional to the square of the lift coefficient. However, in this case the drag at zero lift includes a pressure drag which varies with the thickness of the body or wing. Also, at supersonic speeds, the drag due to lift can no longer properly be called "induced drag." At subsonic speeds the drag arising from the lift can be traced to the influence of the trailing vortex wake on the wing - hence the designation "induced." At supersonic speeds, however, the forward influence of the wake usually constitutes only a small part of the drag arising from the lift and hence

the term "induced drag" does not seem appropriate. Different divisions of the drag due to lift into components of wave drag and induced drag have been proposed, but the proportions allotted in any particular case depend on the method of calculation employed. In the present report the drag is calculated by integrating the pressure distribution in the neighborhood of the body and in this case C_{D_i} appears simply as a pressure drag proportional to the square of the lift coefficient. The subscript i is retained to identify the law of variation with that of the induced drag at subsonic speeds.

Then, for comparison with the subsonic case, we may write

$$C_{D_o} = C_{D_f} + C_{D_t}$$

and

$$C_{D_i} = \left(\frac{C_{D_i}}{C_L^2}\right) C_L^2$$

where C_{D_f} is the total friction drag, and C_{D_t} the total thickness drag, due to wing and fuselage. The factor C_{D_i}/C_L^2 bears no simple relation to the aspect ratio as it does in the subsonic case, but is a complex function of the wing plan form and load distribution.

With the values of C_{D_o} and C_{D_i}/C_L^2, revised for supersonic conditions, equations (10) and (11) for the optimum lift coefficient and maximum value of the lift-drag ratio remain valid. Maximum L/D is obtained when the drag due to lift is equal to the drag at zero lift.

DRAG AT ZERO LIFT

Thickness Drag of Wings

The thickness drag of the wing may be calculated by the methods of reference 4 or 5. Figure 1 shows the variation of thickness drag with Mach number calculated by the method of reference 5 for a rectangular wing and for several swept-back wings. In these cases the airfoil is of symmetrical

biconvex section 5 percent thick. The results for the swept-back airfoils were obtained from reference 6. The curve for the rectangular airfoil is the same as that given for the infinite wing by the Ackeret theory since, as has been demonstrated by J. N. Nielsen in an unpublished application[1] of the same method, the integrated effect of removing outboard portions of the wing on the drag of the remainder of the wing is zero, at least so long as the Mach cone from each tip does not intersect the opposite tip. The thickness drag coefficient of the rectangular airfoil is therefore independent of aspect ratio when

$$A\sqrt{M^2-1}>1$$

where

A = aspect ratio

When the wing is swept well behind the Mach cone the flow over most of the wing is of the subsonic type. (See reference 2.) The pressure drag is small and may be attributed to departures from the subsonic type of flow in the region of the root section. In this condition the outboard sections of the wing have little or no drag, and hence the drag coefficient is inversely proportional to the aspect ratio. At higher speeds, when the Mach angle approaches the leading-edge angle, the distribution of drag changes and the drag coefficient increases rapidly, particularly on the outboard sections. If the leading edge is too near the Mach cone, the drag of the swept wing will exceed that of the straight wing.

Figure 2 shows a plot similar to figure 1 of the variation of drag with Mach number for tapered swept-back airfoils. These results were obtained by K. Margolis of Langley Memorial Aeronautical Laboratory using the method of reference 5. An extensive series of calculations for tapered wings has been given recently by Stewart and Puckett (reference 7). In order to simplify the calculations a double-wedge section was assumed, though it is not to be

[1]Data on file at Ames Laboratory.

supposed that such a section would be desirable in practice. Here the angle of sweepback (60°) is that of the midchord line of the airfoils, which is also the line of maximum thickness. The sharp rises in drag coefficient near $M = 1.52$ and $M = 1.71$ occur when the Mach angle approaches the angle of the trailing edge. Evidently all generators of the wing surface must lie behind the Mach lines to insure favorable drag values.

According to the thin airfoil theory the calculated flow for a given airfoil plan form and Mach number will actually be similar to the flow over another plan form at a different Mach number, provided the two plan forms are oriented similarly with respect to the corresponding Mach lines. This relation may be preserved by changing the x coordinates of the plan form (fig. 3) in the proportion that the x coordinates of the Mach lines are changed, that is, as $\sqrt{M^2-1}$. For plan forms having similar flow patterns the ratio

$$m = \frac{\text{cot leading-edge angle}}{\text{cot sweep angle of Mach lines}}$$ will be constant.

The aspect ratio will then vary with Mach number according to

$$A\sqrt{M^2-1} = \text{constant} \tag{12}$$

and thin airfoil theory shows that the drag coefficient will be proportional to

$$\frac{(t/c)^2}{\sqrt{M^2-1}}$$

or

$$C_{D_t}\sqrt{M^2-1} \sim (t/c)^2 \tag{13}$$

where t/c is the thickness-chord ratio measured in the stream direction. Figure 4 shows the coefficient

$$\frac{C_{D_t}\sqrt{M^2-1}}{(t/c)^2}$$

plotted against m for the constant-chord biconvex airfoils.

Friction Drag of Wing

In general, the friction drag of the wing will be of the same order of magnitude as the thickness drag. At very high speeds a considerable amount of heat is generated in the boundary layer and the resultant temperature variation affects the magnitude of the skin friction. For moderate supersonic speeds, however, the heating effect is not large and the normal relation of skin friction to Reynolds number will not be greatly modified.

For present purposes a conservative value of $C_{D_f} = 0.006$ corresponding to a turbulent boundary layer at a Reynolds number of 10^7 has been used.

Drag of Fuselage

A method for calculating the wave drag of a slender fuselage at supersonic speeds was given by von Kármán in 1935 (reference 8). This method was applied in reference 9 to a series of bodies of parabolic arc shape and estimates of the friction drag added to obtain total drag. More recently the calculations of Haack (reference 10), Sears (reference 11), and Lighthill (reference 12) have become available. These investigators apply Kármán's method to the determination of body forms having a minimum wave drag for certain conditions. The minimum problem is solved for three cases: viz, I, given volume and given length; II, given length and given diameter; and III, given diameter and given volume.

The following equations may be obtained[2] from Haack's report (reference 10). The length l is so chosen that the body lies between +1 and -1 on the x-axis; r/r_o is the radius at any station in terms of the maximum radius r_o and a is the frontal area πr_o^2. The volume is given in terms of the volume of the circumscribed cylinder, and the drag coefficient, which does not include friction, is given in

[2]The formulas given as the final relations in the report are in error. However, the correct relations can easily be derived from the preceding equations.

terms of the frontal area. The factor d/l is the fineness ratio, diameter/length.

Case I: Given length, given volume

$$\left.\begin{aligned} \left(\frac{r}{r_o}\right)^2 &= \left(\sqrt{1-x^2}\right)^3 \\ \text{Volume} &= \frac{3}{16}\,\pi l\,\pi r_o^2 \\ C_D &= \frac{9}{8}\,\pi^2\left(\frac{d}{l}\right)^2 \end{aligned}\right\} \qquad (14)$$

Case II: Given length, given diameter

$$\left.\begin{aligned} \left(\frac{r}{r_o}\right)^2 &= \sqrt{1-x^2} - x^2\cosh^{-1}\frac{1}{x} \\ \text{Volume} &= \frac{\pi}{6}\,l\,\pi r_o^2 \\ C_D &= \pi^2\left(\frac{d}{l}\right)^2 \end{aligned}\right\} \qquad (15)$$

Case III: Given diameter, given volume

$$\left.\begin{aligned} \left(\frac{r}{r_o}\right)^2 &= 3\sqrt{1-x^2} - 2\left(\sqrt{1-x^2}\right)^3 - 3x^2\cosh^{-1}\frac{1}{x} \\ \text{Volume} &= \frac{\pi}{8}\,l\,\pi r_o^2 \\ C_D &= \frac{3}{2}\,\pi^2\left(\frac{d}{l}\right)^2 \end{aligned}\right\} \qquad (16)$$

Figure 5 shows the body shapes computed from these formulas.

Although the wave drag diminishes with increasing slenderness, the friction drag for a given volume or a given cross section tends to increase because of the greater surface area. With usual values of the friction coefficient a favorable balance between the two components requires such a slender body that in most cases the dimensions will actually be governed by the minimum allowable cross section. For a slender body the surface area and hence the friction drag associated with a given cross section is proportional to l/d, while the wave drag is proportional to $(d/l)^2$. It follows that the total drag will be a minimum when the slenderness ratio is such that the friction drag is twice the wave drag.

It will be noted that the body shape for case I actually has very little more drag than the case II body of the same diameter, and since body I has a greater useful volume, it seems a logical choice for practical design. Figure 6 shows the wave drag for case I and also the total drag, based on a skin-friction coefficient of 0.0021, as a function of the fineness ratio. The value of this friction coefficient was obtained from reference 13, and corresponds to a fully turbulent boundary layer and a Reynolds number of 10^8. With this friction coefficient the optimum fineness ratio is about 16 to 1.

DRAG DUE TO LIFT

The drag due to lift is estimated from theoretical solutions for the supersonic flow over thin lifting surfaces. Theoretical solutions are known for cases in which the lifting surface is curved and twisted in such a way as to support a uniform load (reference 14) and, for certain rectangular, triangular, or tapered flat surfaces (references 14 and 15).

Uniformly Loaded Surface

The solution for the uniformly loaded surface may be derived by methods similar to those described in reference 5 for the nonlifting airfoil. In that report the pressure due to thickness on an airfoil oblique to the stream was obtained by superposing the effects of oblique line source in the acceleration potential field. The effect of a line source is

to cause a deflection of the stream lines crossing the source like the deflection caused by a thin wedge-shaped body; that is, the line source is followed by an area over which the vertical velocity w is constant and of opposite sign above and below the chord plane.

Similarly, an oblique vortex gives rise to a constant difference in the horizontal velocity increment u, and therefore in the pressure, above and below the plane of flow crossing the vortex. The corresponding w for a semi-infinite vortex is given by

$$w = \frac{u}{\pi m}\left(\sqrt{1-m^2}\,\cosh^{-1}\frac{x'}{|y'|} - \cosh^{-1}\frac{x}{|y|}\right) \qquad (17)$$

where $x' = x - my$ and y' denotes the absolute value of $y - mx$. (The geometry of the figure has been adjusted, as described in the preceding section and reference 5, to correspond to the case in which the Mach angle is 45°; that is, $\sqrt{m^2-1} = 1$.)

The shape of the surface and the constant pressure are related to the velocity increments by the following formulas:

$$\frac{dz}{dx} = \frac{w}{V} \qquad (18)$$

and

$$\frac{\Delta p}{q} = \frac{2u}{V} \qquad (19)$$

Thus the camber of a triangular airfoil shaped to support a uniform load (fig. 7) may be obtained by superimposing two oblique vortices to form a V coinciding with the leading edge of the triangle. Integration of equation (17) for this case yields:

$$z = \frac{C_L}{4\pi m}\left[\sqrt{\frac{1-m^2}{m}}\left(\bar{y}' \cosh^{-1}\frac{\bar{x}'}{|\bar{y}'|} - y' \cosh^{-1}\frac{x'}{|y'|}\right)\right.$$
$$\left. -2\left(x \cosh^{-1}\frac{x}{|y|} - \sqrt{x^2 - y^2}\right)\right] \qquad (20)$$

where

$$\bar{x}' = x + my \quad \text{and} \quad \bar{y}' = y + mx$$

To obtain a lifting surface of finite chord it is necessary to introduce a negative V-shaped vortex at the desired chord length downstream. (See fig. 8.) Through the use of a finite number of straight vortex segments any plan form bounded by straight lines can be obtained.

The variation of w over the area enclosed by the vortex segments not only gives the camber and twist of the surface required to support a uniform load, but also can be used to calculate the drag arising from the lift. It can be seen that, since the pressure distribution is uniform over the section, the resultant force will lie in a direction at right angles to the chord line, or the line joining the leading and trailing edge, regardless of the camber of the surface. Hence the angle of attack of the chord line at any section times the lift gives the drag due to lift at that section.

In case the leading edge of the airfoil is ahead of the Mach cone the uniformly loaded surface is flat over portions of the wing not influenced by the root or the tip, as is given by the Ackeret theory. More interesting cases are those in which the leading edges are swept behind the Mach cone.

In the case of the swept-back wing it is found that the angle of attack has a logarithmic infinity at the center section. Hence the wing would require an infinite twist to maintain the uniform load across this section. At a distance from the center section the shape of the lifting surface resembles that of the familiar "constant load mean line" used

for subsonic airfoils. The twist and hence the section drag disappear rapidly with distance from the center section. There is consequently a marked reduction of drag coefficient with increasing aspect ratio, just as in the case of the drag due to thickness.

The infinite twist required at the root section of course, makes the construction of such a wing impractical. We may conclude that in a practical wing there will be some falling off of the lift across the center section, and calculations of the lift distribution for flat surfaces show such a loss. The uniformly loaded airfoil gives a useful picture of the variation of drag with plan form, however. In spite of the fact that the local drag coefficient at the root section tends toward infinity, the integrated or over-all drag coefficient of the swept-back wing is finite and at reasonable aspect ratios is considerably lower than that of the flat unswept wing.

Figure 9 shows the coefficient of drag due to lift C_{D_i}/C_L for a series of uniformly loaded airfoils having a constant chord and varying degrees of sweep. To simplify the calculations, an approximation was made for the effect of the wing tip. With the tip cut off parallel to the direction of flight a large twist would theoretically have been required to maintain the uniform load right out to the tip. Instead of calculating this additional twist at the tip, the shape of the infinite wing with uniform load was assumed without modification and a loss in lift within the Mach cone originating at each tip was taken into account. Since the lift will have the full value along the boundary of the cone and will fall to zero at the tip, an average value of half the full load was used over this region. Since the effect of this approximation to a tip effect on the total drag value was small, any error involved in the approximation must also be small. If the tip were cut off along the Mach lines, slightly lower values of C_{D_i}/C_L would have been obtained.

Figure 9 shows that the values of C_{D_i}/C_L at supersonic speed are in general higher than the value corresponding to the same aspect ratio at subsonic speed but approach this value as the angle of sweep is increased (i.e., as $m \to 0$). The practical difficulty of maintaining a given aspect ratio of course increases as the angle of sweep is increased.

Flat Lifting Surfaces

Rectangular plan form. - For a flat rectangular wing of infinite aspect ratio the Ackeret theory gives

$$\frac{\partial C_L}{\partial \alpha} = \frac{4}{\sqrt{M^2-1}} \tag{21}$$

Since the lift is at right angles to the chord,

$$C_{D_i} = C_L \times \alpha \tag{22}$$

and

$$\frac{1}{\sqrt{M^2-1}} \frac{C_{D_i}}{C_L^2} = 0.25 \tag{23}$$

At a Mach number of 1.4 this value is nearly five times the drag due to lift of a subsonic airfoil of aspect ratio 6.

If the wing has a finite aspect ratio there will be a reduction of lift at the tip and a consequent reduction in $\partial C_L/\partial \alpha$ from the value given by equation (21). The distribution of lift over the tip of a flat rectangular wing has been calculated by Busemann (reference 14). The lift over the portion of the wing between the tip Mach cones (fig. 10) is constant and equal to that given by the Ackeret theory. Within either tip cone the lift pressure falls from this value to zero at the tip. If y/x represents the fractional distance from the tip toward the Mach line at a given chordwise position, then the lift pressure varies according to the function

$$\frac{4\alpha}{\sqrt{M^2-1}} \cos^{-1}\left(1 - 2\frac{y}{x}\right) \tag{24}$$

Superposing the effects of the two tip cones where they overlap and integrating the pressure over the whole wing gives for the lift coefficient

$$C_L = \frac{4\alpha}{\sqrt{M^2-1}} \frac{A\sqrt{M^2-1}\ -\frac{1}{2}}{A\sqrt{M^2-1}} \tag{25}$$

and for the drag due to lift

$$\frac{1}{\sqrt{M^2-1}}\left(\frac{C_{D_i}}{C_L{}^2}\right) = \frac{A\sqrt{M^2-1}}{4A\sqrt{M^2-1}\ -2} \tag{26}$$

Busemann's solution is valid for $A\sqrt{M^2-1} \geq 1.0$, that is, so long as the Mach cone from one tip does not cross over the opposite tip. It is interesting to note that when $A\sqrt{M^2-1}=1.0$ the lift falls to zero along the whole trailing edge and the span load distribution is elliptical, as shown in reference 16 for airfoils of very low aspect ratio.

Triangular plan form. - Formulas for the lift distribution and $\partial C_L/\partial\alpha$ for a flat triangular airfoil behind the Mach cone have been given recently by Stewart (reference 15). Stewart finds that the lift distribution as predicted from elementary considerations for very slender triangles (reference 16) actually holds for all leading-edge angles until the leading edge touches the Mach cone. Stewart finds also

$$\sqrt{M^2-1}\ \frac{\partial C_L}{\partial\alpha} = \frac{2\pi m}{E} \tag{27}$$

where $E = E(\sqrt{1-m^2})$ is the elliptic integral.

In the case of the flat surface with the leading edge behind the Mach cone, the chordwise lift distribution has an

infinite value at the leading edge just as it does in the subsonic case. Here the resultant force will be inclined forward relative to the chord plane because of the suction force at the leading edge.

The drag due to lift for the flat triangular airfoil was evaluated by setting up the complex expression for the velocity field u and w by means of Busemann's method (reference 14). The drag was then calculated from the formula

$$C_D = \int_c \frac{2u}{V} \times \frac{W}{V} ds \tag{28}$$

by integrating around a contour c a short distance away from the airfoil surface and enclosing the singularity at the leading edge. The result is

$$\frac{1}{\sqrt{M^2-1}} \frac{C_{D_i}}{C_L{}^2} = \frac{2E - \sqrt{1-m^2}}{4\pi m} \tag{29}$$

A similar formula has been given recently by W. D. Hayes (reference 17).

In this formula, the first term represents a drag equal to the lift times the angle of attack, and the second term represents the thrust at the leading edge. It is noted that this latter term disappears progressively as the edge approaches the Mach cone (i.e., $A\sqrt{M^2-1} \to 4$). At the other limit, the slender triangle near the center of the Mach cone, $E \to 1$, and

$$\frac{C_{D_i}}{C_L{}^2} = \frac{1}{\pi A} \tag{30}$$

as in reference 16. Although the theory shows a forward thrust on the thin plate with a sharp edge, it is not to be expected that this characteristic will be realized in practice unless the leading edge is given a finite radius or camber.

Tapered plan form. - The theoretical lift distribution for a flat untapered swept-back wing with the leading edge behind the Mach cone has not yet been determined. However, the solution for the flat triangular wing may be readily extended to include a special family of tapered wings. This extension is based on the fact that an area of the triangular wing may be removed by making cuts along Mach lines without affecting the flow over the area remaining ahead of the cuts. In particular, the removal of such area will not affect the suction force on the leading edge, as long as the area removed does not include any of the leading edge so that the coefficient of thrust will be increased as area is cut away. Evidently the most efficient members of this family of airfoils are those in which the maximum area is cut out of the triangle, that is, the wing is tapered to a point. (See Fig. 11.)

With the trailing edge fixed at the Mach angle, the angle of taper and hence the aspect ratio of these wings varies with the angle of sweep in such a manner that

$$\sqrt{M^2-1}\ A = \frac{4m}{1-m} \tag{31}$$

as the leading edge approaches the Mach cone $m \to 1.0$ and the aspect ratio approaches infinity.

The lift-curve slope of these airfoils is determined simply by integrating the pressure distribution for the triangular airfoil over the appropriate area. The calculation gives

$$\sqrt{M^2-1}\ \frac{\partial C_L}{\partial \alpha} = \sqrt{\frac{4m}{1-m^2}}\ \frac{1}{E}\left(\frac{\cos^{-1}(-m)}{1+m} + m\sqrt{\frac{1-m}{1+m}}\right) \tag{32}$$

and for the drag due to lift

$$\frac{1}{\sqrt{M^2-1}}\frac{C_{D_i}}{C_L{}^2} = \frac{1}{\sqrt{M^2-1}\,\frac{\partial C_L}{\partial \alpha}} - \sqrt{\frac{1+m}{1-m}}\,\frac{1}{4\pi m}N^2 \tag{33}$$

where N is the ratio of the lift-curve slope of the triangular airfoil to that of the tapered airfoil, that is,

$$N = \frac{(\pi/2)\sqrt{1-m^2}}{\frac{\cos^{-1}(-m)}{1+m} + m\sqrt{\frac{1-m}{1+m}}} \tag{34}$$

Equations (31) through (34) apply to the case of the wing tapered to a point. In subsonic flow such extreme taper is known to lead to high local lift coefficients over the tip portions and to the possibility of tip stalling even at moderate lift coefficients. A similar tendency is evident at supersonic speeds; in fact, the section lift coefficients tend toward infinity at the pointed tip. Hence the extreme taper should not be used in practice and value of $C_{D_i}/C_L{}^2$ calculated for these cases will be somewhat optimistic.

Comparison of Lift and Drag Values for Flat Surfaces

Curves showing the variation of lift-curve slope with Mach number and aspect ratio for the rectangular, triangular, and tapered airfoils are shown in figure 12. At $A\sqrt{M^2-1} = 4$ the leading edge of the triangular airfoil touches the Mach cone and, as shown by Puckett (reference 4), the lift characteristics at higher aspect ratios are identical with those of a rectangular airfoil of infinite aspect ratio.

The drag due to lift versus aspect ratio for the various flat wings is shown in figure 13. According to the Ackeret theory

$$\frac{1}{\sqrt{M^2-1}}\frac{C_{D_i}}{C_L{}^2} = \frac{1}{4} \tag{35}$$

and it is to be noted that both the rectangular and the

triangular airfoils approach this value at higher aspect ratios. At

$$A\sqrt{M^2-1}<4 \tag{36}$$

the leading edges of the triangular airfoil are behind the Mach cone and the drag due to lift is reduced somewhat because of the suction on the leading edge. However, the really favorable values of $C_{D_i}/C_L{}^2$ are obtained only with the swept-back wings of relatively high aspect ratio. The fact that the values for the flat pointed wings agree with those for the cambered, untapered airfoils shown on figure 9 is an indication that the drag due to lift is primarily a function of sweepback and aspect ratio.

RESULTS

The total drag of the supersonic aircraft can now be estimated by adding up the components thus far considered with an allowance for the friction drag of the wing and a small allowance for the tail surfaces.

Since the lift-drag ratio increases with increasing slenderness of the wing, it is necessary to establish some standard of slenderness to obtain comparative values. A rough measure of the structural stiffness of a wing is the maximum spar depth at the wing root divided by the distance, measured along the spar, to the centroid of area of the wing. A value of 1/15 seems to be about the limit of present-day construction.

Airplane with Constant Chord Swept-back Wing

Figure 14 shows lift-drag ratios obtainable at $M = 1.4$ as a function of m with a configuration embodying the constant chord, uniform lift airfoil and a type I body of 15 to 1 fineness ratio. An allowance of $C_{D_f} = 0.006$ was made for the friction drag on the wing and a value equal to 10 percent of the wing drag was allotted to the vertical tail. No horizontal tail is shown, since it is not clear that such a tail would be required with this configuration. The frontal area of the body was assumed to be 4 percent of the wing area. The drag and lift of the wing were assumed to carry across the center sections.

without being modified by the presence of the body.

The airfoil shape is obtained by superimposing a parabolic arc thickness distribution upon a cambered and twisted surface designed, as discussed earlier, to support a uniform load. The varion in sweepback, or m, in this case was assumed to be obtained by rotating the wing panels without changing their length-width ratio, hence the aspect ratio varies with sweep as shown. The wing in the unswept position would have an aspect ratio of 12. If the ratio of the root thickness to the spar length from the root section to the centroid of the wing panel is 1/15, the thickness-chord ratio of the unswept wing would be 0.2. The same wing rotated through 60° ($m = 0.577$) has an aspect ratio of 3 and a t/c (c measured parallel to the stream) of 0.1.

The calculations for the uniformly loaded wings show higher lift-drag ratios for still higher aspect ratios and greater thickness-chord ratios, but it is doubtful that the calculations based on the theory of small disturbances apply in these cases.

Because of the higher aspect ratios attainable with a tapered wing it is found that these configurations are more efficient than the constant chord wings, and therefore they will be discussed in somewhat greater detail.

Airplane with Tapered Wing

Figure 15 shows the lift-drag ratios obtainable at $M = 1.4$ with the flat pointed wing. The proportions of fuselage and tail are the same as in the preceding case, and the same value of C_{D_f} was used. The calculations were made assuming double-wedge sections (as in fig. 2), but an approximate correction factor of 4/3 was inserted into the thickness drag to take account of the greater average slope of the biconvex profile. The quantity 4/3 is the ratio of the wave drag of the biconvex section to that of the double-wedge section in two-dimensional flow. The maximum wing thickness in each case is again 1/15 the distance from the wing root to the centroid of area of the half wing. The variation of t/c (streamwise) is shown in figure 15. Since the trailing-edge angle is fixed on the Mach line, the aspect ratio increases indefinitely as m approaches 1, according to equation (31). The optimum lift coefficient

calculated by equation (10), is also shown in figure 15.

Figure 16 shows the variation of $(L/D)_{max}$ with m at different Mach numbers. It is noted that the optimum value of m is different for different Mach numbers; there appears to be no fixed relation between the sweepback angle and the Mach angle. Evidently relatively greater sweepback angles should be used at smaller Mach numbers. The optimum values of m will, of course, be influenced by the magnitude of the friction drag.

DISCUSSION OF RESULTS

Effect of Plan Form

Figure 17 shows the lift-drag ratios replotted against aspect ratio and compared with values estimated for a straight wing-body combination. It will be noted that up to M = 2 the swept-back wing is much more efficient than the straight wing. The difference is smaller at the higher Mach numbers, however, and the advantages of sweepback at very high Mach numbers may be questioned. In each case the efficiency diminishes with Mach number.

Although the configurations shown in figures 14 and 15 appear from the calculations to give the best lift-drag ratios, it is not to be assumed that these configurations are actually the most suitable for practical use. In practice the wing must of course have a finite tip chord and may also require some camber or twist to avoid the high concentration of load near the tips. Also, as has been previously remarked, the location of the trailing edge on, rather than behind, the Mach lines was chiefly a computational device. It is probable that a greater sweep of the trailing edge would be desirable.

Such modifications will of course cause changes in the lift-drag ratio. However, it is believed that the highest lift-drag values shown can actually be approached with practical configurations. The theoretical values of C_{D_i}/C_L^2 for the wing with its trailing edge along the Mach cone are somewhat more favorable than the values to be expected with a wing having its trailing edge behind the Mach cone. On the other hand, the location of the trailing edge along the Mach line is unfavorable from the standpoint of thickness drag, as shown by figure 2. Hence the net effect of trailing-edge location on

$(L/D)_{max}$ is not expected to be very pronounced. The beneficial effects of tapering the wing indicated by figure 17 may also be assumed to hold qualitatively for more moderate degrees of taper.

Airfoil Section

No attempt was made in the analysis to find an optimum airfoil profile. The section assumed for the calculations has a parabolic thickness distribution. In practice, as previously mentioned, it would be necessary to round or camber the leading edge to achieve the predicted values of $C_{D_i}/C_L{}^2$. It might also be advantageous to use (with the tapered plan form) a cusped trailing edge. This device would enable the designer to take advantage of the high lift to be obtained by placing the trailing edge along the Mach lines, while effectively giving the thickness distribution a greater angle of sweep and thus averting the large wave drag which arises when the generators of the thickness distribution are too near the Mach lines.

Friction Drag

The allowance of 0.006 made for the friction drag coefficient of the wing corresponds to a turbulent boundary layer at a Reynolds number of 10^7. The assumption of turbulent friction for both wing and fuselage is believed to be conservative, since there are indications that large areas of laminar flow can be achieved at supersonic speeds. The importance of maintaining laminar flow or otherwise reducing the friction can be seen from the magnitudes of the various drag components with the best configuration (fig. 15, m = 0.5) at a Mach number of 1.4. The various components are shown in the following table:

(1) Thickness drag of wing	0.0041
(2) Friction drag of wing	.0060
(3) Thickness drag of body	.0020
(4) Friction drag of body	.0036
(5) Drag of vertical tail	.0010
Total drag at zero lift: C_{D_o} =	.0167
Drag due to life C_{D_i} =	.0167
Total drag	0.0334
Friction drag (2) + (4)	0.0096

Note that the friction drag is more than 50 percent of the total drag at zero lift. In this case the maximum lift-drag ratio is 10.7; with completely laminar flow the ratio would increase to about 15.

Optimum Wing Loading and Altitude

The analysis indicates that reasonably good aerodynamic efficiencies are obtainable up to Mach numbers of 1.5. At $M = 1.4$ the best configuration studied should operate near a lift coefficient of 0.35. From equation (5), the wing loading for this case works out to be about one-half the atmospheric pressure. This pressure disturbance can no longer be considered small and the question arises as to whether the linearized theory can be considered applicable in this case. No accurate analysis of this limitation can be given at present. However, an approximate criterion can be deduced by comparing the flow over the swept-back wing with the two-dimensional subsonic flow over a wing section at the same component Mach number as suggested in reference 2. When this comparison is made for configurations near the optimum in figure 15 it is found that the wing sections are operating beyond their critical Mach numbers at the indicated optimum lift coefficient. Thus it appears that the optimum lift coefficient will actually be smaller than is indicated by the linearized theory. For the best configuration at $M = 1.4$, it appears that the optimum lift coefficient may be nearer 0.25 than the 0.357 indicated by figure 15. In this case the L/D_{max} will be diminished from 10.7 to 10, and the optimum wing loading from one-half to approximately one-third atmospheric pressure. At sea level the wing loading required would be 700 pounds per square foot, but for operation at 60,000 feet the much more reasonable figure of 50 pounds per square foot is obtained. At this altitude the true airspeed is 900 miles per hour and the indicated airspeed 290 miles per hour.

Ames Aeronautical Laboratory,
National Advisory Committee for Aeronautics,
Moffett Field, Calif., May 1947

APPENDIX

SYMBOLS

V	flight velocity
V_o	velocity at sea level
ρ	air density
ρ_o	density at sea level
p	atmospheric pressure
T	thrust
W	weight
L	lift
D	drag
M	Mach number $\left(\frac{V}{a}\right)$
a	velocity of sound
C_L	lift coefficient $\left(\frac{L}{\rho/2\ V^2S}\right)$
S	wing area
γ	ratio of specific heats ($\gamma = 1.4$ for air)
C_D	drag coefficient $\left(\frac{D}{\rho/2\ V^2S}\right)$
C_{D_o}	drag coefficient at zero lift
C_{D_t}	coefficient of drag due to thickness
C_{D_i}	coefficient of drag due to lift
C_{D_f}	friction drag coefficient

A	aspect ratio
b	wing span (perpendicular to direction of flight)
x	coordinate along direction of flight
m	parameter indicating relative slope of wing leading edge $\left(m = \frac{\text{cotangent leading-edge angle}}{\text{cotangent sweep angle of Mach lines}}\right)$
t	thickness of wing at midchord
c	wing chord
l	length of fuselage
r	radius of fuselage
r_o	maximum radius
d	maximum diameter of fuselage $(d = 2r_o)$
w	small vertical velocity disturbance
u	small horizontal velocity disturbance
y	lateral (spanwise) coordinate
x'	$x - my$ $\bar{x}' = x + my$
y'	$y - mx$ $\bar{y}' = y + mx$
z	vertical coordinate of wing camber line
α	angle of attack
E	complete elliptic integral of the second kind
N	ratio of lift-curve slope of triangular airfoil to that of the tapered airfoil

REFERENCES

1. Busemann, A.: Aerodynamischer Auftrieb bei Uberschallgeschwindigkeit. Luftfahrtforschung, Bd. 12, Nr. 6, Oct. 3, 1935.

2. Jones, Robert T.: Wing Plan Forms for High-Speed Flight. NACA TN No. 1033, 1946.

3. Korvin-Kroukovsky, B. V.: High Altitude Aviation. Aviation Magazine, April 20, 1929 and May 18, 1929.

4. Puckett, Allen E.: Supersonic Wave Drag of Thin Airfoils. Jour. Aero. Sci., vol. 13, no. 9, Sept. 1946, pp. 475-484.

5. Jones, Robert T.: Thin Oblique Airfoils at Supersonic Speed. NACA TN No. 11Q7, 1946.

6. Harmon, Sidney M. and Swanson, Margaret D.: Calculations of the Supersonic Wave Drag of Nonlifting Wings with Arbitrary Sweepback and Aspect Ratio Wings Swept Behind the Mach Lines. NACA TN No. 1319, 1947.

7. Stewart, H. J. and Puckett, A. E.: Aerodynamic Performance of Delta Wings at Supersonic Speeds. Paper presented at the 15th Annual Meeting of the Institute of the Aeronautical Sciences New York, January 1947.

8. von Kármán, Th.: The Problem of Resistance in Compressible Fluids. GALCIT Pub. No. 75, 1936. (From R. Accad. d'Italia, cl. Sci. fis., mat. e nat., vol. XIV, 1936.)

9. Jones, Robert T. and Margolic, Kenneth: Flow Over a Slender Body of Revolution at Supersonic Velocities. NACA TN No. 1081, 1946.

10. Haack, W.: Geschossformen kleinsten Wellenwiderstandes. Bericht 139 der Lilienthal Gesselschaft.

11. Sears, William R.: On the Minimum Wave Drag of Projectiles. Quarterly of Applied Mathematics. Jan. 1947, pp. 361-366.

12. Lighthill, M. J.: Supersonic Flow past Bodies of Revolution. R. & M. No. 2003, British A.R.C., 1945.

13. Young, A. D.: The Calculation of the Total and Skin Friction Drags of Bodies of Revolution at Zero Incidence. R. & M. No. 1874, British A.R.C., 1939.

14. Busemann, A.: Infinitesimale kegelige Überschallstromung. Sonderdruck. Jahrbuch 1942/43 der Deutschen Akademie der Luftfahrtforschung.

15. Stewart, H. J.: Lift of a Delta Wing at Supersonic Speeds. Quarterly Appl. Math., vol. IV, no. 3, Oct. 1946, pp. 246-254.

16. Jones, Robert R.: Properties of Low-Aspect Ratio Pointed Wings at Speeds below and above the Speed of Sound. NACA TN No. 1032, 1946.

17. Hayes, W. D.: Linearized Theory of Conical Supersonic Flow with Application to Triangular Wings. North American Aviation Co., Engineering Dept. report No. NA-46-818, Oct., 1946.

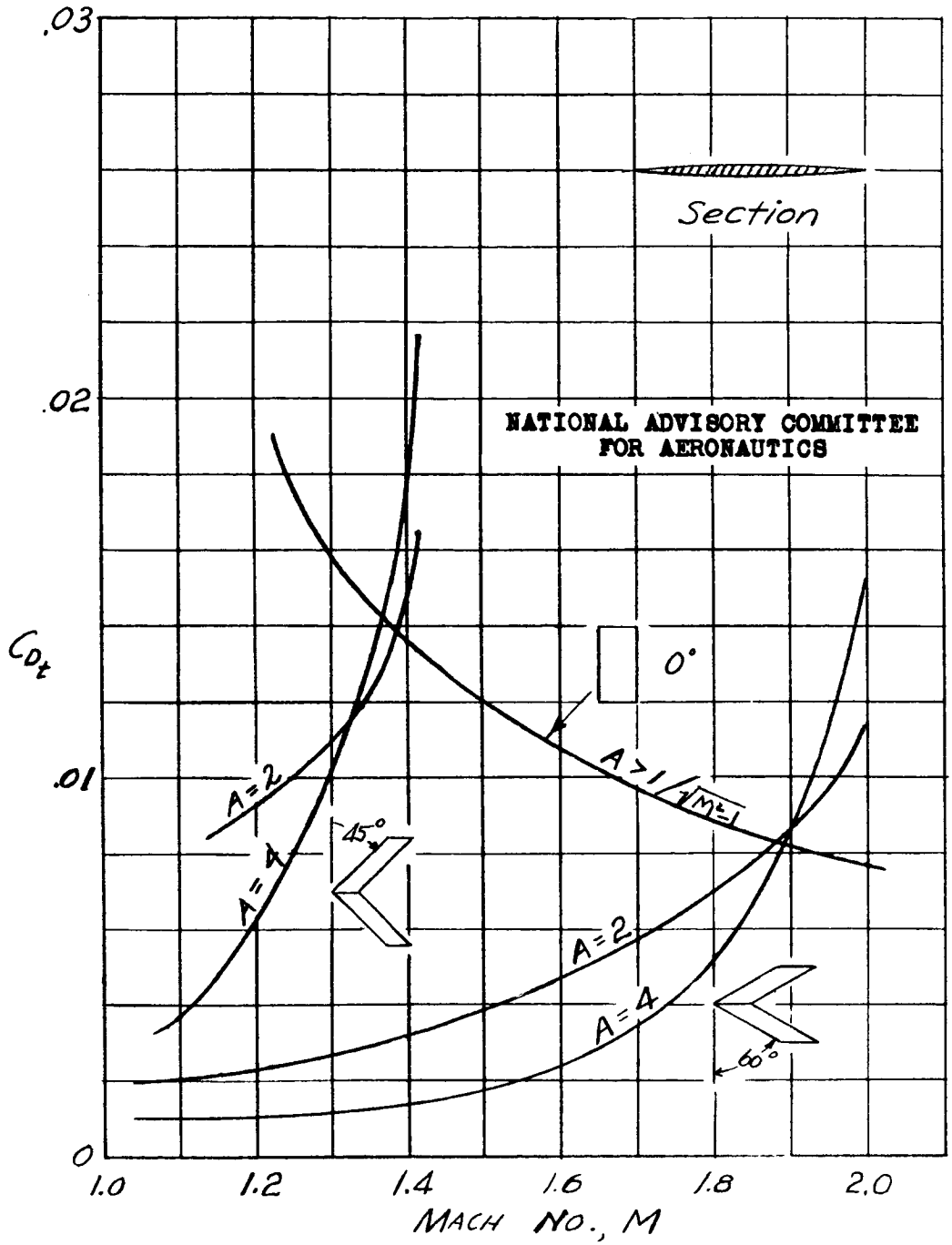

Figure 1. – Thickness drag coefficient for straight and sweptback wings; biconvex section, 5 percent thick.

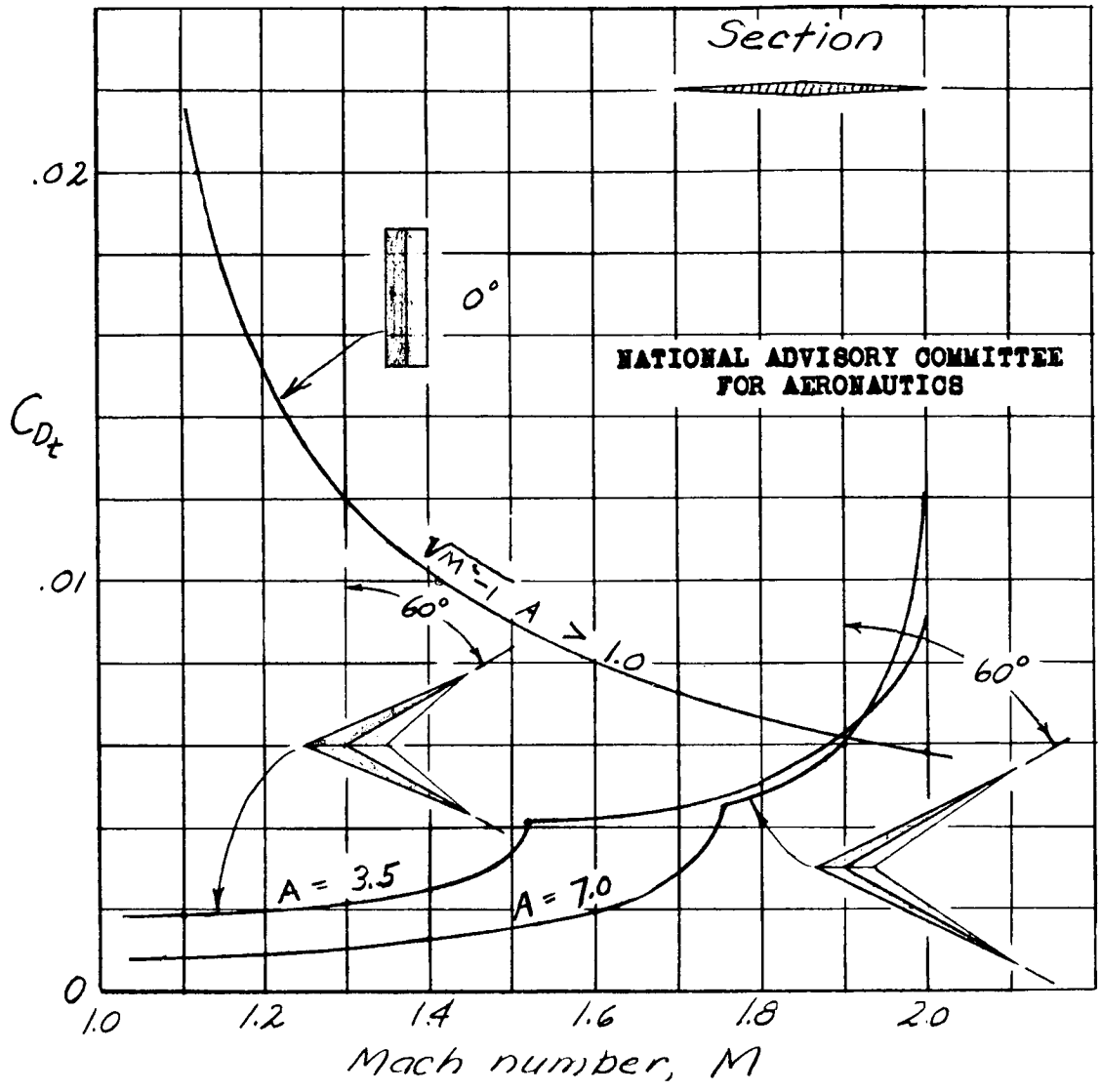

Figure 2.- Thickness drag coefficients for tapered swept-back wings compared with straight wing. Double-wedge sections, 5 percent thick.

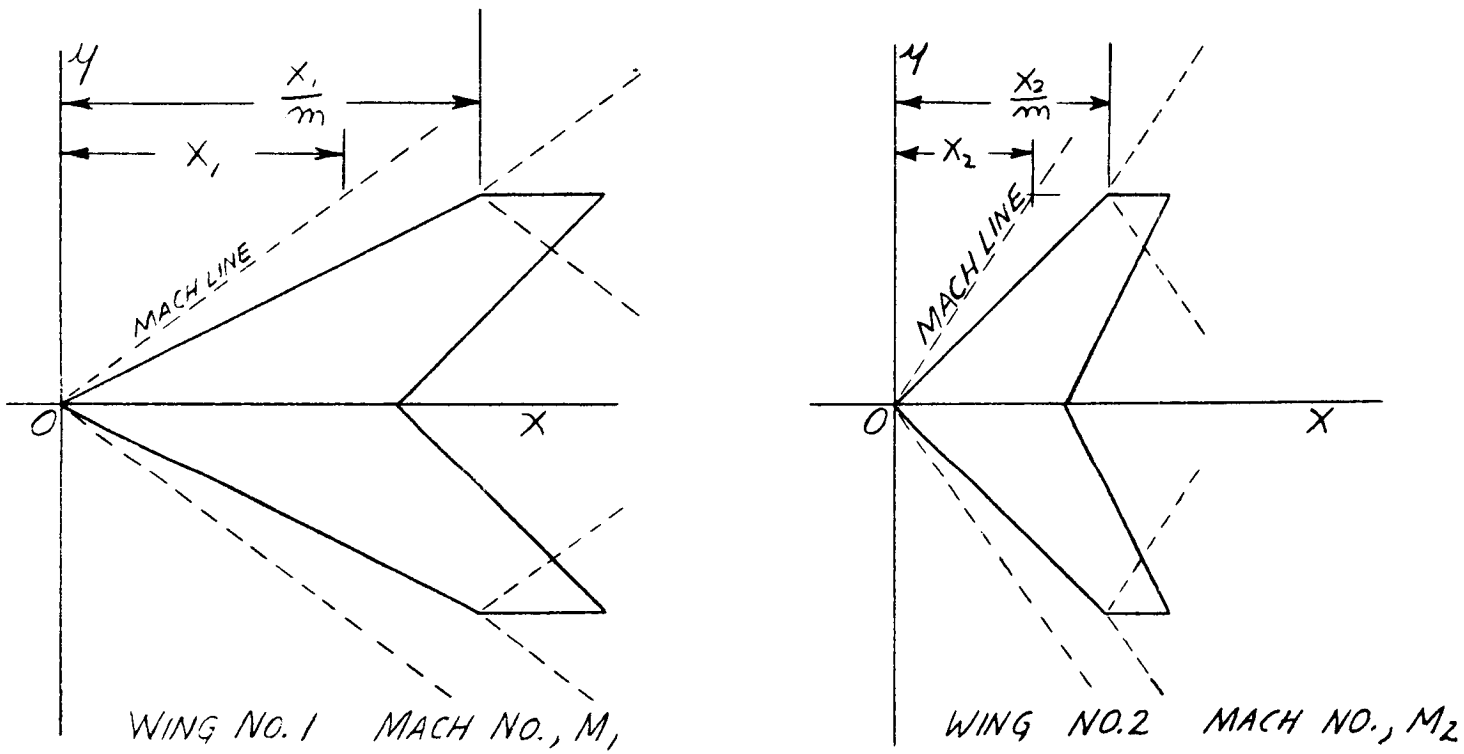

NATIONAL ADVISORY COMMITTEE
FOR AERONAUTICS

$$\alpha_1 = \alpha_2 \; ; \left(\frac{t}{c}\right)_1 = \left(\frac{t}{c}\right)_2 \; ; \left(\frac{\Delta p}{q}\right)_1 = \left(\frac{\Delta p}{q}\right)_2 \quad \frac{x_2}{x_1}$$

FIGURE 3. — WINGS HAVING SIMILAR FLOW PATTERNS AT DIFFERENT MACH NUMBERS.

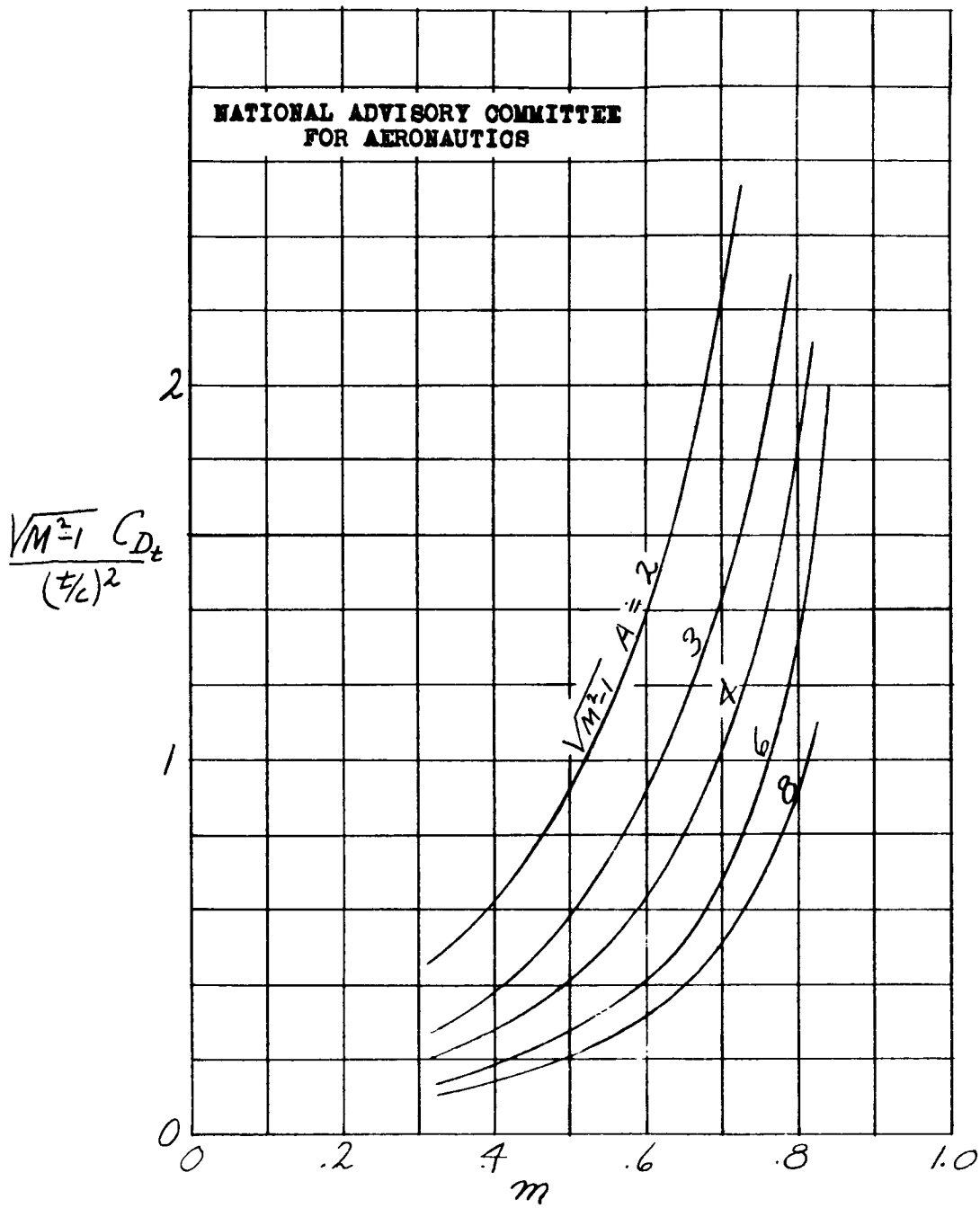

Figure 4 - Thickness drag coefficient for constant-chord sweptback wings of biconvex section.

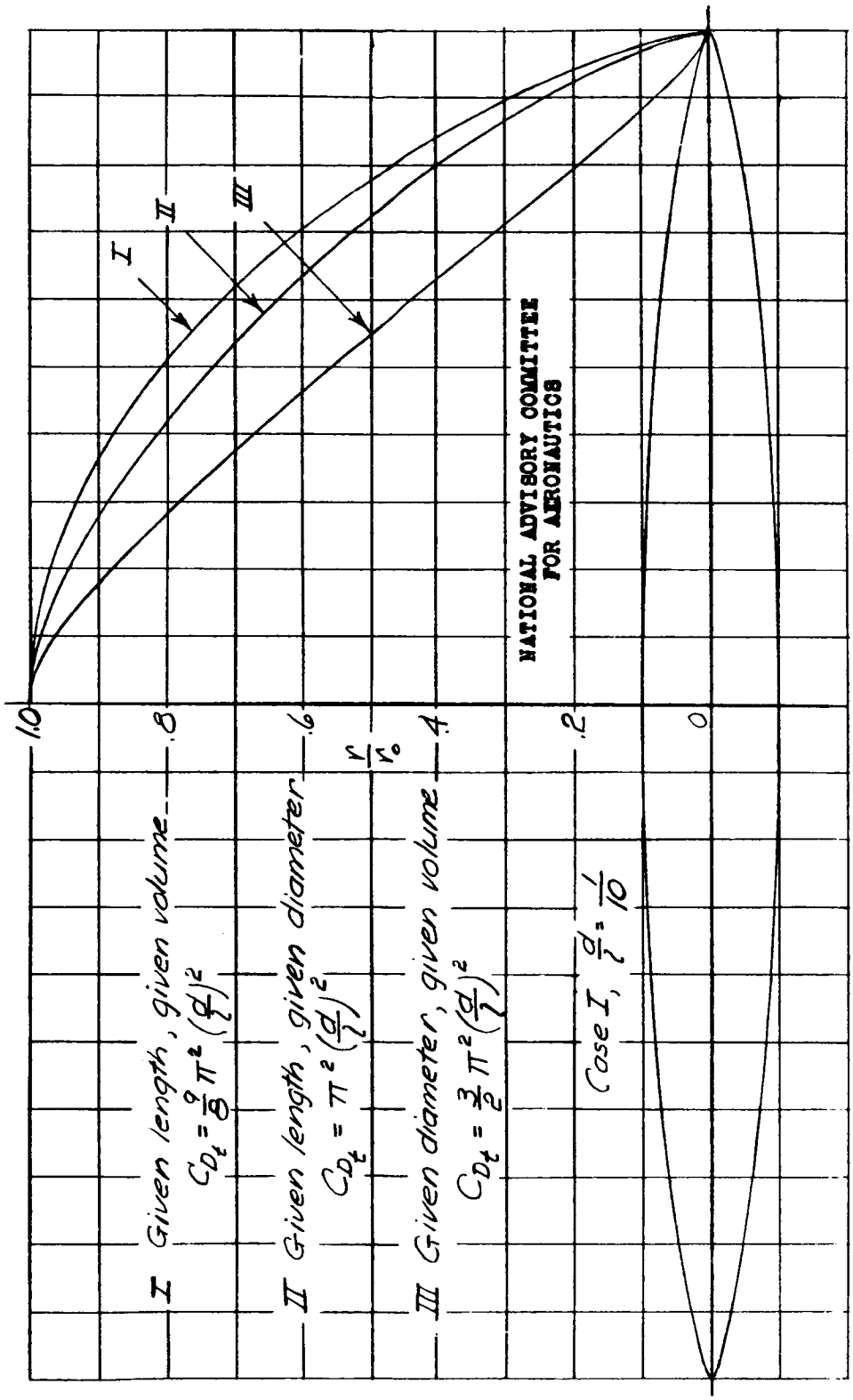

Figure 5 – Bodies of revolution having the minimum wave drag for different specifications of length, diameter and volume. (Ref. 10).

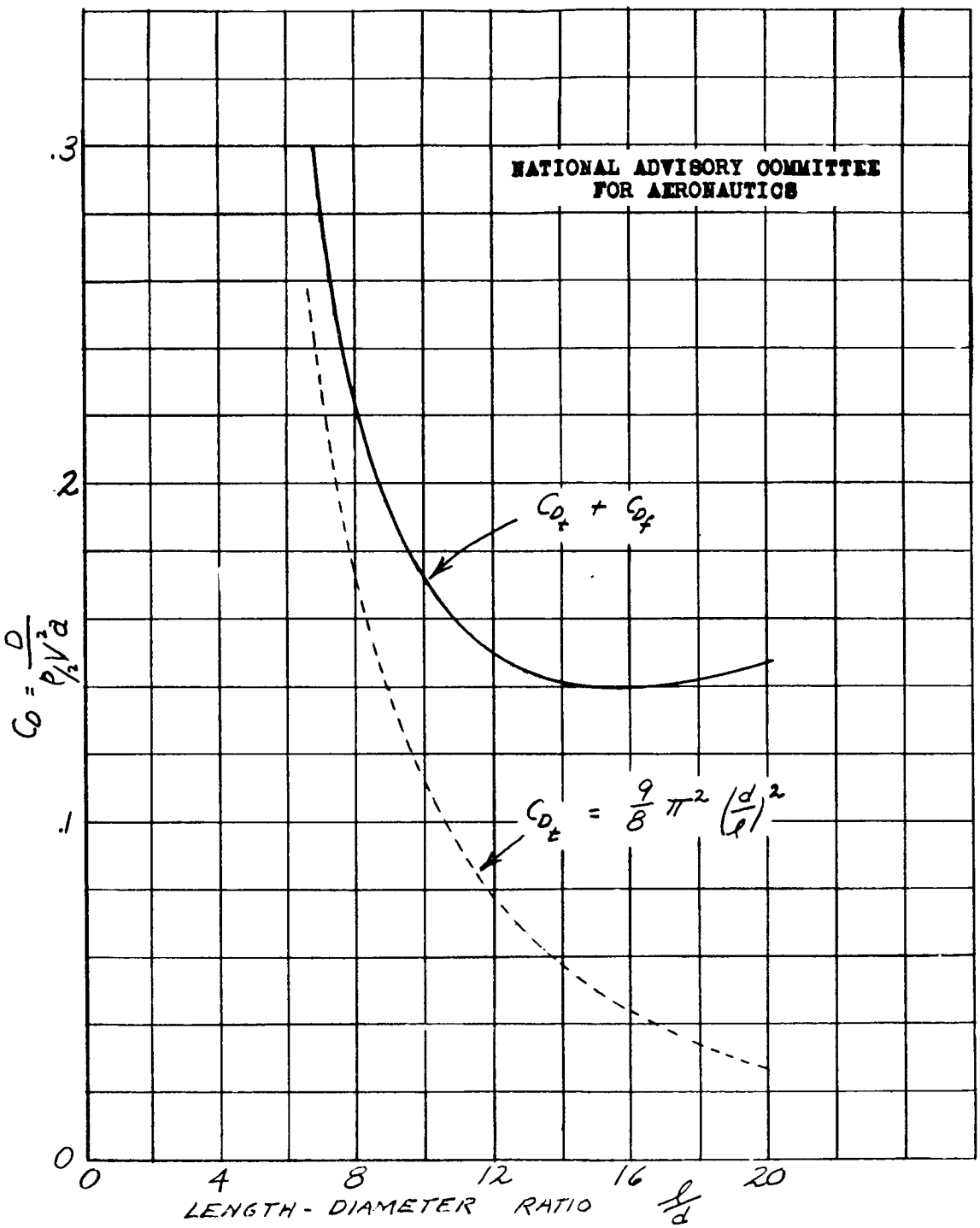

FIGURE 6 — DRAG COEFFICIENT OF FUSELAGE I

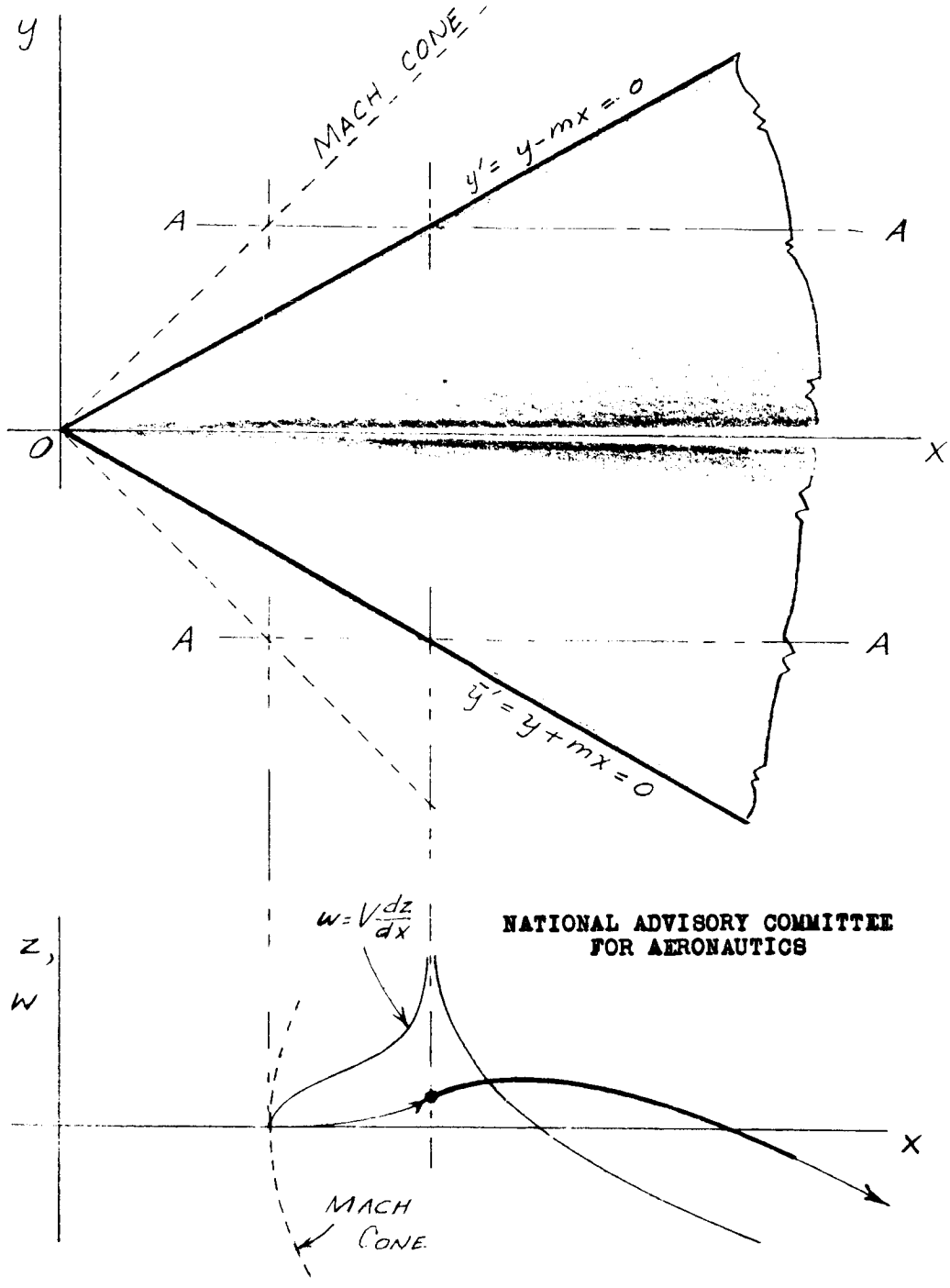

FIGURE 7.- UNIFORMLY LOADED TRIANGLE FORMED BY V-SHAPED VORTEX.

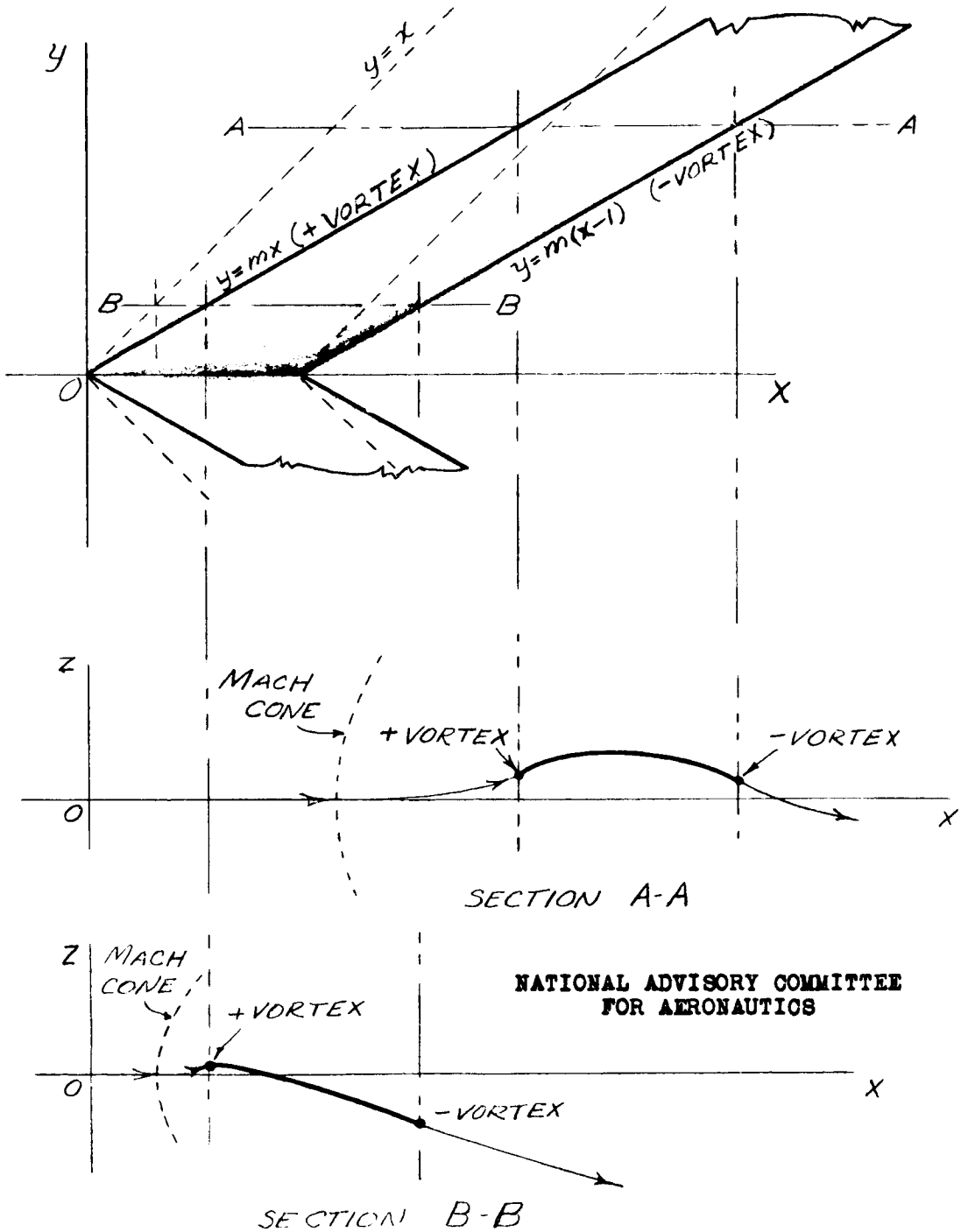

FIGURE 8.- STREAMLINES AND CAMBER SHAPES FOR UNIFORMLY LOADED SURFACE.

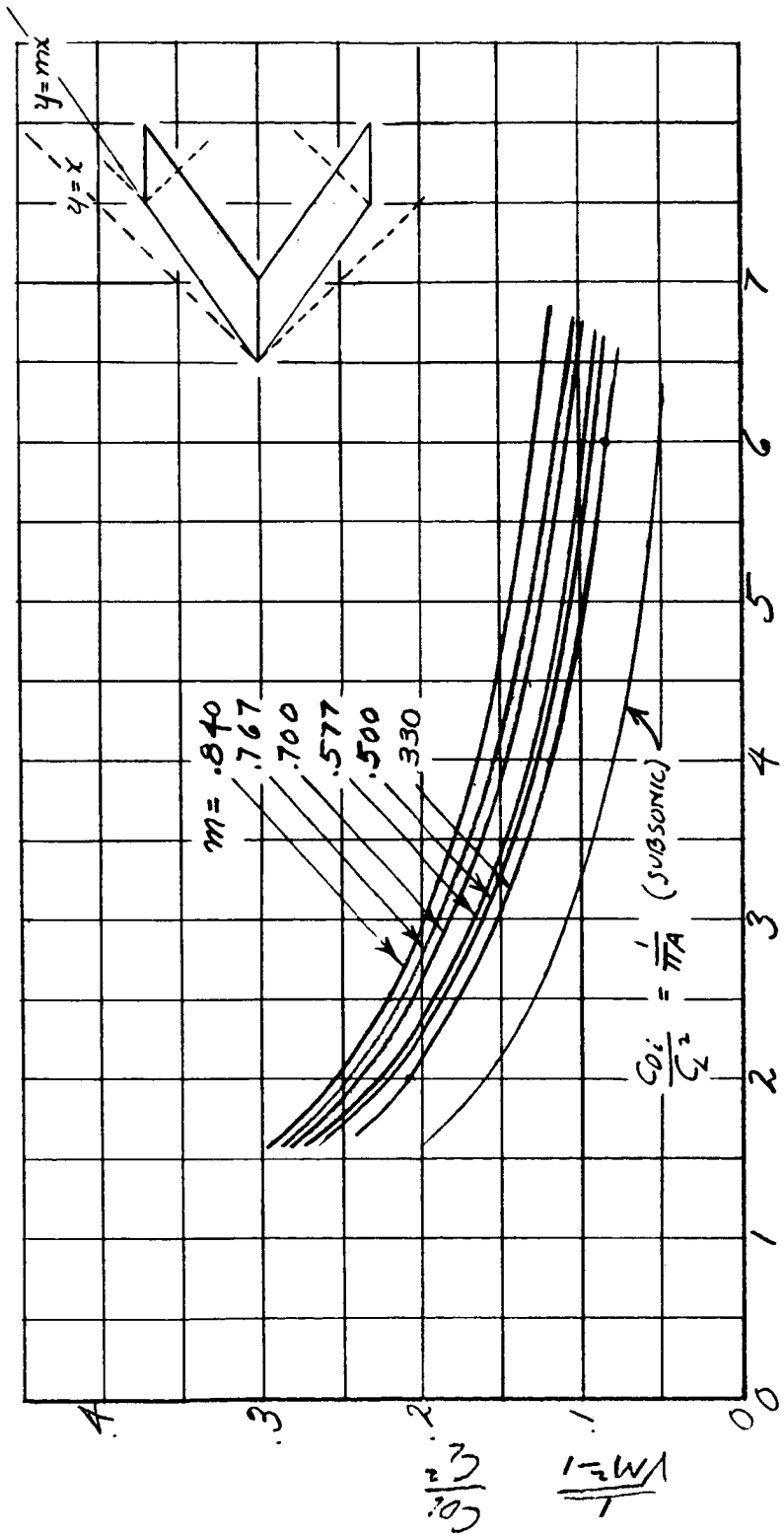

Figure 9. — Coefficient of drag due to lift for swept-back wings with uniform distribution of load.

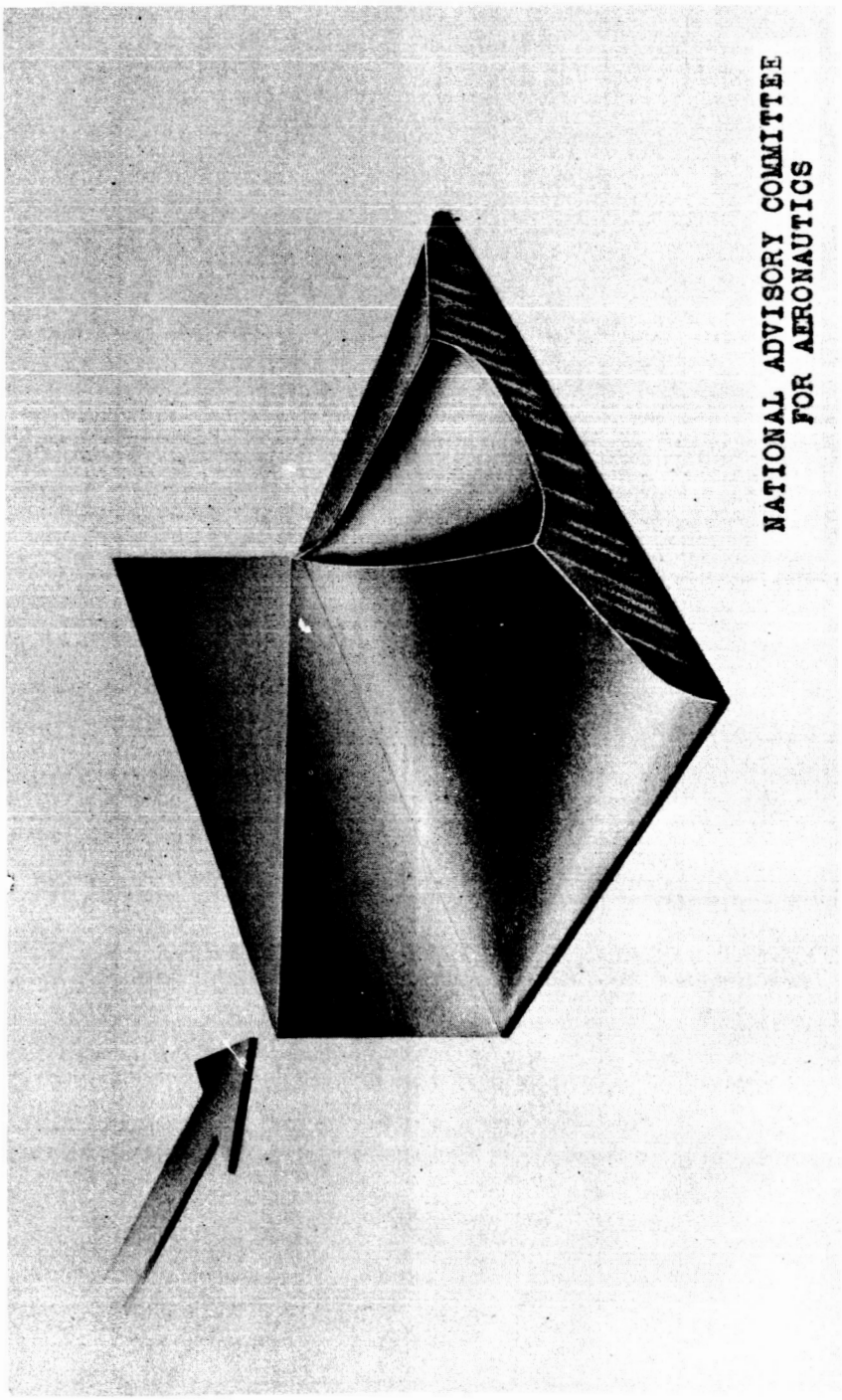

Figure 10.- Lift distribution over flat rectangular surface (ref. 7).

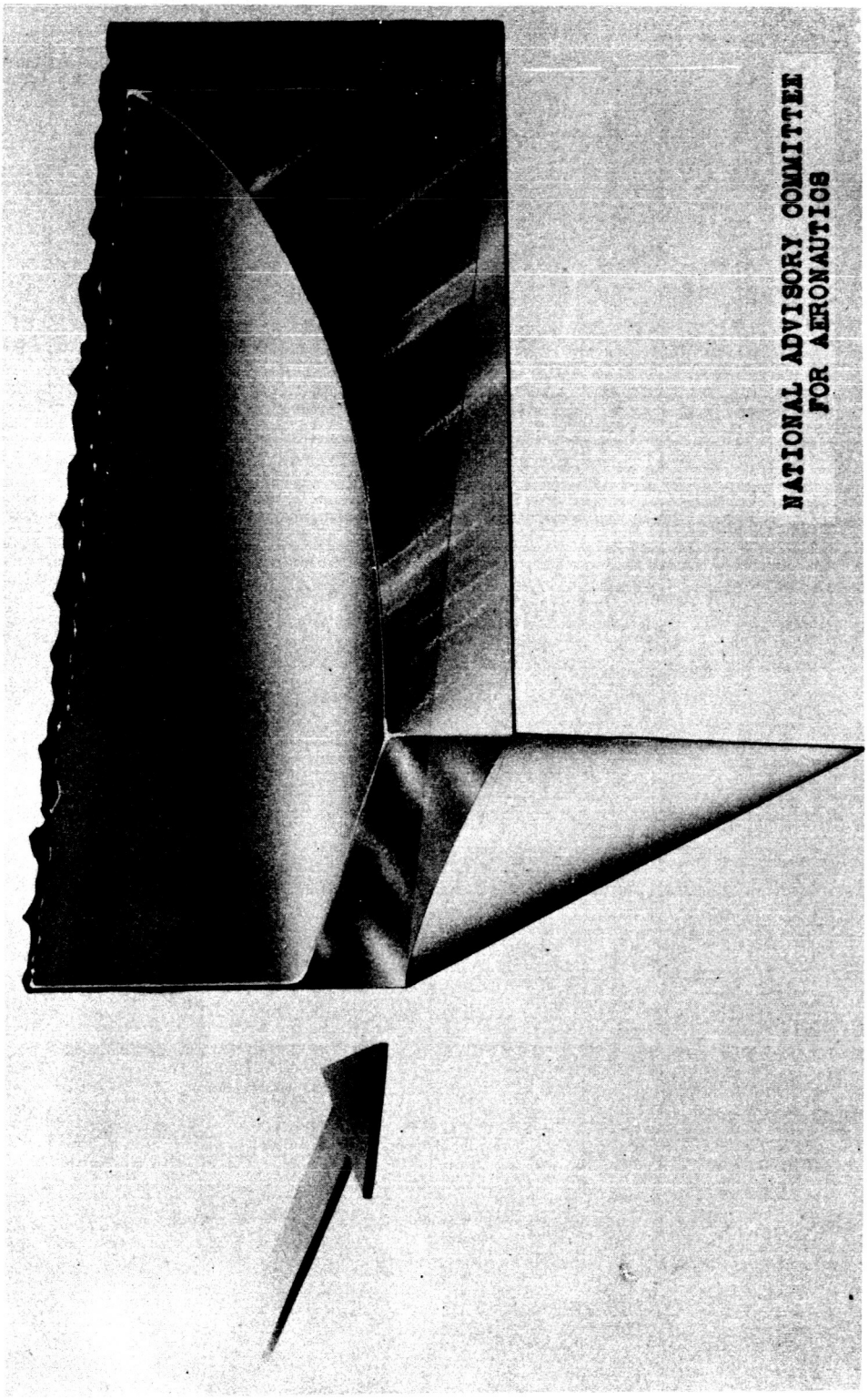

Figure 11.- Lift distribution over swept-back tapered wing with trailing edges along Mach lines.

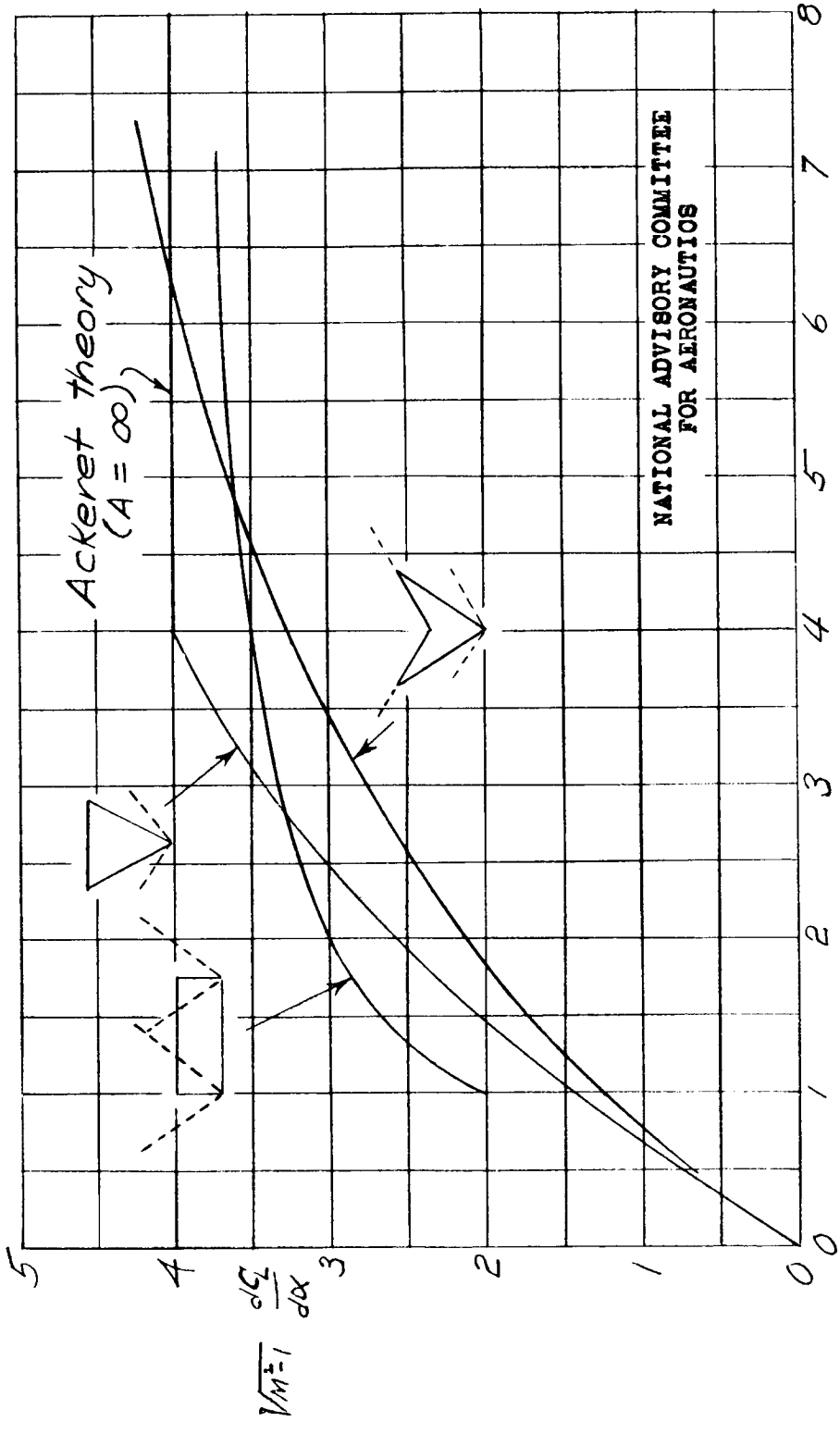

Figure 12. - Lift-curve slope as a function of aspect ratio

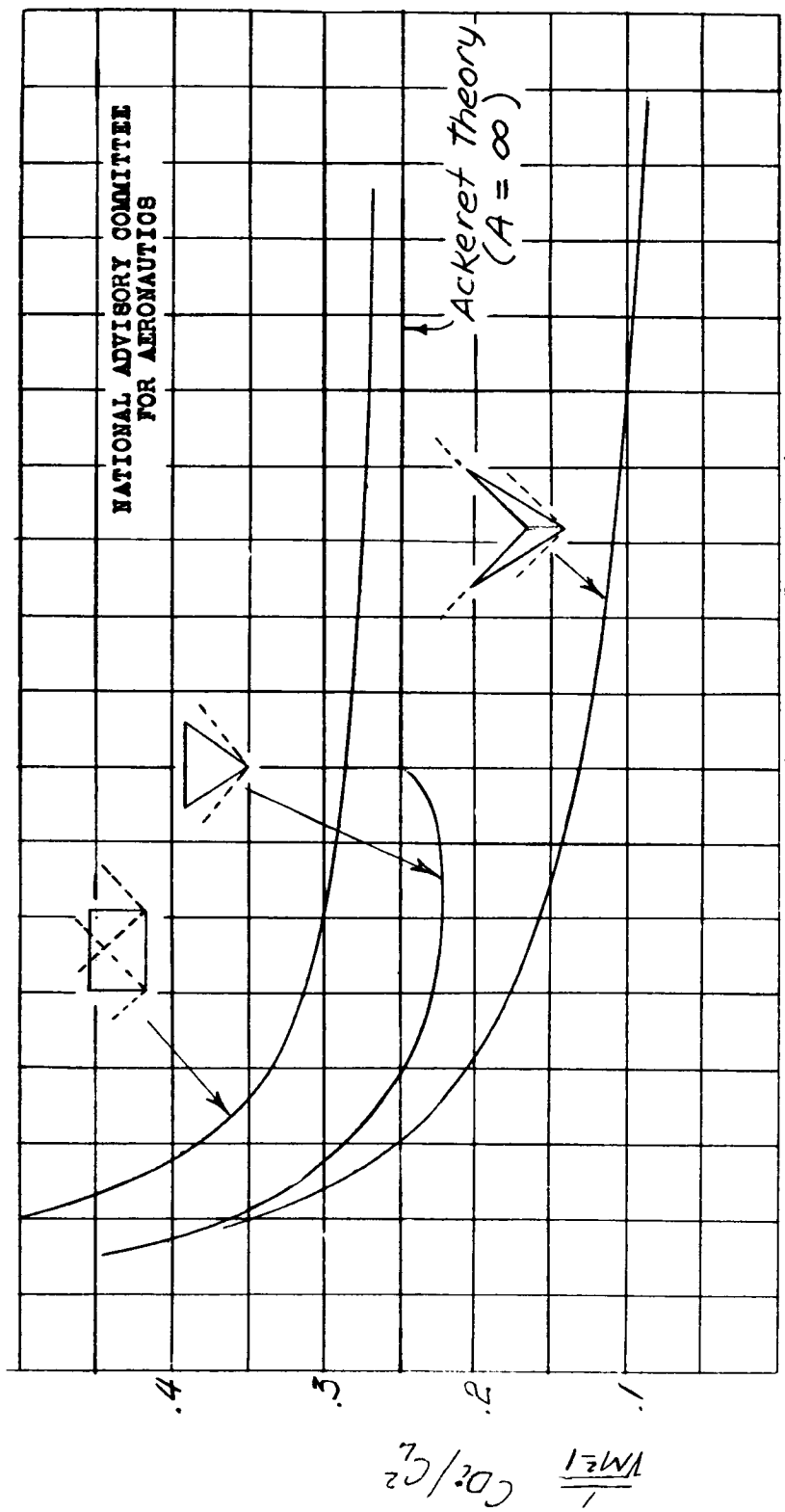

Figure 13 - Drag due to lift as a function of aspect ratio, flat wings

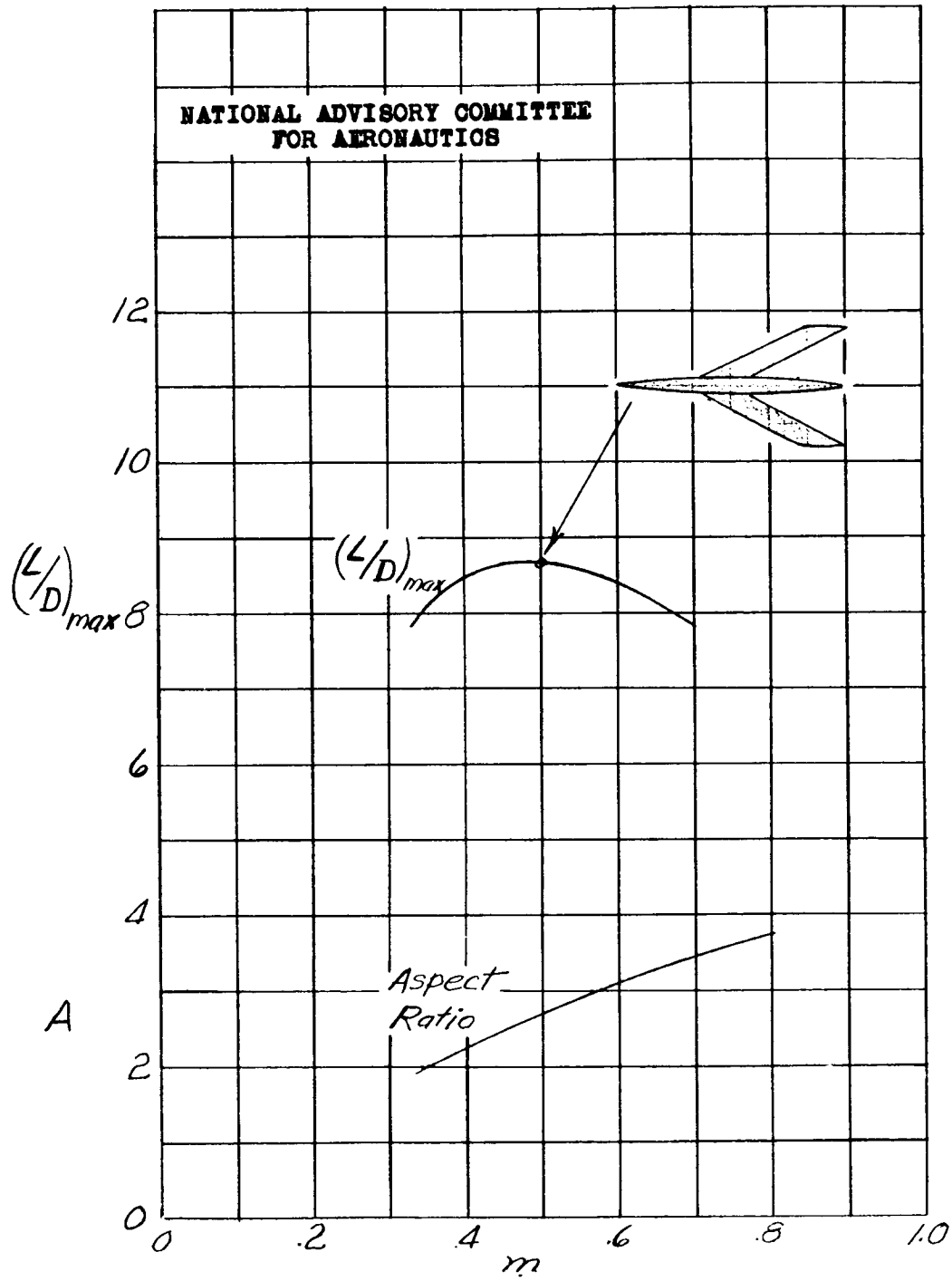

Figure 14 - $(L/D)_{max}$ for airplane with uniformly loaded, constant-chord wings; M = 1.4.

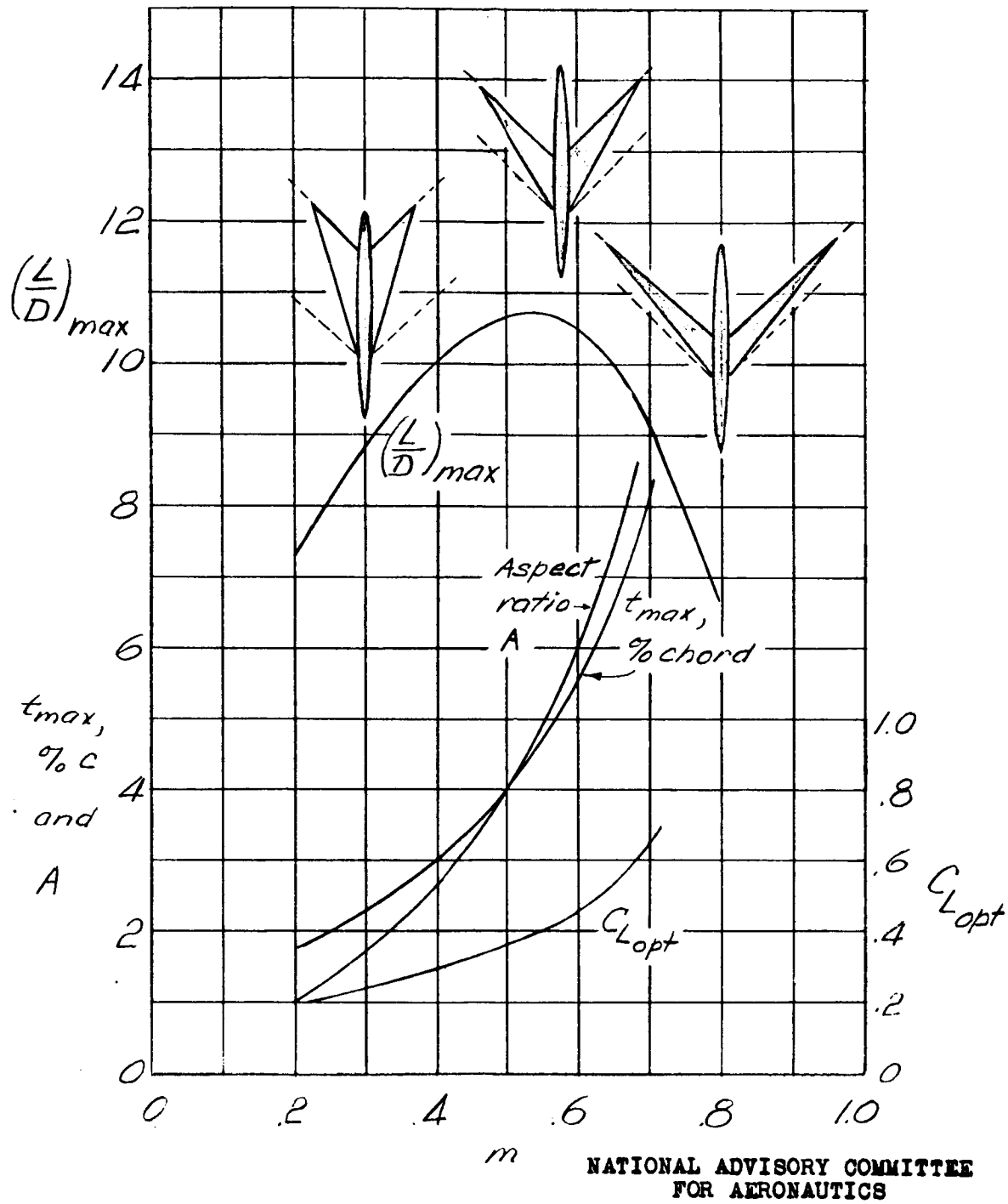

Figure 15.—$(L/D)_{max}$ and $C_{L_{opt}}$ for tapered wing configurations with varying sweep. M=1.4.

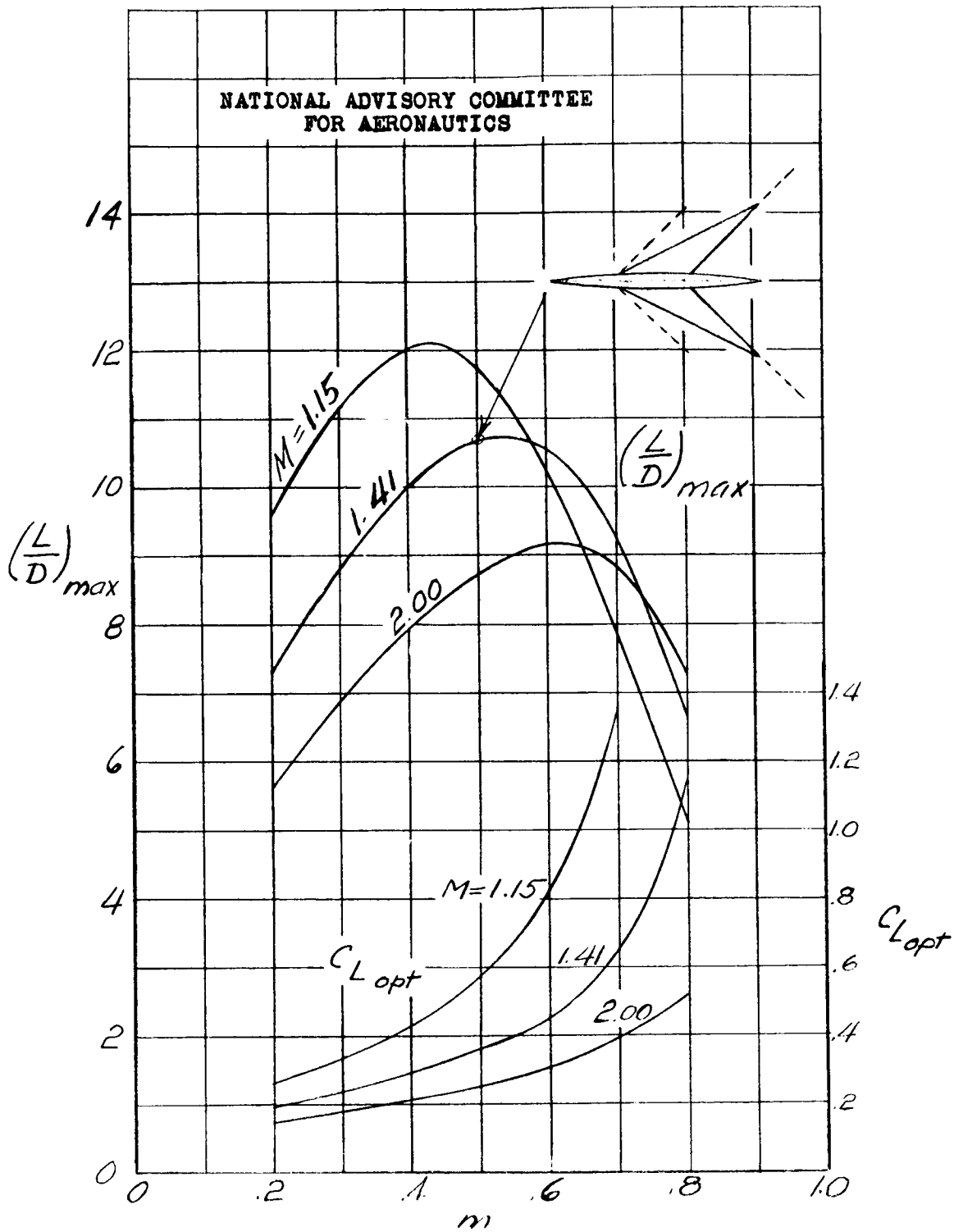

Figure 16.- $(L/D)_{max}$ for airplanes with tapered sweptback wings at various Mach numbers.

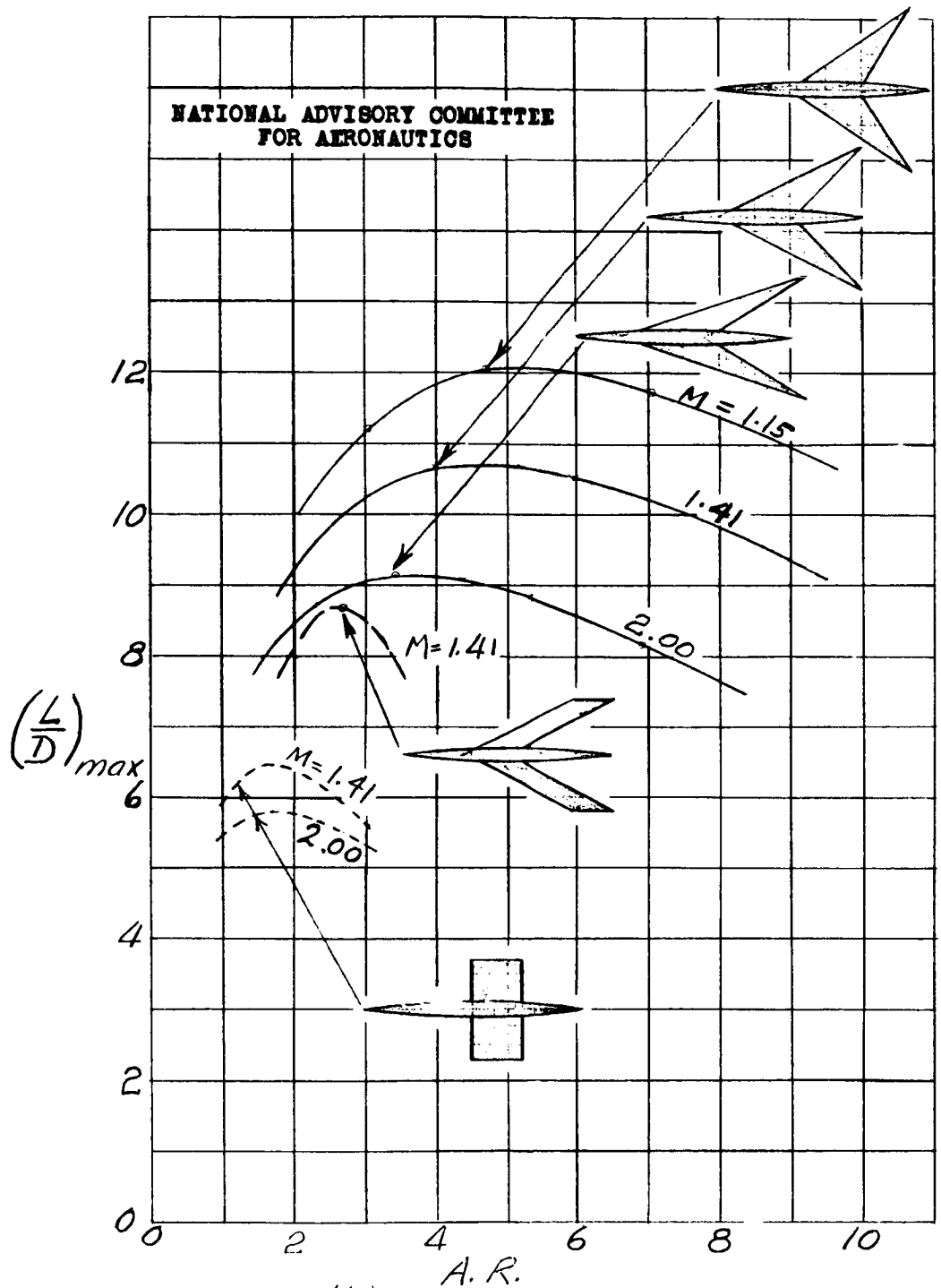

Figure 17.– $\left(\frac{L}{D}\right)_{max}$ at different Mach numbers for airplanes with straight and swept-back wings of varying aspect ratio.

TECHNICAL NOTE 1402

EFFECTS OF SWEEPBACK ON BOUNDARY LAYER AND SEPARATION

Robert T. Jones

Ames Aeronautical Laboratory

July 1947

NATIONAL ADVISORY COMMITTEE FOR AERONAUTICS

TECHNICAL NOTE NO. 1402

EFFECTS OF SWEEPBACK ON BOUNDARY LAYER AND SEPARATION

By Robert T. Jones

SUMMARY

Following the law of stress adopted in the Navier-Stokes equations, the configuration of the viscous flow in planes at right angles to the axis of an infinite cylinder is found to be independent of the axial motion of the cylinder. In the limiting case of a yawed or swept wing of very high aspect ratio, certain boundary-layer and separation phenomena are thus determined independently by the crosswise component of velocity. It follows that the effect of sweepback is to increase the area of stable laminar flow and to decrease the lift coefficient at which flow separation occurs.

INTRODUCTION

Experimental observations of the viscous flow over oblique wings and bodies present such complex phenomena that even the most approximate simplifying principle may be of value in interpreting these observations. In the case of compressible flow, such a simplifying principle was found by studying the idealized problem of the perfectly cylindrical oblique flow, corresponding to the infinite aspect-ratio wing, or the infinitely slender body. In that case, the equations of motion together with the boundary conditions applicable to a moving cylinder in a frictionless fluid showed that (1) the flow pattern and pressure disturbances in planes at right angles to the cylindrical axis are determined solely by the component of velocity in these planes and, (2) the axial motion of the cylinder produces no effect on the flow. Now the question is: Can similar generalizations be made concerning the viscous flow produced by an infinite cylinder moving obliquely? For this case, the Navier-Stokes equations, together with the given boundary conditions, supply a definite answer. It can be shown that proposition (1) still applies while proposition (2), of course, does not. Thus it is to be expected that various features of the viscous flow such as boundary-layer thickness and separation point if observed in planes

at right angles to the cylindrical axis will be determined solely by the component of velocity of the cylinder in these planes.

OBLIQUE VISCOUS FLOW

To verify this feature of the oblique flow, consider first the disturbance produced by a pure crosswise motion of the cylinder. The motion and the state of stress will be the same in all cross sections. Each particle in a given cross section is thus associated with a whole string of particles, or a filament, connecting the various cross sections and moving as a unit. Obviously we may introduce any arbitrary lengthwise translation of these filaments without affecting their progress across the cylinder, since each particle will simply move from one cross section to another similar one. Such a lengthwise motion of the filaments will, of course, introduce shearing stresses in this direction, but these stresses will not affect the rate of shear and hence will not affect the shearing stress in the crosswise direction.

The independence of the cross flow and the axial flow is, of course, the result of the law of shearing stress adopted in the Navier-Stokes equations. The shearing stress in one direction is taken to be proportional to the rate of shearing in this direction and is independent of the rate of shearing in other directions. At high rates of shear where an appreciable temperature rise is involved, the independence of the shearing stresses can no longer be assumed. Such conditions occur at very high Mach numbers and are, of course, beyond the range of validity of the Navier-Stokes equations.

THE LAMINAR BOUNDARY LAYER ON AN OBLIQUE FLAT PLATE

The simplest case of viscous, cylindrical flow is the laminar boundary layer over a flat plate (Blasius flow). The well known result of Blasius shows a parabolic increase of boundary-layer thickness beginning at the leading edge, i.e.,

$$\delta = k\sqrt{\frac{\nu x}{V}}$$

In accordance with the foregoing statements the boundary-layer thickness at any given point will not be affected by the introduction of an additional velocity parallel to the leading edge of the plate. In fact, Blasius' formula shows no change in δ if we change x so that

it is measured along the direction of the new resultant velocity since, in this case, both x and V are changed in the same ratio, figure 1. The resultant drag on the oblique plate lies in the direction of the resultant velocity, but the component force in the direction at right angles to the leading edges can be determined solely from the velocity component in this direction.

An approximate solution for the laminar boundary layer on an oblique plate with a favorable pressure gradient has been given recently by Prandtl in reference 1. On the assumption that the flow in the boundary layer departs only slightly from the direction of the main stream, Prandtl obtains the velocity profile of the boundary layer in two mutually perpendicular directions. It appears that the resultant friction drag is inclined away from the stream direction toward the direction of the favorable pressure gradient.

WIND-TUNNEL TESTS OF CIRCULAR WIRES

With more complex flows involving pressure stresses as well as viscous stresses complete solutions have been obtained only for very low Reynolds numbers. At high Reynolds numbers the pressure stresses predominate but viscosity plays an important part through its effect on separation. Thus in the case of a circular cylinder the flow separates approximately half-way around the surface and a Kármán vortex street is formed in the wake. One would expect that the geometry of this pattern, the vortex frequency, etc., would depend only on the crosswise component of velocity.

Fig. 2 shows the result of a wind-tunnel test on a circular wire at different angles of yaw (reference 2). In these tests the Reynolds number based on the crosswise component varied from 10^2 to 10^3 - a range in which the drag coefficient is nearly constant. Over this range the crosswise component of the drag force on the wire should be proportional to $(V \cos \beta)^2$ and the tests do indicate this variation.

In the case of the circular cylinder there is a certain critical Reynolds number at which the line of separation shifts rapidly to a more rearward position. This shift is accompanied by a marked reduction in the drag coefficient. If the cylinder is oblique, the critical Reynolds number should be delayed to a higher speed such that

$$\frac{V \cos \beta \, d}{\nu} = R_{critical}$$

STABILITY OF LAMINAR FLOW

It is well known that a laminar boundary layer or surface of discontinuity becomes unstable at certain Reynolds numbers. Calculations of the stability of the laminar boundary layer in two-dimensional motion have been made by Tollmein, Schlichting and, more recently, by Lees and Lin. The theoretical predictions have been verified experimentally in important respects by Dryden, Schubauer and Skramstad (references 3 and 4), who find that transition to turbulent flow can result from fluctuations in the laminar layer. In the case of a yawed plate or airfoil the calculated boundary-layer waves would, of course, have their crests and troughs aligned with the leading edge and their stability would be determined by the Reynolds number of the crosswise component of the stream velocity. In case transition is caused by such oscillations one would expect the transition line to recede from the leading edge with increasing angles of yaw in a stream of constant velocity. On the other hand, if transition is caused by roughness of the surface, a cylindrical flow cannot be assumed and the transition may, of course, be affected differently.

An interesting case which departs radically from the usual assumptions made for a cylindrical boundary has been investigated by G. I. Taylor (see reference 5). Taylor investigates the stability of viscous flow in the annular space between two concentric circular cylinders in relative rotation. After a certain Reynolds number is exceeded the cylindrical form of the flow disappears and a regular vortex formation appears with the vortex rotations at 90° to the rotation of the cylinders, and alternating periodically along their length. Gortler and Liepmann find similar three-dimensional disturbances in other cases of boundary-layer flow along convex walls. According to Liepmann(reference 6) transition from laminar to turbulent flow results from this three-dimensional type of instability if the surface is concave, but transition on a plane or convex surface results from the two-dimensional type of wave motion mentioned earlier.

FLOW SEPARATION AND MAXIMUM LIFT

The separation of flow over a straight wing occurs when the adverse pressure increase opposing the motion is sufficient to reverse the momentum of the fluid in the boundary layer (see Fig. 3). In the case of the oblique wing the resultant pressure gradient is of course at right angles to the long axis of the wing and both this pressure and the components of the viscous stress distribution lying in this direction will be determined by the crosswise component of velocity.

Hence the circumstances leading to separation of flow over the straight wing will be reproduced if the crosswise component of motion of the oblique wing is the same as that of the straight wing. In both cases separation will be taken to mean that the fluid in the boundary layer has lost the component of momentum that carries it across the wing. In the oblique case the boundary layer will then flow in a direction parallel to the long axis.

The known adverse effects of sweepback on the lift and drag of a wing can be at least partially explained by this analysis. According to the two-dimensional theory a wing which shows boundary-layer reversal and maximum lift at $C_L - 1.4$, if yawed 45^o, would show separation accompanied by a fully developed lateral motion of the boundary layer at $C_L = .7$. In each case the lift would drop and the resultant force would fall back to a position nearly at right angles to the chord because of the loss of the suction force on the leading edge. At 60^o yaw the predicted maximum lift coefficient would be only .35. Wind-tunnel observations of the boundary-layer flow over swept-back wings agree qualitatively with these predictions in regard to flow separation but do not show the expected loss in maximum lift. Instead of a drop in lift after boundary-layer separation, some experiments indicate an increase in lift curve slope at this point. Ordinarily the forces and moments on the swept wing do begin to show non-linear variations at the separation point, however, and there is a sharp rise in drag at this point indicating that the loss of suction at the leading edge does occur. The tendency to follow the two-dimensional theory up to the point of separation and the partial failure of the theory after separation indicates that the "end effects" are much greater in the separated flow than in the unseparated flow. This situation is not surprising from the physical standpoint, since the influence of the tips would obviously be more extensive in the case of a thick separated region than in the case of a relatively thin boundary layer. It must be supposed, however, that as the aspect ratio of the swept-back wing is increased its maximum lift coefficient will show an increasing tendency to follow the $\cos^2$ law. The experiments on oblique circular wires, which involve large regions of separated flow and yet follow the two-dimensional theory, lend support to this hypothesis.

Ames Aeronautical Laboratory,
National Advisory Committee for Aeronautics,
Moffett Field, Calif.

REFERENCES

1. Prandlt, L.: On Boundary Layers in Three-Dimensional Flow. Reports and Translations No. 64, File No. B.I.G.S. 84, M.A.P. Volkenrode May 1, 1946.

2. Relf, E. H., and Powell, C. H.: Tests on Smooth and Stranded Wires Inclined to the Wind Direction and a Comparison of the Results on Stranded Wires in Air and Water. British A.R.C., R. & M. No. 307, 1917.

3. Schubauer. G. B., and Skramstad, H. K.: Laminar-Boundary-Layer Oscillations and Transition on a Flat Plate. NACA ACR April 1943.

4. Dryden, Hugh L.: Some Recent Contributions to the Study of Transition and Turbulent Boundary Layers. NACA T.N. No. 1168, April 1947.

5. Goldstein, S.: Modern Developments in Fluid Dynamics. The Clarendon Press (Oxford), Vol. I, pp. 196-197, 1938.

6. Liepmann, H. W.: Investigation of Boundary Layer Transition on Concave Walls. NACA ACR No. 4J28.

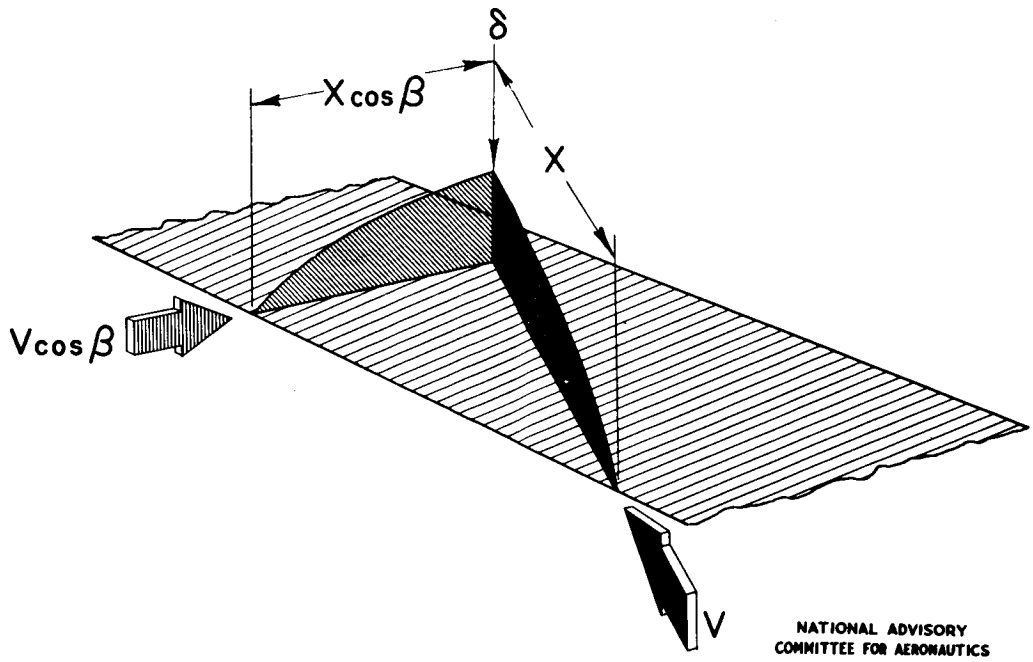

FIGURE 1.- BOUNDARY LAYER ON AN OBLIQUE FLAT PLATE.

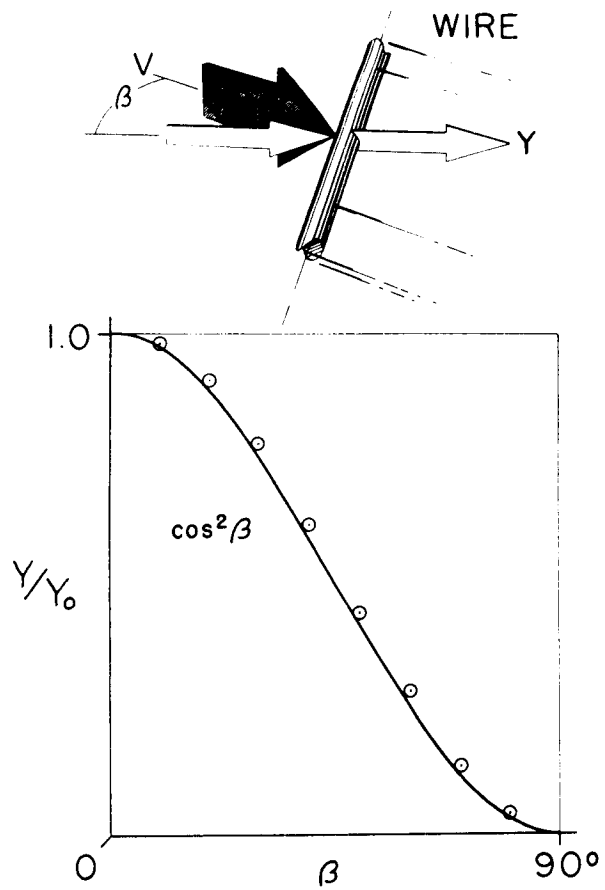

FIGURE 2.- EXPERIMENTAL VARIATION OF CROSS-WISE FORCE ON AN OBLIQUE WIRE. NATIONAL ADVISORY COMMITTEE FOR AERONAUTICS

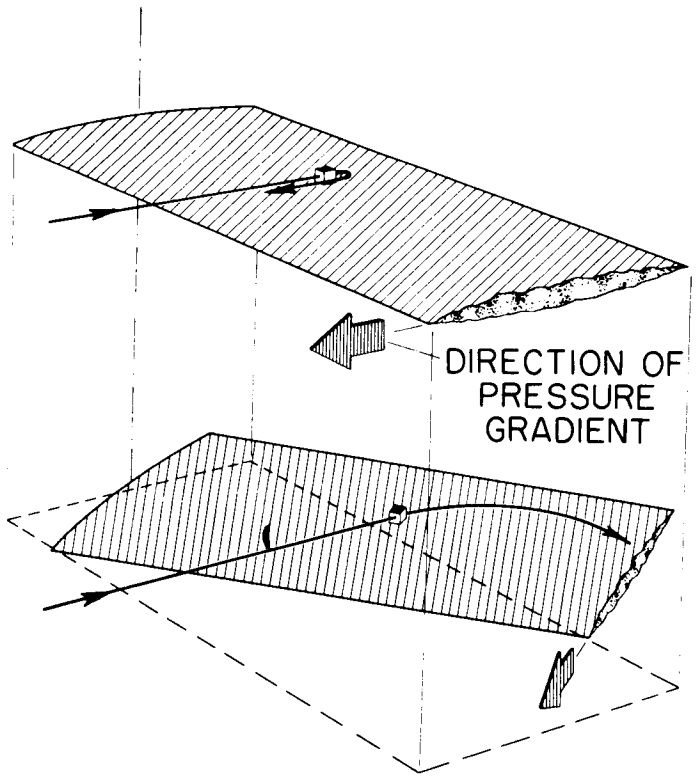

FIGURE 3.- EFFECT OF YAW ON PATHS OF PARTICLES IN SEPARATED BOUNDARY LAYER. NATIONAL ADVISORY COMMITTEE FOR AERONAUTICS

THE USE OF CONICAL AND CYLINDRICAL FIELDS IN SUPERSONIC WING THEORY

Robert T. Jones

Ames Aeronautical Laboratory

June 1948

THE USE OF CONICAL AND CYLINDRICAL FIELDS IN SUPERSONIC WING THEORY

By Robert T. Jones

Ames Aeronautical Laboratory

Some of the recent advances in the theory of thin airfoils are presented with particular reference to extensions of the theory to three-dimensional flows and to supersonic speeds.

The thin-airfoil theory is essentially a linearized theory of small disturbances and the origin of the concepts may be traced back to the older theories of Munk and Ackeret. The present emphasis on three-dimensional flows arose from the discovery that the type of two-dimensional supersonic flow considered by Ackeret is aerodynamically inefficient. The search for aerodynamically efficient forms for supersonic flight also focuses attention on the linear, or small-disturbance, theory since bodies and wings creating large disturbances are thought to be aerodynamically inefficient.

The newer development of the theory is the work of many investigators. The present discussion, however, is based largely on the conical-flow theory first employed by Busemann (reference 1).

The term "thin airfoil" is used to denote a thin, essentially flat body, the surface of which departs only slightly from the xy-plane. In the general problem no restriction is made on the shape of the plan form, but it is essential that the body be thin and flat in all vertical cross sections; hence, slender bodies of revolution are excluded.

The problem discussed herein is the calculation of the small disturbance velocities u, v, and w in the external field produced by the flight velocity V of the airfoil.

As is well known in acoustics, air motions of small amplitude are governed primarily by the simple properties of elasticity of volume and density. In order to depict such motions mathematically, a frictionless, perfectly elastic fluid is, therefore, adopted and a velocity field uvw must be found which is consistent with Newton's laws and which agrees at the airfoil surface with the outward, or normal, velocity imparted by the motion of the airfoil. The application of Newton's laws to the motions of small elements of such a simplified model fluid results in the familiar wave equation for the velocity potential ϕ,

$$\phi_{xx} + \phi_{yy} + \phi_{zz} = \frac{1}{c^2}\phi_{tt} \tag{1}$$

where c is the velocity of sound and $\phi_x = u$, $\phi_y = v$, $\phi_z = w$.

The description of the whole velocity field by a single scalar potential ϕ is, of course, a great simplification and, as explained in text books on hydrodynamics, this scalar potential occurs in every case of frictionless motion in which the density ρ is a function of the pressure only. The elements of such a fluid move only under the action of "buoyancy" or pressure forces. When the density is dependent on the pressure only, variations of density occur only along the direction of the buoyant force. This force then passes through the center of gravity of each element and no rotation is produced. The existence of ϕ follows from the absence of rotation.

Of first interest in the airfoil problem are steady flows. The steady flow consists of a fixed pattern of streamlines attached to the airfoil and moving with it. In order to represent the steady flow, it will be necessary to transform the stationary axes of equation (1) to axes moving with the airfoil at the flight velocity V. The quantity $\frac{1}{c^2}\phi_{tt}$ is then replaced by $\frac{V^2}{c^2}\phi_{xx}$ and the equation becomes, after transposition,

$$\left(1 - \frac{V^2}{c^2}\right)\phi_{xx} + \phi_{yy} + \phi_{zz} = 0 \tag{2}$$

in which $\frac{V}{c}$ is the Mach number M. The problem is now the mathematical one of finding a solution of equation (2) which agrees with the normal boundary velocity imparted by the airfoil. When the thin airfoil as specified is used, it is found sufficient to replace the actual boundary condition by an equivalent condition on the vertical velocity w in the chord plane; that is,

$$(w)_{z=0} = V\frac{dz}{dx}$$

where $\frac{dz}{dx}$ is the slope of the airfoil surface. It is important to note that the sliding component of the airfoil surface imparts no motion to the fluid since the fluid is frictionless. The error made in the equivalent boundary condition at $z = 0$ becomes appreciable only at distances of the order of one wing thickness from the edge. The pressure distribution over the airfoil surface may likewise be taken as the pressure in the chord plane and is obtained from the well-known formula for the pressure in a sound wave

$$\Delta p = -\rho\frac{\partial \phi}{\partial t}$$

or, in steady flow

$$\Delta p = -\rho V \frac{\partial \phi}{\partial x}$$

from which

$$\frac{\Delta p}{q} = -2\frac{u}{V}$$

Thus far, nothing has been said about subsonic- or supersonic-flight velocities. This distinction arises in equation (2) and in the form of its solutions when $M \gtrless 1$.

Except for this distinction, variations of M are of no consequence mathematically since they can be represented by an equivalent change in the scale of x relative to the other coordinates. This change of scale is known as the Prandtl-Glauert transformation and is given as

$$x' = \frac{x}{\sqrt{1 - M^2}}$$

or

$$x' = \frac{x}{\sqrt{M^2 - 1}}$$

The formula to be used depends on whether the flight velocity is subsonic or supersonic. In the latter case, the significance of the transformation is easily seen, since this transformation serves to maintain the correct inclination of the Mach waves to the line of flight at different speeds. It should be noted that the sudden transition of the differential equation from the elliptic to the hyperbolic type at $M = 1.0$ is a feature of the steady-flow equation (equation (2)) and does not, of course, arise in connection with equation (1).

The essential features of the steady flow at subsonic or supersonic speeds can then be ascertained from solutions of the reduced or normalized equations. For $M = 0$,

$$\phi_{xx} + \phi_{yy} + \phi_{zz} = 0 \qquad (3)$$

and for $M = 1.41$,

$$\phi_{xx} - \phi_{yy} - \phi_{zz} = 0 \tag{4}$$

As may be shown by direct differentiation, equations (3) and (4) possess the primary solutions

$$\phi = f(\alpha x + \beta y + \gamma z)$$

where α, β, and γ are quantities determined so that for equation (3)

$$\alpha^2 + \beta^2 + \gamma^2 = 0$$

and so that for equation (4)

$$\alpha^2 - \beta^2 - \gamma^2 = 0$$

The cylindrical flow field, which is the basis of the two-dimensional or wing section theory, is obtained by specializing the primary solution to the two coordinates x and z. In this case for equation (3) $\alpha = 1.0$ and $\gamma = i$; and for equation (4) $\alpha = 1.0$ and $\gamma = 1.0$ so that the general solutions for the cylindrical or two-dimensional flow field become

$$\phi = f(x \pm iz)$$

or

$$u = f'(x \pm iz)$$

$$w = \pm iu$$

The general solution is the basis of the Munk theory, as well as the more exact wing section analyses which depend on the theory of functions of a complex variable. At supersonic speeds the corresponding solutions are

$$\phi = f(x \pm z)$$

or

$$u = f'(x \pm z)$$

$$w = \pm u$$

This latter form of solution, which represents a plane sound wave of arbitrary intensity at 45° to the normalized coordinate axes, is the basis of the Ackeret theory.

The general form of flow field given by solutions of the two foregoing types is illustrated in figure 1. The sketch on the left-hand side is the familiar subsonic streamline pattern for a symmetrical biconvex wing section. In the subsonic pattern the velocity and pressure distrubances diminish uniformly with distance and in the case of steady flow the field possesses a fore and aft symmetry which results in no pressure drag or wave drag. The sketch on the right-hand side (fig. 1) illustrates the marked difference in streamline pattern that arises when the crosswise velocity of the cylindrical field is supersonic. In this case the phase relation of u and w is shifted (from 1 to i) and the pressure distribution is antisymmetric, resulting in a wave drag. This drag appears as the energy in the plane sound waves emanating from the airfoil. The change from subsonic to supersonic type of flow field arises when the rate of progress of the flow pattern through the still fluid exceeds the velocity of sound. With cylindrical flow, the field is not affected by an axial velocity of the cylinder and the pattern progresses at a rate determined only by the crosswise motion of the cylinder. Hence, the subsonic type of flow may persist on a yawed wing even though the flight velocity is supersonic. (See reference 2.)

The sketch in the lower part of figure 1 represents a cross section of a conical flow field of the type originated by Busemann. The particular case used for illustration herein is the flow produced by a flat plate of triangular plan form moving point foremost at a small angle of attack (fig. 2). The Mach cone originates, of course, at the apex of the triangle and the field inside this cone is geometrically the same in all downstream cross sections except for an expansion in scale along the x-axis. The conical flow field may be obtained by the superposition of primary solutions of the form.

$$u = F(\alpha x + \beta y + \gamma z)$$

If $\mu = e^{i\theta}$, then the solution

$$u = F\left[\frac{-2\mu x + (1 + \mu^2)y + i(1 - \mu^2)z}{2\mu}\right]$$

represents a plane sound wave at an angle θ to the y-, z-axes. Superposition of such waves of strength $f'(\mu)$ from $\theta = 0$ to $\theta = 2\pi$ results in a solution analogous to Whittaker's solution; that is,

$$u = \oint f'(\mu)\, F\left[\frac{-2\mu x + (1 + \mu^2)y + i(1 - \mu^2)z}{2\mu}\right] d\mu$$

The quantity $-2\mu x + (1 + \mu^2)y + i(1 - \mu^2)z$ may be factored into $(\mu - \varepsilon)\left(\mu - \frac{1}{\varepsilon}\right)(y - iz)$ where

$$\varepsilon = \frac{y + iz}{x + \sqrt{x^2 - y^2 - z^2}}$$

The general solution of zero degree is obtained when F is replaced by log; that is,

$$u = \oint f'(\mu)\, \log\left[\frac{(\mu - \varepsilon)\left(\mu - \frac{1}{\varepsilon}\right)(y - iz)}{2\mu}\right] d\mu$$

$$= \oint f(\mu)\left[\frac{1}{\mu - \varepsilon} + \frac{1}{\mu - \frac{1}{\varepsilon}}\right] d\mu$$

$$= 2\pi i\left[f(\varepsilon)\right]$$

if the contour does not include $\frac{1}{\varepsilon}$ and if $\oint f(\mu)\, d\mu = 0$ or, in other words, if f is an analytic function (see reference 3).

If the flight velocity is subsonic, the argument ε is replaced by $\frac{y + iz}{x + \sqrt{x^2 + y^2 + z^2}}$. The latter solution was given by W. F. Donkin in 1857 (see reference 4). In either case the form of the argument shows an essential similarity to an expanding cylindrical field (see reference 5). In fact, for the slender conical field, where $y^2 + z^2$ may be neglected in comparison with x^2, the argument becomes simply $\frac{y + iz}{2x}$.

Although no analytic function of ε which removes the distortion of the conical field relative to the cylindrical field can be found, it is possible to transform the field in such a way that the distortion is removed in the neighborhood of the airfoil in the plane $z = 0$. The desired transformation is obtained from the fact that

$$\frac{y + iz}{x} = \frac{2\varepsilon}{1 + \varepsilon\bar{\varepsilon}}$$

Since $\varepsilon\bar{\varepsilon}$ approaches ε^2 near $z = 0$, the analytic variable

$$\mathfrak{z} = \frac{2\varepsilon}{1 + \varepsilon^2}$$

will approach $\frac{y + iz}{x}$ in the neighborhood of the chord plane inside the Mach cone. The new variable $\mathfrak{z}$ greatly simplifies the boundary conditions inasmuch as the Mach cone is transformed into the positive and negative branches of the real axis outside ± 1 and the interior of the Mach cone is mapped into the whole plane. Figure 3 illustrates the effect of this change of variable.

The relation between u and w in the conical field is found from the conditions for irrotational flow; that is,

$$\frac{\partial w}{\partial x} = \frac{\partial u}{\partial z}$$

In terms of the variable ε

$$dw = \frac{i}{2}\left(\varepsilon - \frac{1}{\varepsilon}\right) du$$

or in terms of the variable $\mathfrak{z}$

$$w = -i \int \frac{\sqrt{1 - \mathfrak{z}^2}}{\mathfrak{z}}\, du$$

It is interesting to note that the condition for a flat airfoil surface in two-dimensional flow holds also for the conical field. In the two-dimensional flow $w = iu$ and the condition for a flat surface (constant w) is simply that the function adopted for u has no imaginary part over the region of the real axis covered by the airfoil (assuming that the real

solutions for u and w are used). In the conical flow, the quantity $\frac{\sqrt{1-z^2}}{z}$ is a real number over that part of the real axis between ±1 so that in this region the condition is unchanged.

Figure 4 illustrates the solution for the flat triangular airfoil at a small angle of attack as obtained by H. J. Stewart and M. I. Gurevich (references 6 and 7) and also by Bartels and LaPorte (reference 8). The constant value of w, denoted by w_c, must be calculated to give the relation between the lifting pressure and the angle of attack. The quantity m is the cotangent of the sweepback angle for $M = \sqrt{2}$; for other Mach numbers $m = \sqrt{M^2 - 1}$ times the cotangent of the sweep angle.

Other wing forms generally require the superposition of conical and cylindrical fields. Thus, in the case of the rectangular wing of wedge-shaped section (fig. 5) the field is cylindrical up to the Mach cone originating at the corner of the wing and is conical inside this cone.

The solution for the flat triangular wing can be used as a starting point to obtain the pressure distribution over a sweptback wing. In this process, which is explained in references 9 and 10, the desired wing plan form is, in effect, cut out of the triangle by the superposition of conical fields which cancel the lifting pressure over portions of the triangular area extending beyond the desired outline. The process is simplified in the supersonic case by the limited zone of influence of the superimposed fields. The lifting pressure distribution over a wing with 63° sweepback is shown in figure 6. It will be noted that the lift distribution over the foremost section is flat, as in the Ackeret theory, while farther along the span the subsonic type of pressure distribution appropriate to the reduced crosswise velocity appears. In this example the wing tips were cut off in a direction parallel to the air stream and, in such cases, the lift drops sharply to zero in the region behind the Mach cone from the tip corner.

The solution for a sweptback wing having curvilinear sections cannot be obtained by the superposition of a finite number of conical fields but requires an integration. Such a case is illustrated in figure 7, which shows the pressure distributions at several sections of a symmetrical biconvex wing at 0° angle of attack. This example serves to illustrate the change in proceeding from subsonic to supersonic speed. Since the angle of sweepback is large, the change is not pronounced and occurs primarily at the center sections of the wing. It is interesting to note that the center sections of the wing have a pressure drag at subsonic speeds.

REFERENCES

1. Busemann, A.: Infinitesimal Conical Supersonic Flow. NACA TM No. 1100, 1947.

2. Jones, Robert T.: Wing Plan Forms for High-Speed Flight. NACA TN No. 1033, 1946.

3. Whittaker, E. T., and Watson, G. N.: A Course of Modern Analysis. Fourth ed., Cambridge Univ. Press (London), 1927, p. 403. (Reprinted 1940.)

4. Bateman, H.: Partial Differential Equations of Mathematical Physics. American ed., Dover Publications, 1944, pp. 357-358.

5. Jones, Robert T.: Properties of Low-Aspect-Ratio Pointed Wings at Speeds below and above the Speed of Sound. NACA Rep. No. 835, 1946.

6. Gurevich, M. I.: Lift Force of an Arrow-Shaped Wing. Appl. Math. and Mech. (Moscow), vol. X, no. 4, 1946, pp. 513-520.

7. Stewart, H. J.: The Lift of a Delta Wing at Supersonic Speeds. Quarterly Appl. Math., vol. IV, no. 3, Oct. 1946, pp. 246-254.

8. LaPorte, O., and Bartels, R. C. F.: An Investigation of the Exact Solutions of the Linearized Equations for the Flow past Conical Bodies. Bumblebee Rep. No. 75, Univ. Michigan, Eng. Res. Inst., Feb. 1948.

9. Cohen, Doris: The Theoretical Lift of Flat Swept-Back Wings at Supersonic Speeds. NACA TN No. 1555, 1948.

10. Lagerstrom, P. A.: Linearized Supersonic Theory of Conical Wings. J. P. L. Progress Rep. No. 4-36, Calif. Inst. Tech., 1947.

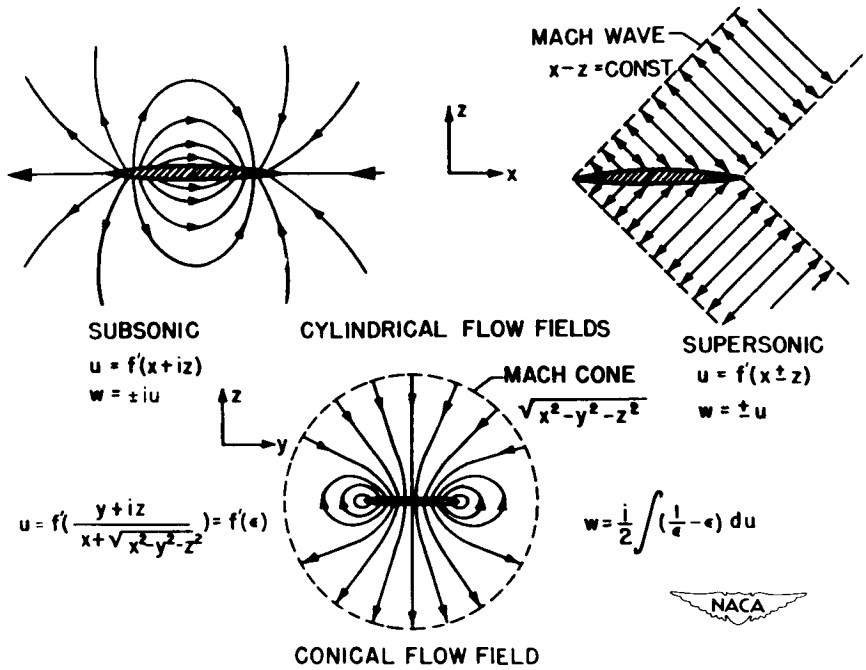

Figure 1.- General form of cylindrical and conical flow fields.

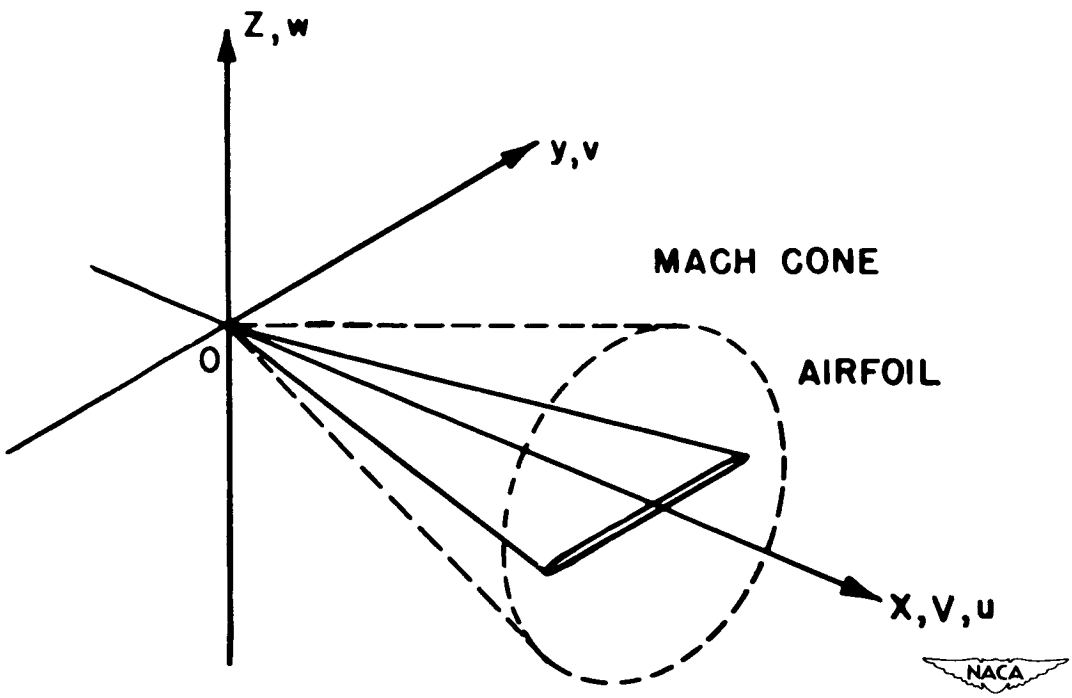

Figure 2.- Flat plate of triangular plan form in conical flow field.

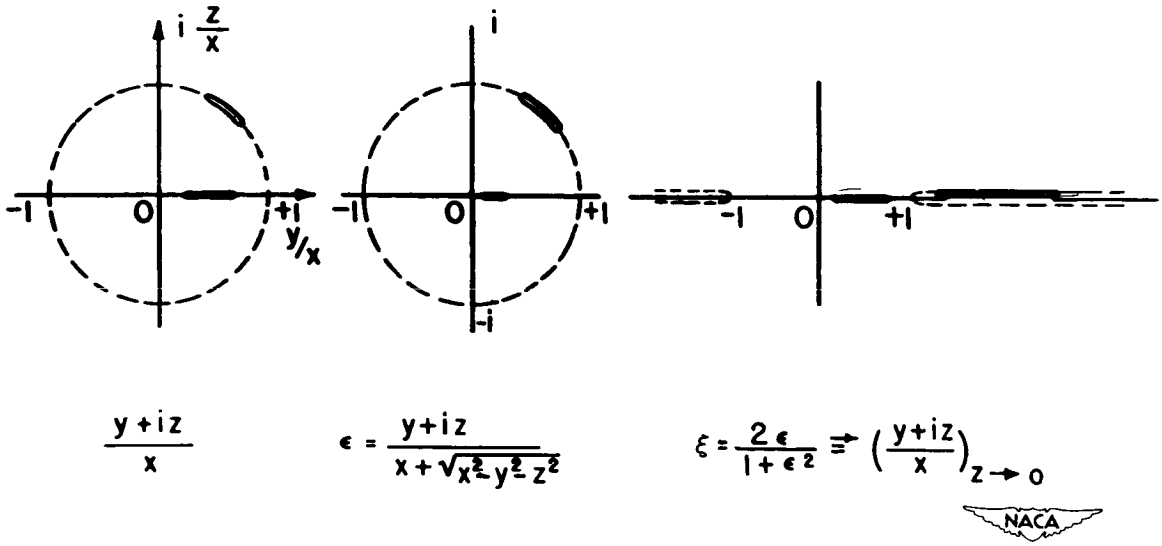

Figure 3.- Transformation of flow field to the ξ plane.

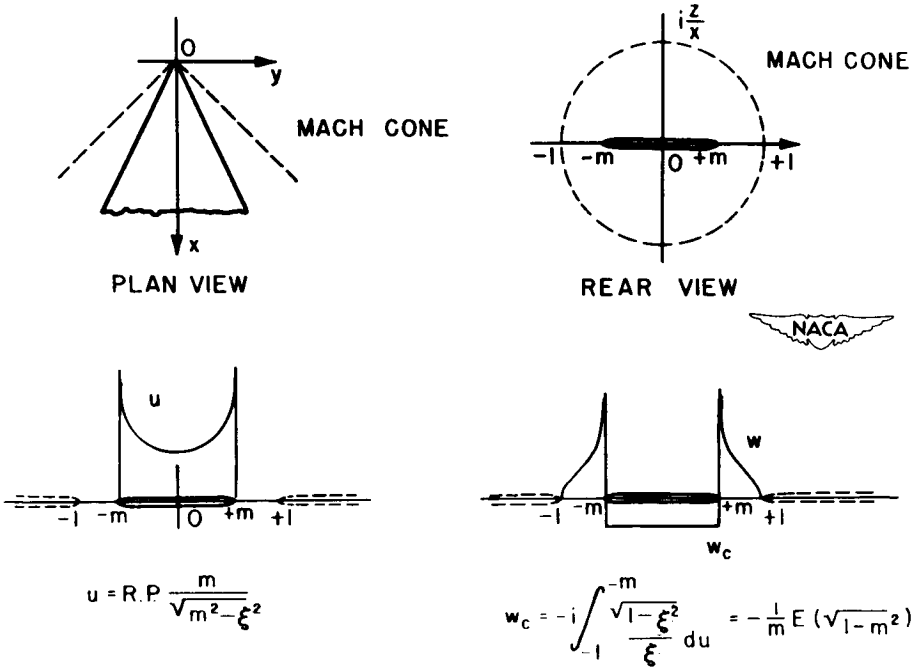

Figure 4.- Solution for flat triangular airfoil at small angle of attack.

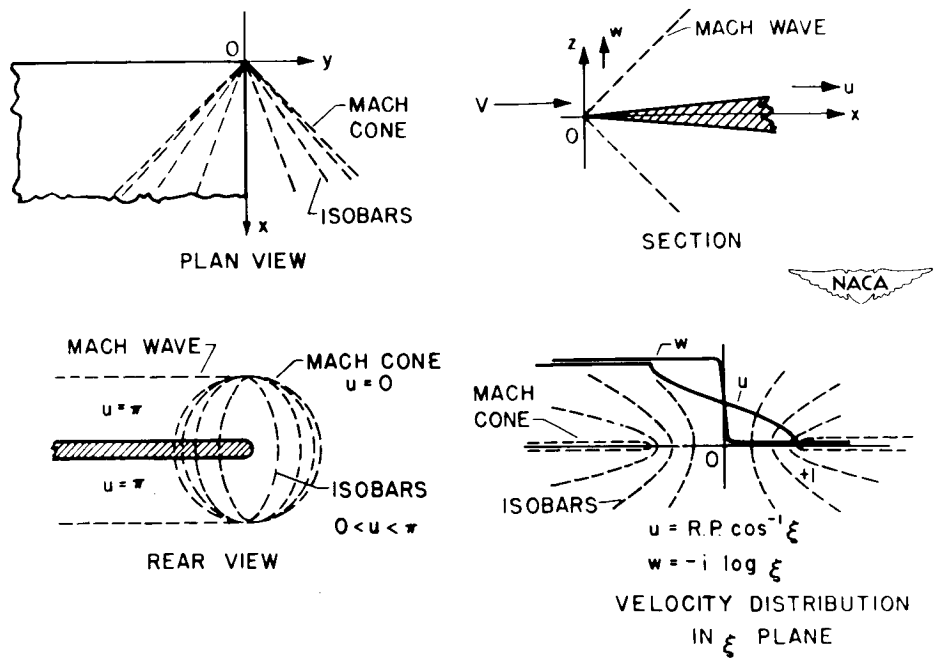

Figure 5.- Cylindrical and conical flow fields about a rectangular wing having a wedge-shape section.

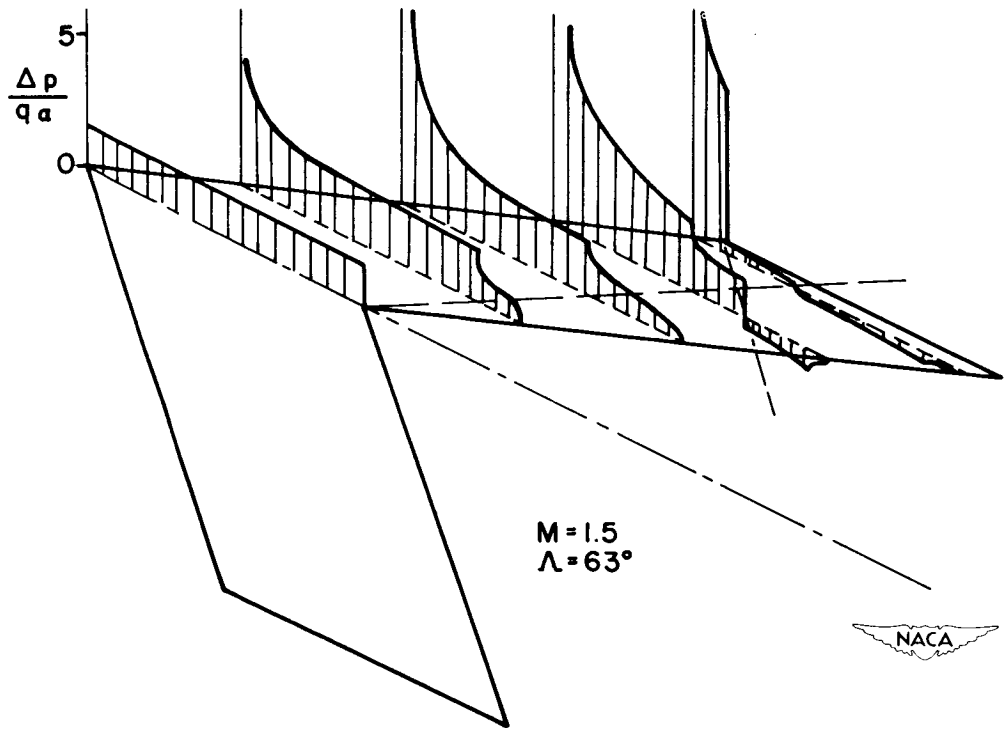

Figure 6.- Lifting pressure distribution over a wing with 63° sweepback.

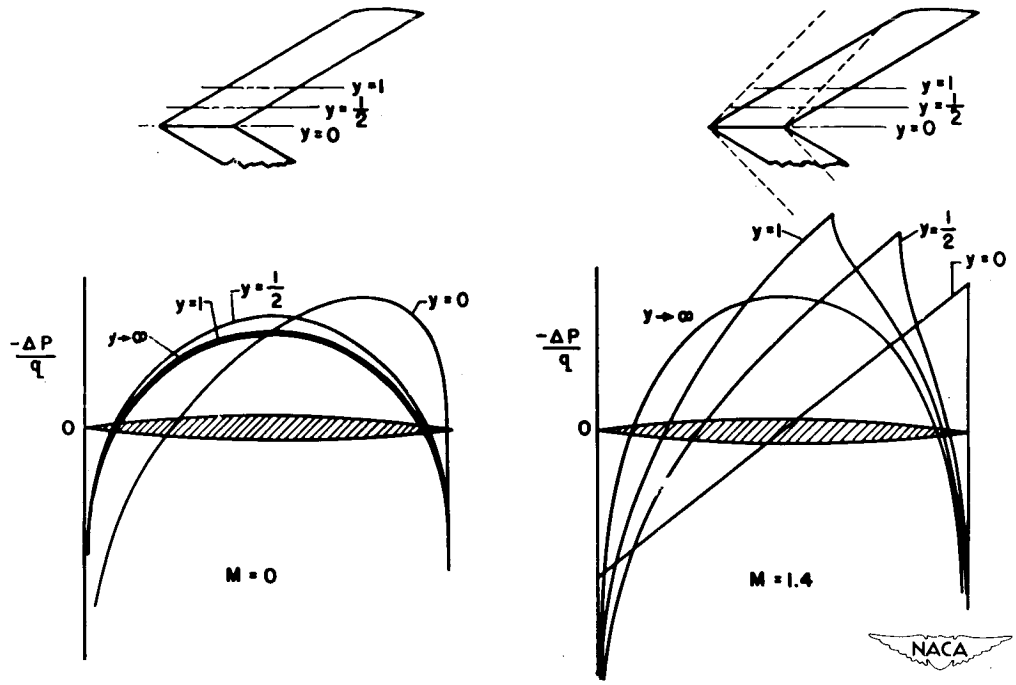

Figure 7.- Pressure distributions at several sections of a symmetrical biconvex wing at 0° angle of attack.

ECONOMY OF FLIGHT AT SUPERSONIC SPEEDS

Robert T. Jones

Ames Aeronautical Laboratory

1948

Economy of Flight at Supersonic Speeds

By Robert T. Jones * Ames Laboratory

The work required to propel an airplane from one place to another in steady flight is equal to its weight times the distance divided by the lift-drag ratio. This simple relation is illustrated in figure 1. A conventional airplane of efficient form may have a lift-drag ratio greater than 20 to 1. The airplane holding the present long-distance record shows a maximum value of 23 to 1 at an angle of attack of about 10°.

The energy required to propel an efficient airplane is much less than that required to propel a rocket. For moderate ranges the rocket requires an amount of energy at least equal to its weight times the distance, hence the equivalent lift-drag ratio is only one - a figure that can be easily surpassed by almost any form of winged body.

If a conventional airplane is maintained at its optimum angle of attack and flown at progressively increasing altitudes the speed necessary for support will increase as the square root of the air density decreases. The lift-drag ratio of the airplane will not be affected by the higher speed, however, until a critical value equal to about seven tenths the speed of sound is reached. Thus the higher speed is gained without the requirement of any additional thrust, and does not necessarily call for greater expenditures of propulsive energy, or fuel, per mile of flight provided the altitude of flight

is properly adjusted and provided the velocity of sound is not approached too closely. This natural increase of cruising speed with altitude is shown in figure 2. An obvious advantage of this method of gaining speed is that it does not interfere with the ability of the airplane to slow down at lower altitudes for landing.

The tendency for the lift-drag ratio to remain unchanged over a wide range of speeds below the speed of sound may be traced to an essential geometric similarity of the airfoil streamline patterns at these subsonic speeds. This similarity appears in the calculated geometry of the frictionless flow field. Figure 3 shows in outline the method of calculation employed to determine the streamline field. The quantity ϕ is the scalar potential of the velocity imparted to the surrounding air by the motion of the wing. The subscripts denote the second partial derivatives with respect to space and time coordinates. The quantity V/c is the ratio of the velocity of flight to the speed of sound; known as the "Mach number." In these calculations of flow geometry we make a new use of the classical wave equation of acoustics. According to this theory, which is outlined more fully in references 1, 2, and 3, the air disturbance produced by the motion of a slender body or wing follows the differential equation of motion of sound waves of small amplitude. If we assume that the disturbance is of fixed pattern traveling with the airfoil and obtain a solution of the differential equation that is consistent with the normal motion of the solid boundary of the airfoil we find, at subsonic

speeds, a pattern of streamlines similar to the flow of an incompressible fluid. An important feature of this subsonic type of flow is the fore and aft symmetry of the pressure distribution over the body, a symmetry which results in almost complete cancellation of the pressure drag. The effect of the elasticity of the air is fully accounted for by an affine transformation (similar to the well known Lorentz contraction in electromagnetic theory) which results in a relative foreshortening of the streamline field, but which does not disturb the fore and aft balance of pressures. The small drag that does arise in such a flow is to be associated with surface friction and with the production of lift.

The equations of motion show a striking change in the pattern of streamlines when the velocity of the pattern exceeds the velocity of sound. At such supersonic speeds the wing travels faster than pressure impulses can be propagated, and hence cannot extend its influence into the region ahead. The fore and aft symmetry of the flow is thus lost and the region of disturbance is bounded by laterally spreading waves or "Mach waves" similar to the bow waves generated by a boat.

The change in the pattern of streamlines on transition to supersonic speeds is most evident in the case of the long narrow wing with its leading edge perpendicular to the direction of flight. The flow field in this case was described many years ago by J. Ackeret and shows two plane waves of sound spreading above and below the wing in a wedge-formation. Ackeret's calculations show positive pressures over the

front of the airfoil and negative pressures over the rear resulting in a "wave drag" which is normally several times as great as the surface friction. (See references 1 and 4.)

Fortunately this sudden increase of drag can be avoided by sweeping the wing back behind the bow wave. With such a swept-back configuration only the foremost section of the wing meets the air without any preparation. (See fig. 4.) Sections farther along the span all lie behind the zone of influence of this foremost section. As described in reference 5 the effect of the laterally spreading zone of influence of the forward sections is to create a flow pattern of the subsonic type over the outer or rearward sections. With such a swept-back wing the unfavorable effect of the supersonic speed thus appears only on the forward sections - while the outer parts of the wing show the dragless type of flow associated with subsonic speeds. In the limiting case of an infinitely long oblique wing there is no change of flow configuration on passing through the speed of sound and the wing behaves simply as if it were flying at the reduced crosswise velocity corresponding to its angle of obliquity.

Maintaining the lift-drag ratio by sweepback requires that the wing be kept well behind the bow wave and, of course, this requires a greater angle of sweep at higher speeds. With acute angles of sweep-back a difficulty arises in that viscosity causes the flow to separate from the upper surface of the wing at relatively small values of the lift. Hence there is a limit to the possibility of maintaining high

lift-drag ratios by the use of sweepback.

Recently a number of investigators have succeeded in applying Prandtl's theory to the determination of the airflow over bodies and wings adapted to supersonic flight. By making use of these results, and by incorporating in them an allowance for the probable skin friction, I have made some estimates of the lift-drag ratios we can expect to achieve at various flight speeds with the best configuration. (See reference 6.) At each speed a slender body and wings having the best angle of sweepback are considered. The results are shown in figures 5 and 6. As shown on figure 5 the angle of sweepback in each case is such that the component velocity normal to the leading edge of the wing is 0.65 times the velocity of sound. I have not extended the calculations beyond 1-1/2 times the speed of sound because of the limitation previously mentioned. However, it does appear that a ratio of lift to drag in excess of 10 to 1 can be maintained up to this speed.

Our estimated values of the lift-drag ratio can be combined with the characteristics of a turbo-jet engine to furnish an overall picture of the probable economy of flight at these speeds. Fortunately the propulsive efficiency of the turbo-jet follows rather simple laws of variation with speed and altitude provided certain requirements are met, so that the characteristics of present day engines can be extrapolated to the speeds we are considering. I have made an estimate of the resultant economy of flight in terms of miles per gallon at various

speeds and the results are shown in figure 7.

Although the results apply to a family of geometrically similar airplanes the values of miles per gallon shown are for an airplane of 40,000 pounds weight, which is about the weight of a 20-passenger transport. I believe these results indicate that supersonic air transportation has possibilities other than purely military ones.

The loss of economy at the lower speeds is the result of the inefficiency of jet propulsion at those speeds. At supersonic speeds the turbo jet is expected to become more efficient than the conventional engine propeller combination - a factor which should partially counteract the unavoidable drop in lift-drag ratio.

For the range of supersonic speeds shown an airplane of normal density and loading would be required to operate at an altitude of the order of 60,000 feet. The limiting value of 1-1/2 times the speed of sound corresponds to a flight speed of 1000 miles per hour. At this speed we should be able to get 1.5 miles per gallon of fuel. It is interesting to note that this value corresponds to a value of more than 15 miles per gallon when the weight is reduced to correspond to that of an ordinary automobile.

REFERENCES

1. Ackeret, J.: Air Forces on Airfoils Moving Faster than Sound. NACA TM No. 317, 1925.

2. Von Kármán, Th.: The problem of Resistance in Compressible Fluids. GALCIT Publication No. 75, 1936. (From R. Accad. d'Italia cl. sci. fis. mat. e nat. Vol XIV 1936)

3. Prandtl, L.: General Considerations on the Flow of a Compressible Fluid. NACA TM No. 805, 1936.

4. Busemann, A.: Aerodynamischer Auftrieb bei Überschallgeschwindigkeit Luftfahrtforschung bd 12, No. 6 Oct. 3, 1935, pp. 210 - 220.

5. Jones, Robert T.: Wing Plan Forms for High Speed Flight. NACA TN No. 1033, 1946.

6. Jones, Robert T.: Estimated Lift-Drag Ratios at Supersonic Speed. NACA TN No. 1350, 1947.

Figure 1

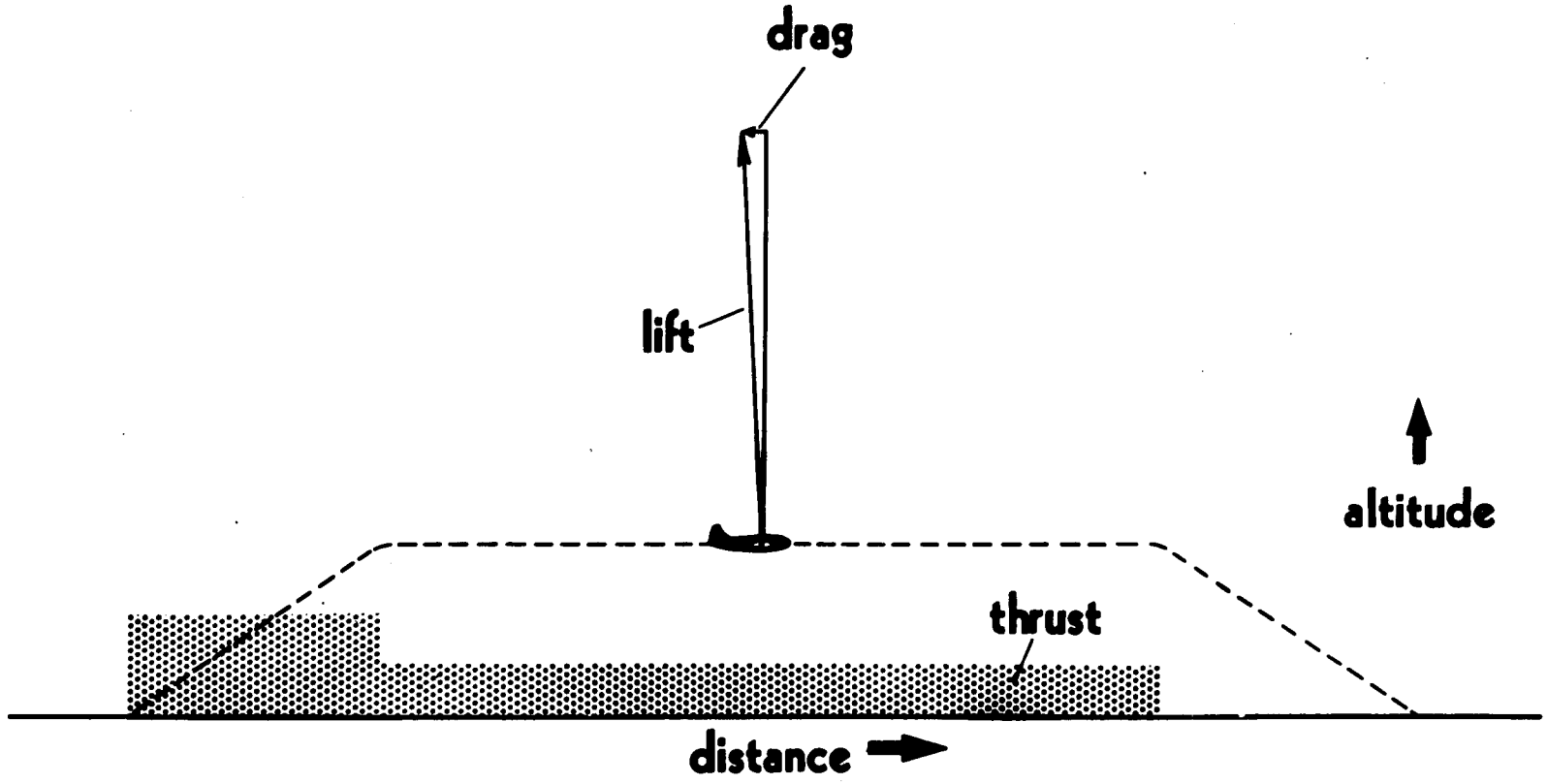

Figure 1

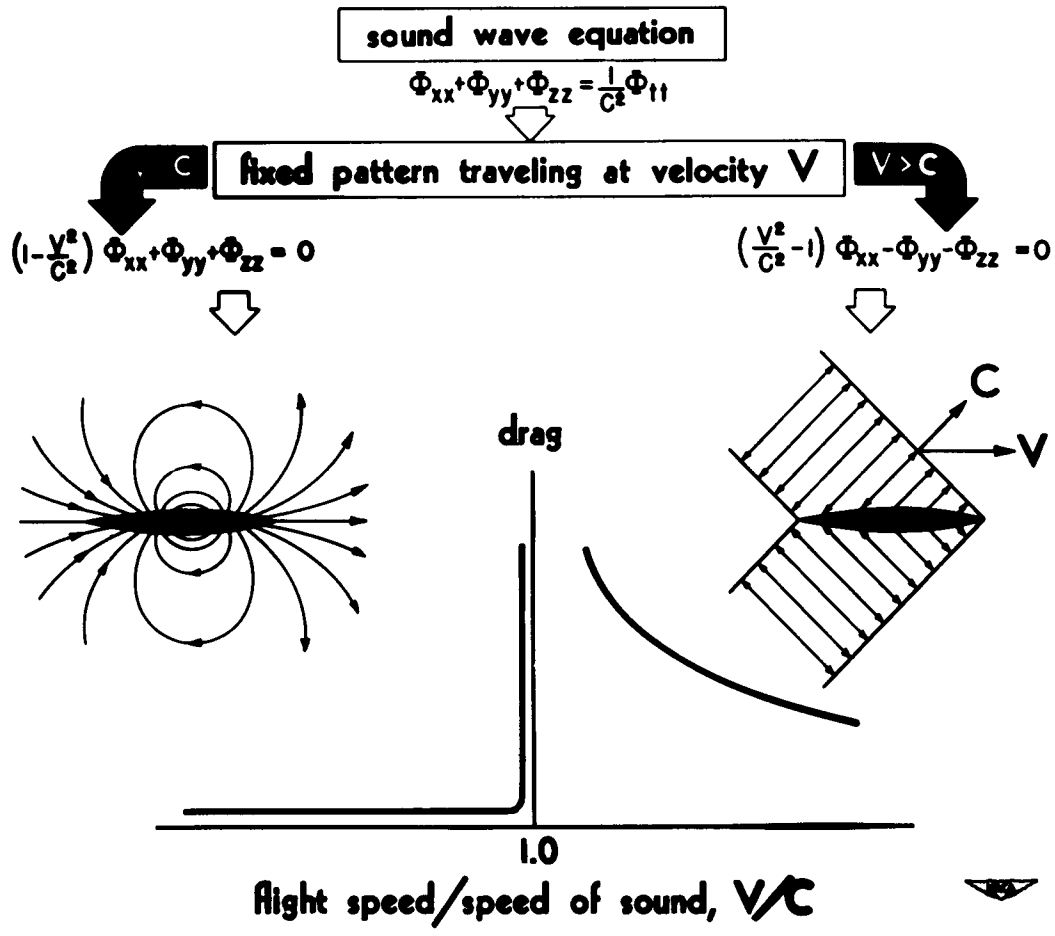
sound wave equation
$\Phi_{xx}+\Phi_{yy}+\Phi_{zz}=\frac{1}{C^2}\Phi_{tt}$
V < C
fixed pattern traveling at velocity V
V > C
$(1-\frac{V^2}{C^2})\,\Phi_{xx}+\Phi_{yy}+\Phi_{zz}=0$
$(\frac{V^2}{C^2}-1)\,\Phi_{xx}-\Phi_{yy}-\Phi_{zz}=0$
drag
C
V
1.0
flight speed/speed of sound, V/C

Figure 3

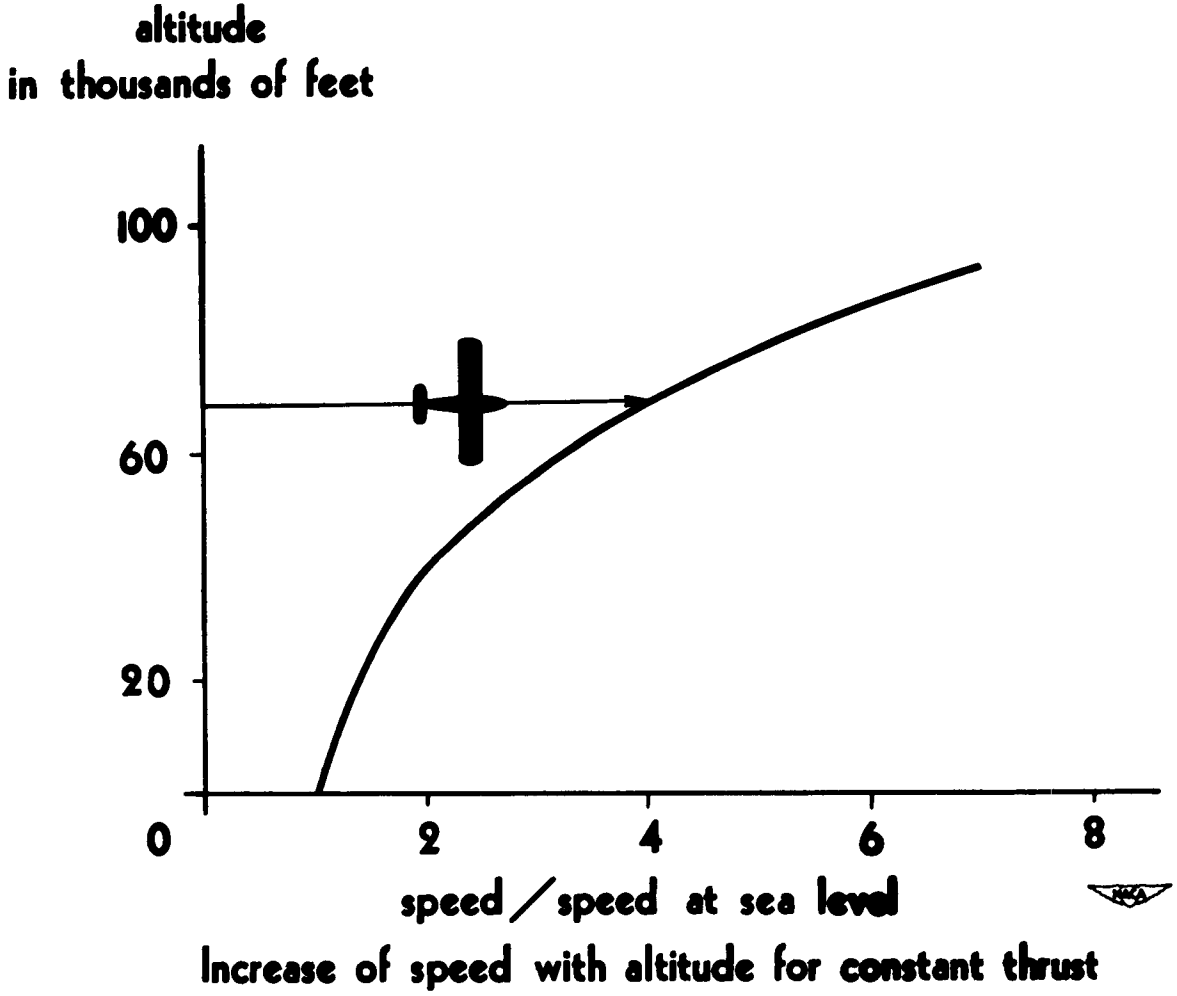

Increase of speed with altitude for constant thrust

Figure 2.

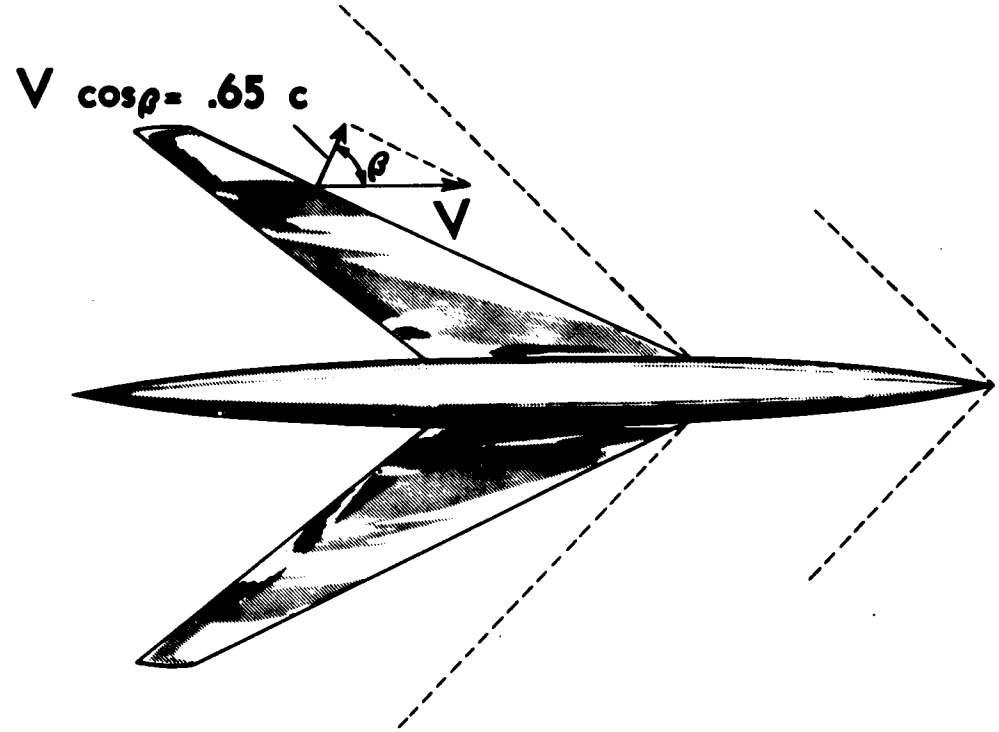

Figure 5

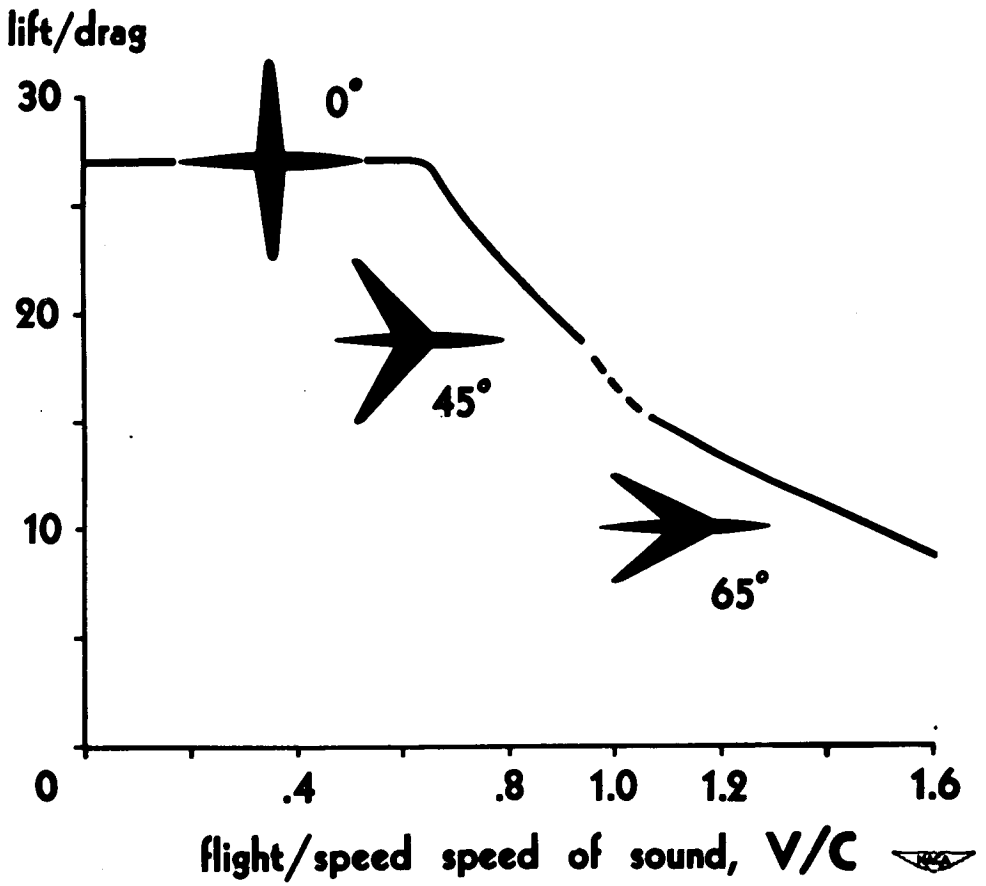
lift/drag
30
20
10
0
0°
45°
65°
.4
.8
1.0
1.2
1.6
flight/speed speed of sound, V/C

Figure 6

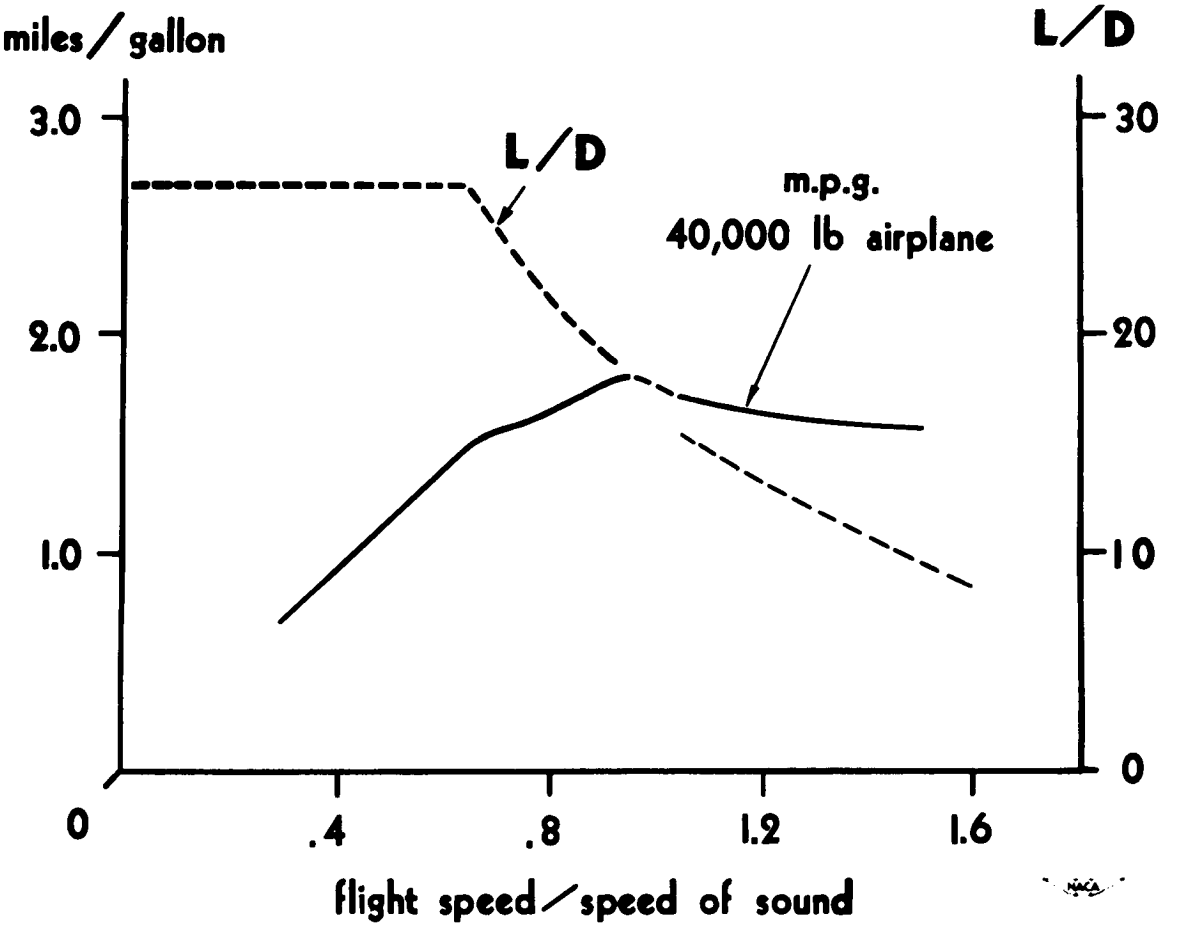
miles / gallon
L/D
3.0
2.0
1.0
0
30
20
10
0
L/D
m.p.g.
40,000 lb airplane
.4
.8
1.2
1.6
flight speed / speed of sound

Figure 7

TECHNICAL NOTE 1901

A METHOD FOR PREDICTING THE STABILITY IN ROLL OF AUTOMATICALLY CONTROLLED AIRCRAFT BASED ON THE EXPERIMENTAL DETERMINATION OF THE CHARACTERISTICS OF AN AUTOMATIC PILOT

Robert T. Jones and Leonard Sternfield

Langley Memorial Aeronautical Laboratory

June 1949

NATIONAL ADVISORY COMMITTEE FOR AERONAUTICS

TECHNICAL NOTE 1901

A METHOD FOR PREDICTING THE STABILITY IN ROLL OF AUTOMATICALLY CONTROLLED AIRCRAFT BASED ON THE EXPERIMENTAL DETERMINATION OF THE CHARACTERISTICS OF AN AUTOMATIC PILOT

By Robert T. Jones and Leonard Sternfield

SUMMARY

A method is suggested for predicting the stability of automatically controlled aircraft by a comparison of calculated frequency-response curves for the aircraft and experimentally determined frequency-response curves for the automatic pilot. The method is applied only to stabilization in roll. The method is expected to be useful as a means of establishing the specifications of the performance required of the automatic control device for pilotless aircraft designed as missiles.

INTRODUCTION

Experience has shown that the provision of automatic stabilization for small pilotless aircraft designed as missiles is extremely difficult. The difficulty is a result of the high-frequency oscillations of small-size aircraft that require rapid control movements and small time lags, characteristics which are difficult to obtain, particularly when the space available for the control servomotors and intelligence units is considered. In an unpublished analysis made at the Langley Aeronautical Laboratory of the NACA, the problem of determining the stability of an automatically controlled aircraft with lag in the control system was analyzed theoretically by assuming a simplified equation for the control motion, this equation being obtained from the knowledge of the behavior of the automatic pilot. Because of the irregular response characteristics often found in automatic pilots, however, the control motion is difficult to represent mathematically and, hence, the simplified equations of the control were found to be inadequate for the analysis.

The present paper suggests a method for predicting the stability of an aircraft based on the experimental determination of the characteristics of its automatic pilot. The procedure consists essentially in calculating the control motion required to maintain a continuous sinusoidal motion of unit amplitude for the degree of freedom being inspected. The motion of the control is obtained for a range of frequencies; the phase angle of the control motion and the ratio of amplitude of control motion to airplane motion are plotted as a function of frequency. Similar curves are established for the autopilot by oscillating it and recording the control motion. The two sets of data are then compared to determine whether the airplane will be stable under control of the automatic pilot. The method is developed in detail only for stabilization in roll. It may be used by the airplane designer for either determining the suitability of an existing automatic pilot for a particular application or specifying the characteristics of the automatic pilot needed for the application.

SYMBOLS

m	mass of airplane, slugs
k_X	radius of gyration of airplane about longitudinal axis, feet
q	dynamic pressure, pounds per square foot
S	wing area, square feet
b	wing span, feet
C_l	rolling-moment coefficient (Rolling moment/qSb)
ϕ	angle of bank, radians
p	angular velocity in bank, radians per second ($d\phi/dt$)
δ	deflection of aileron, radians
C_{l_p}	rate of change of rolling-moment coefficient with angular velocity in bank, per radian ($\partial C_l/\partial p$)
C_{l_δ}	rate of change of C_l with δ, per radian ($\partial C_l/\partial \delta$)
D	differential operation (d/dt)
ω	angular frequency, radians per second

θ phase angle (positive value means lead of δ ahead of ϕ)

ϕ_{max} maximum amplitude of ϕ

K control-amplitude ratio (ratio of control deflection to airplane displacement)

τ lag in seconds between signal for control and its actual motion

t time, seconds

μ real part of root of stability equation

$T_{1/2}$ time for oscillation to damp to one-half its amplitude, seconds

$\delta(t)$ control motion as a function of time

T period of oscillation, seconds

DETERMINATION OF CONDITIONS FOR NEUTRAL STABILITY

The method of determining the conditions for neutral stability is illustrated in figure 1. The calculated phase angle of the control motion and the calculated ratio of the amplitude of control motion to airplane motion are plotted against angular frequency as shown by the solid-line curves. The upper dashed curve is a plot of the experimental ratio of the amplitude of control motion to autopilot motion against angular frequency. The lower three dashed curves are three possible experimental phase-angle curves for the automatic pilot. The intersection of the experimental and calculated control-amplitude curves establishes the approximate frequency of the airplane with the autopilot in operation. If, as in the case of the intermediate experimental phase-angle curve, the intersection of the experimental and calculated phase-angle curves is at the same frequency as the intersection of the control-amplitude-ratio curves, the airplane may be neutrally stable and may be expected to oscillate continuously at this frequency. It is, however, more usual that the intersection of the experimental and calculated phase-angle curves will not be at the same frequency as the intersection of the control-amplitude-ratio curves. If the phase-angle curves, as in one case shown, intersect at a higher frequency than the control-amplitude-ratio curves, the aircraft will be stable. If, as in the remaining case, the intersection of the phase-angle curves is at a lower frequency than the control-amplitude-ratio curves, the aircraft will be unstable. Because of the nonlinear characteristics of the control system, it is generally necessary to

make the experiments for different amplitudes. With a dead spot (insensitivity to small deviations) there will probably be some amplitude below which the system will be unstable.

Calculated frequency-response curves for the aircraft.- In the application of the method to the case of aileron control of an aircraft or a missile independently stabilized about all three axes, the equation of motion for determining the control movement is

$$\left(\frac{mk_X^2}{qbS} D^2 + C_{l_p} D\right)\phi = C_{l_\delta}\delta$$

The calculated steady-state solution of the aircraft in response to a sinusoidal forcing function of unit amplitude $\delta = \sin \omega t$ is $\phi = \phi_{max} \sin (\omega t + \phi)$. (See reference 1.) The values of ϕ_{max} and θ are obtained over the desired range of angular frequencies ω by the substitution of $i\omega$ for D in the equation

$$\frac{\delta}{\phi} = \frac{\frac{mk_X^2}{qbS} D^2 + C_{l_p} D}{C_{l_\delta}}$$

This substitution is equivalent to specifying an undamped sinusoidal motion and results in the expression $A + iB$ from which can be obtained $\frac{1}{\phi_{max}} = \sqrt{A^2 + B^2}$ and $\theta = \tan^{-1}\frac{B}{A}$. The angle θ may denote either a phase lag or lead, depending upon its quadrant. If θ is in the third or fourth quadrant, the control lags behind the displacement, but if θ is in the first or second quadrant, the control leads the motion of the airplane. The ratio of the amplitudes δ and ϕ is $\frac{1}{\phi_{max}}$ and may be defined as the control-amplitude ratio K of the control system, that is, the ratio of maximum control deflection to maximum displacement in bank. A plot of K and θ against ω shows the combination of control-amplitude ratio and phase lag or lead necessary to maintain fixed-amplitude oscillations at any given frequency. These results are the calculated frequency-response curves due to a sinusoidal motion of the aircraft.

Determination of equivalent sine wave for the automatic-pilot response.- The experimental frequency-response curves are obtained by oscillating the automatic pilot sinusoidally at various amplitudes through the desired range of frequencies. The control is assumed to oscillate at the same frequency as the automatic pilot but because of

the physical characteristics of the autopilot the control motion may differ widely from a true sine wave and may show arbitrary phase, amplitude, or wave-form relations (fig. 2). It is necessary, therefore, to determine an equivalent sine-wave response for any arbitrary control motion.

In order to determine the equivalent sine wave for an arbitrary control motion, the following relations are assumed:

(1) The work done per cycle by a control following the equivalent sine wave on an aircraft having a harmonic displacement $\sin \omega t$ must be the same as that done by the actual control variation.

(2) The angular impulse of the equivalent sine wave acting on the airplane over a half cycle must equal the change in angular momentum of the airplane caused by the actual control motion during the same interval.

The work done by a nonharmonic force $\delta(t)$ of frequency ω upon a harmonic motion $\sin \omega t$ is proportional to

$$B_1 = \frac{2}{T}\int_0^T \delta(t) \cos \omega t \, dt$$

where the period of the oscillation is $T = \frac{2\pi}{\omega}$, and B_1 is the coefficient of the component $\cos \omega t$. (See reference 2.) This component of the control motion that is out of phase with the aircraft motion is the only harmonic of the Fourier series representing the forcing function $\delta(t)$ which contributes to the work done on the aircraft. The angular impulse is obtained by integrating the curve of control deflection against time over a half cycle. This component of the control motion in phase with the sinusoidal motion of the aircraft, obtained from the second relation, is

$$A_1 = \frac{\pi}{T}\int_0^{T/2} \delta(t) \, dt$$

where A_1 is the coefficient of the component $\sin \omega t$. The condition of zero net impulse over a series of cycles may be met by adjusting the reference axis for $\delta(t)$ so that $\int_0^T \delta(t) \, dt = 0$. The control motion

may then be expressed as the sum of the in-phase and out-of-phase components:

$$A_1 \sin \omega t + B_1 \cos \omega t$$

or

$$\sqrt{A_1^2 + B_1^2} \sin (\omega t + \theta)$$

The control-amplitude ratio K is equal to $\sqrt{A_1^2 + B_1^2}$ and the phase lag of the system θ is $\tan^{-1} \frac{B_1}{A_1}$. The control-amplitude ratio and the phase lag or lead are determined from records taken of the oscillations and plotted against ω. In contrast to the calculated frequency-response curves which involve the aerodynamic and mass characteristics of the aircraft, these experimentally determined curves will be functions of the dead spots and various types of lag found in the control system. In general, the behavior of the automatic pilot will be nonlinear and hence a family of curves showing different phase and amplitude relations for different amplitudes of disturbance will be obtained.

Comparison of the calculated frequency-response curves of the aircraft and the experimental frequency-response curves of the automatic pilot.- The two sets of frequency-response curves show, on the one hand, the values of K and θ necessary for hunting at a given frequency and, on the other hand, the actual values of K and θ obtained experimentally at this frequency. In order to determine from these curves whether the aircraft will hunt in flight, the following conditions must be satisfied:

(1) At a given frequency and amplitude the experimental values of K and θ must agree with the calculated values.

(2) The motion must be stable for amplitudes larger than the one at which the airplane will hunt (as determined from the first condition).

The first condition indicates that the control-amplitude ratio and phase lag or lead obtained as a result of all types of lag in the control system must agree with the combination of K and θ necessary for hunting to exist. The second condition is essential to prevent instability if the aircraft is displaced to amplitudes larger than the one at which it will hunt. The aircraft is stable at these larger amplitudes if, at the frequency for which the calculated and experimental control-amplitude ratios are equal, the calculated value of the phase lag required for hunting is greater than the experimental value.

In other words, the calculated value of θ is a critical value of the lag necessary to cause the aircraft to hunt. If experimental values of θ are less than the critical value, the aircraft motion is damped, whereas instability occurs if the experimental value of θ exceeds the calculated critical value (fig. 1).

Illustrative case.- The equation of motion in bank of a small experimental aircraft tested in the Langley 7- by 10-foot tunnel was estimated as

$$(0.000245D^2 + 0.00245D)\phi = -0.2645\delta$$

Solving the equation for δ/ϕ and substituting $i\omega$ for D give the expression

$$\frac{\delta}{\phi} = 0.000926\omega^2 - 0.00926\omega i$$

The resultant values of K and θ, that is, the calculated frequency-response curves for the aircraft, are shown as solid lines in figure 3. These curves show that for small values of K, the frequency of the steady oscillation is low and the motion will not be sustained unless the phase lag is large. As K increases, the frequency of the steady oscillation increases but the phase lag required decreases. It is important to note that an automatic pilot with a constant time lag l would be unstable at high angular frequencies since the relation between angular frequency, phase lag, and time lag is θ (radians) = ωl.

The experimental frequency-response curves were obtained by oscillating the automatic pilot at amplitudes of 10° and 20° through the range of desired angular frequencies. The phase lag and control-amplitude ratio for the two amplitudes were determined from records similar to figure 2 and are plotted as a function of ω in figure 3 for two values of control-amplitude ratio K. For this particular automatic pilot, the control-amplitude ratio was independent of amplitude whereas the phase lag varied with amplitude. The results in figure 3 indicate that, for each control-amplitude ratio, the experimental values of θ are greater than the calculated phase lag, and hence the aircraft would be unstable. Unpublished results from wind-tunnel tests indicated that the motion was unstable, as predicted from the curves of figure 3.

In an effort to make the aircraft stable, the parameters of the automatic pilot were modified and additional wind-tunnel tests were performed. The conditions selected for these wind-tunnel tests were, however, different from those conditions for which the experimental frequency-response curves were obtained and hence no direct prediction of the aircraft stability could be made. The results of the wind-tunnel tests with the modified automatic pilot indicated a steady

oscillation, and records taken of the tests showed that the values of K and θ agreed very closely with the combination of K and θ determined from the calculated frequency-response curves. The test points of figure 4 show the combination of K and θ for the cases in which steady oscillations occurred in the roll tests.

CALCULATED FREQUENCY RESPONSE OF THE AIRCRAFT FOR DAMPED OSCILLATIONS

The previous calculations of the frequency-response curves were based on the assumption that the sinusoidal motion of the aircraft is neutrally damped. It is often desirable, however, to determine the performance of an automatic control device required to cause the motion of the aircraft to damp at a sufficiently rapid rate. Although no satisfactory analysis of this problem has been given, a qualitative indication of the rate of damping to be expected in a given case may be obtained by comparing the measured phase and amplitude of the control to the phase and amplitude calculated to be required to enforce a given rate of damping.

Strictly speaking, the assumed exponential damping of the motion would require an exponential decrease in the response of the autopilot at decreasing amplitudes. In general, such a linear response cannot be expected and hence the method will require careful judgment in its application.

The equation of damped motion in bank for the illustrative case may be written by adding a real part μ to the imaginary root $i\omega$

$$\left[0.000245(-\mu + i\omega)^2 + 0.00245(-\mu + i\omega)\right]\phi = -0.2645\delta$$

where μ is given a value as determined by the desired rate of damping. The motion damps to one-half its amplitude in $T_{1/2} = \frac{0.693}{\mu}$ seconds. Solving the equation for δ/ϕ gives the expression

$$\frac{\delta}{\phi} = 0.000926\omega^2 - 0.000926\mu^2 + 0.00926\mu + i(-0.00926\omega + 0.001852\omega\mu)$$

The frequency-response curves shown in figure 5 were calculated for values of μ varying from 0.175 to 8.31. The control-amplitude-ratio curves are only plotted for values of μ equal to 0 and 5 since they are the limiting curves for the values of μ investigated. Figure 5 indicates that the control-amplitude ratio is almost independent of μ

whereas the phase lag decreases as μ increases. For a control system with a given control-amplitude ratio, therefore, the damping of the oscillation increases as the phase lag is reduced. If the oscillation is to damp one-half in less than 1/7.22 second, the control motion must lead the aircraft motion.

In order to predict quantitatively the stability of the motion of an aircraft which damps exponentially, the experimental frequency-response curves would have to be obtained for the condition where the forced oscillation of the automatic pilot also damps exponentially.

CONCLUDING REMARKS

A method for predicting the stability in roll of automatically controlled aircraft by a comparison of calculated frequency-response curves for the aircraft and experimentally determined frequency-response curves for the automatic pilot is presented. The method is expected to be useful as a means of establishing the specifications of the performance required of the automatic control device for pilotless aircraft designed as missiles.

Langley Aeronautical Laboratory
National Advisory Committee for Aeronautics
Langley Air Force Base, Va., June 13, 1946

REFERENCES

1. Jones, Robert T.: A Simplified Application of the Method of Operators to the Calculation of Disturbed Motions of an Airplane. NACA Rep. 560, 1936.

2. Den Hartog, J. P.: Mechanical Vibrations. Second ed., McGraw-Hill Book Co., Inc., 1940, ch. 1, sec. 7.

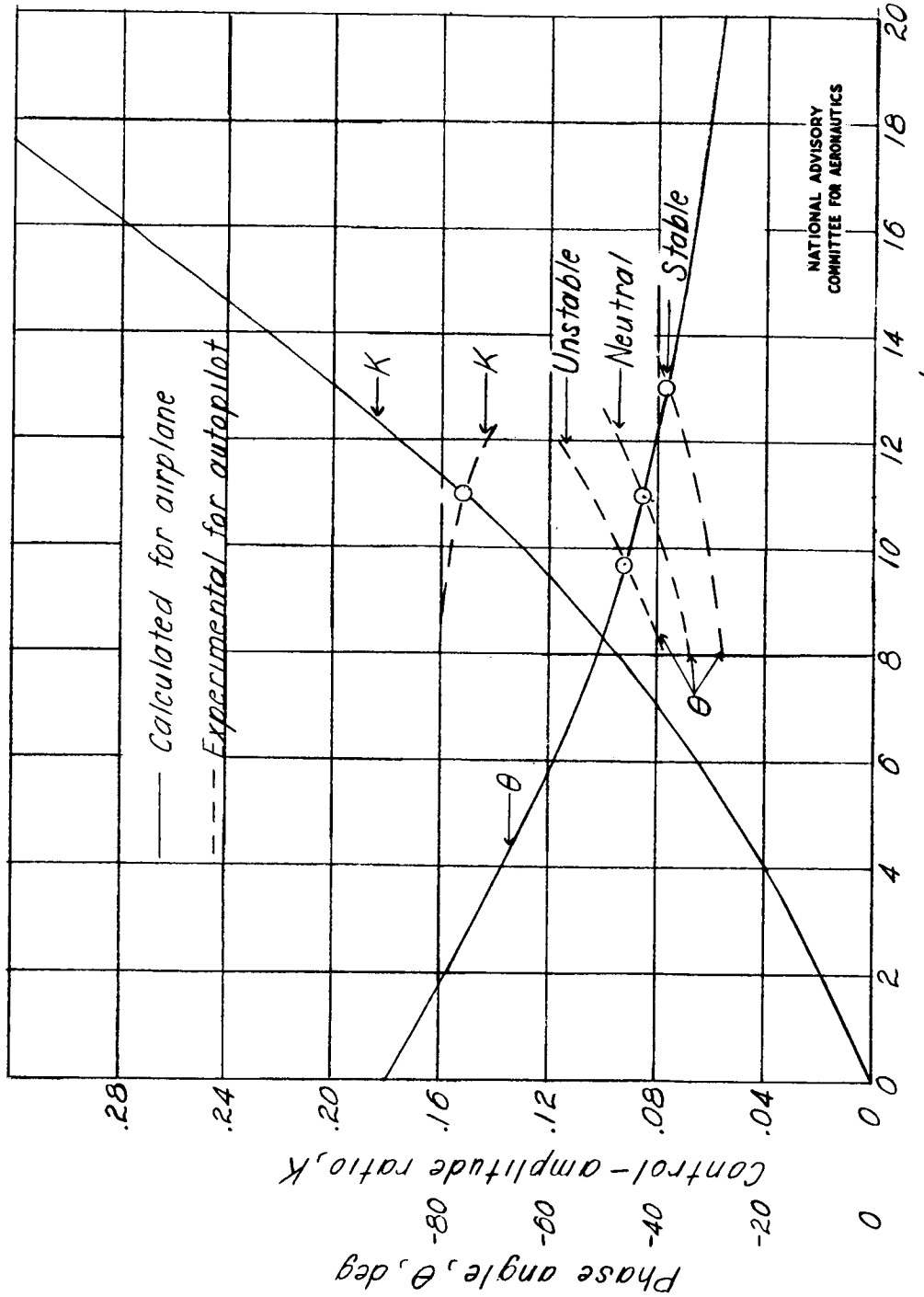

Figure 1.- Frequency-response curves for stable, unstable, and neutrally damped motion of the aircraft.

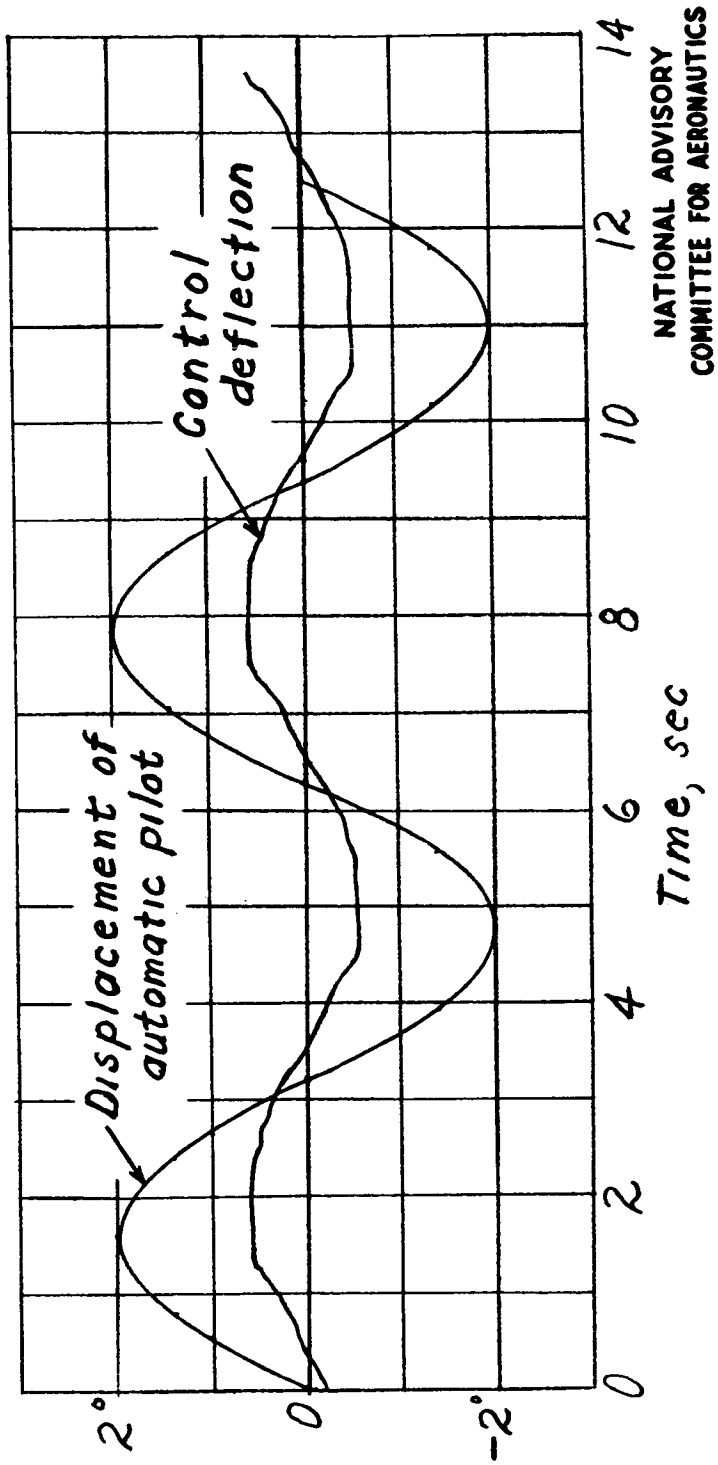

Figure 2.— Typical response of control to sinusoidal oscillation of automatic pilot.

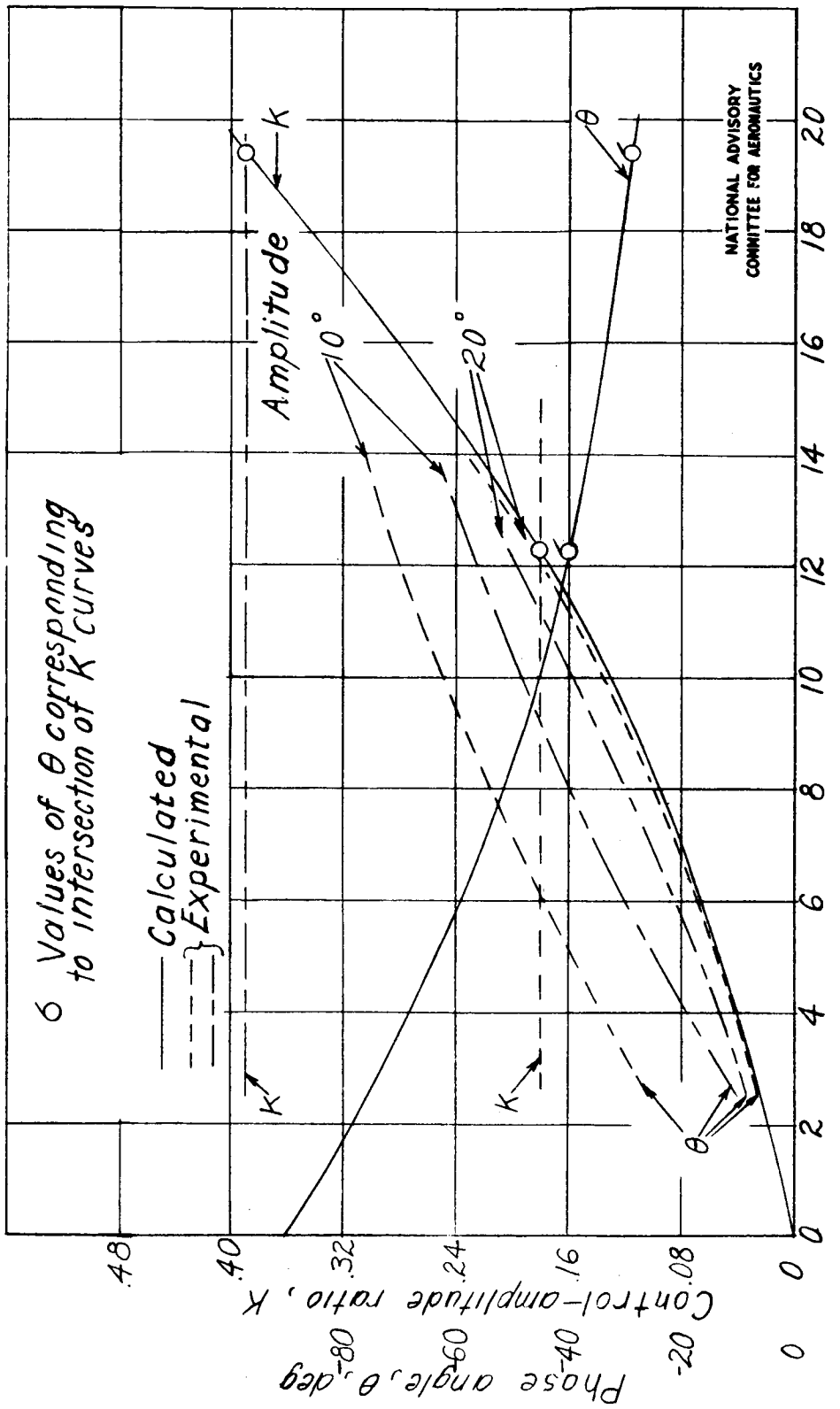

Figure 3.- A comparison of the calculated and experimental frequency-response curves of a small aircraft.

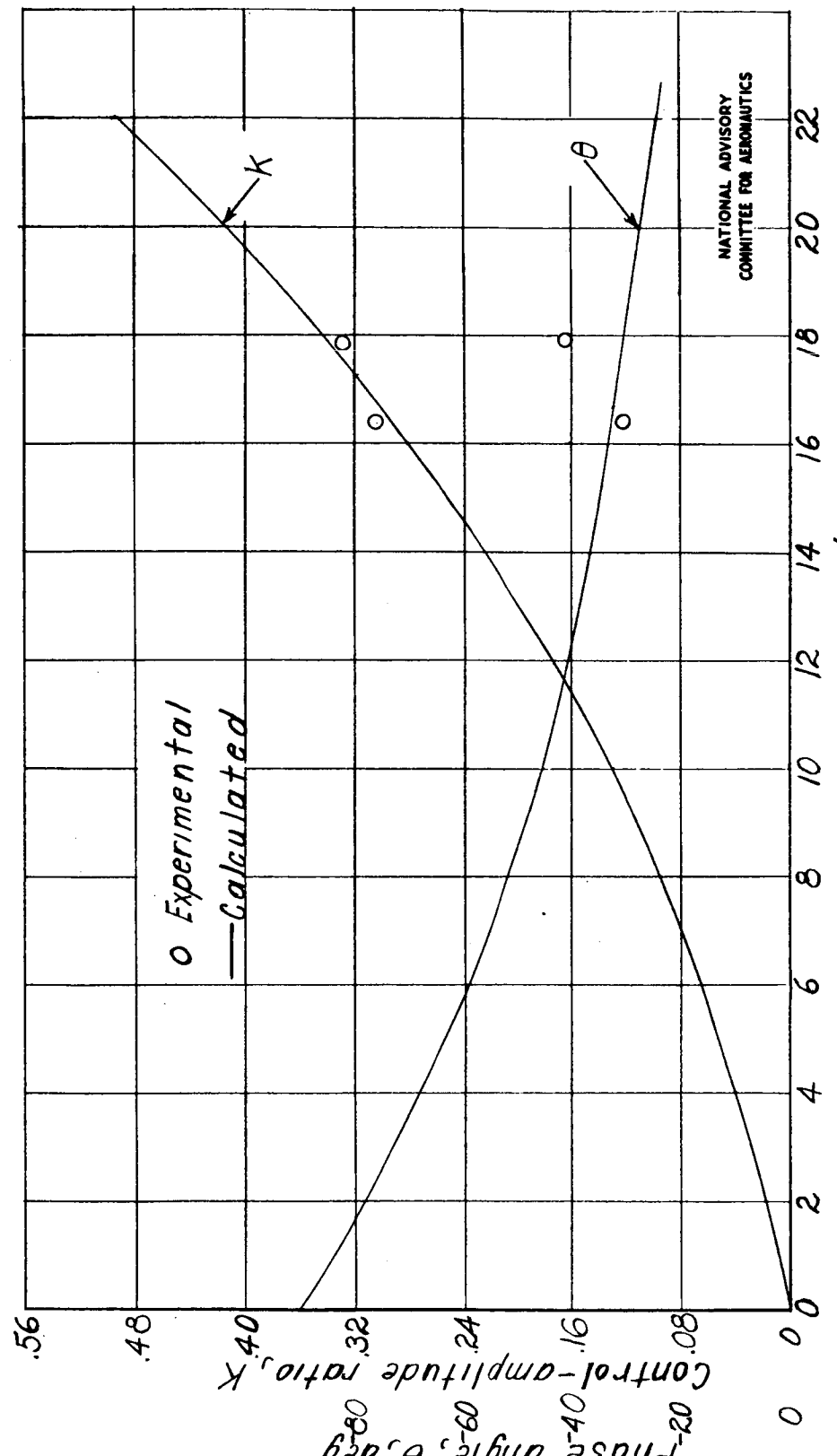

Figure 4.- A comparison between roll-test results and calculated frequency-response curves for a small aircraft.

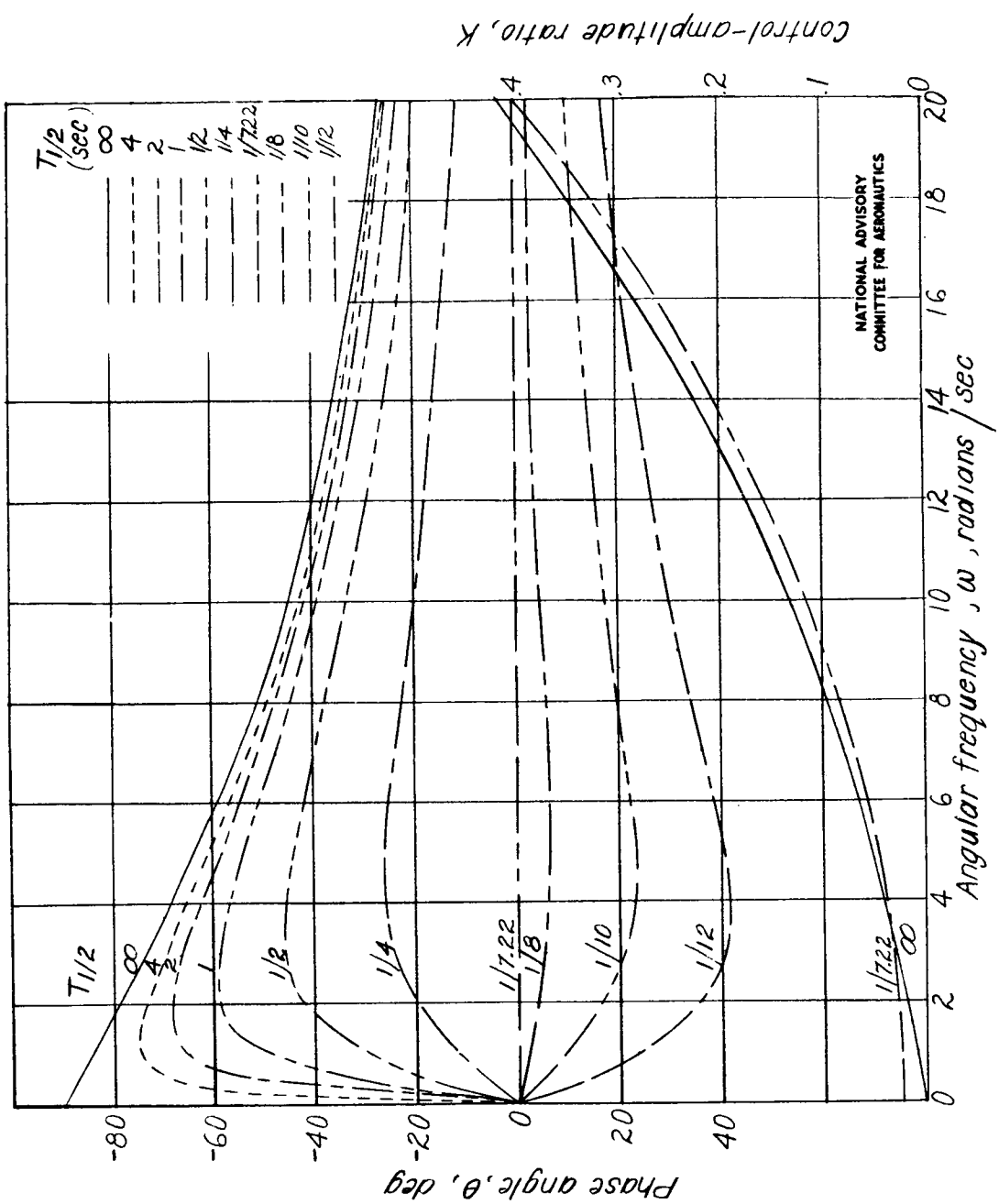

Figure 5.- Calculated frequency-response curves of the aircraft for damped oscillations.

Stability, Dynamic 1.8.1.2

NACA

A Method for Predicting the Stability in Roll of Automatically Controlled Aircraft Based on the Experimental Determination of the Characteristics of an Automatic Pilot.

By Robert T. Jones and Leonard Sternfield

NACA TN 1901
June 1949

(Abstract on Reverse Side)

Controls, Automatic 1.8.2.6

NACA

A Method for Predicting the Stability in Roll of Automatically Controlled Aircraft Based on the Experimental Determination of the Characteristics of an Automatic Pilot.

By Robert T. Jones and Leonard Sternfield

NACA TN 1901
June 1949

(Abstract on Reverse Side)

Jones, Robert T., and Sternfield, Leonard

NACA

A Method for Predicting the Stability in Roll of Automatically Controlled Aircraft Based on the Experimental Determination of the Characteristics of an Automatic Pilot.

By Robert T. Jones and Leonard Sternfield

NACA TN 1901
June 1949

(Abstract on Reverse Side)

NACA

Abstract

A method is suggested for predicting the stability of automatically controlled aircraft by a comparison of calculated frequency-response curves for the aircraft and experimentally determined frequency-response curves for the automatic pilot. The method is applied only to stabilization in roll. The method is expected to be useful as a means of establishing the specifications of the performance required of the automatic control device for pilotless aircraft designed as missiles.

Abstract

A method is suggested for predicting the stability of automatically controlled aircraft by a comparison of calculated frequency-response curves for the aircraft and experimentally determined frequency-response curves for the automatic pilot. The method is applied only to stabilization in roll. The method is expected to be useful as a means of establishing the specifications of the performance required of the automatic control device for pilotless aircraft designed as missiles.

Abstract

A method is suggested for predicting the stability of automatically controlled aircraft by a comparison of calculated frequency-response curves for the aircraft and experimentally determined frequency-response curves for the automatic pilot. The method is applied only to stabilization in roll. The method is expected to be useful as a means of establishing the specifications of the performance required of the automatic control device for pilotless aircraft designed as missiles.

LEADING-EDGE SINGULARITIES IN THIN-AIRFOIL THEORY

Robert T. Jones

Ames Aeronautical Laboratory

May 1950

Leading-Edge Singularities in Thin-Airfoil Theory

ROBERT T. JONES*

Ames Aeronautical Laboratory, N.A.C.A.

SUMMARY

If the thin-airfoil theory is applied to an airfoil having a rounded leading edge, a certain error will arise in the determination of the pressure distribution around the nose. It is shown that the evaluation of the drag of such a blunt-nosed airfoil by the thin-airfoil theory requires the addition of a "leading-edge force," analogous to the well-known leading-edge thrust of the lifting airfoil. The method of calculation is illustrated by application to (1) the Joukowski airfoil in subsonic flow and (2) the thin elliptic cone in supersonic flow. The paper concludes with a general formula for the edge force which is applicable to a variety of wing forms.

INTRODUCTION

IN THE APPLICATION of thin-airfoil theory to airfoils of finite thickness, care must be taken to evaluate the effects of singularities that appear in the thin-airfoil flows. One example of such an effect is the finite force arising from the singularity at the leading edge of a lifting airfoil—that is, the well-known "leading-edge thrust."

Another example is the finite force arising from the singularity in the flow field of a nonlifting airfoil having a blunt leading edge. The latter effect does not appear to have been discussed previously and is of importance at supersonic speeds where it is desired to calculate the "wave drag" arising from the thickness of the airfoil.

THIN JOUKOWSKI AIRFOIL IN SUBSONIC FLOW

A simple example of the leading-edge force is provided by the two-dimensional flow over an airfoil of the Joukowski type. Fig. 1 shows such an airfoil and the coordinate axes used. According to the thin-airfoil theory, the conjugate $u\text{-}iw$ of the perturbation velocity vector will be represented by an analytic function of the complex variable $\xi = x + iz$; that is,

$$u - iw = f(\xi)$$

The function f is chosen to satisfy the desired boundary conditions around the slit $-1 < x < +1$ and to make $u - iw$ vanish at infinity.

By a process of trial, it was found that for the example chosen

$$u - iw = Vt\left[\frac{1-\xi}{\sqrt{\xi^2-1}} + 2(\sqrt{\xi^2-1} - \xi) + 1\right] \quad (1)$$

Near the chord line $\xi = x \pm oi$ and

$$u/Vt \rightarrow 1 - 2x$$

$$\frac{w}{Vt} \rightarrow \pm\left(\frac{1-x}{\sqrt{1-x^2}} - 2\sqrt{1-x^2}\right) \quad (2)$$

The ordinate of the airfoil surface, obtained by integrating $w/V = dz/dx$ is

$$z = t(1-x)\sqrt{1-x^2} \quad (3)$$

The constant t is thus the ordinate of the airfoil at the 50 per cent chord station ($x = 0$). The pressure coefficient is given by

$$\Delta p/(1/2)\rho V^2 = -2(u/V) \quad (4)$$

and, hence, is proportional to $1 - 2x$ in the interval $-1 < x < +1$. At the ends of the interval the terms under the radical change sign and the expression for $u - iw$ become a pure real number, so that $w = 0$ along the streamline ahead of and behind the airfoil. Fig. 2 shows the pressure distribution along this stream-

Received July 7, 1949.

* Aeronautical Engineer.

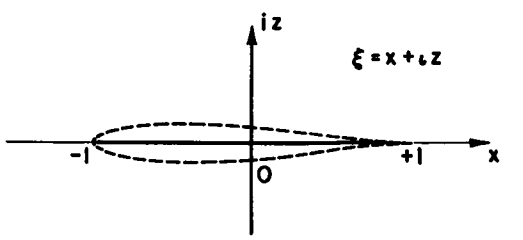

FIG. 1. Thin Joukowski airfoil.

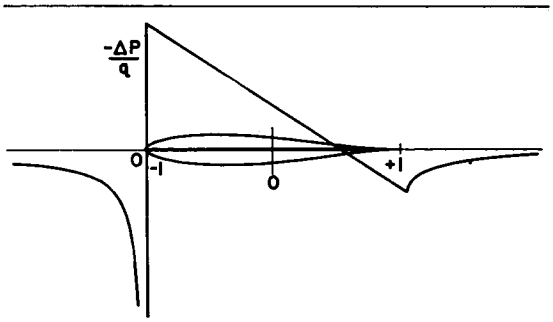

FIG. 2. Pressure distribution for Joukowski airfoil.

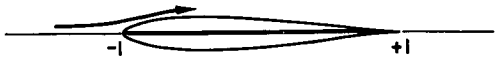

FIG. 3. Contour for evaluation of leading-edge force.

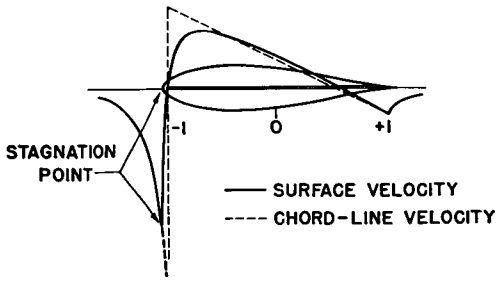

FIG. 4. Comparison of velocity distribution along chord line with velocity at airfoil surface.

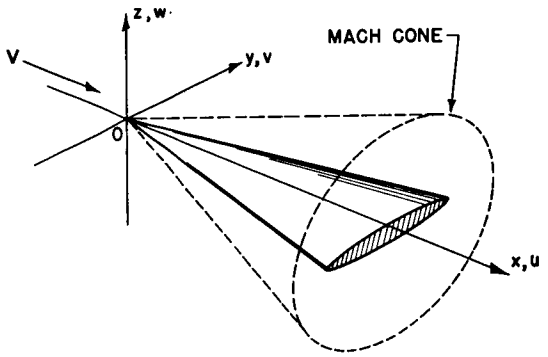

FIG. 5. Elliptic cone in supersonic flow.

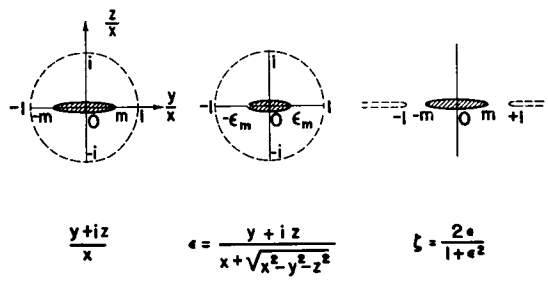

FIG. 6. Transformation of conical flow field.

line and over the airfoil chord between ± 1. An alternate treatment of the thin Joukowski airfoil is given in reference 1.

As is evident from Fig. 2, the thin-airfoil theory shows a negative pressure over the forward three-fourths of the airfoil, changing with a constant gradient to a positive pressure at the trailing edge. Such an increase of pressure toward the rear obviously leads to an upstream buoyancy, or negative drag, in contradiction to D'Alembert's principle. A simple calculation shows that the buoyant force in this case ($D = -\text{volume} \times dp/dx$) corresponds to a drag coefficient of

$$C_D = -2\pi t^2 \tag{5}$$

It will now be shown that this negative drag is exactly canceled by a positive contribution arising from the singularity in the flow field near the leading edge, provided the integration of pressure over the airfoil surface is properly modified by a limiting process to include this singular term. To carry out this limiting process, we select, in preference to the airfoil surface itself, a streamline a short distance above the airfoil surface and, furthermore, allow the integration to extend a short distance ahead of the airfoil nose. The drag is to be obtained from the product of the pressure and the slope of the streamline—that is, the product uw may be formed by noting that

$$(u - iw)^2 = u^2 - w^2 - 2iuw \tag{6}$$

Considering a contour as illustrated in Fig. 3, the drag of a portion of the nose of the airfoil will be given by the integral

$$D_n = \text{I.P. of } \rho \int_c (u - iw)^2 d\xi =$$

$$\text{I.P. of } \rho V^2 t^2 \int_c \left[\frac{1 - \xi}{\sqrt{\xi^2 - 1}} + 2(\sqrt{\xi^2 - 1} - \xi) + 1 \right]^2 d\xi \tag{7}$$

The first term in the square brackets contains the singularity. In the limit as the airfoil thickness approaches zero and the contour approaches the real axis, this term contributes the value

$$C_{D_n} = \text{I.P. of } t^2 \int_c \frac{(1 - \xi)^2}{(\xi - 1)(\xi + 1)} d\xi = 2\pi t^2 \tag{8}$$

over a small length of the path c just above the point -1. This value is equal and opposite the value obtained [Eq. (5)] from the approximate surface pressure distribution. The remaining terms in the integral (7) need not be considered, since they correspond to this previously determined value.

Further insight into the significance of this calculation may be gained by an examination of the velocity field represented by the complex velocity function (1). As illustrated in Fig. 4, the velocity function shows that the horizontal velocity u approaches $-\infty$ at the point -1. Obviously, the leading edge of the airfoil will lie some distance to the left of this singular point, since the additive velocity u becomes equal and opposite to the stream velocity V before the point $\xi = -1$ is reached. The point at which $u = -V$ is the stagnation point and marks the position at which the stream divides to form the upper and lower surfaces of the airfoil. Behind the stagnation point the velocities given by the thin-airfoil theory are, in fact, the velocities of an *internal* flow along the central source-sink distribution of the airfoil. It is evident that the velocity distribution along the source-sink line does not represent a good

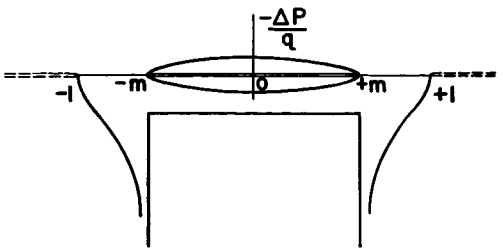

FIG. 7. Pressure distribution over thin elliptic cone in supersonic flow.

approximation to the actual surface velocity distribution in the vicinity of the rounded nose. The exact shape and pressure distribution over the rounded nose are thus not determined by the thin-airfoil theory. The determination of the drag of the nose portion without knowledge of its exact shape or pressure distribution is possible, however, because of the invariant property of the contour integral.

Similar considerations apply in the case of a lifting airfoil. Here, an inclined thin plate is used as an approximation to a lifting airfoil of finite thickness, and the leading-edge force (a forward thrust in this case) is determined from the singularity in the flow around the edge of the plate. The plate in this case represents a line of discontinuity, or a vortex sheet, along the interior of the airfoil.

In either case the application of the theory to compressible flows is made on the assumption that the configuration of the flow exterior to the airfoil remains essentially similar to the corresponding incompressible potential flow. The contour of integration (Fig. 3) is further supposed to lie in a region where the additive velocities are small, so that the velocity u and the corresponding pressure can be corrected by the Prandtl-Glauert rule.

ELLIPTIC CONE IN SUPERSONIC FLOW

As an example of a supersonic flow, consider the case of the flattened elliptic cone which was previously considered by Squire. Adopting a variation of Busemann's method,[3] the velocity field may be described by an analytic function of the variable ζ where

$$\zeta = 2\epsilon/(1 + \epsilon^2) \tag{9}$$

and

$$\epsilon = (y + iz)/(x + \sqrt{x^2 - y^2 - z^2}) \tag{10}$$

As pointed out in reference 3, the variable ϵ is the argument of the general solution of Prandtl's equation, of zero degree (cf. references 4 and 5 for the equivalent solution of Laplace's equation). The variable ζ is an analytic transformation of ϵ that maps the interior of the Mach cone onto the whole complex plane, transforming the Mach cone itself into the positive and negative branches of the real axis outside the points ± 1. The variable ζ approaches the undistorted space coordinate $(y + iz)/x$ near the plane of the airfoil inside the points ± 1 and thus facilitates the choice of functions to represent various airfoil boundary conditions. Figs. 5 and 6 illustrate these relations.

As in the case of the Joukowski airfoil, the elliptic cone requires a singularity of the order $-1/2$ in the expression for the vertical velocity w to represent the rounded leading edge. A trial shows that the simple function*

$$w = -(Vt/2)(m/\sqrt{m^2 - \zeta^2}) \tag{11}$$

satisfies the boundary condition for an elliptic cone of maximum thickness xt having its leading edges along the lines $y = \pm mx$.

The horizontal perturbation velocity u, which determines the pressure distribution ($\Delta p = -\rho u V$), is found from w with the aid of the condition for irrotational motion—that is, $\partial u/\partial z = \partial w/\partial x$. In terms of the variable ζ this relation is equivalent to

$$du/d\zeta = i(\zeta/\sqrt{1 - \zeta^2})(dw/d\zeta)$$

or

$$u = i \int (\zeta/\sqrt{1 - \zeta^2})(dw/d\zeta)d\zeta \tag{12}$$

where the integration begins at a point of zero disturbance.

Integration for the ordinate of the surface yields

$$z = \int \frac{w}{V} dx = -y \int \frac{w}{V\zeta^2} d\zeta = \frac{t}{2} \sqrt{x^2 - (y/m)^2} \tag{13}$$

The constant t is seen to be the maximum thickness of the section at $x = 1.0$.

In the present example, the sweep angle is assumed to be greater than the Mach angle so that the elliptic cone lies entirely within the Mach cone. The velocities u and w then vanish on the Mach cone, and u can be determined by integrating Eq. (12) from -1 to ζ

$$u = \frac{Vt}{2} \frac{m}{1 - m^2} \left[\zeta \sqrt{\frac{1 - \zeta^2}{\zeta^2 - m^2}} + F(\Phi,k) - E(\Phi,k) \right] \tag{14}$$

where

$$\Phi = \arcsin \sqrt{\frac{1 - \zeta^2}{1 - m^2}}, \qquad k = \sqrt{1 - m^2}$$

and F and E are the elliptic integrals. A plot of the real solution for u, which is proportional to the pressure distribution, is shown in Fig. 7. It is interesting to note that the elliptical cross section leads to a constant

* The proper value of the function is selected with the aid of the condition that w is to be discontinuous across the real axis between $\pm m$ and positive on the upper side.

surface pressure distribution. This result has previously been obtained by Squire.

As in the preceding example, the drag is determined by integrating the product $-\rho\overline{uw}$ along a stream surface just above the airfoil surface. Eqs. (11) and (14) for u and w actually contain two (i.e., the real and imaginary) solutions. Since the real solutions are the ones used here, it is necessary to separate the product of the real solutions from the complex product uw. With the aid of Eq. (12), it can be shown that the required product of the real solutions is equal to one-half the real part of the complex product in a limited region near the nose of the airfoil where the term $\zeta/\sqrt{1-\zeta^2}$ can be considered constant.

With this latter point in mind, the expression for the leading-edge force of a section at $x = 1$ can be written

$$D_n = \text{R.P.} \int_c \rho \frac{Vt}{2} \frac{m}{1-m^2} \frac{\zeta\sqrt{1-\zeta^2}}{\sqrt{\zeta^2-m^2}} \times \left(\frac{Vt}{2} \frac{m}{\sqrt{m^2-\zeta^2}} d\zeta\right)$$

$$= \text{R.P.}\, i \frac{\rho V^2 t^2}{4} \frac{m^2}{1-m^2} \int_c \frac{\zeta\sqrt{1-\zeta^2}}{(\zeta-m)(\zeta+m)} d\zeta$$

$$= \pi \frac{\rho}{2} V^2 \frac{t^2}{4} \frac{m^2}{\sqrt{1-m^2}} \qquad (15)$$

or, in coefficient form,

$$C_{D_n} = \pi(t^2/4)(m/\sqrt{1-m^2}) \qquad (16)$$

for both edges.

The contour for Eq. (15) crosses only a limited region near the airfoil nose and involves in the limit only the singular term $\zeta\sqrt{1-\zeta^2}/(\zeta^2-m^2)$. Over the remainder of the interval the contour is equivalent to an evaluation of the surface pressure times the surface slope. Over this interval the pressure is constant, proportional to

$$F(\pi/2, k) - E(\pi/2, k)$$

and the resulting drag is easily computed from the projected area of the cone—that is,

$$\text{partial } C_D = \frac{\pi}{2} t^2 \frac{m}{1-m^2} (F - E) \qquad (17)$$

In this case, both the drag arising from the approximate surface pressure distribution and the leading-edge force act in the same direction so that the total drag amounts to the sum of Eqs. (16) and (17).

$$C_D = \pi \left(\frac{t}{2m}\right)^2 \left[\frac{m^3}{\sqrt{1-m^2}} + 2\frac{m^3}{1-m^2}(F - E)\right] \qquad (18)$$

The quantity $t/2m$ is the "thickness ratio" of the cross sections of the elliptic cone. Eq. (18) does not, of course, include the wake drag that would arise if the cone were cut off so as to have a blunt base.

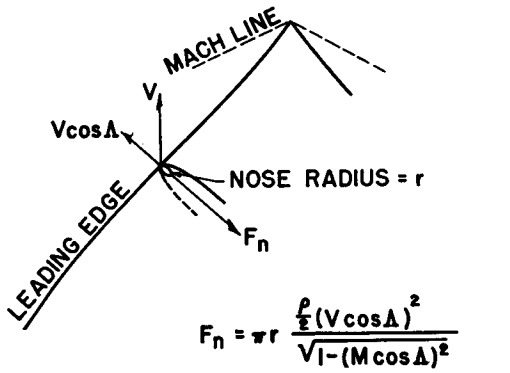

FIG. 8. General expression for force per unit length normal to oblique leading edge.

GENERAL EXPRESSION FOR LEADING-EDGE FORCE

In the foregoing example, the flow field is conical, and the drag coefficient of each section throughout the length of the conical body is the same. In more general examples such as that described by Lighthill,[2] however, this simplifying feature will not appear, and the coefficient of the leading-edge force will vary from point to point along the length of the edge. Furthermore, it will not be possible, in general, to represent the entire geometry of the flow field by a function of a complex variable. However, if the body is sufficiently thin and flat and presents no abrupt changes in the radius of curvature of the leading edge, the flow field in the immediate neighborhood of a point on the leading edge may be considered to have a cylindrical, or two-dimensional, form. In such cases the localized region of the flow field can be represented by a function of a complex variable, and the contour integration for the leading-edge force can be performed. Fig. 8 illustrates the more general relation obtained when this calculation is applied to an elliptical leading edge with nose radius r. It is seen that the force normal to the edge at large angles of sweep is approximately equal to that developed by the impact pressure of the normal stream component acting on the developed area of the circular cylinder having the radius of the leading edge.

REFERENCES

[1] Allen, H. Julian, *General Theory of Airfoil Sections Having Arbitrary Shape or Pressure Distribution*, N.A.C.A. Report No. 833, 1945.

[2] Lighthill, M. J., *Methods for Predicting Phenomena in the High Speed Flow of Gases*, Journal of the Aeronautical Sciences, Vol. 16, No. 2, pp. 69–83, February, 1949.

[3] Jones, Robert T., *The Use of Conical and Cylindrical Fields in Supersonic Wing Theory*, from compilation of papers presented at the N.A.C.A.-University Conference on Aerodynamics, June 21–23, 1948, Langley Field, Va., pp. 341–353. (Durand Reprinting Committee, California Institute of Technology, Pasadena 4, Calif.)

[4] Hobson, E. W., *The Theory of Spherical and Ellipsoidal Harmonics*, pp. 164, 165; The University Press, Cambridge, 1931.

[5] Bateman, H., *Partial Differential Equations of Mathematical Physics*, pp. 356–358; Dover Publications, New York, 1944.

TECHNICAL NOTE 2249

THE SPANWISE DISTRIBUTION OF LIFT FOR MINIMUM INDUCED DRAG OF WINGS HAVING A GIVEN LIFT AND A GIVEN BENDING MOMENT

Robert T. Jones

Ames Aeronautical Laboratory

December 1950

NATIONAL ADVISORY COMMITTEE FOR AERONAUTICS

TECHNICAL NOTE 2249

THE SPANWISE DISTRIBUTION OF LIFT FOR MINIMUM INDUCED DRAG OF WINGS HAVING A GIVEN LIFT AND A GIVEN BENDING MOMENT

By Robert T. Jones

SUMMARY

The problem of the minimum induced drag of wings having a given lift and a given span is extended to include cases in which the bending moment to be supported by the wing is also given. As in the classical problem of induced drag, the theory is limited to lifting surfaces traveling at subsonic speeds. It is found that the required shape of the downwash distribution can be obtained in an elementary way which is applicable to a variety of such problems. Expressions for the minimum drag and the corresponding spanwise load distributions are also given for the case in which the lift and the bending moment about the wing root are fixed while the span is allowed to vary. The results show a 15-percent reduction of the induced drag with a 15-percent increase in span as compared with results for an elliptically loaded wing having the same total lift and bending moment.

INTRODUCTION

In the problem of minimum induced drag as originally treated by Munk (references 1 and 2) the span of the wing and the total lift were supposed to be given and the distribution of lift over the span resulting in a minimum of drag was sought. The solution of this problem thus provided a convenient lower bound for the induced drag of a wing of given dimensions.

In the practical design of wings the requirements for low induced drag and the requirements for structural strength are opposed. Here the bending moment developed by the lift becomes an important consideration - more important in many cases than the actual spanwise dimension of the wing. Such considerations lead to the problem of determining the minimum drag with limitations imposed on the bending moment as well as on the total lift. It is the purpose of the present paper to show how the methods of the earlier analysis can be extended in a very simple way to the solution of problems involving the bending moment of the load distribution.

A complete list of symbols employed in the analysis will be found in the appendix.

GENERAL FORMULAS FOR LIFT, DRAG, AND BENDING MOMENT

Reference may be made to the original papers of Prandtl and Munk (references 1 and 2), or to any of the standard text books on aerodynamics, for the fundamental developments of wing theory which form the basis for the calculations of induced drag. In these developments the over-all lift is given by

$$L = \rho V \int_{-s}^{+s} \Gamma \, dy \tag{1}$$

and the drag is given by

$$D_i = \rho \int_{-s}^{+s} w_i \, \Gamma \, dy \tag{2}$$

In these formulas the wing span is supposed to extend along the y axis between $-s$ and $+s$, Γ is the local circulation or vortex strength, and V is the constant velocity of flight. The induced downwash velocity w_i is variable along the span and is connected with the vortex distribution $\Gamma(y)$ through the relation

$$w_i(y) = \frac{1}{4\pi} \int_{-s}^{+s} \frac{d\Gamma/d\eta}{y-\eta} \, d\eta \tag{3}$$

With this value for w_i the expression for the drag may be converted to a double integral involving the spanwise distribution of lift as represented by the circulation strength Γ

$$D_i = \frac{\rho}{4\pi} \int_{-s}^{+s} \int_{-s}^{+s} \frac{\Gamma(y)\Gamma'(\eta)}{y-\eta} \, dy \, d\eta \tag{4}$$

This integral may be reduced to a more symmetric form if it is integrated by parts on the supposition that Γ falls to zero at the wing tips. Thus[1]

$$D_i = \frac{\rho}{4\pi} \int_{-s}^{+s} \int_{-s}^{+s} \frac{\Gamma(y)\Gamma(\eta)}{(y-\eta)^2} \, dy \, d\eta \tag{5}$$

[1]The validity of equations (3), (4), and (5) can be demonstrated by referring to the limiting values of complex integrals taken along a path a short distance above the singular point on the real axis. In the case of equations (3) and (4) this process yields the Cauchy principal value.

Consider now an initial distribution designed to achieve minimum drag. (See fig. 1.) The drag added by a small additional loading will be composed of three parts, namely:

1. The drag of the additional lift acting alone
2. The drag of the original loading arising from the downwash field of the additional loading
3. The drag of the additional loading induced by the downwash field of the original loading

Item 1 is of second order in terms of the magnitude of the added lift for smooth distributions, that is, so-called "weak variations." (The fact that this second-order term is invariably positive insures that the drag will be a minimum and not a maximum.) Items 2 and 3 are equal by the mutual drag theorem. The first-order variation in drag can then be computed by considering only the drag of the small additional lift acting in the induced downwash field $w_i(y)$ of the original lift.

The conditions of fixed bending moment and fixed total lift are met by allowing only those curves of lift variation that produce no change in these quantities, that is, curves having zero area and zero moment. It can be seen that such curves of variation must have at least three elements to meet the conditions of zero area and zero moment. Furthermore, any curve meeting these conditions can be subdivided into groups of three elements so that the individual groups also satisfy the conditions. Hence, as the representative of such restricted curves of variation we may adopt three small elements having areas l_1, l_2, and l_3 (fig. 1). These elements, together with their positions y_1, y_2, and y_3 and the local values of the downwash w_{i_1}, etc., due to the original loading must satisfy the following three equations:

$$\left.\begin{array}{lll} \text{for} & \delta L = 0, & l_1 + l_2 + l_3 = 0 \\ \text{for} & \delta B = 0, & l_1 y_1 + l_2 y_2 + l_3 y_3 = 0 \\ \text{for} & \delta D_i = 0, & l_1 w_{i_1} + l_2 w_{i_2} + l_3 w_{i_3} = 0 \end{array}\right\} \tag{8}$$

It can be seen that these equations will be consistent if $w_{i_1} \sim a+by_1$, $w_{i_2} \sim a+by_2$ and $w_{i_3} \sim a+by_3$, where a and b are constants to be determined from the given conditions. Since such equations must be satisfied for all positions y_1, y_2, etc., it is concluded that, in general,

$$w_i \sim a + by \tag{9}$$

In mathematical terms the problem is to minimize the double integral, equation (5), while holding fixed values of

$$L = \rho V \int_{-s}^{+s} \Gamma \, dy \tag{6}$$

and

$$B = \rho V \int_{s_o}^{s} (y-s_o) \, \Gamma \, dy \tag{7}$$

where B is the bending moment specified about the point s_o. For the time being s_o will be taken as the origin, or wing root ($s_o = 0$), although later another example will appear.

Although the derivation of the formulas for induced drag makes use of the concept of the lifting line, it is important to note that the results are not actually restricted to this approximation. According to Munk's well-known stagger theorem the induced drag of a lifting surface will be equal to that of a lifting line if the spanwise load distributions are the same.

It should be noted further that the induced drag of a wing having a given lift and a given spanwise load distribution is not affected by the compressibility of the air at subsonic speeds. At supersonic speeds an additional drag associated with the formation of waves arises and the induced drag, which is associated with the vortex wake, becomes only a part of the total pressure drag.

THE DISTRIBUTION OF DOWNWASH FOR MINIMUM DRAG

In general, if the drag is to be a minimum, a small variation in the shape of the curve of spanwise loading will produce no first-order change in the drag. The variation in shape may take the form of a small addition to the original loading; it is then necessary to find conditions under which the drag added by a small additional loading is zero.

The solution of this latter problem is rendered especially simple by the mutual drag theorem (reference 1), which arises from the evident symmetry of the integral to be minimized (equation (5)). The theorem states that if the lift distribution (represented by Γ (y)) is the sum of two distributions Γ_1, and Γ_2, the drag of Γ_1 arising from the downwash field of Γ_2 is exactly equal to the drag of Γ_2 arising from the downwash of Γ_1.

Determination of Span Loading and Induced Drag From the Downwash Distribution

The case of bilateral symmetry with moment specified about the root section will serve as an example of the calculation of the actual span loading and induced drag. It will be evident from the foregoing that the downwash distribution will consist of two straight-line segments with a reversal of slope at the plane of symmetry. It is then necessary to compute the spanwise variation of Γ corresponding to such a curve of downwash.

To perform this calculation by standard methods of airfoil theory, use is made of the idea that at a great distance behind the wing the vortex sheet forms a two-dimensional field of motion, with the discontinuity in the lateral velocity across the sheet given by $d\Gamma/dy$, and the downwash w given by twice the value of the induced downwash w_i at the wing. Hence, the quantity $1/2\ (d\Gamma/dy) - 2iw_i$ can be evaluated by means of the familiar complex velocity function $v - iw$ of the two-dimensional potential theory using for v its value just above the vortex sheet. In this theory if the vertical component of velocity w is given along the line representing the trace of the span, then the velocity vector at any other point in the field $\xi = y + iz$ may be obtained from the relation (reference 4)

$$v - iw = \frac{1}{\pi} \frac{1}{\sqrt{s^2 - \xi^2}} \int_{-s}^{+s} \frac{w(\eta) \sqrt{s^2-\eta^2}}{\eta-\xi} d\eta \tag{11}$$

As noted above,

$$\frac{d\Gamma}{dy} = v(y + oi) - v(y - oi) = 2v(y + oi) \tag{12}$$

Introducing $w = a + by$ for $y > 0$ and $w = a - by$ for $y < 0$ into equation (11) yields, after integration,

$$\frac{d\Gamma}{dy} = -2a \frac{y}{\sqrt{s^2-y^2}} + \frac{4s}{\pi} b \left(\frac{y}{s} \cosh^{-1} \frac{s}{|y|} - \frac{y}{\sqrt{s^2-y^2}} \right) \tag{13}$$

and hence

$$\Gamma = 2 \left(a + \frac{bs}{\pi} \right) \sqrt{s^2-y^2} + \frac{2b}{\pi} y^2 \cosh^{-1} \frac{s}{|y|}$$

The spanwise loading thus contains the elliptical distribution as one component.

Hence, for a minimum induced drag with a given total lift and a given bending moment the downwash must show a linear variation along the span.[2] (See fig. 2.)

The foregoing method may be readily extended to a more general class of problems involving bending moments or rolling moments. Suppose, for example, a braced wing is considered, as in the dotted outline of figure 3. In this case the bending moment developed by that portion of the lift acting inboard of the point of bracing attachment may be of no concern, but it may be desired to limit the bending moment developed by that portion of the spanwise load curve extending between this point and the tip. In this case s_o will not be zero. At least three elements are required to preserve stationary values of the lift and bending moment, and it is evident that at least two of the elements must lie to the right of the point s_o. The three simultaneous equations are (see fig. 2):

$$\left.\begin{aligned} l_1 + l_2 + l_3 &= 0 \\ l_2(y_2-s_o) + l_3(y_3-s_o) &= 0 \\ l_1 w_{i_1} + l_2 w_{i_2} + l_3 w_{i_3} &= 0 \end{aligned}\right\} \tag{10}$$

Here y_2 and y_3 are to the right of the point s_o and y_1 lies to the left of this point. For these equations[3] to be consistent w_i must have the form

$$w_{i_1} \sim a; \quad w_{i_2} \sim a+b(y_2-s_o); \quad w_{i_3} \sim a+b(y_3-s_o)$$

Hence, in general, the downwash will be a constant over the portion of the span for which the moment is not specified, as illustrated in figure 3. If no restriction whatever is placed on the moment there is obtained the solution of Munk's original problem, namely, that the downwash should be constant over the entire span.

---

[2]It may be noticed at this point that, whereas the discussion has emphasized the idea of minimizing the drag, the analysis actually makes no distinction between the lift, bending moment, or drag, in that stationary values of all three are demanded. Thus equation (9) may be considered a necessary condition for the solution of the following problems: (1) given the total lift and the induced drag to find the distribution of lift over the span that will result in a minimum bending moment, and (2) given the bending moment and the induced drag to find the distribution resulting in the maximum total lift.

[3]See reference 3 for a discussion of solutions of such equations.

Equation (13) for the spanwise distribution of circulation enables the determination of the over-all lift, bending moment, and drag in terms of the unassigned constants a and b. The use of equations (2), (6), and (7), together with the wing semispan s, yields the following values:

$$\left.\begin{aligned} L &= \rho V s^2 \left(\pi a + \frac{4}{3} bs\right) \\ B &= \rho V s^3 \left(\frac{2}{3} a + \frac{1}{\pi} bs\right) \\ D_i &= \frac{a}{2V} L + \frac{b}{V} B \end{aligned}\right\} \tag{14}$$

It is convenient to specify the bending moment of the lift in terms of the lateral position of the centroid, or center of pressure, of the load curve. The lateral centroid as a fraction of the semispan s may be denoted by y' (i.e., $y' = 2B/Ls$). Then, solving for a and b,

$$\left.\begin{aligned} a &= \frac{L}{\rho V s^2} 9 \left(\frac{1}{\pi} - \frac{2}{3} y'\right) \\ bs &= \frac{L}{\rho V s^2} 9 \left(\frac{\pi}{2} y' - \frac{2}{3}\right) \end{aligned}\right\} \tag{15}$$

The expression for induced drag in terms of the lift and the lateral center of pressure becomes

$$D_i = \frac{L^2}{\pi \frac{\rho}{2} V^2 (2s)^2} \left(\frac{9}{2} \pi^2 y'^2 - 12\pi y' + 9\right) \tag{16}$$

This equation yields the minimum drag for the given position of y'. If the lateral center of pressure is specified so as to coincide with that for an elliptical loading (i.e., $b = 0$; $y' = 4/3\pi$), then the above formula reduces to

$$D_i = \frac{L^2}{\pi \frac{\rho}{2} V^2 (2s)^2} \tag{17}$$

The optimum distribution of loading for a given position of the centroid y' may be obtained from equation (13) with the aid of equations (15). The result is

$$2s\,\frac{\Gamma\rho V}{L} = \left(\frac{12}{\pi} - 6y'\right)\frac{\sqrt{s^2-y^2}}{s} + \left(18y' - \frac{24}{\pi}\right)\frac{y^2}{s^2}\cosh^{-1}\frac{s}{|y|} \qquad (18)$$

Drag for a Given Bending Moment with Unrestricted Span

The foregoing calculations show, as was to be expected, that the elliptic loading yields a smaller drag than any of the others within a restricted span. However, if the restriction on the span is removed, still lower values of the induced drag can be obtained without any increase in the bending moment at the wing root. The lower values are obtained by permitting the span to increase and at the same time adopting a more tapered form of the loading curve.

Equation (16) which contains the three variables lift, span, and center of pressure can be easily rearranged to show the variation of drag with span when the bending moment and the lift are held at fixed values. In this case, the lateral position of the center of pressure y's will be fixed, while the form and extent s of the load curve will vary. In order to provide a convenient basis for comparison the span and shape of the load curves will be related to the elliptic loading. If s/s_e denotes the ratio of the semispan of the wing to that of an elliptically loaded wing having the same total lift and bending moment, then equation (16) can be rewritten:

$$D_i = \frac{L^2}{\pi\,\frac{\rho}{2}\,V^2(2s_e)^2}\left[8\left(\frac{s_e}{s}\right)^4 - 16\left(\frac{s_e}{s}\right)^3 + 9\left(\frac{s_e}{s}\right)^2\right] \qquad (19)$$

The quantity in the bracket is the ratio of the induced drag to that of the corresponding elliptically loaded wing. This ratio is plotted in figure 4 to show the decrease of drag possible by increase of the span. The forms of load curve required for the minimum drag at various values of s/s_e are shown in figure 5.

It will be noted that a 15-percent reduction of the induced drag below that for elliptic loading can be achieved with a 15-percent increase in span. Further increases of span between 15 percent and 50 percent (s = 1.15 to 1.50) yield no significant reductions, however. At still larger values of s the drag becomes lower, and approaches zero at an infinite value of s. For extreme values of s/s_e the curves begin to show negative loadings at the tips and eventually the bending moment at certain points along the span will exceed that at the wing root.

Ames Aeronautical Laboratory
National Advisory Committee for Aeronautics,
Moffett Field, Calif., Sept. 25, 1950.

APPENDIX

DEFINITIONS OF SYMBOLS

L	total lift
l	element of lift
D_i	induced drag
B	bending moment
ρ	air density
Γ	circulation
w_i	induced downwash velocity at wing
w	downwash velocity, at infinity ($w - 2w_i$)
v	lateral velocity
V	velocity of flight
y,η	distances along wing semispan
s_o	point of origin for bending moment
s	length of wing semispan
y'	lateral position of load centroid as a fraction of s
a,b	constants

REFERENCES

1. Munk, Max M.: The Minimum Induced Drag of Aerofoils. NACA Rep. 121, 1921.

2. Prandtl, L.: Applications of Modern Hydrodynamics to Aeronautics. NACA Rep. 116, 1921.

3. Bocher, Maxime: Introduction to Higher Algebra. The MacMillan Co., N. Y. 1907, p. 49.

4. Munk, Max M.: Elements of the Wing Section Theory and of the Wing Theory. NACA Rep. 191, 1924.

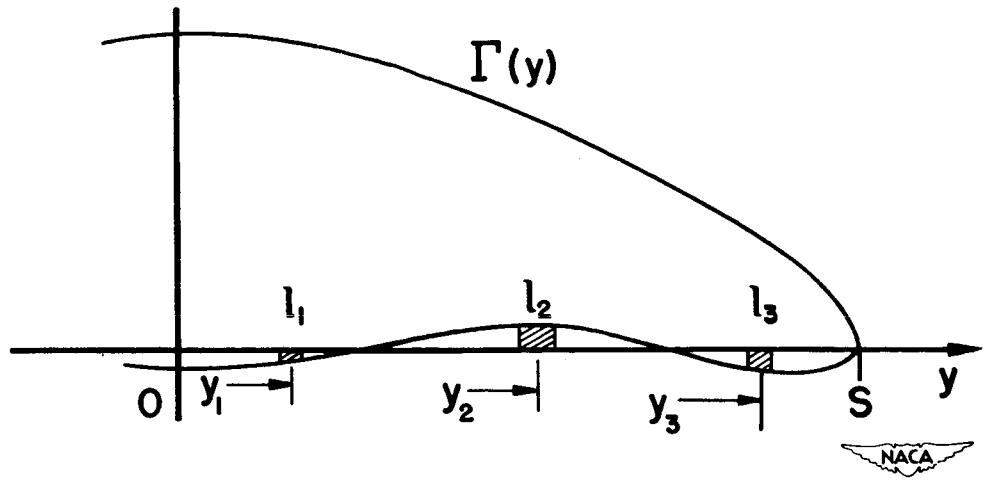

FIGURE 1.- SPANWISE LOAD CURVE WITH THREE ELEMENTS OF VARIATION

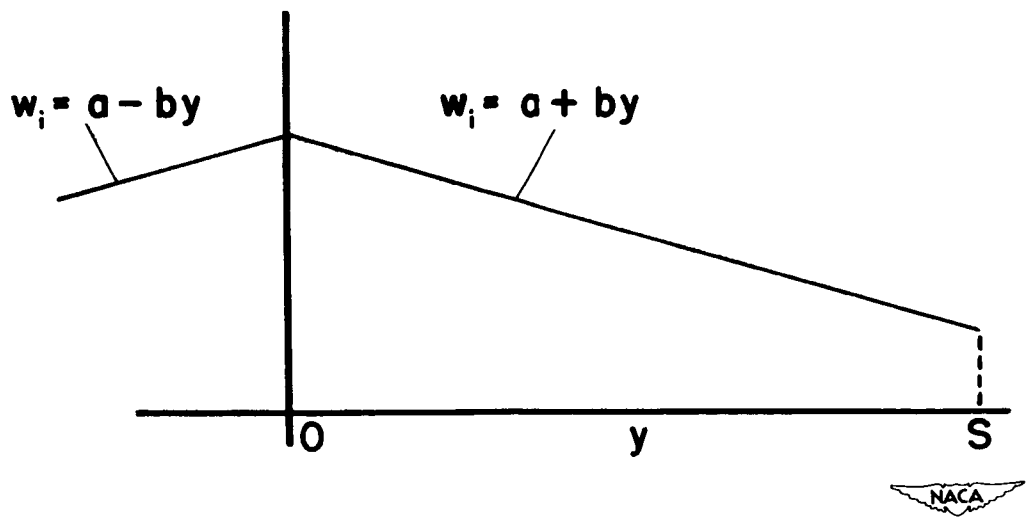

FIGURE 2.- DOWNWASH DISTRIBUTION FOR MINIMUM DRAG WITH RESTRICTED BENDING MOMENT ABOUT CENTER SECTION

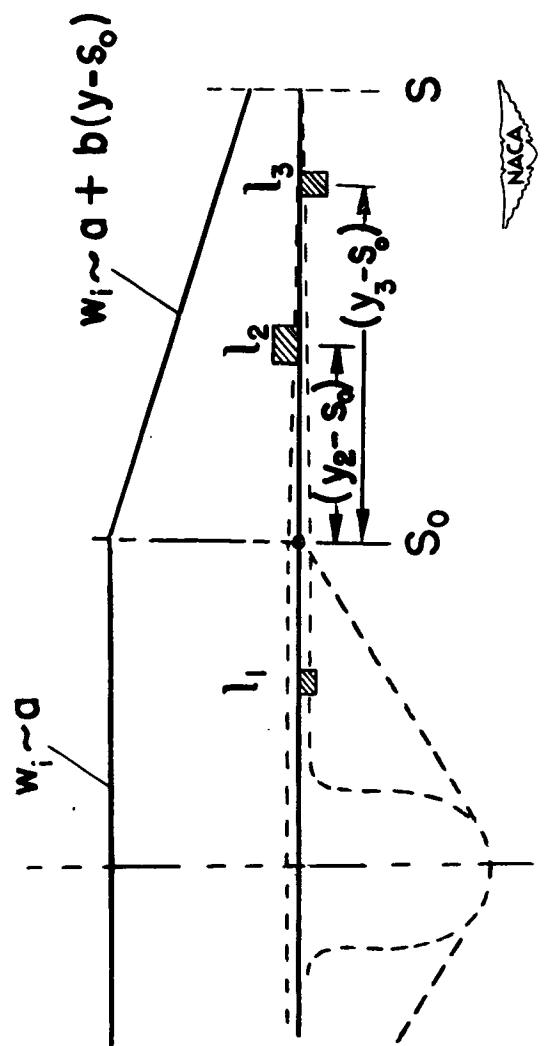

FIGURE 3.- DOWNWASH DISTRIBUTION FOR MINIMUM DRAG WITH RESTRICTION ON BENDING MOMENT OF THE OUTER PORTION OF THE LOAD CURVE

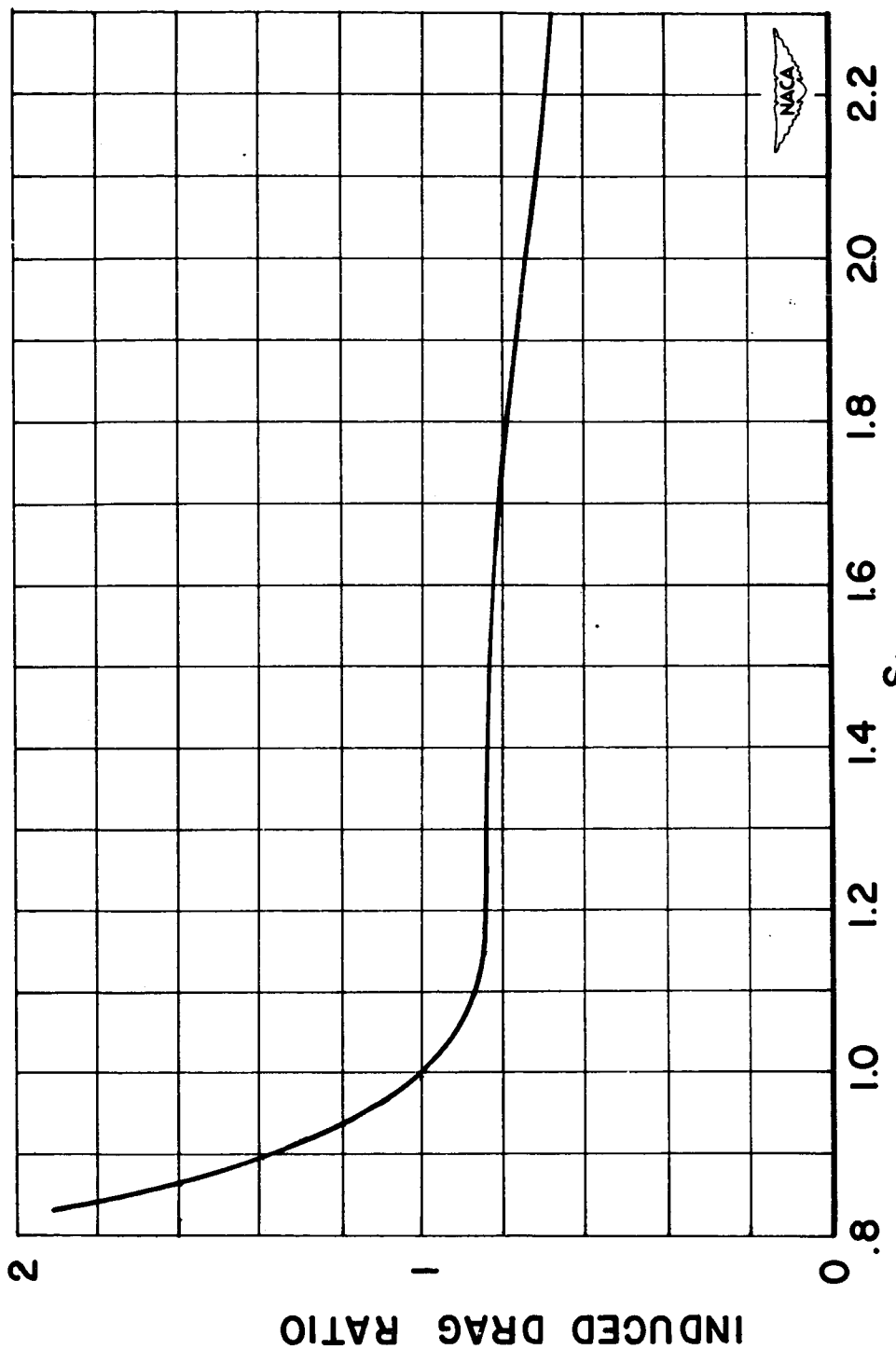

FIGURE 4.- VARIATION OF INDUCED DRAG WITH SEMISPAN RATIO S/Se, FOR WINGS HAVING A FIXED TOTAL LIFT AND A FIXED BENDING MOMENT.

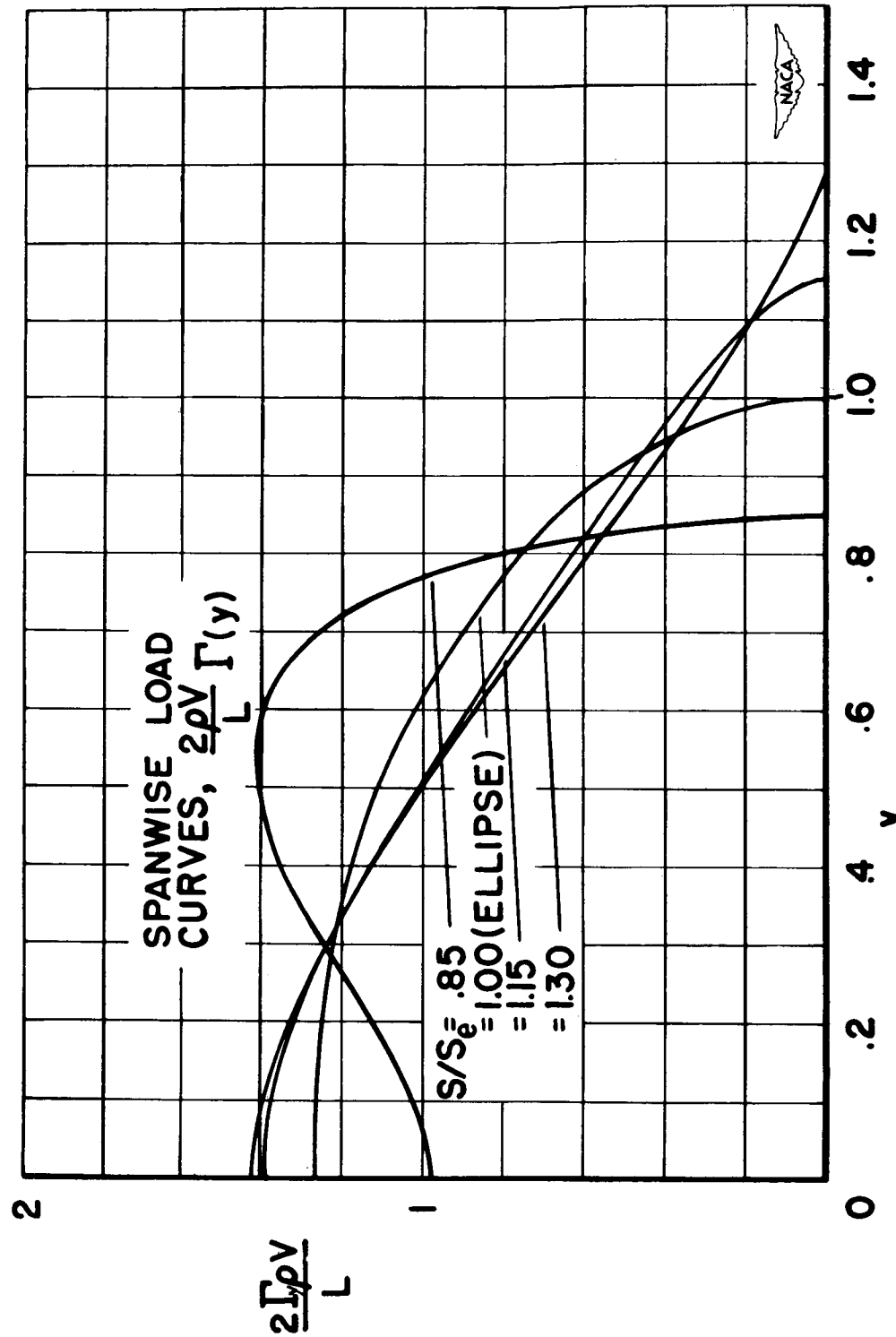

FIGURE 5.- VARIATION OF SHAPE OF THE SPANWISE LOADING CURVE WITH SEMISPAN RATIO S/S_e, FOR WINGS HAVING A FIXED TOTAL LIFT AND A FIXED BENDING MOMENT

Aerodynamics - Fundamental 1.1 The Spanwise Distribution of Lift for Minimum Induced Drag of Wings Having a Given Lift and a Given Bending Moment By Robert T. Jones NACA TN 2249 December 1950 (Abstract on reverse side)	Wings - Complete 1.2.2 The Spanwise Distribution of Lift for Minimum Induced Drag of Wings Having a Given Lift and a Given Bending Moment By Robert T. Jones NACA TN 2249 December 1950 (Abstract on reverse side)
Wing Theory 1.2.2.1 The Spanwise Distribution of Lift for Minimum Induced Drag of Wings Having a Given Lift and a Given Bending Moment By Robert T. Jones NACA TN 2249 December 1950 (Abstract on reverse side)	Jones, Robert T. The Spanwise Distribution of Lift for Minimum Induced Drag of Wings Having a Given Lift and a Given Bending Moment By Robert T. Jones NACA TN 2249 December 1950 (Abstract on reverse side)

Abstract

The problem of the minimum induced drag of wings having a given lift and a given span is extended to include cases in which the bending moment to be supported by the wing is also given. Expressions for the spanwise load distribution and the minimum drag in terms of the lateral position of the load centroid are given. The results show a 15-percent reduction of the induced drag with a 15-percent increase in span over that for an elliptic loading having the same total lift and bending moment.

Abstract

The problem of the minimum induced drag of wings having a given lift and a given span is extended to include cases in which the bending moment to be supported by the wing is also given. Expressions for the spanwise load distribution and the minimum drag in terms of the lateral position of the load centroid are given. The results show a 15-percent reduction of the induced drag with a 15-percent increase in span over that for an elliptic loading having the same total lift and bending moment.

Abstract

The problem of the minimum induced drag of wings having a given lift and a given span is extended to include cases in which the bending moment to be supported by the wing is also given. Expressions for the spanwise load distribution and the minimum drag in terms of the lateral position of the load centroid are given. The results show a 15-percent reduction of the induced drag with a 15-percent increase in span over that for an elliptic loading having the same total lift and bending moment.

Abstract

The problem of the minimum induced drag of wings having a given lift and a given span is extended to include cases in which the bending moment to be supported by the wing is also given. Expressions for the spanwise load distribution and the minimum drag in terms of the lateral position of the load centroid are given. The results show a 15-percent reduction of the induced drag with a 15-percent increase in span over that for an elliptic loading having the same total lift and bending moment.

THE MINIMUM DRAG OF THIN WINGS IN FRICTIONLESS FLOW

Robert T. Jones

Ames Aeronautical Laboratory

February 1951

Jones, R. T., "The Minimum Drag of Thin Wings in Frictionless Flow," Journal of the Aeronautical Sciences, vol. 18, no. 2, Feb. 1951, pp. 75-81.
© 1951 by the Institute of Aeronautical Sciences, Inc.
Reprinted by permission of the American Institute of Aeronautics and Astronautics.

Copyright, 1951, by the Institute of the Aeronautical Sciences and reprinted by permission of the copyright owner

JOURNAL OF THE AERONAUTICAL SCIENCES

VOLUME 18 FEBRUARY, 1951 NUMBER 2

The Minimum Drag of Thin Wings in Frictionless Flow

ROBERT T. JONES*

Ames Aeronautical Laboratory, N.A.C.A.

SUMMARY

The assumptions of the thin airfoil theory are found to provide certain necessary conditions for the minimum drag of airfoils having a given total lift, a given maximum thickness, or a given volume. The conditions are applicable to steady or unsteady motions and to subsonic or supersonic speeds without restriction on the plan form. The computation of drag and the statement of the conditions for minimum drag depend on the consideration of a "combined flow field," which is obtained by superimposing the disturbance velocities in forward and reversed motions.

If the plan form of the airfoil and its total lift are given, it is found that, for minimum drag, the lift must be distributed in such a way that the downwash in the combined field is constant over the entire plan form. If the plan form is given and the thickness of the airfoil is required to contain a specified volume, then the thickness must be distributed over the plan form in such a way that the pressure gradient of the combined field in the direction of flight is constant at all points of the wing. A specification of the thickness along some line drawn on the plan form is found to lead to the requirement that the gradient of the pressure vanishes on either side of this line. For the drag to be a minimum with respect to small changes in the plan form, the foregoing conditions must extend continuously for a small distance beyond the edge of the plan form.

INTRODUCTION

THE DRAG OF A BODY moving through a fluid is attributable partly to the action of tangential, or friction, forces and partly to the action of normal pressures. With well-streamlined bodies, the friction forces are ordinarily confined to a relatively thin boundary layer adjacent to the surface, and in such cases that part of the drag arising from the normal pressures can be determined on the assumption of a frictionless potential motion in the region outside the boundary layer.

A practical way of minimizing the pressure component of the drag is to make the body slender and its angle of attack small. Many of the results of the modern airfoil theory, such as the theory of the induced drag of airfoils, are based on the assumption that the velocities imparted to the air are small in relation to the velocity of flight and, hence, are limited to cases of thin airfoils and small lift coefficients.

In the present paper, certain necessary conditions for the minimum pressure drag of thin airfoils are derived. The analysis makes use of, and extends, certain "reversed flow" theorems originally derived by Hayes[1] and von Kármán[2] and is based on the idea of superimposing the disturbances in forward and reversed motions originally advanced by Munk.[3] Although the analysis is restricted to motions involving small disturbances, the conditions for minimum drag are found to be applicable in a wide variety of circumstances of such motions. Thus, the motion may be steady or unsteady and the velocity of flight may be greater or less than the velocity of sound.

MINIMUM DRAG DUE TO THICKNESS

In the linearized theory the effects of camber, or lift, and thickness can be treated independently and later superimposed in any desired linear combination. Wing problems can therefore be divided into two classes—i.e., those involving thickness but no lift and those involving a distribution of lift over a surface having zero thickness.

Consider first the case of a thin nonlifting body or wing, such as shown in Fig. 1. The surface is assumed to be everywhere nearly parallel to a horizontal plane in the direction of motion. A distribution of thickness, symmetrical above and below this plane, is supposed to be given over the plan form. Computation of the drag of such a body will involve, first, the determination of the pressure distribution over its surface. The drag may then be obtained by one of two methods. In the first method the body is divided into elements of area, and the element of drag is obtained from the in-

Presented at the Aerodynamics Session, Annual Summer Meeting, I.A.S., Los Angeles, July 12–14, 1950.

* Aeronautical Engineer.

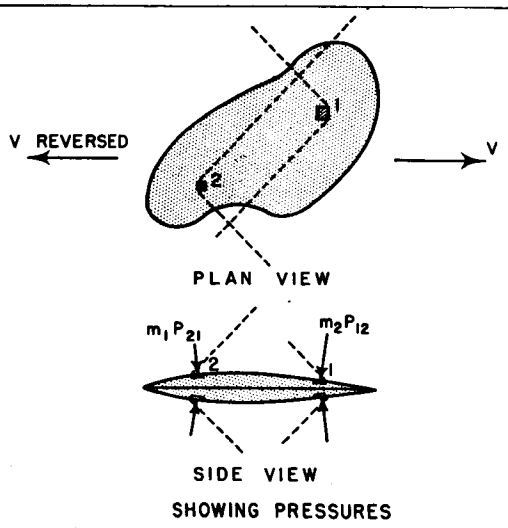

FIG. 1. Thin airfoil with elements representing slope of surface.

clination of the local pressure force. In the second method, which is related to the first through an integration by parts, the body is divided into small elements of volume, and the drag is computed from the force of buoyancy on each element arising from the local gradient of the pressure distribution.

As is well known, the pressure distribution over such a thin, nearly flat body can be calculated by considering only the inclinations or slopes of the surface elements—without regard for the actual displacement of the surface away from the mean plane. The body can then be replaced by a large number of small elementary areas having slopes equal to the local slope of the surface. Each such element can be conceived to create a disturbance field of its own, and the geometric character of this field will depend on the properties of the medium (its elasticity, density, etc.) and on the circumstances of the motion. The disturbance fields of all elements will be alike except for a factor of strength, which is measured by the product of the area of the element and its slope. The total disturbance field of the body may be obtained by superimposing the individual disturbance fields of its elements.

With the aid of this concept of superposition it may be shown that the drag of such a body is unchanged by a reversal of the direction of motion. The pressure at each point of the body is obtained by summing up the influence at this point of every element of the surface. The drag is then obtained by a second summation involving the total pressure force on each element and the slope of its surface in the dragwise direction. Thus, two integrations over the surface are required— or four integrals in all. A typical single element of this sum (see Fig. 1) will be represented by the pressure force on element 2 caused by the pressure field of element 1 and multiplied by the slope of element 2. Now the pressure field of any element, regardless of the distribution or zone of action of the pressure, will be proportional in magnitude to the slope and area of the element. The magnitude of the small contribution to the pressure on element 2 caused by element 1 will therefore be given by the product m_1P_{21}, where m_1 is the "strength" of element 1 as determined from the product of its slope by its elementary area (i.e., m_1 is equal to the frontal area of element 1) and where P_{21} is the pressure arising at element 2 from a unit disturbance at element 1. The increment of drag produced will be equal to the product of the pressure m_1P_{21} by the area and the slope of element 2—i.e., $m_1P_{21}m_2$. In reversed motion, element 1 will lie in the same relation to element 2 formerly occupied by 2 in relation to 1. Hence, P_{21} is equal to P_{12} provided the fluid itself is homogeneous. The signs of m_1 and m_2 are both changed, but their product retains the same sign. The corresponding element of drag in reversed motion is, therefore, $m_2P_{12}m_1$, which is exactly equal to the element of drag in forward motion. Such an equality can be assigned to every pair of elements and therefore must apply to the total drags on forward and reversed motion.

It should be noted that the reversal principle involves hardly any restrictive assumptions aside from those involved in the linearization. It applies, therefore, to steady or accelerated motions and to subsonic or supersonic speeds.

The fact that the drag of the body is the same for either direction of motion leads to the consideration of a method of computing the drag wherein the forward and reversed disturbance fields are considered simultaneously. It is found that the sum of the two drags, or twice the actual drag, can be obtained by superimposing the two fields of disturbance velocities and considering the pressures that would arise from motion of the combined field in the flight direction. The superposition of the two disturbance fields produces a fore-and-aft symmetry in the disturbance field of each element, with the result that the combined flow field is generally simpler in structure than the actual physical field and the calculation of drag is simplified. The pressure in the combined field is simply the difference between the pressures in forward and reversed motions.

It can be shown that in the combined flow field the mutual interference drags of two distributions of thickness are equal. Consider two distributions A and B as illustrated in Fig. 2. The two distributions can be divided into an equal number of elements, and elements from the two distributions may then be paired in an arbitrary way. Considering two elements such as 1 and 2 shown in Fig. 2, it is evident from the symmetry of the combined field of each element that the drag of element 1 caused by element 2 is equal to the drag of element 2 caused by element 1. Since this equality holds for every pair of elements, it must hold for the total distributions A and B.

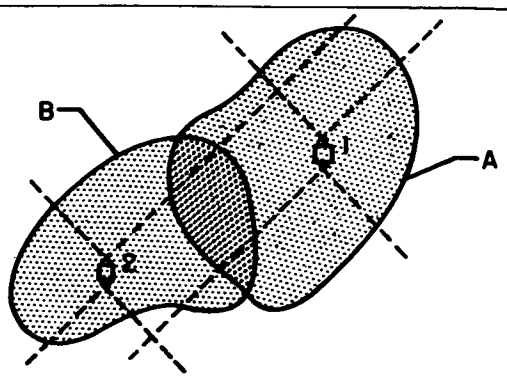

FIG. 2. Elements showing the mutual interference of two wings in combined flow.

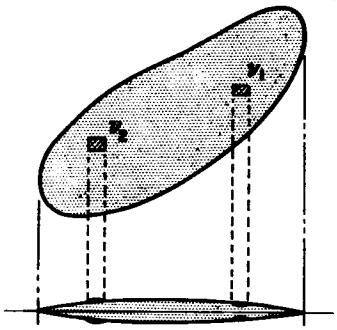

AIRFOIL SHOWING ADDITION OF EQUAL OPPOSITE ELEMENTS OF VOLUME.

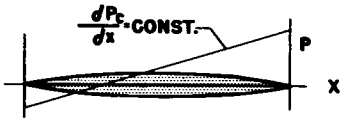

PRESSURE DISTRIBUTION FOR WHICH DRAG OF ADDED ELEMENTS IS ZERO.

FIG. 3a (*top*). FIG. 3b (*bottom*).

We are now in a position to determine the conditions for minimum drag with various specifications of thickness or volume. Consider, first, the following problem: Let the plan form of the wing be given, and suppose that the thickness distribution is required to contain a certain specified volume. What distribution of thickness over the plan form will result in the minimum drag? First, let a distribution of thickness having the specified volume and designed to achieve the minimum drag be given. If the drag is actually a minimum, then a small variation in the shape of the distribution will produce no first-order change in the drag. The variation in shape must not change the original volume and, hence, may be divided into pairs of elements having equal and opposite volumes. The drag of each element is a force of buoyancy equal to the volume of the element multiplied by the local gradient of the pressure. Consider two such elements of volume added to the original distribution as shown in Fig. 3. Following the principle of superposition, the drag added by the elements will be composed of three parts: (1) the drag of the elements in their own pressure fields; (2) the drag added to the original distribution by the pressure fields of the elements; and (3) the drag of the elements in the pressure field of the original distribution. Since the variation in thickness distribution is small compared to the original thickness, item (1) will be of smaller order than (2) or (3).* Furthermore, if use is made of the combined flow field, items (2) and (3) will be equal because of the mutual drag theorem previously demonstrated. The added drag is then equal to twice the buoyancy of the volume elements in the pressure field of the original distribution. Denoting the pressure in the combined field by P_c and the volumes of the elements by ν_1 and ν_2, as in Fig. 3, we have the following two equations:

(1) *For no change in total volume:* $\nu_1 + \nu_2 = 0$

(2) *For no change in drag:* $\nu_1\left(\frac{\partial P_c}{\partial x}\right)_1 + \nu_2\left(\frac{\partial P_c}{\partial x}\right)_2 = 0$

The two equations will be consistent if

$$(\partial P_c/\partial x)_1 = (\partial P_c/\partial x)_2$$

Since such equations must hold for all positions of the elements within the specified plan form, we conclude that the pressure gradient $\partial P_c/\partial x$ must have the same value at all points of the wing. For minimum

* The fact that the second-order variation in drag is always positive ensures that a stationary value will be a minimum and not a maximum.

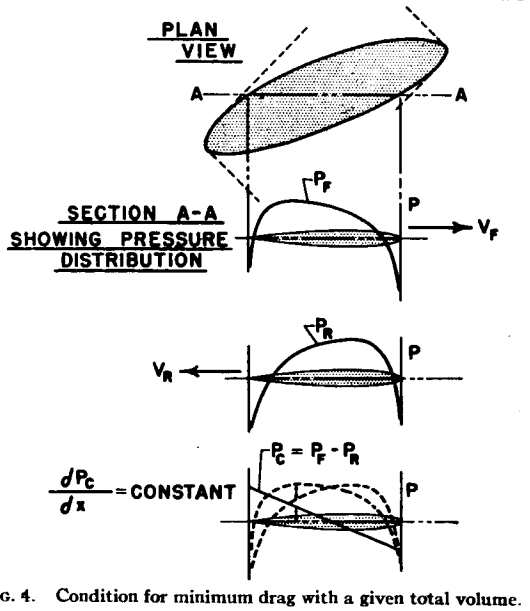

FIG. 4. Condition for minimum drag with a given total volume.

drag, therefore, the thickness must be distributed in such a way that the drag per unit volume is constant over the entire wing in the combined flow field. The significance of this condition in terms of the pressure distributions on an oblique airfoil in supersonic motion is illustrated in Fig. 4.

Examples of bodies satisfying this condition are not difficult to find. One example is that of a thin, flattened ellipsoid accelerating in an incompressible fluid. The drag force in this case is in opposition to the acceleration of the motion and, hence, is attributed to a "virtual additional mass" of the body. The surface pressures due to the acceleration are proportional to $\partial\varphi/\partial t$, where φ is the surface potential. As is well known, the surface potential of any ellipsoid moving in a direction x parallel to a principal axis is of the form $\varphi = KVx$, where K is a constant depending on the proportions of the ellipsoid and V is the velocity. In accelerated motion, $\partial\varphi/\partial t$ and, hence, the pressure are also proportional to x, and this is true for motion in either direction except that the pressures are changed in sign. The pressure distribution in the combined flow, therefore, has a constant gradient in the direction of x, and the ellipsoid satisfies the necessary condition for minimum drag with a given volume. In this case the condition is perhaps better stated as the condition for minimum virtual volume with a given actual volume.

Another example is that of a biconvex airfoil of infinite aspect ratio in steady motion at supersonic speeds. If the upper and lower surfaces are parabolic arcs, the Ackeret theory gives a straight-line distribution of pressure from nose to trailing edge for motion in either direction.

The foregoing method may be readily extended to other problems of minimum drag involving different specifications on the thickness distribution. Perhaps the simplest of these is the case in which the thickness of the wing is specified along some line such as A–B in Fig. 5. Over the remainder of the wing plan form the thickness is to be distributed so as to achieve the minimum drag under the specified conditions.

In this example we wish to consider variations in the thickness distribution which do not alter the shape of the cross section A–B. Any small element of slope having the strength m_1, as in Fig. 5, must therefore be followed by an equal opposite element m_2 at some downstream position ahead of the line A–B so that the thickness along the line A–B is not changed. The two equations determining the necessary condition on the pressure distribution are:

(1) *For no change in thickness along A–B:*

$$m_1 + m_2 = 0$$

(2) *For no change in drag:* $m_1 P_{c1} + m_2 P_{c2} = 0$

and these lead to the relation

$$P_{c1} = P_{c2}$$

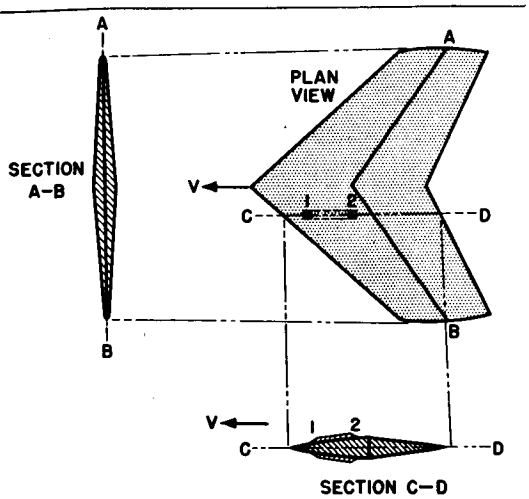

FIG. 5. Wing showing variation of thickness distribution with fixed section A–B.

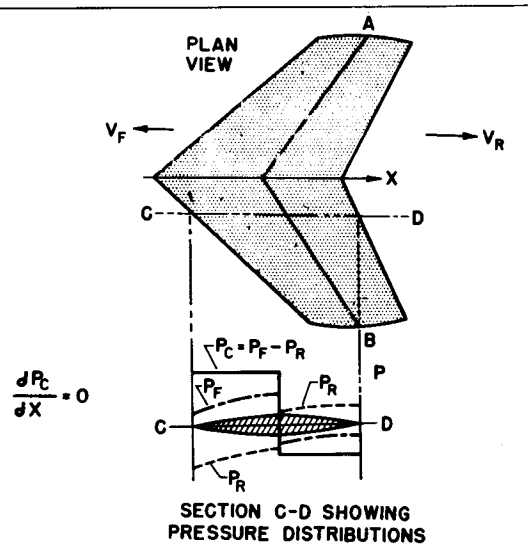

FIG. 6. Condition for minimum drag with given maximum thickness.

Hence, the pressure must not vary in the streamwise direction at points ahead of the section A–B. If the airfoil is further required to close along the trailing edge, a similar condition will be imposed on the pressures in the region behind the line A–B (see Fig. 6).

It will be noted that the condition for minimum drag does not impose a restriction on the spanwise variation of the pressure and that this variation will presumably be determined by the given shape of the section A–B. If the shape of the section A–B is not given exactly but is merely required to have a certain frontal area. then it is found that the pressure in the combined flow field must have the same constant value at all points ahead of this section. The existence of a constant pres-

sure means that the drag per unit of frontal area is constant.

It is interesting to note that the condition for minimum drag with a given frontal area requires that the drag per unit frontal area be constant over the entire wing, while the condition for minimum drag with a given volume requires a constant drag per unit volume. If the maximum thickness of each streamwise section is specified, then the drag per unit thickness must be constant over each section.

Minimum Drag for a Given Lift

The foregoing principles of calculation can be carried over without essential modification to the problem of lift distribution. The drag arising from the lift can be calculated independently of the thickness; hence, the wing can be considered a "lifting surface" slightly cambered or twisted in such a way as to support the desired distribution of lift. A given distribution of lift will induce a certain downwash velocity, and the resultant inclination of the stream lines must agree with the slope of the lifting surface at all points. The drag of the lifting surface will be computed by integrating the product of the local lift by the local inclination of the lifting surface.

The fact that a given distribution of lift has the same drag for either direction of motion can be seen by considering the mutual drags of a pair of lifting elements. Each element of lift produces a distribution of downwash over the plane. The actual configuration of the downwash field does not need to be specified, but its value at all points is assumed to be proportional to the lift of the element. Hence the downwash of an element l_1 at the position of another element l_2 may be expressed in the form $w_{21} = l_1 W_{21}$, where W_{21} is an influence function that depends on the geometric position of element 2 in relation to element 1. The drag of element 2 caused by element 1 is, therefore, $l_1 W_{21} l_2$.

In reversed motion the roles of the elements are reversed and the drag of element 1 caused by element 2 is now $l_2 W_{12} l_1$ and $W_{12} = W_{21}$. Similarly, the drag of element 2 caused by element 1 in reversed motion is equal to the drag of l_1 caused by l_2 in forward motion. These statements do not exclude the possibility that each element lies wholly or partially outside the zone of influence of the other element, and, hence, the reversal principle holds for unsteady or supersonic motions.

Suppose a plan form and a distribution of lift are given, and consider again the field of perturbation velocities obtained by superimposing the fields in forward motion and in reversed motion. The horizontal perturbation velocities that give rise to the lift will be exactly canceled at each point of the surface. However, the downwash velocities over the surface will not, in general, be canceled, and the drag of the given distribution of lift for either direction of motion can be computed by considering this lift to act in the combined downwash field.

If consideration is restricted to the method of calculating drag by combining the flow fields in forward and reversed motion, it is easily seen that the mutual interference drags of any two lifting areas are equal. The drag of a lifting surface A caused by the downwash of lifting surface B is exactly equal to the drag of B caused by the downwash field of A. This theorem follows from the symmetry of the combined flow field of any element and the equality of interference drags of two elements exactly as was previously demonstrated in the case of thickness.

Consider now a lifting surface supporting a given lift L, and suppose that a distribution of lift over the plan form designed to achieve the minimum drag under the stated conditions is given. Any small variation in the shape of the lift distribution which meets the condition of constant total lift can be divided into pairs of elements of equal, opposite lifts. If the drag added by every such pair of elements is zero, then the drag added by any small continuous distribution of the required type will also be zero.

Considering two such elements of a small additional distribution of lift, it is seen that the drag added to the original distribution will again consist of three parts: (1) the drag of the elements alone; (2) the drag added to the original distribution by the downwash fields of the elements; and (3) the drag of the elements in the downwash field of the original distribution. The drag of the elements alone will be of second order but will always be positive so that the second-order variation in drag is positive. Items (2) and (3) will be equal by virtue of the equality of mutual interference drags. For the first-order variation in drag, therefore, we need only consider the elements of lift acting in the downwash of the original distribution. Since the elements of lift are equal and opposite, their drags will be equal and opposite, and the added drag will be zero if the downwash is the same at each element. For all such pairs to contribute zero drag, the downwash must be constant over the whole wing. Hence, for minimum drag the lift must be distributed over the wing in such a way that the downwash in the combined flow field is constant at all points of the plan form. The condition is illustrated in Fig. 7.

Examples of the Minimum Drag of Lifting Surfaces

The stated condition for minimum drag with a given total lift obviously includes the well-known condition for minimum induced drag in steady flight at subsonic speeds.[4] In that case the combined flow field is nothing more or less than the two-dimensional field of motion induced by the vortex wake that is normally trailing but which now extends to infinity both ahead of and behind the wing. The elliptic span loading, which

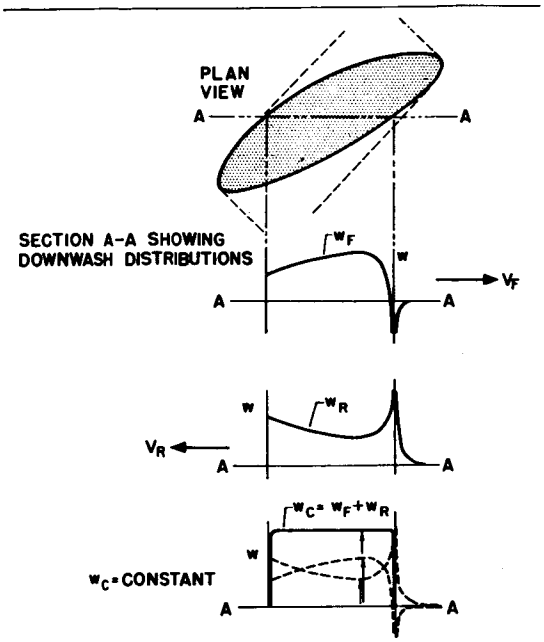

FIG. 7. Condition for minimum drag with a given total lift.

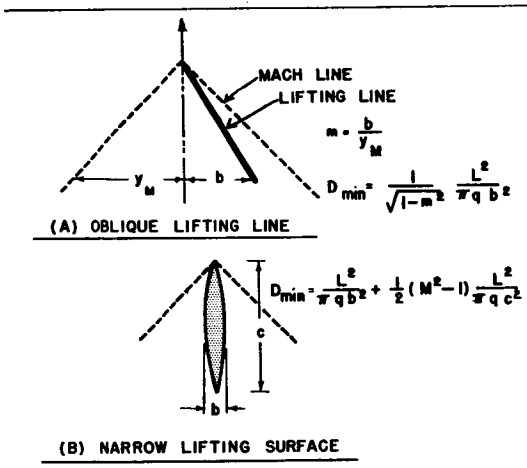

FIG. 8. Examples of minimum drag for a given lift.

yields the minimum drag in this case, produces a uniform downwash not only over the plan form of the wing but over the whole infinite vortex ribbon as well.

In addition to providing the conditions for minimum drag, the combined flow field also provides a simplification of the actual computation of the drag in specific cases. Thus, in the case of steady motion at subsonic speeds, the superposition of the forward and reversed disturbance fields, which are three-dimensional, results in a two-dimensional field of motion. In supersonic motion, the combined field retains its three-dimensional character, but the integration for the downwash is nevertheless considerably simplified when the forward and reversed fields are considered simultaneously.

In the supersonic case, the computation of downwash over the surface involves the superposition of lifting elements whose individual disturbance fields are represented by the potential of an elementary horseshoe vortex that has the form[2, 5]

$$\varphi = \frac{\Gamma\, dy}{2\pi} \frac{xz}{(y^2 + z^2)\sqrt{x^2 - y^2 - z^2}}$$

for an element of lift $\Gamma\rho V\, dy$ located at the origin. The downwash at the position x_2, y_2, z_2 near the plane $z = 0$ arising from an element of lift at the position x_1, y_1 is obtained by differentiating φ with respect to z near $z = 0$ and introducing the displaced origin

$$w_{21} = \frac{\Gamma_1\, dy_1}{2\pi} \times \frac{(x_2 - x_1)}{[(y_2 - y_1)^2 + z_2^2]\sqrt{(x_2 - x_1)^2 - (y_2 - y_1)^2 - z_2^2}}$$

Normally, the computation of downwash over the lifting surface requires that the range of integration be limited to a portion of the plan form so as to exclude the forward branches of the Mach cones, where there is no real disturbance. In the combined flow field, however, both branches of the cones are to be included, and the integration for the downwash at each point can be extended over the entire plan form provided the sign of the radical in the equation is chosen so that the downwash of the lifting element has the same sign in both branches of the cone.

One example that lends itself to calculation is that of an extremely long narrow wing or "lifting line" at an angle of yaw such that the line lies inside the Mach cone originating from its forward tip (see Fig. 8). Here the integration for the downwash in the combined flow field extends from one end of the line to the other, as in the subsonic case, and it is found that an elliptic distribution of lift results in a uniform downwash, yielding the value

$$D = \left(1/\sqrt{1 - m^2}\right)(L^2/\pi q b^2)$$

for the minimum drag. Here, the quantity m is the ratio of the slope of the lifting line to the slope of a Mach line and is less than 1.0 when the crosswise component of velocity of the lifting line is subsonic. As the angle of yaw is decreased so that the lifting line approaches the Mach cone, the drag of this distribution of lift approaches infinity, a fact that must be taken to mean that the concentration of a finite amount of lift within an extremely narrow chordwise dimension is not permissible when the crosswise velocity component is near sonic velocity or is supersonic.

For a lifting surface of narrow proportions lying near the center of the Mach cone, it is found that the expression for the drag can be separated into two components,

one of which depends on the lengthwise distribution of lift while the other depends on the spanwise loading. The minimum value in this case is found to be

$$D = \frac{L^2}{\pi q b^2} + \frac{1}{2}(M^2 - 1)\frac{L^2}{\pi q c^2}$$

where b is the overall span of the wing and c is the overall length. The minimum value of the drag is achieved when both the spanwise and the lengthwise loadings are elliptical.

Determination of Optimum Plan Form

In practice, the determination of the best distribution of lift or thickness for a given plan form may not be so important as the problem of determining the best shape for the plan form. Unfortunately, it is difficult to formulate the latter problem in such a way as to lead to a single definite solution that will be generally useful. The foregoing analysis does, however, provide one important principle concerning wings of minimum drag. Such wings will be characterized by the fact that the drag is stationary not only with respect to variations in the lift or thickness distribution but also with respect to variations in the shape of the outline. Suppose the plan form of such a wing, together with the distribution of lift or thickness satisfying the desired condition for minimum drag, is given. If the drag is to remain unchanged when the outline of the wing is displaced through a small distance, then the distribution of pressure or downwash corresponding to a minimum drag not only must appear over the plan form itself but must also extend for a small distance, without first-order variation, away from the edge of the plan form.

That the foregoing condition leads to a stationary value of the drag can be seen by considering the effect of a small displacement of the outline of a lifting wing, as illustrated in Fig. 9. Supposing the total lifts of the original and the distorted wings to be the same, lift must be removed from the original area and placed on the added area. The first-order variation in drag can again be computed by considering only the effect of the original downwash field on the added distribution of lift. If this downwash, which was required to have a constant value at all points of the original plan form, remains constant in the regions of the added area, then a redistribution of lift from the original to the added area will not affect the total drag.

Curves of variation of the drag with plan-form coefficients seldom show local maxima or minima but show, more often, a monotonic character. As an example

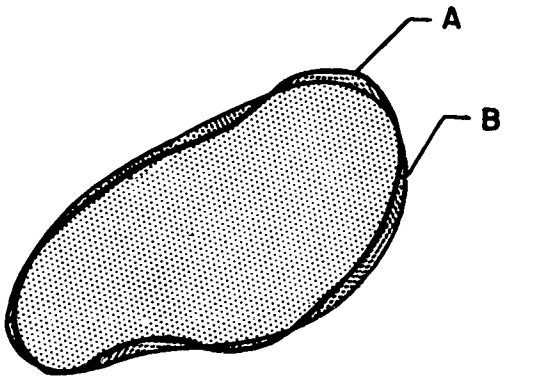

Fig. 9. Condition for drag to be a minimum with respect to variations in plan form.

we may consider the induced drag of wings at subsonic speed. Here, the combined flow field, as previously noted, is simply the two-dimensional motion induced by the vortex wake, and, in the case of minimum drag, the downwash is constant over the whole wake extending ahead of and behind the wing. Since the condition for minimum drag persists along the whole wake, the drag is unaltered by any displacement of the wing boundary in the chordwise direction parallel to the wake. If one proceeds beyond the tip of the wing, however, the downwash changes sign abruptly, and large values of upwash are encountered. The drag is thus not a minimum with respect to changes in the span of the wing but can be continually diminished by removing area from the center portions of the wing and placing it at the tips. At supersonic speeds, the minimum drag for a given area and lift occurs when the wing surface is disposed along narrow lines lying near the center of the Mach cone and having the greatest possible length and span.

References

[1] Hayes, Wallace D., *Linearized Supersonic Flow*, Rep. No. AL-222, North American Aviation, Inc., Los Angeles, June 18, 1947.

[2] von Kármán, Th., *Supersonic Aerodynamics—Principles and Applications*, Journal of the Aeronautical Sciences, Vol. 14, No. 7, pp. 373–409, July, 1947.

[3] Munk, M. M., *The Reversal Theorem of Linearized Supersonic Airfoil Theory*, Jour. Applied Physics, Vol. 21, No. 2, pp. 159–161, February, 1950.

[4] Munk, Max M., *The Minimum Induced Drag of Aerofoils*, N.A.C.A. Report No. 121, 1921.

[5] Heaslet, Max. A., Lomax, Harvard, and Jones, Arthur L., *Volterra's Solution of the Wave Equation as Applied to Three-Dimensional Airfoil Problems*, N.A.C.A. Report No. 889, 1947.

THEORETICAL DETERMINATION OF THE MINIMUM DRAG OF AIRFOILS AT SUPERSONIC SPEEDS

Robert T. Jones

Ames Aeronautical Laboratory

December 1952

Jones, R. T., "Theoretical Determination of the Minimum Drag of Airfoils at Supersonic Speeds," Journal of the Aeronautical Sciences, vol. 19, no. 12, Dec. 1952, pp. 813-822. © 1952 by the Institute of the Aeronautical Sciences, Inc.
Reprinted by permission of the American Institute of Aeronautics and Astronautics.

Reprinted from JOURNAL OF THE AERONAUTICAL SCIENCES
Copyright, 1952, by the Institute of the Aeronautical Sciences and reprinted by permission of the copyright owner
DECEMBER, 1952 VOLUME 19, No. 12

Theoretical Determination of the Minimum Drag of Airfoils at Supersonic Speeds

ROBERT T. JONES*

Ames Aeronautical Laboratory, N.A.C.A.

ABSTRACT

Consider a thin wing in frictionless flow and suppose the plan form of the wing and also the total lift to be given. The drag of the wing will then depend on the way in which the lift is distributed over its surface. In a previous paper, it was shown that the minimum drag occurs when the superposition of the induced disturbance fields in forward and reversed motion results in a constant value of the induced downwash at all points of the wing surface. Similar problems involving the ideal distribution of thickness over the surface were found to lead to similar conditions governing the distribution of pressure in the superimposed or "combined" flow field.

The present paper describes a method for determining mathematically the combined disturbance field, and in certain cases the minimum drag, of wings at supersonic speeds. The simplest analytic example is provided by the wing of elliptic plan form, which achieves its minimum drag when the lift is distributed uniformly over the surface. With a symmetrical distribution of thickness, the requirement of minimum drag for a given total volume is found to lead to profiles of constant curvature.

INTRODUCTION

IN THE THEORY OF WINGS at subsonic speeds, it is shown that the production of lift by a wing of finite span gives rise to a drag force that depends on the distribution of lift over the span. This component of the drag, which arises in frictionless motion, may be related to the energy required for the continual extension of the two-dimensional field of motion induced by the wake of trailing vortices. Alternatively, by examining conditions in the vicinity of the wing sections, the drag may be related to the downward inclination of the air stream induced at the position of the wing by the action of the trailing vortices. Following the latter concept, the drag arising from the lift at subsonic speeds has been termed the "induced drag." It was shown by Munk[1] that this drag is a minimum for a given lift and a given span when the induced downwash is constant at all points of an equivalent lifting line, or vortex, having the same spanwise distribution of lift as the wing. It was further shown by Munk that the induced drag is actually independent of the chordwise distribution of lift.

At supersonic speeds an additional component of drag arises because of the formation of waves by the airfoil, and in this case the drag depends on both the spanwise and chordwise distributions of lift or, in other words, on the actual distribution of lifting pressure over the surface of the wing. In order to extend Munk's problem to wings at supersonic speeds it was necessary therefore to consider not merely the span as given but the actual shape of the wing in plan view. The problem could then be stated in the following form: For a given plan form s and a given total lift L, what distribution of the lift L over the surface s results in the minimum drag?

Furthermore, at supersonic speeds a certain drag arises from the thickness of the airfoil independently of the lift. The two components of drag may, however, be considered separately and later added in any desired combination. To isolate the effect of lift, as distinct from the effect of thickness, it is sufficient to replace the wing by its mean surface, which is supposed to be warped or cambered in whatever way may be required to cause the specified distribution of lift. On the other hand, the drag arising from the thickness may be determined by considering the thickness to be symmetrically disposed above and below a flat mean surface having no lift. In this way additional problems involving the ideal distribution of thickness over the plan form become apparent.

In reference 2 it was shown that all distributions of lift having the minimum drag for a given plan form and a given total lift are characterized by a single condition. If we suppose the wing with its given distribution of lift to be held fixed in a stream of velocity V, then there will arise in the vicinity of the wing and its wake additional small disturbance velocities u, v, and w. Now let the direction of the stream be reversed, but suppose that the curvature and inclination of the surface is so modified as to maintain the original distribution of lift. A new field of disturbance velocities u, v, and w will appear. The wake of trailing vortices will have the same form as before, but the wake will now extend from the wing in the opposite direction. We may now superimpose the two fields of disturbance velocities and obtain by this means a "combined disturbance field," associated with the given distribution of lift. For the drag to be a minimum, the downwash in the combined disturbance field must be constant at all points of the wing surface s.

If the velocity of flight is subsonic, the superposition of the two fields can be shown to result in a two-dimensional field of motion identical in form to the velocity

Presented at the Aerodynamics Session, Annual Summer Meeting, I.A.S., July 16–18, 1952.

* Aeronautical Engineer.

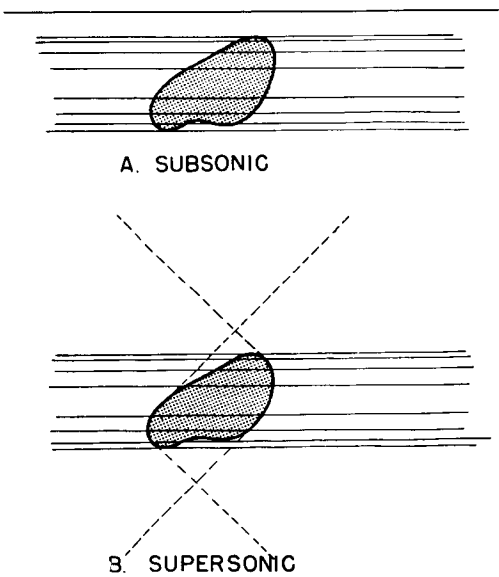

FIG. 1. Lifting surfaces with superimposed disturbance fields.

field of the vortex wake. For distributions of lift having the minimum drag, the downwash induced by the vortex wake in its own plane is a constant, and it will be evident that in this case the downwash is constant not only within the plan form of the wing but at all points of the vortex ribbon ahead of and behind the wing (Fig. 1A).

At supersonic speeds the combination of the forward and reversed disturbance fields again produces an infinite, parallel vortex ribbon, but the field is no longer two-dimensional in character and is bounded by two overlapping zones of influence or wave fronts, as illustrated in Fig. 1B.

By treating the problem of thickness in a similar manner, it was also shown in reference 2 that the minimum drag for a given frontal area of the wing occurs when the pressure in the combined flow field is constant at all points of the wing surface. Similarly, consideration of the minimum drag consistent with a given total volume led to the requirement of a constant streamwise gradient of the pressure in the combined flow.

The present paper describes a method for determining the combined disturbance fields associated with given distributions of lift or thickness. The basic idea of the method is to represent the elementary solutions of the flow equation, such as the solutions for the source and for the horseshoe vortex, by contour integrals, following forms introduced by Whittaker[3] and Bergman[4] rather than the usual forms. The distribution of sources or dipoles over the wing surface is then represented by a triple integral, in which the surface integral, after a change in the order of integration, represents a distribution of two-dimensional disturbances over the surface. The three-dimensional flow is thus obtained finally by the superposition of elementary two-dimensional flows. As will be shown, this method enables the calculation of three-dimensional wing flows that satisfy the conditions for minimum drag and provides, as examples, formulas for the minimum drag of wings of elliptic plan form at supersonic speed.

PRELIMINARY CONSIDERATIONS

As is well known in the thin-airfoil theory, the lift distribution over a thin cambered wing or lifting surface appears as the resultant of two equal, opposite pressures over the upper and lower surfaces With the pressure disturbance given by

$$\Delta p = -\rho u V \tag{1}$$

where u is the longitudinal perturbation velocity, we obtain, for the local lift,

$$l(x,y) = 2\rho V u(x,y,z); \quad z \to +0 \tag{2}$$

The velocity u is discontinuous across the lifting surface and is to be evaluated on the upper side ($z \to +0$). In the lifting case, the downwash velocity $w(x,y)$ is continuous over the whole plane of the wing. The drag is given by

$$D = \int_s \int l(x,y) \frac{w(x,y)}{V} dx\, dy \tag{3}$$

In certain cases, the lift density l and the stream inclination w/V may approach infinite values around the edges of the surface. The integral (3) must then be evaluated by a suitable limiting process, as described in reference 5.

It has been shown by von Kármán[6] and Hayes[7] that the drag of a given distribution of lift is unchanged by a reversal of the direction of motion. Hence, the drag of a specified distribution of lift may be calculated from the corresponding distribution of downwash in either direction of motion or from the combined downwash $\bar{w}$, as indicated by the following formulas:

$$D = \frac{1}{V}\int_s \int \vec{lw}\, dx\, dy = \frac{1}{V}\int_s \int \overleftarrow{lw}\, dx\, dy = \frac{1}{2V}\int_s \int l\bar{w}\, dx\, dy \tag{4}$$

For the minimum drag the combined downwash $\bar{w}$ will be constant over s, and we have

$$D = (1/2)L(\bar{w}/V) \tag{5}$$

where L is the total lift.

Turning to the case of a prescribed distribution of thickness with no lift, it is noted that the velocity u and the pressure as given by Eq. (1) are continuous across the upper and lower sides of the mean plane, but the velocity w has a discontinuity related to the equal and opposite slopes of the upper and lower wing surfaces. If $t(x,y)$ is the prescribed thickness of the wing at the point (x,y), we have

$$w(x,y) = -(1/2)Vt'(x,y); \quad z \to +0 \tag{6}$$

where t' denotes dt/dx. It can be readily verified that the velocity $\bar{w}$, in the combined flow field, vanishes at all points of the wing plan form. A value of $\bar{u}$ remains, however, and determines the drag through the relation

$$D = -\frac{\rho V}{2}\int_s\int t'\bar{u}\,dx\,dy \tag{7}$$

As shown in reference 2 the requirement of minimum drag with various specifications on the maximum thickness or the volume of the wing leads to conditions of the form

$$\bar{u} = \text{constant} \tag{8}$$

or

$$\partial\bar{u}/\partial x = \text{constant} \tag{9}$$

over all or part of the wing plan form.

General Form of the Solution

The field of disturbance velocities surrounding the airfoil will be characterized by a velocity potential satisfying the well-known differential equation

$$(M^2 - 1)\varphi_{xx} - \varphi_{yy} - \varphi_{zz} = 0 \tag{10}$$

The same differential equation holds for the disturbance field in either direction of motion, as well as for the combination of the two fields. Since the fields for different Mach Numbers differ only by an affine transformation, it will be convenient to perform the calculations for $M = \sqrt{2}$.

As may be shown by direct differentiation, the resulting equation possesses the primary solutions[2]

$$\varphi = F(\alpha x - \beta y - \gamma z) \tag{11}$$

where F is an arbitrary, differentiable function and α, β, and γ are parameters determined so that

$$\alpha^2 - \beta^2 - \gamma^2 = 0 \tag{12}$$

Through Eq. (12), α, β, and γ may be made to depend on a single complex parameter λ. Writing $\lambda = e^{i\theta}$ and setting

$$\left.\begin{aligned} \alpha &= 1 \\ \beta &= \cos\theta = (1/2)\,[(1/\lambda) + \lambda] \\ \gamma &= \sin\theta = (i/2)\,[(1/\lambda) - \lambda] \end{aligned}\right\} \tag{13}$$

Eq. (12) is satisfied for values of λ extending over the entire complex plane. For real values of θ ($|\lambda| = 1$), Eq. (11) becomes

$$\varphi = F(x - y\cos\theta - z\sin\theta) \tag{14}$$

and the solution is seen to represent a plane wave of arbitrary form F. The wave front lies at an angle of 45° to the x axis ($M = \sqrt{2}$) but is inclined at an angle θ in the y,z plane. On the other hand, for large values of λ we have

$$\varphi = F[-(\lambda/2)(y - iz)] \tag{15}$$

and the solution here represents a cylindrical or two-dimensional flow with its axis parallel to x. This two-dimensional field is evidently a solution of

$$-\varphi_{yy} - \varphi_{zz} = 0 \tag{16}$$

with φ_{xx} separately equal to zero.

A general solution of Eq. (10) may be constructed by superimposing a number of solutions of the form (11) for various values of the parameter λ. It is clear that the form of the function F need not be the same for all values of λ, so that F may depend on the two variables $\alpha x - \beta y - \gamma z$ and λ. Thus we obtain

$$\varphi = \oint F(\alpha x - \beta y - \gamma z,\lambda)\,d\lambda \tag{17}$$

where C is some contour in the λ plane. Eq. (17) is closely analogous to Whittaker's solution of the Laplaces equation[3] and belongs to the more general class of integral operators studied by Bergman.[4]

Expressions for Elementary Disturbance Fields

As an example of Eq. (17), we may construct the well-known solution for the supersonic point source by means of the superposition of plane waves. This solution can be represented in terms of real values of θ as follows:

$$\varphi_s = \frac{1}{4\pi^2}\int_0^{2\pi}\frac{d\theta}{x - y\cos\theta - z\sin\theta} = \begin{cases} 0, \text{ unless } x^2 > y^2 + z^2 \\ \dfrac{1}{2\pi R} \text{ for } x > 0 \\ \dfrac{-1}{2\pi R} \text{ for } x < 0 \end{cases} \tag{18}$$

(See references 9 and 10.) Here, $R = \sqrt{x^2 - y^2 - z^2}$ and is assumed to have a positive real part. The equation $R = 0$ represents the Mach cone, which extends both ahead of and behind the point source. The integral (18) shows a "zone of silence" in the space between the fore cone and the rear cone.

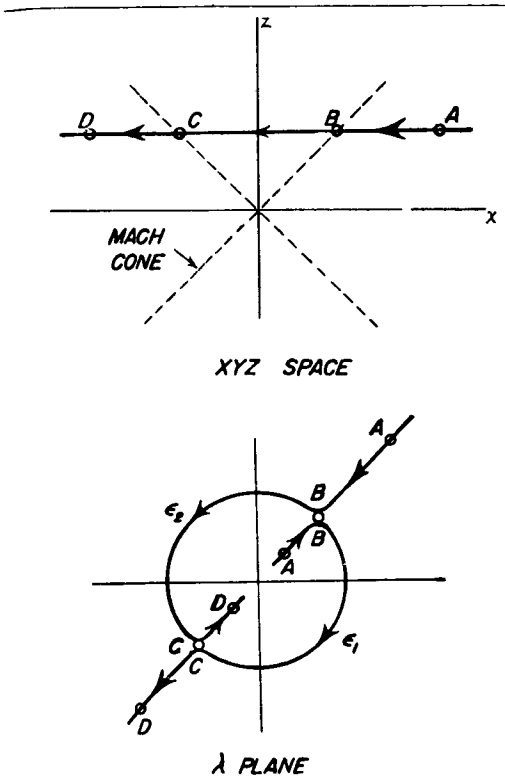

FIG. 2. Course of ϵ_1 and ϵ_2 during variation of point XYZ.

For the purpose of constructing the solution for a complete wing, it is found desirable to represent the elementary solutions in terms of the complex parameter $\lambda = e^{i\theta}$ and to select a contour C which avoids points on the unit circle. It will appear later that the contour C can be selected in a way that simplifies the integration of the elementary solutions over the wing surface.

In terms of λ the potential of the source becomes

$$\varphi_s = \frac{1}{4\pi^2} \oint \frac{d\lambda}{i\lambda\,(\alpha x - \beta y - \gamma z)} \tag{19}$$

The integral may now be evaluated by the method of residues. After expressing α, β, and γ in terms of λ with the aid of Eqs. (13), we have

$$\alpha x - \beta y - \gamma z = (1/2\lambda)\,[2\lambda x - (1 + \lambda^2)y - i(1 - \lambda^2)z] \tag{20}$$

The quantity in the brackets is a quadratic in γ and may be factored so that

$$\alpha x - \beta y - \gamma z = -\frac{(y - iz)\,(\lambda - \epsilon_1)\,(\lambda - \epsilon_2)}{2\lambda} \tag{21}$$

where

$$\left.\begin{aligned} \epsilon_1 &= \frac{x - R}{y - iz} = \frac{y + iz}{x + R} \\ \epsilon_2 &= \frac{x + R}{y - iz} = \frac{y + iz}{x - R} \\ R &= \sqrt{x^2 - y^2 - z^2} \end{aligned}\right\} \tag{22}$$

with the real part of R positive. The integral (19) may now be written

$$\varphi_s = \frac{i}{2\pi^2} \oint \frac{d\lambda}{(y - iz)\,(\lambda - \epsilon_1)\,(\lambda - \epsilon_2)} \tag{23}$$

To evaluate the integral (23) by the method of residues, it is necessary to investigate the positions of the poles ϵ_1 and ϵ_2 in the λ plane as functions of the coordinates x,y,z. Fig. 2 illustrates this correspondence. The three-dimensional x,y,z manifold is represented on the two-dimensional complex plane by the identification of points with rays. This representation was used by Busemann in his conical-flow theory.[11] Each ray drawn from the origin in (x,y,z) space appears as two points ϵ_1 and ϵ_2 in the λ plane. For rays drawn toward the positive direction of x and lying inside the Mach cone ($y^2 + z^2 < x^2$), the point ϵ_1 will lie inside the unit circle, $|\lambda| < 1$, while the point ϵ_2 will lie outside this circle at the reciprocal radius—that is,

$$\epsilon_2 = 1/\bar{\epsilon}_1 \tag{24}$$

Investigation of Eq. (22) shows that for each point (x,y,z) in the space outside the Mach cone ($y^2 + z^2 > x^2$), both ϵ_1 and ϵ_2 lie exactly on the unit circle. Thus, ϵ_1 and ϵ_2 project the space (x,y,z) inside the Mach cone on a surface, while the whole portion of the space (x,y,z) in the "zone of silence" outside the Mach cone is represented on a single line—i.e., the circle $|\lambda| = 1$.

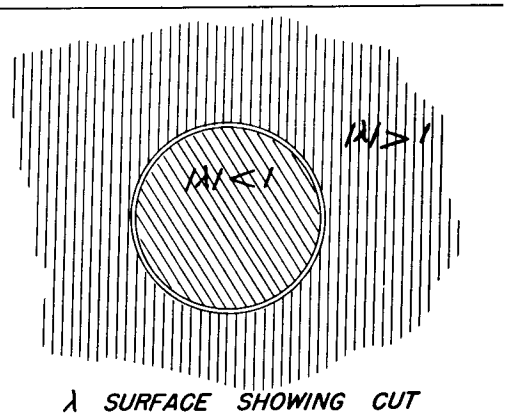

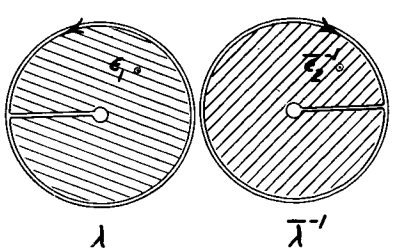

FIG. 3. Representation of λ surface showing two parts of contour C.

This suggests cutting the λ surface into two pieces around the unit circle (see Fig. 3). The gap between the two portions of the surface can then represent the gap between the forward cone of disturbance and the rearward cone of disturbance in the (x,y,z) space. If the outer portion of the λ surface is now mapped onto a second area bounded by a unit circle by means of points at inverse radii, the two circular areas can be related to the circular cross sections of the Mach cone at $x = \pm 1$. Each point on the interior of the unit circle $|\lambda| < 1$ then corresponds to a point $(y + iz)/x$, defined by a ray drawn through the "Mach circle" at $x = +1$. The negative ray that pierces the Mach circle at $x = -1$ then corresponds to a point ϵ_1 on the second surface, $1/|\lambda| < 1$. The center of each surface corresponds to the center of the Mach cone. When both the fore cone and rear cone are considered, it is found that each piece of the λ surface is covered twice, once by ϵ_1 and again by ϵ_2.

Now consider the evaluation of Eq. (19) when the contour is drawn just inside the unit circle, enclosing the surface $|\lambda| < 1$ in the positive direction. For positive values of x such that $x^2 > y^2 + z^2$, the contour will enclose ϵ_1 so that the value of the integral is

$$\frac{-1}{\pi} \frac{1}{(y - iz)(\epsilon_1 - \epsilon_2)} = \frac{1}{2\pi R} \tag{25}$$

For points outside the Mach cone, both ϵ_1 and ϵ_2 lie in the gap between the two portions of the λ surface and are outside the contour, so that the value of the integral is zero. Proceeding toward negative values of x, as soon as the point (x,y,z) reaches the upstream Mach cone, the pole ϵ_1 moves onto the second portion of the λ surface, while the pole ϵ_2 now appears inside the contour $|\lambda| < 1$. The value of the integral is now

$$-\frac{1}{\pi} \frac{1}{(y - iz)(\epsilon_2 - \epsilon_1)} = \frac{-1}{2\pi R} \tag{26}$$

Exactly the same determination of φ_s results from a contour in the negative direction enclosing the remainder of the surface, $1/|\gamma| < 1$. As later calculations will show, changes in the order of integration and differentiation are simplified if the contour C is extended around both portions of the λ surface and if the points $\lambda = 0$ and $1/\bar{\lambda} = 0$ (i.e., poles of β and γ) are excluded by small circles. The two parts of the contour C are shown in Fig. 3.

To describe the flow in the region around a lifting surface we need an expression for the potential field of a "horseshoe vortex" representing the disturbance caused by an element of lift at the origin. This expression may be obtained by the familiar process of integrating the expression for the source in the x direction and then differentiating in the z direction. These operations performed on the integrand of Eq. (19) yield the factor

$$-\gamma d\lambda / i\alpha\lambda = d\beta \tag{27}$$

so that the expression for the horseshoe vortex becomes

$$\varphi = \frac{-1}{8\pi^2} \oint \frac{d\beta}{\alpha x - \beta y - \gamma z} = \begin{cases} 0, \text{ unless } x^2 > y^2 + z^2 \\ \dfrac{+xz}{2\pi R(y^2 + z^2)} \text{ for } x > 0 \\ \dfrac{-xz}{2\pi R(y^2 + z^2)} \text{ for } x < 0 \end{cases} \tag{28}$$

The field is not that of a single horseshoe but of a closely spaced vortex pair extending to infinity in both directions along the x axis. Outside the cone $R = 0$, the disturbance is zero.

Combined Disturbance Field of a Lifting Surface

The combined disturbance field for an entire lifting surface s is obtained by superimposing elementary solutions of the form (28). This superposition amounts to a double integration of elementary horseshoe vortices over the surface, the strength of the vortices at each point being determined by the local lift $l(x_1,y_1)$. After introducing appropriate constants and changing the order of integration so that the contour integral is performed last, the expression for the combined potential $\bar{\varphi}$ of the lifting surface becomes

$$\bar{\varphi} = \frac{-1}{8\pi^2 \rho V} \oint \int_s \int \frac{l(x_1,y_1)\, dx_1\, dy_1}{\alpha(x - x_1) - \beta(y - y_1) - \gamma z} d\beta \tag{29}$$

It will be shown later that the double integral over the surface s in Eq. (29) yields a two-dimensional complex potential function, the form of this function depending on the parameter β. The final integration over β (or) λ then yields the three-dimensional disturbance. By analogy to well-known formulas in two-dimensional potential theory, the integration over the surface s may be defined in such a way as to permit differentiation under the integral. Performing this differentiation for the velocity components $\bar{u}$ and $\bar{w}$, we obtain from Eq. (29)

$$\frac{\bar{u}}{V} = \frac{1}{8\pi^2\rho V^2} \oint \int_s \int \frac{l(x_1,y_1)\, dx_1\, dy_1}{[\alpha(x - x_1) - \beta(y - y_1) - \gamma z]^2}\, \alpha\, d\beta \tag{30}$$

$$\frac{\bar{w}}{V} = \frac{1}{8\pi^2\rho V^2} \oint \int_s \int \frac{l(x_1,y_1)\, dx_1\, dy_1}{[\alpha(x - x_1) - \beta(y - y_1) - \gamma z]^2}\, \gamma\, d\beta \tag{31}$$

The component $\bar{u}/V$ must, of course, vanish at every point of the wing surface.

Relation to Two-Dimensional Flow Theory

It may now be shown that Eq. (31) represents the downwash in the three-dimensional flow by the superposition of the downwash of infinitely many two-dimensional flows. Each two-dimensional flow is associated with an oblique strip drawn in the plane of the wing and having its edges tangent to the outline of the wing plan form. It will appear that the downwash contributed by each strip is given by the familiar "lifting line" formula, the loading on each equivalent lifting line being obtained by an integration of the surface loading on the wing in an oblique direction (see Fig. 4).

For those parts of the contour consisting of the small circles around $\lambda = 0$ and $1/\bar{\lambda} = 0$, the equivalent loading is simply the spanwise loading. It will be evident that these parts of the contour yield the vortex drag of the lifting surface. Considering first the loop around $\lambda = 0$, we have

$$\beta \rightleftharpoons 1/2\lambda, \qquad \gamma \rightleftharpoons i/2\lambda \tag{32}$$

$$\alpha(x - x_1) - \beta(y - y_1) - \gamma z \rightleftharpoons (1/2\lambda)\,[y_1 - (y + iz)] \tag{33}$$

since $\alpha(x - x_1)$ is negligible by comparison. Eq. (31) now becomes

$$\frac{\bar{w}}{V} = \frac{-1}{8\pi^2\rho V^2} \oint \int_s \int \frac{l(x_1,y_1)\, dx_1\, dy_1}{[y_1 - (y + iz)]^2} \frac{i\, d\lambda}{\lambda} \tag{34}$$

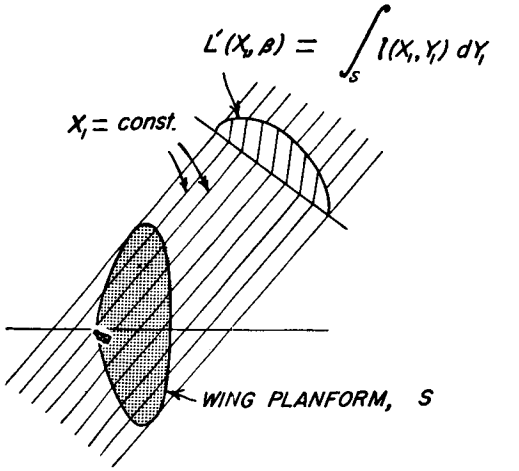

FIG. 4. Integration of surface loading along oblique lines X constant.

The integration along x_1 may now be performed directly and results in the spanwise loading, which may be denoted by

$$\int_s l(x_1,y_1)\, dx_1 = L'(y_1) \tag{35}$$

Now the quantity $l(x_1,y_1)$ represents the lifting pressure, and we may replace it by a quantity that takes equal and opposite values on the upper and lower sides of the wing surface. Similarly, the integrated quantity $L'(y_1)$ may be supposed to take equal and opposite values on the upper and lower sides of the strip, which, for $\lambda = 0$, coincides with vortex wake of the wing. In fact, if we write

$$L'(y_1)/\rho V = \Delta F(y_1) \tag{36}$$

it is clear that ΔF represents the discontinuity in the real part of the two-dimensional complex potential function associated with the trailing vortex wake of the wing.

Instead of integrating ΔF across the strip, we may integrate, using the values of $F = \pm(1/2)\Delta F$, in the positive direction on the upper side and continue in the negative direction on the lower side, forming a closed contour around the strip. Assuming that the function F is smooth and continuous at all points except the points of the strip and does not have a pole at infinity, the contour around the strip may be deformed so as to encircle the point $y + iz$. Then we have, by Cauchy's formula,

$$\frac{1}{\rho V} \int_s \int \frac{l(x_1,y_1)\, dx_1\, dy_1}{[y_1 - (y + iz)]^2} = \oint \frac{F(y_1)\, dy_1}{[y_1 - (y + iz)]^2} = 2\pi i F'(y + iz) \tag{37}$$

The quantity $F'(y + iz)$ is obviously the complex velocity function associated with the vortex wake. Because of the factor i, the real part represents the downwash and the imaginary part represents the lateral velocity v. However, by considering the small loop around the point $1/\bar{\lambda} = 0$ on the second portion of the λ surface, it is found that the quantity $2\pi i F'(y - iz)$ arises instead of Eq. (37). Hence, for the integration in the λ plane around both loops, the lateral velocity v, which is an odd function of z and discontinuous across the strip, vanishes, leaving a real value of the downwash w which is continuous throughout the field.

Returning to Eq. (34), we have, for the integration with respect to the parameter λ,

$$\oint i\, d\lambda/\lambda = 2\pi \tag{38}$$

The same value results for each of the small loops $\lambda \to 0$ and $1/\bar{\lambda} \to 0$. The downwash contributed by these portions of the contour then becomes

$$\frac{w}{V} = \frac{-1}{2\pi\rho V^2}\,\text{R.P.}\int_s \frac{L'(y_1)\,dy_1}{[y_1 - (y + iz)]^2} \tag{39}$$

which is equivalent to Prandtl's formula for the downwash of the trailing vortex wake.

It will now be shown that those portions of the contour C near $|\lambda| = 1$ yield the wave drag of the lifting surface. To illustrate this relation, we replace $\alpha x - \beta y - \gamma z$ by the single variable

$$X = \alpha x - \beta y - \gamma z \tag{40}$$

and for the variable point on the wing we introduce

$$X_1 = \alpha x_1 - \beta y_1 \tag{41}$$

together with the orthogonal variable

$$Y_1 = (\beta x_1 + \alpha y_1)/(\alpha^2 + \beta^2) \tag{42}$$

The factor $\alpha^2 + \beta^2$ in the latter expression preserves the elementary area. Eq. (31) may now be written

$$\frac{w}{V} = \frac{1}{8\pi^2\rho V^2}\oint\int_s\int \frac{l(X_1, Y_1)\,dX_1\,dY_1}{(X - X_1)^2}\,\gamma\,d\beta \tag{43}$$

and the integration with respect to Y_1 may be performed directly by writing

$$\int_s l(X_1, Y_1)\,dY_1 = L'(X_1,\beta) = \rho V \Delta F(X_1,\beta) \tag{44}$$

For $|\lambda| = 1$ the lines $X_1 =$ constant correspond to the intercepts of a system of plane waves at 45° to the x axis ($M = \sqrt{2}$) and at the angle $\theta = \cos^{-1}\beta$ in the yz plane [see Eqs. (13)]. As the angle θ varies from 0 to 2π, the intersections of the plane waves with the lifting surface change their inclination between ±45°. For these various values of θ, Eq. (44) will correspond to an integration of the surface loading of the wing along various oblique directions, as illustrated in Fig. 4. As may be seen by introducing Eq. (44) in the surface integral in Eq. (43), the downwash contributed by each one of these integrated loadings is given by the familiar "lifting line" formula

$$2\pi i\, F'(X,\beta) = \oint \frac{F(X_1,\beta)}{(X - X_1)^2}\,dX_1 \tag{45}$$

In this form the surface integral in Eq. (31) can be recognized as the expression for the downwash arising from a given distribution of lift in two-dimensional flow. In particular, it is known that, if

$$L'(X_1,\beta) = \rho V \Delta F(X_1,\beta)$$

is an ellipse, the downwash, which corresponds to the imaginary part of $F'(X,\beta)$, will be a constant. Hence, if the lift is distributed over the wing in such a way that the integrated loading in every oblique direction between ±45° is elliptical, then the downwash contributed by the outer parts of the contour C (i.e., $|\lambda| \to 1$) will be constant over the entire plan form. If, in addition, the *spanwise* loading is elliptical, then the final integrated value of the downwash will be a constant.

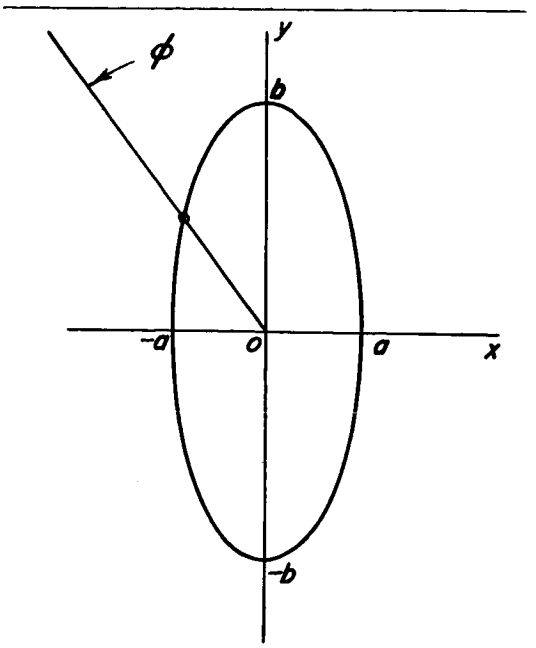

FIG. 5. Elliptic wing.

MINIMUM DRAG OF ELLIPTIC WINGS AT SUPERSONIC SPEED

The foregoing discussion indicated that the downwash will be constant over the plan form if the integrated loading in every oblique direction is elliptical. This condition is, of course, merely a sufficient, and not a necessary, one. The condition is met in the case of the elliptic plan form having a uniform surface distribution of lift. Hence it is concluded that such a uniform surface loading yields the minimum drag in the case of the elliptic wing.

The downwash of the elliptic wing may be calculated directly from Eq. (31). To evaluate the surface integral first, we write

$$\int_s\int \frac{l(x_1,y_1)\,dx_1\,dy_1}{[\alpha(x - x_1) - \beta(y - y_1) - \gamma z]^2} = 2\pi i\rho V F'(X,\beta) \tag{46}$$

After introducing $l = l_0$ and integrating over x_1, there is obtained

$$F'(X,\beta) = \frac{1}{2\pi i\rho V}\int_{-y_s}^{+y_s}\frac{1}{\alpha}\left(\frac{l_0\,dy_1}{X - \alpha x_1 + \beta y_1}\right)_{-x_s}^{+x_s} \tag{47}$$

The subscript s has been introduced to denote the limits of x_1, y_1 corresponding to the edges of the plan form.

For the ellipse with semiaxes a and b, we have, in parametric form (see Fig. 5),

$$y_1 = b\cos\phi; \quad x_s = -a\sin\phi \tag{48}$$

and the integral (47) becomes

$$F'(X,\beta) = \frac{l_0 b}{2\pi i\rho V\alpha}\int_0^{2\pi}\frac{\sin\phi\, d\phi}{X + b\beta\cos\phi + a\alpha\sin\phi} \tag{49}$$

This form is obviously similar to Eq. (18), the complex numbers X, $b\beta$, and $a\alpha$ taking the place of the real numbers x, y, and z in that equation.

The evaluation of integrals of this form has been given by Jacobi, and a complete discussion will be found in reference 10 (see also reference 9). There are two determinations depending on the location of the poles of the integrand, e_1 and e_2, where

$$\left.\begin{aligned} e_1 &= \frac{-X - \sqrt{X^2 - (b\beta)^2 - (a\alpha)^2}}{b\beta - ia\alpha} \\ e_2 &= \frac{-X + \sqrt{X^2 - (b\beta)^2 - (a\alpha)^2}}{b\beta - ia\alpha} \end{aligned}\right\} \tag{50}$$

For real values of $\beta = \cos\theta$, the equation

$$X^2 - (b\beta)^2 - (a\alpha)^2 = 0 \tag{51}$$

determines those values of X which correspond to planes tangent to the edge of the elliptic disc. For points (x,y) inside the elliptic disc,

$$(x^2/a^2) + (y^2/b^2) < 1 \tag{52}$$

and in this case we have the general formula

$$\int_0^{2\pi}\frac{\cos n\phi\, d\phi}{X + b\beta\cos\phi + a\alpha\sin\phi} = \int_0^{2\pi}\frac{i\sin n\phi\, d\phi}{X + b\beta\cos\phi + a\alpha\sin\phi} = \pi\frac{e_1^n - e_2^n}{\sqrt{X^2 - (b\beta)^2 - (a\alpha)^2}} \tag{53}$$

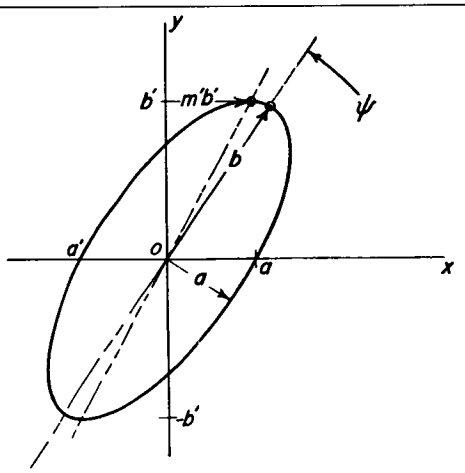

FIG. 6. Oblique ellipse.

Eq. (46) corresponds to $n = 1$,* and the formulas give

$$F'(X,\beta) = \frac{l_0 b}{\rho V\alpha}\frac{1}{b\beta - ia\alpha} \tag{54}$$

For the assumed constant surface loading $F'(X,\beta)$ is thus independent of X, and of x and y, over the surface of the ellipse. Hence the downwash will be constant at these points. The value of the downwash is obtained by introducing the value (54) for (46) in Eq. (31) after making use of the relations

$$\alpha = 1; \quad \gamma = \sqrt{1 - \beta^2} \tag{55}$$

Thus,

$$\frac{\bar{w}}{V} = \frac{-l_0 b}{4\pi i\rho V^2}\oint\frac{\sqrt{1-\beta^2}}{b\beta - ia\alpha}d\beta = \frac{l_0}{\rho V^2}\sqrt{1 + \frac{a^2}{b^2}} \tag{56}$$

Since the value $\beta = i(a/b)$ corresponds to two distinct poles, one on each portion of the λ surface, the value of the integral is twice the residue at this point.

The drag is now given by

$$D_{min.} = (1/2)\,(\bar{w}/V)L \tag{57}$$

where L is the total lift equal to $l_0 S$ for a wing of area S. The formula for the minimum drag of the elliptic wing then becomes

$$D_{min.} = \frac{L^2}{4(\rho/2)V^2 S}\sqrt{1 + \frac{a^2}{b^2}} \tag{58}$$

This relation applies at $M = \sqrt{2}$. The variation of drag with Mach Number may be incorporated in Eq. (55) by applying the Prandtl-Glauert rule. The resulting formula in terms of the coefficients C_L and C_D is

$$C_{D_{min.}} = \sqrt{M^2 - 1}\, C_L^2\sqrt{\left(\frac{1}{4}\right)^2 + \left(\frac{1}{\pi A'}\right)^2} \tag{59}$$

where $A' = \sqrt{M^2 - 1}(A)$ and A is the aspect ratio.

When the aspect ratio is large, Eq. (59) approaches

$$C_D = (\sqrt{M^2 - 1}/4)C_L^2 \tag{60}$$

which is the value given by the Ackeret theory for a flat wing in two-dimensional flow. On the other hand, when A' is small, the wave drag becomes negligible in comparison to the vortex drag, which is given by the well-known formula

$$C_D = C_L^2/\pi A \tag{61}$$

Elliptic Wing at an Angle of Yaw

Eq. (56) indicates that the drag of an elliptic wing of finite aspect ratio is greater than that given by the Ackeret theory (for infinite aspect ratio). Smaller values of the drag can be obtained, however, by placing the wing at an angle of yaw.

* It will be evident that the formulas for $n > 1$ provide extensions to cases of variable loading over the elliptic wing.

The treatment of the yawed wing follows the preceding analysis with only minor modifications. Again the minimum drag occurs when the lift is distributed uniformly over the ellipse. With the symbols defined as in Fig. 6, the equation of the yawed ellipse becomes

$$x_s = m'y_1 \pm (a'/b')\sqrt{b'^2 - y_1^2} \qquad (62)$$

The poles of the integrand in the equation corresponding to Eq. (53) now appear, where

$$\beta = \alpha m' + i(a'/b') \qquad (63)$$

and there are two distinct poles, one on each portion of the λ surface. The value of the integral (31) reduces to

$$\frac{\bar{w}}{V} = \frac{L}{\rho V^2 S}\,\text{R.P.}\,\sqrt{1 - \left(m' + i\frac{a'}{b'}\right)^2} \qquad (64)$$

and we obtain

$$C_{D_{min.}} = \frac{C_L^2}{4}\,\text{R.P.}\,\sqrt{1 - \left(m' + i\frac{a'}{b'}\right)^2} \qquad (65)$$

for the minimum drag of the yawed elliptic wing at $M = \sqrt{2}$.

The variation of drag coefficient with angle of yaw ψ is shown in Fig. 7 for ellipses of various proportions.

The limit $a'/b' \to 0$ corresponds to infinite aspect ratio, and in this case the expression for the drag coefficient reduces to

$$C_{D_{min.}} = (C_L^2/4)\,\text{R.P.}\,\sqrt{1 - m'^2} \qquad (66)$$

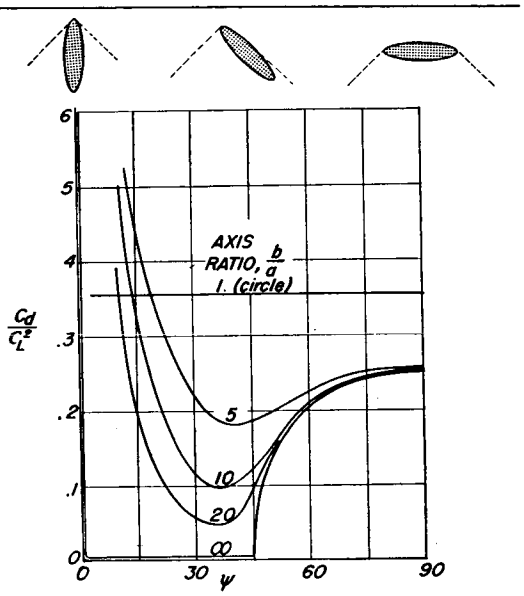

FIG. 7. Minimum drag of elliptic wings at various angles of yaw.

The change of $\sqrt{1 - m'^2}$ from a real number to an imaginary number as m' passes through 1 shows the disappearance of the wave drag when the wing of infinite aspect ratio is yawed behind the Mach cone.

Minimum Drag Due to Thickness

To represent the effect of a symmetrical distribution of thickness, we superimpose elementary solutions of the form (19), corresponding to sources, over the plan form. The expressions for the horizontal and vertical velocities in the combined disturbance field then become

$$\frac{\bar{u}}{V} = \frac{-1}{4\pi^2}\oint\int_s\int \frac{(1/2)t'(x_1,y_1)\,dx_1\,dy_1}{[\alpha(x - x_1) - \beta(y - y_1) - \gamma z]^2}\,\frac{i\,d\lambda}{\lambda} \qquad (67)$$

$$\frac{\bar{w}}{V} = \frac{1}{4\pi^2}\oint\int_s\int \frac{(1/2)t'(x_1,y_1)\,dx_1\,dy_1}{[\alpha(x - x_1) - \beta(y - y_1) - \gamma z]^2}\,\frac{i\gamma\,d\lambda}{\lambda} \qquad (68)$$

where $t'(x_1,y_1) = \partial t/\partial x_1$ and $(1/2)t$ denotes one-half the thickness of the airfoil.

In the case of a symmetrical distribution of thickness, the combined downwash $\bar{w}$ vanishes over the wing surface, while a value of $\bar{u}$ remains. The combined pressure distribution is given by the relation

$$\overline{\Delta p} = -\rho\bar{u}V \qquad (69)$$

The evaluation of the integral (64) is again especially simple in the case of the elliptic plan form. If $t'(x_1,y_1)$ is assumed constant—corresponding to a constant source density over the surface—evaluation of Eq. (64) yields a constant value of $\bar{u}$. The drag therefore has the minimum value for a given frontal area. Since the sections are simple flat-sided wedges, the airfoil does not close at the trailing edge, and the figure is a semi-infinite body rather than a wing. Since the calculations are similar to those given for the lifting wing, they need not be repeated. The result is

$$C_{D_{min.}} = t'^2\,[1/\sqrt{1 + (a^2/b^2)}] \qquad (70)$$

If the source intensity is assumed to vary linearly with x_1 so that $t''(x_1,y_1)$ is a constant, it is found that $\partial\bar{u}/\partial x$ is constant over the area of the wing. In this case the distribution of thickness yields the minimum drag consistent with a given volume—i.e.,

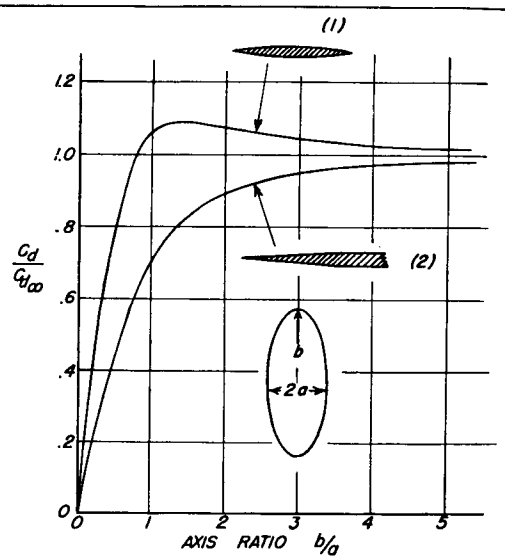

FIG. 8. Minimum drag of elliptic wings having (1) a given volume and (2) a given base area.

$$C_{D_{min.}} = \frac{t_0^2}{a^2}\left(\frac{1}{\sqrt{1 + (a^2/b^2)}}\right)\left(1 + 2\frac{a^2}{b^2}\right) \quad (71)$$

In this case the sections have a constant curvature in the stream direction. Eqs. (70) and (71) are plotted in Fig. 8.

In each case the area of the cross sections has the same distribution along x as that of the corresponding optimum body of revolution. It is interesting to note that each of these figures yields the minimum drag for all distributions of thickness within the space defined by the intersection of its forward and reversed characteristic envelopes.

REFERENCES

[1] Munk, Max. M., *The Minimum Induced Drag of Airfoils*, N.A.C.A. T.R. No. 121, 1921.

[2] Jones, Robert T., *The Minimum Drag of Thin Wings in Frictionless Flow*, Journal of the Aeronautical Sciences, Vol. 18, No. 2, p. 75, February, 1951.

[3] Whittaker, E. T., and Watson, G. N., *Modern Analysis*, pp. 388–403; The Macmillan Company, New York, 1945.

[4] Bergman, Stefan, *Classes of Solutions of Linear Partial Differential Equations in Three Variables*, Duke Mathematical Journal, Vol. 13, No. 3, September, 1946.

[5] Jones, Robert T., *Leading Edge Singularities in Thin Airfoil Theory*, Journal of the Aeronautical Sciences, Vol. 17, No. 5, pp. 307–310, May, 1950.

[6] von Kármán, Th., *Supersonic Aerodynamics—Principles and Applications*, Journal of the Aeronautical Sciences, Vol. 14, No. 7, pp. 373–409, July, 1947.

[7] Hayes, Wallace D., *Linearized Supersonic Flow*, North American Aviation, Inc., Los Angeles, Report No. A.L. 222, June, 1947.

[8] Bateman, H., *Partial Differential Equations*, pp. 95–100; Dover Publications, New York, 1944.

[9] Bierens de Haan, D., *Nouvelles Tables D'Integrals Definies*, Table 68, pp. 104–105; G. E. Stechert & Company, New York, 1939.

[10] Hobson, E. W., *Spherical and Ellipsoidal Harmonics*, pp. 360–364; Cambridge University Press, 1931.

[11] Busemann, A., *Infinitesimale Kegelige Uberschallstromung*, Yearbook of the German Academy for Aeronautical Research, Vol. 713, No. 3, pp. 105–122, 1943.

POSSIBILITIES OF EFFICIENT HIGH-SPEED TRANSPORT AIRPLANES

Robert T. Jones

Proceedings of the Conference on High Speed Aeronautics, Brooklyn

1955

Jones, R. T. "Possibilities of Efficient High-Speed Transport Airplanes," in Conference on High Speed Aeronautics, Polytechnic Institute of Brooklyn, Jan. 20-22, 1955. Proceedings. Edited by A. Ferri, N. J. Hoff, and P. A. Libby. Brooklyn, 1955, pp. 144-156. © 1955 by the Polytechnic Institute of Brooklyn.
Reprinted by permission of its successor, the Polytechnic Institute of New York, Brooklyn, N. Y.

POSSIBILITIES OF EFFICIENT HIGH-SPEED TRANSPORT AIRPLANES

By

Robert T. Jones

National Advisory Committee for Aeronautics

We are accustomed to thinking of the airplane in terms of speed. Less familiar is the fact that the airplane actually achieves its speed with relatively good fuel economy. Recently I flew, together with eighty other passengers, in a scheduled airliner from Kansas City to Los Angeles. On this flight we averaged about 8/10 of a mile per gallon, or 65 miles per gallon for each passenger. Thus we achieved about the same mileage as an ordinary automobile while traveling at six times the speed.

It is easily seen that the efficiency of the subsonic airplane depends on the favorable aerodynamic properties of the wing in this speed range. The possibility of such good lifting efficiency was not obvious to earlier students of hydrodynamic theory—because of an uncertainty in the choice among possible solutions of the flow equations.

Early predictions of airplane performance were based on the choice of the Helmholtz flow. In this flow what is now known as the Kutta condition was applied at both the leading edge and the trailing edge, and the wing was followed by a wake of dead air attached to its upper surface. One of the first text books on aeronautics I studied was entitled "Aeroplane Construction and Operation," by John B. Rathbun (Ref. 1). It was written in 1918 when the wing theory as we now understand it was relatively unknown in this country. On page 93, I find the following statement: "As already explained, the behavior of a body in an air stream cannot be predicted with any certainty by direct mathematical calculation and, for this reason, each and every aerodynamic body must be tested under conditions that are as nearly similar to the actual working conditions as possible. Prior to Professor Langley's first experiments in 1887, mechanical flight with a heavier-than-air machine was derided as an impossibility, even by such scientists as Navier, von Helmoltz, Gay-Lussac, and others who proved by the most intricate calculations that a body larger than a bird could not be supported by its own energy. Such calculations were, of course, based on a wrong understanding of air flow and, as no experimental work had been done up to that time, the flow was assumed according to the individual taste and belief of the demonstrator. The presence of a vacuum on the back of a plate was not understood and, as this contributes

full two-thirds of the lift, it is an easy matter to see why all of the early predictions fell short of the actual lifting forces. To quote one classic absurdity, the scientist Navier proved mathematically that if mechanical flight were possible, then 17 swallows would be capable of developing one horsepower."

Also in 1918, we find in the work of de Bothezat (Ref. 2) (NACA Rep. 28) a theory of airfoils based on the assumption of leading-edge separation and the introduction of a Kármán vortex trail in the wake above and behind the wing. In his consideration of the tip vortices de Bothezat obtains the modern form of the law of induced drag. This component of the drag was, however, negligible in comparison to that induced by the lateral vortices in the wake.

In contrast to these more conservative assumptions, the Kutta-Joukowsky theory predicts large values of the lift without accompanying pressure drag in two-dimensional motion. The degree to which this ideal dragless type of flow can actually be approached under suitable conditions is well illustrated by an experiment made by E. N. Jacobs (Ref. 3) at the NACA's Langley Laboratory a number of years ago. The airfoil in this experiment had a 5-foot chord and extended completely across the (low turbulence) wind tunnel (Fig. 1). At an airspeed of 50 miles per hour and an angle of attack of 7°, a lift force of

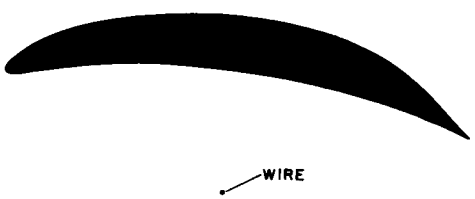

Figure 1 – Airfoil compared with circular wire having equal drag.

100 pounds was measured. The drag amounted to only slightly more than one-third of a pound, so that the lift-drag ratio was nearly 300 to 1. For comparison a round rod or wire having the same drag as the lifting airfoil is also shown.

Flows of the Helmholtz or de Bothezat type are not completely contrary to experience, and yet an airplane designed according to those formulas would have a decidedly unconventional appearance and would require a large thrust. A modern airplane in cruising flight obtains about three times as much thrust from the suction developed in the flow around the leading edge as it does from its engines. This type of assistance from the flow requires a wing of large aspect ratio. In recent years the aspect ratios of transport airplanes have increased to values of 10 or more. Calculations can be made which show that, if

the energy required to transport a given payload were the deciding factor, then still further increases in aspect ratio at the cost of structural weight would be desirable.

As is well known, the fuel consumption of most vehicles increases disproportionately when we try to increase their speed simply by installing more horsepower. The airplane differs from earth-bound vehicles in this respect, however, since, by climbing to a higher altitude, it can increase its speed without necessarily increasing the fuel consumption per mile of flight.

In 1929, B. V. Korvin-Kroukovsky (Ref. 4) published a series of articles in "Aviation" entitled, "The High Altitude Airplane." In that discussion it was pointed out that high economical cruising speeds could be achieved by an ordinary low-speed airplane if this airplane and its power plant could be equipped for operation at high altitudes. Korvin-Kroukovsky's argument was roughly as follows: The ratio of lift to drag of a conventional airplane is determined primarily by its external form and is essentially independent of the airspeed, the wing loading, and the air density. If the airspeed is increased while the airplane is held at a fixed angle of attack, both the lift and the drag will increase with the square of the speed but tend to remain in the same ratio. Now an airplane of conventional form and loading achieves its maximum lift-drag ratio at a rather high angle of attack, which corresponds to a low airspeed at sea level. One method of increasing the speed is to supply more thrust and counteract the increased lift by reducing the angle of attack. Eventually the horsepower required begins to increase as the cube of the speed and the fuel consumption per mile increases, as it does for other vehicles. However, if the airplane is kept trimmed at its optimum angle of attack and the altitude is increased so that the air density diminishes in proportion to the inverse square of the speed, then the air forces, both the lift and the drag, remain constant. In this way the speed can be increased without the requirement of any additional thrust. Since the drag and the thrust required do not increase, then the energy expended per mile of flight remains constant and we can obtain, theoretically, the same number of miles per gallon at progressively higher speeds.

Let us see what happens if we apply this concept to a small lightly loaded airplane of the "Cub" type. Such an airplane might cruise at perhaps 100 miles per hour at a lift-drag ratio of 15 to 1. Suppose a thrust of 1/15 the weight can be supplied at any altitude and that some excess thrust is available for climbing. Figure 2 shows the progressive increase of cruising speed with altitude. At 40,000 feet the speed will have increased to 200 miles per hour and at 68,000 feet the Cub will be traveling at 400 miles per hour. We may ask whether the fabric wings will withstand such a speed or whether there will be difficulty in moving the controls. Of course the indicated airspeed has remained at 100 miles per hour so that the air forces remain essentially unchanged. One effect that might be noticeable is a relative loss in the damping of angular motions. An obvious advantage of this method of

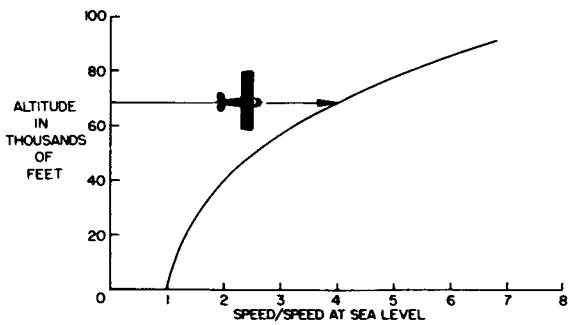

Figure 2 – Increase of cruising speed with altitude for constant thrust.

gaining speed is that it does not interfere with the ability of the airplane to slow down for landing at lower levels.

At first thought one is inclined to ask whether the climb to such a great altitude would be worth-while for any except the longest journeys. Although the increased distance involved in the high altitude path is not important, the time spent at lower altitudes and slower speeds amounts to a considerable fraction of the duration of trips less than 500 miles. However, calculations I have made indicate that, if the means were available, a climb as high as 80,000 feet would save time on a 500 mile flight.

In this connection it is interesting to note that the plan of operation of the Comet airliner, as explained by A. C. Campbell-Orde (Ref. 5) in his paper given at the 20th annual meeting of the Institute of the Aeronautical Sciences, requires a climb to 35,000 feet for the purpose of reaching an alternate airport only 250 miles distant. The saving of time here is essential because of the fuel-burning characteristics of the turbojet engine.

Since density is a relative matter, we might consider, alternatively, increasing the economical cruising speed at low levels simply by increasing the density of the airplane. This method has a marked structural advantage, since the same load would be supported by a more compact structure. A comparison of these methods, that is, increasing altitude vs. increasing airplane density leads to some interesting results. We should also consider the possibility of simply increasing the thrust. This latter method may be thought of as that presently in vogue among automobile manufacturers.

The following table (Fig. 3) shows some results of this comparison—which, needless to say, is made on the simplest possible basis. The numbers listed under the three airplanes to the right show various results of doubling the speed in the subsonic range. In the first method the speed is increased simply by increasing the thrust and the balance between lift and weight maintained by reducing the angle of attack be-

	NORMAL	1 THRUST INCREASED	2 DENSITY INCREASED	3 ALTITUDE INCREASED
SPEED	1	2	2	2
THRUST	1	2	1	1
MILES PER GALLON	1	1/2	1	1
GUST FORCE	1	2	1/2	1/2
LANDING SPEED	1	1	2	1

Figure 3 – Comparison of three methods of increasing speed.

low the optimum value. In the case of a propeller-driven airplane the range in miles per gallon would fall to about one-half and, because of the increased gust force, the ride would be twice as "bumpy." With jet propulsion the range in either case would be rather poor but would not be decreased by going to the higher speed. Of course a considerable increase in the structural stiffness would be required for the higher speed.

In following the second method we would attempt to conceal the same mass and payload in an airplane of one-half the size. If this can be done it is seen that the speed may be doubled without any increase in the required thrust. Thus with jet propulsion the range in miles per gallon will be increased by about the same factor. Furthermore, the riding qualities of the airplane will be improved. The engineering advantage of supporting the given load on a more compact structure is immediately apparent. One difficulty with this method is that the landing speed increases in the same ratio as the cruising speed.

If only the final result is considered, it is clear that an increase of the cruising altitude is the best method of gaining speed. If we can assume that gust velocities diminish at higher altitudes then the gust forces will be even lower than indicated by the table. Each method is essentially limited by the possibilities of engine development. The denser airplane requires the same thrust from engines having one-fourth the normal frontal area, while the engines of the high altitude airplane must develop the required thrust in an atmosphere of one-fourth normal density.

It seems that airplane constructors have actually utilized the benefits of increased density as far as practicable, but the result has been heavier airplanes rather than smaller ones. Figure 4 shows a logarithmic plot of weight versus wing span for a number of successful commercial aircraft. It will be noted that older airplanes and smaller ones, whose design has not changed, tended to follow the law of constant wing loading, that is, $W \propto b^2$. Modern airplanes, especially since restrictions on the landing speed have been removed, tend to follow

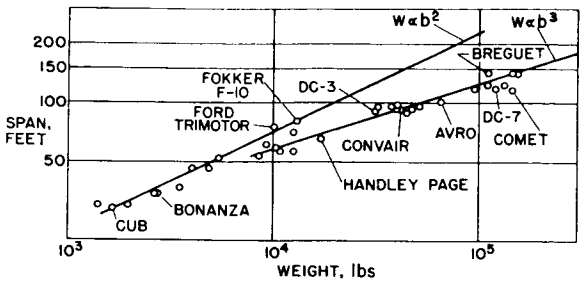

Figure 4 – Airplane weights as a function of a linear dimension.

what might be termed a line of "maximum density." Such a trend, corresponding to constant weight per unit volume, seems to indicate a maximum practical utilization of the space within the airplane. The weight per unit of actual volume along this line approaches that of a loaded railway coach. With the original engine used by Orville and Wilbur Wright the possibility of flight depended on achieving a structure having the minimum density. With present engines it seems that the successful constructor must achieve a maximum density. Although calculations of the landing speed have always occupied an important place in aeronautical engineering, they do not seem to have influenced the final result appreciably.

For many years the airplane designer has advocated a decrease in landing speeds, and yet he has evidently been forced by economic considerations to follow the trend of maximum density according to which the landing speed increases with the size and weight of the airplane. Not long ago landing speeds greater than 65 miles per hour were considered unsafe. Last year, however, approximately 50,000,000 people took off and landed, mostly at speeds of over 100 miles per hour. The landing of transport airplanes at present-day speeds and loadings has proved to be a far safer and more reliable proposition than the landing of early model airplanes, which, with their light wing loadings and slow speeds, could hardly be managed in normal winds and gusts.

There is, of course, a limit to increases of the economical cruising speed of the subsonic airplane and the same limit appears whether we attempt to increase the speed by increasing the density of the airplane or by increasing the altitude of flight. This limit is set by the well-known sudden increase of pressure drag at a critical Mach number. If the optimum lift coefficient and the critical Mach number are given, then we can derive an optimum ratio between the wing loading and the ambient atmospheric pressure P_a. This ratio is

$$\frac{W/S}{P_a} = \frac{\gamma}{2} M_{cr^2} C_{L_{opt}} \qquad (1)$$

and corresponds to the highest cruising speed without loss of efficiency.

At $C_{L_{opt}} = 1.0$ and $M_{cr} = 0.7$ we obtain a wing loading of 1/3 of an atmosphere. Thus, for cruising flight at sea level we require about 700 pounds per square foot. At 60,000 feet, however, the ambient pressure falls to only 150 pounds per square foot, so that the optimum wing loading becomes 50 pounds per square foot. This latter value corresponds to the current density of construction and loading and enables landings to be made at not over 100 miles per hour. It is certainly surprising that our present day heavy wing loadings are really best adapted to the thin air at 60,000 feet.

It has been said that as the speeds of aircraft increase the wings must become proportionately smaller. However, it is hard to discern this trend in the geometric proportions of actual airplanes. Thus, the Comet airliner which flies at about 4-1/2 times the speed of the Ford Trimotor seems to have proportionately even larger wings. Such studies as I have made indicate that if economy of propulsion is to be a major factor, then the relative proportions of the wings will not diminish even at supersonic speeds.

With the velocity given in terms of the Mach number there exists the temptation to think of supersonic speeds in increments of a whole unit. However as our understanding of supersonic wave drag and lift increases it seems increasingly probable that the speeds of commercial aircraft will grow continuously in this range, just as they have in the subsonic range. If we are willing to assume such a continuous transition to the problems of air transportation at supersonic speeds, then it will seem appropriate to follow the trends of loading, density, and altitude disclosed by the preceding development of the subsonic airplane.

The appearance of the wave drag at supersonic speeds does of course require a marked change in the form of an airplane designed for economical flight. Figure 5a illustrates for bodies of revolution the change in the optimum slenderness ratio on going to supersonic speeds. The volume of both bodies is the same and the proportions shown minimize approximately the sum of the drag arising from the normal pressures and from the friction of a turbulent boundary layer. The balance between friction and wave drag is such that a single object 5 feet in diameter requires a fairing 75 feet long.

As a further illustration of the relative magnitude of the wave drag for different forms, I show in Figure 5b two models which, according

Figure 5a – Change in the ideal proportions of a body of revolution on transition to supersonic speeds.

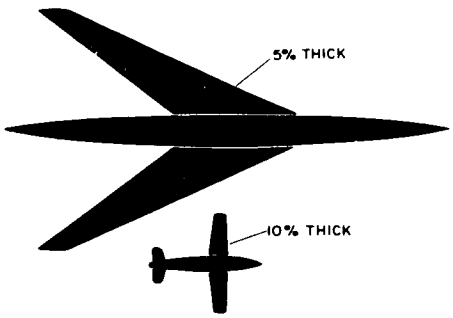

Figure 5b – Models having same drag at low supersonic speed, (zero lift).

to the indications of our experiments, would have the same total drag at a low supersonic Mach number. This comparison of course does not apply to cruising flight since the comparison is made at zero lift.

With regard to the ideal form of the supersonic wing it is interesting to translate the following from Dr. Busemann's paper given 20 years ago at the Volta Congress in Rome (Ref. 6):

"It is clear that the arrow form, quite apart from other considerations, must be favorable since the pressure differences producing lift are fully effective, whilst those producing drag have only a component in the direction of flight. If now a reduction of the effective Mach number makes possible the utilization of a greater surface loading at the same angle of incidence, the relative effect of the shearing forces in the friction layer necessarily decreases." According to our present concept a "subsonic" sweep angle will be required to achieve this objective.

On the basis of the papers of Prandtl (Ref. 7) and von Kármán (Ref. 8) at the 1935 Volta Congress linearized supersonic flow theory has been used to develop the means for estimating the wave resistance of a wide variety of shapes. Even on this simplified basis, however, the formulas often become rather complex so that the trends to be followed by the designer are not clearly displayed. One method of obtaining more instructive formulas is to study the minimum values of the drag under various engineering constraints. As an example we may think of Munk's problem of the minimum induced drag of a wing with a limited span.

At subsonic speeds, even if we allow a large area for the production of lift, the minimum drag can still be achieved by a concentration of the lift along a narrow "lifting line" having a small exposed area and hence small friction. At supersonic speeds the minimum pressure drag usually requires that the given lift be spread over as large an area as allowed by the constraint. An interesting example is provided by the wing of elliptic plan form, which curiously enough seems to have especially simple mathematical properties at supersonic

speeds (Ref. 9). Here the optimum distribution shows no concentration of the lift in any preferred region, but spreads uniformly over whatever elliptical area is allotted. The resulting formula for the pressure drag is

$$D_{min} = \frac{M^2 - 1}{2} \frac{L^2}{\rho V^2 S} \sqrt{1 + \frac{a^2}{b^2}} \tag{2}$$

Here a/b is the axis ratio, subject to the Prandtl-Glauert transformation.

E. W. Graham, H. Luskin, and P. A. Lagerstrom (Ref. 10), in studies made for the Douglas Aircraft Company (Ref. 10 et. seq.), have extended these ideas to distributions of lift in three dimensions. As pointed out to the author by Graham, formula (2) yields the minimum drag not only for the given elliptical area but also for an enlarged area bounded by Mach lines and by lines parallel to the stream direction.

With a straight ellipse the reduction of drag for a given total lift or for a given maximum thickness depends primarily on increasing the exposed wing area S. If we consider an oblique ellipse, then a different form of dependence appears. In this case Eq. (2) is replaced by

$$D_{min} = \frac{M^2 - 1}{2} \frac{L^2}{\rho V^2 S} \operatorname{Re} \sqrt{1 - (m' + i\frac{a'}{b'})^2} \tag{3}$$

Here m is defined by the shearing transformation of the ellipse:

$$x' = x + m'y\,, \quad y' = y,$$

a' is the intercept of the sheared ellipse with the longitudinal x axis and b' is the maximum semispan (see Ref. 9). If we now assume that the area allotted by our constraint is that bounded by the Mach lines and the streamlines as shown in Fig. 6, it is seen that the area actually occupied by the ideal distribution becomes extraordinarily small when the wing is yawed behind the Mach cone. This change coincides with the reappearance of the Kutta-Joukowsky flow, and enables the

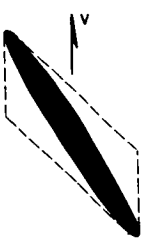

Figure 6—Optimum distribution of lift for area bounded by streamlines and Mach lines tangent to ellipse.

requirements of minimum pressure drag and minimum friction drag to be satisfied simultaneously.

At large angles of sweep or yaw the drag due to lift becomes in a large measure independent of the exact distribution, but depends primarily on the span b and the length l of the wing. For such cases the simpler approximate formula

$$D_{min} = \frac{L^2}{\pi q b^2} + \frac{M^2 - 1}{2} \frac{L^2}{\pi q l^2} \tag{4}$$

shows the essential dependence. The minimum drag occurs when both the lengthwise and the spanwise loadings are elliptical.

For supersonic speed we thus require the maximum span b and the maximum length l, together with the minimum of exposed area. These conditions determine the oblique, elliptically loaded lifting line as an ideal limiting form for the supersonic wing. It seems unfortunate that a bilaterally symmetrical form, such as a swept wing or a V-shaped lifting line could not satisfy the requirement. However if we bend the lifting line at the middle to form a V it is seen that the wave resistance increases considerably.

In order to show the effect of more conventional wing forms on potential supersonic cruising efficiency, I have estimated the lift-drag ratios of several wings in combination with a slender fuselage. Converting these to values of the thrust required by an airplane weighing 50,000 pounds and cruising at 900 miles per hour yields the values shown on Fig. 7. For this comparison the wing thicknesses were selected so as to make possible equal bending stiffness. The order of the comparison would not be changed, however, if a wing of zero thickness were substituted in any one of the examples.

For an operating altitude of 60,000 feet the wing loading in the first two examples should be about 50 pounds per square foot—or the same

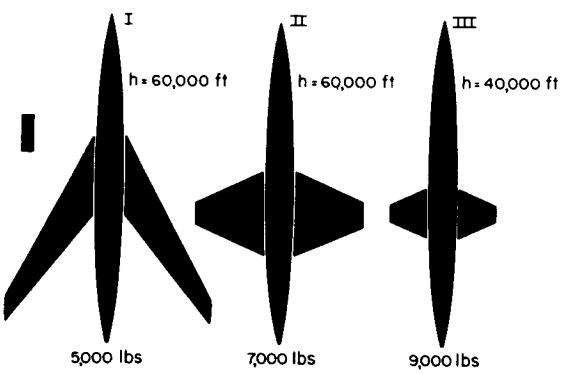

Figure 7—Effect of wing form on required cruising thrust. Values shown are for 50,000-lb. airplane.

as that of a subsonic airplane of this size. Since the indicated airspeed at 60,000 feet is one-third the true airspeed, the structure needs to be sufficiently rigid to withstand—with customary safety margins—a sea-level cruising speed of only 300 miles per hour.

Figure 7 also shows the relative proportions of a conventional turbojet engine designed to produce 10,000 pounds of thrust at sea level. Under our conditions the thrust will be diminished to about one-fourth this value, so that two such engines would be required in the first example. In this case we obtain a specific range of more than one mile per gallon. This latter value compares favorably with that achieved by early model Trimotors, but is of course somewhat less than that obtained with present-day transports operating at subsonic speeds.

We hear a great deal these days about the "heat barrier." However, at 900 miles per hour and 60,000 feet this barrier has not yet been reached. It may be readily calculated that at this speed the aerodynamic heating is no more sufficient to bring the airplane up to room temperature at these levels. Of course, demonstrations of speed at sea level would be rigidly prohibited, both for structural and thermal reasons.

To adapt the airplane to a lower altitude the wing loading needs to be increased. However, if we assume that the maximum density has already been reached in examples I and II, this cannot be done within the limitation of strict geometric similarity. On the other hand, if the airplane is adapted to the lower altitude simply by reducing the size of the wing, then the lift-drag ratio will naturally be reduced. In example III of Figure 7 the wing area was so reduced to suit conditions at 40,000 feet. The thrust required to support the given load then increased to 9000 pounds. Of course if strict geometric similarity could be maintained, a sacrifice of economy would not be involved.

Comparisons of such oversimplified wing-body combinations as shown here may not disclose the full effect of a loss in aerodynamic efficiency. If the thrust needs to be increased at a given altitude then more or larger engines will have to be used and the possibility of concealing them becomes less. In this process the lift-drag ratio of the complete airplane may become still more unfavorable than indicated by the comparison.

These primarily aerodynamic and structural considerations point toward the development of turbojet engines specifically adapted to operation in an atmosphere of one tenth normal density. In addition to the numerous other technological problems associated with operation at these high altitudes, the problems of safe descent and effective limitation to low speeds at low altitudes seem important.

REFERENCES

1. "Aeroplane Construction and Operation," John B. Rathbun, Stanton and Van Vliet (1918).
2. "An Introduction to the Laws of Air Resistance of Aerofoils," George de Bothezat, T. R. No. 28, NACA (1918).
3. "Preliminary Report on Laminar-Flow Airfoils and New Methods Adopted for Airfoil and Boundary Layer Investigations," E. N. Jacobs, W. R. L-345, NACA (1939).
4. "The High Altitude Airplane," B. V. Korvin-Kroukovsky, Aviation (magazine), April 20 (1929) and May 18 (1929).
5. "Some Practical Experiences of Civil Jet Transport Operation and Associated Meteorological Problems," A. C. Campbell-Orde, Paper presented at the 20th annual meeting of the Institute of Aeronautical Sciences, New York, 1952. (Sherman M. Fairchild Preprint no. 355)
6. "Aerodynamischer Auftrieb bei Uberschallgeschwindigkeit," A. Busemann, Luftfahrtforschung, 12, no. 6, 210-220, October 3 (1935). Lecture given at 5th Volta Congress, Rome.
7. "General Considerations on the Flow of a Compressible Fluid," L. Prandtl, NACA T.M. No. 805 (1936).
8. "The Problem of Resistance in Compressible Fluids," Th. von Kármán, GALCIT Publication No. 75 (1936). [From R. Accad. d'Italia cl. sci. fis. mat. e nat. Vol. XIV (1936)].
9. "Theoretical Determination of the Minimum Drag of Airfoils at Supersonic Speeds," Robert T. Jones, Journ. of the Aeron. Sci., 19, no. 12, Dec. (1952).
10. "Reduction of the Drag Due to Lift at Supersonic Speeds," P. A. Lagerstrom, E. W. Graham, B. J. Beane, et. al., WADC Technical Report 54-524.

REPORT NO. 1335

MINIMUM WAVE DRAG FOR ARBITRARY ARRANGEMENTS OF WINGS AND BODIES

Robert T. Jones

Ames Aeronautical Laboratory

1957

REPORT 1335

MINIMUM WAVE DRAG FOR ARBITRARY ARRANGEMENTS OF WINGS AND BODIES [1]

By ROBERT T. JONES

SUMMARY

Studies of various arrangements of wings and bodies designed to provide favorable wave interference at supersonic speeds lead to the problem of determining the minimum possible value of the wave resistance obtainable by any disposition of the elements of an aircraft within a definitely prescribed region. Under the assumptions that the total lift and the total volume of the aircraft are given, conditions that must be satisfied if the drag is to be a minimum are found. The report concludes with a discussion of recent developments of the theory which lead to an improved understanding of the drag associated with the production of lift.

INTRODUCTION

The losses associated with the production of a given lift in frictionless flow are generally diminished by increasing the mass of air entrained or influenced by the wing system. At the same time, however, the loss due to friction becomes greater when the exposed surface area of the wing is increased. To minimize the resultant drag we thus require a lifting system which effects the largest entrainment and yet has the smallest exposed surface area.

At subsonic speeds the mass of air entrained depends only on the lateral dimensions of the wing and is not diminished by concentrating the lift within a narrow chordwise dimension. The fact that a lifting line perpendicular to the direction of flight has such an extensive lateral influence must be considered a peculiarity of subsonic flow; it depends of course on the unlimited propagation of the pressure field ahead of the wing. At supersonic speed the lateral entrainment begins only at the foremost points of the wing surface and is confined to the interior of the rearward-sloping Mach waves from this point. Finally, at extreme speeds for which Newtonian flow may be envisioned, the mass of air affected is limited to the mass coming directly into contact with the wing, so that the area of influence is simply the frontally projected area of the wing.

Another peculiarity of the subsonic inviscid flow is the complete lack of resistance associated with the thickness of the bodies or wings. At supersonic speeds, however, such a component of drag does arise and this drag appears in the energy required for the continual extension of the wave system.

Now the problem of minimizing drag at supersonic speeds may be treated mathematically in several ways, depending on the constraints adopted in the statement of the problem. If, following Munk's problem of the minimum induced drag at subsonic speeds, we impose a constraint merely on the lift L and the span b of the wing, then we obtain the same value for the drag at all Mach numbers, namely the induced drag associated with the vortex wake. However, to achieve this value at supersonic speeds the wing would be required to have an infinitely great length in the flight direction so that the downward momentum associated with the lift could be introduced gradually along the flight path, without appreciable wave formation.

In order to put the problem of drag at supersonic speeds in a definite form the present writer proposed (ref. 1) that the outline or plan form S of the wing be adopted as a constraint rather than single lengthwise or spanwise dimensions. Thus for supersonic speeds we are led to consider the distribution of a given total lift L over a specified plan form S in such a way as to minimize the drag D.

In the latter problem it is presupposed that the lifting system is confined to a plane. However, the possibility of favorable interference with three-dimensional arrangements of airfoils and bodies should not be overlooked. Thus, Busemann has shown (ref. 2) that the wave drag can be completely canceled by reflection between the upper and lower wings of a biplane. Later Ferrari (ref. 3) showed that the drag of a body of revolution could be canceled by the addition of a ring airfoil to catch the wave from the nose and reflect it back to the tail.

The examples in which the wave cancellation is complete are, however, limited to systems in which the net lift and lateral force are zero. Nevertheless, examples cited by Ferri (ref. 4), Lomax and Heaslet (ref. 5), and Graham (ref. 6) indicate that the wave drag associated with the lift can be diminished by various three-dimensional arrangements of wings and bodies. These examples lead to a search for some general statements or criteria regarding the drag of such three-dimensional arrangements.

CONDITIONS FOR MINIMUM DRAG

To put the present question in a definite form it will be assumed the airfoils and bodies are disposed in the interior of a definite three-dimensional region R (see fig. 1). The region R thus represents a geometrical constraint on the dimensions of the aircraft. Three-dimensional problems of a similar type have been considered by E. W. Graham and his colleagues (ref. 6) who give, for example, the optimum distributions of lift in spherical and ellipsoidal regions. Here we assume the total lift L and the volume V to be given. In a typical situation the lift L will be produced

[1] Supersedes NACA TN 3530 by Robert T. Jones, 1956.

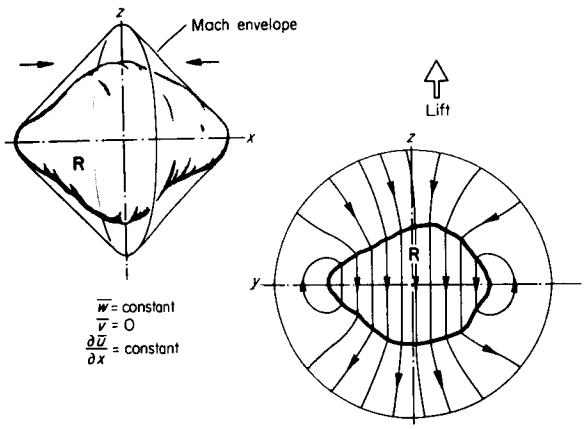

FIGURE 1.—Conditions for minimum drag distributions of lift and volume in region R.

by one or more airfoils while the volume V will represent the internal volume of one or more bodies of revolution plus the volume of the wing. The region R may then be thought of as the region within which the parts of the aircraft may be disposed so as to gain the maximum favorable interference. From a slightly different standpoint, R merely represents the maximum dimensions of the aircraft. We shall be especially interested in structures which minimize the drag for the largest possible region, but which in themselves occupy only a small part of this region.

Suppose a region R together with a distribution of singularities, such as sources or lifting vortices, is given (see fig. 1). Then by Kármán and Hayes' theorem (ref. 7) the drag will be unchanged by a reversal of the whole system. The geometry of the flow, including that of the airfoils and bodies, will be changed by the reversal but the total lift and the total volume will not. The drag for either direction of flow may then be computed by means of a fictitious "combined disturbance field" obtained by superimposing the disturbances in forward and reversed motion. The perturbation velocities in this combined field may be denoted by:

$$2\bar{u}=u_f+u_r$$
$$2\bar{v}=v_f+v_r$$
$$2\bar{w}=w_f+w_r$$

It may be shown that an arrangement of sources or lifting elements, or their combination, which yields the minimum drag is characterized by the following conditions

$$\left.\begin{aligned}\bar{w}&=\text{constant}\\ \bar{v}&=0\\ \frac{\partial \bar{u}}{\partial x}&=\text{constant}\end{aligned}\right\} \tag{1}$$

throughout R.

If conditions (1) are satisfied, then the integrated drag of the whole system will be given simply by

$$D_{min}=L\frac{\bar{w}}{U}+\rho UV\frac{\partial \bar{u}}{\partial x} \tag{2}$$

The first term on the right-hand side of this expression will be recognized as the drag arising from the rearward inclination of the lift vector, whereas the second term is simply the product of the volume and the constant gradient of pressure in the combined flow field.

These conditions may be verified by making use of a "mutual drag relation" (ref. 1), essentially similar to the well-known Ursell-Ward reciprocal relation, which connects the drag of any two interfering distributions of singularities in the combined flow field. According to this relation, the drag of distribution A caused by the interference of a second distribution B is equal to the drag added to B by the interference of A. Now let A be a distribution within R_A satisfying conditions (1). For B select a distribution having zero total lift and zero total volume. If R_B is contained within R_A, then the addition of B will amount simply to a redistribution, without changing the given lift L or volume V of A. The drag of $A+B$ may then be written in shorthand notation

$$D(A+B)=D_{AA}+D_{AB}+D_{BA}+D_{BB} \tag{3}$$

Then, since by the mutual drag relation $D_{AB}=D_{BA}$, this equation may be written as

$$D(A+B)=D_{AA}+2D_{BA}+D_{BB} \tag{4}$$

Here D_{BA} is the drag of B in the combined disturbance field of A. Since $\bar{w}_A=$constant, $\bar{v}_A=0$ and $\left(\frac{\partial \bar{u}}{\partial x}\right)_A=$constant in R_A, this interference drag may be written simply as

$$D_{BA}=L_B\frac{\bar{w}_A}{U}+\rho UV_B\left(\frac{\partial \bar{u}}{\partial x}\right)_A \tag{5}$$

However, since L_B and V_B are both zero D_{BA} vanishes and the added drag is that of distribution B alone, or D_{BB}. Now the drag of an isolated system can never be negative, hence $D(A+B)$ cannot be less than $D(A)$ under the conditions (1).

On the other hand, suppose, for example that the sidewash $\bar{v}_A$ were not zero. A distribution of lateral forces could then be found which would result in a negative interference drag, dominating the quadratic term D_{BB}, so that the total drag could be reduced. Hence, if the drag of distribution A actually is a minimum value, then conditions (1) must be complied with.

The question of uniqueness depends on the existence of distributions of type B for which the drag is zero. As shown by Graham, such distributions exist in three dimensions and hence the minimum drag corresponding to a given region R may be achieved by a variety of arrangements. In the case of a planar region, such as the plan form S of a wing, distributions of lift or volume having zero drag do not exist, and hence in these cases the optimum distributions are unique.

Since $\bar{w}=\frac{\partial \bar{\varphi}}{\partial z}$, $\bar{v}=\frac{\partial \bar{\varphi}}{\partial y}$ and $\frac{\partial \bar{u}}{\partial x}=\frac{\partial^2 \bar{\varphi}}{\partial x^2}$, it can be seen that conditions (1) do not agree with the linearized flow equation

$$(1-M^2)\bar{\varphi}_{xx}+\bar{\varphi}_{yy}+\bar{\varphi}_{zz}=0 \tag{6}$$

in general, but only if

$$\frac{\partial \bar{u}}{\partial x}=0 \tag{7}$$

Since $\frac{\partial \bar{u}}{\partial x}$ is proportional to the drag per unit volume, one concludes that the drag cannot be minimized in an absolute sense unless the drag associated with the volume of the system is zero, or unless the distribution of singularities is continuous throughout R. Examples such as the Busemann biplane satisfy the condition $\frac{\partial \bar{u}}{\partial x}=0$.

It is interesting to note that conditions analagous to $\bar{w}=$ constant and $\bar{v}=0$ were found by Munk in connection with the vortex drag of lifting systems at subsonic speeds. In that problem, the conditions apply to the two-dimensional motion associated with the trace of the wing system in the Trefftz plane. If the idea of superimposed disturbance fields is utilized in the subsonic problem, one finds that the cylindrical flow associated with the Trefftz plane extends along the whole flight path, including the region R. Conditions (1) thus apply at both subsonic and supersonic speeds.

Munk's condition of constant downwash and zero sidewash were used by Hemke (ref. 8) to calculate the effectiveness of end plates in reducing the vortex drag at low speeds. In such problems the condition is usually imposed by the statement that the trace of the airfoil system must move downward as a rigid body. It will be interesting to see how this condition might be used under more general circumstances. This application is illustrated in figure 2 for an end plate on the tip of a wing.

With the wing in forward motion, the lateral velocity v_f at the surface of the end plate is simply the lateral slope of the fin surface multiplied by the stream velocity. The condition $\bar{v}=0$ implies that $v_r=-v_f$ and this condition is obviously satisfied by keeping the geometry of the fin fixed when the flow is reversed. At the same time, however, recall that the distribution of lift and lateral force must be kept the same in forward and reversed flow. Hence, the problem of finding the optimum setting and camber for such a fin is solved by finding that particular shape for which the flow is exactly reversible, that is, the lateral pressure distribution remains unchanged by a reversal of flow direction. At first it seems impossible to satisfy such a requirement, since, for example, the direction of the force on an inclined surface is usually reversed by a reversal of the direction of flow. However, the form of the adjacent wing surface must, in general, change with the reversal, since $\bar{w}\neq 0$ and since the lift distribution on the wing must remain unchanged. Then it is evident that the conditions might be satisfied if the pressures on the fin surface were dominated by the wing pressures through interference.

Recently W. Wilmarth (ref. 9) has found several examples of wings with end plates which minimize the drag for certain prismatic regions.

The conditions for minimum drag are of course simply the result of the constraints adopted in the initial statement of the problem, and these are to a certain extent arbitrary. Nevertheless, experience shows that the study of such problems is likely to disclose essential relations in their clearest form.

With the aid of the combined flow field and the mutual drag theorem, it is a relatively simple matter to extend the

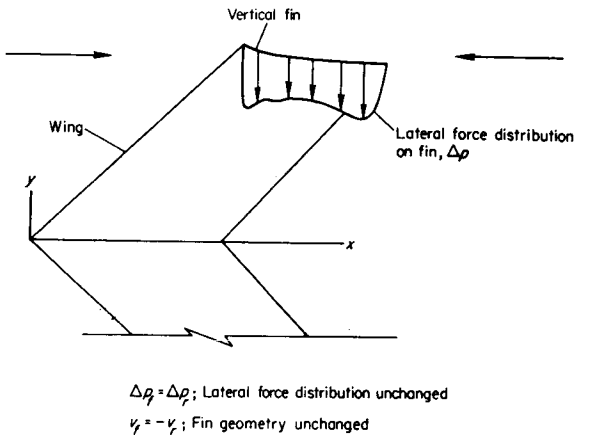

FIGURE 2.—Use of condition $\bar{v}=0$ to determine optimum setting of vertical fin on wing tip.

constraints in various ways. Thus in the case of a planar wing if both the total lift L and the spanwise loading are specified, minimum drag requires that $\bar{w}$ be constant along chordwise strips, but may vary laterally. Here we have

$$\bar{w}=f(y) \tag{8}$$

In case the lengthwise loading is specified we have

$$\bar{w}=f(x) \tag{9}$$

Again, if the first moment of the load distribution about the y axis is specified

$$\bar{w}=a_0+a_1x \tag{10}$$

and so on.

If the conditions on the combined disturbance velocities hold beyond the boundaries of the region R, then the drag cannot be changed by extending the distribution of lift or volume into the new region. In general, this will not be the case, however, and the drag can be continually diminished by increasing the dimensions of R. Thus in the case of a monoplane wing a strong upwash appears beyond the wing tips, indicating that the drag could be diminished by increasing the span. Similarly, sidewash velocities appear just above and below the planar region, and the drag could be reduced by extending vertical fins, or "fences" into this region.

It must be admitted that the considerations have thus far been rather abstract. A more concrete result would yield the actual magnitudes of the drag associated with various regions, as well as the shapes of the bodies or wings. Although no direct method of calculation has been proposed, numerous examples have been found. Thus reference 6 gives the optimum distributions of lift in spherical and ellipsoidal regions.

A rough lower bound for the minimum wave drag associated with any region may be obtained from Hayes' formula (ref. 7) or the formula of Lomax (ref. 5). With these formulas a spatial distribution of lift or volume may be resolved into a number of equivalent linear distributions, the latter obtained from the intersections of the region R by plane

waves lying at various angles θ around the x axis. The wave drag of the system is then the sum of values for the linear distributions integrated from $\theta=0$ to $\theta=2\pi$. The expression for the wave drag of a single linear distribution is the same (except for a constant factor) as the expression for the vortex drag of a lifting line in subsonic flow. Thus, for a single elliptically loaded lifting line of length l parallel to the flight direction the wave drag is:

$$D_{wave}=\frac{M^2-1}{2}\frac{L^2}{\pi q l^2} \tag{11}$$

This value may be used as an approximation for the wave drag of any narrow wing lying near the center of the Mach cone. Deviations are to be expected for wider wings; however, these deviations are not very pronounced, as figure 3 shows. In this figure values of the wave drag obtained from exact theoretical formulas are compared with the values given by the approximate expression (11). The "exact" values were obtained by superimposing uniformly loaded wings of elliptical plan form and are not the minimum values for the resulting plan forms.

A sufficient condition for the wave drag of a lifting system to have a minimum value is that all the projected loadings, in addition to the lengthwise loading, be elliptical. In this case we obtain the formula

$$D_{wave}\geqq\frac{M^2-1}{2}\frac{L^2}{\pi q \bar{l}^2} \tag{12}$$

where

$$\frac{1}{\bar{l}^2}=\frac{1}{\pi}\int_0^{2\pi}\frac{\sin^2\theta\, d\theta}{[l(\theta)]^2} \tag{13}$$

and $l(\theta)$ is the projected length of the region R as defined in figure 4 with $\beta=\sqrt{M^2-1}$.

The value given by equations (12) and (13) is actually attained by elliptic wings and by distributions of lift in spherical or ellipsoidal regions (ref. 6). However, for

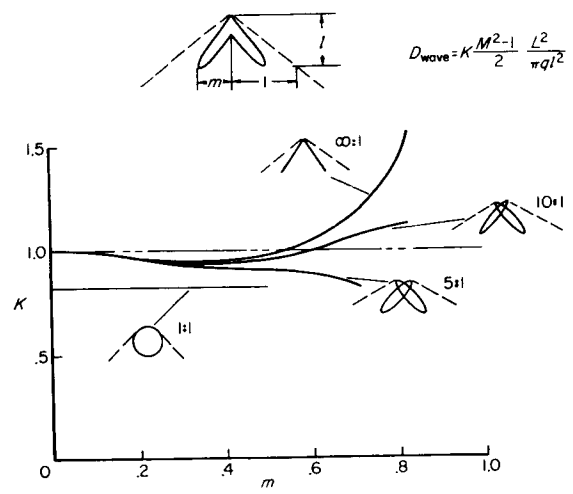

FIGURE 3.—Approximate expression for wave drag of lifting surface.

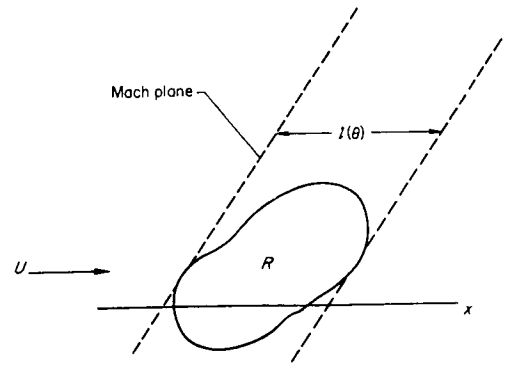

FIGURE 4.—Lower bound for wave drag associated with the region R and the lift L.

triangular or swept wings of the type depicted in figure 3, the values given by the simpler expression equation (11) are more accurate.

In a recent paper (ref. 10) M. I. Kogan has pointed out that determination of the minimum drag of a lifting surface having no subsonic edges can be reduced to the solution of Laplace's equation in the two-dimensional region bounded externally by the trace of the characteristic envelope, and bounded internally by the vortex trace of the wing. In addition to $\varphi_{yy}+\varphi_{zz}=0$, the boundary condition that no disturbance extend beyond the Mach cone corresponds to the condition $\varphi=0$ on the outline of the characteristic trace S_j (i. e., the outer rim of the Mach envelope in fig. 1) while the condition of constant downwash corresponds to $\varphi_z=$constant on the vortex trace.

The result given by Kogan has been derived independently by E. W. Graham (ref. 11) and by G. N. Ward (ref. 12). Graham makes use of the combined flow field, and shows that fields which are two-dimensional throughout the interior of any given characteristic envelope, and which satisfy the condition $\bar{\varphi}_z=\bar{w}=$constant on a vortex trace passing through the region, can be constructed.

Such solutions correspond to our previous conditions (6) and (7) and are not restricted to wings having supersonic edges.

In Ward's analysis the physical flow is used, but the drag is calculated by using the forward-going surface of the characteristic envelope as a control surface. Since $\varphi=0$ there in the reversed flow, it can be seen that the values of φ in the real flow coincide with those in the combined flow on this surface. By a projection of the disturbance velocities on this surface, Ward reduces the integral for drag to Dirichlet's integral, which is a minimum when the derived velocity field satisfies Laplace's equation.

Applications of this method to problems involving thickness and volume have been given by M. A. Heaslet (ref. 13). Problems in which both the lift and the center of pressure are given have been treated by P. Germain (ref. 14).

These theoretical developments provide an interesting intuitive picture of the drag associated with the production of lift at supersonic speeds. At subsonic speeds the lifting wing leaves in its wake a two-dimensional, essentially incompressible downwash flow bounded internally by the

vortex wake, but unbounded externally. According to Kelvin's theorem such an incompressible downwash flow satisfying $\varphi_{yy}+\varphi_{zz}=0$, minimizes the kinetic energy relative to all other streamline motions satisfying the same boundary conditions. For a given lift, (or downward momentum) the kinetic energy, and hence the drag, is minimized when the wake moves with constant downwash. At supersonic speeds we are led to consider not the flow in the Trefftz plane at infinity, but the flow in the last characteristic surface where the zone of influence lies entirely behind the wing. The two-dimensional flow obtained by projection on this surface will be limited laterally by its intersection with the real Mach wave, where φ must vanish, and will be bounded internally by the vortex wake on the the trailing edge of the wing. This flow is certainly not incompressible in general. However, if the wing is to have the minimum drag consistent with the given span and with the given limitations of the lateral zone of influence, then by Kelvin's theorem the flow must imitate the streamlines of an incompressible lateral flow in this intervening limited region. For a given total lift the vortex wake should again move with constant downwash.

The condition $\varphi=0$ on the rim of the characteristic envelope is exactly the same as that imposed at the boundary of an open-jet wind tunnel. Hence, we are led to compare the action of the wing in supersonic flow with that of a wing in a finite jet (fig. 5). Wings having small fore and aft dimensions have a limited lateral entrainment, as shown by the small cross sections of their equivalent incompressible jets (see fig. 6).

In Munk's theory of the minimum induced drag the "area of the additional apparent mass" associated with the vortex trace of the wing plays an important role. Denoting this area by S_w', we have for the drag due to lift

$$D=\frac{1}{2\rho U^2}\frac{L^2}{S_w'} \tag{14}$$

This formula actually applies in perfect fluid flow at all speeds if S_w' is replaced by S_{w_i}', the additional apparent

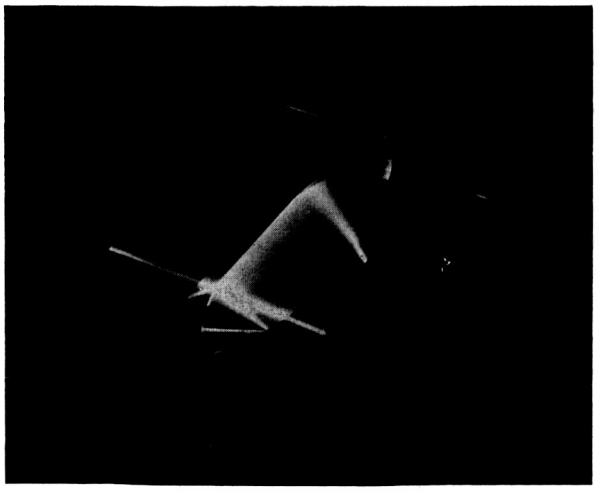

FIGURE 5.—Equivalent incompressible jet for wing at supersonic speed.

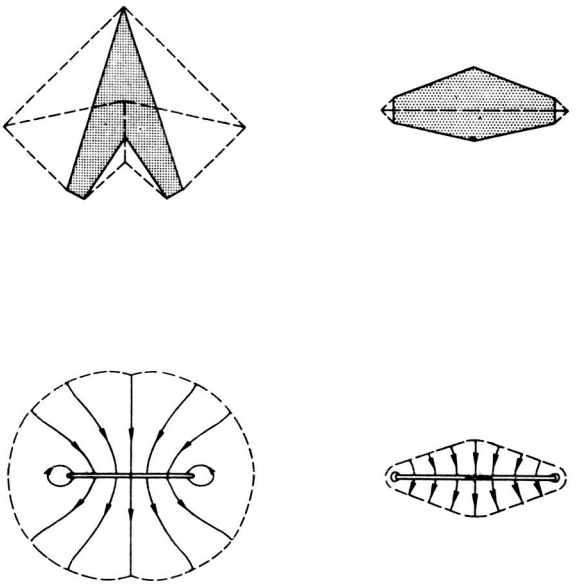

FIGURE 6.—Effect of fore and aft dimension of wing on area of lateral entrainment.

mass of the wing in the limited jet determined by the Mach waves. If the Mach number of the stream is reduced, the waves become more nearly vertical and the equivalent jet expands laterally, reaching an infinite cross section at $M=1.0$. Below $M=1.0$ the wing is operating in unlimited flow and we then have:

$$S_w'=\pi\frac{b^2}{4} \tag{15}$$

which leads to

$$D=\frac{2L^2}{\pi\rho U^2 b^2} \tag{16}$$

On the other hand, at extremely high supersonic speeds, the equivalent jet contracts into a narrow space around the frontal projection of the wing. In this case the streamlines of the downflow in the jet will be nearly straight and parallel, as illustrated in figure 6, and the area S_{w_i}' will be substantially equal to the area of the jet S_j.

In special cases the two-dimensional downflow in the characteristic trace or jet S_j can be readily calculated. Thus in the case of the elliptic wing the envelope of characteristics has an elliptic cross section, with the vortex trace of the wing extending between the foci. Now if a flat plate moves downward (along z) in unlimited flow, the potential at the surface of any confocal elliptic cylinder will be of the form $\varphi_e=kz_e$. Hence the boundary condition $\phi=0$ may be satisfied on any such confocal ellipse by adding a uniform downwash throughout its interior so that $w=-k$ or $\varphi=-kz$. When the downward momentum of the resultant flow is computed, it is found to correspond to a virtual mass with area S_{w_i}' given by

$$\frac{1}{S_{w_i}'}=\frac{1}{S_j}-\frac{1}{S_j+S_j'}+\frac{1}{S_w'} \tag{17}$$

where

$$S_w'=\frac{\pi b^2}{4} \tag{18}$$

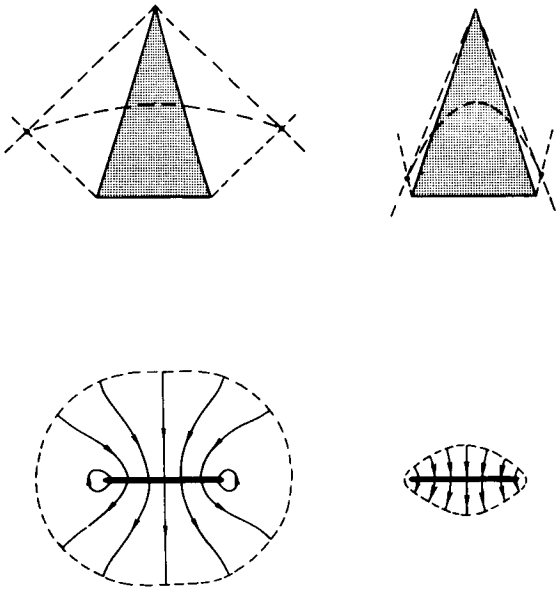

FIGURE 7.—Effect of Mach number on lateral entrainment.

In the case of a long slender wing lying near the center of the Mach cone (slender wing theory) the characteristic trace will be circular. An elliptical lengthwise distribution of lift then produces an incompressible downwash flow resembling that of a dipole at the center of the circle. The added downwash required to make $\varphi=0$ on this circular boundary then yields our formula (11) for the wave drag.

If we try to find the surface loading or shape that corresponds to the drag given by equation (14), we discover that Kogan's analysis has in fact carried us away from our original problem in which the plan form of the wing (or the region R occupied by the lifting system) was given. The information given now concerns only the trace of the wing and its characteristic envelope. Now, the relation between the plan form of a wing and its characteristic trace is certainly not unique. On the other hand the particular form of the two-dimensional flow on the reversed characteristic surface must require a unique distribution of lift in the plane of the wing. Otherwise one could show by superposition that planar distributions of lift having no drag would exist. It must be concluded therefore that of all the plan forms having a given characteristic envelope, only those whose surface area is extensive enough to enclose the required surface distribution of lift can achieve the minimum drag given by equation (14).

AMES AERONAUTICAL LABORATORY
NATIONAL ADVISORY COMMITTEE FOR AERONAUTICS
MOFFETT FIELD, CALIF., *Aug. 14, 1957*

REFERENCES

1. Jones, Robert T.: The Minimum Drag of Thin Wings in Frictionless Flow. Jour. Aero. Sci., vol. 18, no. 2, Feb. 1951, pp. 75–81.
2. Busemann, A.: Aerodynamischer Auftrieb bei Überschallgeschwindigkeit (Supplement). Fifth Volta Congress, Reale Academia D'Italia, 1935.
3. Ferrari, C.: Campi di corrente impersonora attorno a solidi di rivoluzione. L'Aerotecnica, vol. XVII, fasc. 6, June 1937, pp. 507–518. (Also available as Brown Univ. Graduate Div. of Applied Math. Trans. 3965a.)
4. Ferri, Antonio: Recent Work in Supersonic and Hypersonic Aerodynamics at the Polytechnic Institute of Brooklyn. Paper given at the conference on High Speed Aeronautics held by the Polytechnic Institute of Brooklyn, Jan. 22, 1955.
5. Lomax, Harvard, and Heaslet, Max. A.: Recent Developments in the Theory of Wing-Body Wave Drag. I. A. S. Preprint 617, Jan. 23, 1956.
6. Graham, E. W., Lagerstrom, P. A., Licher, R. M., and Beane, B. J.: Theoretical Investigation of the Drag of Generalized Aircraft Configurations in Supersonic Flow. Rep. No. SM–19181, Douglas Aircraft Co., Inc., July 1955.
7. Hayes, Wallace D.: Linearized Supersonic Flow. Rep. AL–222, North American Aviation, Inc., June 18, 1947.
8. Hemke, Paul E.: Drag of Wings With End Plates. NACA Rep. 267, 1927.
9. Wilmarth, William: The Optimum Distribution of Lift in Certain Prismatic Regions at Supersonic Speed. Readers' Forum, Jour. Aero. Sci., vol. 23, no. 8, Aug. 1956, pp. 800–801.
10. Kogan, M. I.: On Bodies of Minimum Drag in a Supersonic Gas Stream. Prikladnaia Matematika i Mechanika, Vol. XXI, 1957, pp. 207–212.
11. Graham, E. W.: The Calculation of Minimum Supersonic Drag by Solution of an Equivalent Two-Dimensional Potential Problem. Rep. SM–22666, Douglas Aircraft Co., Dec. 1956.
12. Ward, G. N.: On the Minimum Drag of Thin Lifting Bodies in Steady Supersonic Flows. Rep. 18,711, F. M. 2459, British A. R. C., 1956.
13. Heaslet, Max. A.: The Minimization of Wave Drag for Wings and Bodies With Given Base Area or Volume. NACA TN 3289, 1957.
14. Germain, Paul: Sur le Minimum de Traînée d'une Aile de Form en Plan Donnée. Compte Rendus. Tome 244, no. 9, 25 Fevrier 1957, pp. 1135–1138.

SOME RECENT DEVELOPMENTS IN THE AERODYNAMICS OF WINGS FOR HIGH SPEEDS

Robert T. Jones

Ames Aeronautical Laboratory

August 1956

Jones, R. T., "Some Recent Developments in the Aerodynamics of Wings for High Speeds," Zeitschrift für Flugwissenschaften, vol. 4, no. 8, Aug. 1956, pp. 257-262. © 1956.
Reprinted by permission of the Deutsche Gesellschaft für Luft- und Raumfahrt and the Deutsche Forschungs- und Versuchsanstalt für Luft- und Raumfahrt, Braunschweig, Germany.

ZEITSCHRIFT FÜR FLUGWISSENSCHAFTEN
ORGAN DER WISSENSCHAFTLICHEN GESELLSCHAFT
FÜR LUFTFAHRT E.V.

4. Jahrgang, Heft 8 | Braunschweig | August 1956

Robert T. Jones, Moffett Field, Calif. (USA.))*

DK 533.691.11.011.5

Some Recent Developments in the Aerodynamics of Wings for High Speeds**)

Übersicht: Die in der vorliegenden Arbeit behandelten Gegenstände betreffen 1. eine kürzlich vorgeschlagene Korrekturformel für den Einfluß der Kompressibilität bei der zweidimensionalen Unterschallströmung, 2. Äquivalenzsatz und Flächenregel für transsonische Strömungen, 3. Reziprozitätsbeziehungen in der linearisierten Tragflügeltheorie und 4. einige allgemeine Ergebnisse, die mit dem Problem des minimalen Wellenwiderstandes zusammenhängen. Die Arbeit schließt mit einem Beispiel über die Einschnürung des Rumpfes zur Erzielung einer günstigen Interferenz mit dem Flügel bei Überschallgeschwindigkeit.

Summary: The items discussed in this summary paper are 1. a recently proposed correction formula for the effect of compressibility in two-dimensional subsonic flow, 2. the equivalence rule and the area rule for transonic speeds, 3. reciprocal relations in linearized wing theory, and 4. some general results connected with the problem of minimum wave resistance. The paper concludes with an example showing indentation of the fuselage to obtain favorable interference with the wing at supersonic speeds.

Résumé: Les problèmes traités dans le travail présent concernent: 1) une formule de correction, récemment proposée, destinée à déterminer l'influence de la compressibilité dans le cas de l'écoulement subsonique bidimensionnel; 2) le théorème de l'équivalence et la règle de la surface des écoulements transsoniques; 3) des relations de réciprocité de la théorie linéarisée des ailes portantes; 4) quelques résultats généraux liés au problème du minimum de la résistance d'ondes. Le travail conclut en relevant un exemple de retrécissement du fuselage destiné à provoquer une interférence plus favorable avec l'aile aux vitesses supersoniques.

The student of fluid mechanics cannot fail to be impressed by the complexity of the phenomena that arise under simple circumstances. Even if we admit only the simplest properties of the fluid together with elementary dynamical laws for the motion, unexpectedly intricate motions may appear. As examples, I may mention the periodic *Taylor-Görtler* vortices that appear when a slightly viscous liquid flows over a concave surface or, again, the characteristic geometrical shapes of the "patches" of turbulence that have recently been observed by *Emmons* and *Schubauer* (NACA TN 3489, Sept. 1955) in regions of transition from laminar to turbulent boundary-layer flow.

In what is commonly understood by the term "airfoil theory" we limit the range and complexity of our investigations considerably by studying particularly simple flows that are apt to be of efficient service in the flight of an airplane. Thus in the *Prandtl* wing theory we study the properties of long, narrow wings, which afford the highest aerodynamic efficiency at ordinary speeds and which at the same time admit a mathematical simplification because of their extreme proportions. Furthermore, in *Prandtl*'s theory we consider only section flows of the *Kutta-Joukowsky* type.

With a different type of section flow, such as might be produced by sharpening the leading edge, the long, narrow wing loses its advantage and the dependence of drag on aspect ratio follows more unfavorable laws. (See, e. g., ref. [1].)

The extraordinary efficiency of a well designed airfoil in two-dimensional flow is illustrated in Fig. 1. Such an airfoil, of conventional form, may show a lift-to-drag ratio of 100 to 1 or at smaller lift coefficients, a drag coefficient of 0,005. The latter coefficient corresponds roughly to the drag of a circular cylinder having a diameter $^1/_{200}$ th of the wing chord.

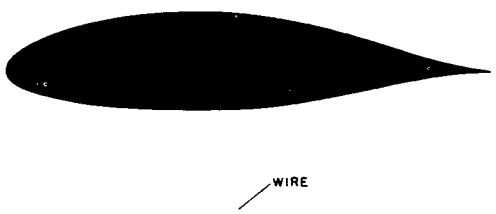

Fig. 1. Airfoil compared with circular wire having equal drag

As is well known, airfoil flows basically similar to the *Kutta-Joukowsky* flow can be maintained up to very high speeds in the subsonic range. Within this range the drag of the wing consists essentially of the induced drag and the surface friction, so that the plan form of the wing is determined, roughly speaking, by the criterion of maximum span together with that of minimum surface

*) National Advisory Committee for Aeronautics, Ames Aeronautical Laboratory.
**) Paper for presentation at the meeting of GAMM, VDI, and WGL at Göttingen, Germany, October 6, 7, 8, 1955.

area. For this range of speeds the straight wing having the highest practicable aspect ratio thus remains the most efficient aerodynamic form.

The efficient operation of airfoils at the upper end of this speed range seems to require primarily that the sections be thin — so that a method of calculation based on expansion in powers of the thickness-chord ratio would appear to be especially appropriate. Such methods are well known through the work of *Görtler* [2], *Hantzsche* and *Wendt* [3], *Kaplan* [4], *Imai* [5], and others. Recently *Van Dyke* [6], utilizing a result of *Hayes* [7], has shown that the pressure distribution around a thin airfoil in two-dimensional motion can be related in a simple way to the corresponding distribution in incompressible flow by this method. If the leading terms in the expansion of the surface pressure coefficient C_p in powers of the thickness-chord ratio t are

$$C_{p\,\mathrm{inc}} = t\,f(x) + t^2\,g(x) \tag{1}$$

for incompressible flow, then *Van Dyke* gives for compressible flow (see Fig. 2)

$$C_{p\,\mathrm{comp}} = K_1\,t\,f(x) + K_2\,t^2\,g(x) \tag{2}$$

with

$$K_1 = \frac{1}{\sqrt{1-M^2}} = \frac{1}{\beta}, \tag{3}$$

$$K_2 = \frac{(\gamma+1)\,M^4 + 4\beta^2}{4\,\beta^4}. \tag{4}$$

This simple rule is found to yield results previously obtained by rather difficult calculations.

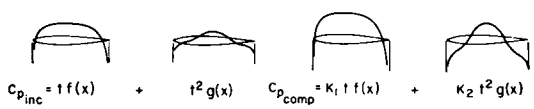

Fig. 2. Pressure correction formula for subsonic flow in two dimensions, Eq. (1) — (4)

As the speed of sound is approached, the three-dimensional wing flow can no longer be approximated by the assumption of locally two-dimensional flows over the wing sections. As shown by the linear *Prandtl-Glauert* theory, the disturbance field of a wing section expands vertically without limit, so that the dimensions of the region of disturbance eventually become large compared to the chord of the wing sections. The section flow is then no longer a local phenomenon but must be modified by the spanwise dimensions of the wing.

In linear theory we treat the disturbance field of a moving wing by the approximations employed in acoustics. Thus the velocity potential of the flow disturbance around the wing at either subsonic or supersonic velocities satisfies the well-known sound wave equation

$$\varphi_{xx} + \varphi_{yy} + \varphi_{zz} - \frac{1}{a^2}\,\varphi_{tt} = 0. \tag{5}$$

To represent disturbances of fixed form travelling in the direction of x with a velocity equal to the speed of sound, a, we may write the solution in the form

$$\varphi = f(y + iz, x - at). \tag{6}$$

Such disturbances thus satisfy, in addition, the relation

$$\varphi_{yy} + \varphi_{zz} = 0 \tag{7}$$

or *Laplace*'s equation for an incompressible flow in planes perpendicular to the direction of propagation of the disturbance. Now, such a disturbance of fixed form may easily be reduced to a steady flow, so that the stream tubes in the oncoming flow must agree with the simple one-dimensional flow equation for stream tubes or channels of slowly varying width. As is well known, the stream tube cross sections reach an absolute minimum at the speed of sound. It is clear then that the "lateral incompressibility" of the flow at sonic speed may be related to this stationary property of the stream tube areas.

The stationary character of the stream tube areas at sonic velocity does not depend on the linearization, but is a characteristic of nonlinear steady flows as well. For such flows the one-dimensional flow equation forms a necessary condition to be satisfied along every stream tube. Here too, we must expect that the lateral flow will agree closely with *Laplace*'s equation for two-dimensional motion in those regions of nearly sonic velocity. These conditions are, of course, not ordinarily sufficient to determine the flow field as a whole but they are of considerable assistance in the intuitive understanding of transonic flow phenomena.

While these elementary considerations do not furnish an exact or detailed picture of the transonic flow, it is possible to determine certain integrated properties such as the lift and moment of slender wings from them. The theory of slender wings is based on just the assumptions implied in equation (7). The applicability of this theory at transonic speeds has been investigated by *Robinson* and *Young* [8] and by *Heaslet, Lomax*, and *Spreiter* [9], following the lines of a theory given by the present writer [10].

It is interesting to note how far the experimental lift and lift distribution follow this simple linear theory in the transonic range. Fig. 3, taken from some experiments made at the NACA's Ames Aeronautical Laboratory by *Nelson* and *McDevitt* [11, 12] shows the variation with aspect-ratio parameter of the lift-curve slope and the pressure drag for a family of rectangular wings at a *Mach* number very close to 1. In spite of the fact that these wings can hardly be considered slender, the linear theory holds well up to an aspect ratio of nearly 3. Another interesting result is the tendency noted in these experiments for the center of pressure to approach the wing leading edge as the aspect ratio is reduced, in accord with the prediction of slender-wing theory.

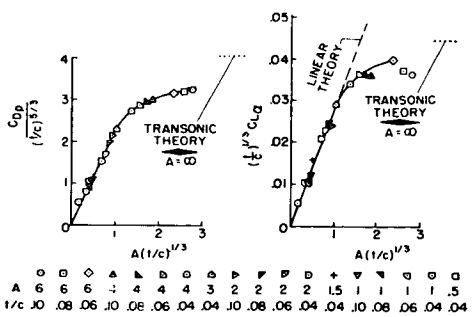

Fig. 3. Drag and lift at $M_0 \approx 1$. Rectangular wings, NACA 65 A 0 XX profiles

At higher aspect ratios the values of lift and drag given by *Guderley* and *Yoshihara* [13] are approached.

When we try to determine the disturbance field produced by a body or wing moving at sonic velocity we face the difficulty that the form of the disturbance is not very definitely connected with the geometry of the body. At this speed extensive longitudinal disturbances can travel almost indefinitely without the assistance of a moving solid. Hence it is perhaps not surprising that a relatively intense longitudinal wave is built up by a solid which travels for some time at this speed. Those who have been in the path of the well-known "sonic boom" have had a direct experience of this longitudinal wave.

According to the "equivalence principle" of *Oswatitsch* [14], the potential, φ, of this large-scale longitudinal disturbance is determined by the longitudinal distribution of areas presented in planes perpendicular to the flight direction. Hence, the potential at large distances reduces to that for an equivalent body of revolution. In *Whitcomb*'s paper [15] on the "area rule" both the form of the wave disturbance and the incremental drag at transonic speeds were shown to depend on this distribution of cross-sectional area. The dependence of wave drag on the area distribution was given by *Hayes* [16] as a formal result of the linear theory at transonic speed. In *Whitcomb*'s experiments it was demonstrated further that the drag associated with the thickness of a wing can be effectively suppressed by removing an appropriate "area distribution" from the fuselage. With these new developments it appears that wing theory at transonic speeds should not be limited to the properties of isolated airfoils.

As a simple test of *Whitcomb*'s drag-equivalence idea, *Spreiter* [17] has analysed the results of experiments made at Ames Laboratory on rectangular airfoils having various aspect ratios and various thickness-chord ratios. To maintain the same area distribution an airfoil having a high aspect ratio and a thin section is compared with one of lower aspect ratio but with a thicker section. For nonlifting wings with symmetrical sections the rule is verified up to aspect ratios of 3 or more. Fig. 4 shows the comparison for aspect ratio 4.

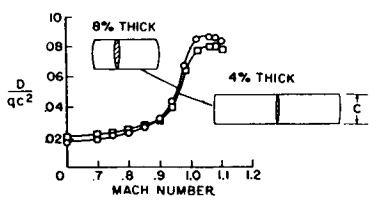

Fig. 4. Drag of wings having same area distribution

Rectangular wings of the forms shown have, of course, a large incremental drag at transonic speeds. Perhaps the most effective practical method of reducing the drag at transonic speeds is the use of extreme angles of sweep, thin sections, and slender bodies. As an illustration of the magnitudes involved I would like to show drawings of two models that have been tested by the NACA (Fig. 5). The two models with the relative dimensions shown would, according to the indication of our experiments, have the same drag at a slightly supersonic *Mach* number.

At the present time the calculation of three-dimensional wing flows at supersonic speed is carried out almost

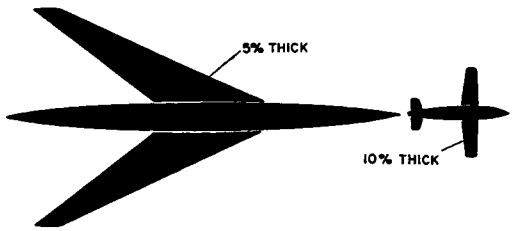

Fig. 5. Models having same drag at low supersonic speed (zero lift)

exclusively by means of the linearized theory. The principles employed in these calculations were brought into sharp focus in the papers of *Prandtl* [18], *von Kármán* [19] and *Busemann* [20] at the 1935 Volta Congress, while the first known application to the three-dimensional lifting wing appeared in *Schlichting*'s paper of 1936 [21].

Linearization of the flow equations brings the three-dimensional wing theory within the realm of classical methods of analysis and so has disclosed a variety of interesting and unexpectedly simple relations. For example, if we consider a thin wing or body whose disturbance field can be produced by the action of simple sources, then the drag of this body will be unchanged by a reversal of the flow direction. Our attention was called to this "reversed flow" relation by *von Kármán* and it was generalized by *Hayes* [16] to include arbitrary distributions of singularities such as lifting elements and sources in three-dimensions. Reversal of the flow may change the geometrical shapes however. In an interesting paper, *Munk* [22] has shown how such reversed flow relations can be derived by considering the abstract disturbance field obtained by superimposing the disturbance velocities generated by the forward motion, and those generated by the reversed motion of the system. Utilizing this idea, *Brown* [23] has been able to show that the lift-curve slope of a wing of any planform is unchanged by a reversal.

A more general form of reversed-flow relation in steady wing flow theory is the reciprocal relation discovered by *Ursell* and *Ward* [24]. Starting with a thin lifting surface of planform S, we may consider the effect of warping or twisting the wing in various ways, represented by permitting the local angle of attack α to vary with the position x, y of a point on the planform. Such a warp or twist $\alpha(x, y)$ will give rise to a distribution of lifting pressure $p(x, y)$ which is a linear functional of α determined by the flow equation and by the outline shape of the wing. Let α_1 and p_1 be two functions so related and let α_2 and p_2 be a different, but similary related, pair of distributions for the wing S in reversed flow; then the *Ursell-Ward* relation is

$$\int_S \alpha_2 p_1 \, d\sigma = \int_S \alpha_1 p_2 \, d\sigma. \tag{8}$$

Fig. 6 illustrates one of the many interesting applications of this theorem. Here α_1 is taken as a constant value, equal to unity, over the whole surface, so that p_1 is the distribution of lift arising when the wing as a whole is given a

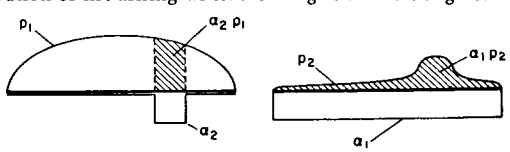

Fig. 6. Reciprocal relation, Eq. (8)

unit angle of attack. α_2 has the value unity over a portion of the wing, or a flap, but has the value zero elsewhere. p_2 then represents the distribution of lift over the whole wing, resulting from the deflection of a flap. The reciprocal relation then tells us that the lift on the wing due to deflecting the flap is equal to the lift on the flap due to deflecting the wing with the flow reversed. This relation is applicable at both subsonic and supersonic speeds. The extension to airfoils in unsteady motion has been given by *Flax* [25] and by *Heaslet* and *Spreiter* [26] who point out its connection with classical reciprocal theorems of *Helmholtz*, *Maxwell*, and *Rayleigh*.

It is interesting to note that extension of the reciprocal theorem to nonstationary motion provided a means for verifying the coincidence between *Kuessner* and *Sears*' "gust lift functions" and *Wagner*'s function describing the growth of circulation around an airfoil starting from rest for wings in three-dimensional flow.

A classical problem in the theory of airfoils is the determination of the form of the wing or the distribution of lift for minimum drag. Thus we may think of *Munk*'s problem of the minimum "induced" drag for a given total lift L and a given span b [27]. At supersonic speeds we have to consider in addition to the induced drag a wave drag which depends in a rather complex way on the distribution of lift over the whole surface. Surprisingly enough, however, we find a continual recurrence of ideas derived from this earlier problem in our studies of wave drag of lifting surfaces at supersonic speeds.

In *Munk*'s problem it was found that minimum drag occurs when the "induced downwash" is constant at all points of the span. To extend these considerations to supersonic speeds we find it essential to specifiy not merely the span, but the plan form of the wing [28]. By making use of the reversibility theorem we are able to express the drag in terms of a fictitious disturbance field, obtained by combining linearly the disturbances produced by a given distribution of lift in forward and in reversed motion. The mean downwash $\bar{w}$, obtained by averaging at each point the values in forward and reverse flow, then takes the place of the "induced downwash" and is quantitatively equal to the latter if the speed is subsonic. The drag is obtained by integrating over the plan form S the product of the local lifting pressure Δp and the mean angle of attack $\bar{\alpha} = \bar{w}/V$. With a given total lift L and a given plan form S the minimum drag occurs when the mean downwash $\bar{w}$ has the same value at all points of S. This result holds whether the speed is subsonic or supersonic.

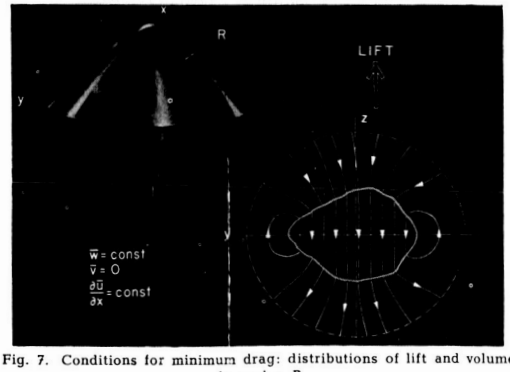

Fig. 7. Conditions for minimum drag: distributions of lift and volume in region R

It is interesting to note that the idea of superimposing the forward and reversed disturbance fields was utilized in *Munk*'s original proof of the so-called stagger theorem.

If we accept the idea of a combined supersonic disturbance field, then the necessary conditions for minimum resistance can be generalized to include interfering distributions of lift and volume in three-dimensional regions. Here we may think of an arrangement of airfoils or lifting elements in space, but limited to the interior of a region R. If the total lift L and the region R are given then the minimum drag occurs when (see Fig. 7)

$$\bar{w} = \text{const}, \quad \bar{v} = 0 \tag{9}$$

throughout R. The value of the minimum drag is then

$$D_{\min} = L\,\bar{w}/V. \tag{10}$$

The computation of the drag of interfering lift distributions is simplified by a reciprocal relation, essentially similar to the *Ursell-Ward* relation, which appears in the combined flow field. Thus if we consider any two distributions of lift represented by $l_a(x, y, z)$ and $l_b(x, y, z)$ then we may write in short-hand notation:

$$D_{a\,b} = D_{b\,a} \tag{11}$$

or, in words, "the drag of a caused by the (combined) disturbance field of b is equal to the drag of b caused by the (combined) disturbance field of a."

In view of this, we may write for the total drag

$$D\,(a + b) = D_{a\,a} + 2\,D_{b\,a} + D_{b\,b}. \tag{12}$$

Now suppose that l_a satisfies conditions (9) and suppose that R_b lies entirely within R_a. Then

$$D_{b\,a} = L_b\,\bar{w}_a/V \tag{13}$$

with

$$\bar{w}_a/V = \text{const} = D_{a\,a}/L_a, \tag{14}$$

so that the total drag, including the interference, is given by

$$D\,(a + b) = D_{a\,a}\,(1 + L_b/L_a) + D_{b\,b}. \tag{15}$$

As is well known, the elliptical spanwise distribution of lift yields the minimum drag for a monoplane wing at subsonic speeds. In our studies of minimum drag at supersonic speeds we have found that the closest connection with the theory for subsonic speeds can be maintained if we employ a special method for the calculation of drag. In this method [29] we make use of *Hayes*' idea of equivalent positions of sources or lifting elements, together with the idea of the combined disturbance field. Following this method, the combined disturbance field of a lifting surface is constructed by the superposition of infinitely many plane waves, all lying at the *Mach* angle, but at varying angles Θ around the flight axis (x axis). At each angle Θ we construct an equivalent "lifting line" by integrating the lift distribution in the direction parallel to these planes. A sufficient condition for the wave drag to be a minimum is that each equivalent litting line be elliptically loaded. I find it quite surprising that the elliptic loading appears again in the problem of minimum drag at supersonic speeds, although *von Kármán* and *Busemann* have already noticed a similar connection with the wave drag of bodies of revolution.

With a wing of elliptic plan form the minimum drag occurs when the lift L is distributed uniformly over the

surface. In this case integration of the surface loading in any oblique direction yields an elliptically loaded lifting line, as shown by Fig. 8. Since the spanwise loading is elliptic, the induced drag or vortex drag is also a minimum.

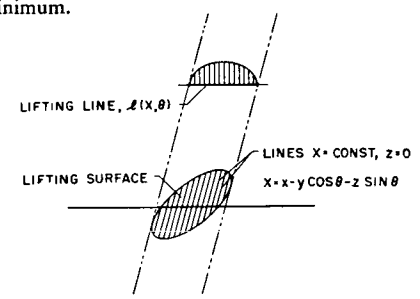

Fig. 8. Integration of surface loading along *Mach* planes

The assumption that the integrated loading for each angle Θ is elliptical can be used to derive a lower bound for the wave resistance associated with a given total lift and a region R. This formula is illustrated in Fig. 9. For the minimum vortex drag under these conditions we may refer to *Munk*'s original paper [27].

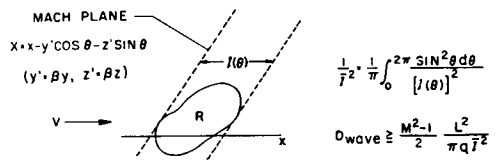

Fig. 9. Lower bound for wave drag associated with the region R and the lift L

For a region R lying everywhere close to the x axis at the center of the *Mach* cone, the loadings integrated along *Mach* planes will all be similar to a "lengthwise loading" obtained by integrating the lift over planes x = const. If this loading is elliptical, we may write for the wave drag

$$D = \frac{M^2 - 1}{2} \frac{L^2}{\pi q \bar{l}^2}. \tag{16}$$

For wider wings the deviation from this value can be taken into account by a factor K. Values of K for several different plan forms are shown in Fig. 10.

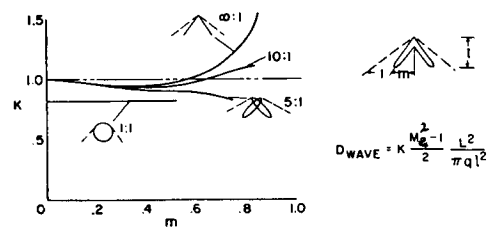

Fig. 10. Approximate expression for wave drag of lifting surface

As is well known, there exists a certain correspondence in airfoil theory between problems involving distributions of lift and those involving distributions of thickness. If the solution of a problem of one type is known, then a corresponding solution of the other type can usually be constructed. Thus our studies of wave drag associated with distributions of lift can readily be extended to problems involving the optimum distribution of thickness or volume within a region R or a plan form S.

Following along the lines of the previous discussion, we suppose that a region R is given and also a certain volume v to be contained in slender, closed bodies or airfoils within R. The condition for minimum drag is then that the pressure gradient, proportional to $\partial \bar{u}/\partial x$, in the combined flow field be constant. Since the total drag is obtained by integrating the product of the local pressure gradient over the volume, we may say that minimum drag for a given volume occurs when the drag per unit volume is constant throughout the region. It must be remembered, however, that the distribution of drag implied in this statement refers to the fictitious disturbance field obtained by averaging the forward and the reversed disturbances.

The drag of interfering bodies and airfoils in three-dimensional regions has been discussed in a recent paper by *Graham*, *Beane*, and *Licher* [30]. For nonlifting systems the wave drag can always be reduced to zero by reflections within the system as, in *Ferrari*'s well-known example of a shrouded body, or the *Busemann* biplane.

The projectile shapes of *von Kármán* [17], *Sears* [31], and *Haack* [32] satisfy the condition $\partial \bar{p}/\partial x$ = const throughout the region R determined by the interior of the "double *Mach* cone" with vertices at the nose and the tail. In this case, of course, the drag is only a relative minimum. However, it is interesting to see how we may simplify the computation of interference drag in such cases as illustrated in Fig. 11. In this example we start with a

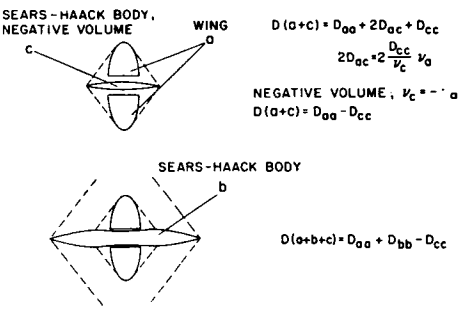

Fig. 11. Use of combined disturbance fields in calculating wing-body drag

planar source distribution, or a nonlifting wing "a", and introduce a linear distribution of sources along the central axis, denoted by "c". For the drag of this combination we may write

$$D(a + c) = D_{aa} + 2D_{ac} + D_{cc}, \tag{17}$$

where D_{ac} is the drag of the wing in the combined disturbance field of the linear source distribution. Now if the combined disturbance field of the linear source distribution satisfies the condition $\partial \bar{p}/\partial x$ = const, as in the case of a *Sears-Haack* body, it will do so throughout the interior of its double *Mach* cone. Furthermore, by making this source distribution sufficiently long, the wing can be contained entirely within this region. The interference drag is then simply the volume of the wing, v_a, times the constant gradient of pressure in the field around the body; or

$$2D_{ac} = 2\frac{D_{cc}}{v_c} v_a. \tag{18}$$

A negative interference drag can be produced by using a source distribution of reversed sign, leading to a "negative volume" for c. If this "volume" is made equal and opposite to the volume of the wing then the distributions a and c can be added to a larger *Sears-Haack* body b without interference. The resultant drag is

$$D(a + b + c) = D_{aa} + D_{bb} - D_{cc}. \tag{19}$$

This equation shows the reduction in over-all drag produced by the source distribution c.

References

[1] *G. de Bothezat:* An introduction to the study of the laws of air resistance of aerofoils. NACA Rep. 28 (1920).

[2] *H. Görtler:* Gasströmungen mit Übergang von Unterschall- zu Überschallgeschwindigkeiten. Z. angew. Math. u. Mech. **20** (1940), pp. 254—262.

[3] *W. Hantzsche* und *H. Wendt:* Der Kompressibilitätseinfluß für dünne wenig gekrümmte Profile bei Unterschallgeschwindigkeit. Z. angew. Math. u. Mech. **22** (1942) pp. 72—86.

[4] *C. Kaplan:* The flow of a compressible fluid past a curved surface. NACA Rep. 768 (1943). (Formerly NACA ARR 3 K 02.)

[5] *I. Imai:* Two-dimensional aerofoil theory for compressible fluids. Rep. No. 294, Aero Res. Inst., Tokyo Imperial Univ. **21** (1944) pp. 283—331. (In Japanese with English abstract.)

[6] *M. D. Van Dyke:* The second-order compressibility rule for airfoils. J. Aeron. Sci. **21** (1954), pp. 647—648.

[7] *W. D. Hayes:* Second-order two-dimensional flow theory and Imai's similitude. British A. R. C. 15, 722, F. M. 1877 (1953). — Also J. Aeron. Sci. **22** (1955), pp. 284—286.

[8] *A. Robinson* and *A. D. Young:* Note on the application of the linearized theory for compressible flow to transonic speeds. Rep. No. 2, The College of Aeronautics, Cranfield A. R. C. 10474 (1947).

[9] *M. A. Heaslet, H. Lomax* and *J. R. Spreiter:* Linearized compressible-flow theory for sonic flight speeds. NACA TN 1824 (1949).

[10] *R. T. Jones:* Properties of low-aspect-ratio pointed wings at speeds below and above the speed of sound. NACA Rep. 835 (1946).

[11] *W. H. Nelson* and *J. B. McDevitt:* The transonic characteristics of 22 rectangular, symmetrical wing models of varying aspect ratio and thickness. NACA TN 3501 (1955).

[12] *J. B. McDevitt:* A correlation by means of the transonic similarity rules of the experimentally determined characteristics of 22 rectangular wings of symmetrical profile. NACA RM A 51 L 17 b (1952).

[13] *G. Guderley* and *H. Yoshihara:* Two-dimensional unsymmetric flow patterns at Mach number 1. J. Aeron. Sci. **20** (1953), pp. 757—768.

[14] *K. Oswatitsch:* Die theoretischen Arbeiten über schallnahe Strömungen am Flugtechnischen Institut der Kungl. Techniska Högskolan, Stockholm. Proc. of Eighth Int. Congress on Theoretical and Applied Mechanics, 1953.

[15] *R. T. Whitcomb:* A study of the zero-lift drag-rise characteristics of wing-body combinations near the speed of sound. NACA RM L 52 H 08 (1952).

[16] *W. D. Hayes:* Linearized supersonic flow. North American Aviation Report AL-222 (1947).

[17] *J. R. Spreiter:* On the range of applicability of the transonic area rule. NACA RM A 54 F 28 (1954).

[18] *L. Prandtl:* Allgemeine Überlegungen über die Strömung zusammendrückbarer Flüssigkeiten. Atti del Convegno della Fondazione Alessandro Volta 1935, pp. 169—198. — Also NACA TM 805 (1936).

[19] *Th. von Kármán:* The problem of resistance in compressible fluids. Atti del Convegno della Fondazione Alessandro Volta 1935, pp. 223—326.

[20] *A. Busemann:* Aerodynamischer Auftrieb bei Überschallgeschwindigkeit. Atti del Convegno della Fondazione Alessandro Volta 1935, pp. 328—360. — Also Luftfahrtforschung **12** (1935), pp. 210—220.

[21] *H. Schlichting:* Tragflügeltheorie bei Überschallgeschwindigkeit. Jahrbuch 1936 der deutschen Luftfahrtforschung, pp. I 181—197.

[22] *M. M. Munk:* The reversal theorem of linearized supersonic airfoil theory. J. Appl. Phys. **21** (1950), pp. 159—161.

[23] *C. E. Brown:* The reversibility theorem for thin airfoils in subsonic and supersonic flow. NACA TN 1944 (1949).

[24] *F. Ursell* and *G. N. Ward:* On some general theorems in the linearized theory of compressible flow. Quart. J. Mech. and Appl. Math. **3** (1950), pp. 326—348.

[25] *A. H. Flax:* Reverse flow and variational theorems for lifting surfaces in nonstationary compressible flow. Cornell Aero. Lab. Report 42 (1952). — Also J. Aeron. Sci. **19** (1952), pp. 352—353.

[26] *M. A. Heaslet* and *J. R. Spreiter:* Reciprocity relations in aerodynamics. NACA TN 2700 (1952).

[27] *M. M. Munk:* Isoperimetrische Aufgaben aus der Theorie des Fluges. Dissertation, Göttingen 1919.

[28] *R. T. Jones:* The minimum drag of thin wings in frictionless flow. J. Aeron. Sci. **18** (1951), pp. 307—310.

[29] *R. T. Jones:* Theoretical determination of the minimum drag of airfoils at supersonic speeds. J. Aeron. Sci. **19** (1952), pp. 813—822.

[30] *E. W. Graham, B. T. Beane* and *R. M. Licher:* The drag of non-planar thickness distributions in supersonic flow. The Aeron. Quarterly **6** (1955), pp. 99—113.

[31] *W. R. Sears:* On projectiles of minimum wave drag. Quart. Appl. Math. **14** (1947), pp. 361—366.

[32] *W. Haack:* Geschoßformen kleinsten Wellenwiderstandes. Lilienthal-Gesellschaft, Bericht 139 (1941), pp. 14—28.

(Received 17. 1. 1956)

REPORT NO. 1284

THEORY OF WING-BODY DRAG AT SUPERSONIC SPEEDS

Robert T. Jones

Ames Aeronautical Laboratory

1956

REPORT 1284

THEORY OF WING-BODY DRAG AT SUPERSONIC SPEEDS [1]

By Robert T. Jones

SUMMARY

The relation of Whitcomb's "area rule" to the linear formulas for wave drag at slightly supersonic speeds is discussed. By adopting an approximate relation between the source strength and the geometry of a wing-body combination, the wave-drag theory is expressed in terms involving the areas intercepted by oblique planes or Mach planes. The resulting formulas are checked by comparison with the drag measurements obtained in wind-tunnel experiments and in experiments with falling models in free air. Finally, a theory for determining wing-body shapes of minimum drag at supersonic Mach numbers is discussed and some preliminary experiments are reported.

DISCUSSION

At subsonic speeds the pressure drag arising from the thickness of the body or wings is negligible so long as the shapes are sufficiently well streamlined to avoid flow separation. In that range there exists no possibility of either favorable or adverse interference on the pressure distributions themselves. If one body is so placed as to receive a drag from the pressure field of another then the second body is sure to receive a corresponding increment of thrust from the first.

At supersonic speeds this tolerance, which was permitted the designer, disappears, and the drag becomes sensitive to the shape and arrangement of the bodies. To be sure, the primary factor here is the thickness ratio, but nevertheless there exist arrangements in which a large cancellation of drag occurs. Examples of the latter are: the sweptback wing and the Busemann biplane.

Recently R. T. Whitcomb (ref. 1) has shown how the drag at transonic speeds may be reduced to a surprising extent by simply cutting out a portion of the fuselage to compensate for the area blocked by the wing. The purpose of the present paper is to discuss some of the theoretical aspects of this method of drag reduction and to show how the basic idea may be extended to higher speeds in the supersonic range.

Whitcomb's deduction of the "area rule" was based on considerations of stream-tube area and the phenomenon of "choking"—which follow from one-dimensional-flow theory. Each individual stream tube of a three-dimensional-flow field must obey the law of one-dimensional flow. While we cannot actually determine the three-dimensional field on this basis alone, nevertheless it provides a good starting point for our thinking. The results demonstrate again the effectiveness of basic and simple considerations.

[1] Supersedes NACA RM A53H18a by Robert T. Jones, 1953.

394915—57

While one-dimensional-flow theory thus provides a clue to the area rule, the necessary principle appears more specifically in the three-dimensional-flow theory. Thus, the formulas for wave drag given by linear theory, if followed toward the limit as M approaches 1.0 (from above), show that the wave drag of a system of wings and bodies depends solely on the longitudinal area distribution of the system as a whole. This was first noted by W. D. Hayes in his 1946 thesis (ref. 2). However, because of the limitations of the theory at transonic speeds, this result was not thought to be of practical significance. Later G. N. Ward (ref. 3), E. W. Graham (ref. 4), and others, restricting themselves to very narrow shapes, expressed the wave drag in terms of the longitudinal area distribution for Mach numbers above 1.0, where the linear theory has a better justification.

It should be noted, however, that both of the problems cited are limiting cases of the more general problem of supersonic drag and it should be borne in mind that only in certain cases has it been possible to reduce the general theoretical formulas to the form of an area rule. It can be shown that the flow field about any system of bodies may be created by a certain distribution of sources and sinks over the surfaces of the bodies. Hayes' formula and the formulas given in reference 5 relate the drag of such a system to the distribution of these singularities. To obtain a formula for the wave drag in terms of area distributions we have to adopt a simplified relation between the source strength and the geometry of the bodies, namely, that the source strength is proportional to the normal component of the stream velocity at the body surface. There are examples (e. g., Busemann biplanes and ducted bodies) for which this assumption is not valid. If, on the other hand, we limit ourselves to thin symmetrical wings mounted on vertically symmetrical fuselages, there are indications that a good estimate of the wave drag at supersonic speeds can be obtained on the basis of the simplified relation assumed.

Following Hayes' method of calculation, we find that at $M=1.0$ the expression for the wave drag of a system of wings and bodies reduces to Kármán's well-known formula (ref. 6) for the wave drag of a slender body of revolution, that is,

$$D_{M=1}=-\frac{\rho V^2}{4\pi}\int_{-x_o}^{+x_o}\int_{-x_o}^{+x_o} S''(x)S''(x_1)\log|x-x_1|\,dx\,dx_1$$

Here $S(X)$ represents the total cross-sectional area intercepted by a plane perpendicular to the stream at the station

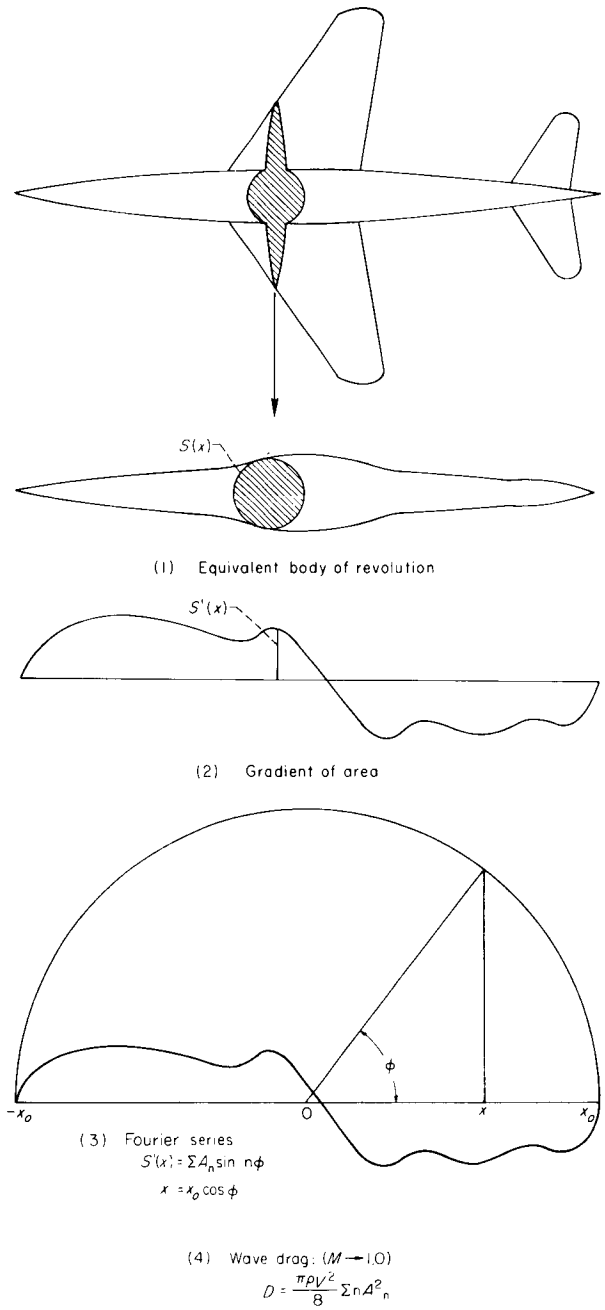

FIGURE 1.—Steps in the calculation of wave drag for $M \rightarrow 1.0$.

x (see fig. 1) and $S''(x)$ is the second derivative of S with respect to x. Following Sears (ref. 7) we may expand $S'(x)$ in a Fourier series and obtain in this way a formula for the drag which is completely analogous to the well-known formula for the induced drag of a wing in terms of its spanwise load distribution. Thus, if we write

$$x = x_0 \cos\phi$$

and

$$S'(x) = \Sigma A_n \sin n\phi$$

we obtain for the wave resistance

$$D = \frac{\pi\rho V^2}{8} \Sigma n A_n^2$$

Of all the terms of the series, each contributes to the drag, but only A_1 and A_2 contribute to the volume or the base area of the system. Thus, to achieve a small drag with a given base area, or with a given over-all volume within the given length, the higher harmonics in the curve $S'(x)$ should be suppressed. This formula enables us to characterize the smoothness of a given shape in a quantitative fashion.

To extend these considerations to supersonic speeds we have to consider a series of cross sections of the system made, not by planes perpendicular to the stream but by planes inclined at the Mach angle, or "Mach planes." By means of

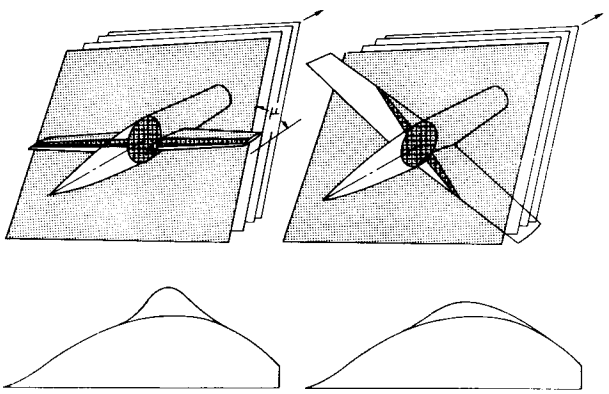

FIGURE 2.—Area distribution given by intersections of Mach planes.

a set of parallel Mach planes (see fig. 2) we construct an "equivalent body of revolution," using the intercepted areas, and compute the drag by von Kármán's formula. The theoretical basis of this step is the fact that the complete three-dimensional disturbance field may be constructed by the superposition of elementary one-dimensional disturbances in the form of plane waves (ref. 8). It is evident that the set of parallel Mach planes may be placed at various angles around the x axis. In constructing the flow field it is necessary to superimpose disturbances at all of these angles and, in computing the drag, to consider the drags of all the equivalent bodies of revolution. The final value of the drag is simply the average of the values obtained through a complete rotation of the Mach planes.

In order to make these statements more specific, we may write the equation of one such Mach plane as follows:

$$X = x - y' \cos\theta - z' \sin\theta$$

where $y' = \sqrt{M^2-1}\, y$, $z' = \sqrt{M^2-1}\, z$, and θ is the angle of rotation of the Mach plane. By assigning different values to X while keeping θ constant, we obtain a series of parallel

planes at the same angle θ around the x axis. By assigning different values to θ while keeping X a constant, we obtain a set of planes enveloping that Mach cone whose apex lies at the point $X=x$.

Selecting a value of θ, we cut through the wing-body system with a series of planes corresponding to different values of X. The total intercepted area in each plane is then equated to the area intercepted by this plane passing through the equivalent body of revolution. If we denote the area intercepted obliquely by $s(X,\theta)$, then the area $S(X,\theta)$ is defined by

$$S=s \sin \mu$$

where μ is the Mach angle (i. e., $\sin \mu=1/M$). Thus, S is the area intercepted by normal planes passing through the equivalent body of revolution on the assumption that this body is slender. Again, we write

$$S'(X,\theta)=\frac{\partial}{\partial X} S(X,\theta)=\Sigma A_n \sin n\varphi$$

with

$$\cos \varphi=\frac{X}{X_o}$$

Here, however, both the length $2X_o$ and the shape of the equivalent body vary with the angle θ. The drag of each equivalent body of revolution, which we may denote by D' (θ) is then determined by applying Sears' formula:

$$D'(\theta)=\frac{\pi\rho V^2}{8} \Sigma n A_n^2$$

The total drag of the wing-body system is the average of all these values between $\theta=0$ and $\theta=2\pi$, that is,

$$D=\frac{1}{2\pi}\int_0^{2\pi} D'(\theta)d\theta$$

In general, the coefficients A_n will be functions of the angle of projection θ. However, calculation shows that the first two coefficients A_1 and A_2 are again related in a simple way to the base area and the volume ν. Thus,

$$A_1=\frac{2}{\pi}\frac{S(X_o)}{X_o}$$

$$A_2=2A_1-\frac{4}{\pi}\frac{\nu}{X_o^2}$$

None of the higher coefficients contribute to the base area of volume, but they invariably contribute to the drag.

The rules for obtaining a low wave drag now reduce to the rule that each of the equivalent bodies obtained by the oblique projections should be as smooth and slender as possible, the "smoothness" again being related to an absence of higher harmonics in the series expression for $S'(X)$. Thus in the case of given length and volume the series should contain only the term $A_2 \sin 2\varphi$ (see fig. 3). It should be noted that in this theory, the equivalent bodies of revolution do not have a physical significance. The concept is simply an aid in visualizing the magnitude of the drag of the complete system.

394915—57——2

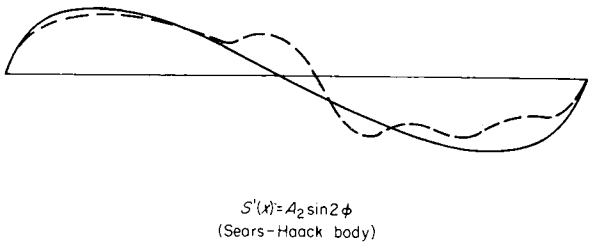

FIGURE 3.—Optimum area distribution for given length and volume.

To check the agreement between these theoretical formulas for the wave drag and experimental values, we have compared our calculations with the results of tests made by dropping models from a high altitude. This comparison was made by George H. Holdaway of Ames Laboratory who supplied the accompanying illustration (fig. 4). In some of these cases it was found necessary to retain more than 20 terms of the Fourier series in order to obtain a convergent expression for the drag.

Considering the variety of the shapes represented here, the agreement is certainly as good as we ought to expect from our linear simplifications. The agreement is naturally better in those interesting cases in which the drag is small.

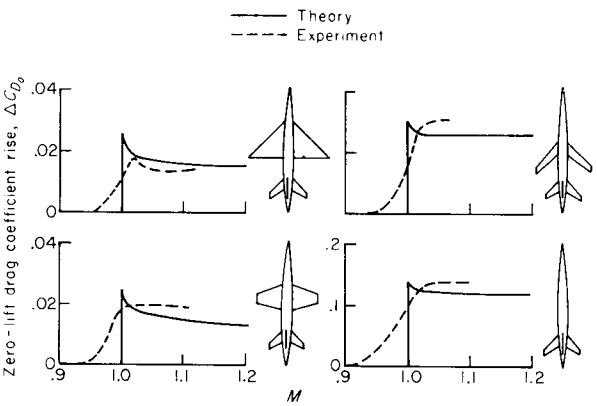

FIGURE 4.—Comparison of theory with results of Ames Laboratory drop tests.

Figure 5 shows an analysis of one of Whitcomb's experiments. The linear theory, of course, shows the transonic drag rise simply as a step at $M=1.0$. We may expect such a variation to be approached more closely as the thickness vanishes. To represent actual values here a nonlinear theory would be needed. For many purposes it will be sufficient to estimate roughly the width of the transonic zone by considerations such as those given in reference 9. In the present case it will be noted that agreement with the linear theory is reached at Mach numbers above about 1.08, and the linear theory clearly shows the effect of the modification.

For further theoretical studies of wing-body drag, shapes have been selected which are especially simple analytically, namely, the Sears-Haack body and biconvex wings of elliptic

plan form, having aspect ratios of 2.54 and 0.635. Figure 6 shows the effect of wing proportions on the variation of wave drag with Mach number, both with and without the Whitcomb modification. In each case the modification has the effect of reducing the wave drag to that of the body alone at $M=1.0$. In the case of the low-aspect-ratio wing this drag reduction remains effective over a considerable range of higher Mach numbers. With the higher aspect ratio, however, the drag increases sharply at higher speeds, so that at $M=1.6$ the modification nearly doubles the wave drag.

The rapid increase of drag in the case of the high-aspect-ratio wing is, of course, the result of the relatively abrupt curvatures introduced into the fuselage lines by the cutout. Such abrupt cutouts are necessarily associated with wings having small fore and aft dimensions, that is, unswept wings of high aspect ratio.

These considerations led to the problem of determining a fuselage shape for such wings that is better adapted to the higher Mach numbers. The first step in this direction is, obviously, simply to lengthen the region of the cutout—thus avoiding the rapid increase of drag with Mach number. The problem of actually determining the best shape for the fuselage cutout at any specified Mach number has been undertaken by Harvard Lomax and Max. A. Heaslet at Ames Laboratory (ref. 10). Their solution of this problem provides a definite method for determining the distribution of sources and sinks along the fuselage axis that will achieve a minimum value of the drag for a given *wing shape* at any specified Mach number. Furthermore, by admitting singularities of higher order quadrupoles, etc., which would distort the rotational symmetry of the fuselage, they have been able to show that the wave drag of a wing-body system can be reduced, in principle at least, to a minimum value associated with the given overall length and volume of the system, that is, to the value for a simple Sears-Haack body containing the whole volume of the system.[2]

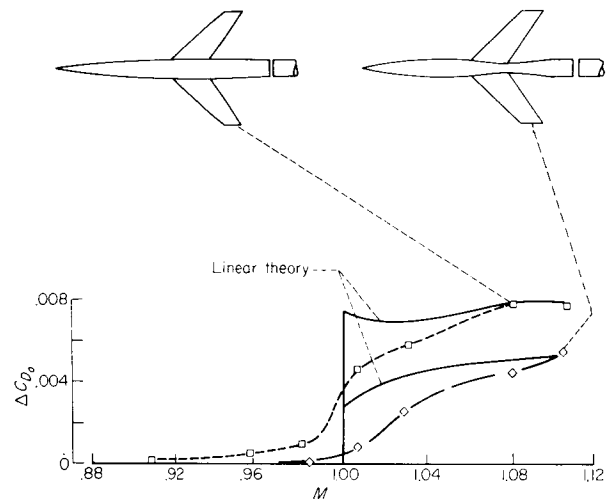

FIGURE 5.—Comparison of Whitcomb's experiments with theory.

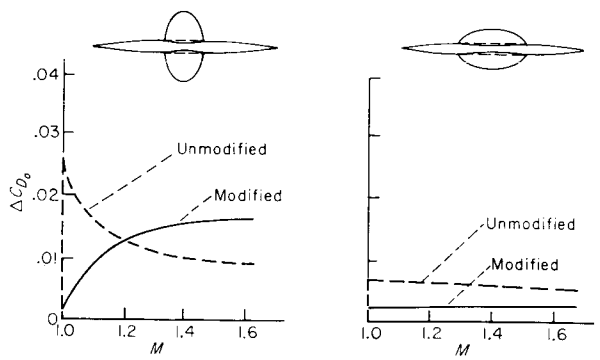

FIGURE 6.—Effect of Whitcomb modification on calculated wave drag.

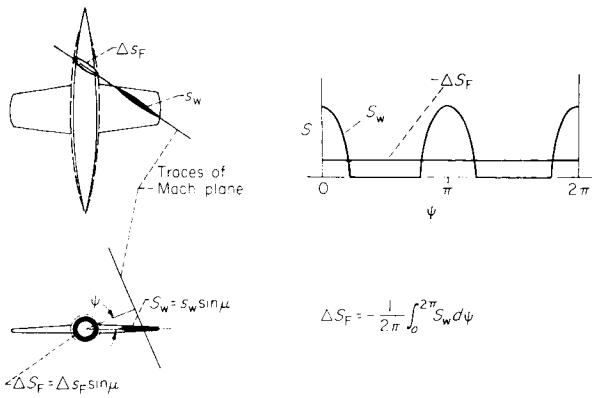

FIGURE 7.—Design of fuselage modification for specified Mach number.

By adopting our simplified relation between the source strength and the body shape, we may describe the result of this theory by a relatively simple concept, which is illustrated in figure 7. For modifications of the first type, the problem is to determine the area ΔS_F to be removed from the fuselage to best compensate for a given wing. (See fig. 7.) Selecting a station along the fuselage axis and a Mach plane passing through this station, we revolve this plane around the axis, measuring at each angle ψ the normal projection, or frontal projection, of the area intercepted where the plane cuts through the wing. After plotting these areas against ψ and integrating between 0 and 2π, we obtain ΔS_F as the average of the values of S_w. At any Mach number the total volume to be subtracted from the fuselage is equal to the wing volume. At higher Mach numbers, since the modification extends over a greater length, the area subtracted at individual cross sections becomes less.

Figure 8 shows the calculated result of designing the fuselage cutout for a specific Mach number, 1.2 in this case. The lower curve is an envelope showing the minimum values that can be achieved by such a radially symmetric cutout.

Figure 9 shows the magnitude of the gain that is theoretically possible by higher order modifications of the fuselage shape. There are three lower bounds here, and the symbols a_0, a_2, etc., attached to them refer to a representation of the fuselage shape by singularities of increasingly higher order.

[2] This value is, of course, not an absolute minimum for a given volume since, as shown by Ferrari, the wave drag of a body can be reduced to zero by special volume distributions (see ref. 11).

The curve labeled a_0 is that given on the previous figure and shows the maximum effect of radially symmetric modifications. While the fuselage shapes for the other curves have not actually been determined, the curve labeled a_0+a_2 may be thought of as referring to a cutout with an additional elliptic modification.

In order to test this theory of determining optimum body shapes we have started a program, using models similar to those investigated theoretically. Several of these models have already been tested in the Ames 2- by 2-foot wind tunnel, with results that agree quite well with calculations made on the assumptions given earlier. Shown in figure 10 are the experimental and theoretical curves. It is evident that the calculated differences are all reproduced approximately in the experimental values.

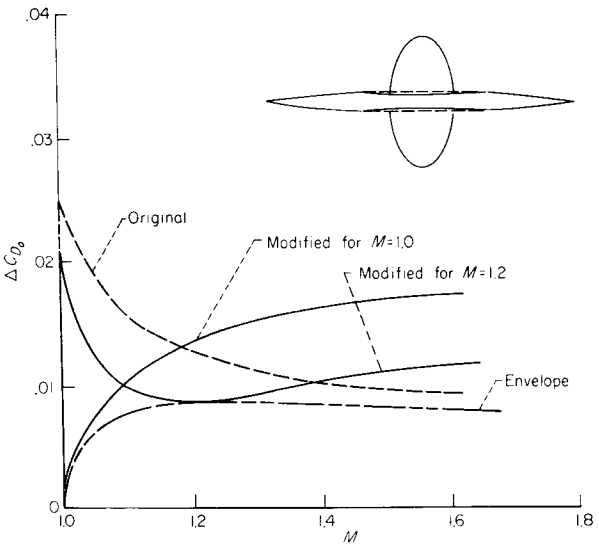

FIGURE 8.—Effect of modification designed for a specified Mach number.

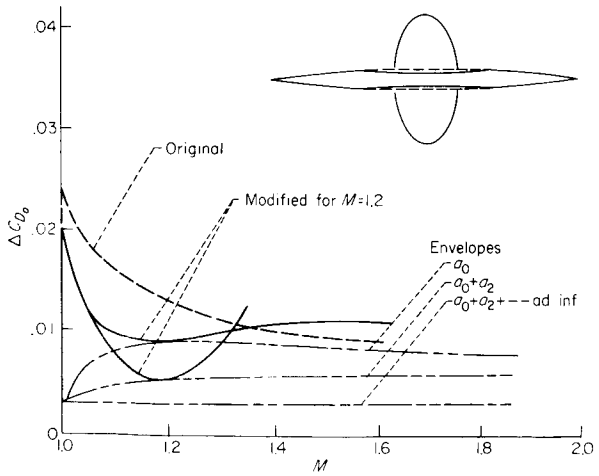

FIGURE 9.—Envelopes for drag at design Mach number.

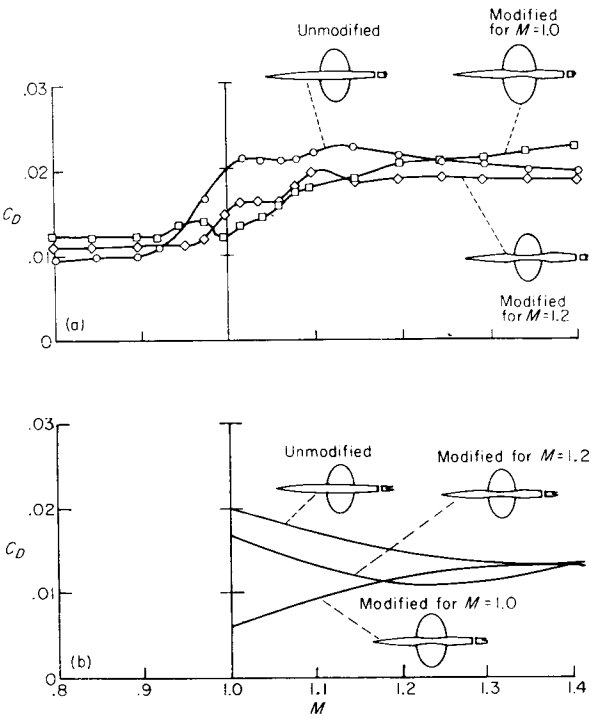

(a) Experimental values.
(b) Calculated values.

FIGURE 10.—Drag of bodies with elliptic wings.

There are, of course, examples of wing-body systems which would hardly benefit by any change in shape of the fuselage. It is easy to decide whether a gain is possible, or worthwhile, by comparing the actual wave drag of the system with that of a Sears-Haack body containing the over-all volume of the system. In the case of 63° the wing-body combination, which has been described in several previous reports, this comparison yields 0.0045 as a lower bound for the wave-drag coefficient and 0.005 for the actual value. In such cases, for which the wave drag is initially very low, further reduction by reshaping the fuselage is not worthwhile.

It is clear from the foregoing, however, that appreciable savings in drag can be made in many cases by a suitable shaping of the fuselage. Unswept wings of high aspect ratio are benefited most and require the most careful consideration of the fuselage shape.

These new developments illustrate, again, the fact that the disturbance fields at transonic and supersonic speeds are essentially three-dimensional phenomena. It was not long ago that our ideas concerning the wing section—which had their origin in the older incompressible flow theory—had to be relinquished because of the predominating effects of the wing plan form. Now we must learn how to design the wing and the fuselage together.

AMES AERONAUTICAL LABORATORY
NATIONAL ADVISORY COMMITTEE FOR AERONAUTICS
MOFFETT FIELD, CALIF., *July 8, 1953*

APPENDIX A

SIMPLIFIED CALCULATION OF DRAG IN SPECIAL CASES

If special shapes such as the Sears-Haack body (ref. 7) and the elliptic wing (ref. 8) are selected for exploratory studies, then the calculation of drag can be greatly simplified.

The radius r of the Sears-Haack body at any station X is given by

$$\frac{r}{r_{max}}=\left[1-\left(\frac{x}{x_0}\right)^2\right]^{3/4} \tag{A1}$$

For this shape

$$S'(X)=A_2 \sin 2\varphi \tag{A2}$$

and the drag has a minimum value for the given volume and length. The value of the drag is given by

$$C_D=\frac{D}{\frac{\rho}{2}V^2S_{max}}=\frac{9}{8}\pi^2\frac{(r_{max})^2}{x_0^2} \tag{A3}$$

The elliptic wing has symmetrical biconvex sections, with ordinates z given by

$$\frac{z}{z_{max}}=1-\frac{x^2}{a^2}-\frac{y^2}{b^2} \tag{A4}$$

where a and b are the semiaxes. The area distribution for every angle of projection is similar to that of the Sears-Haack body, but the projected length varies with the angle. The wing thus yields a minimum value of the wave drag consistent with a given volume and the elliptic plan form. The value of this drag is:

$$C_D=\frac{D}{\frac{\rho}{2}V^2S}=4\frac{(z_{max})^2}{a^2}\frac{1}{\sqrt{M^2-1+\frac{a^2}{b^2}}}\left(2-\frac{M^2-1}{M^2-1+\frac{a^2}{b^2}}\right) \tag{A5}$$

where S is the plan area of the wing.

By making use of the reversal theorem for drag we may compute the wave drag of any body from the fictitious pressure field obtained by superimposing the perturbation velocities for forward and reversed motion (refs. 12 and 13). This process leads to some interesting relations for the shapes selected. Thus in the case of the Sears-Haack body it may be shown that the combined pressure distribution $\bar{p}$ consists of a uniform gradient of pressure over the whole interior R of its "characteristic envelope" defined by the Mach cone from the nose together with the reversed Mach cone from the tail. (See fig. 11.)

By thinking of the characteristic region R as a region of uniform horizontal buoyancy, and of the body b in terms of a certain volume, v_b, we see that the drag is simply the product

$$D_{bb}=v_b\frac{d\bar{p}_b}{dx} \tag{A6}$$

The existence of a constant pressure gradient makes the computation of interference drag particularly simple for such shapes, provided the interfering body lies entirely within the characteristic region R. Thus the additional drag of an airfoil a placed within the double cone of the fuselage will be given by

$$D_{ab}=v_a\frac{D_{bb}}{v_b} \tag{A7}$$

Now, by the mutual drag theorem (ref. 13) we have

$$D_{ab}=D_{ba} \tag{A8}$$

or, "the drag of the fuselage caused by the presence of the wing is equal to the drag of the wing caused by the presence of the fuselage." In this way we obtain the general formula

$$D(a+b)=D_{bb}+2D_{ab}+D_{aa} \tag{A9}$$

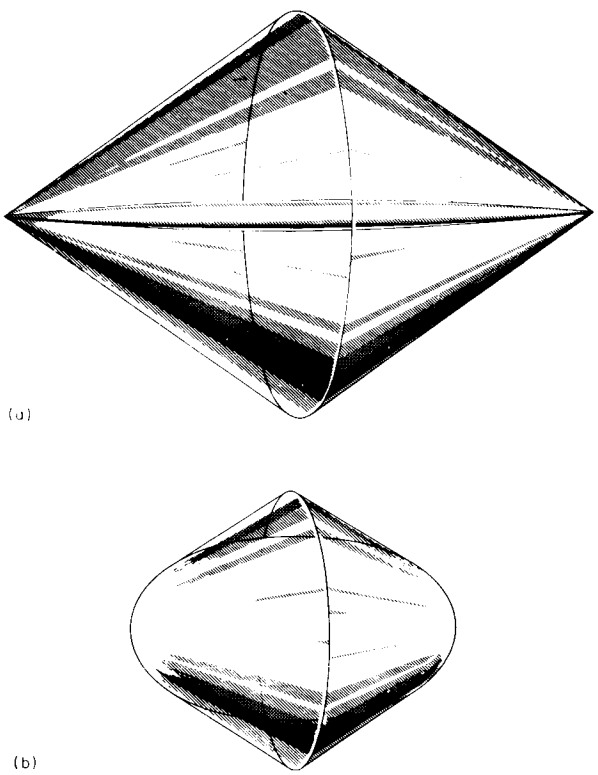

(a)

(b)

(a) Body of revolution.

(b) Elliptic wing.

FIGURE 11.—Characteristic envelopes.

and for the special shapes selected:

$$D(a+b)=D_{bb}\left(1+2\frac{\nu_a}{\nu_b}\right)+D_{aa} \tag{A10}$$

The effect of an indentation or cutout in the fuselage may be calculated by introducing a second "body," c, shorter than the fuselage, and having a negative volume equal to the volume subtracted by the indentation. In order to simplify the situation as much as possible it will be assumed that the wing lies entirely within the characteristic region of the indentation, and furthermore that the latter may be represented by a "negative" Sears-Haack body with volume equal to that of the wing.

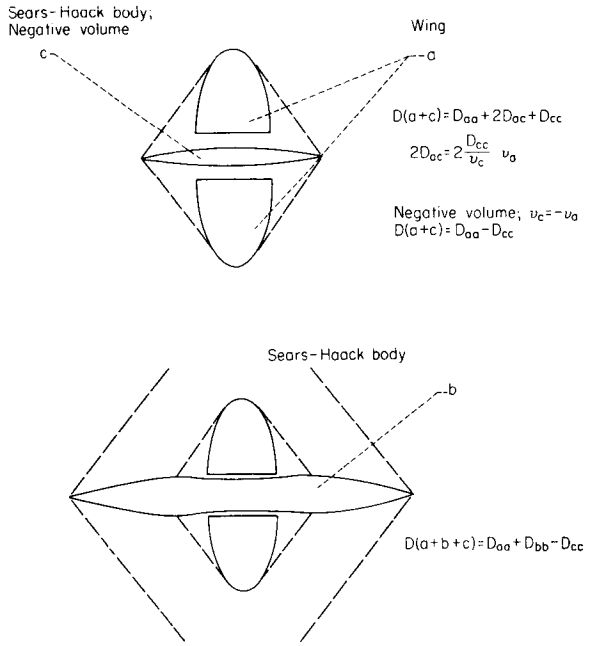

FIGURE 12.—Simplified calculation of interference drag.

The calculation of drag in this case is illustrated in figure 12. For the airfoil and cutout we have

$$\left.\begin{aligned} &D(a+c)=D_{aa}+2D_{ac}+D_{cc}\\ \text{but, since,}\quad &2D_{ac}=-2D_{cc}\\ &D(a+c)=D_{aa}-D_{cc}\end{aligned}\right\} \tag{A11}$$

Now, the combination $(a+c)$ may be placed inside the characteristic region of the body b without interference, since $\nu_a+\nu_c=0$. Hence,

$$D(a+b+c)=D_{aa}+D_{bb}-D_{cc} \tag{A12}$$

This formula yields the minimum drag for the shapes selected under the assumption that ν_{b+c} is fixed. In this case the drag saving is equal to the drag of the indentation alone.

The negative Sears-Haack body is not the optimum shape of the indentation c for the elliptic wing, as shown by the result of Heaslet and Lomax quoted earlier (ref. 10). Again, however, in the case of the optimum shape for c, our previous equation holds. However, the calculation of D_{cc} is more complex in this case and its value is somewhat greater.

REFERENCES

1. Whitcomb, Richard T.: A study of the Zero-Lift Drag Rise Characteristics of Wing-Body Combinations Near the Speed of Sound. NACA RM L52H08, 1952.
2. Hayes, W. D.: Linearized Supersonic Flow. North American Aviation, Inc., Rep. No. AL-222, June 1947, pp. 94-95.
3. Ward, G. N.: Supersonic Flow Past Slender Pointed Bodies. Quart. Jour. Mech. and Appl. Math., vol. II, pt. 1, 1949.
4. Graham, E. W.: Pressure and Drag on Smooth Slender Bodies in Linearized Flow. Douglas Aircraft Co., Rep. SM-13417, 1949.
5. Heaslet, Max. A., Lomax, Harvard, and Spreiter, John R.: Linearized Compressible Flow Theory for Sonic Flight Speeds. NACA Rep. 956, 1950.
6. de Kármán, Th.: The Problem of Resistance in Compressible Fluids. Estratto dagli Atti del V Convegno della Fondazione Alessandro Volta, 1935, Rome, Reale Accademia d'Italia, 1936.
7. Sears, W. R.: On Projectiles of Minimum Wave Drag. Quart. Appl. Math., vol. IV, no. 4, Jan. 1947.
8. Jones, Robert T.: Theoretical Determination of the Minimum Drag of Airfoils at Supersonic Speeds. Jour. Aero. Sci., vol. 19, no. 12, Dec. 1952.
9. Busemann, A.: Application of Transonic Similarity. NACA TN 2687, 1952.
10. Lomax, Harvard, and Heaslet, Max. A.: A Special Method for Finding Body Distortions That Reduce the Wave Drag of Wing and Body Combinations at Supersonic Speeds. NACA Rep. 1282, 1956.
11. Ferri, Antonio: Application of the Method of Characteristics to Supersonic Rotational Flow. NACA Rep. 841, 1946.
12. Munk, Max M.: The Reversal Theorem of Linearized Supersonic Airfoil Theory. Jour. Appl. Phy., vol. 21, no. 2, Feb. 1950, pp. 159-161.
13. Jones, Robert T.: The Minimum Drag of Thin Wings in Frictionless Flow. Jour. Aero. Sci., vol. 18, no. 2, Feb. 1951, pp. 75-81.

THE COMPRESSIBILITY RULE FOR DRAG OF AIRFOIL NOSES

Robert T. Jones and M. D. Van Dyke

Ames Aeronautical Laboratory

March 1958

Jones, R. T. and Van Dyke, M. D., "The Compressibility Rule for Drag of Airfoil Noses," Journal of the Aeronautical Sciences, vol. 25, no. 3, March 1958, pp. 171-172, 180. © 1958 by the Institute of Aeronautical Sciences, Inc. Reprinted by permission of the American Institute of Aeronautics and Astronautics.

Reprinted from JOURNAL OF THE AERONAUTICAL SCIENCES
Copyright, 1958, by the Institute of the Aeronautical Sciences and reprinted by permission of the copyright owner
MARCH, 1958 VOLUME 25, No. 3

The Compressibility Rule for Drag of Airfoil Noses

R. T. JONES* AND M. D. VAN DYKE*

Ames Aeronautical Laboratory, NACA

SUMMARY

It is shown that the drag of any semi-infinite airfoil section in purely subsonic inviscid flow follows precisely the Prandtl-Glauert compressibility rule. The result for the parabola has application to leading-edge corrections in thin airfoil theory.

INTRODUCTION

SEMI-INFINITE BODIES have long been used to represent the noses of elongated aerodynamic shapes. This role assumes increased importance in compressible flow, because the approximate linearized theory must usually be employed, and it breaks down in the neighborhood of stagnation points.[1] It can be corrected, however, if the flow is known past a simple semi-infinite shape (such as a parabola) that matches the actual body near its nose.[2] Except in incompressible flow, the semi-infinite shape itself cannot be treated exactly, but only by another approximation such as the Janzen-Rayleigh method. However, it is shown in the present paper that for the drag itself the effect of compressibility is known exactly.

DRAG OF A PARABOLA IN SUBSONIC FLOW

As discussed by Prandtl and Tietjens,[3] the drag of a semi-infinite body in inviscid flow is understood to be the limit of the pressure drag on a finite section isolated by a transverse slit into which the surrounding pressure penetrates (see Fig. 1). With this definition, the drag (per unit span) of an infinite parabolic cylinder in incompressible flow along its axis is πR times the dynamic pressure, R being the nose radius.

As the free-stream Mach Number increases to any value short of unity, the entire flow field remains subsonic and hence free of shock waves, because a parabola exerts only a retarding influence on the flow. Local pressures do not, of course, follow the Prandtl-Glauert compressibility rule even approximately near the stagnation point. Nevertheless, the particular weighted average of surface pressures that yields the drag does obey that rule exactly. Thus, at any free-stream Mach Number M less than unity, the drag is

$$D = (1/2)\rho U^2 (\pi R/\sqrt{1 - M^2}) \qquad (1)$$

The proof can be based on consideration of any thin airfoil (say, a symmetrical Joukowski section) of thickness τ. If the leading edge is analytic, it has a nose radius proportional to τ^2. Now suppose the airfoil divided into a short nose section of length τ and a remaining tail section (see Fig. 2), and consider the contribution of each to the total drag. The drag vanishes as τ approaches zero, but the drag coefficient remains finite if referred to a length of order τ^2, such as the nose radius. The nose section disappears in the same limit; but if it is magnified so that its nose radius remains constant, it approaches an infinite parabola.

Over the rear section the slope is uniformly small, so that the linearized theory becomes exact in the limit, giving a drag coefficient proportional to $(1 - M^2)^{-(1/2)}$ Over the nose section linearized theory cannot be applied. However, if the flow is purely subsonic, the total drag is zero according to Theodorsen's extension to subsonic flow of d'Alembert's paradox.[4] Hence the drag of the nose also varies as $(1 - M^2)^{-(1/2)}$.

The same compressibility rule holds for the well-known leading-edge suction force associated with angle of attack. This is clear from a repetition of the preceding argument with the airfoil considered to have an angle of attack α that tends to zero in proportion to the thickness τ. In the limit we obtain asymmetric flow past an infinite parabola (see Fig. 3). One cannot speak of the angle of attack, because the slope of all streamlines tends toward zero far upstream, decaying finally like $[s_0/(-x)]^{1/2}$ where s_0 is some characteristic length. However, one can instead characterize the degree of asymmetry of the flow field far upstream by specifying this parameter s_0 in the dimensionless form s_0/R. (In the limiting process just envisioned, the

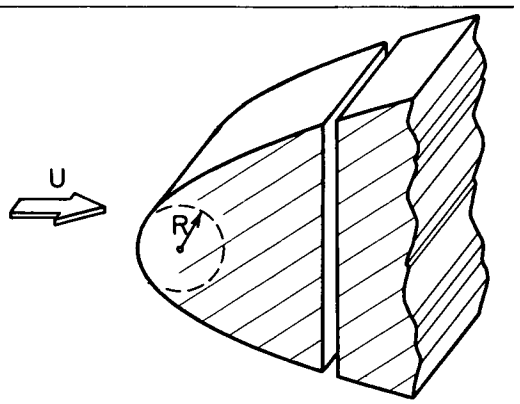

FIG. 1. Flow past a semi-infinite airfoil.

Received December 27, 1956. Revised and received August 20, 1957.

* Aeronautical Research Engineer.

We are indebted to P. A. Lagerstrom for a number of illuminating comments and to Isao Imai for helpful discussions.

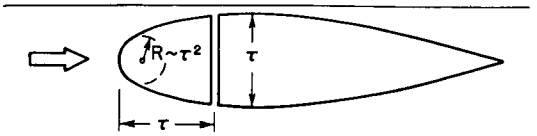

FIG. 2. Division of airfoil into nose and tail sections.

ratio α/τ that was held fixed is proportional to $\sqrt{s_0/R}$.) As indicated in Fig. 3, the stagnation point lies a distance s_0 downstream of the vertex in incompressible flow, but moves nearer the vertex as the Mach Number is increased. Then for a fixed flow pattern far upstream, corresponding to constant s_0, the drag of a parabola is given by

$$D = (1/2)\rho U^2[\pi(R - s_0)/\sqrt{1 - M^2}] \qquad (2)$$

This rule now holds only below the critical Mach Number, which is less than unity for asymmetric flow. At speeds above the critical Mach Number, local supersonic zones appear which undoubtedly terminate in shock waves, and these invalidate the extended d'Alembert paradox on which the argument rests. It may be noted in Eq. (2) that even in nonlinear flow the drag terms are additive.

The rule provides an integral check on detailed approximate solutions. For example, Imai[5] has calculated the Janzen-Rayleigh expansion in powers of M^2 for the surface speed on a parabola in symmetric flow, retaining terms in M^4. Carrying out the complicated integration for the drag gives

$$D/(1/2)\rho U^2\pi R = 1 + (1/2)M^2 + (3/8)M^4 + \ldots \quad (3)$$

This is just the expansion to order M^4 of the Prandtl-Glauert factor $(1 - M^2)^{-(1/2)}$, so that Imai's approximation is in accord with the present rule. Again, Kaplan[6] and others have treated the inclined ellipse by the Janzen-Rayleigh expansion to order M^2, and from that has been extracted the series to M^2 for asymmetric flow past the parabola.[7] Integrating for the drag gives again the compressibility factor $[1 + (1/2)M^2 + \ldots]$. To obtain sufficient accuracy for purposes of correcting compressible thin-airfoil theory for lifting round-nosed wings,[2] this last solution should be extended to include terms in M^4; when that is accomplished the present rule will provide a useful partial check on the formidable calculations involved.

Drag of Other Semi-infinite Bodies

It is clear that the proof given for the parabola will not be invalidated by local changes from parabolic shape near the vertex. Hence any semi-infinite cylinder that approaches a parabola far downstream has (below its critical Mach Number) the drag of that parabola. For example, in Helmholtz' solution for incompressible free-streamline flow past a plate of unit height normal to the stream, the dead-water region far downstream approaches a parabola of nose radius $2/(\pi + 4)$. According to Eq. (1), the dead-water region replaced by a solid body would have a drag of $\pi\rho U^2/(\pi + 4)$, and this is in fact Helmholtz' value for the plate. For the solid body this value would rise with Mach Number as $(1 - M^2)^{-(1/2)}$ until the speed of sound was attained on the surface.

Furthermore, the proof indicates that the rule applies as well to a semi-infinite body that ultimately grows more slowly or more rapidly than a parabola. However, a body has zero drag if it grows more slowly and infinite drag if it grows more rapidly. Hence only the dividing case of a body asymptotic to a parabola provides a significant result.

Similar considerations could be applied to a three-dimensional semi-infinite body—for example, a body of revolution. However, the significant shape that separates axisymmetric bodies of zero and infinite drag has been found by Gurevich[8] to be a peculiar one whose radius varies asymptotically as $x^{1/2}(\ln x)^{-(1/4)}$. As in plane flow, its ultimate form must be the same as that of the dead-water region in axisymmetric free-streamline flow, for which Levinson[9] has indeed found the same form. For a body of noncircular cross section, since the drag depends only on the shape far downstream, where slender body theory becomes accurate, the area rule shows that the drag depends only on the cross-sectional area. Hence, any three-dimensional semi-infinite body having finite drag in subsonic flow grows with cross-sectional area ultimately proportional to $x(\ln x)^{-(1/2)}$.

Application to Subsonic Leading Edges

Thin airfoil theory breaks down near the leading edge of a wing in subsonic flow or in supersonic flow with the edge swept behind the Mach cone. For round edges, the error in pressure is such that the drag can be found correct only by including a leading-edge force associated with the singularity.[1] This force is just the drag of a parabola having the same nose radius, given by Eq. (1). (On swept edges, U and M are to be replaced by their components normal to the edge.) The

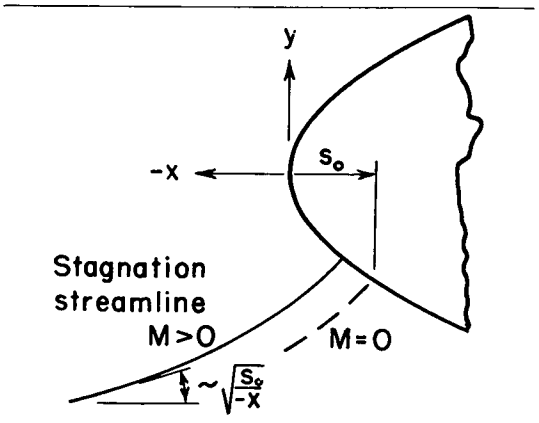

FIG. 3. Asymmetric flow past a parabola.

derivation of these corrections on the basis of thin airfoil theory was, of course, inadequate since the flow is clearly nonlinear in local regions, but when the derivation is based on the extended d'Alembert paradox the corrections are seen to apply to more realistic fluids provided only that the flow remains of the reversible subsonic type.

References

[1] Jones, Robert T., *Leading-Edge Singularities in Thin-Airfoil Theory*, Journal of the Aeronautical Sciences, Vol. 17, No. 5, pp. 307–310, May, 1950.

[2] Van Dyke, Milton D., *Subsonic Edges in Thin-Wing and Slender-Body Theory*, NACA TN 3343, 1954.

[3] Prandtl, L., and Tietjens, O. G., *Applied Hydro- and Aeromechanics*, McGraw-Hill Book Co., Inc., pp. 118–121, 1934.

[4] Theodorsen, Theodore, *The Reaction on a Body in a Compressible Fluid*, Journal of the Aeronautical Sciences, Vol. 4, No. 6, pp. 239–240, April, 1937.

[5] Imai, Isao, *Application of the M^2-Expansion Method to the Subsonic Flow of a Compressible Fluid Past a Parabolic Cylinder*, Proc. 1st Japan Nat. Cong. Appl. Mech., pp. 349–352, 1952.

[6] Kaplan, Carl, *On the Use of Residue Theory for Treating the Subsonic Flow of a Compressible Fluid*, NACA Rep. 728, 1942.

[7] Van Dyke, Milton D., *Second-Order Subsonic Airfoil Theory Including Edge Effects*, NACA Rep. 1274, pp. 7–8, 1956.

[8] Gurevich, M. I., *Flow Past an Axisymmetrical Semi-Body of Finite Drag*, Prikl. Mat. Mech., Akad. Nauk SSSR, Vol. 11, pp. 97–104, 1947 (Russian, English summary).

[9] Levinson, Norman, *On the Asymptotic Shape of the Cavity Behind an Axially Symmetric Nose Moving Through an Ideal Fluid*, I, Ann. of Math. (2), Vol. 47, pp. 704–730, 1946.

AERODYNAMIC DESIGN FOR SUPERSONIC SPEEDS

Robert T. Jones

Ames Aeronautical Laboratory

1959

Jones, R. T., "Aerodynamic Design for Supersonic Speeds," in International Congress in the Aeronautical Sciences, 1st, Madrid, 8-13 September, 1958. Proceedings. Advances in Aeronautical Sciences, v. 1, p. 34-51. New York, London. Pergamon Press, 1959. © 1959.
Reprinted by permission of Pergamon Press, London.

AERODYNAMIC DESIGN FOR SUPERSONIC SPEEDS

By ROBERT T. JONES*

National Advisory Committee for Aeronautics
Ames Aeronautical Laboratory
Moffett Field, California

Summary—The aerodynamic phenomena that may profitably be employed by the designer at subsonic speeds seem now to be well understood. At supersonic speeds such phenomena show a greater and more interesting variety. Search for the minimum number of guiding principles of design thus becomes more difficult and more dangerous.

Studies which can cover an adequate range of geometrical form are at present limited to the linearized version of aerodynamic theory. Such studies, especially those by variational methods, have disclosed certain basic principles of design for aerodynamic efficiency. In present-day experiments, however, the indicated trends are rather quickly confronted with effects of viscosity and nonlinearities. While the theory indicates that good values of aerodynamic efficiency are possible at supersonic speeds it is not yet clear how closely these expectations may be approached in practice.

In the present paper several arrangements of supporting surfaces and bodies are discussed and in some cases comparisons of theory and experiment are made. Finally, certain phenomena connected with lift and drag in a rarefied medium are considered briefly.

INTRODUCTION

IN its earlier development the subsonic airplane showed a great variety in the arrangement of airfoils, bodies, and other parts. For the past 15 or 20 years, however, those airplanes which have passed the tests of experience have shown little alteration in basic form. The aerodynamic principles which have determined this form seem now to be well understood and agreed upon.

The situation is different in the case of the supersonic airplane. Here the aerodynamic rules seem more complex. No clear direction toward a specific form is evident. Our theoretical investigations have taken a rather wide range—seeming in some cases rather far removed from practical questions.

In the present paper we shall review some of the recent theoretical and experimental work in supersonic aerodynamics with its practical application in mind.

*Aeronautical Research Scientist

COMPONENTS OF DRAG

When considering the drag of a complete airplane it is natural to simplify our thinking by dividing the drag into components according to differences in origin. One possibility here is to assign a drag to the individual parts of the airplane and then allow for a certain "interference" between the various components. This scheme is not completely satisfactory at supersonic speeds since the individual drags often tend to be outweighed by the interference. A somewhat more satisfactory division associates a component of the drag with lift-producing elements, elements of volume or thickness, and a component of surface friction. Here again the interference must not be discounted and it is necessary to guard against the acceptance of any such division as having a fundamental significance.

Thus the division of drag according to normal pressure and skin friction or "tangential pressure" seems a natural one, and yet situations arise in which this convention is not appropriate. In the case of a cooled body in a rarefied gas stream the resultant stress acts nearly in the stream direction, independently of the inclination of the surface. Here the resultant affords a simpler description than any of its components.

If we accept tentatively the division according to lift, volume, and surface area, then it is possible to trace the variation in the relative magnitude of these items as the Mach number increases. The range of low supersonic speeds is characterized by the development of large pressures on surfaces having a small inclination. Thus the drag due to thickness or volume is relatively large in comparison with the drag due to lift. At the same time any disturbance causes an extensive lateral influence, giving rise to pronounced interference effects. The surface friction is, however, hardly changed from its subsonic value, provided the increased tendency toward separation can be avoided.

At higher speeds the Mach waves bend back so that the zone of influence is contracted laterally into a smaller space around the body. The pressure developed by a given surface inclination becomes smaller in proportion to the dynamic pressure. For this reason the drag associated with the thickness is reduced. To support a given lift the wing must have a larger angle of attack, so that the drag due to lift is increased. The friction coefficient with either laminar or turbulent flow diminishes, but not as rapidly as the normal pressure.

The drag arising from the volume of the wings or bodies is most pronounced at low supersonic speeds near $M = 1{\cdot}0$. For airplanes intended to fly in this range a proper distribution of volume according to the area rule is important. As in the case of the lift distribution, however, our studies have shown that the minimum of the drag is not a sharp minimum, but there exist many smooth shapes near the optimum which have essentially the minimum drag. From the designer's standpoint the influence of the over-all proportions is perhaps the dominant influence, the wave

drag being reduced most effectively, of course, by extending the volume in the flight direction.

MINIMUM DRAG OF LIFTING SURFACES

In the problem of minimum drag, as previously considered by the present writer[1], the plan form of the wing is assumed to be given as well as the total lift. The result provides a certain unification of subsonic and supersonic airfoil theories through the artifice of a "combined flow field". By considering this problem from a different point of view, M. N. Kogan[2] has recently given a derivation in which the significant quantities seem to have a closer relation to the physical phenomena. Rather than consider a reversed motion of the wing, Kogan utilizes the reversed Mach wave as a control surface in applying the momentum theorem to the calculation of drag. As a result of this choice, the expression for the drag reduces to the Dirichlet integral of the local disturbance velocities projected on this surface. Thus

$$D = \tfrac{1}{2}\rho \int_{\Gamma}\int (\varphi_y^2 + \varphi_z^2)\mathrm{d}y\,\mathrm{d}z \tag{1}$$

while the lift is given by

$$L = \rho U \int_{\Gamma}\int \varphi_z \mathrm{d}y\,\mathrm{d}z \tag{2}$$

Here φ_y and φ_z are the y and z components of the disturbance velocity after projection on the characteristic surface Γ. The lift is thus proportional to the downward momentum of this lateral flow and the drag to its kinetic energy. Now, of flows having a given momentum, the one having the smallest kinetic energy is that one which follows the streamlines of an incompressible fluid. Hence a wing of minimum drag should, if possible, produce on this rear characteristic surface a flow satisfying Laplace's equation in two dimensions, that is:

$$\varphi_{yy} + \varphi_{zz} = 0 \tag{3}$$

The projected velocity distribution on the reversed characteristic surface thus plays a role similar to the lateral velocity distribution in the Trefftz plane in ordinary wing theory. Unlike the Trefftz plane, however, the zone of disturbance on the reversed characteristic surface is limited in extent. Beyond the Mach waves from the leading edge the lateral entrainment of the wing ceases, leading to the boundary condition $\varphi = 0$, so that the wing operates effectively on a limited jet of air. The problem is thus analytically the same as that of a wing at low speed in an open jet wind tunnel (see Fig. 1). The increase of the induced drag which results from the limitation of the wing in the finite jet is exactly equal to the "wave drag" of the wing in unlimited supersonic flow. Wings having

short fore-and-aft dimensions have a small area of entrainment, as shown by Fig. 2. The effect of increasing the Mach number is shown in Fig. 3.

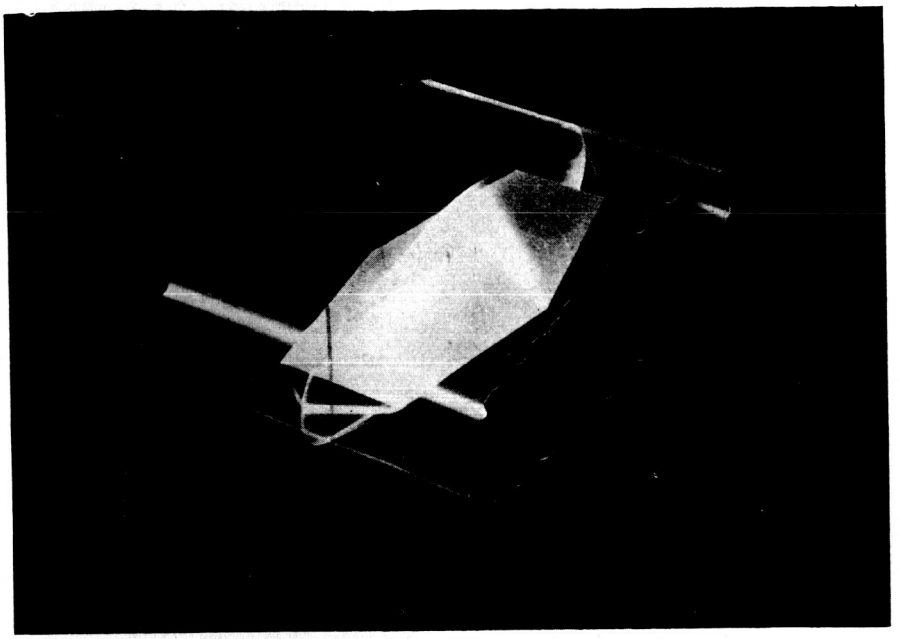

FIG. 1. Equivalent incompressible jet.

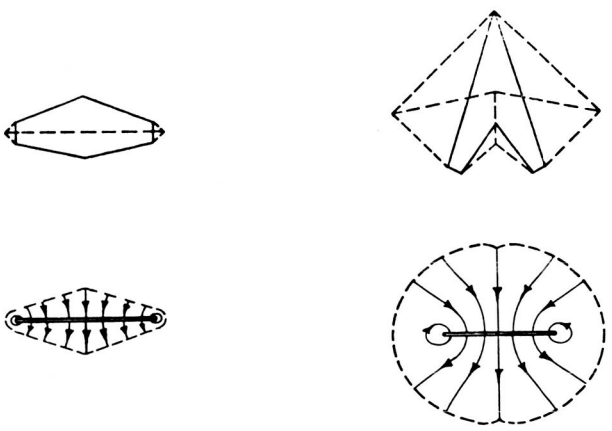

FIG. 2. Effect of fore-and-aft dimension of wing on area of lateral entrainment.

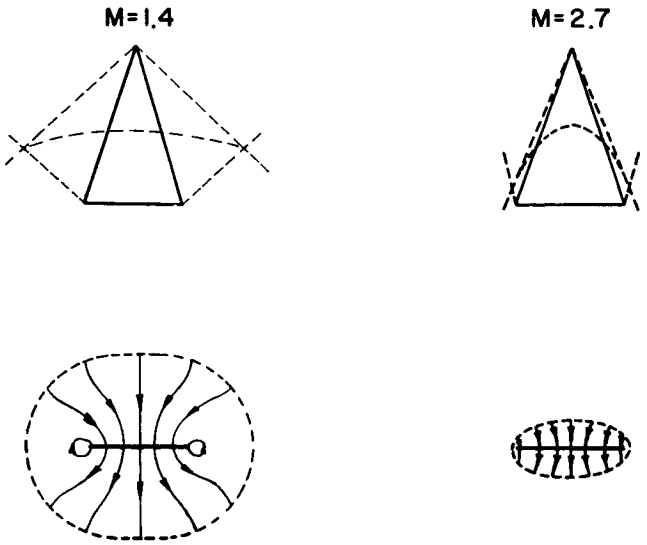

FIG. 3. Effect of Mach number on area of lateral entrainment.

We recall the formulas of Prandtl and Munk for lift and drag of the wing at low speed, that is

$$L = \rho w U S' \tag{4}$$

$$D = \tfrac{1}{2}\rho w^2 S' \tag{5}$$

where w is the downwash and S' is the area of virtual additional mass of the wing's trace. In the new theory these same formulas will apply at supersonic speed if the area S' is replaced by the area of virtual mass of the wing trace in the finite jet as limited by the Mach waves.

It seems unlikely that a result of this kind, referring to principles of momentum and energy, would be strictly limited to the linearized version of the wing theory. Following this thought, M. D. Van Dyke and I have recently found that equations (1), (2), and (3) remain valid even when quantities of second order in the velocities and pressures are retained.

As Ward has indicated[3], the relation between the characteristic trace of the wing and its plan form is not unique. Now Kogan's analysis yields the minimum drag consistent with a given characteristic trace (including the vortex trace) and a given total lift, or, by an obvious extension, a given spanwise load distribution, but it does not give necessarily the minimum drag associated with a given plan form, only a lower bound. For, consider two outline shapes, one lying within the other, yet both having the same characteristic trace, so that the two-dimensional solution is the same for both. Subtract one flow from the other: the disturbance is canceled completely at the characteristic surface, indicating zero drag, yet a dis-

tribution of lift remains in the region of the wings. Thus in determining the minimum drag for a specified characteristic trace we are also determining the associated plan form. For the solution of the minimum problem when the plan form is given we have to return to the criterion of constant downwash given earlier.

E. W. Graham[4] has shown that a result similar to Kogan's can be derived by utilizing the idea of the combined flow field. Graham's analysis provides further a simple determination of the loadings of the wing when integrated in various oblique directions. Graham's analysis brings out the following interesting question: Suppose we have a surface distribution of lift $l(x,y)$ and suppose the projected linear loadings $\mathrm{IL}(x_0,\alpha)$ obtained by integrating $l(x,y)$ along lines in various directions $x = x_0 + \alpha y$ are known. Can the surface distribution $l(x,y)$ be determined from $\mathrm{IL}(x_0,\alpha)$?

Graham[5] gives the following result; if

$$\mathrm{IL}(x_0,\alpha) = \int\int l(x,y)\delta(x-x_0-\alpha y)\mathrm{d}x\,\mathrm{d}y = \int l(x_0+\alpha y,y)\mathrm{d}y \qquad (6)$$

then

$$l(x,y) = \frac{1}{2\pi^2}\int\int \frac{\partial \mathrm{IL}}{\partial x_0}\,\frac{\mathrm{d}x_0\mathrm{d}\alpha}{x-x_0-\alpha y} \qquad (7)$$

A somewhat more symmetrical relation can be achieved if we substitute for the Dirac delta function, δ, its equivalent Cauchy integral formula:

$$\int \mathrm{f}(x)\delta(x-x_0)\mathrm{d}x = \frac{1}{2\pi i}\int_{-\circlearrowright} \frac{\mathrm{f}(x+0i)-\mathrm{f}(x-0i)}{x-x_0}\,\mathrm{d}x = \mathrm{f}(x_0)$$

Then we may write

$$\mathrm{IL}(x_0,\alpha) = \frac{1}{2\pi i}\int_{-\circlearrowright}\int \frac{l(x+0i,y)}{x-x_0-\alpha y}\,\mathrm{d}y\,\mathrm{d}x \qquad (8)$$

The integrations should extend over the largest plan form consistent with the projected lengths of the loadings IL, though the lift distribution $l(x,y)$ may not do so.

Studies by variational methods often establish essential relations with greater clarity than other methods. Here the relation of the drag to the area of entrainment and to the momentum and energy of the downwash flow is perhaps more significant than the relation for the drag to be an absolute minimum. Following this thought we may seek functions for φ which satisfy the condition $\varphi = 0$ on the outer boundary of the characteristic trace and $\varphi_z =$ constant on the wing trace, but which satisfy $\varphi_{yy} + \varphi_{zz} = 0$ only approximately. Thus Heaslet and Fuller[6] find quite simple expressions for the drag of wings having the plan form of a *hyperbola* by relaxing this latter condition. Their solutions correspond to exact minima of the drag for special positions of the center of pressure.

The problem of minimum drag when both the lift and the center of pressure are fixed has been considered by P. Germain[7]. In this case the divergence of the velocity field is not zero as in equation (3) but has a constant value. From the practical standpoint it may be noted that a wing whose width increases toward the rear generally has a smaller drag when the centroid of the lift distribution is placed ahead of the aerodynamic center. Thus we may say that the triangular wing has a "negative trim drag". The optimum loading of wings having fore-and-aft symmetry, however, acts at the middle of the wing, behind the aerodynamic center. Hence wings having fore-and-aft symmetry or wings whose width decreases toward the rear (e.g., a reversed triangular wing) may be expected to have a positive trim drag.

YAWED AND SWEPT WINGS

With planar wings the wave drag is reduced as the lift distribution is extended in the flight direction, while the vortex drag is reduced by extending the span. At the same time the friction drag is reduced by diminishing the exposed area of the wing. At subsonic speeds the last two considerations are effective and they lead to wing forms approaching a lifting line perpendicular to the flight direction. At supersonic speeds the added condition on the length leads to a long, narrow wing placed at an angle of yaw.

It is interesting to analyze the yawed lifting line in terms of its area of entrainment. The forward and reversed Mach waves are simply circular cones drawn from the ends of the line. At subsonic angles of yaw the cones are displaced laterally so that the contour of their inter-section, which outlines the equivalent jet, is an ellipse. The area of this ellipse vanishes rapidly, however, and disappears completely as the lifting line approaches the Mach angle. The area of entrainment is zero and the wave drag given by the theory is infinite at supersonic angles of yaw.

If we convert a yawed wing into a swept wing by bending it at the middle, keeping the same structural slenderness, we see that the length in the flight direction is reduced to about one-half. The wave drag is then increased, so that the potential lift-drag is invariably smaller for the bilaterally symmetric arrangement.

Figure 4 shows the estimated lift-drag ratios for a slender elliptic wing at various angles of yaw. The Mach number considered here is 1·4, so that the transition from flow of the Kutta-Joukowsky type to the Ackeret type occurs in the vicinity of 45°. The best angle of yaw is 30°, placing the wing at a transverse Mach number of approximately 0·70. The lift coefficient required for maximum L/D at this point is, however, too high for the Kutta-Joukowsky type of flow; hence, additional curves have been computed to show the effect of limiting the lift coefficient based on the transverse component of velocity to values of 1·0 in one case and 0·5 in another.

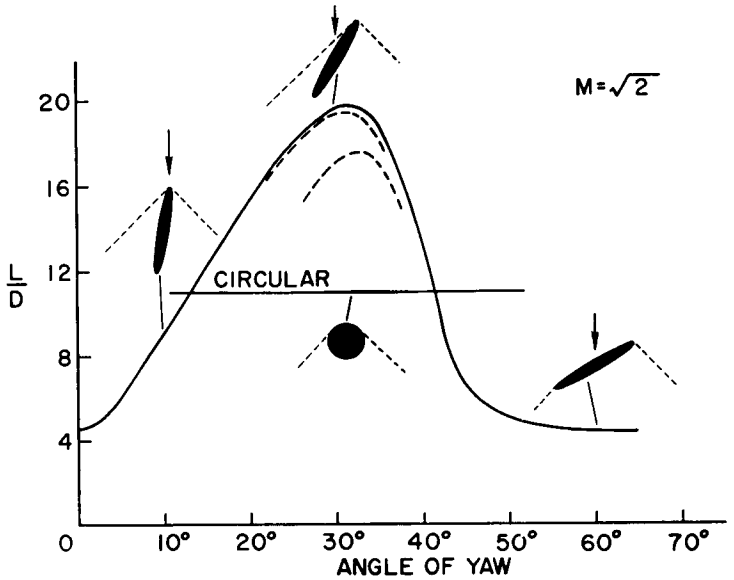

FIG. 4. Effect of yaw on lift–drag ratio of elliptic wing.

Whether the wing is yawed or swept, the potential lift–drag ratio increases almost without limit as the aspect ratio is increased. The practical limit is reached when the lifting pressures become so great that Kutta-Joukowsky flow is no longer possible. A similar situation arises in the design of a sailplane. Here the lift–drag ratio increases rapidly with aspect ratio up to the point at which the optimum lift coefficient begins to exceed the maximum lift coefficient of the wing sections, that is, when Kutta-Joukowsky flow is no longer possible.

Figure 5 shows the results of some experiments made by Robert T.

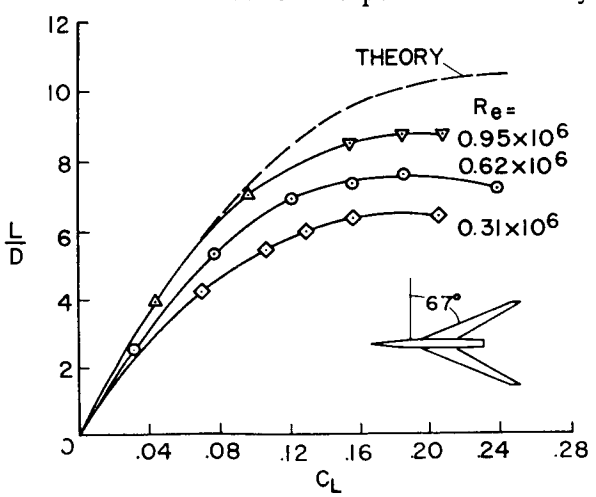

FIG. 5. Effect of Reynolds number on lift–drag ratio; M = 1·53.

Madden at Ames Laboratory on a swept-wing model at a Mach number of 1·53. Here the limitation imposed by the action of viscosity on the performance of the long narrow swept wing is evident—especially at low Reynolds numbers. The sweep angle in this case is 67°.

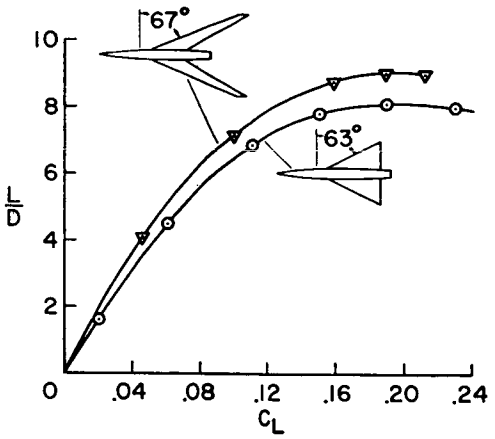

FIG. 6. Effect of wing plan form on L/D.

Figure 6 shows experimental values of L/D obtained by Hall and Heitmeyer[8] for a model having a triangular wing. Their values are compared with the highest curve for the swept wing. The models have the same fuselage and are tested at comparable Reynolds numbers.

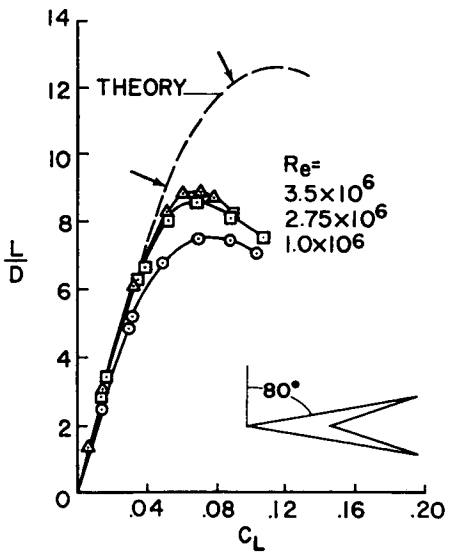

FIG. 7. Effect of Reynolds number on lift–drag ratio; M = 3·0.

Figure 7 shows results of experiments made by Elliott Katzen[9] of Ames Laboratory on a wing having 80° of sweep. The Mach number in

this case is 3·0. The airfoil section of the model shown is the well-known Clark Y, which proved superior to especially cambered sections at these Reynolds numbers.

The curve termed "theory" on the figure (Fig. 7) is simply an estimate in which the limitation on the transverse lift coefficient was not imposed. At the peak of this curve the lift greatly exceeds the maximum lift coefficient of the Clark Y airfoil section in two-dimensional flow. The two arrows shown indicate values of 1·0 and 2·0 for this transverse lift coefficient. There is clearly an uncertainty in our considerations here since the wing has widely different angles of sweep at the leading and trailing edges.

In spite of their limitations, the swept wings nevertheless maintain a margin of superiority over rectangular or triangular plan forms except at the lowest Reynolds numbers. The narrow swept wings, however, have a greater structural weight and a smaller usable lift coefficient for landing. Unless their potential L/D ratios can be approached more closely in practice, their use is difficult to justify in many applications.

REDISTRIBUTION OF LIFT BY FUSELAGE

In steady flow at subsonic speeds the fore-and-aft influence of the wing is complete so that concentration of the lift within a narrow chordwise dimension causes, theoretically, no increase in the pressure drag associated with the lift. At supersonic speeds the unlimited forward influence of the wing is lacking, and the lifting system itself must have an extension in the flight direction if lift is to be produced with a minimum of wave dissipation.

Since the fuselage of a supersonic airplane tends to be long and slender, the question of distributing a part of the lift along the fuselage arises. The possibilities inherent in this suggestion have been studied at Ames

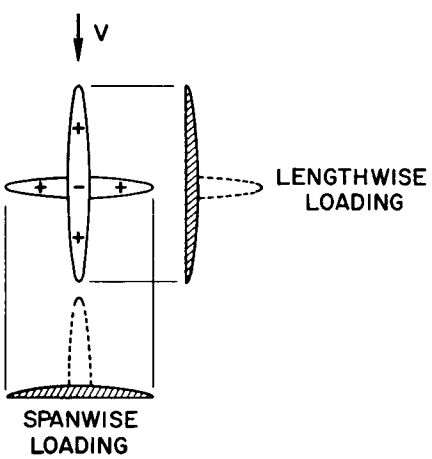

FIG. 8. Distribution of lift along fuselage.

Laboratory and by the theoretical aerodynamics group at the Douglas Aircraft Company[10].

The simplest aspect of the problem appears if we consider distributions of lift on two narrow surfaces in the form of a cross (see Fig. 8). Both the spanwise and the lengthwise loadings should have the form of smooth regular functions. However, if appreciable lift is carried on the "fuselage" then the spanwise loading will show an undesirable concentration at the center. Similarly, a peak in the lengthwise loading appears from the lift carried on the "wing". Desirable loadings appear when the wing and the fuselage each carries a lift approximately equal to the specified value L except at the center, where a downward load of magnitude $-L$ must appear. Hence the fuselage should carry positive lift front and rear but negative lift in the middle.

Detailed calculations show that large gains are to be expected if the theoretical redistribution of lift by the fuselage can be accomplished in practice. The lifting pressures required on the fuselage are, however, of the same order of magnitude as those developed by the wing. According to present experience lifting forces of this magnitude cannot be developed by bending or inclining a slender body of revolution without causing flow detachment and the formation of discrete vortices. Further study of this type of favorable fuselage interference should perhaps include some account of flow detachment or, better still, some means for avoiding it.

HIGH WING ARRANGEMENTS

Interaction between lift and volume begins to appear in the drag when the wing and fuselage are separated vertically. This interference is favorable in the case of a high-wing monoplane, but adverse for the low wing. More generally, we may consider an interaction between surfaces developing forces in a cross-stream direction and elements of volume. Such interactions do not appear at all in the so-called "supersonic area rule". They appear in Hayes' formula[11], however, since the latter is valid quite generally for distributions of singularities in three dimensions. An equally general formulation is given by Lomax and Heaslet[12], which expresses the drag directly in terms of the volume distribution and the lateral forces. In the well-known Ferrari ringed body the interaction between these terms may be considered complete, since the wave drag is canceled exactly.

Such an arrangement may be made to develop lift, but the wave cancellation is then of course incomplete. The most efficient way to gain lift seems to be to omit the lower half of the ring, thus creating a kind of "parasol" monoplane with a highly arched wing (see Fig. 9). The possibility of obtaining high lift–drag ratios with wing-body combinations of this form has been carefully investigated in papers by Lomax and Heaslet of the NACA (ref. 12, and unpublished) and Beane and Ryan of the Douglas Company[13]. Figure 9 illustrates the wing–body arrangement and shows

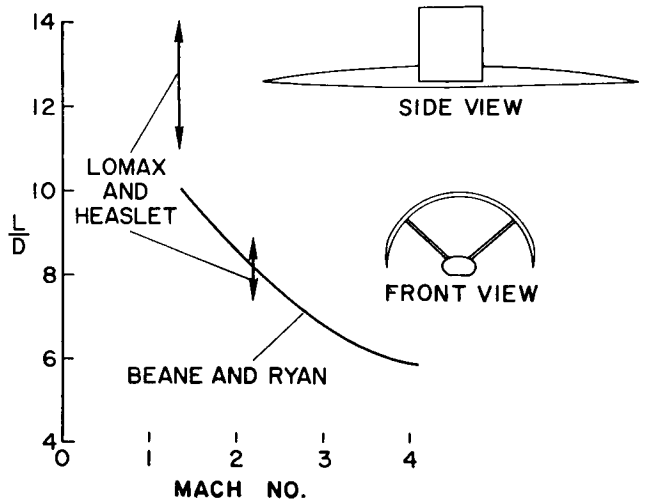

FIG. 9. Estimated lift–drag ratio of body with arched wing.

some typical results at design conditions. As in the case of planar wings, important gains could be shown if the fuselage could be assumed to develop sizeable cross forces. When this possibility is discounted the lift-drag ratios fall considerably but not below those estimated for highly swept wings.

The arrows represent estimates made by Lomax and Heaslet for a wing, a body, and two supporting struts. The flattened body carries no net lift but does support a lift distribution. The wide band covered by the arrows is necessitated by the lack of experimental information on the magnitude of the cross forces that can be generated by body distortions. The curve represents estimates made by Beane and Ryan for a wing and body without the wing support system. Their body, however, was required to carry no lift, even locally. Further, their choice of the turbulent skin-friction drag coefficient was higher, 0·0030 as compared to 0·0025. The conclusion appears to be that the highly arched wing and body can have as high a value of L/D as the swept wing and body.

As in the case of the swept wing, the estimated L/D ratio increases if the wetted area can be reduced by reducing the wing chord. Here again we encounter the limitation imposed by the magnitude of the pressure coefficient. As the wing is made narrower the pressures on the wing increase. The wing pressures are moreover reflected to the rear of the body and increased by a focusing effect. Thus we may expect flow separation at the rear of the body. The influence of these phenomena on the actual characteristics of such an arched wing arrangement will have to be determined experimentally.

In the methods employed by Ferri[14], and Rossow[15], the physical aspect of interference phenomena is made evident. Considering the

interference between planar wings and bodies, these studies have shown definitely favorable effects for high-wing arrangements.

It will be interesting to try and determine a lower bound that might be approached by this method of drag reduction. Referring to Kogan's analysis we find that the conditions imposed on the downwash flow in the "equivalent incompressible jet" are unaltered by the presence of bodies, provided these do not extend beyond the characteristic envelope of the wing. The added bodies may bring the drag of a given wing closer to this lower bound. However, if a wing shape can be found which causes the streamlines of the downwash to follow the pattern of an incompressible flow, then the addition of bodies cannot reduce the drag, except as they may extend the lateral zone of influence of the wing-body system.

CANCELATION OF THICKNESS DRAG

At intermediate supersonic speeds the wave drag due to thickness can be reduced to small values by the phenomenon of wave reflection. There exists a great variety of three-dimensional toroidal shapes for which the wave system is entirely self-contained; that is, the wave resistance is zero at certain Mach numbers, as in the Busemann biplane. One such example with which we have experimented at Ames Laboratory is illustrated in Fig. 10. The model is essentially a tube so shaped as to produce

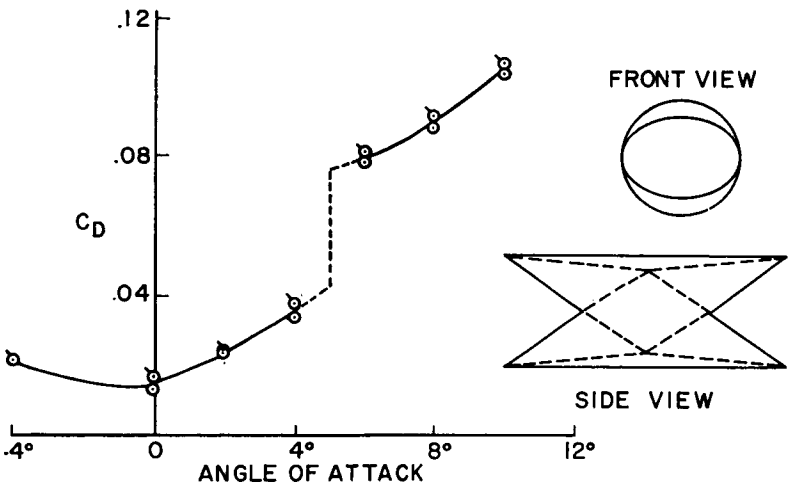

FIG. 10. Drag of tube having a planar wave system.

in its interior a finite portion of the plane wave system between the wings of a Busemann biplane. Such shapes are easily constructed by marking out a stream surface of arbitrary cross section in the undisturbed flow ahead and then calculating the inward deflections of this surface as it passes through the plane wave system of the biplane. Since the wave system has no lateral velocities (i.e., no components in the y direction),

the boundary conditions may be satisfied most conveniently by referring them to sections of the torus made by vertical planes (see Fig. 10).

Tubular bodies having no wave drag can also be made with multiple symmetry, or with complete rotational symmetry. However, such shapes ordinarily enclose regions in which the pressure rises to large values because of focusing. In the case of plane waves the reflection involves only a factor of 2—and this seems to be the smallest value obtainable.

The experiments were made by Loren Bright of Ames Laboratory and showed a negligible wave drag at the design Mach number of 2·0. The most complete wave cancelation, however, occurred at a slightly higher Mach number, $M = 2{\cdot}3$. In Fig. 10 the drag is plotted against angle of attack at $M = 2{\cdot}0$. At about 5° the wave system changes suddenly and the drag increases.

Similar experiments with a torus designed to produce an oblique (i.e., yawed) system of plane waves showed a somewhat more continuous behavior.

While the experiments showed that the wave drag associated with the volume could be eliminated, the tubular bodies developed rather low values of lift-to-drag ratio. It seems that the added surface area required to enclose the wave system increased the friction drag enough to overbalance the gain in wave drag. At still higher Mach numbers the friction drag becomes increasingly important relative to the thickness drag. The use of wave cancelation between interfering bodies or surfaces is more easily justified if the added surfaces are also desirable for some other reason, such as stabilization or control.

LIFT AND DRAG AT HIGH ALTITUDES

In his article "Superaerodynamics" in the *Journal of the Franklin Institute*, Feb. 1934[16], Albert F. Zahm refers to flight in the upper atmospheric layers and states that "Space craft and projectiles must obey new or modified laws of air resistance. These may well be studied in high-vacuum wind tunnels or chambers, under guidance of mathematical theory". I remember Zahm's paper well, since I was a student of his at the time and made drawings for the figures that appear in the paper. I also recall that the paper was not accepted for publication by the journals to which it was first submitted. One is tempted to think that it might be a great service if journals published, in addition to their tables of contents, some notice of the rejected contributions.

Zahm considered the flow of individual particles of a tenuous gas and indicated the modifications needed for diffuse reflection or re-emission of molecules. In later papers[17,18], E. Sänger and H. S. Tsien brought these considerations into closer contact with the physics of gases as based on kinetic theory.

At speeds approaching 20,000 feet per second, we may of course dispense with aerodynamic lift for cruising. However, there are indications

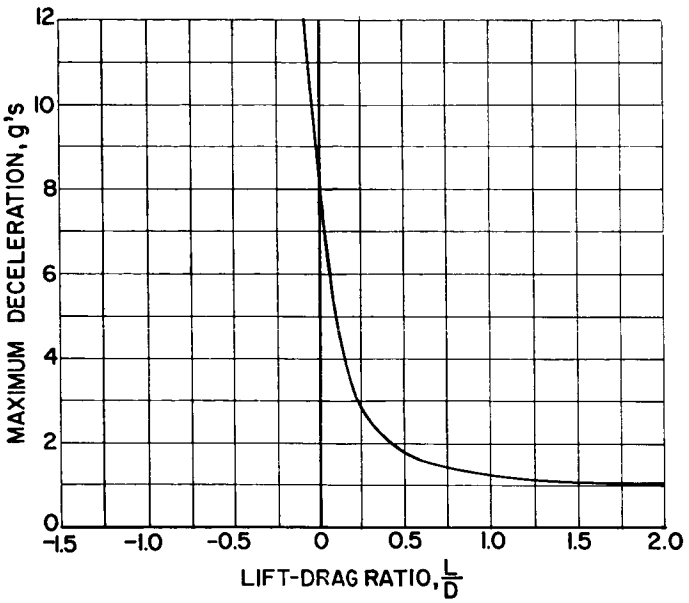

FIG. 11. Effect of lift–drag ratio on maximum deceleration for recovery of satellite.

that aerodynamic forces however small will play an important role in recovery from purely dynamic orbits or trajectories. Figure 11, prepared from calculations made by D. R. Chapman[19] of Ames Laboratory, shows the maximum decelerations encountered in a spiral descent from an initially circular orbit around the Earth. The descent is uncontrolled except that the direction of the resultant aerodynamic force is maintained at a fixed angle to the direction of motion, corresponding to a fixed L/D ratio. If the body develops no lift the maximum deceleration encountered is about $8\,g$. However, even small lift forces result in a much more uniform dissipation of the kinetic energy so that at a lift-drag ratio of one-half the maximum deceleration falls to about $2\,g$.

Even such small values of the L/D may prove difficult to achieve if the deceleration occurs at altitudes above 75 miles. Figure 12 illustrates

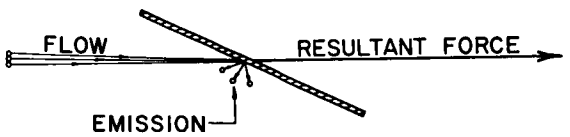

FIG. 12. Aerodynamic force on inclined plate in low-density flow.

the expected reaction on an inclined flat plate in air of extremely low density. The oncoming molecules are deposited on the plate and are emitted with thermal velocities corresponding to its temperature. For a relatively cool surface at high flight velocities the pressure due to emission

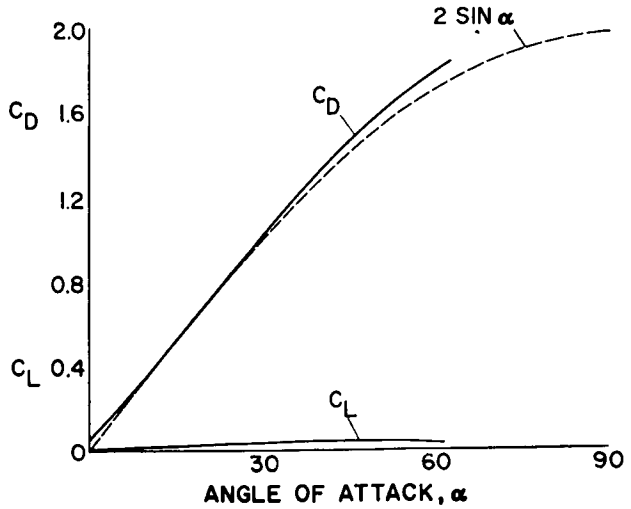

FIG. 13. Drag and lift coefficients on inclined flat plate in low-density flow.

can be neglected. Under these conditions the aerodynamic force is a drag, given by the relation

$$D = \rho U^2 S' \tag{9}$$

Here $S' = S \sin \alpha$, is the frontally projected area of the wing. Figure 13, prepared from data given in ref. 20, shows how closely this simple rule is obeyed by more precise calculations.

The loss of lift in free-molecule flow is a consequence of Knudsen's law, according to which the emission of molecules is independent of their angle of arrival at the surface. Such behavior is closely approximated in experiments conducted thus far[21,22].

It seems unfortunate that the small departures from Knudsen's law have served to characterize a whole regime of rarefied gas dynamics as the region of "slip flow". The main effects seem to be related more directly to the "sticking" of the molecules rather than to their slipping.

Since the pressures developed at high speed are large compared to the ambient pressure, we may expect an extensive range of conditions in which the medium behaves as a gas in the vicinity of the body but as a molecular beam in the exterior flow. The investigation of this semi-continuous regime promises a great variety of yet undiscovered aerodynamic phenomena.

In conclusion, the writer wishes to express appreciation to his colleagues at Ames Laboratory for assistance in preparing this paper and to Prof. H. W. Liepmann of the California Institute of Technology for helpful discussions.

REFERENCES

1. ROBERT T. JONES, The Minimum Drag of Thin Wings in Frictionless Flow. *J. Aeron. Sci.* Vol. 18, No. 2, pp. 75–81, Feb. 1951.
2. M. N. KOGAN, On Bodies of Minimum Drag in a Supersonic Gas Stream. *Prikl. mat. mech.*, Vol. XXI, pp. 207–212, 1957.
3. G. N. WARD, On the Minimum Drag of Thin Lifting Bodies in Steady Supersonic Flows, British A.R.C. 18,711, FM 2459, Oct. 1, 1956.
4. E. W. GRAHAM, The Calculation of Minimum Supersonic Drag by Solution of an Equivalent Two-Dimensional Potential Problem, Rep. SM-22666, Douglas Aircraft Co., Dec. 1956.
5. E. W. GRAHAM, A Geometrical Problem Related to the Optimum Distribution of Lift on a Planar Wing in Supersonic Flow, Rep. SM-23020, Douglas Aircraft Co., Nov. 1957.
6. MAX. A. HEASLET and FRANKLYN B. FULLER, Drag Minimization for Wings and Bodies in Supersonic Flow, NACA Rep., 1958. (Supersedes NACA TN's 3289 and 4227.)
7. PAUL GERMAIN, Sur le Minimum de Traînée d'une Aile de Form en Plan Donnée, *C.R. Acad. Sci., Paris* Vol. 244, No. 9, Feb. 25, 1957.
8. CHARLES F. HALL and JOHN C. HEITMEYER, Lift, Drag, and Pitching Moment of Low-Aspect-Ratio Wings at Subsonic and Supersonic Speeds—Twisted and Cambered Triangular Wing of Aspect Ratio 2 With NACA 0003-63 Thickness Distribution, NACA RM A51E01, 1951.
9. ELLIOTT D. KATZEN, Idealized Wings and Wing-Bodies at a Mach Number of 3, NACA TN 4361, 1958.
10. R. M. LICHER, Reduction of Drag Due to Lift in Supersonic Flight by Distributing Lift Along a Fuselage. *J. Aero. Sci.* Vol. 23, No. 11, pp. 1037–1043, Nov. 1956.
11. WALLACE D. HAYES, Linearized Supersonic Flow. Rep. AL-222, North American Aviation, Inc., June 18, 1947.
12. HARVARD LOMAX and MAX A. HEASLET, Recent Developments in the Theory of Wing-Body Wave Drag. *J. Aero. Sci.* Vol. 23, No. 12, pp. 1061–1074, Dec. 1956.
13. B. J. BEANE and B. M. RYAN, Supersonic Drag Calculations for a Cylindrical Shell Wing of Semi-Circular Cross-Section Combined with a Central Body of Revolution, Rep. SM-22627, Douglas Aircraft Co., Oct. 1956.
14. ANTONIO FERRI, Recent Work in Supersonic and Hypersonic Aerodynamics at the Polytechnic Institute of Brooklyn; Paper given at the Conference on High Speed Aeronautics held by the Polytechnic Institute of Brooklyn, Jan. 22, 1955.
15. VERNON J. ROSSOW, A Theoretical Study of the Lifting Efficiency at Supersonic Speeds of Wings Utilizing Indirect Lift Induced by Vertical Surfaces, NACA RM A55L08, 1956.
16. A. F. ZAHM, Superaerodynamics. *J. Franklin Inst.* Vol. 217, pp. 153–166, 1934.
17. EUGEN SÄNGER, The Gas Kinetics of Very High Flight Speeds, NACA TM 1270, 1950.
18. HSUE-SHEN TSIEN, Superaerodynamics, Mechanics of Rarefied Gases. *J. Aero. Sci.* Vol. 13, No. 12, pp. 653–664, Dec. 1946.
19. DEAN R. CHAPMAN, An Approximate Analytical Method for Studying Entry Into Planetary Atmospheres, NACA TN 4276, 1958.
20. JACKSON R. STALDER and VERNON J. ZURICK, Theoretical Aerodynamic Characteristics of Bodies in a Free-Molecule-Flow Field, NACA TN 2423, 1951.

21. R. G. J. FRASER, *Molecular Rays*, Cambridge University Press, 1931.
22. IMMANUEL EASTERMANN, Molecular Beam Applications to Transport Properties in Gases, Presented at Second Biennial Gas Dynamics Symposium Technological Institute Northwestern University, Evanston, Illinois, Aug. 26–28, 1957.

DISCUSSION

D. W. HOLDER*: Has the author made experiments on wings with subsonic leading edges having sections other than the Clark Y section referred to in the lecture? What improvements of lift/drag ratio does he feel could be achieved by using suitably designed section shapes?

R. T. JONES: The wing having 80° sweep was tested initially with Clark Y sections and with its under surface flat. A cylindrical bending of the wing which increased the angle of attack at the apex and decreased it at the tips resulted in a slight improvement. A further gain might also result from a modification of the section shape, but the direction in which improvement lies is uncertain because of non-linear effects. Further details of these experiments are presented in NACA TN 4361 by Elliott D. Katzen.

G. H. LEE†: The remark by Mr. Jones that there are at present a great many possible layouts for a supersonic aeroplane is one that I should like to endorse. The fact that the designer has such a wide choice from which to select the layout makes his job at present difficult but very interesting; the additional fact that, to-day, there is some doubt regarding military and civil aeroplane requirements, adds to his problems.

In such circumstances, the general work being done by Mr. Jones and discussed in the lecture is very valuable in helping the designer to make his choice by giving him some idea of the relative aerodynamic "attractions", or the performance possibilities, of the different layouts, for example, the relatively small difference, shown in one of the slides, between the maximum L/D ratio for a "swallow-tail" and a delta wing suggests that in many cases L/D ratio would not be the decisive factor, though in certain applications the additional 10% or 15% could be most valuable.

I think we shall find the present paper most useful in making comparisons of this sort and in indicating ways of tackling the various aerodynamic problems which arise.

R. T. JONES: I am grateful to Mr. Lee for his comments and am glad to have my opinions reinforced by those of an experienced airplane designer. Perhaps the present uncertainty in military and civil airplane requirements is simply a reflection of our uncertainty concerning the physical limitation on airplane performance. Such requirements can usually be modified rather quickly following the introduction of a new phenomena or design principle.

* National Physical Laboratory, England
† Deputy Chief Designer, Handley Page Ltd., England

THREE-DIMENSIONAL WINGS OF MINIMUM PRESSURE DRAG

Robert T. Jones

Avco-Everett Research Laboratory

1965

Jones, R. T., "Three-dimensional Wings of Minimum Pressure Drag," in Theory of Optimum Aerodynamic Shapes. Angelo Miele, Editor. New York, Academic Press, 1965. pp. 125-134. © 1965.
Reprinted by permission of Academic Press, Inc., New York.

REPRINTED FROM
THEORY OF OPTIMUM AERODYNAMIC SHAPES
© 1965
ACADEMIC PRESS INC., NEW YORK

CHAPTER 8

THREE-DIMENSIONAL WINGS OF MINIMUM PRESSURE DRAG

by

ROBERT T. JONES*

1. INTRODUCTION

In linearized flow theory, certain very interesting extremal properties of wings can be derived under rather broad conditions without the use of a complicated mathematical apparatus. The present chapter reviews certain results of this theory and indicates some rather obvious extensions to incorporate various auxiliary conditions. Several examples illustrating the relation between the geometrical features of the wing and the lift distribution for minimum drag are given.

2. MINIMUM DRAG PROBLEM

In this section, we consider a thin, cambered lifting surface of given planform and investigate the pressure distribution $p(x, y)$ which yields the minimum drag under various auxiliary conditions (Ref. 1). For this purpose, the drag D in frictionless flow is written in the form

$$D = \iint_S p\alpha \, dx \, dy \tag{1}$$

where x is a chordwise coordinate, y a spanwise coordinate, and $\alpha(x, y)$ the rearward inclination of the normal to the surface element $dS = dx\, dy$ (Fig. 1). With regard to the auxiliary conditions, the following isoperimetric constraints have engineering interest:

$$L = \iint_S p \, dx \, dy \tag{2}$$

if the lift is given,

$$M_x = \iint_S p|y| \, dx \, dy \tag{3}$$

* Principal Research Engineer, Avco-Everett Research Laboratory, Everett, Massachusetts.

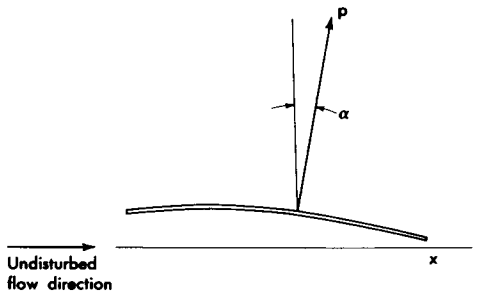

FIG. 1. Cambered lifting surface.

if the bending moment is prescribed, and

$$M_y = \iint_S px\,dx\,dy \tag{4}$$

if the pitching moment is given. Incidentally, the constraints (2) through (4) are particular cases of a more general constraining relationship having the form

$$\iint_S pf(x, y)\,dx\,dy = C \tag{5}$$

where C is a given constant and where $f(x, y)$ is a prescribed weighing function. This weighing function has the values $f = 1$ if the lift is given, $f = |y|$ if the bending moment is prescribed, and $f = x$ if the pitching moment is given.

The problem considered here consists of minimizing the drag integral (1) subject to one or more isoperimetric constraints having the form described by Eq. (5). Clearly, this problem involves two independent variables (x, y) and two dependent variables (p, α). The latter, however, are related through the partial differential equations and boundary conditions describing the flow around the wing or through certain integral relations. Since this method of solution is rather complicated, we abandon it and approach the problem through the use of the reverse flow theorems already established for a wing in linearized supersonic flow (Refs. 2 and 3).

From the linearized theory, it is known that the drag associated with a given distribution of lift remains unchanged when the direction of motion of the wing is reversed. The angle of attack distribution over the wing surface in the reverse flow may be denoted by $\alpha_r(x, y)$ and will, of course, differ from $\alpha(x, y)$ if the pressure distribution $p(x, y)$ is to remain

unchanged. In view of the reverse flow theorem, we may express the drag in terms of a *combined flow field* obtained by superimposing the disturbances created by the given lift distribution in the forward and reverse motions (Fig. 2). Thus, if we write

$$\bar{\alpha} = (\alpha + \alpha_r)/2 \tag{6}$$

the drag may be rewritten in the form

$$D = \iint_S p\bar{\alpha}\, dx\, dy \tag{7}$$

and is stationary provided (see Chapter 3)

$$\iint_S (\bar{\alpha}\, \delta p + p\, \delta\bar{\alpha})\, dx\, dy = 0 \tag{8}$$

where δp and $\delta\alpha$ denote variations calculated at a constant station x, y. On the other hand, the satisfaction of the isoperimetric condition (5) requires that

$$\iint_S f\, \delta p\, dx\, dy = 0 \tag{9}$$

Hence, if λ denotes an undetermined, constant Lagrange multiplier and if Eqs. (8) and (9) are combined linearly, we deduce that

$$\iint_S [(\bar{\alpha} - 2\lambda f)\, \delta p + p\, \delta\bar{\alpha}]\, dx\, dy = 0 \tag{10}$$

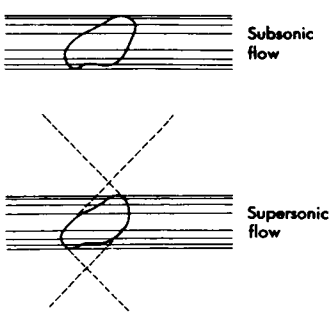

FIG. 2. Lifting surfaces with superimposed disturbance fields.

At this point, we note that the variations δp and $\delta\bar{\alpha}$ are not independent. However, as was shown in Ref. 1, the symmetry introduced by superimposing the forward and reverse disturbance fields is such that the two interference drags are equal, that is,

$$\iint_S p\,\delta\bar{\alpha}\,dx\,dy = \iint_S \bar{\alpha}\,\delta p\,dx\,dy \tag{11}$$

Consequently, after Eqs. (10) and (11) are combined, we obtain the relationship

$$\iint_S (\bar{\alpha} - \lambda f)\,\delta p\,dx\,dy = 0 \tag{12}$$

which involves only the independent variation δp. Because of this, the Euler equation describing the extremal solution is given by

$$\bar{\alpha} = \lambda f(x, y) \tag{13}$$

which has the following significance: *the angle of attack in the combined flow field must be proportional to the weighing function imposed on the pressure distribution.*

A modification of the previous problem arises when several isoperimetric constraints of the form

$$\iint_S p f_j(x, y)\,dx\,dy = K_j\,, \qquad j = 1, \ldots, m \tag{14}$$

are imposed on the wing. Under these conditions, the Euler equation becomes

$$\bar{\alpha} = \sum_{j=1}^{m} \lambda_j f_j(x, y) \tag{15}$$

where each of the multipliers λ_j is an undetermined constant.

3. PARTICULAR CASES

The previous extremal property for the drag is remarkable for the economy of its derivation. It holds for subsonic as well as supersonic flows and is not even restricted to steady motion. Several particular cases are now considered.

3.1. Given Lift. If only the lift is prescribed, Eq. (13) becomes

$$\bar{\alpha} = \lambda \tag{16}$$

meaning that the angle of attack of the combined flow field is constant over the entire planform. Hence, the downwash angle, which is pro-

portional to $\bar{\alpha}$, is constant. Furthermore, for the subsonic flow regime, the spanwise lift distribution is elliptical, as shown by Munk in Ref. 4. Incidentally, a change in the chordwise lift distribution does not cause a modification in the induced drag as long as the spanwise lift distribution is the same (for further comments, see Section 3.2).

It should be noted that the elliptic loading also plays an important role in the minimum drag of supersonic wings. If, following an analogy to Whittaker's solution of Laplace's equation (Ref. 5), we calculate the disturbance field of a supersonic wing by the superposition of two-dimensional fields, we find that the downwash is the sum of the contributions due to a series of two-dimensional loadings obtained by projecting the lift distribution in different directions. Thus, a lower bound for the drag may be obtained by assuming that each projected or integrated loading is elliptical. If the planform is elliptic, this lower bound is the actual minimum value, providing the pressure is constant. As an example, at $M = \sqrt{2}$, the minimum drag of an unyawed wing is given by (Ref. 5)

$$D = \frac{L^2}{2\rho U^2 S}\sqrt{1 + \frac{a^2}{b^2}} \tag{17}$$

where ρ is the free-stream density, U is the free-stream velocity, a and b are the semiaxes of the ellipse, and S is its area. If the wing is yawed, the corresponding minimum drag is given by (Ref. 5)

$$D = \frac{L^2}{2\rho U^2 S}\mathscr{R}\left[\sqrt{1 - \left(m + i\frac{a'}{b'}\right)^2}\right] \tag{18}$$

where i denotes the imaginary unit, $\mathscr{R}$ the real part of the complex number within brackets, and where the quantities a', b', and m are defined in Fig. 3.

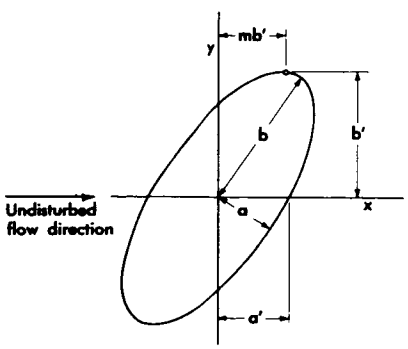

FIG. 3. Oblique ellipse.

3.2. Given Lift and Bending Moment. In steady subsonic flow, the superposition of the forward and reverse disturbance fields results in a purely two-dimensional field of motion identical with the flow produced by the vortex wake in the Trefftz plane. The inclination $\bar{\alpha}$ in the combined flow field may then be identified with the *induced downwash* w_1 of Munk's theory (Ref. 4), that is,

$$\bar{\alpha} = w_1/U \tag{19}$$

In such a two-dimensional field, $\bar{\alpha}$ is independent of the chordwise coordinate x. Therefore, the specification of a weighing function f which depends on x does not lead to a solution of the problem. However, we may impose various conditions on the spanwise distribution of the lift. Thus, following Ref. 6, we may specify both the total lift and the bending moment. In this case, the angle of attack of the combined flow field is given by

$$\bar{\alpha} = \lambda_1 + \lambda_2 |y| \tag{20}$$

In Munk's original problem (Ref. 4), the span b and the total lift were prescribed, and the optimum lift distribution was found to be elliptical. Now, let us consider a family of wings having the same lift and bending moment as Munk's optimum wing, and let us study the effect of the span on the optimum lift distribution as well as on the drag. The analysis, omitted for the sake of brevity (Ref. 6), shows that increasing values of the span cause the lift distribution to become more tapered and the induced drag to become smaller (Fig. 4).

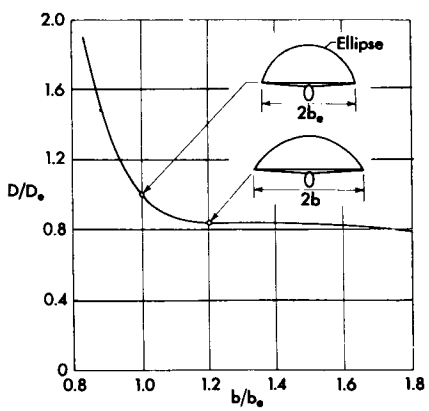

FIG. 4. Minimum vortex drag for wings having a fixed lift and a fixed bending moment.

3.3. Given Lift and Pitching Moment. If an elliptic wing is designed for a given total lift in supersonic flow, the minimum drag occurs when the pressure is uniform. In other words, the center of pressure is identical with the center of the wing. Now, it is known that the centroid of the lift added by a change in the angle of attack is ahead of this point, especially if the wing has a low aspect ratio. Thus, the wing trimmed for flight with the optimum loading is unstable in pitch. These ideas lead us to specify the position of the center of pressure, or the pitching moment, as well as the total lift.

Now, if both the lift and the pitching moment are specified, Eq. (15) becomes

$$\bar{\alpha} = \lambda_1 + \lambda_2 x \tag{21}$$

meaning that the combined angle of attack is a linear function of the chordwise coordinate. By the method of Ref. 5, it can be shown that the associated pressure distribution is also a linear function of the chordwise coordinate, that is,

$$p = p_1 + p_2 x \tag{22}$$

Omitting detailed manipulations, we obtain the following expression for the minimum drag of an unyawed elliptical wing at $M = \sqrt{2}$:

$$D = \frac{L^2}{2\rho U^2 S}\left[\sqrt{\frac{a^2 + b^2}{b^2}} + \left(\frac{\bar{x}}{a}\right)^2 \sqrt{\frac{b^2}{a^2 + b^2}}\right] \tag{23}$$

where $\bar{x}$ is the chordwise displacement of the center of pressure with respect to the centroid of the ellipse.

4. NONPLANAR WINGS

The foregoing derivation is easily extended to nonplanar lifting surfaces such as a wing with upturned or downturned tips (Fig. 5). If the angle of attack is defined as the angle between the free-stream velocity vector

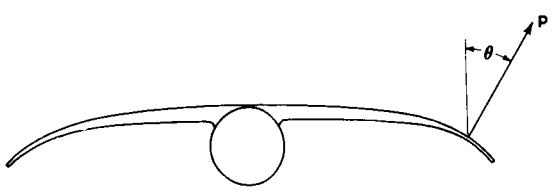

FIG. 5. Wing with drooped tips.

and its projection on the wing surface, the drag is still given by Eq. (7) with the understanding that x is a rectilinear chordwise coordinate and y is a curvilinear spanwise coordinate parallel to the wing surface. Because of the inclination of the pressure, the lift is given by

$$L = \iint_S p \cos \theta(y)\, dx\, dy \tag{24}$$

where the angle $\theta(y)$ is defined in Fig. 5. Consequently, if the lift is the only quantity prescribed, the condition for minimum drag becomes

$$\bar{\alpha} = \lambda \cos \theta(y) \tag{25}$$

For a wing with vertical end plates, $\cos \theta = 0$ over the end plates; hence, the *sidewash* of the combined flow field must vanish.

5. ALTERNATE APPROACH

In Kogan's analysis (Ref. 7), the minimum drag problem is approached from a different point of view. Instead of superimposing the forward and reverse disturbance fields, he utilizes the physically real flow and expresses the drag in terms of quantities integrated over the enveloping characteristic surface of the wing. Such a *characteristic envelope* involves both forward and reverse Mach waves tangent to the edges of the wing (Fig. 6).

With the forward-going characteristic surface Σ as a reference, one obtains the following expression for the drag:

$$D = \frac{\rho}{2} \iint_\Sigma (\varphi_y^2 + \varphi_z^2)\, dy\, dz \tag{26}$$

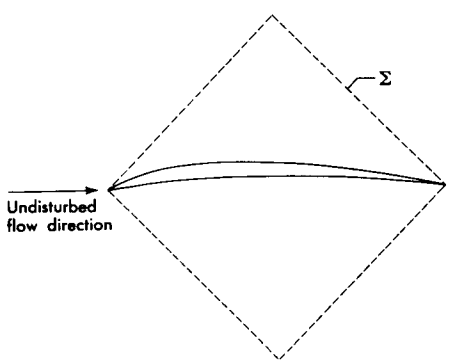

FIG. 6. Characteristic envelope of a wing.

while the total lift is given by

$$L = \rho U \iint_{\Sigma} \varphi_z \, dy \, dz \tag{27}$$

where φ is the velocity potential and where φ_y and φ_z denote the y-component and the z-component of the disturbance velocity after projection on the surface Σ. Thus, the drag is proportional to the kinetic energy of this two-dimensional flow, while the lift is proportional to its downward impulse. Now, among all the flows having a given impulse, the one with the smallest kinetic energy satisfies Laplace's equation (Kelvin's theorem), that is,

$$\varphi_{yy} + \varphi_{zz} = 0 \tag{28}$$

Hence, minimum drag is achieved when the streamlines of this lateral flow on the rear characteristic surface imitate a two-dimensional incompressible flow. The connection between Kogan's analysis and our previous treatment employing the combined disturbance field has been shown by Graham in Ref. 8.

Following Prandtl and Munk, we are accustomed to thinking of the drag of a wing in terms of its *area of entrainment.* As is well known in subsonic steady flow, the equivalent entrainment with optimum loading is represented by a circular jet having a diameter equal to the span of the wing. The drag of the wing at subsonic speeds is small because the area of entrainment is large. At supersonic speeds, however, the lateral influence of the wing is restricted by the Mach waves, so that the downwash associated with a given lift must be greater. Kogan's analysis gives a quantitative value to these intuitive considerations.

References

1. Jones, R. T., *The Minimum Drag of Thin Wings in Frictionless Flow*, JAS, Vol. 18, No. 2, 1951.
2. Von Kármán, T., *Supersonic Aerodynamics—Principles and Applications*, JAS, Vol. 14, No. 7, 1947.
3. Hayes, W. D., *Linearized Supersonic Flow*, North American Aviation, Report AL No. 222, 1947.
4. Munk, M. M., *The Minimum Induced Drag of Aerofoils*, NACA, Report No. 121, 1921.
5. Jones, R. T., and Cohen, D., *High Speed Wing Theory*, Princeton Aeronautical Paperbacks, Princeton University Press, Princeton, New Jersey, 1960.
6. Jones, R. T., *The Spanwise Distribution of Lift for Minimum Induced Drag of Wings Having a Given Lift and a Given Bending Moment*, NACA, TN No. 2249, 1950.

7. KOGAN, M. N., *On Bodies of Minimum Drag in Supersonic Gas Flow* (in Russian), PMM, Vol. 21, No. 2, 1957.
8. GRAHAM, E. W., *The Calculation of Minimum Supersonic Drag by Solution of an Equivalent Two-Dimensional Potential Problem*, Douglas Aircraft Company, Report No. SM-22666, 1956.

REDUCTION OF WAVE DRAG BY ANTISYMMETRIC ARRANGEMENT OF WINGS AND BODIES

Robert T. Jones

Ames Research Center

February 1972

Jones, R. T., "Reduction of Wave Drag by Antisymmetric Arrangement of Wings and Bodies," AIAA Jorunal, vol. 10, no. 2, Feb. 1972, pp. 171-176.
© 1972.
Reprinted by permission of the American Institute of Aeronautics and Astronautics.

Reprinted from AIAA JOURNAL, Vol. 10, No. 2, February 1972, pp. 171-176
Copyright, 1972, by the American Institute of Aeronautics and Astronautics, and reprinted by permission of the copyright owner

Reduction of Wave Drag by Antisymmetric Arrangement of Wings and Bodies

R. T. JONES*
NASA Ames Research Center, Moffett Field, Calif.

In theory, antisymmetric arrangements of wings and bodies can have smaller wave drag than corresponding mirror-symmetric arrangements. Thus, a long narrow oblique wing which presents the same aspect for two opposite directions of flight is potentially more efficient than corresponding (i.e., structurally equivalent) swept wing. The single continuous wing panel also adapts itself more readily to varying angles of obliquity, and hence, to varying flight speeds. The present paper reviews previous work on the aerodynamics and flight stability of oblique wing combinations and suggests a possible mode of application to transport aircraft operating at moderate supersonic speeds.

Introduction

ONE of the unspoken assumptions in aircraft design is that of bilateral or mirror symmetry. At slow flight speeds, this assumption seems on rather secure ground, partly because of the indications of aerodynamic theory, but also because it agrees with the observed evolutionary forms of birds.

Although it is perhaps natural to extrapolate the forms of birds and animals to the supersonic flight regime, there has been no rational discussion of the merits of bilateral symmetry for supersonic flight. In fact, once the velocity of sound is exceeded, the laws of aerodynamics change in such a way as to make it seem inadvisable to arrange the components of an airplane side by side or abreast in a supersonic stream unless there are compelling reasons for such an arrangement.

Both the transonic area rule and the supersonic small disturbance theory show large adverse interference effects for bodies or wings in a mirror-symmetric arrangement. Figure 1 shows the result of applying supersonic wave drag theory to two airplanes flying in close formation at a slightly supersonic Mach number. In the mirror-symmetric arrangement, the drag of each aircraft is doubled by the interference of the other, making a total wave drag of four. In the staggered or antisymmetric arrangement, however, the wave interference is favorable so that the drag of the two airplanes is no greater than that of a single one. Figure 2 shows the same effect for oblique wing panels. The arrow shape, which seems intuitively correct for supersonic speed, nevertheless has a predicted wave drag many times larger than the antisymmetric arrangement.

Elements of lift or volume show favorable wave interference if they are disposed along lines whose normal component of velocity is subsonic. Thus, the wave drag of a long narrow wing tends toward zero if the wing is swept behind the Mach cone.[1] The reversibility of the wave drag,[2,3] however, indicates that a distribution of lift or volume having a minimum drag should show the same aspect for two opposite directions of flight, i.e., would have fore and aft symmetry. Consideration of the vortex drag indicates further that the projected lift distribution should have lateral symmetry (e.g., elliptic-span loading).

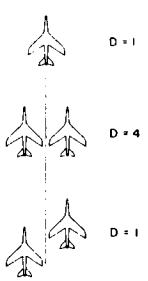

Fig. 1 Wave drag at Mach numbers nears 1.0.

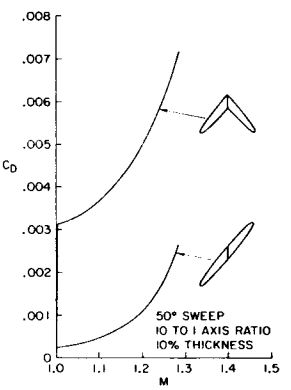

Fig. 2 Calculated wave drag of symmetric and antisymmetric wings.

It is interesting that supersonic theory favors symmetry in both longitudinal and lateral distributions of volume or lift, but evidently not mirror symmetry. Intuitively, one feels that a supersonic airplane should take account of the direction of flight in its shape, i.e., it should somehow "point" in the direction it is going. However, in view of the reversibility of the wave drag, current computer programs must give the same value of the drag with the direction of flight reversed. Figure 3 illustrates this result.†

Review of Aerodynamic Properties of Oblique Elliptic Wings

To obtain a configuration having a minimum wave drag, we suppose first of all that the total lift and volume are given and second a plane area within which the dimensions must be limited.

Received May 3, 1971; revision received August 30, 1971.
Index categories: Airplane and Component Aerodynamics; Aircraft Configuration Design.
* Senior Staff Scientist. Fellow AIAA.

† The reversibility theorems are, of course, limited to the pressure drag and the lift curve slope as determined by linear theory. Thus, the effect of viscosity demands locally different shapes for leading and trailing edges, which are not reversible in practice.

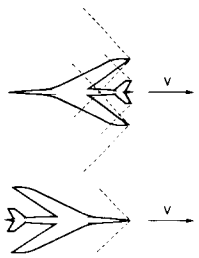

Fig. 3 Computer shows same wave drag for opposite directions of flight.

As a solution of this problem, we find that for any area bounded by two streamlines and two characteristic lines, the distribution of lift and volume yielding the minimum pressure drag (i.e., wave drag + vortex drag) places all the elements of lift and volume near a diagonal lifting line. Such a diagonal line may be considered the limiting configuration of a narrow elliptic wing as illustrated in Fig. 4. Minimum drag occurs when the surface loading of the ellipse is constant and when the thickness is distributed so that the projected cross-sectional areas are those of a Sears Haack body.[4-6]

The foregoing result is of interest not so much as an exact prescription of shape but because it indicates that lift and volume can be concentrated within a narrow dimension having a small wetted area, and hence, small friction drag, provided the "lifting line" extends in a "subsonic" direction. (Linear theory shows an infinite drag if the line becomes supersonic.)

The favorable properties of the oblique wing depend, first of all, on the maintenance of a subsonic type of section flow at supersonic speeds, and this requires that the wing be placed at an angle of yaw such that the component Mach number normal to its long axis be subsonic. If one assumes that the critical "drag divergence" Mach number of the wing sections is 0.7, then the angle of yaw must be such as to reduce the component Mach number to this value. At $M = 1.0$ the angle of yaw required is then 45°.

The advantage of the yawed wing over the swept wing depends on an increased extension of the wing in the flight direction. As is well known, spreading the lift over a greater length diminishes both the sonic-boom intensity and the drag. For a given structural slenderness, the single yawed wing panel may have nearly twice the projected length of the corresponding swept wing.

The foregoing statements may be made more quantitative by referring to various components of the drag as given by linear theory, viz.‡

$$\text{Drag} = C_{D_0} qS_w + \frac{L^2}{\pi q Y^2} + \frac{M^2-1}{2\pi q}\frac{L^2}{\bar{X}_1^{\,2}} + \frac{128q\,\text{Vol.}^2}{\pi\,\bar{X}_2^{\,4}} \qquad (1)$$

Here, S_w is the wing area, Y is the span, $\bar{X}_1$ and $\bar{X}_2$ are

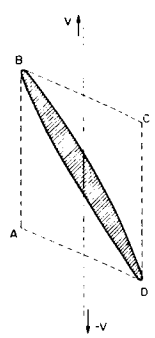

Fig. 4 Optimum distribution of lift and volume within area ABCD.

‡ The distributions of lift and volume assumed in Eq. (1) are those giving the smallest drag consistent with the geometric constraints X and Y.

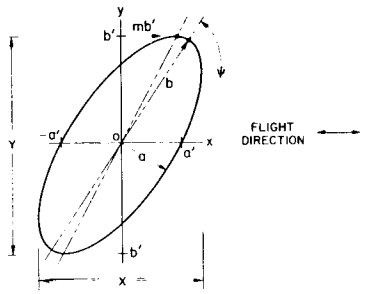

Fig. 5 Oblique ellipse notation.

averaged lengths $X(\theta)$ of the wing as projected by characteristic planes (Mach planes) set at different angles θ around the X axis. The lengths $\bar{X}_1$ and $\bar{X}_2$ are defined by

$$\frac{1}{\bar{X}_1^{\,2}} = \frac{1}{\pi}\int_0^{2\pi} \frac{\sin^2\theta}{X(\theta)^2}\,d\theta \qquad (2)$$

$$\frac{1}{\bar{X}_2^{\,4}} = \frac{1}{2\pi}\int_0^{2\pi} \frac{d\theta}{X(\theta)^4} \qquad (3)$$

At low-supersonic Mach numbers and large angles of sweep or yaw, the lengths $\bar{X}_1$ and $\bar{X}_2$ are close to the actual X-wise extension or length of the wing. Hence, the wave drag due to the lift diminishes approximately as the inverse square of the length while the wave drag due to volume goes down with the inverse fourth power.

The second term of Eq. (1) is the well-known linear formula for the induced drag of a wing having an elliptic span-load distribution. The rules determining the form of large birds, sailplanes, and other subsonic aircraft are evident from the first two terms of Eq. (1). Here, one tries to maximize the span Y and to minimize the wetted area ($2S_w$) by reducing the width of the wing in the flight direction. According to the linear theory (induced drag theory), the drag of the wing at *subsonic* speeds is independent of either the extension or the distribution of lift in the flight direction. Hence, the long narrow straight wing or "lifting line" is ideal at subsonic speeds since it minimizes the wetted area. The success of the rule for increasing L/D by increasing the aspect ratio depends, however, on the maintenance of Kutta-Joukowsky flow. If one tries to approach the "lifting line" too closely, the lifting pressure becomes excessive, and nonlinear effects associated with flow separation or shock losses will intervene. In spite of these limiting phenomena, sailplanes with extreme proportions have achieved L/D ratios as high as 40 or 50 to 1.

The counterpart of the lifting line at supersonic speeds is the oblique lifting line mentioned earlier. Here the appearance of the wave drag [third and fourth terms of Eq. (2)] requires that the wing have as great a length as possible in addition to a wide span and a small surface area. The rules determining the optimum wing form are then similar to those determining the form of a sailplane, except that at supersonic speeds one tries to maximize

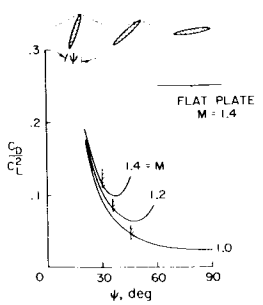

Fig. 6 Drag due to lift; $b/a = 10$.

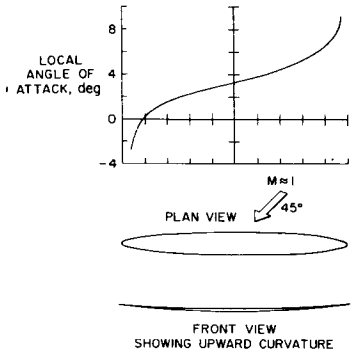

Fig. 7 Upward curvature of wing to maintain uniform lifting pressure $C_L = 0.5$.

both the span and the length in the flight direction together with a minimum surface area.

Again, if one tries to approach the idealized lifting line too closely, nonlinear phenomena will intervene. The lifting pressure may exceed the maximum lift coefficient of the sections, or if the crosswise component Mach number is too high, supercritical shock losses will appear.

For the wing of elliptic planform, the pressure drag associated with the lift (wave drag and vortex drag) is a minimum when the lift is distributed uniformly over the surface. The formula given by linear theory in this case is[5]

$$\Delta C_D = (C_L{}^2/4)\,R.P.\,[\beta^2 - (m + ia/b)^2]^{1/2}$$

where

$$\beta^2 = M^2 - 1$$
$$m = (b^2 - a^2)\sin\psi\cos\psi/b'^2$$
$$b' = (a^2\cos^2\psi + b^2\sin^2\psi)^{1/2}$$
$$a'b' = ab$$

a and b are the major and minor semiaxes of the ellipse and ψ is the complement of the angle of yaw (see Fig. 5).

Figure 6 shows variations of drag due to lift with angle of yaw for an elliptic wing with an axis ratio of 10 to 1. At $M = 1.0$ the value shown is simply the induced drag, or vortex drag, which is, of course, large at large angles of yaw because of the small span. Also, shown on the graphs, are the angles of yaw at which the crosswise Mach number exceeds an assumed critical value of 0.7.

To obtain a reasonably uniform distribution of lifting pressure at large angles of yaw, the wing must be constructed with a certain camber and twist. Calculations of the required camber and twist have been made by R. Carmichael and A. D. Levin of Ames Research Center utilizing the technique of Ref. 6. The amount of twist indicated for a yaw angle of 45°, a lift coefficient of 0.5, and a Mach number near 1.0 is illustrated in Fig. 7. It is seen that the forward going tip must have a positive angle of attack while the angles of the rearmost sections are negative. A practical

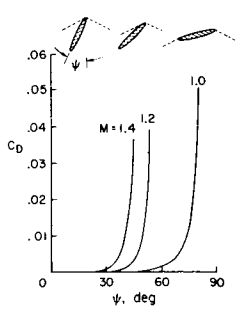

Fig. 8 Drag due to volume; oblique elliptic wings; $t/2a = 0.1$, $b/a = 10$.

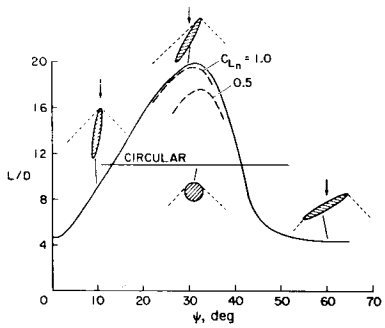

Fig. 9 Estimated lift/drag ratios; $M = 1.4$; $b/a = 10(t/2a) = 1/10$.

way to provide an effective twist that automatically increases with yaw angle is to construct the wing with a certain amount of upward curvature in its unyawed aspect, as shown in the figure. Linear theory is useful for determining gross shape parameters, but cannot, of course, be relied on for critical details. Thus, for the sections of the wing perpendicular to its long axis, one would select airfoil shapes capable of sustaining a high-lift coefficient at a high value of the crosswise component Mach number. Increasing the sweep angle will decrease the component Mach number—but the lift coefficient based on the reduced component velocity will then increase. These considerations involve the critical Mach number and the lift coefficient in combination and point to the choice of airfoil sections that can develop a high ratio of absolute lifting pressure to ambient pressure, i.e.,

$$P_L/P_a = (\gamma/2)M^2C_L$$

without drag penalty.

The minimum wave drag for a given internal volume of the elliptic wing occurs when the thickness ratio of the sections falls off elliptically toward the tips.[5] The formula for the drag due to thickness or volume in the case of the yawed ellipse is given by J. H. B. Smith[7] and the results are plotted in Fig. 8 for an axis ratio of 10 to 1 and a root thickness/chord ratio of 0.1.

The wave drag associated with the volume of the wing shows a steep rise as the long axis of the wing turns into the wind, the influence of the inverse fourth power of the projected length. Here, however, the drag increase associated with nonlinear or supercritical flow over the wing sections may dominate, so that the prediction of linear theory will not be adequate. It is here that the newer developments in supercritical wing sections exemplified by the work of Piercey, Niewland, and Whitcomb may be significant for the antisymmetric wing.

The drag values, given by linear theory together with a suitable estimate of the skin friction, enable the prediction to be made of lift-drag ratios of elliptic wings at varous Mach numbers and yaw angles. Such predictions will be valid if proper account is taken

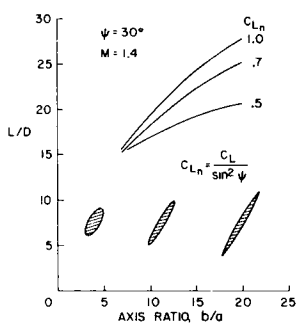

Fig. 10 Variation of L/D with axis ratio showing effect of limitation of the normal lift coefficient C_{L_n}

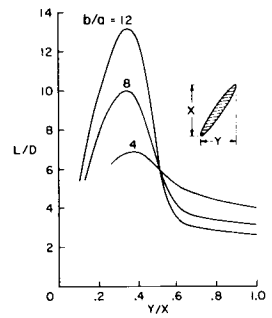

Fig. 11 Estimated L/D ratios for $M = 2.0$ (Refs. 3 and 5).

of the limitations imposed by nonlinear phenomena. Figure 9 taken from Ref. 8 shows such estimates for an ellipse of 10 to 1 axis ratio, 10% thickness and a friction drag coefficient of 0.005. The dotted curves show the effect of limiting the section lift coefficients to values of 1.0 and 0.5, respectively. Figure 10 shows how the increase of L/D with aspect ratio depends on the possibility of achieving rather high section lift coefficients.

Lift-drag values for slanted elliptic wings at $M = 2.0$ have been calculated by J. H. B. Smith[7] and are quoted by D. Kuchemann.[9] Figure 11, adapted from Ref. 7, shows results of this calculation. At $M = 2.0$ peak lift drag ratios occur at $\psi = 15°$–$20°$ corresponding to sweep angles of 70°–75°. The optimum crosswise Mach number indicated by linear theory is approximately 0.7, close to one limit imposed by nonlinear effects.

Wind-Tunnel Tests of Yawed Wing Combinations

Few wind-tunnel experiments have been made to test the predictions for oblique wings of high-aspect ratio. One set of experiments testing yawed and swept wings in conjunction with a fuselage was made by G. H. Holdaway and E. W. Hatfield[10] at Ames Aeronautical Laboratory (now Ames Research Center). The angles of sweep or yaw in these tests was 40° and the wing thickness-chord ratio, approximately 11%. Figure 12 shows the drag at zero lift for two of the combinations tested. At $M = 1.0$ the antisymmetric configuration has much smaller drag, as expected. At $M = 1.15$, however, the normal component of M is approximately 0.88, exceeding the drag rise Mach number of the sections. Beyond this point, the drag of the yawed wing is higher.

Stability and Control of Yawed Wing Aircraft

When the advantages of "subsonic" sweep first became evident, questions were raised about the possibility of flying an airplane with the wing set at a large angle of yaw. Perhaps the earliest experiments to test the flight stability of such an arrangement were made in 1946 by J. P. Campbell and H. M. Drake[11] in the Free-Flight Tunnel at Langley Field, Va.

Campbell and Drake found that the yawed wing avoided the large rolling moment due to sideslip and the consequent short period rolling oscillations of the swept wing. They noted that the flight characteristics of the model remained essentially unchanged up to angles of yaw of 40° and were still satisfactory at 50°. Of special interest is the observation that deflection of the ailerons produced no observable pitching motion in free flight. Evidently, the change of longitudinal lift distribution produced by deflecting the ailerons is almost immediately cancelled by rolling motion of the model. The wing in effect simply follows the helix angle defined by an effective twist associated with the aileron deflection with no significant change in lift distribution. The longitudinal stability and the trimmed lift are then governed by the position of the aerodynamic center and the horizontal tail setting referred to the oblique axis of the wing. Some years later the present writer demonstrated the rather surprising stability of the slanted wing by flying models at the first ICAS meeting in Madrid.

While satisfactory stability can probably be achieved with the yawed wing in the normal flight range, some unusual effects will certainly be apparent. One effect that can be anticipated is a coupling between yaw angle and vertical acceleration, i.e., $\partial L/\partial\psi$. A simple estimate for a wing at 45° yaw shows $(1/L)(\partial L/\partial\psi) = 1$, i.e., 1g per radian of sideslip angle ψ. This value may be compared to the sensitivity of vertical acceleration to angle of attack changes. Assuming $\partial C_L/\partial\alpha = 5$, and a flight-lift coefficient of 1.0 we have $(1/L)(\partial L/\partial\alpha) = 5$; hence, the sensitivity to yaw is about $\frac{1}{5}$ the sensitivity to pitch.

Dynamic coupling between different degrees of freedom is not always undesirable since excessive damping in one mode may be distributed to a mode that would otherwise be deficient. Of course, conventional treatments of stability, which assume bilateral symmetry with the resulting division into "longitudinal" and "lateral" motions, are inapplicable in this case, and a full treatment involving six degrees of freedom as well as aeroelastic deformations will be required.

As is well known, slanted or swept wings tend to stall first at the downstream tips. With the swept wing the loss of lift at the tips leads to a nose-up tendency aggravating the stall. In the case of the slanted wing, the situation would seem worse since the asymmetric stall would lead to bank. The special measures used to control the pitchup tendency of swept wings may quite possibly not be adequate for a yawed wing of high aspect ratio. At best, it is difficult to envision regular landings with the wing in the oblique position, and it seems desirable to incorporate variable geometry so that the wing may be straightened out for landing.

Application to Transport Aircraft

Varying the angle of sweep or yaw has, of course, marked advantages for other flight conditions, such as "holding" at subsonic speeds or adapting the airplane to cruise efficiently at different Mach numbers. Thus, overland flights of a supersonic aircraft will probably be limited to Mach numbers low enough to avoid the sonic boom. The same aircraft may fly much faster over water.

G. H. Lee[12,13] has suggested that the mechanical problems of variable geometry would be effectively eliminated by making an "all-wing" aircraft. Such a step is certainly attractive, but with current densities and loadings seems to be possible only for airplanes of very great size. Lee assumes an airplane designed to cruise at $M = 2.0$ and compares the yawed-wing aircraft with the more conventional delta wing type.

The yawed wing was found capable of carrying twice the payload on the Atlantic flight chiefly because of its better off-design performance. It is anticipated that current supersonic transports may consume as much as 40% of their fuel load in subsonic maneuvers. The ability to cruise or hold efficiently at reduced speed would thus be important for the utility of such aircraft. Current delta wing transports require large amounts of power for takeoff primarily because of large values of weight per unit span. Since the takeoff power diminishes approximately as the $\frac{3}{2}$ power of the span loading, extending the wing span can be very effective in reducing takeoff distance and noise.

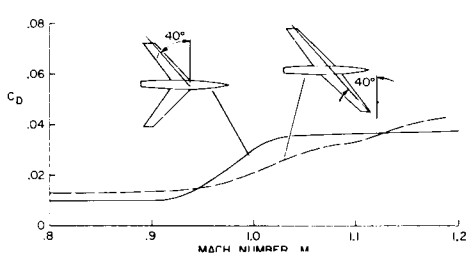

Fig. 12 Drag at zero lift; comparison of yawed and swept wings.[7]

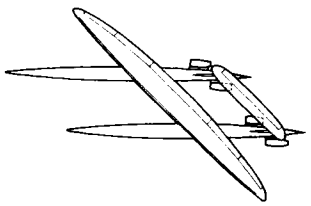

a) Trimmed for $M \cong 1$

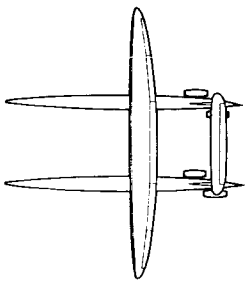

b) Trimmed for $M < 0.7$

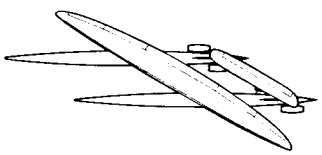

c) Trimmed for $M = 1.3 \sim 1.4$

Fig. 13 Antisymmetric transport aircraft.

Arrangements permitting more conventional values of wing loading and size are shown in Figs. 13(a–c) and 14. The use of two bodies connected across by the wing and horizontal tail in a parallelogram arrangement has certain advantages over the usual arrangement for variable sweep. Shearing the parallelogram does not displace its center of gravity and only slightly displaces the center of lift. The first-order variation of lateral trim with yaw angle can be compensated by constructing the wing with an appropriate curvilinear dihedral as indicated earlier.

As is well known, varying the geometry of the swept wing has several drawbacks. First of all, massive bearings which can carry the wing root bending moment must be used. Secondly, movement of the lifting surface backward at supersonic speeds compounds the normal rearward travel of lifting pressure at these speeds. With the single slanted wing, however, the wing-beam structure is continuous across the pivots and no primary bending loads appear.

Intuitively, one would expect the forward tip of the slanted wing to show a tendency for aeroelastic divergence. Both slanted and swept wings tend to become concave upward when deflected under a gust load, leading momentarily to a tendency to pitch up and increase the load. However, the observation made in the free flight-tunnel[11] is relevant here for the case of the slanted wing. The observation was that increasing the effective angle of attack of the forward wing tip and reducing that of the rearward tip by deflecting the ailerons did not result in observable pitching motion but only in roll.

It can be seen that the elastic deflection of the oblique wing by upward gust is aerodynamically equivalent to a twist, similar to that produced by deflecting ailerons. The air load due to such a twist is, however, almost immediately cancelled by a rolling motion with the helix angle of the roll ($pY/2v$) equal to that of the twist. Hence, the relief provided by the rolling motion should effectively cancel the tendency for aeroelastic divergence in the case of the oblique wing. Stresses that arise during the acceleration of the rolling motion would be proportonal to the inertia in roll of the masses attached to the wing. Since the single fuselage at the center of the wing has almost negligible inertia in roll, one arrives at the surprising conclusion that the one-body arrangement has greater aeroelastic stability than the two-body arrangement. In either case, stability must be assured by adequate wing stiffness and adequate longitudinal stability. Clearly a more complete analysis, taking account of the free motions of the aircraft as well as its elastic deflections will be required.

Table 1 lists estimated components of drag for the arrangement shown in Fig. 13 at $M = 1.0$–1.1 with the wing set at 45°.

Table 1 Drag estimate for antisymmetric-transport aircraft

1)	Wave drag of bodies	$C_D = 0.001$
2)	Wave drag of wing alone	0.0004
3)	Wing-body interference drag	0.0006
4)	Drag + interference of tail surfaces	0.0005
5)	Friction drag of wing	0.004
6)	Nonlinear "form" drag of wing	0.004
7)	Friction drag of bodies	0.0034
8)	Friction drag of tail surfaces	0.0016
9)	Friction drag of engine nacelles	0.0007
		$C_{D_0} = 0.0162$
10)	Lift induced drag at $C_L = 0.575$	$= 0.0162$
		0.0324
	$(L/D)_{max} = 17.7$	

At $M = 1.2$, the yaw angle required is about 50° and the estimated L/D falls to approximately 15. When trimmed for subsonic flight (Fig. 13b) the L/D should exceed 20 to 1.

In conclusion, it is admittedly surprising that aerodynamics and simple mechanics would lead to an antisymmetric form for supersonic flight. The difficulties with such forms may, however, be more conceptual than real and it is hoped that our analysis, though incomplete, will show that such configurations deserve more serious study.

References

[1] Jones, R. T., "Wing Planforms for High Speed Flight," TN 1033, 1946, Rept. 863, 1947, NACA.

[2] von Kármán, T., "Supersonic Aerodynamics Principles and Applications," *Journal of the Aeronautical Sciences*, Vol. 14, No. 7, July 1947, pp. 373–409.

[3] Hayes, W. D., "Linearized Supersonic Flow," Rept. AL 222, June 1947, North American Aviation Inc., Los Angeles; also thesis, California Inst. of Technology.

[4] Jones, R. T., "Possibilities of Efficient High-Speed Transport Airplanes," *Proceedings of Conference on High-Speed Aeronautics*, Polytechnic Inst. of Brooklyn, 1955.

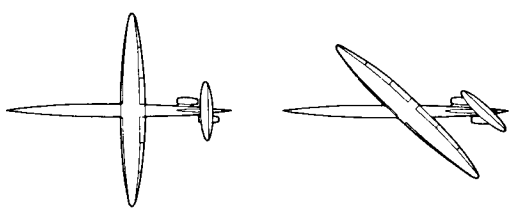

Fig. 14 Oblique winged aircraft with single fuselage.

[5] Jones, R. T., "Theoretical Determination of the Minimum Drag of Airfoils at Supersonic Speeds," *Journal of the Aeronautical Sciences*, Vol. 19, No. 12, Dec. 1952, pp. 813–822.

[6] Carmichael, R. L., Castellano, C. R., and Chen, C. F., "The Use of Finite Element Methods for Predicting the Aerodynamics of Wing-Body Combinations," *Analytic Methods in Aircraft Aerodynamics*, NASA SP 228, 1969, pp. 37–51.

[7] Smith, J. H. B., "Lift/Drag Ratios of Optimized Slewed Elliptic Wings at Supersonic Speeds," *The Aeronautical Quarterly*, Vol. XII, Aug. 1961, pp. 201–218.

[8] Jones, R. T., "Aerodynamic Design for Supersonic Speeds," *Proceedings of the First International Congress in the Aeronautical Sciences, Advances in Aeronautical Sciences*, Pergamon Press, New York, 1959, pp. 34–51.

[9] Kuchemann, D., "Aircraft Shapes and Their Aerodynamics," *Proceedings of the 2nd I.C.A.S., Advances in Aeronautical Sciences*, Vol. 3–4, Pergamon Press, New York, 1962, pp. 221–252.

[10] Holdaway, G. H. and Hatfield, E. W., "Transonic Investigation of Yawed Wings of Aspect Ratios 3 and 6 With a Sears-Haack Body and With Symmetrical and Asymmetrical Bodies Indented for a Mach Number of 1.2," RM A58C03, 1958, NACA.

[11] Campbell, J. P. and Drake, H. M., "Investigation of Stability and Control Characteristics of an Airplane Model With Skewed Wing in the Langley Free-Flight Tunnel," TN 1208, 1947, NACA.

[12] Lee, G. H., comments appended to Kuchemann, D., "Aircraft Shapes and Their Aerodynamics," *Proceedings of the 2nd I.C.A.S. Advances in Aeronautical Sciences*, Vol. 3–4, Pergamon Press, New York, 1962, pp. 221–252.

[13] Lee, G. H., "Slewed Wing Supersonics," *The Aeroplane*, Vol. 100, March 1961, pp. 240–241.

NEW DESIGN GOALS AND A NEW SHAPE FOR THE SST

Robert T. Jones

Ames Research Center

December 1972

Jones, R. T., "New Design Goals and a New Shape for the SST," Astronautics and Aeronautics, vol. 10, no. 12, Dec. 1972, pp. 66-70. © 1972.
Reprinted by permission of the American Institute of Aeronautics and Astronautics.

New Design Goals and a New Shape for the SST

By ROBERT T. JONES
NASA Ames Research Center

A wing which pivots as a whole would permit supersonic aircraft that both avoid sonic boom and reduce noise around airports

New demands on the SST for better economy and less noise make it seem appropriate to consider a radically different concept of design. The shape suggested here: an almost perfectly conventional subsonic aircraft equipped with a straight wing of high aspect ratio, but with the wing arranged so that it can be turned to different oblique angles for flight at different Mach numbers.

Not a new idea at all, turning the wing as a whole instead of sweeping it back from the middle has been proposed several times in the past by the present writer and others.[1-3,10] J. P. Campbell and H. M. Drake studied the stability and control of oblique-winged aircraft in the NACA Free Flight Tunnel more than 25 years ago.[4] Early in the 1960s G. H. Lee considered the advantages of an "all-wing" aircraft arranged so that it could be steered by flying at varying oblique angles.[3,5] In addition to American work, it appears that German aerodynamicists made classified studies of such configurations during WW II. Specifically, Richard Vogt of the Blohm and Voss Company proposed designs of this type, but the projects did not reach the stage of flight test.

ROBERT T. JONES (F) is a senior staff scientist at Ames. He has played a major part in raising the speed of aircraft through developing theory for swept and slender delta wings. In 1946 the AIAA gave him its Sylvanus Albert Reed Award. He has remained with NACA-NASA since 1934, except for seven years with the AVCO Everett Research Lab, where he directed work on cardiac-assist devices. He has also professionally followed an interest in optics.

These proposals do not seem to have been taken very seriously by aircraft designers. In this article, consequently, I would like to call attention to some rather remarkable properties of the oblique wing, report some new discoveries concerning the shape of such wings, and discuss their adaptation to a practical aircraft.

To determine an optimum wing shape, or a shape having a minimum of drag, the designer must first of all adopt some constraint on the dimensions of the wing. Thus in Munk's problem of minimum induced drag the span of the wing is supposed to be limited. With the total lift given, the induced drag or vortex drag is then found to be a minimum when the lift is distributed elliptically over the span. Furthermore, the vortex drag is independent of the distribution of lift in the direction of flight. If a limitation on the maximum lift coefficient is recognized and if the skin friction is taken into account, the optimum wing planform turns out to be a narrow ellipse with its long axis perpendicular to the direction of flight.

For supersonic speeds, in addition to the vortex drag and the friction, the designer must weigh a wave drag associated with the thickness or volume of the wing as well as with the lift distribution. These latter components are not independent of the distribution in the flight direction, but diminish rapidly and continuously as the length of the wing in the flight direction is increased. So the designer must adopt a limitation on the length of the wing as well as the span. In spite of the additional sources

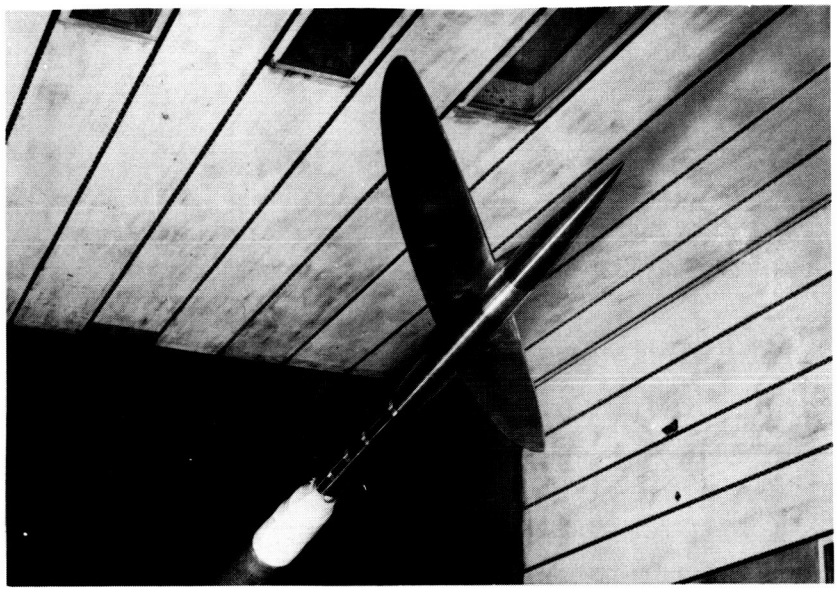

F-2 OBLIQUE-WINGED MODEL IN AMES 11-ft TUNNEL

of drag, the additional constraint, and the fact that the flow equation is now hyperbolic instead of elliptic, the *subsonic elliptic wing reappears as the optimum for supersonic speeds.* The wing merely takes up the greatest "subsonic sweep" angle permitted by the constraints. The minimum drag again occurs when the spanwise loading is elliptical and when the thickness-chord ratio of the wing sections falls off elliptically toward the tips.[1,6]

The optimum supersonic wing planform thus does not have the bilateral (mirror) symmetry of the subsonic wing. It is easy to show that the optimum thin planar wing cannot have the usual arrow or delta form. According to the reversibility theorems of Karman and Hayes a given distribution of lift or volume must have the same wave drag when flying in the opposite direction.[7-8] According to Munk's theorem the vortex drag must be the same also. Hence, if the arrow wing were the optimum, the reversed arrow would also be the optimum.

The reversibility theorems thus indicate that an optimum shape should have fore and aft symmetry, i.e., should look the same for either direction of flight. The oblique ellipse satisfies this criterion, having both longitudinal and lateral symmetry but not bilateral symmetry. The indication of fore and aft symmetry is certainly remarkable since neither the supersonic flow field nor the local distribution of the drag shows this kind of symmetry. Small-disturbance theory identifies a limitation here. Local details of the airfoil section shape are strongly influenced by nonlinear effects, and are, of course, not reversible.

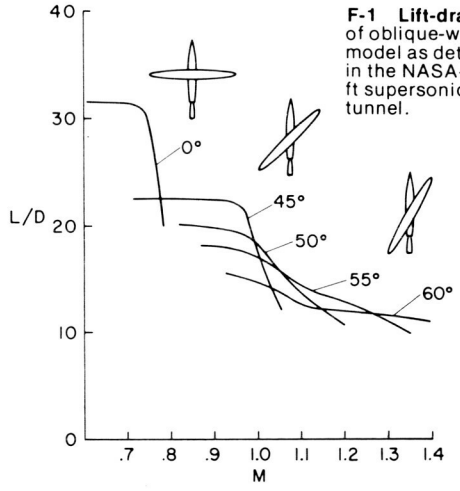

F-1 Lift-drag ratios of oblique-winged model as determined in the NASA-Ames 11-ft supersonic wind tunnel.

Wind-tunnel experiments at NASA Ames Research Center have specifically tested the foregoing theoretical predictions (F-1). The wing has a quasi-elliptic planform of 10-to-1 axis ratio (aspect ratio 12.7). It was attached in the high wing position to a fuselage of 12-to-1 fineness ratio. The airfoil sections, 10% thick, were derived by the conventional NACA "4-digit" formula. To maintain the desired symmetry of the lift distribution in the yawed position, the wing was constructed without twist but with a calculated amount of upward curvature, i.e., a "curvilinear dihedral" in the unyawed position. The wing thus has bilateral symmetry in the unyawed position.

December 1972

With the wing in the oblique positions the curvilinear dihedral has an aerodynamic effect equivalent to that of twist.

A photo here (F-2) shows the elliptic wing-body model in the Ames 11-ft supersonic tunnel. The tests confirmed the theoretical predictions in a very satisfactory way. With the wing straight the maximum lift-drag ratio L/D_{max} exceeded 30 to 1 at Mach numbers (M) up to 0.7, but fell abruptly to 11 at M = 0.8. The wing was then turned to 45 deg and L/D_{max} increased to 20 at M = 0.98. At M = 1.4 and a wing angle of 60 deg, L/D was approximately 11. In every case these values run significantly higher than those previously obtained with arrow wing or delta wing-body combinations.

Since the oblique wing does not have the customary bilateral symmetry, questions of stability and control immediately present themselves. Perhaps the earliest experiments on the controllability of such a configuration were made by H. M. Drake and J. P. Campbell in the NACA's Free Flight Tunnel at Langley Field.[4] They found that the oblique-winged model did not have the lateral rolling oscillations characteristic of swept-wing models and showed satisfactory stability and control up to wing angles of 50 deg. At 60 deg however, the ailerons become ineffective and lateral control could not be maintained.

With the wing set at a large angle, the ailerons are in a position to cause a relatively large pitching moment in addition to their normal rolling action. Campbell and Drake found, however, that aileron deflection in free flight did not produce observable pitching motions. Evidently the rolling motion quickly cancels the unsymmetrical lift distribution produced by the ailerons and the resulting pitching moment.

To gain further experience in the control and stability of oblique winged aircraft, I have made and tested radio-controlled flying models, taking advantage of the highly sophisticated techniques and equipment developed in recent years by model-airplane builders. Photos (F-3 and F-4) show one of the models. The radio control[9] gives linear, proportional deflection of all surfaces and in addition permits variation of the wing skew angle in flight. Takeoffs and landings were made with the wing straight. An enlarged 16-mm movie frame (F-

F-3 RADIO-CONTROLLED FLYING MODEL

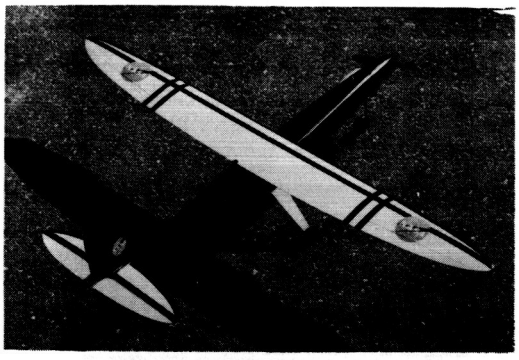

F-4 OBLIQUE WINGED AIRCRAFT

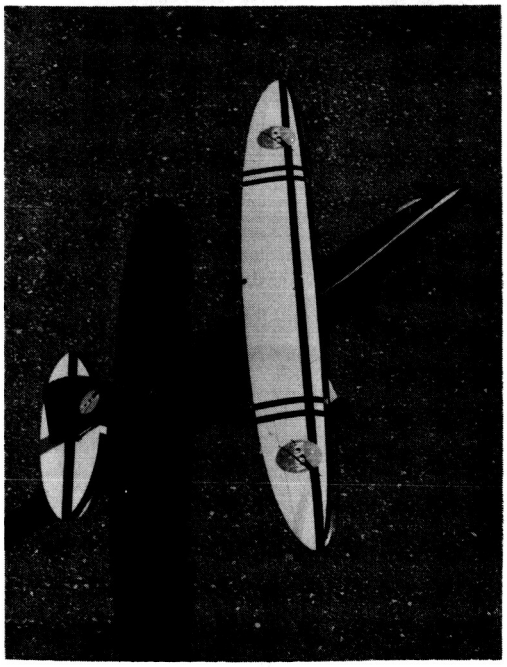

F-5 ENLARGED 16-MM MOVIE FRAME OF R. C. MODEL IN FLIGHT

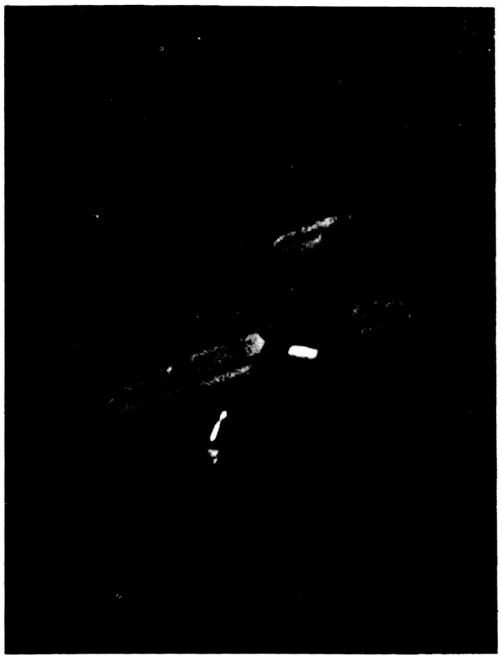

5) shows the model in flight with the wing at 45 deg. Burnett L. Gadeberg of Ames controlled the model.

Variations of wing angle up to and beyond 45 deg produced no apparent changes in stability and only a slight change in lateral trim—requiring a 1- or 2-deg offset of the ailerons. Elevator and aileron effectiveness remained normal and we observed no change in longitudinal trim.

Ordinary maneuvers such as loops and rolls were performed without difficulty at wing angles of 45 deg. Coupling between longitudinal and lateral motions did not appear in aileron rolls, but was quite apparent in the response to elevator control. Thus loops performed with the wing at 45 deg appeared to take the form of a 45-deg helix, indicating that the rotation produced by the elevator tends to align with the long axis of the wing. With the left tip forward, use of the elevator in a left turn tended to steepen the bank angle. Analysis shows that in this case a certain amount of aileron deflection must be employed with the elevator to prevent banking toward the forward tip.

Varying the sweep by turning the wing as a whole has several practical advantages over the usual "swing wing" design. It keeps the wing structure continuous across the pivot and makes the primary load on the pivot tension. With separate wing panels pivoted at the root, however, much greater loads develop on the pivots (F-6). Also, sweeping the wing panels back for high-speed flight displaces the center of lift rearward, compounding the normal rearward center-of-pressure shift at these speeds. Turning the wing as a whole, however, does not displace the centroid of area relative to the center of gravity (F-7). Even with fixed geometry the structure of the bilaterally symmetric wing is less favorable because of the unbalanced torsion at the wing root. The unbalanced torsion may be equated approximately to increase in beam length for the swept wing (F-8). Finally, conforming to the "area rule," the swept wing requires a rather localized and deep indentation of the fuselage. The optimum fuselage shape for the oblique wing, however, is much more nearly cylindrical (F-9).

The artist's rendering on the last page of this article shows a conceptual version of a long-range supersonic transport utilizing the oblique wing. By attaching the wing to the fuselage so that it can be turned to different angles, flight at different Mach numbers can be made with the utmost efficiency. Thus, for overland flights at speeds slow enough to avoid the sonic boom (M 1.0-1.2) the wing angle must be 45-55 deg. For overwater flights at M 1.4, 60-65 deg would be needed. It is anticipated that landings and takeoffs would be made with the wing in the straight

F-6 CONTINUOUS WING STRUCTURE; NO BENDING LOAD ON PIVOTS

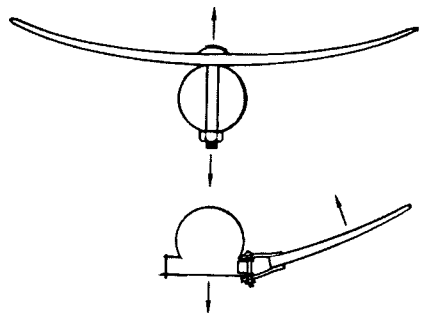

F-7 CENTROID OF LIFTING AREA NOT DISPLACED BY ROTATION

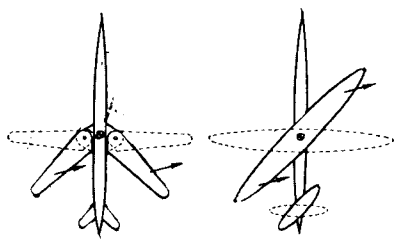

F-8 STRAIGHT-BEAM STRUCTURE.

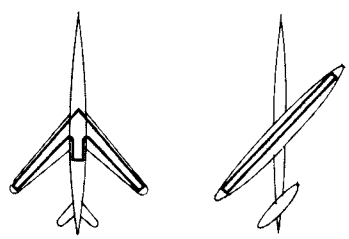

F-9 SMOOTH AREA DISTRIBUTION FOR FUSELAGE

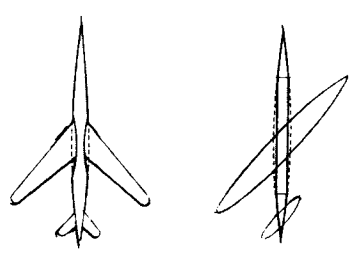

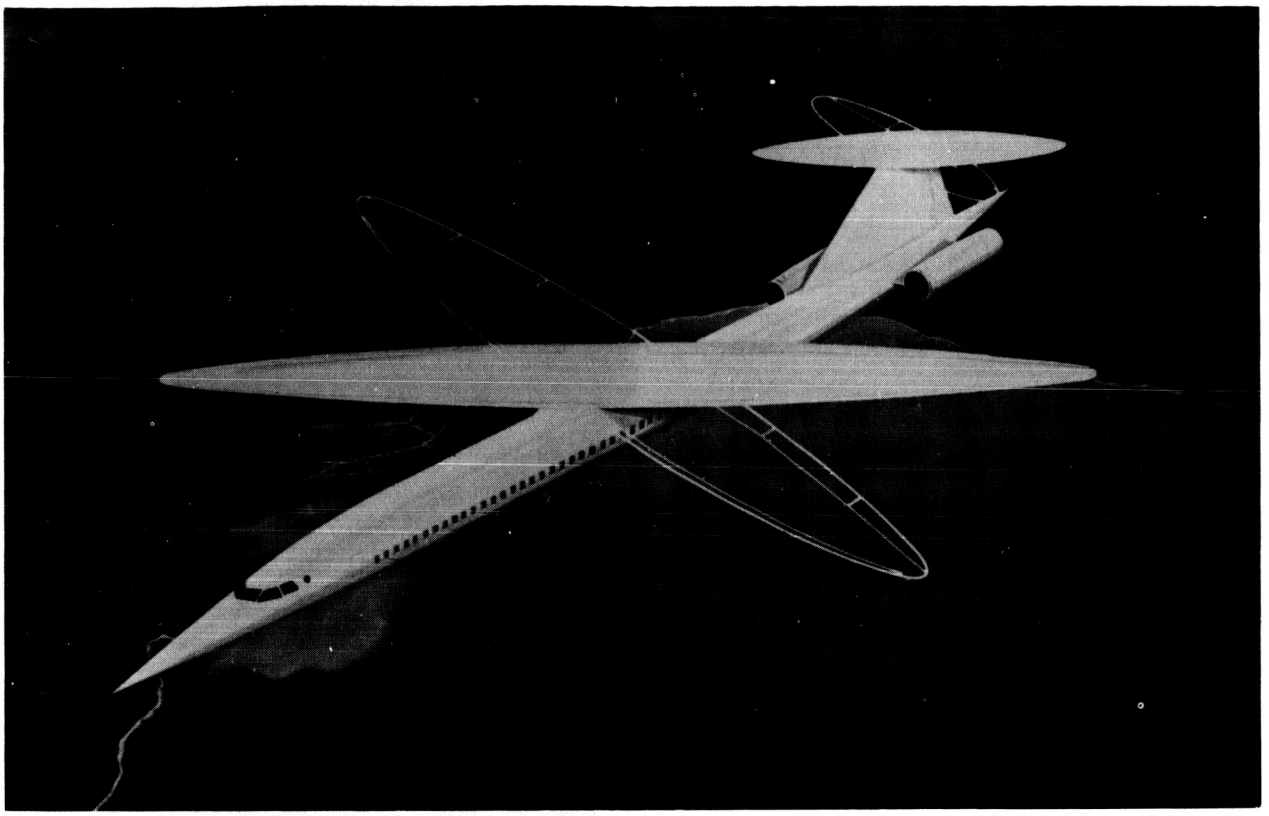

Concept of a pivoting-wing SST for commercial operations.

position. With a straight wing of high aspect ratio, the energy required for takeoff should be less than that required by conventional *subsonic* jets and about one-fourth that required by current supersonic transports. And limiting the maximum cruise Mach number to 1.4 will permit the use of inherently quiet fanjet engines. Thus it seems that a design of the type considered could effectively meet current demands for voiding sonic boom and reducing noise around airports.

References

1. Jones, R. T., "Theoretical Determination of the Minimum Drag of Airfoils at Supersonic Speeds," *Journal of the Aeronautical Sciences*, Vol. 19, No. 12, Dec. 1952, pp. 813-822.

2. Jones, R. T., "Aerodynamic Design for Supersonic Speeds," Proceedings of the First International Congress in the Aeronautical Sciences, Madrid, Sept. 1958, *Advances in Aeronautical Sciences*, Pergamon Press, N.Y., 1959, pp. 34-51.

3. Lee, G. H., comments appended to Kuchemann, D., "Aircraft Shapes and Their Aerodynamics," Proceedings of the 2nd ICAS, *Advances in Aeronautical Sciences*, Vol. 3-4, Pergamon Press, N.Y., 1962, pp. 221-252.

4. Campbell, J. P. and Drake, H. M., "Investigation of Stability and Control Characteristics of an Airplane Model with Skewed Wing in the Langley Free-Flight Tunnel," TN1208, 1945, NACA.

5. Lee, G. H., "Slewed Wing Supersonics," *The Airplane*, Vol. 100, March 3, 1961 pp. 240-241.

6. Smith, J. H. B., "Lift/Drag Ratios of Optimized Slewed Elliptic Wings at Supersonic Speeds," *The Aeronautical Quarterly*, Royal Aeronautical Quarterly, Royal Aeronautical Society, Vol. XII, Aug. 1961, pp. 201-218.

7. Von Karman, Th., "Supersonic Aerodynamics Principles and Applications," *Journal of the Aeronautical Sciences*, Vol. 14., No. 7, July 1947, pp. 373-409.

8. Hayes, W. D., "Linearized Supersonic Flow," Rep. AL 222, June 1947, North American Aviation, Inc., Los Angeles, also Thesis, California Institute of Technology.

9. Kraft Systems, Inc., 450 W. California Avenue, Vista, Calif. 92083.

10. Jones, R. T., "Reduction of Wave Drag by Antisymmetric Arrangement of Wings and Bodies," *AIAA J.*, Vol. 10, No. 2, Feb. 1972, pp. 171-176. ■

TECHNICAL MEMORANDUM X-62,256

AN EXPERIMENTAL INVESTIGATION OF THREE OBLIQUE-WING AND BODY COMBINATIONS AT MACH NUMBERS BETWEEN 0.60 AND 1.40

Lawrence A. Graham, Robert T. Jones and Frederick W. Boltz

Ames Research Center

April 1973

CONTENTS

	Page
SUMMARY	1
INTRODUCTION	1
NOMENCLATURE	2
TEST FACILITY	4
MODEL DESCRIPTION	5
TESTING AND PROCEDURE	5
RESULTS AND DISCUSSION	5
REFERENCES	7
TABLES	
1. MODEL GEOMETRY	8
2. WING GEOMETRIC DATA	9
3. BODY DIMENSIONAL DATA	16
4. TEST CONDITIONS	22
5. INDEX OF DATA FIGURES	23
FIGURES	
1. AXIS SYSTEMS	24
2. OBLIQUE-WING/BODY MODEL DETAILS AND PHOTOGRAPH	25
3. WING-SECTION DRAWINGS	30
4. DATA	31

(THIS PAGE INTENTIONALLY LEFT BLANK)

AN EXPERIMENTAL INVESTIGATION OF THREE OBLIQUE-WING AND BODY COMBINATIONS AT MACH NUMBERS BETWEEN 0.60 AND 1.40

By Lawrence A. Graham, Robert T. Jones and Frederick W. Boltz

Ames Research Center

SUMMARY

An experimental investigation was conducted in the Ames 11- by 11-Foot Transonic Wind Tunnel to determine the aerodynamic characteristics of three oblique high aspect ratio wings in combination with a high fineness-ratio Sears-Haack body. The three wings had the same elliptical planform and base line curvature but had different airfoil sections. One wing had an airfoil section designed to have a lift coefficient of 1.0 at a Mach number of 0.7, another to have shock-free supersonic flow over the upper surface, and the other to have a lift coefficient of 1.3 at a Mach number of 0.6.

Longitudinal and lateral-directional stability data were obtained at wing yaw angles of 0°, 45°, 50°, and 60° over a test Mach number range from 0.6 to 1.4 for angles of attack between -7°and 9°. Reynolds numbers for the study were 4 and 6 million per foot. Flow-visualization studies were made to examine the nature of the flow on the wing surfaces.

Notable differences were found in the aerodynamic characteristics of the three wing-body combinations, particularly in the lateral-directional characteristics. The aerodynamic efficiency of the three wing-body combinations was in most instances about the same, with two of the wings generally exhibiting slightly higher maximum values. The other wing was slightly more efficient at Mach numbers where supercritical flow existed on the wings.

INTRODUCTION

Theoretical predictions and indications related to the oblique-wing concept have been extensively discussed (as in references 1 and 2) and recently investigated experimentally in the NASA-Ames 11- by 11-Foot Transonic Wind Tunnel.

Theory indicates that in order to achieve maximum efficiency the oblique angle of the wing must be varied with Mach number in such a way that the component of velocity normal to the long axis of the wing remains subsonic

and below the "drag rise" Mach number of the wing sections. The sections taken in the planes perpendicular to the long axis then have a "subsonic" shape with a rounded leading edge and camber to produce a high lift coefficient at a high critical Mach number. Three wings, having different airfoil sections in the planes perpendicular to the long axis of the wing, have been tested in the Ames 11- by 11-Foot Transonic Wind Tunnel. All wings have the same elliptical planform with an elliptic axis ratio of 10 to 1, an unswept aspect ratio of 12.7 and a thickness-chord ratio of 0.1.

One wing has an airfoil section derived by the well known NACA "4 digit" formula (see reference (3)). The shape parameters for the airfoil were selected on the basis of previous wind tunnel experience with the intention of achieving as high a lift coefficient as possible at a critical Mach number of 0.7. The section has a relatively blunt leading edge with a radius of 2 percent of the chord.

Another airfoil tested was designed by Bauer, Garabedian and Korn of the Courant Institute, New York University using a hodograph method to obtain a shock-free supersonic zone over the upper surface. Data on this airfoil are given as example 1 (figure 5 in Reference (4)).

The other airfoil was designed for purely subsonic flow at a Mach number Of 0.60. This airfoil has more camber and a design lift coefficient of 1.3 (based on the normal component velocity).

NOMENCLATURE

The axis systems and sign convention are shown in figure 1. Lift and drag are presented in the stability-axis coordinate system and all other forces and moments are presented in the body-axis coordinate system. Because the data were computer plotted the corresponding plot symbol, where used, is given together with the conventional symbol.

Symbol	Plot Symbol	Definition
b		wing span
c		wing chord
c_{root}		wing root chord
C_D	CD	drag coefficient, drag/qS

C_ℓ	CBL	rolling-moment coefficient, rolling moment/qSb
C_L	CL	lift coefficient, lift/qS
C_m	CLM	pitching-moment coefficient, pitching moment/qSc_{root}
C_n	CYN	yawing-moment coefficient, yawing moment/qSb
C_Y	CY	side-force coefficient, side force/qS
H		maximum vertical distance from wing reference plane to wing base line at 0.4c for W_1
L		longitudinal distance along the body from body maximum diameter
(L/D)	L/D	lift-drag ratio
M	MACH	free-stream Mach number
q		free-stream dynamic pressure
Re	RN/L	unit Reynolds number, million per foot
S		wing area
t		wing thickness
W		body width
x		Cartesian coordinate
Y-Up		maximum distance from wing base line to wing upper surface measured perpendicular to the wing base line
Y-Lo		maximum distance from wing base line to wing lower surface measured perpendicular to the wing base line
Z-Up		vertical distance from wing chord to wing upper surface
Z-Lo		vertical distance from wing chord to wing lower surface
z		Cartesian coordinate
α	ALPHA	angle of attack

β	BETA	angle of sideslip
Λ	LAMBDA	angle between a perpendicular to the body longitudinal axis and the 0.25 chord line of the wing measured in a horizontal plane
ϕ		angle between vertical plane and the intersection of the circular portion of the body with the rectangular portion of the body

Subscripts

max	maximum value
0	zero trailing edge deflection
1	denotes original wing
2	denotes wing number 2, wing with 0.013c leading edge radius
4	denotes wing number 4, wing with 0.005c leading edge radius

Configuration Code

W	W	wing
F	F	trailing edge segment
B	B	body

TEST FACILITY

The tests were conducted in the Ames 11- by 11-Foot Transonic Wind Tunnel, which is a variable density, closed return, continuous flow type. This tunnel has an adjustable nozzle (two flexible walls) and a slotted test section to permit transonic testing over a Mach number range continously variable from 0.4 to 1.4.

MODEL DESCRIPTION

The model consisted of an elliptical planform wing mounted on top of a Sears-Haack body as shown in figure 2(a). Pertinent dimensions of the wings investigated and of the Sears-Haack body, which was common to all configurations, are given in tables 1 through 3 and in figures 2(a) through (d). A photograph of the model is shown in figure 2(e). The wing was pivoted in the horizontal plane about the 0.4 root chord point to obtain oblique angles of 0°, 45°, 50°, and 60°as shown in figure 2(a).

All wings had elliptical planforms with a straight 25-percent chord line (fig. 2(a)). Wing number 1, W_1, (see ref. 1) had an NACA 3610-02,40 airfoil section (fig. 2(d)) perpendicular to the unswept chord line. The second wing tested (wing number 2, W_2) had an airfoil section (fig. 3 (a)) designed using a hodograph method to obtain a shock-free supersonic zone over the upper surface. The third wing tested (wing number 4, W_4) had a subsonic airfoil section (fig. 3(b)) designed for a lift coefficient of 1.3 at a Mach number of 0.60. Airfoil coordinates for the three wings are given in table 2.

TESTING AND PROCEDURE

The models were sting mounted through the base of the model body as shown in figures 2(a) and 2(c), and force and moment data were obtained from an internally mounted six-component strain-gage balance. The moment center was on the body center line and longitudinally at the wing pivot point ($0.4c_{root}$). Tests were conducted at Reynolds numbers of 4 and 6 million per foot. The angle-of-attack range, selected to define maximum lift-to-drag ratio for each configuration, was nominally ± 8 degrees. Six component force and moment data were obtained for the wing at oblique angles of 0°, 45°, 50°, and 60°.

The measured balance data were adjusted to a condition corresponding to free-stream static pressure on the model base. The Mach number range for each oblique angle tested is shown in table 4.

RESULTS AND DISCUSSION

A complete index to the data figures is given in table 5. Among the noteworthy results of these experiments are the exceptionally high lift-drag ratios obtained in the transonic and low supersonic speed ranges.

Lift-to-drag ratios for the three wings are shown in figures 4 through 7 for the test Mach numbers and wing-sweep angles. Wing number 2 shows a maximum L/D value of 31 for M = 0.80 and zero wing sweep (fig. 4, pg. 21). Wing numbers 1 and 4 both had a maximum L/D value of 11 at M = 1.40 and 60° of wing sweep (fig. 7, pg. 140).

Wing number 2, which was designed to operate with shock-free supersonic flow over the upper surface showed the expected behavior. At zero wing sweep this airfoil extended the useful Mach number from 0.70 to approximately 0.80. At 60° sweep, however, the crosswise component of Mach number at M = 1.40 is only 0.70, not sufficient to achieve the design condition of this wing. Further refinement of airfoil selection for such oblique wings will depend on the extension of three dimensional wing theory beyond the linearized formulas now in use and probably also on more detailed wind tunnel studies.

Another noteworthy feature of the test results is the remarkably small shift of center of pressure for wing sweep variations from 0° to 60°. Comparing the pitching moment of the straight wing at M = 0.70 (fig. 4, pg. 9) with that of the same wing turned 60° shows only moderate changes in spite of the fact that the fore and aft dimension (streamwise chord) of the wing increased almost ten-fold when the wing was swept.

A similar result can be observed in the rolling moment measurements. Figure 4, page 13 shows rolling moments measured on the wings in the unyawed position. Presumably such moments arise from accidental manufacturing irregularities of the models. Figure 7, page 104 shows rolling moments of the same wings turned 60°. In the normal flight range these are only slightly greater than those developed on the straight, supposedly symmetrical wings. At larger angles of attack, however, effects of premature stalling of the downstream tip are observed on the oblique wings. This behavior may be compared with the premature tip stalling encountered with more conventional swept-back wings. With conventional swept-back wings stalling of the tips causes the airplane to pitch up. With the oblique wing only one tip stalls and the airplane may be expected to roll.

Ames Research Center
National Aeronautics and Space Administration
Moffett Field, California 94035

April 2, 1973

REFERENCES

1. Graham, Lawrence A.; Jones, Robert T.; and Boltz, Frederick W.: An Experimental Investigation of an Oblique-Wing and Body Combination at Mach Numbers Between 0.60 and 1.4. NASA TM X-62,207, December 1972.

2. Jones, R. T.: New Design Goals and a New Shape for the SST. Astronautics and Aeronautics, December, 1972.

3. Abbott, Ira H.; and Von Doenhoff, Albert E.: Theory of Wing Sections. Dover Publications 60-1601, New York, 1959.

4. Bauer, F.; Garabedian, P.; and Korn, D.: Supercritical Wing Section. Lecture Notes in Economics and Mathematical Systems, No. 66. Springer Verlag, Berlin, Heidelberg, New York, 1972.

TABLE 1. - MODEL GEOMETRY

Body (Sears-Haack)	
Length	
Closed	45.25 in
Cut-off	36.00 in
Maximum Diameter	3.37 in
Wing	
Planform 10:1 ellipse about c/4	
Span (reference)	60.00 in
Area (reference)	278.00 in^2
Root chord	6.00 in
Aspect ratio	12.7
Maximum t/c	0.10
Incidence	0°
0.25c sweep	0°
Maximum thickness location, percent chord	40
Section	
W_1	NACA 3610-02,40
W_2	Garabedian, 0.013c nose radius
W_4	Garabedian, 0.005c nose radius

TABLE 2. - WING GEOMETRIC DATA*

Wing 1, W_1

Semi-Span	Chord	Y-Up/c	Y-Lo/c	H/c
0.000	6.000	.0775	.0298	.0000
1.000	5.997	.0775	.0298	-.0002
2.000	5.987	.0775	.0298	-.0008
3.000	5.970	.0775	.0298	-.0017
4.000	5.946	.0775	.0298	-.0029
5.000	5.915	.0775	.0298	-.0042
6.000	5.879	.0775	.0298	-.0056
7.000	5.834	.0775	.0298	-.0072
8.000	5.783	.0775	.0298	-.0090
9.000	5.724	.0775	.0298	-.0107
10.000	5.657	.0775	.0298	-.0124
10.986	5.583	.0775	.0298	-.0140
11.850	5.512	.0775	.0298	-.0154
12.635	5.442	.0775	.0298	-.0162
13.356	5.373	.0775	.0298	-.0175
14.024	5.304	.0775	.0298	-.0185
14.645	5.237	.0775	.0298	-.0193
15.226	5.170	.0775	.0298	-.0199
15.772	5.104	.0775	.0298	-.0206
16.286	5.039	.0775	.0298	-.0210
16.772	4.975	.0775	.0298	-.0213
17.233	4.911	.0775	.0298	-.0218
17.671	4.849	.0775	.0298	-.0221
18.087	4.787	.0775	.0298	-.0221
18.483	4.726	.0775	.0298	-.0222
18.862	4.666	.0775	.0298	-.0225
19.224	4.606	.0775	.0298	-.0224
19.570	4.548	.0775	.0298	-.0224
19.902	4.490	.0775	.0298	-.0225
20.220	4.432	.0775	.0298	-.0223
20.977	4.289	.0775	.0298	-.0219
21.533	4.178	.0775	.0298	-.0215
22.046	4.069	.0775	.0298	-.0209
22.523	3.963	.0775	.0298	-.0202
22.966	3.860	.0775	.0298	-.0194
23.379	3.760	.0775	.0298	-.0186
23.763	3.662	.0775	.0298	-.0177

* Semispan and chord are in inches

TABLE 2. - WING GEOMETRIC DATA - Continued.

Wing 1, W_1

Semi-Span	Chord	Y-Up/c	Y-Lo/c	H/c
24.123	3.567	.0775	.0298	-.0168
24.459	3.474	.0775	.0298	-.0158
24.773	3.384	.0775	.0298	-.0148
25.068	3.296	.0775	.0298	-.0137
25.344	3.210	.0775	.0298	-.0125
25.604	3.127	.0775	.0298	-.0112
25.848	3.046	.0775	.0298	-.0098
26.077	2.966	.0775	.0298	-.0088
26.293	2.889	.0775	.0298	-.0076
26.495	2.814	.0775	.0298	-.0060
26.686	2.741	.0775	.0298	-.0047
26.866	2.670	.0775	.0298	-.0034
27.036	2.600	.0758	.0292	-.0023
27.196	2.533	.0738	.0284	-.0008
27.347	2.467	.0721	.0276	.0008
27.489	2.403	.0703	.0270	.0022
27.624	2.340	.0688	.0265	.0034
27.751	2.279	.0671	.0259	.0048
27.870	2.220	.0653	.0252	.0063
27.984	2.163	.0643	.0245	.0079
28.091	2.106	.0613	.0237	.0095
28.345	1.965	.0590	.0229	.0137
28.524	1.859	.0565	.0221	.0167
28.684	1.758	.0546	.0210	.0205
28.825	1.662	.0529	.0205	.0241
28.952	1.572	.0515	.0197	.0274
29.064	1.487	.0504	.0195	.0309
29.164	1.406	.0491	.0185	.0349
29.254	1.330	.0481	.0180	.0383
29.333	1.258	.0469	.0183	.0429
29.405	1.190	.0462	.0176	.0471
29.468	1.125	.0453	.0178	.0516
29.529	1.064	.0442	.0169	.0555
29.600	.977	.0440	.0174	.0624
29.700	.846	.0449	.0165	.0757
29.800	.692	.0448	.0173	.0968
29.900	.489	.0450	.0163	.1431
30.000	.000	.0000	.0000	∞

TABLE 2. - WING GEOMETRIC DATA - Continued.

Wing 2, W_2

x/c	z/c	x/c	z/c	x/c	z/c
-.000259	.002799	.014919	.020037	.044480	.032330
-.000253	.003206	.014942	.020032	.044901	.032450
-.000245	.003358	.016227	.020802	.045314	.032567
-.000236	.003508	.016719	.021082	.045720	.032681
-.000225	.003655	.017617	.020584	.046122	.032792
-.000213	.003800	.018626	.022130	.046523	.032902
-.000198	.003941	.019108	.022389	.046935	.033011
-.000183	.004080	.020538	.023127	.047351	.033125
-.000156	.004281	.020582	.023202	.047772	.033236
-.000117	.004537	.022320	.024010	.048201	.033349
-.000068	.004814	.023832	.024723	.048640	.033462
-.000004	.005114	.024277	.024927	.049093	.033578
.000077	.005437	.025427	.025443	.049562	.033696
.000181	.005788	.026636	.025968	.050049	.033818
.000313	.006172	.027858	.026482	.050556	.033943
.000482	.006592	.031474	.027994	.051086	.034072
.000690	.007047	.031980	.028189	.051640	.034205
.000939	.007531	.032497	.028386	.052221	.034343
.001226	.008037	.032945	.028555	.052829	.034485
.001500	.008482	.033498	.028761	.053467	.014633
.001816	.008963	.034020	.028953	.054135	.034785
.002177	.009476	.034543	.029143	.054835	.034943
.002581	.010017	.035082	.029337	.055566	.035106
.003024	.010576	.035537	.029499	.056330	.035273
.003584	.011242	.036082	.029691	.057127	.035445
.003741	.011420	.036601	.029872	.057955	.035623
.003823	.011512	.037112	.030047	.058816	.035803
.004052	.011764	.037619	.030220	.059707	.035987
.004286	.012016	.038349	.030423	.060629	.036175
.004774	.012520	.038942	.030619	.061578	.036366
.005286	.013023	.039521	.030809	.062555	.036559
.005821	.013524	.040086	.030991	.063556	.036754
.006380	.014024	.040636	.031166	.064581	.036954
.006993	.014548	.041171	.031335	.065628	.037148
.007703	.015127	.041689	.031496	.066694	.037346
.008523	.015766	.042191	.031650	.067779	.037543
.009472	.016473	.042677	.031798	.068883	.037743
.010371	.017251	.043148	.031939	.070005	.037942
.011837	.018106	.043605	.032074	.071146	.038140
.013283	.019037	.044048	.032204	.072311	.038339

TABLE 2. - WING GEOMETRIC DATA - Continued.

Wing 2, W_2

x/c	z/c	x/c	z/c	x/c	z/c
.073503	.038540	.420081	.058866	.950000	.030800
.074730	.038742	.437854	.059084	.955000	.029550
.076001	.038949	.455795	.059249	.960000	.028400
.077328	.039260	.473858	.059360	.965000	.027150
.078729	.039379	.491996	.059416	.970000	.026000
.080223	.039609	.510163	.059416	.975000	.024800
.081835	.039851	.528315	.059362	.980000	.023150
.083594	.040110	.546409	.059253	.985000	.021750
.085532	.040390	.564404	.059088	.990000	.020000
.087689	.040654	.582260	.058870	.995000	.018350
.090107	.040976	.599941	.058599	1.000000	.016250
.092832	.041331	.617410	.058275	1.000000	.011500
.095916	.041721	.634633	.057900	.996930	.012309
.099411	.042151	.651577	.057474	.992183	.013346
.103374	.042623	.668211	.056998	.984458	.014902
.107860	.043139	.684502	.056473	.974208	.016590
.112926	.043700	.708417	.055897	.969617	.017227
.118625	.044307	.715919	.055271	.964869	.017799
.125010	.044957	.730965	.054590	.959372	.018372
.132127	.045650	.745497	.053849	.953100	.018917
.140017	.046380	.759430	.053036	.946064	.019625
.148713	.047144	.772646	.052143	.938325	.020235
.158242	.047936	.785031	.051216	.935056	.020502
.168619	.048749	.796561	.050304	.930826	.020947
.179851	.049576	.807278	.049408	.918220	.021598
.191936	.050410	.817242	.048524	.902981	.021796
.204859	.051244	.826502	.047657	.892173	.021526
.218596	.052066	.835095	.046812	.888918	.021610
.233111	.052876	.874772	.042382	.880800	.021338
.248369	.053661	.881389	.041550	.873936	.021038
.261499	.054286	.886521	.040890	.867017	.020651
.275210	.054893	.893973	.039903	.860072	.020179
.289481	.055476	.898775	.039245	.853133	.019744
.304289	.056033	.905727	.038267	.839225	.018253
.319605	.056559	.907539	.038022	.829378	.016944
.335396	.057049	.917272	.036560	.821363	.015678
.351625	.057502	.923762	.035541	.816907	.014932
.368251	.057912	.932355	.034142	.808726	.013456
.385233	.058278	.936350	.033414	.804319	.012614
.402526	.058597	.946280	.031675	.799694	.011703

TABLE 2. - WING GEOMETRIC DATA - Continued.

Wing 2, W_2

x/c	z/c	x/c	z/c	x/c	z/c
.794844	.010726	.511412	-.035139	.121072	-.037610
.789767	.009690	.502244	-.035896	.116816	-.037243
.784463	.008599	.492898	-.036626	.113390	-.036946
.778938	.007454	.483403	-.037324	.105636	-.036223
.773195	.006281	.473787	-.037990	.103263	-.035985
.770172	.005655	.464063	-.038623	.098167	-.035466
.767702	.005121	.454281	-.039217	.097820	-.035434
.762277	.004017	.444445	-.039774	.093341	-.034950
.760899	.003714	.434573	-.040292	.088930	-.034484
.756939	.002880	.419722	-.041001	.982042	-.033633
.751239	.001707	.404842	-.041625	.078825	-.033212
.747425	.000931	.389941	-.042168	.071082	-.032134
.746296	.000679	.375014	-.042632	.066312	-.031417
.741604	-.000291	.360044	-.043017	.064241	-.031090
.736259	-.001371	.342450	-.043369	.060793	-.030528
.735732	-.001500	.327518	-.043585	.058050	-.030061
.729835	-.002691	.326625	-.043595	.055317	-.029577
.727639	-.003147	.316009	-.043698	.053273	-.029201
.722656	-.004155	.310610	-.043734	.051242	-.028817
.718286	-.005028	.307293	-.043753	.049218	-.028421
.716080	-.005470	.294383	-.043786	.047205	-.028014
.713785	-.005940	.291384	-.043785	.045207	-.027596
.707523	-.007170	.279420	-.043752	.043227	-.027167
.706231	-.007440	.277862	-.043743	.041267	-.026727
.698425	-.008951	.264209	-.043634	.039329	-.026276
.696716	-.009296	.248682	-.043426	.037419	-.025814
.687638	-.011037	.245962	-.043375	.035541	-.025341
.687600	-.011037	.233501	-.043129	.033698	-.024858
.679061	-.012627	.229561	-.043038	.032960	-.024651
.674766	-.013435	.217370	-.042719	.032547	-.024546
.658057	-.016407	.203264	-.042270	.031022	-.024119
.643396	-.018887	.194206	-.041935	.029605	-.023700
.627219	-.021469	.185170	-.041562	.029466	-.023667
.609744	-.024068	.176128	-.041149	.027631	-.023102
.591249	-.026591	.167067	-.040695	.027484	-.023056
.591100	-.026613	.157951	-.040190	.027462	-.023057
.575291	-.028602	.151106	-.039779	.026683	-.022817
.557428	-.030667	.143697	-.039302	.025394	-.022392
.537560	-.032741	.136226	-.038784	.024693	-.022149
.520372	-.034358	.128686	-.038222	.024151	-.021972

TABLE 2. - WING GEOMETRIC DATA - Continued.

Wing 2, W_2

x/c	z/c	x/c	z/c	x/c	z/c
.022570	-.021413	.008173	-.013944	.002392	-.006487
.021473	-.021007	.008077	-.013865	.002258	-.006226
.021444	-.020997	.007909	-.013723	.002052	-.005812
.020750	-.020723	.007763	-.013599	.001912	-.005522
.020483	-.020627	.007667	-.013515	.001770	-.005221
.019814	-.020355	.007626	-.013479	.001557	-.004748
.018965	-.020017	.007561	-.013422	.001190	-.003936
.018883	-.019975	.007471	-.013340	.000948	-.003315
.017959	-.019583	.007085	-.012984	.000745	-.002757
.017228	-.019263	.007007	-.012909	.000576	-.002257
.016508	-.018936	.006963	-.012866	.000437	-.001812
.015799	-.018603	.006744	-.012655	.000321	-.001417
.015105	-.018266	.006485	-.012390	.000246	-.001147
.014428	-.017925	.006207	-.012094	.000172	-.000871
.013772	-.017582	.005911	-.011701	.000098	-.000589
.013138	-.017239	.005596	-.011390	.000000	-.000000
.012530	-.016898	.005266	-.010982	-.000009	.000317
.011950	-.016559	.004928	-.010542	-.000081	.000604
.011401	-.016226	.004591	-.010082	-.000131	.000896
.010882	-.015900	.004263	-.009613	-.000170	.001188
.010397	-.015583	.003950	-.009146	-.000201	.001475
.009945	-.015276	.003655	-.008688	-.000225	.001757
.009526	-.014982	.003399	-.008278	-.000243	.002032
.009140	-.014700	.003141	-.007841	-.000254	.002297
.008787	-.014433	.002886	-.007397	-.000260	.002553
.008465	-.014181	.002636	-.006944		

TABLE 2. - WING GEOMETRIC DATA - Concluded.

Wing 4, W_4

x/c	z/c	x/c	z/c	x/c	z/c
.99596	-.02586	.01149	-.00620	.00709	.01538
.98615	-.02306	.00943	-.00570	.01197	.01878
.96854	-.01899	.00774	-.00519	.02179	.02443
.94348	-.01488	.00674	-.00481	.03187	.02928
.91595	-.01191	.00592	-.00445	.04250	.03373
.89717	-.01051	.00467	-.00382	.06373	.04113
.87054	-.00923	.00343	-.00308	.09353	.04969
.82243	-.00837	.00257	-.00249	.13389	.05882
.77611	-.00873	.00165	-.00176	.17545	.06612
.74682	-.00927	.00104	-.00120	.22415	.07277
.71655	-.01008	.00048	-.00058	.28227	.07863
.68122	-.01118	0.00000	0.00000	.34741	.08291
.65330	-.01209	-.00045	.00079	.41444	.08502
.61351	-.01340	-.00073	.00146	.48168	.08487
.57465	-.01459	-.00086	.00191	.55738	.08191
.54359	-.01545	-.00097	.00244	.62052	.07704
.50010	-.01647	-.00103	.00290	.68276	.06982
.45495	-.01727	-.00106	.00345	.72012	.06433
.38597	-.01791	-.00104	.00403	.75413	.05845
.31761	-.01781	-.00098	.00463	.82318	.04432
.25034	-.01714	-.00077	.00572	.85663	.03610
.19880	-.01620	-.00052	.00653	.89115	.02678
.13965	-.01462	-.00021	.00732	.92448	.01698
.09339	-.01288	-.00026	.00830	.95410	.00764
.06022	-.01116	-.00073	.00909	.97175	.00178
.03967	-.00970	.00163	.01033	.99163	-.00516
.02583	-.00837	.00276	.01161	.99988	-.00810
.01539	-.00694	.00464	.01340	1.00000	-.01725

TABLE 3. - BODY DIMENSIONAL DATA

L	x	Dia	Area	W	z	Φ
.00	22.62	3.036	8.909	3.036	.000	90.0
.10	22.52	3.036	8.909	3.036	.000	90.0
.20	22.42	3.035	8.908	3.035	.000	90.0
.30	22.32	3.035	8.907	3.035	.000	90.0
.40	22.22	3.035	8.905	3.035	.000	90.0
.50	22.12	3.034	8.903	3.034	.000	90.0
.60	22.02	3.033	8.900	3.033	.000	90.0
.70	21.92	3.032	8.896	3.032	.000	90.0
.80	21.82	3.032	8.892	3.032	.000	90.0
.90	21.72	3.030	8.888	3.030	.000	90.0
1.00	21.62	3.029	8.883	3.029	.000	90.0
1.10	21.52	3.028	8.878	3.028	.000	90.0
1.20	21.42	3.026	8.872	3.026	.000	90.0
1.30	21.32	3.025	8.865	3.025	.000	90.0
1.40	21.22	3.023	8.858	3.023	.000	90.0
1.50	21.12	3.021	8.850	3.021	.000	90.0
1.60	21.02	3.019	8.842	3.019	.000	90.0
1.70	20.92	3.017	8.834	3.017	.000	90.0
1.80	20.82	3.015	8.825	3.015	.000	90.0
1.90	20.72	3.013	8.815	3.013	.000	90.0
2.00	20.62	3.010	8.805	3.010	.000	90.0
2.10	20.52	3.008	8.794	3.008	.000	90.0
2.20	20.42	3.005	8.783	3.005	.000	90.0
2.30	20.32	3.002	8.771	3.002	.000	90.0
2.40	20.22	2.999	8.759	2.999	.000	90.0
2.50	20.12	2.996	8.746	2.996	.000	90.0
2.60	20.02	2.993	8.733	2.993	.000	90.0
2.70	19.92	2.989	8.719	2.989	.000	90.0
2.80	19.82	2.986	8.705	2.986	.000	90.0
2.90	19.72	2.982	8.690	2.982	.000	90.0
3.00	19.62	2.979	8.675	2.979	.000	90.0
3.10	19.52	2.975	8.659	2.925	.000	90.0
3.20	19.42	2.971	8.643	2.971	.000	90.0
3.30	19.32	2.967	8.626	2.967	.000	90.0
3.40	19.22	2.962	8.609	2.962	.000	90.0
3.50	19.12	2.958	8.591	2.958	.000	90.0
3.60	19.02	2.953	8.573	2.953	.000	90.0
3.70	18.92	2.949	8.554	2.949	.000	90.0

* All dimensions are inches except Area, in^2, and Φ, degrees

TABLE 3. - BODY DIMENSIONAL DATA - Continued.

L	x	Dia	Area	W	z	Φ
3.80	18.82	2.944	8.535	2.944	.000	90.0
3.90	18.72	2.039	8.515	2.939	.000	90.0
4.00	18.62	2.934	8.495	2.934	.000	90.0
4.10	18.52	2.929	8.474	2.929	.000	90.0
4.20	18.42	2.924	8.452	2.924	.000	90.0
4.30	18.32	2.918	8.431	2.918	.000	90.0
4.40	18.22	2.913	8.400	2.913	.000	90.0
4.50	18.12	2.907	8.386	2.907	.000	90.0
4.60	18.02	2.902	8.362	2.900	.059	87.7
4.70	17.92	2.899	8.338	2.889	.119	85.3
4.80	17.82	2.896	8.314	2.878	.160	83.7
4.90	17.72	2.894	8.289	2.867	.199	82.1
5.00	17.62	2.891	8.264	2.854	.230	80.0
5.10	17.52	2.889	8.239	2.841	.262	79.6
5.20	17.42	2.886	8.212	2.828	.289	78.4
5.30	17.32	2.884	8.186	2.813	.318	77.3
5.40	17.22	2.882	8.158	2.798	.346	76.1
5.50	17.12	2.880	8.131	2.782	.372	75.0
5.60	17.02	2.877	8.103	2.766	.397	74.0
5.70	16.92	2.875	8.074	2.748	.423	72.9
5.80	16.82	2.873	8.045	2.730	.448	71.8
5.90	16.72	2.872	8.016	2.711	.474	70.7
6.00	16.62	2.870	7.986	2.691	.499	69.7
6.10	16.52	2.868	7.955	2.671	.523	68.6
6.20	16.42	2.866	7.924	2.649	.547	67.6
6.30	16.32	2.864	7.893	2.627	.571	66.5
6.40	16.22	2.863	7.861	2.604	.596	65.4
6.50	16.12	2.861	7.829	2.580	.619	64.4
6.60	16.02	2.859	7.796	2.554	.642	63.3
6.70	15.92	2.857	7.763	2.528	.665	62.2
6.80	15.82	2.856	7.729	2.501	.689	61.1
6.90	15.72	2.854	7.695	2.473	.712	60.1
7.00	15.62	2.853	7.660	2.444	.736	59.0
7.10	15.52	2.851	7.625	2.414	.758	57.9
7.20	15.42	2.849	7.590	2.383	.781	56.8
7.30	15.32	2.848	7.554	2.350	.804	55.6
7.40	15.22	2.846	7.518	2.317	.827	54.5
7.50	15.12	2.854	7.481	2.282	.857	53.1

TABLE 3. - BODY DIMENSIONAL DATA - Continued.

L	x	Dia	Area	W	z	Φ
7.60	15.02	2.861	7.444	2.245	.887	51.7
7.70	14.92	2.867	7.406	2.207	.915	50.3
7.80	14.82	2.873	7.368	2.168	.943	49.0
7.90	14.72	2.878	7.330	2.127	.969	47.7
8.00	14.62	2.883	7.291	2.085	.996	46.3
8.10	14.52	2.888	7.252	2.040	1.022	44.9
8.20	14.42	2.891	7.212	1.994	1.047	43.6
8.30	14.32	2.895	7.172	1.946	1.072	42.2
8.40	14.22	2.898	7.131	1.895	1.096	40.8
8.50	14.12	2.900	7.090	1.843	1.120	39.4
8.60	14.02	2.902	7.049	1.787	1.143	38.0
8.70	13.92	2.903	7.007	1.729	1.166	36.6
8.80	13.82	2.904	6.965	1.668	1.189	35.0
8.90	13.72	2.905	6.923	1.603	1.211	33.5
9.00	13.62	2.903	6.880	1.534	1.232	31.9
9.10	13.52	2.902	6.836	1.461	1.254	30.2
9.20	13.42	2.901	6.793	1.383	1.275	28.5
9.30	13.32	2.899	6.749	1.298	1.296	26.6
9.40	13.22	2.996	6.704	1.207	1.316	24.6
9.50	13.12	2.892	6.659	1.106	1.336	22.5
9.60	13.02	2.888	6.614	.992	1.356	20.1
9.70	12.92	2.883	6.568	.863	1.376	17.4
9.80	12.82	2.877	6.522	.707	1.394	14.2
9.90	12.72	2.870	6.476	.502	1.413	10.1
10.00	12.62	2.861	6.429	.000	1.431	.0
10.10	12.52	2.851	6.382			
10.20	12.42	2.840	6.335			
10.30	12.32	2.829	6.287			
10.40	12.22	2.819	6.239			
10.50	12.12	2.808	6.191			
10.60	12.02	2.796	6.142			
10.70	11.92	2.785	6.093			
10.80	11.82	2.774	6.044			
10.90	11.72	2.763	5.994			
11.00	11.62	2.751	5.944			
11.10	11.52	2.739	5.893			
11.20	11.42	2.727	5.843			
11.30	11.32	2.716	5.792			

TABLE 3. - BODY DIMENSIONAL DATA - Continued.

L	x	Dia	Area
11.40	11.22	2.704	5.740
11.50	11.12	2.691	5.689
11.60	11.02	2.679	5.637
11.70	10.92	2.667	5.585
11.80	10.82	2.654	5.532
11.90	10.72	2.641	5.480
12.00	10.62	2.629	5.427
12.10	10.52	2.616	5.373
12.20	10.42	2.603	5.320
12.30	10.32	2.589	5.266
12.40	10.22	2.576	5.212
12.50	10.12	2.563	5.158
12.60	10.02	2.549	5.103
12.70	9.92	2.535	5.048
12.80	9.82	2.521	4.993
12.90	9.72	2.507	4.938
13.00	9.62	2.493	4.883
13.10	9.52	2.479	4.827
13.20	9.42	2.465	4.771
13.30	9.32	2.450	4.715
13.40	9.22	2.436	4.659
13.50	9.12	2.421	4.602
13.60	9.02	2.406	4.546
13.70	8.92	2.391	4.489
13.80	8.82	2.375	4.432
13.90	8.72	2.360	4.374
14.00	8.62	2.345	4.317
14.10	8.52	2.329	4.260
14.20	8.42	2.313	4.202
14.30	8.32	2.297	4.144
14.40	8.22	2.281	4.086
14.50	8.12	2.265	4.028
14.60	8.02	2.248	3.970
14.70	7.92	2.232	3.912
14.80	7.82	2.215	3.853
14.90	7.72	2.198	3.795
15.00	7.62	2.181	3.736
15.10	7.52	2.164	3.677

TABLE 3. - BODY DIMENSIONAL DATA - Continued.

L	x	Dia	Area
15.20	7.42	2.146	3.619
15.30	7.32	2.129	3.560
15.40	7.22	2.111	3.501
15.50	7.12	2.093	3.442
15.60	7.02	2.075	3.383
15.70	6.92	2.057	3.324
15.80	6.82	2.039	3.265
15.90	6.72	2.020	3.206
16.00	6.62	2.002	3.147
16.10	6.52	1.983	3.088
16.20	6.42	1.964	3.029
16.30	6.32	1.944	2.970
16.40	6.22	1.925	2.911
16.50	6.12	1.905	2.852
16.60	6.02	1.886	2.793
16.70	5.92	1.866	2.734
16.80	5.82	1.845	2.675
16.90	5.72	1.825	2.616
17.00	5.62	1.805	2.558
17.10	5.52	1.784	2.499
17.20	5.42	1.763	2.441
17.30	5.32	1.742	2.382
17.40	5.22	1.720	2.324
17.50	5.12	1.699	2.266
17.60	5.02	1.677	2.208
17.70	4.92	1.655	2.151
17.80	4.82	1.633	2.093
17.90	4.72	1.610	2.036
18.00	4.62	1.587	1.979
18.10	4.52	1.564	1.922
18.20	4.42	1.541	1.866
18.30	4.32	1.518	1.809
18.40	4.22	1.494	1.753
18.50	4.12	1.470	1.697
18.60	4.02	1.446	1.642
18.70	3.92	1.421	1.587
18.80	3.82	1.397	1.532
18.90	3.72	1.372	1.478

TABLE 3. - BODY DIMENSIONAL DATA - Concluded.

L	x	Dia	Area
19.00	3.62	1.346	1.424
19.10	3.52	1.321	1.370
19.20	3.42	1.295	1.317
19.30	3.32	1.269	1.264
19.40	3.22	1.242	1.212
19.50	3.12	1.215	1.160
19.60	3.02	1.188	1.108
19.70	2.92	1.160	1.057
19.80	2.82	1.132	1.007
19.90	2.72	1.104	.957
20.00	2.62	1.075	.908
20.10	2.52	1.046	.860
20.20	2.42	1.017	.812
20.30	2.32	.987	.765
20.40	2.22	.956	.718
20.50	2.12	.926	.673
20.60	2.02	.894	.628
20.70	1.92	.862	.584
20.80	1.82	.830	.541
20.90	1.72	.797	.499
21.00	1.62	.763	.457
21.10	1.52	.729	.417
21.20	1.42	.694	.378
21.30	1.32	.658	.340
21.40	1.22	.621	.303
21.50	1.12	.583	.267
21.60	1.02	.545	.233
21.70	.92	.505	.200
21.80	.82	.464	.169
21.90	.72	.422	.140
22.00	.62	.378	.112
22.10	.52	.332	.086
22.20	.42	.283	.063
22.30	.32	.231	.042
22.40	.22	.175	.024
22.50	.12	.111	.010
22.60	.02	.029	.001
22.62	.00	.000	.000

TABLE 4. - TEST CONDITIONS

Configuration	Λ deg.	$Re/10^6$, per ft.	Mach Numbers										
			0.60	0.70	0.80	0.95	0.98	1.05	1.10	1.15	1.20	1.30	1.40
W_1 F_0 B	0	6	x	x	x								
	45	6		x	x	x	x	x					
	50	6			x	x	x		x	x	x		
W_1 F_0 B	60	6			x	x			x		x	x	x
W_2 F_0 B	0	4	x	x	x								
	45	4		x	x	x	x	x	x	x			
	50	4			x	x	x		x	x	x	x	
W_2 F_0 B	60	4			x	x			x		x	x	x
W_4 F_0 B	0	6	x	x	x								
	45	6	x	x	x	x	x	x					
	50	6			x	x	x		x	x	x		
W_4 F_0 B	60	6			x	x		x	x		x	x	x

TABLE 5. - INDEX OF DATA FIGURES

Figure	Title	Page
4	Effect of wing airfoil section for an oblique wing angle of 0 degrees.	1
5	Effect of wing airfoil section for an oblique wing angle of 45 degrees.	22
6	Effect of wing airfoil section for an oblique wing angle of 50 degrees.	57
7	Effect of wing airfoil section for an oblique wing angle of 60 degrees.	99

Note:
1. Positive directions of force coefficients, moment coefficients, and angles are indicated by arrows

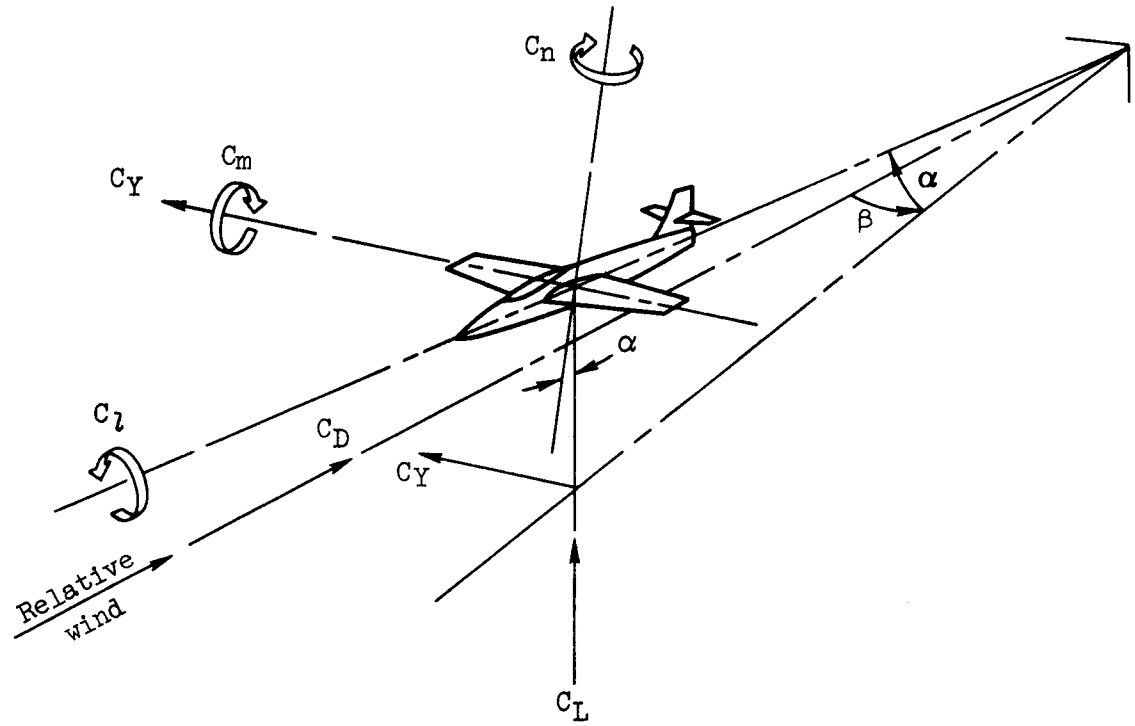

Figure 1.- Axis systems.

Note: All dimensions are in inches except as noted

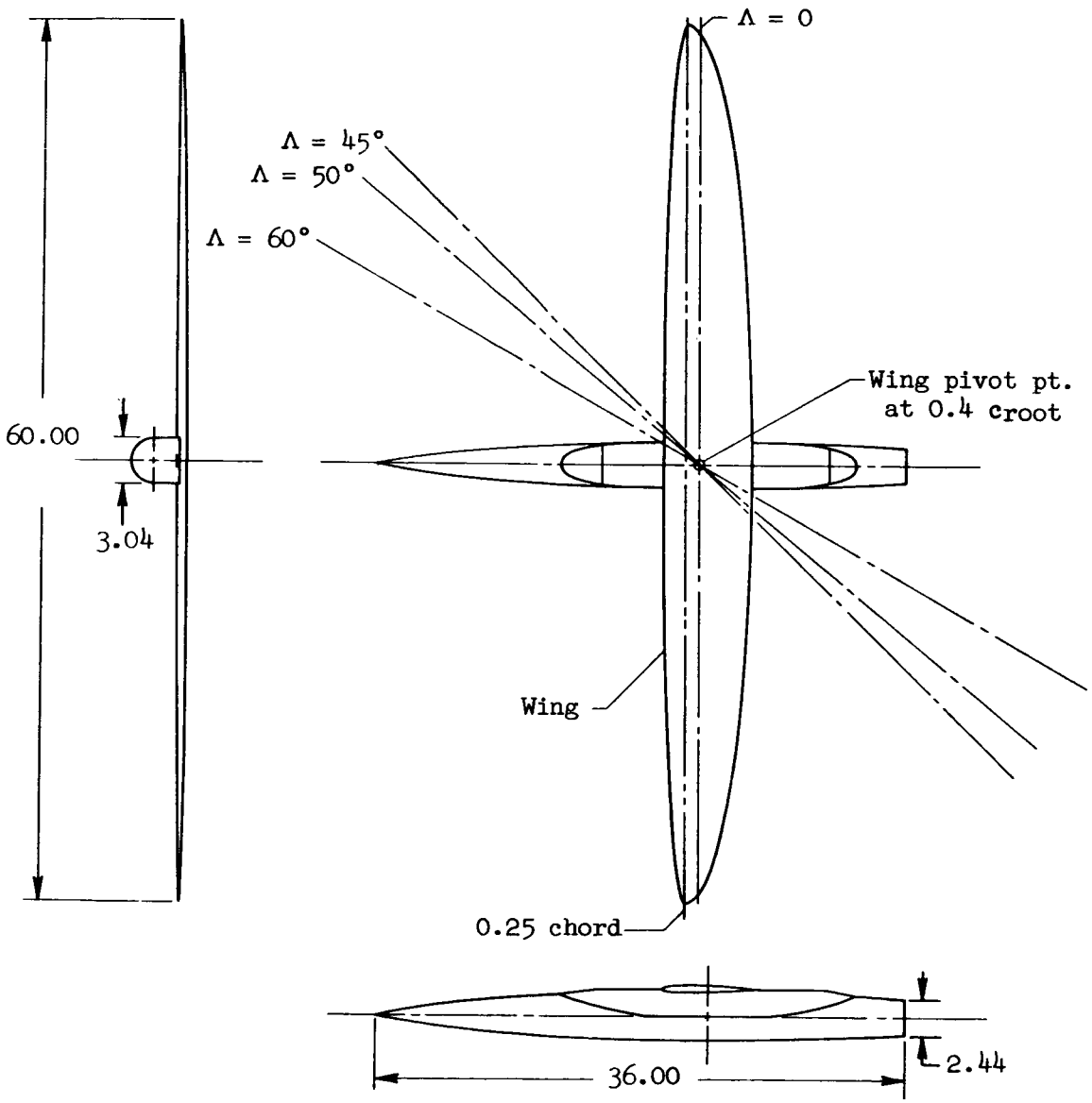

(a) Model drawing

Figure 2.- Oblique-wing/body model details and photograph.

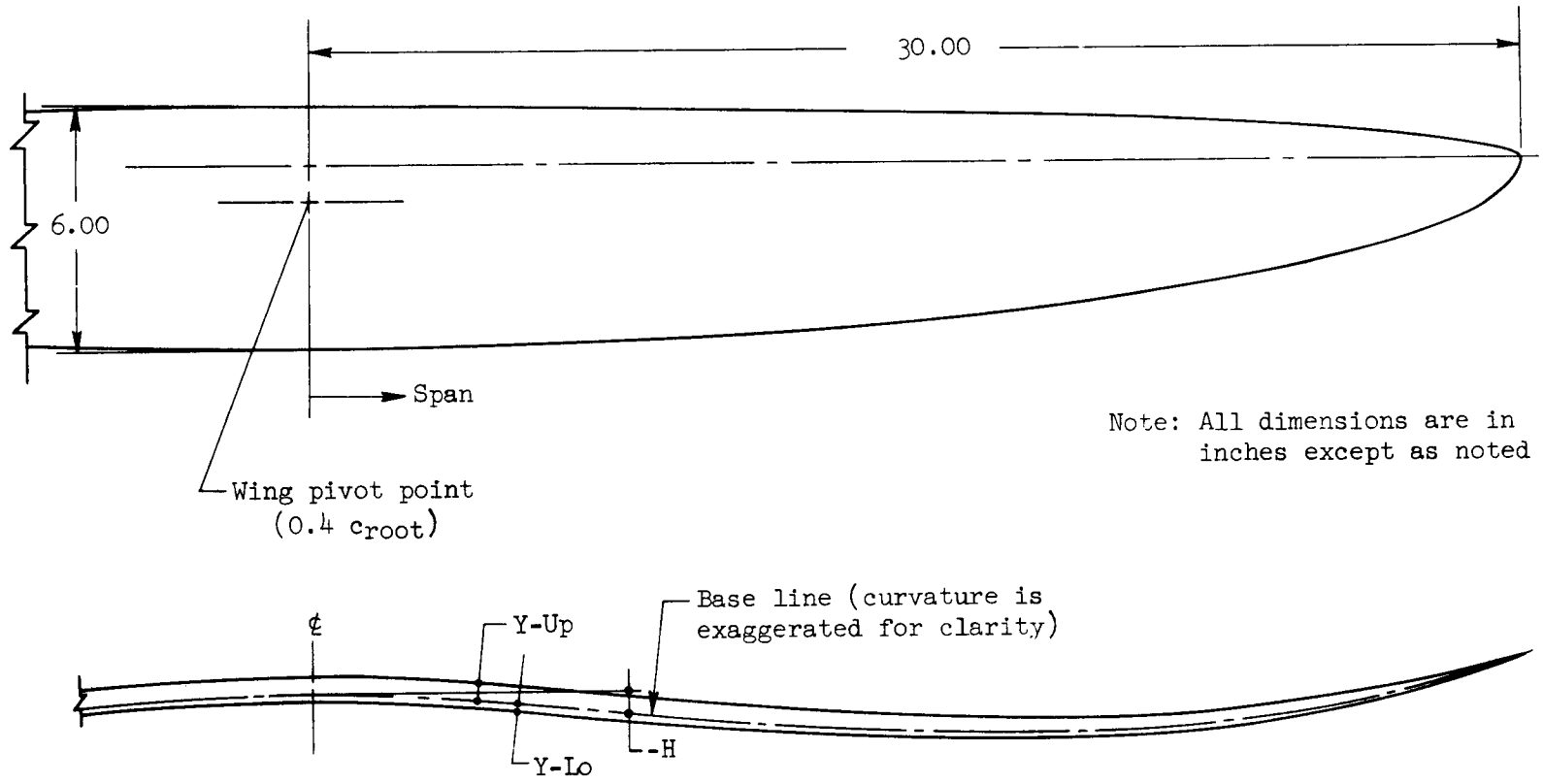

(b) Wing planform and base line curvature

Figure 2.- Continued.

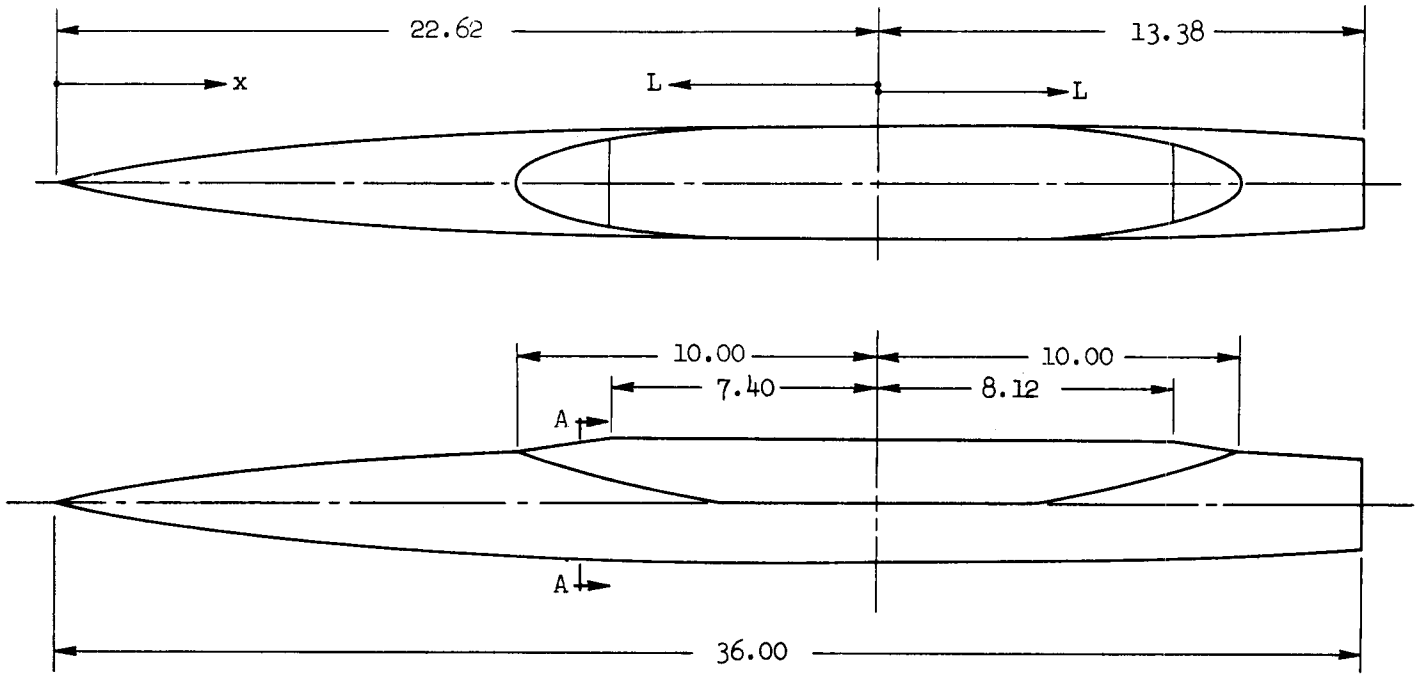

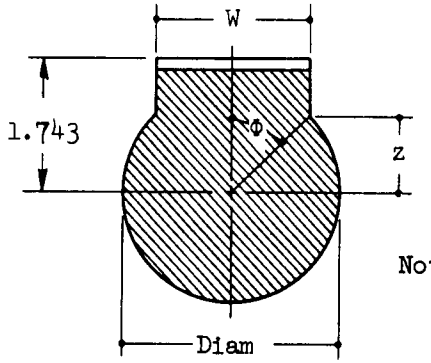

Section A-A

Note: See table 3 for body-section dimensional details. Section taken at L = 8.10

All dimensions are in inches, angles are in degrees

(c) Body dimensional data

Figure 2.- Continued.

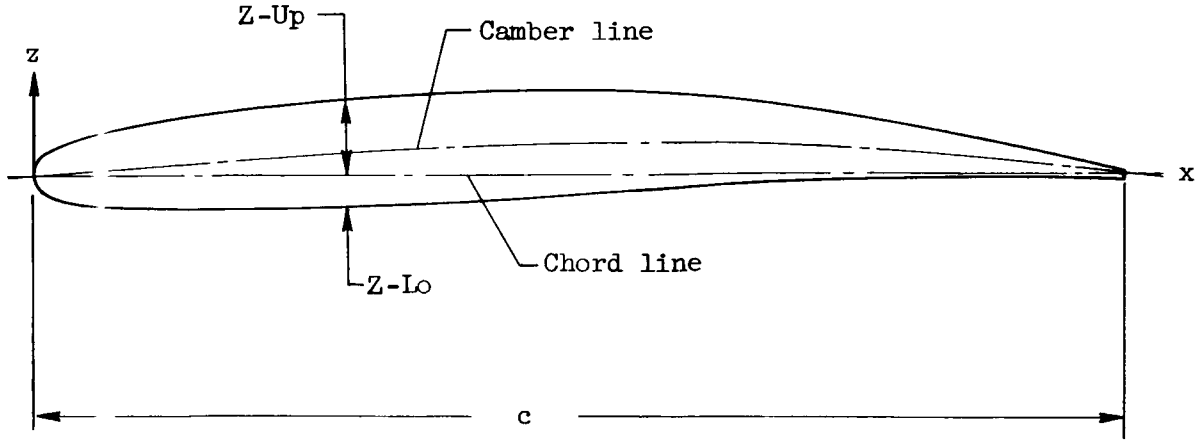

$\frac{x}{c}$	$\frac{t}{c}$	$\frac{\text{Camber}}{c}$	$\frac{\text{Z-Up}}{c}$	$\frac{\text{Z-Lo}}{c}$
.001	.01203	.00008	.00609	-.00594
.010	.03394	.00078	.01775	-.01619
.025	.04849	.00195	.02619	-.02230
.050	.06119	.00389	.03449	-.02671
.075	.06891	.00582	.04027	-.02864
.100	.07446	.00772	.04495	-.02951
.150	.08250	.01144	.05269	-.02981
.200	.08852	.01498	.05924	-.02928
.300	.09689	.02129	.06974	-.02715
.400	.10000	.02621	.07621	-.02379
.500	.09647	.02925	.07749	-.01899
.600	.08560	.02995	.07275	-.01285
.700	.06796	.02785	.06182	-.00613
.800	.04568	.02246	.04531	-.00038
.900	.02255	.01334	.02461	.00207
1.000	.00400	.00000	.00200	-.00200

(d) ' ing section drawing and tabulated airfoil section data for wing number 1, W_1

Figure 2.- Continued.

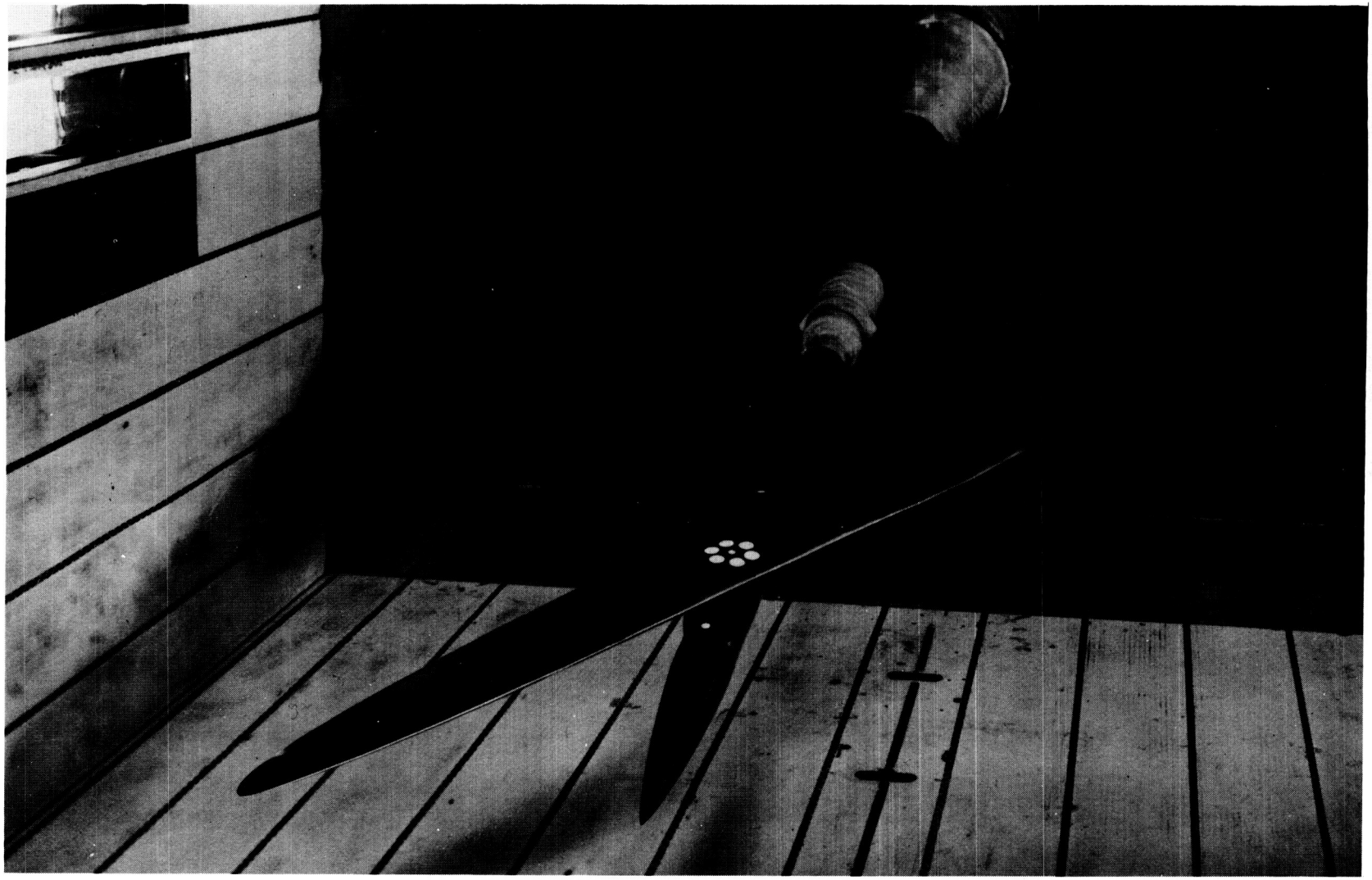

(e) Photograph of the model in the Ames 11- by 11-Foot Wind Tunnel, $\Lambda = 60^{\circ}$

Figure 2. - Concluded.

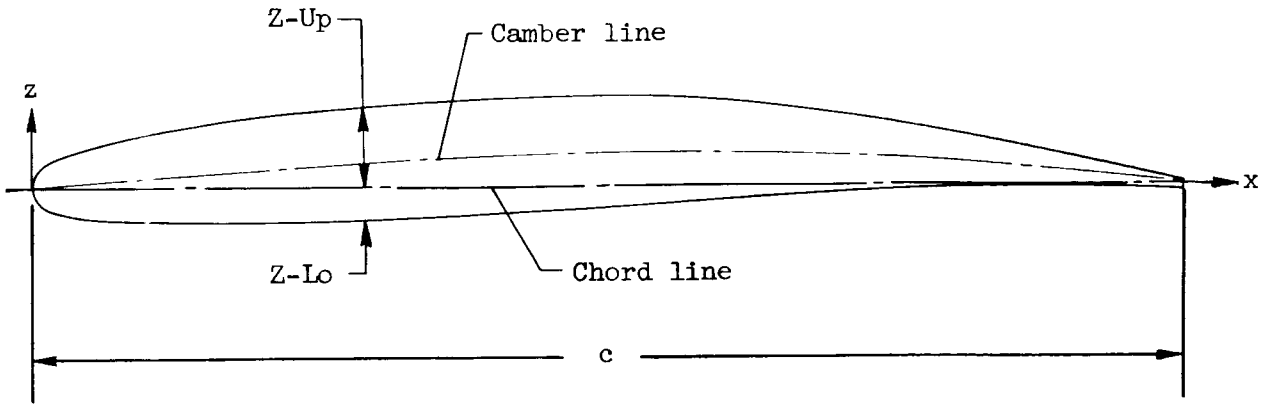

(a) Wing number 2, W_2
(see table 2 for section coordinates)

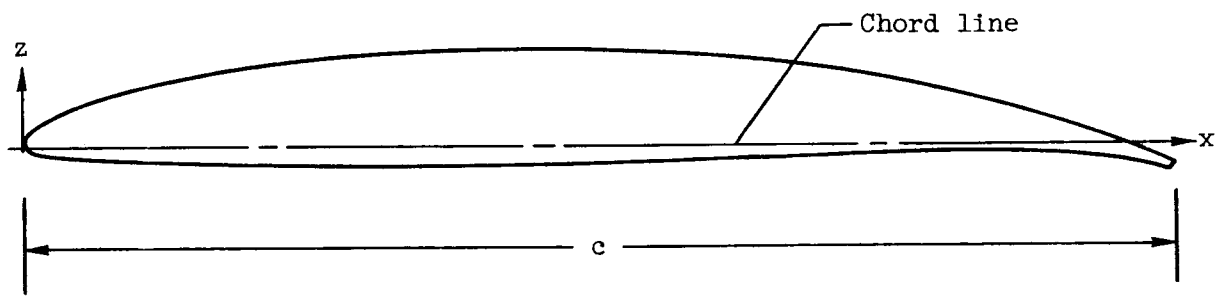

(b) Wing number 4, W_4
(see table 2 for section coordinates)

Figure 3.- Wing-section drawings.

DATA

DATA SET	SYMBOL	CONFIGURATION DESCRIPTION	BETA	LAMBDA	RN/L
(1AE005)	○	W1 F0 B	0.000	0.000	6.000
(1AE040)	△	W2 F0 B	0.000	0.000	6.000
(1AE065)	◇	W4 F0 B	0.000	0.000	6.000

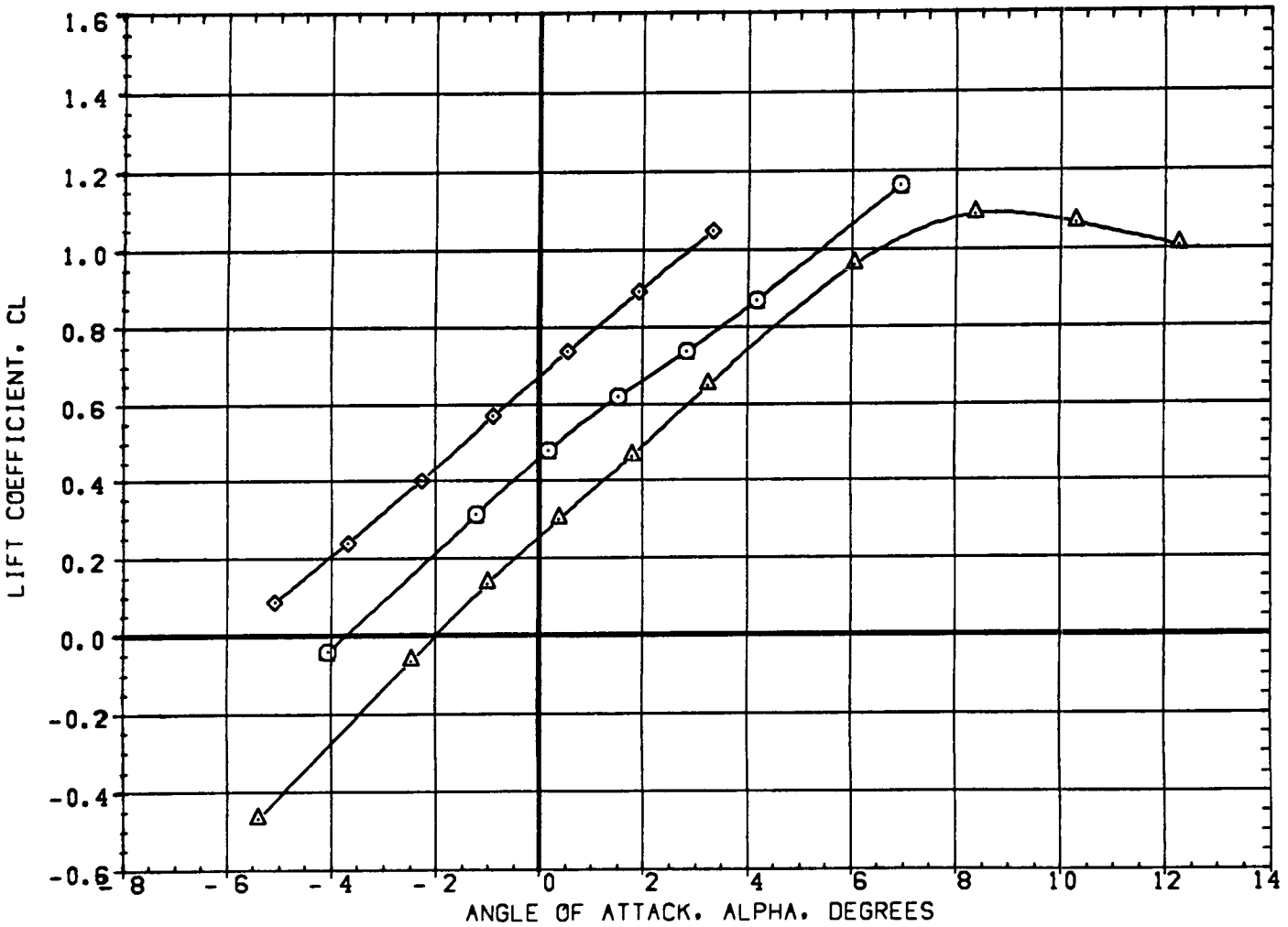

FIGURE 4 EFFECT OF WING AIRFOIL SECTION FOR AN OBLIQUE WING ANGLE OF 0 DEGREE

(A)MACH = .60

DATA SET	SYMBOL	CONFIGURATION DESCRIPTION	BETA	LAMBDA	RN/L
(1AE003)	○	W1 F0 B	0.000	0.000	6.000
(1AE040)	△	W2 F0 B	0.000	0.000	6.000
(1AE065)	◇	W4 F0 B	0.000	0.000	6.000

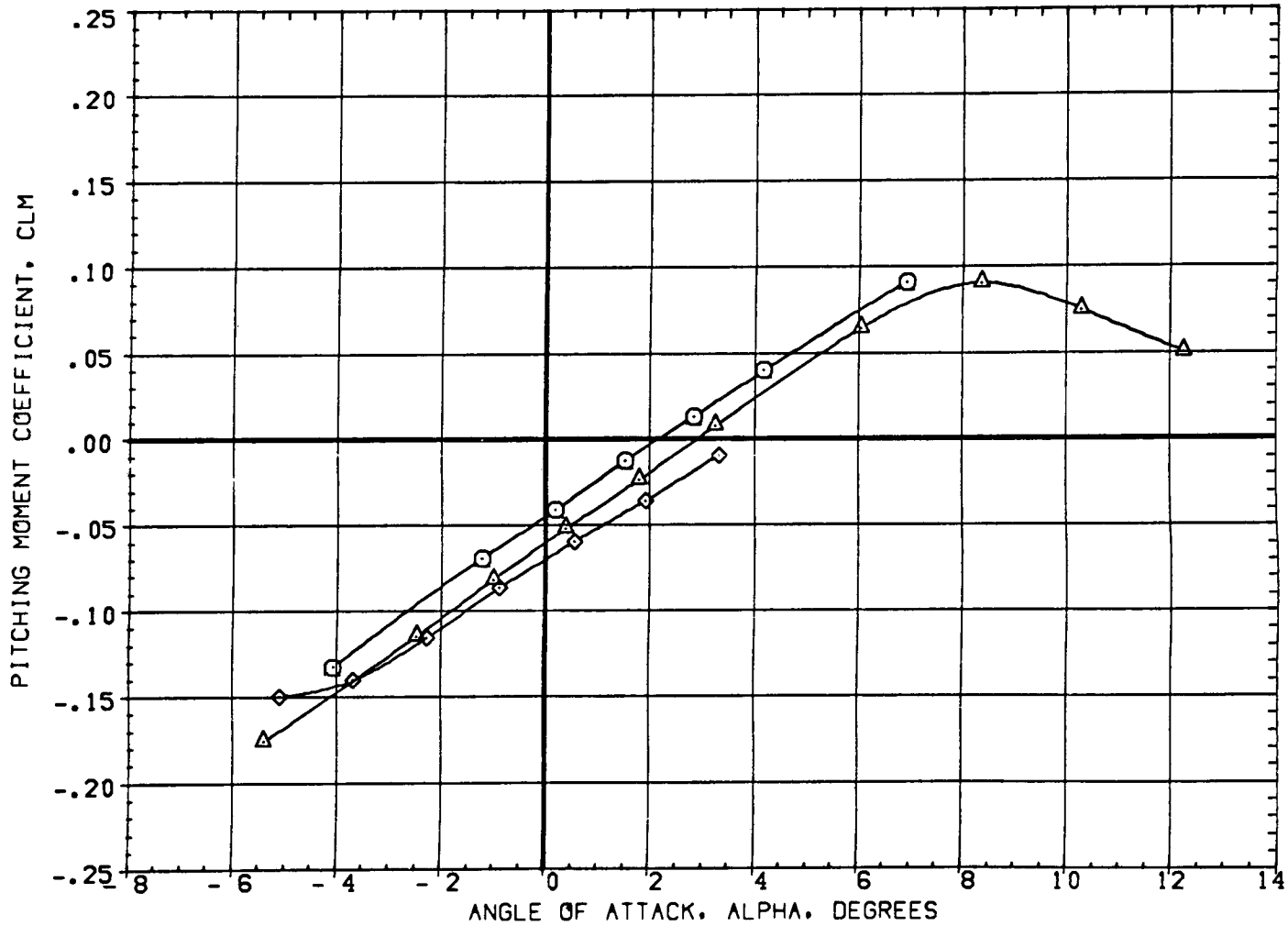

FIGURE 4 EFFECT OF WING AIRFOIL SECTION FOR AN OBLIQUE WING ANGLE OF 0 DEGREE

(A)MACH = .60

DATA SET	SYMBOL	CONFIGURATION DESCRIPTION	BETA	LAMBDA	RN/L
(1AE003)	○	W1 F0 B	0.000	0.000	6.000
(1AE040)	△	W2 F0 B	0.000	0.000	6.000
(1AE065)	◇	W4 F0 B	0.000	0.000	6.000

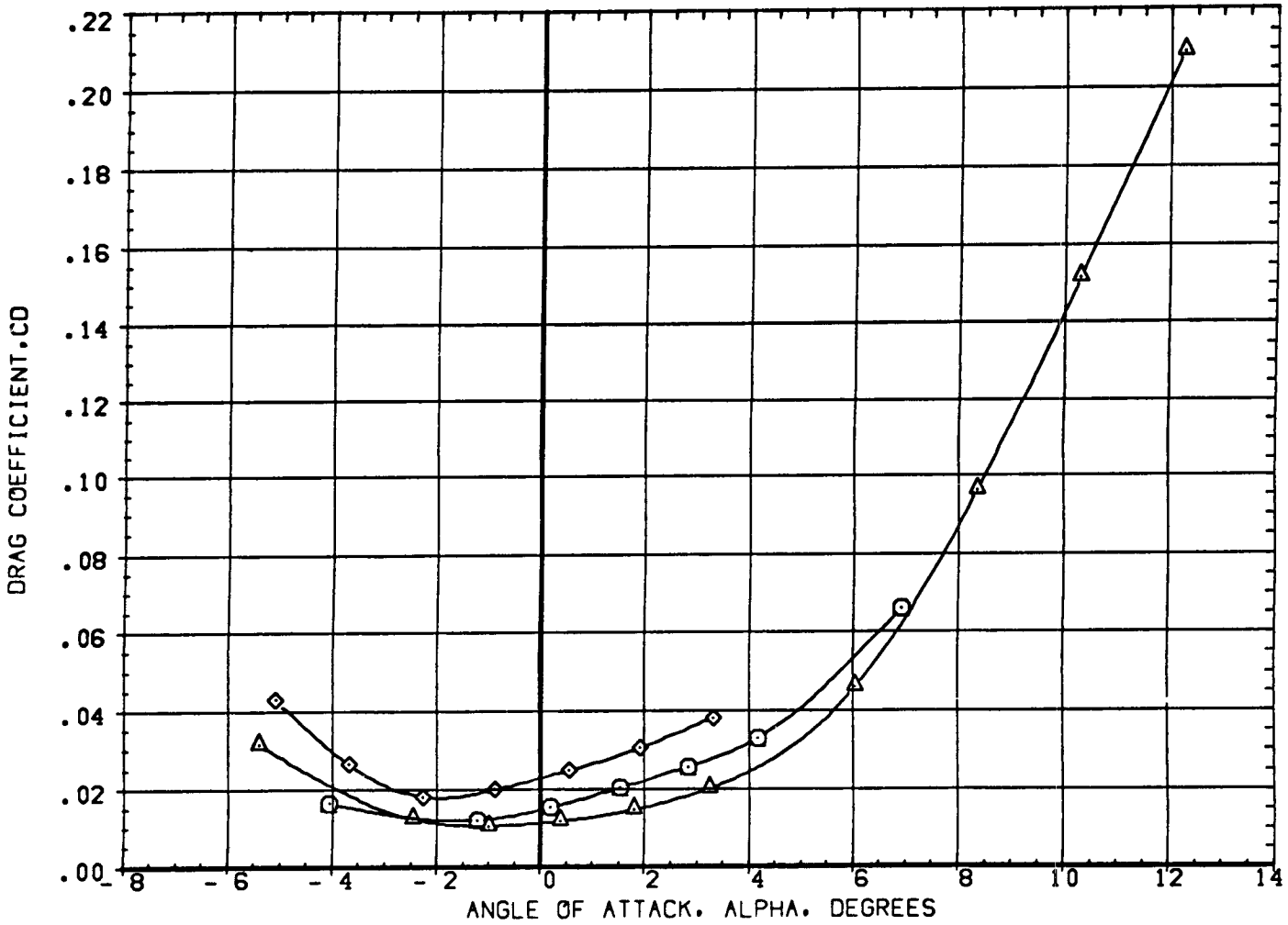

FIGURE 4 EFFECT OF WING AIRFOIL SECTION FOR AN OBLIQUE WING ANGLE OF 0 DEGREE

(A)MACH = .60

DATA SET	SYMBOL	CONFIGURATION DESCRIPTION	BETA	LAMBDA	RN/L
(1AE003)	○	W1 FO B	0.000	0.000	6.000
(1AE040)	△	W2 FO B	0.000	0.000	6.000
(1AE065)	◇	W4 FO B	0.000	0.000	6.000

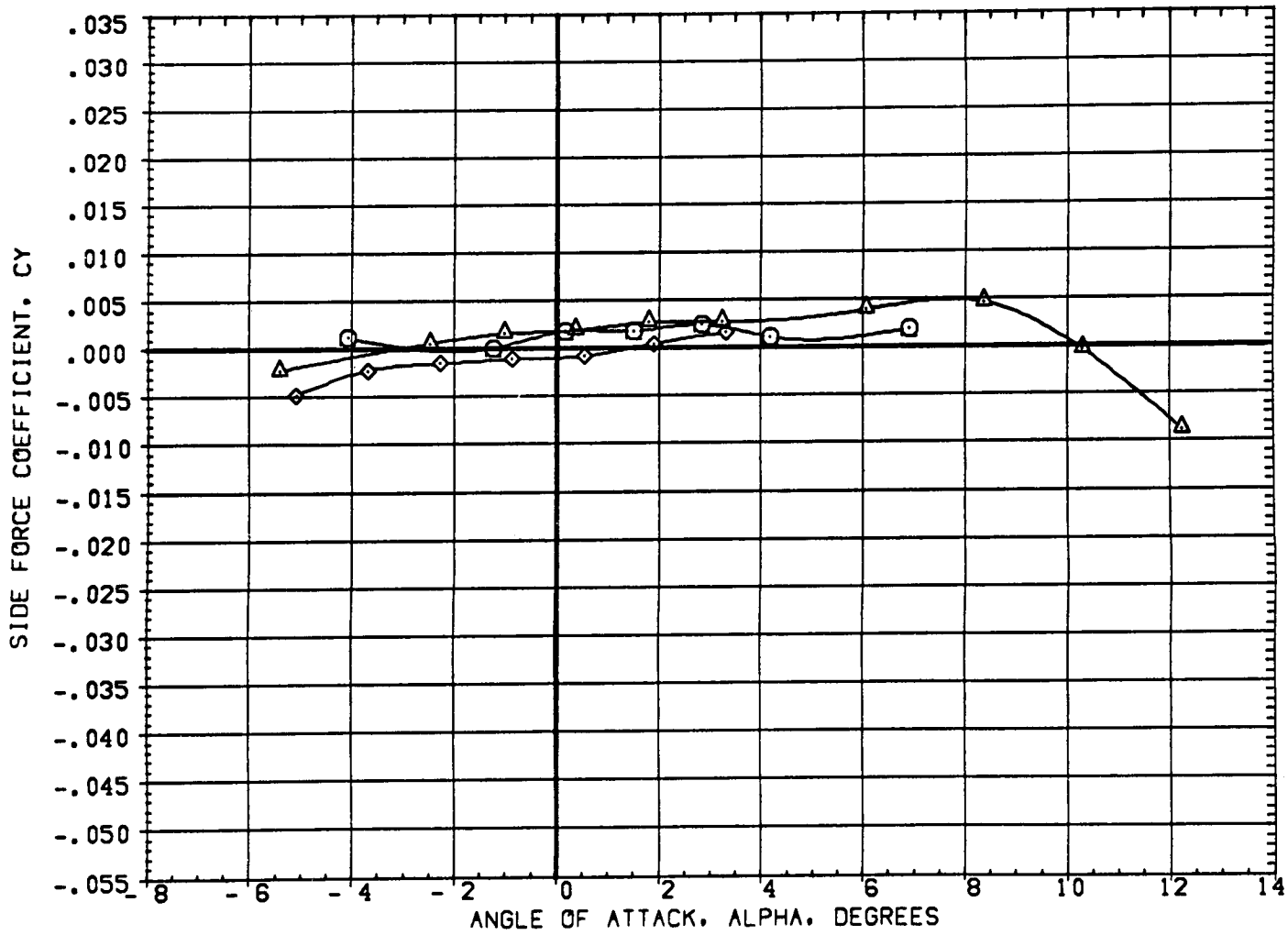

FIGURE 4 EFFECT OF WING AIRFOIL SECTION FOR AN OBLIQUE WING ANGLE OF 0 DEGREE

(A)MACH = .60

DATA SET	SYMBOL	CONFIGURATION DESCRIPTION	BETA	LAMBDA	RN/L
(1AE003)	○	W1 FO B	0.000	0.000	6.000
(1AE040)	△	W2 FO B	0.000	0.000	6.000
(1AE065)	◇	W4 FO B	0.000	0.000	6.000

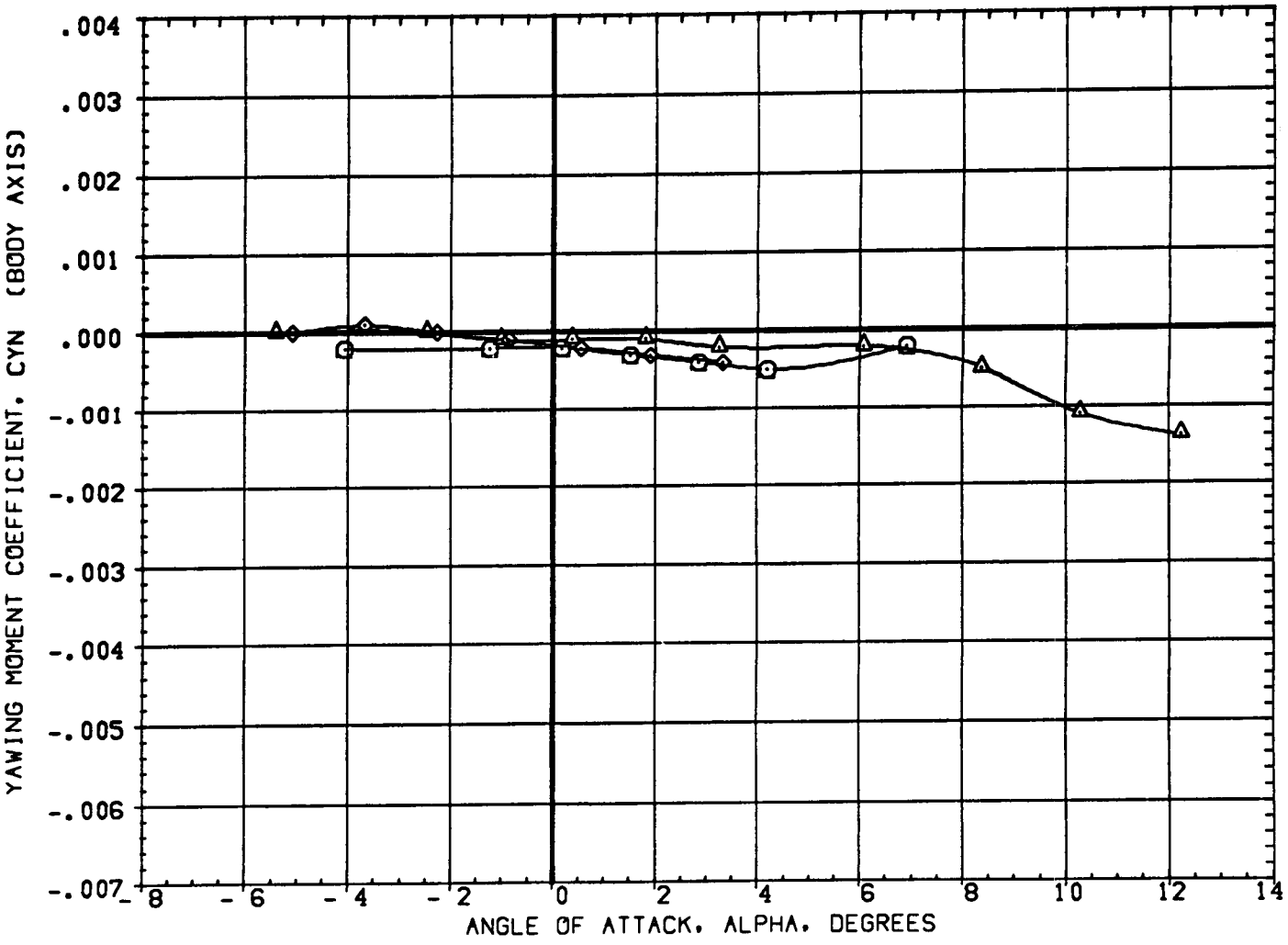

FIGURE 4 EFFECT OF WING AIRFOIL SECTION FOR AN OBLIQUE WING ANGLE OF 0 DEGREE

(A)MACH = .60

DATA SET	SYMBOL	CONFIGURATION DESCRIPTION	BETA	LAMBDA	RN/L
(1AE003)	○	W1 F0 B	0.000	0.000	6.000
(1AE040)	△	W2 F0 B	0.000	0.000	6.000
(1AE065)	◇	W4 F0 B	0.000	0.000	6.000

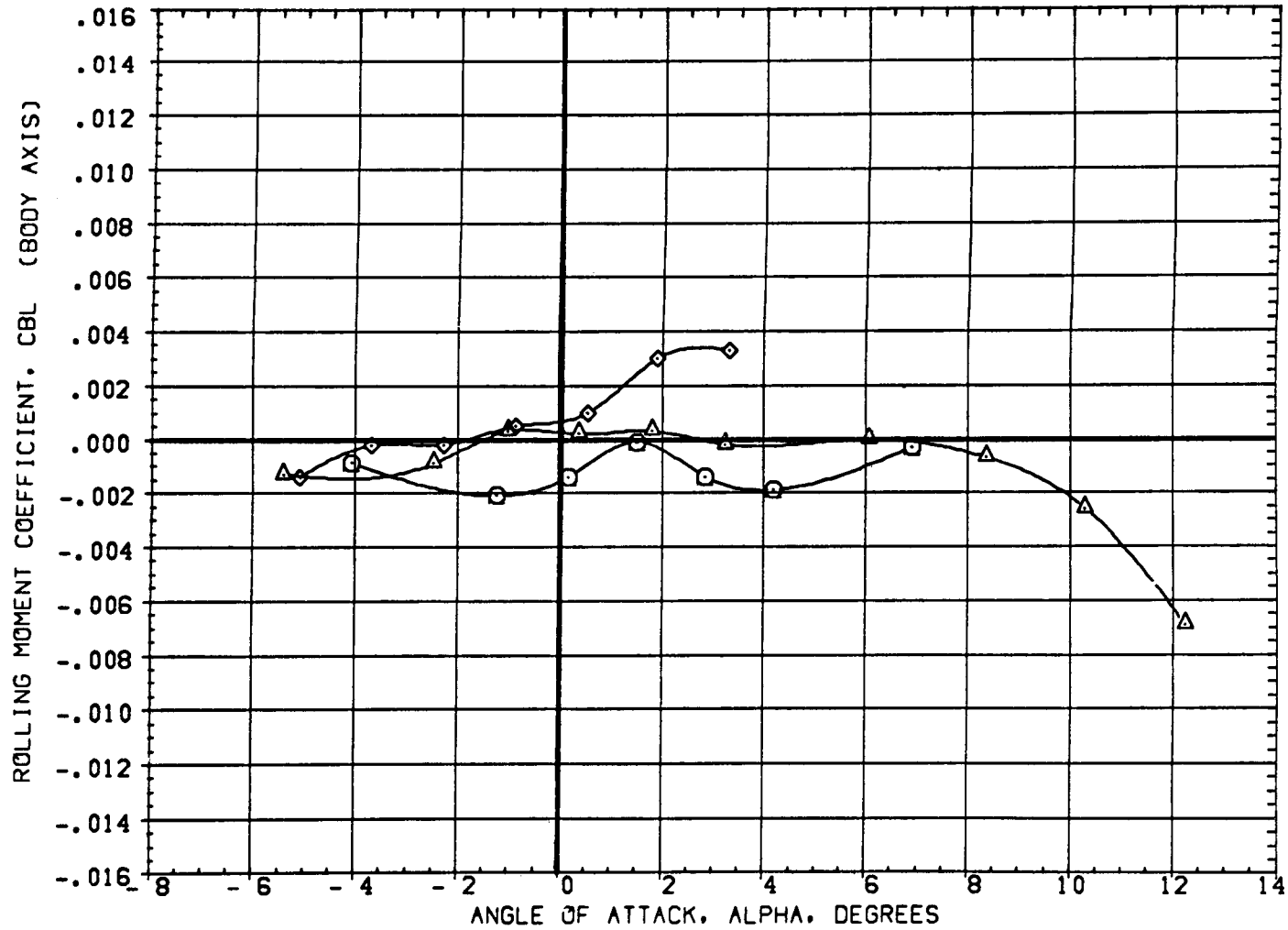

FIGURE 4 EFFECT OF WING AIRFOIL SECTION FOR AN OBLIQUE WING ANGLE OF 0 DEGREE

(A)MACH = .60

DATA SET SYMBOL		CONFIGURATION DESCRIPTION	BETA	LAMBDA	RN/L
(1AE003)	○	W1 F0 B	0.000	0.000	6.000
(1AE040)	△	W2 F0 B	0.000	0.000	6.000
(1AE065)	◇	W4 F0 B	0.000	0.000	6.000

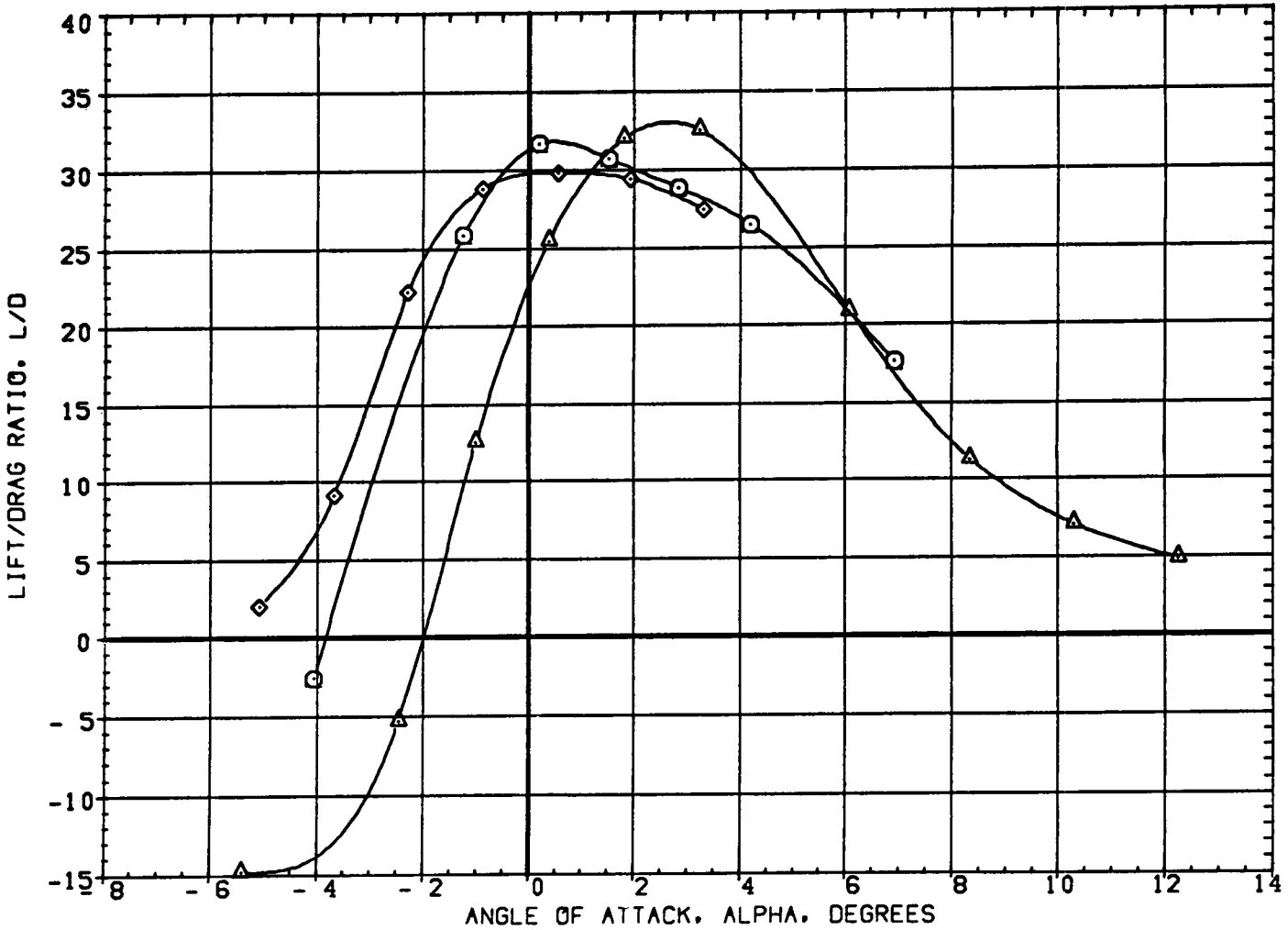

FIGURE 4 EFFECT OF WING AIRFOIL SECTION FOR AN OBLIQUE WING ANGLE OF 0 DEGREE

(A)MACH = .60

DATA SET	SYMBOL	CONFIGURATION DESCRIPTION	BETA	LAMBDA	RN/L
(2AE003)	○	W1 F0 B	0.000	0.000	6.000
(2AE039)	△	W2 F0 B	0.000	0.000	4.000
(2AE065)	◇	W4 F0 B	0.000	0.000	6.000

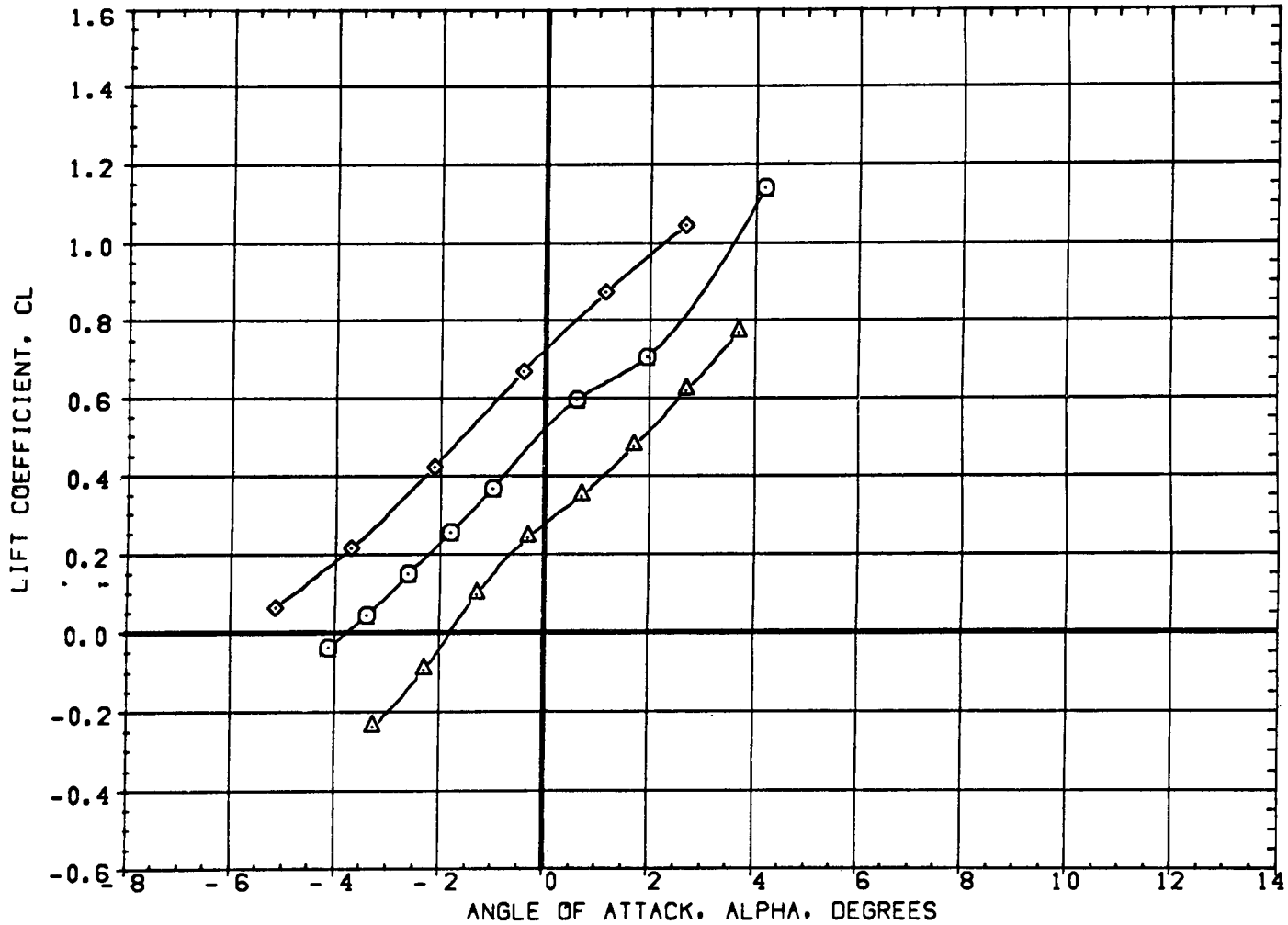

FIGURE 4 EFFECT OF WING AIRFOIL SECTION FOR AN OBLIQUE WING ANGLE OF 0 DEGREE

(A)MACH = .70

DATA SET	SYMBOL	CONFIGURATION DESCRIPTION	BETA	LAMBDA	RN/L
(2AE003)	○	W1 F0 B	0.000	0.000	6.000
(2AE039)	△	W2 F0 B	0.000	0.000	4.000
(2AE065)	◇	W4 F0 B	0.000	0.000	6.000

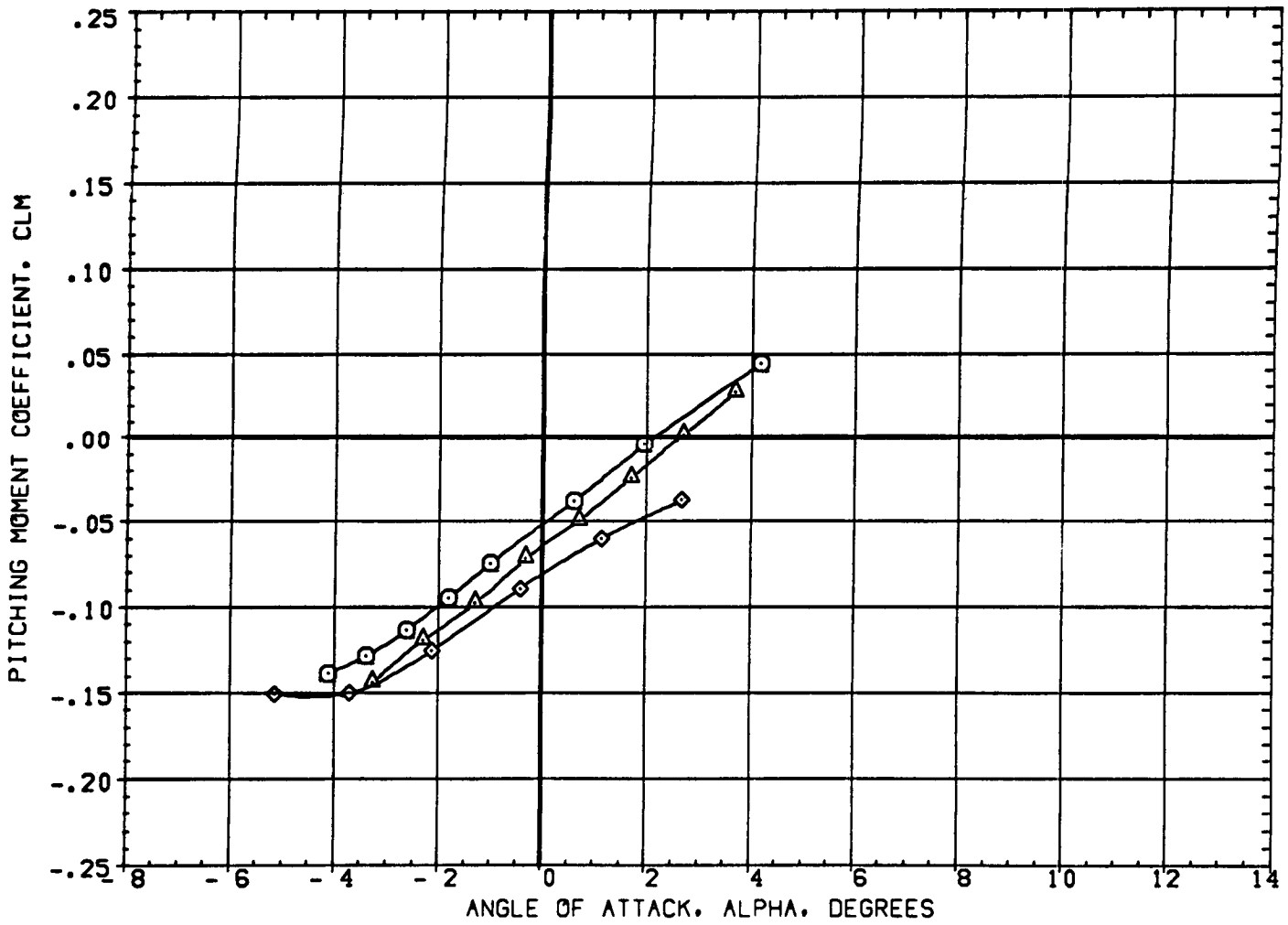

FIGURE 4 EFFECT OF WING AIRFOIL SECTION FOR AN OBLIQUE WING ANGLE OF 0 DEGREE

(A)MACH = .70

DATA SET	SYMBOL	CONFIGURATION DESCRIPTION	BETA	LAMBDA	RN/L
(2AE003)	○	W1 FO B	0.000	0.000	6.000
(2AE039)	△	W2 FO B	0.000	0.000	4.000
(2AE065)	◇	W4 FO B	0.000	0.000	6.000

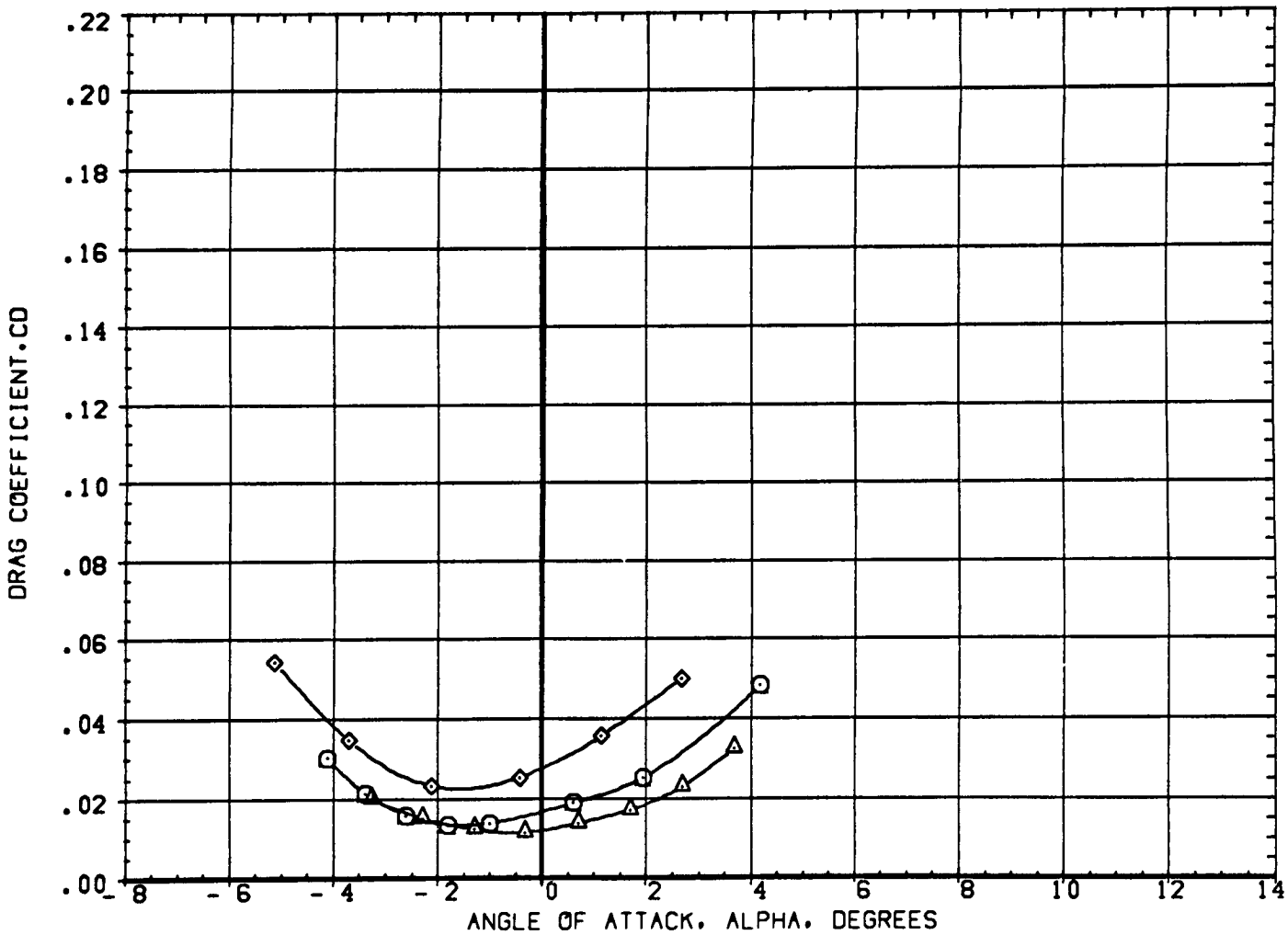

FIGURE 4 EFFECT OF WING AIRFOIL SECTION FOR AN OBLIQUE WING ANGLE OF 0 DEGREE

(A)MACH = .70

DATA SET	SYMBOL	CONFIGURATION DESCRIPTION	BETA	LAMBDA	RN/L
(2AE003)	○	W1 F0 B	0.000	0.000	6.000
(2AE039)	△	W2 F0 B	0.000	0.000	4.000
(2AE065)	◇	W4 F0 B	0.000	0.000	6.000

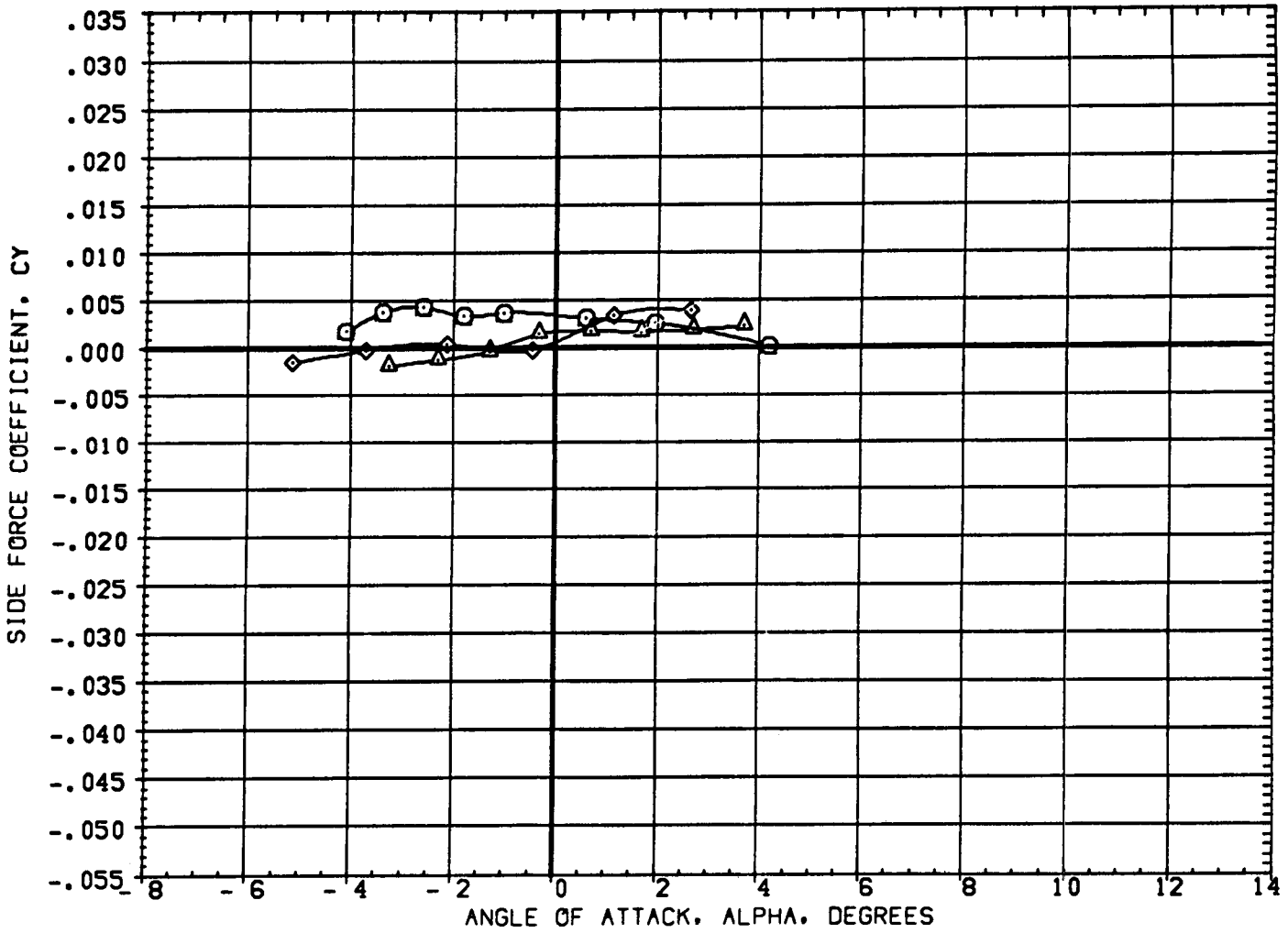

FIGURE 4 EFFECT OF WING AIRFOIL SECTION FOR AN OBLIQUE WING ANGLE OF 0 DEGREE

(A)MACH = .70

DATA SET	SYMBOL	CONFIGURATION DESCRIPTION	BETA	LAMBDA	RN/L
(2AE003)	○	W1 F0 B	0.000	0.000	8.000
(2AE039)	△	W2 F0 B	0.000	0.000	4.000
(2AE065)	◇	W4 F0 B	0.000	0.000	6.000

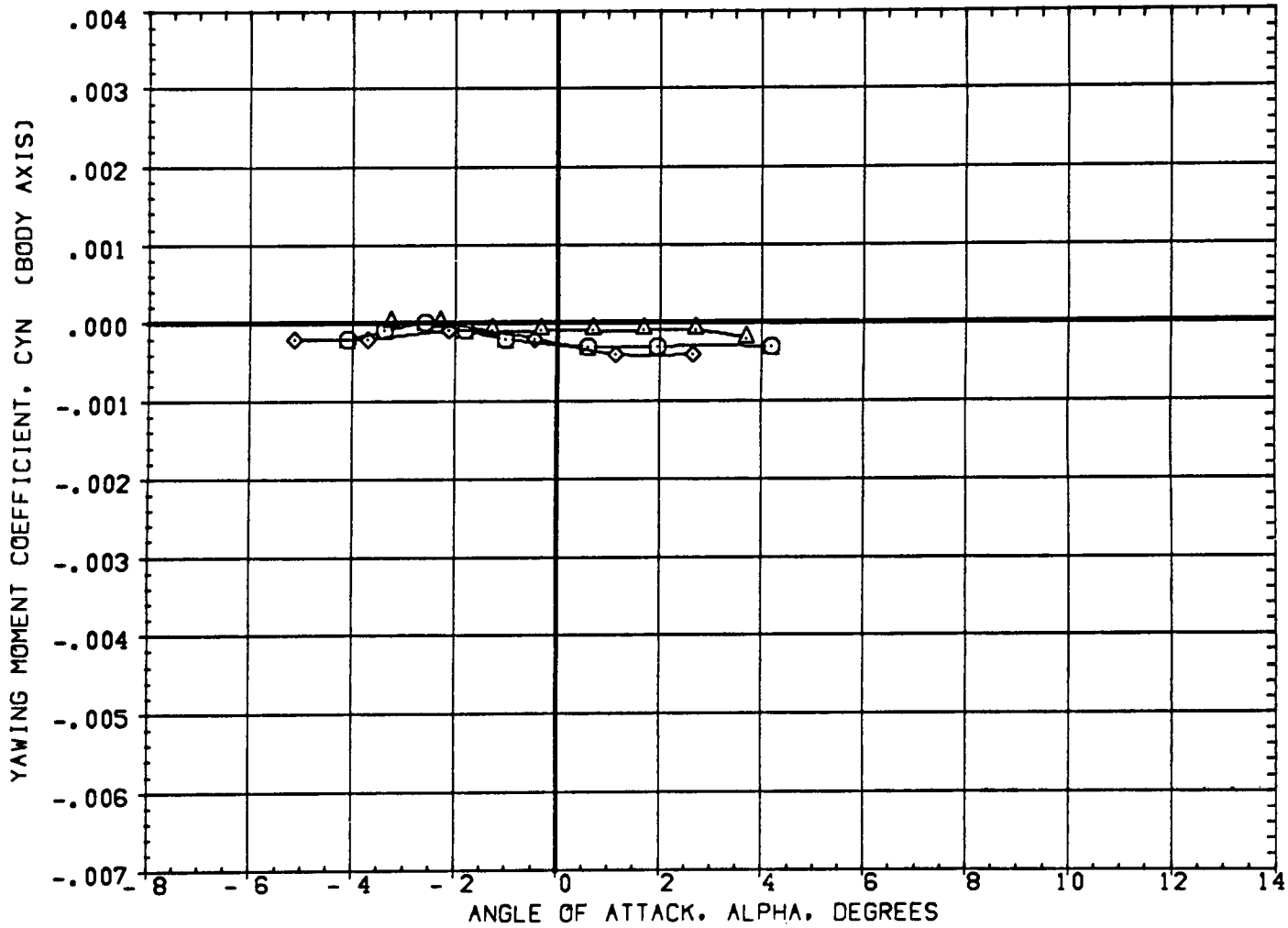

FIGURE 4 EFFECT OF WING AIRFOIL SECTION FOR AN OBLIQUE WING ANGLE OF 0 DEGREE

(A)MACH = .70

DATA SET	SYMBOL	CONFIGURATION DESCRIPTION	BETA	LAMBDA	RN/L
(2AE003)	○	W1 FO B	0.000	0.000	6.000
(2AE039)	△	W2 FO B	0.000	0.000	4.000
(2AE065)	◇	W4 FO B	0.000	0.000	6.000

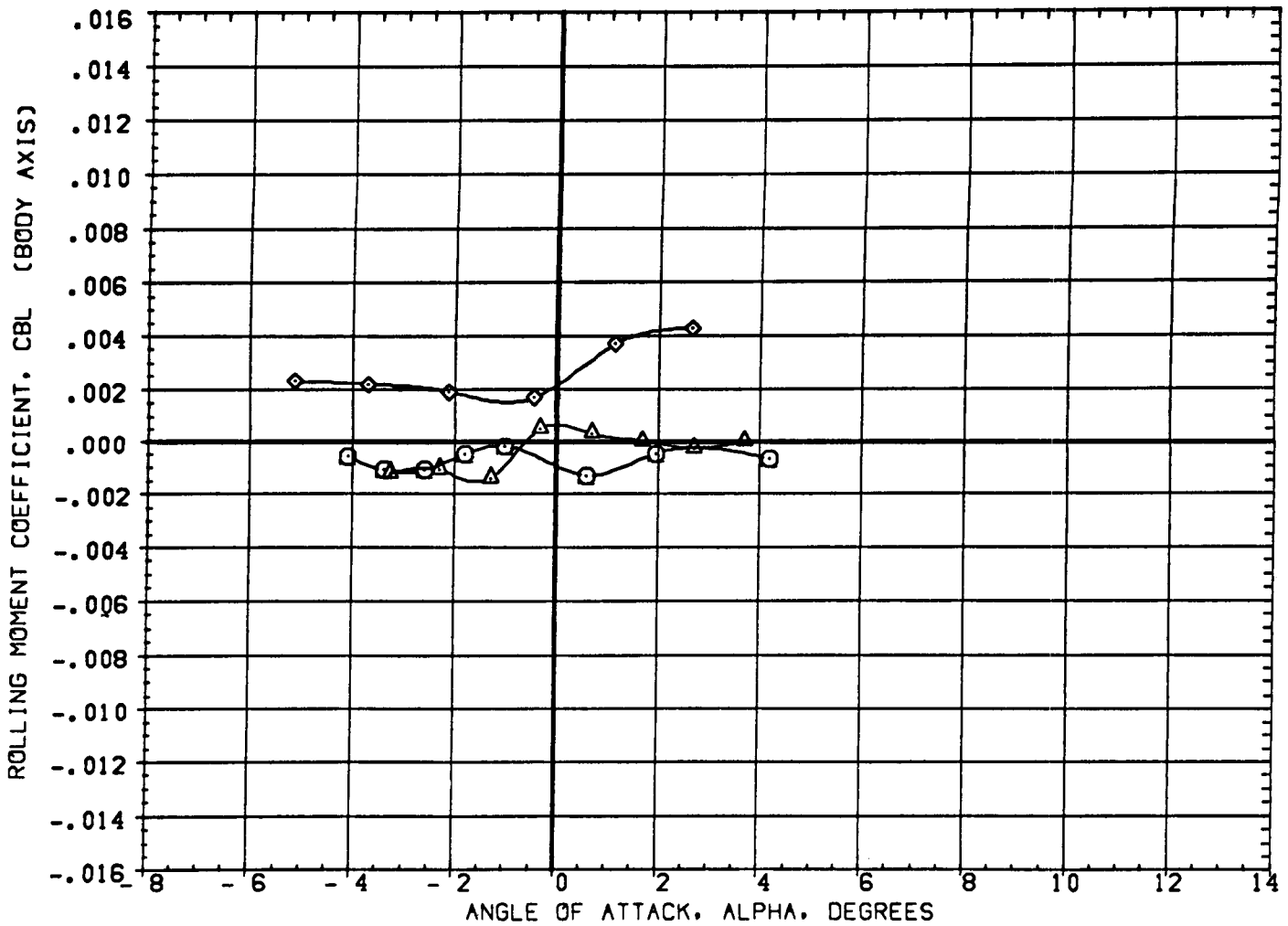

FIGURE 4 EFFECT OF WING AIRFOIL SECTION FOR AN OBLIQUE WING ANGLE OF 0 DEGREE

(A)MACH = .70

DATA SET	SYMBOL	CONFIGURATION DESCRIPTION	BETA	LAMBDA	RN/L
(2AE003)	○	W1 FO B	0.000	0.000	6.000
(2AE039)	△	W2 FO B	0.000	0.000	4.000
(2AE065)	◇	W4 FO B	0.000	0.000	6.000

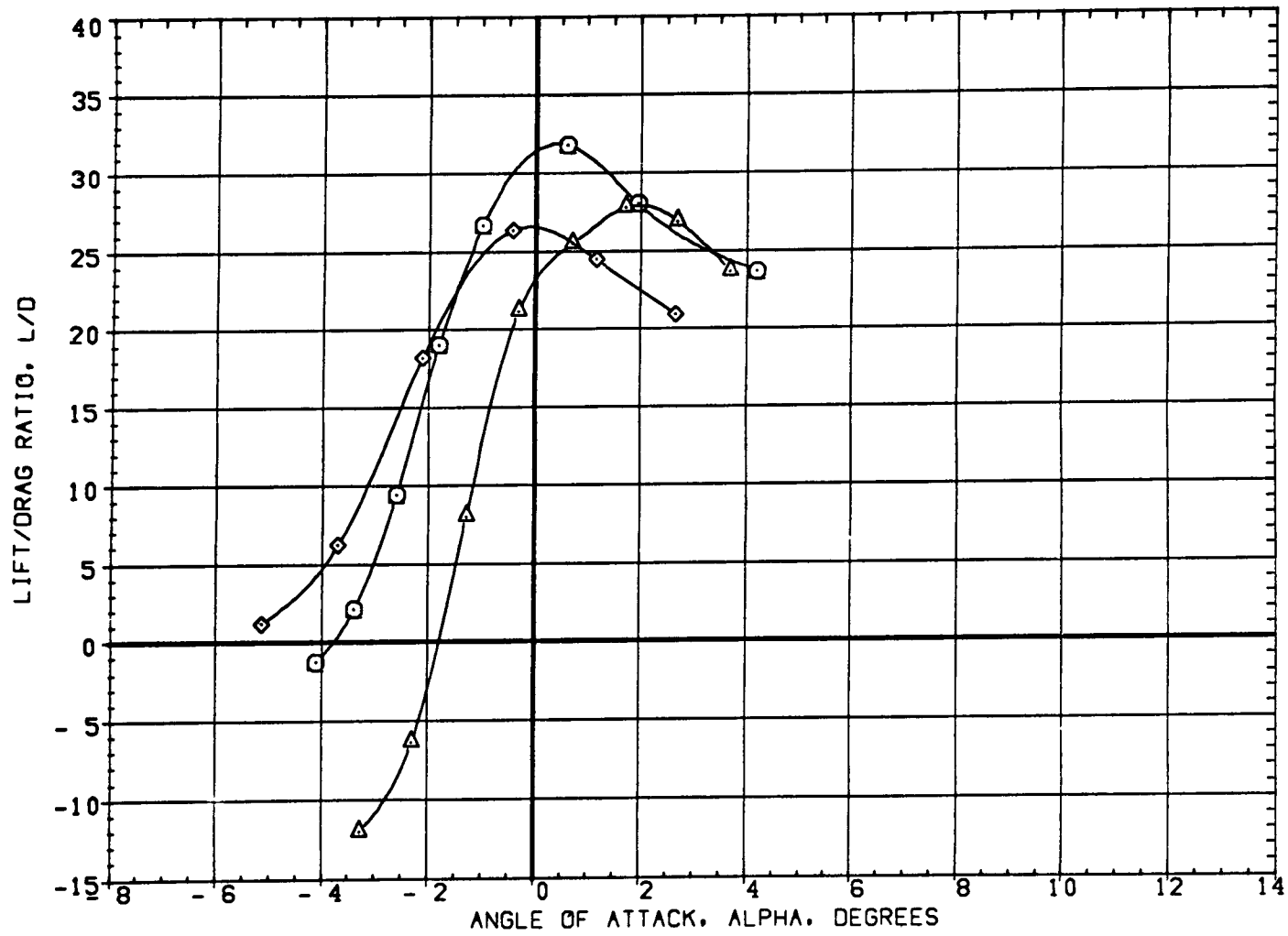

FIGURE 4 EFFECT OF WING AIRFOIL SECTION FOR AN OBLIQUE WING ANGLE OF 0 DEGREE

(A)MACH = .70

DATA SET	SYMBOL	CONFIGURATION DESCRIPTION	BETA	LAMBDA	RN/L
(3AE003)	○	W1 FO B	0.000	0.000	6.000
(3AE039)	△	W2 FO B	0.000	0.000	4.000
(3AE065)	◇	W4 FO B	0.000	0.000	6.000

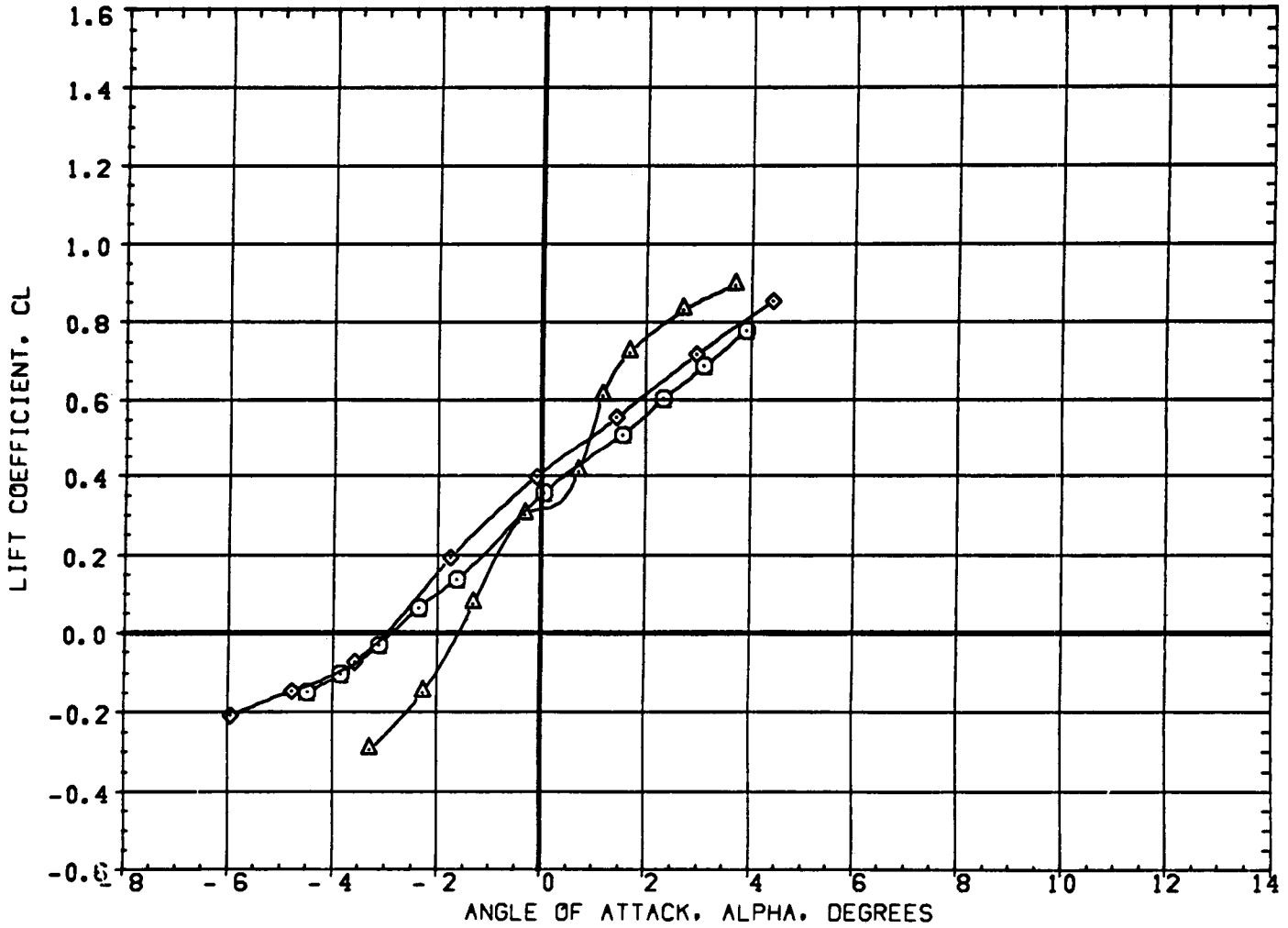

FIGURE 4 EFFECT OF WING AIRFOIL SECTION FOR AN OBLIQUE WING ANGLE OF 0 DEGREE

(A)MACH = .80

DATA SET	SYMBOL	CONFIGURATION DESCRIPTION	BETA	LAMBDA	RN/L
(3AE003)	○	W1 F0 B	0.000	0.000	6.000
(3AE039)	△	W2 F0 B	0.000	0.000	4.000
(3AE065)	◇	W4 F0 B	0.000	0.000	6.000

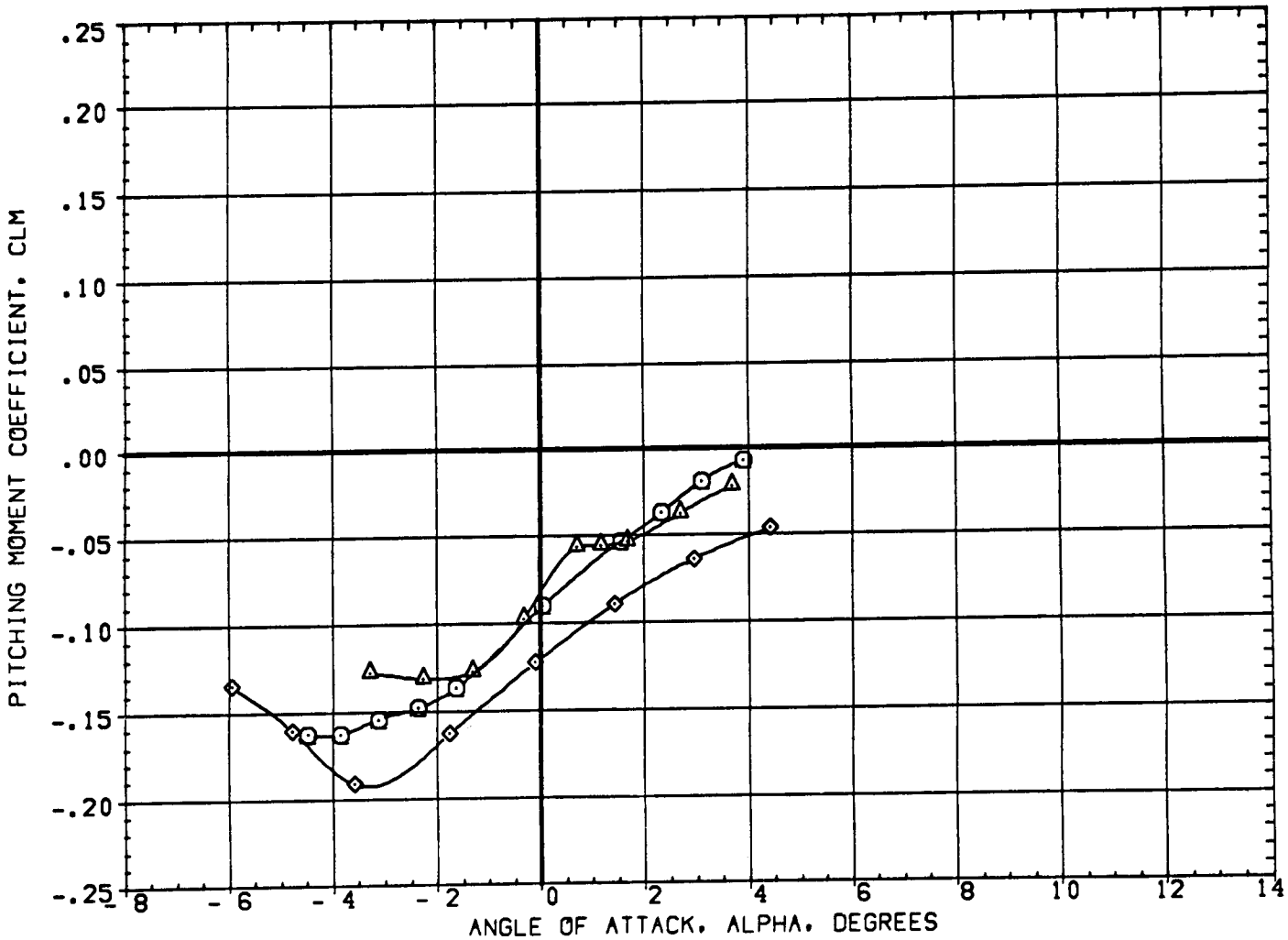

FIGURE 4 EFFECT OF WING AIRFOIL SECTION FOR AN OBLIQUE WING ANGLE OF 0 DEGREE

(A)MACH = .80

DATA SET	SYMBOL	CONFIGURATION DESCRIPTION	BETA	LAMBDA	RN/L
(3AE003)	○	W1 F0 B	0.000	0.000	6.000
(3AE039)	⊠	W2 F0 B	0.000	0.000	4.000
(3AE065)	◇	W4 F0 B	0.000	0.000	6.000

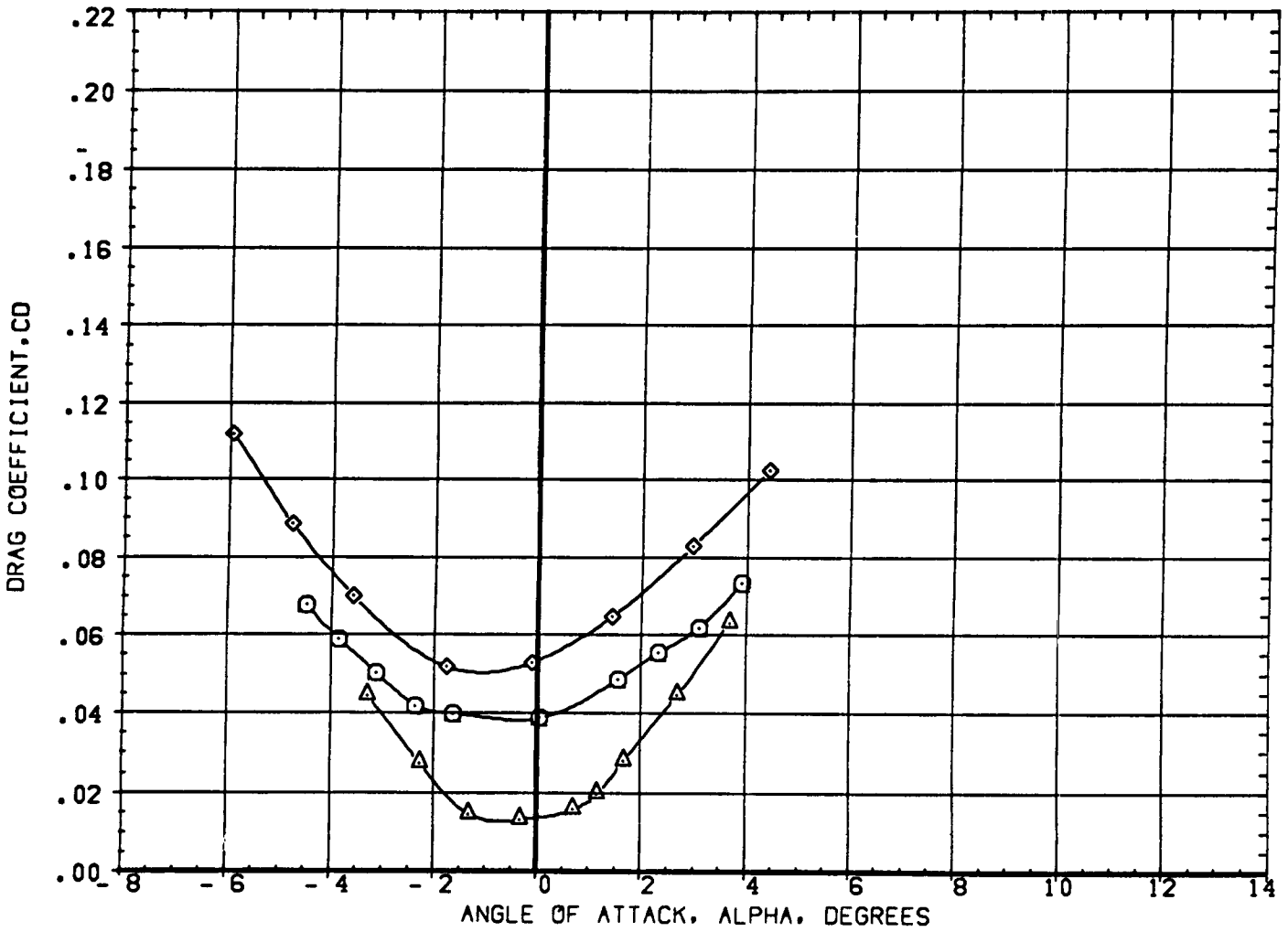

FIGURE 4 EFFECT OF WING AIRFOIL SECTION FOR AN OBLIQUE WING ANGLE OF 0 DEGREE

(A)MACH = .80

DATA SET	SYMBOL	CONFIGURATION DESCRIPTION	BETA	LAMBDA	RN/L
(3AE003)	○	W1 F0 B	0.000	0.000	6.000
(3AE039)	△	W2 F0 B	0.000	0.000	4.000
(3AE065)	◇	W4 F0 B	0.000	0.000	6.000

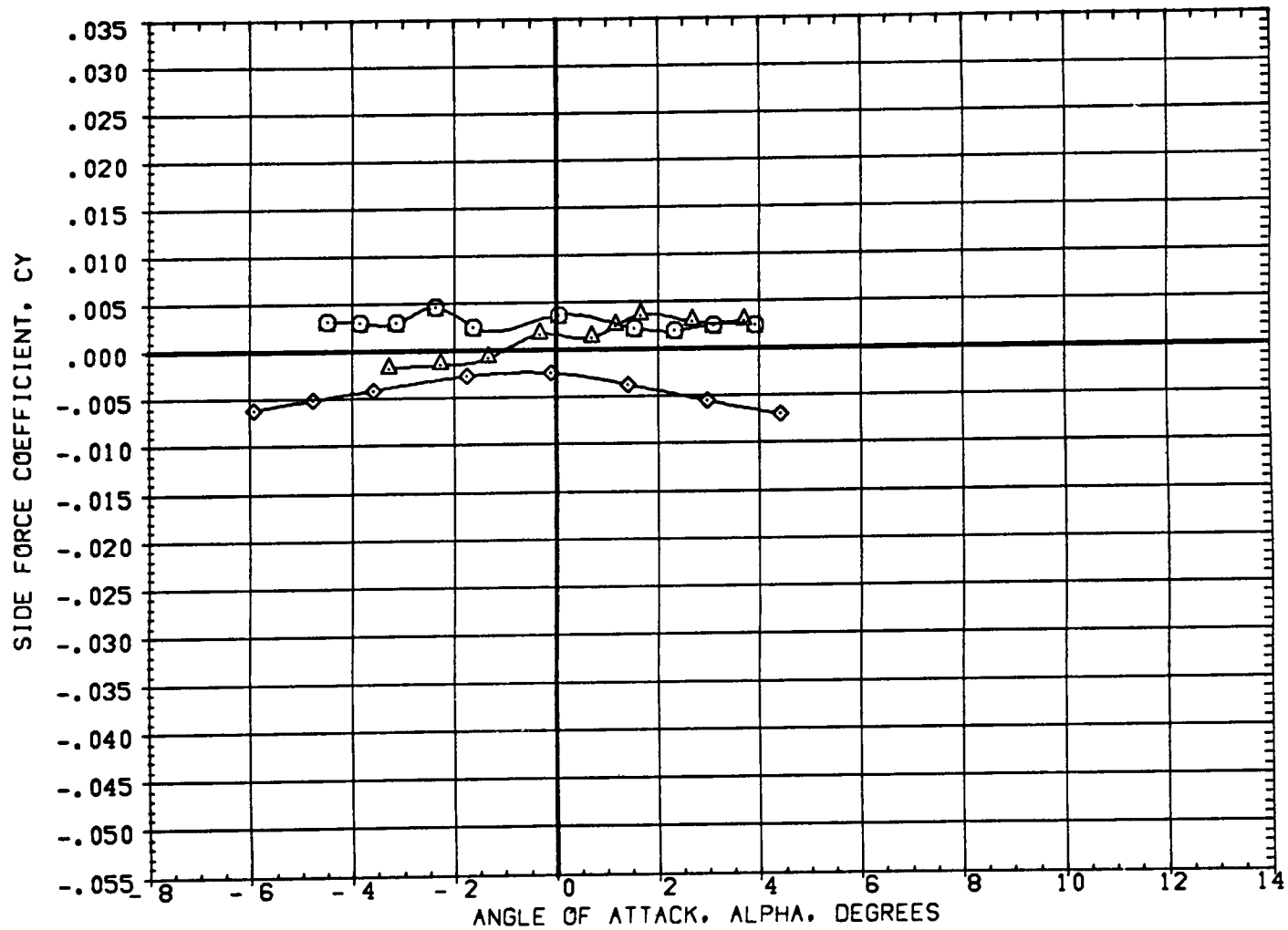

FIGURE 4 EFFECT OF WING AIRFOIL SECTION FOR AN OBLIQUE WING ANGLE OF 0 DEGREE

(A)MACH = .80

DATA SET	SYMBOL	CONFIGURATION DESCRIPTION	BETA	LAMBDA	RN/L
(3AE003)	○	W1 F0 B	0.000	0.000	6.000
(3AE039)	△	W2 F0 B	0.000	0.000	4.000
(3AE065)	◇	W4 F0 B	0.000	0.000	6.000

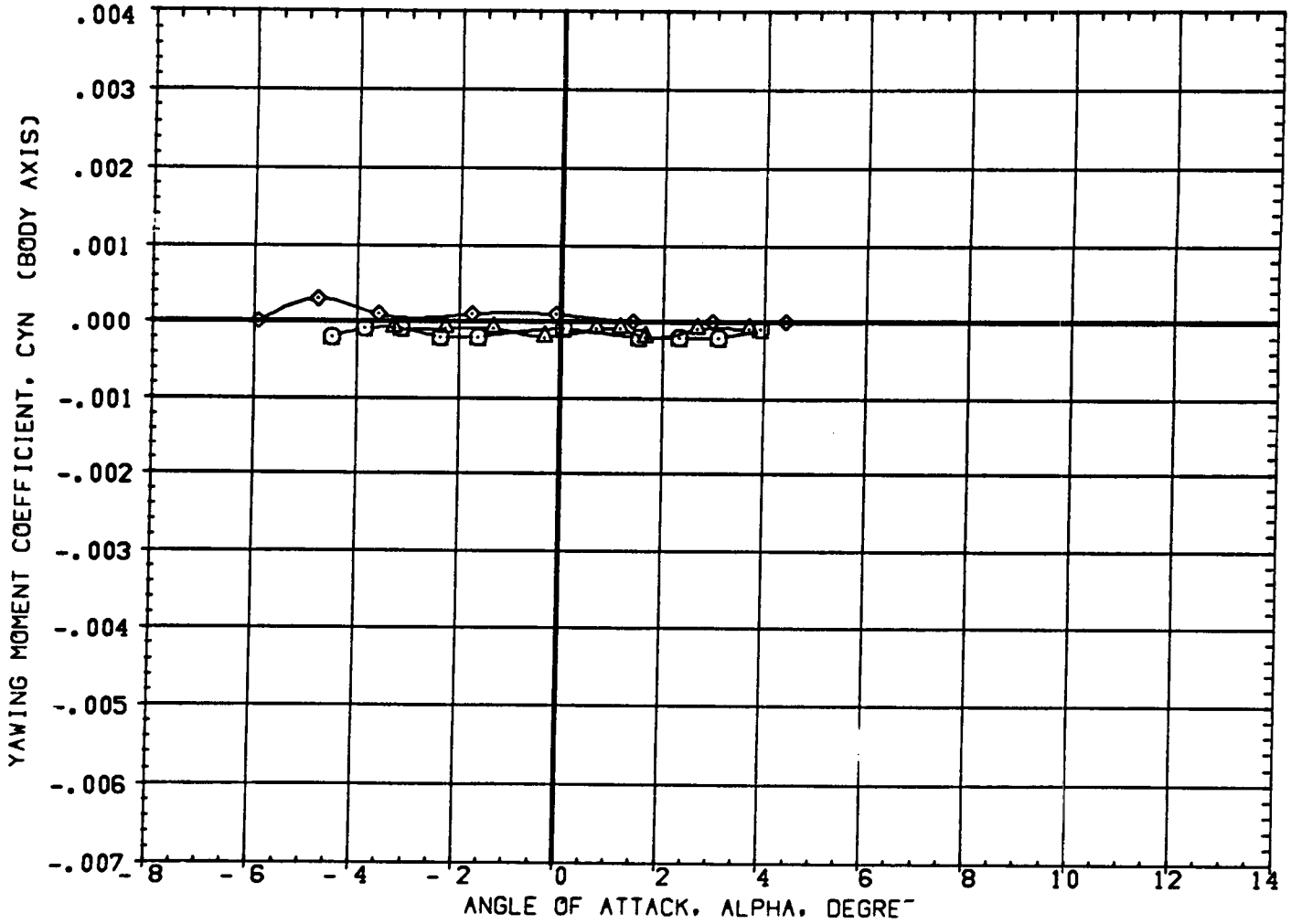

FIGURE 4 EFFECT OF WING AIRFOIL SECTION FOR AN OBLIQUE WING ANGLE OF 0 DEGREE

(A)MACH = .80

DATA SET	SYMBOL	CONFIGURATION DESCRIPTION	BETA	LAMBDA	RN/L
(3AE003)	○	W1 F0 B	0.000	0.000	6.000
(3AE039)	△	W2 F0 B	0.000	0.000	4.000
(3AE065)	◇	W4 F0 B	0.000	0.000	6.000

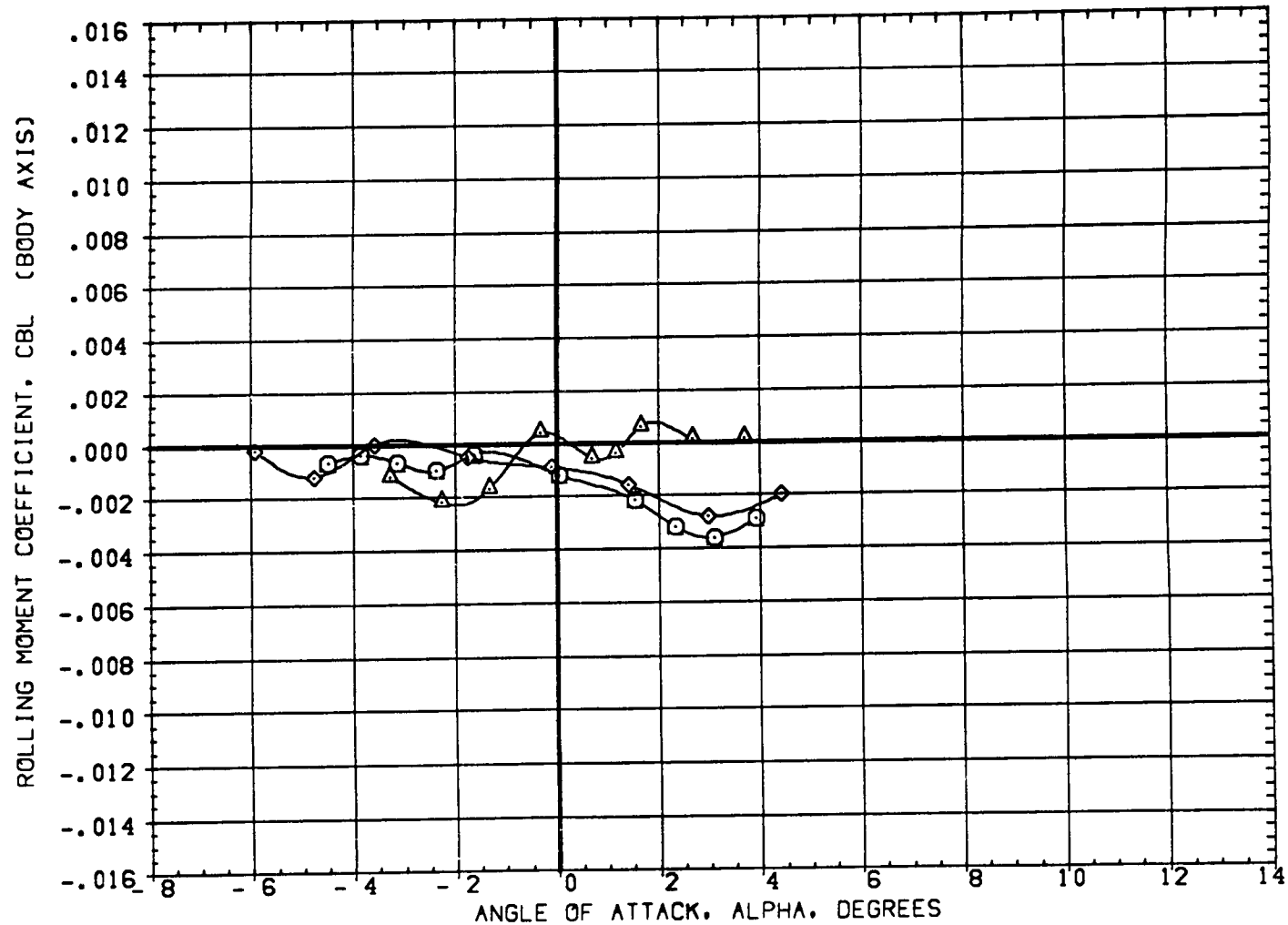

FIGURE 4 EFFECT OF WING AIRFOIL SECTION FOR AN OBLIQUE WING ANGLE OF 0 DEGREE

(A)MACH = .80

DATA SET	SYMBOL	CONFIGURATION DESCRIPTION	BETA	LAMBDA	RN/L
(3AE003)	○	W1 FD B	0.000	0.000	6.000
(3AE039)	△	W2 FD B	0.000	0.000	4.000
(3AE065)	◇	W4 FD B	0.000	0.000	6.000

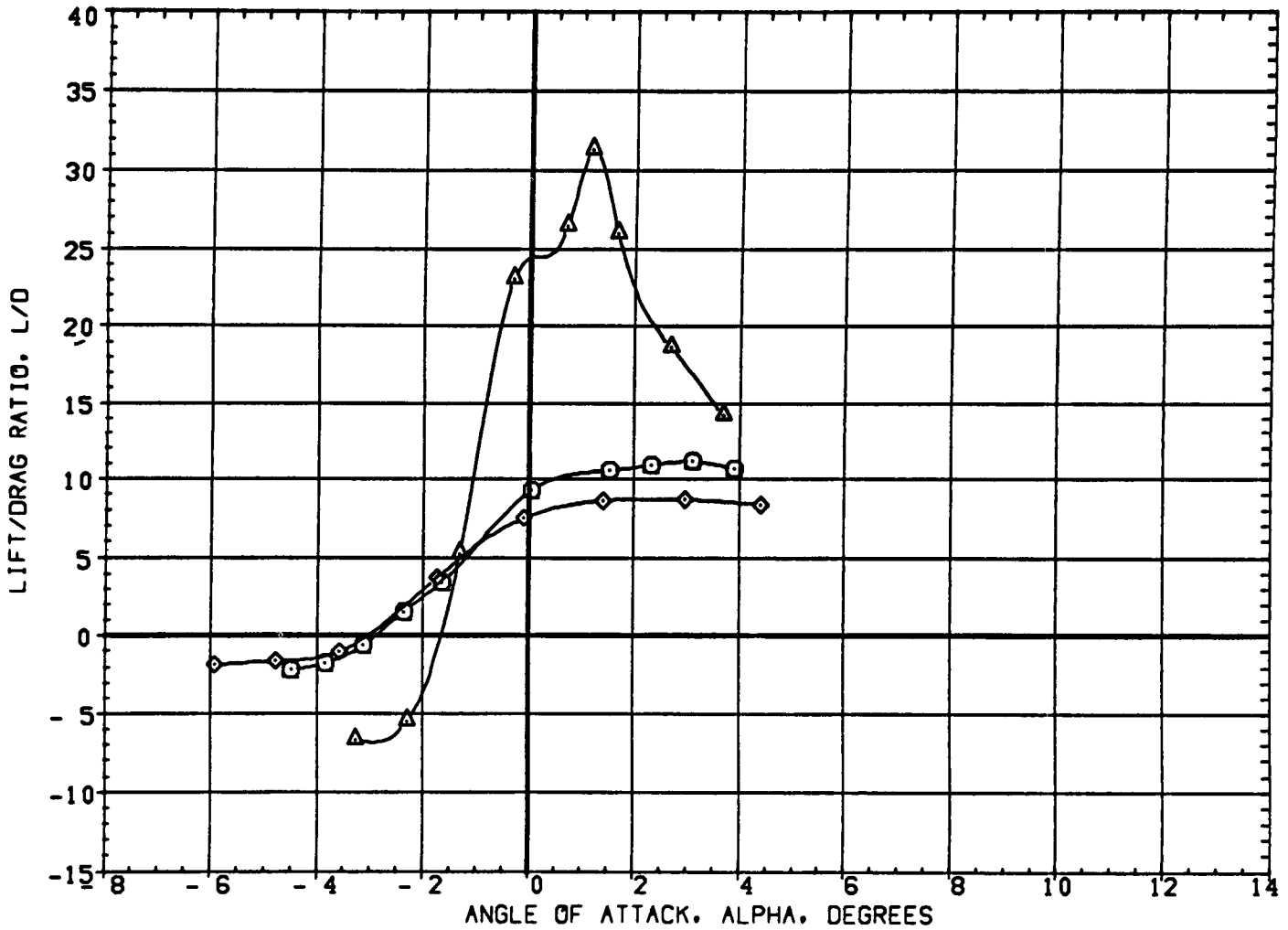

FIGURE 4 EFFECT OF WING AIRFOIL SECTION FOR AN OBLIQUE WING ANGLE OF 0 DEGREE

(A)MACH = .80

DATA SET	SYMBOL	CONFIGURATION DESCRIPTION	BETA	LAMBDA	RN/L
(2AE005)	○	W1 F0 B	0.000	45.000	6.000
(2AE041)	△	W2 F0 B	0.000	45.000	4.000
(2AE066)	◇	W4 F0 B	0.000	45.000	6.000

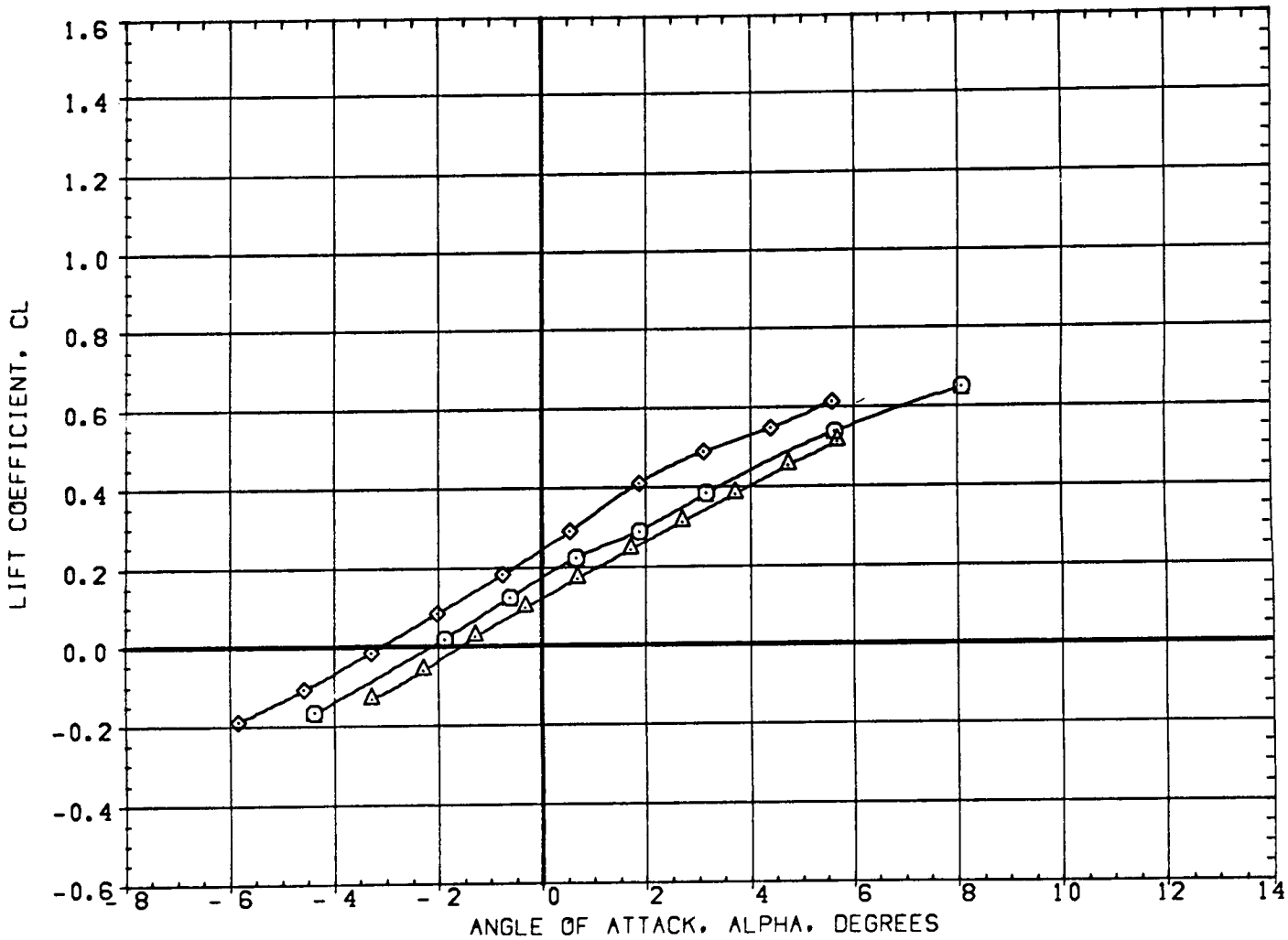

FIGURE 5 EFFECT OF WING AIRFOIL SECTION FOR AN OBLIQUE WING ANGLE OF 45 DEGREES

(A)MACH = .70

DATA SET	SYMBOL	CONFIGURATION DESCRIPTION	BETA	LAMBDA	RN/L
(2AE005)	○	W1 F0 B	0.000	45.000	6.000
(2AE041)	△	W2 F0 B	0.000	45.000	4.000
(2AE066)	◇	W4 F0 B	0.000	45.000	6.000

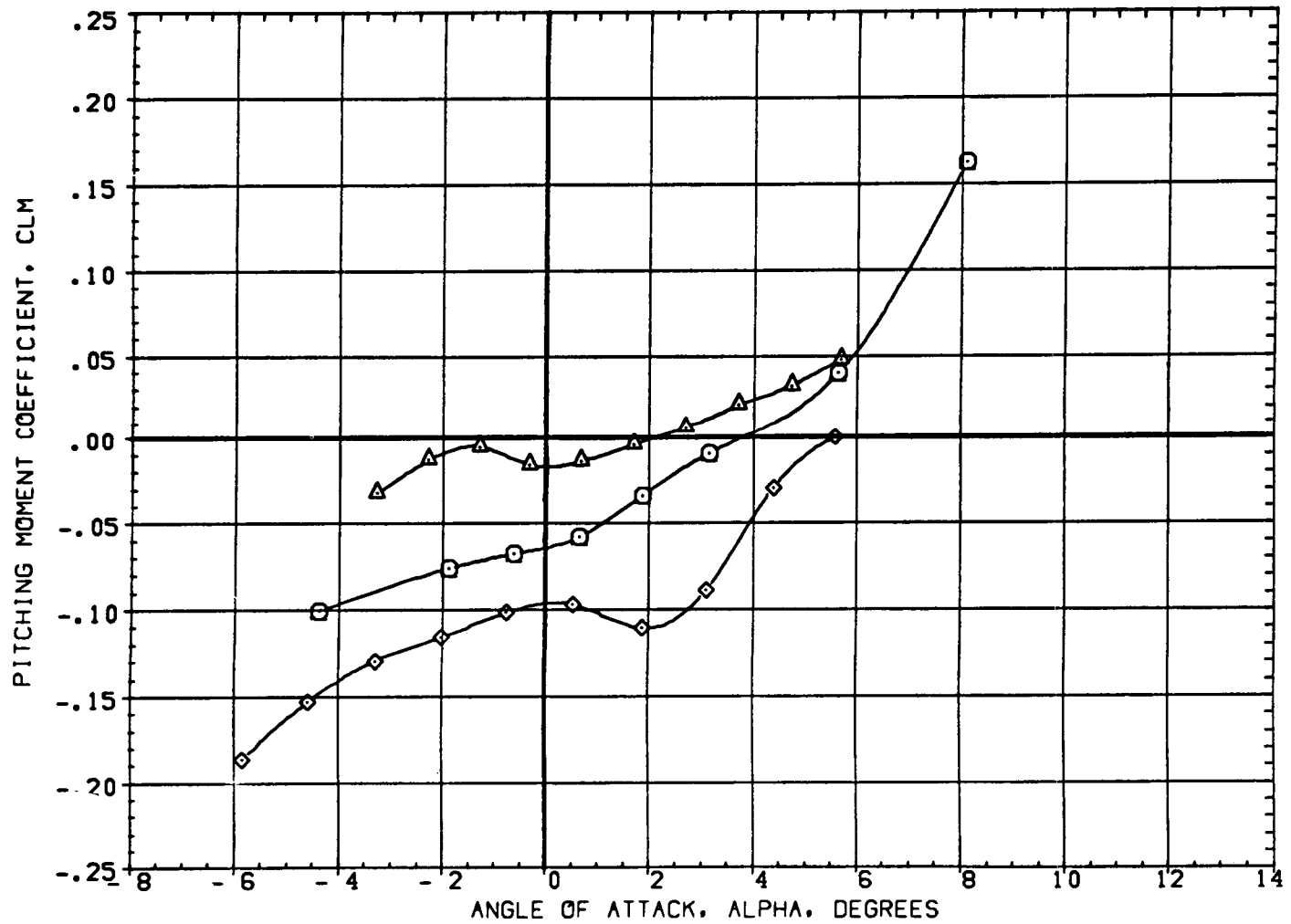

FIGURE 5 EFFECT OF WING AIRFOIL SECTION FOR AN OBLIQUE WING ANGLE OF 45 DEGREES

(A)MACH = .70

DATA SET	SYMBOL	CONFIGURATION DESCRIPTION
(2AE005)	○	W1 F0 B
(2AE041)	△	W2 F0 B
(2AE066)	◇	W4 F0 B

BETA	LAMBDA	RN/L
0.000	45.000	6.000
0.000	45.000	4.000
0.000	45.000	6.000

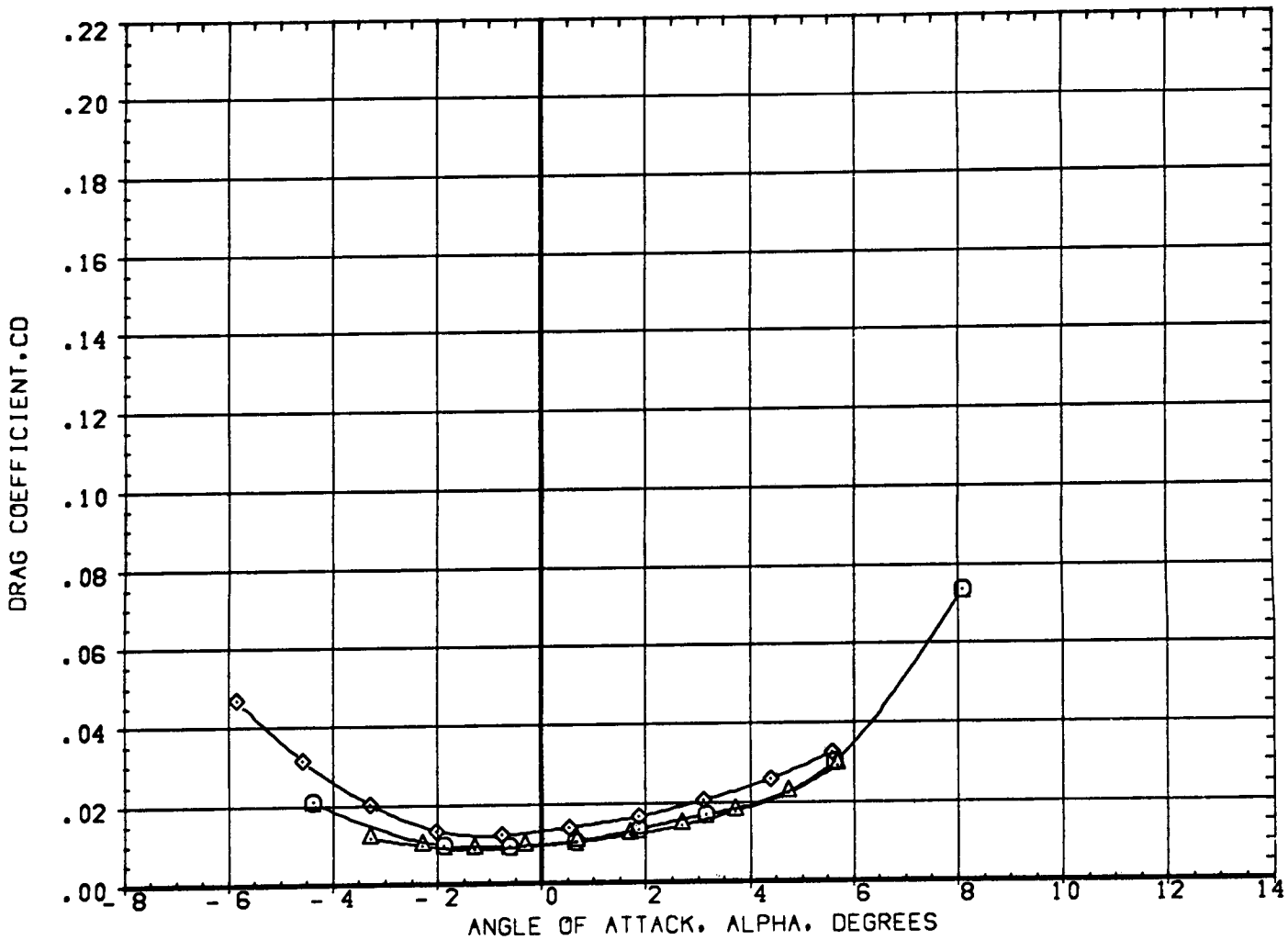

FIGURE 5 EFFECT OF WING AIRFOIL SECTION FOR AN OBLIQUE WING ANGLE OF 45 DEGREES

(A)MACH = .70

DATA SET	SYMBOL	CONFIGURATION DESCRIPTION	BETA	LAMBDA	RN/L
(2AE005)	○	W1 F0 B	0.000	45.000	6.000
(2AE041)	△	W2 F0 B	0.000	45.000	4.000
(2AE066)	◇	W4 F0 B	0.000	45.000	6.000

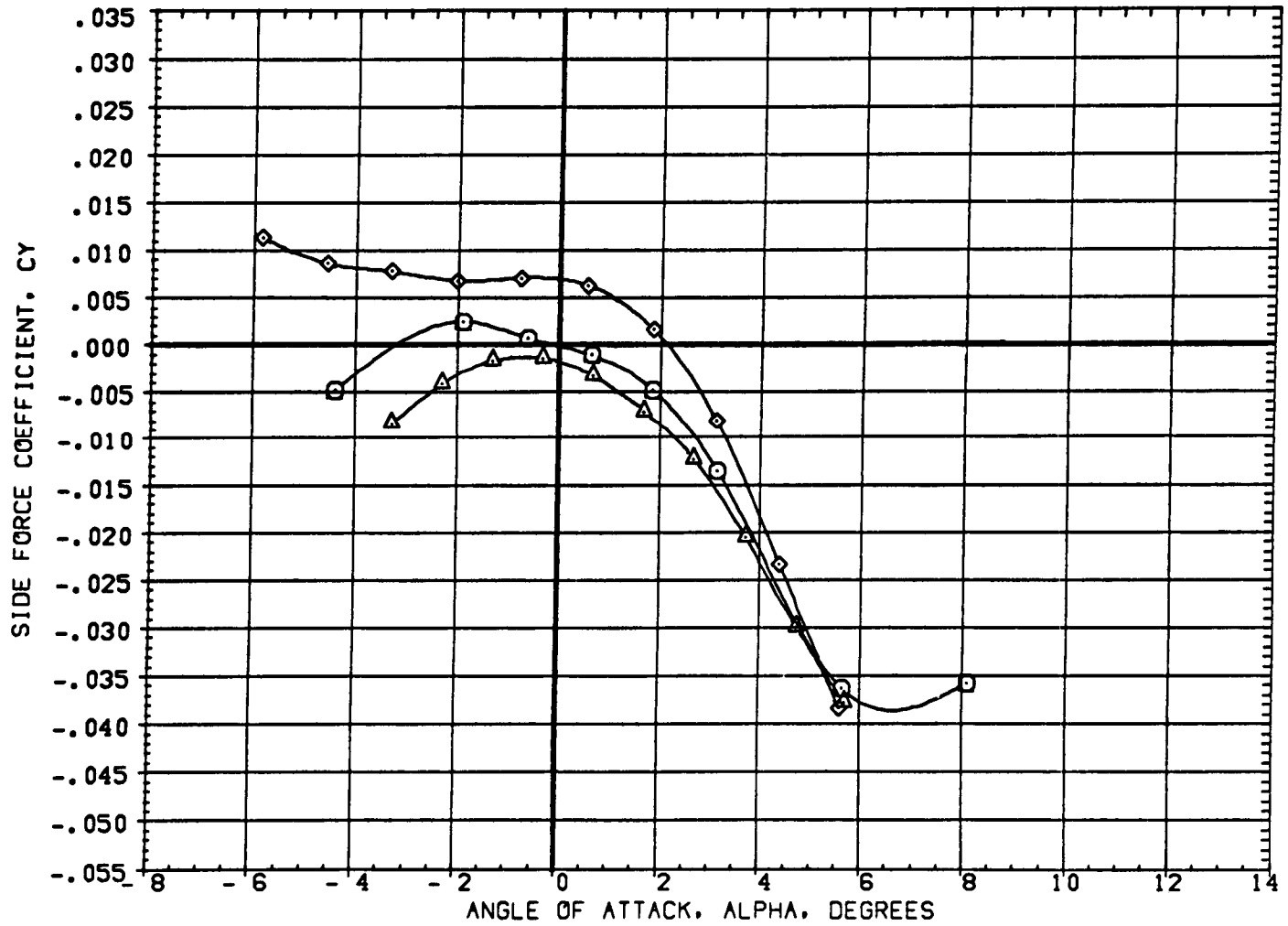

FIGURE 5 EFFECT OF WING AIRFOIL SECTION FOR AN OBLIQUE WING ANGLE OF 45 DEGREES

(A)MACH = .70

DATA SET	SYMBOL	CONFIGURATION DESCRIPTION	BETA	LAMBDA	RN/L
(2AE005)	○	W1 FD B	0.000	45.000	6.000
(2AE041)	△	W2 FD B	0.000	45.000	4.000
(2AE066)	◇	W4 FD B	0.000	45.000	6.000

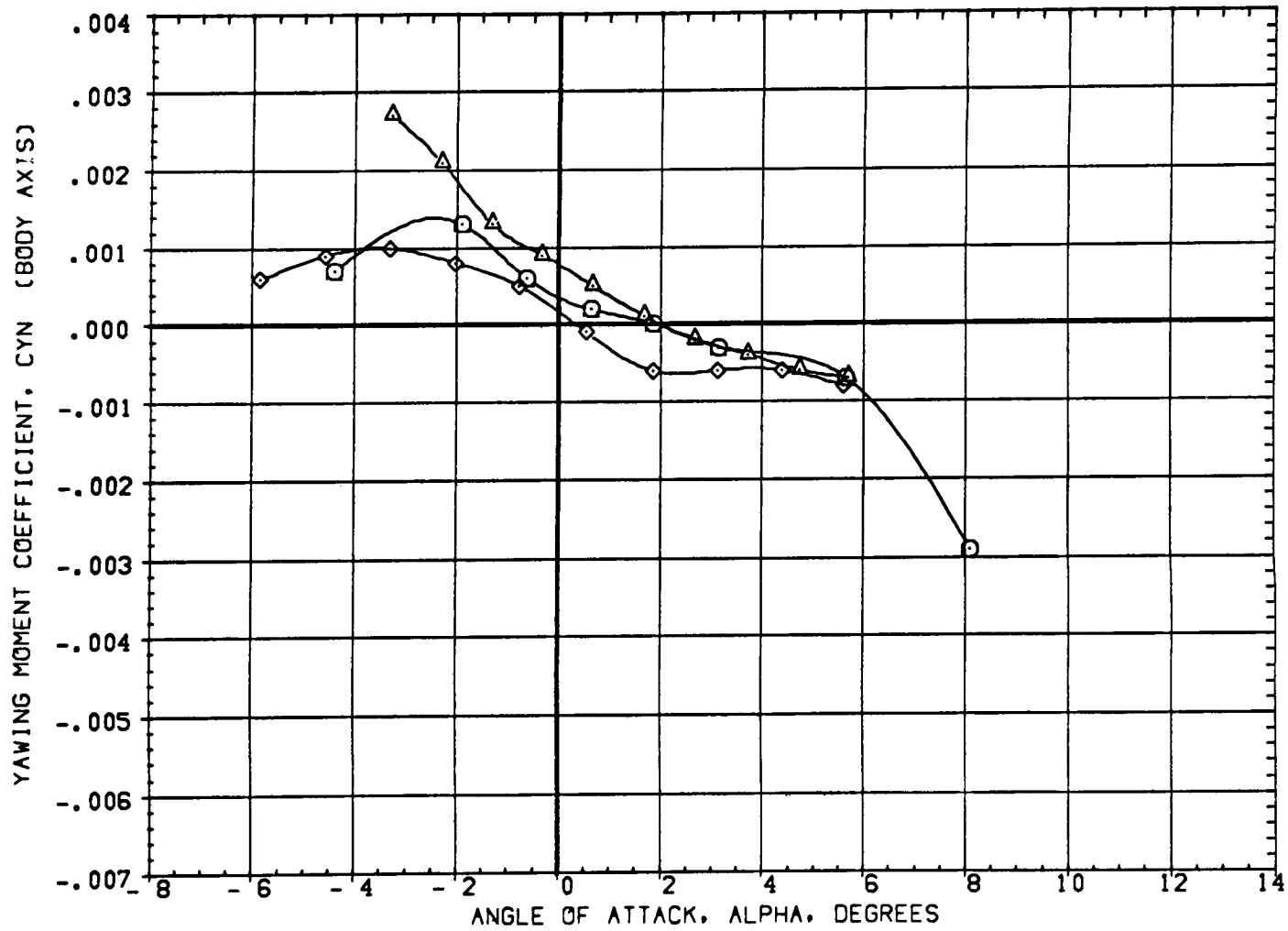

FIGURE 5 EFFECT OF WING AIRFOIL SECTION FOR AN OBLIQUE WING ANGLE OF 45 DEGREES

(A)MACH = .70

DATA SET	SYMBOL	CONFIGURATION DESCRIPTION	BETA	LAMBDA	RN/L
(2AE005)	○	W1 F0 B	0.000	45.000	6.000
(2AE041)	△	W2 F0 B	0.000	45.000	4.000
(2AE066)	◇	W4 F0 B	0.000	45.000	6.000

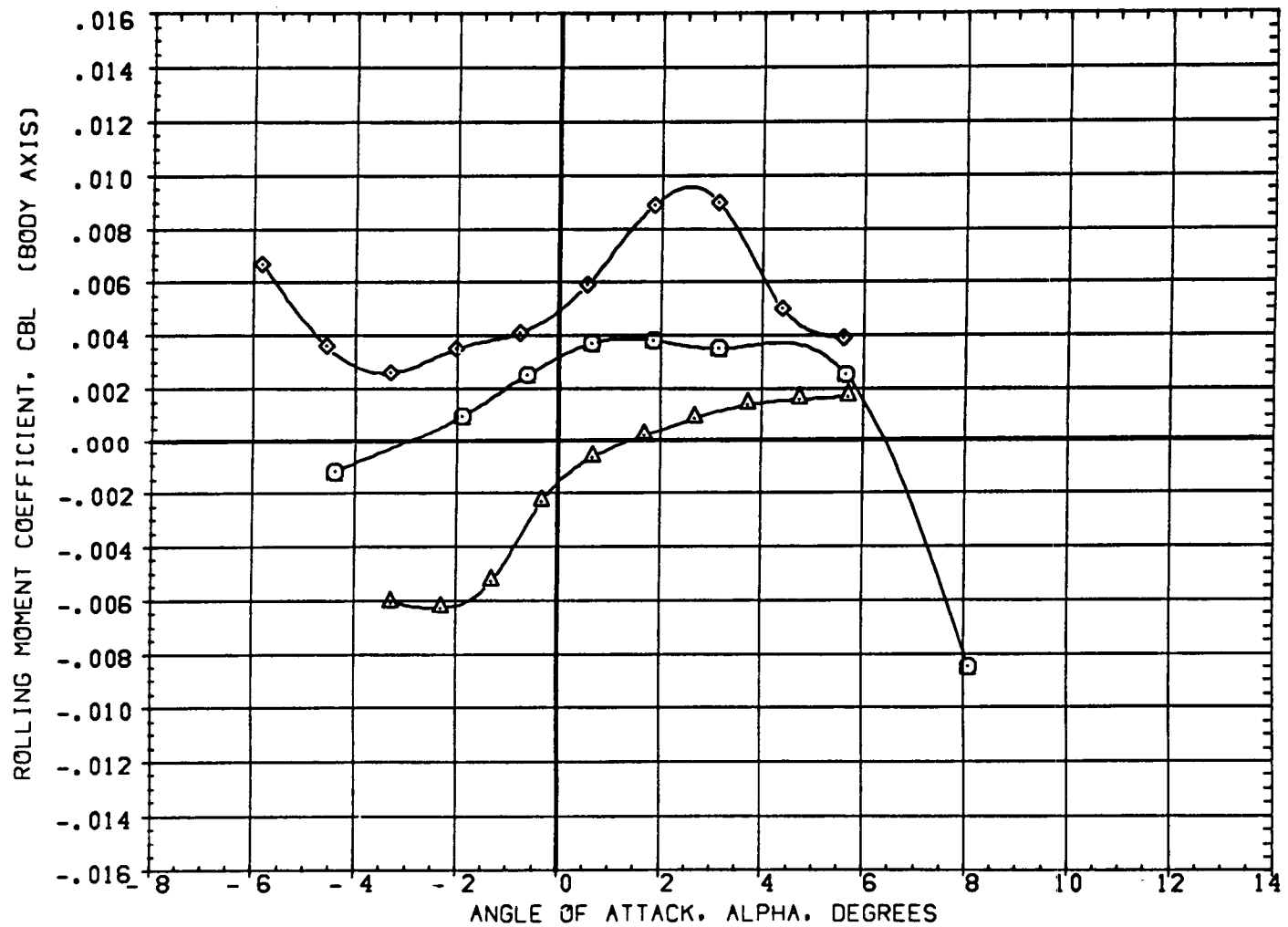

FIGURE 5 EFFECT OF WING AIRFOIL SECTION FOR AN OBLIQUE WING ANGLE OF 45 DEGREES

(A)MACH = .70

DATA SET	SYMBOL	CONFIGURATION DESCRIPTION	BETA	LAMBDA	RN/L
(2AE005)	○	W1 F0 B	0.000	45.000	6.000
(2AE041)	△	W2 F0 B	0.000	45.000	4.000
(2AE066)	◇	W4 F0 B	0.000	45.000	6.000

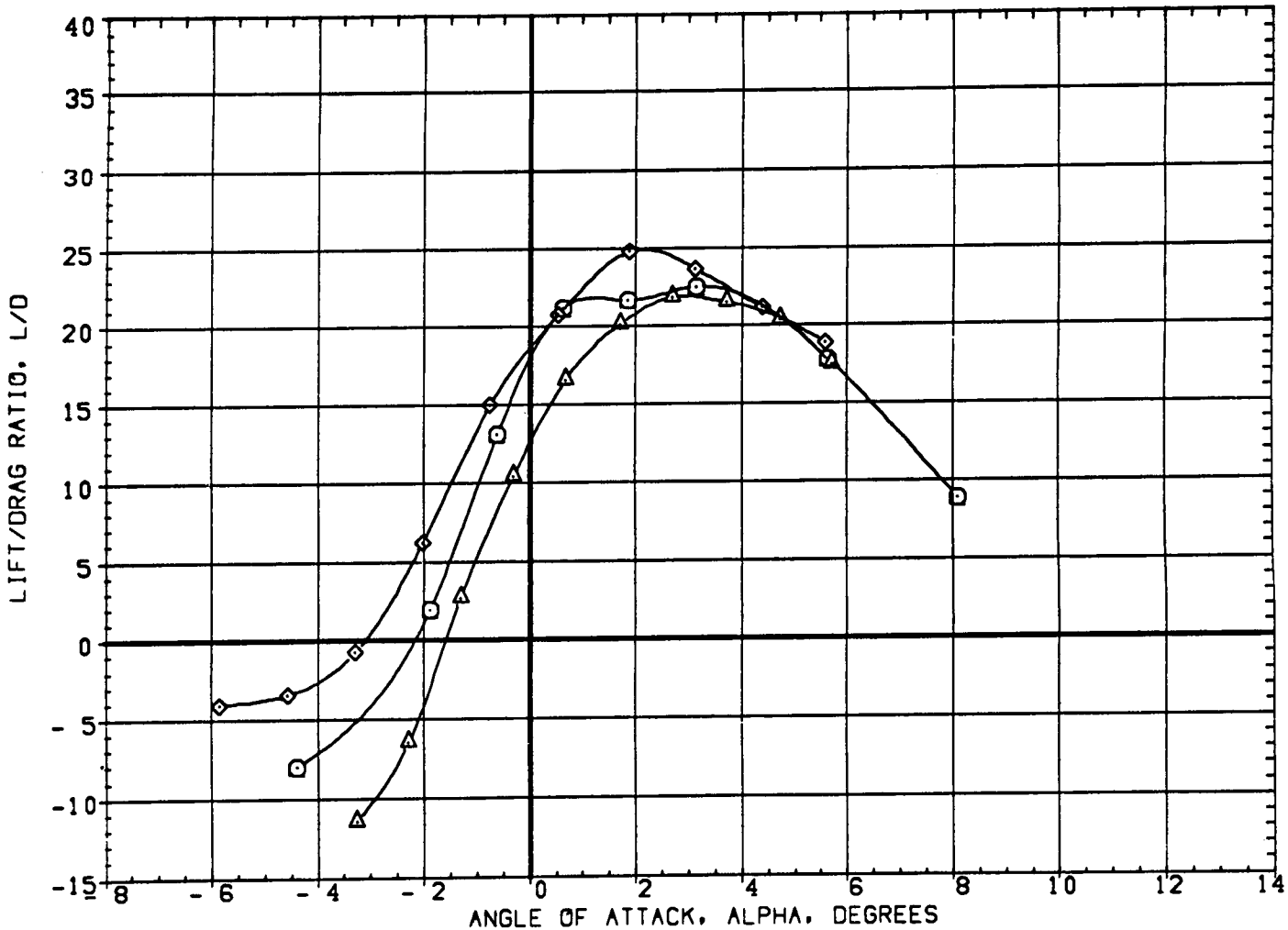

FIGURE 5 EFFECT OF WING AIRFOIL SECTION FOR AN OBLIQUE WING ANGLE OF 45 DEGREES

(A)MACH = .70

DATA SET	SYMBOL	CONFIGURATION DESCRIPTION	BETA	LAMBDA	RN/L
(3AE008)	○	W1 FO B	0.000	45.000	6.000
(3AE041)	△	W2 FO B	0.000	45.000	4.000
(3AE066)	◇	W4 FO B	0.000	45.000	6.000

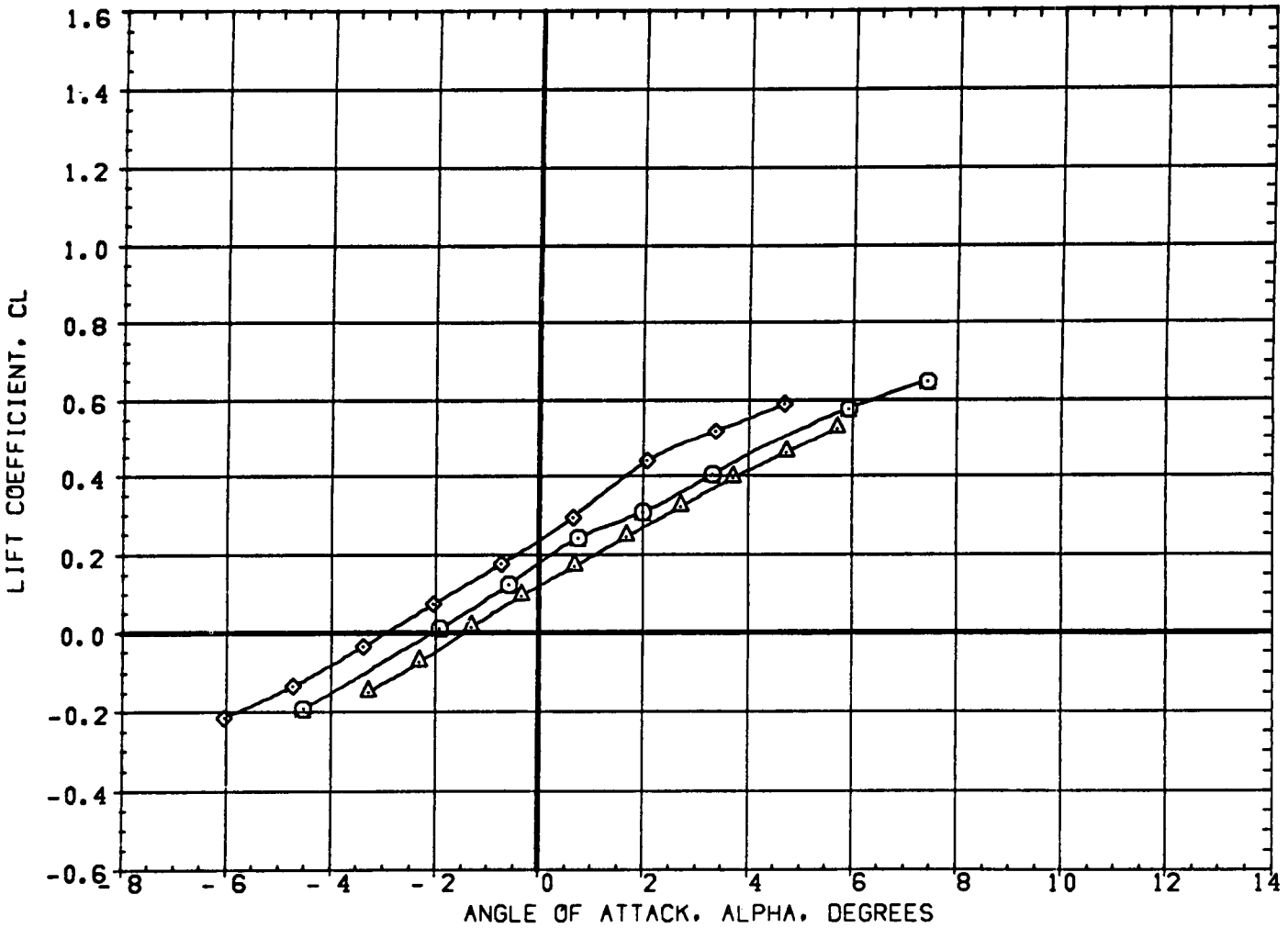

FIGURE 5 EFFECT OF WING AIRFOIL SECTION FOR AN OBLIQUE WING ANGLE OF 45 DEGREES

(A)MACH = .80

DATA SET	SYMBOL	CONFIGURATION DESCRIPTION	BETA	LAMBDA	RN/L
(3AE005)	○	W1 FO B	0.000	45.000	6.000
(3AE041)	△	W2 FO B	0.000	45.000	4.000
(3AE066)	◇	W4 FO B	0.000	45.000	6.000

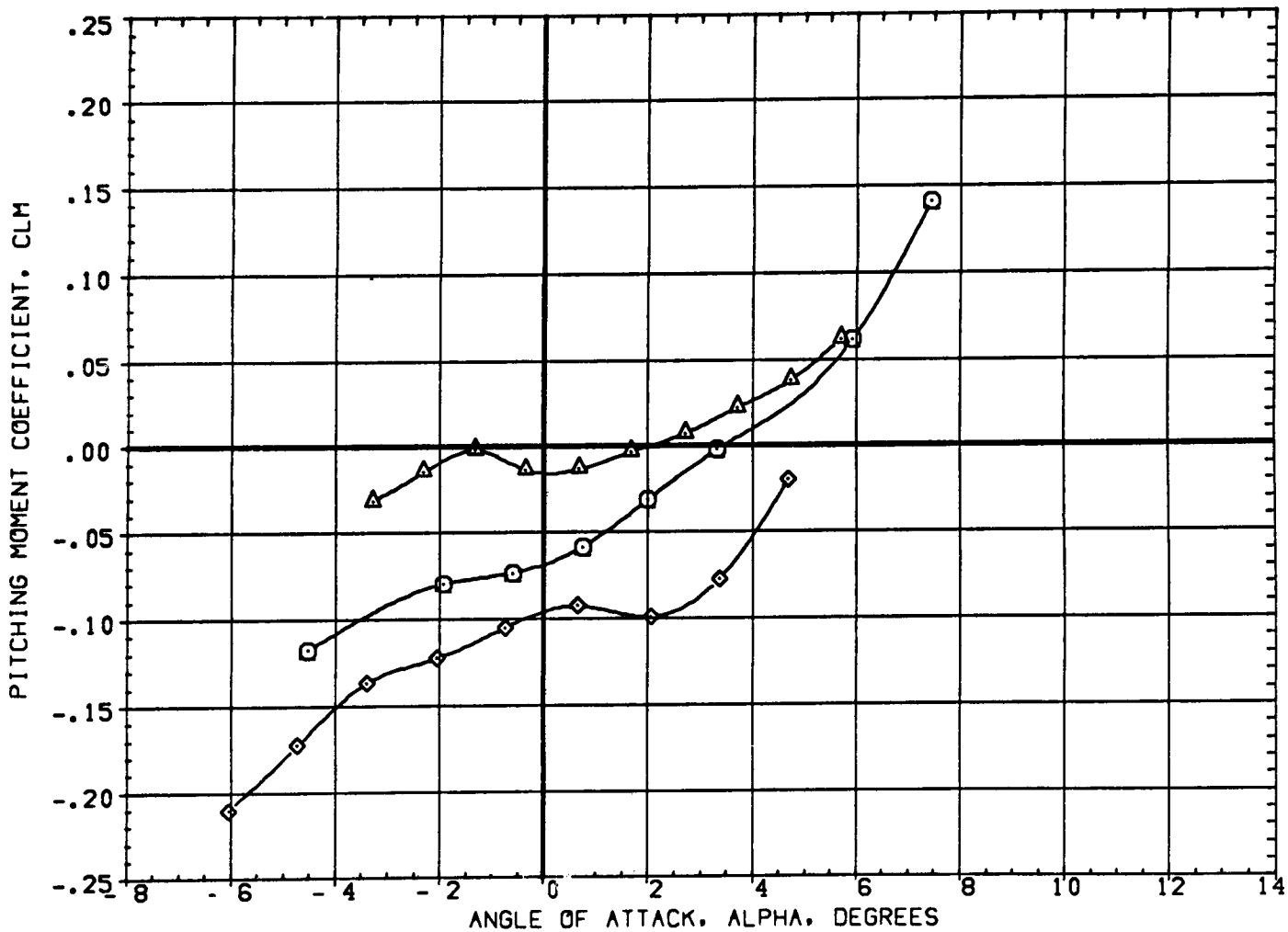

FIGURE 5 EFFECT OF WING AIRFOIL SECTION FOR AN OBLIQUE WING ANGLE OF 45 DEGREES

(A)MACH = .80

DATA SET	SYMBOL	CONFIGURATION DESCRIPTION	BETA	LAMBDA	RN/L
(3AE005)	○	W1 F0 B	0.000	45.000	6.000
(3AE041)	△	W2 F0 B	0.000	45.000	4.000
(3AE066)	◇	W4 F0 B	0.000	45.000	6.000

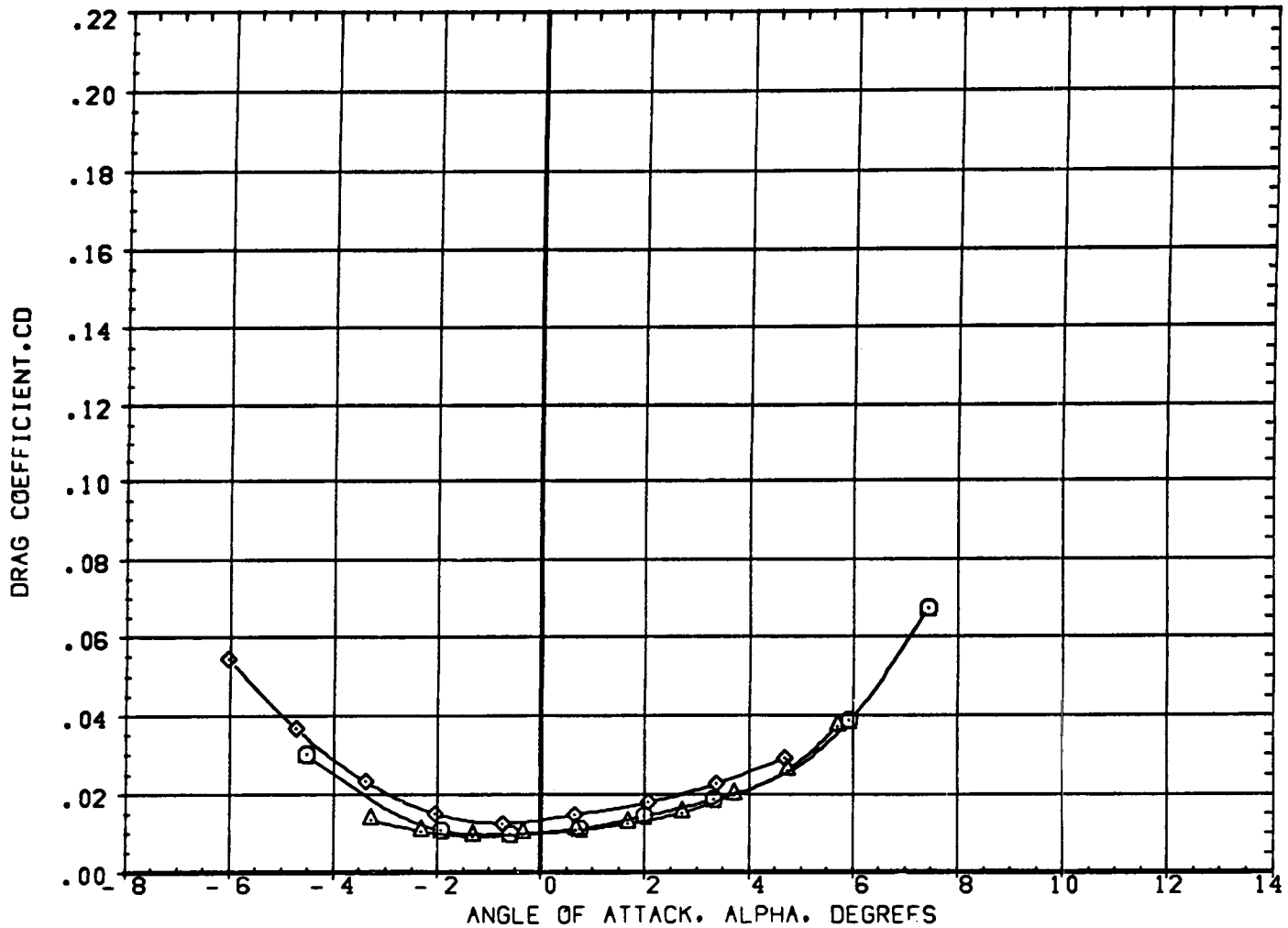

FIGURE 5 EFFECT OF WING AIRFOIL SECTION FOR AN OBLIQUE WING ANGLE OF 45 DEGREES

(A)MACH = .80

DATA SET	SYMBOL	CONFIGURATION DESCRIPTION	BETA	LAMBDA	RN/L
(3AE005)	○	W1 FO B	0.000	45.000	0.000
(3AE041)	△	W2 FO B	0.000	45.000	4.000
(3AE066)	◇	W4 FO B	0.000	45.000	6.000

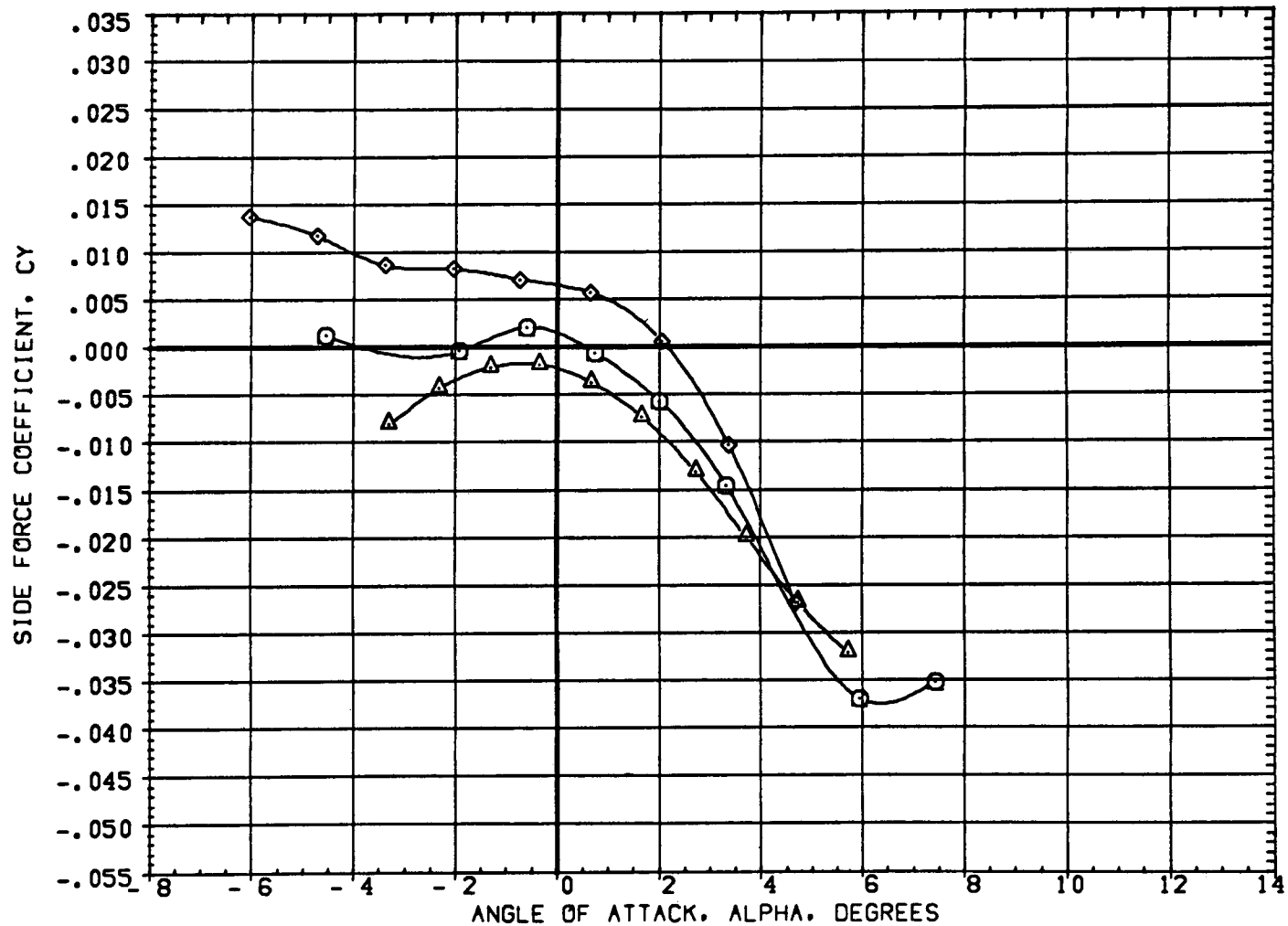

FIGURE 5 EFFECT OF WING AIRFOIL SECTION FOR AN OBLIQUE WING ANGLE OF 45 DEGREES

(A)MACH = .80

DATA SET	SYMBOL	CONFIGURATION DESCRIPTION	BETA	LAMBDA	RN/L
(3AE005)	○	W1 FO B	0.000	45.000	6.000
(3AE041)	△	W2 FO B	0.000	45.000	4.000
(3AE066)	◇	W4 FO B	0.000	45.000	6.000

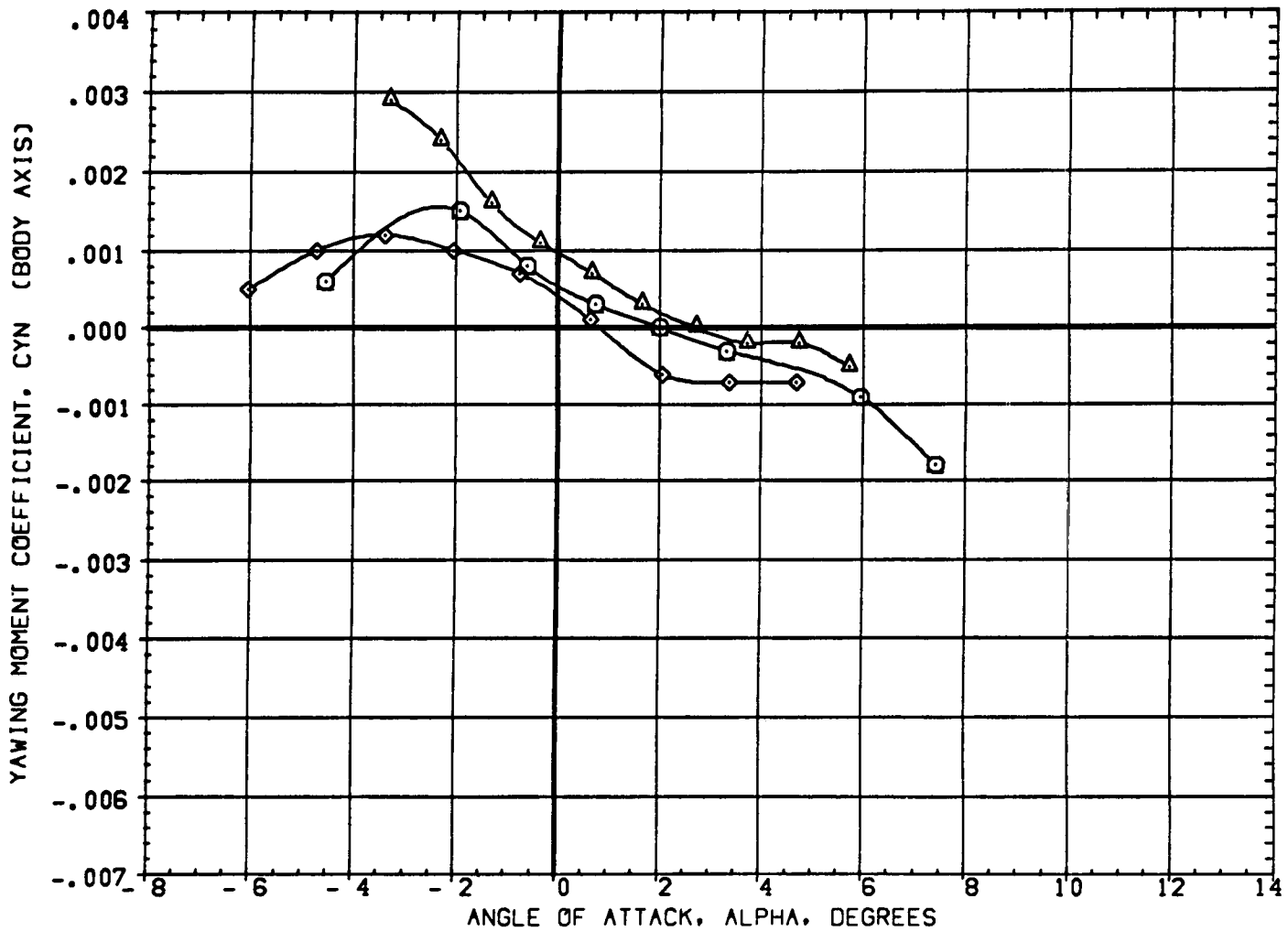

FIGURE 5 EFFECT OF WING AIRFOIL SECTION FOR AN OBLIQUE WING ANGLE OF 45 DEGREES

(A)MACH = .80

DATA SET	SYMBOL	CONFIGURATION DESCRIPTION	BETA	LAMBDA	RN/L
(3AE005)	○	W1 F0 B	0.000	45.000	6.000
(3AE041)	△	W2 F0 B	0.000	45.000	4.000
(3AE066)	◇	W4 F0 B	0.000	45.000	6.000

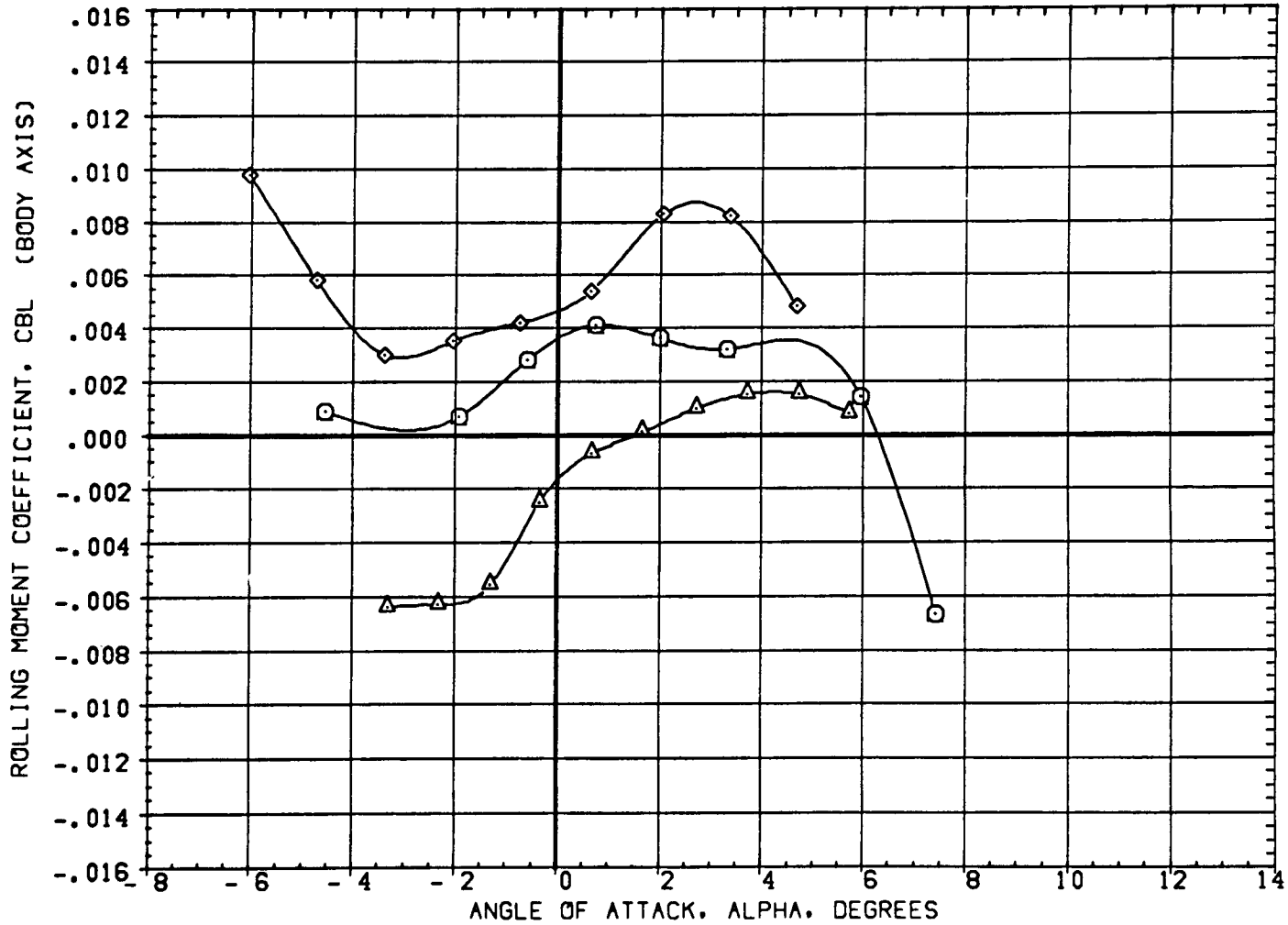

FIGURE 5 EFFECT OF WING AIRFOIL SECTION FOR AN OBLIQUE WING ANGLE OF 45 DEGREES

(A)MACH = .80

DATA SET	SYMBOL	CONFIGURATION DESCRIPTION	BETA	LAMBDA	RN/L
(3AE005)	○	W1 F0 B	0.000	45.000	6.000
(3AE041)	△	W2 F0 B	0.000	45.000	4.000
(3AE066)	◇	W4 F0 B	0.000	45.000	6.000

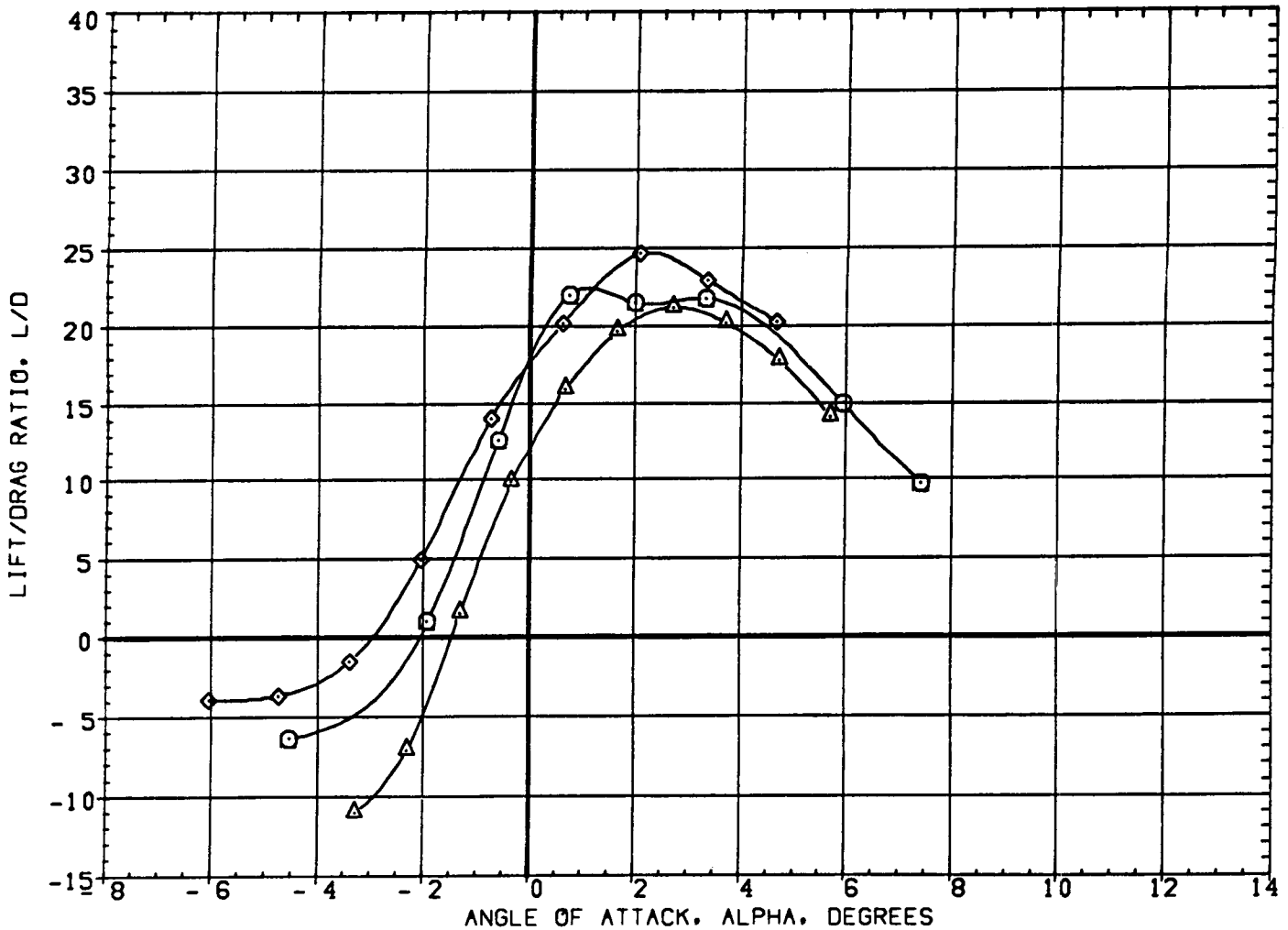

FIGURE 5 EFFECT OF WING AIRFOIL SECTION FOR AN OBLIQUE WING ANGLE OF 45 DEGREES

(A)MACH = .80

DATA SET	SYMBOL	CONFIGURATION DESCRIPTION
(4AE005)	○	W1 FO B
(4AE041)	△	W2 FO B
(4AE066)	◇	W4 FO B

BETA	LAMBDA	RN/L
0.000	45.000	6.000
0.000	45.000	4.000
0.000	45.000	6.000

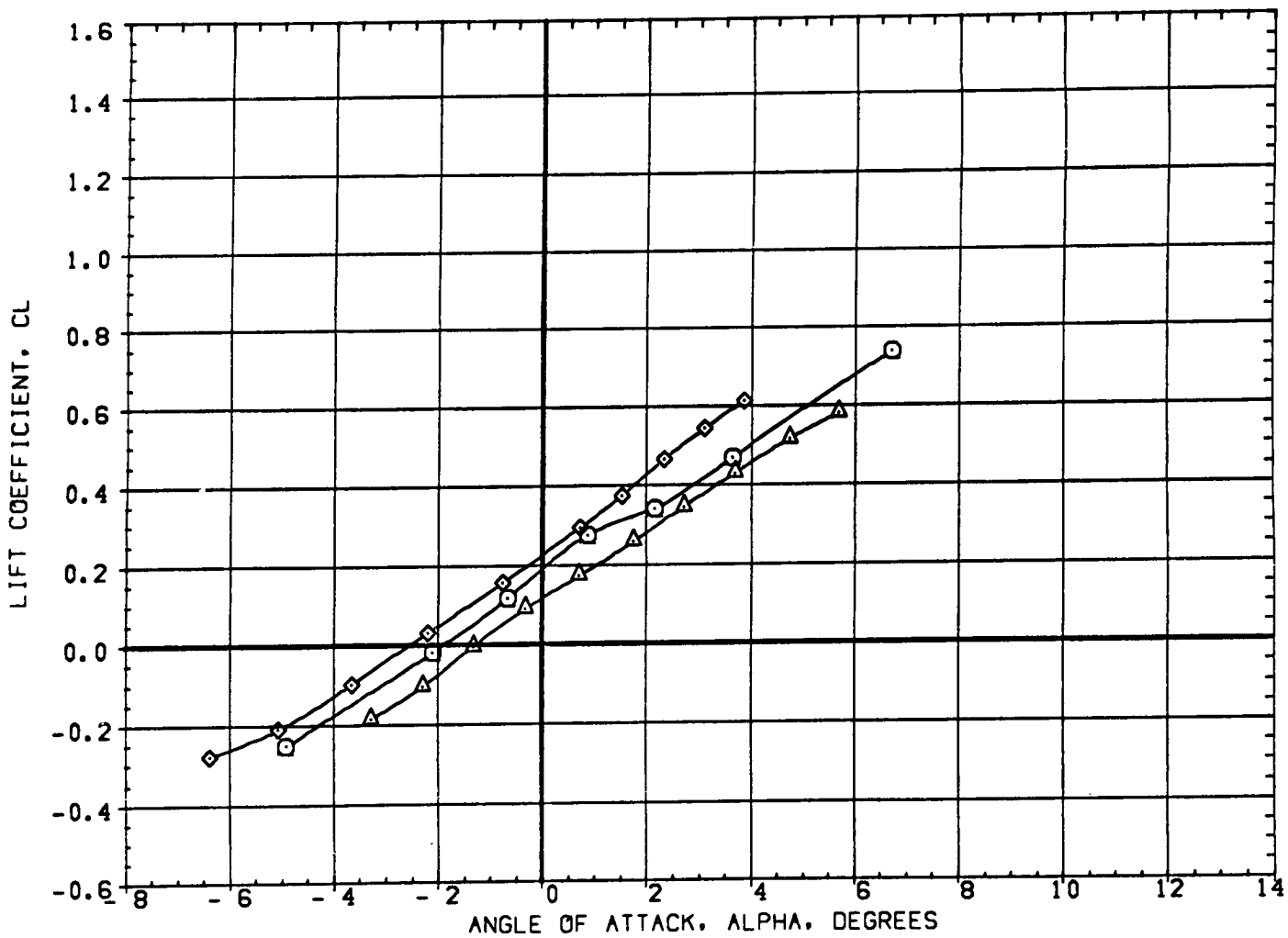

FIGURE 5 EFFECT OF WING AIRFOIL SECTION FOR AN OBLIQUE WING ANGLE OF 45 DEGREES

(A)MACH = .95

DATA SET	SYMBOL	CONFIGURATION DESCRIPTION	BETA	LAMBDA	RN/L
(4AE005)	○	W1 F0 B	0.000	45.000	6.000
(4AE041)	△	W2 F0 B	0.000	45.000	4.000
(4AE066)	◇	W4 F0 B	0.000	45.000	6.000

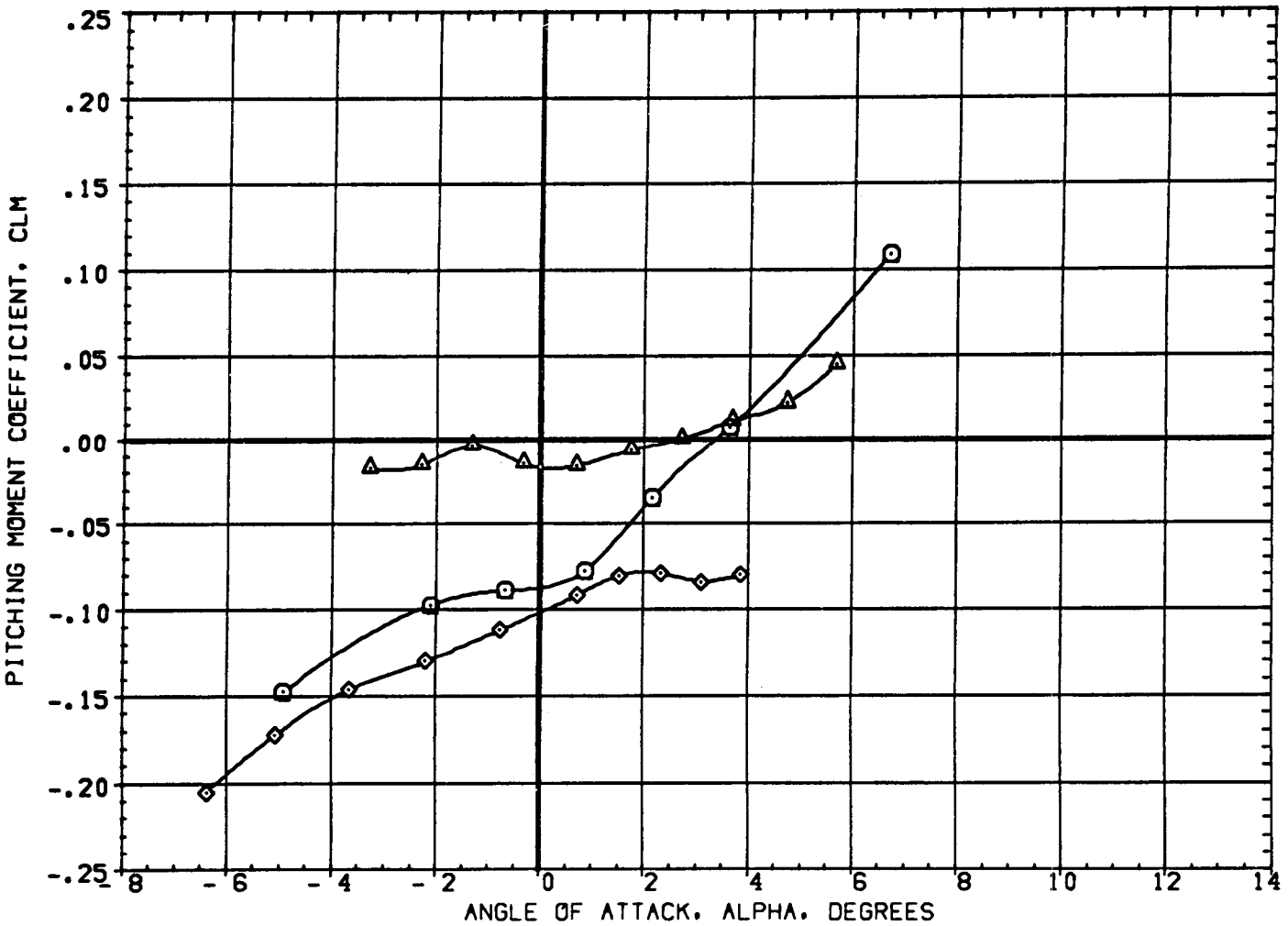

FIGURE 5 EFFECT OF WING AIRFOIL SECTION FOR AN OBLIQUE WING ANGLE OF 45 DEGREES

(A)MACH = .95

DATA SET	SYMBOL	CONFIGURATION DESCRIPTION	BETA	LAMBDA	RN/L
(4AE005)	○	W1 F0 B	0.000	45.000	6.000
(4AE041)	△	W2 F0 B	0.000	45.000	4.000
(4AE066)	◇	W4 F0 B	0.000	45.000	6.000

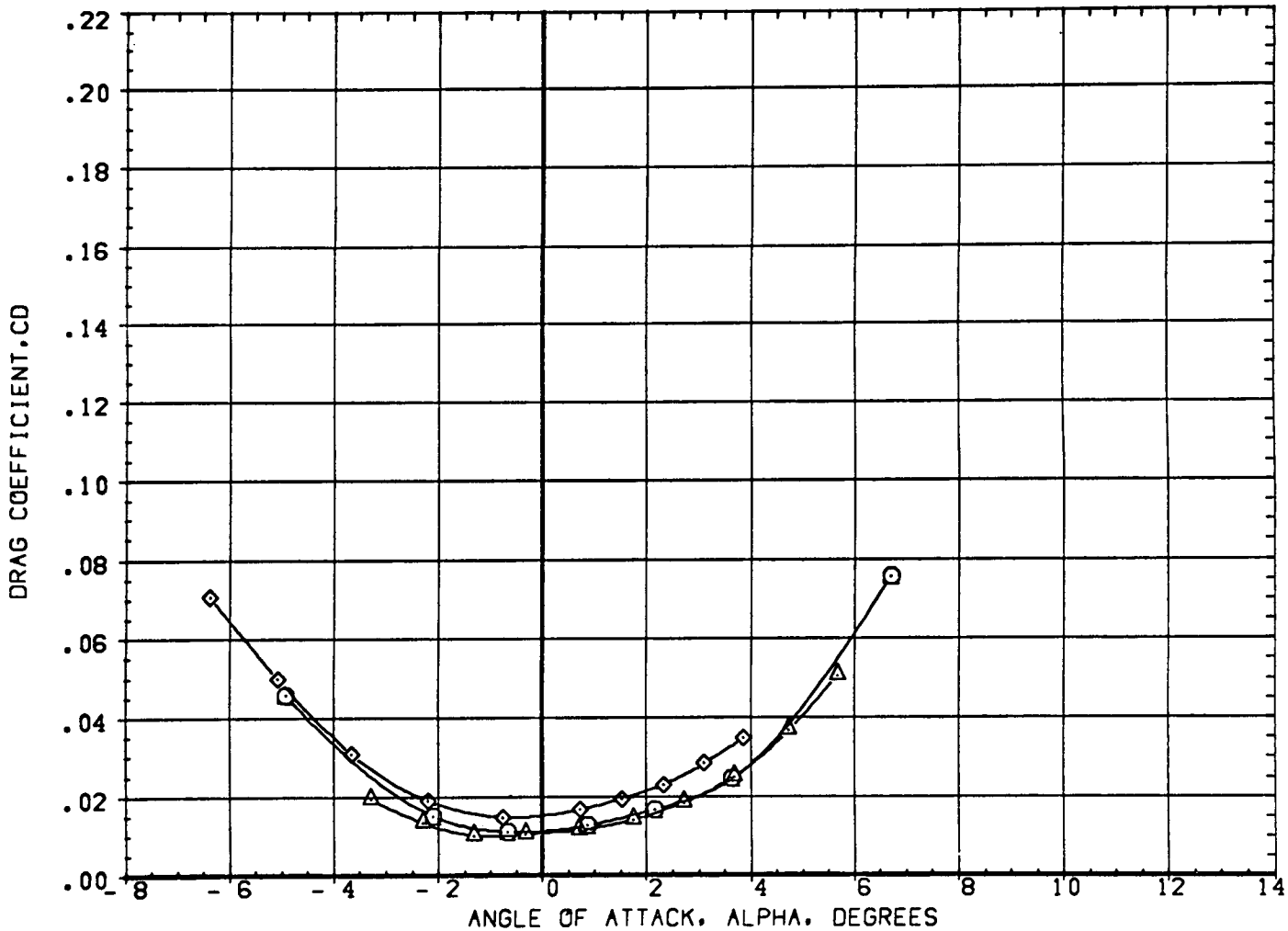

FIGURE 5 EFFECT OF WING AIRFOIL SECTION FOR AN OBLIQUE WING ANGLE OF 45 DEGREES

(A)MACH = .95

DATA SET	SYMBOL	CONFIGURATION DESCRIPTION	BETA	LAMBDA	RN/L
(4AE005)	○	W1 F0 B	0.000	45.000	6.000
(4AE041)	△	W2 F0 B	0.000	45.000	4.000
(4AE066)	◇	W4 F0 B	0.000	45.000	6.000

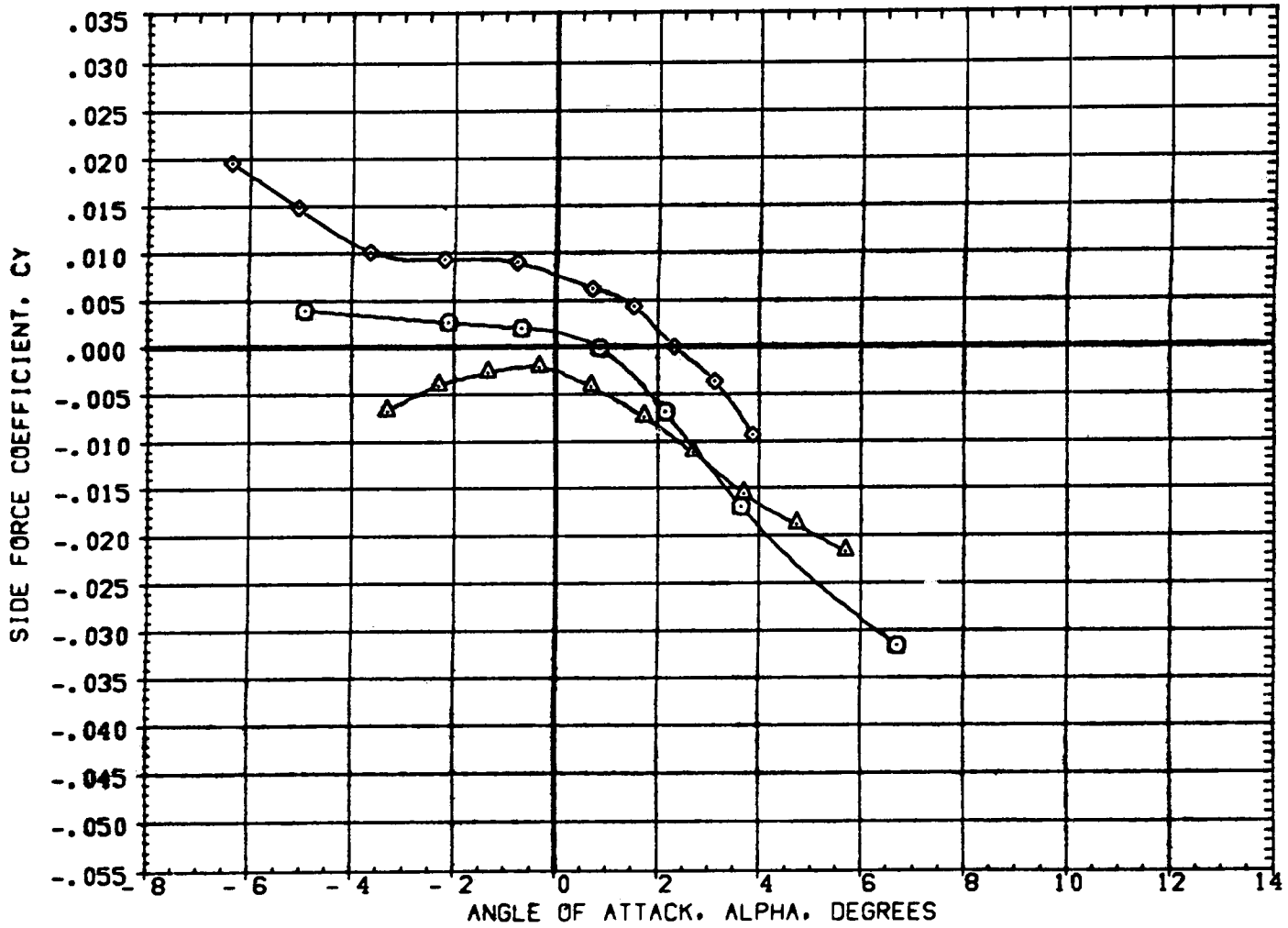

FIGURE 5 EFFECT OF WING AIRFOIL SECTION FOR AN OBLIQUE WING ANGLE OF 45 DEGREES

(A)MACH = .95

DATA SET	SYMBOL	CONFIGURATION DESCRIPTION	BETA	LAMBDA	RN/L
(4AE005)	○	W1 F0 B	0.000	45.000	6.000
(4AE041)	△	W2 F0 B	0.000	45.000	4.000
(4AE066)	◇	W4 F0 B	0.000	45.000	6.000

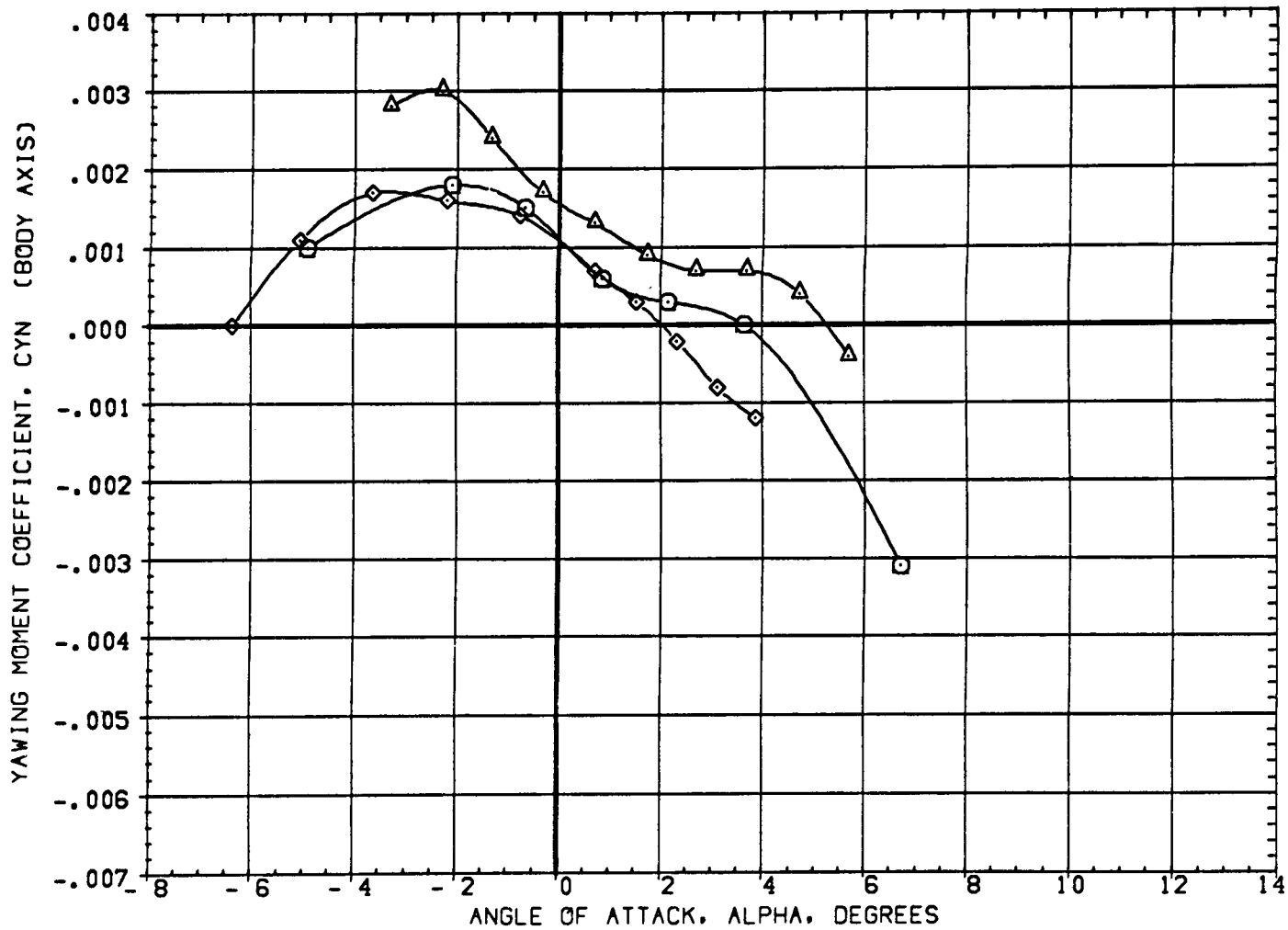

FIGURE 5 EFFECT OF WING AIRFOIL SECTION FOR AN OBLIQUE WING ANGLE OF 45 DEGREES

(A)MACH = .95

DATA SET	SYMBOL	CONFIGURATION DESCRIPTION	BETA	LAMBDA	RN/L
(4AE005)	○	W1 F0 B	0.000	45.000	6.000
(4AE041)	△	W2 F0 B	0.000	45.000	4.000
(4AE066)	◇	W4 F0 B	0.000	45.000	6.000

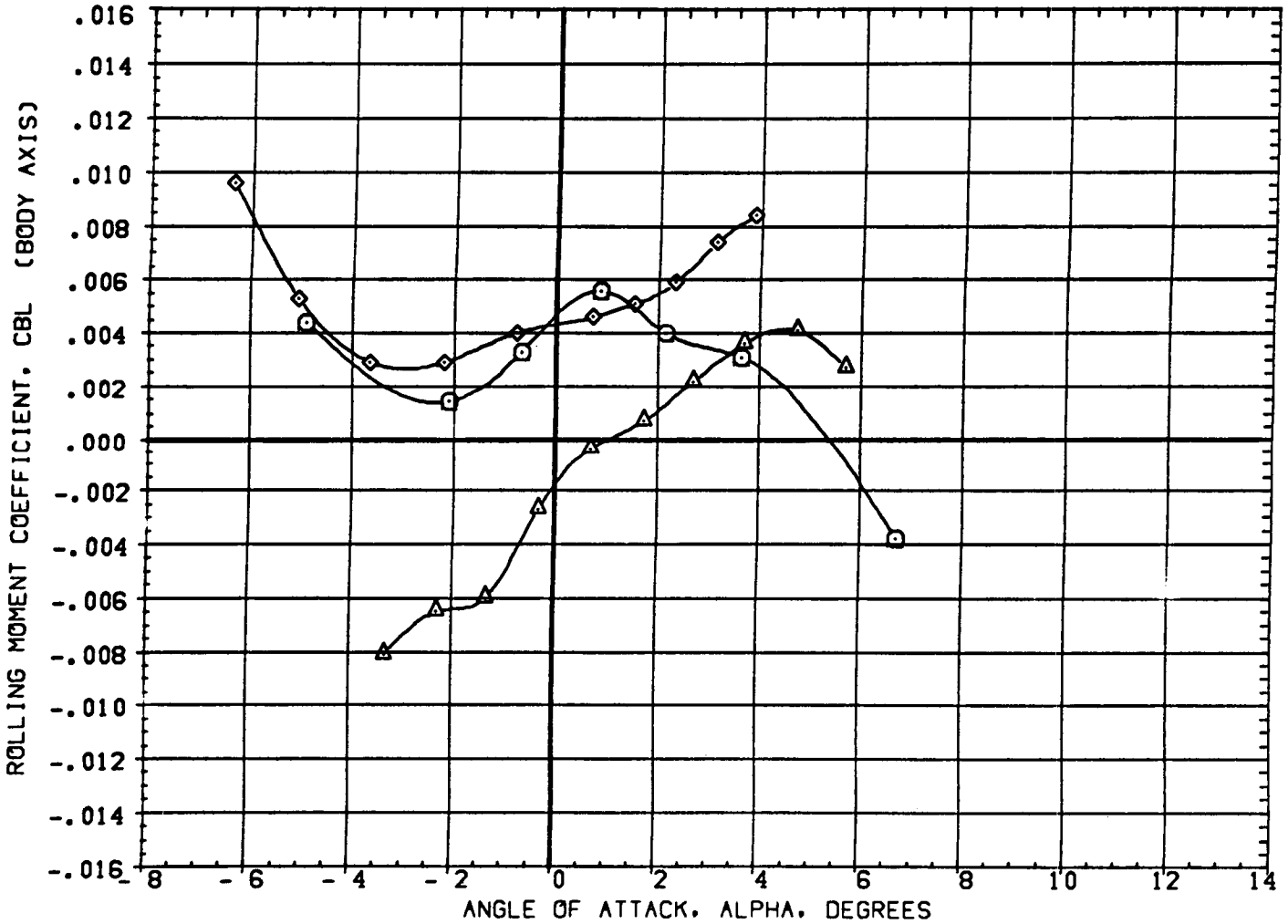

FIGURE 5 EFFECT OF WING AIRFOIL SECTION FOR AN OBLIQUE WING ANGLE OF 45 DEGREES

(A)MACH = .95

DATA SET	SYMBOL	CONFIGURATION DESCRIPTION	BETA	LAMBDA	RN/L
(4AE005)	○	W1 FO B	0.000	45.000	6.000
(4AE041)	△	W2 FO B	0.000	45.000	4.000
(4AE066)	◇	W4 FO B	0.000	45.000	6.000

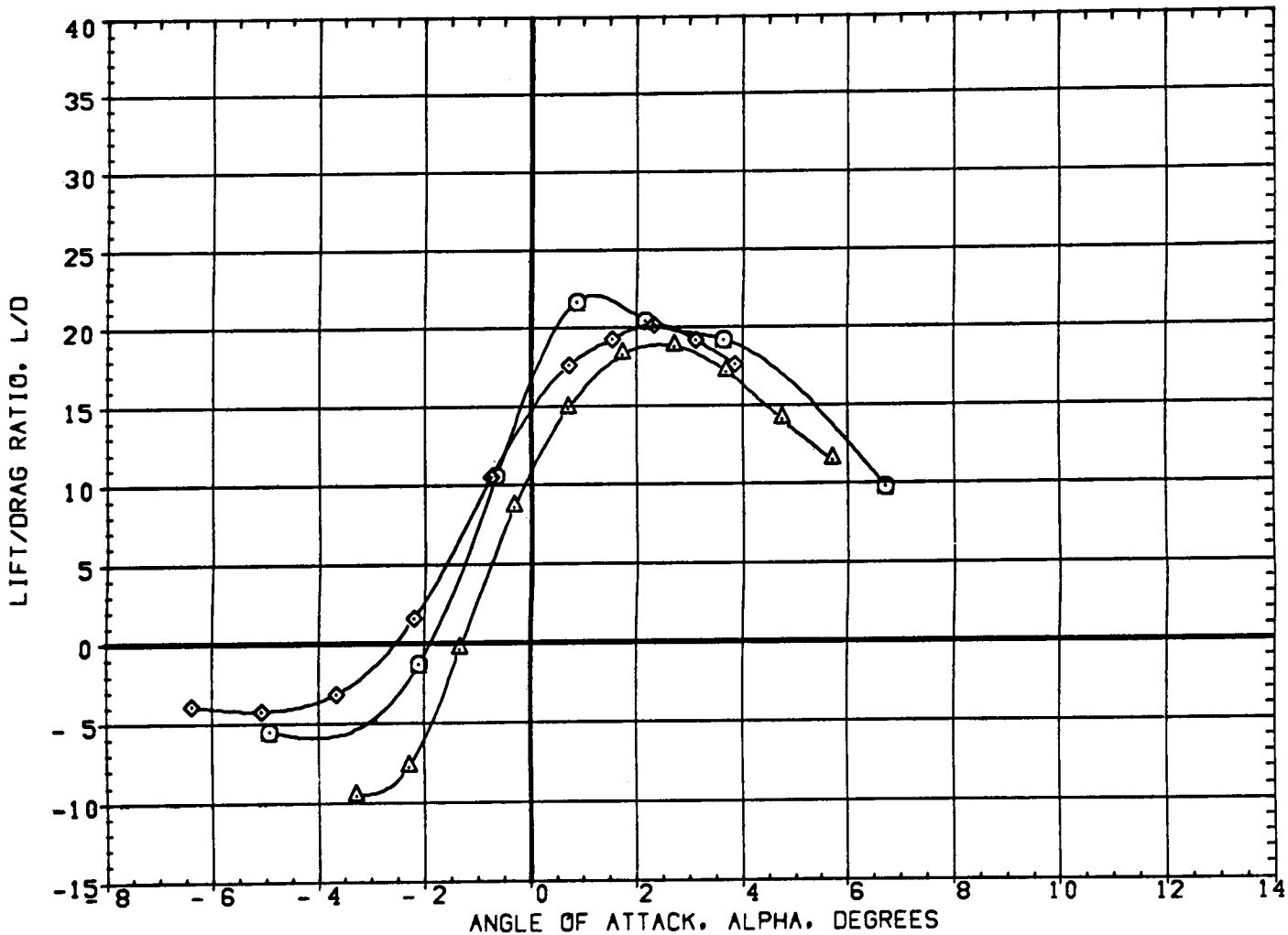

FIGURE 5 EFFECT OF WING AIRFOIL SECTION FOR AN OBLIQUE WING ANGLE OF 45 DEGREES

(A)MACH = .95

DATA SET	SYMBOL	CONFIGURATION DESCRIPTION	BETA	LAMBDA	RN/L
(SAE005)	○	W1 F0 B	0.000	45.000	6.000
(SAE041)	△	W2 F0 B	0.000	45.000	4.000
(SAE066)	◇	W4 F0 B	0.000	45.000	6.000

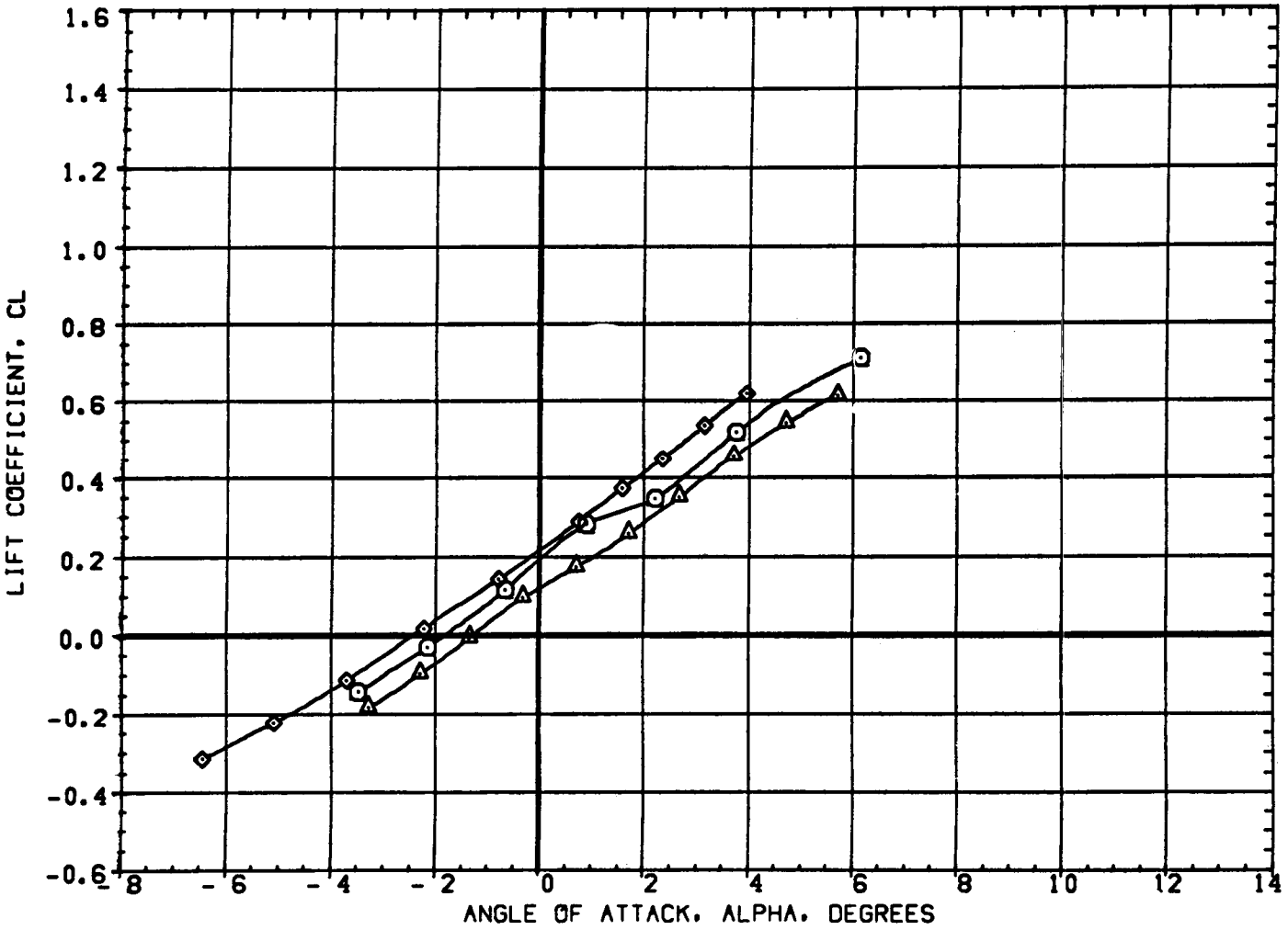

FIGURE 5 EFFECT OF WING AIRFOIL SECTION FOR AN OBLIQUE WING ANGLE OF 45 DEGREES

(A)MACH = .98

DATA SET	SYMBOL	CONFIGURATION DESCRIPTION	BETA	LAMBDA	RN/L
(SAE005)	○	W1 F0 B	0.000	45.000	6.000
(SAE041)	△	W2 F0 B	0.000	45.000	4.000
(SAE066)	◇	W4 F0 B	0.000	45.000	6.000

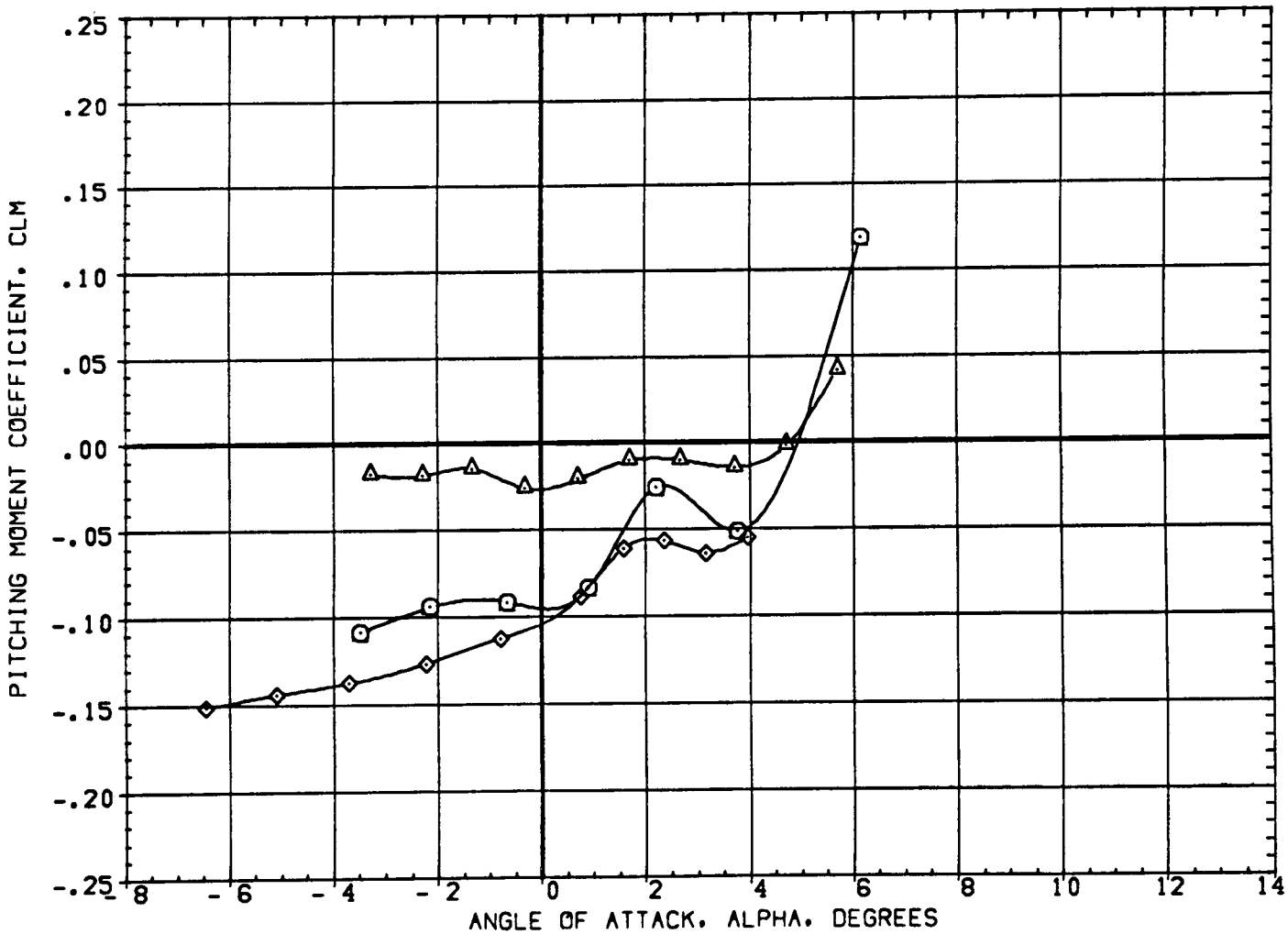

FIGURE 5 EFFECT OF WING AIRFOIL SECTION FOR AN OBLIQUE WING ANGLE OF 45 DEGREES

(A)MACH = .98

DATA SET	SYMBOL	CONFIGURATION DESCRIPTION	BETA	LAMBDA	RN/L
(SAE005)	○	W1 F0 B	0.000	45.000	6.000
(SAE041)	△	W2 F0 B	0.000	45.000	4.000
(SAE066)	◇	W4 F0 B	0.000	45.000	6.000

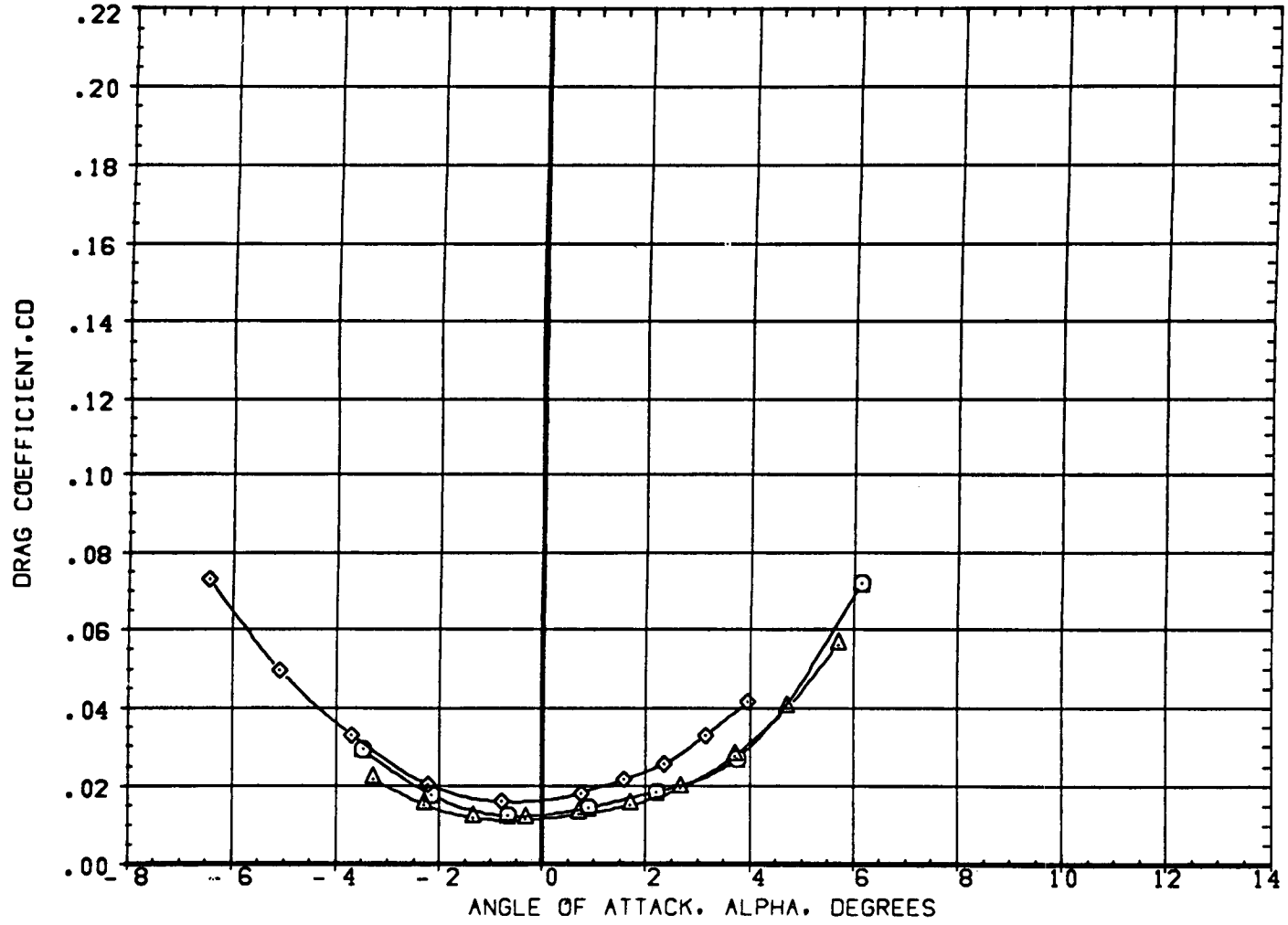

FIGURE 5 EFFECT OF WING AIRFOIL SECTION FOR AN OBLIQUE WING ANGLE OF 45 DEGREES

(A)MACH = .98

DATA SET	SYMBOL	CONFIGURATION DESCRIPTION	BETA	LAMBDA	RN/L
(SAE008)	○	W1 FO B	0.000	45.000	6.000
(SAE041)	□	W2 FO B	0.000	45.000	4.000
(SAE066)	◇	W4 FO B	0.000	45.000	6.000

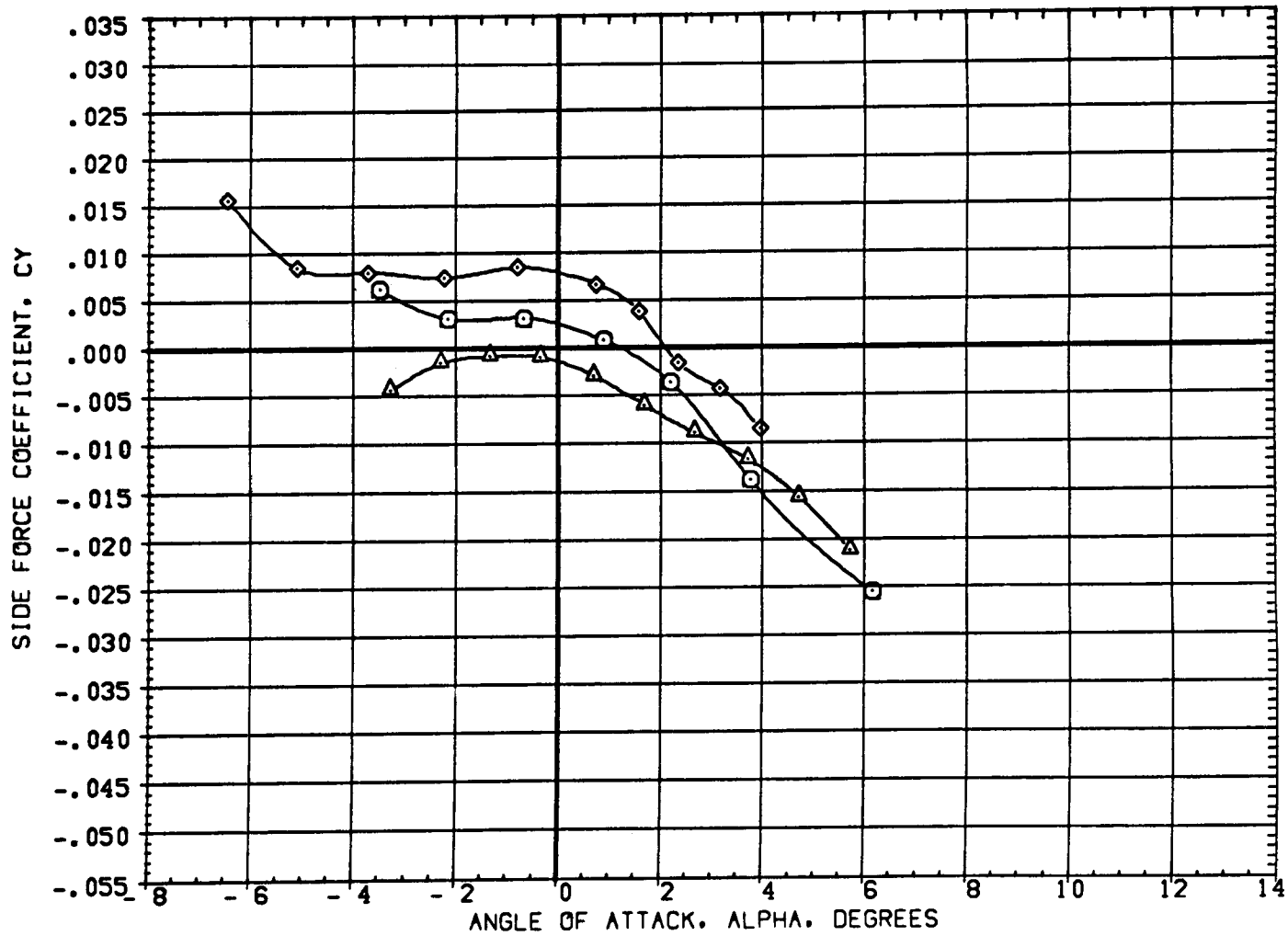

FIGURE 5 EFFECT OF WING AIRFOIL SECTION FOR AN OBLIQUE WING ANGLE OF 45 DEGREES

(A)MACH = .98

DATA SET	SYMBOL	CONFIGURATION DESCRIPTION	BETA	LAMBDA	RN/L
(SAE005)	○	W1 F0 B	0.000	45.000	6.000
(SAE041)	△	W2 F0 B	0.000	45.000	4.000
(SAE066)	◇	W4 F0 B	0.000	45.000	6.000

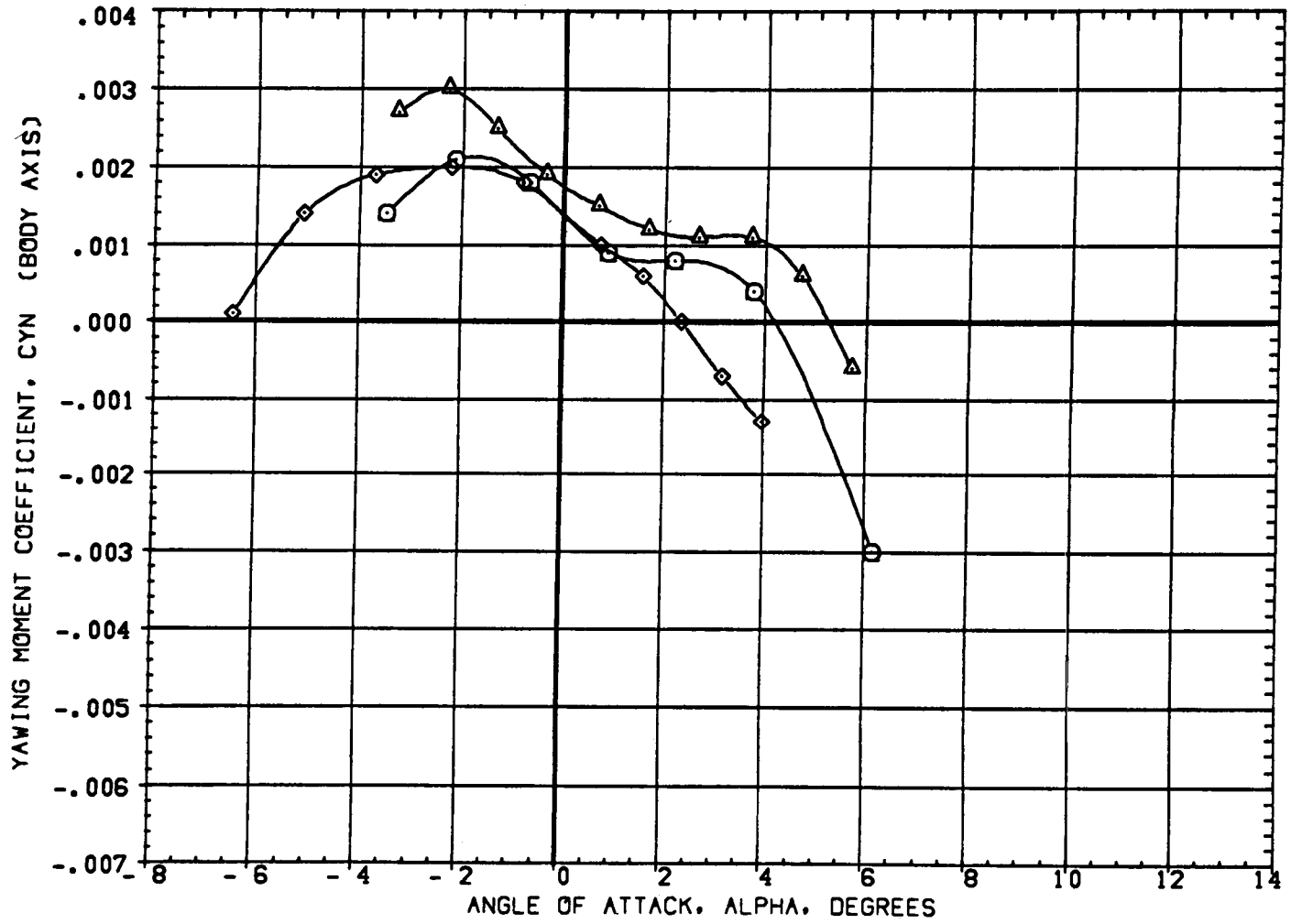

FIGURE 5 EFFECT OF WING AIRFOIL SECTION FOR AN OBLIQUE WING ANGLE OF 45 DEGREES

(A)MACH = .98

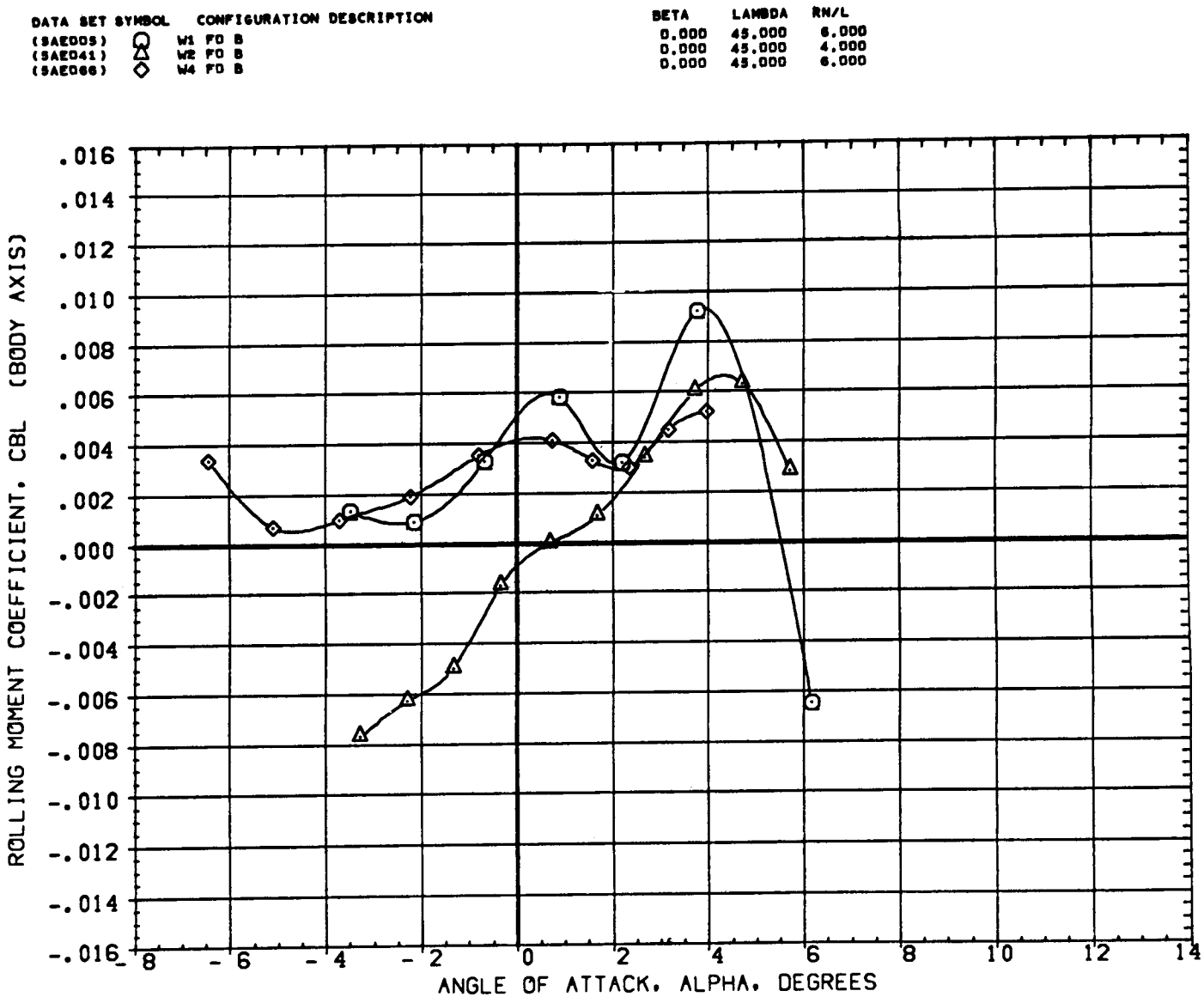

FIGURE 5 EFFECT OF WING AIRFOIL SECTION FOR AN OBLIQUE WING ANGLE OF 45 DEGREES

(A)MACH = .98

DATA SET	SYMBOL	CONFIGURATION DESCRIPTION	BETA	LAMBDA	RN/L
(3AE005)	○	W1 F0 B	0.000	45.000	6.000
(3AE041)	△	W2 F0 B	0.000	45.000	4.000
(3AE066)	◇	W4 F0 B	0.000	45.000	6.000

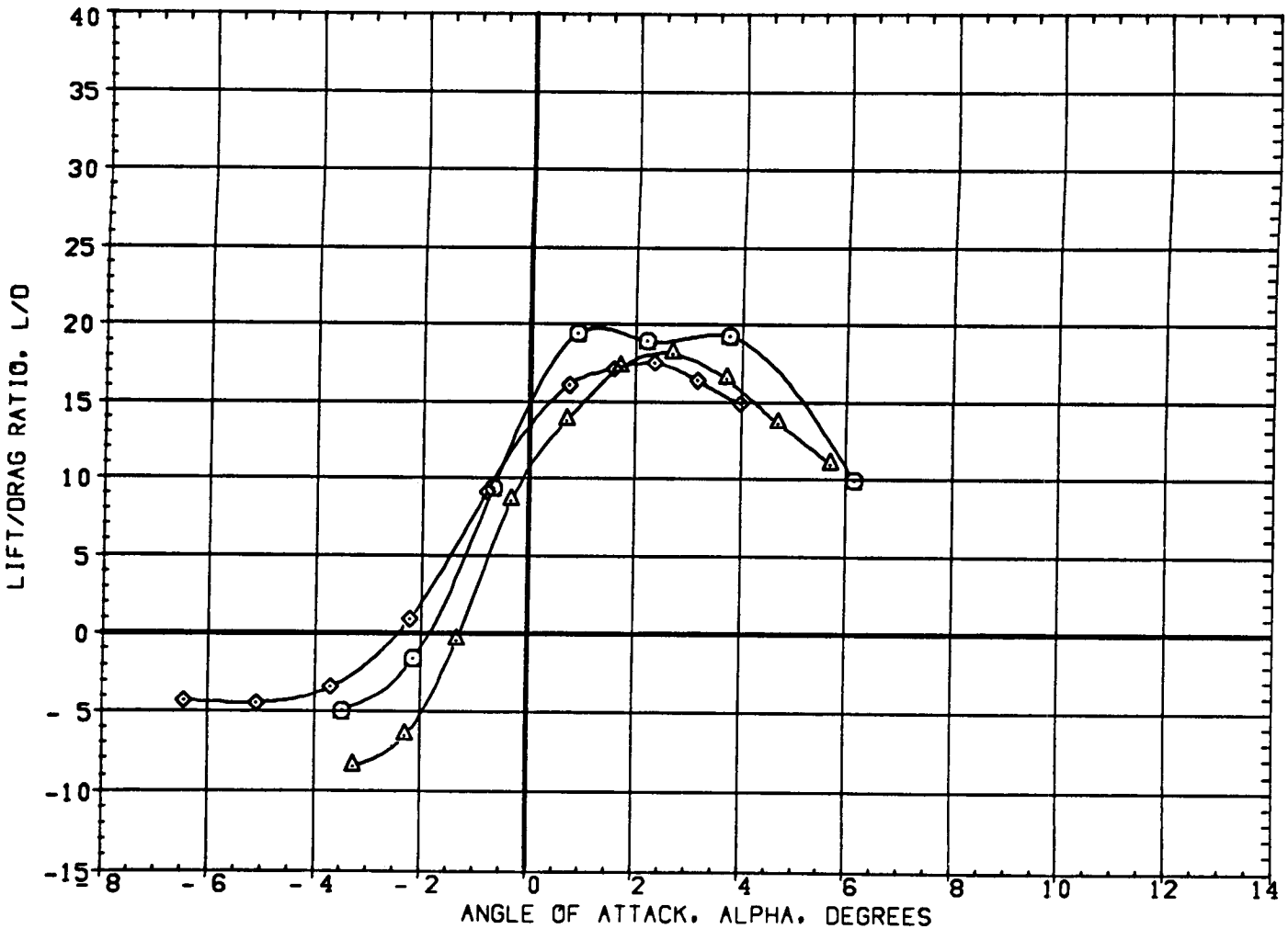

FIGURE 5 EFFECT OF WING AIRFOIL SECTION FOR AN OBLIQUE WING ANGLE OF 45 DEGREES

(A)MACH = .98

DATA SET	SYMBOL	CONFIGURATION DESCRIPTION
(6AE005)	○	W1 FO B
(6AE041)	△	W2 FO B
(6AE066)	◇	W4 FO B

BETA	LAMBDA	RN/L
0.000	45.000	6.000
0.000	45.000	4.000
0.000	45.000	6.000

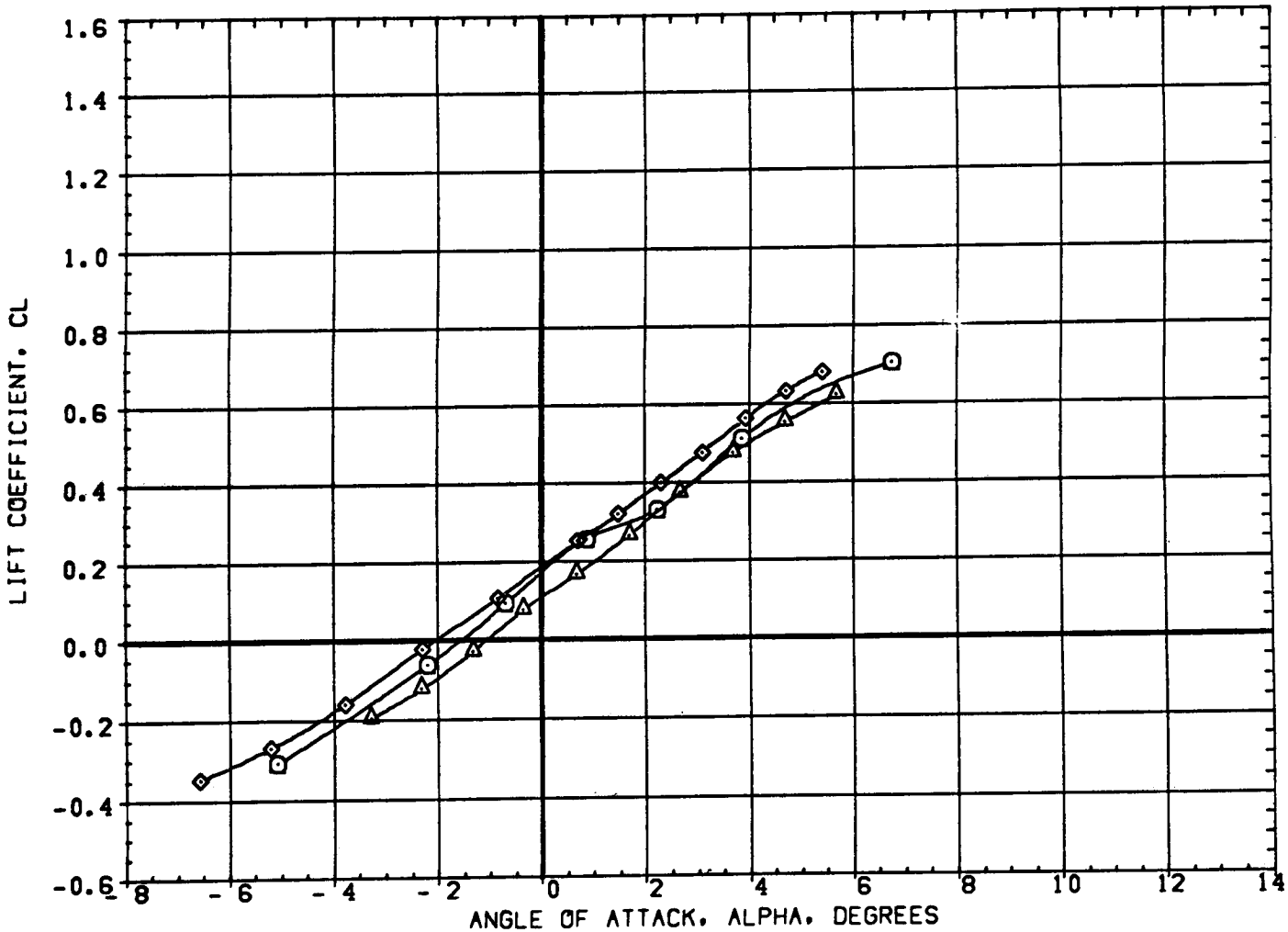

FIGURE 5 EFFECT OF WING AIRFOIL SECTION FOR AN OBLIQUE WING ANGLE OF 45 DEGREES

(A)MACH = 1.05

DATA SET	SYMBOL	CONFIGURATION DESCRIPTION	BETA	LAMBDA	RN/L
(6AE005)	○	W1 F0 B	0.000	45.000	6.000
(6AE041)	△	W2 F0 B	0.000	45.000	4.000
(6AE066)	◇	W4 F0 B	0.000	45.000	6.000

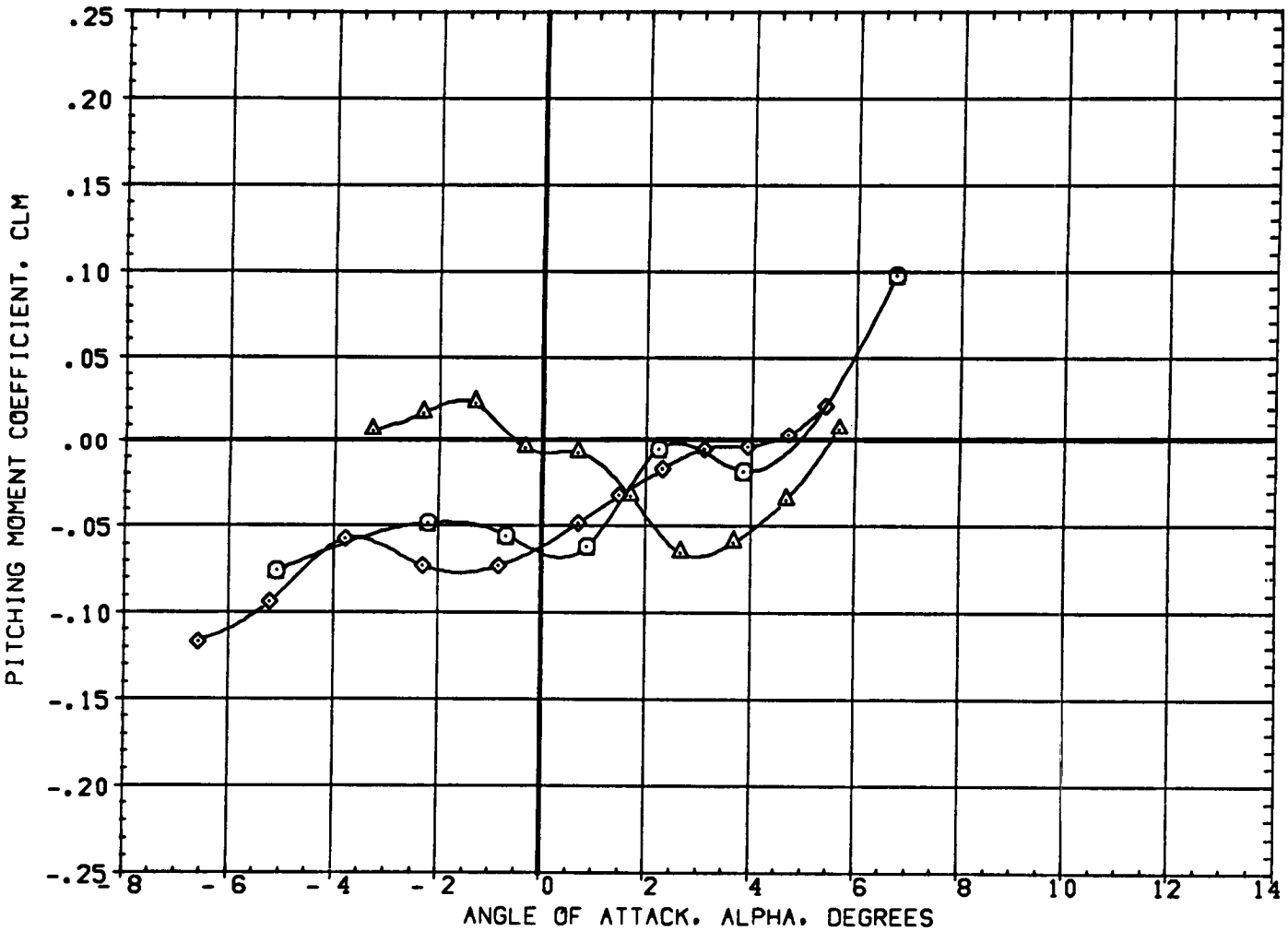

FIGURE 5 EFFECT OF WING AIRFOIL SECTION FOR AN OBLIQUE WING ANGLE OF 45 DEGREES

(A)MACH = 1.05

DATA SET	SYMBOL	CONFIGURATION DESCRIPTION	BETA	LAMBDA	RN/L
(6AE005)	○	W1 F0 B	0.000	45.000	6.000
(6AE041)	△	W2 F0 B	0.000	45.000	4.000
(6AE066)	◇	W4 F0 B	0.000	45.000	6.000

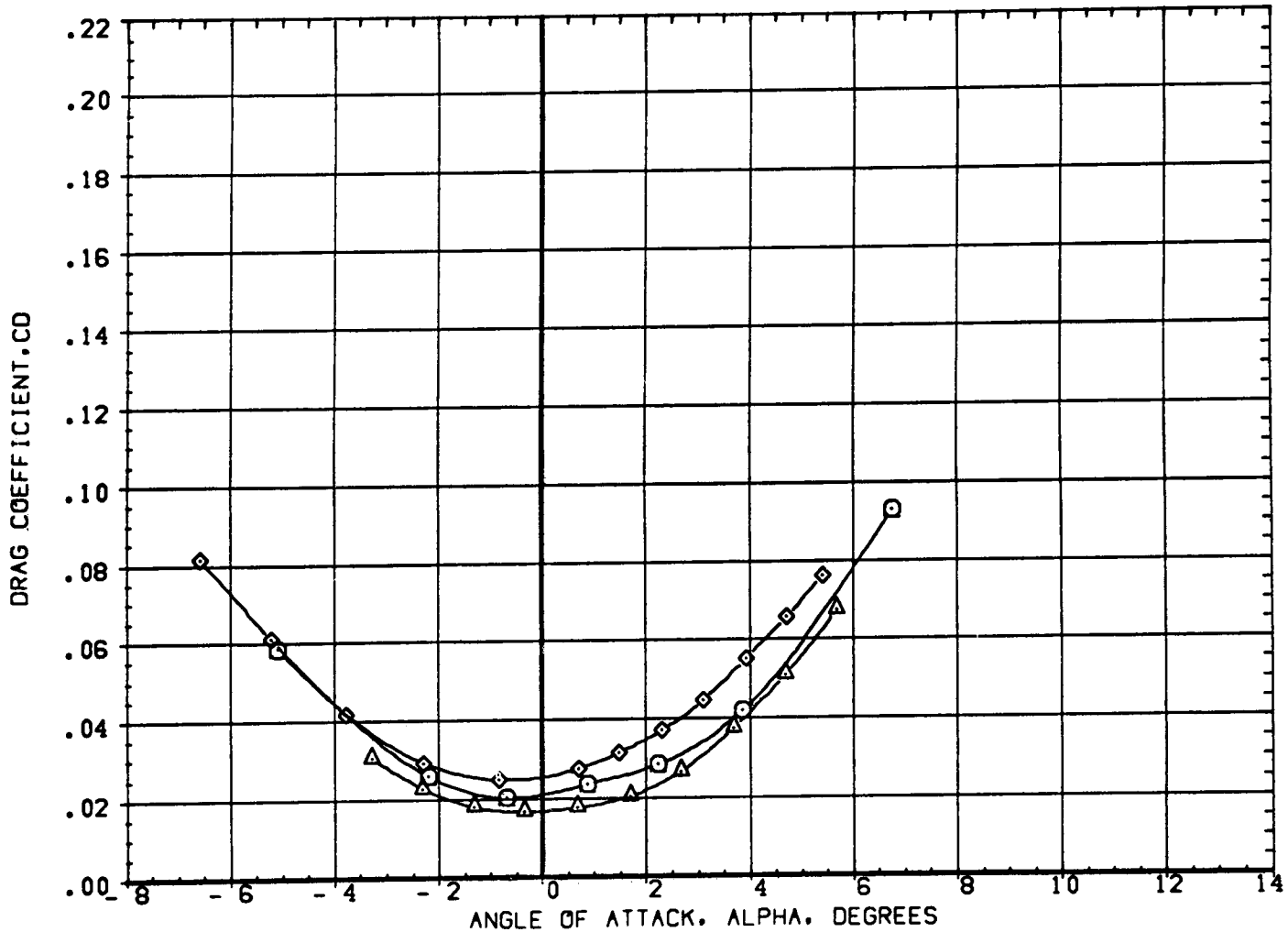

FIGURE 5 EFFECT OF WING AIRFOIL SECTION FOR AN OBLIQUE WING ANGLE OF 45 DEGREES

(A)MACH = 1.05

DATA SET	SYMBOL	CONFIGURATION DESCRIPTION	BETA	LAMBDA	RN/L
(@AE005)	○	W1 FD B	0.000	45.000	6.000
(@AE041)	△	W2 FD B	0.000	45.000	4.000
(@AE066)	◇	W4 FD B	0.000	45.000	6.000

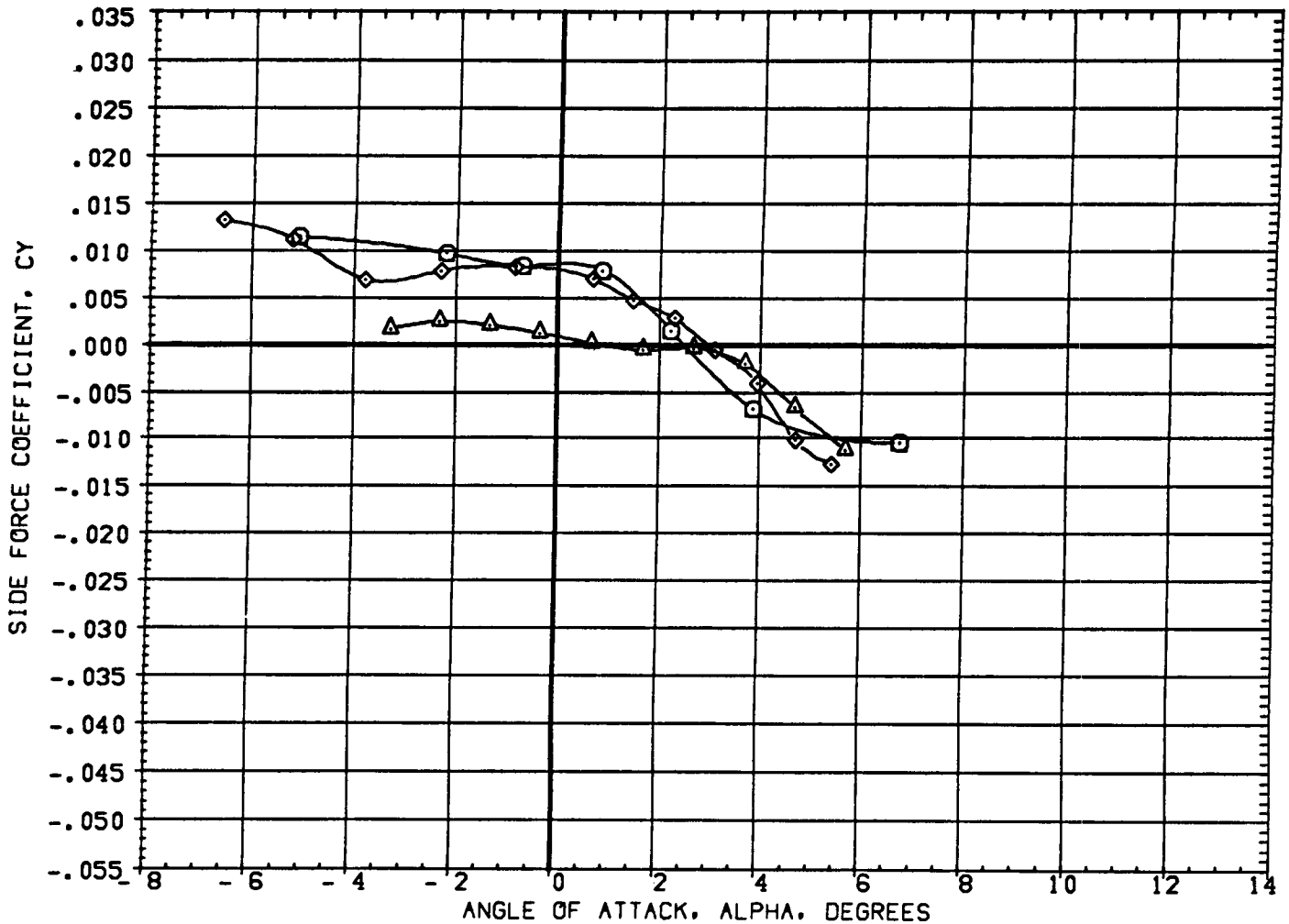

FIGURE 5 EFFECT OF WING AIRFOIL SECTION FOR AN OBLIQUE WING ANGLE OF 45 DEGREES

(A)MACH = 1.05

DATA SET	SYMBOL	CONFIGURATION DESCRIPTION	BETA	LAMBDA	RN/L
(8AE005)	○	W1 F0 B	0.000	45.000	6.000
(8AE041)	△	W2 F0 B	0.000	45.000	4.000
(8AE066)	◇	W4 F0 B	0.000	45.000	6.000

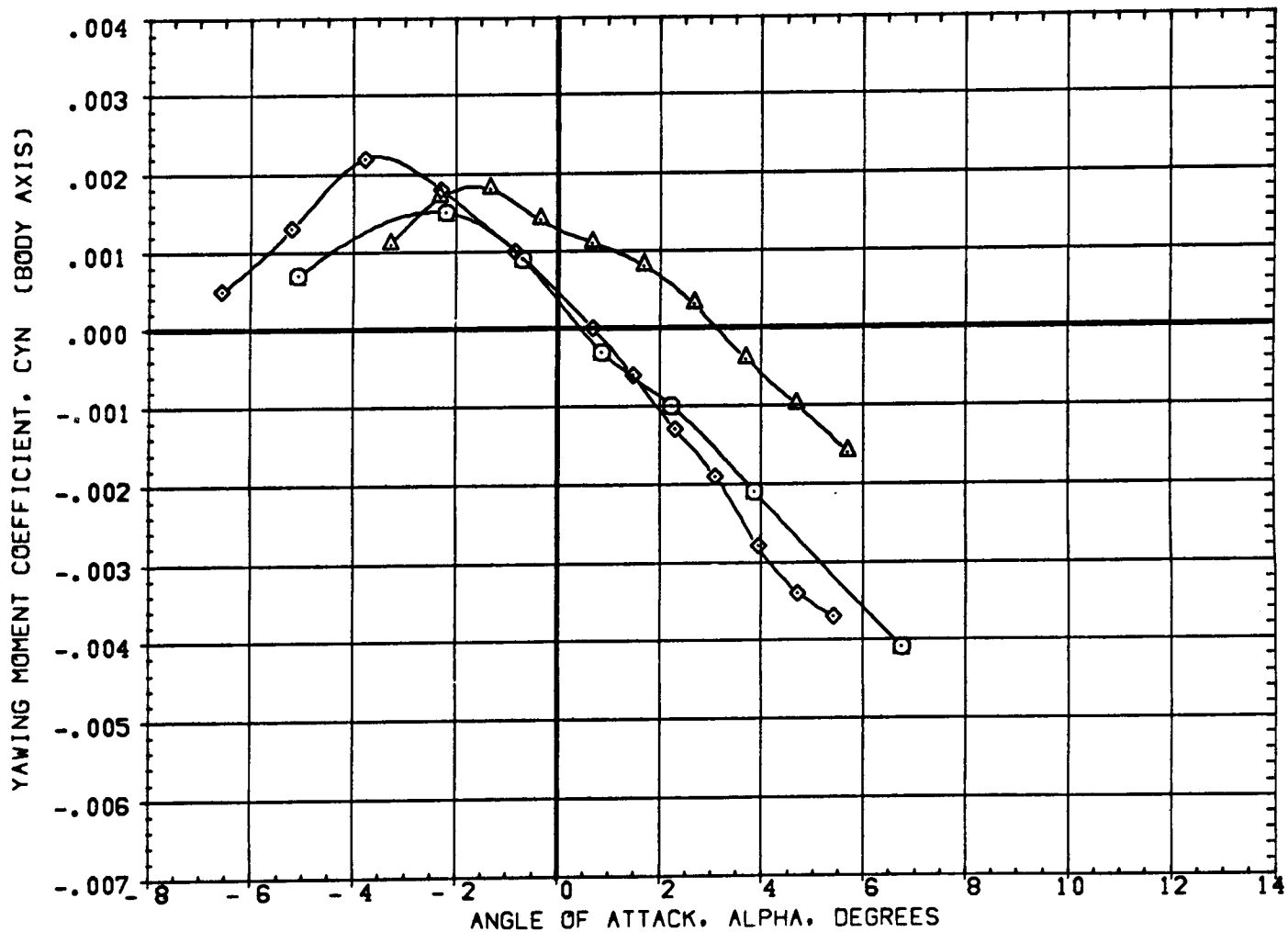

FIGURE 5 EFFECT OF WING AIRFOIL SECTION FOR AN OBLIQUE WING ANGLE OF 45 DEGREES

(A)MACH = 1.05

DATA SET	SYMBOL	CONFIGURATION DESCRIPTION	BETA	LAMBDA	RN/L
(6AE005)	○	W1 F0 B	0.000	45.000	6.000
(6AE041)	△	W2 F0 B	0.000	45.000	4.000
(6AE066)	◇	W4 F0 B	0.000	45.000	6.000

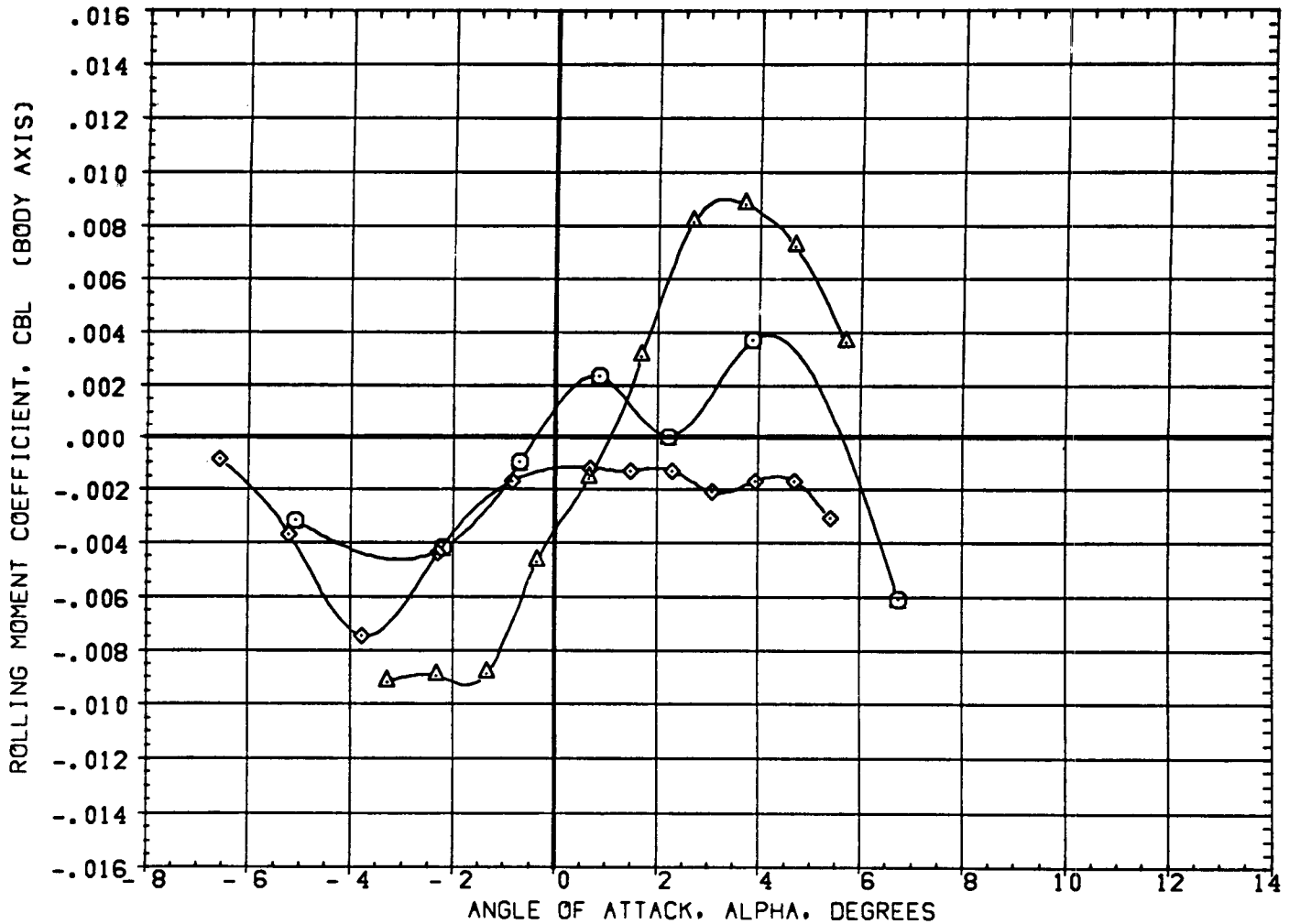

FIGURE 5 EFFECT OF WING AIRFOIL SECTION FOR AN OBLIQUE WING ANGLE OF 45 DEGREES

(A)MACH = 1.05

DATA SET	SYMBOL	CONFIGURATION DESCRIPTION	BETA	LAMBDA	RN/L
(SAE005)	○	W1 F0 B	0.000	45.000	6.000
(SAE041)	△	W2 F0 B	0.000	45.000	4.000
(SAE006)	◇	W4 F0 B	0.000	45.000	6.000

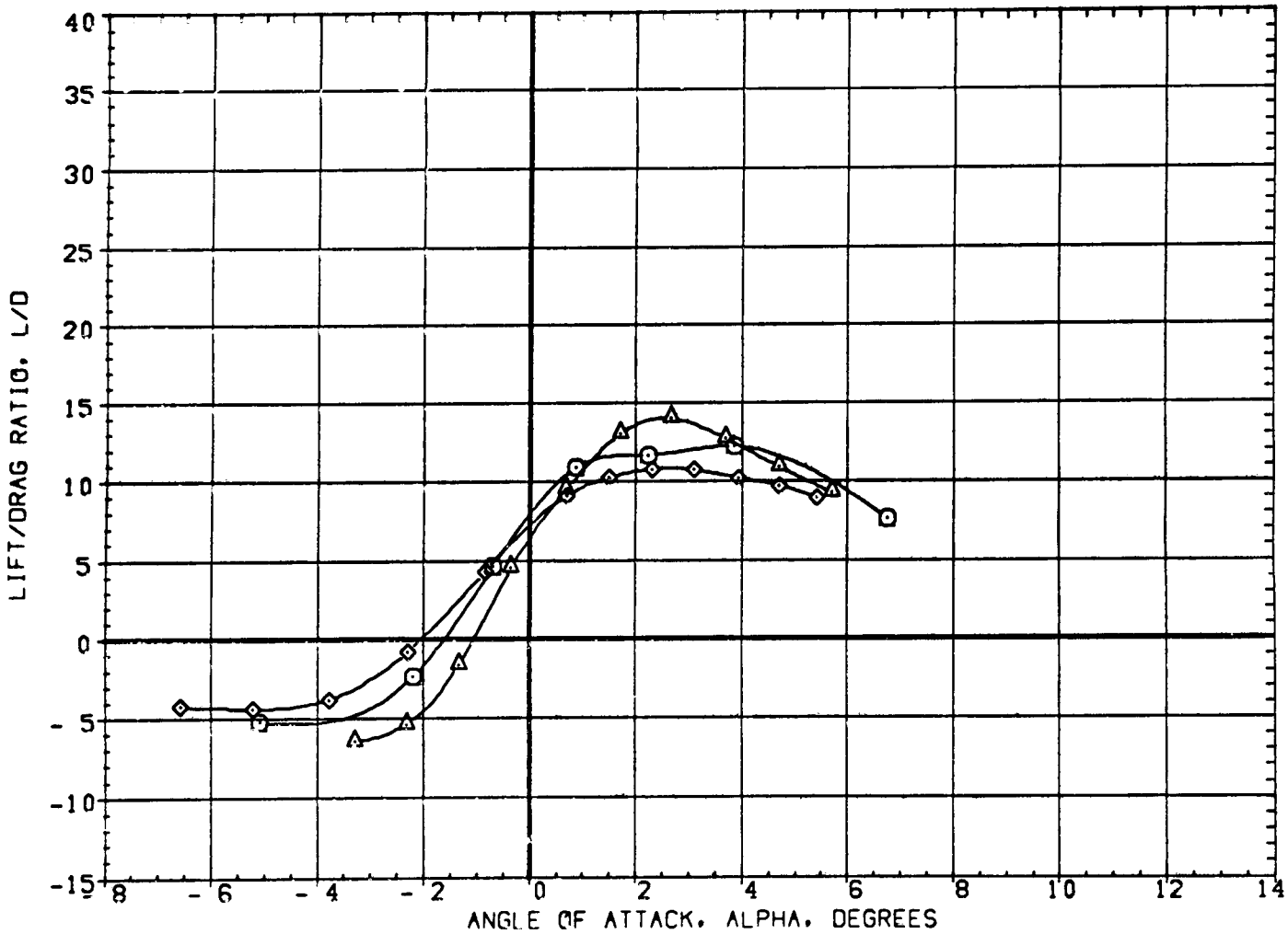

FIGURE 5 EFFECT OF WING AIRFOIL SECTION FOR AN OBLIQUE WING ANGLE OF 45 DEGREES

(A)MACH = 1.05

DATA SET	SYMBOL	CONFIGURATION DESCRIPTION	BETA	LAMBDA	RN/L
(3AE007)	○	W1 F0 B	0.000	50.000	6.000
(3AE042)	△	W2 F0 B	0.000	50.000	4.000
(3AE068)	◇	W4 F0 B	0.000	50.000	6.000

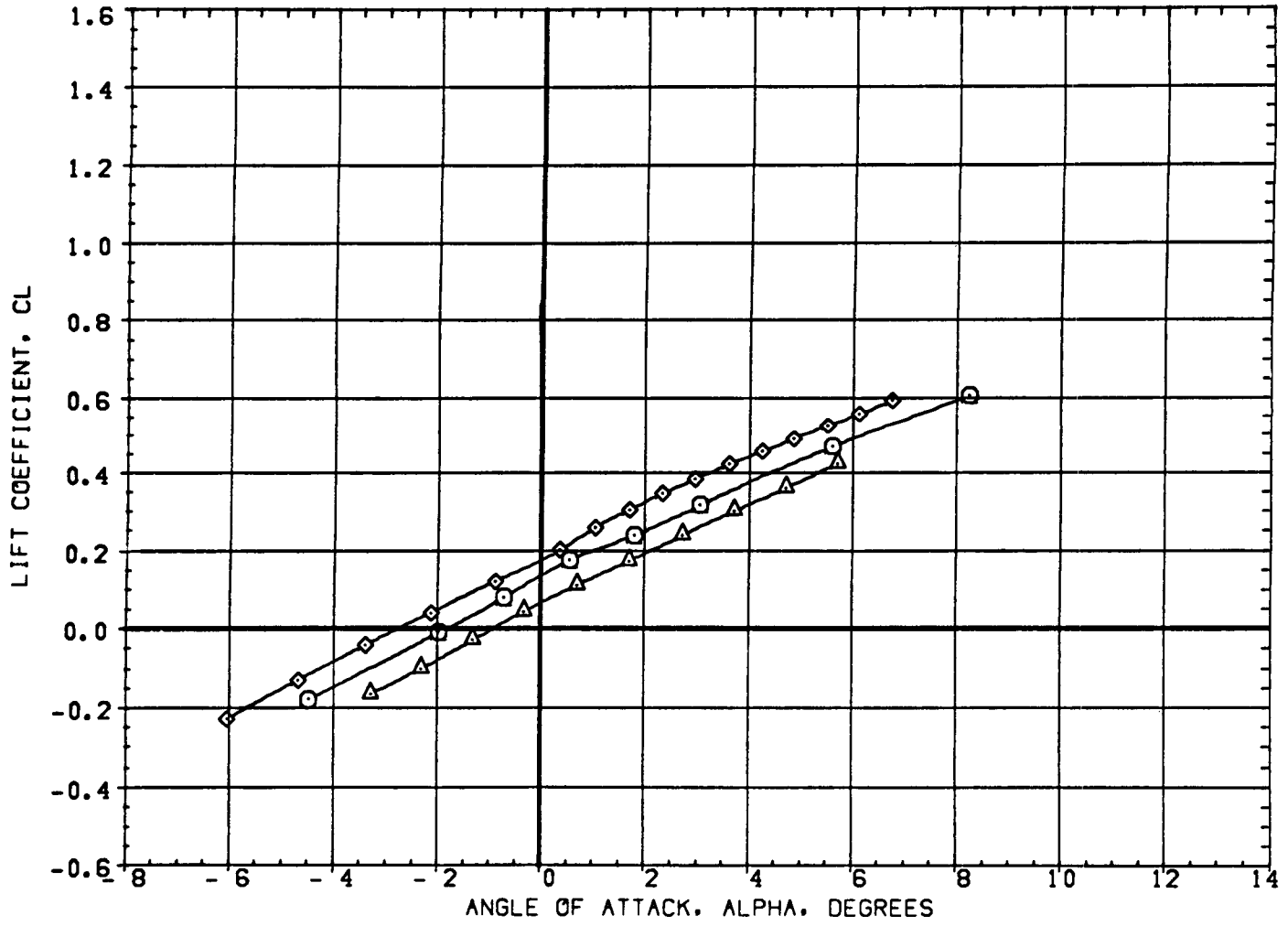

FIGURE 6 EFFECT OF WING AIRFOIL SECTION FOR AN OBLIQUE WING ANGLE OF 50 DEGREES

(A)MACH = .80

DATA SET	SYMBOL	CONFIGURATION DESCRIPTION
(3AE007)	○	W1 F0 B
(3AE042)	□	W2 F0 B
(3AE068)	◇	W4 F0 B

BETA	LAMBDA	RN/L
0.000	50.000	6.000
0.000	50.000	4.000
0.000	50.000	6.000

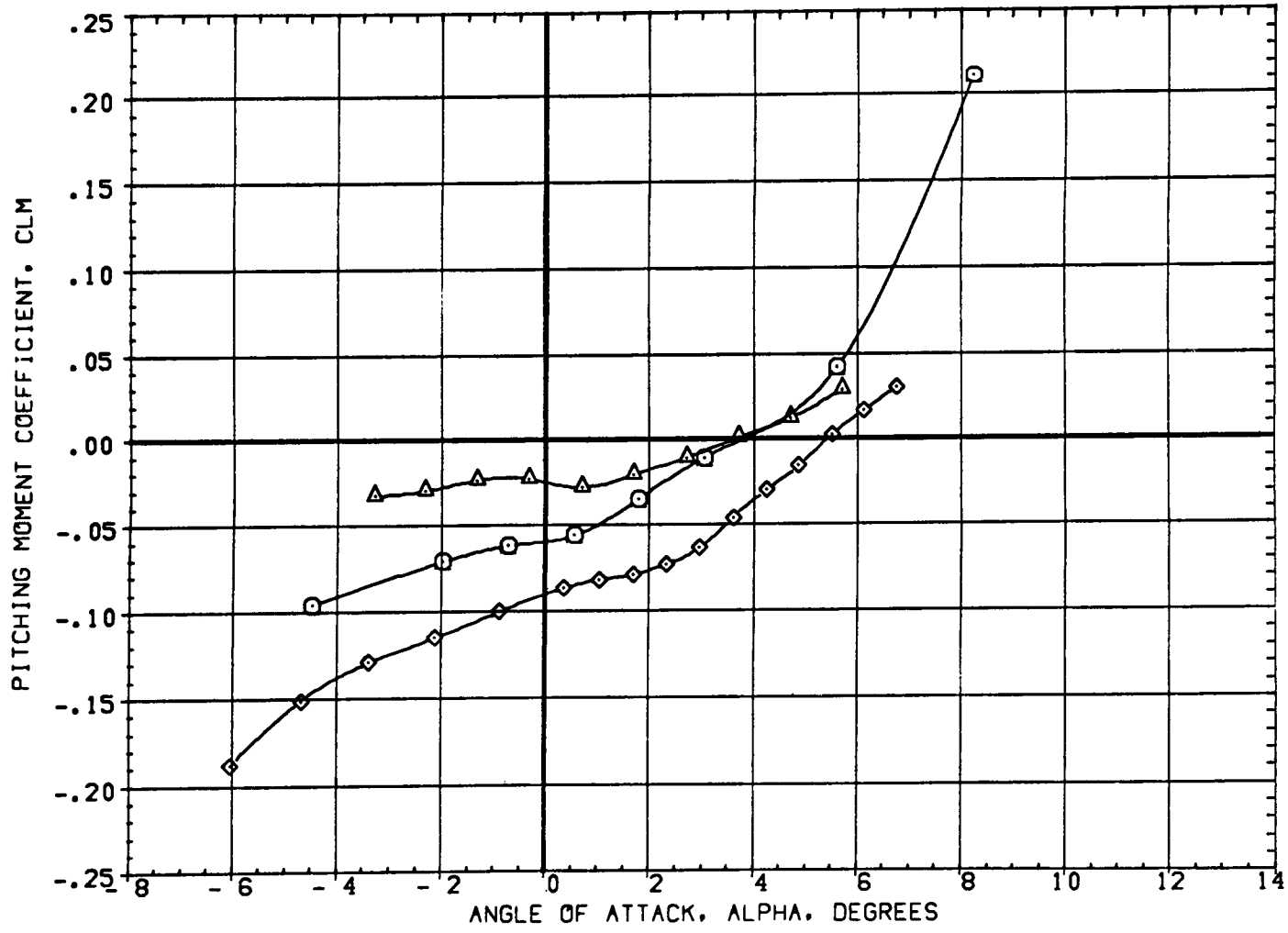

FIGURE 6 EFFECT OF WING AIRFOIL SECTION FOR AN OBLIQUE WING ANGLE OF 50 DEGREES

(A)MACH = .80

DATA SET	SYMBOL	CONFIGURATION DESCRIPTION	BETA	LAMBDA	RN/L
(3AE007)	○	W1 F0 B	0.000	50.000	6.000
(3AE042)	△	W2 F0 B	0.000	50.000	4.000
(3AE068)	◇	W4 F0 B	0.000	50.000	6.000

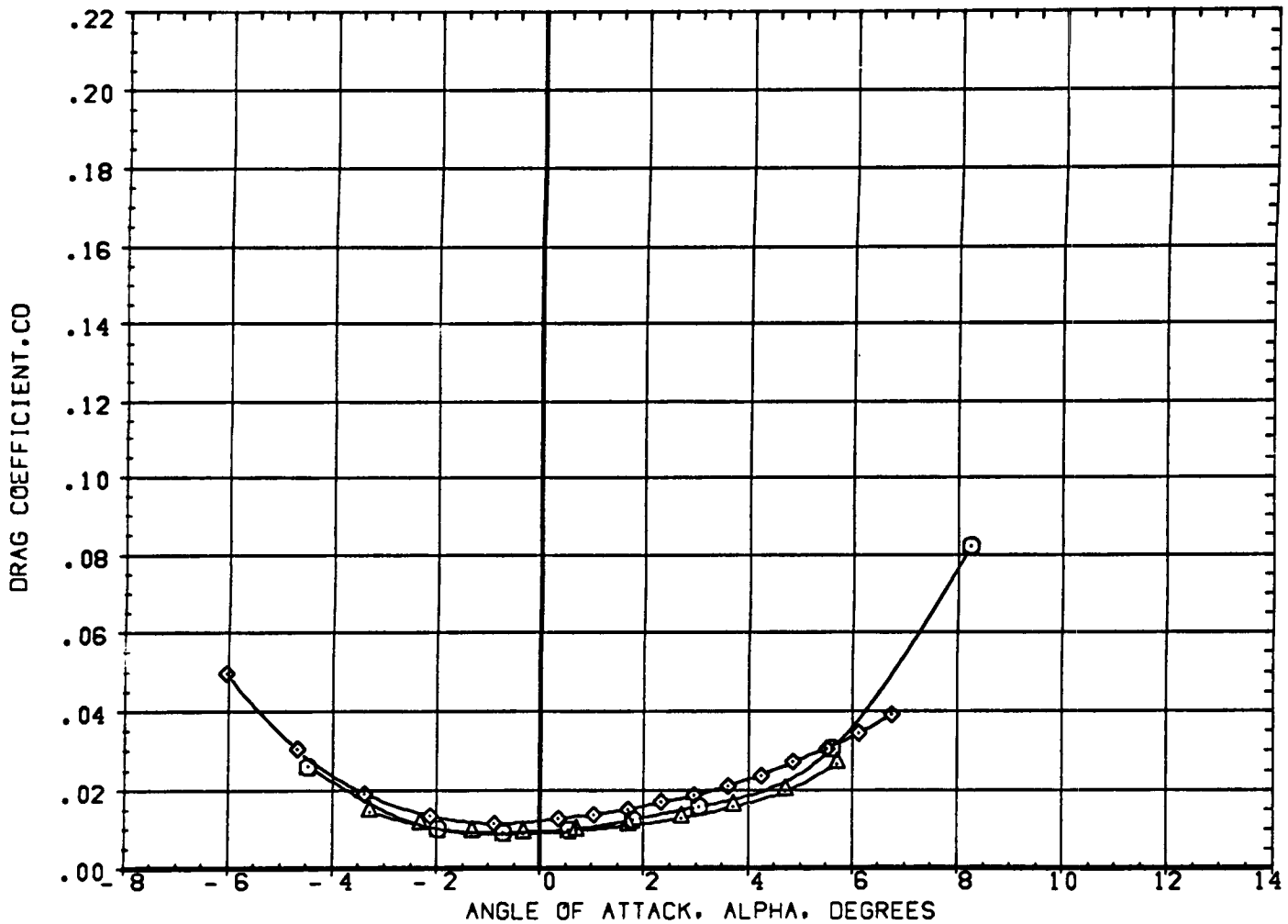

FIGURE 6 EFFECT OF WING AIRFOIL SECTION FOR AN OBLIQUE WING ANGLE OF 50 DEGREES

(A)MACH = .80

DATA SET	SYMBOL	CONFIGURATION DESCRIPTION	BETA	LAMBDA	RN/L
(3AE007)	○	W1 F0 B	0.000	50.000	6.000
(3AE042)	△	W2 F0 B	0.000	50.000	4.000
(3AE06L)	◇	W4 F0 B	0.000	50.000	6.000

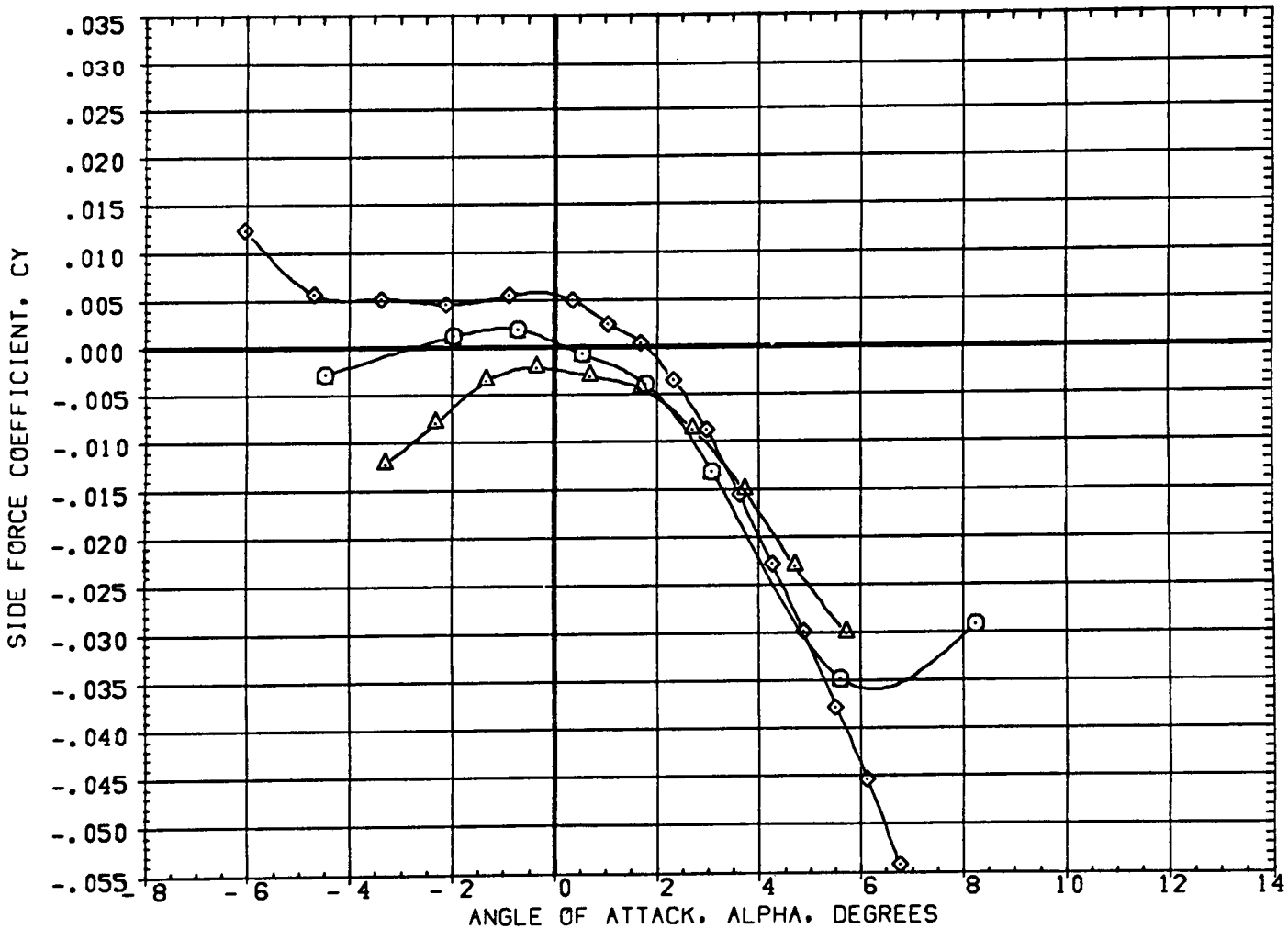

FIGURE 6 EFFECT OF WING AIRFOIL SECTION FOR AN OBLIQUE WING ANGLE OF 50 DEGREES

(A)MACH = .80

DATA SET	SYMBOL	CONFIGURATION DESCRIPTION	BETA	LAMBDA	RN/L
(3AE007)	○	W1 F0 B	0.000	50.000	6.000
(3AE042)	△	W2 F0 B	0.000	50.000	4.000
(3AE068)	◇	W4 F0 B	0.000	50.000	6.000

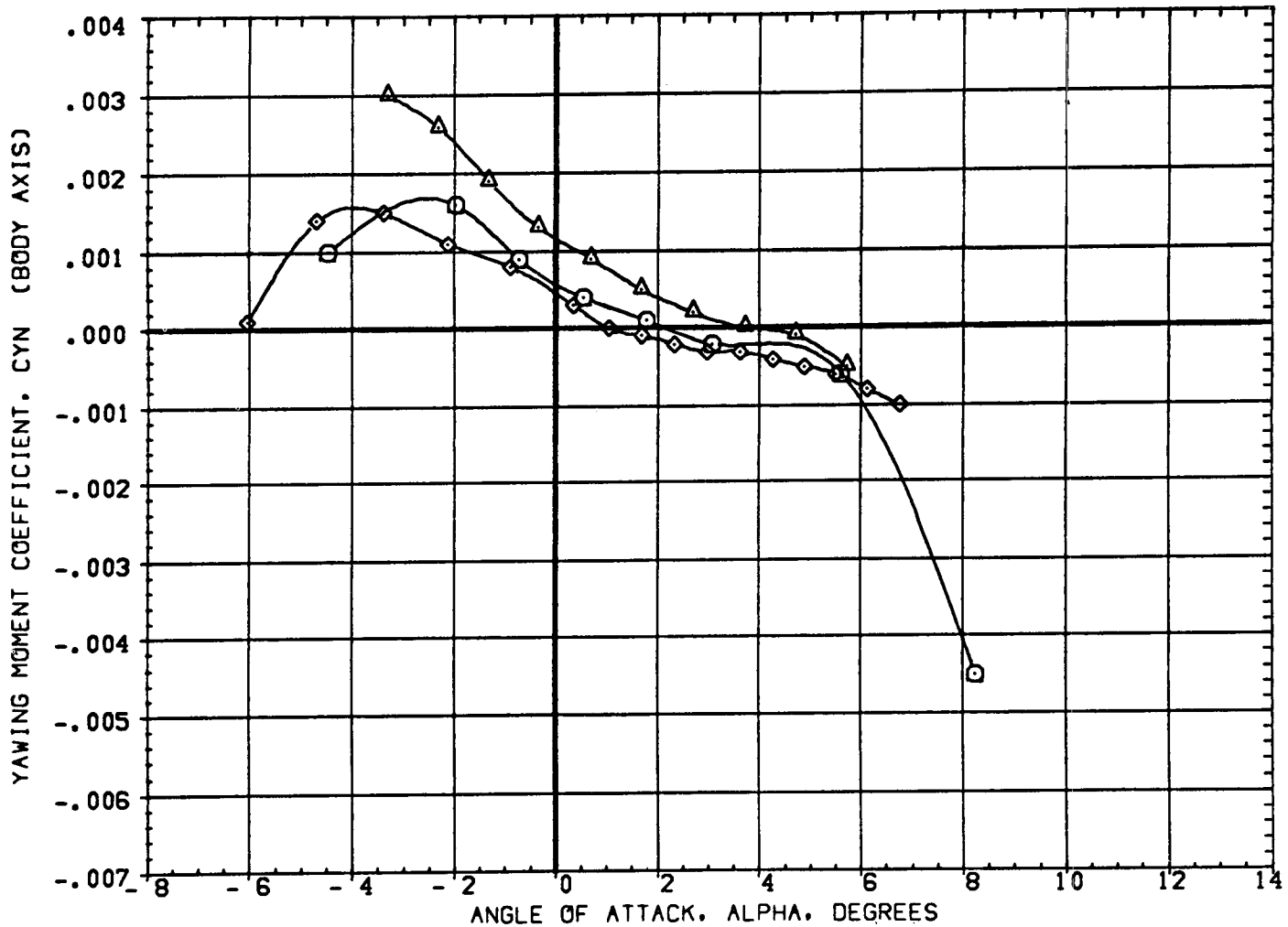

FIGURE 6 EFFECT OF WING AIRFOIL SECTION FOR AN OBLIQUE WING ANGLE OF 50 DEGREES

(A)MACH = .80

DATA SET	SYMBOL	CONFIGURATION DESCRIPTION	BETA	LAMBDA	RN/L
(3AE007)	○	W1 F0 B	0.000	50.000	6.000
(3AE042)	△	W2 F0 B	0.000	50.000	4.000
(3AE068)	◇	W4 F0 B	0.000	50.000	6.000

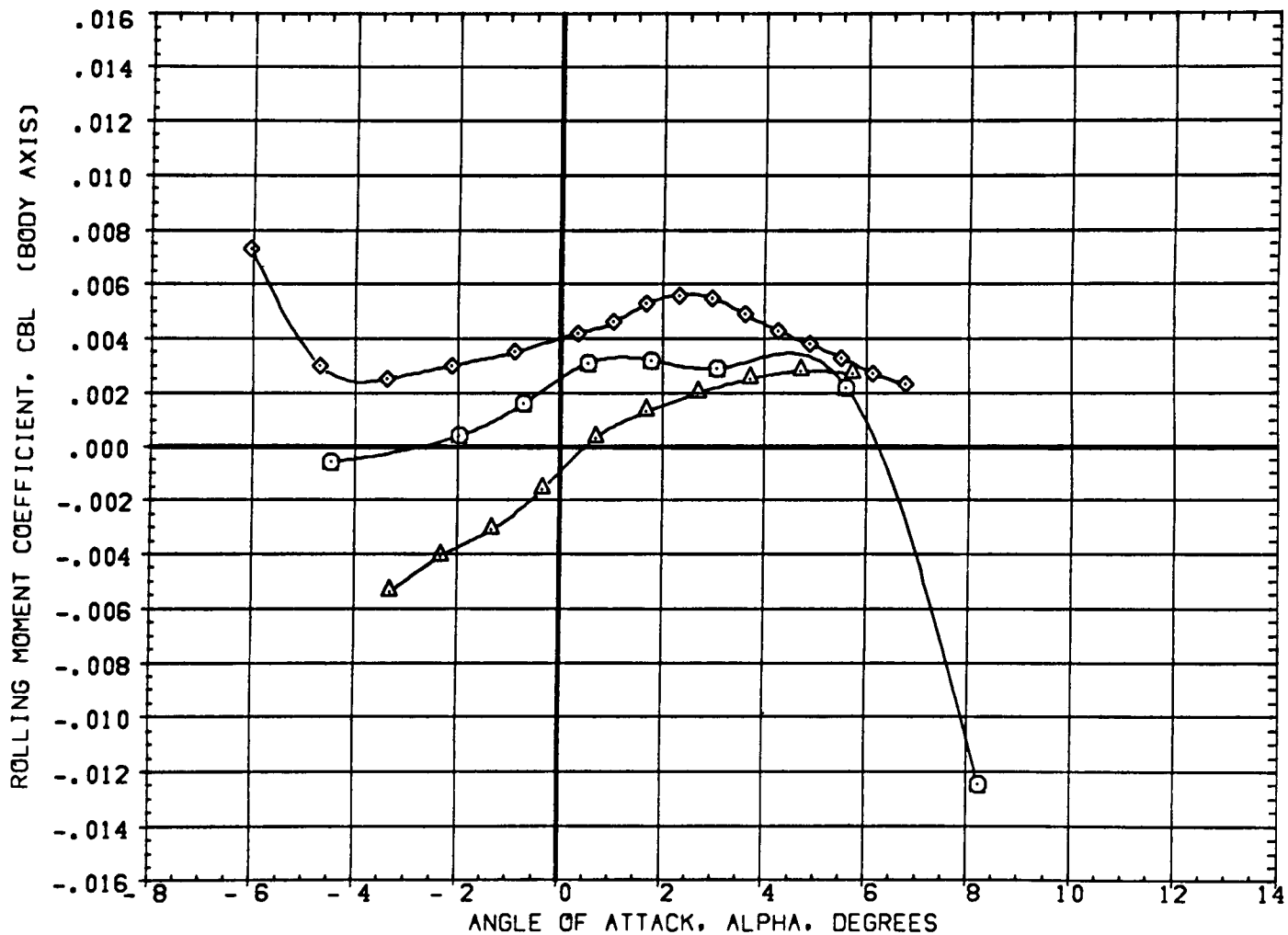

FIGURE 6 EFFECT OF WING AIRFOIL SECTION FOR AN OBLIQUE WING ANGLE OF 50 DEGREES

(A)MACH = .80

DATA SET	SYMBOL	CONFIGURATION DESCRIPTION	BETA	LAMBDA	RN/L
(3AE007)	○	W1 F0 B	0.000	50.000	6.000
(3AE042)	△	W2 F0 B	0.000	50.000	4.000
(3AE068)	◇	W4 F0 B	0.000	50.000	6.000

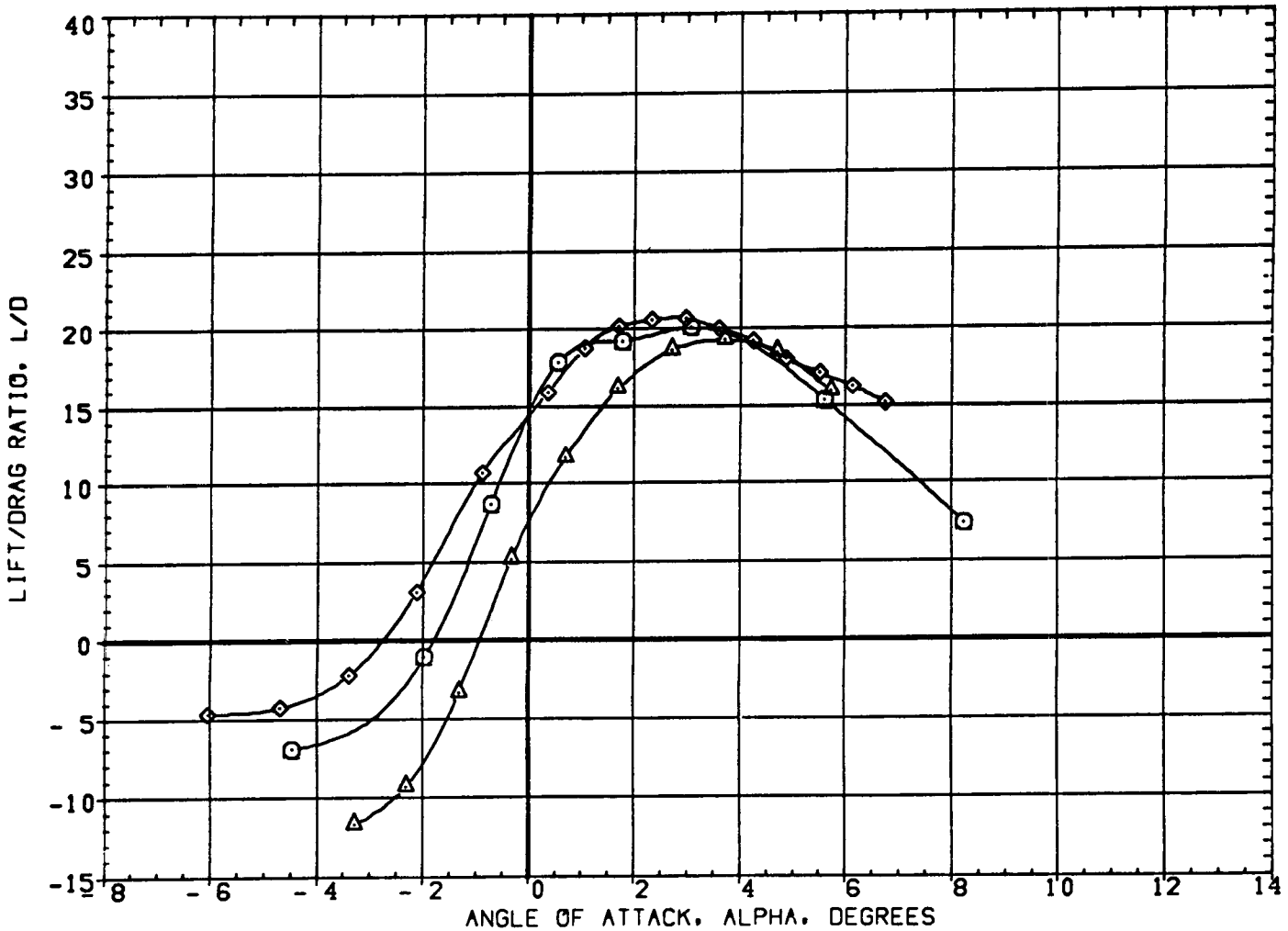

FIGURE 6 EFFECT OF WING AIRFOIL SECTION FOR AN OBLIQUE WING ANGLE OF 50 DEGREES

(A)MACH = .80

DATA SET	SYMBOL	CONFIGURATION DESCRIPTION	BETA	LAMBDA	RN/L
(4AE007)	○	W1 F0 B	0.000	50.000	6.000
(4AE042)	△	W2 F0 B	0.000	50.000	4.000
(4AE068)	◇	W4 F0 B	0.000	50.000	6.000

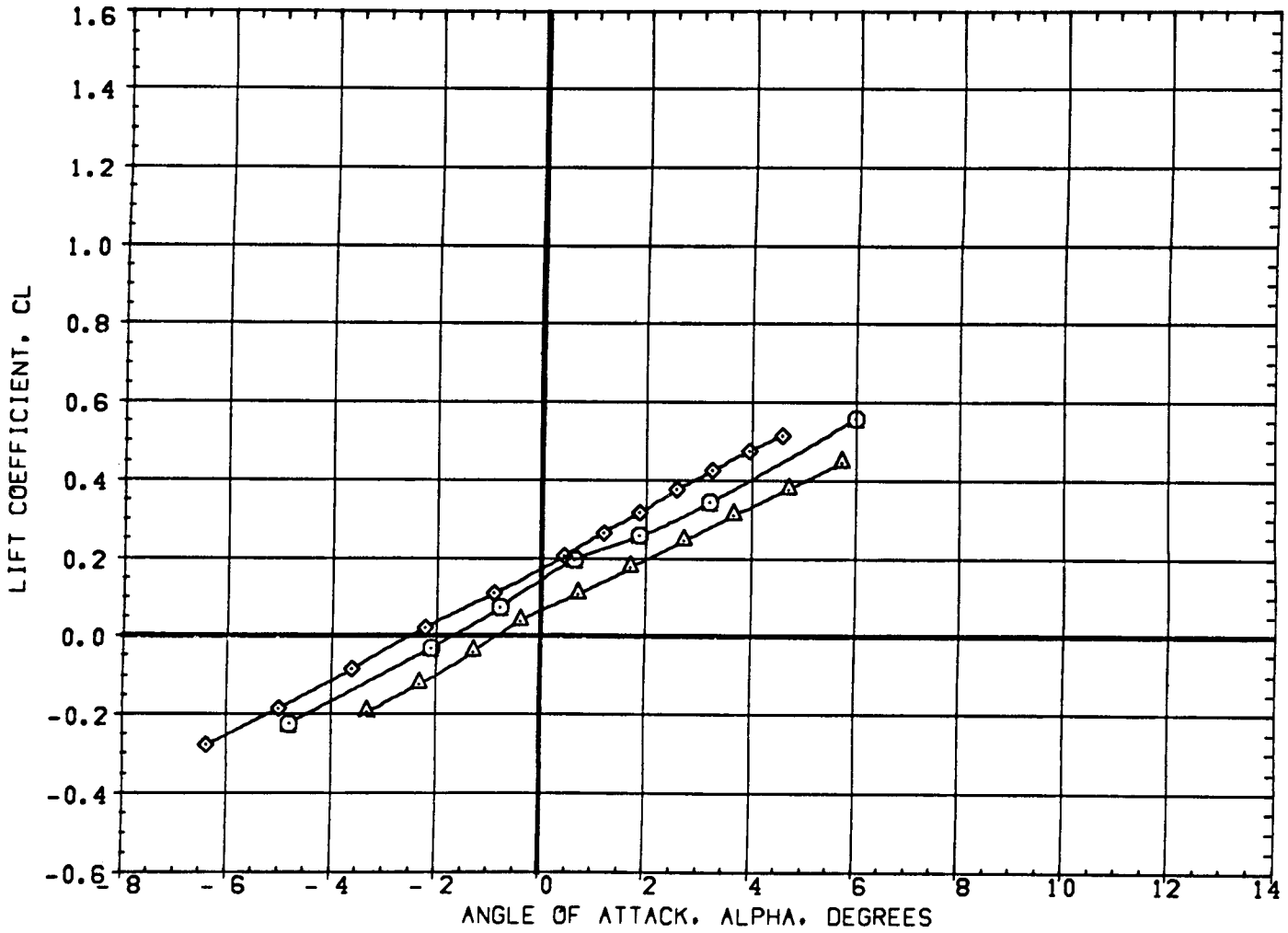

FIGURE 6 EFFECT OF WING AIRFOIL SECTION FOR AN OBLIQUE WING ANGLE OF 50 DEGREES

(A)MACH = .95

DATA SET	SYMBOL	CONFIGURATION DESCRIPTION	BETA	LAMBDA	RN/L
(4AE007)	○	W1 F0 B	0.000	50.000	6.000
(4AE042)	△	W2 F0 B	0.000	50.000	4.000
(4AE068)	◇	W4 F0 B	0.000	50.000	6.000

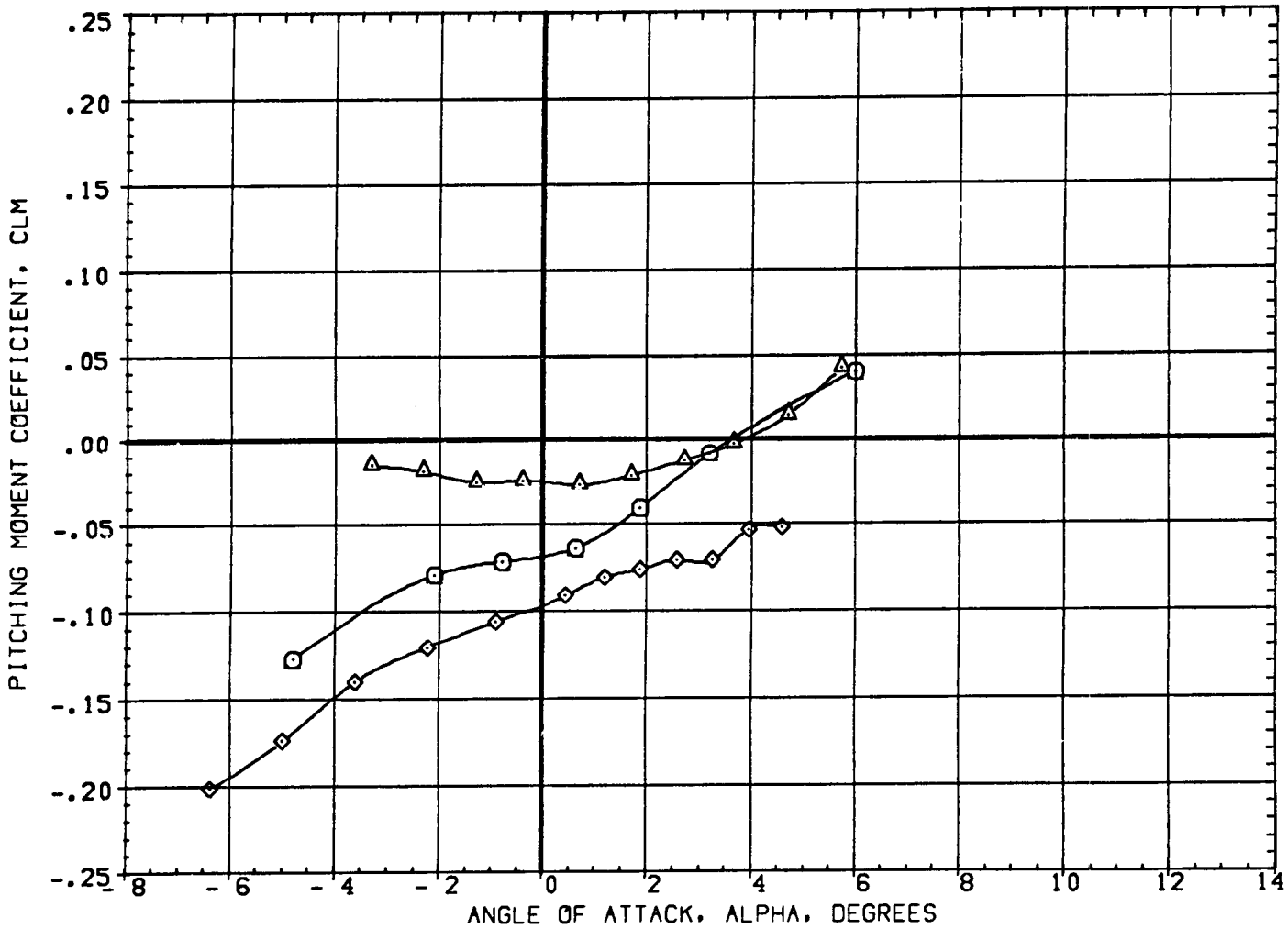

FIGURE 6 EFFECT OF WING AIRFOIL SECTION FOR AN OBLIQUE WING ANGLE OF 50 DEGREES

(A)MACH = .95

DATA SET	SYMBOL	CONFIGURATION DESCRIPTION	BETA	LAMBDA	RN/L
(4AE007)	○	W1 FO B	0.000	50.000	6.000
(4AE042)	△	W2 FO B	0.000	50.000	4.000
(4AE068)	◇	W4 FO B	0.000	50.000	6.000

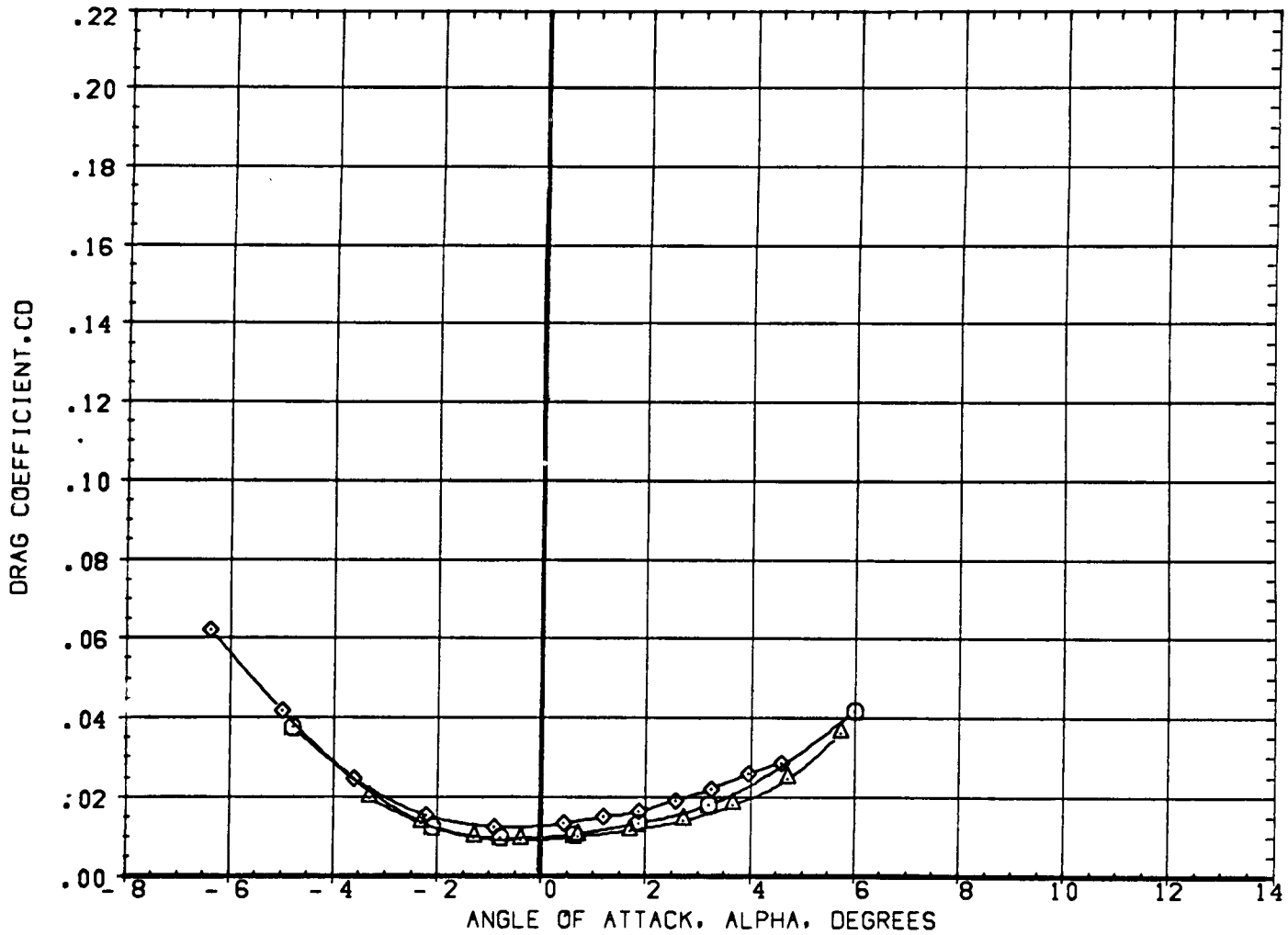

FIGURE 6 EFFECT OF WING AIRFOIL SECTION FOR AN OBLIQUE WING ANGLE OF 50 DEGREES

(A)MACH = .95

DATA SET SYMBOL		CONFIGURATION DESCRIPTION	BETA	LAMBDA	RN/L
(4AE007)	○	W1 F0 B	0.000	50.000	6.000
(4AE042)	△	W2 F0 B	0.000	50.000	4.000
(4AE068)	◇	W4 F0 B	0.000	50.000	6.000

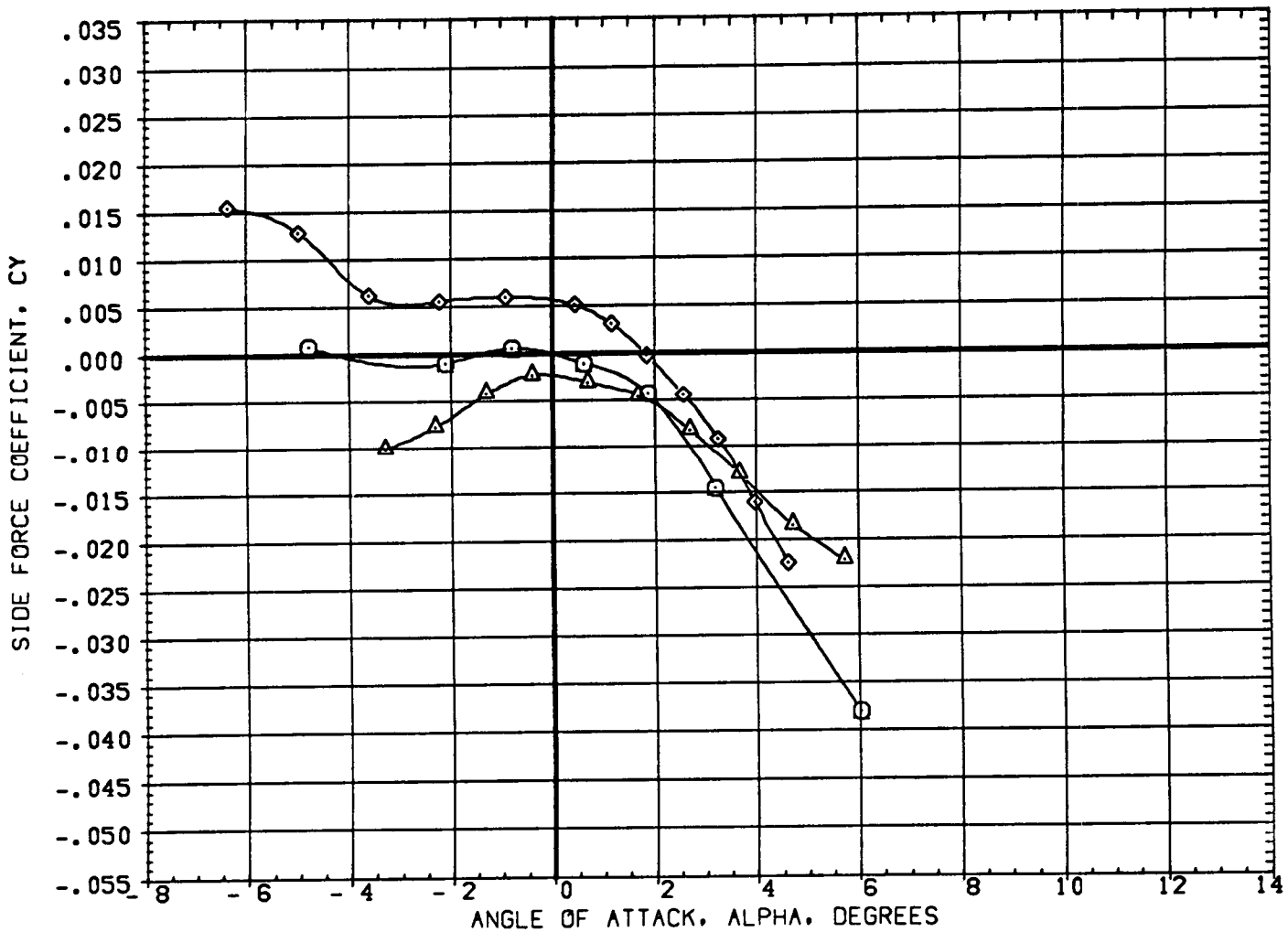

FIGURE 6 EFFECT OF WING AIRFOIL SECTION FOR AN OBLIQUE WING ANGLE OF 50 DEGREES

(A)MACH = .95

DATA SET	SYMBOL	CONFIGURATION DESCRIPTION	BETA	LAMBDA	RN/L
(4AE007)	○	W1 FO B	0.000	50.000	6.000
(4AE042)	△	W2 FO B	0.000	50.000	4.000
(4AE068)	◇	W4 FO B	0.000	50.000	6.000

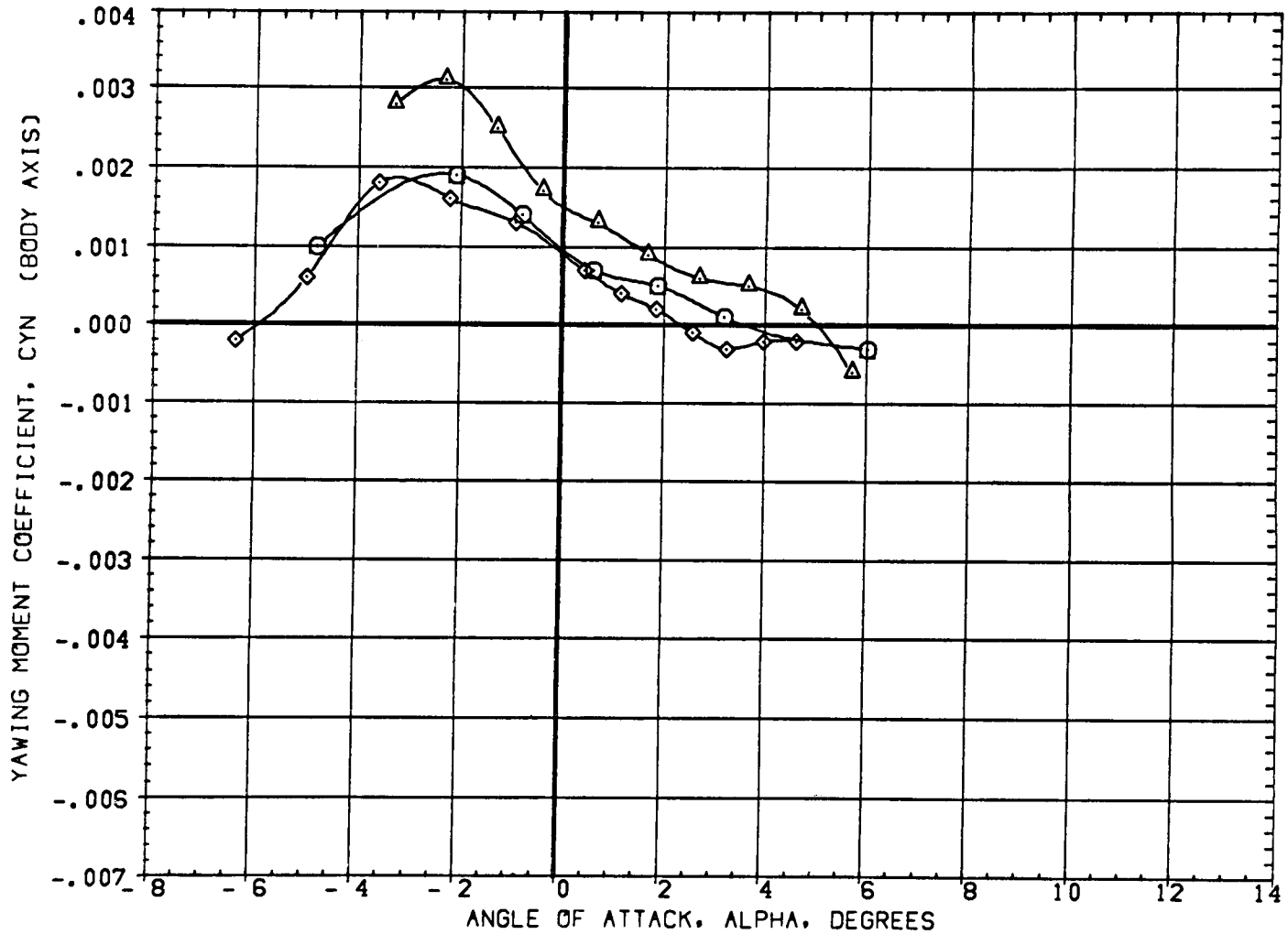

FIGURE 6 EFFECT OF WING AIRFOIL SECTION FOR AN OBLIQUE WING ANGLE OF 50 DEGREES

(A)MACH = .95

DATA SET	SYMBOL	CONFIGURATION DESCRIPTION	BETA	LAMBDA	RN/L
(4AE007)	○	W1 F0 B	0.000	50.000	6.000
(4AE042)	△	W2 F0 B	0.000	50.000	4.000
(4AE068)	◇	W4 F0 B	0.000	50.000	6.000

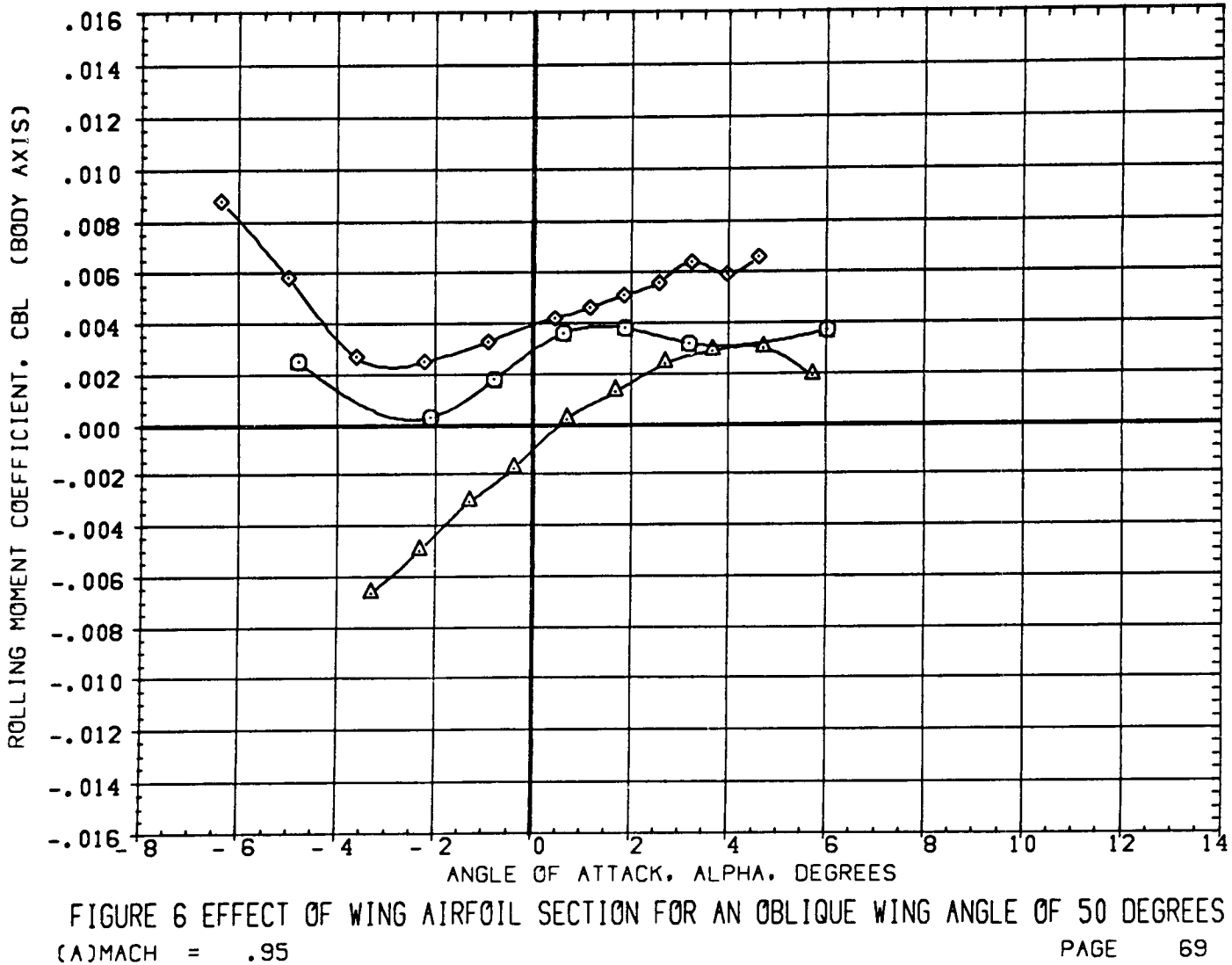

FIGURE 6 EFFECT OF WING AIRFOIL SECTION FOR AN OBLIQUE WING ANGLE OF 50 DEGREES

(A)MACH = .95

DATA SET	SYMBOL	CONFIGURATION DESCRIPTION	BETA	LAMBDA	RN/L
(4AE007)	○	W1 F0 B	0.000	50.000	6.000
(4AE042)	△	W2 F0 B	0.000	50.000	4.000
(4AE068)	◇	W4 F0 B	0.000	50.000	6.000

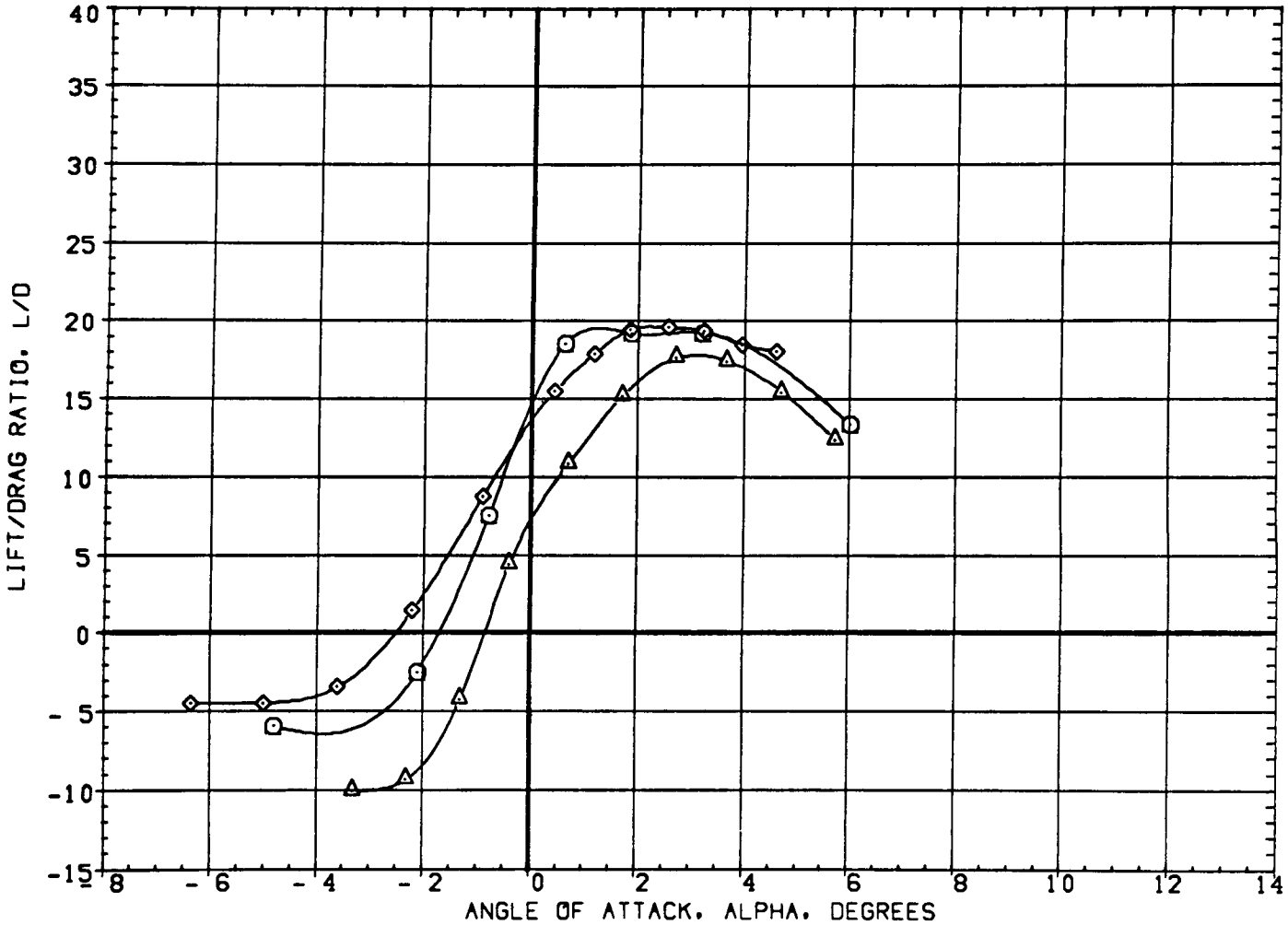

FIGURE 6 EFFECT OF WING AIRFOIL SECTION FOR AN OBLIQUE WING ANGLE OF 50 DEGREES

(A)MACH = .95

DATA SET	SYMBOL	CONFIGURATION DESCRIPTION	BETA	LAMBDA	RN/L
(SAE007)	○	W1 F0 B	0.000	50.000	6.000
(SAE042)	⊠	W2 F0 B	0.000	50.000	4.000
(SAE068)	◇	W4 F0 B	0.000	50.000	6.000

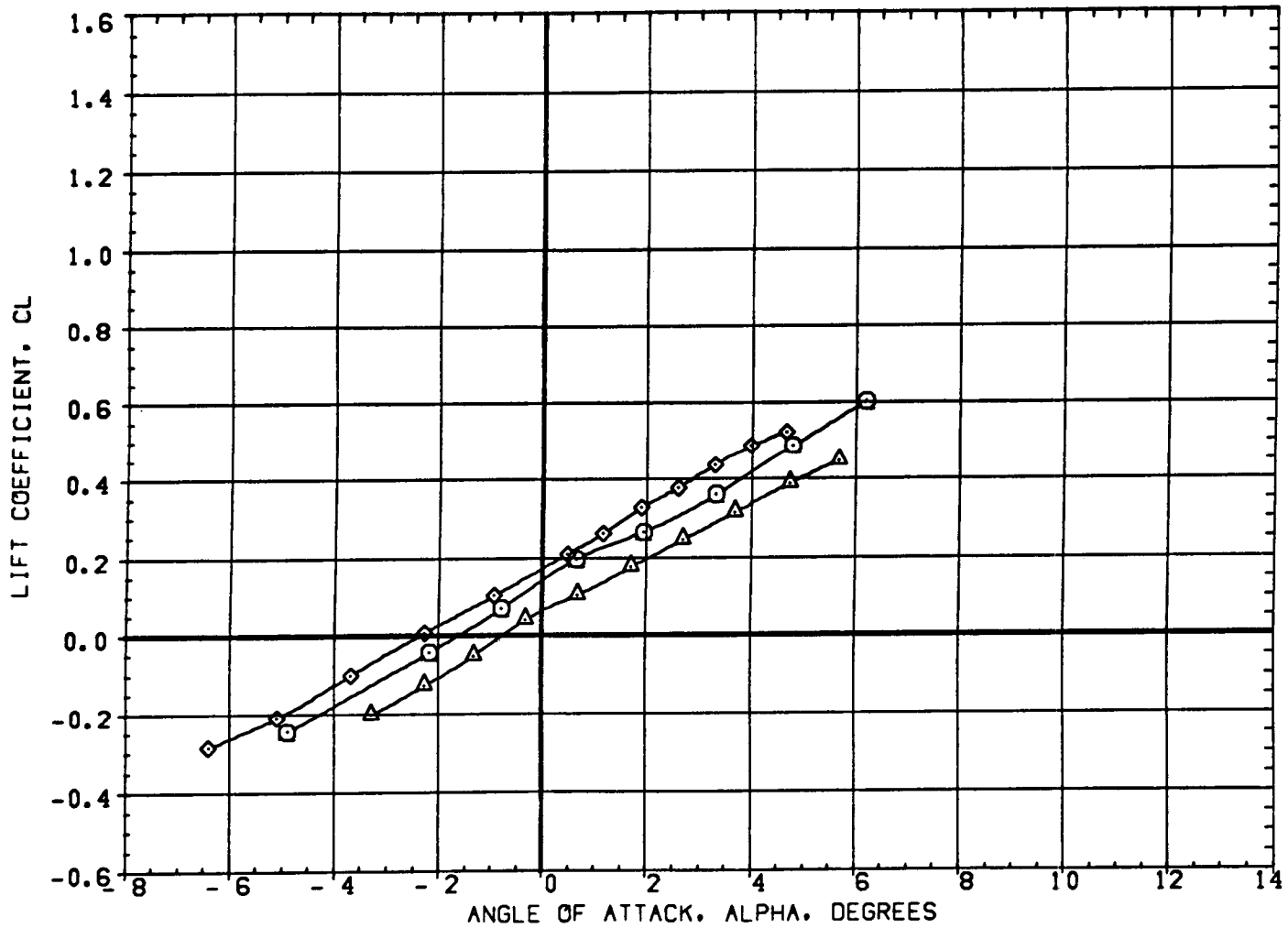

FIGURE 6 EFFECT OF WING AIRFOIL SECTION FOR AN OBLIQUE WING ANGLE OF 50 DEGREES

(A)MACH = .98

DATA SET	SYMBOL	CONFIGURATION DESCRIPTION	BETA	LAMBDA	RN/L
(5AE007)	○	W1 F0 B	0.000	50.000	6.000
(5AE042)	△	W2 F0 B	0.000	50.000	4.000
(5AE068)	◇	W4 F0 B	0.000	50.000	6.000

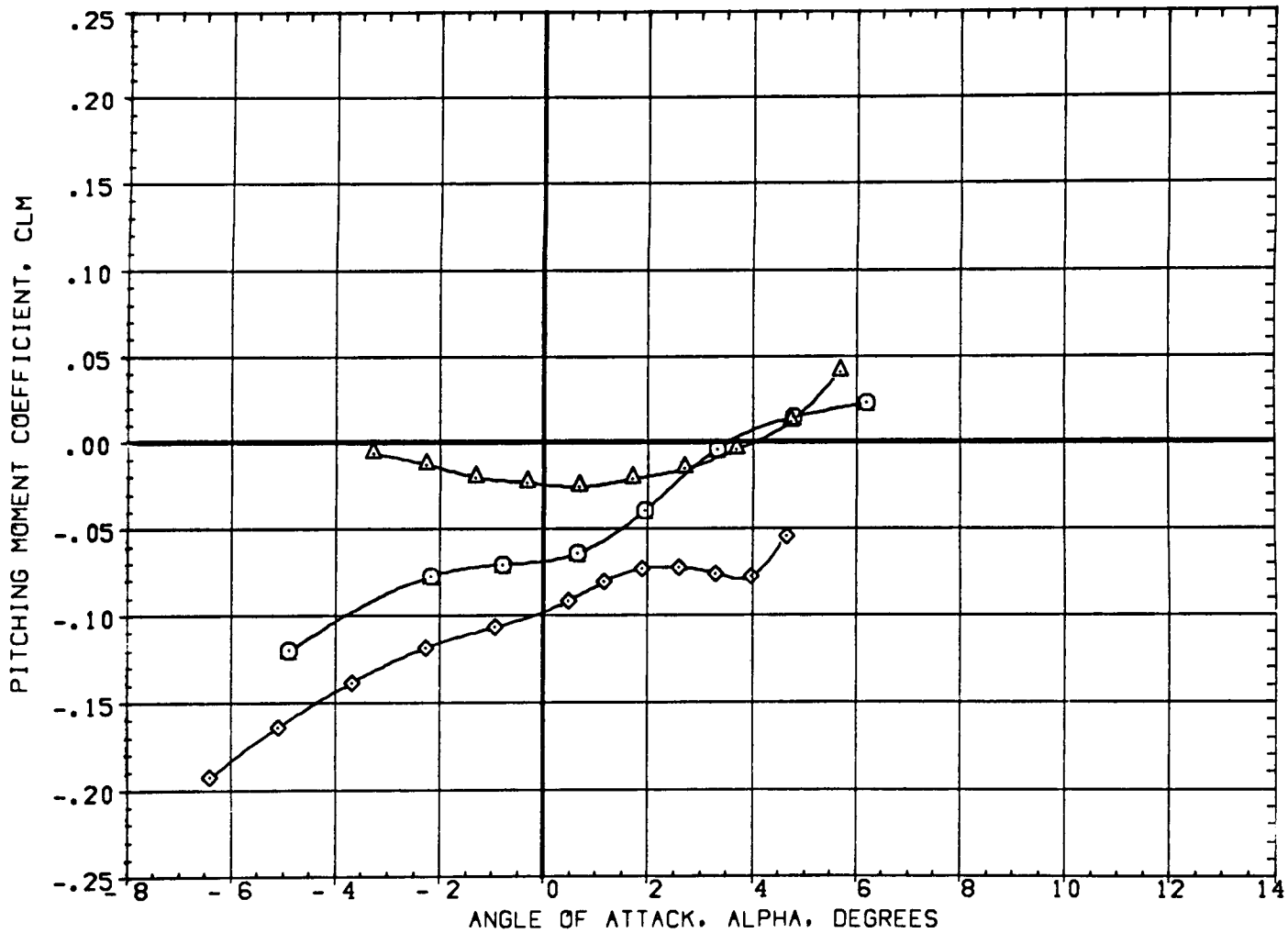

FIGURE 6 EFFECT OF WING AIRFOIL SECTION FOR AN OBLIQUE WING ANGLE OF 50 DEGREES

(A)MACH = .98

DATA SET	SYMBOL	CONFIGURATION DESCRIPTION	BETA	LAMBDA	RN/L
(5AE007)	○	W1 F0 B	0.000	50.000	6.000
(5AE042)	△	W2 F0 B	0.000	50.000	4.000
(5AE068)	◇	W4 F0 B	0.000	50.000	6.000

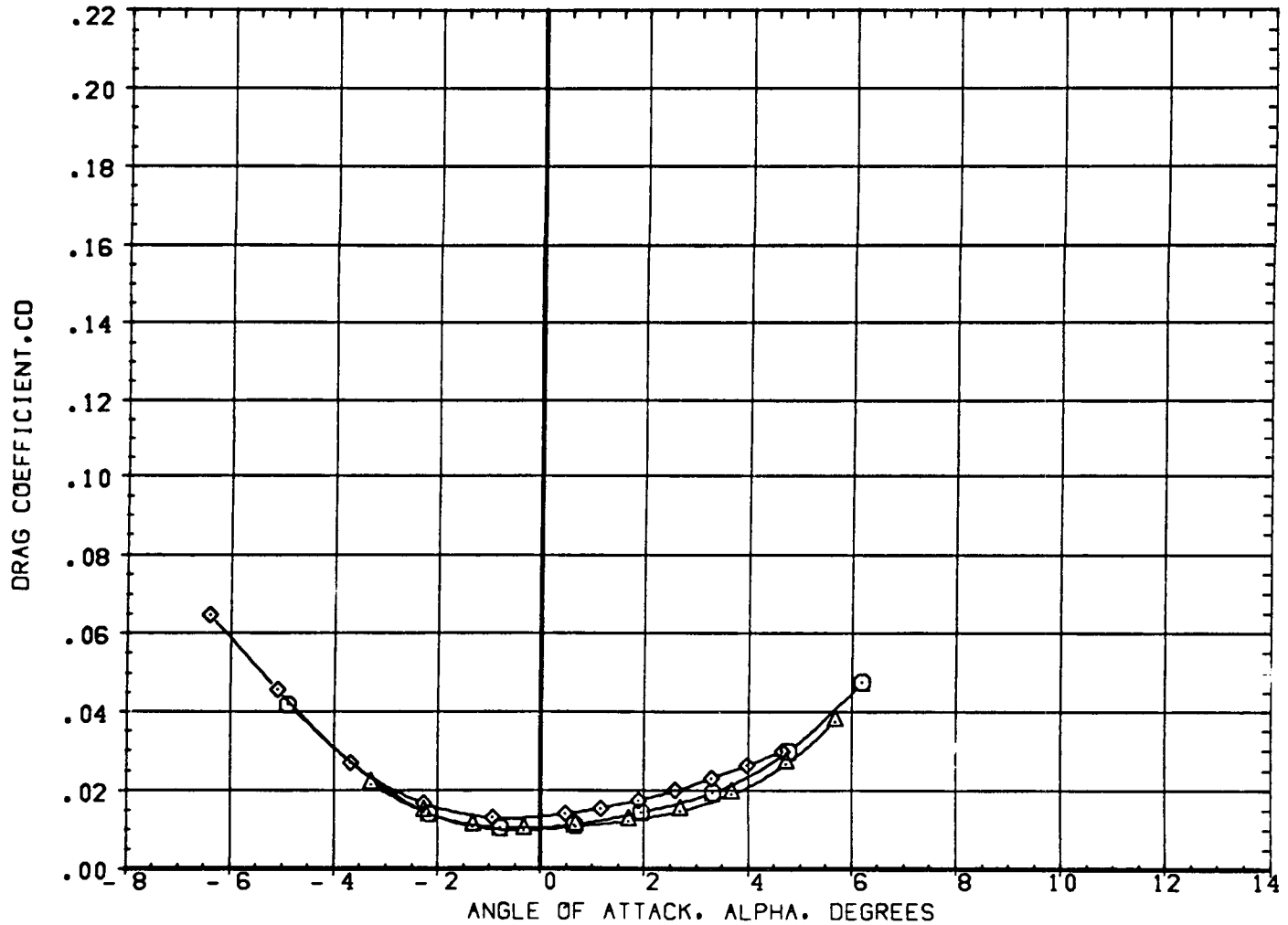

FIGURE 6 EFFECT OF WING AIRFOIL SECTION FOR AN OBLIQUE WING ANGLE OF 50 DEGREES

(A)MACH = .98

DATA SET	SYMBOL	CONFIGURATION DESCRIPTION	BETA	LAMBDA	RN/L
(5AE007)	○	W1 F0 B	0.000	50.000	6.000
(5AE042)	△	W2 F0 B	0.000	50.000	4.000
(5AE068)	◇	W4 F0 B	0.000	50.000	6.000

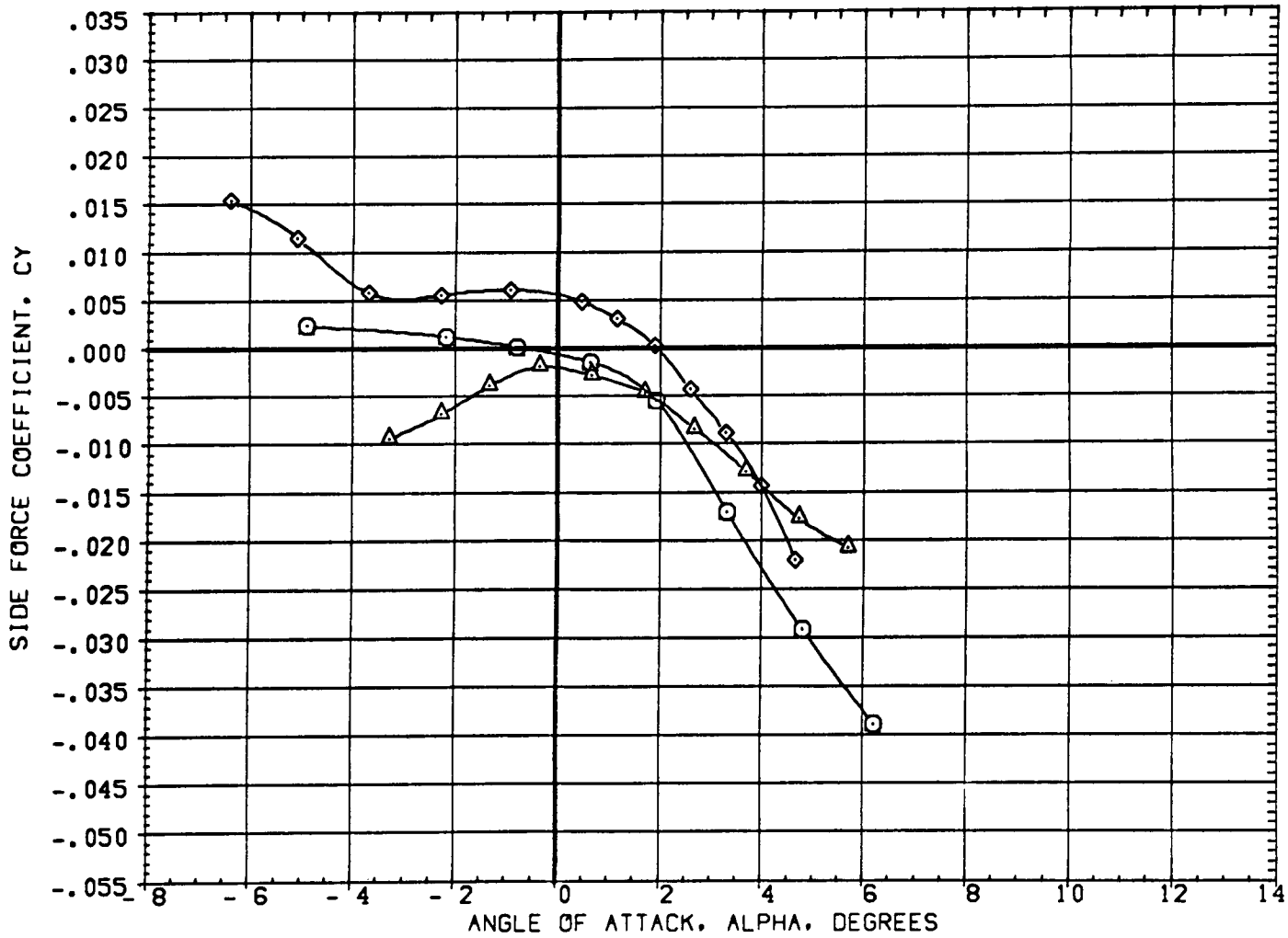

FIGURE 6 EFFECT OF WING AIRFOIL SECTION FOR AN OBLIQUE WING ANGLE OF 50 DEGREES

(A)MACH = .98

DATA SET	SYMBOL	CONFIGURATION DESCRIPTION	BETA	LAMBDA	RN/L
(5AE007)	○	W1 F0 B	0.000	50.000	6.000
(5AE042)	△	W2 F0 B	0.000	50.000	4.000
(5AE068)	◇	W4 F0 B	0.000	50.000	6.000

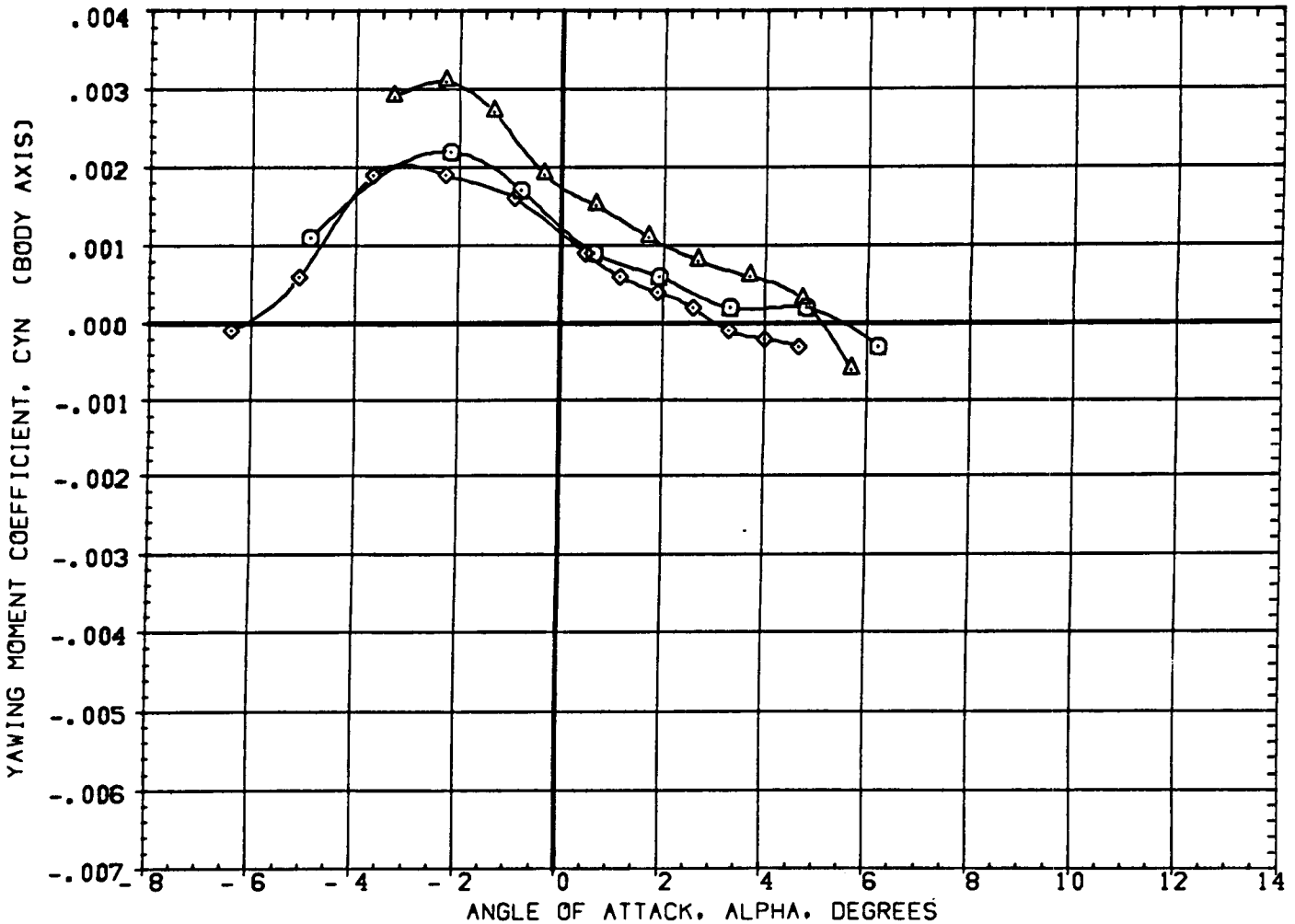

FIGURE 6 EFFECT OF WING AIRFOIL SECTION FOR AN OBLIQUE WING ANGLE OF 50 DEGREES

(A)MACH = .98

DATA SET	SYMBOL	CONFIGURATION DESCRIPTION	BETA	LAMBDA	RN/L
(5AE007)	○	W1 F0 B	0.000	50.000	6.000
(5AE042)	△	W2 F0 B	0.000	50.000	4.000
(5AE068)	◇	W4 F0 B	0.000	50.000	6.000

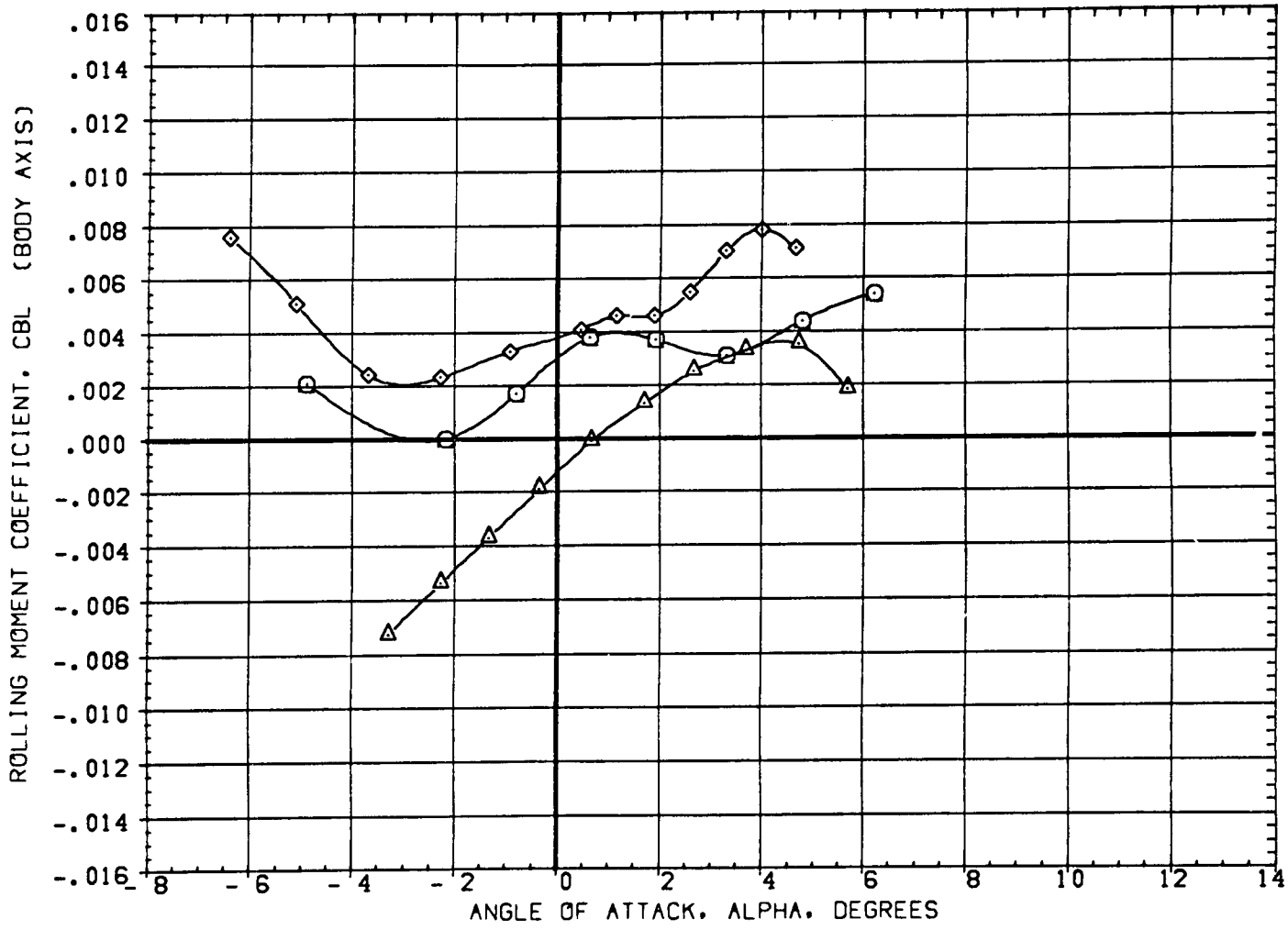

FIGURE 6 EFFECT OF WING AIRFOIL SECTION FOR AN OBLIQUE WING ANGLE OF 50 DEGREES

(A)MACH = .98

DATA SET	SYMBOL	CONFIGURATION DESCRIPTION	BETA	LAMBDA	RN/L
(SAE007)	○	W1 F0 B	0.000	50.000	6.000
(SAE042)	△	W2 F0 B	0.000	50.000	4.000
(SAE066)	◇	W4 F0 B	0.000	50.000	6.000

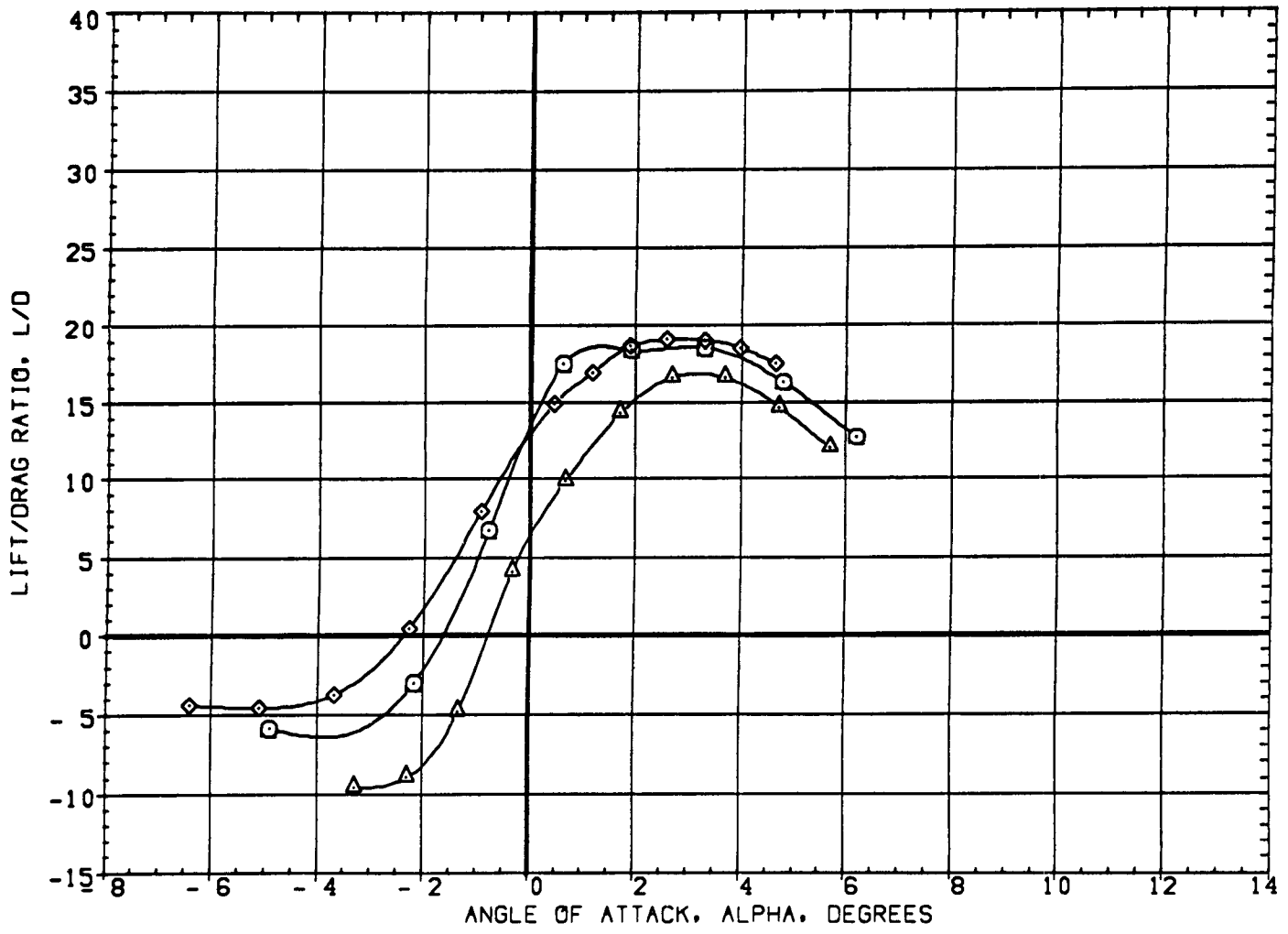

FIGURE 6 EFFECT OF WING AIRFOIL SECTION FOR AN OBLIQUE WING ANGLE OF 50 DEGREES

(A)MACH = .98

DATA SET	SYMBOL	CONFIGURATION DESCRIPTION	BETA	LAMBDA	RN/L
(7AE007)	○	W1 F0 B	0.000	50.000	6.000
(7AE042)	△	W2 F0 B	0.000	50.000	4.000
(7AE068)	◇	W4 F0 B	0.000	50.000	6.000

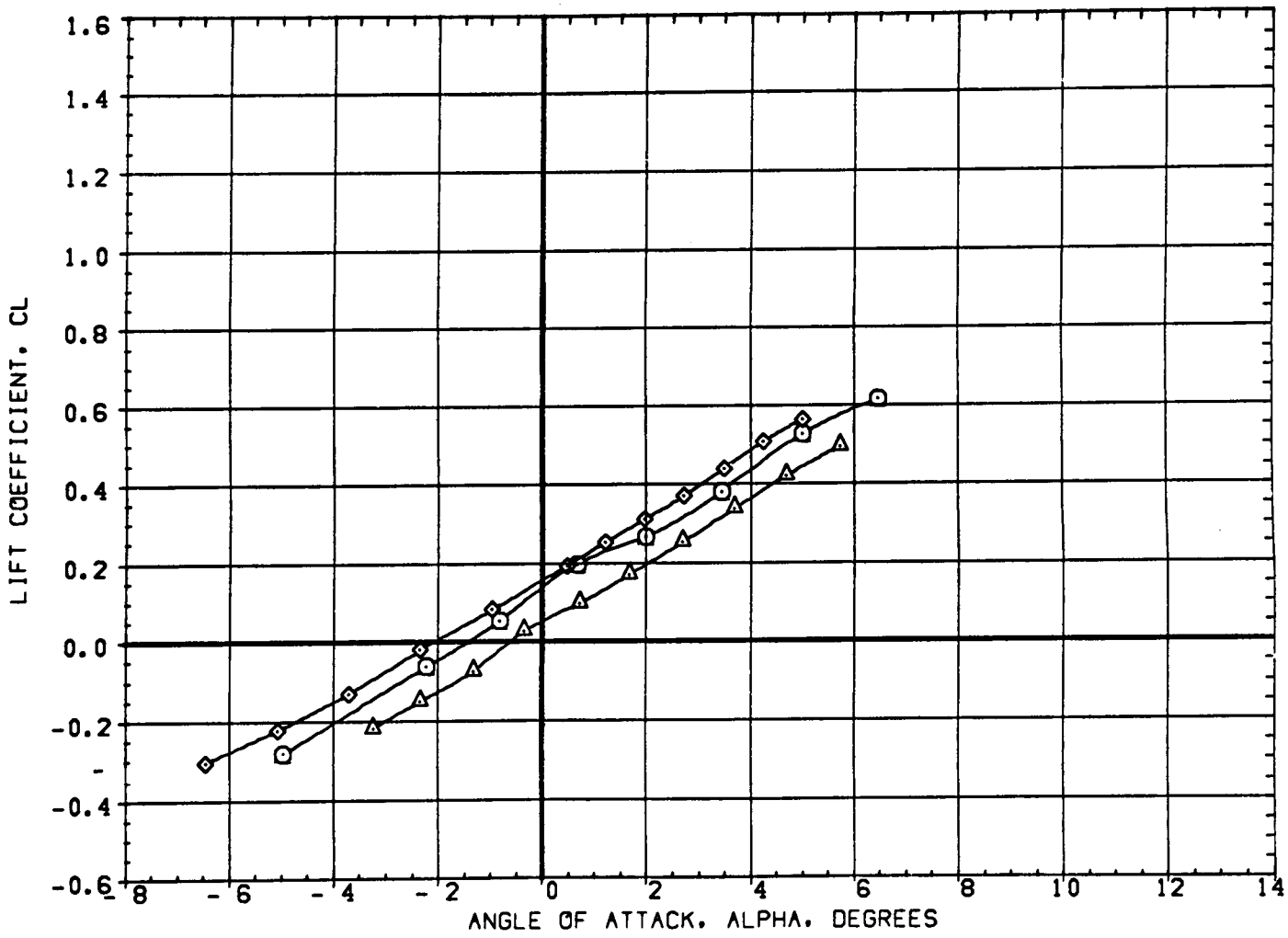

FIGURE 6 EFFECT OF WING AIRFOIL SECTION FOR AN OBLIQUE WING ANGLE OF 50 DEGREES

(A)MACH = 1.10

DATA SET	SYMBOL	CONFIGURATION DESCRIPTION	BETA	LAMBDA	RN/L
(7AE007)	○	W1 FD B	0.000	50.000	6.000
(7AE042)	△	W2 FD B	0.000	50.000	4.000
(7AE068)	◇	W4 FD B	0.000	50.000	6.000

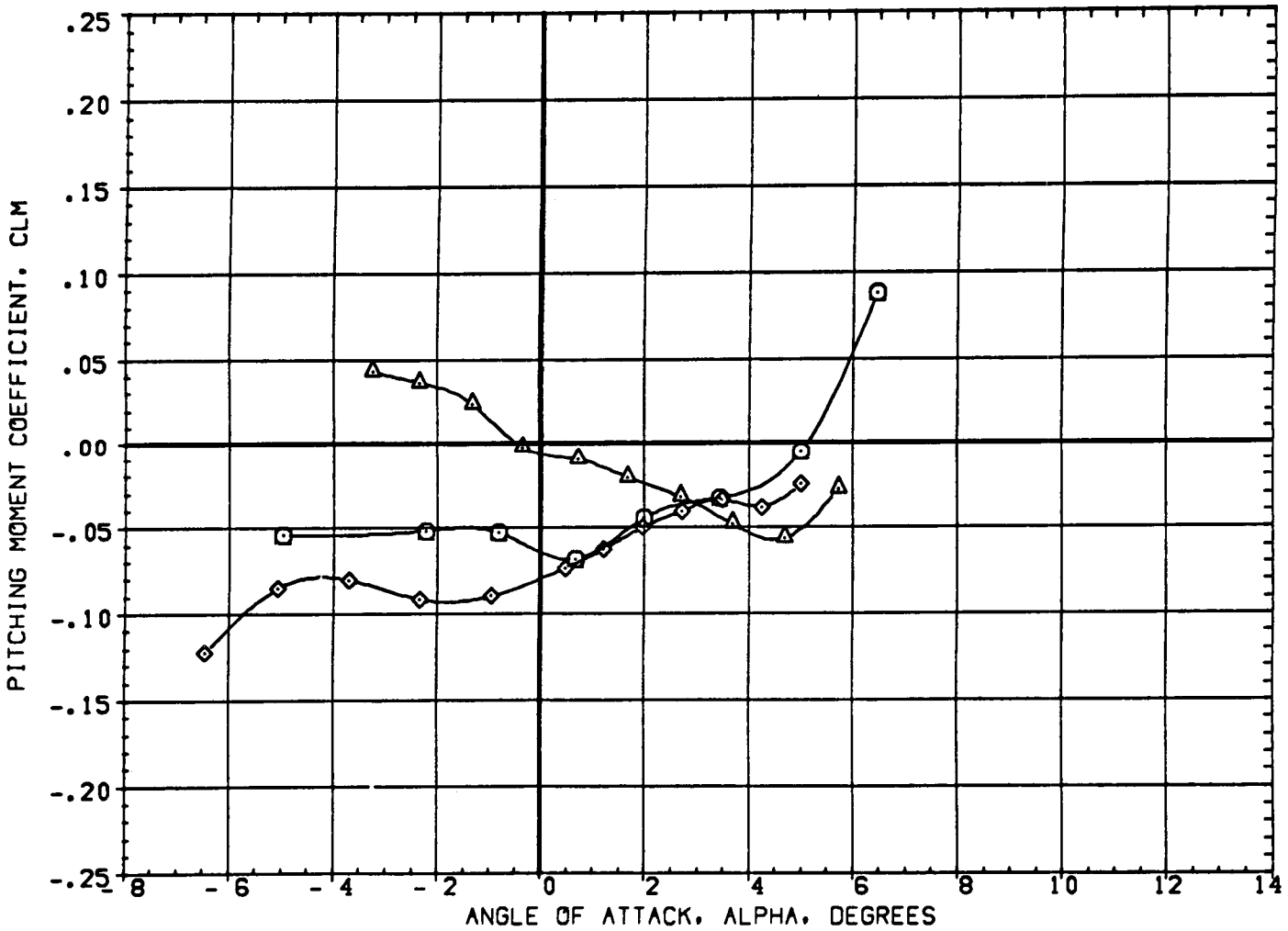

FIGURE 6 EFFECT OF WING AIRFOIL SECTION FOR AN OBLIQUE WING ANGLE OF 50 DEGREES

(A)MACH = 1.10

DATA SET	SYMBOL	CONFIGURATION DESCRIPTION	BETA	LAMBDA	RN/L
(7AE007)	○	W1 F0 B	0.000	50.000	6.000
(7AE042)	△	W2 F0 B	0.000	50.000	4.000
(7AE068)	◇	W4 F0 B	0.000	50.000	6.000

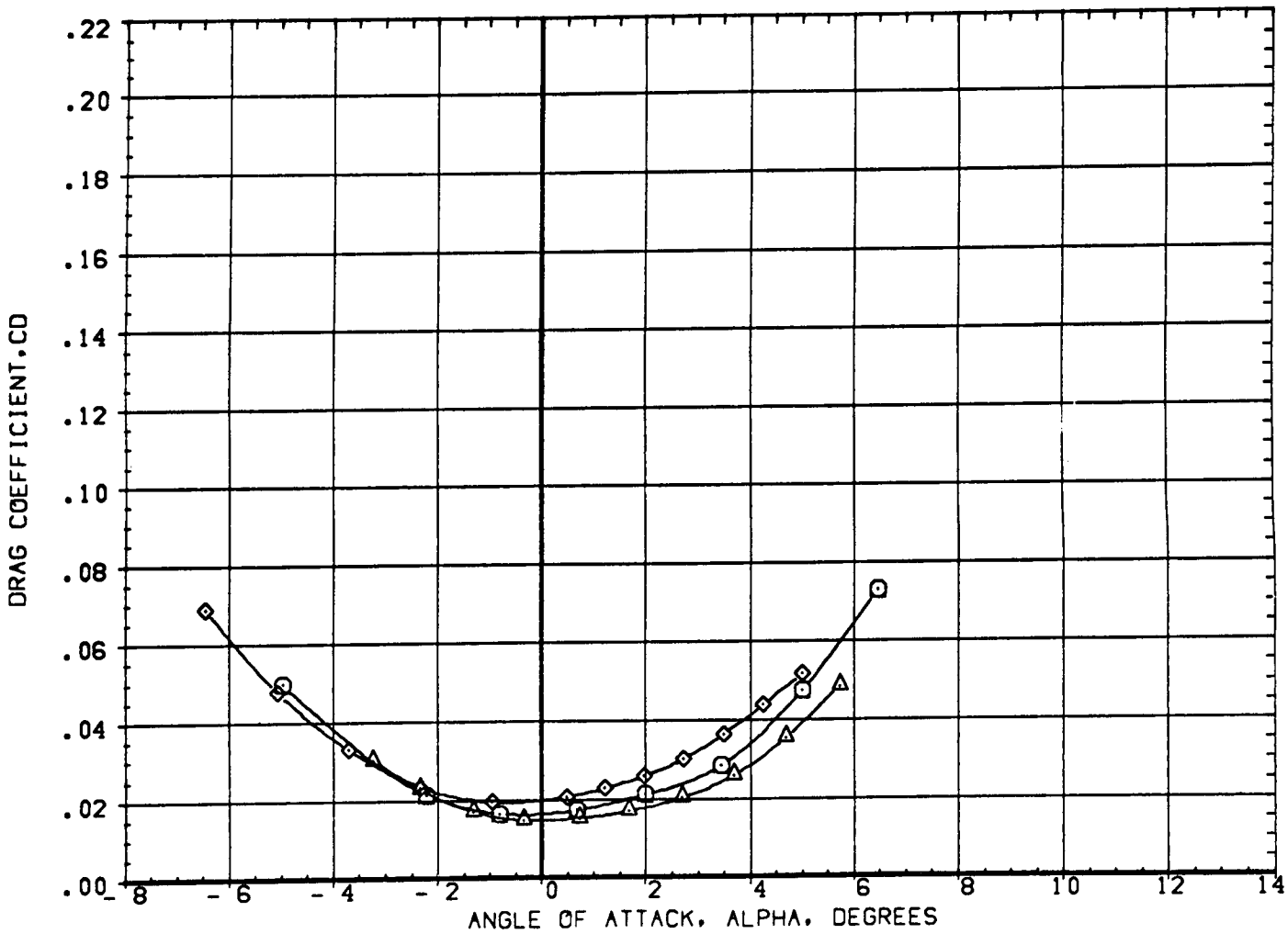

FIGURE 6 EFFECT OF WING AIRFOIL SECTION FOR AN OBLIQUE WING ANGLE OF 50 DEGREES

(A)MACH = 1.10

DATA SET	SYMBOL	CONFIGURATION DESCRIPTION	BETA	LAMBDA	RN/L
(7AE007)	○	W1 F0 B	0.000	50.000	6.000
(7AE042)	△	W2 F0 B	0.000	50.000	4.000
(7AE068)	◇	W4 F0 B	0.000	50.000	6.000

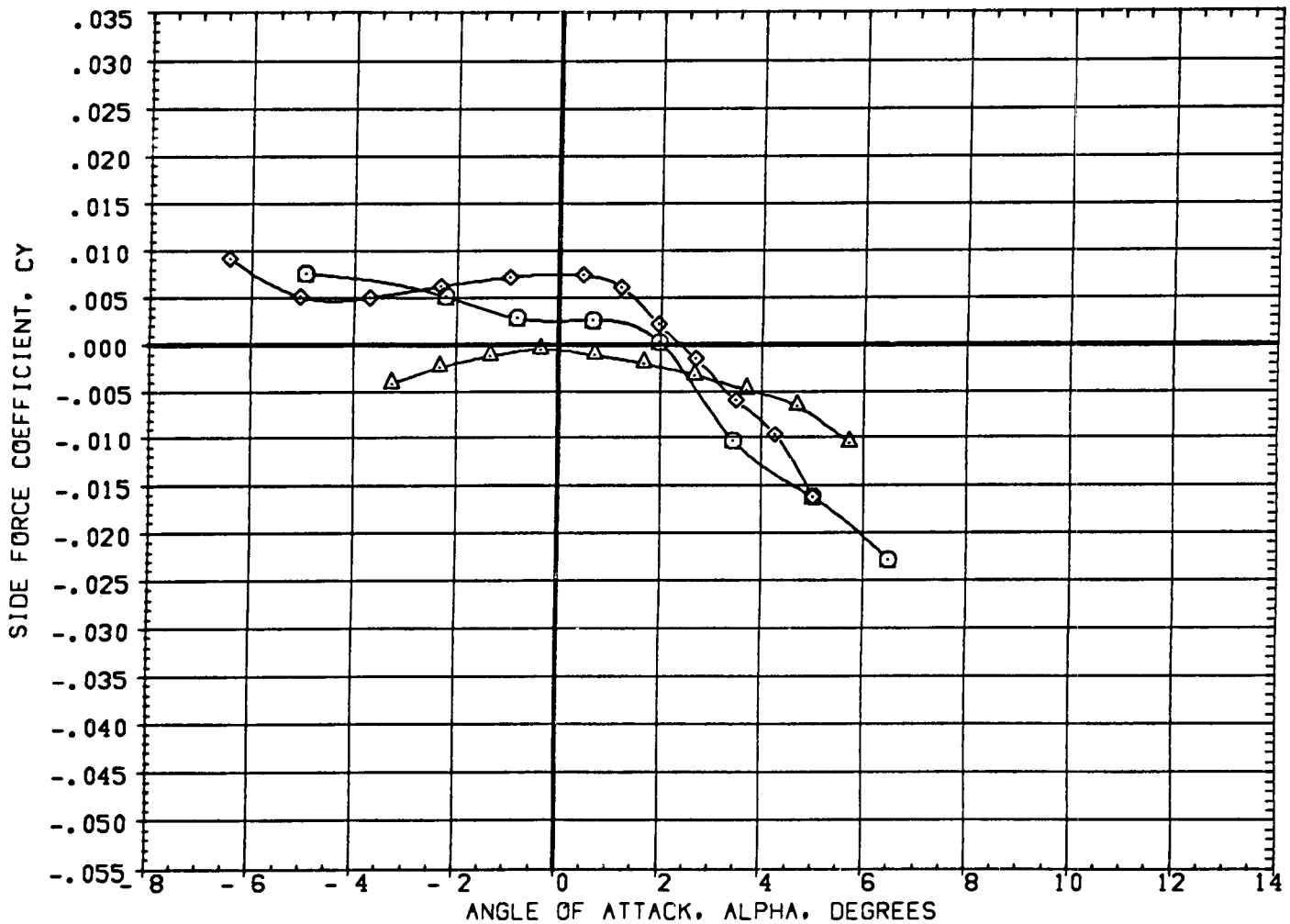

FIGURE 6 EFFECT OF WING AIRFOIL SECTION FOR AN OBLIQUE WING ANGLE OF 50 DEGREES

(A)MACH = 1.10

DATA SET	SYMBOL	CONFIGURATION DESCRIPTION
(7AE007)	○	W1 F0 B
(7AE042)	△	W2 F0 B
(7AE068)	◇	W4 F0 B

BETA	LAMBDA	RN/L
0.000	50.000	6.000
0.000	50.000	4.000
0.000	50.000	6.000

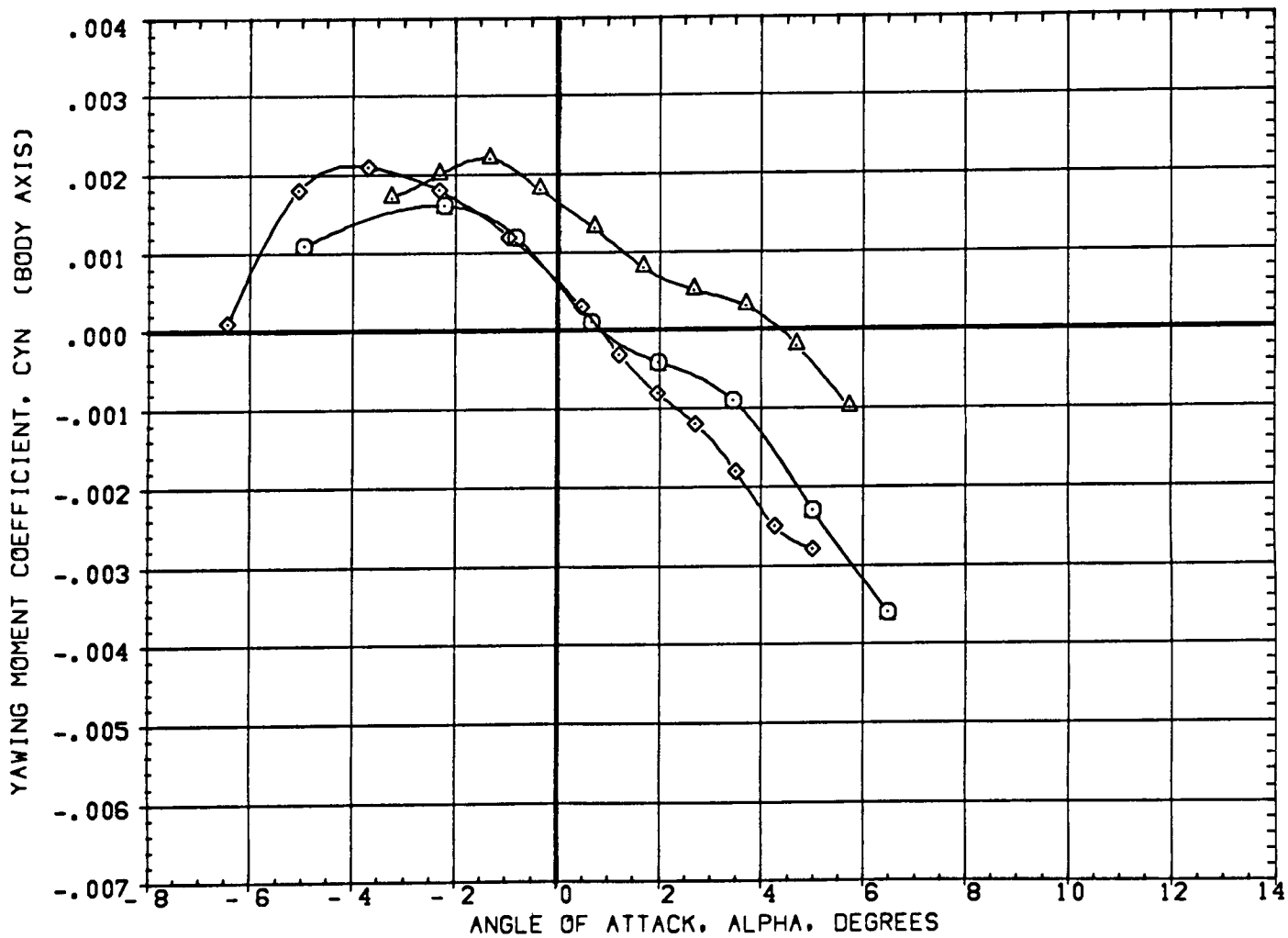

FIGURE 6 EFFECT OF WING AIRFOIL SECTION FOR AN OBLIQUE WING ANGLE OF 50 DEGREES

(A)MACH = 1.10

DATA SET	SYMBOL	CONFIGURATION DESCRIPTION	BETA	LAMBDA	RN/L
(7AE007)	○	W1 F0 B	0.000	50.000	6.000
(7AE042)	△	W2 F0 B	0.000	50.000	4.000
(7AE068)	◇	W4 F0 B	0.000	50.000	6.000

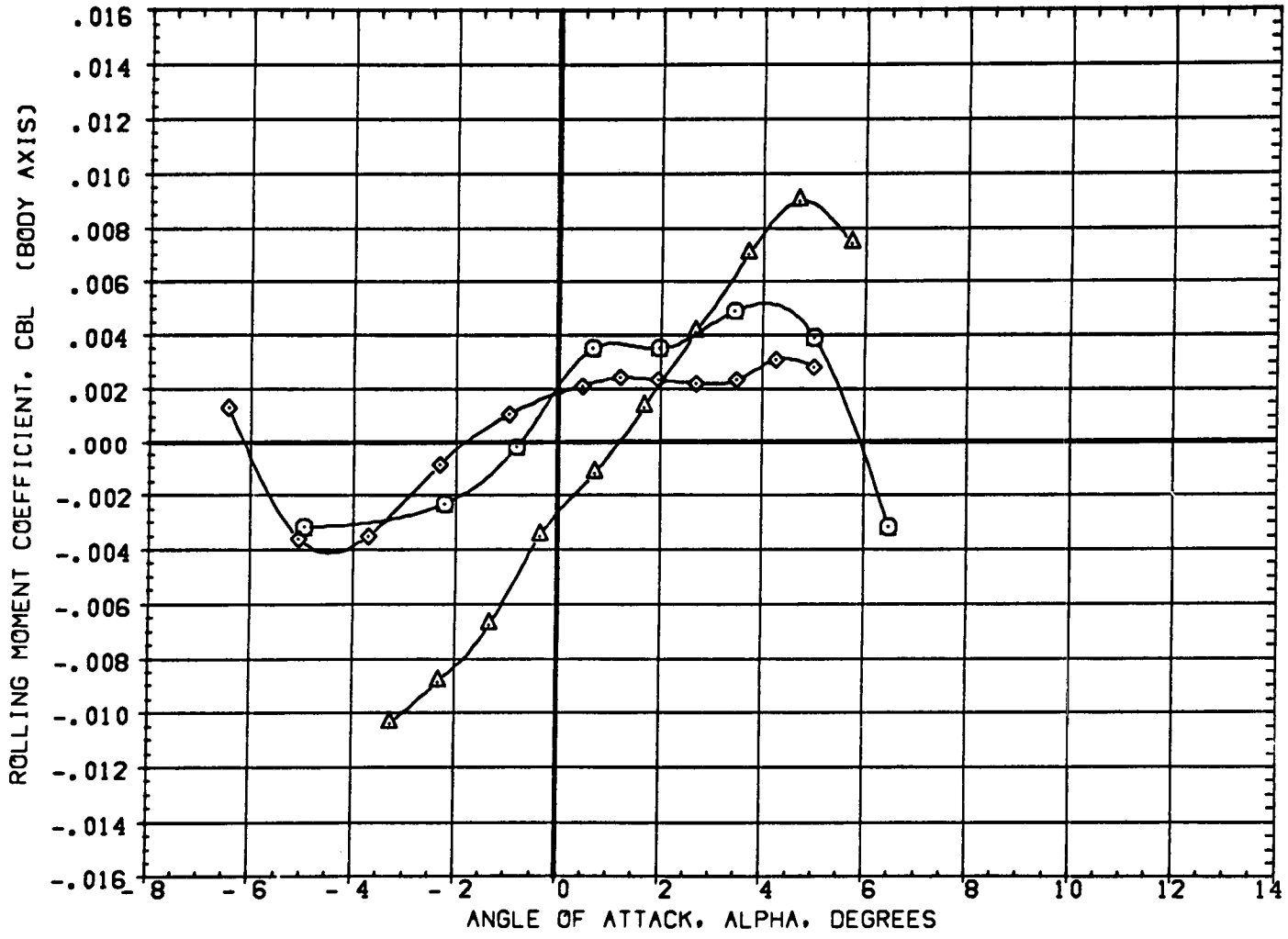

FIGURE 6 EFFECT OF WING AIRFOIL SECTION FOR AN OBLIQUE WING ANGLE OF 50 DEGREES

(A)MACH = 1.10

DATA SET	SYMBOL	CONFIGURATION DESCRIPTION	BETA	LAMBDA	RN/L
(7AE007)	○	W1 F0 B	0.000	50.000	6.000
(7AE042)	△	W2 F0 B	0.000	50.000	4.000
(7AE066)	◇	W4 F0 B	0.000	50.000	6.000

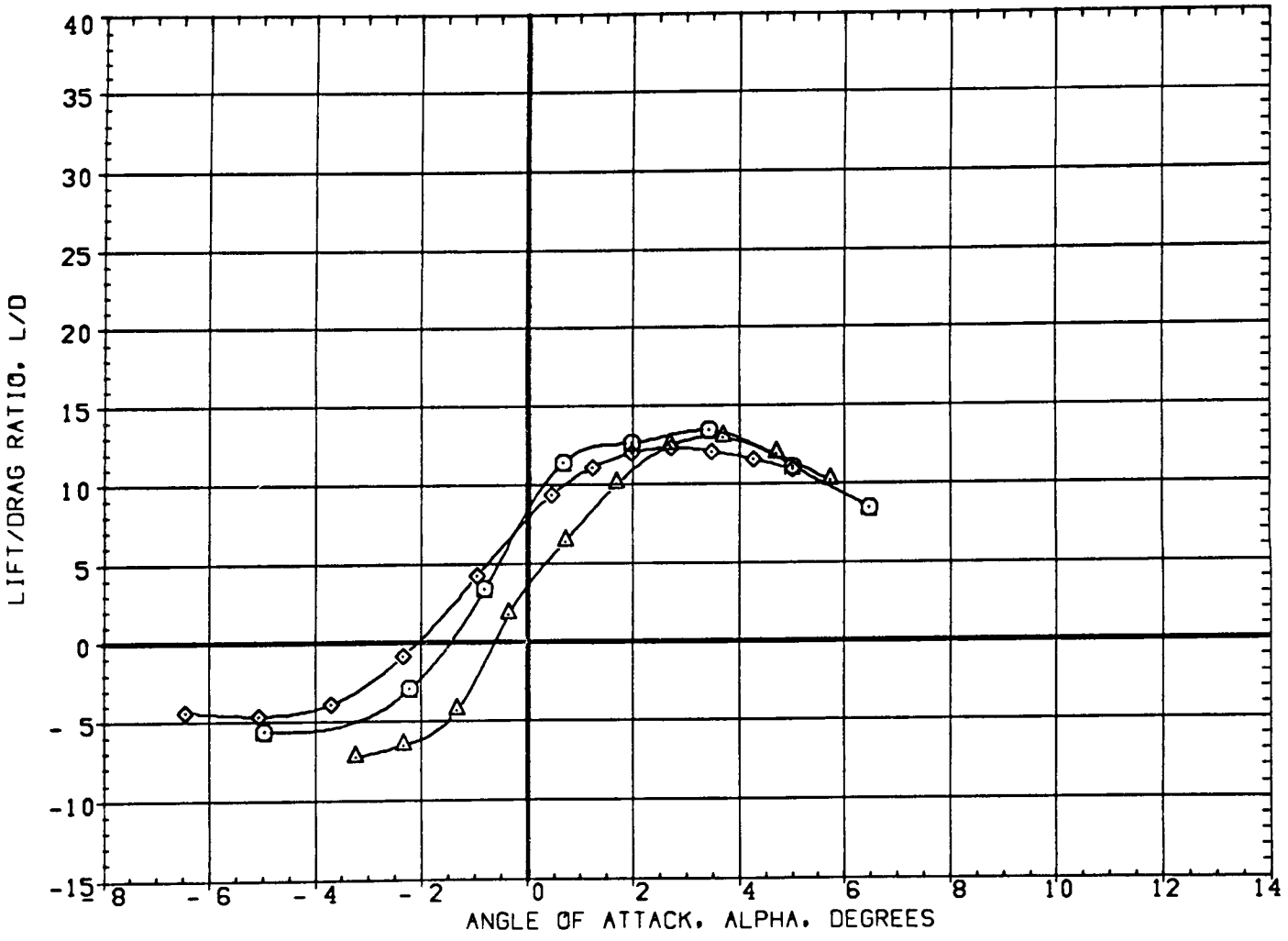

FIGURE 6 EFFECT OF WING AIRFOIL SECTION FOR AN OBLIQUE WING ANGLE OF 50 DEGREES

(A)MACH = 1.10

DATA SET	SYMBOL	CONFIGURATION DESCRIPTION	BETA	LAMBDA	RN/L
(8AE007)	○	W1 F0 B	0.000	50.000	6.000
(8AE042)	△	W2 F0 B	0.000	50.000	4.000
(8AE068)	◇	W4 F0 B	0.000	50.000	6.000

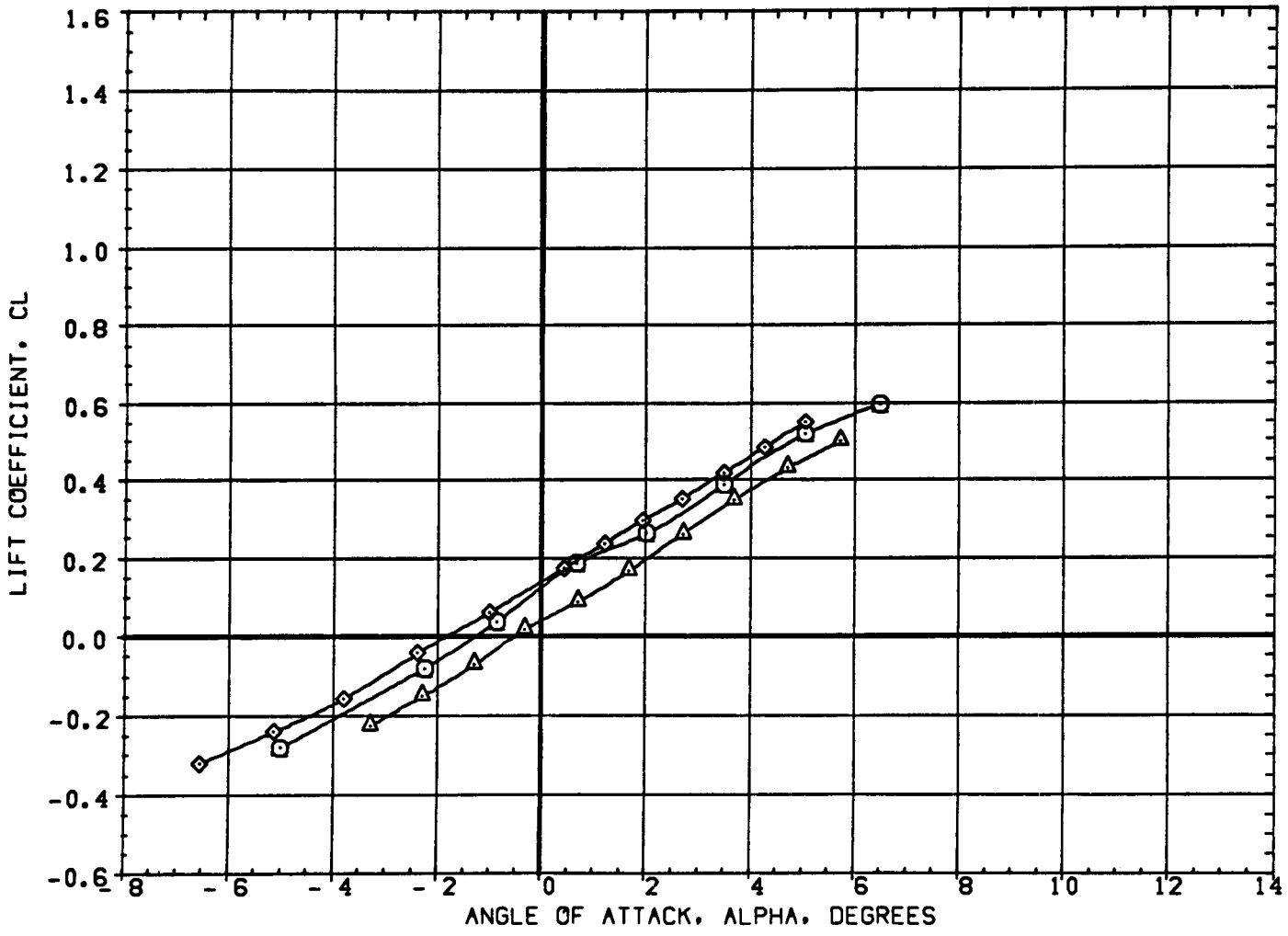

FIGURE 6 EFFECT OF WING AIRFOIL SECTION FOR AN OBLIQUE WING ANGLE OF 50 DEGREES

(A)MACH = 1.15

DATA SET	SYMBOL	CONFIGURATION DESCRIPTION	BETA	LAMBDA	RN/L
(8AE007)	○	W1 F0 B	0.000	50.000	8.000
(8AE042)	△	W2 F0 B	0.000	50.000	4.000
(8AE068)	◇	W4 F0 B	0.000	50.000	6.000

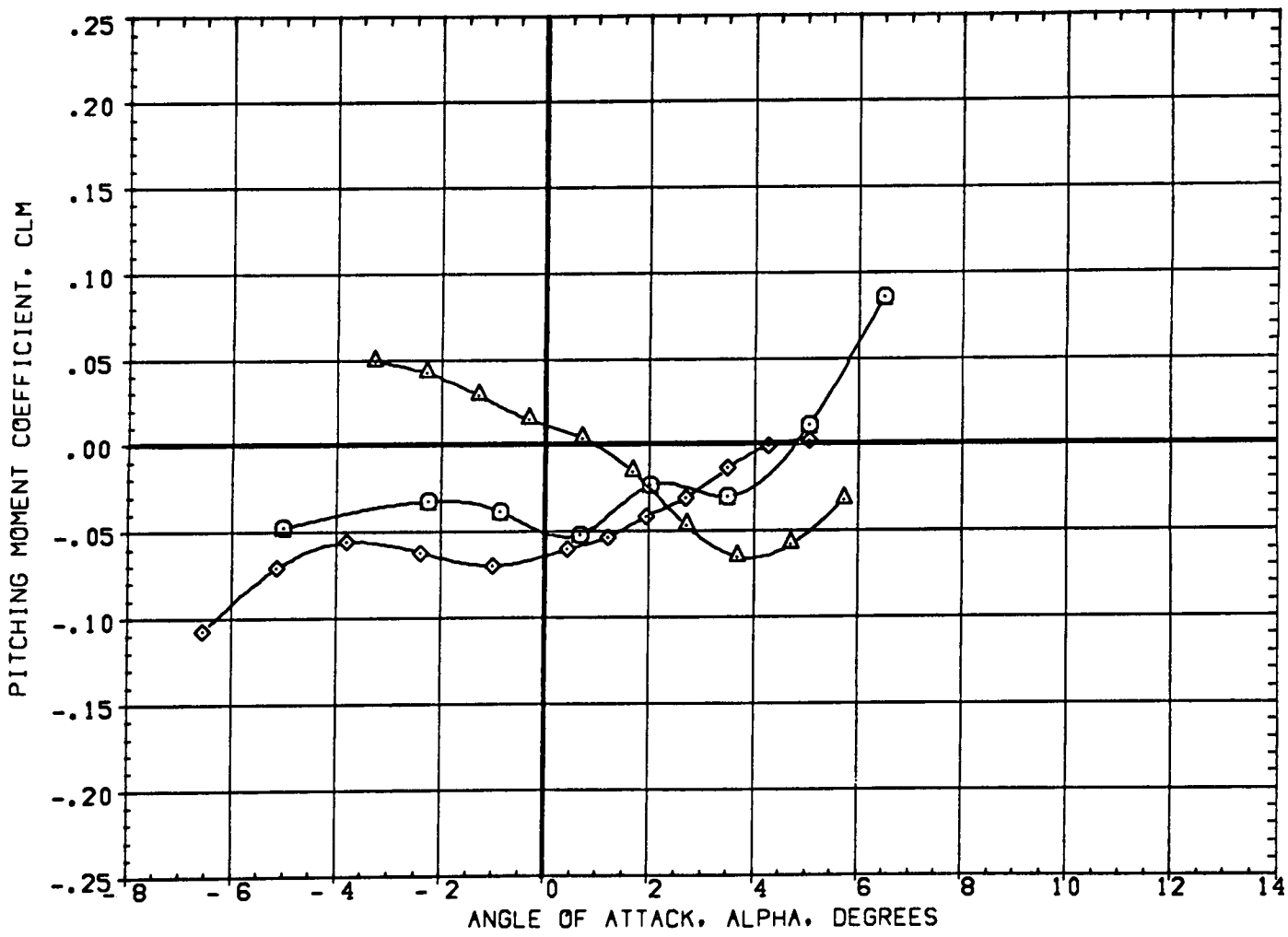

FIGURE 6 EFFECT OF WING AIRFOIL SECTION FOR AN OBLIQUE WING ANGLE OF 50 DEGREES

(A)MACH = 1.15

DATA SET	SYMBOL	CONFIGURATION DESCRIPTION	BETA	LAMBDA	RN/L
(8AE007)	○	W1 F0 B	0.000	50.000	6.000
(8AE042)	△	W2 F0 B	0.000	50.000	4.000
(8AE066)	◇	W4 F0 B	0.000	50.000	6.000

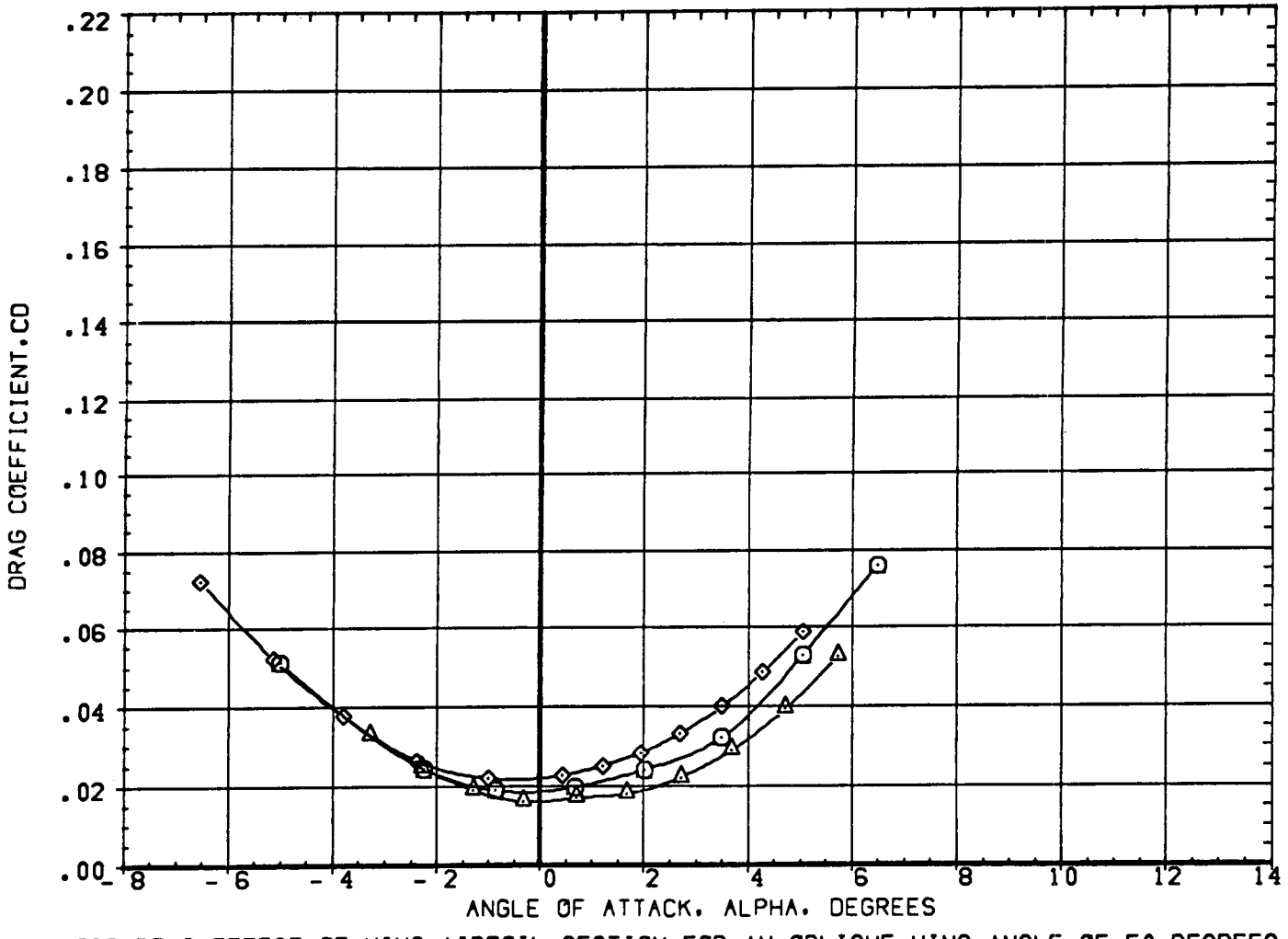

FIGURE 6 EFFECT OF WING AIRFOIL SECTION FOR AN OBLIQUE WING ANGLE OF 50 DEGREES

(A)MACH = 1.15

DATA SET	SYMBOL	CONFIGURATION DESCRIPTION	BETA	LAMBDA	RN/L
(SAE007)	○	W1 F0 B	0.000	50.000	6.000
(SAE042)	△	W2 F0 B	0.000	50.000	4.000
(SAE068)	◇	W4 F0 B	0.000	50.000	6.000

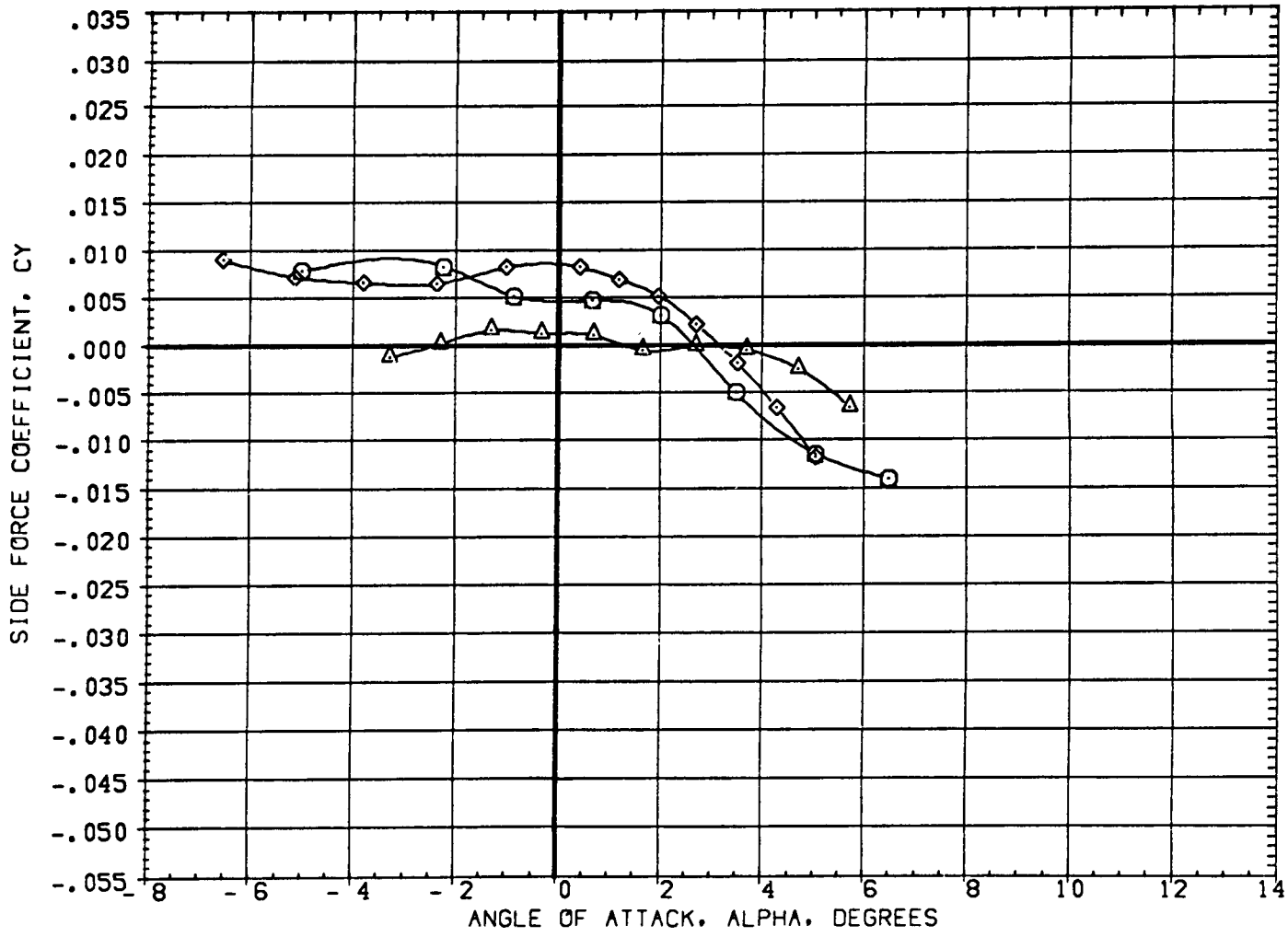

FIGURE 6 EFFECT OF WING AIRFOIL SECTION FOR AN OBLIQUE WING ANGLE OF 50 DEGREES

(A)MACH = 1.15

DATA SET	SYMBOL	CONFIGURATION DESCRIPTION	BETA	LAMBDA	RN/L
(8AE007)	○	W1 F0 B	0.000	50.000	6.000
(8AE042)	△	W2 F0 B	0.000	50.000	4.000
(8AE068)	◇	W4 F0 B	0.000	50.000	6.000

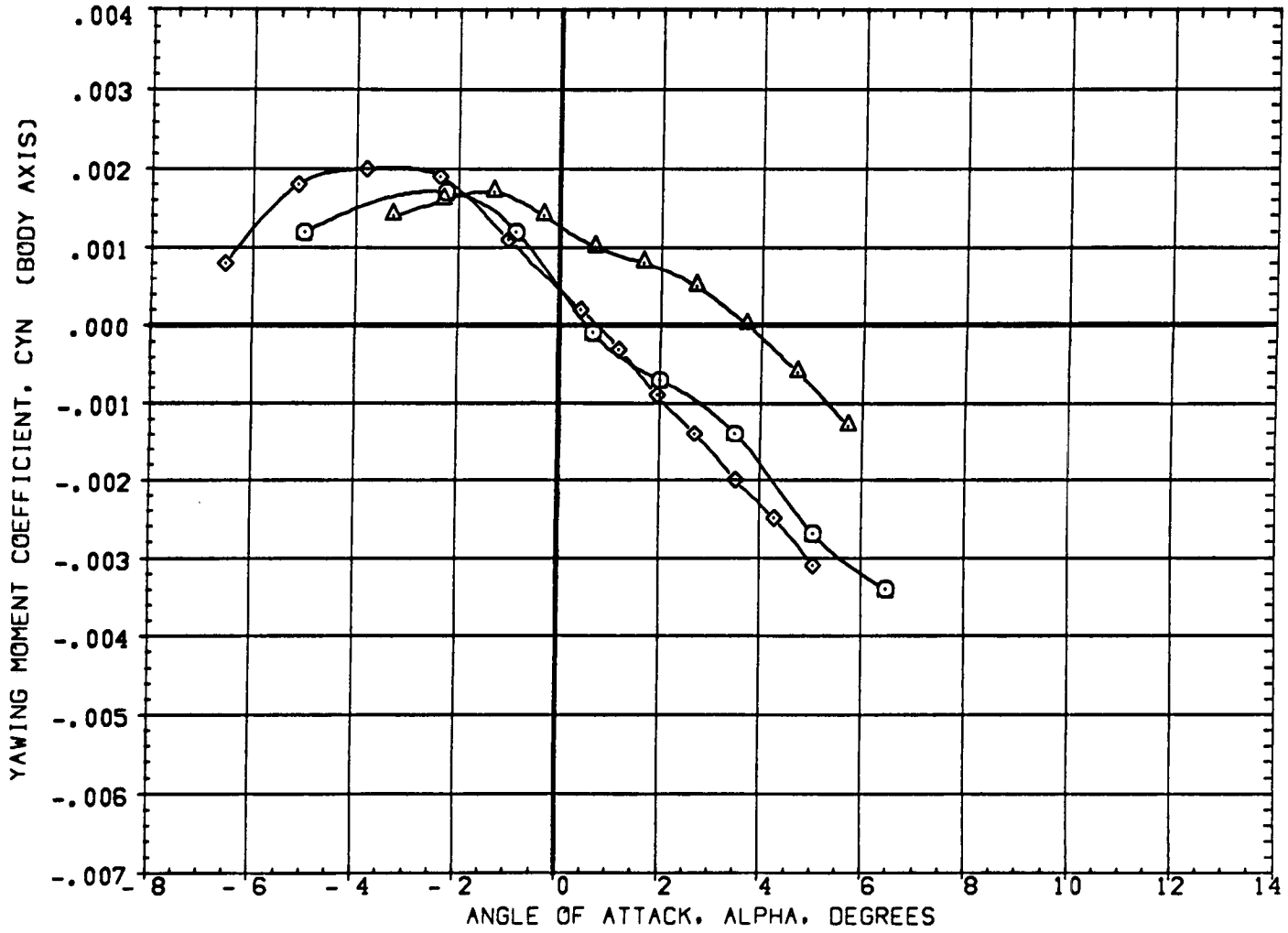

FIGURE 6 EFFECT OF WING AIRFOIL SECTION FOR AN OBLIQUE WING ANGLE OF 50 DEGREES

(A)MACH = 1.15

DATA SET	SYMBOL	CONFIGURATION DESCRIPTION	BETA	LAMBDA	RN/L
(8AE007)	○	W1 F0 B	0.000	50.000	6.000
(8AE042)	△	W2 F0 B	0.000	50.000	4.000
(8AE068)	◇	W4 F0 B	0.000	50.000	6.000

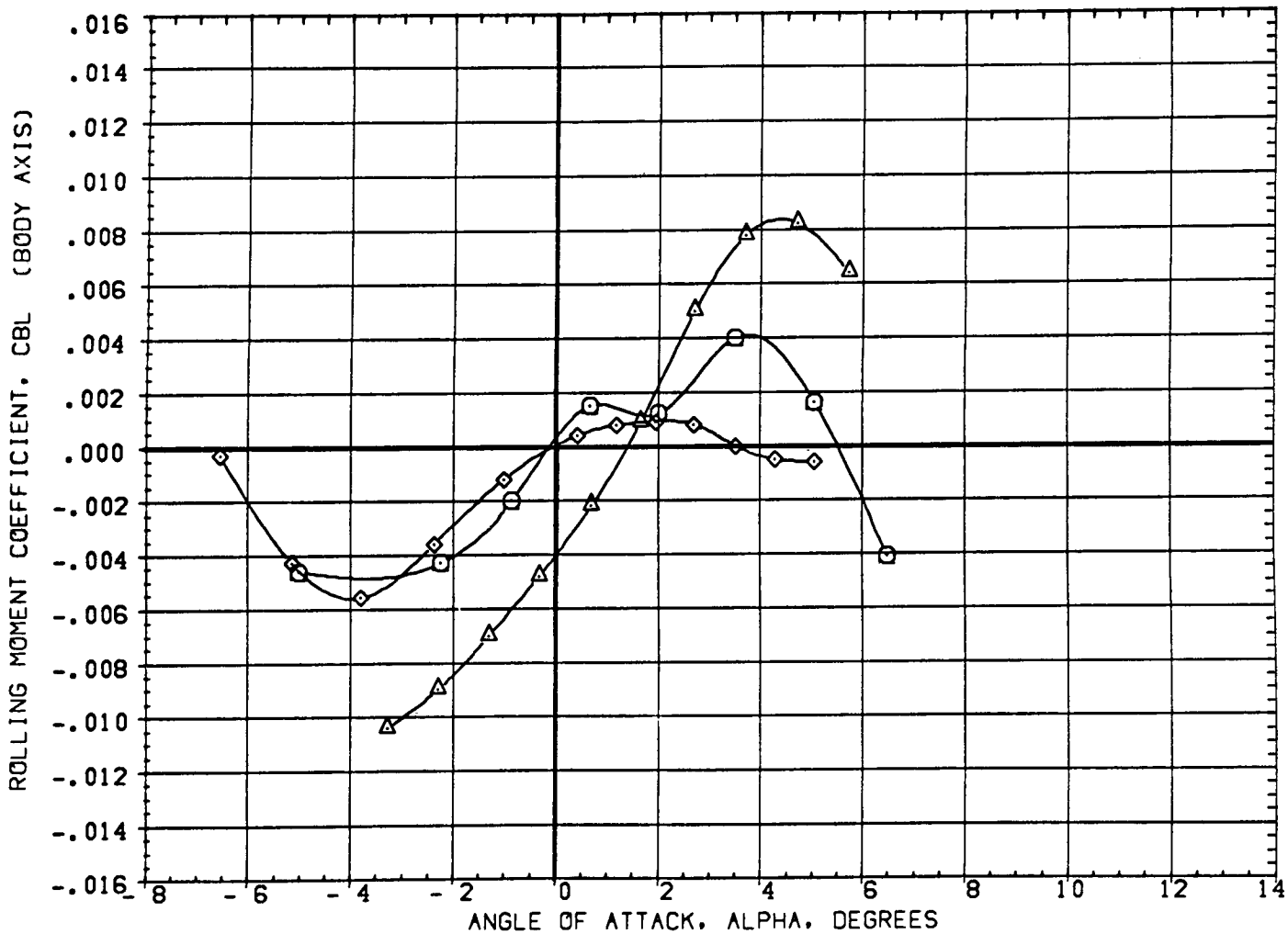

FIGURE 6 EFFECT OF WING AIRFOIL SECTION FOR AN OBLIQUE WING ANGLE OF 50 DEGREES

(A)MACH = 1.15

DATA SET	SYMBOL	CONFIGURATION DESCRIPTION	BETA	LAMBDA	RN/L
(8AE007)	○	W1 FO B	0.000	50.000	6.000
(8AE042)	△	W2 FO B	0.000	50.000	4.000
(8AE068)	◇	W4 FO B	0.000	50.000	6.000

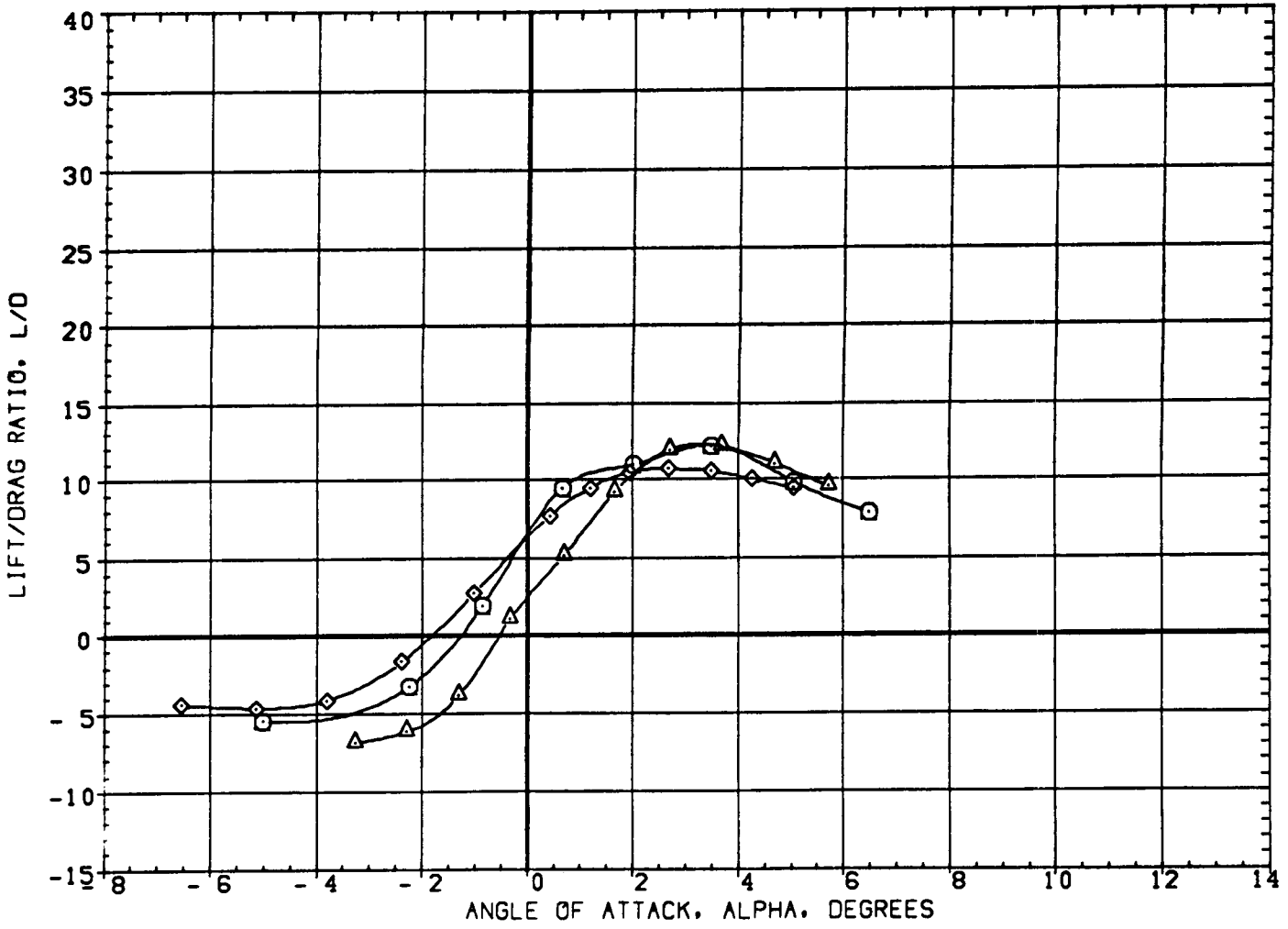

FIGURE 6 EFFECT OF WING AIRFOIL SECTION FOR AN OBLIQUE WING ANGLE OF 50 DEGREES

(A)MACH = 1.15

DATA SET	SYMBOL	CONFIGURATION DESCRIPTION	BETA	LAMBDA	RN/L
(9AE007)	○	W1 FO B	0.000	50.000	6.000
(9AE042)	△	W2 FO B	0.000	50.000	4.000
(9AE068)	◇	W4 FO B	0.000	50.000	6.000

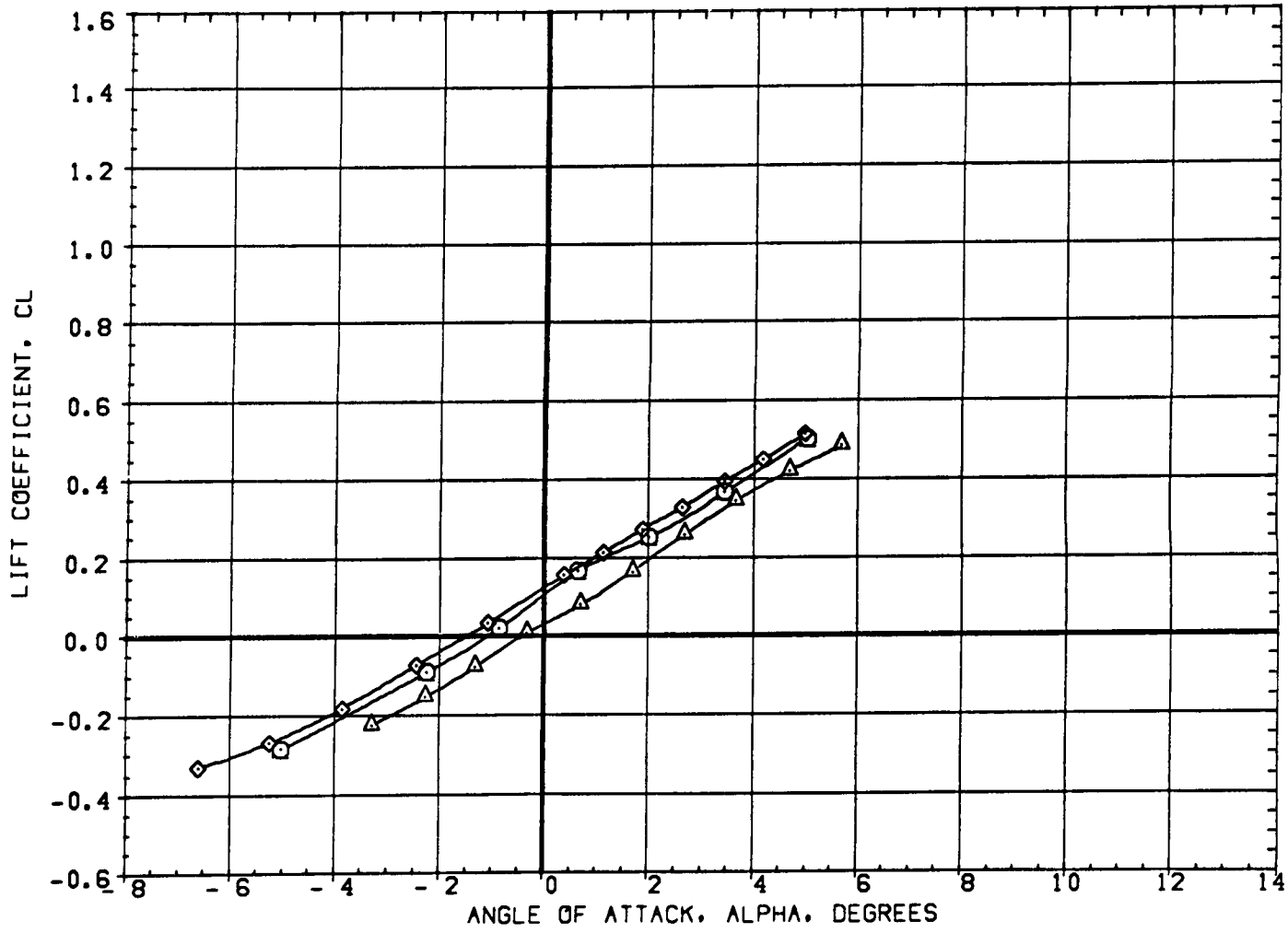

FIGURE 6 EFFECT OF WING AIRFOIL SECTION FOR AN OBLIQUE WING ANGLE OF 50 DEGREES

(A)MACH = 1.20

DATA SET	SYMBOL	CONFIGURATION DESCRIPTION	BETA	LAMBDA	RN/L
(9AE007)	○	W1 F0 B	0.000	50.000	6.000
(9AE042)	△	W2 F0 B	0.000	50.000	4.000
(9AE068)	◇	W4 F0 B	0.000	50.000	6.000

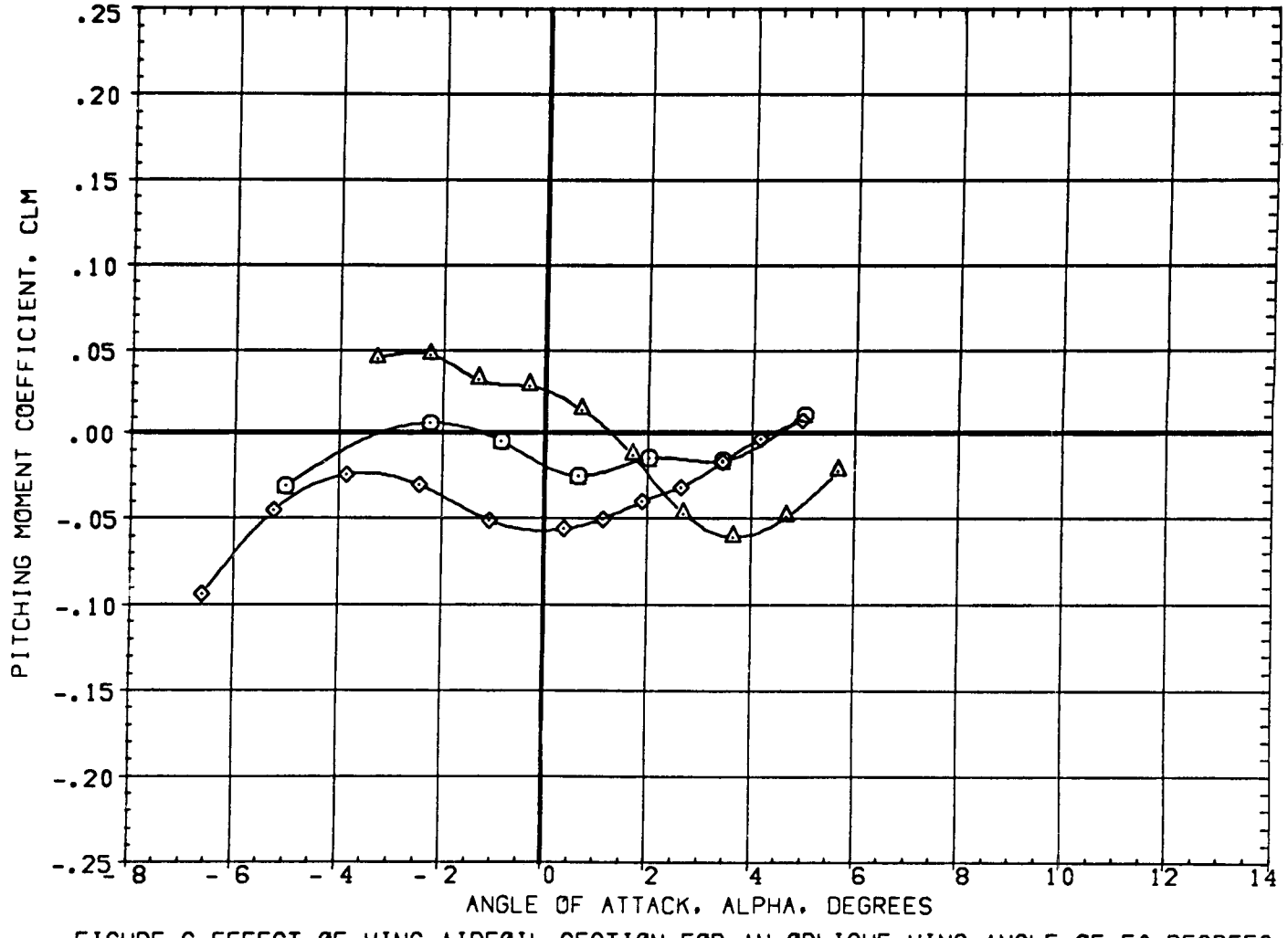

FIGURE 6 EFFECT OF WING AIRFOIL SECTION FOR AN OBLIQUE WING ANGLE OF 50 DEGREES

(A)MACH = 1.20

DATA SET	SYMBOL	CONFIGURATION DESCRIPTION	BETA	LAMBDA	RN/L
(9AE007)	○	W1 FO B	0.000	50.000	6.000
(9AE042)	△	W2 FO B	0.000	50.000	4.000
(9AE068)	◇	W4 FO B	0.000	50.000	6.000

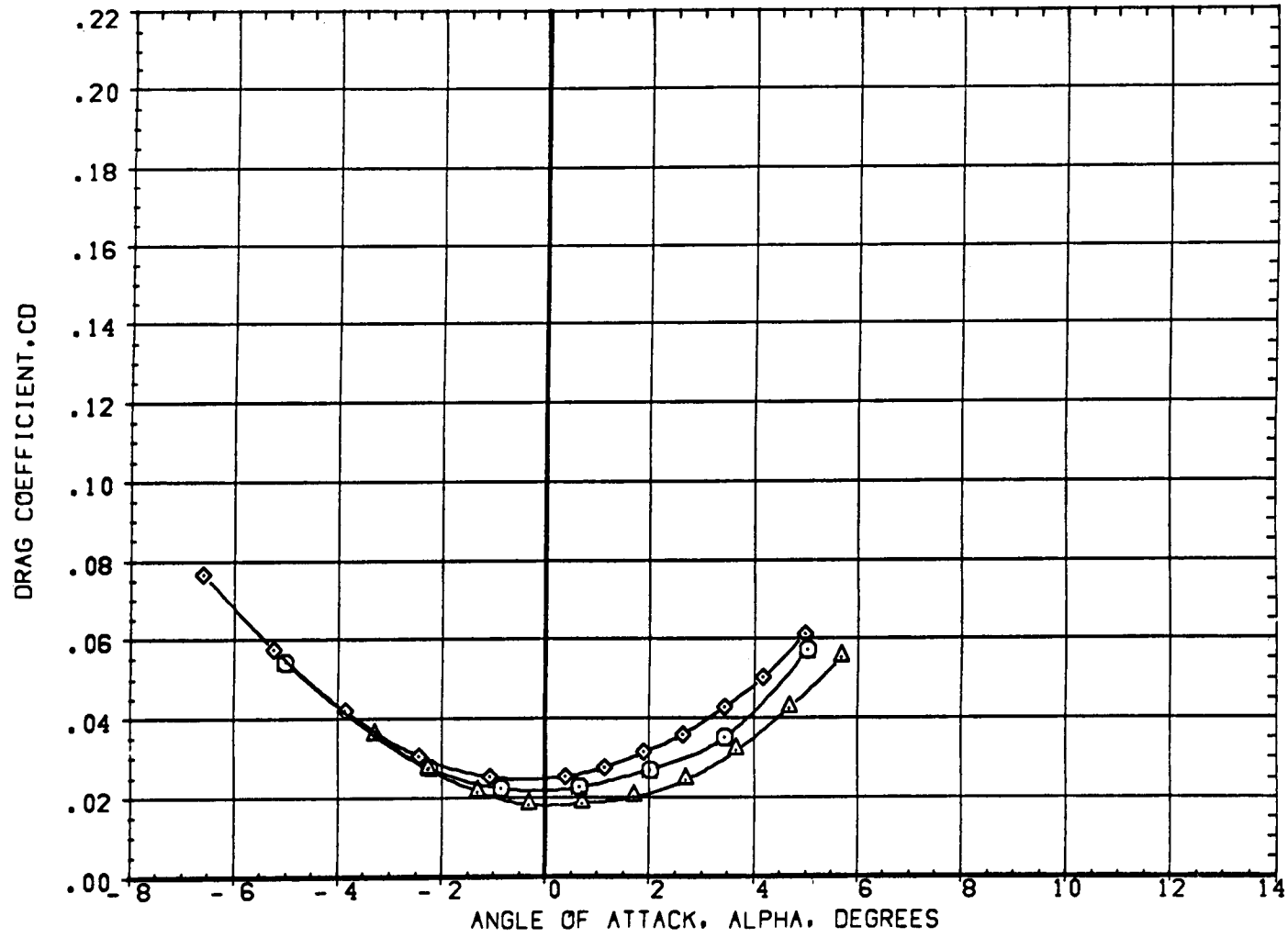

FIGURE 6 EFFECT OF WING AIRFOIL SECTION FOR AN OBLIQUE WING ANGLE OF 50 DEGREES

(A)MACH = 1.20

DATA SET	SYMBOL	CONFIGURATION DESCRIPTION	BETA	LAMBDA	RN/L
(9AE007)	○	W1 F0 B	0.000	50.000	6.000
(9AE042)	△	W2 F0 B	0.000	50.000	4.000
(9AE068)	◇	W4 F0 B	0.000	50.000	6.000

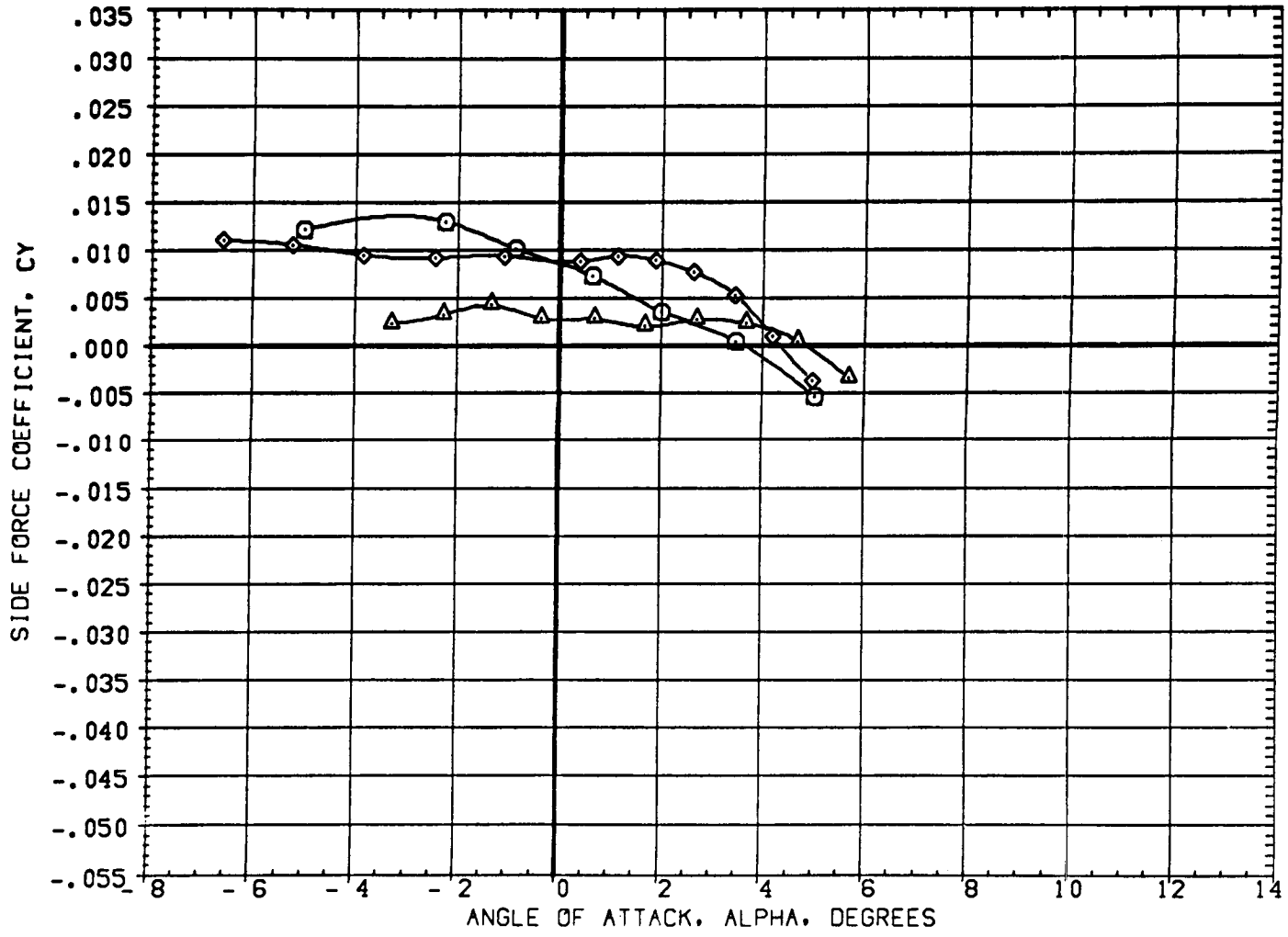

FIGURE 6 EFFECT OF WING AIRFOIL SECTION FOR AN OBLIQUE WING ANGLE OF 50 DEGREES

(A)MACH = 1.20

DATA SET	SYMBOL	CONFIGURATION DESCRIPTION	BETA	LAMBDA	RN/L
(9AE007)	○	W1 F0 B	0.000	50.000	6.000
(9AE042)	△	W2 F0 B	0.000	50.000	4.000
(9AE068)	◇	W4 F0 B	0.000	50.000	6.000

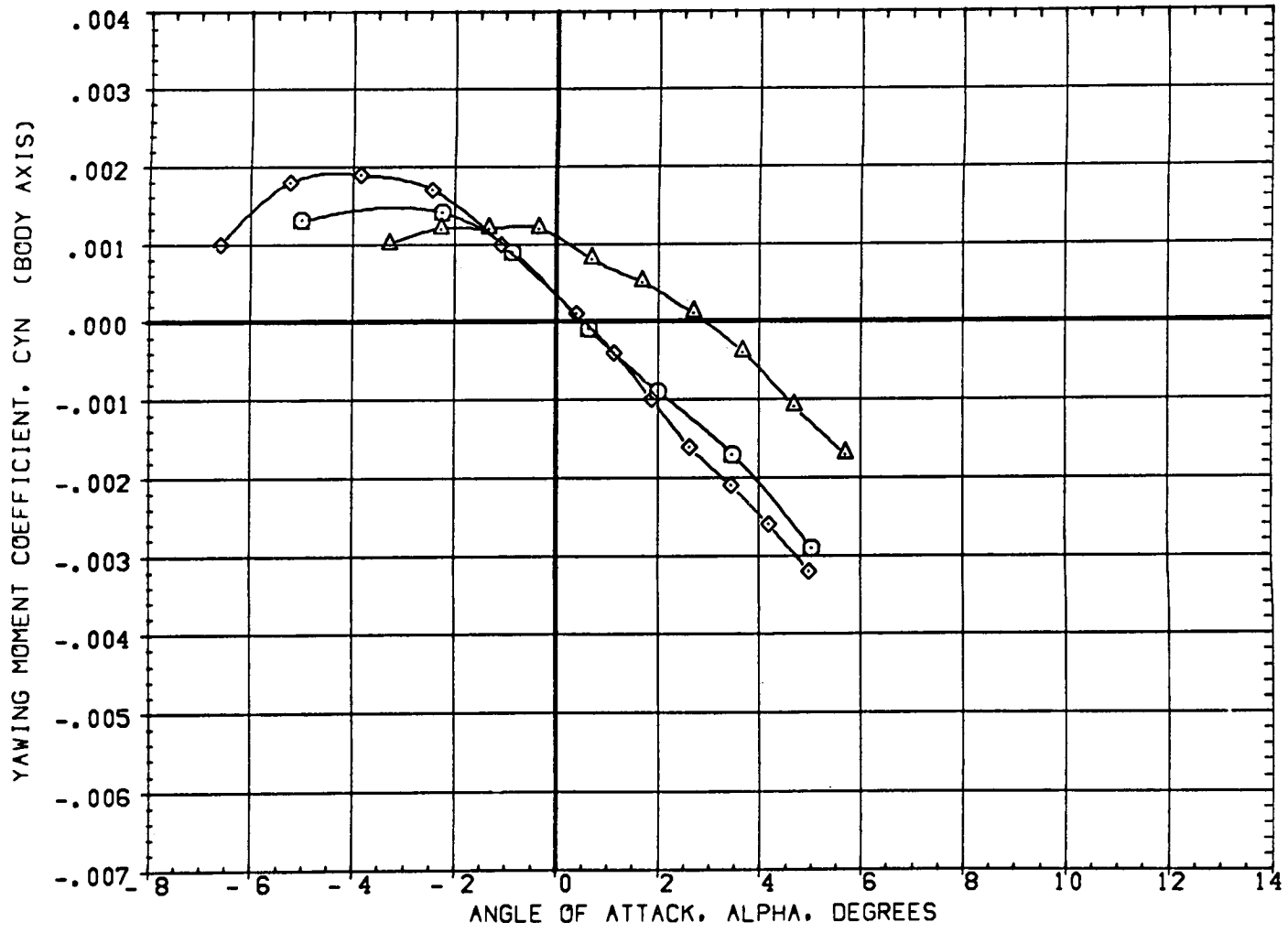

FIGURE 6 EFFECT OF WING AIRFOIL SECTION FOR AN OBLIQUE WING ANGLE OF 50 DEGREES

(A)MACH = 1.20

DATA SET	SYMBOL	CONFIGURATION DESCRIPTION	BETA	LAMBDA	RN/L
(9AE007)	○	W1 F0 B	0.000	50.000	6.000
(9AE042)	△	W2 F0 B	0.000	50.000	4.000
(9AE068)	◇	W4 F0 B	0.000	50.000	6.000

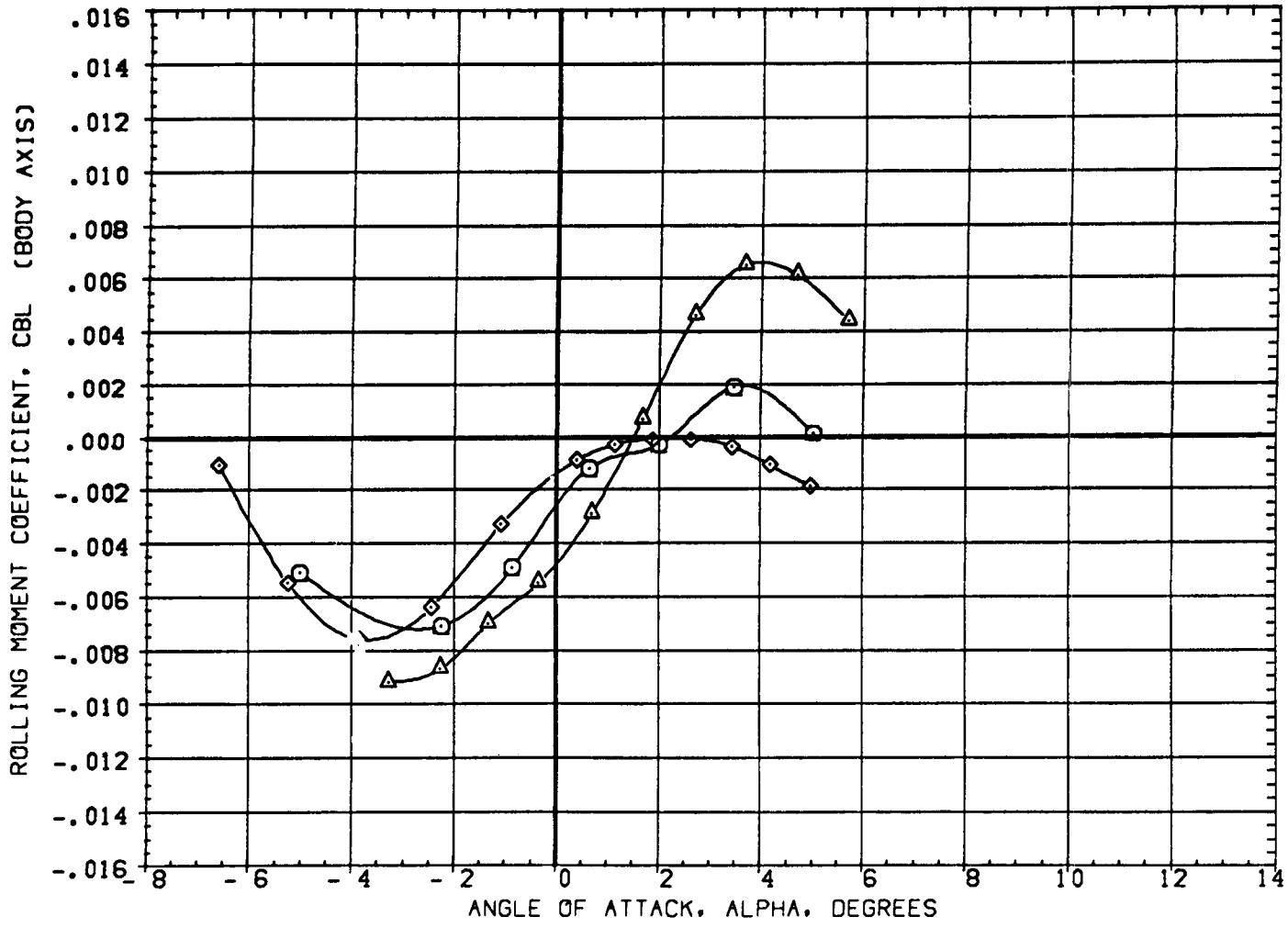

FIGURE 6 EFFECT OF WING AIRFOIL SECTION FOR AN OBLIQUE WING ANGLE OF 50 DEGREES

(A)MACH = 1.20

DATA SET	SYMBOL	CONFIGURATION DESCRIPTION	BETA	LAMBDA	RN/L
(9AE007)	○	W1 F0 B	0.000	50.000	6.000
(9AE042)	△	W2 F0 B	0.000	50.000	4.000
(9AE068)	◇	W4 F0 B	0.000	50.000	6.000

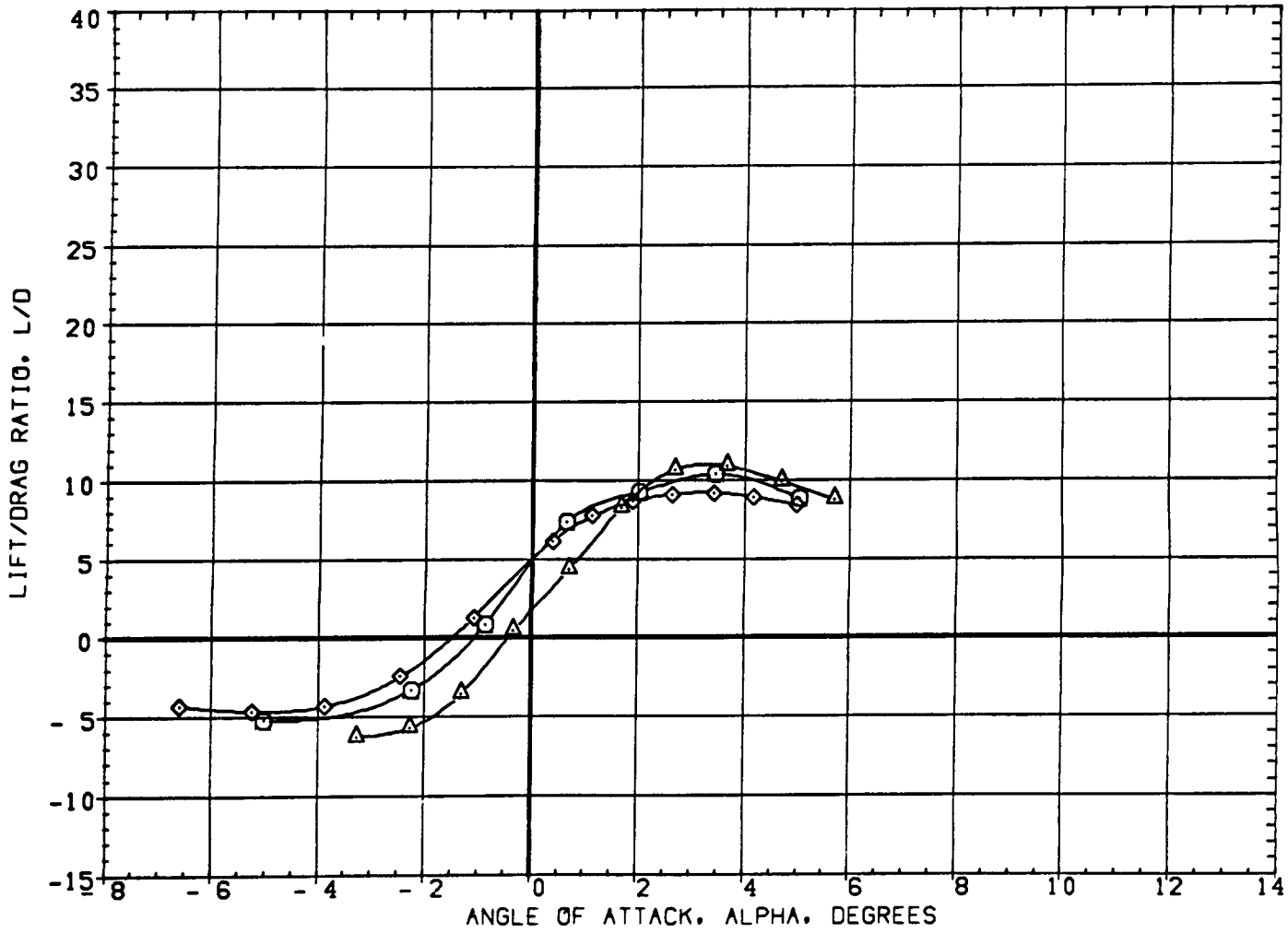

FIGURE 6 EFFECT OF WING AIRFOIL SECTION FOR AN OBLIQUE WING ANGLE OF 50 DEGREES

(A)MACH = 1.20

DATA SET	SYMBOL	CONFIGURATION DESCRIPTION	BETA	LAMBDA	RN/L
(3AE012)	○	W1 FD B	0.000	60.000	6.000
(3AE043)	△	W2 FD B	0.000	60.000	4.000
(3AE067)	◇	W4 FD B	0.000	60.000	6.000

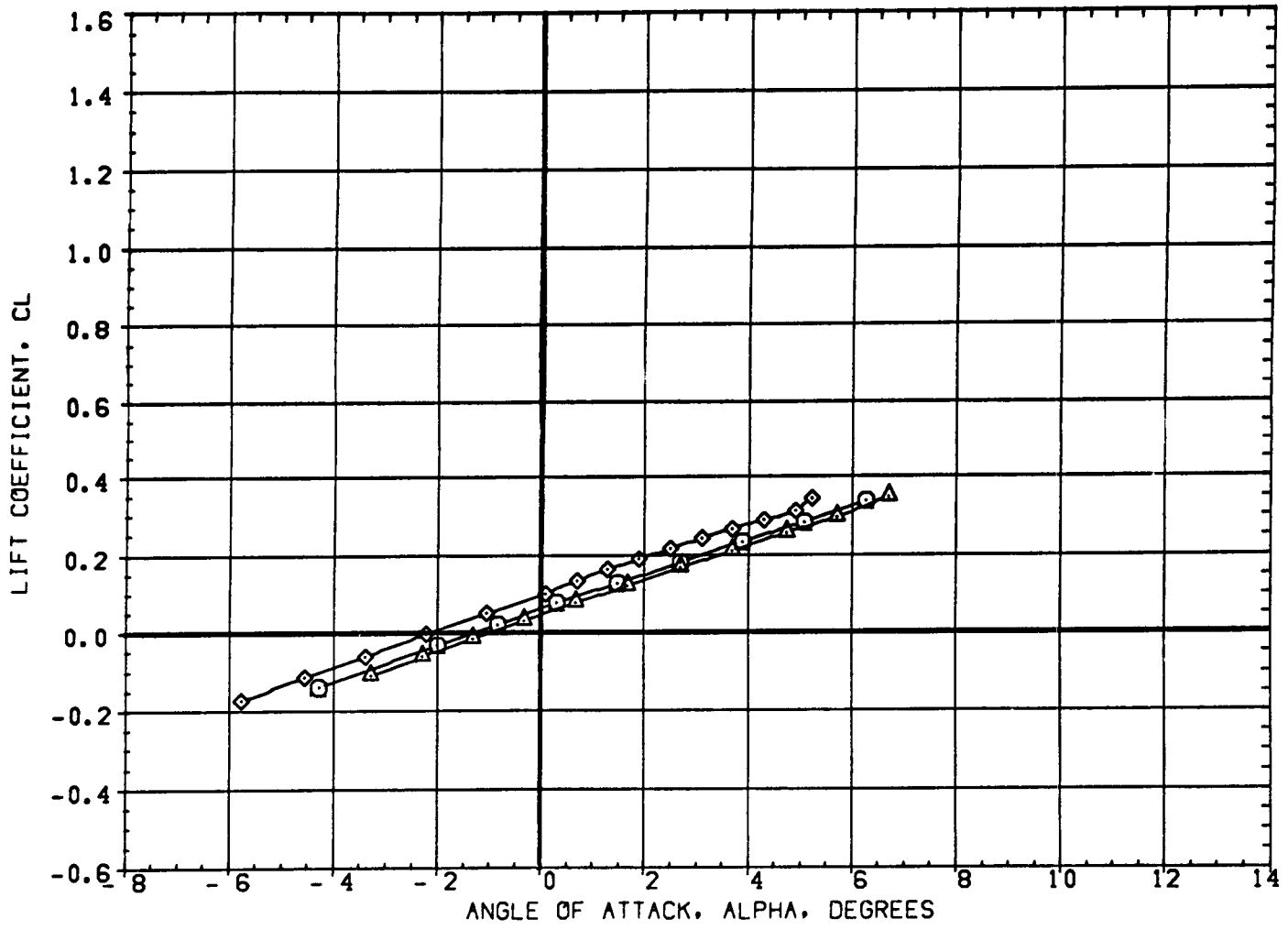

FIGURE 7 EFFECT OF WING AIRFOIL SECTION FOR AN OBLIQUE WING ANGLE OF 60 DEGREES

(A)MACH = .80

DATA SET	SYMBOL	CONFIGURATION DESCRIPTION	BETA	LAMBDA	RN/L
(3AE012)	○	W1 F0 B	0.000	60.000	6.000
(3AE043)	△	W2 F0 B	0.000	60.000	4.000
(3AE067)	◇	W4 F0 B	0.000	60.000	6.000

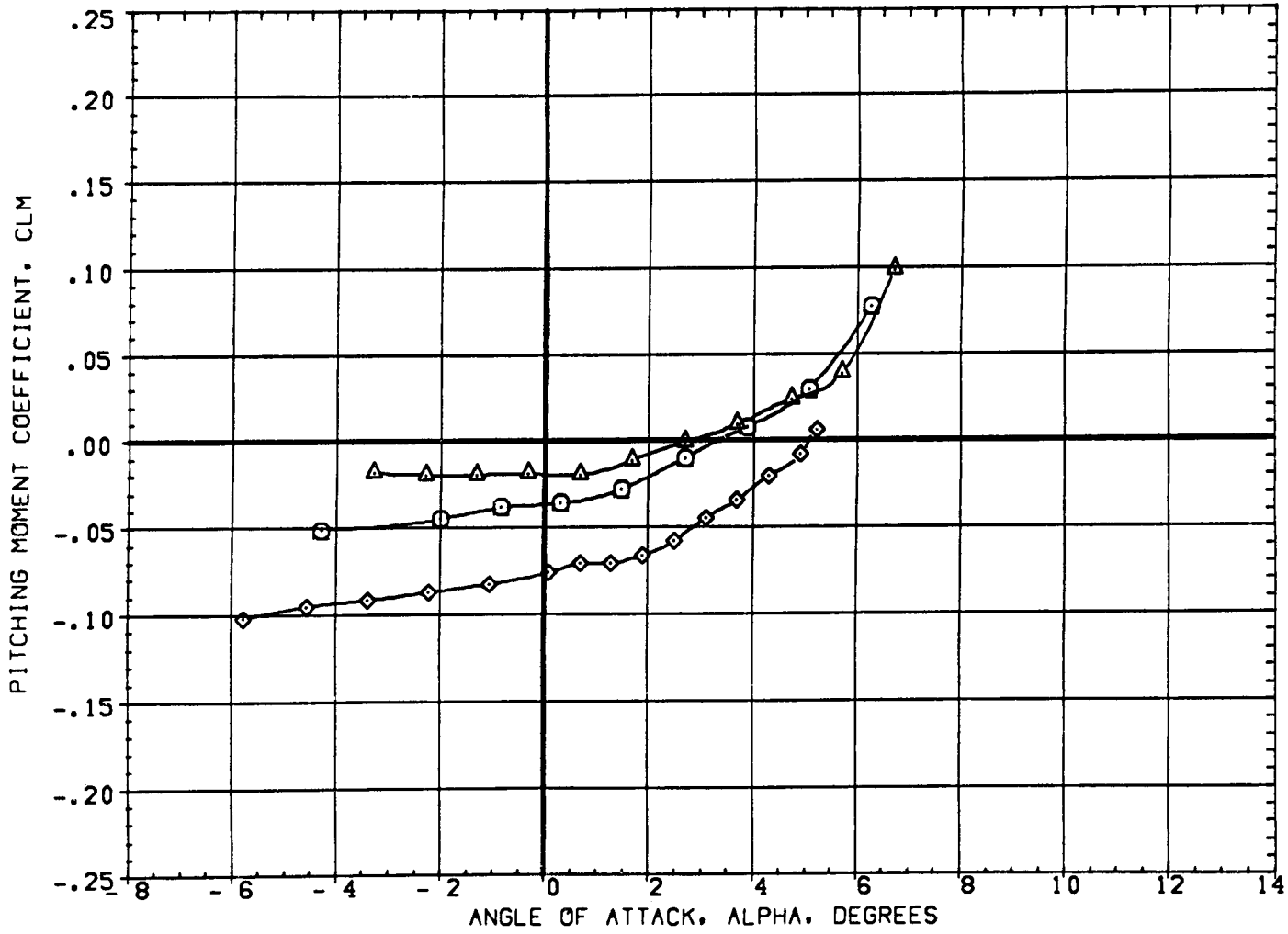

FIGURE 7 EFFECT OF WING AIRFOIL SECTION FOR AN OBLIQUE WING ANGLE OF 60 DEGREES

(A)MACH = .80

DATA SET	SYMBOL	CONFIGURATION DESCRIPTION	BETA	LAMBDA	RN/L
(3AE012)	○	W1 F0 B	0.000	60.000	6.000
(3AE043)	△	W2 F0 B	0.000	60.000	4.000
(3AE067)	◇	W4 F0 B	0.000	60.000	6.000

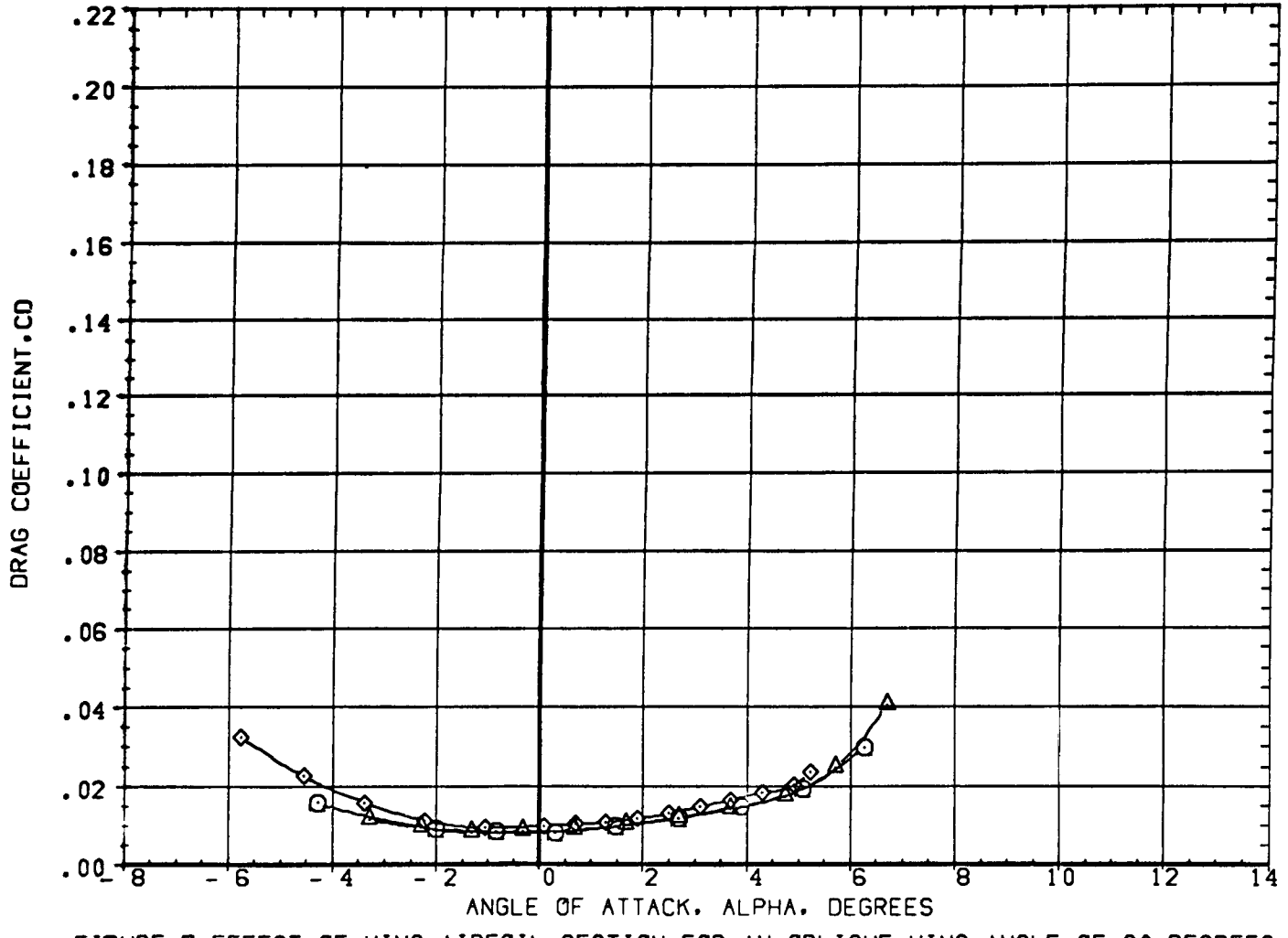

FIGURE 7 EFFECT OF WING AIRFOIL SECTION FOR AN OBLIQUE WING ANGLE OF 60 DEGREES

(A)MACH = .80

DATA SET	SYMBOL	CONFIGURATION DESCRIPTION	BETA	LAMBDA	RN/L
(3AE012)	○	W1 F0 B	0.000	60.000	6.000
(3AE043)	△	W2 F0 B	0.000	60.000	4.000
(3AE067)	◇	W4 F0 B	0.000	60.000	6.000

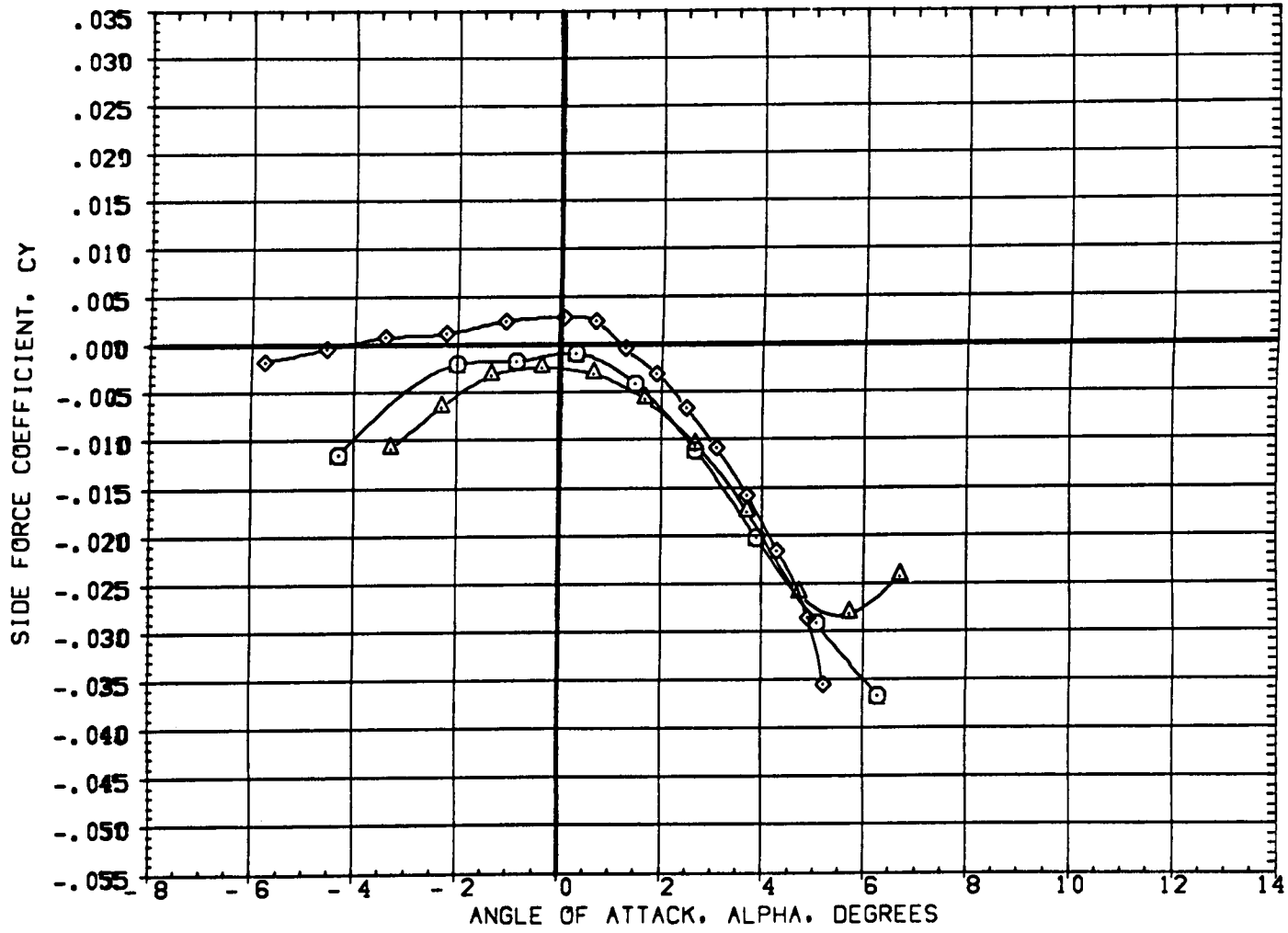

FIGURE 7 EFFECT OF WING AIRFOIL SECTION FOR AN OBLIQUE WING ANGLE OF 60 DEGREES

(A)MACH = .80

DATA SET	SYMBOL	CONFIGURATION DESCRIPTION	BETA	LAMBDA	RN/L
(3AE012)	○	W1 FD B	0.000	60.000	8.000
(3AE043)	△	W2 FD B	0.000	60.000	4.000
(3AE087)	◇	W4 FD B	0.000	60.000	6.000

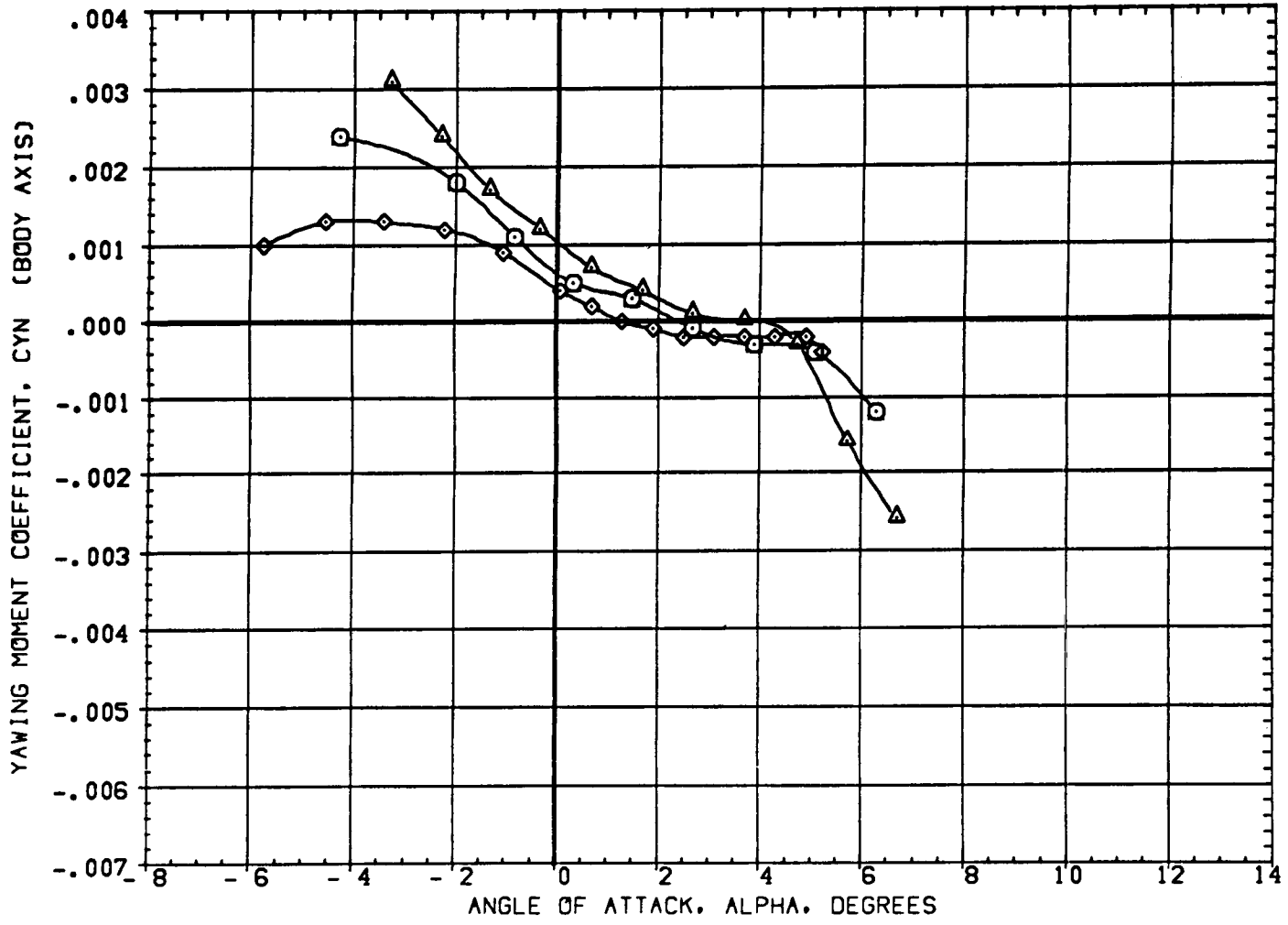

FIGURE 7 EFFECT OF WING AIRFOIL SECTION FOR AN OBLIQUE WING ANGLE OF 60 DEGREES

(A)MACH = .80

DATA SET	SYMBOL	CONFIGURATION DESCRIPTION
(3AE012)	○	W1 F0 B
(3AE043)	△	W2 F0 B
(3AE067)	◇	W4 F0 B

BETA	LAMBDA	RN/L
0.000	60.000	6.000
0.000	60.000	4.000
0.000	60.000	6.000

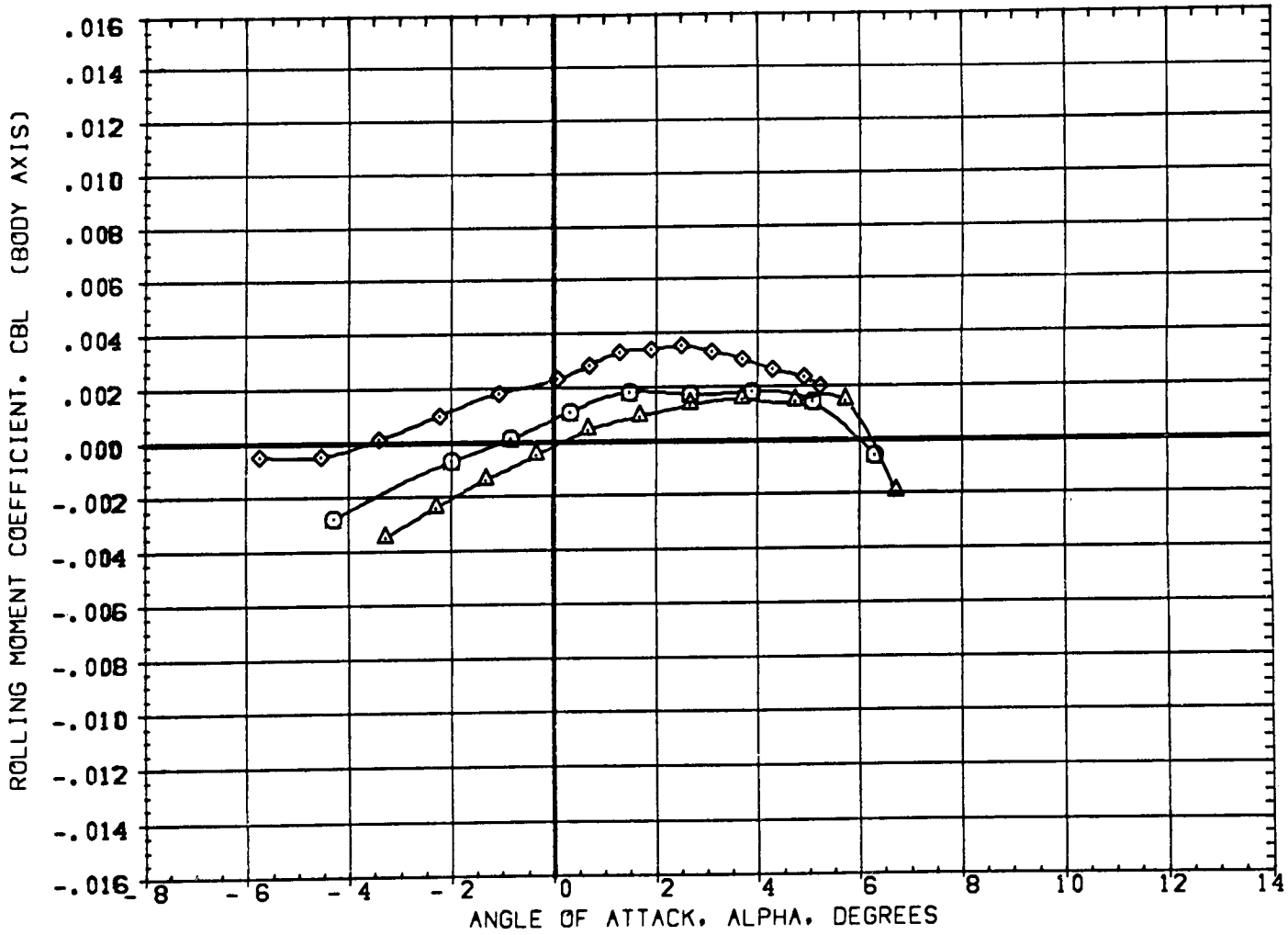

FIGURE 7 EFFECT OF WING AIRFOIL SECTION FOR AN OBLIQUE WING ANGLE OF 60 DEGREES

(A)MACH = .80

DATA SET	SYMBOL	CONFIGURATION DESCRIPTION	BETA	LAMBDA	RN/L
(3AE012)	○	W1 FD B	0.000	60.000	6.000
(3AE043)	△	W2 FD B	0.000	60.000	4.000
(3AE067)	◇	W4 FD B	0.000	60.000	6.000

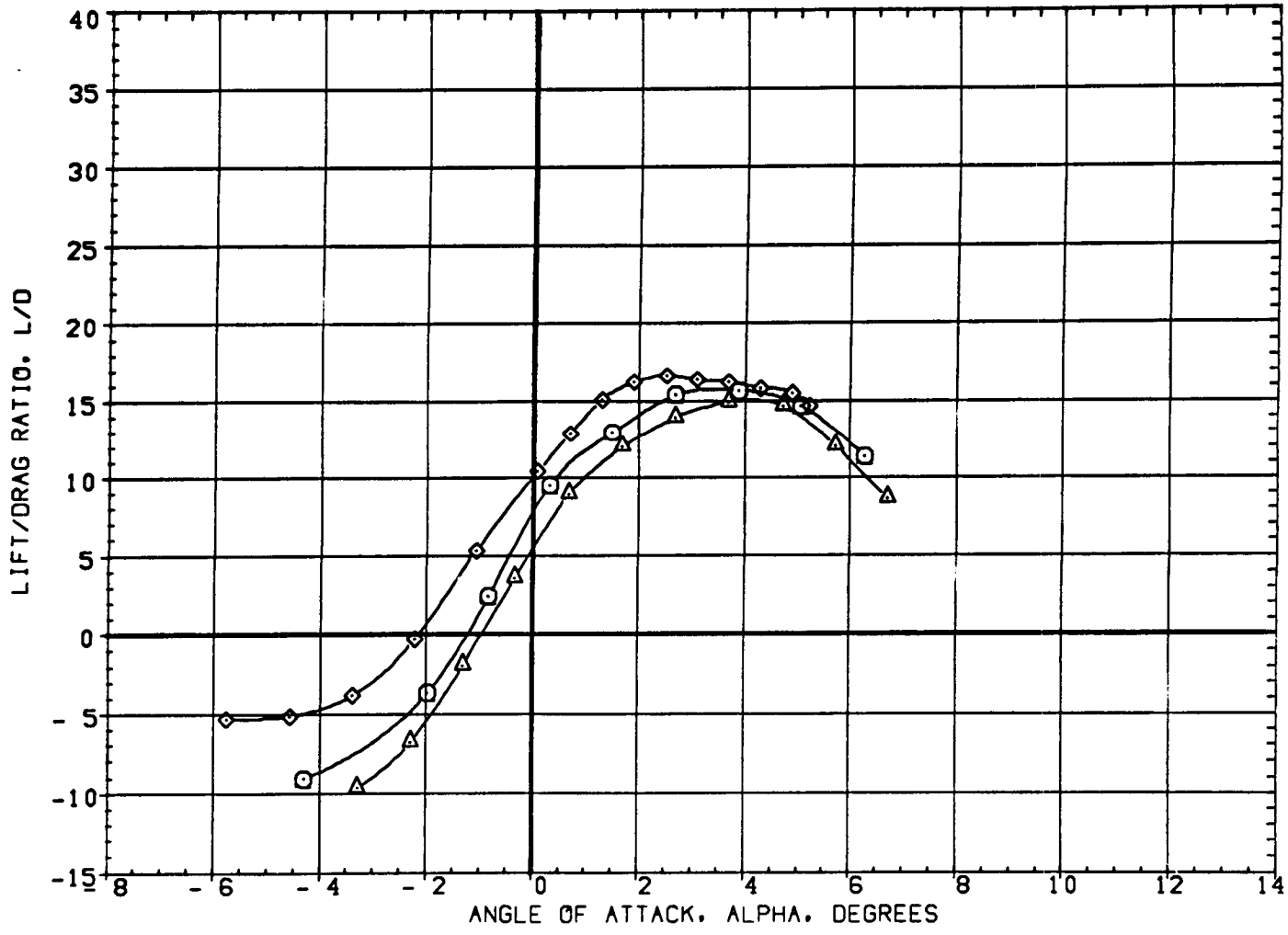

FIGURE 7 EFFECT OF WING AIRFOIL SECTION FOR AN OBLIQUE WING ANGLE OF 60 DEGREES

(A)MACH = .80

DATA SET	SYMBOL	CONFIGURATION DESCRIPTION	BETA	LAMBDA	RN/L
(4AE012)	○	W1 F0 B	0.000	60.000	6.000
(4AE043)	△	W2 F0 B	0.000	60.000	4.000
(4AE067)	◇	W4 F0 B	0.000	60.000	6.000

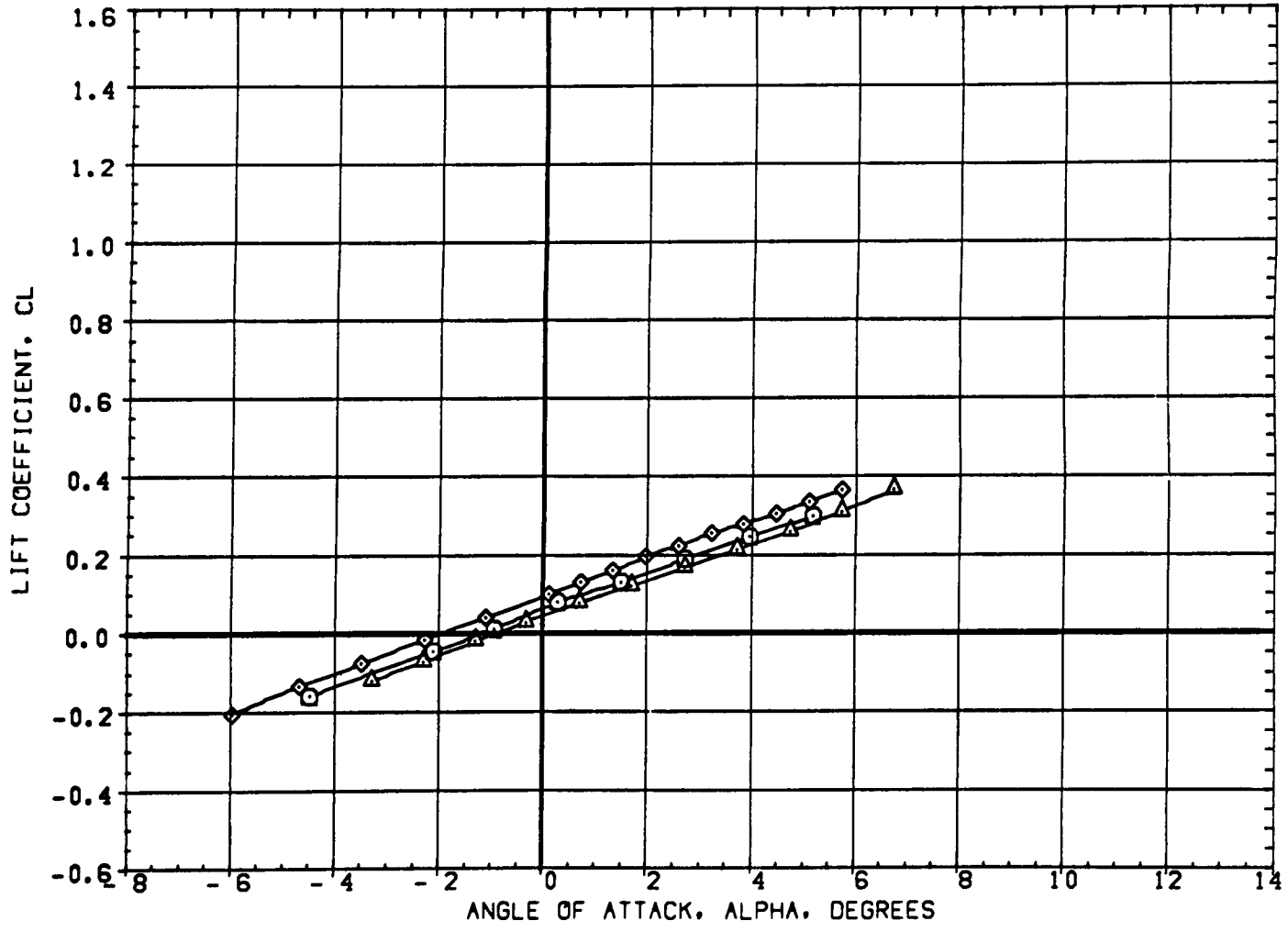

FIGURE 7 EFFECT OF WING AIRFOIL SECTION FOR AN OBLIQUE WING ANGLE OF 60 DEGREES

(A)MACH = .95

DATA SET	SYMBOL	CONFIGURATION DESCRIPTION	BETA	LAMBDA	RN/L
(4AE012)	○	W1 F0 B	0.000	60.000	6.000
(4AE043)	△	W2 F0 B	0.000	60.000	4.000
(4AE067)	◇	W4 F0 B	0.000	60.000	6.000

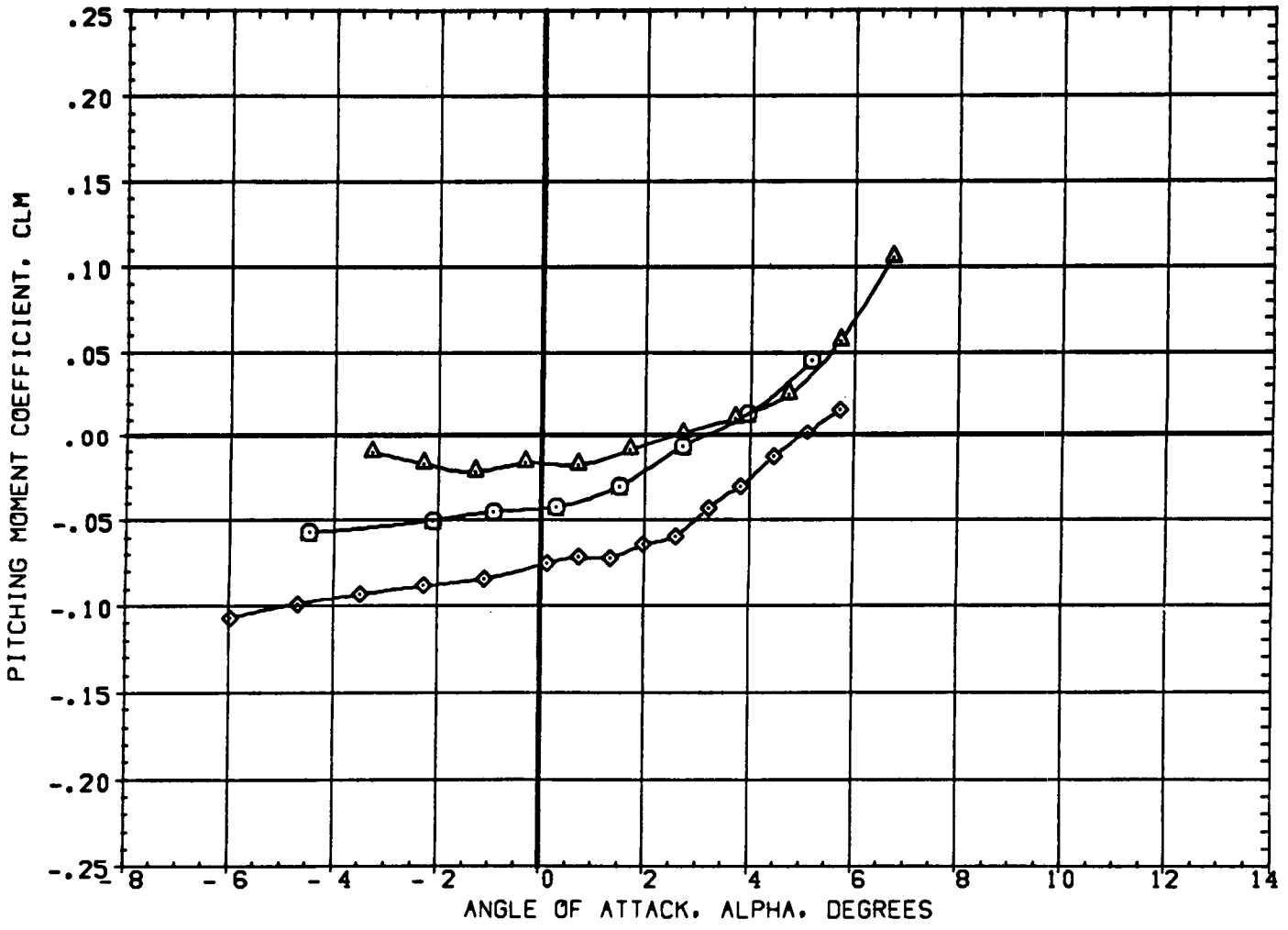

FIGURE 7 EFFECT OF WING AIRFOIL SECTION FOR AN OBLIQUE WING ANGLE OF 60 DEGREES

(A)MACH = .95

DATA SET	SYMBOL	CONFIGURATION DESCRIPTION	BETA	LAMBDA	RN/L
(4AE012)	○	W1 F0 B	0.000	60.000	6.000
(4AE043)	△	W2 F0 B	0.000	60.000	4.000
(4AE067)	◇	W4 F0 B	0.000	60.000	6.000

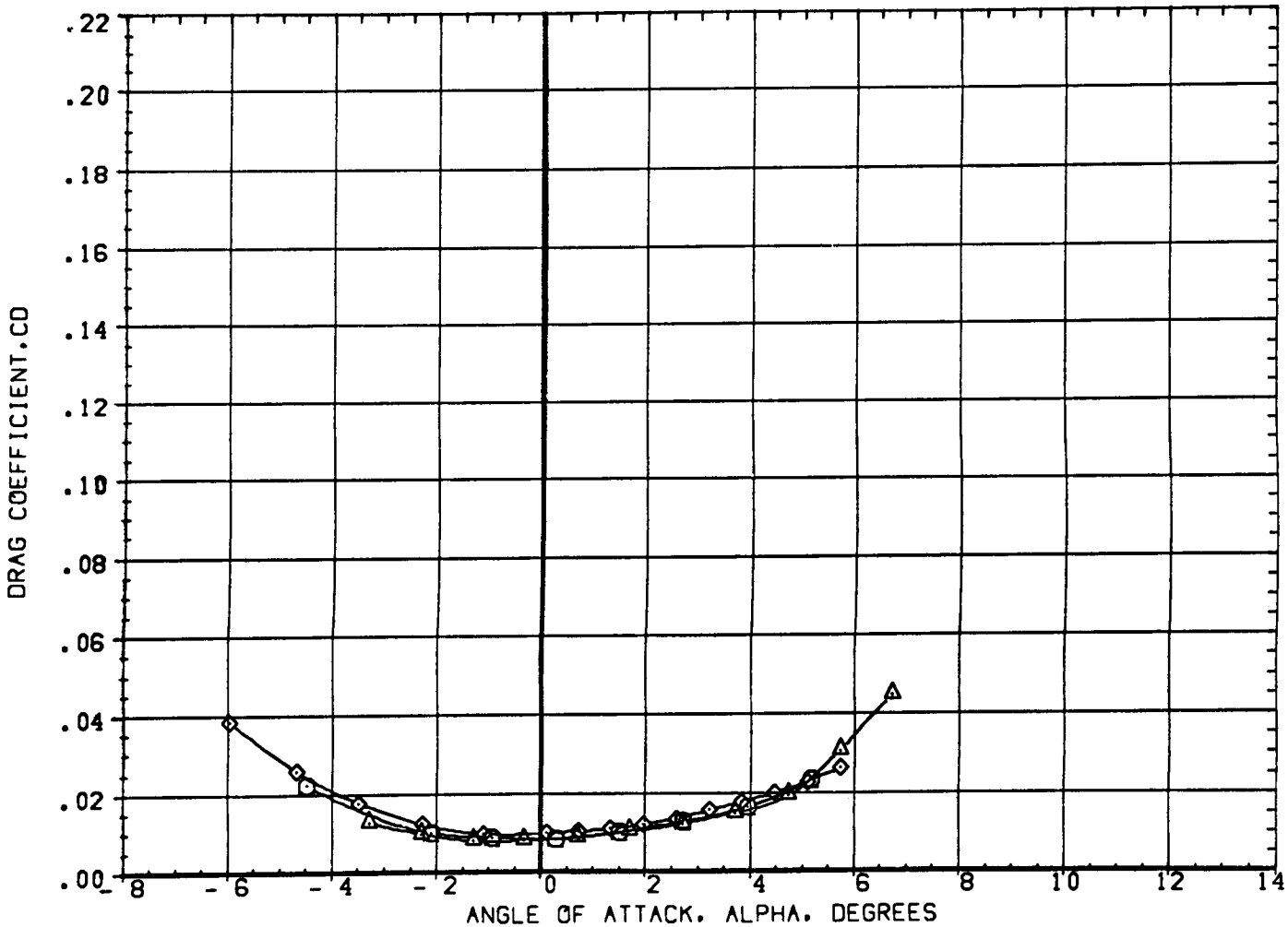

FIGURE 7 EFFECT OF WING AIRFOIL SECTION FOR AN OBLIQUE WING ANGLE OF 60 DEGREES

(A)MACH = .95

DATA SET	SYMBOL	CONFIGURATION DESCRIPTION	BETA	LAMBDA	RN/L
(4AE012)	○	W1 F0 B	0.000	60.000	6.000
(4AE043)	△	W2 F0 B	0.000	60.000	4.000
(4AE067)	◇	W4 F0 B	0.000	60.000	6.000

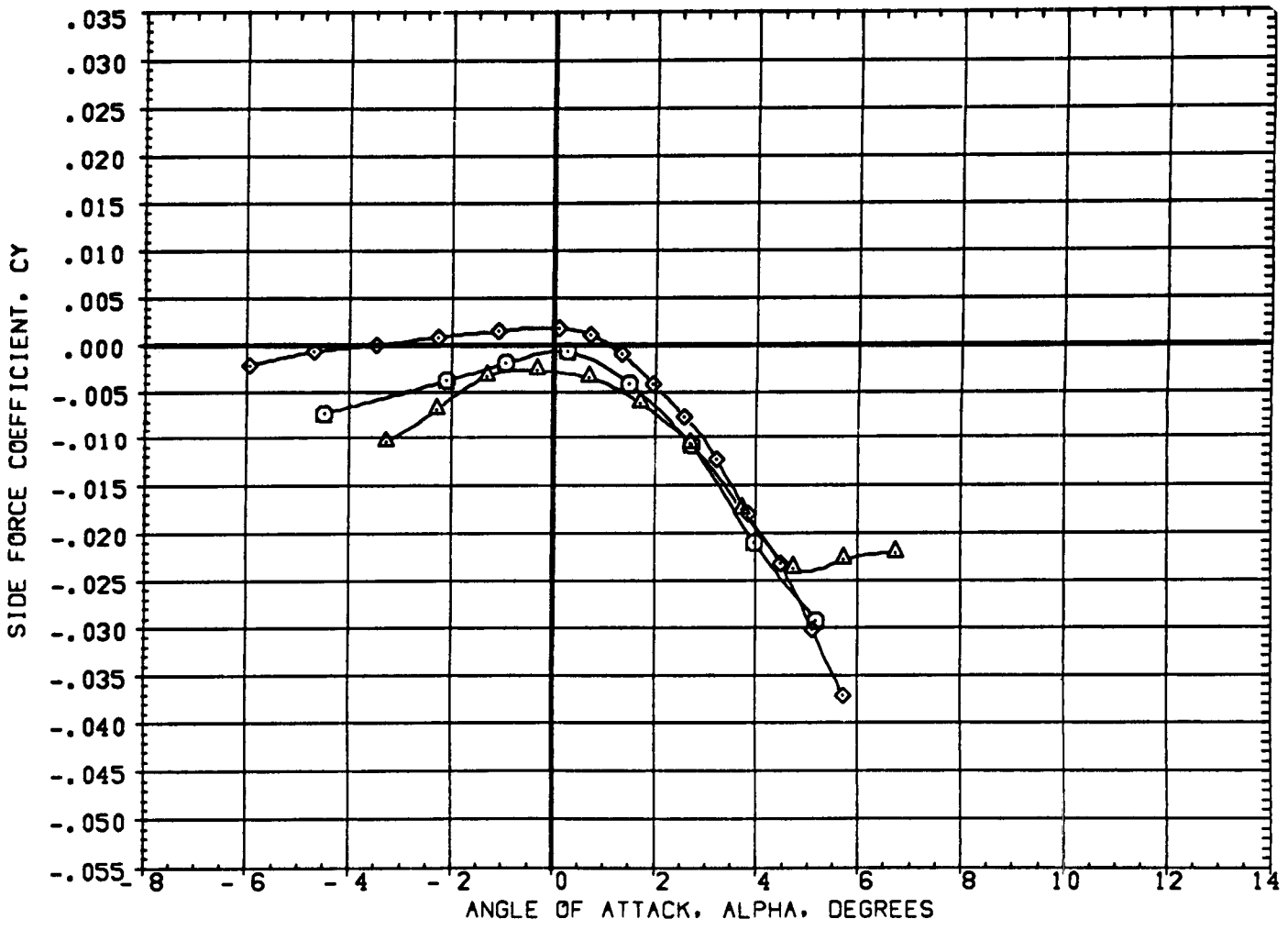

FIGURE 7 EFFECT OF WING AIRFOIL SECTION FOR AN OBLIQUE WING ANGLE OF 60 DEGREES

(A)MACH = .95

DATA SET	SYMBOL	CONFIGURATION DESCRIPTION
(4AE012)	○	W1 F0 B
(4AE043)	△	W2 F0 B
(4AE067)	◇	W4 F0 B

BETA	LAMBDA	RN/L
0.000	60.000	6.000
0.000	60.000	4.000
0.000	60.000	6.000

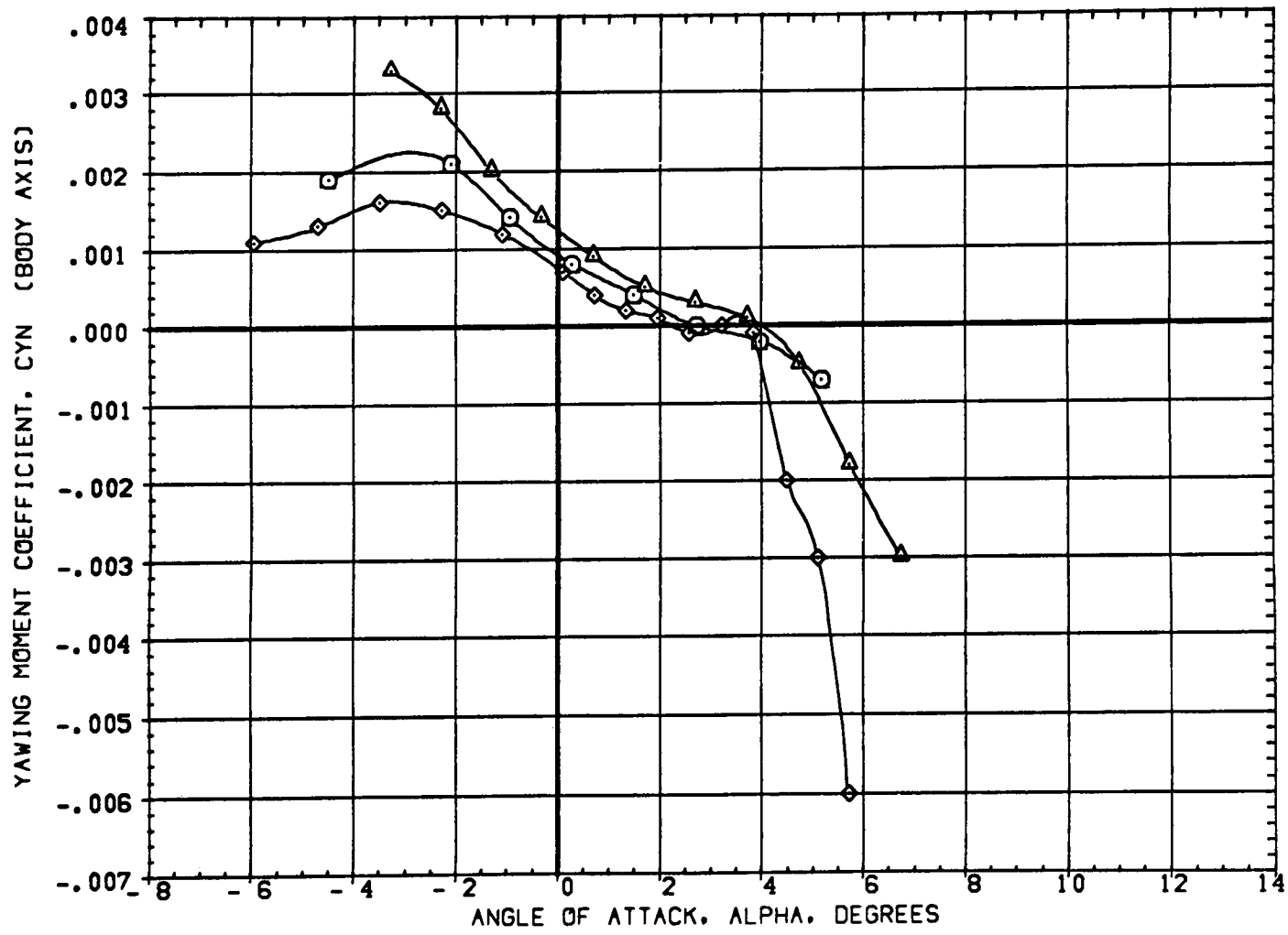

FIGURE 7 EFFECT OF WING AIRFOIL SECTION FOR AN OBLIQUE WING ANGLE OF 60 DEGREES

(A)MACH = .95

DATA SET	SYMBOL	CONFIGURATION DESCRIPTION	BETA	LAMBDA	RN/L
(4AE012)	○	W1 F0 B	0.000	60.000	6.000
(4AE043)	△	W2 F0 B	0.000	60.000	4.000
(4AE067)	◇	W4 F0 B	0.000	60.000	6.000

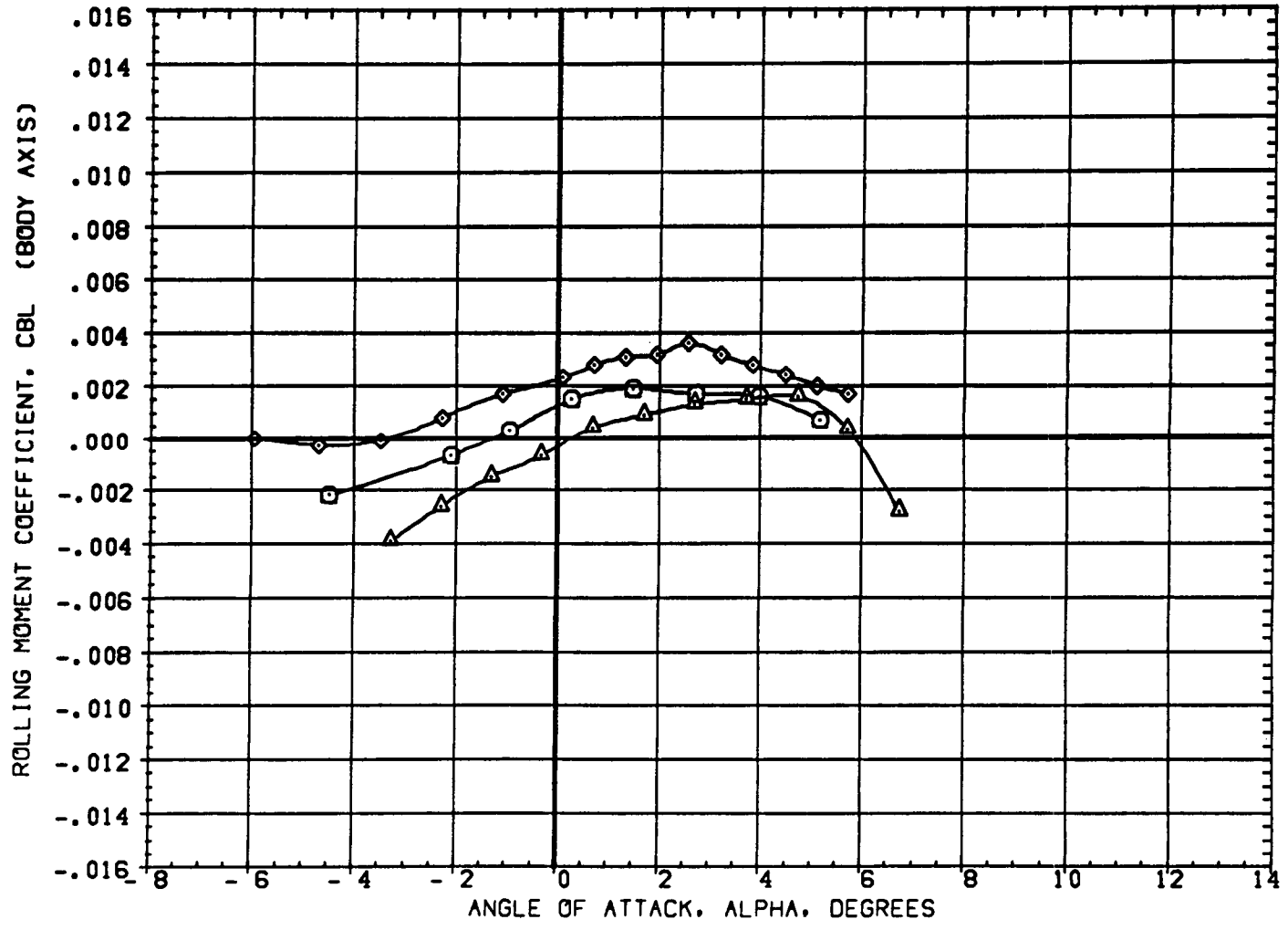

FIGURE 7 EFFECT OF WING AIRFOIL SECTION FOR AN OBLIQUE WING ANGLE OF 60 DEGREES

(A)MACH = .95

DATA SET	SYMBOL	CONFIGURATION DESCRIPTION
(4AE012)	○	W1 FD B
(4AE043)	△	W2 FD B
(4AE067)	◇	W4 FD B

BETA	LAMBDA	RN/L
0.000	60.000	6.000
0.000	60.000	4.000
0.000	60.000	6.000

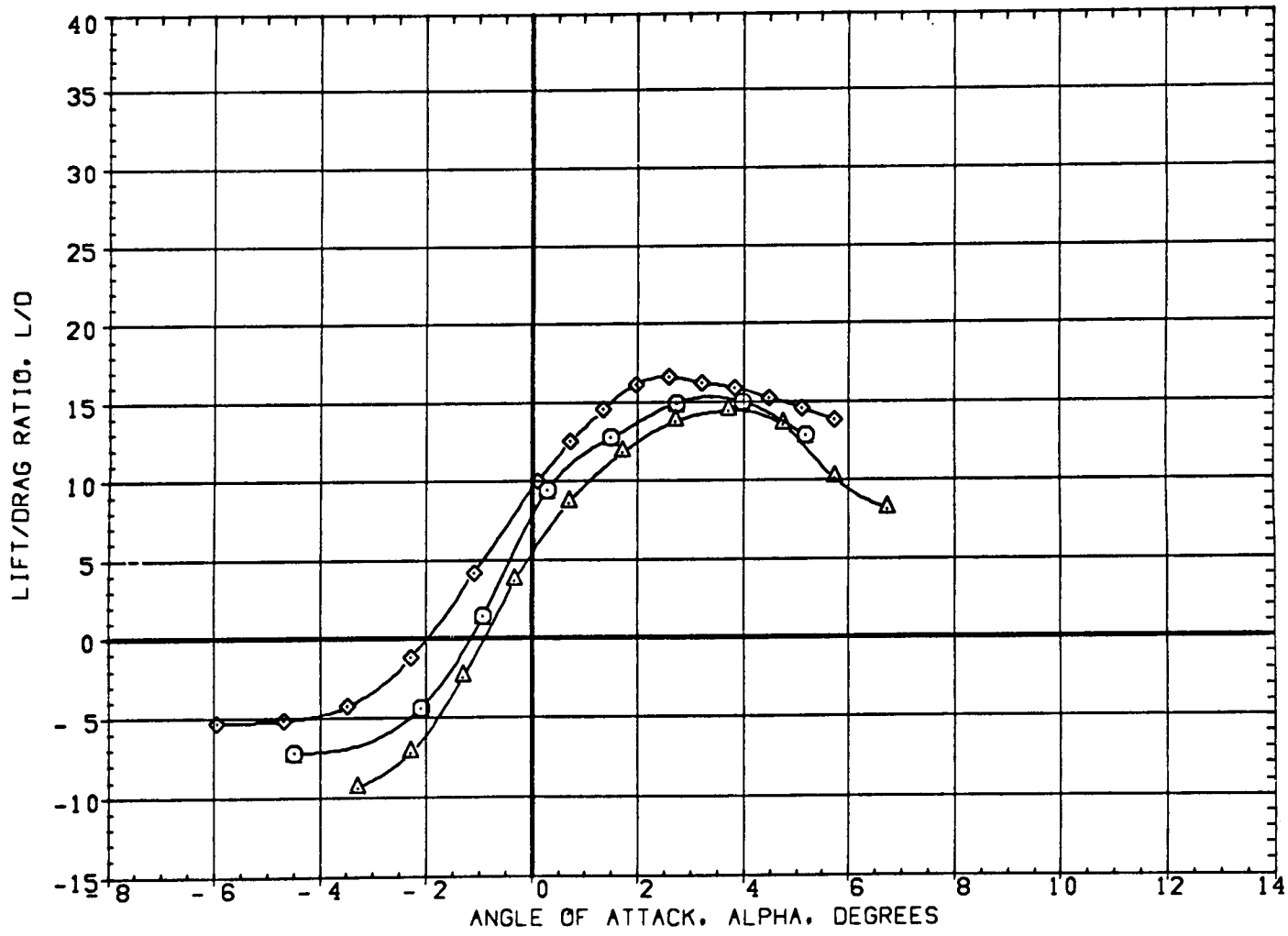

FIGURE 7 EFFECT OF WING AIRFOIL SECTION FOR AN OBLIQUE WING ANGLE OF 60 DEGREES

(A)MACH = .95

DATA SET	SYMBOL	CONFIGURATION DESCRIPTION	BETA	LAMBDA	RN/L
(7AE012)	○	W1 F0 B	0.000	60.000	6.000
(7AE043)	△	W2 F0 B	0.000	60.000	4.000
(7AE067)	◇	W4 F0 B	0.000	60.000	6.000

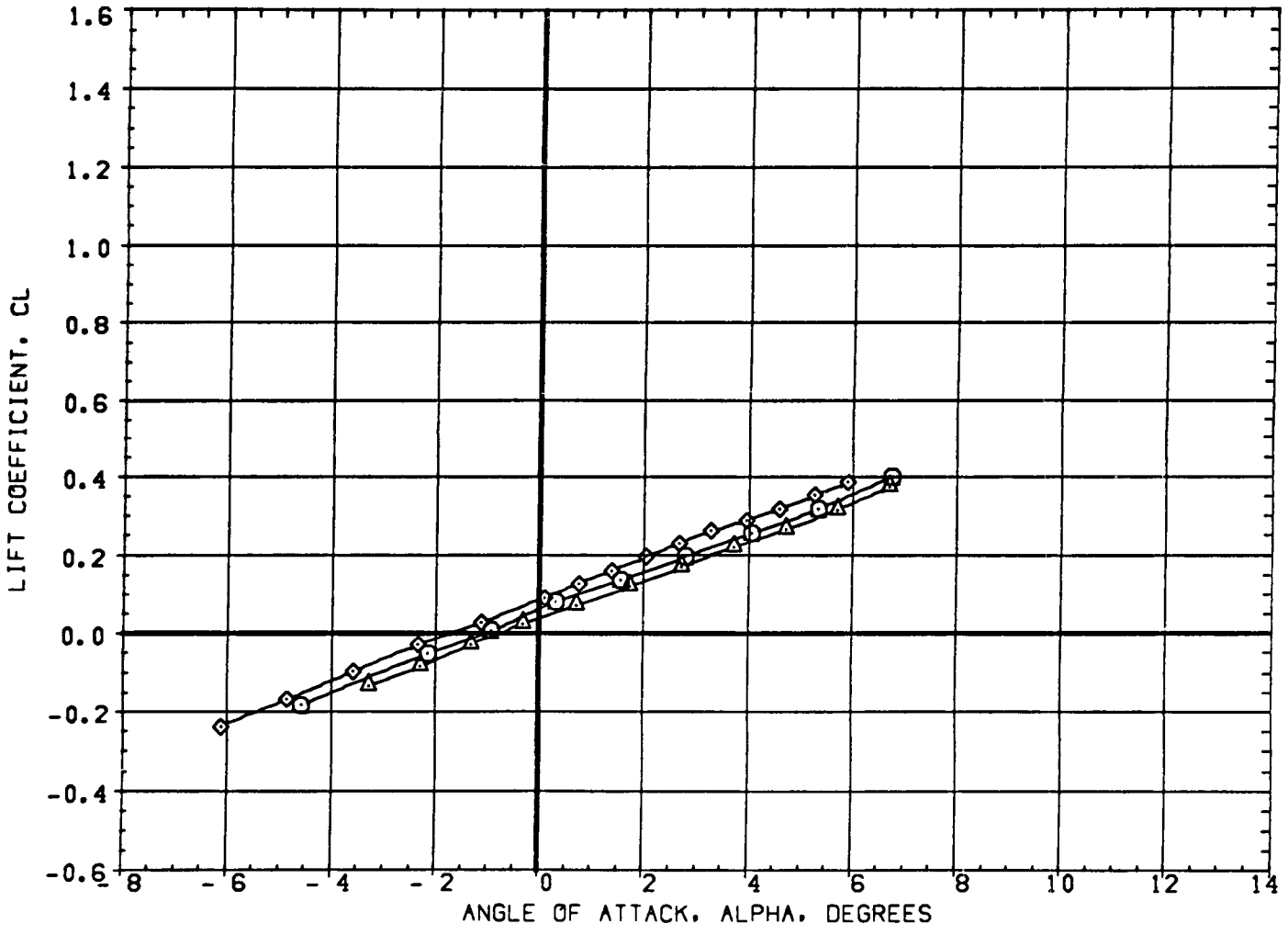

FIGURE 7 EFFECT OF WING AIRFOIL SECTION FOR AN OBLIQUE WING ANGLE OF 60 DEGREES

(A)MACH = 1.10

DATA SET	SYMBOL	CONFIGURATION DESCRIPTION	BETA	LAMBDA	RN/L
(7AE012)	○	W1 F0 B	0.000	60.000	6.000
(7AE043)	△	W2 F0 B	0.000	60.000	4.000
(7AE067)	◇	W4 F0 B	0.000	60.000	6.000

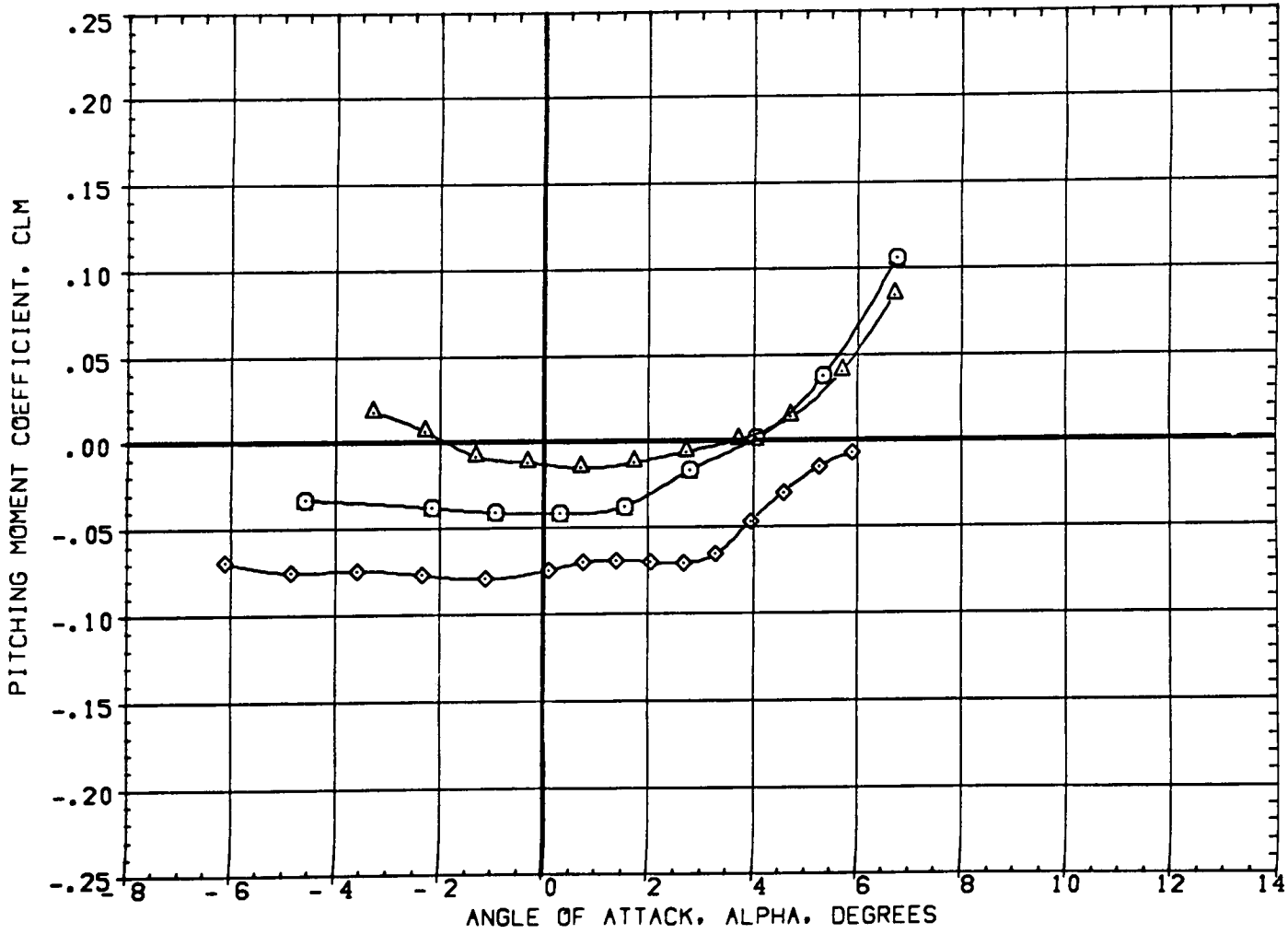

FIGURE 7 EFFECT OF WING AIRFOIL SECTION FOR AN OBLIQUE WING ANGLE OF 60 DEGREES

(A)MACH = 1.10

DATA SET	SYMBOL	CONFIGURATION DESCRIPTION	BETA	LAMBDA	RN/L
(7AE012)	○	W1 F0 B	0.000	60.000	6.000
(7AE043)	△	W2 F0 B	0.000	60.000	4.000
(7AE067)	◇	W4 F0 B	0.000	60.000	6.000

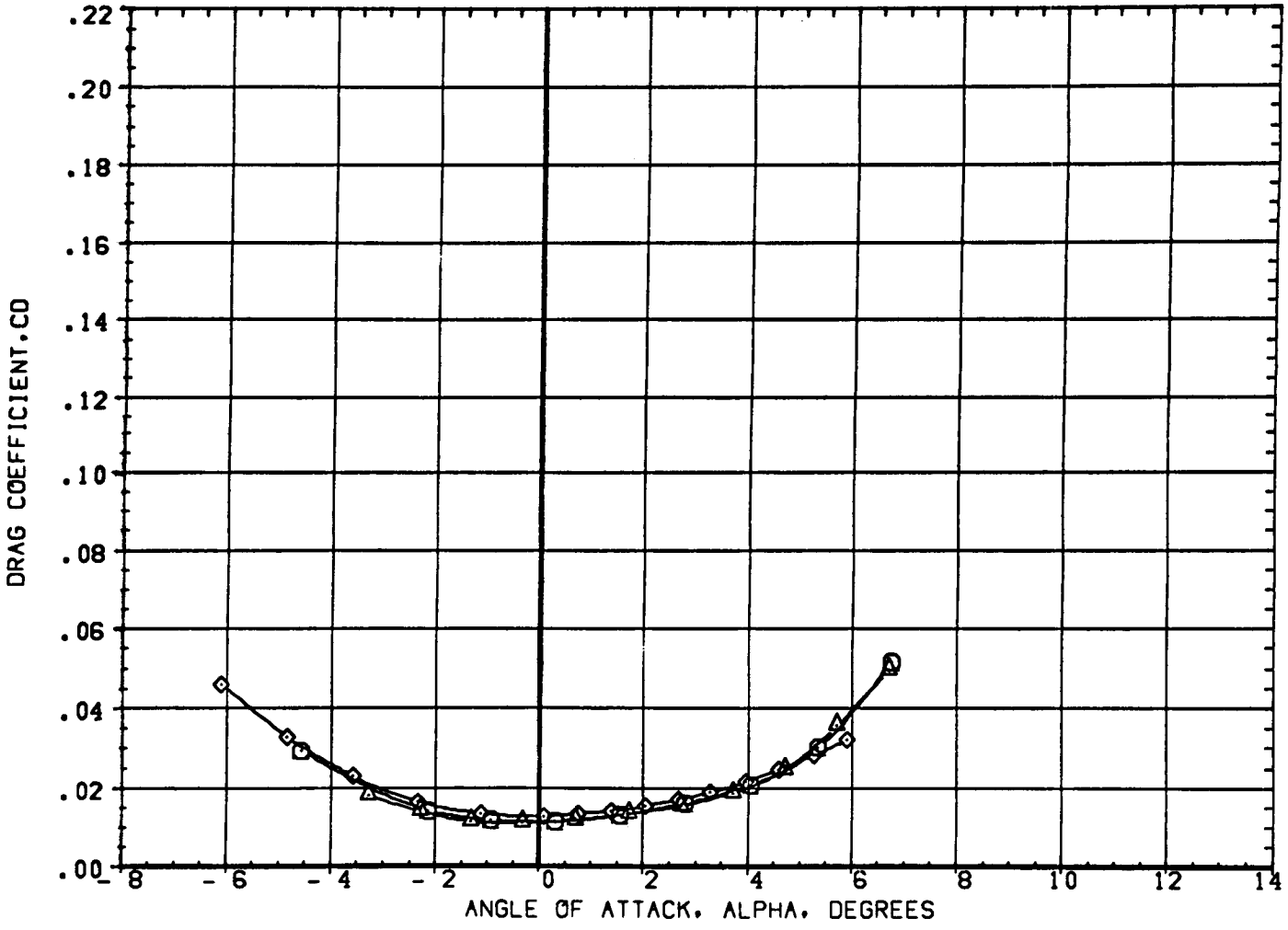

FIGURE 7 EFFECT OF WING AIRFOIL SECTION FOR AN OBLIQUE WING ANGLE OF 60 DEGREES

(A)MACH = 1.10

DATA SET	SYMBOL	CONFIGURATION DESCRIPTION	BETA	LAMBDA	RN/L
(7AE012)	○	W1 F0 B	0.000	60.000	6.000
(7AE043)	△	W2 F0 B	0.000	60.000	4.000
(7AE067)	◇	W4 F0 B	0.000	60.000	6.000

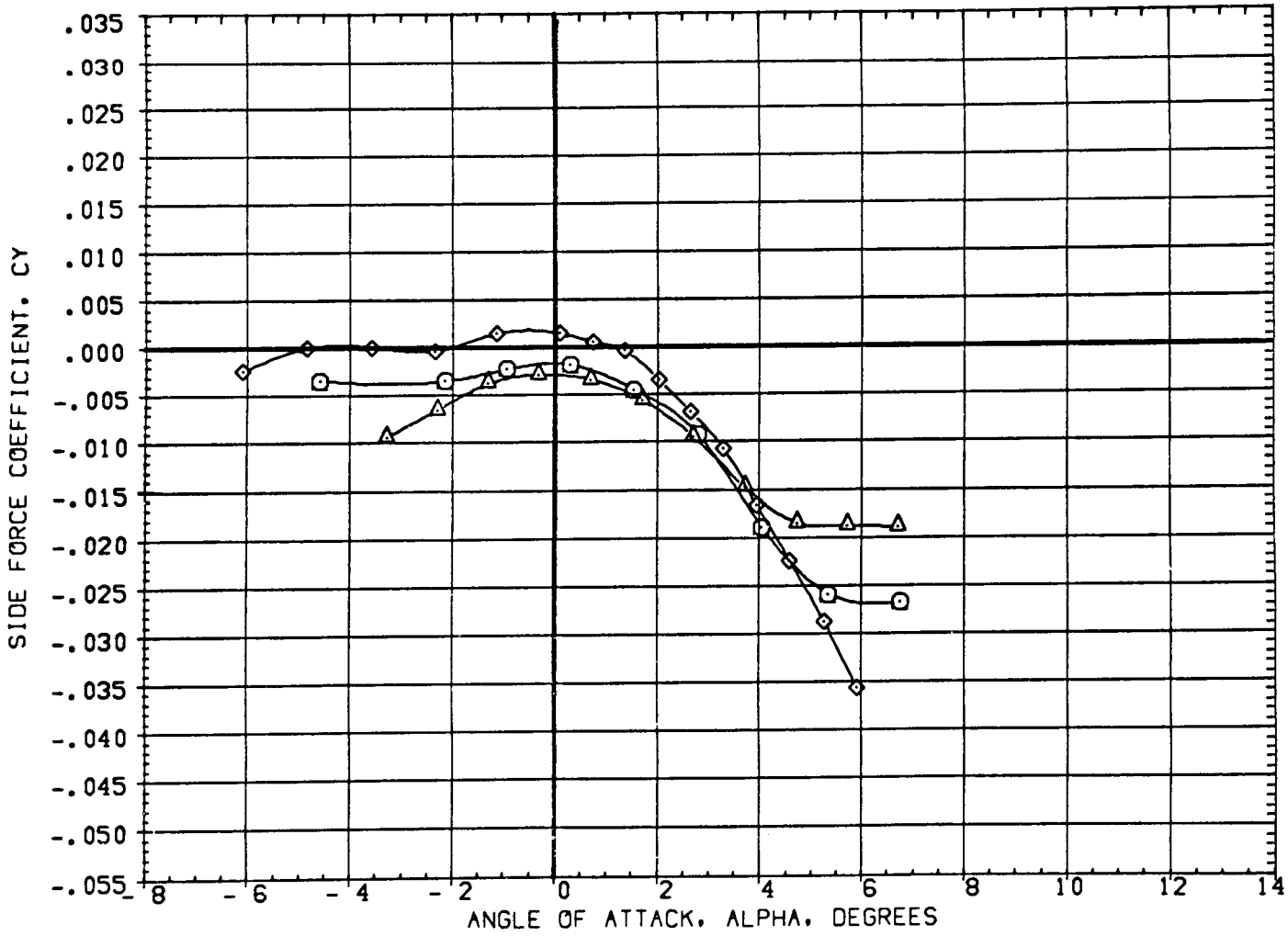

FIGURE 7 EFFECT OF WING AIRFOIL SECTION FOR AN OBLIQUE WING ANGLE OF 60 DEGREES

(A)MACH = 1.10

DATA SET	SYMBOL	CONFIGURATION DESCRIPTION	BETA	LAMBDA	RN/L
(7AE012)	○	W1 F0 B	0.000	60.000	6.000
(7AE043)	△	W2 F0 B	0.000	60.000	4.000
(7AE067)	◇	W4 F0 B	0.000	60.000	6.000

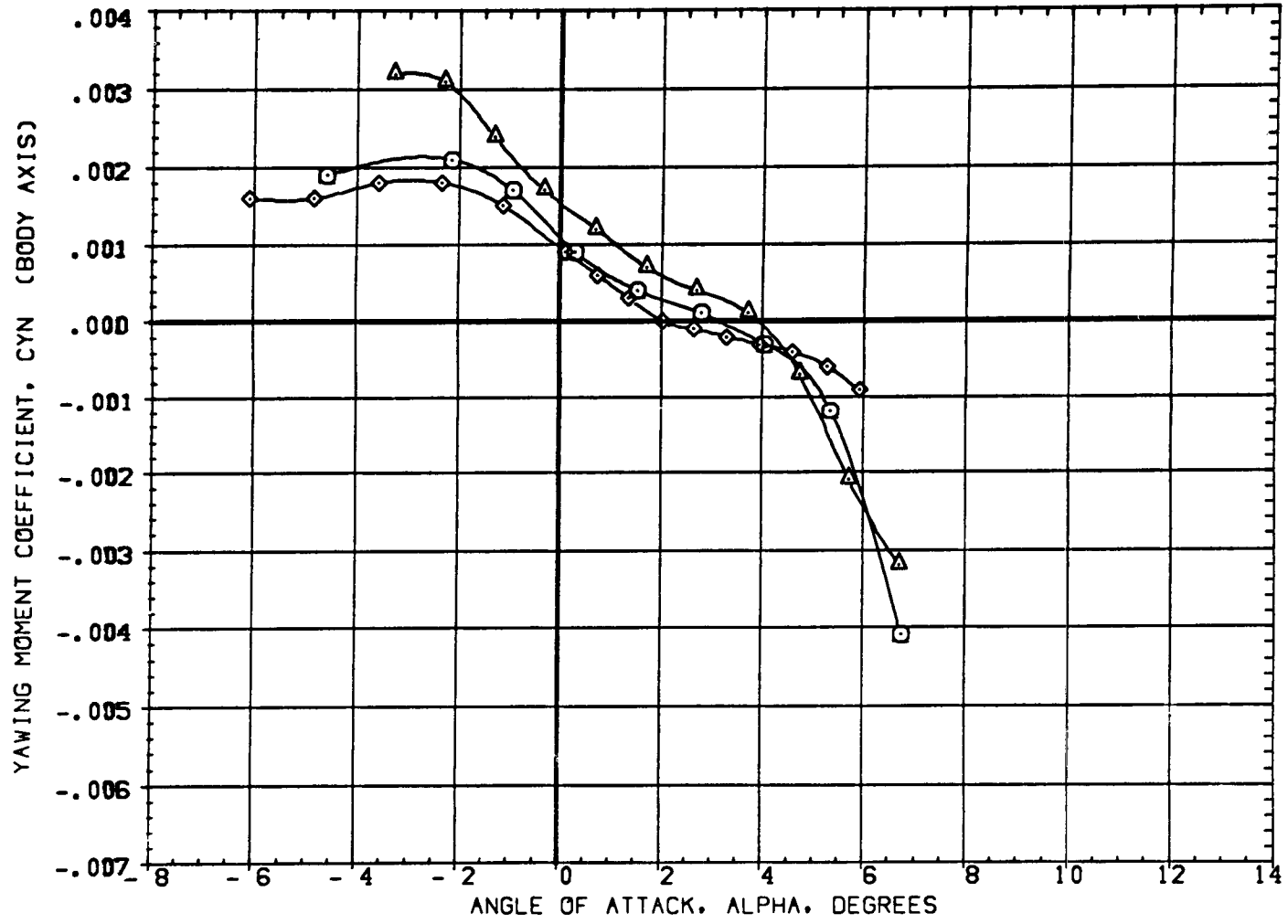

FIGURE 7 EFFECT OF WING AIRFOIL SECTION FOR AN OBLIQUE WING ANGLE OF 60 DEGREES

(A) MACH = 1.10

DATA SET	SYMBOL	CONFIGURATION DESCRIPTION	BETA	LAMBDA	RN/L
(7AE012)	○	W1 F0 B	0.000	60.000	6.000
(7AE043)	△	W2 F0 B	0.000	60.000	4.000
(7AE067)	◇	W4 F0 B	0.000	60.000	6.000

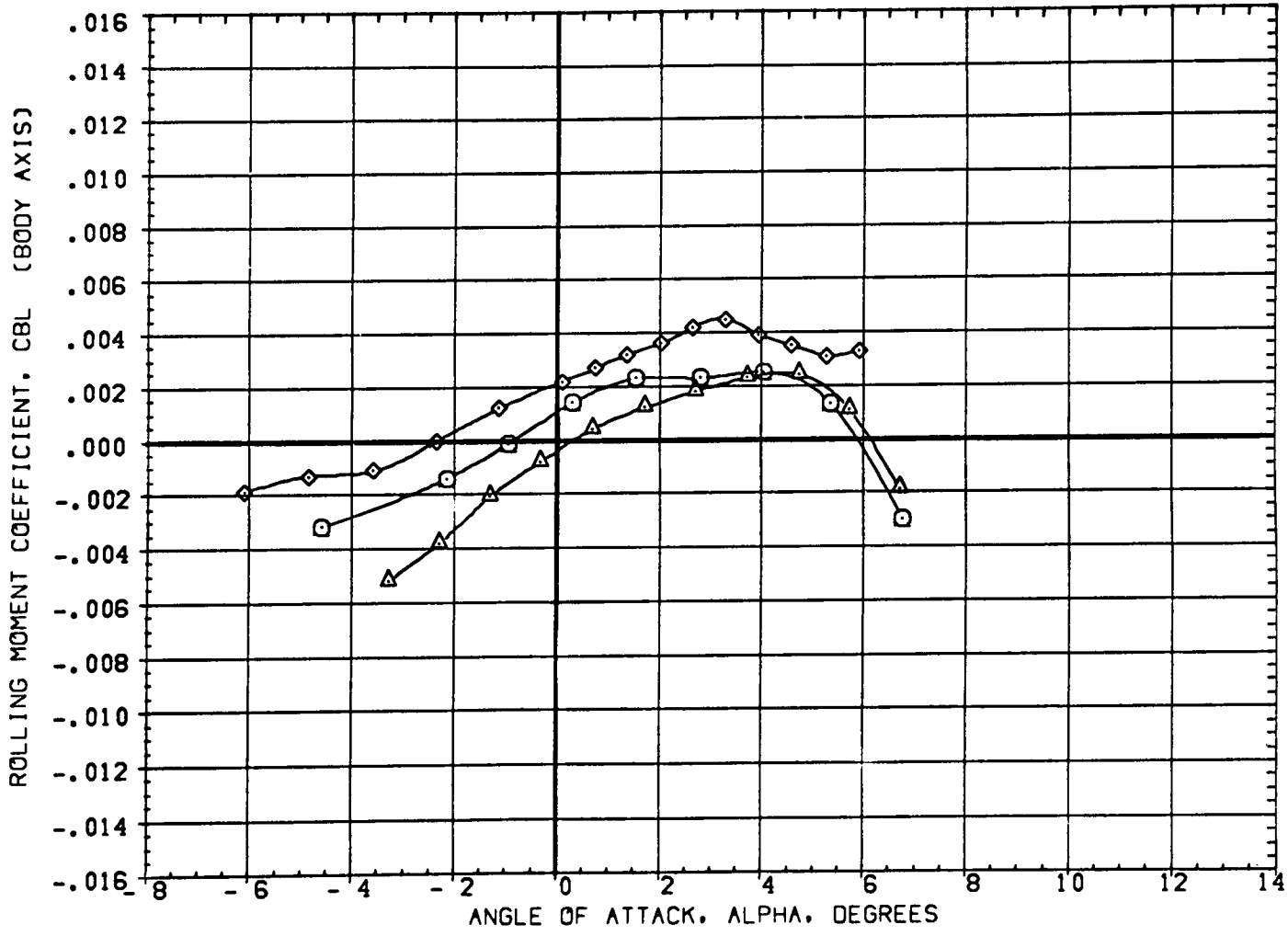

FIGURE 7 EFFECT OF WING AIRFOIL SECTION FOR AN OBLIQUE WING ANGLE OF 60 DEGREES

(A)MACH = 1.10

DATA SET	SYMBOL	CONFIGURATION DESCRIPTION	BETA	LAMBDA	RN/L
(7AE012)	○	W1 F0 B	0.000	60.000	6.000
(7AE043)	△	W2 F0 B	0.000	60.000	4.000
(7AE067)	◇	W4 F0 B	0.000	60.000	6.000

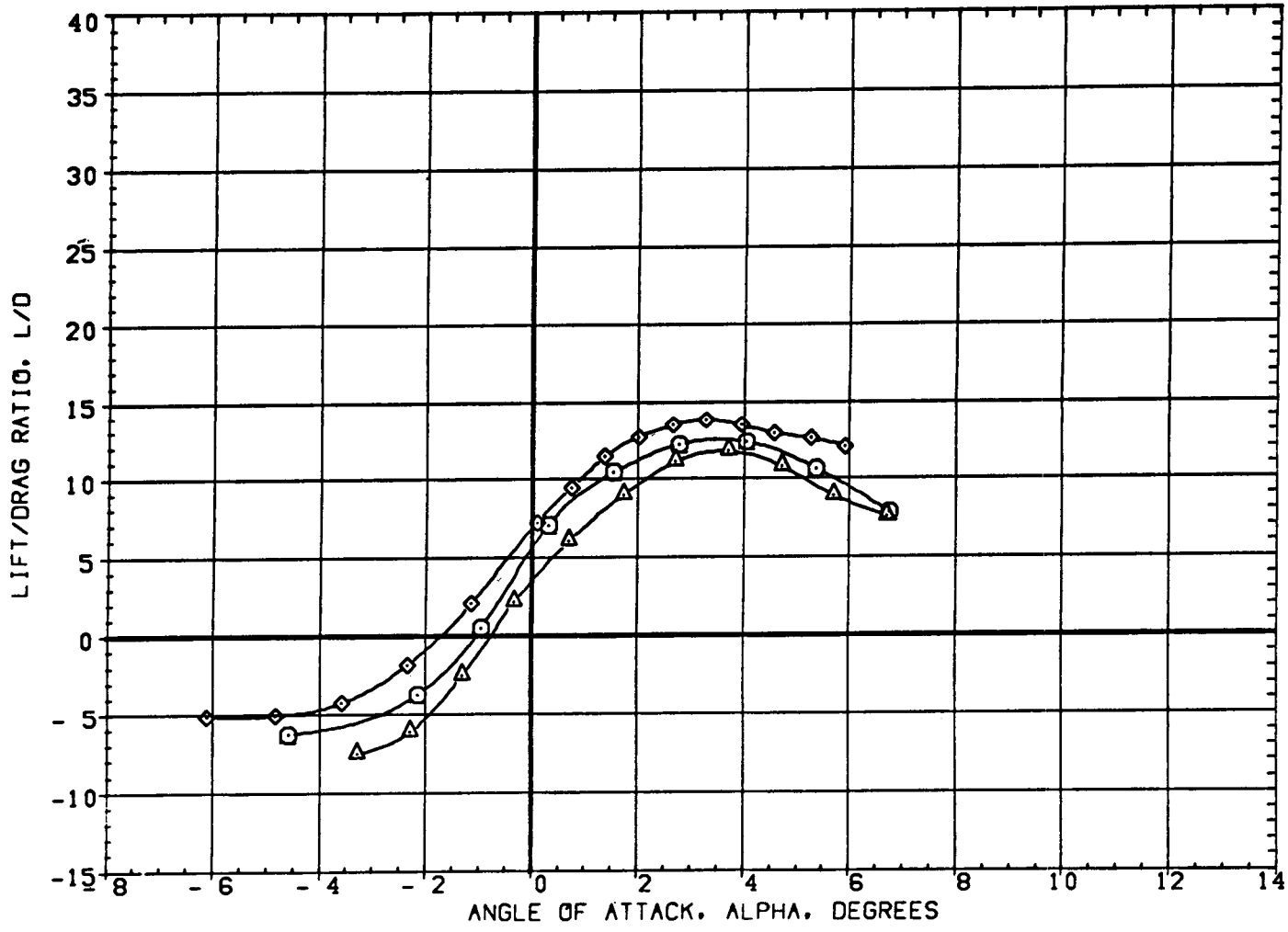

FIGURE 7 EFFECT OF WING AIRFOIL SECTION FOR AN OBLIQUE WING ANGLE OF 60 DEGREES

(A)MACH = 1.10

DATA SET	SYMBOL	CONFIGURATION DESCRIPTION	BETA	LAMBDA	RN/L
(9AE012)	○	W1 F0 B	0.000	60.000	6.000
(9AE043)	△	W2 F0 B	0.000	60.000	4.000
(9AE067)	◇	W4 F0 B	0.000	60.000	6.000

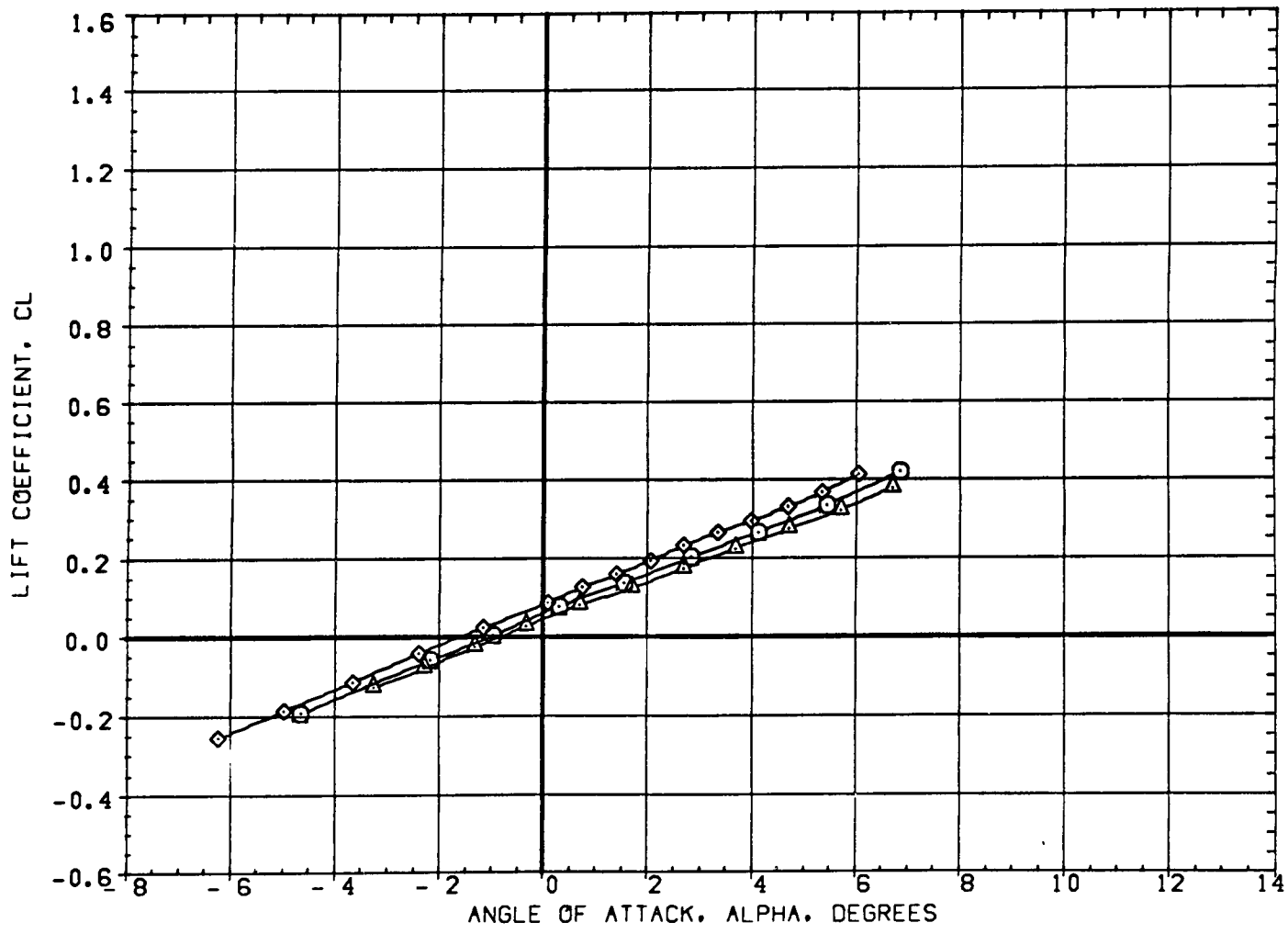

FIGURE 7 EFFECT OF WING AIRFOIL SECTION FOR AN OBLIQUE WING ANGLE OF 60 DEGREES

(A)MACH = 1.20

DATA SET	SYMBOL	CONFIGURATION DESCRIPTION	BETA	LAMBDA	RN/L
(9AE012)	○	W1 F0 B	0.000	60.000	6.000
(9AE043)	△	W2 F0 B	0.000	60.000	4.000
(9AE067)	◇	W4 F0 B	0.000	60.000	6.000

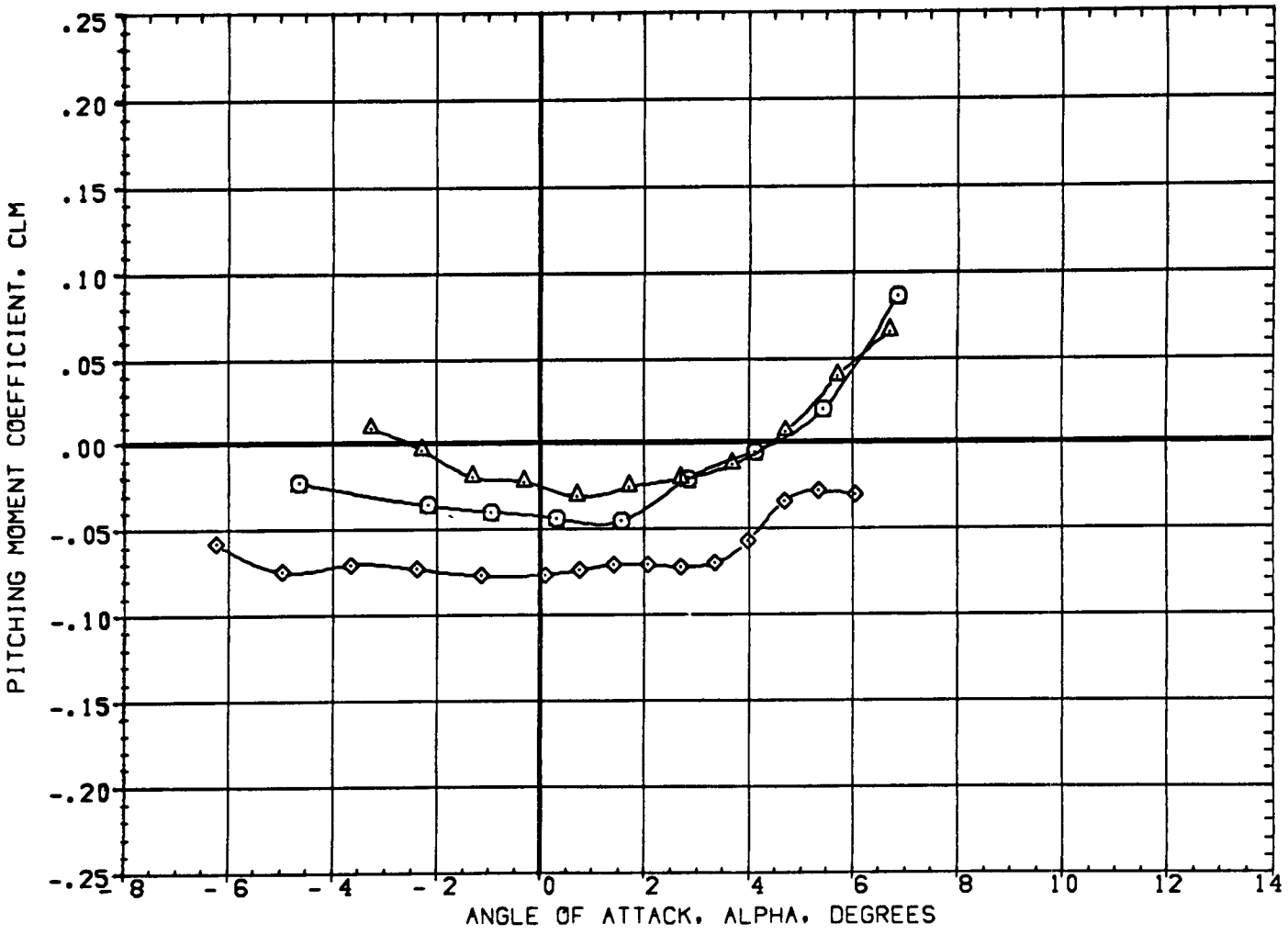

FIGURE 7 EFFECT OF WING AIRFOIL SECTION FOR AN OBLIQUE WING ANGLE OF 60 DEGREES

(A)MACH = 1.20

DATA SET	SYMBOL	CONFIGURATION DESCRIPTION	BETA	LAMBDA	RN/L
(9AE012)	○	W1 F0 B	0.000	60.000	6.000
(9AE043)	△	W2 F0 B	0.000	60.000	4.000
(9AE067)	◇	W4 F0 B	0.000	60.000	6.000

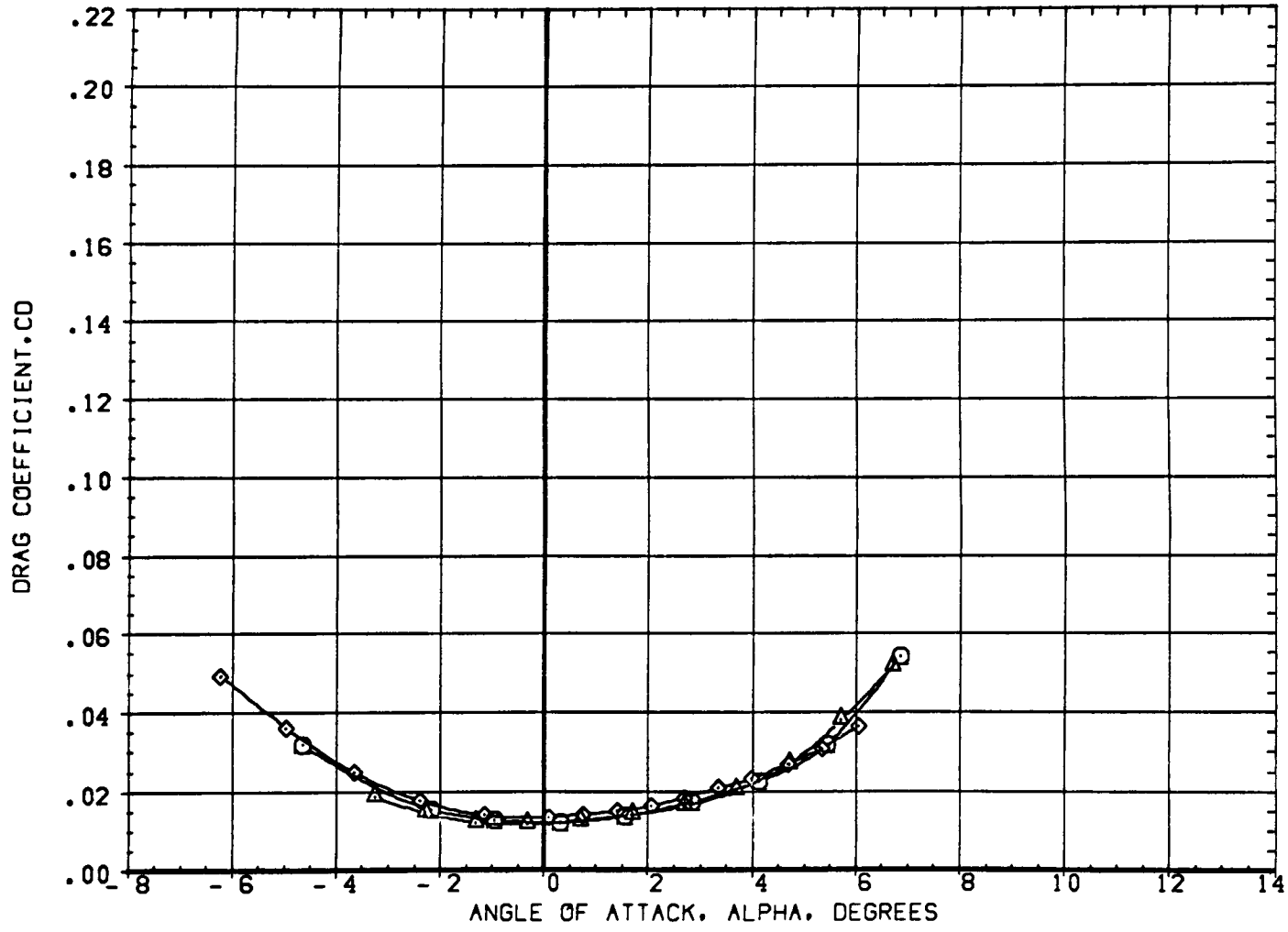

FIGURE 7 EFFECT OF WING AIRFOIL SECTION FOR AN OBLIQUE WING ANGLE OF 60 DEGREES

(A)MACH = 1.20

DATA SET	SYMBOL	CONFIGURATION DESCRIPTION	BETA	LAMBDA	?N/L
(9AE012)	○	W1 F0 B	0.000	60.000	6.000
(9AE043)	△	W2 F0 B	0.000	60.000	4.000
(9AE067)	◇	W4 F0 B	0.000	60.000	6.000

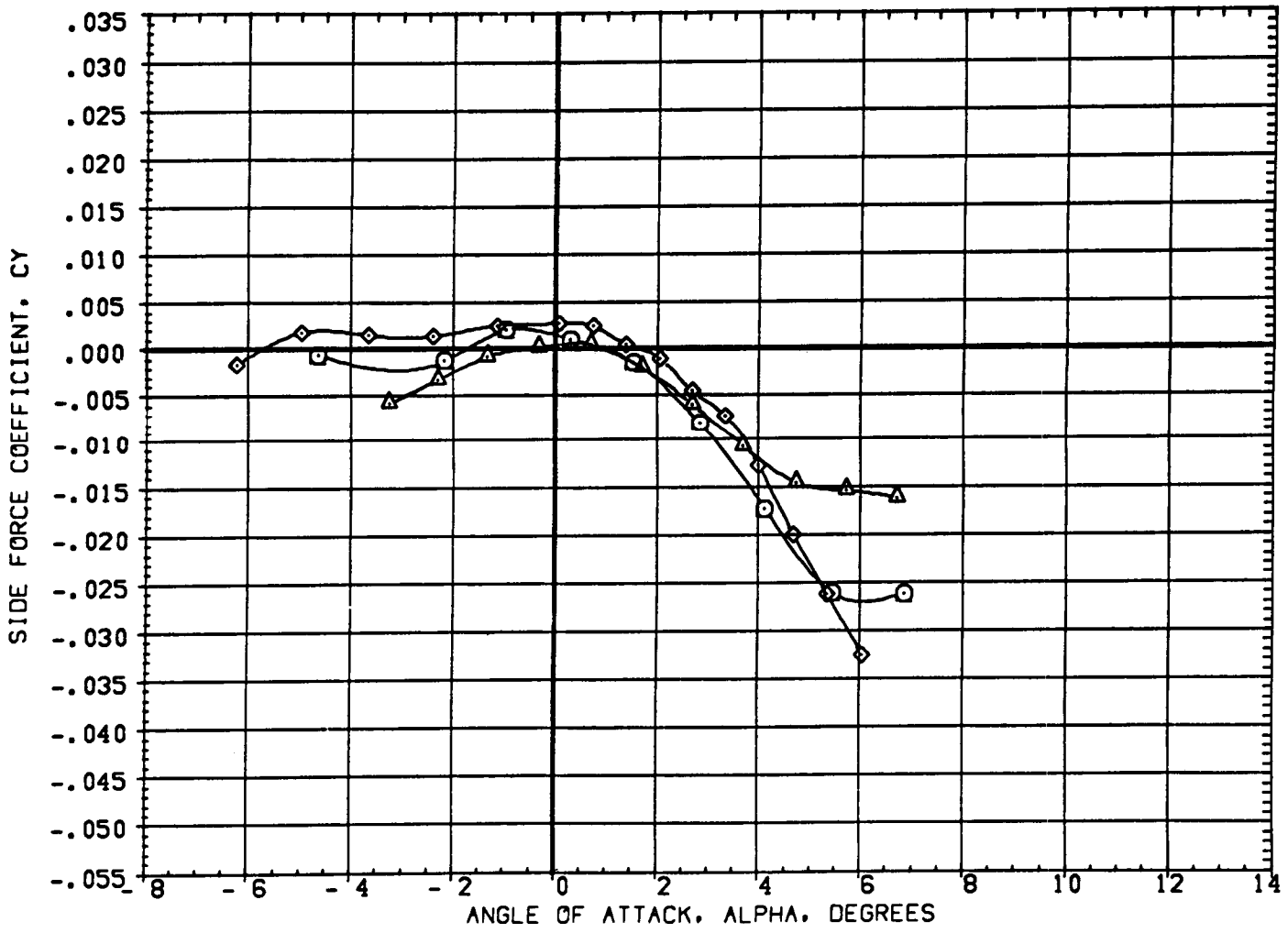

FIGURE 7 EFFECT OF WING AIRFOIL SECTION FOR AN OBLIQUE WING ANGLE OF 60 DEGREES

(A)MACH = 1.20

DATA SET	SYMBOL	CONFIGURATION DESCRIPTION	BETA	LAMBDA	RN/L
(9AE012)	○	W1 F0 B	0.000	60.000	6.000
(9AE043)	△	W2 F0 B	0.000	60.000	4.000
(9AE067)	◇	W4 F0 B	0.000	60.000	6.000

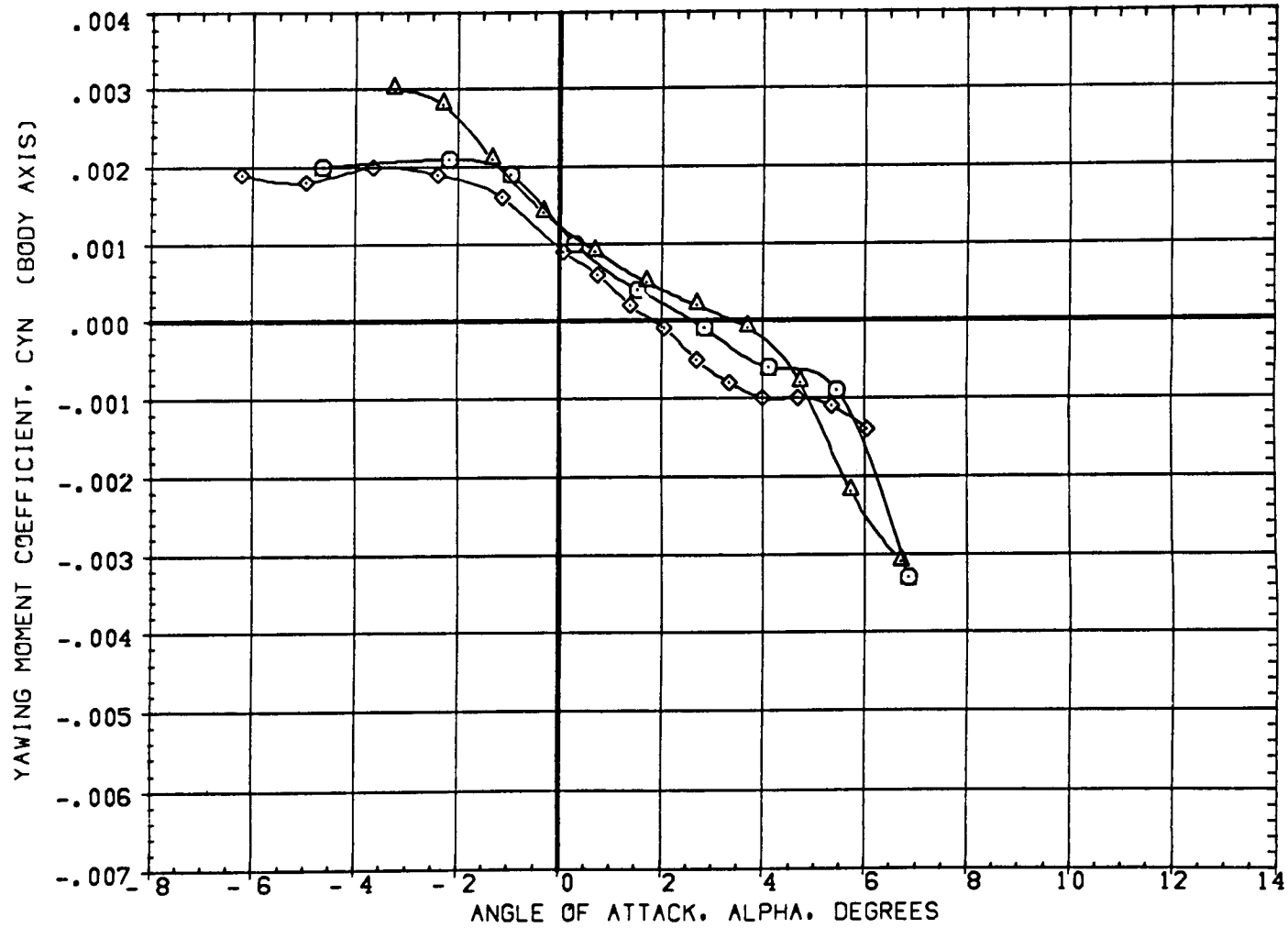

FIGURE 7 EFFECT OF WING AIRFOIL SECTION FOR AN OBLIQUE WING ANGLE OF 60 DEGREES

(A)MACH = 1.20

DATA SET	SYMBOL	CONFIGURATION DESCRIPTION	BETA	LAMBDA	RN/L
(9AE012)	○	W1 F0 B	0.000	60.000	6.000
(9AE045)	△	W2 F0 B	0.000	60.000	4.000
(9AE067)	◇	W4 F0 B	0.000	60.000	6.000

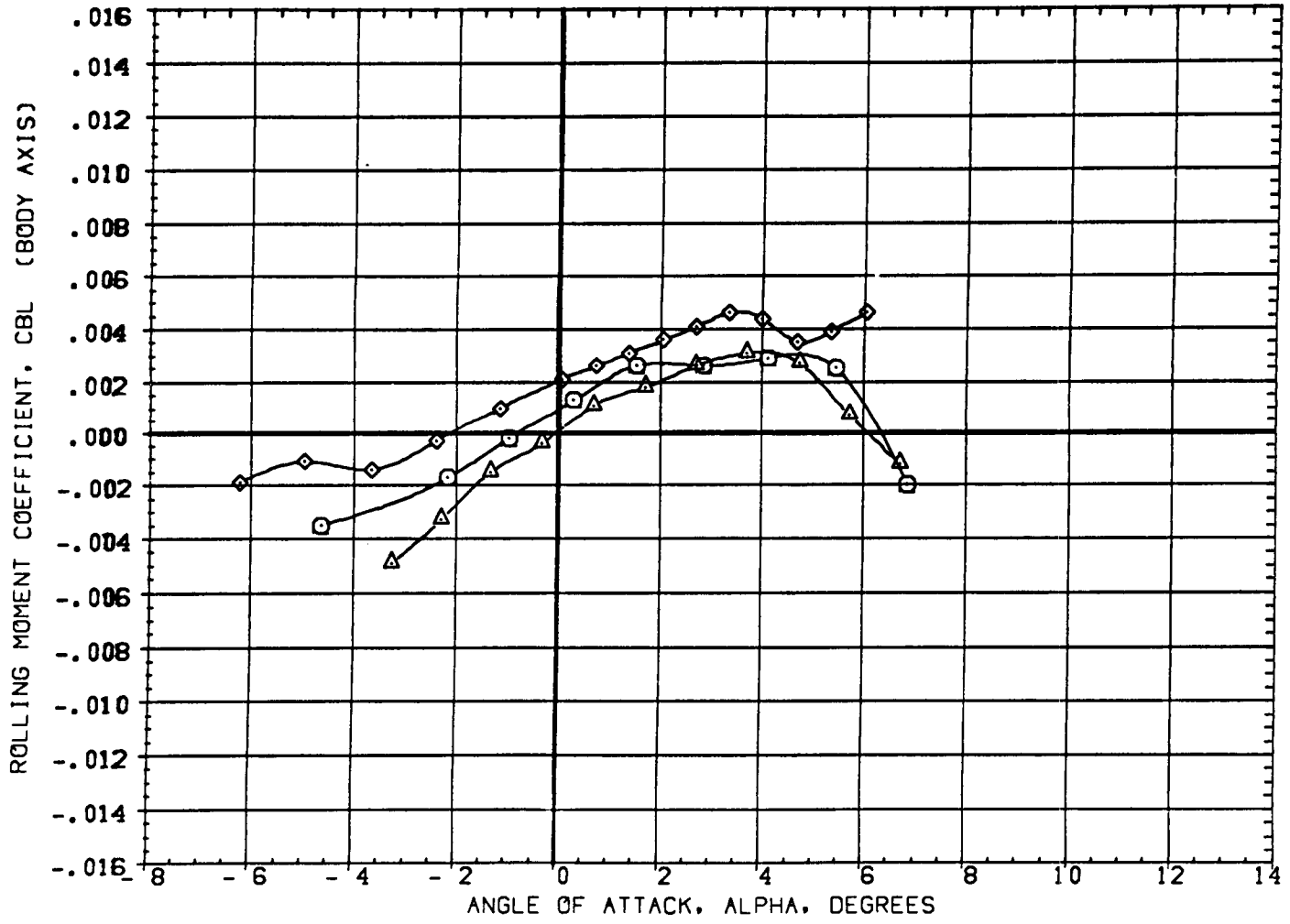

FIGURE 7 EFFECT OF WING AIRFOIL SECTION FOR AN OBLIQUE WING ANGLE OF 60 DEGREES

(A)MACH = 1.20

DATA SET	SYMBOL	CONFIGURATION DESCRIPTION	BETA	LAMBDA	RN/L
(9AE012)	○	W1 F0 B	0.000	60.000	6.000
(9AE043)	△	W2 F0 B	0.000	60.000	4.000
(9AE067)	◇	W4 F0 B	0.000	60.000	6.000

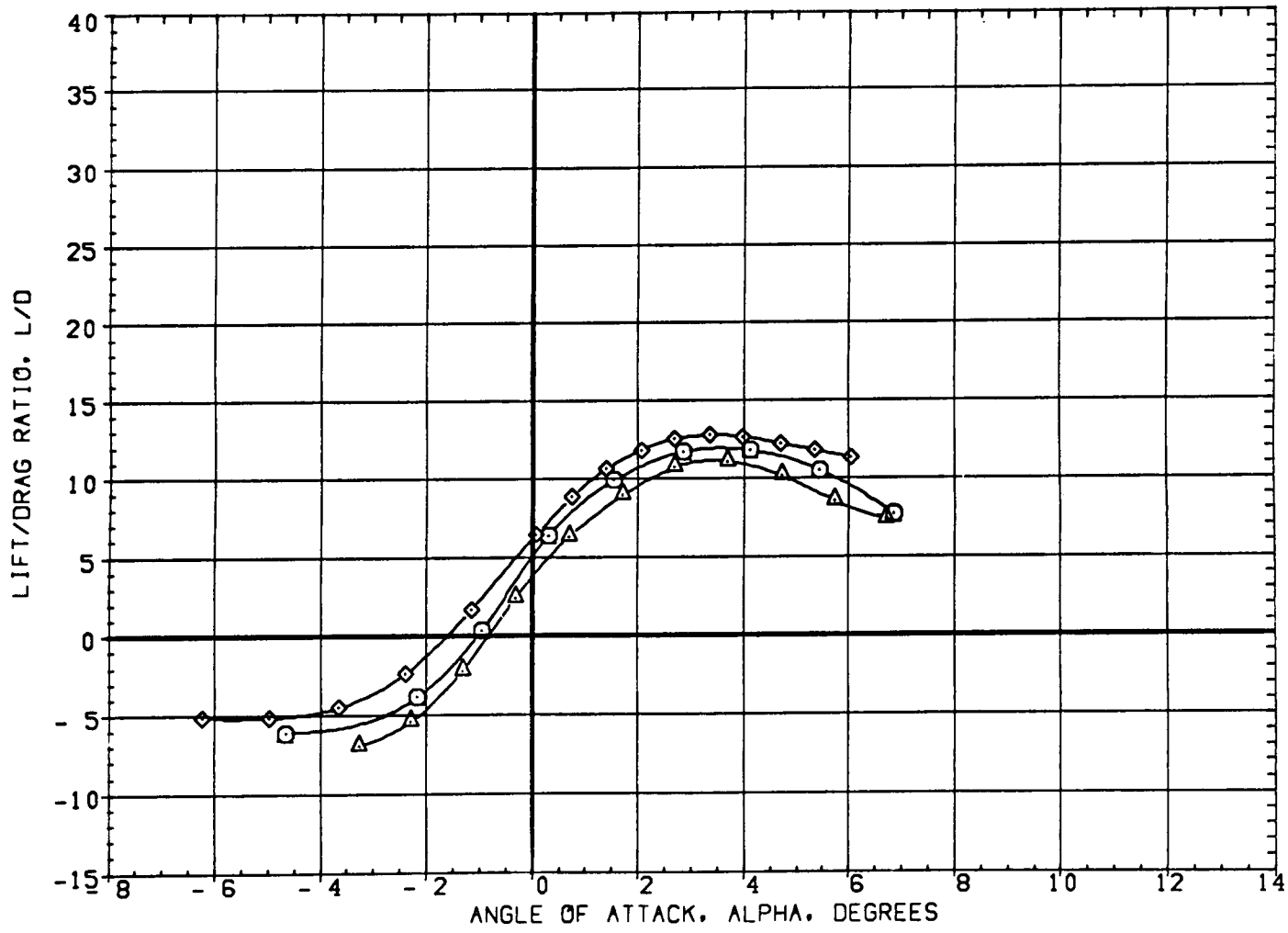

FIGURE 7 EFFECT OF WING AIRFOIL SECTION FOR AN OBLIQUE WING ANGLE OF 60 DEGREES

(A)MACH = 1.20

DATA SET	SYMBOL	CONFIGURATION DESCRIPTION	BETA	LAMBDA	RN/L
(0AE012)	○	W1 F0 B	0.000	60.000	6.000
(0AE043)	△	W2 F0 B	0.000	60.000	4.000
(0AE067)	◇	W4 F0 B	0.000	60.000	6.000

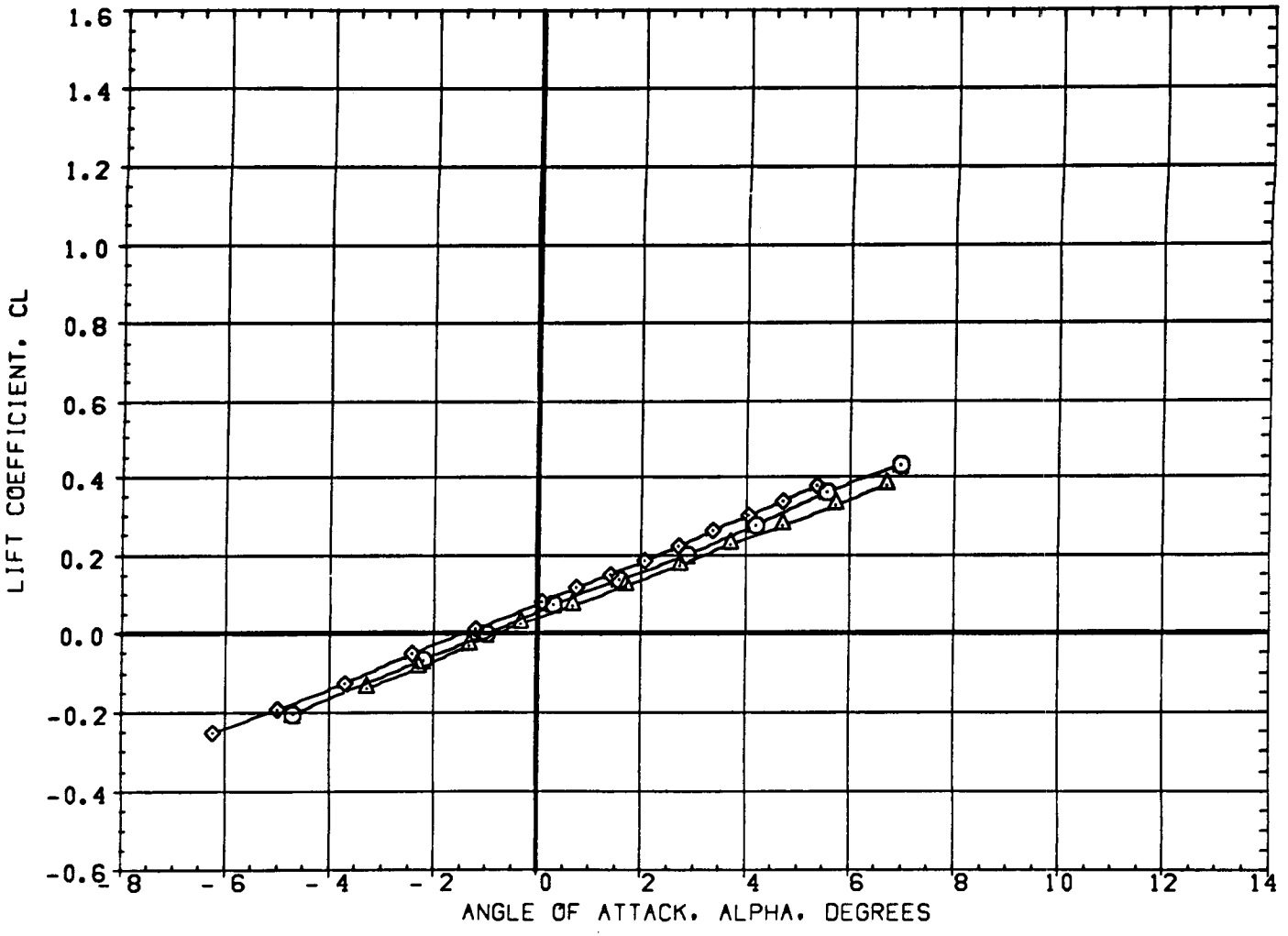

FIGURE 7 EFFECT OF WING AIRFOIL SECTION FOR AN OBLIQUE WING ANGLE OF 60 DEGREES

(A)MACH = 1.30

DATA SET	SYMBOL	CONFIGURATION DESCRIPTION	BETA	LAMBDA	RN/L
(0AE012)	○	W1 F0 B	0.000	60.000	6.000
(0AE043)	△	W2 F0 B	0.000	60.000	4.000
(0AE067)	◇	W4 F0 B	0.000	60.000	6.000

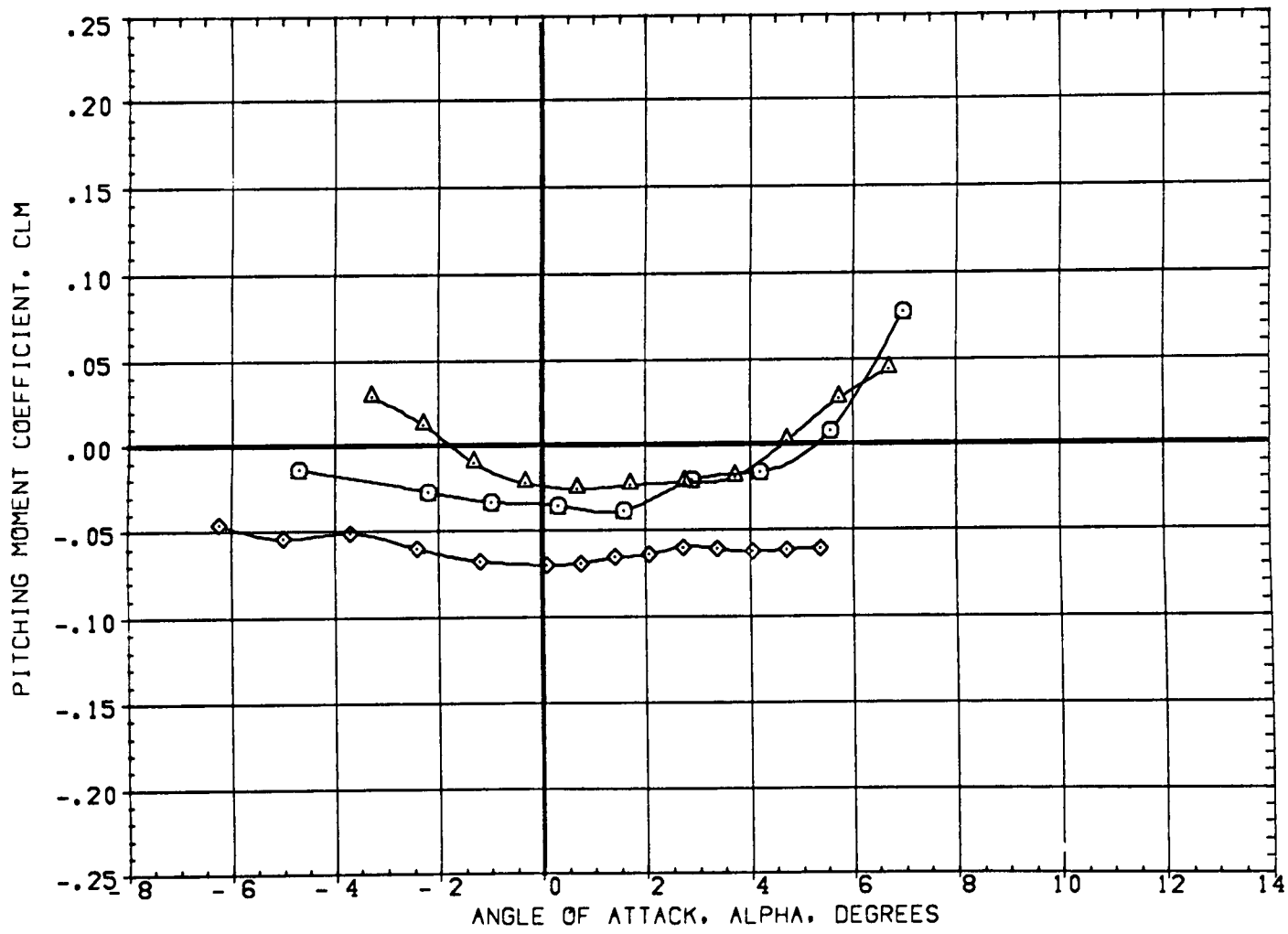

FIGURE 7 EFFECT OF WING AIRFOIL SECTION FOR AN OBLIQUE WING ANGLE OF 60 DEGREES

(A)MACH = 1.30

DATA SET	SYMBOL	CONFIGURATION DESCRIPTION	BETA	LAMBDA	RN/L
(0AE012)	○	W1 F0 B	0.000	60.000	6.000
(0AE043)	△	W2 F0 B	0.000	60.000	4.000
(0AE067)	◇	W4 F0 B	0.000	60.000	6.000

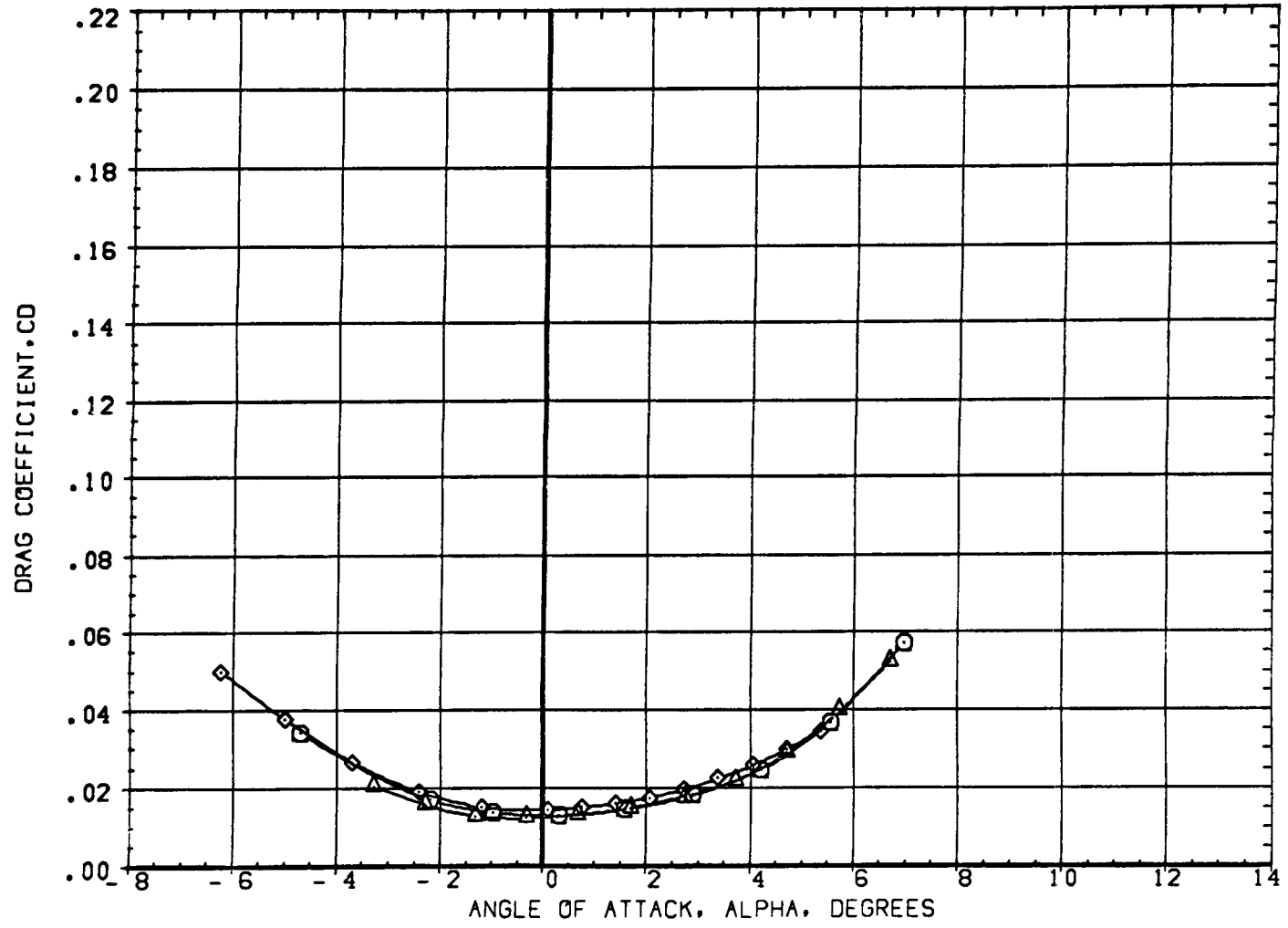

FIGURE 7 EFFECT OF WING AIRFOIL SECTION FOR AN OBLIQUE WING ANGLE OF 60 DEGREES

(A)MACH = 1.30

DATA SET	SYMBOL	CONFIGURATION DESCRIPTION	BETA	LAMBDA	RN/L
(0AE012)	○	W1 F0 B	0.000	60.000	6.000
(0AE043)	△	W2 F0 B	0.000	60.000	4.000
(0AE067)	◇	W4 F0 B	0.000	60.000	6.000

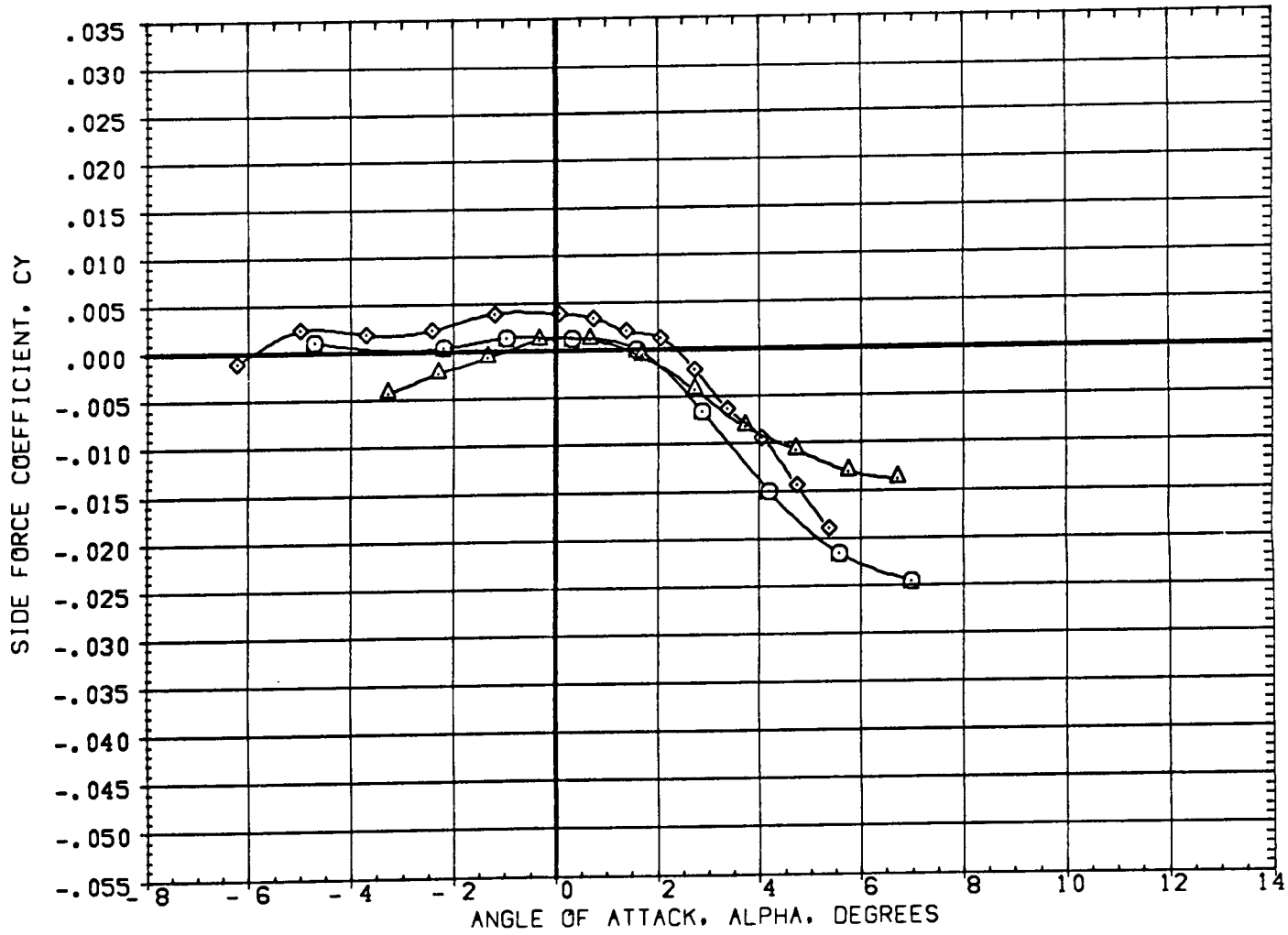

FIGURE 7 EFFECT OF WING AIRFOIL SECTION FOR AN OBLIQUE WING ANGLE OF 60 DEGREES

(A)MACH = 1.30

DATA SET	SYMBOL	CONFIGURATION DESCRIPTION	BETA	LAMBDA	RN/L
(0AE012)	○	W1 F0 B	0.000	60.000	6.000
(0AE043)	△	W2 F0 B	0.000	60.000	4.000
(0AE067)	◇	W4 F0 B	0.000	60.000	6.000

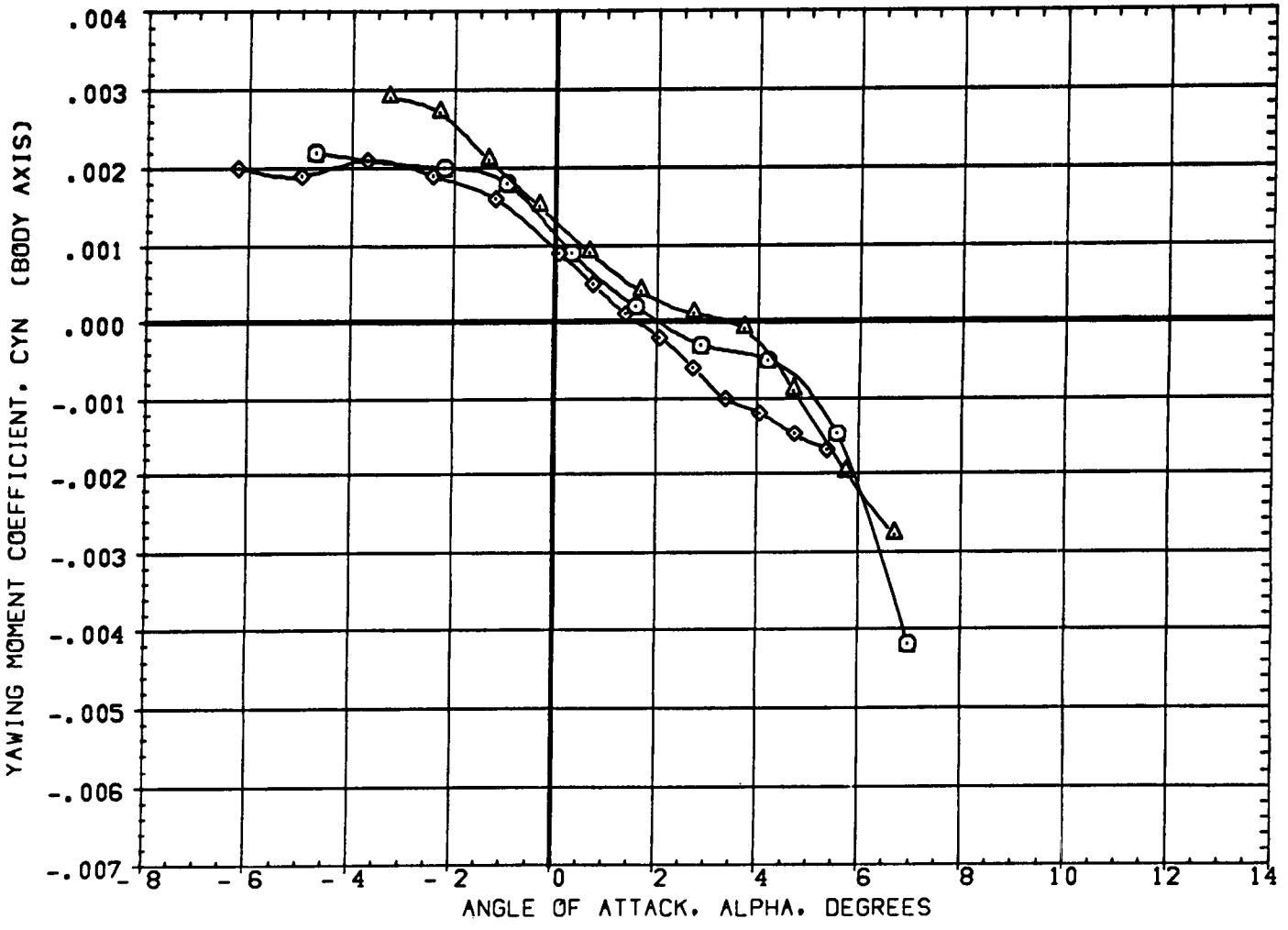

FIGURE 7 EFFECT OF WING AIRFOIL SECTION FOR AN OBLIQUE WING ANGLE OF 60 DEGREES

(A)MACH = 1.30

DATA SET	SYMBOL	CONFIGURATION DESCRIPTION	BETA	LAMBDA	RN/L
(0AE012)	○	W1 F0 B	0.000	60.000	6.000
(0AE043)	△	W2 F0 B	0.000	60.000	4.000
(0AE067)	◇	W4 F0 B	0.000	60.000	6.000

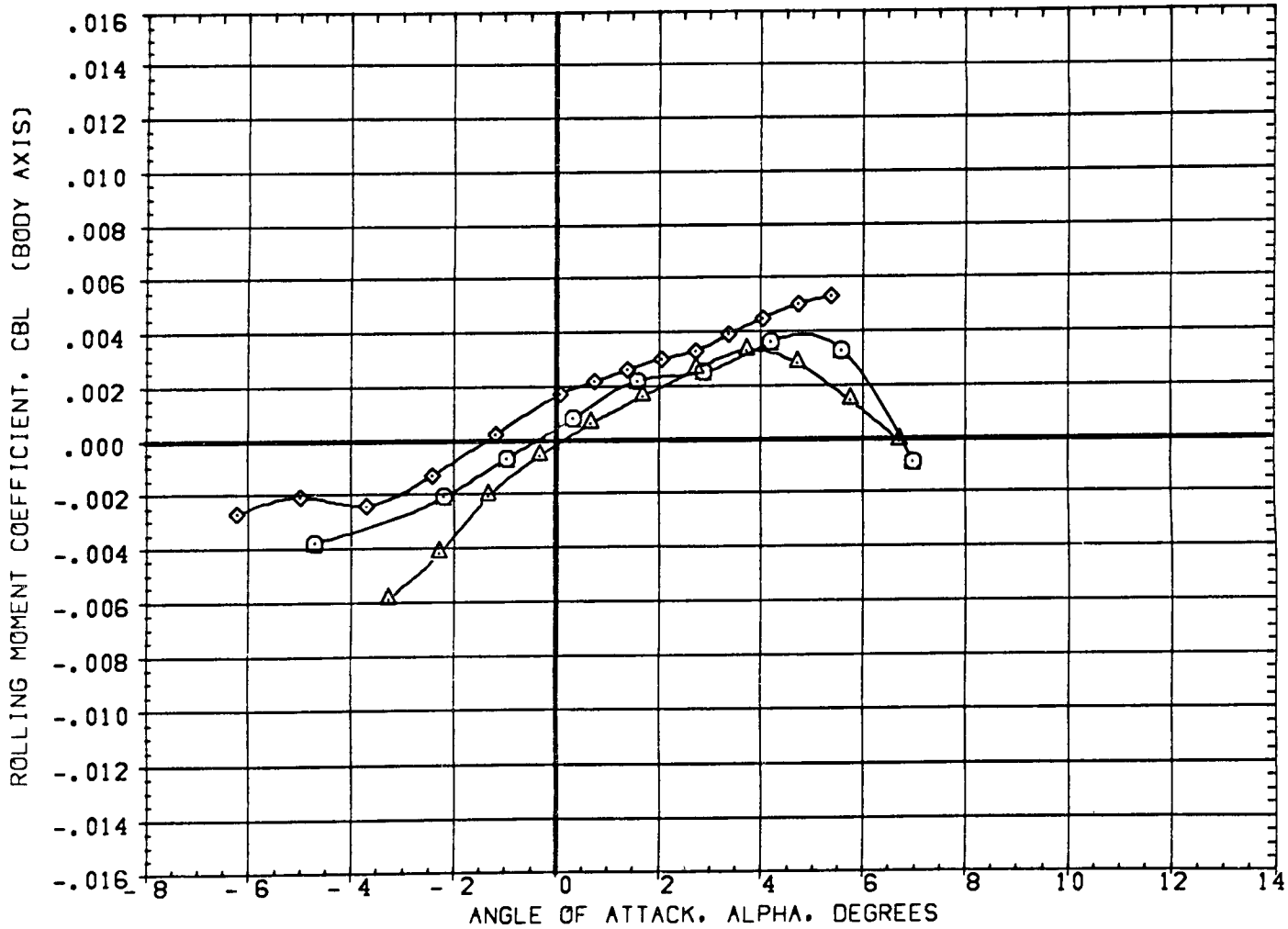

FIGURE 7 EFFECT OF WING AIRFOIL SECTION FOR AN OBLIQUE WING ANGLE OF 60 DEGREES

(A)MACH = 1.30

DATA SET	SYMBOL	CONFIGURATION DESCRIPTION	BETA	LAMBDA	RN/L
(0AE012)	○	W1 F0 B	0.000	60.000	6.000
(0AE043)	△	W2 F0 B	0.000	60.000	4.000
(0AE067)	◇	W4 F0 B	0.000	60.000	6.000

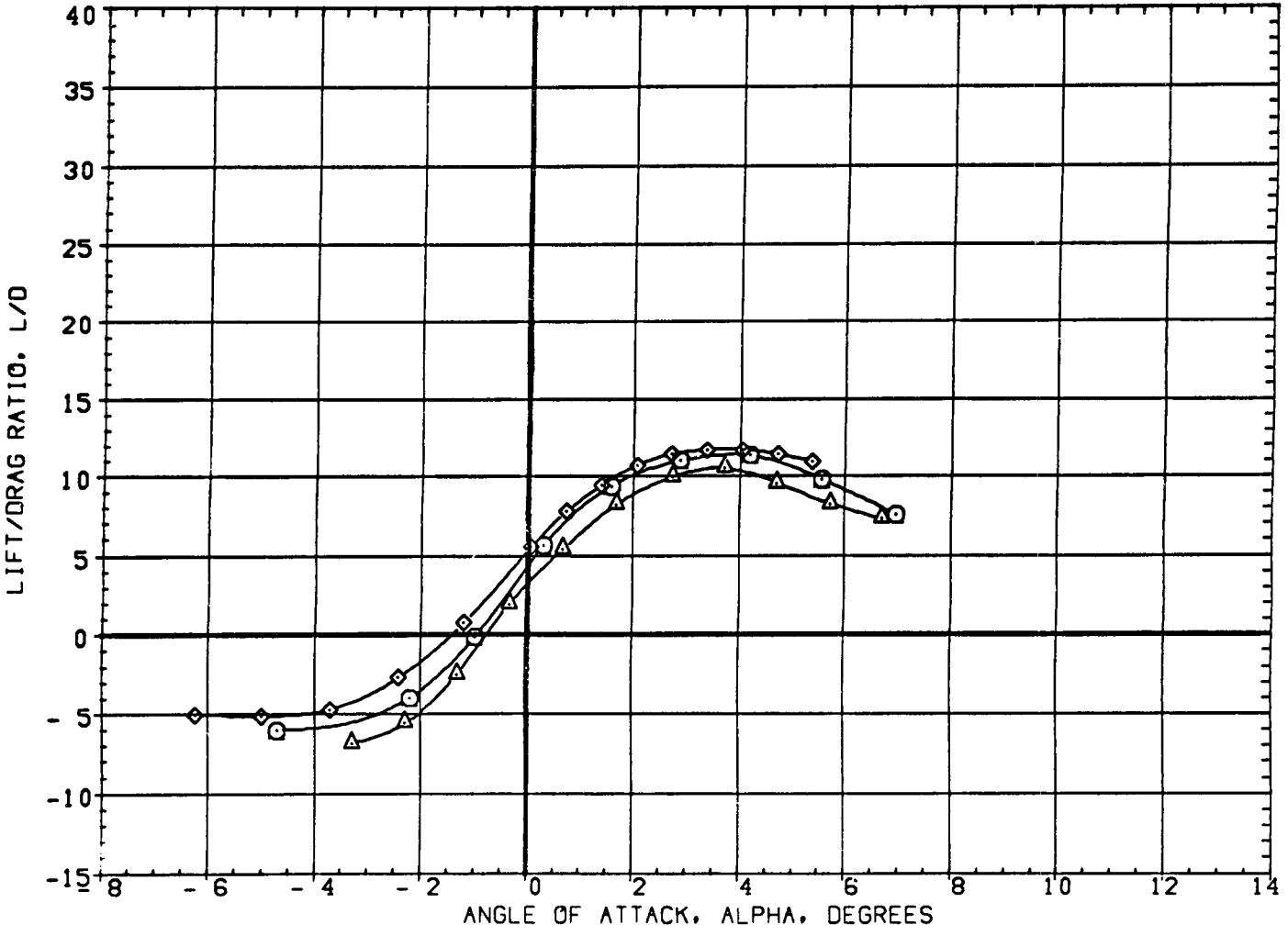

FIGURE 7 EFFECT OF WING AIRFOIL SECTION FOR AN OBLIQUE WING ANGLE OF 60 DEGREES

(A)MACH = 1.30

DATA SET	SYMBOL	CONFIGURATION DESCRIPTION	BETA	LAMBDA	RN/L
(ZAE012)	○	W1 F0 B	0.000	60.000	6.000
(ZAE043)	△	W2 F0 B	0.000	60.000	4.000
(ZAE067)	◇	W4 F0 B	0.000	60.000	6.000

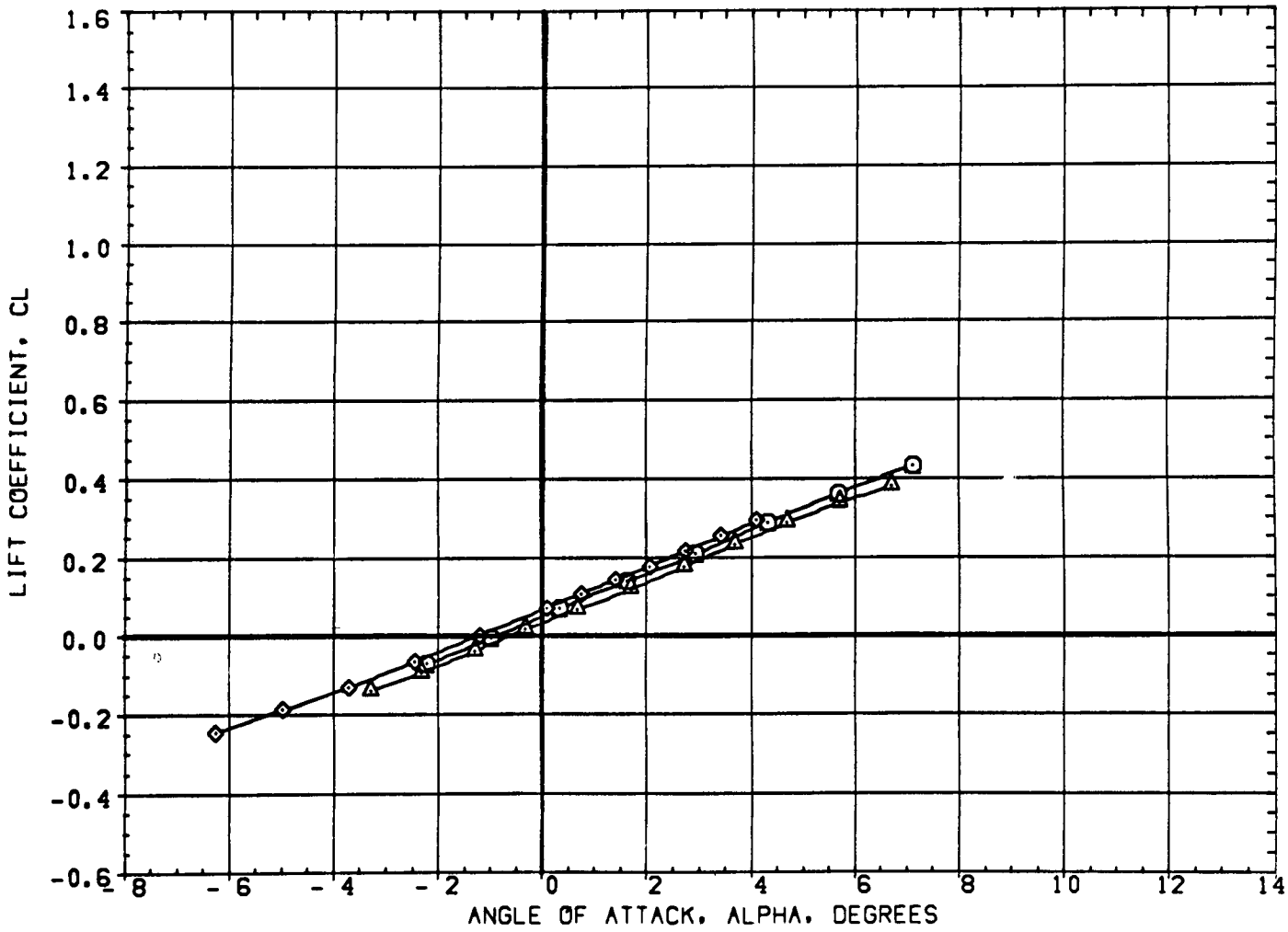

FIGURE 7 EFFECT OF WING AIRFOIL SECTION FOR AN OBLIQUE WING ANGLE OF 60 DEGREES

(A)MACH = 1.40

DATA SET	SYMBOL	CONFIGURATION DESCRIPTION	BETA	LAMBDA	RN/L
(ZAE012)	○	W1 FO B	0.000	60.000	6.000
(ZAE043)	△	W2 FO B	0.000	60.000	4.000
(ZAE067)	◇	W4 FO B	0.000	60.000	6.000

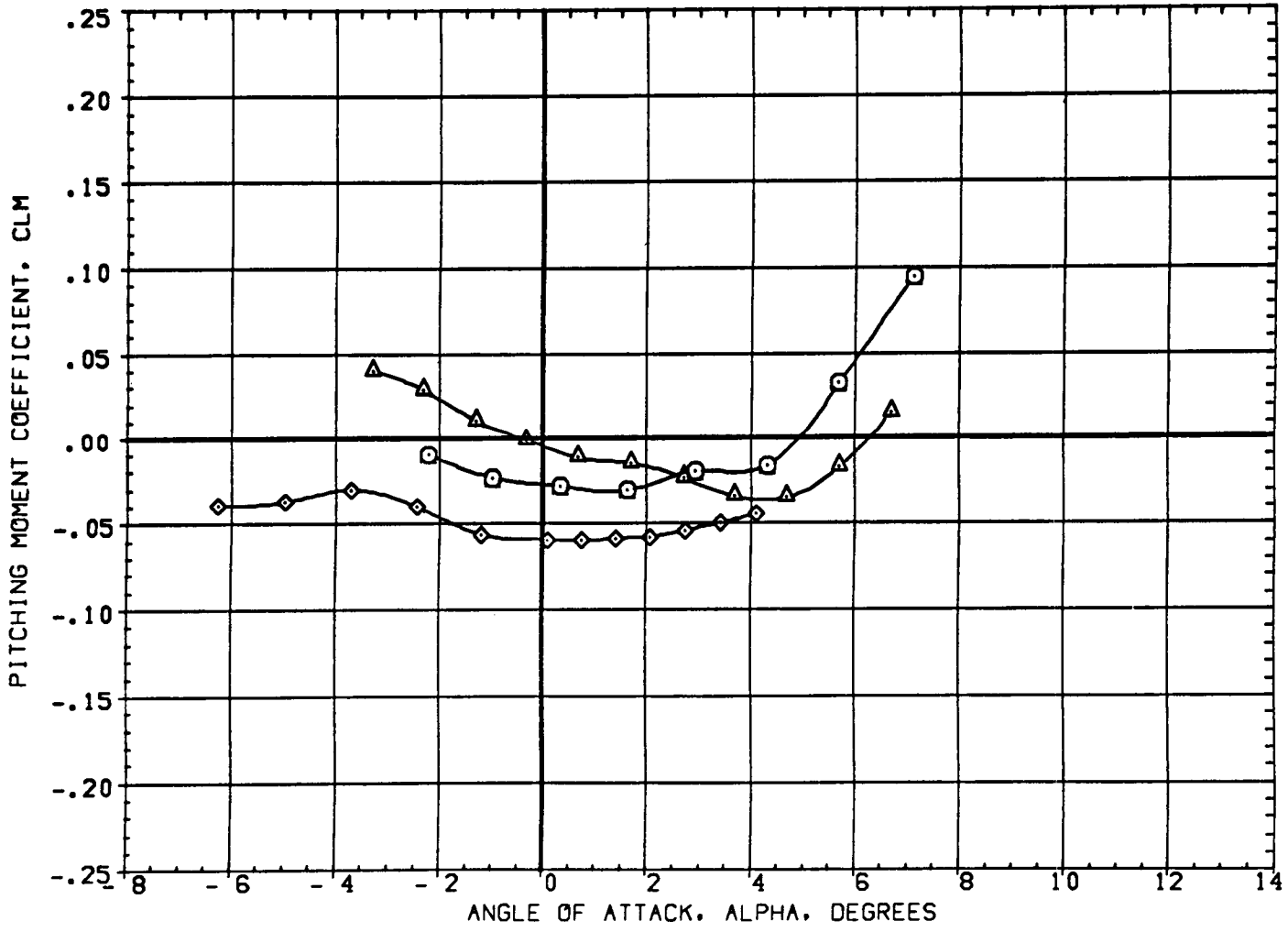

FIGURE 7 EFFECT OF WING AIRFOIL SECTION FOR AN OBLIQUE WING ANGLE OF 60 DEGREES

(A)MACH = 1.40

DATA SET	SYMBOL	CONFIGURATION DESCRIPTION	BETA	LAMBDA	RN/L
(ZAE012)	○	W1 F0 B	0.000	60.000	6.000
(ZAE043)	△	W2 F0 B	0.000	60.000	4.000
(ZAE067)	◇	W4 F0 B	0.000	60.000	6.000

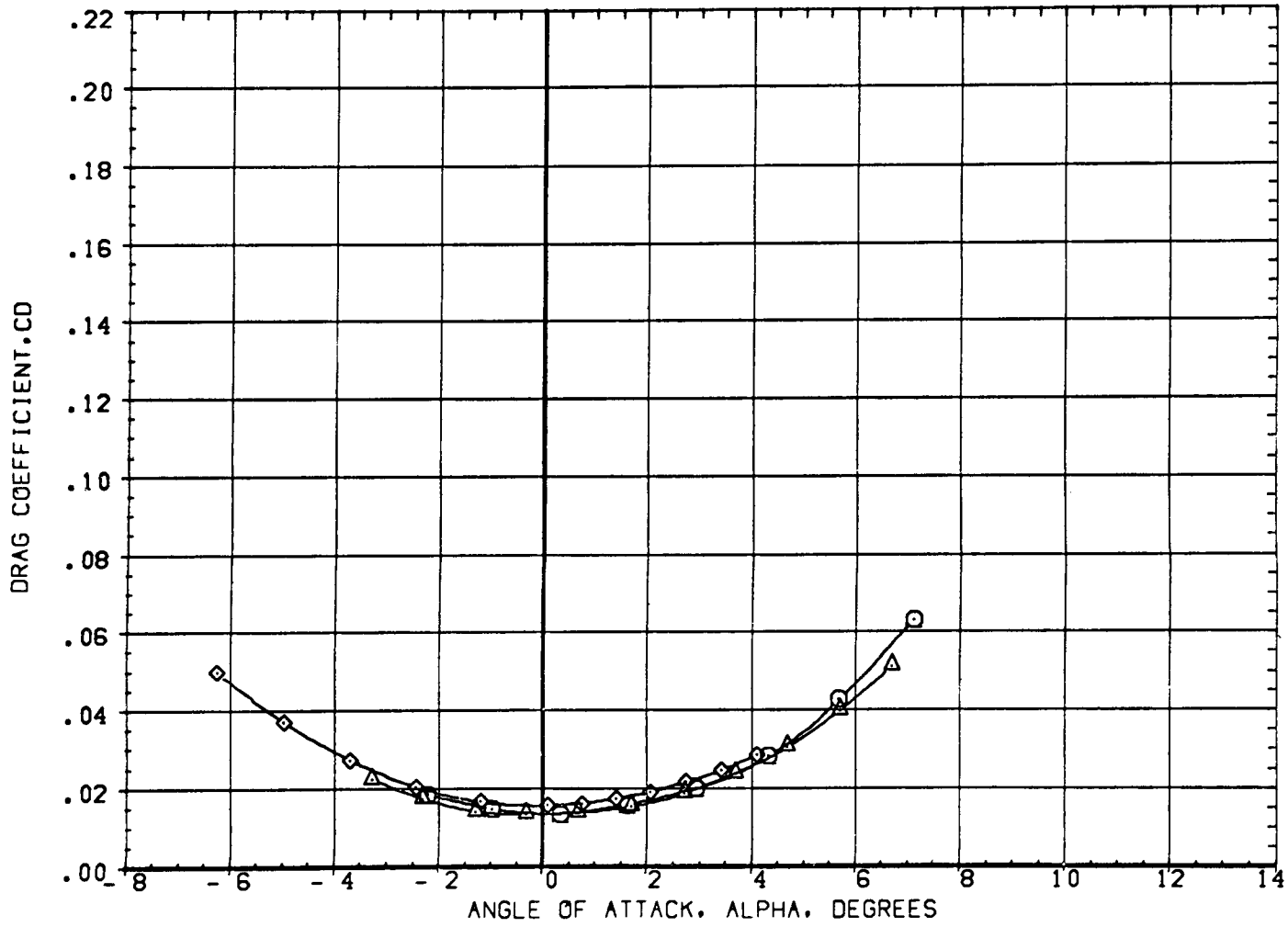

FIGURE 7 EFFECT OF WING AIRFOIL SECTION FOR AN OBLIQUE WING ANGLE OF 60 DEGREES

(A)MACH = 1.40

DATA SET	SYMBOL	CONFIGURATION DESCRIPTION	BETA	LAMBDA	RN/L
(ZAE012)	○	W1 F0 B	0.000	60.000	6.000
(ZAE043)	△	W2 F0 B	0.000	60.000	4.000
(ZAE067)	◇	W4 F0 B	0.000	60.000	6.000

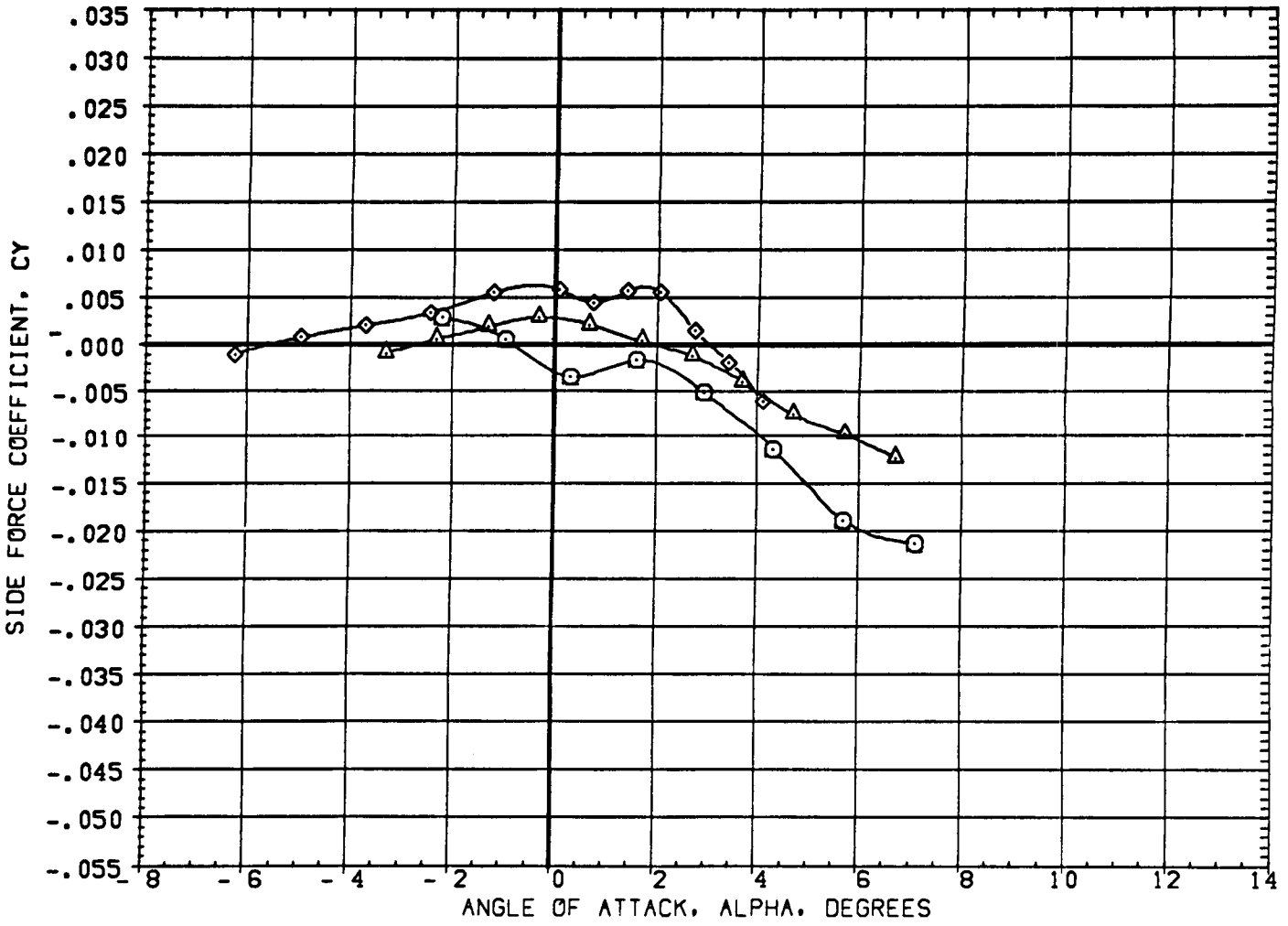

FIGURE 7 EFFECT OF WING AIRFOIL SECTION FOR AN OBLIQUE WING ANGLE OF 60 DEGREES

(A)MACH = 1.40

DATA SET	SYMBOL	CONFIGURATION DESCRIPTION	BETA	LAMBDA	RN/L
(ZAE012)	○	W1 FO B	0.000	60.000	6.000
(ZAE043)	△	W2 FO B	0.000	60.000	4.000
(ZAE067)	◇	W4 FO B	0.000	60.000	6.000

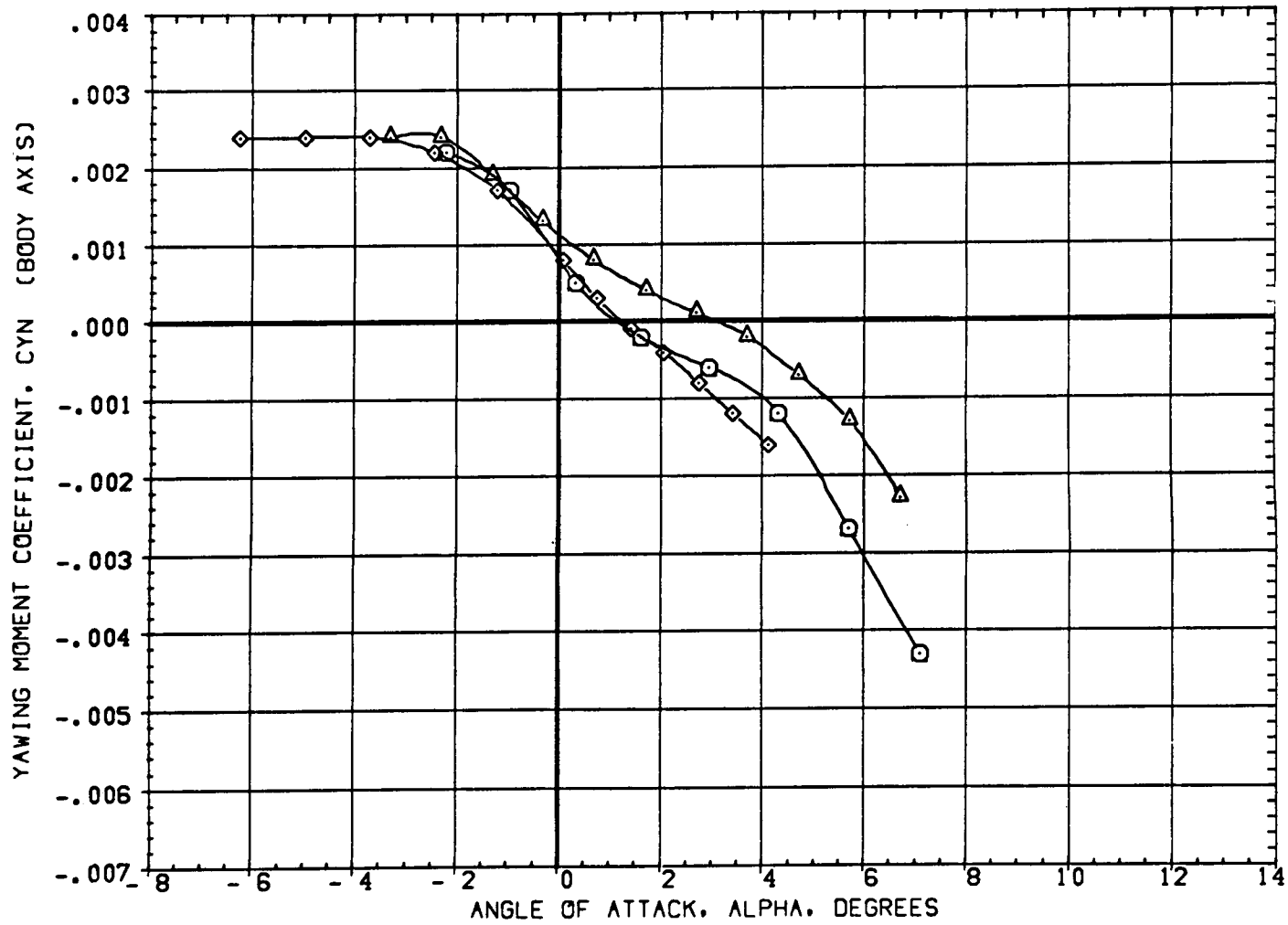

FIGURE 7 EFFECT OF WING AIRFOIL SECTION FOR AN OBLIQUE WING ANGLE OF 60 DEGREES

(A)MACH = 1.40

DATA SET	SYMBOL	CONFIGURATION DESCRIPTION	BETA	LAMBDA	RN/L
(ZAE012)	○	W1 F0 B	0.000	60.000	6.000
(ZAE043)	△	W2 F0 B	0.000	60.000	4.000
(ZAE067)	◇	W4 F0 B	0.000	60.000	6.000

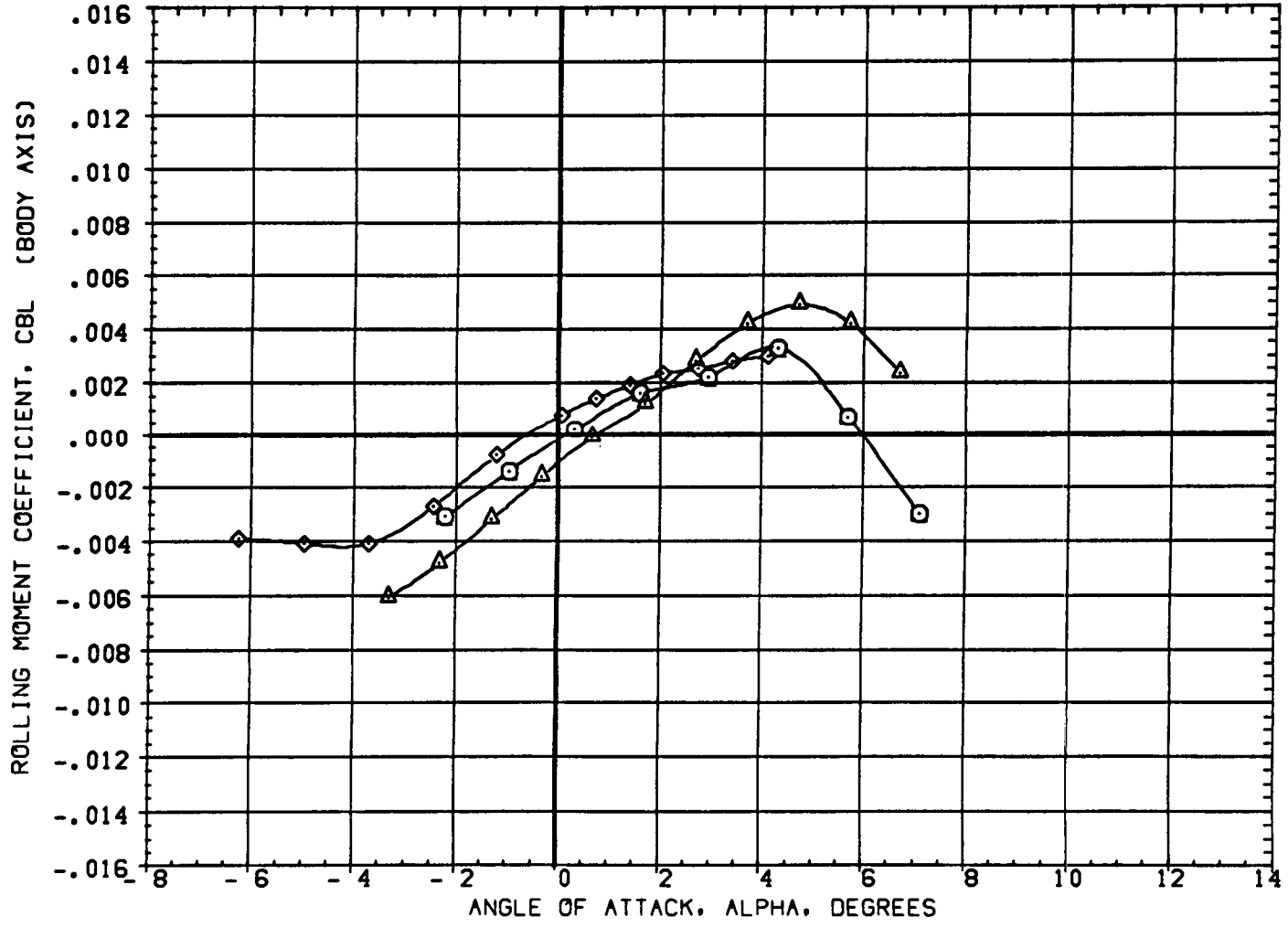

FIGURE 7 EFFECT OF WING AIRFOIL SECTION FOR AN OBLIQUE WING ANGLE OF 60 DEGREES

(A)MACH = 1.40

DATA SET	SYMBOL	CONFIGURATION DESCRIPTION	BETA	LAMBDA	RN/L
(ZAE012)	○	W1 FO B	0.000	60.000	6.000
(ZAE043)	△	W2 FO B	0.000	60.000	4.000
(ZAE067)	◇	W4 FO B	0.000	60.000	6.000

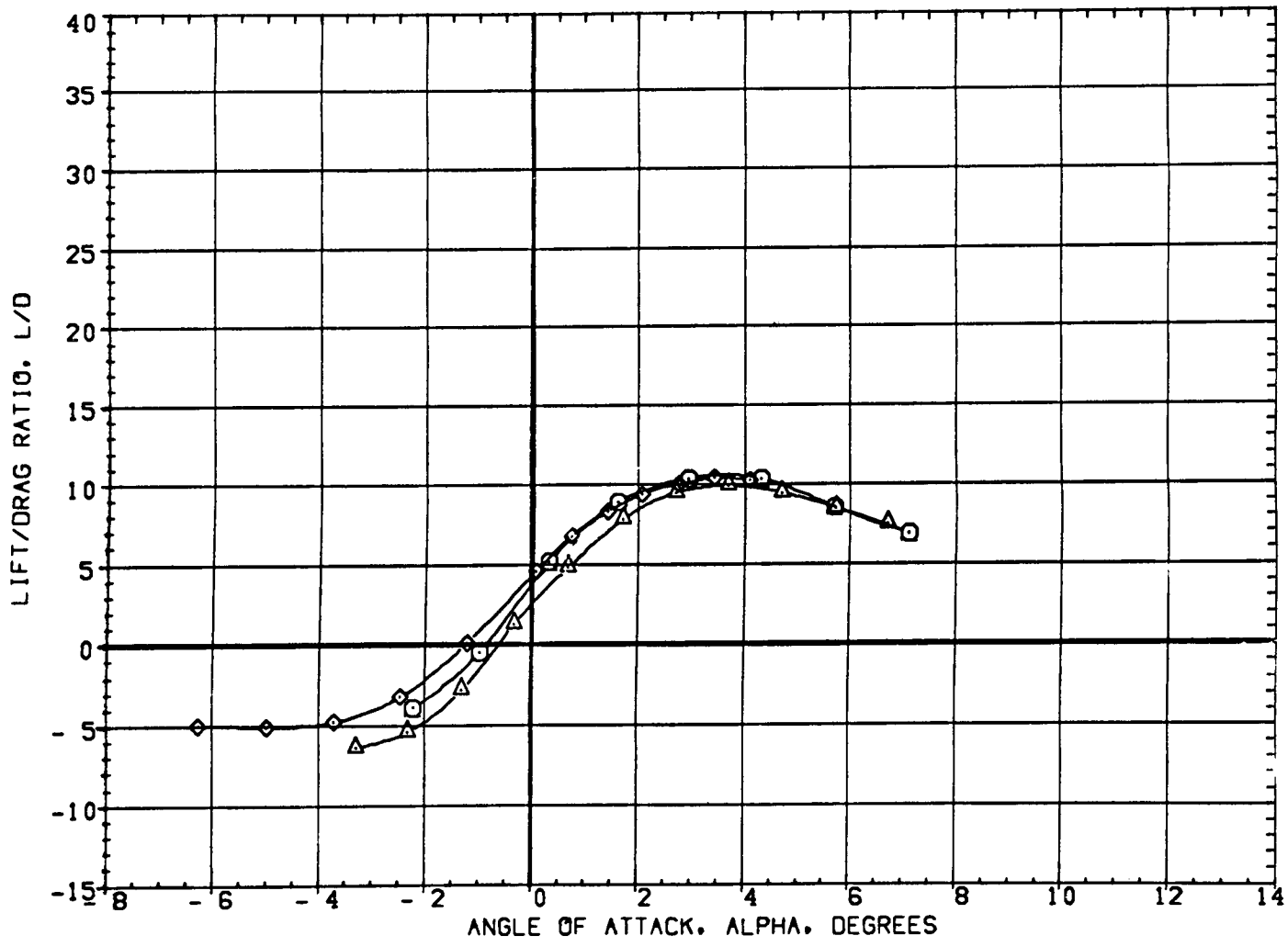

FIGURE 7 EFFECT OF WING AIRFOIL SECTION FOR AN OBLIQUE WING ANGLE OF 60 DEGREES

(A)MACH = 1.40

TRANSONIC TRANSPORT WINGS–OBLIQUE OR SWEPT?

Robert T. Jones

Ames Research Center

and

John W. Nisbet

Boeing Commercial Airplane Company

January 1974

Jones, R. T. and Nisbet, J. W., "Transonic Transport Wings — Oblique or Swept?"
Astronautics and Aeronautics, vol. 12, no. 1, Jan. 1974, pp. 40-47.
© 1974.
Reprinted by permission of the American Institute of Aeronatuics and Astronautics, New York, N.Y.

Transonic Transport Wings—Oblique or Swept?

By **ROBERT T. JONES**
NASA Ames Research Center
and
JAMES W. NISBET
Boeing Commercial Airplane Co.

In terms of gross weight, fuel consumption, and aircraft noise, an oblique-wing aircraft looks best, and it shows acceptable aeroelastic stability; but its design characteristics and economic implications need further study

In transonic-aircraft design, one naturally thinks of highly swept arrow or delta-wing shapes. An article in the December 1972 *A/A*, however, proposed a radically different wing form for such aircraft[1]: a conventional unswept subsonic wing that can be turned to different oblique angles for different flight speeds. Tests in the 11-ft supersonic wind tunnel at NASA Ames Research Center confirmed the superior aerodynamic efficiency of the oblique wing.

While it seems clear that the oblique wing can generate higher lift-to-drag ratios in the transonic speed range, it is not clear that such an unusual arrangement could be successfully adapted to a real airplane. Factors such as increased structure weight, aeroelastic instability, or other configurational considerations might nullify a purely aerodynamic advantage.

To answer such practical questions, a comparative study of transonic and low-supersonic transport aircraft was undertaken by the Boeing Commercial Airplane Co. under NASA contract. The study covered five different wing designs (see the sketches in F-1 at right).

1. Swept wing; fixed geometry.
2. Swept wing; variable sweep.
3. Fixed delta wing.
4. Oblique wing with two bodies.[2]
5. Oblique wing with single body.

The study covered aerodynamic and engine performance analysis, preliminary structural calculations and weight estimates, and dynamic-stability and aeroelastic-stability analysis, as well as configurational work. (Aerodynamic and performance considerations: R. M. Kulfan, E. C. Noble, J. R. Stalter, and J. K. Murakami. Propulsion and noise characteristics: defined by M. B. Sussman. Weight and balance estimates: J. P. McBarron. Flight stability of the unsymmetrical configurations: A. R. Mullally. Structural and aeroelasticity studies: J. W. Nisbet and D. W. Gimmestad. The general arrangements were worked out by F. D. Neumann.)

It was found that the assigned flight mission could be performed by any one of the five design concepts, although airplane size and weight varied considerably.

ROBERT T. JONES (F), (far left), a senior staff scientist at NASA-Ames, played a major part in raising the speed of aircraft through developing theory for swept and slender delta wings. In 1946 the AIAA gave him its Sylvanus Albert Reed Award. He has been with NACA and NASA since 1934, except for seven years with the AVCO Everett Research Laboratory, where he directed work on cardiac-assist devices. Besides aerodynamics, he has maintained a professional interest in optics. **JAMES W. NISBET**, during 13 years at Boeing, has worked on nearly all of the current jet airplanes as well as in preliminary design and research. Currently responsible for aeroelastic loads in airplane exploratory design, he has long been involved in analysis, wind-tunnel testing, and airplane testing regarding aeroelasticity and structural dynamics. Before joining Boeing, he spent four years with Canadian Westinghouse on the design of electrical system controls.

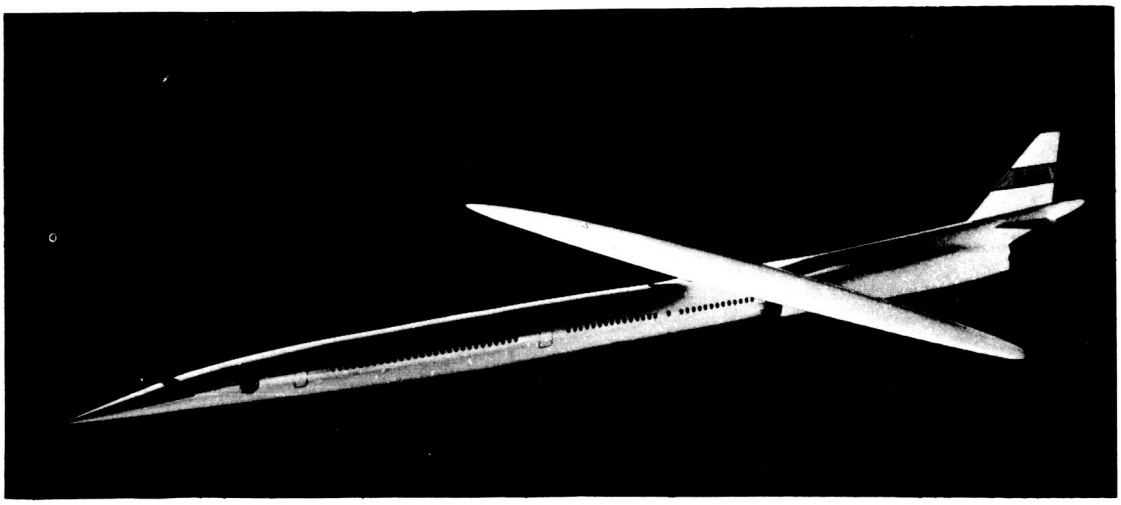

F-1 CONFIGURATION CONCEPTS

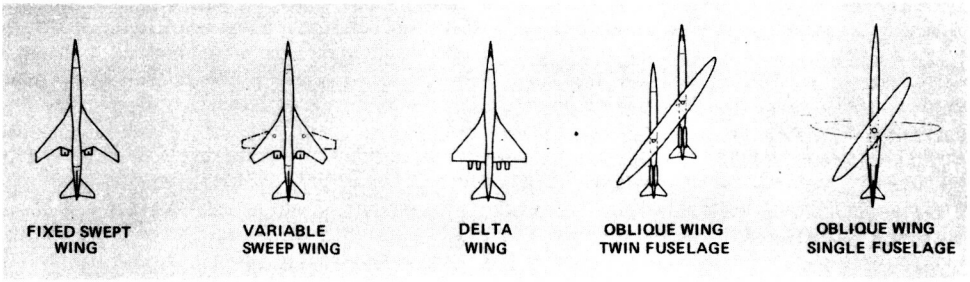

Complete results and the assumptions employed in the study are contained in NASA CR 114658.[3] This article emphasizes certain results characterizing oblique-wing designs.

Each airplane was designed to carry 195 passengers 3000 n. mi. at a speed near the sonic ground speed. Operation just below sonic ground speed eliminates the sonic boom associated with overland supersonic flight. As shown in F-2 (from Ref. 4) the shock fronts curve slightly as they progress to lower altitude. This curvature, caused by the change in speed of sound with temperature, establishes the maximum speed at which a transonic transport can fly without producing a boom at ground level. When the shock front becomes vertical the boom does not extend to the ground; this would permit boom-free flight at speeds nearly 50% greater than subsonic jets make today—*a saving of some 2 hr on east-to-west and 1 hr on west-to-east transcontinental U.S. flights.*

The aerodynamic characteristics of all five configurations were developed using similar procedures. The planform parameters were selected to exploit the aerodynamic benefits of each concept. The wing thickness distributions were derived from past weight-drag tradeoff studies on transonic transports. The camber and twist distributions were developed by linear theory. The body designs for all configurations were area-ruled to yield minimum cruise drag. The nacelle shape and location was strongly influenced by the engine size and the configurational arrangement.

Engine performance, size, and weight characteristics were consistent with the results of the Advanced Transport Technology (ATT) study.[5] Engine selection was based on an engine-bypass-ratio tradeoff study. The penalty of reducing the jet noise by increasing bypass ratio was compared to the penalty associated with jet suppression of lower-bypass-ratio installations. A bypass-ratio-of-1 engine with jet suppression was selected for all configurations as the most efficient means of achieving low noise levels.

The swept-wing, variable-sweep wing, and delta-wing configurations had the advantage of considerable previous study; and it seems probable that the arrangement of landing gear, engine, etc. was near the optimum in those cases.

The oblique-winged aircraft introduced some new problems, and considerable effort was devoted to finding a good general arrangement. The emphasis was on the engine and landing-gear placement. There was considerable flexibility in locating the landing gear because takeoff rotation and high-angle landing flare were not required. F-3 shows the arrangement adopted in the final stage of the study.

A balance and loading analysis of the oblique-wing configuration indicated the need for a center-of-gravity range of 25% MAC (mean aerodynamic

F-2 AVOIDING SONIC BOOM

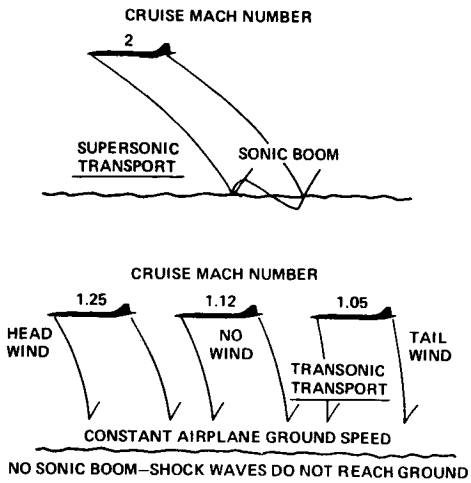

chord). Forward body ballast was required for low payloads. Selective fuel management with an aft body fuel tank allowed minimizing cruise trim-drag.

Control, trim, and aerodynamic stability characteristics were evaluated with the wing in the oblique position. Aerodynamic coupling between the longitudinal and lateral motions does exist and was considered. The effect of wing flexibility on this coupling is currently being evaluated. It appears that the flight characteristics do not present any insurmountable problems, although modified control techniques will be required.

Structural weight of the oblique wing received considerable attention because of the concern over aeroelastic stability. This phase of the study will be presented in some detail because of its potential impact on oblique-wing performance and because of the unique oblique-wing aeroelastics.

Wind-tunnel results given last January in *A/A* represented an elliptic wing having an aspect ratio of 12.7 (10:1 ellipse) with airfoil sections of 10% thickness/chord ratio.[1] The beam slenderness ratio (length/max thickness) in that case ran 50 to 1, whereas 17 to 1 might typify current transport aircraft. It was discovered rather early in the studies reported here that such proportions would lead to excessive structural weight. Reducing the aspect ratio to 10.2 (8:1 ellipse) and increasing the wing root thickness to 12% improved the situation considerably, and for the remainder of the studies these proportions characterized the oblique wing.

Structural materials were selected for all configurations based on the Advanced Transport Technology (ATT) study results.[5] F-4 identifies the materials selected for the single-fuselage oblique-wing configuration and gives an estimate of the percent weight savings of the advanced materials relative to conventional aluminum skin-stringer construction.

Graphite-epoxy honeycomb was selected for the wing, fuselage, and vertical-tail primary structure. Titanium was selected for the wing pivots and pivot-support structure. For configurations other than the oblique wing, the primary wing-structure weightsaving was estimated to be 25%. Primary-structure weight savings for the oblique wing was determined by analysis of both an aluminum and a graphite-epoxy structure. The aluminum oblique wing was stiffness- rather than strength-critical; the graphite-epoxy oblique wing was strength-critical. This resulted in a weightsaving of 35% for the advanced material as compared to aluminum.

Structural analysis of the graphite-epoxy oblique wing involved these conditions:

A ply arrangement—considering external load distributions and the bending stiffness required for aeroelastic stability.

Isotropic structural parameters (such as ultimate strength and stiffness modulus) simulating the anisotropic ply arrangement.

An estimated compression-buckling curve for built up panels.

Allowables and stiffness moduli were determined from material data in the Air Force Advanced Composites Design Guide.[6] High-modulus graphite was used. Fiber orientations were selected to enhance wing-bending strength and stiffness, while retaining adequate strength in the other directions. Ply orientation in the graphite-epoxy face sheets was 60% (0°), 30% (±45°) and 10% (90°). An allowance of 15% for aluminum and 25% for graphite-epoxy was added to the wing's primary structural weight to account for fittings, fasteners, and joints.

In F-5 you see a conceptual design (cross section) for the oblique-wing pivot. It differs significantly from a variable-sweep wing pivot. A variable-sweep wing pivot must transfer wing-bending moments through the pivot bearings. This was avoided on the oblique-wing pivot by placing the bearings below the wing and maintaining continuous upper and lower wing-surfaces to transfer the bending moments. In addition, the pivot diameter was made as large as possible to keep the bearing loads low. Vertical loads, rolling moments, and pitching moments were transferred through the bearings on the circumference of the pivot. Drag loads and side loads were transferred through bearings on the pin in the middle of the pivot. Systems going from the body to the wing were routed through the center of the pivot.

As is well known, swept-forward wings show a

tendency for aeroelastic divergence. Bending of a swept-forward wing panel creates an aerodynamic force which acts to increase the deflection in opposition to the structural stiffness. At a sufficiently high flight speed or dynamic pressure the aerodynamic destabilizing force can overpower the structural stiffness, leading to aeroelastic divergence.

The behavior of the oblique wing differs from the bilaterally symmetric swept-forward wing's: the coupled rolling motion exerts a *stabilizing influence.* Aeroelastic instability of the oblique wing occurs as an oscillatory instability; there is a progressive lengthening of the period and loss of damping of the elastic bending oscillations of the wing combined with rolling motion.

F-6 illustrates the dynamic model used to study the aeroelastic stability of the oblique wing. The wing mass was represented by a series of point masses. The aerodynamic lift distribution was represented by a section lift coefficient for each of the wing panels. Wing flexibility was represented by beam bending and beam torsion, although it was found in the analysis that torsional stiffness had little effect on the stability of a wing with an oblique angle of 45 deg. Airplane roll was treated as a separate degree of freedom in the analysis.

F-7 shows the results of the analysis of a wing with an aspect ratio of 12.7 (10:1 ellipse) designed for strength alone. For comparison, it also shows stability with the fuselage clamped to prevent rolling (as in a wind-tunnel test). At zero flight speed (or, equivalently, zero dynamic pressure) the frequency of the unrestrained airplane as well as both wings of the restrained airplane was 0.93 Hertz. As the speed was increased, the damping ratio initially increased.

With the fuselage clamped, the frequency of the forward wing decreased while the frequency of the aft wing increased. The damping ratio of the forward wing decreased rapidly at higher speeds. (The so-called "static" divergence speed is the speed at which both the frequency and damping ratio become zero.)

F-3 OBLIQUE-WING AIRPLANE

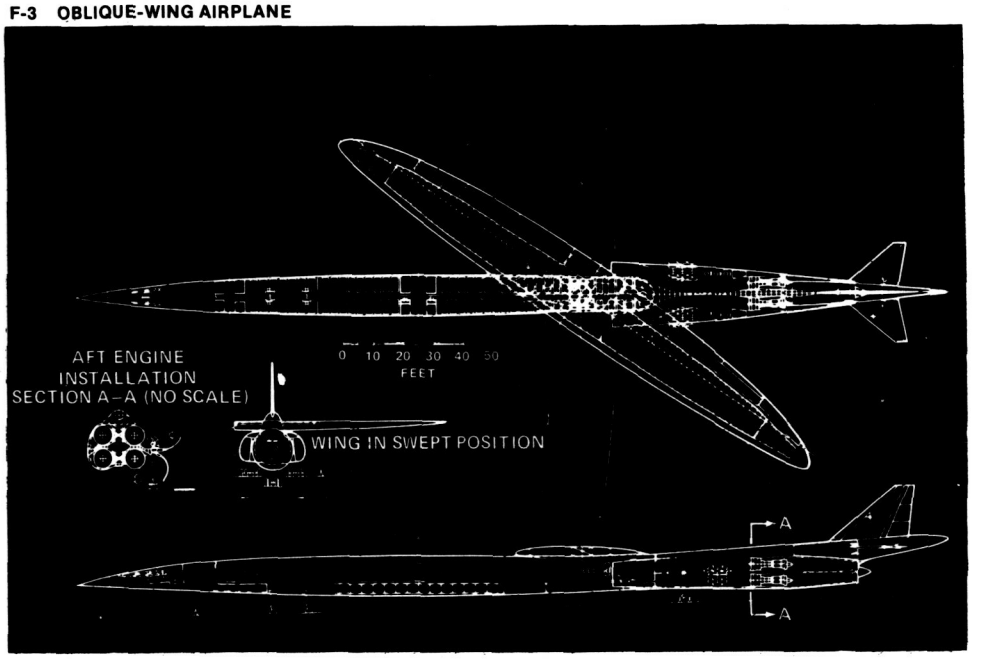

F-4 MATERIALS SELECTION FOR AN ADVANCED-TECHNOLOGY OBLIQUE-WING AIRCRAFT

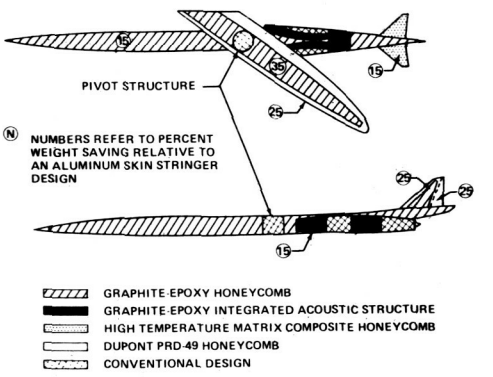

F-5 STRUCTURAL ARRANGEMENT OF OBLIQUE-WING PIVOT

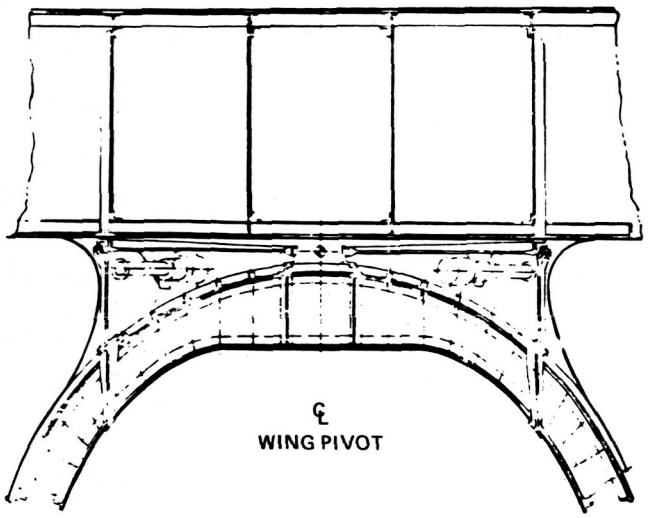

OBLIQUE WING PIVOT CONCEPT

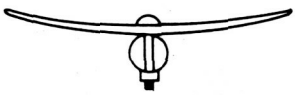

VARIABLE SWEEP WING PIVOT CONCEPT

The unrestrained airplane did not exhibit this static instability. As speed was increased, the frequency decreased and the bending deflection of the forward wing increased relative to the aft wing. The wing-bending deflections introduced roll participation into the oscillation. The oscillatory aeroelastic instability occurred at a higher speed than the speed at which the clamped fuselage static instability occurred.

Analyses of aeroelastic behavior which assume that the fuselage is clamped at the wing root appear to be conservative for most oblique-wing configurations. The aspect-ratio-12.7 oblique wing designed for strength alone became unstable at about 90% of the airplane's speed. FAA criteria require stability up to 120% of the design speed. It is evident that a wing of this high an aspect ratio would require considerable additional structure for stiffness.

Reducing the aspect ratio to 10.2 (8:1 ellipse) improved this situation considerably. F-8 compares the stability of *strength*-designed aluminum and graphite-epoxy wings of aspect ratio 10.2. The aluminum wing designed for strength alone still did not satisfy the requirement for aeroelastic stability; it would have to be stiffened with more material to improve the stability. On the other hand, the graphite-epoxy wing designed for strength alone had adequate stability.

The advantage of using graphite-epoxy rather than aluminum for construction of an oblique wing, and the importance of aspect ratio, can be seen in F-9. A graphite-epoxy wing satisfying only the strength requirements offers about 20% weight advantage. Considering the aeroelastic stability indicated, the graphite-epoxy should have an even greater advantage over aluminum. Reducing the aspect ratio of the wing gave lower weight and improved stability. These results, however, should not be considered as the last word since only an elliptic planform was included in this study.

F-6 STABILITY - ANALYSIS MODEL

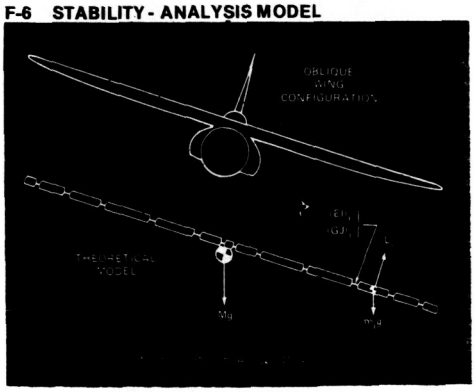

Astronautics & Aeronautics

F-7 ELASTIC STABILITY: ASPECT-RATIO-12.7 OBLIQUE WING

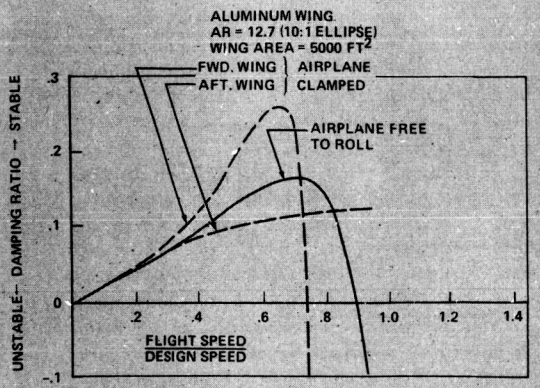

NOTE: MINIMUM SPEED REQUIRED FOR STABILITY IS 1.2 TIMES THE DESIGN SPEED

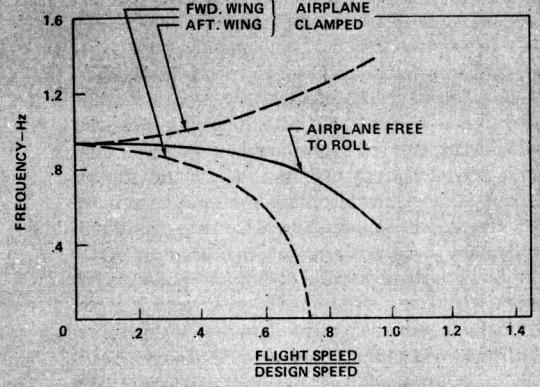

F-8 ELASTIC STABILITY: ASPECT-RATIO-10.2 OBLIQUE WING

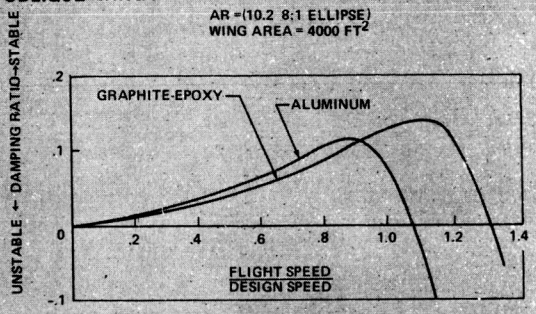

NOTE: MINIMUM SPEED REQUIRED FOR STABILITY IS 1.2 TIMES THE DESIGN SPEED

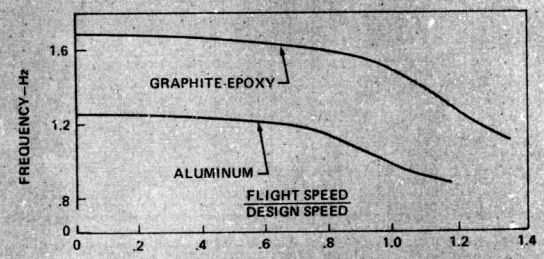

F-9 WEIGHT EFFECT OF ASPECT RATIO AND STRUCTURAL MATERIALS ON OBLIQUE WING

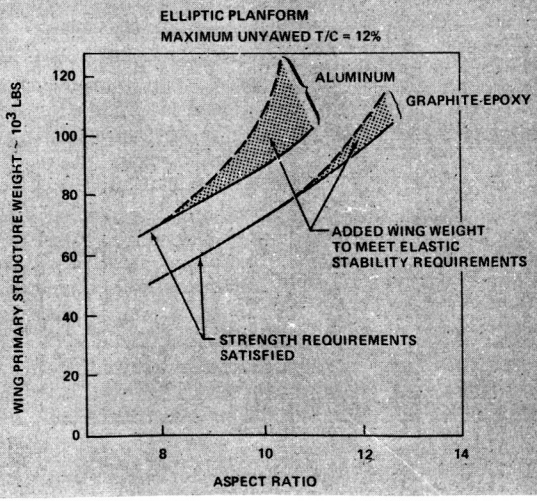

F-10 GROSS-WEIGHT SUMMARY

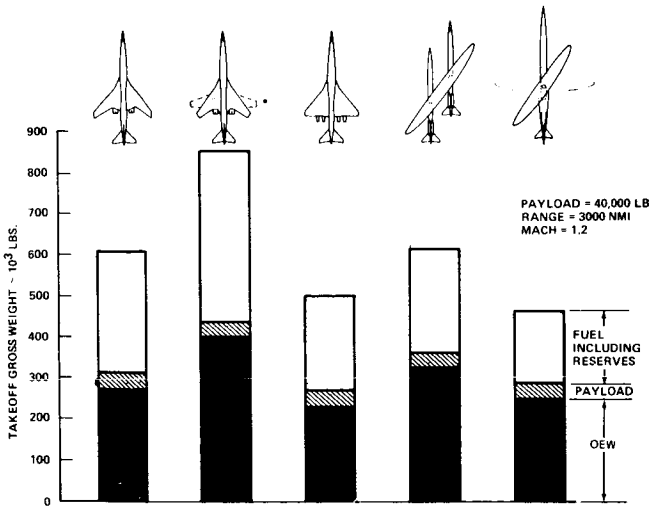

F-11 WEIGHT COMPARISON

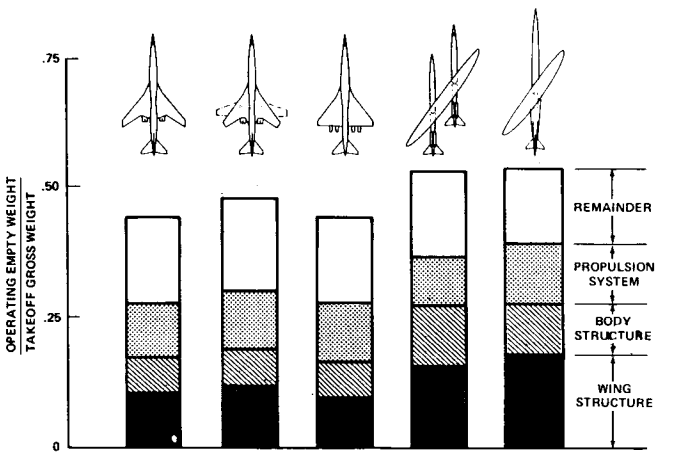

F-12 CRUISE-DRAG COMPARISON

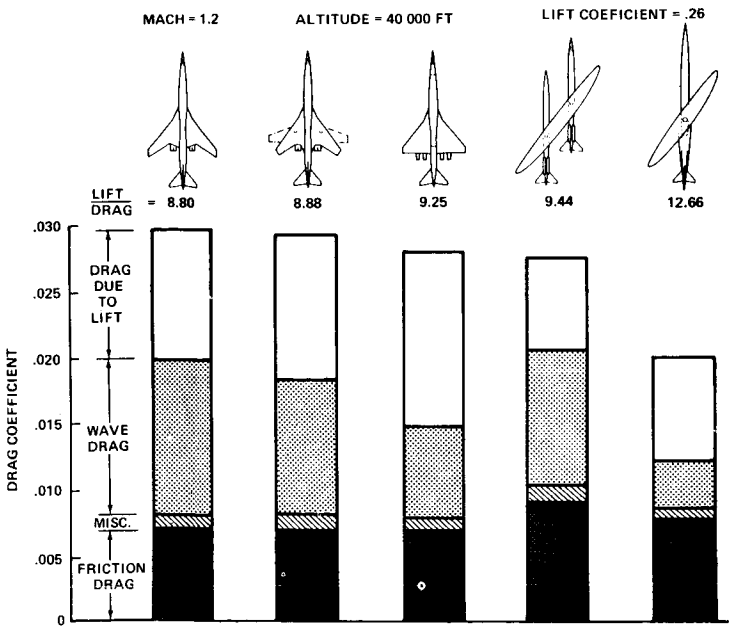

Further planform studies considering the distribution of mass and stiffness as well as the aerodynamic characteristics of the wing would seem to be most important.

Minimum gross weight (F-10) required to perform the 3000-n. mi. mission was determined for airplanes based on the five configurational concepts in this study. Additional work established the gross weight penalty for noise reduction.

Substantially lower gross weights were required for the delta-wing and single-body, oblique-wing configurations than for any of the others. The delta-wing configuration had the advantage of a low structural weight and thus a low operating empty weight, as shown in F-11. The single-body, oblique-wing airplane (F-10) had a smaller gross weight because of its lesser fuel requirements. It is interesting to note that the structural weight penalty of the oblique wing was not primarily associated with the peculiar features of the design nor the variable geometry, but rather it was the result of the basic strength requirements of a high-aspect-ratio wing.

The single-body oblique wing has the advantage in aerodynamic efficiency, as shown by the cruise-drag comparison in F-12. The effect of the higher aspect ratio in reducing drag due to lift is quite evident for the oblique-wing configurations. Another major difference in drag of the configurations was found to be the wave drag due to volume. The double-pod installation was primarily responsible for the high wave drag on the fixed- and variable-sweep-wing configurations. The low wave drag of the single-body oblique wing reflects the integrated body-nacelle arrangement and the inherent characteristics of the oblique wing.[2]

F-13 describes the impact on takeoff gross weight of achieving lower noise levels by engine-nacelle treatment. The takeoff-gross-weight increase reflects weight added for acoustical treatment and the associated engine-performance losses. Only the oblique-wing configurations could achieve a noise level of FAR 36 minus 15 EPNdB.

This technically orientated study has yielded, we believe, a realistic performance comparison of the five wing-planform concepts and gives insight into areas unique to the oblique-wing configuration. The oblique wing offers desirable performance, but further analysis and wind-tunnel work will be needed to develop a rounded picture of its potential. In particular, future work should include an economic evaluation of the consequences of oblique wing's ability to increase today's cruise speeds 50%.

In terms of the transonic concepts it covers, the most significant conclusions of this study might be summarized as follows:

F-13 IMPACT OF NOISE TREATMENT ON TAKEOFF GROSS-WEIGHT

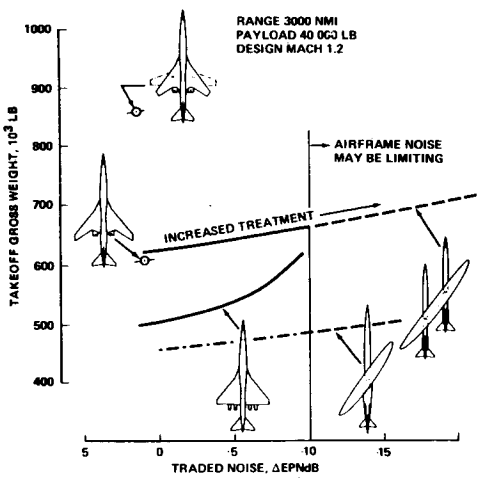

1. The oblique-wing airplane had the smallest gross weight and the lowest fuel consumption.
2. Only the oblique-wing airplane could achieve a noise level of FAR 36 minus 15 EPNdB.
3. The oblique wing is aeroelastically less stable than a sweptback wing but more stable than a swept-forward wing. For the designs considered, an aluminum oblique wing would require a moderate amount of additional stiffness to meet stability requirements. For graphite-epoxy no additional stiffness would be required.
4. Further development studies supported by wind-tunnel tests will be needed to develop the full potential of the oblique-wing concept. This should be followed by an economic evaluation treating productivity.

References

1. Jones, R. T., "New Design Goals and a New Shape for the SST," *Astronautics & Aeronautics*, Vol. 10, No. 12, Dec. 1972, pp. 66-70.
2. Jones, R. T., "Reduction of Wave Drag by Antisymmetric Arrangement of Wings and Bodies," *Astronautics & Aeronautics*, Vol. 10, No. 2, Feb. 1972, pp. 171-176.
3. Kulfan, Robert M., et al., "High Transonic Speed Transport Aircraft Study," NASA CR-114658, Sept. 1973.
4. Goodmanson, Lloyd T., "Transonic Transports," *Astronautics & Aeronautics*. Vol. 9, No. 11, Nov. 1971, pp. 46-56.
5. NASA Contracts NAS1-1071, NAS1-1072, NAS1-1073, "Study of the Application of Advanced Technologies to Long-Range Transport Aircraft".
6. "Advanced Composites Design Guide," Advanced Composites Division, Air Force Material Laboratory, Air Force Systems Command, Wright-Patterson Air Force Base, Ohio, Nov. 1971. ■

AIRCRAFT DESIGN FOR FLIGHT BELOW THE SONIC BOOM SPEED LIMIT

Robert T. Jones

April 1974

Jones, R. T., "Aircraft Design for Flight Below the Sonic Boom Speed Limit,"
Canadian Aeronautics and Space Journal, vol. 20, no. 5, May 1974,
pp. 225-230.
Reprinted by permission of the Canadian Aeronautics and Space Institute,
Ottawa, Can.

Reprinted in Canada from CANADIAN AERONAUTICS AND SPACE JOURNAL

AIRCRAFT DESIGN FOR FLIGHT BELOW THE SONIC BOOM SPEED LIMIT†

by Dr. R.T. Jones*

NASA Ames Research Center

SUMMARY

The avoidance of sonic booms places a constraint on aircraft design and can lead to unusual new configurations. From a comparison among several candidate designs, it is shown that an oblique winged aircraft offers many advantages when structure, stability, flight efficiency, and airport noise are considered jointly.

To avoid the sonic boom, overland flights must be limited to a subsonic ground speed, i.e. approximately 1200 km per hour. Since the speed of sound at low levels is normally 160 km/hr faster than it is at flight altitudes the airplane must fly supersonically in its own medium in order to reach this overland speed limit. Under standard conditions the flight Mach number is about 1.15. However, the flight speed for constant ground speed varies considerably with meteorological conditions.

With a strong headwind aloft and a high temperature at ground level the aircraft Mach number may be as high as 1.3. Under these conditions the waves made by the airplane are refracted by wind and temperature gradients, become vertical and disappear before reaching the ground (Figure 1). Under other (exceptional) conditions even a subsonic airplane might produce a sonic boom. Flying down wind in a fast jet stream the lifting pressure may be transmitted to a region where the relative velocity is supersonic.

More complete analyses of flight conditions and schedules at the sonic boom speed limit will be found in References (1) and (2). It appears that east to west flights across the US could be shortened by two hours and west to east flights by about one hour. Flight at constant ground speed, of course, tends to equalize schedules in all directions.

An airplane designed for such service should be capable of efficient flight at various speeds from subsonic to supersonic. Unfortunately, flight at supersonic speed entails some loss of aerodynamic efficiency. However, the loss at transonic and low supersonic speeds need not be as great as the loss at higher supersonic speeds. It seems possible that the increased utilization of the aircraft and the time saving for the passengers could make up for a moderate increase of energy consumption per mile of flight.

The specific range R_{sp} of an airplane in payload pound-miles per pound of fuel (or kilogram-kilometers per kilogram) is given by

$$R_{sp} = R_o \times \eta \times L/D \times \frac{W_{payload}}{W_{airplane}}$$

Here R_o is the specific range corresponding to the thermal energy content of the fuel — about 2700 miles or 4400 kilometers for kerosene (i.e. one kilogram of kerosene contains enough energy to exert a force of one kilogram for a distance of 4400 kilometers). L/D is the aerodynamic lift to drag ratio of the airplane, typically 15 to 20 or higher in the subsonic range (below M = 0.8) and 7 to 10 in the supersonic range. η is the conversion efficiency of thermal energy to thrust. With the development of the fan jet engine it has become possible to obtain a conversion efficiency η of 40 percent or more over a wide range of speeds — subsonic or supersonic.

The quantities displayed in the formula are not, of course, independent. Thus, a loss in aerodynamic L/D such as occurs at supersonic speed will call for a greater fuel load and hence a smaller ratio of payload to gross weight. Similarly, measures taken to increase the aerodynamic efficiency usually result in increased structure weight.

It is important to note that the basic equation for energy economy does not contain the flight speed directly but only indirectly as it may affect the L/D or other factors. By adjust-

†Presented at the Quarter Century Symposium, University of Toronto, on the 1st April, 1974.

*Senior Scientist

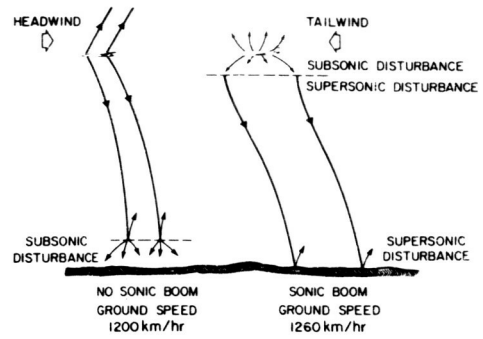

Figure 1

Flight below sonic boom speed limits

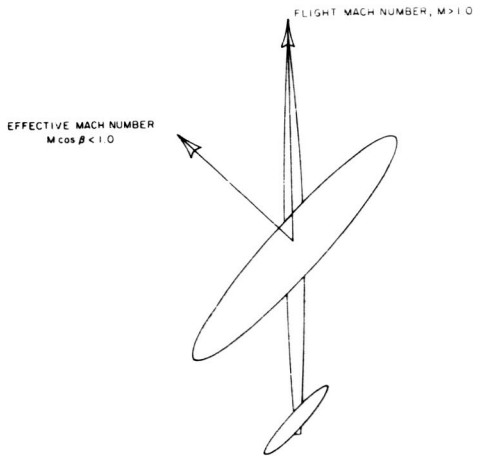

Figure 2

Reduction of effective mach number by oblique motion

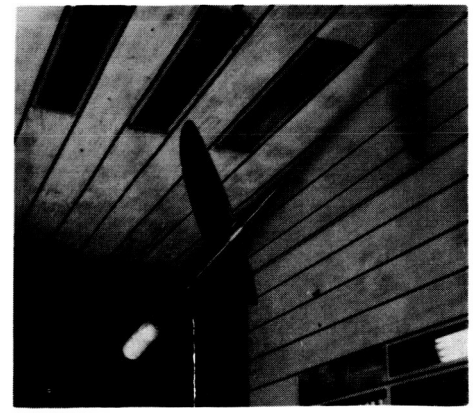

Figure 3

Oblique wing model in Ames 11-ft. tunnel

ment of altitude and wing loading the subsonic airplane can maintain its high lift to drag ratio at any speed up to about M = 0.8. Hence, contrary to a popular opinion, the subsonic airplane does not have to pay for its speed in terms of miles per gallon. Following the above relations, current subsonic jets could get 60 or more passenger miles per gallon, though they have often operated profitably in the range 20 to 30 PMPG. At transonic and low supersonic speeds it appears that with suitable design one could at least equal or exceed the latter figure.

The loss of lift/drag ratio begins at M = 0.7 or 0.8. To minimize the loss at higher speeds we must ask what wing shape can give the highest lift to drag ratio at transonic and supersonic speeds? The surprising answer given by aerodynamic theory is that the narrow straight wing of high aspect ratio, ideal for low speed flight, already has the right shape for supersonic speeds provided it can be turned so as to move through the air obliquely.

With such a long narrow wing moving at an oblique angle it is permissible to divide the flight velocity into two components, one showing the air movement across the wing and the other along the length of the wing (Figure 2). The component of motion along the length of the wing has little effect and so the wing behaves as though it were flying at reduced speed, corresponding to the reduced component of the flight velocity in the direction perpendicular to the leading edge. By increasing the angle as the speed is increased the effective component velocity can be kept subsonic, even though the flight velocity is supersonic.

While the theoretical properties of the oblique wing have been known for many years References (3), (4), (5), it is only recently that we have obtained experimental verification of the theory in the 11-ft. supersonic wind tunnel at NASA Ames Research Center[6]. In these tests we employed rather conventional subsonic wings of quasi-elliptic planform, mounted on a slender body (Figure 3). By pivoting the wing on the body and setting it at different angles of yaw so that the component Mach number remained below 0.7 we were able to demonstrate lift-drag ratios higher than either the delta wing or the bilaterally symmetric swept back wing at all speeds between M = 0.6 and 1.4. Thus, at M = .98 and 45° yaw we obtained an L/D of 20 to 1. At M = 1.4, 60° of yaw was required and the L/D had fallen to 11 — about 10% greater than that of a comparable swept wing model. At still higher Mach numbers, the relative superiority of the oblique wing over more familiar shapes is expected to diminish further.

Figure 3a shows the maximum lift/drag ratios obtained in these tests. The wings were of quasi-elliptic planform having an aspect ratio of 12.7. The results for three different airfoil sections of 10 percent thickness are shown. Airfoil 1 is a conventional NACA "4-digit" shape having a critical Mach number of .7. Airfoil 2 is a newer type designed by Bauer Garabedian and Korn,[7] following the suggestion of R.T. Whitcomb. Airfoil 2 was designed for a Mach number of 0.8 and

maintained a lift/drag ratio of 31 at this Mach number with the wing unyawed. At 60° yaw and M = 1.2 to 1.4 the highly cambered section No. 3 was superior, however.

Subsequent studies have shown that the wings employed in these tests are somewhat too slender to satisfy the requirements of strength and aeroelastic stability. By reducing the aspect ratio to 10 and increasing the root thickness to 12% it appears that the requirements of strength and stability can be satisfied with a small loss of L/D.

The elliptic planform satisfies the condition for minimum drag (i.e. wave drag + vortex drag) when the overall dimensions of the wing are limited. A more appropriate auxiliary condition would be a limitation on the wing root bending moment[8]. The resulting planform and span loading is then somewhat more tapered than the elliptical. The potential gains in this direction are now being investigated.

The really significant advantage of the oblique wing lies in the ease with which the sweep angle can be varied to suit flight conditions. Thus, during landing, take-off or holding the wing should be straight and in this configuration the L/D ratio was approximately 30 to 1 — a value which could lead to a very low power requirement and thus minimize the unwanted display of energy in the airport environment.

Can an airplane with its wing at such an angle be stable or controllable in flight? A preliminary answer to this question was given many years ago by J.P. Campbell and Hubert M. Drake, who tested an oblique winged model in the NACA Langley Free Flight Tunnel in 1946[9]. Campbell and Drake found their model to be more stable against lateral oscillations than highly swept bilaterally symmetric models. Even though the ailerons on the oblique wing are in a position to produce large pitching moments, no pitching motion was observed in flight — the ailerons producing essentially pure roll. Stability and control were satisfactory up to wing angles of 50°. At 60°, however, ailerons became too weak for adequate control.

More recently the present writer with the assistance of Mr. Burnett L. Gadeburg of Ames Research Center has made experiments with larger (6 ft. span) radio-controlled models in free flight. In addition to the normal control channels the radio was equipped with an extra channel to permit variations of wing and horizontal tail angle in flight. Figure 4 shows one of the models in flight with the wing and tail at 45°. Yaw angles greater than 45° were not attempted because of the speed of the model (50 to 100 mph) and the difficulty of visual orientation. The results of the free flight tests may be summarized as follows:

• Changing the wing and horizontal tail angle from 0 to 45 in level flight resulted in no perceptible change in longitudinal trim and a barely perceptible change in lateral trim. The model nosed down and gained speed to compensate for the loss of lift due to yaw.

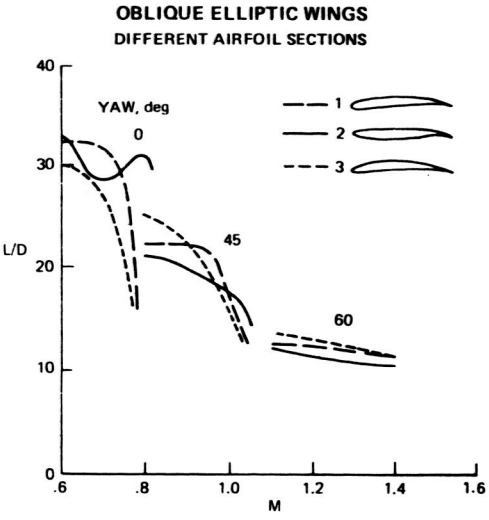

Figure 3a
Oblique elliptic wings – different airfoil sections

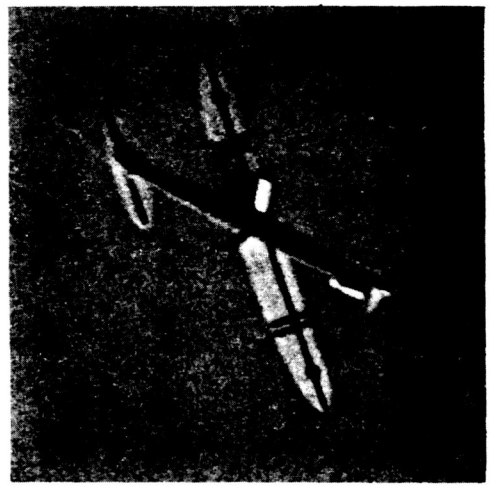

Figure 4
Radio controlled flight model

• Aileron rolls were performed with normal control movements and without appreciable coupled pitching motion — as observed by Campbell and Drake.

• Elevator control was accompanied by strongly coupled rolling motion. Use of the elevator tends to produce a rotation about the long axis of the wing — which is oblique — instead of about the normal pitch axis. Loops performed by pulling back the elevator took the form of a helix.

• The coupled rolling motion produced by the elevator results in differing behavior in right

MACH 1.2
PAYLOAD = 18 143 KG (40 000 LB)
RANGE = 5560 Km (3000 NMI)
INITIAL CRUISE ALTITUDE =
11,887 m (39,000 FT)
TAKE OFF FIELD LENGTH
3505 m (11 500 FT)
PERIPHERAL NOISE TREATMENT

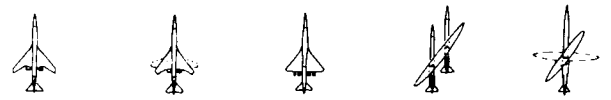

AIRPLANE CONFIGURATION	1-2a	2-2a	3-2a	4-2a	5-3a
TAKE OFF GROSS WEIGHT KG (LBS)	275283 (607000)	388283 (857000)	226796 (500000)	280726 (619000)	211828 (467000)
OPERATING EMPTY WEIGHT KG (LBS)	122626 (270500)	180726 (398500)	103855 (229000)	146804 (322600)	113832 (251000)
WING AREA m^2 (FT^2)	433.8 (4670)	612.2 (6590)	436.6 (4700)	442.2 (4760)	319.6 (3440)
ENGINE THRUST RATING					
SEA LEVEL STATIC N (LBS)	284241 (63900)	406123 (91300)	216184 (48600)	226859 (51000)	156113 (35100)
NUMBER OF ENGINES/BYPASS RATIO	4/1	4/1	4/1	4/1	4/1
THRUST LOADING (T/W)	0.42	0.43	0.39	0.33	0.30
WING LOADING (W/S) N/m^2 (LB/FT^2)	6224 (130)	6224 (130)	5075 (106)	6224 (130)	6512 (136)
L/D CRUISE	8.1	8.1	8.9	10.6	12.3
TAKE OFF FIELD LENGTH: MAX FLAPS m (FT)	2438 (8000)	1554 (5100)	3505 (11500)	2225 (7300)	2179 (7150)
REDUCED FLAPS m (FT)	3353 (11000)	2286 (7500)	3505 (11500)	3078 (10100)	2947 (9670)
L/D COMMUNITY: REDUCED FLAPS	8.8	9.2	6.3	22	6.9
APPROACH SPEED: REDUCED FLAPS Km/HR (KT)	333 (180)	296 (160)	317 (171)	261 (141)	254.5 (137.4)
COMMUNITY NOISE Δ EPNdB FROM FAR PART 36					
● TAKE OFF WITH THRUST CUTBACK AT NOISE STATION	-6.0	-10.2	+1.8	-15.0	-0.4
● SIDE LINE	+3.0	+ 3.5	+3.4	+ 3.1	+2.0
● APPROACH	-0.7	- 1.9	-0.5	- 2.8	-2.0
● TRADED	+1.0	+ 1.5	+1.4	+ 1.1	0.

Figure 5
Aircraft characteristics and performance

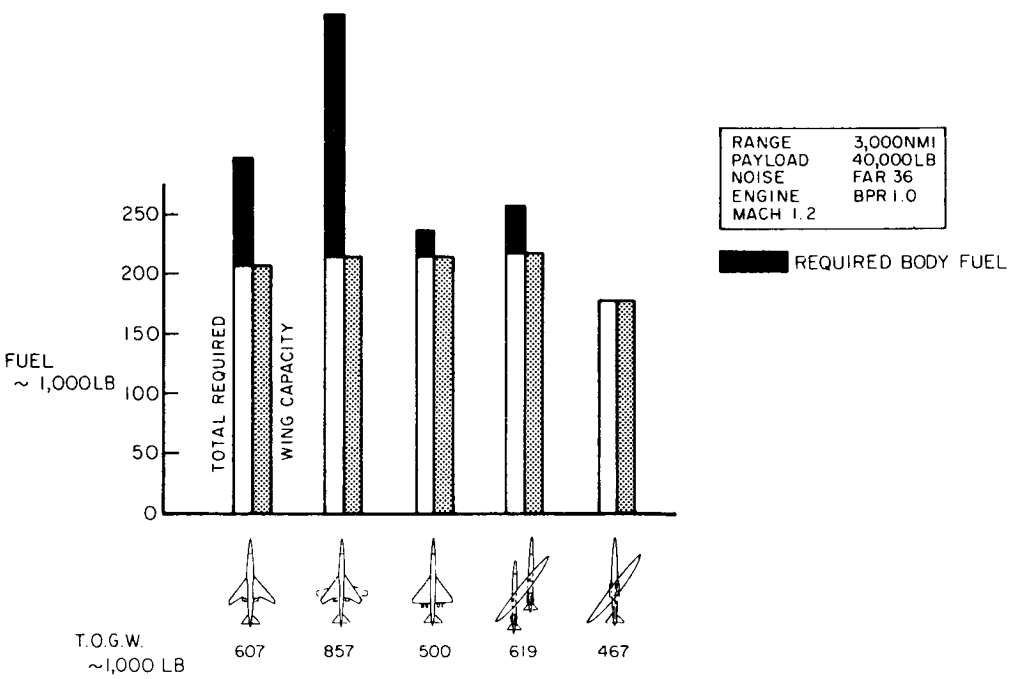

Figure 5a
Fuel volume comparison

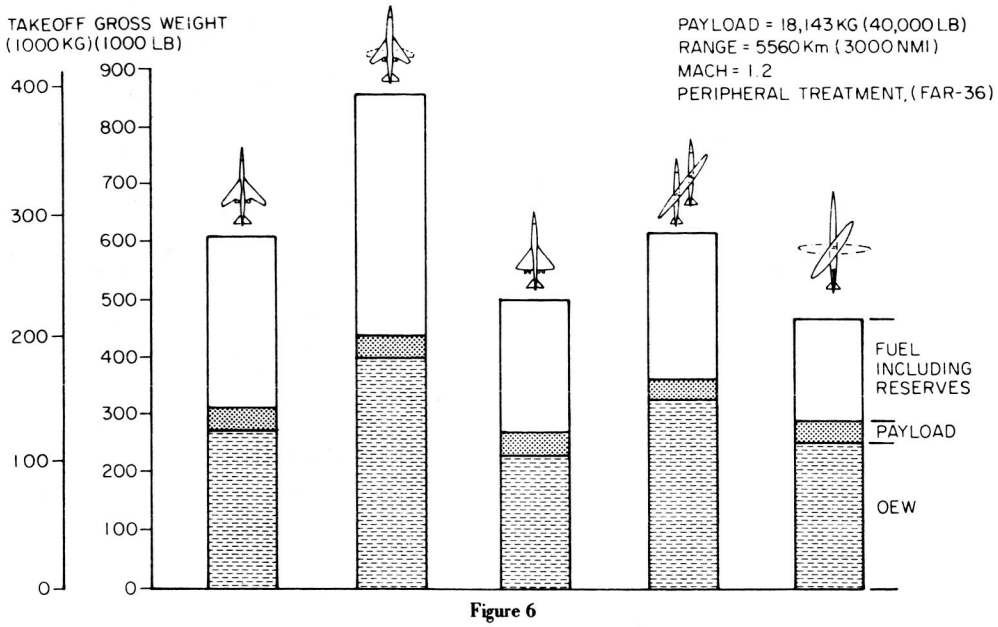

Figure 6

Boeing estimate of gross weights for the five designs

and left turns. Thus, in turning toward the forward wing tip, use of the elevator tends to steepen the bank; for turns in the opposite direction the elevator has the opposite effect.

• While unusual control effects were prominent in rapid manoeuvres they were not noticeable in the use of controls to maintain steady level flight. Hence, the lack of bilateral symmetry though interesting theoretically, may not be important for high altitude cruising flight where oblique wing angles would be used.

Following our experiments at Ames Research Center the Boeing Commercial Aircraft Company has made, under NASA contract, a comparative design study of transonic transport aircraft intended to operate at speeds below the sonic boom cut-off speed. One of the objectives of the study was to determine whether the apparent advantages of the pivoted wing might be realized in a practical airplane.

The study included consideration of four different wing designs (Figure 5); (1) sweptback wing with fixed geometry, (2) sweptback wing with variable geometry, (3) fixed delta wing and (4) pivoted oblique wings. Details and results of the Boeing study will be found in Reference (8).

Prominent in the Boeing analysis were considerations of structural design and weight, including the use of newer composite materials. The oblique wing designs required a new analysis of aeroelastic stability as well as the design of a suitable pivoting structure.

Each airplane was sized to carry 195 passengers for 3000 nautical miles at a flight Mach number of 1.2. It was found that this mission could be performed by any one of the five designs but the gross weight and size of the airplane needed varied considerably. A fuel volume comparison for these configurations is made in Figure 5a. Figure 6 shows the Boeing estimate of gross weights for the five designs. It is seen that the swept back wing with variable sweep required the highest gross weight for the mission, while the oblique winged design had the lowest. Varying the sweep in bilaterally symmetric fashion imposes severe requirements of mechanical strength, leading to excessive weight of the wing pivot structure. In the oblique design the wing structure is continuous across the pivot and very little additional weight is introduced by the pivot structure. The analysis did show, however, that the oblique wing would be rather heavy, primarily because of its high aspect ratio. Of all the designs the delta wing configuration gave the smallest empty weight. The oblique-winged airplane had a smaller take-off weight, however, because of its lower fuel consumption. Figure 7 shows the configuration suggested by the Boeing study for an oblique-winged transport.

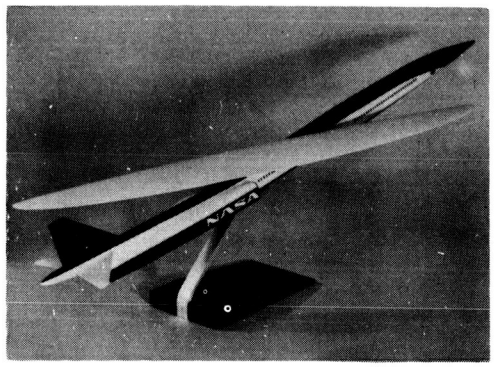

Figure 7

Configuration suggested by the Boeing study for an oblique-winged transport

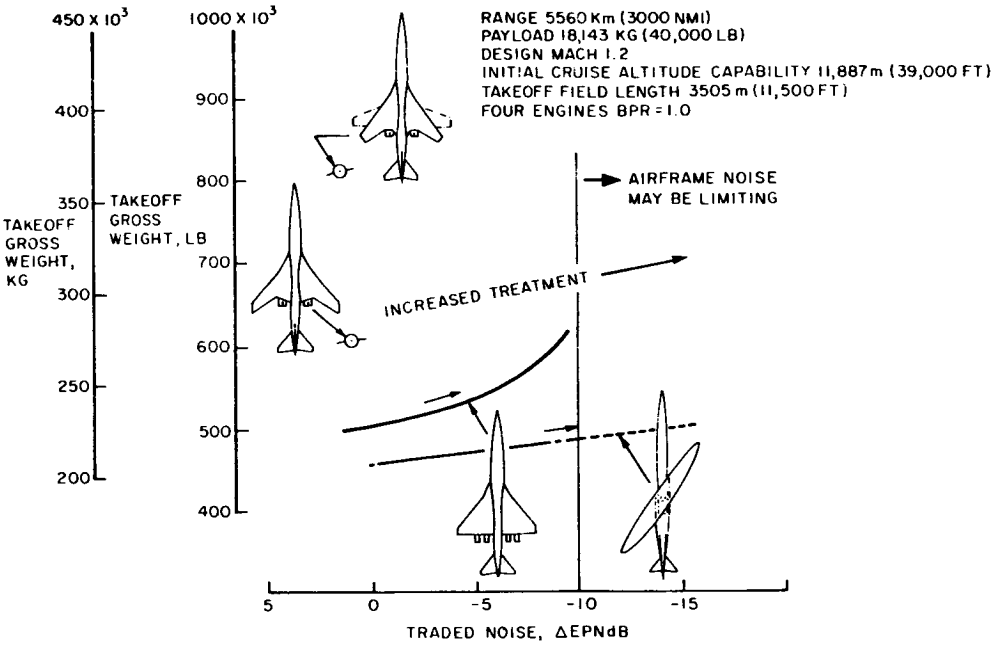

Figure 8

Estimated increases in gross weight required to meet increasingly stringent noise requirements

It seems possible that future restrictions on the noise made by airplanes may become more stringent. Figure 8 shows the estimated increases in gross weight that would be required to meet such increasingly stringent noise requirements. It appears from this study that the oblique wing, which can straighten itself out for landing or takeoff could achieve the lowest noise levels.

In summary, the investigations made thus far, which have included considerations of structure, stability, and flight efficiency as well as noise in the airport environment, point to the oblique winged aircraft as the optimum design for flight approaching the sonic boom speed limit.

REFERENCES

(1) Haglund, G.T.: *A Preliminary Climatology of the Threshold Mach Number and Implications for Boomless Supersonic Flight.* 4th Conference on Aerospace Meteorology, American Meteorological Society and AIAA, Las Vegas, Nevada, May 1970.

(2) Goodmanson, L.T.: Transonic Transports, Astronautics and Aeronautics, Vol. 9, No. 11, November 1971.

(3) Jones, R.T.: *Theoretical Determination of the Minimum Drag of Airfoils at Supersonic Speeds.* Journal of the Aeronautical Sciences, Vol. 19, No. 12, December 1952, pp. 813-822.

(4) Jones, R.T.: *Possibilities of Efficient High Speed Transport Airplanes.* Proceedings of the Conference on High Speed Aeronautics, Polytech. Institute of Brooklyn, Jan. 20-22, 1955.

(5) Jones, R.T,: *Reduction of Wave Drag by Antisymmetric Arrangement of Wings and Bodies.* AIAA Journal, Vol. 10, No. 2, pp. 171-176, February 1972.

(6) Graham, L.A.; Jones, R.T.; and Boltz, F.W.: *An Experimental Investigation of Three Oblique-Wing and Body Combinations at Mach Numbers Between 0.60 and 1.40.* NASA TM X-62, 256, Ames Research Center, Moffett Field, California 94035, April 1973.

(7) Bauer, F.; Garabedian, P.; and Korn, D.: *Supercritical Wing Sections.* Lecture Notes in Economics and Mathematical Systems, Springer-Verlag Berlin-Heidelberg-New York, 1972.

(8) Jones, R.T.: *The Spanwise Distribution of Lift for Minimum Induced Drag of Wings having a Given Lift and a Given Bending Moment.* NACA TN 2249, 1950.

(9) Campbell, J.P., and Drake, H.M.: *Investigation of Stability and Control Characteristics of an Airplane Model with a Skewed Wing in the Langley Free Flight Tunnel.* Technical Note 1208, US National Advisory Committee for Aeronautics, 1947.

(10) Kulfan, R.M., et al: High Transonic Speed Transport Aircraft Study. Prepared by Boeing Commercial Airplane Company, NASA CR 114, 658, September 1973. For sale by the National Technical Information Service, Springfield, Va. 22151.

AEROELASTIC CHARACTERISTICS OF AN OBLIQUE WING

Robert T. Jones

Ames Research Center

and

John W. Nisbet

Boeing Commercial Airplane Company

AEROELASTIC CHARACTERISTICS OF AN OBLIQUE WING

R. T. JONES

J. W. NISBET

In theory, the most efficient wing shape for transonic and low supersonic speeds is simply a long narrow straight "subsonic" wing turned at an oblique angle to the flight direction. This theory has recently been verified by tests at Mach numbers from .6 to 1.4 in the NASA-Ames 11' Supersonic Wind Tunnel (see reference 1) and by comparative studies of transonic transport designs made by the Boeing Commercial Airplane Company (see Fig. 1) (see ref. 2).

In considering the oblique wing, it is perhaps natural to try to relate its behavior to well known phenomena associated with swept forward and swept aft wings. This approach would lead one to expect severe static divergence and roll trim requirements. Figure 2 shows the effect of bending an oblique wing with the fuselage clamped as in a wind tunnel model. When the wing tips bend up as a result of an aerodynamic lift increment, the structural sections AB and A'B' tend to move together. Since the point C' does not move up as much as B', there is a reduction in the angle of attack of the section C'B'. This reduction in section angle of attack on the aft wing leads to a loss of lift. For the forward wing, the point C moves up more than the point B, causing an increase in angle of attack of the section CB. This leads to an increase in lift, more bending and a further increase in

the section angle of attack. Aeroelastic divergence results when the increase in lift overcomes the restoring moment due to wing stiffness.

After further consideration of the oblique wing configuration, one wonders if divergence of the free flying airplane can actually occur. The effect of aeroelasticity is to increase the lift on the forward wing and decrease the lift on the aft wing. This antisymmetrical lift distribution causes the airplane to roll. The lift caused by the roll rate tends to cancel the aeroelastic lift. (See Fig. 3)

Alternatively, if aileron control is applied to prevent roll the lift distribution produced by the ailerons also tends to cancel the aeroelastic lift increment.

With bilaterally symmetric swept forward wings, the free motions of the airplane show no such relieving or stabilizing influence, but rather aggravate the unstable tendency of the wing. Thus, bending swept-forward tips upward increases the lift on both tips symmetrically causing a pitching moment which tends to increase the angle of attack of the whole airplane, adding to the aeroelastic increment.

Clearly, the behavior of the oblique wing in free flight, will be different from that of the swept-forward wing because of its different symmetry. Analyses of the oblique wing which assume that the wing is clamped at the root section or that the fuselage is restrained in roll, turn out to be misleading for this reason.

The foregoing discussion leads to three questions:

(1) Does a free-flying oblique winged airplane exhibit the divergent instability characteristic of a swept-forward wing configuration?

(2) Does the elasticity of the wing affect the aileron control adversely?

(3) How much aileron deflection will be required to maintain trim at different speeds?

By exploring a simple dynamic model we hope to provide insight into these questions.

Figure 4 shows the simplified model assumed in our calculations. The model consists of two rigid wing panels hinged near the center of the wing with elastic restraining springs. Assuming the hinge axes perpendicular to the long axis of the wing, the stiffness of the springs will represent the stiffness of the wing in pure bending, without torsion. Since the rolling motion has an important influence on the behavior, the airplane is assumed free to roll. There are then three degrees of freedom corresponding to deflections ψ_u and ψ_o of the upstream and downstream wing panels and the bank angle ϕ (see figure 4). The equations of motion of the system are:

$$I_\psi \ddot{\psi}_u + K_a m_a \dot{\psi}_u + (K_e - K_e)(\psi_u - \phi \cos \Lambda) = 0$$

$$I_\psi \ddot{\psi}_o + K_a m_a \dot{\psi}_o + (K_e + K_a)(\psi_o - \phi \cos \Lambda) = 0$$

$$I_\phi \ddot{\phi} + 2K_e \cos^2 \Lambda \phi - K_e \cos \Lambda (\psi_u + \psi_o) = 0$$

where

I_ψ = Moment of inertia of wing panel about hinge axis

I_ϕ = Moment of inertia of fuselage and center wing portion about roll axis

K_e = Elastic spring stiffness about hinge (bending moment per unit deflection angle)

K_a = Aerodynamic bending moment per unit deflection angle

$m_a K_a$ = Aerodynamic damping moment due to angular velocity, assumed proportional to K_a

Both K_e and K_a are taken as positive. The first of the three equations refers to the upstream wing panel and it will be noted that the aerodynamic moment represented by K_a diminishes the apparent stiffness of the upstream wing panel but increases the apparent stiffness of the downstream panel.

Subjecting any of the three degrees of freedom to an initial disturbance and solving the equations by standard methods we will find

$$\psi_u \ \psi_o \quad \text{or} \quad \phi = \Sigma \, An \, e^{\lambda nt}$$

where the λ_n are the complex "eigenvalues" or roots of the characteristic determinant of the equations. There are 6 such eigenvalues and if the real part of any one of them is positive the motion following an initial disturbance will grow in unstable fashion. Since the system has neutral stability in bank angle ϕ one of the eigenvalues will be zero.

Values of the quantities appearing in equations (1) have been estimated for a 200 passenger transport airplane designed to fly at Mach number 1.2 with a wing yaw angle of 55° (see ref. 2). Figure 5 shows how the damping of the least stable mode varies with flight dynamic pressure for several assumed values of fuselage roll inertia. The case $I_\phi = \infty$ corresponds to a lack of roll freedom (fuselage fixed, as in a wind tunnel test) and in this case the instability occurs as a straight non-oscillatory divergence (so called "static"

divergence) at about 1.6 times the cruising dynamic pressure q_{cr} (= $0/2\ V^2$). With a finite value of roll inertia (I_ϕ) direct divergence does not occur and instability takes the form of increasing oscillations, beginning at two to three times cruise dynamic pressure.

The aeroelastic stability boundary, or boundary for neutrally damped oscillations may be obtained from equations (1) by setting the real part of a complex eigenvalue equal to zero. If the imaginary part of the eigenvalue is also zero then the instability will be non-oscillatory. More generally, the value of the imaginary part determines the frequency of marginally stable oscillations. Setting the eigenvalue equal to $iu\ell$, we obtain

$$\begin{vmatrix} -u\ell^2 + iu\ell u\ell_o^2 Km_a + u\ell_o^2(1-K) & 0 & -u\ell_o^2(1-K)\cos\Lambda \\ 0 & -u\ell^2 + iu\ell u\ell_o^2 Km_a + u\ell_o^2(1+K) & -u\ell_o^2(1+K)\cos\Lambda \\ \dfrac{-m u\ell_o^2}{2\cos\Lambda} & \dfrac{-m u\ell_o^2}{2\cos\Lambda} & +m u\ell_o^2 - u\ell^2 \end{vmatrix} = 0$$

where

$$u\ell_o^2 = \frac{K_e}{I_\psi} = \text{natural bending frequency of wing panel}$$

$$\frac{K_a}{K_e} = K$$

$$2\,\frac{I_\psi}{I_\phi}\cos^2\Lambda = m$$

Setting both real and imaginary parts of the determinant equal to zero results in expressions for the stiffness ratio K and the frequency ratio $\frac{u\ell}{u\ell_o}$ at the stability boundary.

$$K^2 = \frac{1+\sqrt{1+m^2}}{2+u\ell_o^2 m_c^2 (1-m-\sqrt{1+m^2})}$$

$$\frac{u\ell^2}{u\ell_o^2} = \frac{1}{2}\,(1+m-\sqrt{1-m^2})$$

Figures 6(a and b) show stability boundaries for various values of the inertia ratio $m = 2\,\frac{I_\psi}{I_\phi}\cos^2\Lambda$ and the stiffness ratio $K = \frac{K_a}{K_e}$.

The value $K = 1$ corresponds to the so-called "static divergence" case and to the actual stability boundary when the roll inertia of the fuselage approaches infinity $(m = 0)$. Normally, the roll inertia I_ϕ of the fuselage is small compared with that of the wing panels I_ψ. Since K_a is proportional to the dynamic pressure $q = \rho/2\ V^2$ and K_e is constant it may be shown that

$$K = \frac{q}{q_s}$$

where q_s is the dynamic pressure for divergence with the fuselage clamped.

AILERON CONTROL AND TRIM OF OBLIQUE WING

Assuming the wing is aeroelastically stable we have still to investigate the effect of bending flexibility on aileron control and trim.

Figure (7) shows measured rolling moments produced by an oblique elliptic wing model in the NASA-Ames 14 foot transonic tunnel at a Mach number of 1.2. The wing has an aspect ratio of 10, an airfoil section 12% thick and is equipped with conventional ailerons. The results shown were obtained with the wing at 60^{o} yaw.

The model was constructed with an upwardly curved chord plane, resulting in a dihedral angle at the tips of approximately 6^{o}. The intention here was to provide roll trim at a cruising lift coefficient of .3 to .35. At zero lift, the rolling moment is in the direction to raise the forward tip and may be attributed to the built in dihedral of the wing. The downward slope of rolling moment curve with increasing lift coefficient shows that the lift curve slope of downstream sections is greater than that of upstream sections. This effect arises from an upwash induced by the upstream portions of the wing and is predicted by linear lifting surface theory. Extrapolation of the linear portion of the curve would show trim with ailerons neutral at the intended lift coefficients C_L .3. Evidently viscous effects intervened, causing a loss of lift on the downstream sections so that roll trim was not attained at $\delta_a = 0$ with this amount of dihedral. Aileron deflections within the range $\pm 10^{o}$ could, however, provide trim over a wide range of lift coefficients. Deflections within this range produced no significant increments of drag, as might be expected because of the oblique angle (60^{o}) of the hinge lines. Presumably, a smaller dihedral angle (i.e., smaller upward tip angle) would have lowered the curve for $\delta_a = 0$ so that even smaller aileron angles would suffice for trim.

The model used in the 14 foot tunnel tests was of solid steel and was, of course, relatively much stiffer than a full-sized wing. There remains the problem of the influence of bending flexibility of a full-sized wing on the roll and trim effectiveness.

The simplified aeroelastic model (fig. 4) used in the study of stability boundaries can provide some insight into the effect of wing bending on roll control and trim. Assuming that the stiffness of the wing is sufficient to provide dynamic stability (i.e., is within the stable range of figure 6) transient oscillations will die out and the ability of the ailerons to provide a steady roll rate or trim can be studied by omitting the inertia terms from the equations of motion (1).

To determine the roll effectiveness of the ailerons, we rewrite the equations of motion omitting the inertia terms and introduce moments δM_δ proportional to the aileron deflections δ_u and δ_d applied at $t = 0$.

$$M_{\dot\psi}\dot\psi_u + (K_e - K_a)(\psi_u - \phi\cos\Lambda) = \delta_u M_\delta$$

$$M_{\dot\psi}\dot\psi_d + (K_e + K_a)(\psi_o - \phi\cos\Lambda) = \delta_d M_\delta$$

$$2K_e\cos^2\Lambda\phi - K_e\cos\Lambda(\psi_u + \psi_d) = 0$$

where $M_{\dot\psi} = K_a m_a$ is the damping coefficient for angular motions $\dot\psi$, analogous to the damping in roll. Assuming step input aileron deflections and solving for the roll rate $\dot\phi$, we obtain

$$\dot\phi = \frac{M_\delta}{2\cos\Lambda M_{\dot\psi}}\left[(\delta_u + \delta_d) + (\delta_u - \delta_d)\frac{K_a}{K_e}(1 - e^{-\lambda t})\right]$$

where $\lambda = \dfrac{K_e}{M_{\dot\psi}}$

Evidently, if the ailerons are used together with $\delta_u = \delta_d$ (equal up and down deflections) bending elasticity of the wing has no effect on the roll rate. In this situation, the spanwise loading produced by the ailerons is effectively cancelled by the rolling motion as illustrated in figure (3).

A different picture emerges, however, if we attempt to control roll by using a single aileron alone on either tip. In these cases, wing distortions appear, and it is found that an aileron on the downstream tip alone ceases to be effective at the speed for static divergence $K_e - K_a = 0$, or $K = 1$. Figure (8) summarizes the behavior at $K = 1$.

In the foregoing, we have considered bending distortions only. In practice, the elasticity of the wing in torsion must be considered also, and it is to be expected that torsion will reduce the aileron effectiveness at high values of the dynamic pressure. It should be borne in mind, however, that the dynamic pressure effective in producing torsion is greatly reduced by the sweep.

In conclusion, these results show that aeroelastic divergence, which is characteristic of swept forward wings, does not occur in the case of the oblique wing. Aeroelastic instability of the oblique wing evidently appears in the form of undamped oscillations at a dynamic pressure which may be considerably greater than that for "static" divergence of a swept forward wing.

The stability of the oblique wing shows an important dependence on the moment of inertia of the fuselage in roll. In a more realistic

model, a similar influence of the distribution of mass along the wing span may be expected.

SUMMARY

The aeroelastic stability of an oblique wing is studied by means of a simple model having three degrees of freedom. It is found that freedom in roll exerts a stabilizing influence on the behavior of the oblique wing so that aeroelastic bending divergence which is typical of swept forward wings does not occur in the case of the oblique wing. Instability of the oblique wing appears in the form of undamped oscillations at a flight speed which may be considerably greater than that for static divergence of a swept forward wing. Stability is dependent on the roll inertia of the fuselage and on the distribution of mass along the wing. Bending elasticity of the wing has little effect on aileron control and trim of the oblique wing provided equal opposite aileron deflections are employed.

REFERENCES

1. Graham, Lawrence A., Jones, Robert T., and Boltz, Fredrick W. "An Experimental Investigation of an Oblique-Wing Body Combination at Mach Numbers between 0.60 and 1.40." NASA TMX-62, 207 Dec. 1972. See also NASA TMX-62, 256 Apr. 1973.

2. Kulfan, Robert M. et al
   Study of the Single Body Yawed Wing Aircraft Concept
   Boeing Commercial Airplane Co. NASA CR 137483 May 1974

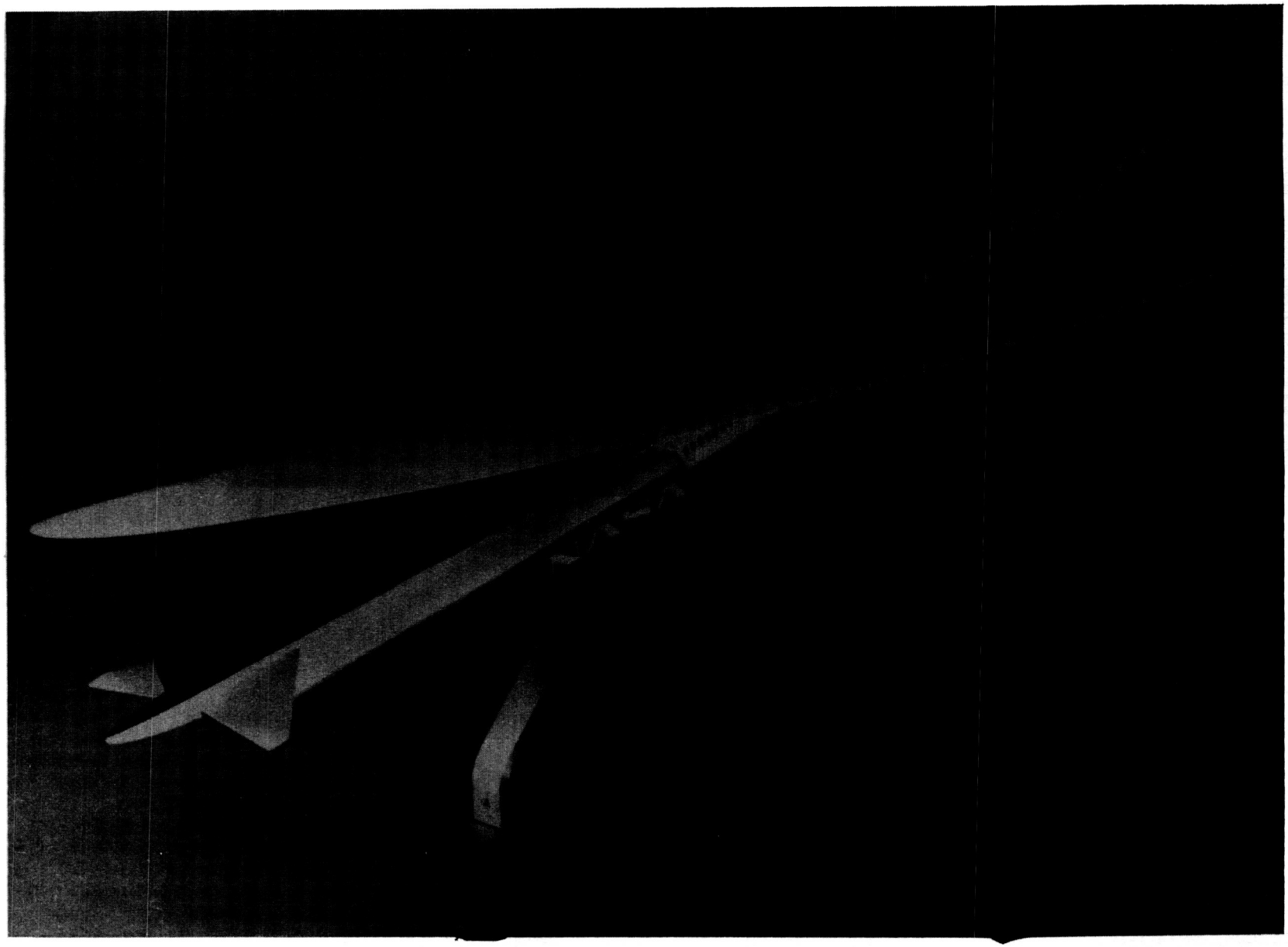

Figure 1

OBLIQUE WING AEROELASTICS

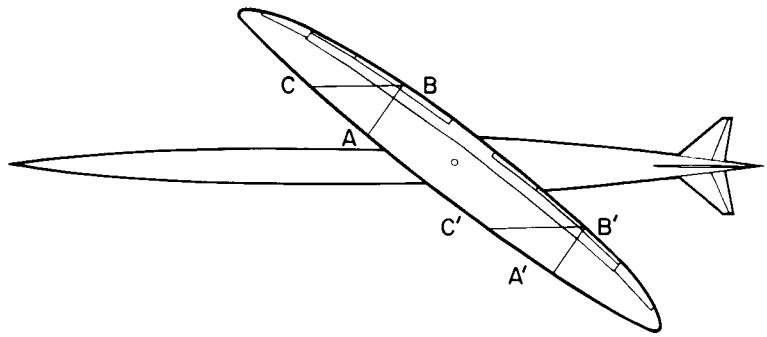

Figure 2

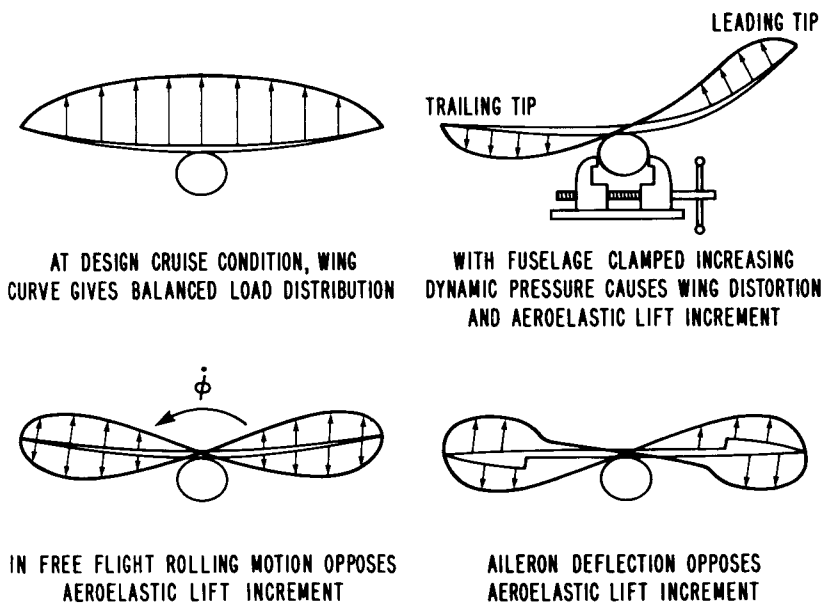

Figure 3

SIMPLIFIED MODEL FOR AEROELASTIC ANALYSIS

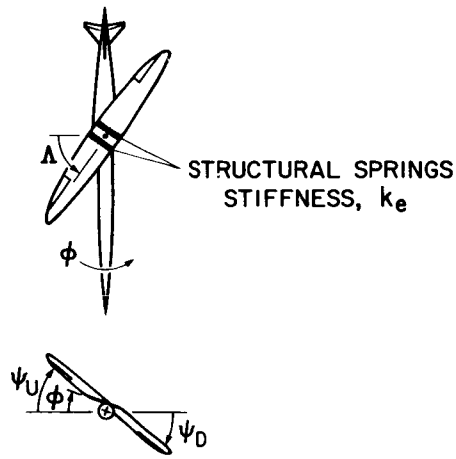

Figure 4

EFFECT OF FUSELAGE INERTIA ON AEROELASTIC STABILITY OF OBLIQUE WING

$\lambda = \alpha \pm i\beta$

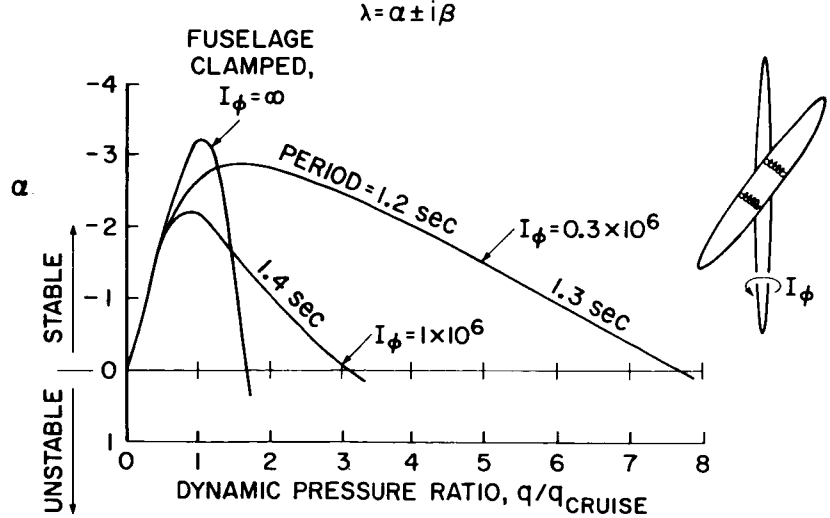

Figure 5

STABILITY BOUNDARIES FOR SIMPLIFIED AEROELASTIC MODEL

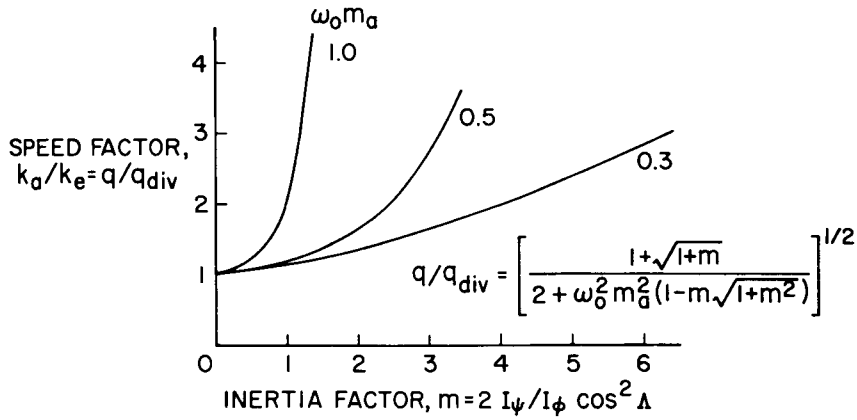

Figure 6a

FREQUENCY OF NEUTRALLY STABLE OSCILLATIONS COMPARED WITH NATURAL BENDING FREQUENCY

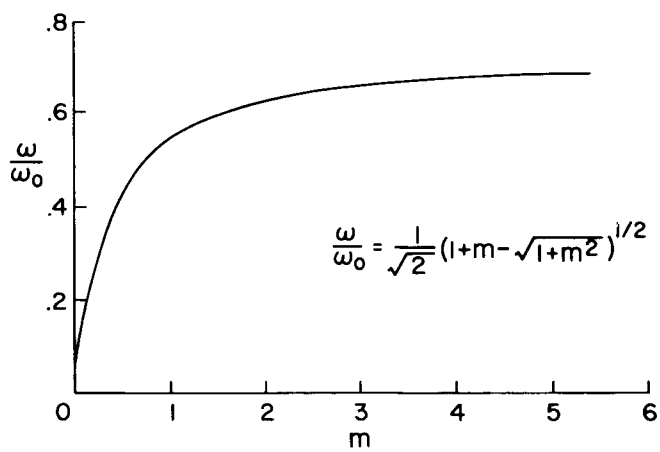

Figure 6b

EFFECT OF AILERONS ON ROLLING MOMENTS OF OBLIQUE WINGED MODEL

NASA-AMES 14ft TRANSONIC WIND TUNNEL

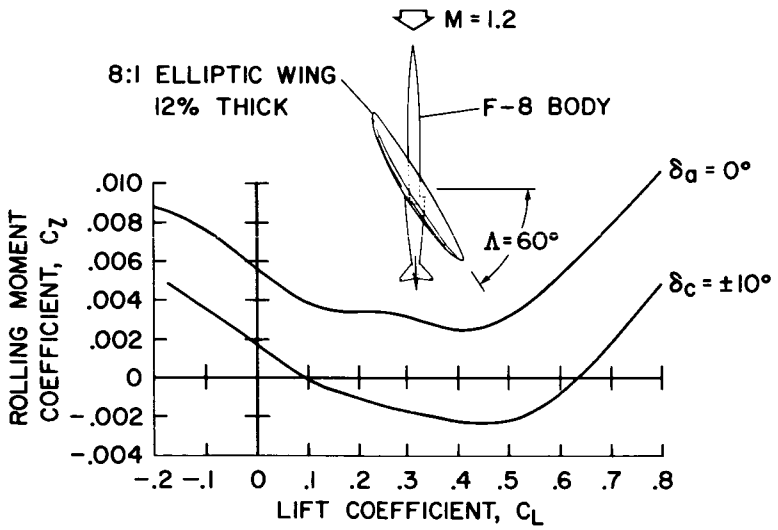

Figure 7

AILERON CONTROL BEHAVIOR AT SPEED FOR STATIC DIVERGENCE

$k_e - k_a = 0$

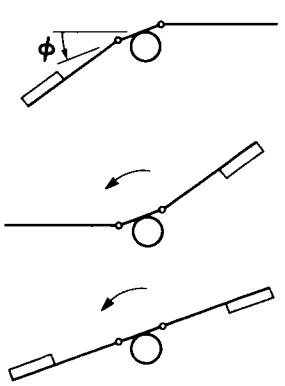

AILERON ON DOWNSTREAM TIP ONLY
- ZERO ROLL RATE
- STATIC BANK ANGLE +
- WING DISTORTION

AILERON ON UPSTREAM TIP ONLY
- FULL ROLL RATE
- DISTORTED WING SHAPE

EQUAL AILERONS ON BOTH TIPS
- FULL ROLL RATE
- NO WING DISTORTION

Figure 8

COMA OF MODIFIED GREGORIAN AND CASSEGRAINIAN MIRROR SYSTEMS

Robert T. Jones

August 1954

Jones, R. T., "Coma of Modified Gregorian and Cassegrainian Mirror Systems,"
Optical Society of America, vol. 44, no. 8, Aug. 1954, pp. 630-633.
Reprinted by permission of the Optical Society of America, Washington, D.C.

Reprinted from JOURNAL OF THE OPTICAL SOCIETY OF AMERICA, Vol. 44, No. 8, 630–633, August, 1954
Printed in U. S. A.

Coma of Modified Gregorian and Cassegrainian Mirror Systems

ROBERT T. JONES
Ames Aeronautical Laboratory, National Advisory Committee for Aeronautics, Moffett Field, California
(Received February 8, 1954)

The equivalence of the classical Newtonian, Cassegrainian, and Gregorian mirror systems with respect to the first two Seidel aberrations is rederived by means of a simple congruence. The effects of arbitrary small modifications of the two-mirror systems are then studied and general formulas are derived for the effects of such modifications on the spherical aberration and coma. Spherical aberration is corrected to the third order if the amount of glass removed from one surface is replaced at the corresponding zone of the other surface (approximate expression of Fermat's principle). Modifications in which one surface is made spherical while the other is adjusted to eliminate spherical aberration result in large increases of coma for systems having the usual amplifying ratios.

IN the standard forms of the Cassegrainian and Gregorian telescopes the curves of the primary and secondary mirrors are confocal conic sections, so that, insofar as geometrical optics is concerned, rays parallel to the axis of the system will be brought to a perfect focus at the axial image point. There remains, however, a slight variation in the equivalent focal length of the various rays throughout the aperture of the instrument, so that the magnification is greater for the outer zones of the aperture than for the central part. Such a variation also appears in the Newtonian telescope, with a single parabolic reflector, and produces the aberration known as "coma."

It was shown by A. C. Lunn[1] that in any combination of mirrors having confocal conic sections, the zonal magnification error will be exactly the same as that of a single parabolic reflector having the equivalent focal length of the compound system. Since the magnification error of a long-focus paraboloid is slight, and furthermore diminishes with the inverse square of the focal ratio, it follows that the comatic aberration in the conventional Cassegrainian or Gregorian forms is ordinarily extremely small.

Practical experience has shown, however, that the excellence of the calculated properties of these compound-mirror systems is difficult to achieve in actual construction. To overcome these difficulties several modifications of the standard Cassegrainian and Gregorian forms have been proposed. Perhaps the best known of these is the construction employed by Dall and Kirkham.[2] Here the secondary is made spherical and the spherical aberration is corrected by modifying the primary. Descriptions of this and other possible modifications have been given by Allyn J. Thompson[3] and quoted by Albert G. Ingalls.[4] Recently Yoder, Patrick, and Gee[5] have presented calculations of all the third-order aberrations for an example of the Dall-Kirkham type.

The present paper extends the previous discussions by giving general formulas for the effects of various modifications on the coma of two-mirror systems. The formulas are based, of course, on geometrical optics and are limited to small apertures such that the fifth and higher powers of the aperture ratio are negligible. Within this limitation they agree with the formulas given by Schwarzschild for the aplanatic case (zero coma), but show in addition the effects of departures from aplanatism while maintaining zero spherical aberration.

Consider first the unmodified Cassegrainian with a parabolic primary mirror p and a hyperbolic secondary mirror s (see Fig. 1). Denoting the paraxial equivalent focal length by F_0, the "oblique focal lengths" $F_y=fp'$ of the zones y may be found by extending the rays from the focal point f straight through the secondary mirror and noting the intersections p' of these rays with the incoming parallel rays. The Abbé sine condition will be satisfied if the intersection points lie on a sphere centered at f. In this case the oblique focal lengths F_y, and hence the magnification, would be constant for all zones. However, it is easily verified that in the case of the Cassegrainian this intersection surface is not a sphere, but is a paraboloid having a focal length equal to F_0. Referring again to Fig. 1, consider the conjugate reflecting system formed on the reversed side of the secondary by the extended rays together with the rays extended from the primary toward its focal point f'. Denoting by A the amplification of the original system, it is seen that the concave side of the hyperboloid forms the secondary of a conjugate Cassegrainian system having the amplification $1/A$, and having its focal point

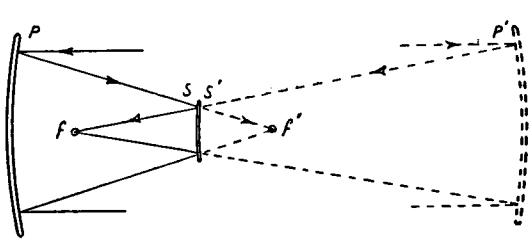

FIG. 1. Congruence of rays in the Cassegrainian and the rays from a reversed parabolic reflector.

[1] A. C. Lunn, Astrophys. J. 27, 280–285 (1908).
[2] Alan R. Kirkham, Sci. American 158, No. 6, 374 (1938).
[3] Allyn J. Thompson, Sky and Telescope (May, 1948, *et seq.*).
[4] Albert G. Ingalls, Sci. American (June, 1933, *et seq.*).
[5] Yoder, Patrick, and Gee, J. Opt. Soc. Am. 43, 1200 (1953).

at f'. The surface p' may be considered the primary of this system if the incoming parallel rays are reversed. However, the only primary surface that will produce a focus at f' after reflection at the hyperboloid s' is a paraboloid. It follows that the Abbé surface p' is a paraboloid having its focus at f. A similar construction (Fig. 2), but with the paraboloidal surface p' located behind the primary, is available in the case of the Gregorian form. Thus in each of these cases the rays in the vicinity of the focal point may be brought into congruence with the rays from a simple parabolic reflector having the same equivalent focal length. The Newtonian, the Gregorian, and the Cassegrainian are thus all equivalent as far as coma is concerned.

As was shown by A. C. Lunn[1] this equivalence holds for compound systems comprising any number of mirrors, provided all the mirrors have such curves (conic sections) that the spherical aberration is perfectly corrected at each focus (or virtual focus) within the system.

In the case of the single parabolic reflector a well-known derivation[6] yields for the departure from the

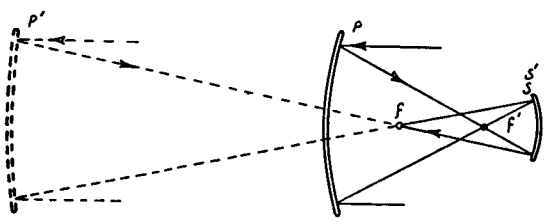

FIG. 2. Congruence of rays in the Gregorian and the rays from a parabolic reflector.

sine condition

$$(F_y/F_0)-1=(y^2/4F_0^2). \tag{1}$$

The quantity $(F_y/F_0)-1$ may be thought of as the percent error in magnification at the zone y. In the case of the Gregorian or Cassegrainian the same formula applies, but since the equivalent focal length is A times the focal length of the primary, the coma is reduced by the factor $1/A^2$ relative to that of the primary mirror alone.

To study the effects of various modifications of the Cassegrainian we write for the equation of the primary:

$$x_1=\frac{y_1^2}{2R_1}+P\frac{y_1^4}{(2R_1)^3}, \tag{2}$$

and for the secondary:

$$x_2=\frac{y_2^2}{2R_2}+\left[S-\frac{4A}{(A-1)^2}\right]\frac{y_2^4}{(2R_2)^3}. \tag{3}$$

Here R_1 and R_2 are the radii of the respective surfaces

[6] L. C. Martin, *Technical Optics* (Pitman and Sons, Ltd., London, 1948), Vol. II.

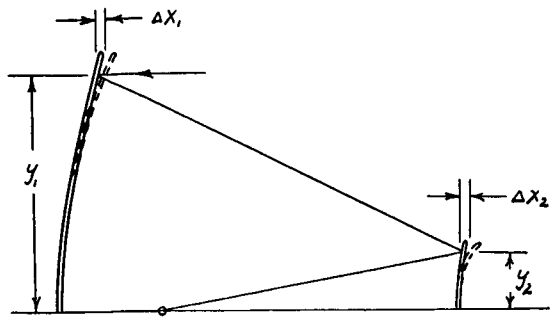

$$\Delta X_1 = \Delta X_2$$

FIG. 3. Relation between fourth-degree deformations for zero spherical aberration.

at $y=0$, and the coordinates of each surface are measured from its intersection with the x axis. The quantities

$$\Delta x_1=P[y_1^4/(2R_1)^3], \tag{4}$$

and

$$\Delta x_2=S[y_2^4/(2R_2)^3], \tag{5}$$

represent deviations of the primary and secondary mirrors from their original parabolic and hyperbolic forms. Thus, setting $P=1$ makes the primary spherical instead of parabolic. If S is set equal to $1+4A/(A-1)^2$, the secondary will be spherical.

Analysis of paraxial rays shows that the spherical aberration will be corrected if a simple relation is maintained between the deformations of the primary and secondary mirrors. This relation is (see Fig. 3)

$$\Delta x_1=\Delta x_2, \tag{6}$$

where the increments in x are measured at the corresponding zones y_1 and y_2—i.e., zones touched by the same ray in the undistorted Cassegrainian. This relation obviously amounts to an approximate expression of Fermat's principle. If the primary is bent slightly toward the object point, the shortening of the light time between the primary and secondary must be compensated by bending the secondary away from the primary an equal distance where the ray touches. Within the fixed approximate form of Eqs. (2) and (3), the focusing of a time signal is not merely necessary, but is also sufficient for the focusing of all four coordinates of a point event. The approximation here obviously involves a small shift of the rays from those of the undeformed Cassegrainian.

When the equations given by Schwarzschild for the surfaces of an aplanatic telescope[7] are converted to the form of deviations from the standard Cassegrainian, it is found that they agree with the foregoing rule.

A similar comparison is found to hold in the case of the formulas given by Kirkham.[2]

[7] K. Schwarzschild, Abhandl. Ges. Wiss. Göttingen Math. physik. Kl. 2 (1905).

If D_2 is the nominal diameter of the secondary* we have for the undeformed Cassegrainian the simple proportion

$$D_2/D_1=y_2/y_1. \tag{7}$$

From Eqs. (4), (5), (6), and (7) we obtain

$$P=S(R_1/R_2)^3(D_2/D_1)^4, \tag{8}$$

as the relation between P and S for zero spherical aberration.

To study the effect of the deformations P and S on the coma we have to consider the changes in inclination and intersection points of the rays. Referring to Fig. 1, the law of sines yields

$$F_y=(l_1/l_2)l_3, \tag{9}$$

where $l_1=pf'$, $l_2=s'f'$, $l_3=sf$. Carrying through the analysis for paraxial rays, we find

$$\frac{F_y}{F_0}-1=C\frac{y^2}{4F_0^2}, \tag{10}$$

where

$$C=1+\frac{(A-1)^3}{2A}\left(1-\frac{D_2}{D_1}\right)S, \tag{11}$$

or, in terms of P,

$$C=1+\frac{A^2}{2}\left(\frac{D_1}{D_2}-1\right)P, \tag{12}$$

P and S being, of course, related through Eq. (8)

As shown by Schwarzschild, both spherical aberration and coma may be eliminated by a special shaping of the two mirror surfaces. To obtain Schwarzschild's formulas we set $C=0$ and solve Eqs. (11) and (8) for the shape parameters S and P. The result is

$$S=-\frac{2A}{(A-1)^3[1-(D_2/D_1)]}, \tag{13}$$

$$P=-\frac{2}{A^2[(D_1/D_2)-1]}. \tag{14}$$

When these values are introduced into Eqs. (2) and (3) it is found that they require, for amplifying ratios greater than 1.0, a slight overcorrection of the primary (hyperbolic primary) and an increase in the eccentricity of the hyperbolic secondary. For values of A less than 1.0 the secondary is concave and with certain proportions approaches a spherical shape.

In the construction employed by Dall and Kirkham[2] the amplifying ratio is greater than one (convex secondary) and the secondary is made spherical for ease of construction and adjustment. For this case we find

$$S=1+[4A/(A-1)^2], \tag{15}$$

and for the departure from the sine condition,

$$\frac{F_y}{F_0}-1=\left[1+\frac{(A-1)(A+1)^2}{2A}\left(1-\frac{D_2}{D_1}\right)\right]\frac{y^2}{4F_0^2}. \tag{16}$$

For $D_2/D_1=\frac{1}{4}$ and $A=4$, the quantity in the brackets (C) is 8. Thus with these proportions the coma is increased by a factor of 8 when compared with the standard Cassegrainian having a hyperbolic secondary. In spite of this, the coma is only half as great as that for the primary mirror alone. Figure 4 shows values of C for various values of D_2/D_1 and A. Since the factor C diminishes rapidly with amplifying ratio, it seems advisable to use somewhat smaller values of A in this type if a large field of view is required. The tolerance to misalignment is also enhanced if the focal length of the primary is made longer (and A smaller), since the effect of misalignment must be related to the coma of the individual mirrors.

Turning now to the case in which the primary is made spherical, we set $P=1$ and obtain

$$S=\left(\frac{A}{A-1}\right)^3\frac{D_1}{D_2}, \tag{17}$$

$$\frac{F_y}{F_0}-1=\left[1+\frac{A^2}{2}\left(\frac{D_1}{D_2}-1\right)\right]\frac{y^2}{4F_0^2}. \tag{18}$$

For $D_1/D_2=4$ and $A=4$, $C=24$. The coma is thus $1\frac{1}{2}$ times that of the primary alone. The excessive coma of a telescope of this type has been noted by Thompson.[3]

To treat modifications of the Gregorian we write for the equation of the secondary:

$$x_2=-\frac{y_2^2}{2R_2}-\left[S+\frac{4A}{(A+1)^2}\right]\frac{y_2^4}{(2R_2)^3}. \tag{19}$$

The condition for zero spherical aberration becomes

$$S=-P(R_2/R_1)^3(D_1/D_2)^4, \tag{20}$$

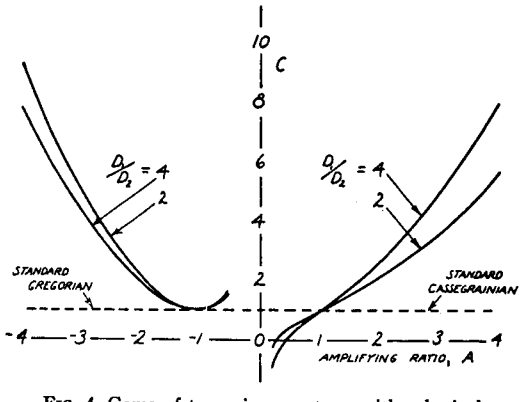

FIG. 4. Coma of two-mirror systems with spherical secondary mirrors.

* Here D_2 is the diameter of the secondary illuminated by the full aperture D_1 of the primary from an axial object point. The actual diameter of the secondary should of course be slightly greater than this to allow for a finite image dimension.

while the factor of increase C in the zonal magnification error reads

$$C=1-\frac{A^2}{2}\left(1+\frac{D_1}{D_2}\right)P. \tag{21}$$

In these equations the amplifying ratio A is considered positive. However, in Figs. 4 and 5 the values of C for the Gregorian have been plotted on the negative side of the axis to distinguish them from the values for the Cassegrainian. The partial obstruction of the aperture by the secondary mirror has not been taken into account in these calculations.

To obtain a quantitative idea of the effect of the zonal magnification error we may compute the elongation of an off-axis star image. The result is

$$\delta=3\beta\left[\frac{F_y}{F_0}-1\right]_{\max} \tag{22}$$

Here β is the angle of the star away from the axis of the telescope and δ is the extreme angular elongation (tangential coma) of the image in the same units. Setting $y_{\max}=D/2$ and making use of Eq. (10) we obtain

$$\delta=\tfrac{3}{16}C(D/F_0)^2\beta. \tag{23}$$

Formulas (22) and (23) are, of course, based on geometrical optics. Studies of the wave-diffraction pattern associated with the coma image[8] show that little effect is apparent until the elongation given by Eq. (22) is about three times the radius of the normal Airy diffraction disk, or

$$\delta/3\leqq 1.22(\lambda/D),$$

where λ is the wavelength. With a radio telescope the comatic elongation might be allowed to reach several inches, since the normal diffraction disk will be of that

[8] R. Kingslake, Proc. Phys. Soc. (London) **61**, pt. 2, No. 344 (1948).

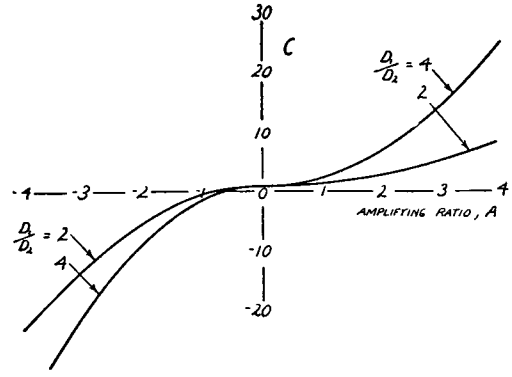

FIG. 5. Coma of two-mirror systems having spherical primary mirrors.

diameter. For ordinary light we have

$$\delta/3\leqq 5.5/D,$$

where δ is now in seconds of arc and D is in inches. Using this value of δ, we may solve Eq. (23) for β and obtain an expression for the angular radius of the field of view unaffected by coma:

$$\beta=\frac{16}{C}\left(\frac{F_0}{D}\right)^2\frac{5.5}{D}$$

in seconds.

The foregoing criterion corresponds approximately to the Rayleigh limit. In many applications a considerably wider tolerance is permissible. Regardless of the tolerance adopted, however, the radius of the field of good definition will be inversely proportional to the coefficient C.

ACKNOWLEDGMENT

The author wishes to thank Mr. Franklin B. Wright for providing a comparison with his unpublished derivations, and for helpful suggestions.

A PORTABLE 12-INCH

Robert T. Jones

February 1956

Jones, R. T., "A Portable 12-Inch," Sky and Telescope, vol. 15, no. 4, Feb. 1956, pp. 181-183.
Reprinted by permission of Sky and Telescope, Cambridge, Mass.

A PORTABLE 12-INCH

Relatively light weight and easy portability are features of my 12-inch Newtonian. As the picture shows, it is mounted on a system of large-diameter aluminum alloy tubes. The small wheels permit raising one end to push the instrument under shelter in my garage, as well as to nearby star parties of the Peninsula Astronomical Society.

Gusset plates and 5/16" bolts hold the mounting parts together. Extremely strong connections are not required to develop the full rigidity of the members. The polar axle is 5" in diameter, but is of thin (0.040") tubing, and hence is extremely light and more rigid than the customary solid steel axle. The declination axle turns on ball bearings inside a 4" diameter tube which pierces the upper end of the polar axis at right angles. A tight press fit was achieved there with the aid of a paper template, a hacksaw blade, and a round file. The rectangular gusset plates on opposite sides of the polar axis tube restored some of its strength after this operation. Aluminum alloy is ideal for this type of construction because it is easily worked with simple tools.

The slow-motion control consists of a hand crank adapted from a pilot's radio tuner and a speedometer cable which drives a tangent screw through a worm-gear reduction. The latter is of the type commonly found in war-surplus radio tuners. The tangent screw, which incorporates a spring-loaded half-nut for resetting, was made by sawing up an ordinary C-clamp. This arrangement has proved adequate for visual use.

The main tube is 14" in diameter and was made from 18-gauge 24ST aluminum alloy sheet. The three stiffening rings were cast by the local foundry, using a rather simple pattern made from 1/8" thick Masonite. The tube can be rotated to bring the eyepiece into a convenient position for young observers.

The mirror has a focal length of 78", and is used with an aperture of 12". The diagonal flat was cut from a 4" diameter pyrex blank 3/4" thick. I first attempted to make this mirror from a crown glass blank 1/2" thick, but this suffered from thermal distortion and flexure. With the thick pyrex blank, production of the flat was a straightforward matter.

Especially long eyepiece tubes have been made to carry Barlow lenses. These are 1.6" in diameter, and are placed 4" inside of focus; one amplifies the image 2x, the other 3x. The last provides an effective focal length for the telescope of nearly 20 feet. With the types of glass chosen, it was found that both spherical aberration and coma could be canceled almost exactly, even though the lenses are cemented. When used with a large-diameter Erfle eyepiece, this design provides an exceptionally wide field of view at high power.

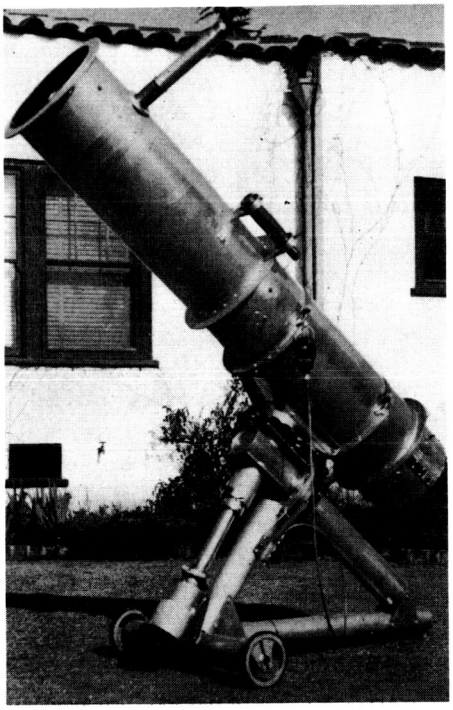

The Jones portable 12-inch reflector.

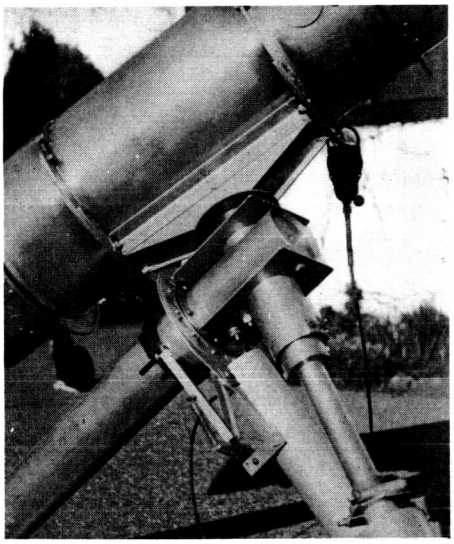

The rectangular gusset plates and details of the spring-loaded slow motion are seen in this picture.

When the telescope was first tried, rather pronounced thermal effects were noticed. Out-of-focus star images had a downward elongation that was not altered by rotating the optical system. Tests with smoke showed a slow current of air, inward along the bottom of the tube and out along the top. Subsequently, six 2" diameter openings were made in the tube directly in front of the mirror. Although the effects are perhaps not completely eliminated, it is interesting to watch the star images become approximately round when these ventilators are opened. In the photograph, the vents are covered by thin plates.

ROBERT T. JONES
840 Lincoln Ave.
Palo Alto, Calif.

A WIDE–FIELD TELESCOPE WITH SPHERICAL OPTICS

Robert T. Jones

September 1957

Jones, R. T., "A Wide-Field Telescope with Spherical Optics," vol. 16, no. 11, Sept. 1957, pp. 548-550.
Reprinted by permission of Sky and Telescope, Cambridge, Mass.

GLEANINGS FOR ATM's

CONDUCTED BY ROBERT E. COX

A WIDE-FIELD TELESCOPE WITH SPHERICAL OPTICS

Utilizing a doublet lens to correct the aberrations of a spherical mirror, the writer has designed and constructed a small f/8 telescope for visual use. The lens has considerable negative power, so that it serves as a Barlow lens as well as a corrector.

The lens is 2" in diameter, placed 6" inside the mirror's normal focal point. Extremely small star images are produced, and difficult double stars can be separated at surprisingly low power. With an Erfle eyepiece, images are sharp and colorless over a wide field.

Usually, the construction of an optically corrected, compact telescope presents some difficult problems for the amateur. Short-focus paraboloidal mirrors require increased accuracy of zonal measurements, as shown by this table for the conventional Foucault test:

Focal ratio of mirror, F/D	*Tolerable error of knife-edge reading, in inches*
f/3	0.006
f/4	0.010
f/6	0.023
f/8	0.041

For example, to verify the figure accuracy of an f/4 paraboloidal mirror of any diameter, the knife-edge setting must be read to 1/100 of an inch.

Even assuming that the spherical aberration of a short-focus mirror can be perfectly corrected, there is always the matter of off-axis aberrations, which increase rapidly as the focal length is reduced. An excellent discussion of these aberrations is contained in the article by James G. Baker in *Amateur Telescope Making-Book III*. The following table, adapted in part from Dr. Baker's article, gives the size of the field outside of which "the comatic flare becomes of such a size as to be apparent over the graininess of the [photographic] emulsion or larger than the seeing disk."

Focal ratio of mirror, F/D	*Diameter of good field, in inches*
f/3	0.36
f/4	0.64
f/6	1.44
f/8	2.56

Again, the dimension listed in independent of the absolute size of the instrument.

A well-known expedient for increasing the angular field of a Newtonian reflector is a neutral doublet correcting lens near the focus. Lenses of this type are used with the Mount Wilson and Palomar telescopes and other large reflectors. It has been pointed out by Baker and by C. G. Wynne, however, that such a doublet cannot correct spherical aberration, coma, and astigmatism simultaneously *if* the spherical aberration is already corrected at the primary.

Therefore, in the reflector-corrector designed by Baker, spherical aberration is introduced into the system by a figured plate, permitting subsequent complete correction by the lens. This arrangement has been used to adapt a conventional paraboloid to wide-angle photography (see *Sky and Telescope*, January, 1954, page 73), but it does not lend itself easily to amateur use.

In the design presented here, ordinary achromatism is achieved by the use of closely spaced elements of crown and flint glass, while the radii of the four surfaces have been adjusted to cancel the spherical aberration and coma of the primary mirror. The secondary spectrum (expressed as a fraction of the over-all focal length of the system) introduced by the power of the lens is less than half that of a comparable refractor, that is, an achromat having an aperture and focal length equal to the equivalent focal length of the new system.

The diagram shows the optical arrangment, which in my case incorporates a 6-inch spherical primary with a focal length of 24". The correcting lens is mounted in a tube that also contains the diagonal mirror. The first element (nearest the primary) is made of ordinary crown glass, 517645, while the second element is flint, 649338. (It should be noted that this arrangement is the reverse of that in the conventional Barlow lens.)

Radii of the four surfaces have been computed for positions of the lens 5" and 6" inside the focus of the primary and for a fixed amplifying ratio of 1.92 to 1:

Inches inside focus	*Radii of curvature in inches*			
	R_1	R_2	R_3	R_4
5	-8.33	3.74	2.98	5.73
6	-12.69	4.11	3.54	6.76

Although the radii in the table were worked out for a primary focal length of 24" (equivalent focal length 46"), they may be adapted to larger or smaller instruments by a proportionate scaling factor. For the particular amplifying ratio chosen, the (Gaussian) rays emerging from the crown lens into the space between the elements are parallel to the optical axis, so the correction is not extremely sensitive to the spacing of the components.

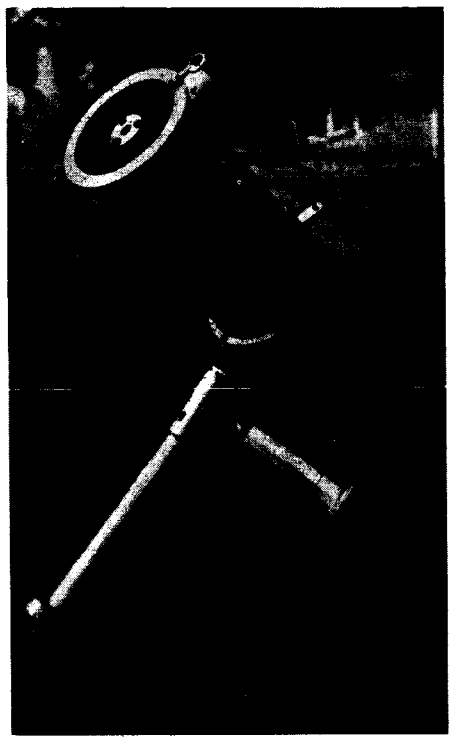

Only spherical optical surfaces are used in this compact reflector constructed by Robert T. Jones.

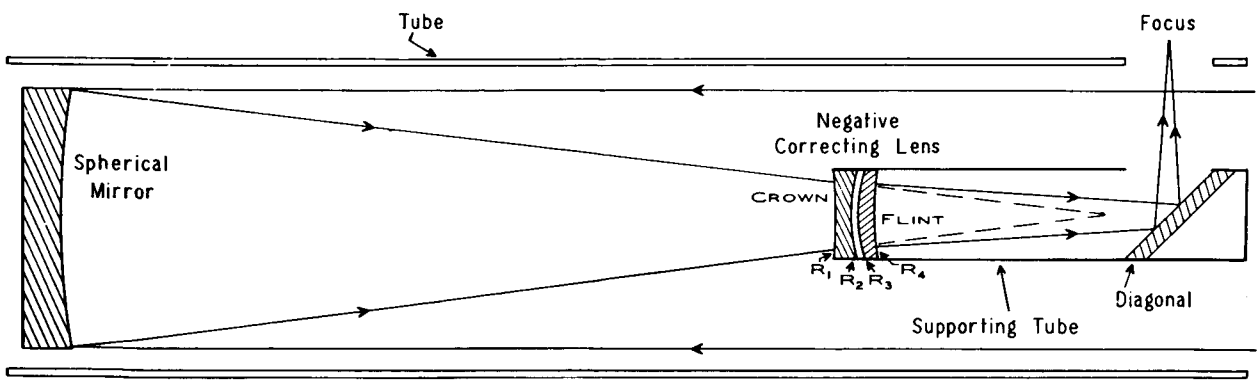

The optical system of Mr. Jones' telescope

The calculations were made first by thin-lens theory and then verified in several instances by Seidel sums for the individual surfaces, allowing a thickness of 0.33" for each element. The reader interested in the methods employed in such calculations should consult the article by C. G. Wynne in the *Proceedings* of the Physical Society (London). *62*, 360B, December 1949.

In my first experiments with this design, a 1.4" lens was placed only 4" inside the focus (20" ahead of the primary). The lens was made from standard blanks, using a small lathe and a miniature Draper-type polishing machine. Careful fine grinding and polishing resulted in spherical curves that required hardly any corrective figuring. The f/4 spherical primary is, I believe, easier to make than the conventional f/8 paraboloid.

The necessity of precise collimation in any compact optical system was forcibly demonstrated by the first observations with the newly assembled instrument. In my later experiments, the optical axis of the mirror has been permanently set by an aluminum ring machined so as to make a narrow contact with the optical surface just inside the mirror's edge. This ring, together with the spider supporting the secondary-lens tube, was then assembled permanently in the main tube with the aid of a machined jig.

The latter consists essentially of a steel tube threaded at one end to screw into the lens cell, and having a disk at the other end to hold the mirror ring in position. The ring and the spider are bolted in the main tube while still attached to the jig. Since the jig is made to run true on the lathe, it insures alignment.

This first telescope, however, was not definitely superior to a well-corrected Newtonian of the same equivalent focal length, since the angular field was not noticeably wider and some color and de-focusing were apparent at the edges of the field.

When a larger corrector, 2" in diameter, was installed 6" inside the primary focus, these defects were removed — the field curvature was reduced and the correction of the remaining aberrations was extended over a wider field. It was found that a 1.6" aperature stop in front of the 2-inch lens caused no obvious loss of performance, so that the corrector could probably be made that size advantageously, for there would be less diffraction and loss of light.

Since completion of this second modification, further studies of the design have indicated that, for particular amplifying ratios, a cemented doublet would reduce coma over a wide field to values below Baker's limit. The cemented design requires that the flint element be placed nearest the primary, so its surfaces are R_1 and R_2. Using the same types of optical glass as in the previous lens, and with the elements finished to a thickness of 0.33", the cemented design requires the following radii: R_1 -7.58", R_2 -3.32", R_3 -3.32", R_4 +10.50". This corrector is to be placed 6" inside the focus of a spherical mirror having a 24" focal length, and gives an amplifying ratio of 2.5 to 1.

As many readers know, results similar to mine may be achieved, theoretically at least, with a Cassegrainian type of reflector. The present design, however, with only spherical surfaces, permits this theoretical performance to be approached more closely in an instrument that can be easily made by the amateur. (Commercial rights are reserved by me.)

ROBERT T. JONES
840 Lincoln Ave.
Palo Alto, Calif.

SPACE SCIENCE–SOME SELECTED PROBLEMS AND ACCOMPLISHMENTS

Robert T. Jones

Ames Research Center

May 1960

Abstract of paper to be presented at Foothill College,
Space Lecture Series, May 16, 1960

SPACE SCIENCE - SOME SELECTED PROBLEMS AND ACCOMPLISHMENTS

By Robert T. Jones*

National Aeronautics and Space Administration
Ames Research Center
Moffett Field, Calif.

In this last lecture of our Foothill series we shall try to extend our viewpoint in two directions, looking forward and also backward in time for the scientific origins of some of our present day exploits.

It is interesting that the possibility of creating an artificial earth satellite is discussed rather extensively in Newton's Principia Mathematica. Modern space scientists do not often delve into such old textbooks, but if they were to do so they would find many interesting theorems - concerning, for example, the effect of air resistance on the spiraling "re-entry" of a satellite.

Newton's artificial satellite was launched by a cannon. The rocket is of course better for this purpose. By starting with a sufficiently large rocket and ending up with a sufficiently small pay load an almost unlimited speed can be acquired. Having a thorough understanding of

*Aeronautical Research Scientist

National Aeronautics and Space Administration
Ames Research Center
Moffett Field, Calif.

these principles the Russian scientists have evidently developed the largest rocket boosters. Military pressures from the sides have undoubtedly provided some inspiration to them in this task.

Looking toward improvement of the rocket, we seek means for increasing the velocity of the exhaust. At the present time acceleration of the exhaust by electromagnetic forces is being studied extensively. The ion rocket and the plasma rocket utilize such forces. The photon rocket, which propels itself simply by expelling electromagnetic field energy has been the subject of much speculation. Here the exhaust velocity is equal to the velocity of light. It is a well founded tradition of physicists that a body alone in empty space cannot change the position of its center of gravity. With the photon rocket this tradition is preserved in an unusual way through the equivalent weight of the expelled energy. The thrust developed by the photon rocket is however disappointingly small.

Present day technology contains many hints and clues regarding propulsive devices beyond the rocket. To go into the possibilities here would be, for me at least, a reckless venture. We may however arrive at some interesting conclusions if we suppose that the invention of such devices succeeds absolutely - so that we have available a thrust of comfortable magnitude for as long a period as required. Several years ago, following this thought, I published calculations of the times required to travel to various planets of the solar system at an acceleration of 1 g. The human organism is known to survive upwards of 70 years under this acceleration, but only 36 hours are required to get to Venus. A

rectilinear acceleration of 1 g in free space produces a velocity of the order of the velocity of light in one year (32 ft/sec^2 ≅ 1 light year/year^2). Survival at such cosmic ray velocities does indeed raise questions far beyond our present experience.

Finally I would like to mention one experiment which seems to me the most exciting and perhaps the most portentous experiment our scientists have performed to date. To understand this experiment we must go back to the development of the theory of earth's aurora by Stormer, Alfven and Poincaré in the early 1900's. In one experiment, performed in 1896, Birkeland made a small magnetized iron model of the earth. Suspending this magnetic "earth" in a primitive cathode ray tube and exposing it to a stream of electrons, supposed similar to those emanating from the sun, he observed bands of radiation which, as you will see from his illustration, are strikingly similar to those discovered around the real earth recently by James A. Van Allen. About the time of Van Allen's discovery a number of our local scientists were engaged in carrying out an experiment similar to, but much bolder than Birkeland's - suggested by N. C. Christofolos. In Christofolos' experiment a shell of relativistic electrons was created enclosing the earth along a surface defined by its magnetic field. It was found necessary to impose a limitation on the number of electrons injected into the magnetic shell to ensure that no radiation hazard would be produced. The experiment did however produce artificial auroras at points separated by thousands of miles over the earth.

This ability on the part of the scientists to create conditions which involve an interaction with the whole earth as a planet will clearly

call for increasing attention on the part of national leaders. We can hardly suppose that our past disputes will be resolved by these new things, but it may become necessary to neglect some of them - particularly those that have already begun to appear somewhat conventional. Thus progress is accompanied not so often by the solution of old problems as by their replacement with new ones.

NEWTON'S SYSTEM OF THE WORLD 551

force which is directed towards some centre; and as it regards
force as it is simply a body in that centre, we call it circumsolar, circum-
particularly centrimental; and so in respect of other central bodies.

The action of centripetal forces.

centripetal forces the planets may be retained in certain
The action of centripetal forces the planets may be retained in certain
easily understand, if we consider the motions of projectiles
a stone that is projected is by the pressure of its own weight
the rectilinear path, which by the initial projection alone it
pursued, and made to describe a curved line in the air; and

PHILOSOPHIÆ
NATURALIS
PRINCIPIA
MATHEMATICA

Auctore *J. S. NEWTONO*, Trin. Coll. Cantab. Soc. Matheseos
Professore Lucasiano, & Societatis Regalis Sodali.

IMPRIMATUR
S. PEPYS, Reg. Soc. PRÆSES.
Julii 5. 1686.

LONDINI,
Jussu Societatis Regiæ ac Typis Josephi Streater. Prostat apud
plures Bibliopolas. Anno MDCLXXXVII.

MOTION OF ROCKET IN FREE SPACE
V ROCKET / V NOZZLE
0
1
2
3
.5
1.0
1.5
W FINAL / W INITIAL

INTERPLANETARY FLIGHT AT 1g
REVERSE MANEUVER

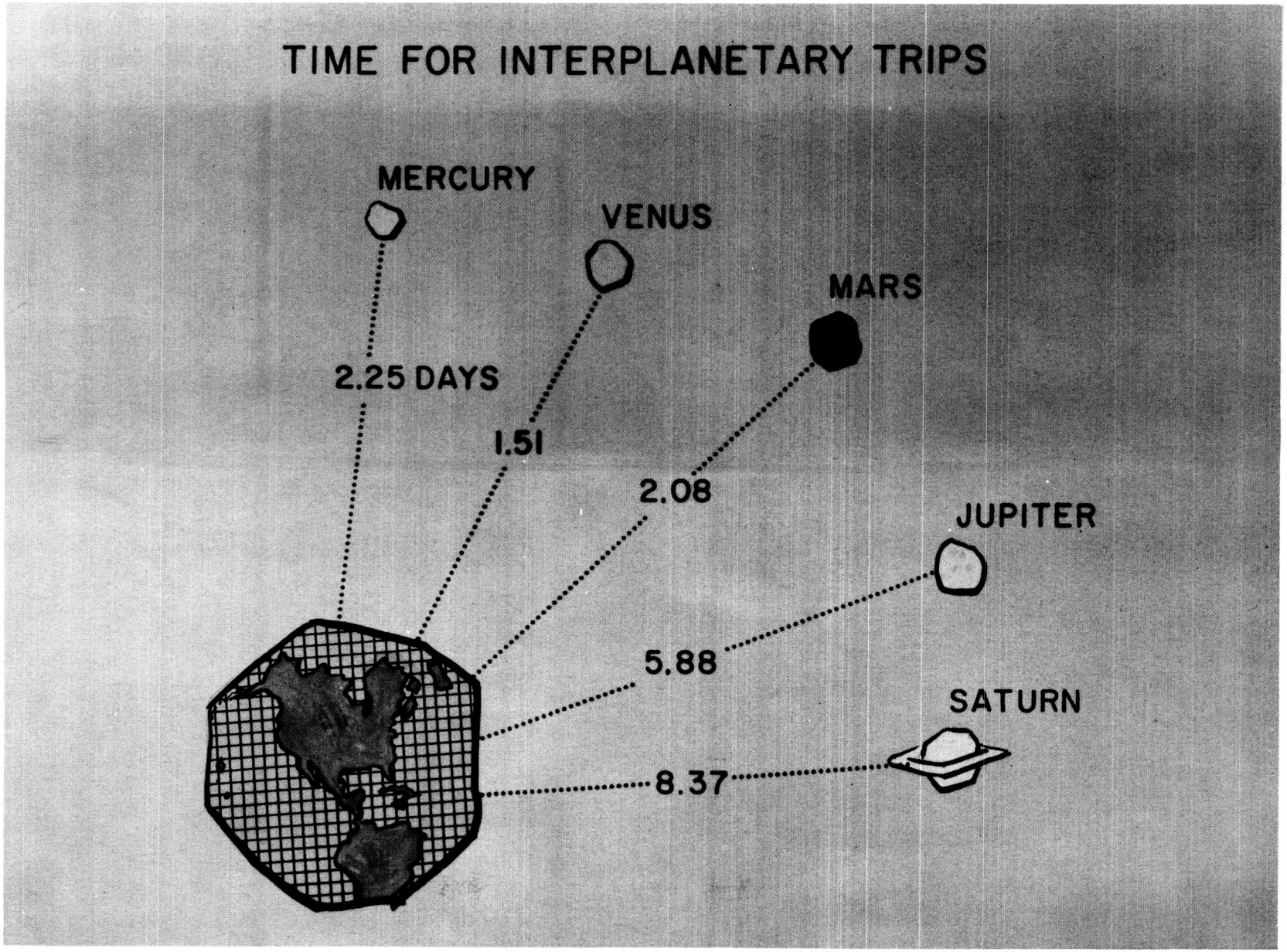
TIME FOR INTERPLANETARY TRIPS
MERCURY
VENUS
MARS
2.25 DAYS
1.51
2.08
JUPITER
5.88
SATURN
8.37

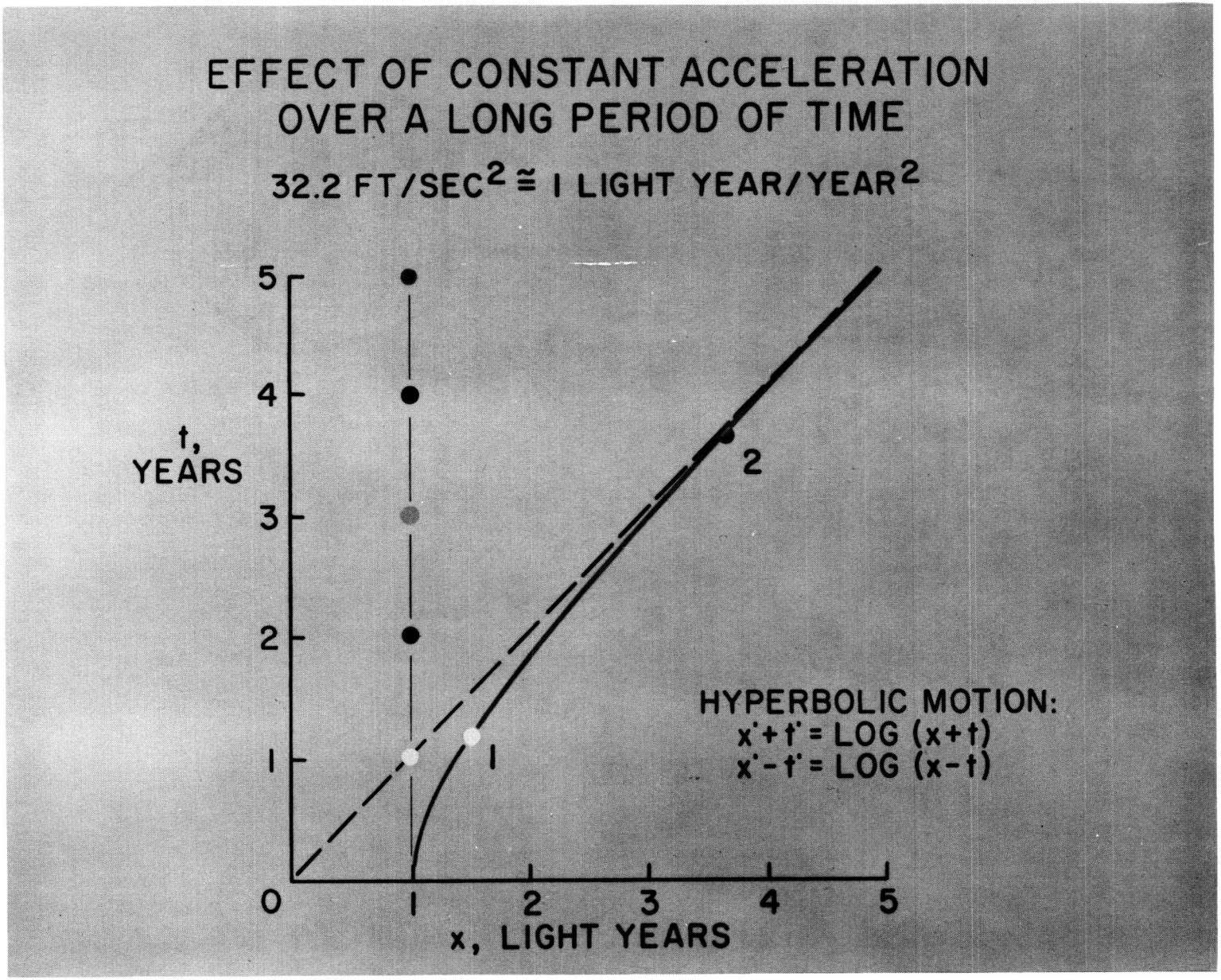
EFFECT OF CONSTANT ACCELERATION
OVER A LONG PERIOD OF TIME
32.2 FT/SEC^2 ≅ 1 LIGHT YEAR/YEAR^2
t, YEARS
5
4
3
2
1
0
1
2
3
4
5
x, LIGHT YEARS
2
1
HYPERBOLIC MOTION:
x'+t' = LOG (x+t)
x'-t' = LOG (x-t)

BIRKELANDS ORIGINAL EXPERIMENT
1896

ARGUS EXPERIMENT - CHRISTOFOLOS
1959

WIDE ANGLE LENSES WITH ASPHERIC CORRECTING SURFACES

Robert T. Jones

Avco-Everett Research Laboratory

November 1966

Jones, R. T., "Wide Angle Lenses with Aspheric Correcting Surfaces," Applied Optics, vol. 5, no. 11, Nov. 1966, pp. 1846-1849. © 1966.
Reprinted by permission of the Optical Society of America, Washington, D.C.

Reprinted from APPLIED OPTICS, Vol. 5, page 1846, November 1966
Copyright 1966 by the Optical Society of America and reprinted by permission of the copyright owner

Wide Angle Lenses with Aspheric Correcting Surfaces

Robert T. Jones

Refracting elements having aspheric correcting surfaces near the center of curvature are analyzed. As in the case of the Schmidt reflector, such systems can have a wide aperture and a wide field of view; in addition, they are free from obstructing surfaces. Being uncorrected for dispersion, however, the refracting systems are restricted to nearly monochromatic radiation. Typical forms of the correcting surfaces have been determined, both by third-order theory and by numerical integration of exact equations.

I. Introduction

In *La Geometrie*[1], Descartes shows how lens surfaces may be shaped to achieve axial stigmatism. The curves devised by Descartes for this purpose have since become known as Cartesian Ovals. Later, Huygens[2] showed how the rear surface of a lens could be shaped to correct the spherical aberration of preceding surfaces.

These measures, of course, leave uncorrected oblique aberrations such as coma and astigmatism. In 1930, Bernhard Schmidt pointed out that the oblique aberrations of a spherical mirror could be eliminated by placing a stop at the center of curvature of the mirror. Since the central ray of a pencil always meets the mirror at perpendicular incidence, there are, in effect, no *oblique* rays in such an arrangement. Spherical aberration is then corrected by placing a thin aspheric lens at the stop. The correcting lens, of course, introduces oblique aberrations of its own, but since it has only enough power to correct the spherical aberration of the mirror, these are reduced to small values.

Such a principle, utilizing the symmetry of the sphere and with correction at the center of curvature, may be adapted to refracting elements as well as to the reflector. Though restricted to monochromatic radiation, such refracting systems have advantages in certain applications.

Figure 1 shows two dioptric systems of this nature. In Fig. 1(a), the thickness of the lens is equal to the radius of the rear surface, and the aspheric correction together with the stop are placed at the front surface. The image is formed in air on a surface whose radius is equal to the distance between an axial image point and the stop.

The author is with Avco Everett Research Laboratory, Everett, Massachusetts 02149.

Received 8 June 1966.

This work was supported by U.S. Air Force under a contract.

II. Type A Lens

An approximate form for the correcting surface in Fig. 1(a)* may be obtained by computing the optical path difference between the spherical rear surface and an appropriate Cartesian oval. The Cartesian oval for stigmatic refraction of parallel rays at the rear surface is an hyperboloid of eccentricity n(n = index of refraction). Expanding the equation of this surface in terms of the vertex radius r, one obtains

$$x = a + (y^2/2r) - [y^4/(2r)^3](n^2 - 1) + \ldots, \quad (1)$$

while for the sphere

$$x = a + (y^2/2r) + [y^4/(2r)^3]. \quad (2)$$

The difference in optical path is then

$$\Delta x = -n^2\,[y^4/(2r)^3], \quad (3)$$

and this is the equation of the front surface, to the accuracy of third-order theory. Somewhat better correction can be obtained if this fourth degree curve is combined with a second degree curve in order to bring the slope of the correcting surface to zero at some specified zone y_m of the lens. In this case, we would have

$$\Delta x = [(2n^2y_m^2y^2)/(2r)^3] - n^2[y^4/(2r)^3] \quad (4)$$

The foregoing relations, determined by third-order theory, will not be sufficiently accurate for lenses of wide aperture. Therefore, we have programmed the exact determination of the shape of the correcting surface on the Avco Everett Research Laboratory IBM

* The lens design shown in Fig. 1(a) has been suggested independently by R. Gelles in a paper presented at the 1966 Spring meeting of the Optical Society of America (paper WH 17). Gelles' report (as yet unpublished) gives field aberration curves determined by geometric ray traces and suggests an interesting application of the Schmidt principle in a spectroscope.

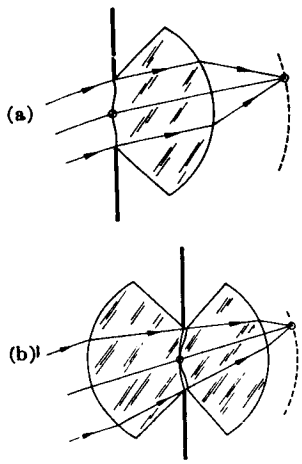

Fig. 1. Lenses with correction at center of curvature.

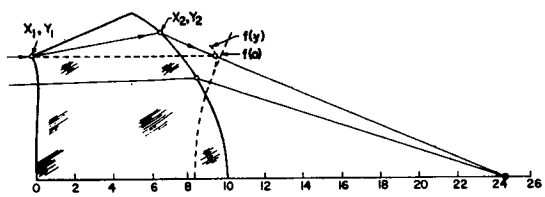

Fig. 2. Type A lens, showing departure from sine condition: $n = 1.52$, $R = 1.0$, $f(0) = 1.606$ (see Table I).

7040 computer. Figure 2 and Table I give a typical result of these calculations.

With wide apertures and small field angles, the most serious oblique aberration will be coma. In the absence of spherical aberration, the extreme width of the coma patch for a field angle β is given by $\delta = 3\beta\,[f(y) - f(0)]$. Here y is the semi-aperture, $f(0)$ is the paraxial focal length, and $f(y)$ is the focal length of the zone y obtained by producing the incoming parallel ray to its intersection with the converging ray (see Fig. 2). The difference $f(y) - f(0)$ is a measure of the departure from the sine condition.

Figure 2 shows the calculated departures from the sine condition for the lens shape of Fig. 1(a). It is noted that the sine condition holds to a high degree of accuracy for apertures considerably greater than those accessible to third-order theory. Appreciable departures do not occur until value of $y > 0.6$.

With coma eliminated, there remains an aberration proportional to the square of the field angle β. Following an analysis by Caratheodory[3], it is found that this aberration depends on the slope and curvature of the correcting surface and, at a given zone y, is identical with the ordinary astigmatism of an equivalent simple lens.

In the case of the Schmidt reflector, the local power of the correcting surface is ordinarily quite small, and the higher order astigmatism is usually negligible. However, the spherical aberration of the refractor is much greater than that of the reflector, so the power of the correcting surface required may no longer be negligible. Thus, in Fig. 2, the curvature of the correcting surface exceeds that of the main refracting surface for values of $y > 0.47$. If the aperture is allowed to exceed this value, one would expect the astigmatism associated with these zones to be as great as that of a simple uncorrected lens.

III. Type A Lens Reversed

In addition to the shapes illustrated in the first figure, one might also consider a lens in which the main refraction occurs at the front surface and with the *rear* surface figured, but nearly flat. Such a surface, however, lacks the essential properties of the correcting lens since rather large oblique aberrations arise in the converging rays. Figure 3 shows the third-order astigmatism for several arrangements. In Fig. 3(a), the rear lens surface is flat; it is to be noted that the sagittal and tangential focal surfaces curve rather sharply toward the lens. Such curvature cannot be avoided by aspheric figuring.

Coma and astigmatism can be avoided by a suitable curvature of the rear lens surface, however. The theory gives $r_2 = r_1[n/(n^2 - 1)]$. For the usual values of n, the second surface has considerable negative power, so the resultant power of the lens is rather small. Figure 3(c) corresponds to Fig. 1(a); in this case, both third-order astigmatism and coma vanish.

As is well known[3,4] aspheric shapes can be found for two refracting surfaces that will eliminate both spherical aberration and coma. A free parameter in such shapes is the thickness of the lens. By selecting thicknesses approximately equal to the radius of one of the surfaces, we obtain forms for these *aplanatic* lenses approximating the forms illustrated in Fig. 3. Figure 4

Table I. Coordinates of Surfaces and Rays; Lens Fig. 1(a)

x_1 / y_1	x_2 / y_2	$f(y)$
0.0	1.0	1.606086
0.0	0.0	
0.001799	0.994987	1.605898
0.110773	0.100000	
0.005914	0.981784	1.605527
0.207266	0.190000	
0.010954	0.960000	1.605252
0.298160	0.280000	
0.015826	0.916515	1.605626
0.407434	0.400000	
0.014472	0.854166	1.607595
0.500538	0.520000	
0.008904	0.803725	1.610152
0.549880	0.595000	
−0.003427	0.728543	1.615800
0.600030	0.685000	
−0.018830	0.649923	1.625010
0.634677	0.759999	

$n = 1.52$, $R = 1.0$, $f(0) = 1.606$.

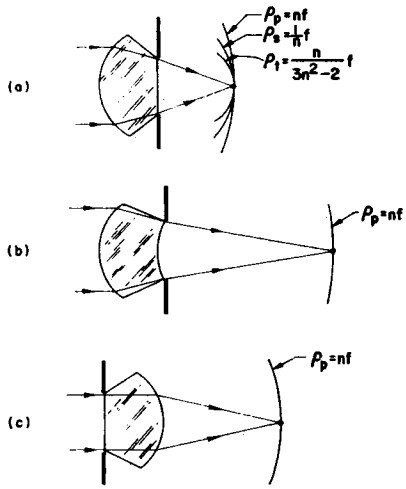

Fig. 3. Astigmatism of lenses with stop at center of curvature.

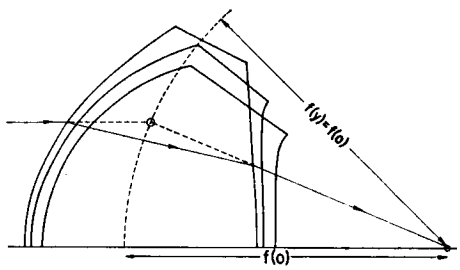

Fig. 4. Aplanatic lens shapes for $t \simeq r$.

shows several aplanatic lenses having the required thickness.

The shapes illustrated in Fig. 4 were calculated with the aid of the Avco Everett Research Laboratory's IBM 7040 computer, utilizing equations given by A. K. Head.[5] Such lenses, having two aspheric surfaces, can achieve rather wide apertures with correction of third-order coma. Astigmatism will not be corrected, however, unless the rear surface has considerable negative power, as in Fig. 3(b).

Since the main refracting surfaces in Fig. 4 are approximately spherical, it is of interest to determine the magnitude of the error in the sine condition that would be introduced by making the first surface exactly spherical. Figure 5 shows such a Huygens lens compared with a neighboring, perfectly aplanatic lens. The small change in shape results in a surprisingly large departure from the sine condition. Aspheric figuring does not affect the coma of a single surface, but the transfer of distortions between two surfaces separated by a large distance can evidently produce quite a large effect.

IV. Type B Lens

The arrangement of Fig. 1(b) seems to afford the widest apertures and field angles. Here, by third-order theory, we obtain

$$\Delta x = G(n)[2y_m^2y^2/(2r)^3 - y^4/(2r)^3], \qquad (5)$$

where Δx is the thickness of the *air lens* and $G(n) = n[n - (2 - n)(2n - 1)]$. These equations refer to the case in which the front and rear surfaces are portions of the same sphere. Since the air lens lies in the path of converging rays, it seems preferable to curve its mean line about their center of convergence.

In order to determine the shape of the correcting surfaces for wider apertures than permitted by third-order theory, we have used the method of Wasserman and Wolf[4], programming the calculation for the IBM 7040 computer. These calculations yield two surfaces, Σ and Σ', which, together with the two spherical surfaces, make the system aplanatic. Figure 6 shows a typical result of these calculations. As might be expected, the aspheric surfaces Σ and Σ' curve backward,

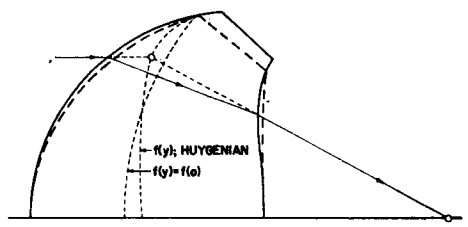

Fig. 5. Comparison of Huygenian and aplanatic lenses.

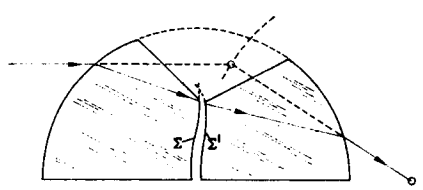

Fig. 6. Spherical lens with aplanatic correcting surfaces.

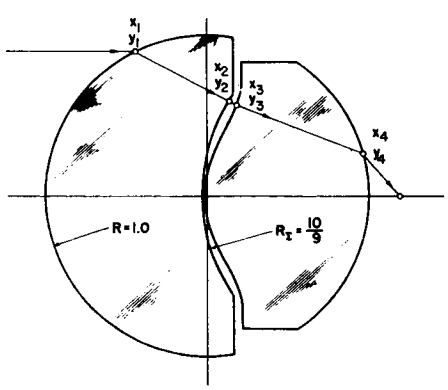

Fig. 7. Spherical lens with approximately aplanatic correcting surfaces: $n = 1.52$ $R_\Sigma = 10/9$, $f(0) = 1.2$ (see Table II).

Table II. Coordinates of Surfaces and Rays; Lens Fig. 1(b)

x_1	x_2	x_3	x_4	$f(y)$
y_1	y_2	y_3	y_4	
−1.000000	−0.025000	−0.011832	1.000000	1.200000
0.0	0.0	0.0	0.0	
−0.988771	−0.020536	−0.004185	0.999683	1.198802
0.149438	0.099504	0.098986	0.025167	
−0.955337	−0.007527	0.017720	0.998681	1.195709
0.295520	0.196272	0.194601	0.051349	
−0.900447	0.012913	0.050774	0.996825	1.192091
0.434966	0.287773	0.283734	0.079623	
−0.837345	0.035035	0.084161	0.994325	1.189906
0.546675	0.360286	0.352980	0.106385	
−0.780506	0.053742	0.109972	0.991682	1.789347
0.625148	0.410830	0.400332	0.128711	
−0.370000	0.069436	0.129594	0.988967	1.189568
0.683447	0.448263	0.434922	0.148135	
−0.685327	0.082624	0.144462	0.986224	1.189998
0.728236	0.477055	0.461329	0.165413	
0.610223	0.103425	0.164562	0.980690	1.190335
0.792230	0.518552	0.499402	0.195567	
−0.521892	0.125925	0.181135	0.971954	1.188204
0.853012	0.559115	0.537521	0.235173	
−0.450757	0.142743	0.189489	0.961641	1.182566
0.892647	0.587048	0.565432	0.274310	
−0.389937	0.156396	0.193113	0.947501	1.173333
0.920842	0.608438	0.588941	0.319753	
−0.309448	0.173742	0.190704	0.896886	1.152821
0.950917	0.634153	0.623372	0.442262	

$n = 1.52$, $R = 1$, $R_\Sigma = 10/9$, $f(0) = 1.2$.

making the air lens more or less normal to the converging rays.

The Σ and Σ' curves determined in this way provide exact correction of third-order coma. Furthermore, if the Σ and Σ' surfaces are nearly parallel, the higher order aberrations introduced by them will be quite small. If the Σ and Σ' curves actually do satisfy this latter condition, it will not be essential to make both curves aspheric. One curve (Σ, for instance) can be made spherical, and the small difference in optical path length can be transferred to the other surface.

Following this latter thought, we have made calculations for the shape of the Σ' surface on the assumption that Σ has a spherical shape generally similar to that of the aplanatic curve. Figure 7 and Table II show one of the shapes determined in such a way for a focal length of 1.2 times the radius of the sphere. Also shown are the slight departures from the sine condition $f(y) - f(0)$. Here the transfer of elements of the optical path has occurred over a small distance separating the Σ and Σ' surfaces, with the result that the sine condition is hardly disturbed. It is noted that the example provides a high degree of correction up to an aperture of $f/0.66$.

The author would like to acknowledge the assistance of J. D. Teare of Avco Everett Research Laboratory in formulating the problem of aspheric lens shapes, and of H. Kachadorian, Paul Kasperovics, and R. Johnson for helping in the programming of the calculations.

References

1. R. Descartes, *La Geometrie;* see *The Geometry of Descartes*, by D. E. Smith and M. L. Latham (Open Court Publishing Company, La Salle, Ill., 1925), pp. 352–353.
2. C. Huygens, *Treatise on Light* (Dover Publications, Inc., New York, 1962).
3. E. H. Linfoot, *Recent Advances in Optics* (Clarendon Press, Oxford, 1955), pp. 180–181.
4. M. Born and E. Wolf, *Principles of Optics* (Pergamon Press, Inc., New York, 1959), pp. 196–201.
5. A. K. Head, Proc. Phys. Soc., **74**, 731 (1959).

TIMES FOR INTERPLANETARY TRIPS

Robert T. Jones

Ames Research Laboratory

November 1955

Jones, R. T., "Times for Interplanetary Trips."
Reprinted by permission from Jet Propulsion, v. 26, no. 2, February 1956, page 102.

Times for Interplanetary Trips

ROBERT T. JONES[1]

Ames Laboratory, NACA, Palo Alto, Calif.

THE writer found it interesting to calculate the times required to travel to the various planets at an acceleration of one "g," or 8×10^4 mph/h.

Of course, with a thrust of such comfortable magnitude one can neglect surrounding gravitational fields except for a relatively short distance near take-off or landing. The "orbit" consists of an essentially straight line with the thrust directed toward the destination up to the halfway point, but in the opposite direction for the remainder so that the velocity is zero on arrival.

The following table lists the approximate times required, and also the maximum velocities acquired in light units v/c.

	t, in days	v/c
Mercury	2.25	0.0032
Venus	1.51	0.0021
Mars	2.08	0.0029
Jupiter	5.88	0.0083
Saturn	8.37	0.0118
Uranus	12.07	0.017
Neptune	15.45	0.022
Pluto	17.80	0.025

In spite of the small values of v/c the energy expended is certainly large by present standards. Nevertheless, it is interesting to see how quickly even "astronomical" distances succumb to the application of a thrust force of such a reasonable magnitude.

Received Nov. 14, 1955.

[1] Senior Aeronautical Scientist.

EXTENDING THE LORENTZ TRANSFORMATION BY CHARACTERISTIC COORDINATES

Robert T. Jones

Ames Research Center

February 1960

Jones, R. T., "Extending the Lorentz Transformation by Characteristic Coordinates," American Journal of Physics, vol. 28, no. 2, Feb. 1960, pp. 109-111. © 1960 held by the American Association of Physics Teachers. Reprinted by permission of the American Journal of Physics, New York, N.Y.

Reprinted from AMERICAN JOURNAL OF PHYSICS, Vol. 28, No. 2, 109–111, February, 1960
Printed in U. S. A.

Extending the Lorentz Transformation by Characteristic Coordinates

ROBERT T. JONES*
National Aeronautics and Space Administration, Ames Research Center, Moffett Field, California
(Received May 28, 1959)

The problem considered is that of rectilinear motion with variable velocity. The paper gives, by an elementary construction, a system of coordinates which is conformal in a restricted region near the axis of the motion. In such coordinates the velocity of light remains invariant even for observers moving with variable velocity. By a particular choice of the scale relation the restricted conformal transformations can be made to reduce to the Lorentz transformation everywhere in the case of constant velocity and locally in the case of variable velocity.

IN the *American Journal of Physics*, November, 1958, Leffert and Donahue call attention to irregularities that appear when the Lorentz transformation is extended to problems of variable motion. Figure 1 illustrates the difficulty alluded to. Here the moving origin of a system B is plotted as a curvilinear world line on a rectangular system which is not shown, but which we may designate as A. In such a diagram the lines $t'=$constant associated with B are oblique and if they are continued as straight lines they will cross, leading to a nonuniform correspondence of events between the A and B systems. This lack of uniformity appears in the conventional treatments of the problem, as, for example, in the analysis given by Møller.[1]

A uniform correspondence can be achieved, however, if the Lorentz transformation is extended by means of characteristic lines, rather than along straight t' lines. An extension along straight t' lines amounts to the assumption that the Lorentz transformation propagates instantaneously in the B system and at the electromagnetic phase velocity c^2/v in the A system. The characteristic lines, however, have the same slope in either system, and of course propagate at the velocity of light. The use of the characteristic lines establishes a conformal correspondence between the two systems x, it and x', it'. As is well known, such transformations preserve a constant velocity of light during accelerated motions, even in three-dimensional space, if they can be established.[2,3] This note shows how such coordinates can be established in the vicinity of the line of motion for a system with variable rectilinear velocity.

Figure 2 shows the curvilinear coordinates obtained in the xt plane when the Lorentz

* Aeronautical Research Scientist.
[1] C. Møller, *The Theory of Relativity* (Clarendon Press, Oxford, 1952), pp. 258–263.
[2] H. Bateman, *Electrical and Optical Wave Motion* (Dover Publications, New York, 1955), S14.
[3] L. Infeld and A. Schild, Phys. Rev. 26, 250–272 (1945).

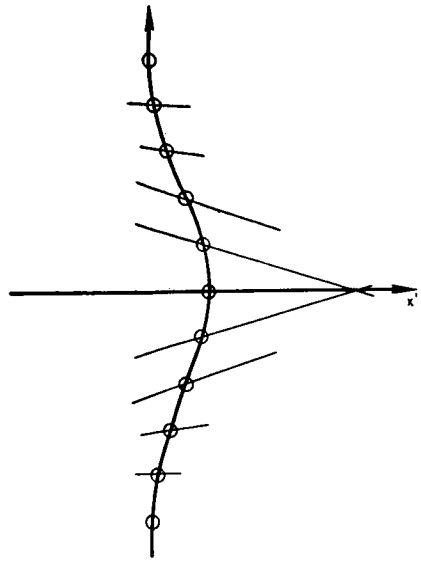

FIG. 1. Continuation of the Lorentz transformation along straight time lines, $t'=$const.

transformation is extended by means of the characteristic lines. For convenience the velocity of light is chosen so that these lines are at 45°. The spacing of the lines (Doppler frequencies), and the extended x', t' coordinates may be obtained from time signals originated in the moving system. Thus we may suppose that a clock at the origin of $B(x'=0)$ emits signals at equal intervals of its proper time. Each pulse is marked by two characteristic lines, $x-t=$const and $x+t=$const. By extending the pulses in the negative time direction, we represent also the signals arriving at the origin from the other clocks of the system. Such waves, identified with length and time signals, are stationary or "standing" relative to the moving clock as far as length and time measurements are concerned. The surfaces of constant phase and constant amplitude in such a wave pattern form the level surfaces of a conformal coordinate system, valid at least in a small region of space around the x axis. The construction thus provides a particular example of the group of conformal transformations introduced by Bateman and discussed by Milne and others. The particular transformation obtained by our construction differs from those previously given in that it reduces to the Lorentz transformation locally in the case of variable velocity and everywhere in the case of uniform velocity.

Omitting y and z for the moment, we may write the Lorentz transformation in the form

$$x'-t'=[(1+v)/(1-v)]^{\frac{1}{2}}(x-t),$$
$$x'+t'=[(1-v)/(1+v)]^{\frac{1}{2}}(x+t).$$

The extended transformation is

$$x'-t'=G(x-t),$$
$$x'+t'=F(x+t).$$

Here F and G are functions partly determined by the variable motion of B. Setting

$$\frac{dF}{d(x+t)}=f;\quad \frac{dG}{d(x-t)}=g,$$

we obtain for the velocity

$$v=\left(\frac{dx}{dt}\right)_{x'=\text{const}}=\frac{g-f}{g+f}.$$

For the composition of two velocities v_1 and v_2 we write

$$v_1=\frac{g_1-f_1}{g_1+f_1},$$
$$v_2=\frac{g_2-f_2}{g_2+f_2},$$

and from the composition of two transformations

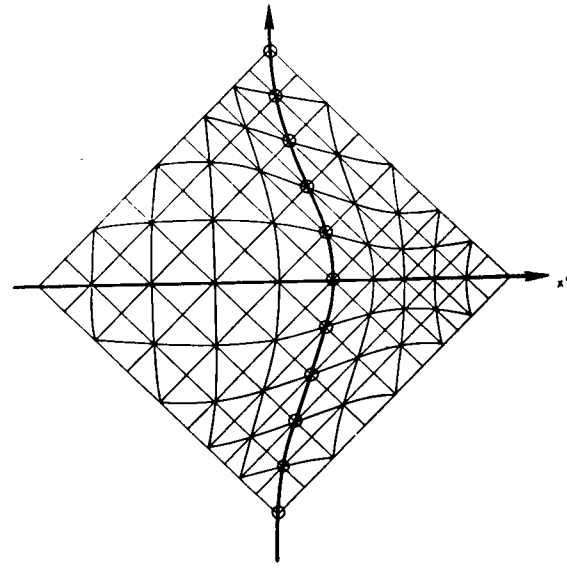

FIG. 2. Continuation of the Lorentz transformation along conformal coordinates.

there results

$$v_3=\frac{g_1g_2-f_1f_2}{g_1g_2+f_1f_2},$$

a form which illustrates the group property by its symmetry. In the more usual form,

$$v_3=\frac{v_1+v_2}{1+v_1v_2}.$$

To calculate the deficit in elapsed time for system B, we need the formula

$$(dt')_{x'=\text{const}}=(fg)^{\frac{1}{2}}(1-v^2)^{\frac{1}{2}}dt.$$

The result is the same as that given by the restricted relativity theory since our construction makes the factor fg equal to unity along the line $x'=0$. For other clocks of the B system the time discrepancy is a function of position. However, these displacements ultimately adjust themselves to the same value if the system comes to rest. There is also a discrepancy in elapsed distances, obtained by integrating the formula

$$(dx')_{t'=\text{const}}=(fg)^{\frac{1}{2}}(1-v^2)^{\frac{1}{2}}dt.$$

The foregoing one-dimensional analysis may be extended to three-dimensional space at least over a small region in the vicinity of the axis of motion. If we write

$$y'=(fg)^{\frac{1}{2}}y,$$
$$z'=(fg)^{\frac{1}{2}}z,$$

then

$$-(ds'^2)=fg(dx^2+dy^2+dz^2-dt^2) \quad \text{as} \quad y^2+z^2\to 0.$$

Such restricted conformal transformations permit arbitrary motions. Unrestricted transformations, which preserve a constant velocity of light throughout space, seem to admit only special types of accelerated motion.

To preserve the condition of complete equivalence demanded by E. A. Milne,[4] we should require that the scale factor fg reduce to unity along the line $x=0$ and also along the line $x'=0$. It does not seem possible to meet this requirement by conformal transformations except in the case of uniform velocity (Lorentz transformation). The construction given above makes the scale factor equal to one in the vicinity of the origin of $B(x'=0)$; A and B are hence not equivalent in Milne's sense, but A is here distinguished as an inertial system.

In the analysis of Donahue and Leffert the gravitational waves associated with the acceleration of B travel instantaneously in the B system and at the electromagnetic phase velocity c^2/v in the A system. As Fig. 2 shows such waves travel at the velocity of light in the conformal coordinate system. However, a physical interpretation of these distortions seems difficult, since both incoming and outgoing waves are present. Such questions could hardly be answered by the elementary considerations we have employed.

Additional details of this analysis will appear in a forthcoming NASA Memorandum.[5]

In conclusion, the writer wishes to acknowledge helpful discussions with Professor Paul R. Garabedian of Stanford University and Barrett S. Baldwin of Ames Research Center.

[4] E. A. Milne, *Relativity, Gravitation, and World Structure* (Clarendon Press, Oxford, 1935).

[5] Robert T. Jones, "Extending the Lorentz Transformation to Motion with Variable Velocity," NASA MEMO 7-9-59A (1959).

ANALYSIS OF ACCELERATED MOTION IN THE THEORY OF RELATIVITY

Robert T. Jones

Ames Research Center

June 1960

Jones, R. T., "Analysis of Accelerated Motion in the Theory of Relativity,"
Nature, vol. 186, no. 4727, June 4, 1960, p. 790. © 1960.
Reprinted by permission of Macmillan Journals, Ltd., London.

ANALYSIS OF ACCELERATED MOTION IN THE THEORY OF RELATIVITY

Conventional treatments of accelerated motion in the theory of relativity have led to certain difficulties of interpretation. Thus, Crampin, McCrea and McNally[1] mention the lack of uniformity in the correspondence of events as depicted by the transformation of Born and Biem. Again, Donahue and Leffert[2] and Moller[3] discuss certain reversals in the apparent gravitational field of an accelerated body. I have found[4] that these difficulties may be avoided by simpler analysis based on the use of restricted conformal transformations. In the conformal theory the velocity of light remains constant even for experimenters in accelerated motion.

The problem considered is that of rectilinear motion with a variable velocity v. I introduce two coordinate systems, A, (x,t) and B, (x',t'). The motion takes place along the x or x' axis.

The correspondence between the xt and $x't'$ systems may be expressed quite simply by the transformation:

$$\begin{aligned} x' + t' &= F(x + t) \\ x' - t' &= G(x - t) \end{aligned} \tag{1}$$

The velocity is given by:

$$v = \frac{g - f}{g + f} \tag{2}$$

Here f and g are the derivatives of F and G with respect to their arguments $x \pm t$. I now suppose that A, (x,t) is an inertial system, and in order to satisfy the relation of equivalent scale in the vicinity of B, I apply the boundary condition:

$$fg = 1 \text{ along } x' = 0 \tag{3}$$

If the motion of B is given then this relation, together with equation (2), is sufficient to determine the functions F and G. As determined in this way, this transformation becomes tangent to instantaneous Lorentz transformations all along the path of B and in the case of uniform velocity reduces to the Lorentz transformation everywhere.

Fig. 1 shows how such $x't'$ co-ordinates may be constructed graphically with the aid of periodic time signals originating in the B system. Such

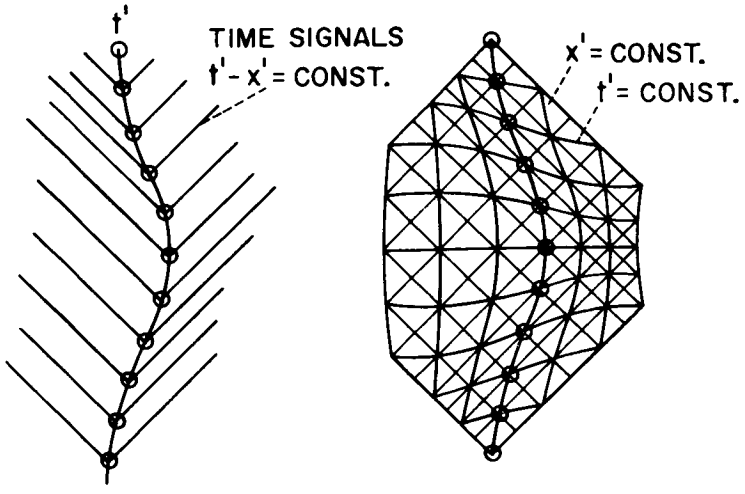

Figure 1. A system of conformal co-ordinates associated with non-uniform motion

signals generate a family of outgoing waves, represented by the characteristic lines $t \pm x$ = constant. If these lines are now extended backward, a corresponding family of incoming signals will be represented. Intersections of the characteristic lines may then be identified with the events of synchronization of the various clocks of the B system.

Extension of the theory of relativity by conformal transformations in four dimensions was considered many years ago by Bateman[5]. It seems that the group $C4$ admits only restricted motions, and of these the Lorentz transformation alone maintains equality in the scale relation. Therefore, we do not speak of a conformal transformation of the whole space. However, by restricting attention to a narrow cylindrical region around the x-axis,

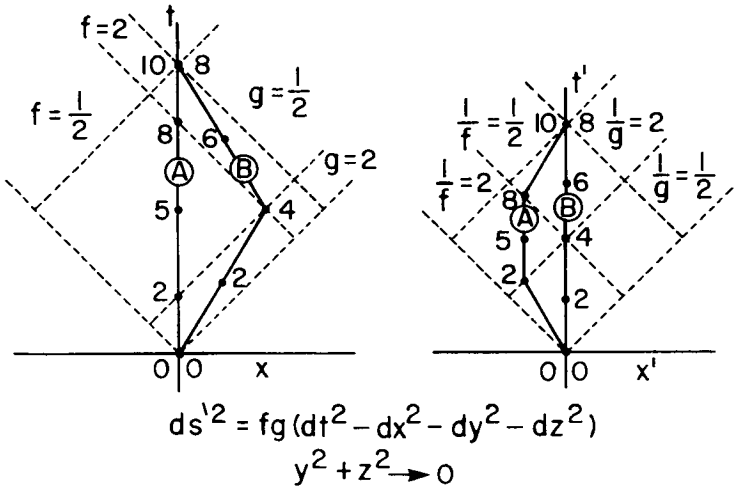

Figure 2. Example showing application of restricted conformal transformations

conformal mappings can be employed locally, so that:

$$ds'^2 = fg(dt^2 - dx^2 - dy^2 - dz^2) \qquad (4)$$
$$\text{for } y^2 + z^2 \to 0.$$

Fig. 2 illustrates a simple example of the type discussed in connexion with the clock paradox. At $t = 0$, B starts away from A at the velocity 3/5. At $t = 5$, B reverses its motion and returns. Values of f and g in various regions are indicated between characteristic signal lines. The condition of local scale equivalence, $fg = 1$, results in a 20 per cent reduction of the elapsed time along the path of B. In addition to the time discrepancy, there appears also a discrepancy in the relative spatial displacements.

ROBERT T. JONES

National Aeronautics and Space Administration,
Ames Research Center,
Moffett Field, California.
Jan. 20.

REFERENCES

1. Crampin, Joan, McCrea, W. H., and McNally, D., *Proc. Roy. Soc.*, A, 252, 156 (1959).

2. Leffert, C. B., and Donahue, T. M., *Amer. J. Phys.*, 26, No. 8 (1958).

3. Moller, C., *Amer. J. Phys.*, 27, No. 7 (1959).

4. Jones, Robert T., "Extending the Lorentz Transformation to Motion with Variable Velocity", NASA Memo 7-9-59*A* (1959).

5. Bateman, H., *Proc. Lond. Math. Soc.*, ii, 8, 223 (1910).

CONFORMAL COORDINATES ASSOCIATED WITH UNIFORMLY ACCELERATED MOTION

Robert T. Jones

Ames Research Center

February 1961

Jones, R. T., "Conformal Coordinates Associated with Uniformly Accelerated Motion," American Journal of Physics, vol. 29, no. 2, Feb. 1961, pp. 124-125. © 1961 held by the American Association of Physics Teachers. Reprinted by permission of American Journal of Physics, New York, N. Y.

Reprinted from AMERICAN JOURNAL OF PHYSICS, Vol. 29, No. 2, 124–125, February, 1961
Printed in U. S. A.

Conformal Coordinates Associated with Uniformly Accelerated Motion

ROBERT T. JONES
National Aeronautics and Space Administration, Ames Research Center, Moffett Field, California

DISCUSSION of specific problems in the theory of relativity is often simplified by an appropriate choice of the coordinate system. Thus the restricted conformal coordinates described in a previous communication[1] provide an especially simple analysis of motion with uniform acceleration, known as "hyperbolic motion".[2]

Conformal coordinates x', t' may be obtained from Cartesian coordinates x, t by the transformation

$$x'+ct'=F(x+ct)$$
$$x'-ct'=G(x-ct), \tag{1}$$

where c is the velocity of light. A variable motion of the x' system will be determined by the choice of the functions F and G. However, since a function remains constant whenever its argument is constant, light signals have the same velocity c in both x and x' systems.

The scale factor of the transformation is given by the product fg, where f and g are the ordinary derivatives of F and G. The line $x'=0$ may be taken as the world line of a particle. To satisfy the principle of relativity in the vicinity of this particle, we impose the boundary condition,

$$fg=1 \quad \text{along} \quad x'=0. \tag{2}$$

With this boundary condition, the functions F and G are determined so that both the transformation and its inverse have the same scale along $x'=0$.

As an example, try

$$x'+ct'=\log(x+ct)$$
$$x'-ct'=\log(x-ct). \tag{3}$$

By addition,

$$2x'=\log(x^2-c^2t^2).$$

The world line $x'=0$ is then given by the hyperbola

$$x^2-c^2t^2=1.$$

After differentiating Eqs. (3), we obtain

$$fg=1/(x^2-c^2t^2),$$

which has the value 1 along $x'=0$. Equations (3) thus yields the conformal coordinates associated with uniformly accelerated motion. The acceleration here has the value one light-year/year,[2] or approximately one "g"; however, the formula is easily generalized.

It is interesting to note that the gravitational field in the $x't'$ system is singular at the origin of the xt system. Such singularities arise when simple analytic formulas are employed. In the present case, the singularity disappears if the acceleration is not continued for an infinite time.

As is well known, conformal transformations in Euclidean space are carried out with the aid of functions of a single complex variable. Such a conformal map may represent the streamlines and equipotential lines of a fluid motion. On using the customary φ and ψ for the potential function and the stream function, we may write

$$\varphi+i\psi=F(x+iy).$$

The complex potential for a vortex is given by

$$\varphi+i\psi=i\log(x+iy).$$

This formula is clearly analogous to our Eq. (3) for hyperbolic motion. Thus the conformal coordinates associated with hyperbolic motion in Minkowski space become the circular paths of a vortex motion in Euclidean space.

Now the vortex motion is merely the simplest example of a wider class of fluid motions known as "free streamline flows". The boundary condition of such flows is that the scale factor of the mapping reduce to unity along a (free) streamline $\psi=0$. This condition is clearly analogous to our condition $fg=1$, along $x'=0$. Thus, every free streamline may be transformed into an analytic world line with its associated conformal coordinates. The converse is not true, however, since the possibilities in Euclidean space are limited to analytic functions of a single (complex) variable.

[1] Robert T. Jones, Am. J. Phys. 28, 109 (1960).
[2] W. Pauli, *Theory of Relativity* (Pergamon Press, New York, 1958)

CONFORMAL COORDINATES ASSOCIATED WITH SPACE-LIKE MOTIONS

Robert T. Jones

Ames Research Center

January 1963

Jones, R. T., "Conformal Coordinates Associated with Space-Like Motions," Franklin Institute. Journal, vol. 275, no. 1, Jan. 1963, pp. 1-12.
© 1963.
Reprinted by permission of the Franklin Institute, Philadelphia, Pa.

Journal
of
The Franklin Institute
Devoted to Science and the Mechanic Arts

Vol. 275 JANUARY, 1963 No. 1

CONFORMAL COORDINATES ASSOCIATED WITH SPACE-LIKE MOTIONS

BY

ROBERT T. JONES[1]

ABSTRACT

Conformal transformations in two dimensions provide a simple extension of the Lorentz transformation. The velocity of light appears in such transformations as a singular velocity rather than as an upper limit for the velocity. A well-ordered branch of the theory exists for velocities in excess of the velocity of light.

If the velocity of a point exceeds the singular velocity in an inertial system, then the conformal representation of the motion is no longer uniform, but contains a folded region. However, the branching of the transformation may be determined so that the elapsed time along the path of such a motion remains positive.

Kinematic relations on the other side of the singular velocity seem to complement the usual results of relativity theory in an interesting way. Thus it is known that motion at the speed of light occurs along a null geodesic, and hence corresponds in a certain sense to motion at infinite velocity (that is, in the sense of proper time elapsed). The complementary relation is that a motion of infinite velocity corresponds in the same sense to motion at the speed of light.

INTRODUCTION

In the world of the physicist everything moves, but always at speeds less than the speed of light. The astronomer's world, too, is filled with moving objects, moving at $v < c$. In the world of the mathematician, however, anything is possible, provided only that it is a consequence of something else.

Strangely enough, writers on physics would like to refer the nonexistence of velocities greater than light to a mathematical demonstration—connecting it with the transition of the Lorentz factor $1/\sqrt{1 - v^2/c^2}$ to imaginary values, or to a supposed continuity of the conformal scale factor. It is

[1]Research Scientist, National Aeronautics and Space Administration, Ames Research Center, Moffett Field, Calif.

(Note—The Franklin Institute is not responsible for the statements and opinions advanced by contributors in the JOURNAL.)

known, however, in the theory of Cerenkov radiation and also in supersonic aerodynamics that the wave equation remains invariant under transformations having the factor $1/\sqrt{v^2/c^2 - 1}$ for velocities v in excess of the characteristic velocity c.

Several years ago N. Rosen (1)[2] pointed out that different theories of relativity could be formulated for media having different dielectric properties. For an observer whose experience is confined to such a medium, the retarded velocity of light $c' = c/n$ appears again as a limit for the velocity to which a body can be accelerated by electrodynamic action. As Rosen pointed out, a particle might, however, enter such a region with a velocity in excess of c' (as in the phenomenon of Cerenkov radiation) and its behavior could not be accounted for by such a theory.

A theory for particles travelling faster than light may thus be viewed simply as a mathematical formality, or it might be considered a physical theory for the inhabitants of Rosen's c' land. There is one additional point, however, and this refers to the elements of idealization in the classical theory. As is well known, relativistic dynamics depends on the linearity of the wave equation and on the assumption of point particles. These assumptions are enough to lead to infinite field energy, and in the aerodynamic analogue they are just sufficient to give the sonic barrier an infinite rigidity.

If one of the foregoing points of view is adopted, then it becomes of interest to investigate kinematic relations on the other side of the singular velocity $v = c$. Following a conventional terminology, such motions, with velocity $v > c$, may be termed "space-like."

For the investigation of space-like motions we restrict ourselves first of all to purely kinematic relations, and we adopt the simplest possible mathematical model, namely, conformal coordinates and their transformations in two dimensions x, t.

CONFORMAL TRANSFORMATIONS IN TWO DIMENSIONS

In conformal coordinates the velocity of light remains constant for all experimenters, whether moving or fixed. The invariance here is not merely a local relation, but holds also for finite displacements. Thus it has been shown (2) that an expanding light pulse continues to maintain spherical symmetry about its point of origin.

Figure 1 shows how this invariant property of electromagnetic signals may be used by two experimenters, A and B, to establish identical Cartesian coordinate systems x, t and x', t'. In our units the velocity of light is taken as unity and a signal pulse is thus represented by lines expanding at 45°. Though A and B may be in relative motion, each assumes that there is no "upstream" or "downstream" influence on his signals and sets every distant clock at a time halfway between the times of departure and return of an electromagnetic signal from the origin—in accordance with

[2] The boldface numbers in parentheses refer to the references appended to this paper

Einstein's well-known rules. We have no need here for the assumption that the electromagnetic velocity is the maximum possible. If a faster mode of transmission existed, we might still prefer to use electromagnetic signals because of their supposed invariant property.

If A and B are in uniform relative motion, we may establish a conformal correspondence between their coordinate systems by means of the Lorentz transformation. In Fig. 2 this correspondence is illustrated graphically by an artificial distortion of the B coordinate system so that its corresponding points coincide with those of an undistorted (that is, rectangular Cartesian) A system. In such a diagram the lines $t' = \text{const}$ are inclined so as to represent B's position at the center of an expanding signal pulse.

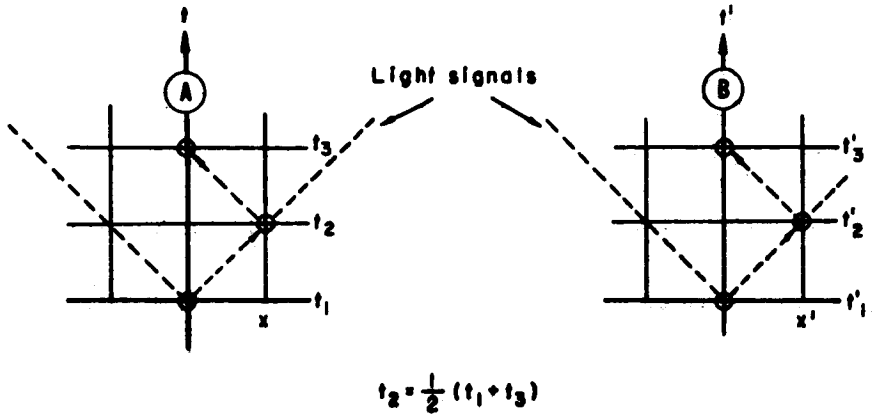

FIG. 1. Coordinates established by light signals.

The Lorentz transformation is of course limited to motion at constant velocity. A transformation which maintains the conformal property for variable motions in two dimensions is given by (3)

$$\left.\begin{aligned} x' + t' &= F(x + t) \\ x' - t' &= G(x - t) \end{aligned}\right\} \tag{1}$$

The lines $x' \pm t' = \text{constant}$ may be identified with signal pulses emitted by a periodic oscillator or a clock in the B system. The transformation thus amounts to a specified variation of the Doppler frequency of time signals emitted by B as they might be received in the A system. The Doppler frequencies are in fact the derivatives:

$$\left.\begin{aligned} f &= \frac{dF}{d(x + t)} \\ g &= \frac{dG}{d(x - t)} \end{aligned}\right\} \tag{2}$$

Such variable Doppler frequencies will correspond to a certain variation of the velocity of the B coordinate system. The velocity is given by

$$v = \left(\frac{dx}{dt}\right)_{x' = \text{const}} = \frac{g - f}{g + f}. \tag{3}$$

The velocity of the "world line" $x' = 0$ may be taken as the velocity of the oscillator B in the A system. The other coordinate points $x' = \text{const}$, though at rest relative to B, move with varying velocities in the A system.

Figure 3 shows a correspondence of the type given by Eqs. 1 for an example in which B moves to the right of A at a velocity 3/5 the velocity of light and comes to rest at the time $t = 5$, $t' = 4$. It is seen that in spite of the motion, B remains at the center of the signal pulse emitted at the beginning of the trip.

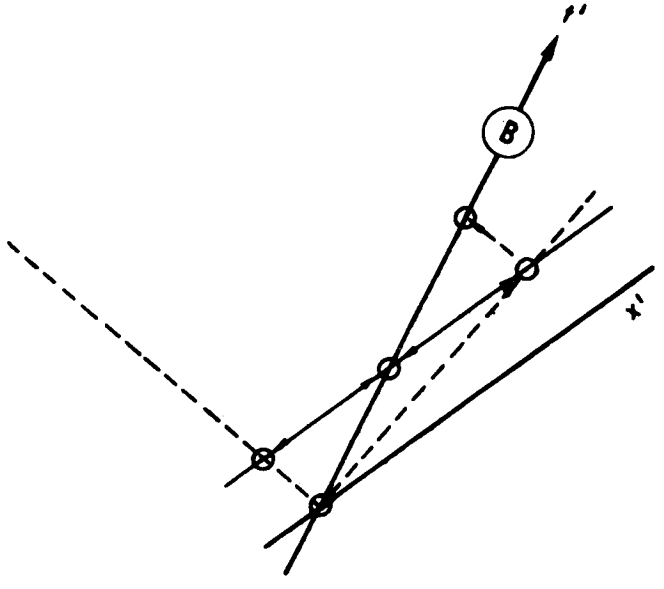

FIG. 2. Lorentz transformation.

If we invert the transformation (Eqs. 1), we find that the velocity is reversed at every point. Thus, as would be expected, the velocity of B relative to A is the reverse of the velocity of A relative to B. This relativity of velocities is, however, merely a local relation. Reversal of a field of variable velocities does not in general reverse the displacements. Thus if B moves three units to the right of A, it does not follow that A has moved three units to the left of B. Similarly, finite time displacements of the two systems are not equal and there arises a time discrepancy, as is well known.

COMPOSITION OF TRANSFORMATIONS

To explore the group properties of the transformation (1) we consider three systems A, B, and C, and apply two such transformations in succession. For the velocity v_1 between A and B there is obtained

$$v_1 = \frac{g_1 - f_1}{g_1 + f_1} \tag{3a}$$

and a similar expression for v_2 between B and C. For the resultant velocity of C relative to A the composition of two transformations yields

$$v_3 = \frac{g_1 g_2 - f_1 f_2}{g_1 g_2 + f_1 f_2} = \frac{v_1 + v_2}{1 + v_1 v_2}. \tag{4}$$

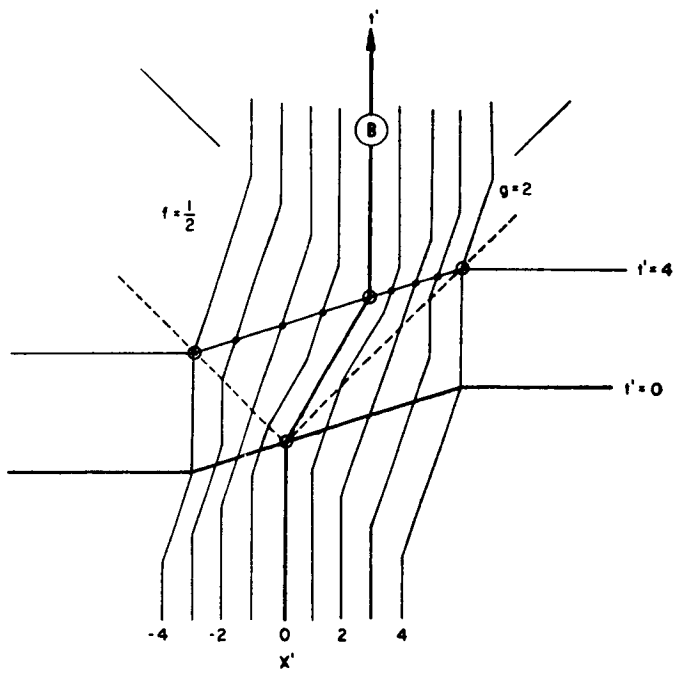

FIG. 3. Conformal transformation, $v = 3/5$.

The latter formula is, of course, the well-known law for the "addition" of velocities. Evidently this law does not depend on the principle of relativity, but only on the constancy of the speed of light.

Figure 4 illustrates graphically the law of composition given by Eq. 4. In its usual context the formula is of course limited to the range $v < 1$. However, our extended diagram seems to show more clearly the singular nature of the velocity of light. It is evident here that the value $v = 1$ is not altered by composition with *any* other velocity. If Eq. 4 is interpreted as a

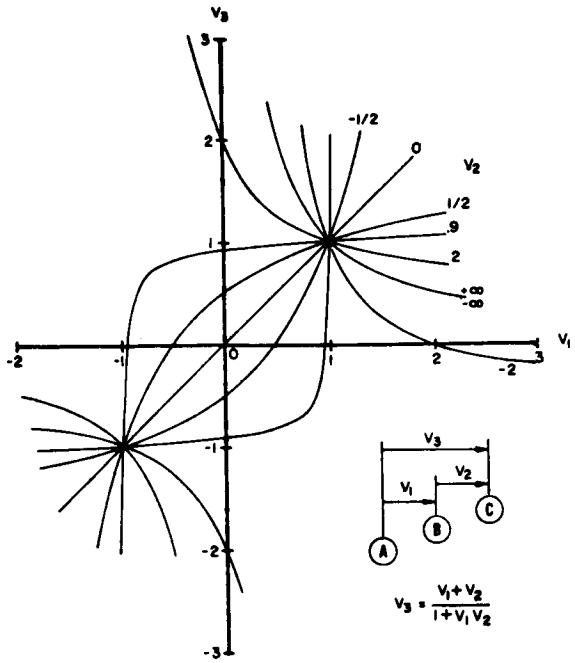

FIG. 4. Composition of velocities in conformal coordinates.

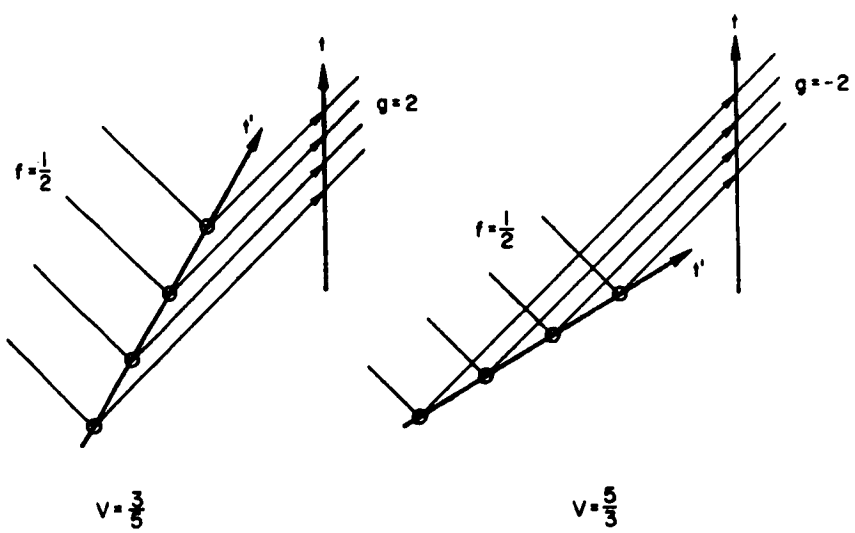

FIG. 5. Doppler shift of time signals.

formula for "addition," it is seen that the value 1 has the property ordinarily associated with an infinite value. On the other hand, the value $v = \infty$ does not have its usual property as an infinite magnitude but is reduced to finite value by addition of (that is, composition with) any finite value. In spite of these unusual relations, it will be observed that the composition of two transformations corresponding to $v_2 = -v_1$ yields the identical transformation (that is, $v_3 = 0$) except for the singular value $v_1 = 1$. There is thus no rest system associated with the velocity 1.

The law of composition of velocities has been cited to show the nonexistence of velocities greater than light. However, we find in this law merely an expression of the invariance of the velocity of light, valid for any velocity of the coordinate system.

SINGULAR BEHAVIOR OF THE DOPPLER FREQUENCY

Conformal transformations do not, in general, satisfy the principle of relativity because of an unsymmetrical scale relation. Thus it is found that

$$dx'^2 - dt'^2 = fg(dx^2 - dt^2). \tag{5}$$

To make the scale change symmetrical we should have

$$fg = \frac{1}{fg} \tag{6}$$

or

$$fg = \pm 1. \tag{7}$$

There are thus two values of the scale factor fg which lead to symmetry in the relations A to B and B to A. The negative value corresponds to velocities greater than light.

Of course, if the motion occurs with variable velocity, one cannot specify a fixed value of the scale factor for the whole coordinate transformation. However, if we identify A as an inertial system then the relation of equivalent scale may be satisfied locally all along the path of B in the A system. Hence, we impose the following boundary condition along the line $x' = 0$:

$$fg = \begin{cases} +1 \text{ where } v < 1 \\ -1 \text{ where } v > 1. \end{cases} \tag{8}$$

As Eq. 3 shows, if the velocity of a motion is to exceed 1 then one of the Doppler frequencies f or g must become negative. The transition to a negative frequency may be readily understood with the aid of a simple wave diagram as shown in Fig. 5. As the velocity increases toward 1 the signals from an approaching oscillator shift to higher and higher frequencies while those on the receding side become slower, approaching zero at a rate determined by the relation $f = 1/g$. The high frequency received from the approaching oscillator persists on transition through $v = 1$, but the signals

now arrive at the stationary oscillator suddenly and in reversed order. The transition of g from positive to negative values thus takes place by way of infinity (see Fig. 6). The frequency f shows no such singular behavior but retains positive values on each side of the value zero at $v = 1$. The discontinuous change of the scale factor fg from $+1$ to -1 on transition through the critical velocity may thus be explained simply in terms of the expected behavior of the Doppler signals. The possibility of such a discontinuous change seems to have been overlooked in the literature. Thus in (3) and (4) the negative value is omitted in the derivation. In (5) the negative value is discarded by an argument based on the supposed continuity of the scale factor as a function of velocity.

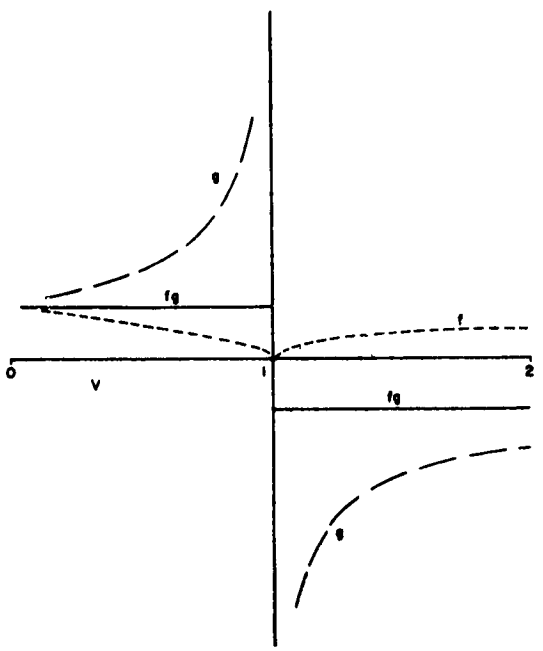

FIG. 6. Behavior of the Doppler frequencies f and g on transition through $v = 1$.

If we suppose that the path of B involves a transition through the speed of light, then several sets of time signals will appear simultaneously in A. Since the transformation (1) is expressed in terms of the Doppler shift of time signals, it is evident that the correspondence between x,t and x',t' will become multiple-valued. This multiple correspondence may be seen in another way from a simple plot of the function F or G. If the derivative of a function changes sign, then either the function itself or its inverse must become multiple-valued.

Figure 7 shows the conformal correspondence for a space-like motion of B in the inertial system A. It has been assumed that B remains at rest until

$t = t' = 0$ and then moves to the right of A with the velocity $v = 5/3$, coming to rest at $x = 5$, $t = 3$. This particular example may be obtained from the previous one for which $v = 3/5$ by a folding of the diagram (Fig. 3) along lines $x - t = \text{const}$.

Though B moves faster than light in the A system, we have nevertheless supposed that the propagation of electromagnetic signals takes place in the B system exactly as in Fig. 1. The "upstream" propagation of signals in such a system is, of course, an intuitively difficult concept—but not essentially different from that employed in the usual range of the theory.

Since we have supposed that the conformal property is retained for such motions, the point B must at every instant lie at the center of light pulses emitted along its path. In Fig. 7 the marked x' coordinates illustrate

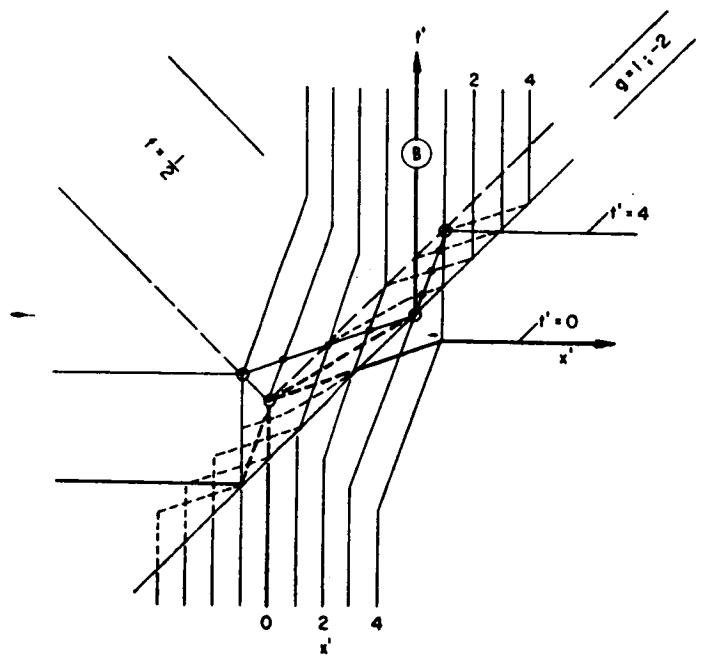

FIG. 7. Conformal transformation, $v = 5/3$.

this property for the instant $t' = 4$. The function g is of course multivalued in this region, but according to our convention the values $0 < x' < 4$, $0 < t' < 4$ are assigned to the branch $g = -2$. This convention, which maintains the conformal property, is evidently also sufficient to avoid the occurrence of negative time intervals along the path of B in the A system. Such negative intervals, or time reversals, do occur, however, along the path of A in the noninertial system B.

Recently R. Penrose (6) and J. Terrell (7) have shown that the contrac-

tion of length indicated by the Lorentz transformation is not a visually observed phenomenon. It is interesting also to speculate on the visual appearance of a superlight particle. As Heaviside (8) has shown, such a particle would appear suddenly at a point and then split into two particles which appear to recede from each other. This double appearance is illustrated in Fig. 8. In three dimensions the boundary of sensible disturbance expands along a cone behind the body. Such a cone may be thought of as an envelope of spherical waves emitted by the body. It is readily seen that any point within the cone lies on the intersection of two such spheres and is thus affected by two apparent sources of disturbance.

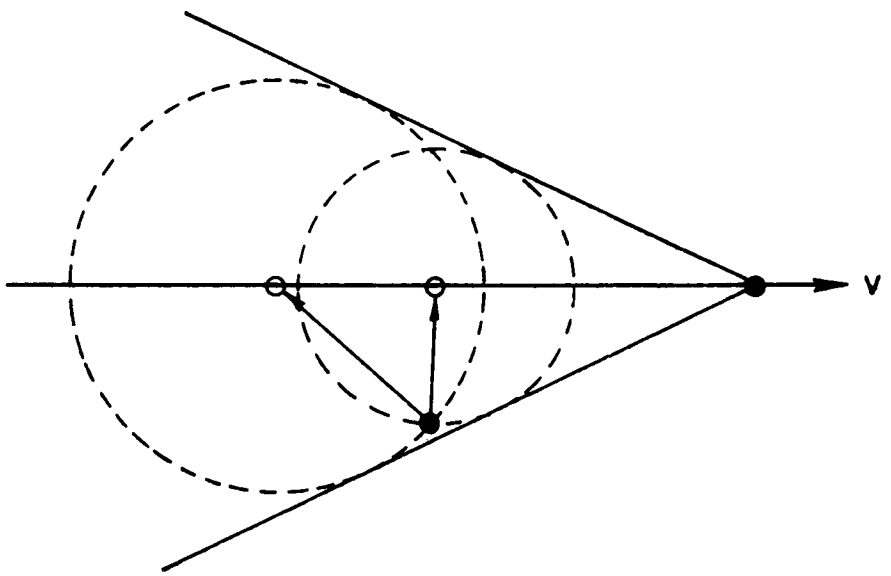

FIG. 8. Double appearance of particle travelling at $v > 1$.

RELATIONS OF ELAPSED TIME

Equation 5 may be used to obtain an analytic expression for the elapsed time along a space-like world line. Since $dx' = 0$ we have

$$-dt'^2 = fg(dx^2 - dt^2). \tag{9}$$

After introducing $dx = v\,dt$, there is obtained

$$dt' = \sqrt{fg(1 - v^2)}. \tag{10}$$

The boundary condition (8) then yields for $v > 1$

$$(dt')_{x'=0} = \sqrt{v^2 - 1}\,dt. \tag{11}$$

The discontinuous change in sign of the Doppler frequency g thus prevents the radical from becoming imaginary.

The range of values $v > 1$ provides relations which seem to complement those of the usual range of the theory. These relations are illustrated in Fig. 9, which shows the times elapsed in both $A(x,t)$ and $B(x',t')$ systems

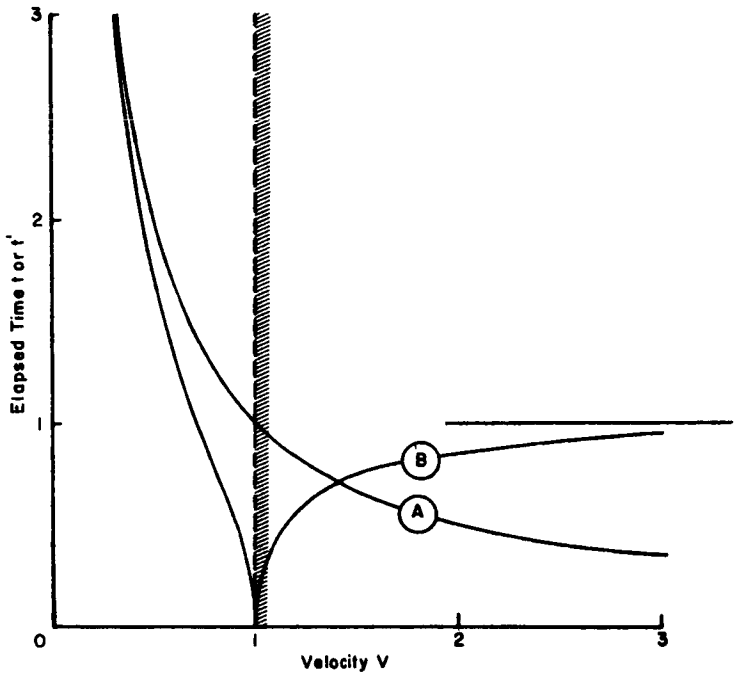

FIG. 9. Elapsed times at various velocities.

for a trip covering one light year in the A system. For velocities less than 1 the elapsed time along an accelerated path (B) is always less than that in the inertial system and reaches a minimum value of zero at $v = 1$. Travel at the velocity of light is thus equivalent to infinite velocity. In our theory superlight velocities offer no advantage to the traveller. At velocities greater than $v = \sqrt{2}$ the travelling twin of the well-known paradox comes back older instead of younger. At higher velocities the elapsed time increases and becomes equal to the light time at $v = \infty$. Thus infinite velocity in the inertial system is equivalent to the velocity of light for the traveller. These dual relations do not make the world of electromagnetic signals any less strange, but they seem to make it more symmetrical.

REFERENCES

(1) N. ROSEN, "Special Theories of Relativity," *Am. J. Phys.*, Vol. 20, pp. 161–164 (1952).

(2) H. BATEMAN, "Electrical and Optical Wave Motion," New York, Dover Publications, Inc., 1955, p. 145, ex. 11.

(3) R. T. JONES, "Extending the Lorentz Transformation by Characteristic Coordinates," *Am. J. Phys.*, Vol. 28, pp. 109–111 (1960).
(4) A. EINSTEIN AND OTHERS, "The Principle of Relativity," New York, Dover Publications, Inc., 1923, pp. 47–48.
(5) L. LANDAU AND E. LIFSHITZ, "The Classical Theory of Fields," Reading, Addison-Wesley Press, Inc., 1951, p. 6.
(6) R. PENROSE, "The Apparent Shape of a Relativistically Moving Sphere," *Proc. Cambridge Phil. Soc.*, Vol. 55, p. 137 (1959).
(7) J. TERRELL, "Invisibility of the Lorentz Contraction," *Phys. Rev.*, Vol. 116, pp. 1041–1045 (1959).
(8) O. HEAVISIDE, "Electromagnetic Theory," New York, Dover Publications, Inc., 1950, p. 378.

MOTIONS OF A LIQUID IN A PULSATING BULB WITH APPLICATION TO PROBLEMS OF BLOOD FLOW

Robert T. Jones

Avco-Everett Research Laboratory

March 1970

Jones, R. T., "Motions of a Liquid in a Pulsating Bulb with Applications to Problems of Blood Flow," Medical and Biological Engineering, vol. 8, no. 1, Jan. 1970, pp. 45-51. © 1970.
Reprinted by permission of Pergamon Press, Ltd., Oxford, Eng.

Med. & biol. Engng. Vol. 8, pp. 45–51. Pergamon Press, 1970. Printed in Great Britain

MOTIONS OF A LIQUID IN A PULSATING BULB WITH APPLICATION TO PROBLEMS OF BLOOD FLOW*

ROBERT T. JONES

Avco Everett Research Laboratory, Everett, Mass., U.S.A.

Abstract—Potential flows of the form $\phi = (ax^2 + by^2 + cz^2)f(t)$ may be utilized to represent motions produced in pulsating bulbs. While the initial bulb shape may be arbitrary, sequential shapes are related by affine transformations. Two components appear in the distribution of pressure, one dependent on the instantaneous velocity and the other on the acceleration. For flows with stationary streamlines the inertial impedance is that of a simple mass, and is proportional to the first moment of the actual mass of fluid contained within the bulb. Examples treated are: (1) expanding and collapsing circular cylinders and (2) elliptical cylinders in which the perimeter is held constant.

The thickness of the pulsatile laminar boundary layer is found to be approximately one millimeter for conditions in the vicinity of the heart. Conditions for separation and turbulence differ from those in steady flow.

FLOWS in pulsating or squeezing bulbs are of very common occurrence, and yet they seem to have received but little attention from fluid dynamicists. As an example we may mention the heart, which receives and expels blood nearly forty million times a year.

If the shape of the heart or bulb were given precisely, or if the course of its motion could be prescribed exactly, then one might attempt an accurate mathematical analysis of the flow, treating the phenomenon conventionally as a boundary value problem of a well-known type. However, the accuracy with which such biological phenomena reproduce themselves can hardly justify great pretension to accuracy in their mathematical treatment. It seems that in these cases one should use the analysis rather more as a guide to the intuition than as a means for producing quantitative results in specific cases.

Considerable insight into the squeezing bulb problem may be gained by considering flows of a very simple type. Using Cartesian coordinates x, y, z, and denoting component velocities of the fluid at a point u, v, w, we write:

$$\left.\begin{aligned} u &= 2x \\ v &= -y \\ w &= -z \end{aligned}\right\} \times \frac{u_0}{2L} \times f(t). \qquad (1)$$

Such a velocity distribution represents the irrotational flow of an incompressible liquid, and is of course a trivial solution of the Navier–Stokes equations as well as of Laplace's equation. Figure 1 shows the streamlines associated with this velocity distribution, which will be recognized as an axially symmetric flow with a stagnation point at the origin, TIETJENS (1957).

Figure 2 shows how this velocity distribution may be adapted to give the streamlines inside the bulb. To make the equations dimensionally correct the velocities given by (1) are multiplied by the ratio of a characteristic velocity u_0 to a characteristic length L. u_0 may be the velocity at the exit of the bulb and L may be the distance of the mouth of the bulb from the origin.

* *Received* 5 *May* 1969

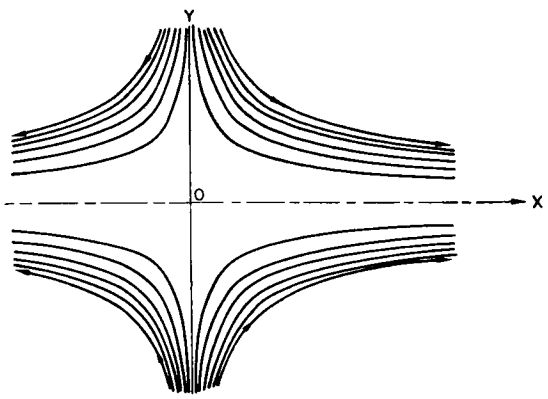

FIG. 1. Axially symmetric flow with stagnation point at origin.

Furthermore, in order to represent the unsteady or pulsatile character of the flow we have introduced a function of the time, $f(t)$ as a factor in (1). The potential of the flow is then

$$\Phi = \phi f(t) = \left(x^2 - \frac{y^2 + z^2}{2}\right) \frac{u_0}{2L} f(t). \quad (2)$$

The velocity profiles given by (1) are flat in all three directions. Thus the flow contains no

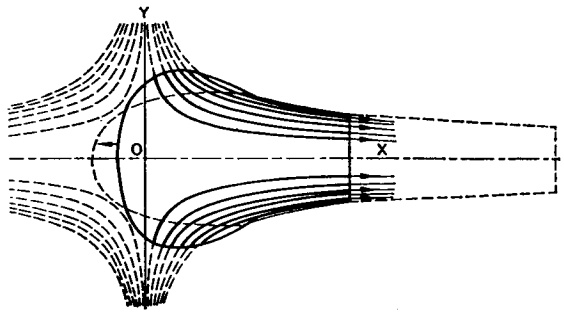

FIG. 2. Streamlines associated with collapsing bulb.

shearing motion and imaginary plane surfaces convected with the fluid remain plane and parallel. Thus the flow satisfies the boundary condition of a rectangular box whose sides are collapsing toward the x-axis and whose ends are moving outward along the x-axis in such a way as to maintain a constant volume. Similarly the flow satisfies the boundary condition of a circular cylinder collapsing toward the axis or expanding away from it, and the cylinder may have plane ends.

The fact that plane surfaces convected with the fluid remain plane and parallel means of

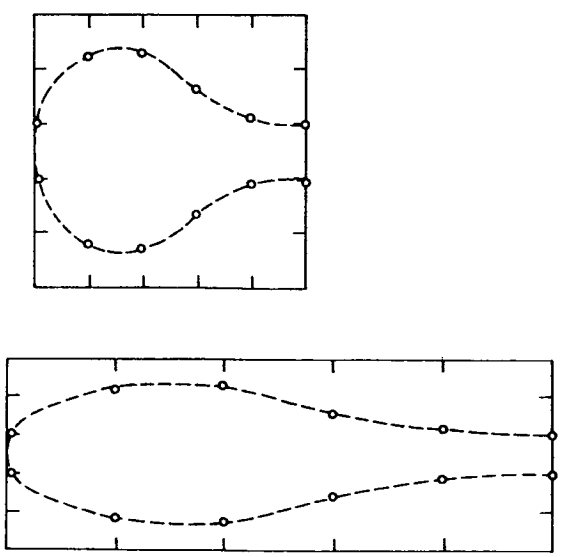

FIG. 3. Successive shapes of bulb.

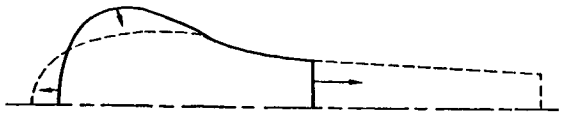

FIG. 4. Examples of bulb shape obtained by affine transformation.

course that a set of coordinate planes will be transformed to a new set related to the first by an "affine" transformation. Thus, starting with a bulb of arbitrary shape, one may represent motions in which the successive shapes are related by a simple stretching transformation. Figure 3 illustrates this process. In order to approximate the condition of a fixed outlet or mouth of the bulb the shape must be drawn so that it becomes tangential to the streamlines in the neighborhood of the exit. It is surprising how well a fixed exit can be represented without mathematical complication. Figure 4 shows one example.

Omitting the effect of viscosity, the pressure at points within the bulb will be given by

$$p = p_0(t) - p/2\,(u^2 + v^2 + w^2)\,f(t)^2 - \rho\phi f'(t). \tag{3}$$

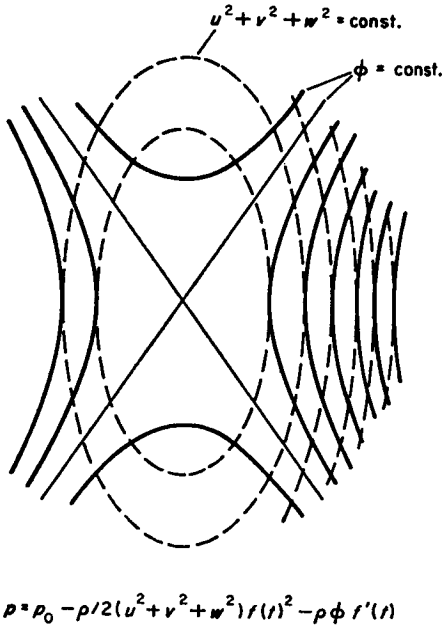

FIG. 5. Components of the pressure in bulb flow.

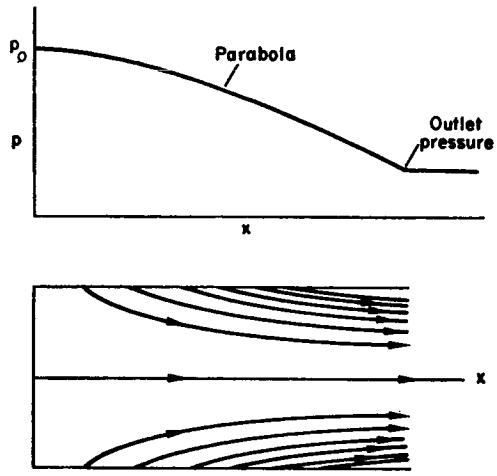

FIG. 6. Distribution of pressure on surface of collapsing cylinder.

The first term $p_0(t)$ is the pressure imposed by the environment into which the bulb works. The second term is of course the "Bernoulli" pressure, proportional to the square of the instantaneous velocity. The last term is proportional to the instantaneous acceleration of the flow and is responsible for its inertial impedance.

For the velocity term we have

$$u^2 + v^2 + w^2 = (4x^2 + y^2 + z^2)\left(\frac{u_0}{2L}\right)^2 \times [f(t)]^2. \tag{4}$$

This component of the pressure is constant on ellipsoidal surfaces having a 2 to 1 axis ratio.

For the last term we have

$$\frac{\partial \Phi}{\partial t} = \left(x^2 - \frac{y^2 + z^2}{2}\right)\frac{u_0}{2L} f'(t), \tag{5}$$

and the surfaces are hyperboloids. Figure 5 shows these isobaric surfaces.

Figure 6 shows the distribution of surface

pressure over an expanding and collapsing circular tube having one closed end. The distribution along the tube is parabolic and in the limit approaches the value given by one-dimensional flow theory. If the tube pulses in a cyclic fashion the pressure associated with the velocity will oscillate at twice the frequency of that associated with the acceleration.

The dynamics of flow within the bulb determine only the gradients of pressure and not the pressure itself. Hence we may introduce an arbitrary variation of pressure at the mouth of the bulb and the pressure inside will rise and fall accordingly, and will be felt uniformly over the surface of the bulb. The most interesting case is that in which the bulb expels its fluid into a long elastic tube such as an artery. According to a well-known theory the pressure at the end of the tube will be given by

$$p = p_0 + \rho\, u_0\, c, \tag{6}$$

where c is the pulse wave velocity in the tube, YOUNG (1808, 1809). Here the pressure at the bulb exit will vary with the outflow velocity u and the pressures given by (3) are simply to be added to this pressure. In the case of the left heart the component given by (6) is much larger than the variations of pressure developed by dynamic motions within the heart.

The horizontal or x-component of momentum of the flow is easily computed since the horizontal component of velocity of each fluid element is simply proportional to x. Thus the virtual inertia or virtual mass of the flow is proportional to the first moment of the volume of the fluid within the bulb. More specifically the virtual mass is equal to the actual mass times the ratio of the centroid of mass $\bar{x}$ to the length L, i.e.

$$m' = m\frac{\bar{x}}{L}. \tag{7}$$

The virtual inertia is referred to the acceleration at the exit plane L.

By placing the bulb at a large distance from the origin, so that $\bar{x} \rightrightarrows L$, we approach the situation of a sac of fluid accelerating back and forth along the x-axis without sensible change of shape. The virtual mass here is simply the actual mass of the fluid within the sac.

It should be noted that while the forms of the streamlines and the isobaric surfaces are stationary, the fluid itself may oscillate back and forth along the streamlines and the magnitude of the pressures will vary in accordance with the function $f(t)$.

It will have been noted also that while the initial shape of the bulb is arbitrary, the sequential shape changes are restricted to those obtainable by affine transformations. However, the variation in time of these changes is arbitrary. The axially symmetric flow does not exhaust the possibilities for affinely related shape changes. Thus if we wish to represent the flow in a bulb which flattens its shape as it contracts we may utilize a flow of the type

$$\phi = \alpha\, x^2 + \beta\, y^2 + \gamma\, z^2, \tag{8}$$

where α, β, γ are any constants such that

$$\alpha + \beta + \gamma = 0. \tag{9}$$

The successive shapes of the bulb, related by affine transformations may be conveniently expressed by the Lagrangian coordinates

$$\begin{aligned} \zeta &= x\, e^{\alpha\tau} \\ \eta &= y\, e^{\beta\tau} \\ \xi &= z\, e^{\gamma\tau} \end{aligned} \tag{10}$$

where $(\partial\tau/\partial t) = f(t)$.

For continuity the stretched coordinate planes must contain the same volume as the initial coordinates planes, that is

$$xyz = \zeta\eta\xi, \tag{11}$$

and we have from (10)

$$\zeta\eta\xi = xyz\, e^{(\alpha+\beta+\gamma)\tau} \tag{12}$$

so that $\alpha + \beta + \gamma = 0$.

As an example we may mention the flow in an initially circular tube which flattens into an elliptical shape. Supposing at first that the major diameter remains unchanged; we would set $\gamma =$

0 so that $\xi = z$. Then $\alpha = 1$ and $\beta = -1$ and the potential function is

$$\phi = (x^2 - y^2)\frac{u_0}{2L}. \tag{13}$$

An interesting example is one in which the perimeter of the tube remains constant during the flattening process. In this case, the quantities α, β, γ are functions of the time and the flow does not have stationary streamlines.

In certain cases it is desirable to represent the flow produced by inflating one bulb inside another. MOULOPOULOS, *et al.* (1962) proposed a method for assisting the circulation by inserting a long narrow rubber balloon into the abdominal aorta. The balloon is inflated and deflated through an external air pipe and expels blood from the aorta in such a way as to assist the pumping action of the heart. To represent this situation crudely we may consider the flow in the space between two circular cylinders, produced by expansion and contraction of the inner cylinder.

Returning to our first example

$$\phi = \left(x^2 - \frac{y^2 + z^2}{2}\right)\frac{u_0}{2L}, \tag{14}$$

we have already noted that it satisfies the boundary condition appropriate to a circular cylinder collapsing toward the axis, i.e.

$$\phi_r = -\,r\,\frac{u_0}{2L} \text{ where } r = (\sqrt{y^2 + z^2}). \tag{15}$$

Since there is no liquid within the inner tube, we are at liberty to introduce singularities there and by so doing we can obtain a second flow which satisfies the boundary condition of a cylinder expanding radially. Superpositions of the two flows, one expanding and one collapsing, will result in zero radial velocity at a certain fixed radius. For the expanding flow we may utilize the potential $\log r$ of a line source along the x-axis. For the two flows we then have

$$\frac{2L}{u_0}\phi = A\left(x^2 - \frac{r^2}{2}\right) + B\log r, \tag{16}$$

so that

$$\frac{2L}{u_0}\phi_r = \frac{B}{r} - Ar. \tag{17}$$

The radial velocity is zero when

$$\frac{B}{r_0} = A\,r_0, \tag{18}$$

or where $r_0 = (\sqrt{B/A})$. (19)

Flow produced by an expanding cylinder within a fixed cylinder

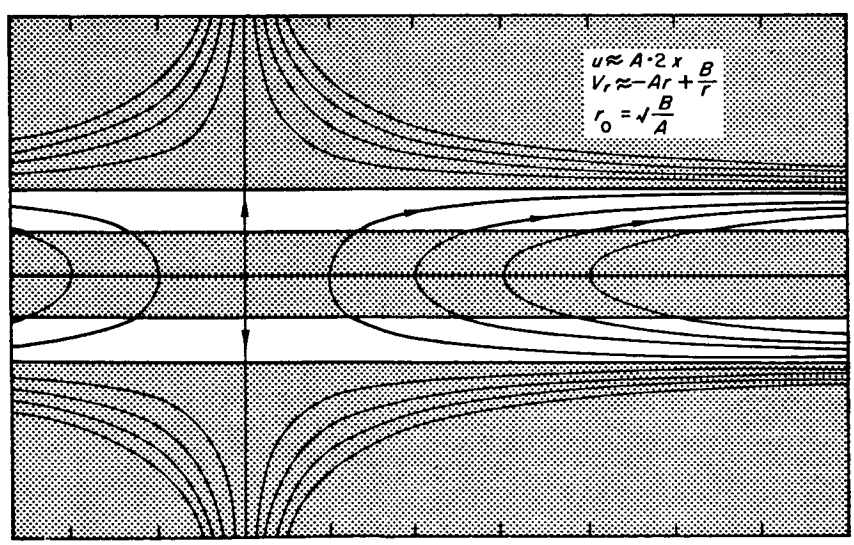

FIG. 7. Streamlines of flow between concentric circular cylinders.

Cylindrical surfaces convected with the fluid approach the fixed cylinder from both sides. Figure 7 shows the streamlines of this flow.

In the affinely related shapes we have considered that the surface of the bulb moves with the fluid at every point. Thus the flow satisfies not only the boundary condition of normal velocity, but also the condition of no slip at the surface. If the surface of the bulb actually moves in this fashion then the flows discussed above will apply to viscous as well as non-viscous fluids, since the potential flows are in this case exact solutions of the Navier–Stokes equations. The addition of viscosity to the fluid will require additional normal and tangential pressures at the surface of the bulb.

It is of interest to estimate the magnitude of the additional stresses introduced by viscosity. Since the shearing strains $(\partial u/\partial y)$, $(\partial v/\partial x)$, etc. vanish, the only surviving terms in the viscous stress tensor are

$$2\mu \frac{\partial u}{\partial x},\ 2\mu \frac{\partial v}{\partial y},\ 2\mu \frac{\partial u}{\partial z}.$$

The latter two terms require an additional compression from the surface of the bulb acting toward the x-axis while the term $2\mu(\partial u/\partial x)$ requires a tension along the x-axis. Comparing this term with the Bernoulli pressure at the exit of the bulb we have

$$\rho/2\, u^2 \cong \rho/2\, {u_0}^2$$

$$2\mu \frac{\partial u}{\partial x} = 2\mu \frac{u_0}{L}$$

and their ratio is $1/4\ (\rho u_0 L/\mu)$

or 1/4 the Reynolds number based on the length of the bulb. Since the Reynolds numbers in the vicinity of the heart are between 1000 and 10,000, we see that the additional stresses introduced within the fluid by viscosity are very small when compared with the dynamic pressures.

While the affine transformations can yield realistic bulb shapes, the requirement that the surface of the bulb move with the fluid both in tangential and normal directions is unrealistic. In practice we may suppose that the boundary condition of normal velocities is satisfied and that shearing motions arise in a thin boundary layer at the surface.

Since the boundary layer is thin we may consider a portion of the inner surface of the bulb to be locally flat. In this way the boundary layer development in a pulsatile flow within the bulb can be reduced to the problem of shearing motions produced by tangential oscillations of a flat plate. The solution of this latter problem is given in TIETJENS (1957) and shows that the oscillatory shearing motions diminish exponentially with distance from the surface. The decay is given by

$$u \cong \exp^{-(\sqrt{\rho\omega/2\mu})y}.$$

Taking $\mu/\rho = 0{\cdot}04$ for blood and $0{\cdot}8$ sec for the period $(= 2\pi/\omega)$, then

$$y_{1/e} = 0{\cdot}1 \text{ cm}.$$

Hence shearing motions decay by the factor 1/e within a distance of one millimeter from the wall. In other words, the boundary layer has time to grow to a thickness of one millimeter during the period of one heart beat. The stresses developed by viscosity within this thin layer will of course be much greater than those calculated earlier for the body of fluid within the bulb.

More difficult questions are those of the transition to turbulence and flow separation. Reynolds numbers in the vicinity of the heart regularly exceed those found by Reynolds for transition in a straight smooth pipe. However, comparisons of the flow in the heart and aorta with standard hydraulic experiments should be made with caution because of the unsteady nature of the flow. It seems doubtful that anything resembling fully developed turbulent pipe flow will appear in the larger arteries. Transitory separation accompanied by the formation of jets and vortices may appear, however, but their prediction will require a deeper study than we have undertaken here.

Acknowledgment—This work was supported in part by the Office of Naval Research, Department of the Navy, Washington, D.C.

REFERENCES

TIETJENS, O. G., *Fundamentals of Hydro- and Aeromechanics* (based on lectures of L. Prandtl). Dover Publications, New York (1957).

MOULOPOULOS, S. D., TOPAZ, S. and KOLFF, W. J. Diastolic balloon pumping (with carbon dioxide) in the aorta: A mechanical assistance to the failing circulation. *Am. Heart J.* **63,** 669 (1962).

YOUNG, T. Croonian lectures: On the functions of the heart and arteries. *Phil. Trans. Roy. Soc. (Lond.)* **98,** 164–186 (1808); **99,** 1–31 (1809).

ELEMENTARY THEORY OF SYNCHRONOUS ARTERIO-ARTERIAL BLOOD PUMPS

Robert T. Jones, Harry E. Petscheck and Arthur R. Kantrowitz

Avco-Everett Research Laboratory

December 1967

Jones, R. T., Petschek, H. E. and Kantrowitz, A. R., "Elementary Theory of Synchronous Arterio-Arterial Blood Pumps," Medical and Biological Engineering, vol. 6, no. 3, June 1968, pp. 303-308. © 1968.
Reprinted by permission of Pergamon Press, Ltd., Oxford, Eng.

Med. & biol. Engng. Vol. 6, pp. 303–308. Pergamon Press, 1968. Printed in Great Britain

ELEMENTARY THEORY OF SYNCHRONOUS ARTERIO-ARTERIAL BLOOD PUMPS*

ROBERT T. JONES, HARRY E. PETSCHEK and ARTHUR R. KANTROWITZ

Avco Everett Research Laboratory, Everett, Mass.

Abstract—In the technique of arterio-arterial pumping, a volume of fluid is withdrawn from the aorta during systole and reinjected during diastole, thereby reducing the systolic pressure of the heart and adding energy to the systemic circulation. It is found that an upper bound for the effectiveness of such devices is given by the formula

$$\frac{\Delta Q_h}{Q_{hu}} - \frac{\Delta P_1}{P_{1u}} = \frac{Q_b}{Q_{hu}} \frac{P_{1u} - P_{2u}}{P_{1u}}$$

where Q_{hu} is the stroke output of the unaided heart and ΔQ_h is the increment caused by the pump with a stroke Q_b. P_{1u} and P_{2u} are the systolic and diastolic pressures (unaided). ΔP_1 is normally negative and represents the reduction in ventricular pressure. The division of effort of the pump between the reduction of pressure and the increase of flow depends on the physiological–mechanical impedance of the heart. The total effect is, however, independent of the impedance.

ARTERIO-ARTERIAL pumping provides artificial assistance to the circulation by withdrawing fluid from the aorta during systole and reinjecting it during diastole.

The arterio-arterial pump may take the form of a simple pulsating bulb attached to the aorta and may operate without valves of its own provided the natural aortic valve is competent and provided the pump is synchronized with the natural heart. During systolic ejection from the heart the bulb is expanded, deflating the aorta so that the outflow from the heart is received at a reduced pressure. During diastole, when the aortic valve is closed, the bulb is compressed inflating the aorta and providing increased pressure for the systemic circulation. Conventionally, these events are timed by using the *R*-wave of the ECG complex as a signal. This principle of synchronous pumping is utilized in the Kantrowitz-Avco auxiliary ventricle (Fig. 1A) and in the technique of intra-aortic balloon pumping proposed by Kolff, Moulopoulis and Topaz (see Fig. 1C).

The action of such devices is obviously complicated by their dependence on the natural heart. Thus, the auxiliary ventricle (or balloon) may both reduce the pressure in the left ventricle and may permit the natural ventricle to eject a greater volume. The particular division between these two effects will depend on the mechanical impedance of the heart as a generator, a quantity which, in turn, depends on the pathologic physiology of the heart. The purpose of the present paper is to indicate that a simple relation for the sum of these effects can be derived independently of the mechanical impedance of the natural ventricle.

Without trying to settle any physiological questions, it is of interest to attempt to understand the mechanical action of the synchronous arterio-arterial pump on as simple a basis as possible. For this purpose we shall employ a simple "windkessel" model of the aortic system and assume linear peripheral resistances. In this model the incremental pressure in the aorta is simply proportional to the volume of blood

* *First received* 25 *September* 1967 *and in revised form* 20 *December* 1967.

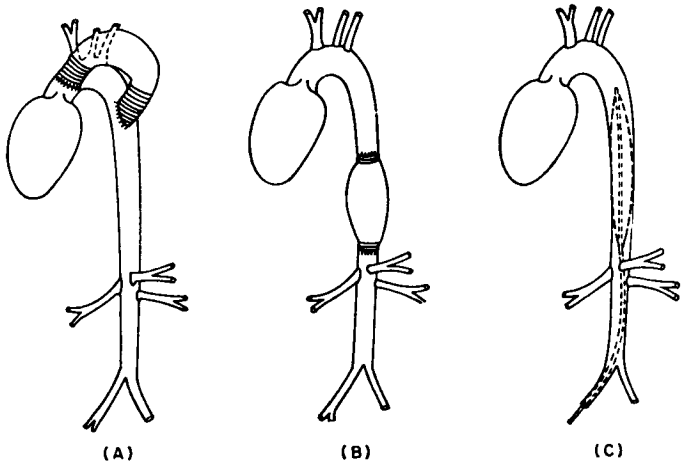

FIG. 1. Arterio-arterial pumps. A, Thoracic auxiliary ventricle; B, Auxiliary ventricle in descending aorta; C, Intra-aortic balloon pump.

injected into it.* The pressure and volume decay exponentially with flow through the peripheral resistances. Typical physiological values of the resistance R and the capacitance C give values of RC between 0·7 and 1·5 sec.

Consider first the effect of an arterio-arterial pump with the natural heart completely inactive. We assume here that the left ventricle and the atrium present no impedance to flow and provide a reservoir of blood at a low but constant (atrial) pressure and that both the aortic and mitral valves open when the pressure in the aorta falls below this value (see Fig. 2). During the intake stroke the pump must first withdraw enough blood from the aorta to reduce the pressure to the atrial level and thus to open the valves. The remainder of the stroke is then effective in withdrawing blood from the reservoir. Following completion of the intake stroke we assume that the pump quickly ejects its contents Q_b into the aorta, closing the aortic valve and raising the pressure by an amount

$$P_1 = \frac{Q_b}{C} \qquad (1)$$

where C is the capacitance of the aorta, i.e.

$$C = \frac{1}{(dP/dQ)}$$

During the interval τ_2 following ejection the pressure in the aorta will give rise to flow

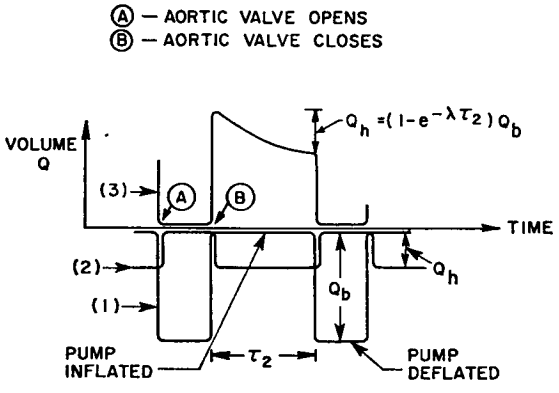

FIG. 2. Stroke cycle of arterio-arterial pump. Aortic valve opens at A, closes at B. (1) is the pump stroke, (2) is the volume ejected from the heart into the aorta, (3) is the instantaneous volume in the aorta which is proportional to the aortic pressure.

* As an approximate correction for the position of the pump along the aorta one should make allowance for the elay in wave propagation by altering the phase of the pump cycle.

through the peripheral resistances and the pressure will fall to the value P_2 such that

$$P_1 - P_2 = \frac{Q_b}{C}(1 - e^{-\lambda\tau_2}) \qquad (2)$$

where $\lambda = \frac{1}{RC}$ and R is the peripheral resistance.

Clearly, if the interval τ_2 were sufficiently long the aorta would deflate completely and the whole stroke volume Q_b of the pump would find its way into the systematic circulation. However, if the diastolic intervals τ_2 are short, the valveless pump will expend most of its effort simply inflating and deflating the aorta. The outflow during a cycle will be

$$Q_h = C(P_1' - P_2') = Q_b(1 - e^{-\lambda\tau_2}) \qquad (3)$$

The quantity $1 - e^{-\lambda\tau_2}$ is thus a measure of the stroke effectiveness of the pump* assuming that the pump is operated in the manner specified. For $\lambda = 1{\cdot}0$ and $\tau_2 = 0{\cdot}5$ we have $Q_h = 0{\cdot}4\ Q_b$ so that the effectiveness in this case is 40 per cent. It is clear that the value given by equation (3) is an upper bound for the effectiveness since we have assumed that no time is wasted in expelling the pump volume Q_b into the aorta.

It is interesting that in the case of the active heart the flow contributed by the pump is still given by equation (3) provided the flow impedance of the heart is negligible.

Figure 3 compares the pressure pulse for the unaided and aided heart. P_1 is defined here as the pressure just following closure of the aortic valve. At the instant of closure we assume that the auxiliary pump ejects its contents Q_b into the aorta. This ejection raises the aortic pressure from P_1 to P_1'

$$P_1' = P_1 + \frac{Q_b}{C} \qquad (4)$$

(This equation is a modification of equation (1) taking into account that the pressure at the initiation of pump ejection is P_1 rather than zero.) During the diastolic interval τ_2 an outflow through the peripheral resistances takes place reducing the pressure in the aorta from P_1' to P_2'.

$$P_1' - P_2' = P_1'(1 - e^{-\lambda\tau_2}) \qquad (5)$$

The total outflow Q_h during a cycle will be

$$Q_h = Q_s + (P_1' - P_2')C \qquad (6)$$

where Q_s is the outflow to the peripheral resistance during the systolic interval. Substituting from (1) and (2) we obtain

$$Q_h = Q_s + P_1C(1 - e^{-\lambda\tau_2}) + Q_b(1 - e^{-\lambda\tau_2}) \qquad (7)$$

In case the heart is *pressure-limited* but offers no impedance to additional flow P_1 will not be affected by the auxiliary pump ($P_1 = P_{1u}$) and the contribution to the flow will be given by the term

$$\Delta Q_h = Q_b(1 - e^{-\lambda\tau_2}) \qquad (8)$$

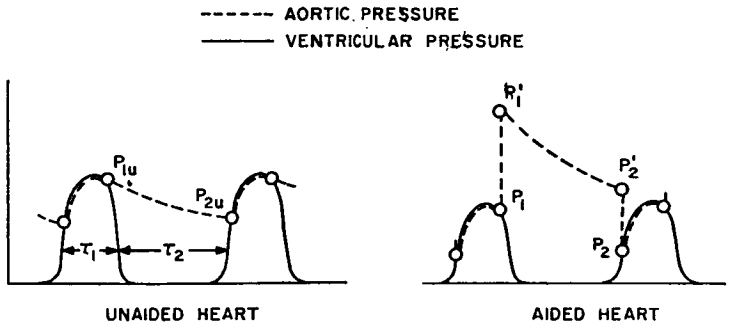

FIG. 3. Effect of arterio-arterial pumping on ventricular and aortic pressures.

* In spite of a decrease of stroke effectiveness the total flow volume increases when the pump is operated at a faster rate, however.

as before. The quantity $1 - e^{-\lambda\tau_2}$ may be conveniently expressed as the ratio of the natural pulse pressure to the systolic pressure of the unaided heart. Relations for the unaided heart can be obtained by taking $Q_b = 0$, i.e. no pump stroke, in the above equations. In this case $P_1' = P_1 = P_{1u}$ and $P_2' = P_2 = P_{2u}$ and equation (5) can be rewritten as

$$1 - e^{-\lambda\tau_2} = \frac{P_{1u} - P_{2u}}{P_{1u}} \tag{9}$$

so that

$$\frac{\Delta Q_h}{Q_b} = \frac{P_{1u} - P_{2u}}{P_{1u}}$$

or expressed as a fractional change in stroke output

$$\frac{\Delta Q_h}{Q_{hu}} = \frac{Q_b}{Q_{hu}} \frac{P_{1u} - P_{2u}}{P_{1u}} \tag{10}$$

The concept of a "source impedance" of the heart as it is to be understood in our analysis is perhaps not a conventional physiological concept and deserves some elaboration. A heart supposed to have a very high, or infinite, impedance will eject a fixed volume with each stroke and this volume will not be affected by the pressure in the aorta. Thus, in this extreme the excursion of the heart muscle is supposed to be unaffected by the tension developed in the muscle. In this case the artificial reduction of pressure in the aorta by the auxiliary pump will not lead to any increase of flow but will result solely in a reduction of ventricular pressure.

At the other extreme one can envision a heart muscle which develops its maximum possible tension on each stimulus, but which is capable of greater or smaller excursion.

In the more general case the heart will present a finite impedance to flow and the effort of the pump will be divided between a reduction of pressure in the left ventricle and an increase of flow. It is interesting, however, that a relation combining the two effects is independent of the impedance. For the unaided heart equation (7) reduces to

$$Q_{hu} = Q_{su} + P_{1u} C (1 - e^{-\lambda\tau_2}) \tag{11}$$

We now assume that the flow into the peripheral resistances during systole is proportional to the systolic pressure P_1, and that the intervals τ_1, τ_2 are unchanged by the pump. Thus,

$$Q_s = P_1 \frac{\tau_1}{R} \times k \tag{12}$$

where τ_b is the systolic interval and k is a constant of proportionality. We then have

$$Q_h = P_1 C \left[\frac{k\tau_1}{RC} + 1 - e^{-\lambda\tau_2}\right] + Q_b (1 - e^{-\lambda\tau_2}) \tag{13}$$

and

$$Q_{hu} = P_{1u} C \left[\frac{k\tau_1}{RC} + 1 - e^{-\lambda\tau_2}\right] \tag{14}$$

Subtracting (14) from (13) and substituting

$$C \left[\frac{k\tau_1}{RC} + (1 - e^{-\lambda\tau_2})\right] = \frac{Q_{hu}}{P_{1u}}$$

we obtain

$$Q_h - Q_{hu} = \frac{P_1 - P_{1u}}{P_{1u}} Q_{hu} + Q_b (1 - e^{-\lambda\tau_2})$$

and finally

$$\frac{Q_h - Q_{hu}}{Q_{hu}} - \frac{P_1 - P_{1u}}{P_{1u}} = \frac{Q_b}{Q_{hu}} (1 - e^{-\lambda\tau_2}) \tag{15}$$

or

$$\frac{\Delta Q_h}{Q_{hu}} - \frac{\Delta P_1}{P_{1u}} = \frac{Q_b}{Q_{hu}} \frac{P_{1u} - P_{2u}}{P_{1u}} \tag{16}$$

Thus the total effect of the auxiliary pump is proportional to its stroke volume ratio and to the pulse pressure ratio of the unaided heart.

The determination of either ΔQ_h or ΔP_1 alone requires, of course, a second relation for the source impedance of the heart which is at present unknown.

Equation (16) may be considered an upper bound for the effectiveness since we have assumed instantaneous withdrawal and ejection from the pump. If the pump stroke occupies a finite time interval, then the effectiveness will fall below that given by (16). Since our relations are linear it is not difficult to extend this result to cases of prescribed injection or withdrawal. An interesting example which illustrates the

effect of finite ejection time is provided by the case in which withdrawal and ejection by the pump imitate those of the natural unaided heart exactly. Assuming the heart to have infinite impedance, the aortic pressure variation will then be left unchanged in form but will be shifted in phase by the systolic interval τ_1. The ventricular pressure will follow the variation of diastolic pressure over an interval τ_1 near the

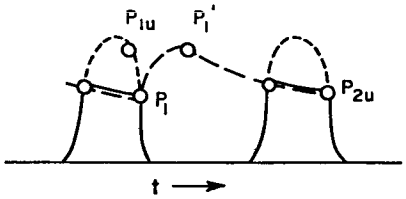

FIG. 4. Idealized operation of pump to shift aortic pressure curve
$P_1' = P_{1u}$
$P_1 = P_{2u}$.

end of diastole. Figure 4 shows the construction of this pressure curve. The result is

$$\frac{P_{1u} - P_1}{P_{1u}} = \frac{P_{1u} - P_{2u}}{P_{1u}} \text{ with } \frac{Q_b}{Q_h} = 1 \quad (17)$$

and is precisely equal to our upper bound for the effectiveness. However, it should be noted that the form of the ventricular pressure curve has been changed by the pump (i.e. the proportionality factor k has been changed) so that its typical magnitude is no longer proportional to P_1, but is somewhat higher, showing the effect of finite ejection time.

Limited experience acquired thus far suggests that the undamaged or healthy heart acts as a constant flow generator so that the effect of artificial pumping is chiefly to reduce the left ventricular pressure ($\Delta Q_h \to 0$). There are indications, however, that the failing heart may be pressure-limited and not flow-limited so that the flow can be increased by the artificial pump. In this case the reduction of left ventricular pressure will not be so great but the beneficial effect on the patient may be greater.

In our analysis we have emphasized the simplest possible relations and have obtained a result which is obviously capable of refinement in several respects. Thus in equation (12) the outflow during systole could be represented more accurately by an integral involving the average pressure during systole. Various programs for the rate of withdrawal or ejection by the pump might also be incorporated by means of a convolution integral. Perhaps more serious is our assumption that the ventricular pressure curves remain similar, and similarly related to the pressures at which the aortic valve closes (equations 13 and 14). It appears, however, that a further refinement of this hypothesis will require a deeper study of the physiological response of the heart to the artificial assist device.

Acknowledgements—This investigation was supported by the Department of the Air Force under Contract AF 49(638)–1657 and the National Heart Institute under Contract PH 43–66–1131.

BLOOD FLOW

Robert T. Jones

Avco-Everett Research Laboratory

1969

soidal particles. The values obtained for nonspherical particles are larger than those for spheres, becoming logarithmically infinite for extreme proportions. For flattened ellipsoids of 6 to 1 axis ratio (about the proportions of a red blood cell) (4) gives

$$\mu' = \mu(1 + 5c) \qquad 3.$$

For a concentration of 40 per cent we obtain $\mu' = 3\mu$. Taking the viscosity of plasma as $\mu = .015$, the result is $\mu' = .045$. Though the concentration is by no means small, it can be seen that there is rough agreement with measured values.

Theories of suspensions lead to a linear, Newtonian, viscosity. Experiments with whole blood (6) show, however, an increasing value of μ at small rates of deformation. Thus, at shear rates of 1 per sec, the viscosity is about doubled. The stress level at which the non-Newtonian component begins to be evident is thus about 1/10 dyne/cm^2. On the other hand, the normal stress corresponding to a pressure of 1 mm Hg is about 1000 dynes/cm^2.

The relative stiffening of the fluid at low rates of strain will lead to a modification of the parabolic velocity profile in Poiseuille flow, and in the extreme case (Bingham fluid) to a blunt-nosed profile or "plug flow." It is of interest to estimate the size of this plug in the case of a typical small blood vessel. For Poiseuille flow we have

$$\frac{du}{dr} = -u_{\text{mean}} \frac{r}{r_0^2} \qquad 4.$$

Assuming a vessel of radius $r_0 = 1$ mm with u_{mean} equal to 10 cm/sec, we obtain $r = .001$ cm, or 100μ. The effect of non-Newtonian viscosity is evidently quite negligible in vessels of 1 mm or larger. The effect on wall friction in oscillatory or pulsatile flow has been studied by M. G. Taylor (7).

The anomalous viscosity of blood becomes more prominent in the smaller vessels and capillaries, and it is in these vessels that the primary dissipation of energy in the circulatory system occurs. According to Zweifach (8) the collective length of capillaries in the human body amounts to about 60,000 miles. The chief pressure drop evidently occurs, however, in somewhat larger vessels, arterioles, which control the peripheral flow by means of precapillary sphincters [see (9)]. A preliminary study of the mechanical properties of these small vessels has been reported by Y. C. Fung (10).

In such small vessels the flow is greatly complicated by the relatively large size of the suspended particles, which may occupy the whole cross section of the vessel. In this regime, rheological concepts become inappropriate and one must analyze the phenomena in detail. An analysis of viscous flow in a tube with large spherical particles has been given by Wang & Skalak (11).

Flow and Pressure in the Heart and Large Arteries

In the heart and the larger arteries the flow is dominated by normal pressures and by the elasticity of the vessels.

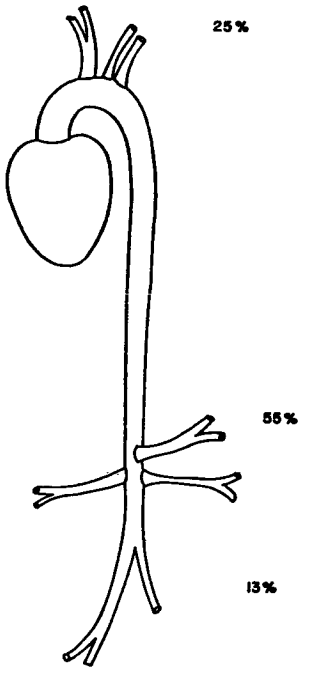

FIG. 1. Left heart, aorta, and main branches.

Figure 1 shows a greatly simplified sketch of the heart and the aorta together with some of the main branches. Also shown are typical percentages of flow to various organs. The total outflow from the heart, as well as its distribution, vary widely under different physiological circumstances.

Figure 2 shows some features of a typical pulse of the left heart. Ejection from the heart into the aorta is remarkably rapid, occurring with an acceleration of 1000 to 5000 cm/sec^2 (i.e., 1 to 5 "g's") and with a peak velocity v as high as 100 cm/sec [see (12, 13)]. In spite of this, the kinetic energy of flow is but a small fraction of the energy of the heart beat. Thus $\rho/2v^2$ may have a peak value of 3 to 4 mm Hg, while the aortic pressure varies from 70 to 120 mm. The major fraction of the pulse energy appears as elastic inflation of the aorta.

Pressure developed in the right heart and the pulmonary artery is considerably smaller than the pressures in systemic arteries. The flow energy is thus a larger fraction of the total on the right side, but in neither case does it dominate. The dominant role of the pressure may be seen in the architecture of the arterial system. Branching arteries show no consistent tendency to come off in the direction of flow, 90° being a common branching angle.

Since the flow in the upper part of the aorta occurs in short spurts fol-

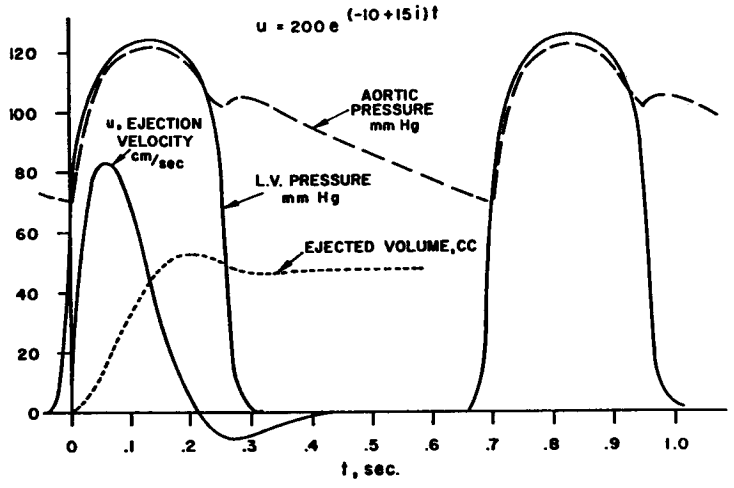

FIG. 2. Typical pulse of left heart.

lowed by longer periods of near zero velocity, it is of interest to estimate the unsteady growth of the viscous boundary layer during this period. Such an estimate shows that the boundary layer can grow to a thickness of approximately 1 mm during the ejection period. Since the aorta is two or more centimeters in diameter in this region, the flow is evidently far from that described by Poiseuille's law.

The Reynolds number corresponding to an ejection velocity of 100 cm/sec and a diameter of 2 cm is approximately 5000, higher than the Reynolds number for transition to turbulence in steady pipe flow. However, since the wall vorticity has diffused inward only one tenth of the arterial radius, transition in the usual sense can hardly occur.

Flow near the heart and in the larger arteries is thus dominated by inertial stresses and is not turbulent in the usual statistical sense. Flows in this regime are nevertheless greatly modified by the action of viscosity (separation, vortical flow), though they are typically insensitive to the magnitude of the viscosity.

Figure 3 shows the resistance of a sphere, approximately the size of an artificial heart valve, plotted against the relative viscosity. Without viscosity the sphere would have no drag, yet a 100-fold variation in μ hardly affects the magnitude.

Although the flow in the heart is probably quite irregular, it is nevertheless instructive to examine some simplified mathematical models of flow in a pulsating bulb [see (14)]. For this purpose we consider flows with a potential ϕ given by

$$\phi = \alpha x^2 + \beta y^2 + \gamma z^2 \qquad 5.$$

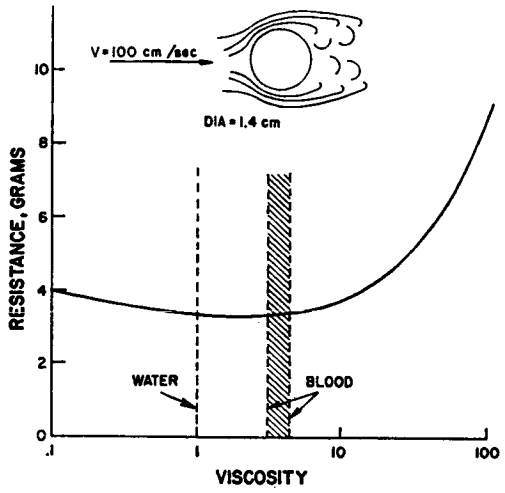

FIG. 3. Effect of viscosity on resistance of sphere.

where α, β, γ are functions of the time with

$$\alpha(t) + \beta(t) + \gamma(t) = 0 \tag{6.}$$

and x, y, z are Cartesian coordinates. Such flows have the property that initially plane surfaces convected with the fluid remain plane. Successive changes in the shape of a bulb are thus related to an (arbitrary) initial shape by affine transformations.

If the time dependence in Equation 5 is represented by a single function, as in

$$\phi = f(t)[ax^2 + by^2 + cz^2] = f(t)\phi(x, y, z) \tag{7.}$$

where a, b, c are constants with

$$a + b + c = 0 \tag{8.}$$

then the streamlines will be stationary though the flow is time dependent. Figure 4 shows streamlines for a flow of this type. Here $a = 2$, $b = -1$, $c = -1$, and the flow is axially symmetric with a stagnation point at the origin. Starting with a bulb of arbitrary shape, successive shapes are obtained by a simple stretching transformation. Figure 4 illustrates this process. In order to approximate the condition of a fixed outlet or mouth of the bulb, the shape should be drawn so that it becomes a tangent to the streamlines in the neighborhood of the exit.

With the effect of viscosity omitted, the pressure at points within the bulb will be given by

$$P = P_0(t) - (\rho/2)(u^2 + v^2 + w^2)[f(t)]^2 - \rho f'(t) \tag{9.}$$

where $u = \phi_x$, $v = \phi_y$, $w = \phi_z$. The expression for the pressure contains an arbi-

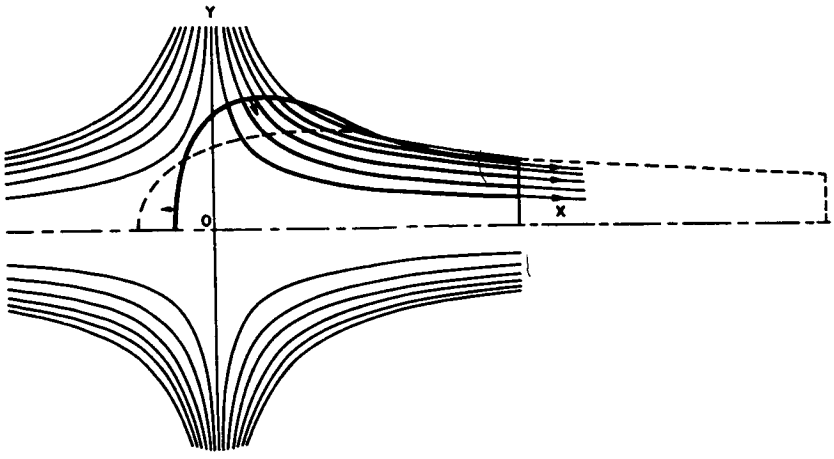

FIG. 4. Streamlines for collapsing bulb.

trary function of the time, $P_0(t)$, which must be determined by the impedance into which the bulb works.

For flows with stationary streamlines the isobaric surfaces given by $u^2+v^2+w^2$ and ϕ in Equation 7 are also stationary. Figure 5 shows these

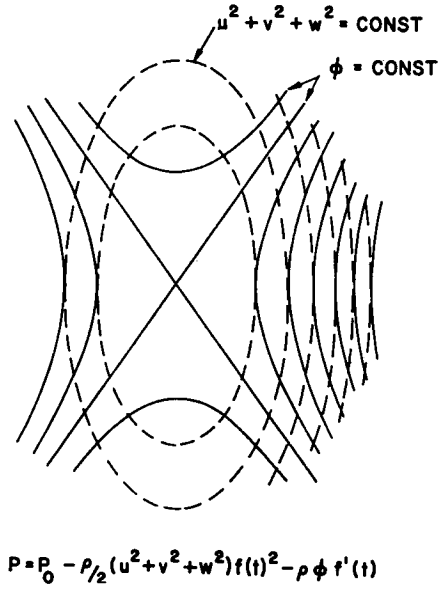

FIG. 5. Isobaric surfaces.

isobaric surfaces for flows with axial symmetry. The component associated with ϕ may be termed the "acceleration pressure" while $(\rho/2)(u^2+v^2+w^2)$ $[f(t)]^2$ is the "Bernoulli pressure." In an oscillatory flow the latter component will oscillate at twice the frequency of the former.

Figure 6 shows pressures computed by the above formulae for the initial instant of collapse of the bulb shown. Here $u^2+v^2+w^2=0$, and the pressures are entirely due to acceleration of the flow $[P=P_0-\rho(d\phi/dt)]$. For an ejection curve of the type shown on Figure 2, the pressure changes within the bulb

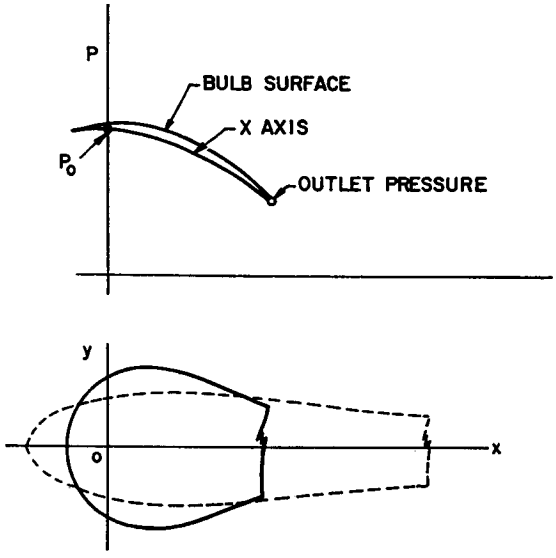

FIG. 6. Initial distribution of pressure within collapsing bulb.

amount to 4 or 5 mm Hg, while the outlet pressure may be 70 mm. Pressures due to the acceleration of flow within the heart are thus of the same order as the "Bernoulli" pressures.

If the aorta behaved as a rigid pipe, the inertial reaction would lead to excessive outlet pressures. The elastic compliance of the aorta serves an important function in smoothing out pressure fluctuations from the heart. Thus the simplest theory of the action of the aorta is known as the "*windkessel* theory" (15), relating its action to that of the pneumatic chamber formerly used to smooth the impulses from fire engine pumps.

According to the *windkessel* theory, the aorta acts simply as an elastic bag or, in electrical terms, as a capacitor. The incremental pressure developed in the aorta is then proportional to the volume ejected into it. Typically, the ejection of 50 cc of blood into the aorta will raise the pressure from 70 mm to 120 mm, or by 62×10^3 dynes/cm^2, so that $dP/dQ=(62\times10^3)/50$.

Considered together with a "lumped" peripheral resistance, the *windkessel* theory leads to a simple exponential decay of pressure in the aorta during diastole according to the formula

$$P_d = P_e e^{-\lambda t} \qquad 10.$$

where $\lambda = (1/R)(dP/dQ)$.

Values for R may be estimated from data given in textbooks on physiology. For a mean aortic pressure of 100×10^3 dynes/cm^2 and a cardiac output of 70 cc/sec, the value of R works out to 1400. The time constant $1/\lambda$ is then approximately 0.9 sec.

The *windkessel* theory gives remarkably good predictions of pressure in the larger arteries during diastole. The inflation of the arterial system is, however, complicated by the phenomenon of wave propagation and reflection, which involves the lengths of the arteries. The propagation of pulse waves was first investigated mathematically in 1808 by T. Young (16) who gave the basic formulation.

Pulse Wave Phenomena

Perhaps the most comprehensive recent analysis of pulse wave phenomena is that by Womersley (17). An excellent review of modern work is given by Skalak (18).

An instructive derivation of Young's formula results if one chooses axes in which the pulse waves are stationary and the flow steady. Consider a long elastic tube filled with incompressible liquid flowing at a velocity c. Small wavelike changes in diameter of the tube will be opposed by changes in the elastic tension of the wall. In addition to the pressure developed by elastic stress, bulges in the tube will also cause changes in the flow velocity and, hence, the pressure developed in the fluid. For small flow velocities the elastic pressure will dominate, restoring the tube to its initial straight form. However, for a sufficiently high velocity c, the changes in fluid pressure can overcome the elastic restoring tension. At this speed the tube is neutrally stable and variations in cross-sectional area will retain whatever form is given them. The internal pressure associated with circumferential tension T in the tube wall is

$$P = \frac{T}{R} \qquad 11.$$

and

$$\frac{dP}{dR} = \frac{1}{R^2} E\tau$$

or

$$\frac{dP}{dA} = \frac{E\tau}{2AR} \quad \text{where} \quad A = \pi R^2$$

Here E is the elastic modulus, and τ is the thickness of the wall.

Turning to the pressure developed by the motion of the fluid we can write

$$P = P_0 - (\rho/2)(c + u)^2 \qquad 12.$$

so that

$$\Delta p = -\rho uc \qquad 13.$$

Here u is the perturbation (assumed small) produced by the change in cross-sectional area. From continuity we may write

$$cdA = -uA$$

so that $dp = \rho c^2(dA/A)$, or

$$\frac{dp}{dA} = \frac{\rho c^2}{A}$$

Equating this "Bernoulli pressure" to the pressure developed elastically (Equation 11) we obtain

$$c^2 = \frac{E\tau}{2\rho R} \qquad 14.$$

If the flow velocity exceeds c, then the Bernoulli pressures will dominate the elastic restoring pressures and stationary waves will grow in amplitude. It may be expected that attempts to force fluid through an elastic tube (with fixed ends) at a velocity greater than c will result in unstable distortions.

Transforming to axes moving at the velocity $-c$ we obtain Young's formula for the wave speed, Equation 14, in a tube with zero mean velocity. More generally, if the mean velocity is U_0 we find that the waves travel at the velocity c in either direction relative to axes moving at the velocity U_0, i.e., the waves are convected with the fluid. The pressure is now given by Equation 13 with the sign reversed if we adopt the convention that u is positive in the direction of the wave.

The foregoing analysis presents the problem in its simplest terms. Olsen & Shapiro (19) have investigated several of the nonlinear effects associated with waves of larger amplitude. One interesting result of their analysis is that the nonlinear elasticity of a material like rubber cancels the nonlinear component of the hydrodynamic pressure, producing a "linear" behavior for large-amplitude waves.

Our analysis has assumed one-dimensional flow. However, solutions that show the effect of radial motions of the liquid are available in the hydrodynamic literature [e.g., Lamb (20a) p. 472]. Figure 7 shows the effect of radial motions in reducing the speed of shorter waves. A more complete treatment, including unsymmetrical modes, will be found in the paper by Anliker & Maxwell (20).

Since the arteries are imbedded in tissue, an estimate of the effect of a surrounding medium on the pulse is of interest. Figure 8 shows the influence of a surrounding liquid on the wave velocity of tubes filled with the same

liquid. Such an effect simulates the inertial impedance of the surrounding tissue, but does not simulate viscous or elastic effects.

A treatment of the tapered artery based on the assumption of constant wave speed c leads to the well-known differential equation used in the study of acoustic horns. An analysis of an exponentially tapered artery, on this basis, has been given by R. L. Evans (21). A somewhat simpler analysis, adaptable to a conical taper, utilizes the spherical wave equation; i.e.,

$$\phi = \frac{1}{R} f\left(t \pm \frac{R}{C}\right)$$

In this case, pressure pulses retain their shape but vary in amplitude inversely as the vessel diameter. The velocity, given by $d\phi/dR$, shows a more complicated dependence.

Branching Arteries: Peripheral Impedance

Proceeding from the large arteries to smaller branching vessels, viscosity begins to play an increasingly important role. A very complete treatment of the effects of viscosity in pulsatile flow has been given by Womersley. In the larger arteries vorticity can diffuse only a short distance into the flow during a pulse. In smaller arteries, however, the unsteady boundary layer begins to

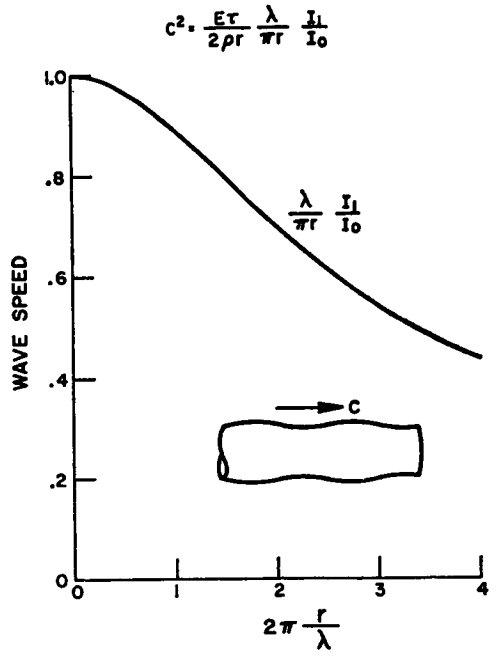

Fig. 7. Effect of radial motions on pulse wave velocity.

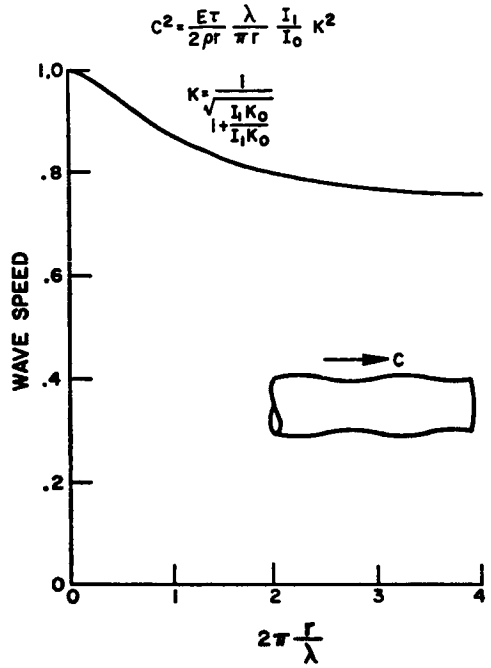

FIG. 8. Effect of surrounding liquid on pulse wave velocity.

occupy the total cross section of the artery. As an introduction to Womersley's results, it is instructive to consider the oscillatory shearing motion of a viscous liquid produced by a flat surface oscillating in its own plane. In this case a well-known solution gives

$$u = u_n e^{-ky}\cos(nt - ky) \qquad 15.$$

where $k = (n/2\nu)^{1/2}$. Here u is the velocity (parallel to the plate), y is the distance normal to the surface, and ν is the kinematic viscosity. For a normal heart rate n is about 10. Taking ν as 0.05 we obtain $k = 10$; hence, the oscillatory shearing motions diminish to $1/e$ of the surface value at $y = 0.1$, or 1 mm.

For a vessel 2 cm in diameter the viscosity hardly modifies the velocity profile. Such a thin boundary layer, however, leads to values of wall-shearing stress considerably higher than those for steady Poiseuille flow. The shearing stress on the oscillating plate is given by

$$\tau = \rho\sqrt{n\nu}\,u_n\cos\left(nt + \frac{\pi}{4}\right) \qquad 16.$$

and is thus 45° out of phase with the velocity. For a peak velocity u_n of 100 cm/sec, $\nu = 0.05$, $k = 10$ as above, we obtain

$$\tau_{max} = 140 \text{ dynes/cm}$$

For an artery 50 cm long, this value corresponds to a pressure drop of approximately 11 mm Hg at peak flow—about 7 times that associated with steady Poiseuille flow.

Our rough calculation is intended only to give an intuitive picture of the problem. For rigorous theory and results one should refer to Womersley's paper. Oscillatory shearing motion adjacent to a flat surface is simply a damped sinusoid with surface traction 45° out of phase with the velocity for all frequencies. In a circular tube the oscillations are described by Bessel functions and the phase shift is a function of the frequency.

For blood vessels below a certain diameter, the diffusion of vorticity is essentially complete at every stage of an oscillatory flow. Since the Reynolds number is quite small, the flow is dominated by viscosity. In this limiting case the equation of motion is simply Poiseuille's formula

$$\frac{\partial P}{\partial x} = -\frac{8\mu}{r^2} u \qquad 17.$$

The continuity relation is, however, modified by the elasticity of the vessel; i.e.,

$$\frac{\partial A}{\partial t} = -\frac{\partial}{\partial x} \rho A u \qquad 18.$$

Introducing the relation between the pressure and the elastic distension of the cross section by means of the pulse wave velocity c, we write

$$\frac{\partial A}{\partial P} = \frac{A}{c^2} \qquad (A = \pi r^2) \qquad 19.$$

so that Equation 18 becomes

$$\frac{1}{c^2} \frac{\partial P}{\partial t} + \rho \frac{\partial u}{\partial x} = 0 \qquad 20.$$

Eliminating u between Equations 17 and 20 we obtain for the pressure

$$k \frac{\partial^2 P}{\partial x^2} - \frac{\partial P}{\partial t} = 0 \qquad 21.$$

which is the well-known diffusion equation. Evidently in vessels of this size the pulse no longer travels as a wave, but is reduced to a diffusion of pressure by the action of viscosity. Equation 21 has a one-parameter family of solutions corresponding to a step input of pressure, viz.,

$$\frac{\Delta P}{\Delta P_\infty} = Erfc \frac{x}{2r} \sqrt{\frac{8\mu}{\rho c^2 t}} \qquad 22.$$

The phenomenon of diffusion of pressure is evidently restricted to vessels smaller than 1 mm in diameter. To determine the critical size, we may compare the pressure at a point along the artery with the pressure that would arrive at that point if the pulse wave were unimpeded. Hence, we set t in

Equation 22 equal to x/c. For $c=1000$, $r=0.05$ we find that the pulse is reduced to one half in a distance of 6 cm.

Perhaps the most doubtful quantity in the foregoing estimate is the magnitude of c in such small vessels. A constant value of c would correspond to a constant ratio of wall stress to pressure and, hence, would give large and small vessels the same margin of safety. Measurements show, however, that the wave speed is higher in branching arteries than in the aorta. Whether this tendency persists to very small vessels in not known.

Aortic Pressure Pulse

Since the collective area of the arterial branches increases with distance from the heart, the average flow velocity must decrease. Thomas Young supposed that the pulse pressure would decrease also. However, D. McDonald (22, 23) and others have shown that pulsatile components of the pressure actually increase for a certain distance in going toward the periphery. The increase of harmonic components with distance from the heart corresponds to the well-known sharpening of the pulse in the distal radial and femoral arteries.

The phenomenon of pulse sharpening can be demonstrated quite well with a simple physical model of the aortic system. Figure 9 shows such a model in use at Avco Everett Research Laboratory (see 24). This model consists of an untapered rubber tube having geometric and elastic properties

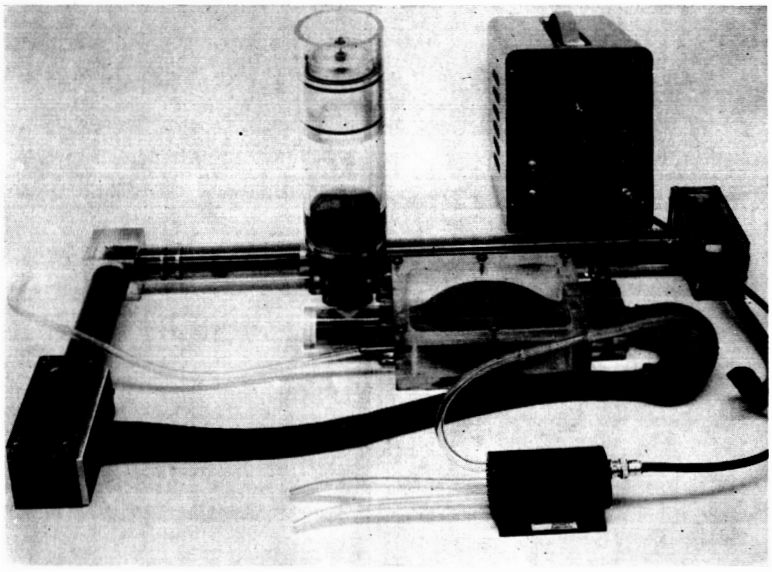

FIG. 9. Simplified physical model of aorta.

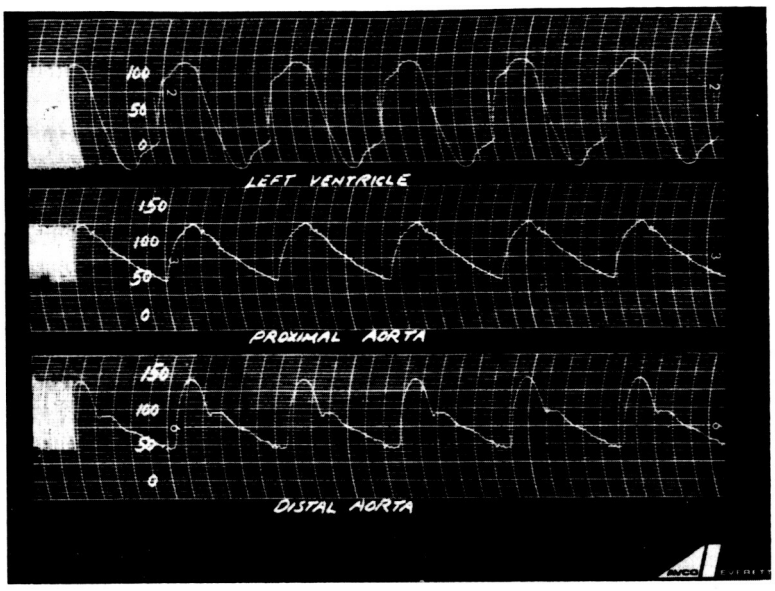

FIG. 10. Proximal and distal pulse shapes produced by simplified model.

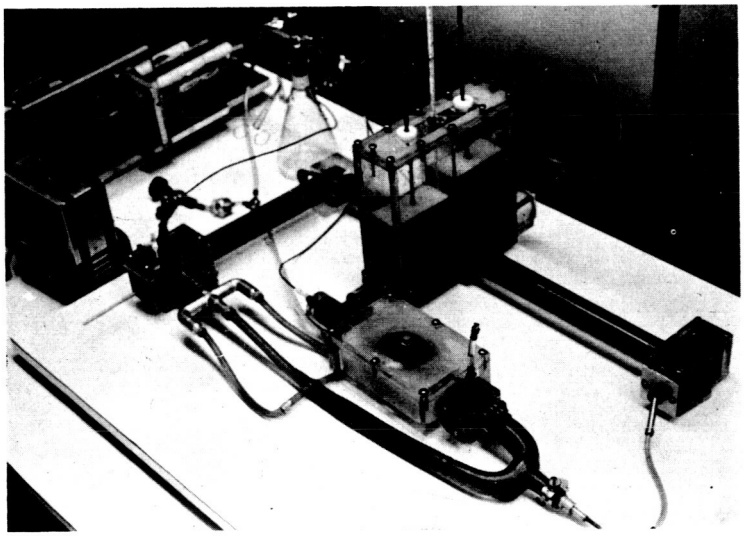

FIG. 11. Later version of aortic model.

similar to those of the aorta. Pulsatile flow is produced by an electric motor and a mechanical linkage that imitates the ejection curve of the heart. At its lower end the rubber "aorta" enters a box filled with plastic sponge, intended to simulate the peripheral resistance. Aortic and mitral valves are plastic flaps. Figure 10 shows the forms of the pressure curves in the aorta for positions near the (rubber) "heart" and near the peripheral resistance. These curves show a striking similarity to physiological pressure pulses.

A direct physical model such as described above has been found useful in isolating and studying purely mechanical phenomena connected with the circulation. Figure 11 shows a later version in which the aorta (silicone rubber) is tapered and is equipped with rudimentary carotid and renal-celiac

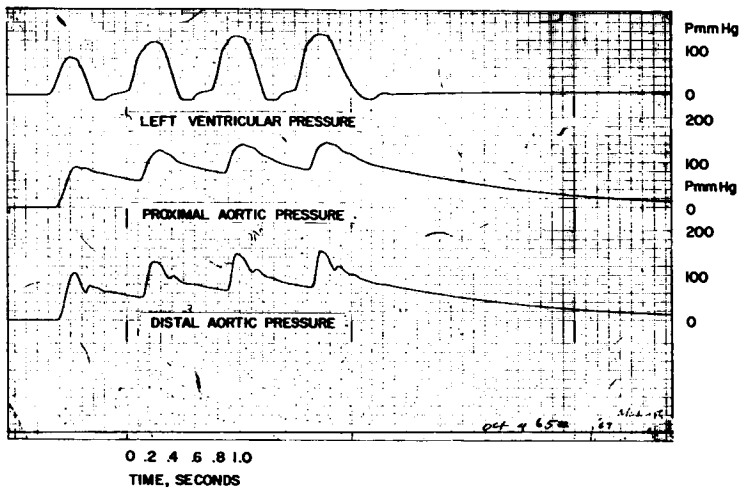

FIG. 12. Transient pulses produced by model.

branches. The rectangular reservoirs that supply the ventricle are separated by an orifice plate so that the difference in level is an indication of mean flow. This model has been used at Avco Everett Research Laboratory for the investigation of various "circulatory assist" devices.

Figure 12 shows transient pulses in the left ventricle and the aorta, obtained by starting and stopping the drive motor. About four strokes are required to build the aortic pressure up to its steady value. When the motor is stopped the pressure decays exponentially, accompanied by outflow through the peripheral resistances. Evidently the *windkessel* theory gives a good representation of the phenomenon except during the early part of the pulse, where the pressures are complicated by wave reflections and vary with position.

Before proceeding to the discussion of reflections, it is useful to consider

the effect of a stepwise input of flow (assumed frictionless) into an elastic tube. Figure 13 illustrates this phenomenon. The injection of "new" fluid into the tube sets into motion a part of the fluid already there, creating a bulge which travels at the velocity c, greater than u. The new fluid is separated from the old by a "contact surface." The change in momentum at the wave front is ρu and occurs at the velocity c, so that the pressure is

$$\Delta p = \rho u c \qquad 23.$$

Since $(\rho/2)u^2$ is usually small compared with ρuc, the pulse is not very sensitive to variations in the velocity profile of the injection, depending primarily on the volume influx.

If A is the cross-sectional area of the tube, the volume flow will be $Q = uA$.

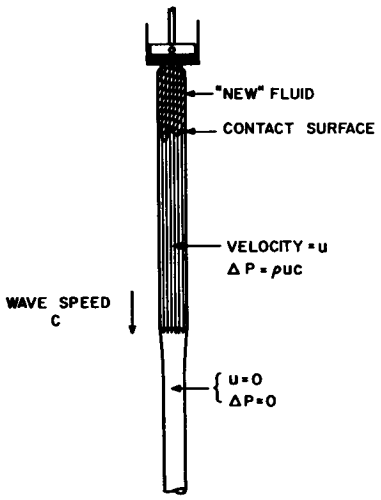

FIG. 13. Injection of fluid into an elastic tube.

The pressure required is in phase with the flow rate and, hence, the elastic tube without reflections and with frictionless flow presents a simple resistive impedance

$$Z_c = \frac{P}{Q} = \frac{\rho c}{A}$$

In the electrical analogue, Z_c is termed the "characteristic" or "surge" impedance.

Typical values of mean flow to various organs, together with the mean aortic pressure, may be used to estimate the resistive impedance associated with various branching arteries. Values corresponding to Figure 1 are shown on Figure 14. It will be seen that the resistance associated with the capillary beds is an order of magnitude greater than the pulse impedance of the aorta.

Figure 15 shows by means of a characteristics diagram how the aortic

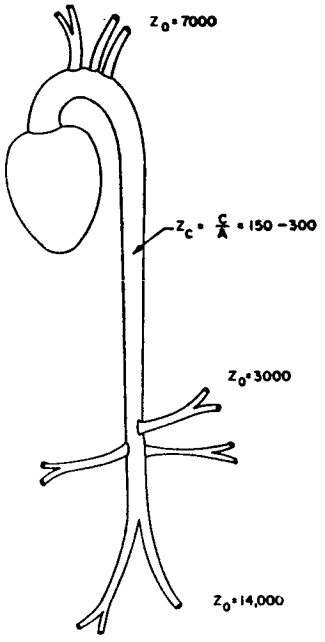

FIG. 14. Pulse impedance of aorta compared with peripheral resistances.

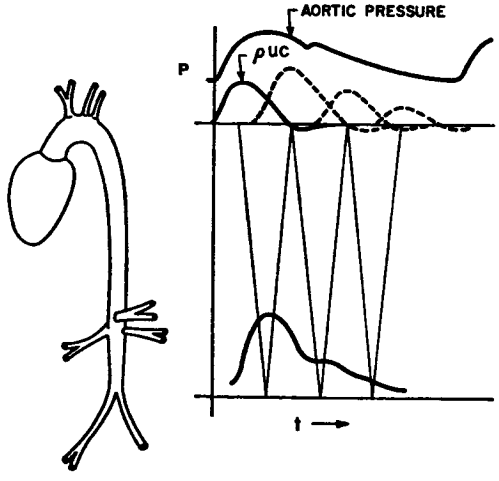

FIG. 15. Superposition of reflected pulses in proximal and distal aorta.

pressure appears as the superposition of a series of partially reflected pulse waves of the form

$$\rho uc = f(t) \tag{24.}$$

where $u = u(t)$ is the original ejection curve. Assuming, for the moment, perfect reflections (i.e., no outflow), the pressure at a position x along the aorta will be

$$\begin{aligned} P - P_0 = {} & f\left(t - \frac{x}{c}\right) + f\left(t - \frac{x}{c} - \frac{2L}{c}\right) + f\left(t - \frac{x}{c} - \frac{4L}{c}\right) + \cdots \\ & + f\left[t + \left(\frac{x}{c} - \frac{2L}{c}\right)\right] + f\left[t + \left(\frac{x}{c} - \frac{2L}{c}\right) - \frac{2L}{c}\right] \\ & + f\left[t + \left(\frac{x}{c} - \frac{2L}{c}\right) - \frac{4L}{c}\right] + \cdots . \end{aligned} \tag{25.}$$

The superposition of functions repeated with a small shift is equivalent, in the limit, to the process of integration. Thus, the Euler-Maclaurin summation formula gives

$$f(t) + f(t - \Delta t) + f(t - 2\Delta t) + \cdots = \int_0^t f(\tau)\frac{\partial \tau}{\Delta t} + \frac{1}{2}f(t) + \cdots \tag{26.}$$

This equivalence may be used to show the relation between the pulse wave theory and the *windkessel* theory of the aorta. The Euler-Maclaurin series will further provide a first-order correction of the *windkessel* theory for the effect of finite length of the aorta. As Equation 26 implies, the correction amounts simply to the addition of the term $\frac{1}{2}f(t) = \frac{1}{2}\rho uc$ to the pressures computed from the *windkessel* theory.

The integral on the right-hand side of Equation 26 may be rewritten as (since $\Delta t = 2L/c$)

$$\int_0^t \rho uc \frac{\partial \tau}{\Delta t} = \frac{1}{2}\frac{\rho c^2}{LA}\int_0^t uA\,d\tau \tag{27.}$$

where A is the cross-sectional area of the aorta. The term uA is then the volume flow and $\rho c^2/LA$ is the reciprocal of the volume compliance or "capacitance" of the aorta:

$$\frac{\rho c^2}{LA} = \frac{\rho c^2}{\Delta Q_0} = \rho\frac{\partial P}{\partial Q} \tag{28.}$$

The integral, Equation 27, is thus seen to be simply the pressure developed by static inflation of the tube as a *windkessel*.

When the origin is shifted to take account of the delay in onset of the pressure $[t - (x/c) = 0$ or $t + (x/c) - (2L/c) = 0]$ and when Equation 26 is applied to the downgoing and upgoing waves independently, the formula

$$P = P_{windkessel} + \tfrac{1}{2}\rho uc \tag{29.}$$

will show the steepening of the pulse along the length. Figure 16 illustrates

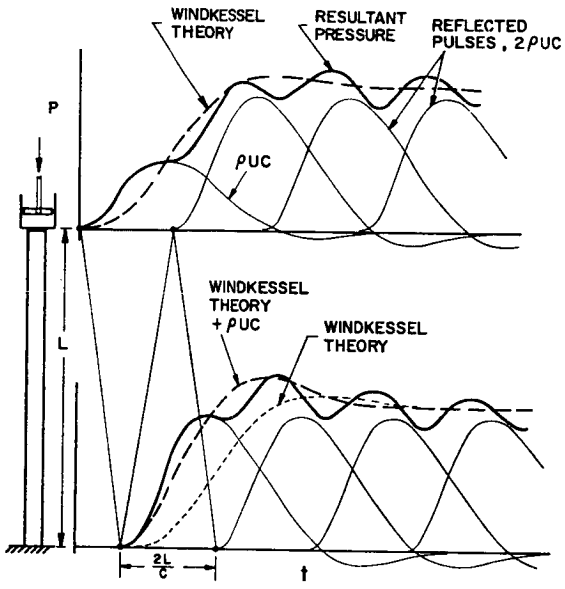

INFLATION OF AN ELASTIC TUBE

FIG. 16. First-order correction of *windkessel* theory for tube of finite length.

an application of the corrected *windkessel* theory to the inflation of an elastic tube of finite length with no outflow.

To take account of outflow at the proximal and distal ends, reflection coefficients k' and k may be introduced into Equation 25. Thus

$$k = \frac{Z_2 - Z_c}{Z_2 + Z_c} \tag{30.}$$

where Z_2 is the distal terminating impedance and Z_c is the characteristic impedance of the aorta. Equation 25 now becomes

$$P - P_0 = f\left(t - \frac{x}{c}\right) + kk'f\left(t - \frac{x}{c} + \frac{2L}{c}\right) + (kk')^2 f\left(t - \frac{x}{c} + \frac{4L}{c}\right) + \cdots + k\left\{f\left(t + x - \frac{2L}{c}\right) + kk'f\left(t + \frac{x}{c} - \frac{4L}{c}\right) + \cdots\right\} \tag{31.}$$

Equations 25 and 31 are analogous to equations for electromagnetic waves in transmission lines and are most conveniently treated by Heaviside's method (25). Using Heaviside's method we may write

$$f(t - \Delta t) = e^{-\Delta t D} f(t) \tag{32.}$$

where D is the differential operator $\partial/\partial t$. The right-hand side of Equation 32 is termed the "shift operator." The "repeat operator" is

$$\frac{1}{1 - e^{-\Delta t D}} f(t) = f(t) + f(t - \Delta t) + f(t - 2\Delta t) + \cdots \qquad 33.$$

while

$$\frac{1}{1 - ke^{-\Delta t D}} f(t) = f(t) + kf(t - \Delta t) + k^2 f(t - 2\Delta t) + \cdots \qquad 34.$$

With these rules Equation 31 becomes

$$P - P_0 = \frac{e^{-(x/c)D} + ke^{((x/c)-(2L/c))D}}{1 - kk'e^{-2L/cD}} f(t) \qquad 35.$$

A similar analysis yields for the velocity u

$$u = \frac{e^{-(x/c)D} - ke^{((x/c)-(2L/c))D}}{1 - kk'e^{-2L/cD}} \frac{f(t)}{\rho c} \qquad 36.$$

where $u = u(x, t)$ and $f \otimes = \rho c u(0, t)$. The flow and pressure in arteries are often analyzed by Fourier's series. In this case the terms of the series will involve

$$f_n(t) = A_n e^{int} \qquad 37.$$

The substitution of in for D in Equation 35 will then yield the "complex impedance" as a function of frequency [see (25)].

Expansion of Equation 36 for small values of L/c yields again the *windkessel* theory with a correction for transient wave reflections. In this case the formula incorporates the effect of an exponentially-decaying outflow through the peripheral resistances by virtue of the reflection coefficients k and k'.

The above treatment is frankly heuristic and by no means complete. Thus we have assumed that the impedance of the aortic branches is purely resistive. A more precise treatment would incorporate reactive components in the reflection coefficients k and k', and, of course, more branching arteries. A considerable improvement in accuracy might be achieved by treating the main branching arteries as small *windkessels* interposed between the aorta and the terminal capillary resistances. Taking, for example, a carotid artery (26) gives as the wave velocity 1800 cm/sec, or about 3 times that in the aorta. Assuming a length of 20 cm and a heart rate of 80/min, we find the carotid artery is about 1/70 of a wave in length. Evidently, even the larger branching arteries may be treated approximately as lumped capacitors. The capacitance will be given by

$$\left(\frac{\partial P}{\partial Q}\right)^{-1} = \left(\frac{\rho c^2}{LA}\right)^{-1} = \frac{1}{216\ 000}$$

or about 0.6 cc change in volume for 100 mm change in pressure. Such a branching artery may terminate in a resistance of 8000 (cgs) and the "RC" time constant will then be approximately 0.04 sec. Evidently the capacitance of the branching arteries, though small, is great enough to modify the shapes of the reflected pulses significantly.

More detailed treatment of arterial flow leads rapidly to a great increase in analytical complexity. Thus, Womersley (17) has calculated the impedance and reflection at a branching artery on the basis of time-dependent viscous flow. The actual impedance at a branch of the larger arteries will be determined primarily, however, by smaller branching arteries farther down. Hence, Womersley's analysis must be continued for several stages to obtain the true impedance at a branch. For such detailed calculations, the electrical analogue [see (27)] becomes useful. In this connection Jager, Westerhof & Noordergraaf (28) have succeeded in devising an electrical circuit to approximate Womersley's formula.

LITERATURE CITED

1. Goldsmith, H. L., Mason, S. G., *The Microrheology of Dispersions in Rheology*, **4** (Eirich, F. R., Ed., Academic Press, New York, 1967)
2. Einstein, A., *Investigations on the Theory of the Brownian Motion* (Dover, New York, S 304, 36–54, 1956)
3. Taylor, G. I., *Proc. Roy. Soc. London, Ser. A*, **138**, 41 (1932) [See also (1) above]
4. Lauffer, M. A., in *Currents in Biochemical Research*, 241–60 (Green, David E., Ed., Interscience, New York, 1946)
5. Frisch, H. L., Simha, R., in *Rheology*, **I**, 525–613 (Eirich, F. R., Ed., Academic Press, New York, 1956)
6. Merrill, E. W., *J. Appl. Physiol.*, **18**, 255 (1963)
7. Taylor, M. G., *Phys. Med. Biol.*, **3**, 273 (1959)
8. Zweifach, B. W., *Sci. Am.*, **200**, 54–60 (1959)
9. Zweifach, B. W., *Am. J. Med.*, **23**, P. 684–96 (1957)
10. Fung, Y. C., in *Biomechanics*, 151–66 (Fung, Y. C., Ed., Am. Soc. Mech. Engrs., 1966)
11. Wang, H., Skalak, R., *Viscous Flow in a Cylindrical Tube Containing a Line of Spherical Particles* (Dept. Civil Eng. Eng. Mech., Columbia Univ., New York, 1967)
12. Porje, I. G., Rudenwald, B., *Opuscula Med.*, **2**, 280–93 (1957)
13. Schultz, D. L., Turnstall-Pedoe, D. S., Lee, G. J., Gunning, A. J., Bellhouse, B. J., *Velocity Distribution and Transition in the Arterial System* (Univ. Oxford, Dept. Eng. Sci. Rept. 1968)
14. Jones, R. T., *Motions of a Liquid in a Pulsating Bulb with Application to Problems of Blood Flow* (Avco Everett Res. Lab. Res. Rept. 237 December 1965)
15. Taylor, M. G., Wave Travel in Arteries and the Design of the Cardiovascular System, in *Pulsatile Blood Flow*, 343–72 (Attinger, E., Ed., McGraw-Hill, New York, 1964)
16. Young, T., *Phil. Trans. Roy. Soc. London*, **98**, 164–86 (1808), **99**, 1–31 (1809)
17. Womersley, J. R., *Mathematical Analysis of the Arterial Circulation* (Wright Air Develop. Center Tech. Rept. WADC TR 56-614)
18. Skalak, R., *Wave Propagation in Blood Flow* Biomechanics, ASME, 20 (1966)
19. Olsen, J. H., Shapiro, A. H., *J. Fluid Mech.*, **29**, 513–38 (1967)
20. Anliker, M., Maxwell, J. A., *The Dispersion of Waves in Blood Vessels* (Environ. Biol. Div., Ames Res. Ctr., NASA, Dept. Aeron. Astronaut., Stanford Univ., Stanford, Calif.)

20a. Lamb, H., *Hydrodynamics*, 6th Ed. (Cambridge Univ. Press, 1932)

21. Evans, R. L., *Nature*, **186**, 290 (1960)
22. McDonald, D., *Blood Flow in Arteries* (Williams & Wilkins Co., Baltimore, 1960)
23. McDonald, D., Taylor, M. G., *Progr. Biophys. Biophys. Chem.*, **9**, 107 (1959)
24. Jones, R. T., Laird, J. D., in *Prospects for Simulation and Simulators of Dynamics Systems*, 151–62 (Shapiro, G. & Rogers, M., Eds., Spartan Books, New York, McMillan, London)
25. McLachlan, N. W., *Complex Variable Theory and Transform Calculus* (Cambridge Univ. Press, 1955)
26. Patel, D. S., Greenfield, J. C. Jr., Fry, D. L., in *Pulsatile Blood Flow* (See Ref. 15)
27. Noordergraaf, A., in *Pulsatile Blood Flow* (See Ref. 15)
28. Jager, G. N., Westerhof, N., Noordergraaf, A., Oscillatory Flow Impedance in Electrical Analog of Arterial System *Circulation Res.*, **16**, 121–133 (1965)

FLUID DYNAMICS OF HEART ASSIST DEVICES

Robert T. Jones

May 1970

Jones, R. T. "Fluid Dynamics of Heart Assist Devices," in Biomechanics: Its Foundations and Objectives. Edited by Y. C. Fung, N. Perrone, and M. Anliker. Englewood Cliffs, N. J., Prentice-Hall, 1972. © 1972. Reprinted by permission of Prentice-Hall, Inc., Englewood Cliffs, N. J.

From BIOMECHANICS: ITS FOUNDATIONS AND OBJECTIVES,
Y. C. Fung, N. Perrone and M. Anliker, editors.
© Prentice-Hall, Inc., Englewood Cliffs, New Jersey.
All rights reserved. Printed in the United States of America.

21

Fluid Dynamics of Heart Assist Devices

ROBERT T. JONES

In this article certain hemodynamic phenomena that arise in connection with the use of artificial blood pumping devices will be reviewed. Among these are: 1) flows produced by collapsing bulbs, 2) the impedance presented by the aorta, 3) limiting velocities and instability of flow in elastic vessels, 4) effectiveness of valveless arterio-arterial pumps, and 5) wave reflection phenomena and instabilities associated with the intra-aortic balloon pump.

* * *

Maintenance of life by an artificial blood pump is an everyday occurrence in most large hospitals. The pump-oxygenator which takes over the function of both the heart and the lungs during surgery seems, however, to be limited in use to a maximum of several hours. Beyond this time one looks for certain symptoms which are taken as evidence of changes in the physiological constituents of the blood, that is, loss of red blood cells (hemolysis) and platelets as well as denaturation of protein components. In spite of this deficiency the pump-oxygenator is considered adequate for most surgical procedures, though not suited in its present form to chronic support of a weakened or failing heart.

Pending the development of an ideal total heart replacement, there have been numerous attempts to provide partial assistance to the heart (see references) for periods longer than the few hours available with the pump oxygenator. These have generally taken the form of pumps to assist the left ventricle, since left ventricular function is most critical and evidently most often deficient.

Several types of left ventricular assist pumps are illustrated in Fig. 1. In Fig. 1*a* the pump is equipped with inflow and outflow valves and is placed in parallel with the ventricle (atrio-arterial pump) where it may divert all or part of the flow around the left heart. By contrast, pumps placed in series with the ventricle may not significantly alter the flow but may be expected to relieve all or part of the systemic pressure from the heart. It is interesting that the series pump may accomplish this function even without valves if it is properly phased with the pulsatile outflow from the ventricle. The centrifugal pump described by Dorman et al (1969) operates by magnetic coupling through the intact skin and, of course, requires no valves.

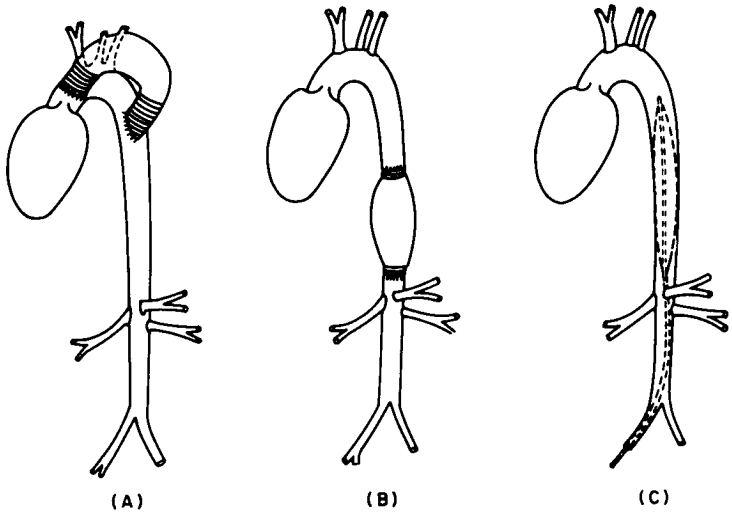

Fig.1: Heart assist devices

In order to understand the operation of such devices, it is first of all necessary to gain at least a crude understanding of the function of the left ventricle and the aorta in mechanical terms.

Our first curiosity here is in the flow produced by a collapsing or squeezing bulb since both the natural and the artificial ventricles operate in this fashion. As has been shown (Jones, 1969) potential flows of the type

$$\Phi(x, y, z, t) = \alpha x^2 + \beta y^2 + \gamma z^2 \tag{1}$$

provide perhaps the simplest starting point for mathematical modeling of the

bulb flows. Here Φ is the velocity potential, x, y, z are cartesian coordinates and α, β, γ are constants or functions of the time such that

$$\alpha + \beta + \gamma = 0 \tag{2}$$

Such flows are trivial solutions of the Navier-Stokes equations and, of course, of Laplace's equation. If x, y and z are taken as the initial coordinates of a particle of fluid (or of the boundary) we have

$$\zeta = xe^{\int \alpha\, dt} \tag{3}$$

$$\eta = ye^{\int \beta\, dt} \tag{4}$$

$$\xi = ze^{\int \gamma\, dt} \tag{5}$$

for the Lagrangian coordinates. The Lagrangian coordinates are thus related to the initial coordinates by simple affine transformations. Plane surfaces remain plane and a bulb of initially arbitrary shape undergoes distortions that can be represented by stretching its coordinates in different directions while preserving a constant volume.

Figure 2 shows streamlines emanating from a collapsing bulb together with pressures calculated by the foregoing method on the assumption of frictionless flow. The motion of the liquid in a bulb does not completely determine the pressures, but there remains an arbitrary function of the time to be determined by the impedance into which the bulb works, that is, the relation between pressure and flow in the aorta.

In a typical case the diastolic pressure in the aorta will be 70–80 mm Hg and the ejection of blood from the ventricle will raise this pressure by 60–70 mm. Pressures arising from dynamic motions within the bulb, however, are of the order of 3–4 mm only. Thus it seems that very little of the effort of the heart is directed against the inertia of the blood but appears initially in elastic distension of the arteries; later to be dissipated in frictional resistance through the capillaries.

Examination of the heart cavity shows a surface far from streamlined form, with deep furrows (trabeculae) and tendons to support the mitral valve. Similarly, the architecture of the aortic system shows little disposition toward flow dynamics as ordinarily understood. Branching arteries often show no preference for the flow direction. Here again we find but a small fraction of the pressure in kinetic form; $\rho u^2/2$ is of the order of a few millimeters.

In prosthetic heart pumps streamlining does not play an important role in the purely mechanical function, though the flow does seem most important in relation to clotting. The clotting phenomenon is at present a dominant factor in the success or failure of artificial heart devices including prosthetic valves and assist pumps. Though beyond the scope of the present discussion,

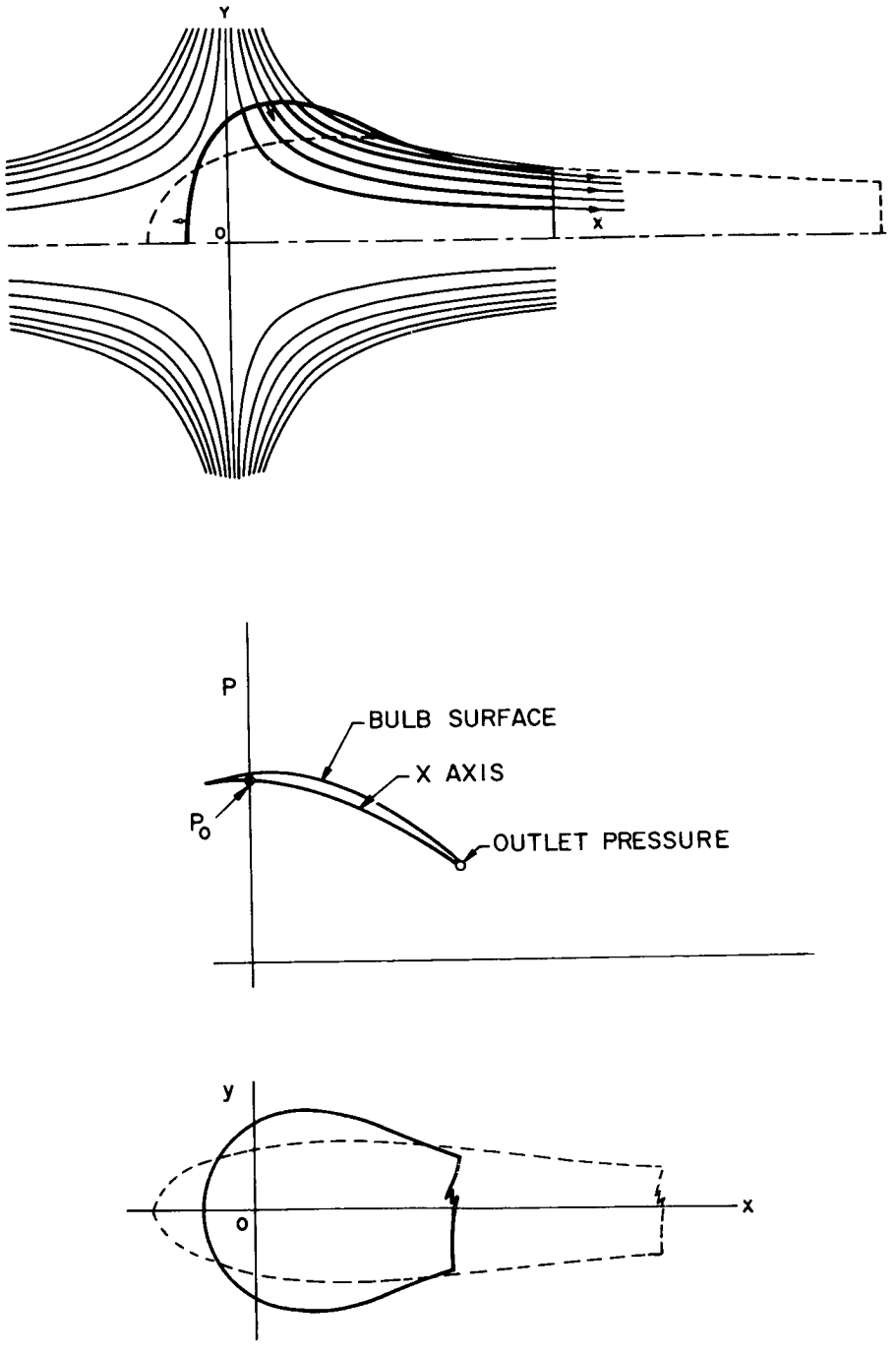

Fig. 2: Streamlines and pressures in collapsing bulb.

the relation between clotting and flow has become a major item of research at our laboratory and elsewhere.

Nearly all current heart assist pumps operate by pneumatically driven plastic bulbs. In our experience we have found it essential that the bulb not change its volume by stretching but rather by folding. The bulb must undergo a change of extrinsic geometry without altering the intrinsic geometry of the surface. The solution appears by reflection of the convex surface in a plane so that progressively larger areas of the surface change from convex to concave, along a singular curve determined by the intersection of the plane. In practice the bulb has finite thickness and the surface bends to a finite radius along this curve. In spite of the concentration of bending strain, bulbs of silicone rubber have very satisfactory fatigue life in this mode of deformation.

Such bulbs are occasionally made by fitting initially flat sheets of fabric and silicone rubber over a convex form. Here one encounters a problem well known to tailors and known to mathematicians from the properties of the Tschebyschev net. It seems that such a net (as a handkerchief) can be fitted over a convex surface whose integrated solid angle does not exceed 2π.

The function of the aorta and the major vessels as an elastic compliance is well characterized by the simplest theory of aortic impedance known as the "windkessel" theory (Taylor, 1965). Here the aorta acts simply as a lumped capacitance, and if the peripheral resistance is linear, one obtains an exponential decay of pressure following ejection of a volume of blood from the heart.

Figure 3 illustrates our attempt to make a direct physical model of the aortic system. In medical circles such devices are known by the term "mock circulation." We have found such a model useful in studying and isolating the purely mechanical effects of cardiac assist devices. The model aorta is made of silicone elastomer with compliance determined so as to lie within the physiological range. The substitute ventricle is made of the same material and is placed in an air tight box so that it can be actuated pneumatically by a linkage and piston drive as shown. Figure 4 shows the type of pressure pulse produced by our model compared with natural pulses taken from a textbook on physiology.

With such a model one has control of various parameters such as source impedance of the heart, cardiac output, wave speed and diameter of the aorta, and peripheral resistance. In addition, since the aorta is transparent, we have been able to observe visually the action of the intra-aortic balloon pump.

Fortunately, because of the high Reynolds number of the flow in the larger arteries, one is not required to duplicate the detailed rheological properties of the blood in such experiments. A rough calculation will show that the unsteady laminar boundary layer on the inner wall of the aorta has time to grow to a thickness of only about one millimeter during the heart beat. Separation vortices of the order of a centimeter in diameter may be expected

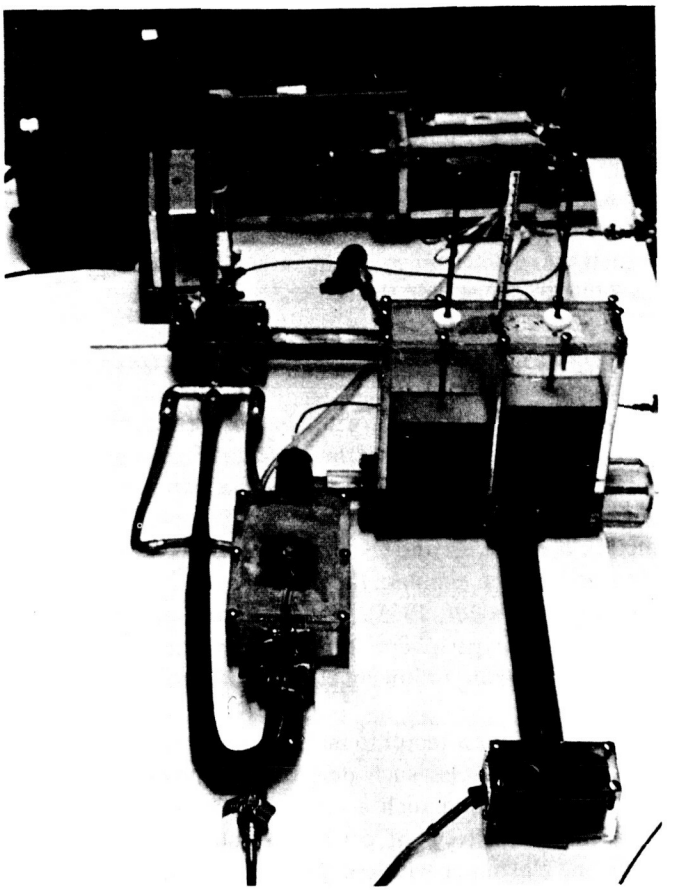

Fig. 3: Aortic circulation model.

to persist for two or more heart beats. It should be borne in mind, however, that the dynamic pressure associated with the flow is small compared with the actual pressure. Hence, flow irregularities do not normally have a great influence on the mechanical performance of heart assist pumps. They may, however, influence the behavior of artificial valves and, of course, the formation of thrombi.

In our early effort at Avco Everett Research Laboratory, we sought to develop and perfect the Kantrowitz auxiliary ventricle, illustrated in Fig. 1*b*. This device comprises a simple compliant pumping chamber which is fitted inside a more rigid plastic case. The space between the bulb and the case communicates by a small gas tube through a percutaneous connector to the control system outside the body. The bulb can then be alternately compressed and

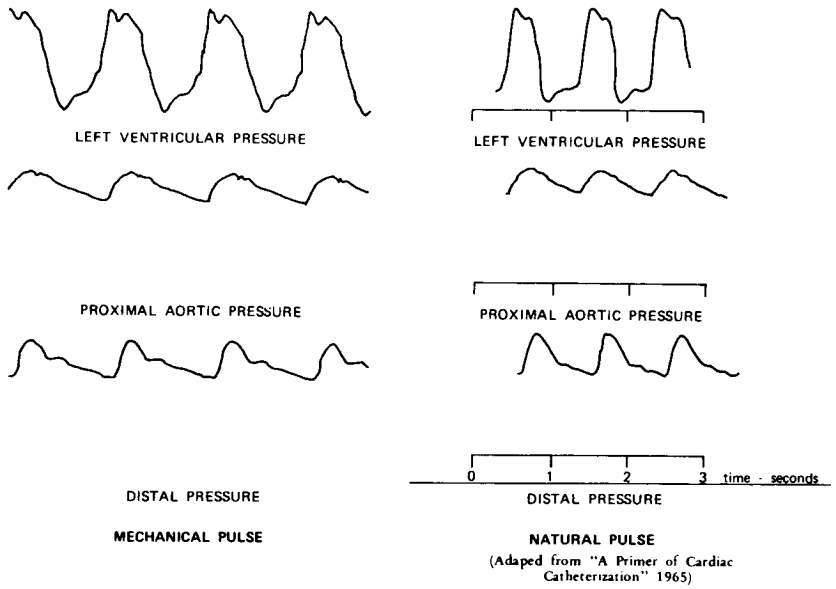

Fig. 4: Comparison of pulses produced by model with physiologic pulse.

expanded by pneumatic pressure from an external power source. Since the blood pumping chamber has no valves, it is necessary that its stroke be synchronized and properly phased with the action of the heart. This synchronization was accomplished with the aid of electrocardiac signals obtained from electrodes attached to the heart muscle. By withdrawing blood from the aorta prior to systole the pressure required for ejection by the heart can be reduced, thus lessening the effort of the heart. After the ejection from the natural heart is complete and the aortic valve is closed, the blood withdrawn into the auxiliary ventricle can be pumped back into the aorta, raising the pressure and supplying energy for the systemic circulation. This technique has the advantage of creating higher pressures in the aorta during diastole and hence the possibility of increased coronary perfusion (in practice the coronary flow has in some cases been observed to diminish, perhaps because the assisted heart requires less). If we suppose, for example, that the stroke volume of the artificial ventricle Q_b is as great as the output stroke of the natural ventricle Q_h then it is clear that the pressure rise during systole may be suppressed and the pressures in the natural ventricle need hardly exceed diastolic pressure. This special situation requires that the withdrawal stroke of the AV imitate the ejection stroke of the natural ventricle in reverse. In practice somewhat better results are obtained by reducing the pressure in the aorta prior to systole, permitting the aortic valve to open at a lower pressure and reducing the pressure during isometric contraction.

The intra-aortic balloon pump (Fig. 1*c*), functions by a similar principle (Moulopoulos et al, 1962) since inflation and deflation of the balloon affects aortic pressures in much the same way as injection and withdrawal of a corresponding quantity of blood. The balloon pump has the advantage that it can be inserted through a femoral artery under local anesthesia. In this case electric signals for timing are obtained from skin electrodes.

The reduction of outflow pressure during systole may, of course, permit the heart to eject a greater flow quantity. Hence, the auxiliary ventricle (or the balloon pump) may increase the cardiac output as well as effect a reduction in left ventricular pressure. The precise division of effort between flow and pressure will depend on what may be termed the "source-impedance" of the heart. Animal experiments with such pumps indicate that a healthy heart has a very high source impedance (is flow-limited). The primary effect of the auxiliary pump then appears as a reduction of pressure in the left ventricle. However, experience with human patients in cardiac distress indicates that the weakened heart may be pressure limited. In such cases the arterio-arterial pump will act primarily to increase the cardiac output.

Because of its dependence on pathology, it seems unlikely that any universal relation for cardiac impedance can be found. However, the reduction of ventricular pressure and the increase of flow can be combined linearly into a quantity which may be thought of as total effectiveness and which can be simply related to the stroke volume of the pump and to the unassisted aortic pulse (Jones et al, 1968). This cycle analysis of the arterio-arterial pump is based on the windkessel theory of aortic impedance. Figure 5 illustrates the essential idea of the cycle analysis. Here the pump injects its stroke

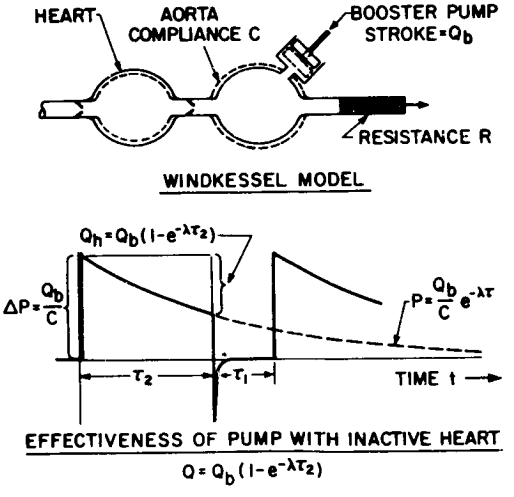

Fig. 5: Analysis of arterio-arterial pump.

volume into the aorta which distends as a windkessel. The pressure increment so produced then decays exponentially as the volume flows out through the peripheral resistances. All of the added volume would ultimately find its way into the periphery if enough time were available. However, the pump must withdraw volume and lower the pressure in the aorta prior to the next heart beat. It must therefore withdraw a portion of the blood previously injected, namely the fraction

$$e^{-\lambda t_d} \times Q_b \tag{6}$$

where $\lambda = 1/RC$. R is the peripheral resistance and C the aortic compliance or capacitance. Q_b is the stroke volume of the pump and t_d is the diastolic interval. The complete analysis, which entails the assumption that operation of the pump does not change systolic or diastolic intervals, leads to the formula

$$\frac{\Delta Q}{Q} - \frac{\Delta P}{P} = \frac{Q_b}{Q_h}(1 - e^{-\lambda t_d}) \tag{7}$$

The quantity $(1 - e^{-\lambda t_d})$ may be conveniently replaced by the quantity $(P_1 - P_2)/P_1$ where P_1 and P_2 are systolic and diastolic pressures with the unaided heart. In this form it is evident that the operation of such valveless pumps depends on the pulsatile character of the aortic pressure. In order to obtain an upper bound for the effectiveness, it has been assumed that the pump displaces its volume Q_b instantaneously. Other variations of the stroke Q_b as a function of the time will require a convolution of Q_b with the decay factor $e^{-\lambda t}$.

The use of the windkessel theory for aortic impedance corresponds to an assumption that the arterio-arterial pump will be equally effective at any position along the aorta. Experiments with animals and with our artificial circulation model tend to support this assumption provided the timing of the pump cycle is adjusted to account for the delay in wave propagation.

Figure 6 shows the result of an experiment made in the circulation model to check this assumption. Here the pumping effect of an intra-aortic balloon placed in the descending thoracic aorta is compared with the effect of an auxiliary ventricle placed near the heart. In each case the same stroke volume was used, but the timing of the balloon was advanced slightly. The curves on the left of the chart recordings show the rather large aortic pressure produced by the pump during diastole. Near the center of each diagram the chart speed was reduced, compressing the pulses. The rise in left ventricular pressure when the pumps were turned off is clearly evident here and is approximately the same for the balloon and the AV. During the compressed portions of the records an integrating circuit was switched on to record mean aortic pressures. The mean pressures are an indication of the flow, and it will be noted that each

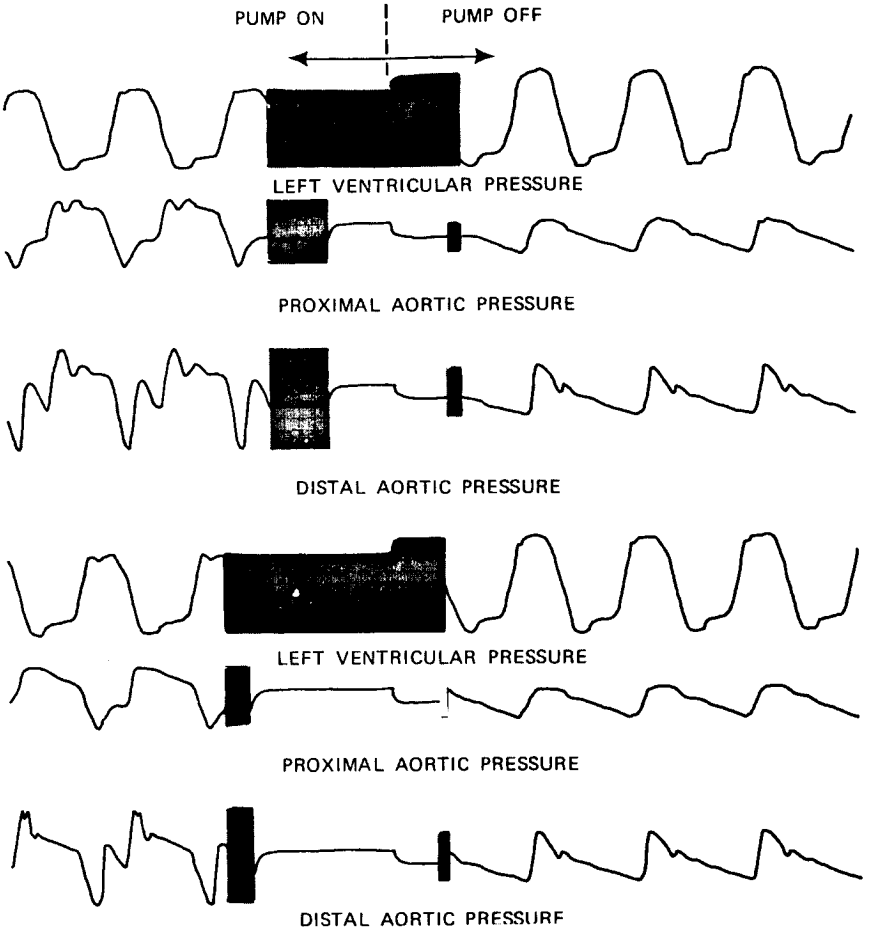

Fig. 6: Comparative effects of balloon pump and auxiliary ventricle.

pump increased the cardiac output by the same amount. In spite of the obstruction presented by the balloon in the aorta, the distal mean pressure is very effectively increased.

The action of the arterio-arterial pump will evidently depend not only on the source impedance of the heart, but also on the complex impedance presented by the aortic system. The impedance of the aorta is, of course, complicated by the phenomenon of pulse wave propagation. (McDonald, 1960; Young, 1808, 1809; Womersley; 1956 Anliker and Maxwell, 1966). The elastic tube, except for reflections, presents a characteristic resistive impedance. With an injection velocity u the pressure developed is

$$\Delta p = \rho u c$$

where c is the wave propagation velocity of the order of 500–1000 cm/sec. The flow quantity will be uA where A is the cross-sectional area of the artery. The characteristic impedance is then

$$Z_c = \frac{\rho c}{A} \tag{9}$$

For a wave speed of 600 cm/sec and an area A of 4 sq cm, we obtain

$$Z_c = 150 \text{ (cgs)} \tag{10}$$

Estimates of the capillary resistance associated with the various outlets may be made from data on mean pressures and flow to various organs given in physiology textbooks. Values of peripheral resistance vary over a wide range, especially in pathologic conditions such as shock. However, it is significant that the values are an order of magnitude greater than either the pulse impedance or the frictional resistance of the aorta. Hence, we may suppose that the pulse wave will be strongly reflected by large resistances which are rather closely coupled through the main branching arteries. Furthermore, since the time for a pulse wave to traverse the length of the aorta is short compared with the duration of the heart beat one can expect the pressure and flow to be dominated by multiple reflections from the periphery during a single heart beat.

The foregoing characteristics of the aortic system lead us to what might be termed a "slender windkessel" theory of aortic impedance. Clearly, if an elastic tube of finite length is inflated sufficiently slowly it will behave simply as a compliance. With more rapid inflation waves and their reflections from the ends will become prominent (Fig. 7). The important parameter here is the characteristic time for reflection along the length of the tube, ℓ/c, compared with the time scale of the inflation process. By expanding the wave reflection formulas in ascending powers of ℓ/c, one obtains, first of all, the result of the windkessel theory followed by a succession of terms which correct the windkessel theory for the finite length of the aorta (Jones, 1969). Curiously, the first correction does not involve the length of the windkessel at all but merely takes account of the fact that the windkessel is an elastic tube. By considering one of the two families of characteristics, there is obtained

$$\Delta p = \frac{1}{2} P_{\text{windkessels}} + \frac{1}{2} \rho u c + \cdots \tag{11}$$

Thus the first correcting term is simply 1/2 the characteristic pressure, ρuc. Figure 7 illustrates the process of inflation of an elastic tube for the case of a stepwise inflow velocity $u(t)$ and shows the nature of the correction. Applying this calculation to the aorta, one should take account of outflow at the reflection sites. Such outflow leads to progressive diminution of the reflected

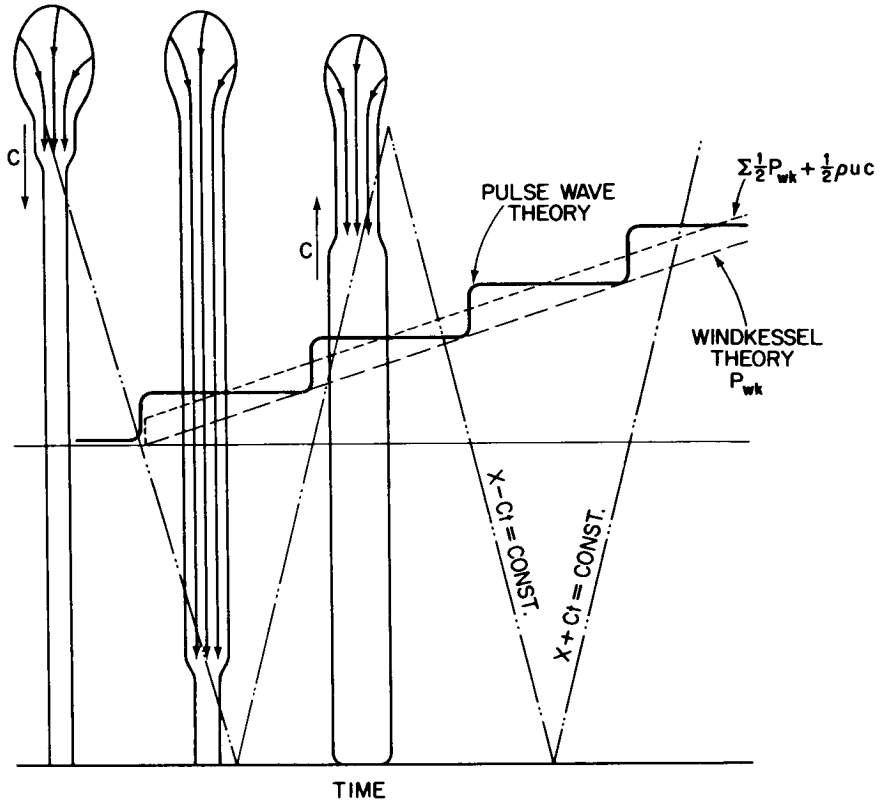

Fig. 7: Inflation of an elongated windkessel.

pulses by a fixed fraction (reflection coefficient K) and thence to an exponential decay of aortic pressure. The windkessel theory (P_{wk}) shows this behavior by a convolution of the inflow pulse with the factor $e^{-\lambda t}$. However, since it depends on the integral curve of the inflow pulse, P_{wk} shows too slow an initial rise of pressure. This behavior is illustrated in Fig. 8.

A method of arterio-arterial pumping not illustrated in Fig. 1 consists of withdrawing blood directly through cannulae inserted in the femoral arteries and reinjecting the same blood during diastole. While the effect of distance from the heart is rather small in the case of the balloon or the abdominal ventricle, such effects will certainly be larger here. In particular, the taper of the artery will be significant since the femoral vessels may be only 6 mm in diameter while the aorta near the heart is approximately 20–25 mm.

The pulse wave phenomenon in a tapered elastic tube leads, in the case of constant wave speed, to an equation similar in form to that employed in the analysis of acoustic horns. A treatment of the exponentially tapered tube has

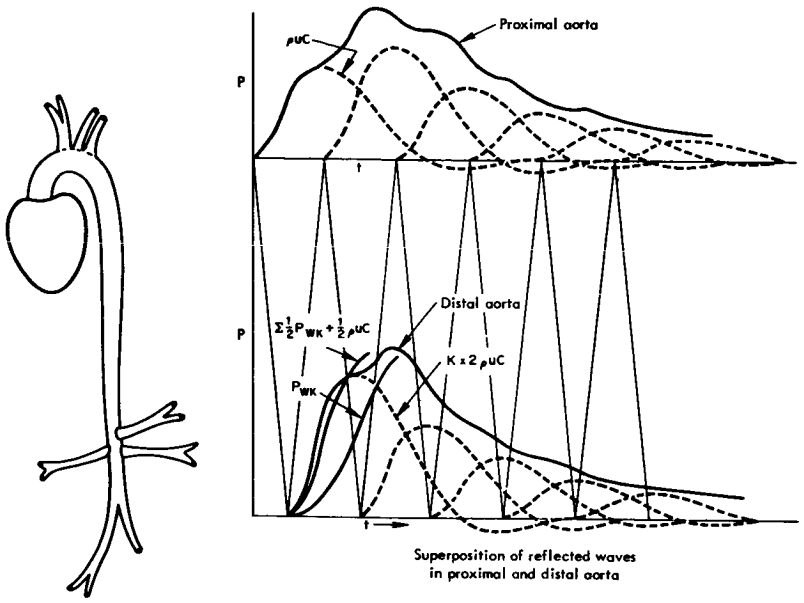

Fig. 8: Superposition of reflected waves in proximal and distal aorta.

been given (Evans, 1960). A transformation which yields a one-parameter family of solutions in which the wave speed and the tube diameter vary together is described by McMahon et al (1969).

Perhaps the simplest treatment is that employing the spherical wave equation as suggested by Thomas Young (1808, 1809) for a straight conical taper. Here the velocity potential will have the well-known form

$$\phi = \frac{1}{R} f\left(t \pm \frac{R}{c}\right) \tag{12}$$

where R is the distance from the virtual apex of the aorta. Figure 9 shows a calculation on this basis which illustrates the transformation between pressure and flow effected by a conically tapered elastic tube. Here we have assumed that a quantity $\Delta Q = 10$ cc is withdrawn from the narrow (6 mm) end of the conical tube, following the pressure and velocity variations shown. At the upper, wider end of the tube the pressure pulse is much reduced, although the flow quantity temporarily withdrawn has increased to 40 cc.

Pulsatile pumping by direct withdrawal and injection through a small artery must evidently be restricted to certain levels of pressure and velocity in order to avoid blood damage. The flow velocity is in any case limited to values less than the pulse wave velocity. In the balloon pump the fluid withdrawn can be a light gas such as helium, enabling greater volumes to be

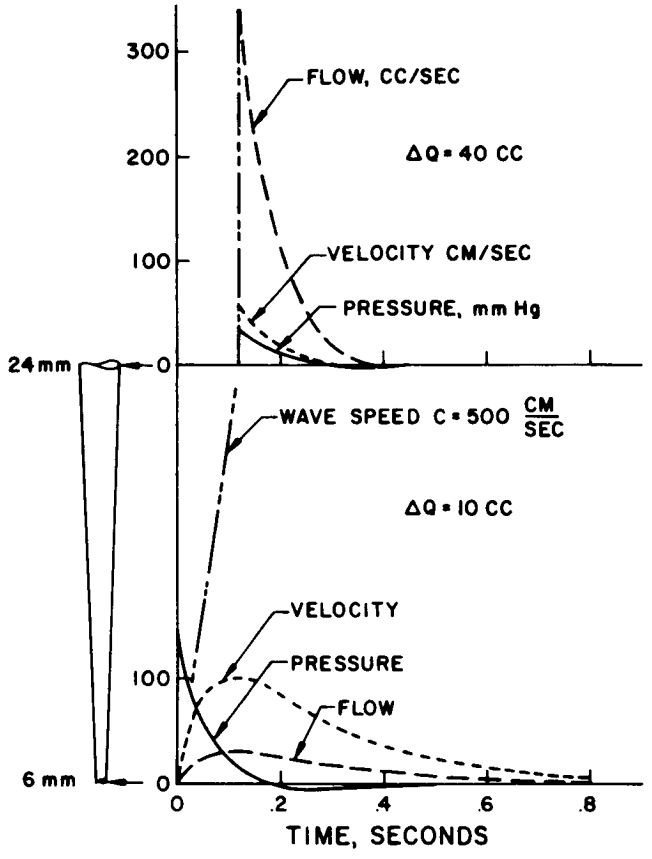

Fig. 9: Transmission of pulse in tapered artery.

pumped. The balloon, however, has its own peculiar instability which we have termed "bubble trapping." The origin of this phenomenon becomes evident when we attempt to calculate the flow and pressure produced by an expanding cylindrical balloon in a circular tube. For this purpose we use the potential

$$\phi = A\left(x^2 - \frac{1}{2}r^2\right) + B\log r \tag{13}$$

which satisfies the boundary condition for a cylinder expanding within a fixed cylinder of radius $r_o = \sqrt{B/A}$. Calculation shows a parabolic pressure distribution along the length of the expanding cylinder with pressures at the center as much as 100 mm higher than the pressures at the ends. An ordinary limp balloon cannot, of course, support such pressure gradients, and the

inflating gas simply rushes toward the ends of the balloon inflating them first and sealing off the aorta. As Professor Shapiro of M. I. T. has pointed out, any manner of expelling blood from the space around the balloon must involve such a falling pressure gradient and will lead to bubble trapping unless corrective measures are taken.

Figure 10 shows the bubble trapping phenomenon as it appears in our Avco circulation model. The blood trapped between the ends of the balloon is, of course, not effective in the pumping cycle, and the aorta in this region may be subjected to high pressures of the order of the drive pressure.

One method we have found successful in limiting this phenomenon is to divide the balloon along its length into a number of compartments, inflating the compartments selectively through orifices of different size. Figure 11

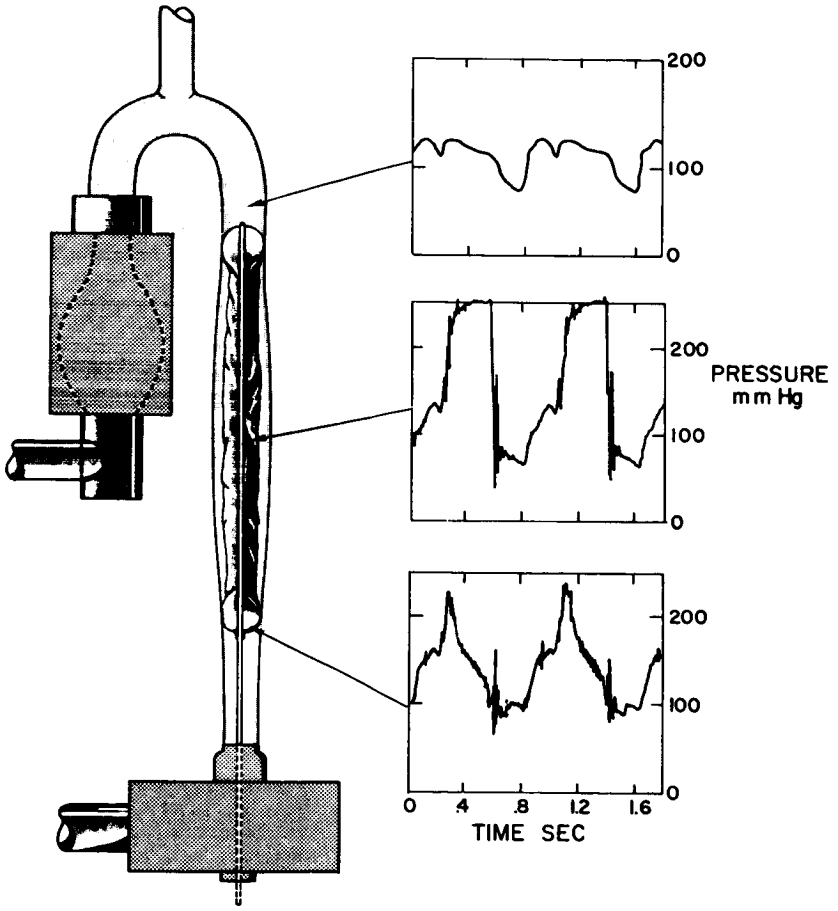

Fig. 10: Bubble trapping phenomenon.

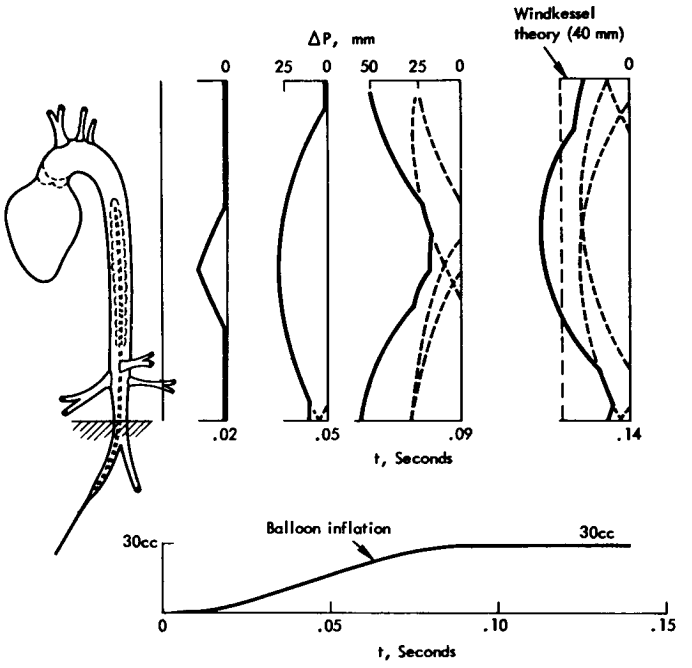

Fig. 11: Calculated pressures with controlled balloon inflation.

shows pressures calculated for such a controlled balloon in an elastic artery. Here it has been assumed that the pulse wave velocity is not modified by the presence of the balloon, an assumption permissable only if uncontrolled movements of the gas along the length of the balloon are effectively impeded.

Acknowledgment. *The work described herein was supported in part by the U.S. Air Force Office of Scientific Research. This paper was presented at a Specialists Meeting on "Fluid Dynamics of Blood Circulation and Respiratory Flow," May 4–6, 1970 in Naples, Italy, under the sponsorship of the Fluid Dynamics Panel of the AGARD, NATO, the Advisory Group for Aerospace Research and Development.*

REFERENCES

Anliker, M. and J. A. Maxwell 1966. The dispersion of waves in blood vessels. Biomechan. Sym. ASME, New York.

Birtwell, W. C., M. S. Soroff, M. Wall, A. Bisgerg, M. J. Levine and R. A. Deterling 1962. Assisted circulation-improved method for counterpulsation. Trans. Amer. Soc., Artif. Int. Organs. 8: 35.

Clauss, R. H., W. C. Birtwell, S. Albertal Lunzer, W. T. Taylor, A. F. Fosberg and D. E. Harken 1961. Assisted circulation: I. arterial counterpulsator. J. Thoracic and Cardiovas. Surg. 41: 447.

Dennis, C., J. R. Moreno, D. P. Hall, C. Grosz, S. M. Ross, S. A. Wesolowski and A. Senning 1963. Studies on external counterpulsation as a potential measure for acute left heart failure. Trans. Amer. Soc. Artif. Int. Organs 9: 186.

Dorman, F., E. F. Bernstein, P. L. Blackshear, R. Sovilj and D. R. Scott 1969. Progress in the design of a centrifugal cardiac assist pump with trans-cutaneous energy transmission by magnetic coupling. Trans. Amer. Soc. Artif. Int. Organs 15:

Evans, R. L. 1960 Nature, 186–290.

Gradel, F., T. Akutsu, P. A. Chaptal and A. Kantrowitz 1965. Successful hemodynamic results with a new U-shaped auxiliary ventricle. Trans. Amer. Soc. Artif. Int. Organs.

Jones, R. T. 1969. Blood Flow. Ann. Rev. Fluid Mechanics Vol. 1. Annual Rev. Inc., Palo Alto, Calif.

Jones, R. T., H. E. Petschek and A. R. Kantrowitz 1968. Elementary theory of synchronous arterio-arterial blood pumps. Med. & Biol. Eng. 6: 303–308.

Kantrowitz, A. and A. Kantrowitz, 1953. Experimental augmentation of coronary flow by retardation of the arterial pressure pulse. Surgery 34: No. 4: 678–87.

Liotta, D., C. W. Hall, D. A. Cooley and M. E. DeBakey 1964 Prolonged ventricular bypass with intrathoracic pumps. Trans. Amer. Soc. Artif. Int. Organs, 10: 154.

McDonald, D. 1960. Blood Flow in Arteries. Williams and Wilkins Co., Baltimore.

McMahon, T. A., V. S. Murthy, C. Clark, M. Y. Jaffrin and A. H. Shapiro 1969. The dynamics and fluid mechanics of the intra-aortic balloon heart assist device. M. I. T. Fluid Mech. Lab. Pub. No. 69-11.

Moulopoulos, S. D., S. Topaz and W. J. Kolff 1962. Diastolic balloon pumping (with carbon dioxide) in the aorta: A mechanical assistance to the failing circulation. Amer. Heart J., 63: 669.

Taylor, M. G. 1965. Wave travel in arteries and the design of the cardiovascular system. *In* E. Attinger (ed.), Pulsatile Blood Flow. McGraw-Hill Book Company, New York.

Womersley, J. R. 1956. Mathematical analysis of the arterial circulation. Wright Air Develop. Center Tech. Rept. WADC TR 56-614. Dayton, Ohio.

Young, T. 1808. Hydraulic investigations. Subservient to an intended Croonian lecture on the motion of the blood. Phil. Trans. Roy. Soc. (London) 98: 164–86.

Young, T. 1809. On the functions of the heart and arteries. The Croonian Lecture. Philos. Trans. Roy. Soc., London. M1355, 99: 1–31.

A SIMPLE VIOLIN OSCILLATOR

Robert T. Jones

A SIMPLE VIOLIN OSCILLATOR

Robert T. Jones

For acoustic tests the violin may be driven laterally at the bridge by a small speaker of the type commonly found in pocket transistor radios. To reduce the radiation from the speaker itself I remove the cone, leaving the small voice coil supported by the corrugated diaphragm under the cone. A narrow (half inch diameter) stiff paper (IBM card paper) cone is then made and cemented to the voice coil projecting forward. At the tip of this cone a narrow strip of fiber is cemented. The fiber strip extends forward an additional half inch or so and can be inserted under one of the strings (A or D) at the top of the bridge. All of this is made possible by a marvelous substance known as "five minute epoxy." The flat base of the speaker is secured to its mount by a type of "double-sticky" tape known in model airplane shops as "servo-mounting" tape. With the fiber strip clamped between the string and the bridge and the driving current from the oscillator turned on it will normally be found that the voice coil is off center. This is easily corrected by small adjustments of position, but it is essential that such adjustments be permitted by the mounting. I use the type of mounting used by machinists in setting up a dial gauge (see photograph) though there are other possibilities. In order to record the driving force I place a four ohm resistor in series with the voice coil and measure the voltage drop. Though these speakers cost only a dollar or two, it seems safe to assume that Faraday's laws still apply, and that the magnetism is of the same quality as would be obtained in a more expensive arrangement.

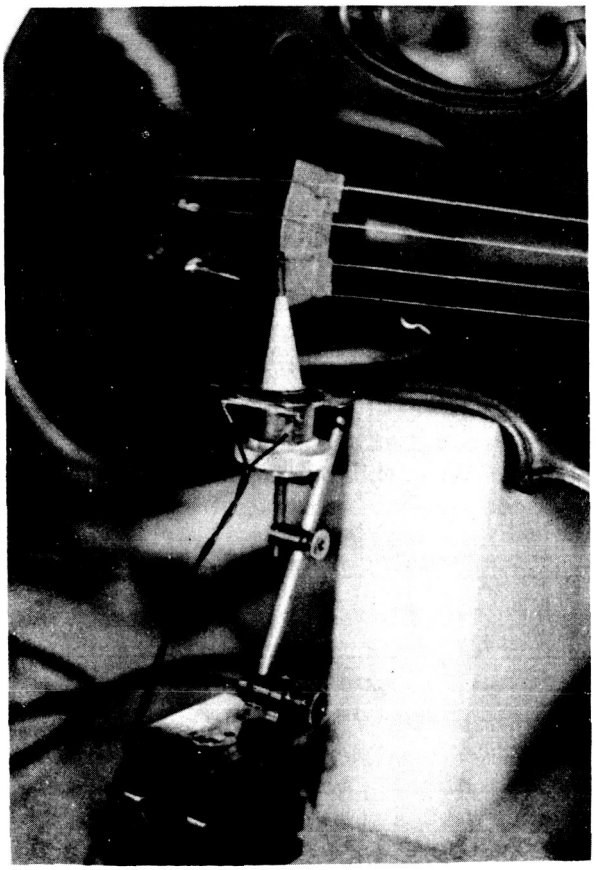

For saw tooth excitation I use the sweep voltage of an oscilloscope. By turning the frequency down to one or two cycles per second one can obtain an impulsive or "delta function" input. For pure tone excitation, a Hewlett-Packard audio oscillator is employed and the sound is picked up by a G.R. sound level meter.

Figures 1 and 2 show sound level peaks in the range above 74 db from two violins, one I made in 1956 and the other more recently. The tests were made in a rather reverberant room, making it necessary to interpret the higher frequencies more or less statistically. These violins were made following early recommendations of Prof. Saunders and Mrs. Hutchins, and they have large amplitudes in the low frequency range.

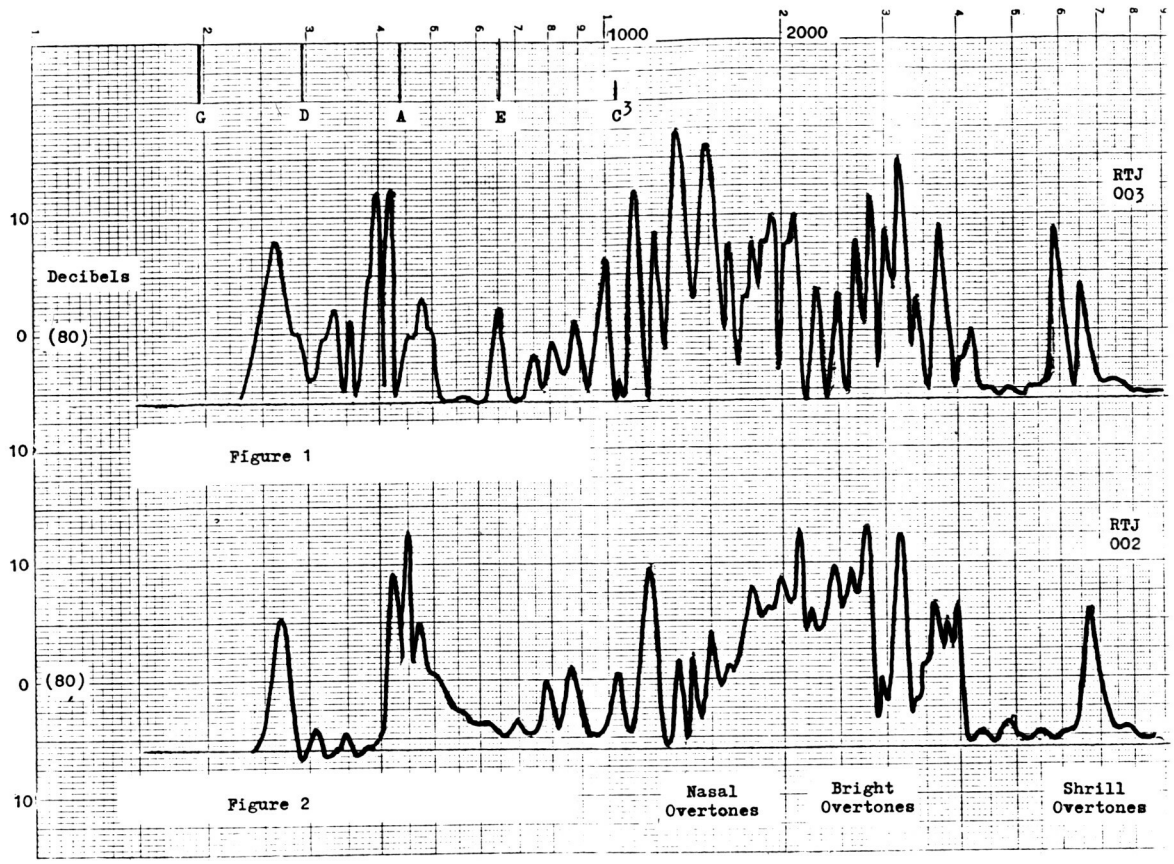

Response to pure tone excitation
G.R. Sound Level Meter

Although both violins have a powerful tone and easy response, the first one is judged not acceptable because of too much emphasis in the bass region and because of a "nasal" quality. It will be noted that in this case the overtone peaks are highest in the 1500 cylce region, corresponding to the observation by Meinel (J. Acous. Soc. Amer., vol. 29, July 1957) that overtones in this range produce a nasal quality.

In order to test Meinel's statement more specifically, I arranged to mix the tones from two audio oscillators and played them through an ordinary loudspeaker. My son and daughter, who have considerable musical experience and who did not know the expected outcome of the experiment, definitely preferred 500 plus 2000 Hz to the combination 500 plus 1500.

Actually (as mentioned for example by Möckel in Die Kunst des Geigenbaues) the nasal range is probably between 1350 and 1700 Hz. My tests in which various distorted wave shapes were played through a loudspeaker both with and without an LC filter centered in this range tend to confirm this impression.

It will be noted that the second violin has accentuated overtones in the 2000 to 3000 Hz range, the main body resonance is at 450 Hz, and the air resonance peak is somewhat lower in amplitude. This violin is preferred by musicians who have tried both.

Production and interpretation of Chladni patterns - To calculate the sound radiation from a violin one would like to know the vibration amplitude as a function of position over the top and bottom surfaces. The holographic technique permits this, but not everyone has access to such equipment. Gross patterns of the vibration modes can be obtained very simply however by the old-fashioned Chladni method. The fact that the violin plates are curved introduces some difficulty and most powders will be influenced too much by gravity. The pictures shown were taken with the aid of pumice powder which seems to have just the right amount of "stickiness" and will flow uphill away from a vibrating area.

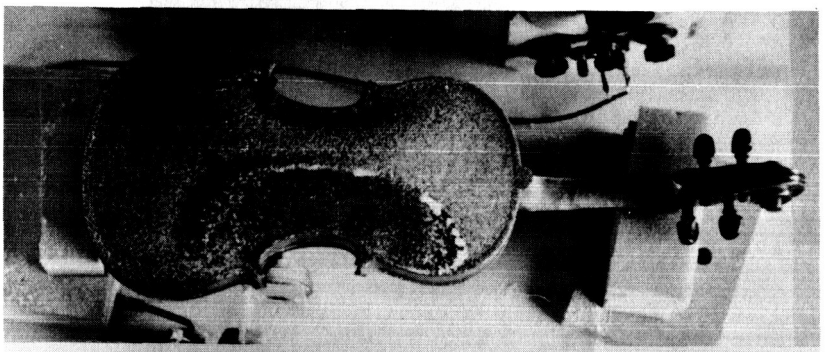

390 Hz

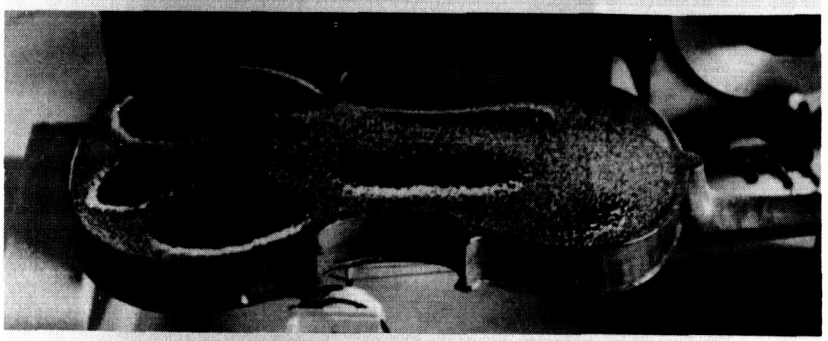

1300 Hz

At 390 Hz, it will be noted that a portion of the back plate opposite the bass bar is vibrating. This vibration is evidently being communicated through the ribs and is doubtless just in phase with the vibration of the top.* Following John Schelleng's analysis (Newsletter No. 16, Nov. 1971) it can be seen that this motion of the back plate, far from adding to the sound, will actually subtract from it, since it subtracts from the volume changes of the violin. The pattern at 1300 Hz is remarkably symmetrical. It is tempting to associate the perfection of visual symmetry in these vibration patterns with acoustic perfection of the violin. A little thought will show however that the sound radiation might well be enhanced if the Chladni pattern were not so symmetrical.

---

*This statement turns out to be incorrect. The vibration of the back at 390 Hz is in opposite phase to that of the top. The vibration of the area appearing in the photo does contribute volume changes and is responsible for a significant portion of the output at 390 Hz.